UNCLASSIFIED

AD NUMBER
AD377073
CLASSIFICATION CHANGES
TO: **UNCLASSIFIED**
FROM: **CONFIDENTIAL**
LIMITATION CHANGES
TO: **Approved for public release; distribution is unlimited.**
FROM: **Distribution authorized to U.S. Gov't. agencies and their contractors; Administrative/Operational Use; OCT 1966. Other requests shall be referred to Air Force Rocket Propulsion Lab., Edwards AFB, CA.**
AUTHORITY
AFRPL ltr 31 Aug 1973 ; AFRPL ltr 31 Aug 1973

THIS PAGE IS UNCLASSIFIED

SECURITY MARKING

The classified or limited status of this report applies to each page, unless otherwise marked.
Separate page printouts MUST be marked accordingly.

THIS DOCUMENT CONTAINS INFORMATION AFFECTING THE NATIONAL DEFENSE OF THE UNITED STATES WITHIN THE MEANING OF THE ESPIONAGE LAWS, TITLE 18, U.S.C., SECTIONS 793 AND 794. THE TRANSMISSION OR THE REVELATION OF ITS CONTENTS IN ANY MANNER TO AN UNAUTHORIZED PERSON IS PROHIBITED BY LAW.

NOTICE: When government or other drawings, specifications or other data are used for any purpose other than in connection with a definitely related government procurement operation, the U. S. Government thereby incurs no responsibility, nor any obligation whatsoever; and the fact that the Government may have formulated, furnished, or in any way supplied the said drawings, specifications, or other data is not to be regarded by implication or otherwise as in any manner licensing the holder or any other person or corporation, or conveying any rights or permission to manufacture, use or sell any patented invention that may in any way be related thereto.

CONFIDENTIAL

AFRPL-TR-66-239

327078

(TITLE UNCLASSIFIED)

REINFORCED GRAIN ADVANCED DEVELOPMENT PROGRAM

ROCKETDYNE, A DIVISION OF
NORTH AMERICAN AVIATION, INC.
SOLID ROCKET DIVISION
McGREGOR, TEXAS

OCTOBER 1966

DDC
NOV 28 1966
D

AIR FORCE ROCKET PROPULSION LABORATORY
RESEARCH AND TECHNOLOGY DIVISION
AIR FORCE SYSTEMS COMMAND
EDWARDS AIR FORCE BASE, CALIFORNIA

CONFIDENTIAL

When U.S. Government drawings, specifications, or other data are used for any purpose other than a definitely related Government procurement operation, the Government thereby incurs no responsibility nor any obligation whatsoever, and the fact that the Government may have formulated, furnished, or in any way supplied the said drawings, specifications, or other data, is not to be regarded by implication or otherwise, or in any manner licensing the holder or any other person or corporation, or conveying any rights or permission to manufacture, use, or sell any patented invention that may in any way be related thereto.

AFRPL-TR-66-239

(TITLE UNCLASSIFIED)

REINFORCED GRAIN ADVANCED DEVELOPMENT PROGRAM

ROCKETDYNE, A DIVISION OF
NORTH AMERICAN AVIATION, INC.
SOLID ROCKET DIVISION
McGREGOR, TEXAS

OCTOBER 1966

DOWNGRADED AT 3 YEAR INTERVALS;
DECLASSIFIED AFTER 12 YEARS.
DOD DIR 5200.10

This document contains information affecting the national defense of the United States within the meaning of the Espionage Laws, Title 18, U.S.C., Sections 793 and 794. Its transmission or the revelation of its contents in any manner to an unauthorized person is prohibited by law.

AIR FORCE ROCKET PROPULSION LABORATORY
RESEARCH AND TECHNOLOGY DIVISION
AIR FORCE SYSTEMS COMMAND
EDWARDS AIR FORCE BASE, CALIFORNIA

NOTICE

UNITED STATES PATENT OFFICE SECRECY ORDER

A patent application has been filed in the U.S. Patent Office by North American Aviation, Inc. based upon subject matter included herein or related hereto, and the Secrecy Order appended hereto has been issued thereon pursuant to Title 35, United States Code (1952) Sections 181-188. Further dissemination of said subject matter is prohibited except in strict compliance with said order. The recipient of this document is requested to notify all persons who will have access to this material of the Secrecy Order. Penalties for violation of a Secrecy Order include a fine of up to $10,000 or imprisonment for not more than two years, or both.

DEPARTMENT OF COMMERCE
United States Patent Office
Washington

SECRECY ORDER

NOTICE: To the applicant above named, his heirs and any and all his assignees, attorneys and agents, hereinafter designated principals:

You are hereby notified that your application as above identified has been found to contain subject matter, the unauthorized disclosure of which might be detrimental to the public safety or defense, and you are ordered in nowise to publish or disclose the invention or any material information with respect thereto, including hitherto unpublished details of the subject matter of said application, in any way to any person not cognizant of the invention prior to the date of the order, including any employee of the principals, but to keep the same secret except by written permission first obtained of the Commissioner of Patents, under the penalties of 35 U.S.C. (1952) 182, 186.

Any other application which contains any significant part of the subject matter of the above identified application falls within the scope of this order. If such other application does not stand under a secrecy order, it and the common subject matter should be brought to the attention of the Patent Security Division, Patent Office.

If prior to the issuance of the secrecy order any significant part of the subject matter has been revealed to any person, the principals shall promptly inform such person of the secrecy order and the penalties for improper disclosure.

This order should not be construed in any way to mean that the Government has adopted or contemplates adoption of the alleged invention disclosed in this application; nor is it any indication of the value of such invention.

DEPARTMENT OF COMMERCE
United States Patent Office
Washington

PERMIT FOR PATENT APPLICATION

CLASSIFIED BY GOVERNMENT CONTRACT

This permit authorizes the principals, as designated in the secrecy order, to take any action with regard to the subject matter of the application , to the extent authorized by the security requirements of the Government contract which imposes the highest security classification on the subject matter of this application, except that this permit does not authorize export of this application or the subject matter thereof, whether for the foreign filing of corresponding applications or otherwise. Permission for such export must be specifically obtained from the Patent Office.

FOREWORD

This report was prepared at Rocketdyne, A Division of North American Aviation, Inc., Solid Rocket Division, McGregor, Texas, to document work accomplished under Contract AF 04(611)-9090. The document carries the contractor's library serial number R-4233-22.

Air Force monitor for this effort is Richard E. Spann/RPMM. The term of the basic contract of this Advanced Development Program was from April, 1963, to March 1965.

This report, which contains no classified information extracted from other classified documents, was submitted for approval in August, 1966. This technical report has been reviewed and is approved.

Richard E. Spann
Motor Development Branch

UNCLASSIFIED ABSTRACT

The program originally outlined the development of three designs of lightweight, upper-stage motors using wire as grain reinforcement. During the course of the program, one of the original three upper-stage designs was replaced by a test-weight air-launched demonstration motor with extreme environmental requirements. One of the upper-stage designs included a supersonic split-line gimbaled nozzle. Static firing data of the upper-stage motors showed the design approach yielded high mass fraction goals. However, fabrication experience proved that unusual care and development approaches were necessary. Limitations and areas of risk, as well as preferred approaches, were established from the wide range of tests conducted during this Advanced Development Program.

PREVIOUS PAGE WAS BLANK, THEREFORE WAS NOT FILMED

TABLE OF CONTENTS

Section I

Introduction 1

1. Objective 1

2. Specific Requirements 10

a. Original Program Requirements 10

b. Revisions To Program Requirements 13

3. Program Plan 17

a. Task I--Program Plan (Motors A, B, and D) 21

b. Task II--Design and Fabrication Development 21

c. Task III--Fabrication and Test of Full-Scale Motors 22

Section II

Summary 25

Section III

Conclusions and Recommendations 29

1. Conclusions 29

2. Recommendations 32

Section IV

Motor A 35

1. Design and Development 36

a. Ballistic Design 39

b. Structural Design 63

c. Components 99

d. Process Development 183

e. Processing Procedure 242

f. Development of Quality Control and Non-destructive Test Requirements and Techniques 275

TABLE OF CONTENTS
(Continued)

Section V

Motor A--Full-Scale Fabrication and Test 283
1. Development Motor A-1002 283
a. Fabrication 283
b. Testing 293
2. Development Motor A-1001 309
a. Fabrication 312
b. Testing 330
3. Development Motor A-1002 337
a. Fabrication 340
b. Testing 351
4. Development Motor A-1003 382
a. Fabrication 387
b. Testing 395
5. Development Motor A-1004 412
a. Fabrication 416
b. Testing 434
6. Development Motor A-1005 473
a. Fabrication 474
b. Testing 488

Section VI

Motor B 515
1. Design and Development of Motor B 515
a. Ballistic Design 519
b. Structural Design 532
c. Components 542
d. Process Development 621
e. Processing Procedure 643
f. Aerospace Ground Equipment 644

TABLE OF CONTENTS
(Continued)

Section VII

Motor B Full-Scale Fabrication and Test 647

1. Motor B-2001 647

a. Fabrication 647

b. Testing 657

2. Motor B-2002 682

a. Fabrication 682

3. Motor B-2003 701

Section VIII

Motor C 705

1. Beryllium Wire Technology 705

2. Design 706

3. Hygiene and Saftey 708

Section IX

Motor C-1 709

1. Requirements 709

2. Design 709

Section X

Motor B' 713

1. Requirements 714

2. Design Approach 714

3. Fabrication 720

4. Flightweight Design 725

TABLE OF CONTENTS
(Continued)

Section XI

Motor D 731

1. Ballistic Design 737
   a. Parametric Study 737
   b. Charge Desigh 740
   c. Matrix Propellant 746
2. Structural Design 748
   a. Boost Grain Analysis 750
   b. Sustain and Restart Grain Analysis 754
3. Components 763
   a. Case, Closure, and Nozzle 763
   b. Insulation and Grain Support System 778
   c. Igniter
4. Process Development 806
   a. Cylindrical Grain Design 806
   b. Grain Fabrication 811
   c. Grain Assembly 813
   d. Case Insulation 816
   e. Motor Assembly 817

Appendix I

Design and Hydrotest of 20-Inch Reinforced Grain/Glass Filament Wound 7205/7403 823

Appendix II

Heat Transfer Methods of Analysis 853

Appendix III

Thrust Vector Control System 865

TABLE OF CONTENTS

(Continued)

Appendix IV

Estimation of Energy Required for Solid Propellant Motor Ignition 889

Appendix V

Winding Machines 899

Appendix VI

Cam Design 907

Appendix VII

Automatic Propellant Feed System 917

Appendix VIII

Wire Feed System for Reinforced Grain 927

FIGURES

SECTION I

1	Program Schedule	2
2	Motor A Schematic	3
3	Motor B Schematic	4
4	Motor C Schematic	5
5	Motor D Schematic	7
6	Motor B Thrust Vector Control System	9
7	Program Planning and Status Chart	19
8	RFG Program Plan and Status Chart, March 1965	20

SECTION II

9	RFG Motor A Firing Summary	27

SECTION IV

10	Motor A Assembly	37
11	Nominal Liquid Strand Burning Rate as a Function of Fine Oxidizer Loading	44
12	Strand Burning Rates of an 87.5% Solids-Loaded Propellant (Nonaluminum) with Various Ratios of Strontium Carbonate and Calcium Citrate at Total Level of 5%	46
13	Nominal Liquid Strand Burning Rate as a Function of Depressant Level in RDS-514 Propellant	47
14	Nominal Liquid Strand Burning Rate as a Function of Depressant Level in RDS-523 Propellant	48
15	Estimated Variation of Specific Impulse With Motor Burning Rate	50
16	Estimated Variation of c* With Motor Burning Rate	51
17	Estimated Variation of Pressure Exponent (n) with Burning Rate at 1000 psia, RDS-514 and -523	52

FIGURES

(Continued)

18	Motor Burning Rate vs Pressure, RDS-514 and -523	53
19	Product of Motor Burning Rate at Chamber Pressure and c* vs Chamber Pressure	54
20	Motor A Core Grain Schematic	61
21	GFW Case 10-016 After Rupture	70
22	RFG-Filament Wound Case Design Criteria	76
23	Motor A Layer Detail	83
24	Motor A Core Grain Configuration	96
25	Propellant Spectrum, RDS-526	98
26	Forward and Aft Polar Bosses	101
27	Load Ring Stress Distributions	103
28	Polar Boss Stress Modes	104
29	Polar Boss Design with Integral Load Ring	105
30	Revised Polar Boss Design	106
31	Tensile Test Specimen	109
32	Compressive Test Specimen and Fixture	111
33	Interlaminar Shear Specimen	111
34	Polar Boss Tensile, Shear, and Compression Tests	115
35	Polar Boss Static Load Test	120
36	Polar Boss Hydrotest	122
37	Aft Polar Boss Ablation Loss and Char Depth at End of Firing	129
38	Ablation Loss-vs-Time for Aft Polar Boss Stations	129
39	Aft Polar Boss Temperature Distribution at End of Firing	130
40	Ablation Losses and Char Depth of Forward Closure and Polar Boss at End of Firing	131
41	Ablation Loss-vs-Time for Forward Closure and Polar Boss Stations	132

FIGURES

(Continued)

42	Temperature Distribution of Forward Closure and Polar Boss at End of Firing	133
43	Typical Load Ring Section, Motor A	135
44	Motor A Aft Polar Boss Area	137
45	10-Inch Subscale Polar Boss	139
46	20-Inch Polar Boss	140
47	Static Test of Load Ring	141
48	Load Ring Failure Mode	142
49	Static Load Ring Test, Before and After Test (20 Inch Motor Load Ring)	145
50	Typical Propellant Load Ring Interface Temperature-vs-Exposure Time for Various Thicknesses of a Steel Load Ring	147
51	Temperature-vs-Time for Various Thickness of Load Ring Materials	149
52	Heavyweight Nozzle Configuration	154
53	Flightweight Nozzle Configuration	155
54	Heavyweight Nozzle Configuration With Composite Throat	156
55	Predicted Ablation Loss-vs-Time for Nozzle Stations	160
56	Predicted Ablation Losses and Char Depth of the Aft Polar Boss and Nozzle at the End of Firing	161
57	Predicted Bond Line Temperature-vs-Time Between 101-Graphite and FM5067	164
58	Predicted Bond Line Temperature-vs-Time at Nozzle Station 5	165
59	Predicted Aft Polar Boss and Nozzle Temperature Distribution at End of Firing	167
60	Predicted Corrosion Loss-vs-Time Nozzle Station 3 (Throat)	169
61	Motor A Igniter	171

FIGURES
(Continued)

62	Igniter Development, TO 8001	176
63	Igniter Development, TO 8002	177
64	Igniter Development, TO 8003	178
65	Igniter Development, TO 8004	179
66	Igniter Development, TO 8005	180
67	Igniter Development, TO 8006	181
68	Multi-Helix Angle Concept	186
69	Winding Pattern, First Cycle of Motor A RFG	187
70	Calculation of Buildup at Pole	190
71	Dome and Pole Layer Thickness	191
72	Filament Length on Dome	193
73	Polar Buildup	194
74	Dome Section of Two Cycles of Reinforced Grain	204
75	Before Hydrotest of Case A-1412	220
76	Typical GFW Case Instrumentation	223
77	After Hydrotest of Case A-1412	225
78	Pressure-vs-Hoop Strain for GFW A-1412	227
79	Pressure-vs-Longitudinal Strain for GFW A-1412	228
80	Before Hydrotest of Case A-1413	231
81	After Hydrotest of Case A-1413	232
82	Pressure-vs-Average Strain for GFW A-1413	234
83	Case/Skirt Buildup on Case A-1414	236
84	A-1414 Before Testing	239
85	A-1414 After Testing	240
86	Pressure-vs-Average Strain for GFW A-1414	241
87	Application of Tenite to Surface of Sand/PVA Mandrel	247
88	Spraying RTV Over the Tenite Coated Sand/PVA Mandrel	248

FIGURES

(Continued)

89	Installing Aft Polar Boss Into Mandrel Assembly	249
90	Wrapping Mandrel Assembly With Polyken Tape	250
91	Winding of Check-out Pattern on Mandrel Assembly	251
92	RFG For Winding of High Angle Fill Layer	253
93	Installation of Load Ring During Winding of RFG	254
94	Reinforced Grain Ready for Restriction	255
95	Restricted RFG Readied for Winding of GFW Case	257
96	Glass Roving Threading Sequence	260
97	Helix Winding of a Heavyweight GFW Case	261
98	Glass Cloth Reinforced Being Wrapped on GFW Skirt	263
99	Completed GFW Case Prior to Removal From Winding Machine	264
100	Washout of Soluble Mandrel	265
101	Removal of Liner From RFG/GFW After Mandrel Washout	267
102	Core Mandrel Assembly	269
103	Motor in Casting Pit Readied for Casting of Core Grain	270
104	Casting of Core Propellant into RFG	271
105	Installing Nozzle	273
106	Full Assembled Motor	274
107	Quality Control History Card	276

SECTION V

108	Pantograph Tracing for RFG A-1212	291
109	GFW-1415 Skirt Buildup	295
110	Pressure-vs-Time for Motor A-1006	298
111	Location of Strain Gages and Linear Potentiometers for Motor A-1212	301

FIGURES

(Continued)

112	Pressure-vs-Hoop Strain in GFW Case Motor A-1006	304
113	Pressure-vs-Hoop Strain in Inner Surface of RFG Motor A-1006	306
114	Composite Hoop Stress (GFW Case) vs Composite Hoop Strain (GFW Case) Motor A-1006	307
115	Estimated Thrust and Pressure Time, A-1001 and Flightweight Design	312
116	Reinforced Grain of A-1001	315
117	Motor A-1001 GFW Case Dome Section, Aft End	323
118	Motor A-1001 GFW Case Dome Section, Forward End	324
119	"Bumps" on RFG of A-1001	326
120	Dome Restrictions of RFG, A 1001	327
121	Cylindrical Restriction of A-1001	329
122	A-1001 in Firing Stand	330
123	Estimated Pressure-Time, A-1001	333
124	Pressure vs Time for Motor A-1001	334
125	Pressure and Strain vs Time for Motor A-1001	336
126	Estimated Thrust and Pressure vs Time, A-1002	338
127	A-1002 Before Firing	352
128	A-1002 During Firing	353
129	A-1002 After Firing	354
130	Pressure-vs-Time, A-1002	357
131	Location of Strain Gages and Linear Potentiometers, A-1002	359
132	Strain vs Time, A-1002	360
133	Strain vs Time, A-1002 (Gage 29)	361
134	Strain vs Time, A-1002	362
135	Deflection vs Time, A-1002 (Gages 1 and 2)	363
136	Pressure and Hoop Strain vs Time, A-1002	365

FIGURES

(Continued)

137	Temperature vs Time from Thermocouples on Motor A-1002 Forward Dome	366
138	Temperature vs Time for Thermocouples on Motor A-1002 Aft Dome	367
139	Temperature vs Time from Thermocouples Located at the Forward and Aft Tangent of the Cylindrical Section of Motor A-1002	368
140	Section GFW Case, A-1002	369
141	Section Forward End of GFW Case, A-1002	370
142	Sectioned Nozzle, A-1002	372
143	Temperature vs Time from Thermocouples on Motor A-1002 Nozzle Exit Cone	373
144	Location of Thermocouples on Motor A-1002 Nozzle Exit Cone	374
145	Temperature vs Time from Thermocouples Embedded Motor A-1002 Nozzle Exit Cone	375
146	Nozzle Materials Losses and Char Depths after Firing, A-1002	377
147	Ignition Transient for Motor A-1002, Utilizing Igniter P/N 802476	379
148	Doubler for A-1003	383
149	Estimated Thrust and Pressure-vs-Time for Motor A-1003 and Flightweight Design	385
150	A-1003 on Firing Stand	396
151	Thrust and Pressure-vs-Time, A-1003	397
152	Location of Strain Gages and Linear Potentiometers for Motor A-1003	399
153	Location of Thermocouples for Motor A-1003	400
154	Strain-vs-Time in Cylindrical Section for Strain Gages 1 Through 6 for Motor A-1003	402
155	Strain-vs-Time in Cylindrical Section for Strain Gages 7 through 12 for Motor A-1003	403

FIGURES

(Continued)

156	Strain-vs-Time in Forward Dome for Strain Gages 13 through 16 for Motor A-1003	404
157	Strain-vs-Time in Forward Dome for Strain Gages 17 and 18 for Motor A-1003	405
158	Strain-vs-Time in Aft Dome for Motor A-1003	406
159	Deflection-vs-Time for Motor A-1003	407
160	Temperature-vs-Time for Motor A-1003	408
161	A-1003 Ignition, Pressure-vs-Time	410
162	Estimated Thrust- and Pressure-vs-Time Motor A-1004	415
163	Forward Polar Boss, Showing Added Load Ring Lock	421
164	Aft Polar Boss, Showing R-142 "Boot"	421
165	Aft Polar Boss, Showing Test Failure Location	422
166	Aft Polar Boss, Showing Increased Boss Insulation	423
167	Cracked Aft Polar Boss of Motor A-1004	427
168	Motor A-1004 Aft Polar Boss After Removal of Cracked Material	428
169	Two Cracked Pieces Removed from Motor A-1004 Aft Polar Boss	429
170	Repaired Aft Polar Boss, Motor A-1004	430
171	Estimated Material Loss, Char Depth, and 500 F Isotherm for RFG Motor A-1004 Aft Polar Boss	431
172	Motor A-1004 Before Test	435
173	Motor A-1004 Before Test, Looking in Nozzle	436
174	Motor A-1004 Test Firing	437
175	Pressure- and Thrust-vs-Time for Motor A-1004	439
176	Pressure- and Thrust-vs-Time for Motors A-1002 and A-1004	440
177	RFG Ignition, Motors A-1002, 1003, and 1004	443
178	Location of Strain Gages and Linear Potentiometers for Motor A-1004	444

FIGURES

(Continued)

179	Aft Dome Strain-vs-Time for Motor A-1004	445
180	Cylinder Strain-vs-Time for Motor A-1004 (Gages 9 and 10)	446
181	Cylinder Strain-vs-Time for Motor A-1004 (Gages 3, 4, and 8)	447
182	Cylinder Strain-vs-Time for Motor A-1004 (Gages 5, 6, 11, and 12)	448
183	Forward Dome Strain-vs-Time for Motor A-1004	449
184	Forward and Aft Dome Deflection-vs-Time for Motor A-1004	450
185	Cylinder Longitudinal Deflection-vs-Time for Motor A-1004	451
186	Location of Thermocouples on Nozzle Exit Cone of Motor A-1004	453
187	Location of Thermocouples for Motor A-1004	454
188	Forward Dome Temperature-vs-Time for Motor A-1004 (Thermocouples 1, 2, and 3)	455
189	Forward Dome Temperature-vs-Time for Motor A-1004 (Thermocouples 4, 5, and 6)	456
190	Forward Closure Temperature-vs-Time for Motor A-1004	457
191	Cylinder Temperature at Forward Tangent Plane-vs-Time for Motor A-1004	458
192	Cylinder Temperature at Center-vs-Time for Motor A-1004	459
193	Cylinder Temperature at Aft Tangent Plane-vs-Time for Motor A-1004	460
194	Aft Dome Temperature-vs-Time for Motor A-1004 (Thermocouples 9, 10, and 11)	461
195	Aft Dome Temperature-vs-Time for Motor A-1004 (Thermocouples 12, 13, and 14)	462
196	Aft Dome Insulation Exterior Temperature-vs-Time for Motor A-1004	464

FIGURES

(Continued)

197	Nozzle Exit Cone Temperature-vs-Time for Motor A-1004	465
198	Material Loss and Char Depth of Forward Polar Boss and Closure for Motor A-1004	466
199	Material Loss and Char Depth of Aft Polar Boss for Motor A-1004	467
200	Material Loss and Char Depth of Nozzle Assembly for Motor A-1004	469
201	Motor A-1005 Case Change	473
202	Estimated Thrust and Pressure vs Time Motor A-1005	476
203	Bi-Propellant Interfaces	485
204	Pressure and Thrust vs Time for Motor A-1005	491
205	Strain Gage and Linear Potentiometer Locations for Motor A-1005	493
206	Pressure and Thrust vs Time for Motor A-1005	495
207	Forward Dome Strain vs Time for Motor A-1005	496
208	Forward Dome Strain vs Time (Expanded Time Scale) for Motor A-1005	497
209	Aft Dome Strain vs Time for Motor A-1005	498
210	Aft Dome Strain vs Time (Expanded Time Scale) for Motor A-1005	499
211	Cylinder Strain vs Time for Motor A-1005	500
212	Cylinder Strain vs Time (Expanded Time Scale) for Motor A-1005	501
213	Displacement vs Time for Motor A-1005	502
214	Displacement vs Time (Expanded Time Scale) for Motor A-1005	503
215	Forward Closure Temperature vs Time for Motor A-1005	504
216	Internal Thermocouple Locations for Motor A-1005	507
217	Nozzle Thermocouple Locations for Motor A-1005	508
218	Case Thermocouple Locations for Motor A-1005	509
219	Forward Closure Temperature vs Time for Motor A-1005	511

FIGURES

(Continued)

SECTION VI

220	Motor B General Arrangement	517
221	Motor B Core Grain Cross Section and Conicyl Configuration	522
222	Motor B Estimated Performance - Flightweight Motor (-75 F)	524
223	Motor B Estimated Performance - Flightweight Motor (60 F)	525
224	Motor B Estimated Performance - Flightweight Motor (170 F)	526
225	Motor B Estimated Performance - Flightweight Motor, Nozzle Ratio 10:1 (-75 F)	528
226	Motor B Estimated Performance - Flightweight Motor, Nozzle Ratio 10:1 (60 F)	529
227	Motor B Estimated Performance - Flightweight Motor, Nozzle Ratio 10:1 (170 F)	530
228	Forward End, Core Grain--Motor B	534
229	Aft End, Core Grain--Motor B	535
230	Strain Capability and Thermally Induced Strain vs Temperature	536
231	Strain Capability and Pressure - Induced Strain vs Temperature	537
232	Thermal and Pressure Margin of Safety vs Temperature	538
233	Margin of Safety for Combined Loads vs Temperature	539
234	Longitudinal Stresses in Forward End, Model for -75 F	540
235	Longitudinal Stresses in Aft End, Model for -75 F	541
236	Motor B Forward Polar Boss	543
237	Motor B Aft Polar Boss	544
238	Aft Polar Boss Material Loss and Char Depths at End of a -75 F Firing	549

FIGURES

(Continued)

239	Aft Polar Boss Material Loss and Char Depths at End of a 60 F Firing	550
240	Aft Polar Boss Material Loss and Char Depths at End of a 170 F Firing	551
241	Aft Polar Boss Temperature Distribution at the End of a -75 F Firing	552
242	Aft Polar Boss Temperature Distribution at the End of a 60 F Firing	553
243	Aft Polar Boss Temperature Distribution at the End of 170 F Firing	554
244	Material Loss vs Time and Various Firing Temperatures and the 7.45 Inch and 8.25 Inch Nozzle Entrance Diameter at Nozzle Station 11	555
245	Material Loss vs Time for Various Firing Temperatures for the 7.45 Inch and 8.25 Inch Nozzle Entrance Diameter at Nozzle Station 12	556
246	Material Loss vs Time for Various Firing Temperatures for the 7.45 Inch and 8.25 Inch Nozzle Entrance Diameter at Nozzle Station 13	557
247	Material Loss vs Time for Various Firing Temperatures for the 7.45 Inch and 8.25 Inch Nozzle Entrance Diameter at Nozzle Station 14	558
248	Material Loss vs Time for Various Firing Temperatures for the 7.45 Inch and 8.25 Inch Nozzle Entrance Diameter at Nozzle Station 15	559
249	Material Loss vs Time for Various Firing Temperatures at Nozzle Station 16	560
250	Material Loss vs Time for Various Firing Temperatures at Nozzle Station 17	560
251	Material Loss vs Time for Various Firing Temperatures at Nozzle Station 18	560
252	Material Char Depth vs Time for Various Firing Temperatures at Nozzle Station 19	561

FIGURES

(Continued)

253	Material Char Depth vs Time for Various Firing Temperatures at Nozzle Station 20	561
254	Material Loss and Char Depth at the End of Firing of the Forward Polar Boss for a -75 F Firing	563
255	Material Loss and Char Depth at End of Firing of the Forward Polar Boss for a 60 F Firing	564
256	Material Loss and Char Depth of the Forward Polar Boss at the End of Firing for a 170 F Firing	565
257	Temperature Distribution of Forward Polar Boss at End of -75 F Firing	566
258	Temperature Distribution of Forward Polar Boss at End of 60 F Firing	567
259	Temperature Distribution of Forward Polar Boss at End of 170 F Firing	568
260	Char Depth vs Time for Various Firing Temperatures, Forward Polar Boss, Station 1	569
261	Char Depth vs Time for Various Firing Temperatures at Forward Polar Boss Station 2	569
262	Char Depth vs Time for Various Firing Temperatures at Forward Polar Boss Station 3	570
263	Char Depth vs Time for Various Firing Temperatures at Forward Polar Boss Station 4	570
264	Char Depth vs Time for Various Firing Temperatures at Forward Polar Boss Station 5	571
265	Char Depth vs Time for Various Firing Temperatures at Forward Polar Boss Station 6	571
266	Char Depth vs Time for Various Firing Temperatures at Forward Polar Boss Station 7	572
267	Char Depth vs Time for Various Firing Temperatures at Forward Polar Boss Station 8	572
268	Char Depth vs Time for Various Firing Temperatures at Forward Polar Boss Station 9	573
269	Char Depth vs Time for Various Firing Temperatures at Forward Polar Boss Station 10	573

FIGURES

(Continued)

270	Temperature vs Time for Forward Polar Boss Station 1 for Various Firing Temperatures	574
271	Section View: Forward Polar Boss	576
272	Typical Load Ring Section	577
273	Motor B Nozzle Assembly	581
274	TVC Program Schedule	587
275	Strengths of Plastics vs Temperature	591
276	Strength of Graph-I-Tite "G" vs Temperature	592
277	Strength of Pyrolitic Graphite vs Temperature	593
278	TVC System Block Diagram	594
279	Results of Temperature Cycling and Vibration Tests	602
280	Results of Longitudinal and Transverse Frequency Surveys, Longitudinal Axis	607
281	Results of Longitudinal and Transverse Frequency Surveys, Transverse Axis	608
282	Igniter Development, TO 8010	609
283	Igniter Development, TO 8011	610
284	Forward Doubler, Motor B	614
285	Aft Doubler, Motor B	615
286	Variation of Flow Port Diameter with Net Reverse Thrust for Four Ports at Angles of 30, 35 and 40 Degrees	617
287	Variation of Flow Port Diameter with Net Reverse Thrust for Three Ports at Inclination Angles of 30, 35, and 40 Degrees	618
288	GFW Case B-2415 Before Hydrotest	631
289	GFW Case B-2415 After Hydrotest	632
290	Motor B GFW Skirt-to-Case Fill	633
291	GFW Case B-2416 Before Test	637
292	GFW Case B-2416 After Test	638

FIGURES

(Continued)

293	Pressure vs Strain for GFW A-1416	639
294	Average Force vs Strain	641
295	Average Force vs Strain	642

SECTION VII

296	Closeup of Motor Prior to Testing Cycle 1 (B-2001)	658
297	Location of Strain Gages and Linear Potentiometers for Motor B-2001	661
298	Forward Dome, Internal, After First Pressure Cycle	663
299	Aft Dome, Internal, After First Pressure Cycle	664
300	Pressure vs Time for Motor B-2001	665
301	Aft Dome, Internal, After Second Pressure Cycle	666
302	Forward Dome, Internal, After Second Pressure Cycle	667
303	Pressure vs Time for Motor B-2001	668
304	External View After Third Pressure Cycle	670
305	Forward Dome, Internal, After Third Pressure Cycle	671
306	Aft Dome, Internal, After Third Cycle	672
307	Aft Dome, Internal, After Third Pressure Cycle With LAGZ Coating Removed	673
308	Forward Dome, Internal, With LAGZ Liner Removed After Third Pressure Cycle	674
309	Pressure vs Time for Motor B-2001	675
310	Pressure vs Hoop Strain in Glass Case	676
311	Pressure vs Hoop Strain at Inner Surface of RFG	678
312	Composite Hoop Stress (GFW) vs Composite Hoop Strain (GFW)	680
313	Composite Hoop Stress on Inner Surface of RFG vs Composite Hoop Strain at Inner Surface of RFG	681

FIGURES

(Continued)

314	Ring and Doubler Installation; Motor B-2002 Aft Polar Boss Area	685
315	Motor B-2002, Thermocouple Locations (Forward End)	690
316	Boss Movement	696
317	Low Density Areas Near Bosses	696
318	Forward Doubler Tear	697
319	Star Valley Crack in B-2002	698
320	Forward Conicyl Crack in B-2002	699
321	Location of Crack in Star Valley of B-2002 Core	702
322	Motor B Photoelastic Study	703

SECTION X

323	Motor B Testweight Design	715
324	Pressure and Thrust vs Time for Motor B	718
325	4-Slot Burning Pattern	719
326	Dome Contouring Device-Schematic	721
327	Slotter	722
328	Slotted Motor B Type Grain (2530 pounds)	724
329	Motor B Flightweight Design	727

SECTION XI

330	Motor D General Arrangement	735
331	Variation of RFG Burning Rate with Wire Angle	741
332	Motor D Grains	742
333	Estimated Thrust and Pressure vs Time at 70 F	745
334	Stress vs Strain for Aluminum Wire in Motor D	757
335	Motor D Insulated Case Assembly	765

FIGURES

(Continued)

336	Case Temperature vs Time For The Forward and Aft Ends, Motor D	767
337	Motor D Forward Closure Assembly	768
338	Forward Head/Motor Case Interface Joint	769
339	Motor D Nozzle Assembly	770
340	Nozzle/Case Interface Joint	771
341	Temperature vs Time, Motor D Nozzle Throat Section	773
342	Thermal Stress vs Time For Motor D Nozzle Insert, Graph-I-Tite G	774
343	Erosion Loss vs Time for Motor D Nozzle Throat with Graph-I-Tite G Insert	775
344	Temperature vs Time Comparison of Pyrolytic and Monolythic Throat Inserts	776
345	Erosion Loss vs Time Comparison of Pyrolytic and Monolythic Throat Inserts	777
346	Insulation-to-Case Interface Temperature vs Time When Exposed to 650 F Environment	781
347	Insulation Material Performance Prediction	783
348	Deflection vs Pressure for General Electric Co. Sponge Rubber	786
349	Deflection vs Time Controlled Pressure for General Electric Co. Sponge Rubber	787
350	Insulation/Propellant Interface Temperature vs Time at the Restart Grain (Forward End)	790
351	Frame-Mounted Thermesh Test Sample	792
352	Test Motor and Igniter	794
353	Formulation Optimization Tests, 6-Inch Test Motors, Thermesh Igniters	796
354	Nine Motor Evaluation of Thermesh Design Variables	798
355	Six-Inch Test Motors, Thermesh Igniter Evaluation; Test Motors -41 and -31	799
356	Six-Inch Test Motors, Thermesh Igniter Evaluation	800

FIGURES

(Continued)

357	Installation of Thermesh Igniter Within a Typical Boost Grain on an Unrelated Program	801
358	Assembly of Typical Sustain Grain and Integral Thermesh Igniter on an Unrelated Program	802
359	Boost-Sustain Igniter, Motor D	804
360	Restart Igniter Concept, Motor D	805
361	Preliminary Process Flow Sheet for Motor D	807
362	Low-Angle Cylindrical Grain Fab Method	808
363	Layer Design Calculation Chart	810
364	Temperature vs Time for Conditioning Motor D RFG to Cure Temperature	814
365	Motor D Grain Assembly and Restrictor Mandrel	815
366	Motor D Loading Pressure Chamber	819
367	Temperature vs Time for Conditioning Motor D During Temperature Cycling	821
368	Temperature vs Time for Conditioning Motor D During Temperature Cycling	822

TABLES

SECTION II

I	Motor A - Summary of Test Results	26
II	Motor B - Summary of Test Results	28

SECTION IV

III	Summary of Motor A Parameter Evaluation	41
IV	Propellant Compositions Developed (And Used) for Reinforced Grains	43
V	Motor A RFG Propellant Weight and Burning Rate Data	57
VI	Motor A Design Weight Summary	63
VII	Properties Used in Filament Wound Case Design	67
VIII	IR&D Resin Study	68
IX	Results of Ignition Pressurization Stress Analysis for Motor A Core Grain	99
X	Tensile Properties, FTMS L-P-406	110
XI	Compressive Properties, Per FTMS L-P-406	112
XII	Interlaminar Shear Properties, FTMS L-P-406	113
XIII	Tensile Test Results	116
XIV	Interlaminar Shear Test Results	117
XV	Compressive Test Results	118
XVI	Static Load Test Results on Motor A Polar Bosses and Load Rings	119
XVII	Physical and Mechanical Properties MX-2646 Molding Compound	124
XVIII	Calculated Linear Coefficients of Expansion for MX-2646	125
XIX	Calculated Linear Coefficients of Expansion for MX-2646	126

TABLES

(Continued)

XX	Effect of Aging Propellant RDS-526 with Fiberite MX-2646 Propellant Mechanical Properties	127
XXI	Load Ring Material Study	143
XXII	Motor A Static Load Ring Tests	144
XXIII	Material Properties	159
XXIV	Development Igniter Prefiring and Firing Characteristics	182
XXV	Weights and Dimensional Data of GFW Case A-1412	218
XXVI	Weights Data of GFW Case A-1413	230

SECTION V

XXVII	Propellant for RFG A-1212	285
XXVIII	Grain Winding Data for RG-1212	287
XXIX	Motor A-1006, Layer Construction for RG-1212	290
XXX	Motor A-1006 Winding Parameters, Glass Filament Case GFW 1415 on RG-1212	294
XXXI	Motor A-1006, Weights and Dimension of Case GFW 1415	296
XXXII	Processing Weights for Motor A-1006	297
XXXIII	Maximum and Minimum Recorded RFG and GFW Case Strains, RFG A-1006	299
XXXIV	Estimated Performance Summary, A-1001 and Flightweight Design	310
XXXV	Estimated Weight and Mass Fraction, A-1001 and Flightweight Design	311
XXXVI	Winding Data	317
XXXVII	RFG A-1201 Propellant Properties	321

TABLES

(Continued)

XXXVIII	Estimated Performance RFG Motor A-1001	332
XXXIX	Estimated Performance Summary, Motor A-1002	339
XL	Estimated Weight and Mass Fraction for A-1002 and Flightweight Design	339
XLI	Propellant Properties, Motor A-1002	341
XLII	RFG A-1201 Winding Parameters and Cylindrical Buildup	343
XLIII	Motor A-1002 GFW Case Fabrication Data (GFW 1402)	346
XLIV	Core Propellant Properties	349
XLV	Motor Weight History	350
XLVI	Performance Summary for A-1002	355
XLVII	Weight Summary for Motor A-1002	356
XLVIII	Estimated Performance Summary Motor A-1003 and Flightweight Design	384
XLIX	Estimated Weight and Mass Fraction Motor A-1003 and Flightweight Design	386
L	Construction of Motor A-1003, by Propellant Layers	389
LI	Construction of Motor A-1003, by Wire Layers	390
LII	Weight Summary for A-1003 and Flightweight Design	394
LIII	Estimated Weight and Mass Fraction A-1004 Flightweight Motor	413
LIV	Estimated Performance Summary A-1004	414
LV	A-1004 Propellant Burning Rates and Ambient Mechanical Properties	417
LVI	Winding Data, Motor A-1004	418

TABLES

(Continued)

LVII	Burning Rate Summary for Motors A-1002 and A-1004	420
LVIII	Dimensions and Weights of Motor A-1004 GFW Case	425
LVIX	Motor A-1004 Weight and Mass Fraction Summary	433
LX	Performance Summary for Motor A-1004	438
LXI	Estimated Performance Summary Motor A-1005	475
LXII	Design Estimated Weight and Mass Fraction, Motor A-1005	477
LXIII	A-1005 Processing Data	478
LXIV	A-1005 Propellant Mechanical Properties	479
LXV	Burning Rate Summary for Motors A-1004 and A-1005	480
LXVI	A-1005 Case Dimensions and Weights	483
LXVII	RDS-501 and RDS-526 Formulation	486
LXVIII	Weight and Mass Fraction Summary for Motor A-1005	487
LXIX	Performance Summary for Motors A-1002, A-1004, and A-1005	490

SECTION VI

LXX	Motor B Performance Estimate - Flightweight Motor	523
LXXI	Motor B Performance Estimate - Flightweight Motor	527
LXXII	Motor B Design Weight Summary - Flightweight Motor	531
LXXIII	Motor B Polar Boss Design and Process Considerations	545

TABLES

(Continued)

LXXIV	Motor B Polar Boss Design Parameters	546
LXXV	Motor B Polar Boss Structure Margins	547
LXXVI	Load Distribution (Load Rings)	575
LXXVII	TVC System Requirements	579
LXXVIII	TVC System Schedule	579
LXXIX	TVC Component Requirements	596
XXC	Motor B Nozzle Design	598
XXCI	Weight Breakdown, Test Configuration TVC Systems	599
XXCII	Flight Configuration TVC Systems Weight Breakdown	600
XXCIII	Dimensions and Weights of GFW Case B-2415	629
XXCIV	Dimensions and Weights of GFW Case B-2416	636

SECTION VII

XXCV	Motor B-2001 Grain Winding Data	649
XXCVI	Motor B-2001 Dimensional Changes	651
XXCVII	RFG Propellant Burning Rates	651
XXCVIII	Motor B-2001 Ambient Propellant Physicals	652
XXCIX	Dimensions and Weights of GFW Case B-2401, Motor B-2001	654
XC	Motor B-2001 Weight History and Aluminum Percent	656
XCI	Maximum Recorded RFG and GFW Case Strains	660
XCII	Motor B-2002 Estimated Ballistic Performance	683
XCIII	Motor B-2002 Estimated Weight Summary and Mass Fraction	684
XCIV	Motor B-2002 Grain Winding Data	687

TABLES

(Continued)

XCV	B-2002 RFG Propellant Burning Rates and Ambient Mechanical Properties	691
XCVI	Dimensions and Weights of Motor B-2002 GFW Case	693
XCVII	Core Processing Data, Motor B-2002 and Motor A	700
	SECTION VIII	
XCVIII	Design Requirements for Motor C	706
XCIX	Motor C Estimated Performance from Preliminary Design	707
	SECTION IX	
C	Design Requirements for Motor C-1	710
CI	Performance Summary for Motor C-1 at 60 F in Vacuum	711
CII	Weight and Mass Fraction Summary Motor C-1	712
	SECTION X	
CIII	Motor B and Motor B' Characteristics	730
	SECTION XI	
CIV	Summary of Design Objectives for Motor D	732
CV	Miscellaneous Physical Data	743
CVI	Ballistic Performance	744
CVII	Burning Rates Required with Uncured Matrix Rates	747
CVIII	Matrix Propellant Data (RDS-531)	748
CIX	Matrix Propellant RDS-531 and 532	749

TABLES

(Continued)

CX	Pertinent Characteristics of Reinforced Propellants for Motor D	749
CXI	Pertinent Data for Boost Grain Structural Analysis-Motor D	751
CXII	Pertinent Data for Restart Grain Structural Analysis	758
CXIII	Ablation Evaluation	778
CXIV	Heat Exposure Evaluation	779
CXV	Effects of Heat Exposure on Physical Properties of R-124	780
CXVI	Compression Data for General Electric Co. Sponge Rubber	785
CXVII	Compression Set of General Electric Co. Sponge Rubber	788
CXVIII	Motor D Winding Requirements	812

REFERENCES

As indicated by the title and nature of this program, few reference works on this subject are available. The majority of the limited number available were originated within Rocketdyne. Therefore, this document contains no separate table of references per se. The few "references" used are included in the numbered footnotes, in accordance with MIL-STD-847.

SECTION I

INTRODUCTION

This report describes progress and results of advanced development effort under the Reinforced Grain Program, Contract AF 04(611)-9090, conducted under sponsorship of Solid Rocket Division, Rocket Propulsion Laboratory, Research and Technology Directorate, Air Force Systems Command, Edwards Air Force Base, California. Contract period was April 1963 to March 1965.

1. OBJECTIVE

(C) The objective of the primary Advanced Development Program (see Fig. 1) was to fabricate and test full-scale motors so that an engineering development program utilizing reinforced grain motors tailored to a specific mission could be initiated subsequently with minimum risk. Two motor types, representing typical upper stage and air-launched missile motors, were investigated. Performance requirements for Motor A, B, and C, (high mass fraction units, utilizing ultra-thin fiberglass cases wound over wire filament reinforced grains) were based generally on upper stage Scout (Motor A) and second stage Skybolt requirements (Motors B and C), with payloads patterned after upper stage ICBM requirements. Severe flight loads and temperature range (-75 to 170 F) were specified. Motor C requirements were similar to Motor B, with increased total impulse to be obtained by replacing aluminum with beryllium in the propellant. Motor D, a cartridge-loaded reinforced grain in a steel case, typifies an advanced air-launched rocket motor incorporating stop-restart capability. Figures 2 through 6 present introductory schematics of all four motors and the Motor B thrust vector control system.

(C) Initially the program was directed entirely toward demonstration of full-scale, high mass fraction motors for upper stage application. This application uses the proven pressure-carrying capability and stiffness of the RFG to supplement the strength of the glass filament wound case, thus reducing inert weight. Three distinct motor designs, designated Motors A, B, and C, were included in the program. In the Motor C design, beryllium wire and powder replaces the conventional powdered aluminum to obtain a predicted significant increase in propellant impulse. Means of thrust reversal and thrust vector control were planned as integral parts of Motors B and C. However, the requirement for thrust reversal was later deleted because future systems probably will not require ports in the forward dome as a means of achieving thrust reversal.

CONFIDENTIAL

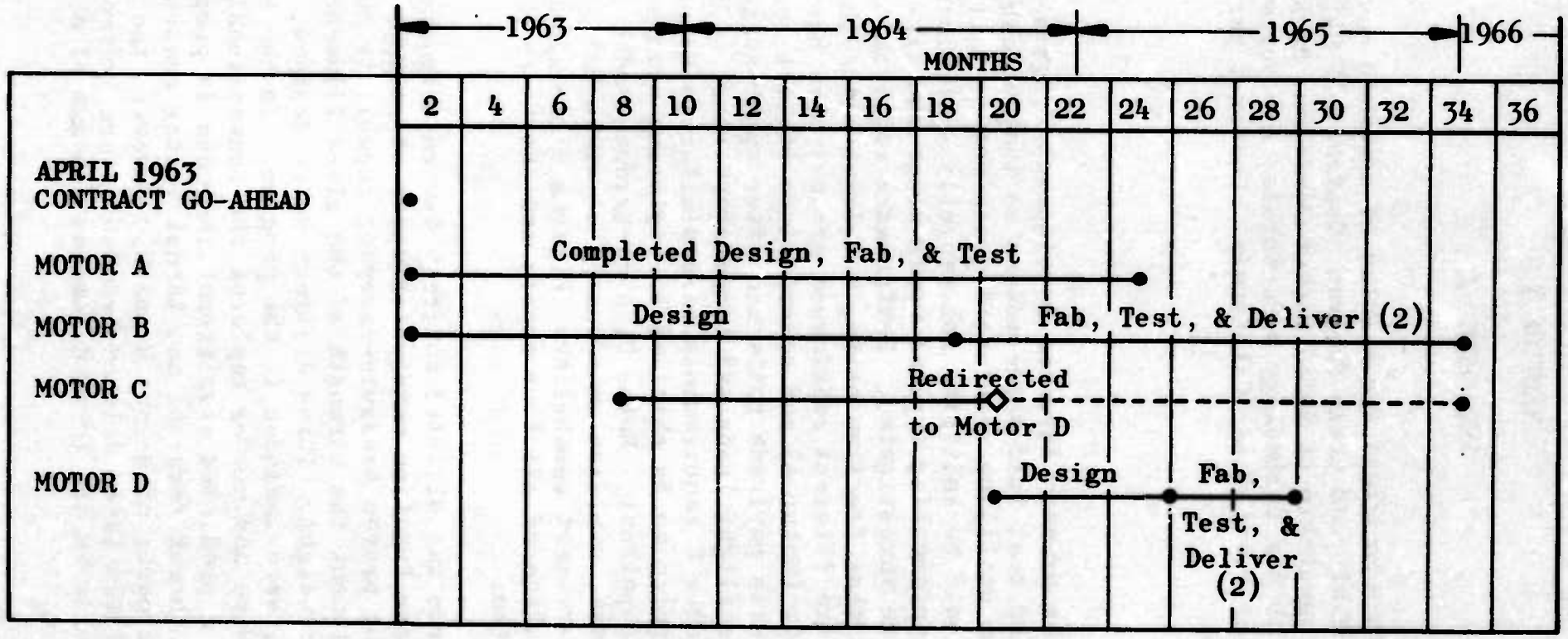


Figure 1. Program Schedule

CONFIDENTIAL

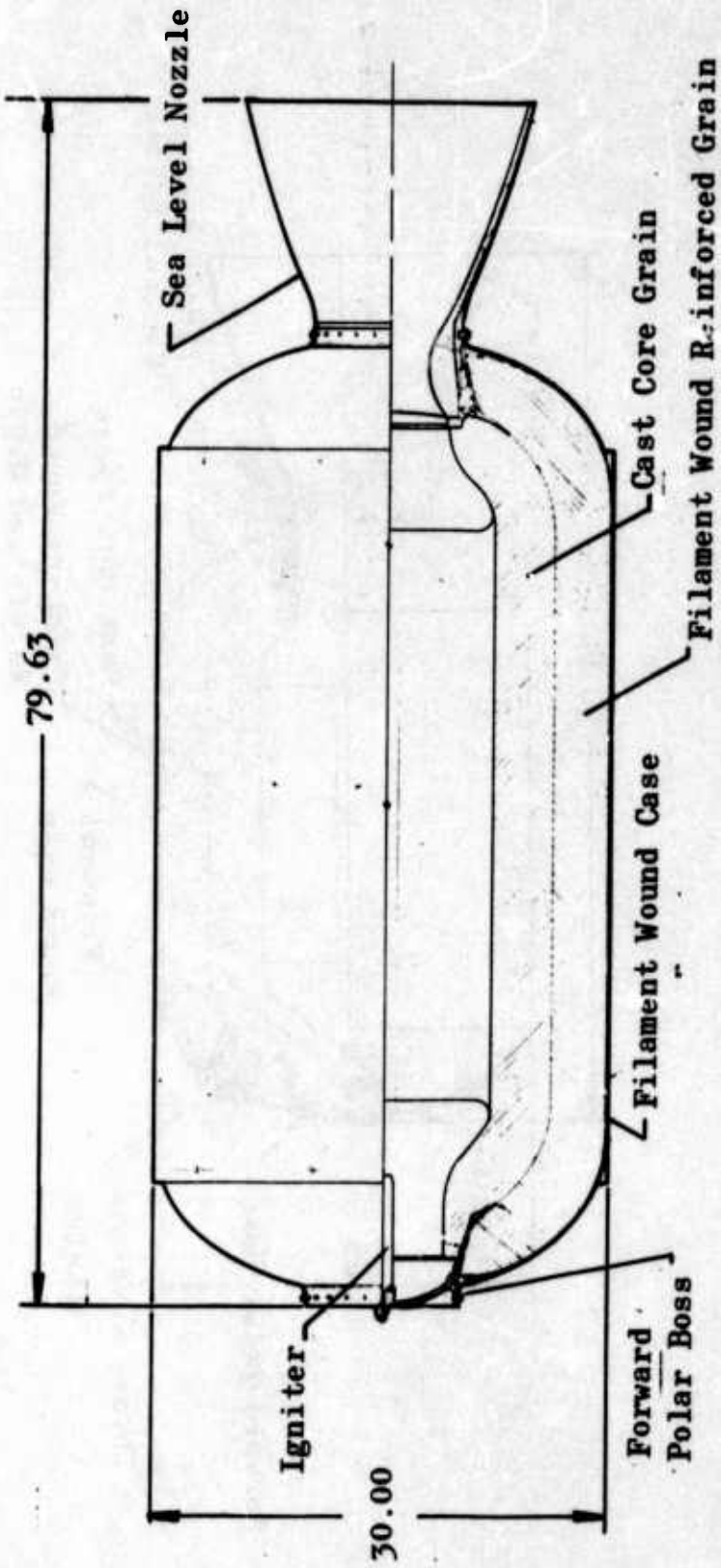


Figure 2. Motor A Schematic

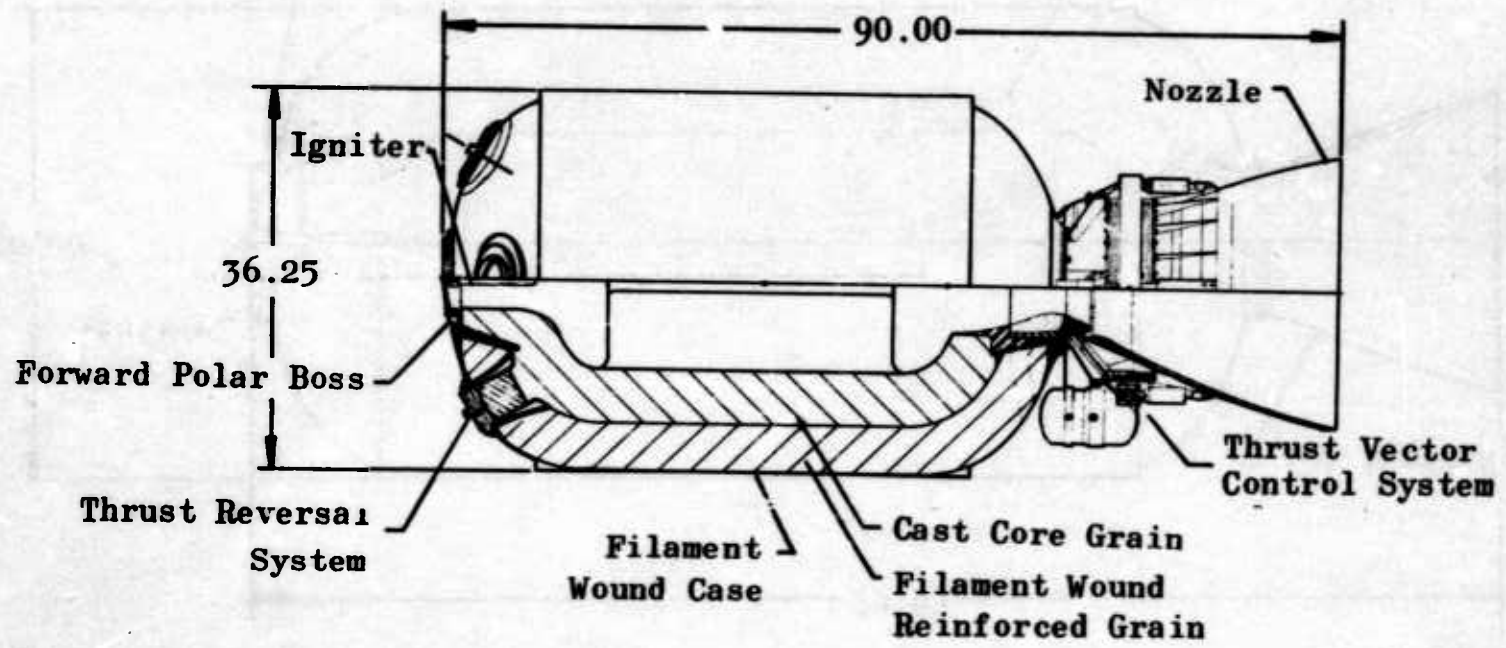


Figure 3. Motor B Schematic

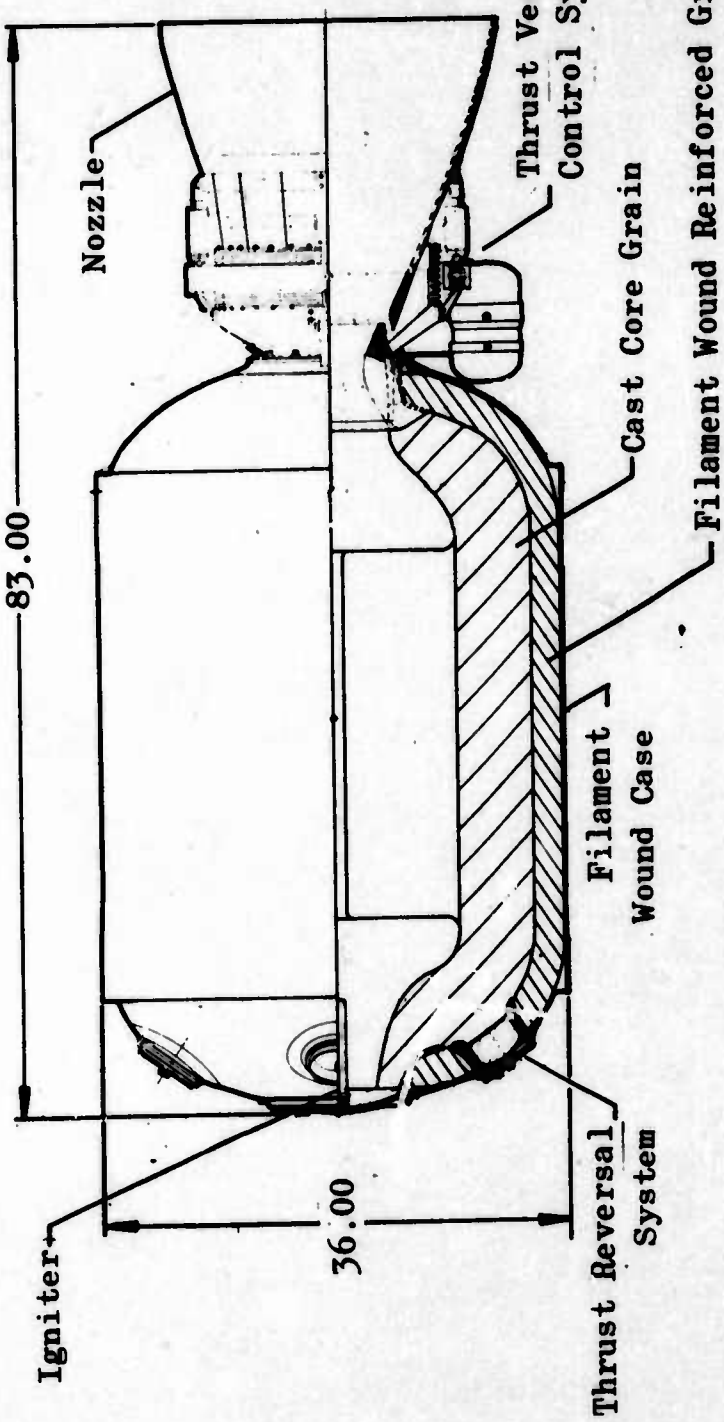
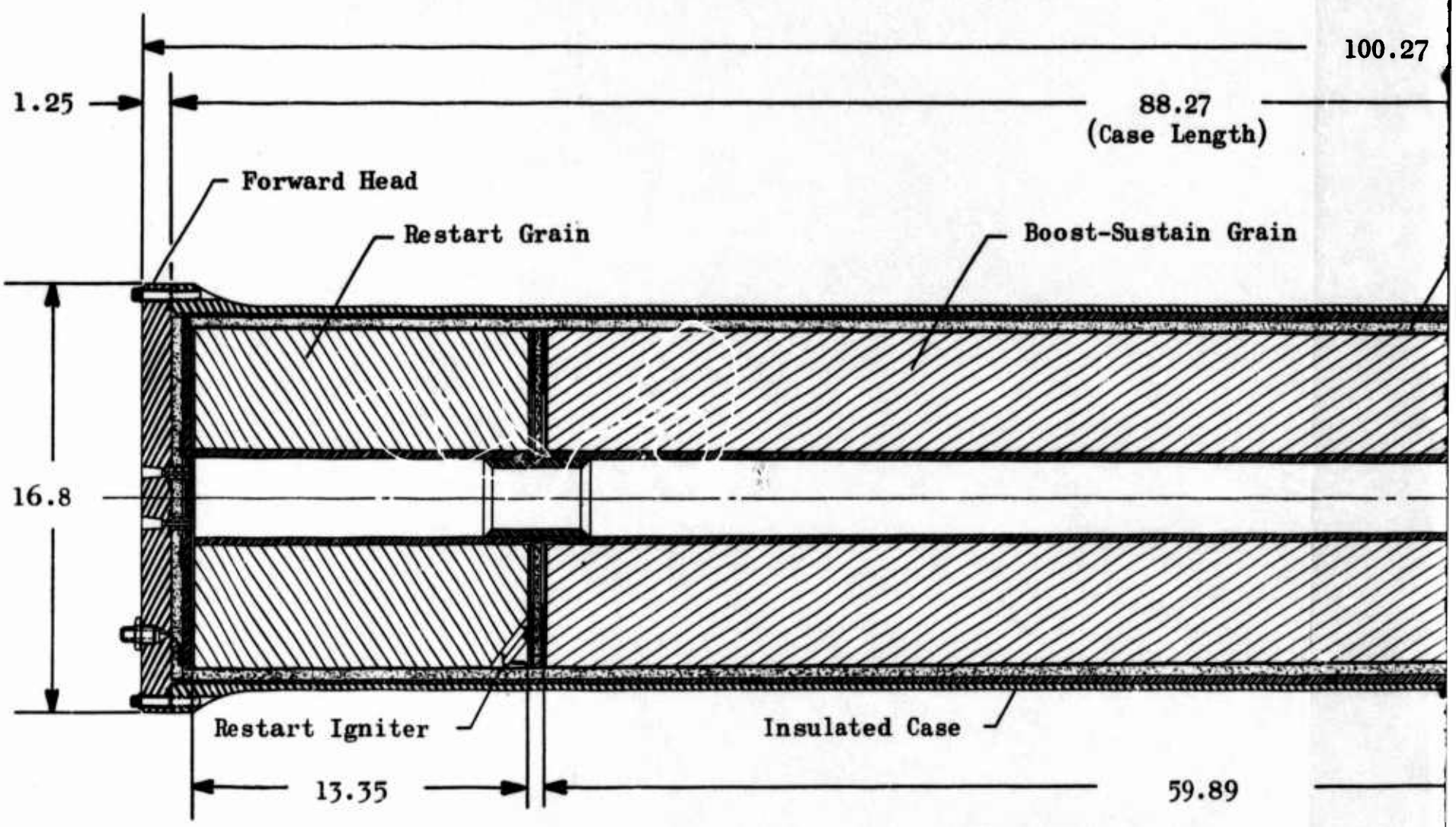


Figure 4. Motor C Schematic


100.27
1.25
88.27
(Case Length)
Forward Head
Restart Grain
Boost-Sustain Grain
16.8
Restart Igniter
Insulated Case
13.35
59.89

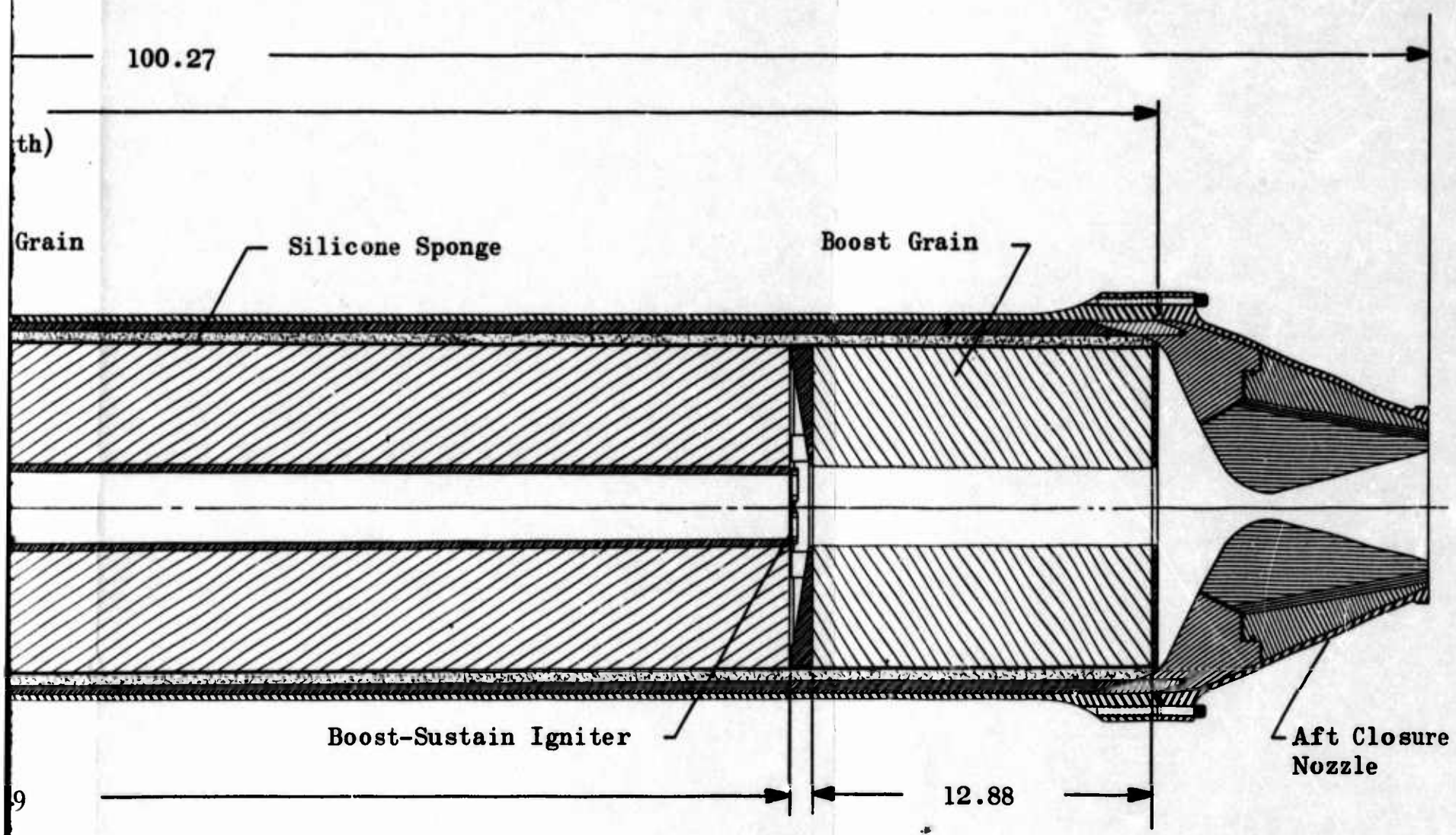


Figure 5. Motor D Schematic

CONFIDENTIAL

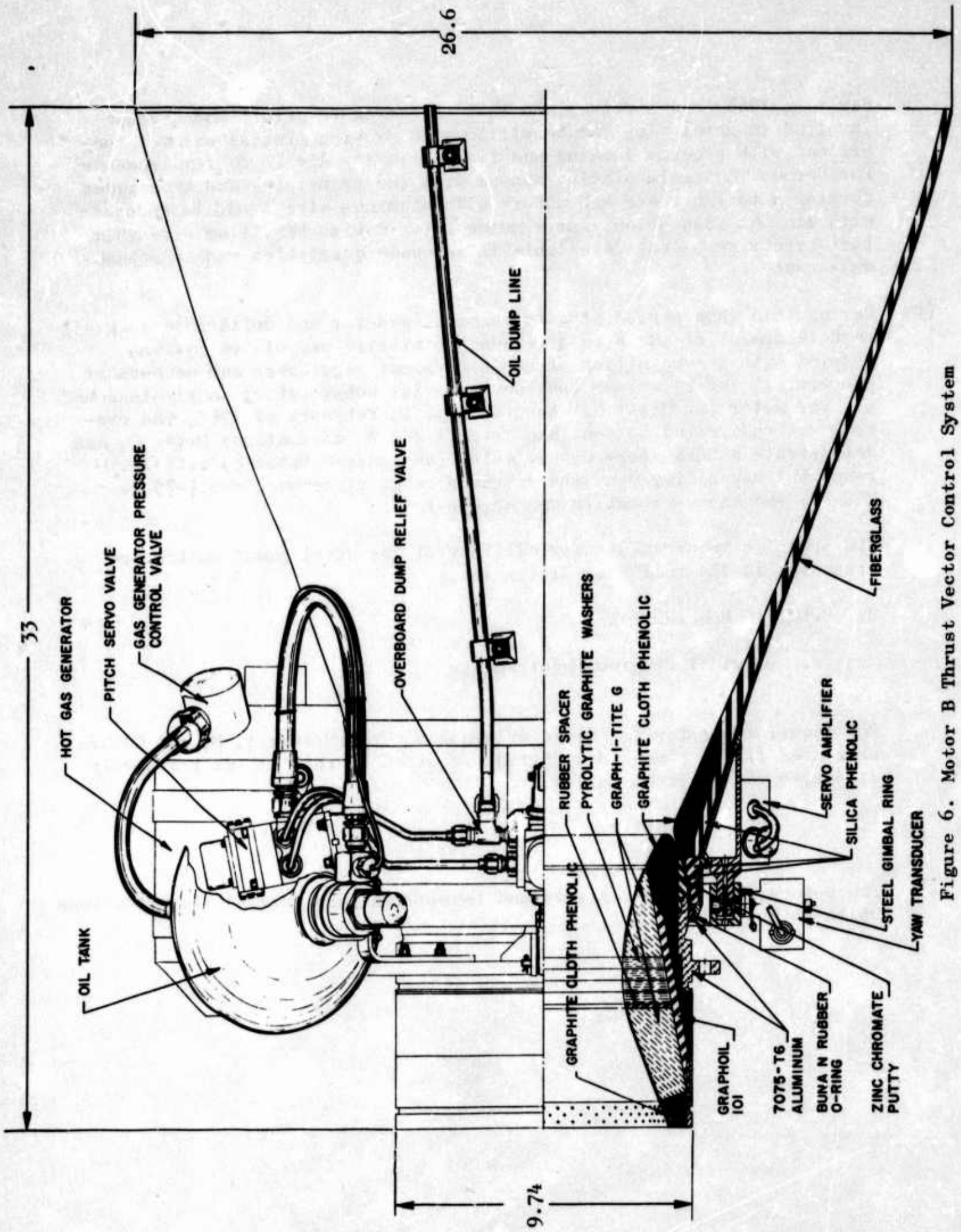


Figure 6. Motor B Thrust Vector Control System

Early in 1964 it was determined that the extended effort and expense involved in developing the beryllium wire drawing process was not consistent with program funding and first-priority Air Force requirements. Furthermore, experimentation showed that the principles and techniques developed to fabricate RFG motors with aluminum wire would be adequate, with minimum adaptation, for winding Motor C with beryllium wire when this type wire becomes available in adequate quantities and at reasonable cost.

(C) During this same period, the increasing need for and deliberate emphasis on development of advanced air-launched missile propulsion systems, coupled with a recognition of RFG's physical ruggedness and mechanical properties, led to strong consideration for substituting an air-launched missile motor for Motor C. Accordingly, in February of 1964, the program was redirected to continue Motor A and B, discontinue Motor C, and demonstrate an RFG stop-restart motor (designated Motor D) with environmental capability over the extended range of temperature (-75 to 250 F), endurance-vibration and aeroheat.

The specific requirements for all four of the development motors are presented in the following discussion.

2. SPECIFIC REQUIREMENTS

a. Original Program Requirements

The requirements for the three original motors (Motors A, B, and C) are presented first. The modifications required to reflect the previously discussed redirections follow.

(1) Dimensions

The motors were to be designed and fabricated according to the dimensions which follow:

	Flightweight Motors	
	A	B & C
Outside Diameter, in. (max)	30	36.25*
(C) Length, in.		
Over-all (max)	100	90
Skirt to Skirt (min)	51	40
Weight, lb		
Total (max)	2600	3200
Mass Fraction (min)	0.96*	0.937**

*With skirts; cylindrical section--36 in.
**Total motor weight shall include: skirts, igniters, thrust reversal system, altitude nozzle, and complete thrust vector control system including gas generator, actuating devices, hydraulic oil, and tank. In the event that a heavyweight gas generator is utilized, the gas generator weight used in calculating mass fraction will be 10.9 lb.

(2) Mechanical and Physical

Flight and payloads loading--buckling criteria, simultaneously applied to forward thrust skirt faces, were specified as follows:

(C) (a) Motor A

Axial Compression Load, lb	40,000
Bending Moment, in.-lb	800,000
Shear Load, lb	7,500
Torsional Moment, in.-lb	110,000

(b) Motor B Loads Simultaneously Applied to Aft Skirt

Axial Compression Load, lb	3,000
Bending Moment, in.-lb	1,500,000
Shear, lb	30,500

(c) Motor C Loads Simultaneously Applied to Aft Skirt

Axial Compression Load, lb	15,000
Bending Moment, in.-lb	500,000
Shear, lb	10,160

(C) (d) Vibration (Motor B only)--Procedure 1 of MIL-R-25534A

Exception: Survey and endurance testing to be conducted at ambient temperature.

Temperature cycling (Motors B and C) was to be conducted in accordance with MIL-R-25534A. The temperature range was -75 to 170 F.

(C) (e) Operational Temperature Range

Motor A	50 to 90 F
Motor B & C	-75 to 170 F

(3) Performance

(C) The rated performance at 60 F and applicable altitude shall be as follows:

	Motor		
	A	B	C
Altitude Condition	Sea Level	Vacuum	Vacuum
Thrust, lb			
Average	16,750	21,000	23,000
Maximum	28,000	30,000	31,000
Minimum Action Time Total Impulse, lb-sec	540,000	800,000	800,000
Ignition			
Maximum Ignition Delay, sec	0.100	0.100*	0.100*
Deliver Specific Impulse, lb-sec/lb (1000 psia at 0° Half Angle)	250 (S.L.)	250 (S.L.)	300 (Vac)
Nozzle Expansion Ratio	Optimum	25:1	25:1

(C) *Additional requirement--shall be capable of ignition to 90,000 feet altitude. Tests of Motors B and C to be conducted at simulated altitude of 100,000 feet or greater.

(4) Thrust Vector Control

(C) Motors B and C shall have a TVC system capable of vectoring the thrust line of action a minimum of plus or minus 4 degrees from centerline in both the pitch and yaw directions.

(5) Thrust Reversal

(C) Motors B and C shall have thrust reversal capabilities according to the following criteria:

1. Port location shall be in accordance with the design as mutually agreed upon between the contractor and the Contracting Officer or his designee.
2. Actuation shall be anytime after 10 seconds of burning.
3. The initial net reverse thrust level, excluding any transient thrust peak at time of actuation, shall be at least 200 pounds when port actuation occurs at a pressure level equivalent to the average chamber pressure at 60 F. Subsequent to port actuation a net reverse thrust shall be continuously maintained. The initial transient net reverse thrust peak shall be nominally 1000 pounds.
4. Must achieve reverse thrust within 5 milliseconds (± 2 milliseconds) after signal.
5. Thrust reversal ports must withstand reverse thrust for seven seconds, regardless of time of activation in motor firing cycle.

b. Revisions To Program Requirements

As the program progressed, the requirements changed and these modifications were necessary:

1. Because RPL mission analysis studies showed no need for thrust termination ports, direction was given to delete the thrust reversal ports in Motors B and C.

2. The slow progress in beryllium wire drawing technology, and its high costs, coupled with the recognition of the need for a rugged, extreme environment, air-launched missile, resulted in the replacement of Motor C with Motor D.

3. A better definition of the Motor B external load requirements, required expanding the original specification.

These modifications changed the original specifications as listed below:

(1) Dimensional Requirement Revisions

Motors A and B were unchanged.

All requirements for Motor C were deleted.

(2) Mechanical and Physical Requirement Revisions

Motor A requirements were unchanged.

(C) These design loads were added for Motor B:

(C)

	Compression, lb	Shear, lb	Bending Moment, in.-lb
Pressurized Condition			
Forward Skirt	15,000	3,000	300,000
Case	15,000	3,000	300,000
Aft Skirt	--	--	--
Unpress Condition (Max Long Accel)			
Forward Skirt	15,000	5,000	500,000
Case	61,500	10,160	823,300
Aft Skirt	61,500	10,160	823,300
Unpress Condition (Max Lat Accel)			
Forward Skirt	3,000	15,000	1,500,000
Case	12,300	30,500	2,469,000
Aft Skirt	12,300	30,500	2,469,000

(C) The requirement "Motor B simultaneously applied to aft skirt" was changed to read "Test loads simultaneously applied to aft skirt" shall be:

Axial Compression Load, lb	3,000
Bending Moment, in.-lb	1,500,000
Shear, lb	30,500

The Motor B vibration, temperature cycling, and operating temperature range are unchanged.

All requirements and references to Motor C were deleted.

(3) Performance Revisions

Motor A performance was unchanged.

Motor B performance was changed as follows:

(C)

	Motor B
Altitude Condition	Vacuum
Thrust, lb	
Average	24,000
Maximum	31,000
Minimum Action Time Total Impulse, lb-sec/lb	800,000
Ignition	
Maximum Ignition Delay, sec	0.100*
Deliver Specific Impulse, lb-sec/lb	283**
Nozzle Expansion Ratio	25:1

*Additional requirement--shall be capable of ignition up to 90,000 feet altitude. Tests of Motor B to be conducted at simulated altitude of 100,000 feet or greater.

**Vacuum at motor pressure, actual expansion ratio and half angle.

All requirements for Motor C were deleted.

(4) Thrust Vector Control Revisions

Motor B requirements were unchanged.

All Motor C requirements and references were deleted.

(5) Replacement of Motor C with Motor D

(C) This required the following summary of design objectives and nominal values for the new motor:

1.	Action Time Total Impulse, lb-sec (Sea Level Optimum Expansion)	155,000
2.	Thrust, Average	
	Boost	5,000
	Sustain	1,400
	Restart, minimum	1,400
3.	Outside Diameter, in.	15
4.	Over-all Length, in.	100
5.	Length, Grain, in.	80
6.	Propellant Weight, maximum, lb	680
7.	Delivered Specific Impulse, lb-sec/lb (Corrected to Optimum 1000/14.7 psia Expansion and 0° Half Angle)	250
8.	Boost Grain Design Suitable for Ignition From Sea Level to 80,000 Feet	
9.	Restart Grain Design and Restart Suitable for Ignition From Sea Level to 80,000 Feet	
10.	Action Time, sec	
	Boost	12
	Sustain	50
	Restart, minimum	10
11.	Storage, years	5

(C) 12. Thermal Environment Demonstration--
Design Considerations

Environment: -75 to 170 F (Storage)
250 F—60 min (Captive Flight)
650 F—2 min (Captive Flight)

Demonstration: Temperature Cycling -75 to 250 F 20 times Military Specification MIL-R-25534A requirement (2 1/2 cycles), end at 250 F, subject to 650 F (hold for 2 min), fire at 650 F ambient air temperature

13. Case structure will be heavyweight

14. Ignition delay for boost and restart, minimum, 0.100 sec

15. Vibration design considerations for motors of the D configuration shall include the capability of withstanding vibration in accordance with Procedure 1 of MIL-R-25534A.

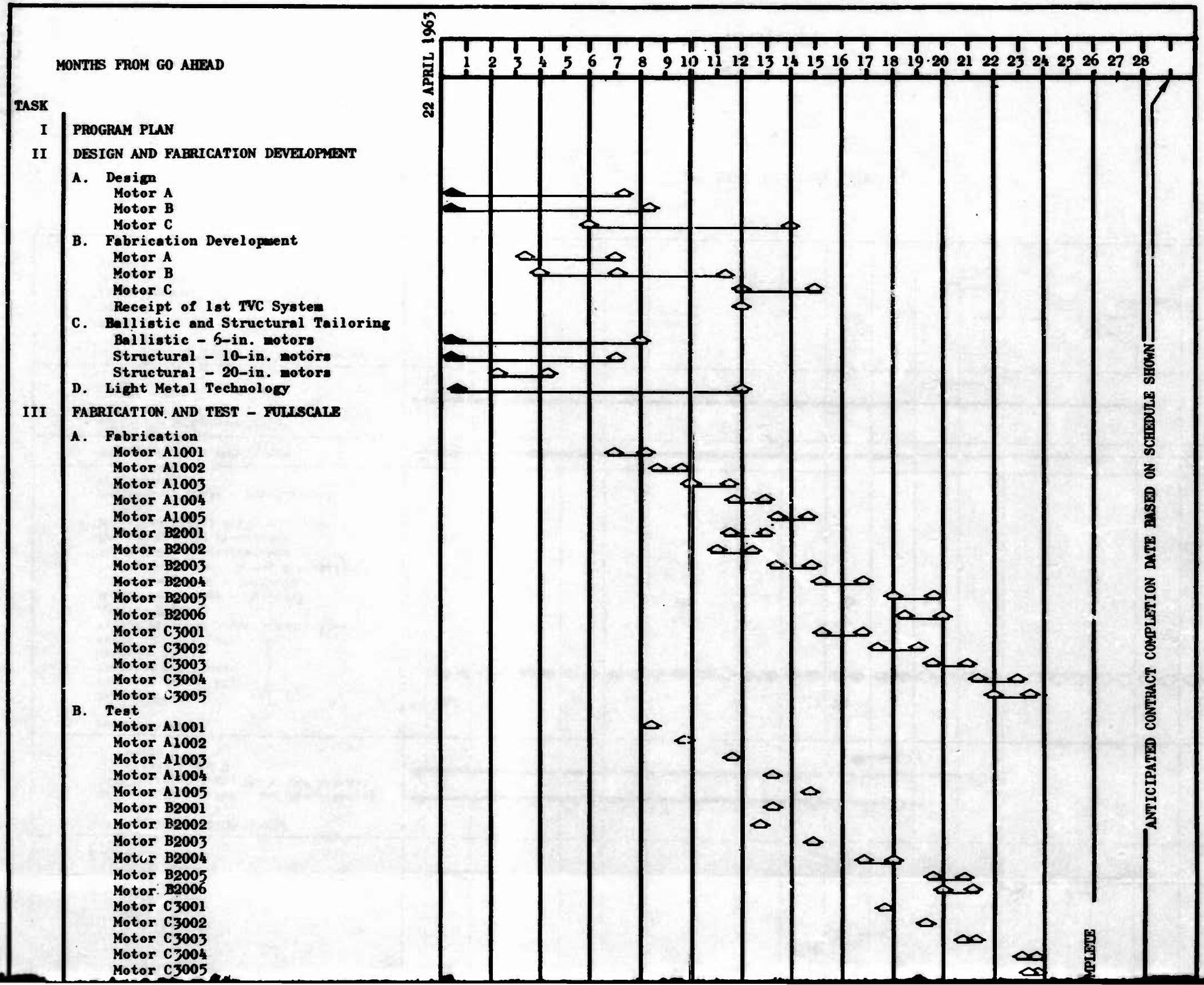
(C) In addition to the design considerations specified above, the design included the capability of the motors to withstand a ±3g input through 6 log-sweeps of 10 minutes each over the frequency range of 30 to 2000 cps; and through log-sweeps of 10 minutes duration over the frequency range of 5 to 28 cps at 0.100 inch double amplitude and from 28 to 300 cps at ±4g input. (A sweep is defined as either increasing frequency or decreasing frequency, and shall extend over a 10-minute period.) The Motor D configuration shall be capable of surviving the above vibration requirements at the following ambient air temperatures: -75, 70, 170, and 250 F.

3. PROGRAM PLAN

Based on the specification for the three separate motors, Rocketdyne proceeded to establish the design, development, and test program necessary to accomplish these objectives. Because of the similarity of the missions for Motors A and B, and the different mission for Motor D (also because of its late addition), the program was aligned to conduct tests that supported both Motors A and B, with some additional tests required for Motor D.

To facilitate program control it was divided into nine distinct tasks. Figures 7 and 8, respectively, show the two-year evolution of the

CONFIDENTIAL



PREVIOUS PAGE WAS BLANK, THEREFORE WAS NOT FILMED

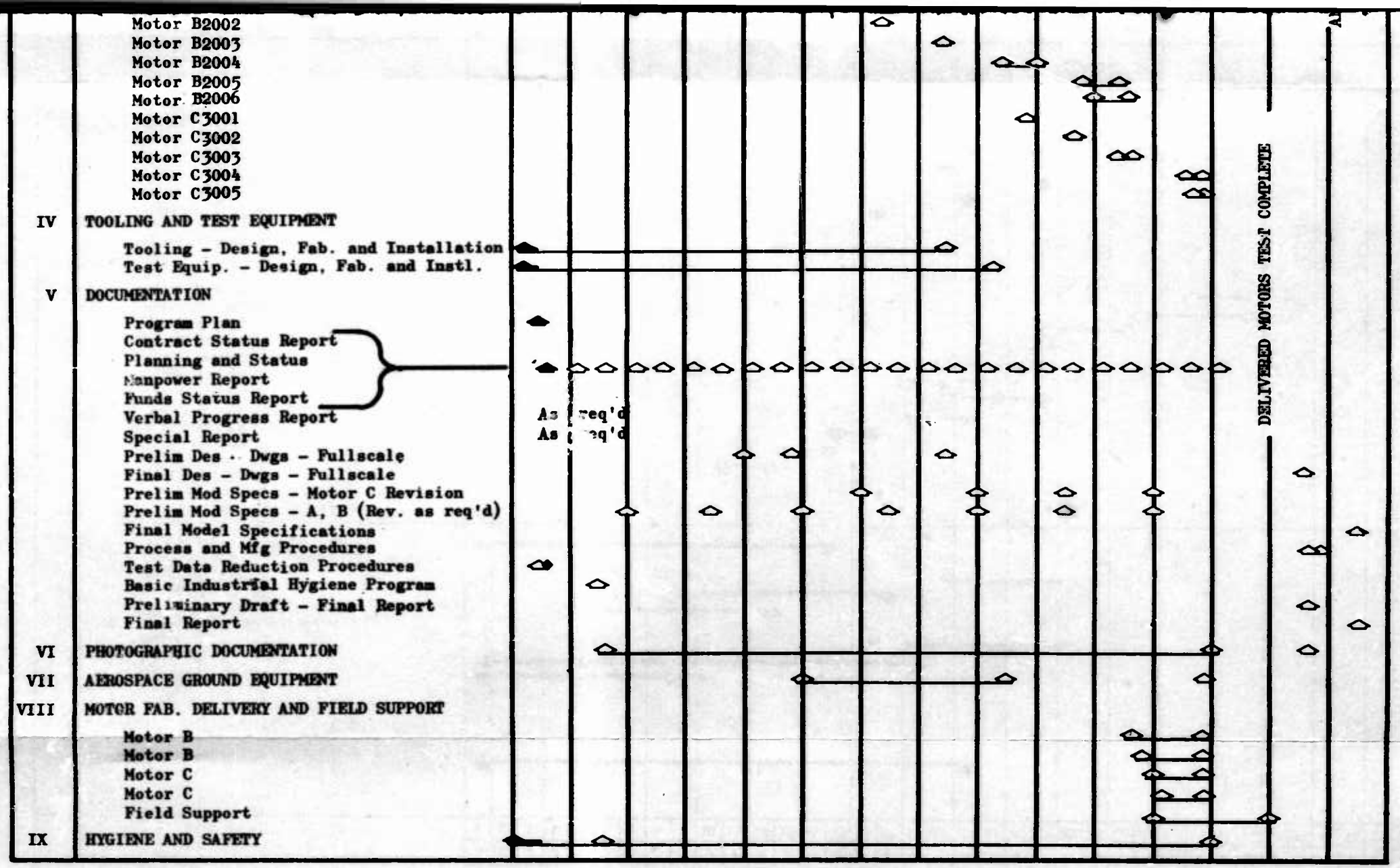


Figure 7. Program Planning and Status Chart
(For the Original Program)

CONFIDENTIAL

	1963									1964										1965												1966					
	A	M	J	J	A	S	O	N	D	J	F	M	A	M	J	J	A	S	O	N	D	J	F	M	A	M	J	J	A	S	O	N	D	J	F	M	A	M	J
	1	2	3	4	5	6	7	8	9	10	11	12	13	14	15	16	17	18	19	20	21	22	23	24	25	26	27	28	29	30	31	32	33	34	35	36	37	38	39
TASK																																						
I. PROGRAM PLAN																																						
II. DESIGN AND FABRICATION DEVELOPMENT																																						
A. Design																																						
Motor A (Complete)																																						
Motor B																																						
Motor D																																						
B. Fabrication Development																																						
Motor A																																						
Motor B																																						
Motor D																																						
C. Ballistic and Structural Tailoring																																						
Structural--10-inch motors																																						
III. FABRICATION AND TEST--FULLSCALE																																						
A. Fabrication																																						
Motor A-1001																																						
Motor A-1002																																						
Motor A-1003																																						
Motor A-1004																																						
Motor A-1005																																						
Motor B-2001																																						
Motor B-2002																																						
Motor B-2003																																						
Motor B-2004																																						
Motor B-2005																																						
Motor B-2006																																						
Motor D-1																																						
B. Test																																						
Motor A-1001																																						
Motor A-1002																																						
Motor A-1003																																						
Motor A-1004																																						
Motor A-1005																																						
Motor B-2001																																						
Motor B-2002																																						
Motor B-2003																																						
Motor B-2004																																						
Motor B-2005																																						
Motor B-2006																																						
Motor D-1																																						
IV. TOOLING AND TEST EQUIPMENT																																						
Tooling-Design, Fab., and Installation																																						
Test Equip.-Design, Fab., and Install																																						
Motors A and B																																						
Motor D																																						
V. DOCUMENTATION																																						
Program Plan																																						

Motors A and B

"D"

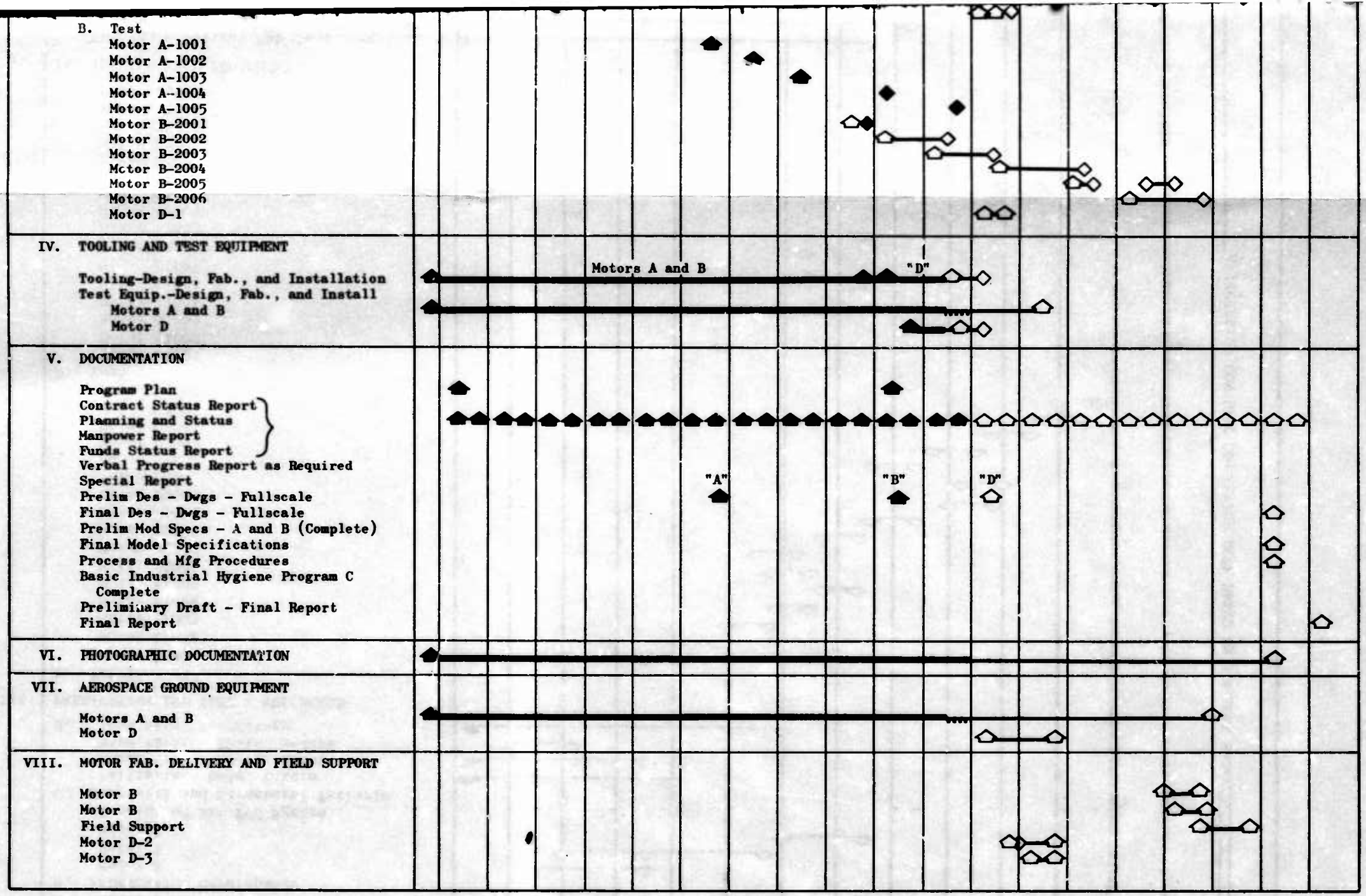


Figure 8. RFG Program Plan and Status Chart, March 1965

CONFIDENTIAL

(C) program from its origin with Motors A, B, and C to its final structure of Motors A, B, and D. Tasks I through VII included the design, development, fabrication, and testing of two different flightweight motors, A and B, and one heavyweight Motor D. Task VIII covered the fabrication and delivery of two each Motors B and D. Task IX covered the industrial hygiene and occupational medicine programs for beryllium motor fabrication and testing (related to Motor C only). A brief discussion of each task follows.

a. Task I—Program Plan (Motors A, B, and D)

This task requires the preparation, submittal and maintaining an up to date program plan. The plan is to be updated monthly and will include, but not be limited to the following:

1. Master Schedule
2. Plan for testing of subscale specimens and full-scale motors
3. Full-scale motor performance parameter definitions which conform to MIL-R-25532A; the method of testing for full-scale motors shall be as specified in MIL-R-25532A and data shall be reported in general conformance with requirements of MIL-R-25532A
4. Identification of major component subcontractors

b. Task II—Design and Fabrication Development

Conduct design analysis and design Motor A, B and D including the reinforced grain, core grain, glass filament wound and steel cases, nozzle and associated systems (thrust vector control) where applicable. Conduct grain winding and case winding fabrication development to advance reinforced grain processing techniques and fabrication techniques for glass filament case winding for Motors A and B; test fire igniters to determine and evaluate ignition characteristics. Accomplish, through fabrication and test of small test specimens, that structural and ballistic characterization is associated directly with design and fabrication of full-scale Motors A, B, and D.

c. Task III--Fabrication and Test of Full-Scale Motors

(1) Motor A, 30-inch Diameter

Five complete full-scale motors will be fabricated and tested. Testing shall consist of:

Motor	Type of GFW Case	RFG	Core Grain	Test Requirements
A	Test Weight	Al	None	Static Test Fire--Ambient
	Test Weight	Al	Al	Static Test Fire--Ambient
	Test Weight	Al	Al	Static Test Fire--Ambient
	Flightweight	Al	Al	Static Test Fire--Ambient
	Flightweight	Al	Al	Combined Loads and Static Test Fire--Ambient

(2) Motor B, 36-inch Diameter

Six full-scale motors will be fabricated and subjected to the following tests:

Motor	Type of GFW Case	RFG	Core Grain	Test Requirements
B	Flightweight	Al	None	Pressure Burst
	Test Weight	Al	Al	Static Test Fire--Ambient
	Flightweight	Al	Al	Static Test Fire--Ambient
	Flightweight	Al	Al	Temperature cycle test, static test fire at ambient, hydraulically actuate TVC with hydraulic cart.
	Flightweight	Al	Al	Vibrate, static fire at -75 F hydraulically actuate TVC with hydraulic test stand.
	Flightweight	Al	Al	Temperature cycle, vibrate, combined loads test, static fire at +170 F. Hydraulically actuate TVC with hydraulic cart.

(3) Motor D, 15-inch Diameter

One full-scale motor will be fabricated and tested at ambient temperature (70 ± 10 F). This motor will be testweight in design and is intended to prove concept feasibility.

d. Task IV--Tooling and Special Test Equipment (Motors A, B, and D)

Design, develop, fabricate, and/or procure tools, fixtures and special test equipment necessary to perform the work provided for under this program.

e. Task V--Documentation and Drawings (Motors A, B, and D)

Specified drawings and documentation shall be prepared, maintained, and submitted. (Submittal of drawings was deleted when contract was terminated.)

f. Task VI--Photographic Documentation

Provide photographic coverage of Motors A and B consisting of one complete 16mm audio visual report in color, not exceeding 20 minutes in length. (Submittal of final film report was deleted.)

g. Task VII--Aerospace Ground Equipment (Motors A and B)

Design, fabricate, and/or procure aerospace ground equipment necessary for handling, transporting, and testing of the motors. (This task was not completed since the program never developed a need for the equipment.)

h. Task VIII--Motor Delivery and Field Test Support

Deliver to the Air Force two motors of the B configuration with altitude nozzles complete with thrust vector control system. Deliver to the Air Force two testweight D motors. Provide field support for testing of delivered motors. Deliver the necessary aerospace ground equipment for support of testing the deliverable B and D motors at a designated Air Force test facility. (No motors were delivered to the Air Force.)

i. Task IX--Hygiene and Safety

(C) Perform an industrial hygiene and occupational medicine program for beryllium motor fabrication and testing. (This task was related only to Motor C, which was replaced by Motor D.)

SECTION II

SUMMARY

(C) The original Reinforced Grain Advanced Development Program, initiated in April 1963, was to develop three different designs of lightweight, upper-stage motors designated Motors A, B, and C. Motors A and B used aluminum wire as grain reinforcement and Motor C used beryllium wire. In early 1964 the high cost and limited availability of beryllium wire required the redirection of the program. At this time Motor C was replaced with Motor D, a testweight air-launched demonstration motor with extreme environmental requirements. The specific requirements for all four motors are listed in the Introduction.

(C) The initial design and development was on Motor A, a 30-inch diameter, 100 inch long, 2600 pound motor. Early development consisted of subscale tests and partial full-scale fabrication. Six full-scale motors were fabricated and tested. The test plan was to begin with a heavyweight conservative motor (to obtain an initial successful firing to evaluate ballistic and other data); and then reduce the weight to the flightweight configuration. The results of the motor firings are summarized in Table I and Fig. 9.

(C) The Motor B program was initiated after the Motor A program to take advantage of the experience. Motor B was similar in design concept to Motor A, was 36 inches in diameter by 90.00 inches in length, and weighed 3200 pounds. The motor was initally intended 'o have thrust reversal ports, but these were deleted at USAF direction. It also had a supersonic split-line, gimbaled nozzle. Like Motor A, six motors were scheduled for development testing on Motor B, starting with a heavyweight motot for initial firing and reducing the weight on subsequent motors to the flightweight design.

TABLE I
MOTOR A - SUMMARY OF TEST RESULTS

Motor No.	Type of Test	Summary of Design	Test Results
A-1006	Hydrotest at ambient environment	Flightweight design on RFG and GFW case, thick liner (0.099 inch), no core grain	Ultimate failure pressure 1345 psi, design pressure 1170 psi.
A-1001	Static fire at ambient environment, vertical test position	Heavyweight design on GFW case and liner (0.66 inch); mass fraction 0.90, water damage to RFG ID	Malfunction after 670 ms; failure probably due to damage of motor during fabrication
A-1002	Static fire at ambient environment, vertical test position	Testweight design on GFW case and liner (0.284 inch); mass fraction 0.911	Successful firing for full duration, 34.0 sec
A-1003	Static fire at ambient environment, horizontal test position	Testweight design on GFW case and liner (0.186 inch); mass fraction 0.933; loose forward polar boss	Malfunction after 3.388 sec; failure most likely due to loose forward polar boss or doubler on aft polar boss
A-1004	Static fire at ambient environment, horizontal test position	Flightweight RFG and GFW case; liner (0.060 inch); mass fraction 0.942	Malfunctioned after 25.04 sec; failure attributed to poor combustion efficiency and erosive burning
A-1005	Static fire at ambient environment, horizontal test stand	Heavyweight case and liner (0.147 inch); mass fraction 0.938; dual core grain	Malfunctioned after 9.8 sec; probably due to separation between two core grain propellants

CONFIDENTIAL

CONFIDENTIAL

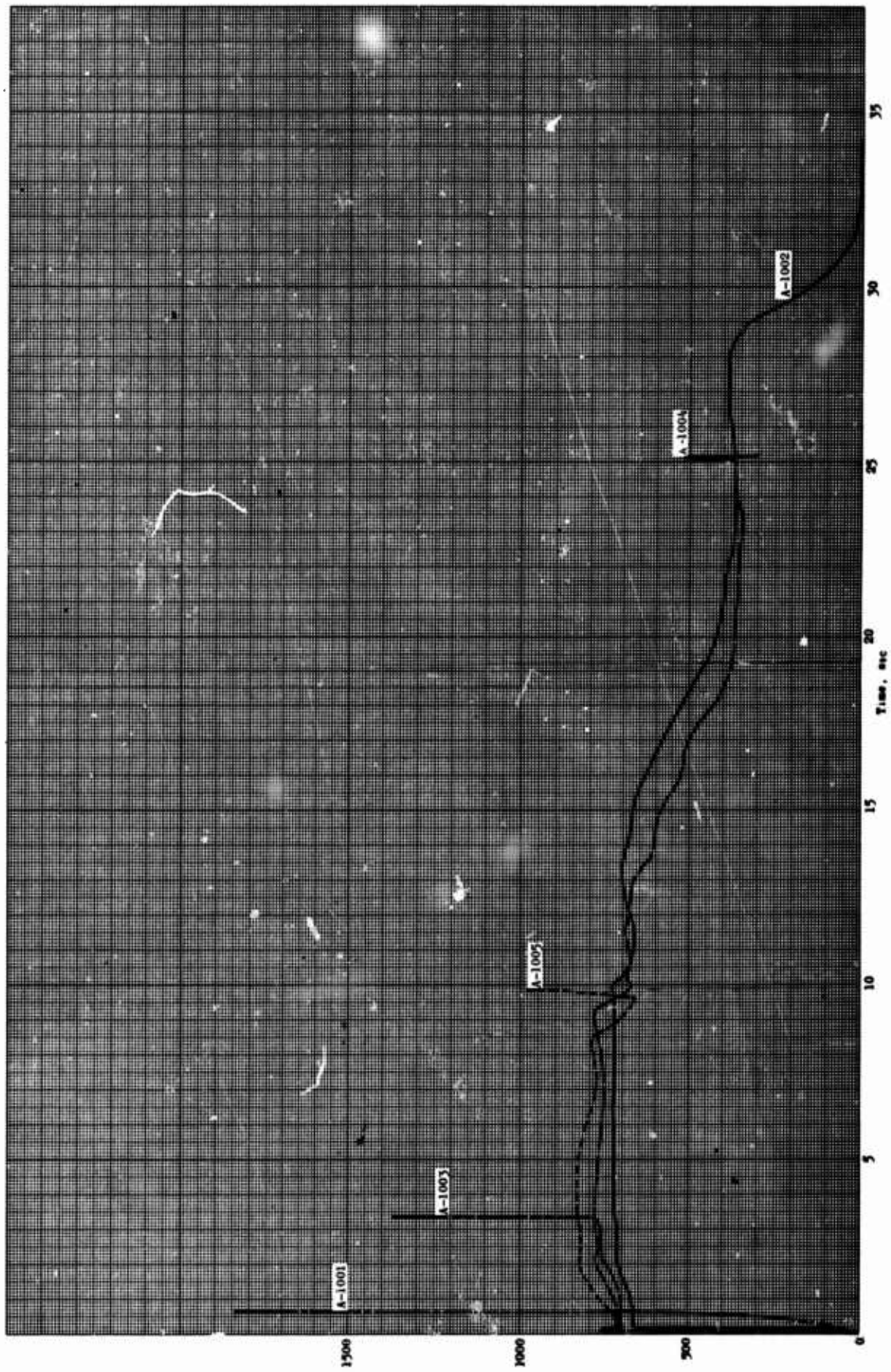


Figure 9. RFG Motor A Firing Summary

The contract was terminated after completing fabrication of the second Motor B. For a summary of the Motor B results, see Table II.

TABLE II

MOTOR B--SUMMARY OF TEST RESULTS

Motor No.	Type Test	Summary of Design	Test Results
B-2001	3 cycle-hydrotest	Flightweight RFG, GFW case, & liner (0.210 inch); no core grain	1st cycle: 1150 psi 2nd cycle: 1160 psi 3rd cycle: 1430 psi; failure design pressure 1650 psi (one cycle) Successful cycle test with grain plastic strain indicated after first cycle
B-2002	Static fire at ambient on horizontal test stand	Testweight RFG, GFW case, and liner (0.38 inch)	Never subjected to testing due to cracks in cast propellant core grain
B-2003		Only component fabrication was initiated prior to contract termination	

Motor D was initiated when Motor C was cancelled. It was a 15-inch diameter x 100-inch long testweight, air-launched motor featuring a duty cycle of boost-sustain/stop-restart-sustain. Three motors were planned to be fabricated with one static fired and the other two to be delivered to RPL. The design was nearing completion when a program review was held with RPL. Subsequently, the contract was terminated, effective 15 March 1965.

SECTION III

CONCLUSIONS AND RECOMMENDATIONS

1. CONCLUSIONS

(C) Test results from static firings of Motors A and B showed that the design approach used in both motors to achieve high mass fraction goals (Motor A, 0.96; Motor B, 0.937) through the use of a composite RFG/GFW structure and a cast core grain is feasible. This was demonstrated by the successful test firing of Motor A at a mass fraction level of over 0.91. However, fabrication experience proved that this particular type of motor requires unusual care in fabrication and is subject to performance degradation arising from the addition of burning rate depressants in RFG propellant formulations to achieve regressive pressure-time characteristics. The program provided a foundation upon which to base designs for a variety of RFG motors for specific applications. Limitations and areas of risk, as well as preferred approaches, were established from the wide range of tests conducted during the course of this Advanced Development Program.

(C) Engineering and fabrication technology was developed which is directly applicable to any future programs utilizing reinforced propellants. These are the main achievements:

1. New machines and techniques were devised for fabricating thick wall, helically wound pressure vessels with geodesic isotensoid domes, using 7.5 mil aluminum wire filaments and FLEXADYNE* (CTL polybutadiene) propellant binder.
2. Methods and materials for overwrapping glass cases on propellant grains were developed.
3. Analytical techniques were evolved for handling complex viscoelastic fields in wire-wrapped domed structures, and for combining them with structurally thin (0.032 inch) filament wound glass cases.
4. Methods were developed for designing the motor components to simultaneously satisfy the ballistic, structural, and processing (fabrication) requirements of a design wherein the propellant grain is a working structural member.

*Trademark

5. End closure attachments (polar bosses) utilizing the support of both the grain and the case were designed, developed, and proof tested. The end closures also provided nozzle and igniter attachment points.

6. Testing methods were developed to evaluate reinforced grain and motor reaction to both internal pressure loads and bending, compression and torsional flight loads.

7. A very lightweight omni-axial, supersonic split line gimbaled nozzle applicable to conventional motors was developed for Motor B.

8. Two nozzles and a thrust vector control system were delivered to AFRPL for test.

9. All components critical to the final design except the ultimate flightweight case and liner were proven in separate tests, although not combined in one motor.

10. There is an indication of a solution of the major structural and fabrication technique problems with the case/grain composite and the polar end bosses joining them.

11. Smooth progression of burning during core-to-RFG transition and through the multi-layered RFG was successfully demonstrated in Motor A-1002.

12. Reinforced propellant specific impulse levels and burning rates, in formulations without depressants, were shown to be essentially the same (within measurement accuracy) as that of similar powdered aluminum formulations.

13. Adequacy of Motor A nozzle and igniter performance were demonstrated in static tests.

A flightweight configuration Motor A was successfully hydrotested to well beyond motor operating pressure limits (over 15%), and the first Motor B was successfully hydrotested to 14% over motor operating pressure limits after two pressure cycles.

The first Motor B scheduled for static firing exhibited cast core grain cracking. Subsequent contractual decisions and actions precluded further effort toward correcting this by design or process changes.

(C) The use of beryllium wire in Motor C did not progress far enough to evaluate combustion efficiency or to permit full-scale experimentation. Subscale winding of the small amounts of beryllium wire procured indicates

(C) that the currently available beryllium wire is considerably more brittle, even in the annealed state, than aluminum wire. However, grains can be fabricated from beryllium wire with minor modification of aluminum wire winding equipment to increase the bend radius. Known future mission requirements at this time do not appear to warrant further work with beryllium RFG. However, the potential performance increases prompting the inclusion of Motor C in the program remains for possible future consideration.

Although the program was terminated before the Motor D design could be tested, all data acquired and analyses conducted on the program indicate that the strength and ruggedness inherent in wire reinforced propellants can be utilized effectively to provide motors with extended vibration, shock and temperature cycling capability. Based on data from tests of smaller motors, and optimization studies of Motor D design, there is considerable evidence that characteristics such as volumetric loading, delivered impulse, and service life/initial cost tradeoffs, are competitive with conventional cast propellants.

When reflecting on the practicality rather than the feasibility of the concepts under development, the processing and fabrication difficulties encountered would have to be considered greater than normally expected. Error free fabrication of the motors presented many problems in process control and operator training throughout the program.

A review of program objectives, progress and funding was made by the Air Force at the conclusion of the Motor A phase. The Motor B program was viewed in the light of Motor A experience and the similarity of the two designs. At the same time, Motor D objectives were closely scrutinized and compared with contemporary air-launched missile specifications and projected requirements.

As a result of the reassessment, in early 1965, the Air Force determined that while Motor B program objectives might be met or closely approached, the final product as designed would be largely unrewarding. The cost to achieve these objectives would not be warranted in light of probable advancements in conventional solid propulsion system performance (mass fraction, specific impulse) criteria. Serious doubt was also expressed by the Air Force as to the real need in the foreseeable future for air-launched missile propulsion systems possessing environmental capability appreciably beyond the then current Military Specification requirements, that could not be achieved using conventional cast propellants.

The review culminated in an Air Force decision to terminate the program, on the basis that program progress and results to date did not warrant its continuance. Remaining funds were stated to be inadequate to attain suitable and worthwhile objectives in applying RFG technology to foreseeable Air Force needs. Also, serious questions were raised as to the wisdom of further pursuing any type of grain reinforcement, until such time as a future specific system has requirements for ruggedness or other properties not attainable by conventional propellants.

Termination of program effort, except for final report preparation, was effective 15 March 1965.

2. RECOMMENDATIONS

It is Rocketdyne's opinion that (1) future air-launched system may well demand propellant grains and support systems with properties permitting application of higher g loadings and greatly increased vibration endurance cycles, as well as extended temperature range, and (2) that reinforced grain appears, on the basis of experimentation, test results and analysis, to offer a most promising solution to these challenging and perhaps even formidable technical barriers. For upper stage, high mass fraction motors capable of operating over extended environmental ranges and resisting severe flight load conditions, an all-reinforced grain motor, cylindrically-wound and slotted, without a cast core (Motor B design) offers a promising application of RFG. The geodesic method of grain fabrication, although largely unrewarding for conventional ballistic missiles, will be most useful in applications where the motor should be entirely consumable (no case at all) for other than performance reasons (for example, when the last missile stage disappears for penetration reasons, and for clandestine delivery of payloads). In the ensuing period and during review of program data and progress in the course of preparing this report, no information or conclusions have been reached which change Rocketdyne's viewpoint.

In retrospect, several deficiencies in the planning and conduct of the ADP program are evident. The program objectives, as originally agreed upon by Rocketdyne and the Air Force, were quite ambitious for advanced development. In the light of the considerable and sometimes unpredicted problems of various types encountered, it is apparent that a less ambitious program in terms of types of motors would have been desirable and additional exploratory development prior to or concurrent with the ADP would have been of great benefit. This would permit illumination and solution or circumvention of the more fundamental deterrents to smooth program pro ess, and would help prevent the costly and time consuming effort of ing approaches in the course of a full-scale, ADP effort. Dual app s, which would have offered some assurance against redirection, coul be taken in most instances in this program because of program scope a unding limitations.

The initial primary goal of the program was to reach for the ultimate performance levels predicted for the RFG concept. This carries an inherently higher risk than an incremental approach. Contract incentives were placed entirely on motor performance on the basis of the highest attained in any one successful (full duration) firing. Although a more conservative viewpoint stressing test motor success and stepwise approach to program objectives, indicating "attainability" vs "attainment" prevailed in the latter program phases, the predominant motivation was actual demonstration of advanced objectives at recognized high risk.

Although valuable design information was obtained on this program many additional unknowns have been encountered. Therefore, future applications of the reinforced grain concept should be approached with additional experimental attention to the phenomena which surrounds the variables intrinsic to the concept. From these basic experiments, the concept can be exploited to its fullest potential.

SECTION IV

MOTOR A

The design, development, fabrication, and test of the RFG Motor A are presented in this section. It is divided into seven subsections. The first part discusses design and development; the second part the first development motor; and the remaining five parts discuss the static fired development motors.

The major portion of the contract effort was devoted to this motor because of the similarity between it and Motor B. As is common with large motor (30-inch, 36-inch diameter) development programs, the new or novel components and techniques are tested in less-expensive subscale models. This large motor design and development effort was oriented in a similar manner. The basic design description is presented first, including a parametric study which established the basic motor goals. This is followed by a ballistic design discussion which includes the ballistic design of the RFG and core grain and the necessary propellant development; next, a structural design is discussed, presenting the acquisition of required design data and fabrication techniques and the method for analyzing the RFG/GFW composite structure. The subscale test results necessary to supporting the various design areas are presented within the discussion on the particular area.

Throughout the actual ballistic and structural design, certain component requirements were developed. Some of these components are common to all solid rocket motors and others are unique to the RFG motor. Such components as the polar bosses and load rings are unique to the RFG motor but the nozzle, igniter, and restrictor are common to all solid rocket motors. The development of the components to fulfill their specific requirements is discussed after the structural presentation in this order--polar bosses, load rings, nozzles, igniters, and insulators.

After the discussion on the preliminary design and component verification, the fullscale 30-inch diameter motor process development is presented. This includes the reinforced grain fabrication techniques, application of the restrictor to the RFG, and overwrap of a glass filament case on a live grain. The process development concluded with a recommended processing procedure which is presented next. Along with the process development of the motor, inspection techniques were developed to ensure the quality of the final product. These techniques are presented after the process procedures.

The culmination to all the design, development, and subscale testing is the fabrication and structural test of the first fullscale RFG motor (A-1006 . This motor's discussion precedes the subsections discussing the fabrication and static test firing of the five development motors.

1. DESIGN AND DEVELOPMENT

Motor A (Fig. 10) is 30 inches in diameter by 100 inches long with dome shaped ends. A filament-wound skirt is made to integrate with, and attach to, the motor case at the case-head junctions. A metal ring flange is bolted to the skirts to provide a mounting for missile interstage coupling and to transfer external loads into the case and grain assembly.

An opening is provided through the forward end of the motor to permit installation of the igniter. Another opening is provided through the aft end where a static, bell contour nozzle is installed.

The grain is made in two sections. The outer section which is also the load carrying grain, or RFG, is a thick layer of propellant matrix with a uniform winding of high strength aluminum wire passing helically through the layer, much like a wound ball of yarn. The inside section is a cast conventional composite propellant.

Special fittings, or polar bosses, are wound in both the forward and aft RFG openings to provide a means of attaching the igniter and nozzle, to seal the spindle opening during RFG winding, and to transmit loads into the case and grain.

Thin metal rings, called load rings, are fitted to the polar bosses between each primary RFG layer. The purpose of the load ring is to reduce unit bearing loads in order that maximum joint strength may be obtained.

The case, which is a thin shell of glass reinforced epoxy, serves as a primary structure to contain hot gases and to transfer external loads. The igniter is a conventional basket design.

The RFG provides extra strength to aid the case in carrying pressure and external loads during the initial motor burning phase and acts as an ordinary propellant to provide thrust during the final burn phase. The core grain provides thrust for the initial or boost phase.

CONFIDENTIAL

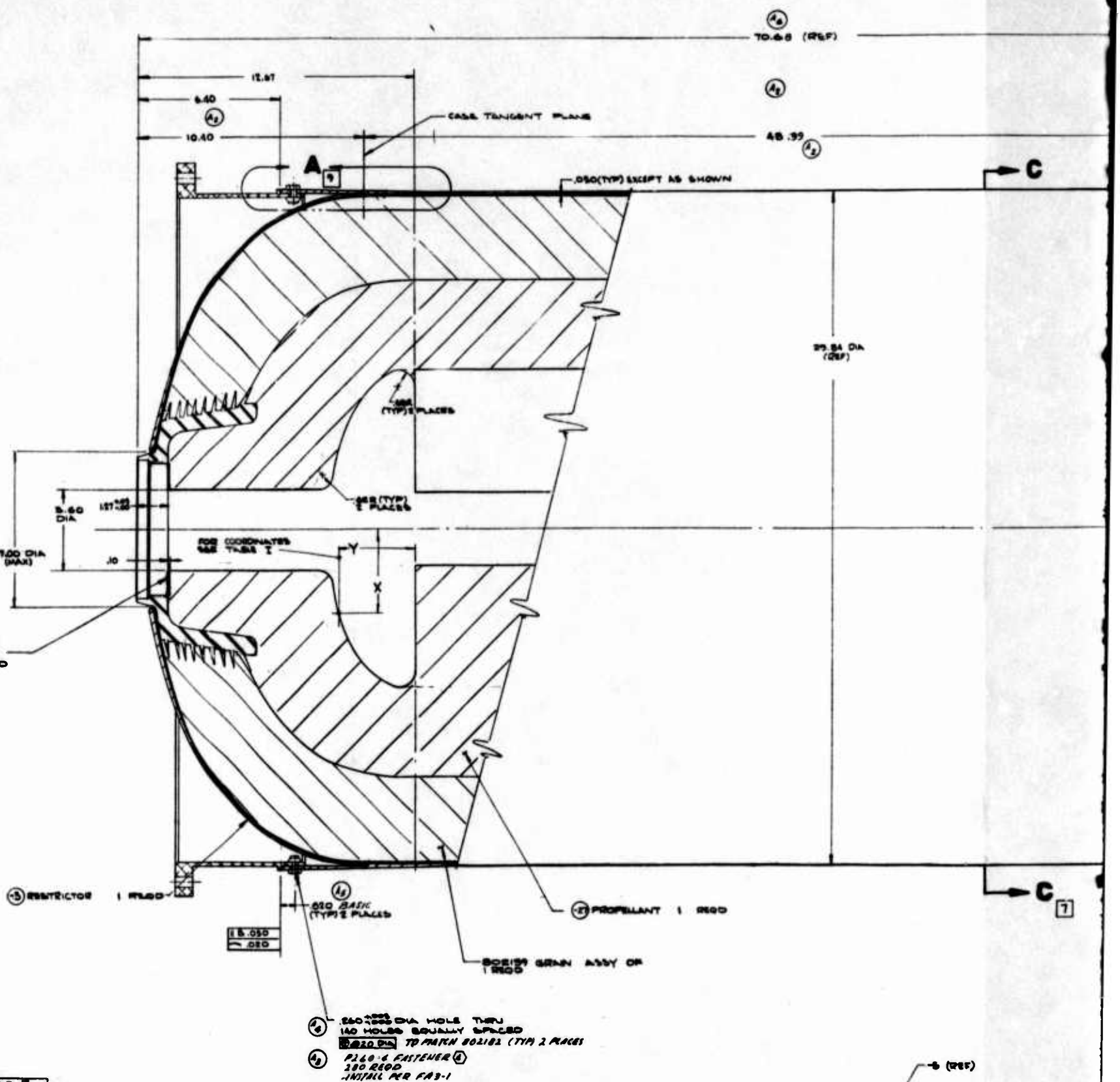
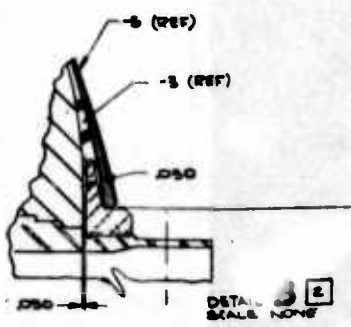
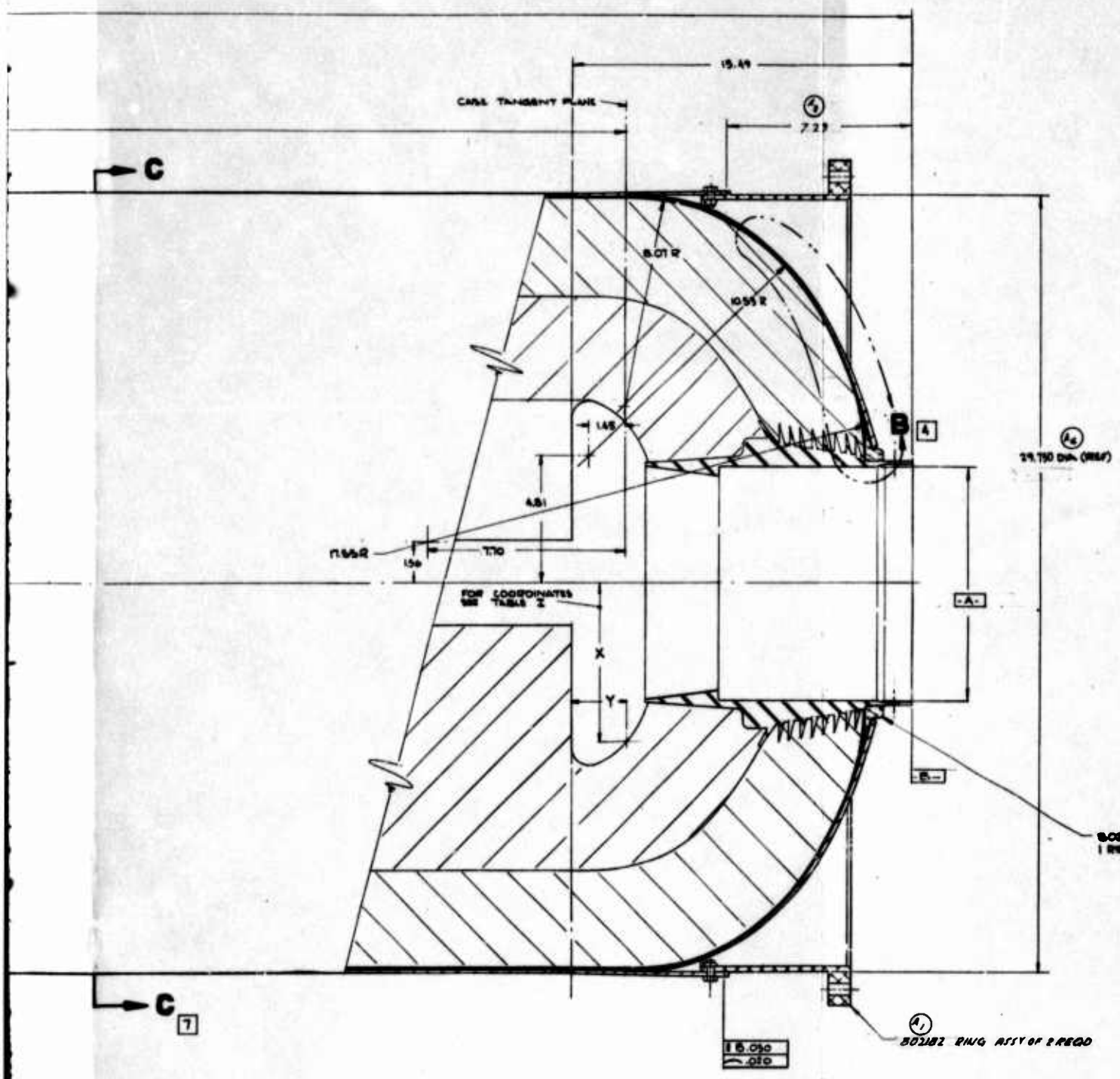


TABLE I	
X (in)	Y (in)
2.50	8.09
3.00	8.58
4.00	8.89
5.00	9.10
5.22	9.24
6.70	1.51
6.90	.48



1



4. 9 NATIONAL SCREW & MFG. CO., LOS ANGELES, CALIF.
8. BALLISTIC PERFORMANCE SHALL MEET RAD BIO-ST1
7. PROCESS PER RAD 310-850
3. 6. 795 ENDS PER INCH (TOTAL HELICAL WRAPS)
2. 5. 850 ENDS PER INCH (TOTAL CIRCUMFERENTIAL WRAPS)

1. 6. EACH ORIENTED WITH [illegible] PARALLEL TO MOTOR LONGITUDINAL [illegible]
5. FOR LIST OF MATERIALS SEE S/NA DRAWING
COORDINATES PLOT MACHINE
2. INTERFACE DIMENSIONS AND TOLERANCES PER RS-MD-6.
1. IDENTIFY PER RAD/N-850. DO NOT OBSCURE MARKING.

Figure 10. Motor A Assembly

CONFIDENTIAL

The floating restrictors provide stress relief to areas of high stress at the end of the core grain while the primary restrictor acts as a high pressure seal and protects vulnerable components from hot gases.

a. Ballistic Design

In considering the ballistic design of Motor A it must be remembered that the reinforced portion of the grain is utilized as a structural member, and that the strength of the RFG is reduced as the grain is consumed. Therefore, to utilize this unique structural feature to its fullest, the chamber pressure must be maintained at a maximum that is commensurate with the strength in the combined RFG and glass filament wound case. However, since the RFG is consumed during the motor firing (and the combined case and grain strength reduced), the chamber pressure must be decreased in proportion to the reduction in the case-RFG structural capability. This is accomplished by reducing the propellant burning rate. The rest of the propellant (core grain) is a conventional composite and is selected and designed with convention techniques.

(C) In determining the operating pressure limits of Motor A, a parametric study was conducted to optimize the mass fraction. By varying the RFG initial pressure while holding the final pressure constant, the mass fraction was optimized at an average core pressure and RFG initial pressure of 800 psi for Motor A. Of necessity another variable in this parametric study was the RFG web thickness, the web thickness of 3.82 inches corresponded to the 800 psi pressure.

This ballistic section is divided into three topics: (1) Parametric Study, (2) Propellant Development, and (3) Ballistic Design RFG and Core Grain.

(1) Parametric Study

System analysis of Motor A was initiated to provide data for selection of operating characteristics. This analysis included evaluating pressure level, which would have a subsequent effect on mass fraction and total impulse. The over-all ballistic requirements for Motor A are summarized below:

(C)

Action time total impulse, lb-sec	540,000
Average thrust, lb	16,750
Maximum thrust, lb	28,000
Nozzle expansion ratio	Opt @ sea level
Total motor weight, lb (max)	2,600
Mass fraction	0.96
Delivered spec impulse (I_{sps}), lb-sec/lb	250

(C) Of primary consideration was the mass fraction of 0.96. Of secondary importance was the burning rate required in the outer layers. For increasing operating pressures in the core, the nozzle areas required were smaller; hence, the burning rates required in the outer layers of the RFG became smaller. Difficulty was encountered in obtaining the low rates, because the specific impulse of these propellants decreased with the addition of depressants. Under certain simplifying assumptions the RFG outer layer burning rate can be shown as a function of core pressure. Core pressure is a function of propellant properties, grain geometry, and nozzle throat area. In the study, propellant properties and core flow channel geometries were essentially fixed. Variations of core pressure required variation of the RFG thickness and, consequently, the core web. However, average burning surface of the core was essentially constant. With these assumptions the average core pressure is a function of throat area only.

$$P_c = \left(\frac{K_1}{A_t}\right)^{1/1-n}$$

where P_c = chamber pressure
A_t = throat area, average cone
n = burning rate exponent
K_1 = constant

Similarly, the final pressure in the RFG is a function of its propellant properties, geometry, and throat area. The latter is fixed by the envelope, and only the burning rate in the final layer was considered as a variable, along with throat area. Hence, the final pressure can be shown as follows:

$$P_f = \left(\frac{K_2 r_b}{A_t}\right)^{1/1-n}$$

where P_f = final chamber pressure
A_t = throat area
n = burning rate exponent
K_2 = constant
r_b = burning rate

(C) As the study was performed for a final pressure of 400[1] psia (P_f), the two equations can be combined and the rate required in the outer layer can be shown as a function of core pressure.

$$r = f\left(\frac{K_3}{P_c}\right)$$

where r = burning rate in outer RFG layer
P_c = chamber pressure, average core
K_3 = constant

These data were calculated and are shown in Table III.

TABLE III

SUMMARY OF MOTOR A PARAMETER EVALUATION

RFG[1] Initial Pressure (psia)	RFG[2] Final Pressure (psia)	Total Impulse (lb-sec)	Relative Variation in Mass Fraction	Final Burning Rate, in./sec at 1000 psi
1200	400	566,700	0.003	0.137
1100	400	566,300	0.002	0.151
1000	400	565,400	0.001	0.161
900	400	563,800	--	0.180
800	400	561,700	--	0.195
700	400	560,500	--	0.241
600	400	551,700	--	0.286
500	400	540,300	0.001	0.356
400	400	521,200	0.001	0.482

(1) Also, Core Grain Design Pressure
(2) Also, GFW Design Pressure

Propellant weight is essentially constant; however, inert weight from point to point varies as a result of nozzle throat and closure modifications accommodating the pressure levels. Generally, the nozzle throat area (and, hence, weight of the nozzle insert) decreases as pressure increases. Higher pressures, however, required the increase structural

(1) This was considered the minimum pressure that the outer RFG layer could efficiently burn.

(C) support in the areas of the nozzle and polar bosses. This increased the over-all motor weight. Along with the varying weight of the components was the limitations of attainable burning rates required in the outer layers of the reinforced grain. The minimum outer-layer RFG burning rate that could be assured corresponded to a core average pressure of 800 psia. At this pressure the mass fraction was at a maximum, and estimated total impulse was well over the stipulated minimum of 540,000 lb-sec. Hence, the level of pressure was taken as 800 psia; this was defined as nominal maximum pressure. On this basis average pressure for the core was set at 750 psia.

(C) With this initial RFG pressure the structural requirements of the composite RFG-GFW case were established (and, therefore, the RFG web). An RFG with 20% aluminum wire weight percentage and an ID of 22 inches corresponded to the 800 psi nominal pressure. After testing Motor A-1002, the average pressure was adjusted to 775 psia, when the pressure-time record was found to be more neutral than originally estimated.

(2) Propellant Development

The burning rate of the reinforced propellant was controlled by the burning rate of the nonaluminized propellant used as the binder composition in fabricating the reinforced propellant. Since the binder composition is the prime influence on the resulting burning rate of the reinforced sections, company-sponsored activities were concerned principally with developing binder propellants that had a wide range of burning rates without sacrificing performance; that is, the oxidizer loadings were maintained as high as possible to achieve a high oxidizer/fuel ratio.

(C) As a result of this development, binder compositions containing 87% or 88% by weight of solids were formulated for the RFG application. These compositions exhibited burning rates from 0.135 in./sec at 400 psi to 0.590 in./sec at 1000 psi. An upper range of burning rates (0.31 to 0.59 in./sec at 1000 psi) was accomplished with a single composition by varying the ratio of the fine-to-coarse oxidizer fractions. This composition is identified as RDS-512; the formulation is given in Table IV, with the burning rate (shown as a function of the oxidizer ratios) given in Fig. 11.

TABLE IV

PROPELLANT COMPOSITIONS DEVELOPED (AND USED) FOR REINFORCED GRAINS

Formulation	RDS-512	RDS-514	RDS-523	RDS-526
Usage	Binder in Reinforced Section	Binder in Reinforced Section	Binder in Reinforced Section	Core Propellant
Ingredient	Weight Percent, Typical			
Butarez CTL Type 1	9.82	9.82	11.59 10.64 9.83	11.00
MAPO	0.22	0.22	0.25 0.23 0.22	0.26
Conoco H-25	1.96	1.96	1.16 2.13 2.95	2.74
	12.00	12.00	13.00	14.00
Ammonium Perchlorate				
400 micron, avg	63--30	34	34	--
200 micron, avg	--	33	32	48.30
10 micron, avg (spherical)	--	14.00--20.90	21--14	--
7--11 micron, avg Grind	25--58	--	--	20.70
Aluminum Powder	--	--	--	16.00
Burning Rate Additive (50-50 mixture of Strontium Carbonate and Calcium Citrate)	--	7.00--0.10	0--7	--
Ferric Oxide	--	--	--	--
Total Solids	88.00	88.00	87.00	86.00
Burning Rate Range	See Fig. 1	See Fig. 3	See Fig. 4	0.35 to 0.47 in./sec @ 750 psia

CONFIDENTIAL

CONFIDENTIAL

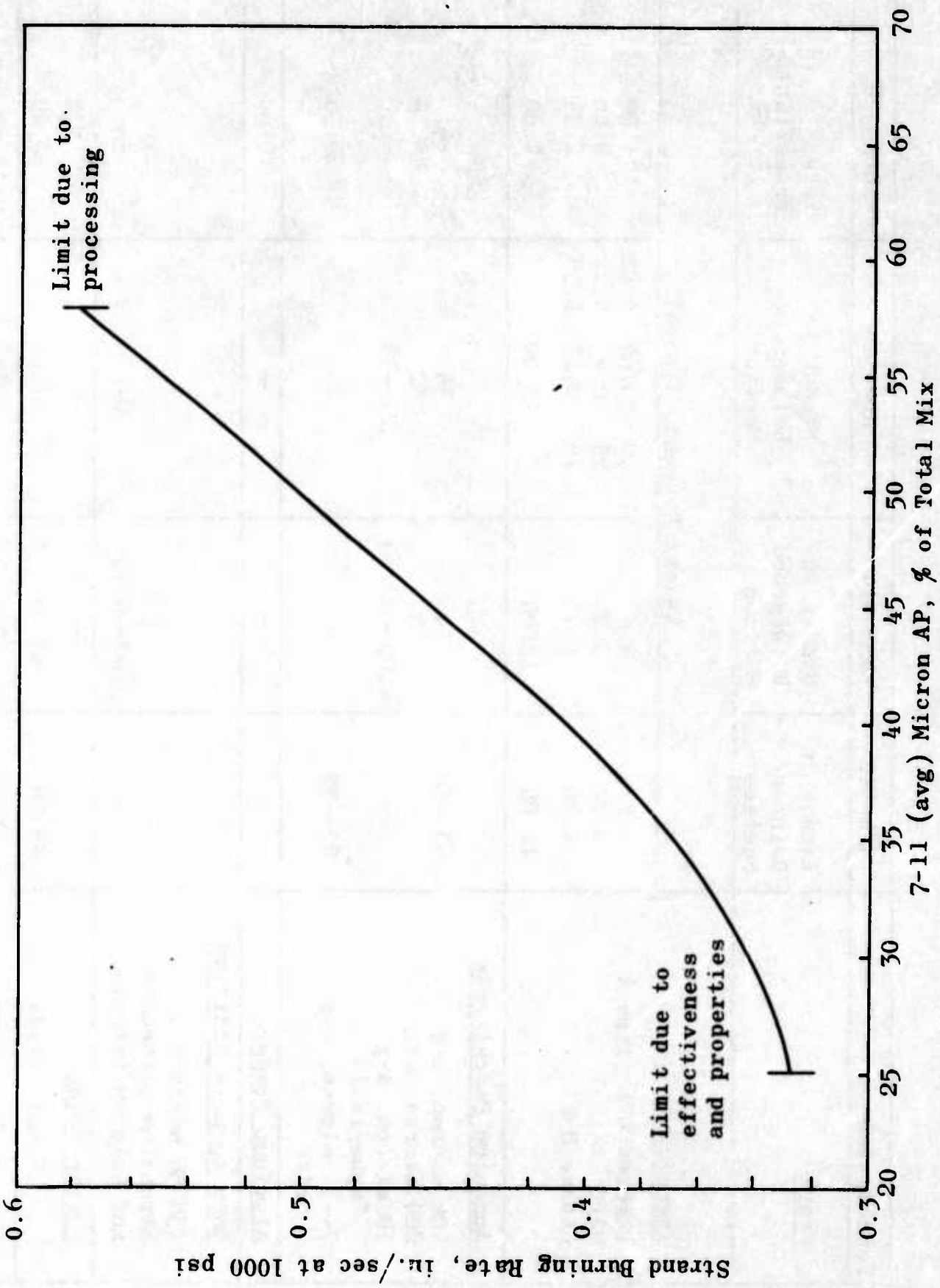


Figure 11. Nominal Liquid Strand Burning Rate as a Function of Fine Oxidizer Loading.

Binder compositions with burning rates below that of RDS-512 require the use of burning-rate modifiers, or depressants. Since the RFG designs required more extensive use of propellants with lower burning rates, the company-sponsored phases of the propellant development were also concerned with burning-rate depressants, solid particle size ratios, and/or materials to reduce burning rate at low pressures by increasing the burning-rate exponent. Over 40 individual ingredients and combinations of these ingredients were evaluated for their effectiveness in reducing the burning rate in actual compositions. In general, the most promising burning-rate depressants investigated were salts of metals from Group III of the periodic table, which includes barium, strontium and calcium. Indications were that the salt should be one that produces carbon dioxide (such as the citrates, oxalates, and carbonates).

From this study, the greatest reduction in burning rate from a control value for a given amount of burning-rate depressant was accomplished with strontium carbonate up to a 3% by weight level. However, increased quantities, above 3%, failed to reduce the burning rate still further. On the other hand, calcium citrate at increased levels continued to decrease the burning rate, even though at the 3% level, the citrate was not as effective as the strontium carbonate. By using a combination of calcium citrate and strontium carbonate, a slight reduction in burning rate below the individual ingredients could be achieved. This is illustrated in Fig. 12.

A low burning rate composition, RDS-514, was issued for reinforced grain application. It contained (1) 88% solids and (2) a depressant (50-50 ratio of calcium citrate and strontium carbonate) level varying from 0.1 to 7.0%. The burning rates that can be achieved by this composition (formulation given in Table IV) when using the allowable range of depressant levels are illustrated in Fig. 13. Using this composition at the higher depressant levels resulted in processing problems associated with increased rheological properties. To improve the processing considerations with propellants at the lowest burning rates (higher depressant levels), a second low-burning-rate composition was issued for this program. This binder composition, RDS-523, contained the same depressants as RDS-514 but with the solids loading reduced to 87% and with three optional levels (10, 20, and 30 parts per hundred rubber of plasticizers, for flow considerations); RDS-523 composition is given in Table IV. The burning rate as a function of depressant level is illustrated in Fig. 14.

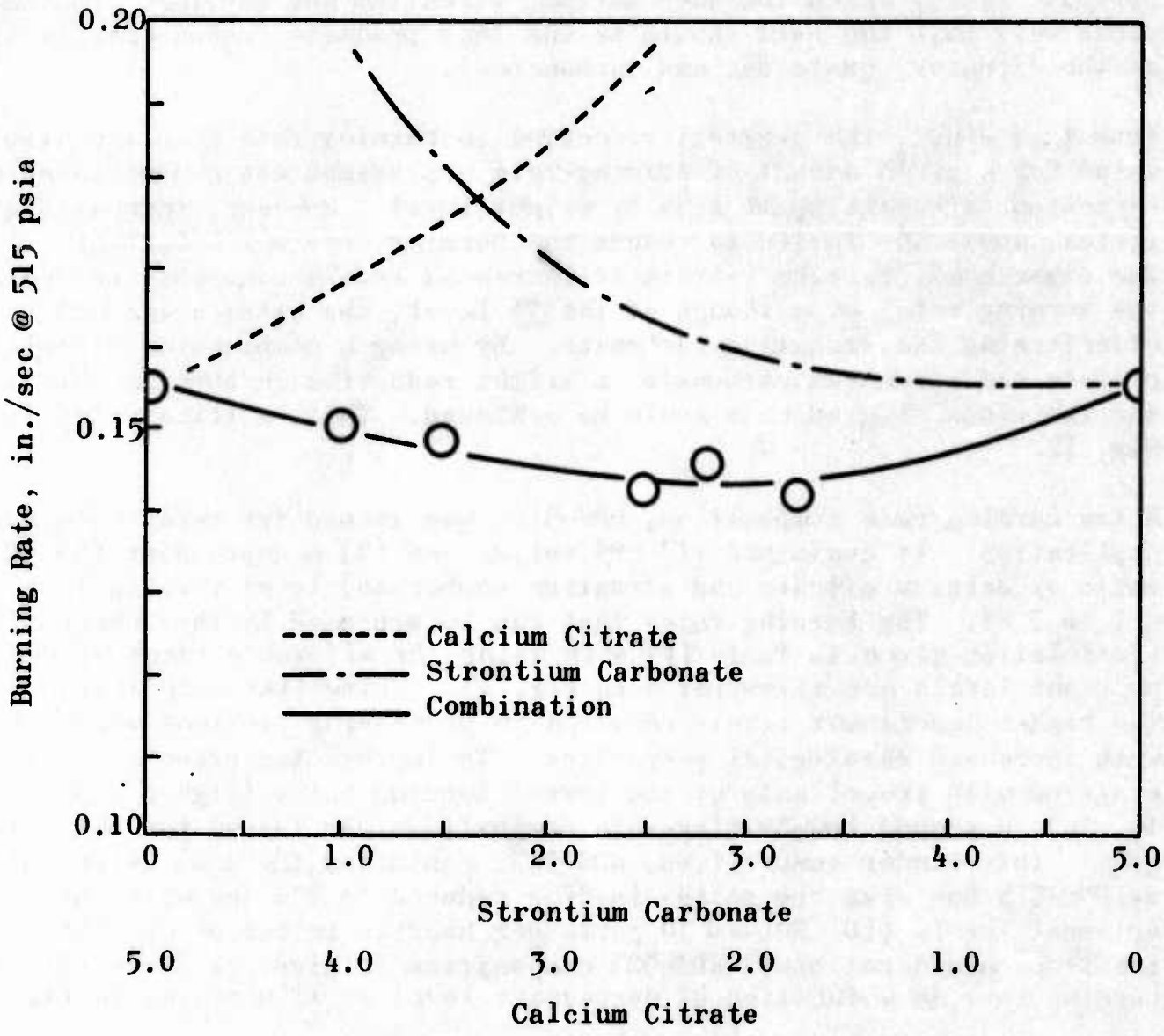


Figure 12. Strand Burning Rates of an 87.5% Solids-Loaded Propellant (Nonaluminum) with Various Ratios of Strontium Carbonate and Calcium Citrate at Total Level of 5%

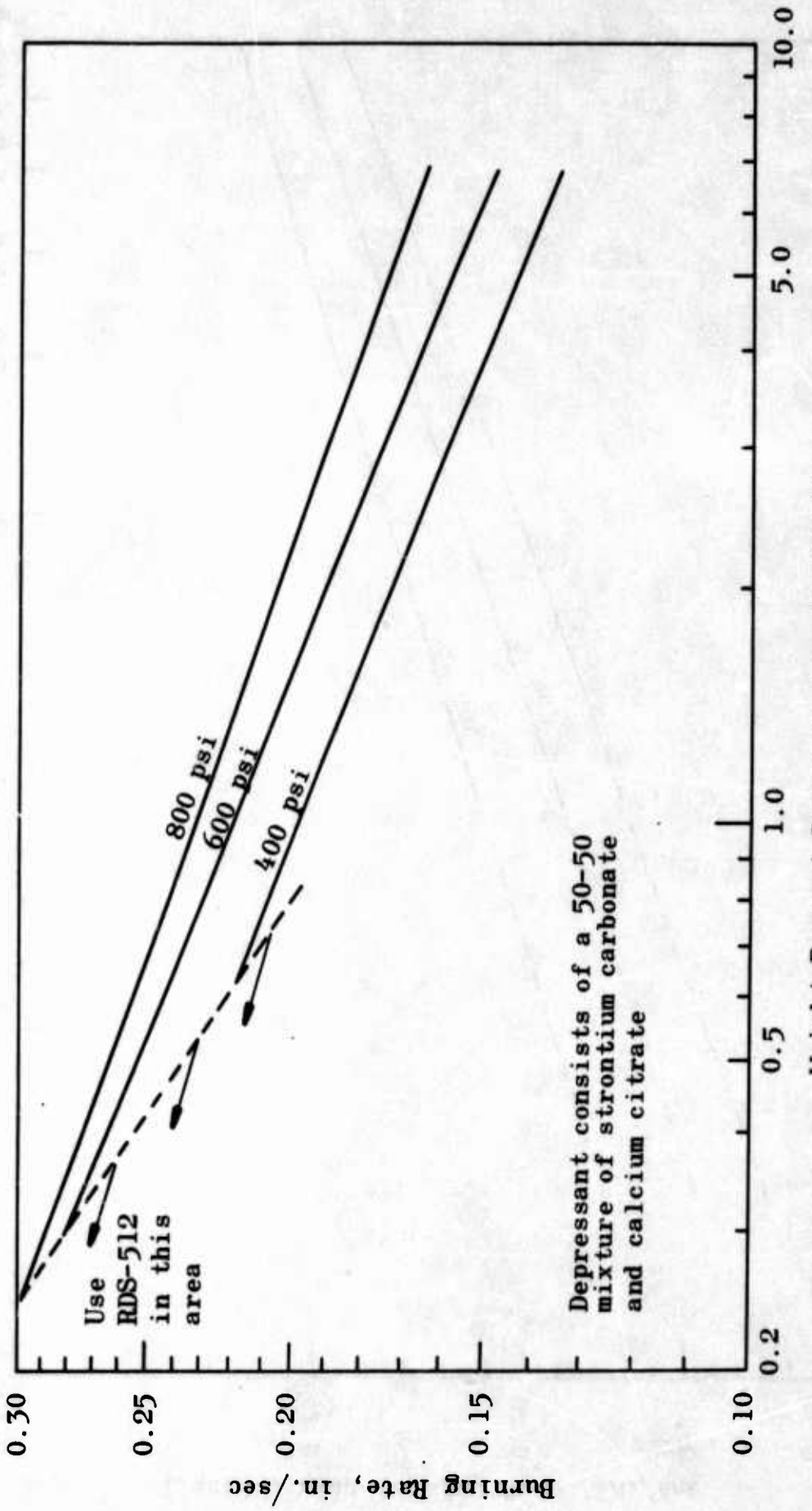


Figure 13. Nominal Liquid Strand Burning Rate as a Function of Depressant Level in RDS-514 Propellant

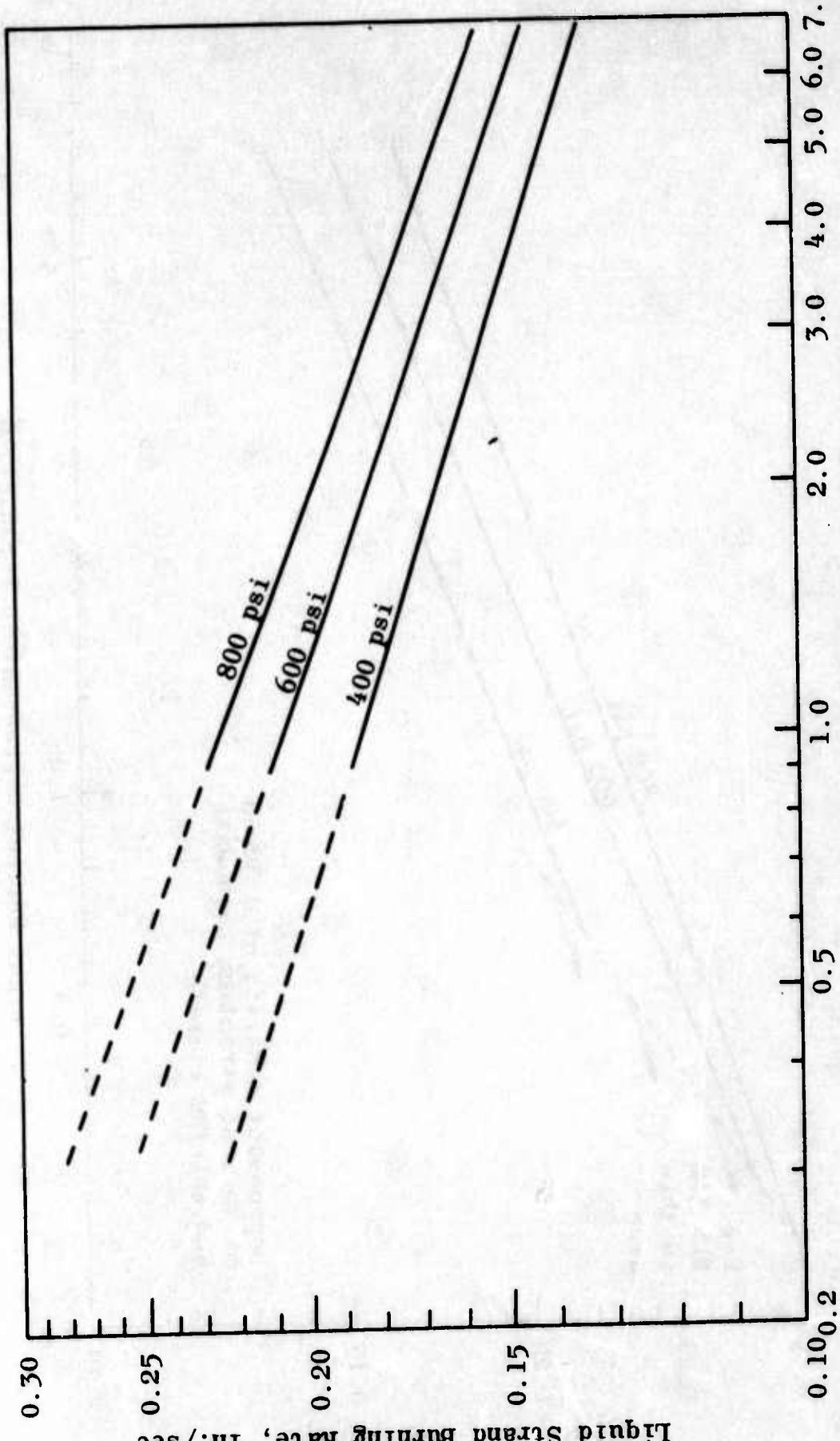


Figure 14. Nominal Liquid Strand Burning Rate as a Function of Depressant Level in RDS-523 Propellant

A fourth propellant composition was issued for usage in this reinforced grain program. This propellant, RDS-526, is a conventional aluminized Flexadyne composition containing 86% total solids with a burning rate modifier to achieve the design burning rate. This composition is used as the core grain and is processed by normal casting techniques.

(3) Ballistic Design of RFG and Core Grain

The actual design of this motor differs from conventional motors. Knowing the charge configuration in a conventional motor design, the required burning rate (r) to yield a particular pressure, with other parameters known, can be determined explicity. However, in the reinforced grain the specific impulse and characteristic exhaust velocity (c*) vary with the amount of depressant added for burning-rate control. This burning-rate variation is required by the decreasing chamber pressure. To facilitate the design analysis, the following parametric curves were established.

1. The relation of specific impulse vs burning rate was established, based on 6-inch motor firings. From this curve a curve of c* vs r at 1000 psia was drawn (Figs. 15 and 16).
2. From the same 6-inch motor data, the variation of pressure exponent vs r at 1000 psia was determined (Fig. 17).
3. From the above, rate vs pressure curves were drawn, with varying pressure exponents depending on r at 1000 psia (Fig. 18).
4. From this information a parametric curve of the product of c* x r at chamber pressure vs chamber pressure, with r at 1000 psia as a parameter, was prepared (Fig. 19).

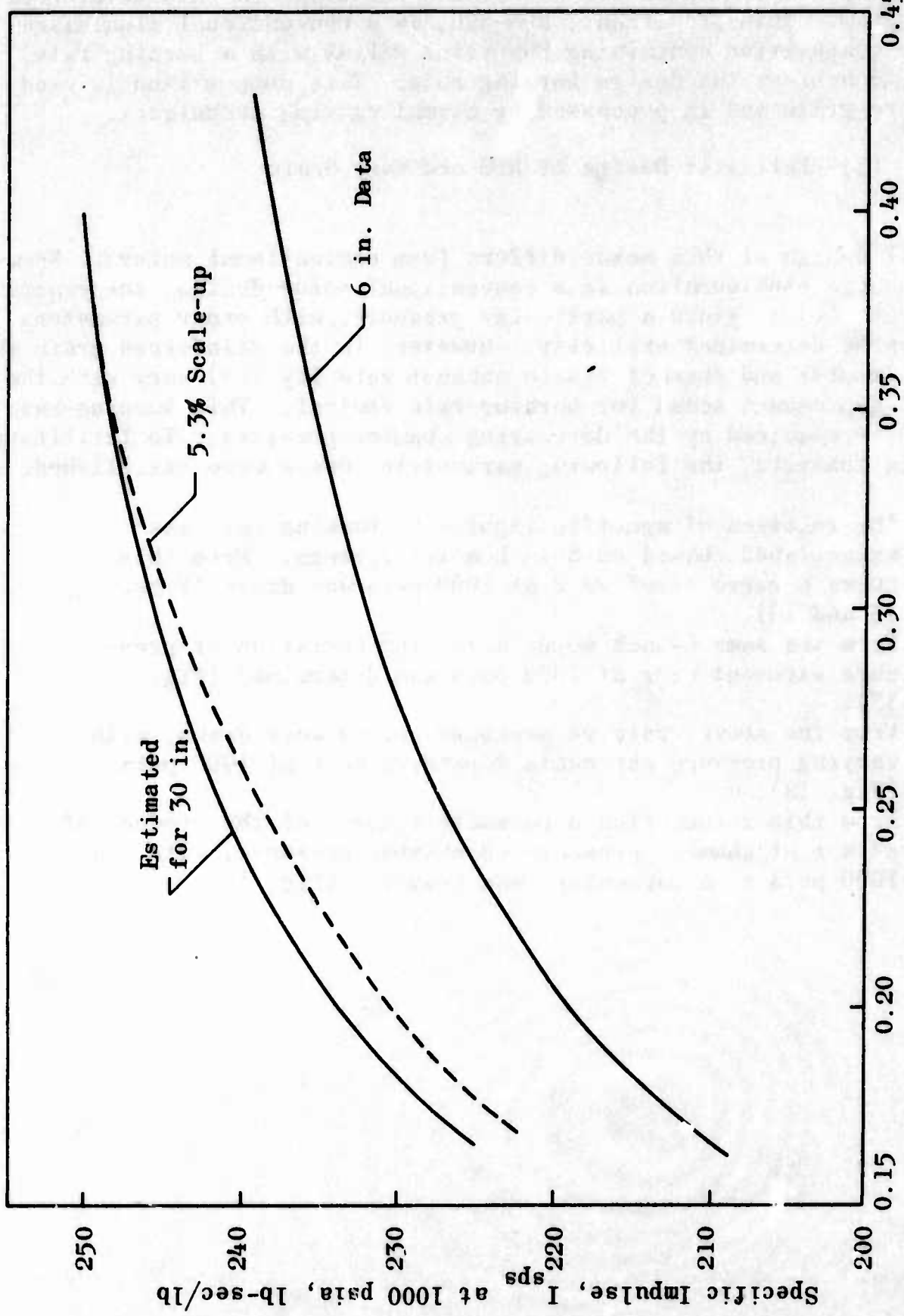


Figure 15. Estimated Variation of Specific Impulse With Motor Burning Rate

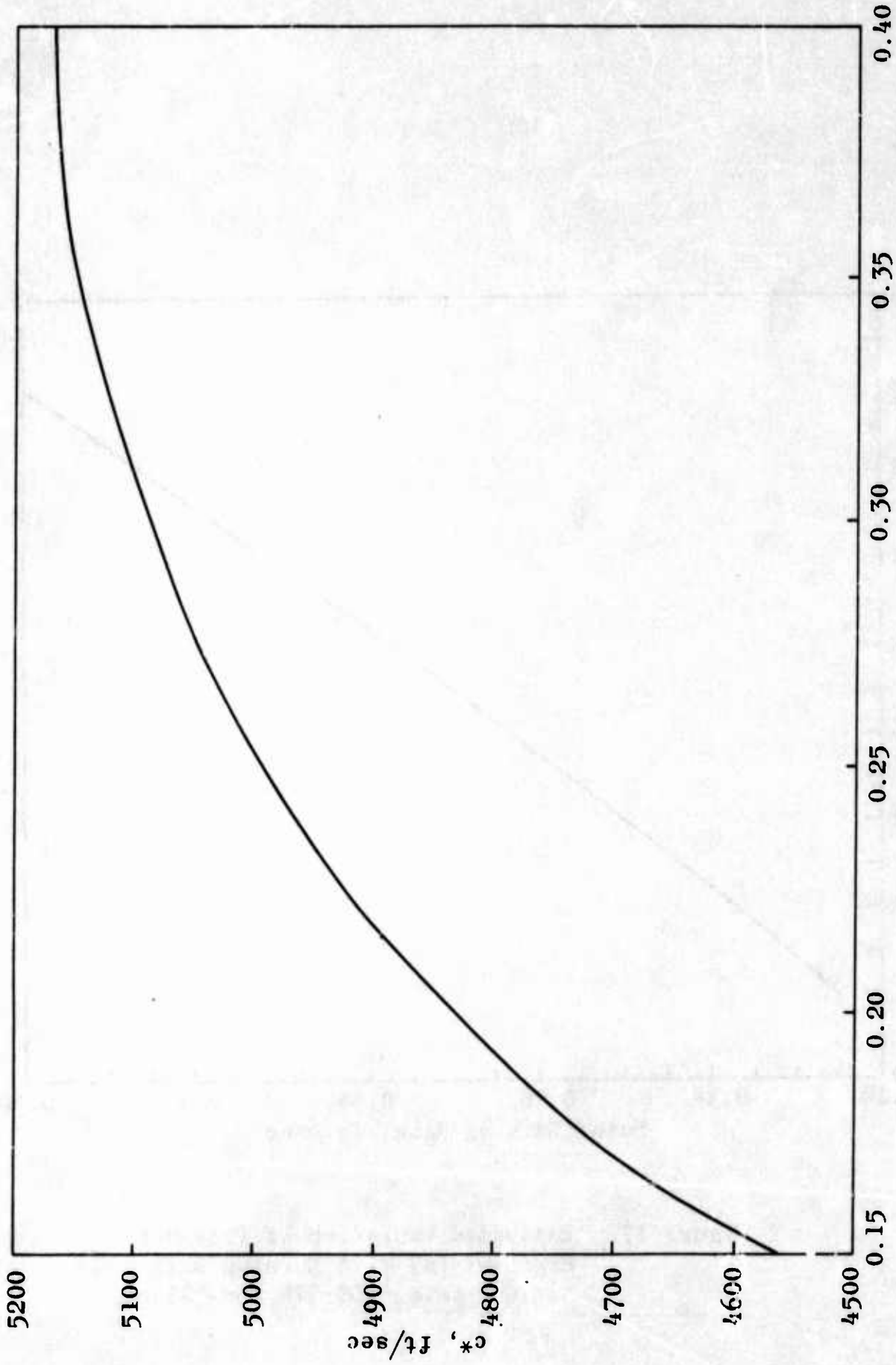


Figure 16. Estimated Variation of c* With Motor Burning Rate

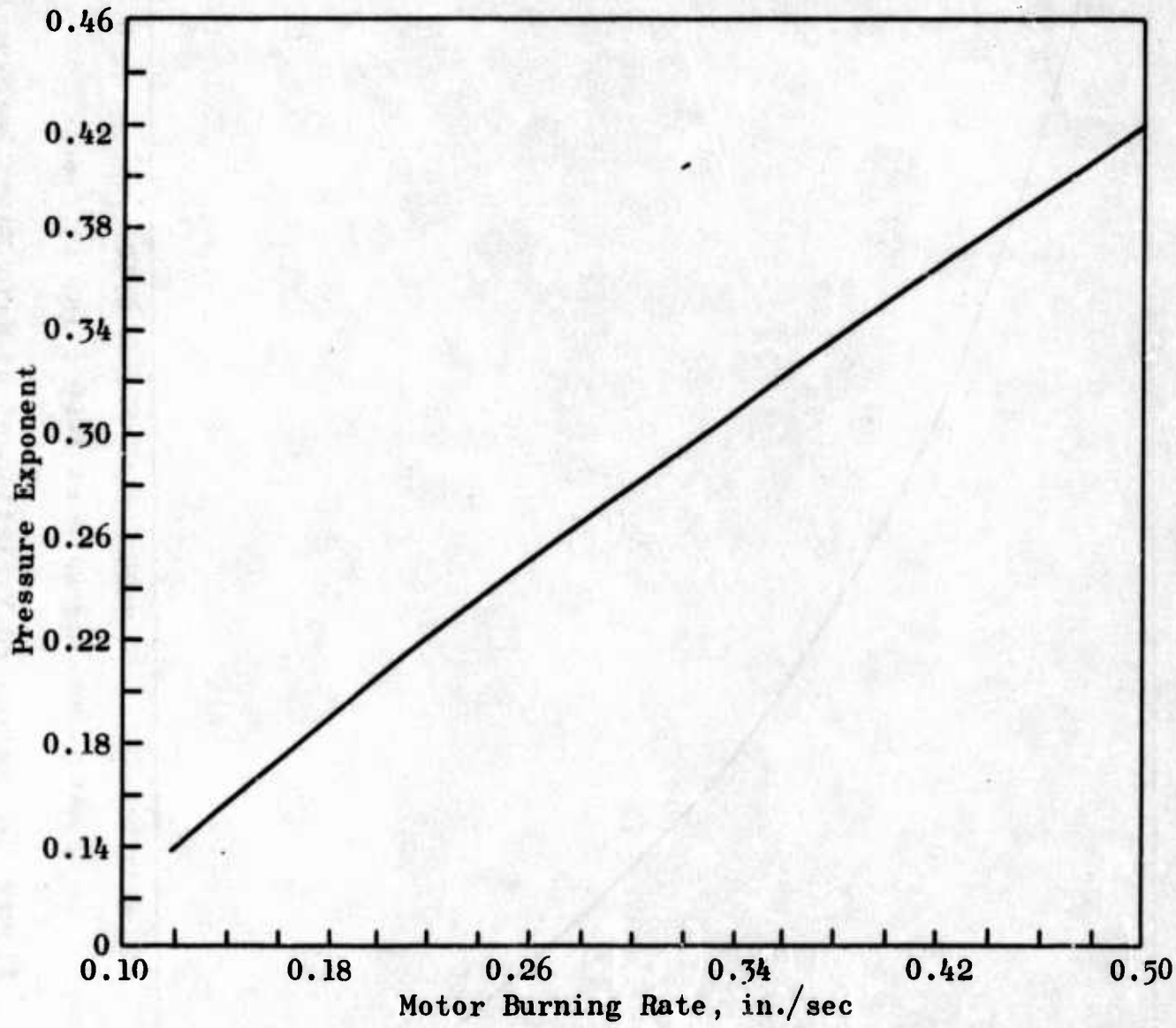


Figure 17. Estimated Variation of Pressure Exponent (n) with Burning Rate at 1000 psia, RDS-514 and-523

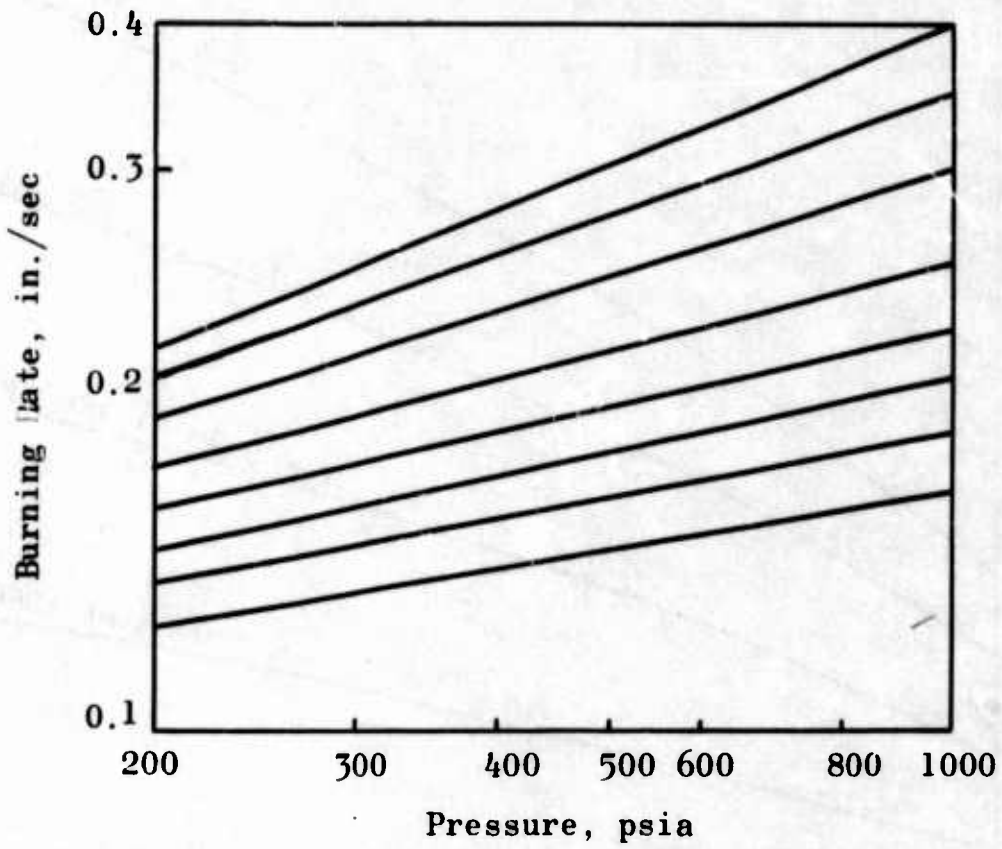


Figure 18. Motor Burning Rate vs Pressure, RDS-514 and -523 (Refer to Fig. 17 for Exponent Value)

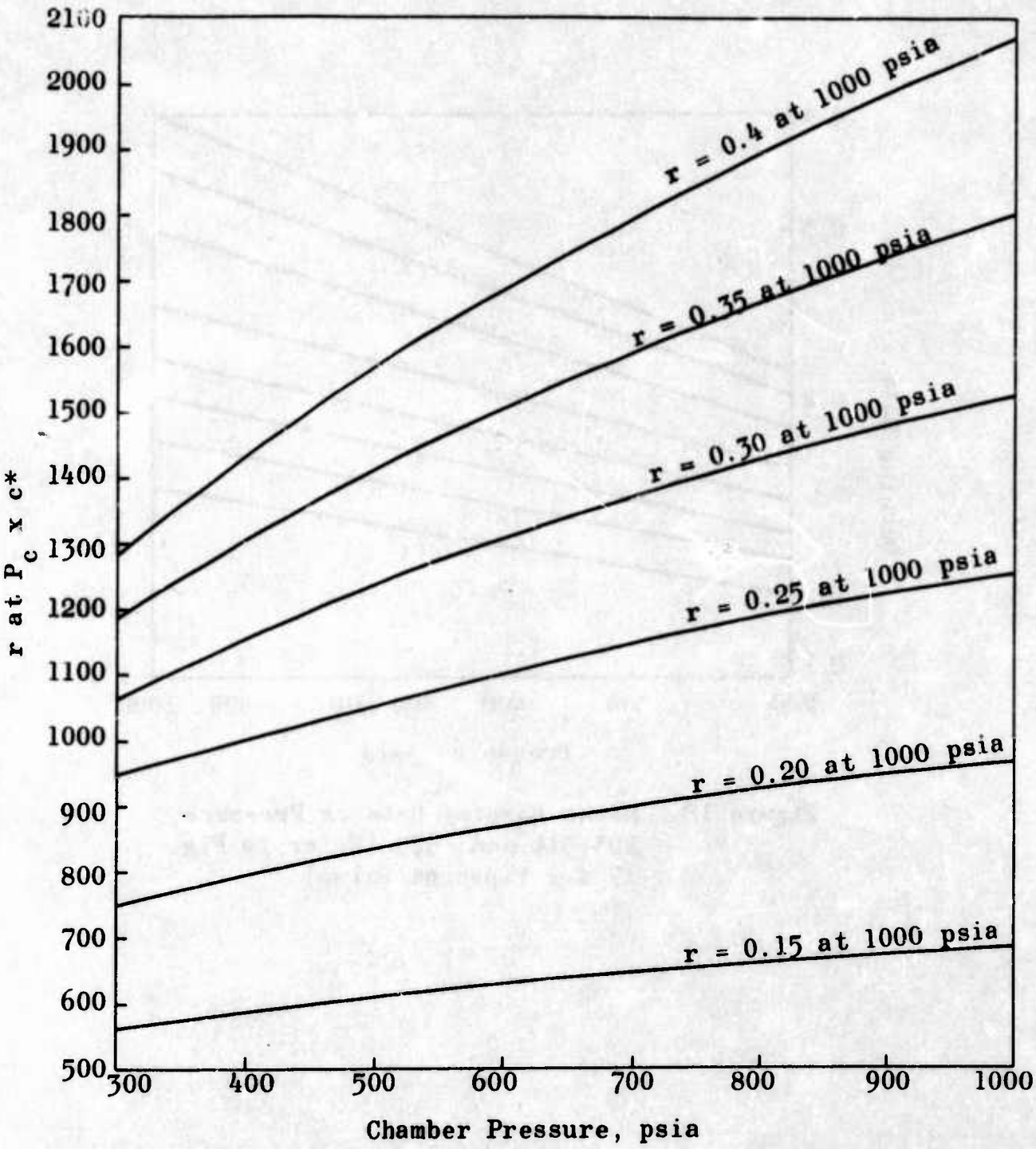


Figure 19. Product of Motor Burning Rate at Chamber Pressure and c* vs Chamber Pressure

From the equation:

$$P = \frac{s\rho c^* r \ @ \ P}{gA_t}$$

where

g = Gravity constant
A_t = Throat area
S = Burning surface area
ρ = Propellant density
c^* = Characteristic exhaust velocity
r = Burning rate
P = Chamber pressure

the product of $c^* \times r \ @ \ P$ can be solved explicitly and can be shown as a function of burning surface.

Motor burning rate was estimated from the uncured-strand burning rate. The strand rate was found to be approximately 18% lower than the motor rate.

The functions described above were used as a basis for selecting the required rate in each layer of the RFG. The calculations were straightforward except for the allowance made for core propellant (sliver) which burns simultaneously with the RFG. (Details of this method are discussed in the core grain subsection.)

(C) Having established these relationships, the ballistic design for the RFG was initiated from the data provided by the parametric study. The envelope available for the reinforced grain of Motor A was defined by an outside case diameter of 30 inches. Case thickness and insulation requirements reduced the diameter to 29.64 inches. The original case liner thickness was set at 0.30 inch, however, the minimum attainable was found to be about 0.060 inch, and this was used as a final target. The RFG inside diameter was set at 22.00 inches. Hence, the cylindrical web, based on the liner thickness of 0.060 inch, was 3.79 inches.

(C) The trade-off studies defined the nominal chamber pressure at the start of RFG burning to be 800 psia at 60 F. As the motor was to be fired only at 60 F, 800 psia was used as the design nominal. The design nominal pressure-time requirement was defined by a straight line (pressure vs web burned) from 800 psia at the start of RFG burning to 400 psia at a web remainder of one inch. The design nominal pressure during the last inch of web was constant at 400 psia. Thus, the configuration and amount of propellant was obtained for the RFG. This left the major effort in ballistic design in determining the burning rates for the propellant layers and estimating the performance of the RFG.

Essentially all surface-burning modes in Motor A RFG are in the radial direction. Because of the decrease in layer thickness in the domes, the flame front is burning more than one layer simultaneously. However, the burning modes initiated in this manner were assumed to contribute little toward additional weight flow rate. All burning in the cylindrical portion is theoretically normal to the initial surface. The flame front in the domes was scaled, based on normal burning through these layers, their burning rates and thickness. The total web through the RFG in the domes is significantly less than in the cylindrical section. To provide simultaneous burnout of all surfaces of the RFG, the conicyl in the core grain was dimensioned such that at the burnout of core web, a sufficient portion of core propellant remains in the domes to provide the simultaneous burnout of surfaces in the domes and cylinder.

(C) Performance estimates were based on instantaneous burning surfaces and associated burning rates. Surfaces were first calculated for the RFG as if no core propellant were present. Actually, at core burnout with all surfaces burning completely normal, 128 pounds of core propellant remains. Most of this comes from the star configuration, which has a cross-section sliver fraction[2] of 0.16, based on the 22-inch OD of the core grain. A portion of this 128 pounds is in the domes. To account for this in the estimate of performance, an area equivalent to the volume of 128 pounds was added to the curve of RFG surface vs web. The equivalent surface from the web then was used with the parametric curves in determining the burning rates of the grain.

Miscellaneous propellant weight and burning rate data for the RFG for Motor A, with a liner thickness of 0.060 inch are presented in Table V.

---

(2)Cross-section sliver fraction is defined as the cross-sectional area ratio of remaining core propellant to original core propellant, when the core burn front first reaches 22 inches diameter.

TABLE V

MOTOR A RFG PROPELLANT WEIGHT AND BURNING RATE DATA

Helical Layer No.	Uncured Strand Rate @ P, in./sec	Estimated Motor Rate @ P, in./sec	Propellant Weight, lb	Propellant RDS Number	Percent Depressant
1	0.260 @ 735 psia	0.305	133	514	0.5
2	0.220 @ 670 psia	0.258	139	514	1.1
3	0.179 @ 600 psia	0.210	156	514	2.5
4	0.170 @ 540 psia	0.200	156	523	2.6
5	0.145 @ 470 psia	0.170	178	523	5.5
6-9	0.132 @ 400 psia	0.155	575	523	6.0
			—		
		Total Propellant	1337		
		Propellant in Domes	448		
		Propellant in Cylinder	889		

Pressure and thrust-time were calculated by conventional methods, using properties of the respective propellant layers. At the interfaces of two layers with different burning rates, there is theoretically a discontinuity in the pressure-time function, as two pressures can be calculated for one time point. This of course, will not occur, primarily because a degree of propellant blending will occur in the manufacture of the RFG. As a method for constructing the curves, the pressure-time curve with discontinuities was first drawn. The degree of propellant blending was then estimated and its effect on pressure-time was drawn. Pressure-time integrals were made to coincide with propellant weight and ballistic properties.

The total impulse was calculated for each layer based on its propellant weight and average pressure over the particular interval. The average pressure was based on the pressure-time curve with its discontinuities. Portions of the core sliver were included with initial layers in determining the total impulse. Detailed evaluations of each test and a discussion of reinforced grain performance for each motor are given under the full-scale motor tests reports.

Although the specific ballistic performance requirements for the core grain were not specified, they are implied in the total motor performance specification and other considerations.

(C) Physical dimensions of the core envelope were fixed by the over-all motor envelope and the RFG structural considerations. The outside diameter of the grain was 22.00 inches, corresponding to the inside diameter of the reinforced grain. The optimum initial RFG pressure from the trade off studies was 800 psia and from this the core average operating pressure for the core propellant was established at 750 psia.

Propellant RDS-526 was selected for the core propellant and was tailored slightly for burning rate requirements. Properties of the propellant applicable to Motor A core are:

Temp coefficient of pressure (π_k), %/deg F	0.12
Pressure exponent (n)	0.30
Motor burning rate at 1000 psia, 60 F	0.393
Characteristic exhaust velocity, (c*), ft/sec	5168
Spec impulse (I_{sp}) at 1000 psia, zero deg half angle	250
Ratio of specific heats(*)	1.191
Theoretical flame temp, deg F(*)	5725
Density, lb/cu in.	0.0629

(*)Based on shifting equilibrium

With thrust and pressure levels essentially defined for the core burning duration, weight flow rate was limited to a particular level. Within the range of burning rates available in RDS-526, average burning surface of the core grain was established commensurate with the pressure level and nozzle throat area. From stress considerations and grain-design requirements the core-web value was determined to be 4 inches.

Within these boundaries, grain design studies were undertaken to obtain the highest feasible volumetric loading. Experience had shown that a conventional star configuration would be best, and this was taken as the final design configuration. However, other configurations were considered, such as modified-star or dogbone configurations. In the studies, port-to-throat ratios, erosive burning, and other variables affecting maximum pressure were considered.

(C) Pressure neutrality was a primary consideration in the grain design, as the more neutral design could operate closer to 800 psia; thereby, it could deliver more impulse. Conicyls (circumferential slots) in both forward and aft ends of the grain were incorporated for this purpose as well as stress considerations.

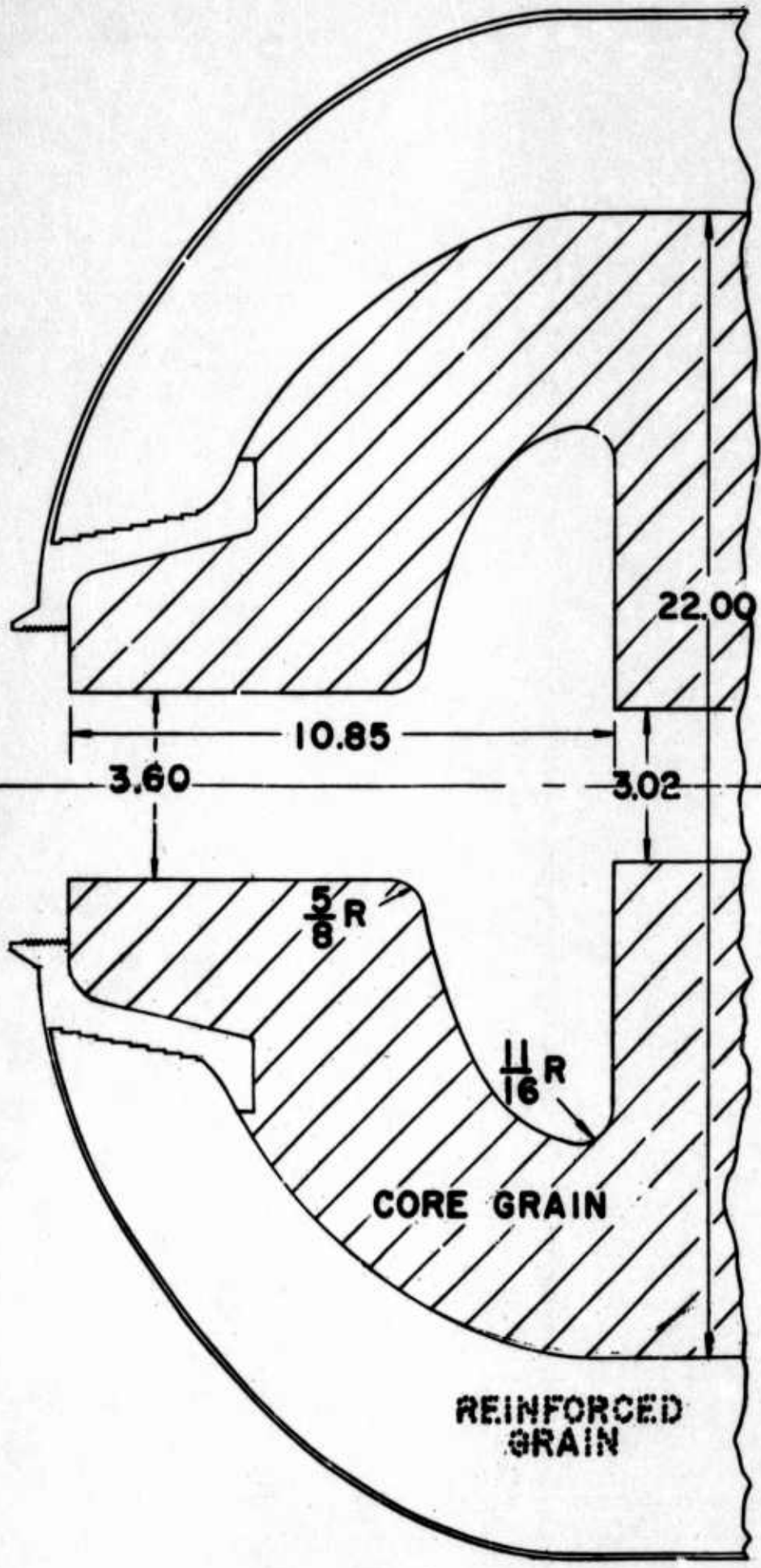
As a concept requirement, the reinforced grain was a pressure load-carrying member; this called for keeping the core flame front away from the reinforced grain in the dome areas prior to the transition from core to RFG in the cylindrical section. Initial design analyses considered restricting a portion of the core propellant to provide this feature, when both aft and forward polar bosses were the same. However, design features of the aft polar boss enabled the core configuration to be made without restrictor in this area.

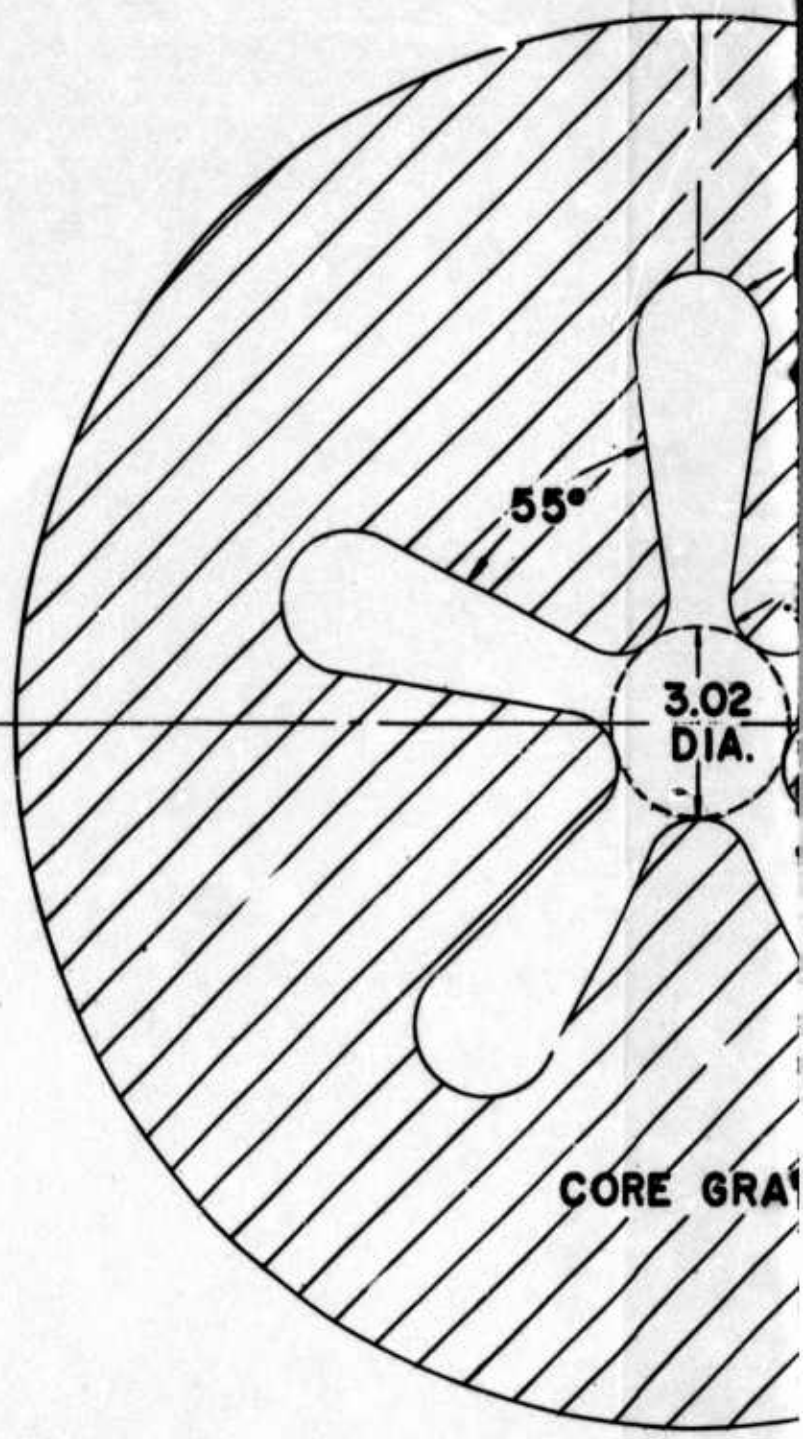
(C) A five-point, conventional star cross-section was determined to be the optimum design (see Fig. 20). The star angles were determined from the ballistic design analysis. The fillet radius of 1.10 inch was primarily a stress consideration, and the 0.87-inch radius at the star tip was the minimum radius which mandrel design would tolerate.

(C) With this core design, and based on the 22-inch diameter of the core grain, the cross sectional sliver content is 16%. However, this propellant is not sliver as such, as evidenced by data from A-1002 firing, where the tail-off impulse represented 3.4% of the total impulse. Most of this cannot be attributed to the cross-sectional sliver content of the core grain. As the flame front progresses into the RFG, the propellant remaining from the core has a relatively higher burning rate than the RFG, and it will be consumed well before the end of RFG burning.

CONFIDENTIAL

PREVIOUS PAGE WAS BLANK, THEREFORE WAS NOT FILMED





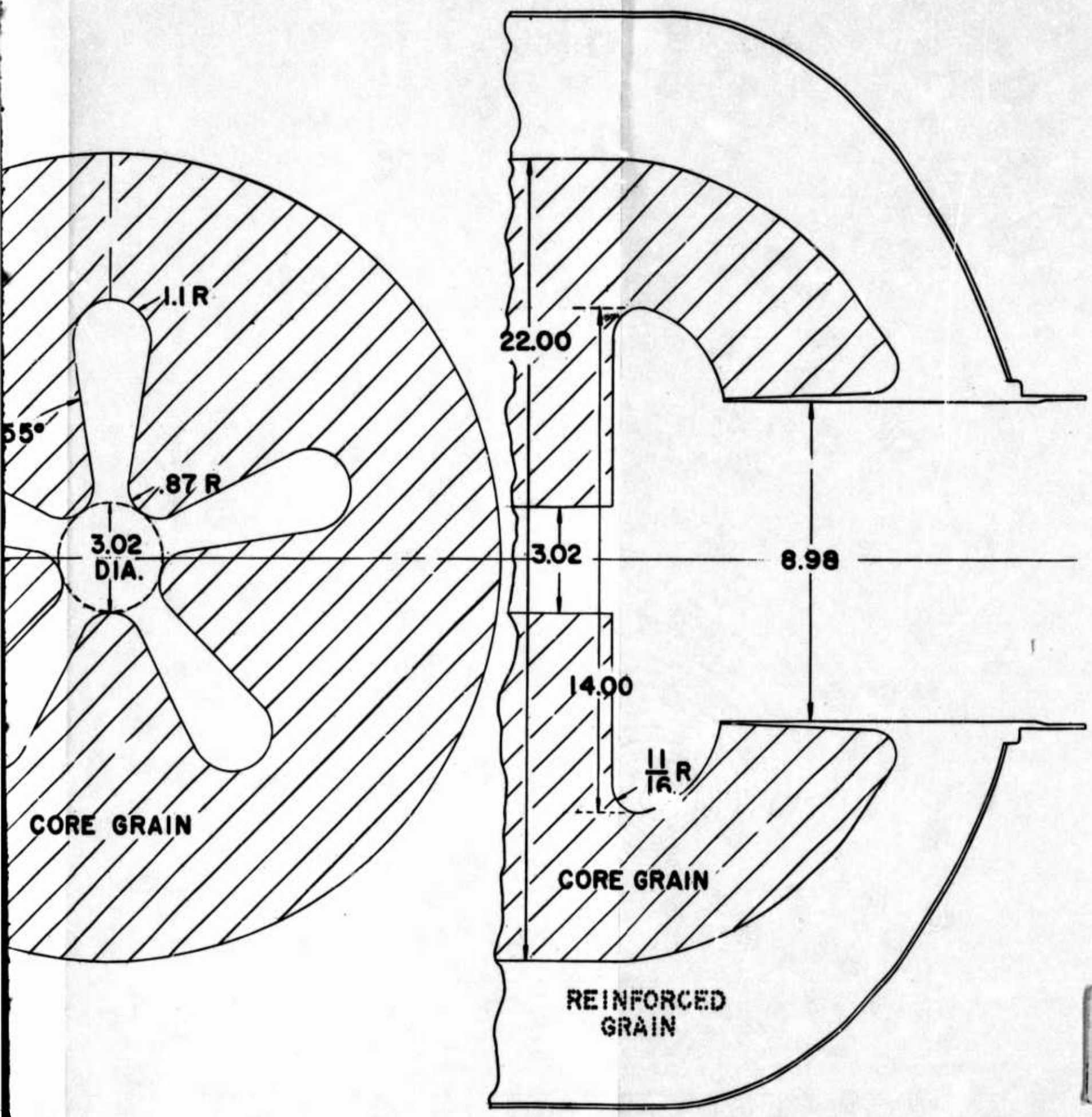


Fig. 20 Motor A
Core Grain Schematic

CONFIDENTIAL

PREVIOUS PAGE WAS BLANK, THEREFORE WAS NOT FILMED

The final flightweight Motor A design weight summary is presented in Table VI.

TABLE VI

MOTOR A DESIGN WEIGHT SUMMARY (FLIGHTWEIGHT MOTOR)

	Wt, lb
Propellant	
Core Grain	1,133.00
RFG	1,349.00
Igniter	0.55
Total Propellant	2,482.55
Inert	
Case and Skirt	34.0
Liner	12.0
Nozzle	26.77
Aft Polar Boss, Load Ring, Flange, Pins	19.07
Forward Polar Boss and Load Rings	14.95
Igniter Assy	3.08
Total Inerts	109.87
Total Motor	2,592.42
Mass Fraction	0.958

b. Structural Design

The case-grain structure was designed to support maximum chamber pressure as well as ultimate flight loads, whereas the filament-wound glass case was only designed to contain chamber pressure near the end of burning combined with flight bending loads. Buckling of the thin fiberglass case would have been the critical load condition if a conventional grain had been used in these motors. However, because of the relatively high modulus and inherent rigidity of the reinforced grain, the case was stabilized in a manner similar to a pressurized case.

The design of the reinforced grain-case combination provided a composite structure with a greater structural efficiency throughout the burning time than conventional grain-case combinations. Design of the motor involved a balance between structural and ballistic performance and compatibility of the entire composite.

The glass filament wound case/reinforced grain composite structure for Motor A was designed as a mutually interacting pressure vessel. The GFW case consisted of S-994-HTS glass fiber-reinforced epoxy resin which was bonded through an R-143 rubber liner to a series of interlayers of filament-wound, wire-reinforced Flexadyne propellant. Structural support fittings of titanium and glass/phenolic insulation were provided at the forward and aft ends for support during the winding and for attachment of the forward head closure and nozzle. The GFW case had integral forward and aft skirts.

The specific requirements for Motor A establish the maximum geometric envelope and externally applied loads. In addition to these loads, motor internal pressure and thrust loads also had to be considered in the structural design. Magnitude of the thrust load was small enough in comparison with the externally applied bending moment that it did not influence the design of Motor A.

(C) Trade-off studies conducted early in the program dictated these maximum initial and burn-out pressures for the motor:

	Maximum Initial Pressure, psia*	Maximum Burn-out Pressure, psia*
Motor A	880	440

*Includes 10% for variation in ballistic reproducibility

(C) These values were for 60 F operating temperatures. Although it was only required that Motor A be fired at 60 F, it was decided to design the RFG/GFW structure so it could be fired at 90 F. This increased the maximum initial and burn-out pressure for Motor A to 935 and 468 psia, respectively.

The structural design conformed to the requirements called out in MIL-R-25532A in that it was based on an internal pressure which was 1.25 times greater than the maximum hot operating pressure with a 10% assumed maximum variation in ballistic performance. This value has proven slightly conservative on other preliminary motor designs. Flight loads were interpreted as the maximum operating loads and the structure was designed not to fail at ultimate flight loads which were 1.25 times greater than the maximum operating loads. Thus, the safety factors used were:

S_{F_u} = 1.25 internal pressure

S_{F_u} = 1.25 flight loads

This gave the following design ultimate structural loads for Motor A:

	Initial	Burnout
Pressure, psia	1,170	585
Compression, lb	50,000	50,000
Bending moment, in.-lb	1,000,000	1,000,000
Shear, lb	9,375	9,375
Torsion, in.-lb	137,500	137,500

The RFG was capable of supporting the major portion of the internal pressure until just prior to burnout. Therefore, the critical design condition for this motor was determined to be the simultaneous combination of the following ultimate loads (which occurred just prior to burn-out of the RFG):

Pressure, psia	585
Bending moment, in.-lb	1,000,000
Shear, lb	9,375
Torsion, in.-lb	137,500

The GFW case was designed to withstand these loads at 90 F.

(1) Design Data Acquisition

At program initiation the proposed methods to be used in the structural analysis were still in need of improvement, and some materials and fabrication changes were indicated by a previous RFG contract (AF04-611-8193). These voids were planned to be filled by joint Air Force and Rocketdyne subscale programs.

(a) Resin and Glass Studies

One area of concern was in the glass filament wound cases. Although glass filament wound cases have been used in the solid propellant rocket industry for a number of years, the reinforced grain application required a new resin system with somewhat unique qualities. Consequently, Rocketdyne made a study of many different systems before selecting one for RFG cases. Since the glass filament wound case was wrapped directly onto the grain, the resin had to be one which would cure at a relatively low temperature and still retain good mechanical properties when the rocket motor was subjected to a high temperature environment.

After testing many different resin and glass combinations, seven were selected for final evaluation. All seven were tested at room temperature and all resins (but not all glasses) were tested at 200 F. Owens-Corning, 20-end, X994 (now S994), HTS glass roving with DER 332 resin and APCO 320 curative were selected for preliminary design because of the high ultimate strength attainable. The DER 332/APCO 320 resin was tested at room temperature with S994 glass, and at 200 F with Owens-Corning "E" glass. These tests, conducted on standard, Rocketdyne, 3-inch, open-end cylinders, showed an ultimate hoop stress of 352,000 psi. One 18-inch diameter glass filament wound case, fabricated and tested at room temperature, ruptured during a biaxial test at a composite hoop stress of 300,000 psi. Based on tests performed the following ultimate properties (Table VII) were used for design of filament wound cases for reinforced grains. These mechanical properties were used in the preliminary design of Motors A and B.

Further resin studies continued on a Rocketdyne IR&D program where better values of all material properties were obtained for final full-scale, flightweight designs. Of the many low-temperature curing resins studied, a few were subjected to final laboratory tests. Dow Chemical Company's resin, DER 332, was retained and all tests used the new Owens-Corning S994 fiberglass with the new resin curative EMI. Comparative test results are shown in Table VIII.

TABLE VII

PROPERTIES USED IN FILAMENT WOUND CASE DESIGN

Materials		
Fiberglass:	Owens-Corning, 20-end, S994 (HTS) Roving	
Resin:	Dow Chemical Co. DER 332	
Curative:	Applied Plastics Co. APCO 320	
Mechanical Properties	**Temperature, deg F**	
	80	**200**
Ultimate Tensile Stress, psi (circumferential wraps)	270,000	216,000
Ultimate Tensile Stress, psi (helical wraps, in the direction of the fiber)	230,000	184,000
Ultimate Compressive Stress, psi (in the direction of the fiber)	180,000	144,000
Young's Modulus, psi (in the direction of the fiber)		
Tension, million psi	10.0	8.0
Compression, million psi	9.0	7.2
Ultimate Interlaminar Shear Stress, psi	3000	2400
Poisson's Ratio	0.12	0.12
Composite Density	0.074	0.074

TABLE VIII

IR&D RESIN STUDY

Resin DER 332	Curative	
	APCO 320	EMI
Ultimate Composite Tensile Stress, psi		
at 80 F	293,000	304,000
at 200 F	231,000	267,000
Ultimate Interlaminar Shear Stress, psi		
at 80 F	10,270	9,510
at 200 F	6,450	6,210
at 250 F	2,250	5,580

Because of its slightly better tensile stress and much better inte - laminar shear stress, particularly at elevated temperature, the EMI curative was selected for testing in subscale GFW cases. Two 10-inch diameter GFW cases without skirts, 10-019 and 10-020, were fabricated and tested at 200 F to determine the ultimate allowable stress at this temperature for the glass-resin composite. Pertinent fabrication data for these cases are as follows:

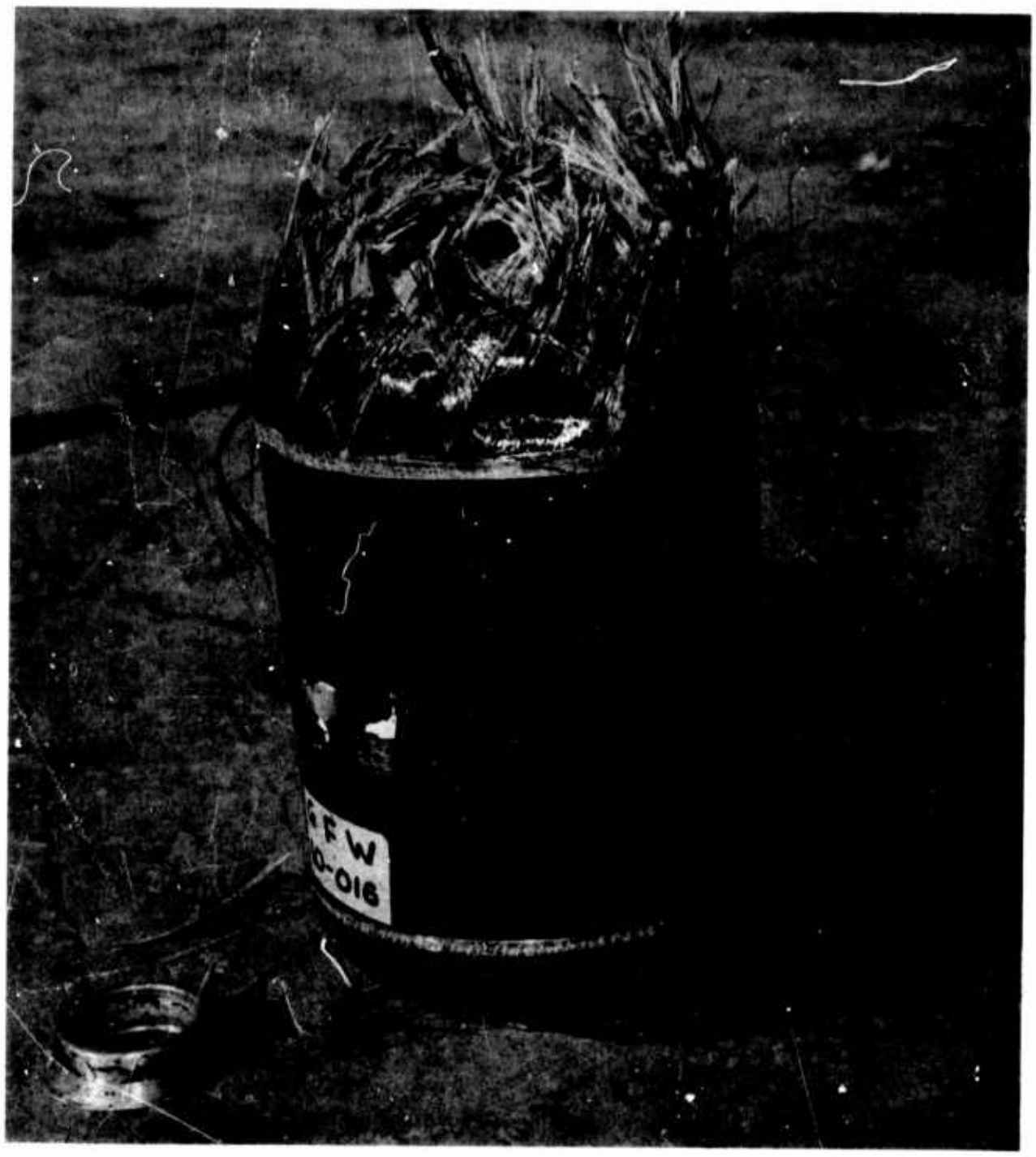
Fiberglass	12 End S994
Resin/Curative	DER 332/EMI
Length-to-Diameter	1.0/1.0
Winding Pattern	Polar-4 Cycle-2 Covers
Polar Wrap Angle	20^{o} 43'
Glass Density, ends per inch	
Polar Wrap	414
Circ Wrap	585

Burst pressure only was recorded for these cases. It occurred at 1308 and 1277 psi for Cases 10-019 and 10-020, respectively. These tests not only confirmed that the preliminary fiberglass ultimate stress values were realistic, but also indicated that the decrease in ultimate stress at elevated temperature (200 F) was not going to present as large a problem as anticipated. Figure 21 shows the GFW case after rupture. Initial rupture was in the cylindrical section.

Two more 10-inch cases (10-021 and 10-022) were fabricated with skirts and hydrotested to verify the design stress allowables and to determine the effect of the skirts on the rupture pressure. Pertinent design and fabrication data for these cases are shown below:

Fiberglass	12 End S994
Resin/Curative	DER 332/EMI
Length-to-Diameter Ratio	1.5/1.0
Winding Pattern	Polar-4 Cycle-2 Covers
Polar Wrap Angle	17^{o} 42'
Glass Density, ends per inch	
Polar Wrap	419
Circ Wrap	503

Calculated burst pressure at 70 F for these cases was 1016 psi in the circular wrap assuming the same maximum values of ultimate stress and no degradation for the skirt stress concentration factor. Rupture occurred at 1108 and 1145 psi in GFW Cases 10-021 and 10-022, respectively and was in the hoop wraps. These cases were not balanced for a pressure loading because they were designed for combined pressure, bending, torsion, and compression.



2YA25-9/25/63M1B

Figure 21. GFW Case 10-016 After Rupture

Critical external load conditions for Motor A were expected to be unpressurized bending and compression of the motor. Compression and bending tests of additional 10-inch motors which were scaled similar to Motor A showed the critical buckling load on the RFG/GFW combinations to be approximately 4.9 times as high as the critical buckling load for the identical GFW case only. These tests confirmed previous laboratory test results of 6-inch motors on a Rocketdyne-sponsored program. The ratio of critical buckling loads for the 6-inch motor tests was 3.53:1. However, these laboratory specimens were cylinders only and a higher ratio was expected for the dome-ended motors. Extrapolation of the 10-inch motor test data to the full-scale motors indicated no buckling problem would be encountered with the full-scale motors as a result of external loads. The only problem concerning external loads which remained unsolved when the contract was terminated was the inability of the GFW case skirts to transmit the loads to the case without tearing out. This problem is discussed in the full-scale motor fabrication and test sections of this report.

(b) Aluminum Wire

(C) Another problem area that developed early in the initial phase of the program was with the reinforcing wire. Reinforced grains for Motor A were planned to be fabricated with approximately 0.0075-inch diameter and 20% by weight aluminum wire (this percent was established in the trade-off studies). Tests were conducted with 5056 aluminum wire furnished by the Hudson Wire Company. Minimum guaranteed properties for this wire are as follows:

Minimum Ultimate Tensile Stress, psi	70,000
Minimum Elongation, %	1.0

Composite properties as determined by tests conducted at Rocketdyne[3] for reinforced grains fabricated with low elongation 5056 aluminum wire were:

(C)

Maximum Hoop Stress at the Inside Surface, psi	4500
Maximum Hoop Strain at the Inside Surface, in./in.	0.01
Young's Modulus, psi	6.0×10^5

(3) Under Contract AF04(611)-8193 and Company IR&D

Current tests had shown poor structural compatibility of the RFG and GFW on several 10-inch diameter tests which had been attributed to the low elongation of the aluminum wire. Rupture of 10-inch diameter GFW cases was consistently occurring at 3% strain. However, when RFG/GFW combination motors were tested, rupture of the RFG was occurring when strain in the GFW case was only 0.3 to 0.7%. Calculations showed that this strain in the case, and therefore outside diameter of the RFG indicated approximately 0.6 to 1.4% strain in the aluminum wire on the inside diameter of the grain. It was surmised that failure was initating at the inside surface and propagating to the GFW case as a result of the wires reaching the maximum strain capability.

Efforts to obtain a higher elongation aluminum wire without decreasing the ultimate tensile strength were unsuccessful. It was evident that a wire with at least 2.5% elongation (strain in GFW case at RFG burnout) would have to be obtained to be compatible with the fiberglass case for ballistic testing. Consequently, it was decided to obtain aluminum wire with a minimum elongation of 5% to exclude rupture of the RFG at the inner surface prior to rupture of the GFW case.

A survey of potential vendors showed the best available wire had a minimum ultimate tensile strength of 50,000 psi with a minimum elongation of 5%. Some of this wire was purchased on a company-sponsored program and a 10-inch diameter RFG/GFW motor was hydrotested. This motor was identical to previous 10-inch motors except high-elongation (5%) aluminum wire was substituted for the low-elongation (1%) aluminum wire. Although the ultimate tensile strength of the wire was decreased from 70,000 to 50,000 psi, the motor burst pressure was increased 38%. The high-elongation (5%) wire was selected for use in the design of all subscale and full-scale motors for this contract.

(C) Although 5% elongation was considered high for this high-strength aluminum wire, it was still well below the minimum elongation of Flexadyne propellant and resulted in a much lower reinforced grain composite modulus of elasticity. Based on composite properties obtained with low-elongation wire, the following were estimated mechanical properties of reinforced grains fabricated with high-elongation wire:

Maximum Hoop Stress at the Inside Surface, psi	3215
Maximum Hoop Strain at the Inside Surface, in./in.	0.05
Young's Modulus, psi	1.5×10^5

One variable in the aluminum wire which was not investigated on this program was the influence on structural efficiency of wire diameter with the high-elongation wire. Ballistic testing on the previous contract had shown combustion efficiency with 5-mil wire to be slightly higher than with 7.5-mil wire. Structural testing, however, with samples of 2, 6, and 10 inches in diameter had shown a structural advantage of nearly 100% by using 7.5-mil wire. However, since these tests were all conducted with low-elongation wire, the effect of the wire diameter on structural efficiency when using high-elongation wire was unknown. It was decided that structural efficiency of the 7.5-mil, high-elongation wire was probably better than, but certainly equal to, the 5-mil wire and since the difference in combustion efficiency was small, the 7.5-mil, high-elongation wire was selected for the remainder of the work on this program.

(c) Localized Buckling or Crippling

Another area of investigation was that of problems of buckling and crippling. The correct buckling coefficient for fiberglass cases and reinforced grains in combination was to have been determined experimentally. (The forward and aft skirt design, however, were similar to current fiberglass case design.) Several experiments were completed by the Structural Plastics Department of Rocketdyne to determine the correct buckling coefficient, C_{cr}, to be used in the conventional cylindrical buckling equation:

$$\bar{\sigma}_{cr} = \frac{C_{cr} E_{c_z} t_c}{R} \qquad (1)$$

Tests were conducted on Owens-Corning S994 fiberglass cylinders with an R/t ratio of 50. Based on test results, Rocketdyne recommended a C_{cr} value of 0.49 for cylinders of this material which had an R/t ratio of 50 and were wound with two circumferential wraps for each helical wrap. This value was extrapolated for other R/t ratios by using the buckling coefficient vs R/t ratio curve in the "North American Aviation Structures Manual." For R/t ratios of interest, the following values of the buckling coefficient C_{cr} were determined:

Radius to thickness (R/t) ratio	50	100	150	200
Buckling coefficient (C_{cr})	0.49	0.47	0.45	0.43

The original program plan was to subject ten 10-inch GFW cases to external bending, compression, and torsional loads and to compare these with 10-inch RFG/GFW motors subjected to the same type of loading. Only three of the cases were fabricated and tested. Two of these, 6401 and 6402, were subjected to axial compression at 170 F and the third was subjected to bending. The bending test fixture was designed to apply a uniform bending moment over the entire length of the motor but a pin, which was used for compression loading, was inadvertently left in the fixture during the test and, therefore, loaded the case in a statically indeterminate manner. Subsequent compression tests of the RFG/GFW combination showed the compressive ultimate strength of the 10-inch motors was improved by a factor of approximately three and, therefore, the critical design condition for the full-scale motors was determined to be the combination of pressure and bending.

(d) Fabrication Modifications

The structural problem associated with fabrication was investigated on the 20-inch motor because the design, winding cams, and winding techniques were already worked out for a partial-web, 20-inch RFG.

Ballistic considerations made it necessary to design and fabricate an RFG having very near uniform thickness in the cylinder and the domes. With conventional filament winding techniques this was not possible because of the inherent buildup as the filament was wound on a smaller adjacent radius, as in the domes. A technique of staggering the opening diameter on the dome of each layer in the RFG was developed which gave a very near uniform dome thickness.

Previous hydrotests of RFG/GFW motors had shown that the method of analysis which treated the motor as a thick-wall, composite pressure vessel was slightly conservative in the cylinder, but these tests indicated a severe structural incompatibility in the region of the polar openings. The polar bosses on RFG's prior to this contract had been retained by two flanges or "load rings." One of these was located on the inside surface of the RFG and the other between the outside surface of the RFG and the GFW case.

To provide better load distribution across the web of the RFG, a load ring was positioned between each helical layer that was wound with the same opening as the diameter of the polar boss. The original design of the load rings used plastic to provide additional flexibility as well as better load distribution. To evaluate the loading concept one 20-inch RFG and one 20-inch RFG/GFW motor were fabricated and scheduled for hydrotest. Primary objectives of these tests also included further evaluation

of high-elongation wire, evaluation of structural capability of RFG's fabricated with uniform web thickness, evaluation of structural compatibility of RFG/GFW composite structure, and evaluation of polar boss, RFG, GFW interaction.

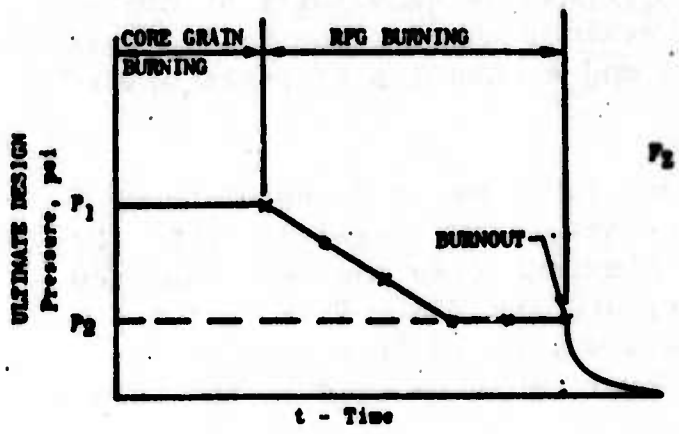
The first 20-inch hydrotest (RFG/GFW 7202/7401) was a disappointment in that rupture occurred at a very low pressure. Investigation after the test, however, revealed that the wrong aluminum wire had been supplied by the vendor and had been used to fabricate the RFG. This test and subsequent design and fabrication changes which led to a completely successful 20-inch, RFG/GFW motor hydrotest are discussed in Appendix I.

(2) Design Approach, GFW and RFG

To obtain maximum structural efficiency, it was desirable to have the RFG and case stressed as near as possible to their ultimate for the duration of the burning time. Thus, since the RFG structure burned away as a function of time it was necessary to design for a regressive pressure-time history. Since the case and grain had different moduli and different failure points, it was important to consider the structure as an interacting, two-element, redundant structure.

The analytical approach to the RFG and GFW case structural compatibility during internal pressurization loading was to consider the reinforced grain as a thick wall elastic cylinder contained in (and supported at its outer diameter by) a thin elastic case. Infinitesimal elastic theory using a plain strain end consideration was applied to predict the stresses, strains, and deflections of the RFG and filament wound case at intervals during the pressurized burning period.

Composite case and RFG hoop moduli were determined during hydrostatic pressurization testing of RFG's and filament wound cases. These test values along with other dimensional parameters were then used as inputs to a computer program which determined the required case thickness, the initial RFG web thickness, and the required web thickness-vs-pressure curve necessary to maintain a sound structure until burnout. Figure 22 illustrates the RFG and case design procedure. The case was first designed to withstand an internal pressure equal to the motor burnout pressure (P_2) and the ultimate flight loads. An RFG web thickness was then calculated to ensure the composite structure would contain the maximum initial pressure (P_1). The following discussion on the GFW design, fullscale tests, and the RFG design presents the design procedure for the individual elements and the composite structure.

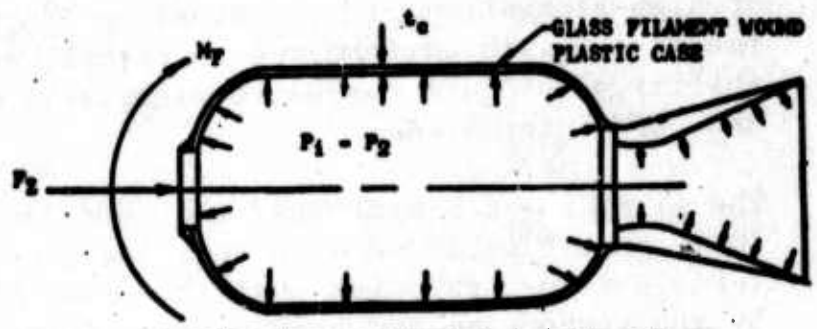


(a) DIAGRAMMATIC RFG MOTOR PRESSURE-TIME TRACE

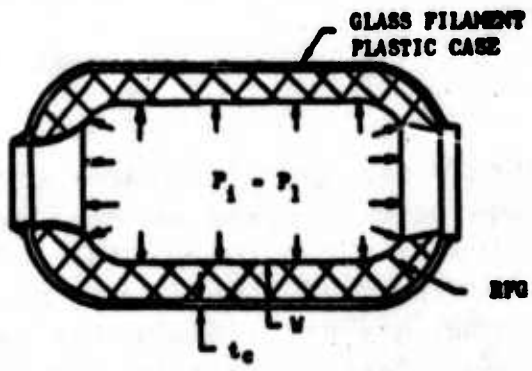
P_1 = INTERNAL DESIGN PRESSURE, psi

P_1 = ULTIMATE DESIGN PEAK PRESSURE. EQUAL TO THE INITIAL MAXIMUM HOT OPERATING PRESSURE (INCLUDING AN ASSUMED DEVIATION FROM NOMINAL) MULTIPLIED BY THE APPROPRIATE SAFETY FACTOR.

P_2 = ULTIMATE DESIGN PRESSURE JUST PRIOR TO MOTOR BURNOUT. EQUAL TO THE MAXIMUM HOT OPERATING PRESSURE JUST PRIOR TO BURNOUT (INCLUDING AN ASSUMED DEVIATION FROM NOMINAL) MULTIPLIED BY THE APPROPRIATE SAFETY FACTOR.



(b) COMPOSITE CASE THICKNESS (t_c) DESIGNED FOR BURNOUT PRESSURE (P_2) AND FLIGHT LOADS (F_Z & M_F).



(c) RFG WEB THICKNESS (W) DESIGNED TO INSURE THAT THE COMPOSITE STRUCTURE WILL CONTAIN THE MAXIMUM PRESSURE (P_1).

Figure 22. RFG-Filament Wound Case Design Criteria

(a) GFW Case

The case loads were calculated as follows (Ref. Fig. 22)(4)

$$N_{z_T} = \frac{P_2\, C}{2} + \frac{M_F}{\pi\, C^2} - \frac{F_z}{2\,\pi\, C}$$

$$N_{\theta_T} = P_2\, C$$

(4) Symbols are defined on pages 87 through 93, and may be folded out for convenience in reading.

With the case wrapped on a goedesic-isotensoid contour around the heads, the cylindrical helical angle was defined by:

$$\alpha = \sin^{-1}\left(\frac{R_o}{C}\right)$$

The helical wrap thickness necessary to withstand the longitudinal loads was calculated as follows:

$$t_z = \frac{N_{z_T}}{\overline{\sigma}_{\alpha_z} \cos^2 \alpha}$$

The circumferential (circ) wrap thickness required was calculated as follows:

$$t_\theta = \frac{P_2\, C}{\overline{\sigma}_{\alpha_\theta}} - (t_z \sin^2 \alpha)\left(\frac{\overline{\sigma}_{\alpha_z}}{\overline{\sigma}_{\alpha_\theta}}\right)$$

The composite case thickness was:

$$t_c = t_z + t_\theta$$

The composite modulus of the case was calculated as follows:

$$E_{c_\theta} = \frac{E_{c_\alpha}}{t_c}\left[t_\theta + t_z \sin^2 \alpha\right]$$

The composite allowable hoop stress for the case was:

$$\bar{\sigma}_{c_\theta} = \frac{P_2\, C}{t_c}$$

(C) The conventional netting analysis was used to calculate burst strength for GFW cases. Hoop and longitudinal strength was approximately balanced based on an ultimate fiberglass stress at 70 F of 388,000 and 422,000 psi in the polar and circ wraps respectively. Burst pressure in the hoop and circ directions was calculated by the following equations:

$$P_c \text{ (Max. Hoop)} = \frac{2}{D_i}\left[N_c\, \bar{\sigma}_{g_c}\, \bar{A}_e + N_p\, \bar{\sigma}_{g_p}\, \bar{A}_e \sin^2 \alpha_p\right]$$

$$P_c \text{ (Max. Longitudinal)} = \frac{4}{D_i}\left[N_p\, \bar{\sigma}_{g_p}\, \bar{A}_e \cos^2 \alpha_p\right]$$

where

N_c and N_p = the number of fiberglass ends per inch in the circ and geodesic wraps respectively

$\bar{\sigma}_{g_c}$ and $\bar{\sigma}_{g_p}$ = ultimate allowable stress in the fiberglass in the circ and geodesic wraps respectively

$\bar{A}_e$ = the average cross-sectional area of a single end of fiberglass roving

(C) Because the 10-inch GFW cases exceeded the design ultimate stress by approximately 10%, it was decided to use the same ultimate fiberglass stress in the first full-scale GFW case tests as well as in a 20-inch RFG/GFW motor hydrotest. These values of ultimate stress in the fiberglass, (422,000 psi-circ wrap and 388,000 psi-helical wrap) although considered to be optimistic at the time, were demonstrated on numerous 10-inch cases after all the various fabrication problems were solved.

(b) Reinforced Grains

All RFG motors designed on this contract were designed specifically to utilize the structural capabilities of the RFG to resist the internal pressure and applied external loads.

(C) Trade-off studies showed that to obtain the highest possible mass fraction, the core grain of Motor A should burn at 800 psi and that burning of the RFG should regress from an initial nominal value of 800 psi to 400 psi at burnout. Therefore, the GFW case was designed to support the internal pressure at RFG burnout and the RFG/GFW composite was designed to support the initial chamber pressure. Outside diameter of the case was set by contract at a maximum of 30 inches. Allowance for the GFW case skirt thickness and liner thickness set the outside diameter of the Motor A at approximately 29.6 inches.

The maximum tensile stress and strain in the RFG occurred at the inside surface and in a tangential direction. Calculations using the conventional thick wall cylinder equations were used to determine the first approximation of the web thickness:

$$\sigma_{g_\theta} = \frac{1}{b^2 - a^2} \left[P_i \ (a^2 + b^2) - 2 \ b^2 \ P' \right] \qquad (1)$$

$$\epsilon_{g_\theta} = \frac{1 + \mu_g}{E_{g_\theta} \ (b^2 - a^2)} \ P_i \ (a^2 + b^2 - 2 \ \mu_g \ a^2) -$$

$$2 \ g^2 \ P' \ (1 - \mu_g) \qquad (2)$$

(C) In equation (1), 3215 psi was considered the maximum allowable hoop-stress value. This value was determined from subscale motor testing and has proven to be slightly conservative. P_i is the ultimate chamber pressure, considering reproducibility limits and a 1.25 load factor. P' is the external pressure on the RFG or the pressure between the RFG and the GFW case and is given by the following equation:

$$P' = \frac{A}{1 + \frac{B}{a^2} + \frac{D}{a^2}\,\frac{b^2}{c^2 - b^2} - \frac{D}{c^2 - b^2}} \qquad (3)$$

where

$$A = 2\,P_i\,(1 + \mu_g)$$

$$B = b^2\,(1 - 2\,\mu_g)$$

$$D = \frac{E_{g_\theta}}{E_{c_\theta}}\,\frac{1 + \mu_c}{1 + \mu_g}\,b^2\,(1 - 2\,\mu_c) + C^2$$

a = inside radius of RFG

b = outside radius of RFG

C = outside radius of GFW case

Eg_θ, Ec_θ are Young's modulus of the RFG and GFW case respectively in the hoop direction.

μ_g, μ_c are Poisson's ratio of RFG and GFW case respectively.

(C) Various values of "a" were substituted into Eq. 1, 2, and 3 for an ultimate pressure (P_i) of 1170 psi. These calculations showed the RFG inside radius should be approximately 11.0 inches, which gave a web thickness of 3.82 inches.

The preceding RFG equations were concerned with the calculation of circumferential stresses and strains only. The RFG structure, however, was made up of helical wraps as well as circumferential wraps to encure a proper longitudinal pressure carrying capability.

The RFG web was divided into 9 geodesic isotensoid (GI) layers and 8 fill layers, Fig. 23. Only the GI layers were considered in determining the longitudinal strength of the RFG because all the fill layers terminate before reaching the load rings on the polar boss. For the same reason, only the GI layers were effective in resisting shearout of the polar bosses. The fill layers were designed to provide hoop strength in the cylindrical part of the grain as well as to fill in between the GI layers on the dome and provide a near-uniform web thickness.

Once the RFG preliminary web thickness had been determined, the final grain design was established by balancing the maximum pressure capability for the following conditions.

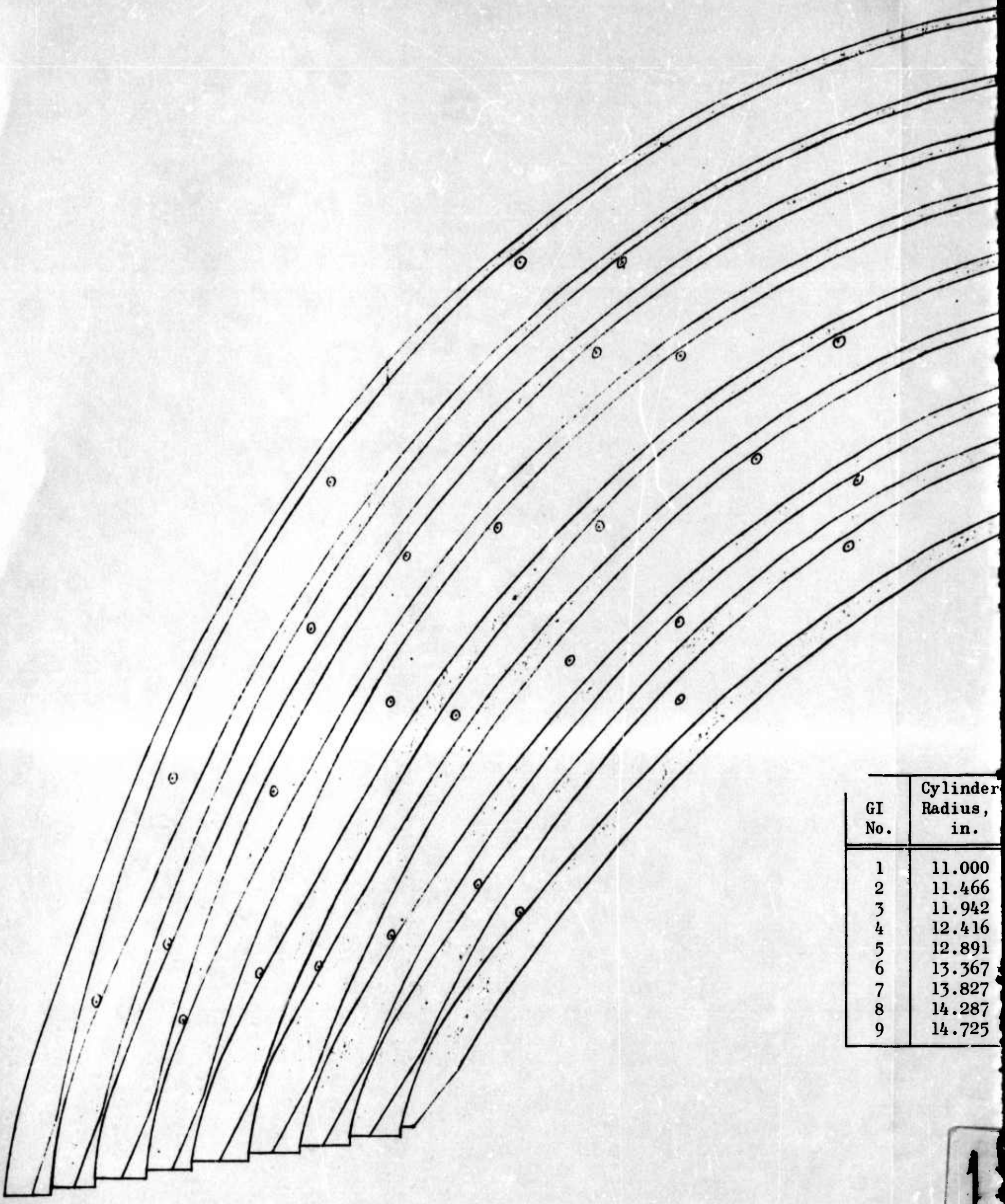
Considering the RFG as a thick wall isotropic cylinder gave a longitudinal stress σ_{g_z} of

$$\sigma_{g_z} = \frac{P_i\, a^2}{b^2 - a^2} \tag{4}$$

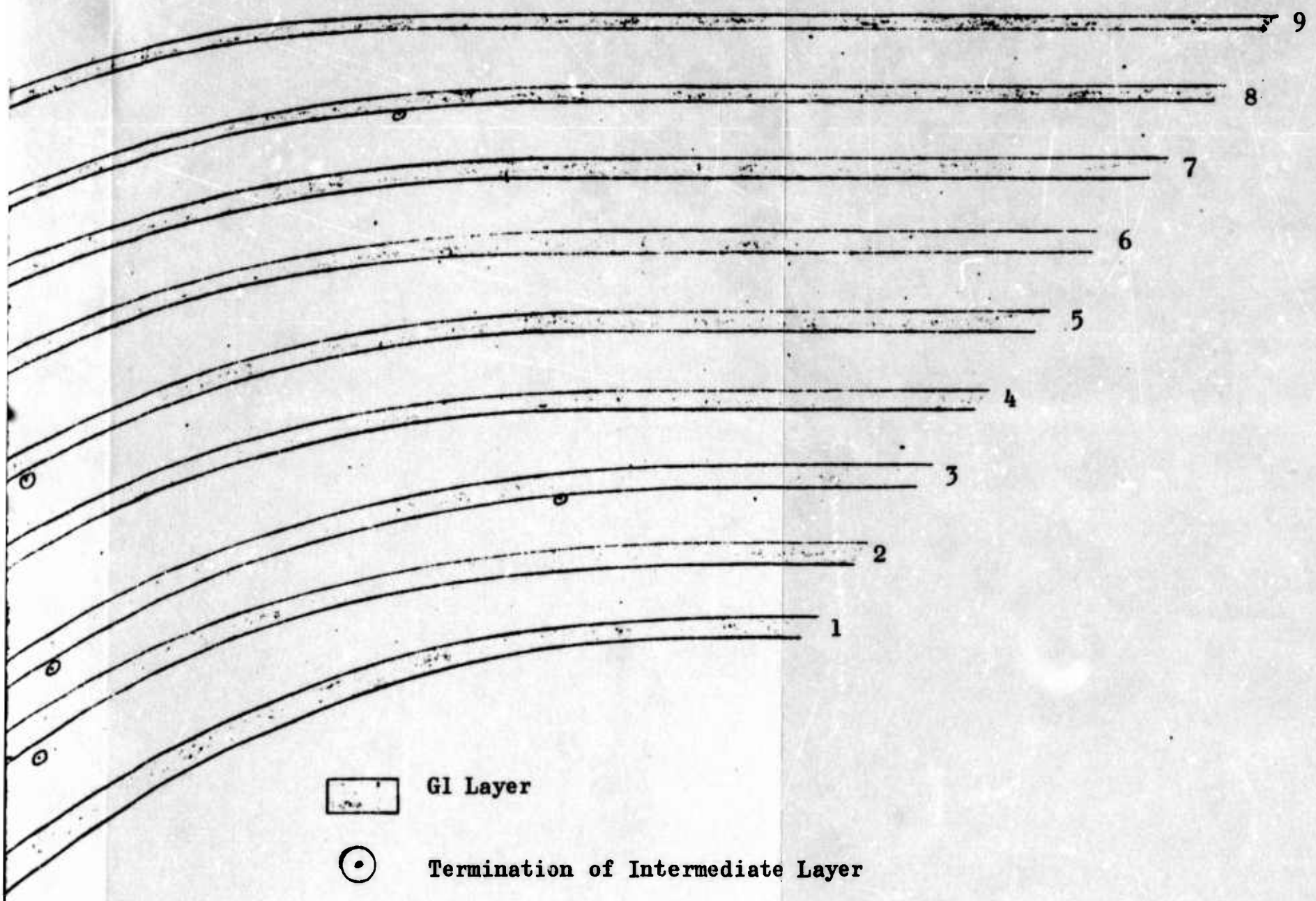
For a series of concentric thin cylinders, the maximum value of σ_{g_z} was given by the following:

$$\sigma_{g_z}\ (\max) = \frac{fw\ \bar{\sigma}_w}{t_{g_t}} \sum_{n=1}^{n=i} \cos^2 \alpha_n\ t_n \tag{5}$$

PREVIOUS PAGE WAS BLANK, THEREFORE WAS NOT FILMED



GI No.	Cylinder Radius, in.
1	11.000
2	11.466
3	11.942
4	12.416
5	12.891
6	13.367
7	13.827
8	14.287
9	14.725



GI No.	Cylinder Radius, in.	Thickness, in.	Helix Angle, deg
1	11.000	1.133	31.20
2	11.466	0.133	30.10
3	11.942	0.133	28.60
4	12.416	0.133	26.50
5	12.891	0.133	25.04
6	13.367	0.114	23.70
7	13.827	0.114	22.40
8	14.287	0.095	21.46
9	14.725	0.095	20.40

Figure 23. Motor A Layer Detail

CONFIDENTIAL

PREVIOUS PAGE WAS BLANK, THEREFORE WAS NOT FILMED

Near the polar bosses, only the 9 GI layers supported the longitudinal load and σ_{g_z} could be determined from the values of the material properties and winding geometry. After σ_{g_z} had been determined, the maximum value of P_i from Eq. 4 could be easily obtained. Maximum internal pressure, based on shear of the wires at the polar boss, was given by the following:

$$P_i \text{ (max)} = 2 \bar{\sigma}_{w_s} N_w \left(\frac{D_w}{D_b}\right)^2 \tag{6}$$

In the hoop or tangential direction, the stress was a maximum at the inside surface and was given by the following:

$$\sigma_{g_\theta} \text{ (max)} = \frac{P_i (b^2 + a^2)}{b^2 - a^2} \tag{7}$$

The maximum hoop stress which the RFG could withstand was given by the following equation:

$$\sigma_{g_\theta} = \frac{\bar{\sigma}_w f_w}{t_{g_t}} \sum_{n=1}^{n=i} \sin^2 \alpha_n \, t_n \tag{8}$$

In Eq. 8, every wrap angle must be included because every layer, whether GI or fill, contributed to the hoop strength. The value of σg_θ was determined from RFG geometry and material properties. Substituting this value into Eq. 7 gave the maximum internal pressure the RFG could withstand in the hoop direction. The number and thickness of the various layers were modified until the value of internal pressure from Eq. 4, 6, and 7 were approximately equal.

Modifications to the individual RFG layers was done with discretion because all internal layers affected the outside contour of the grain. This contour must be maintained near the design contour to make the most efficient use of the GFW case. Figure 108 shows the actual and design contour for the Motor A-1006 RFG.

SYMBOLS

DIMENSIONS

a = Inside radius of cylindrical portion of RFG, in.

b = Outside radius of cylindrical portion of RFG, in.

c = Radius of outside surface of the case, in.

e = Radius to the inside of the core grain web (Radius to base of core grain star point), in.

t_z = Thickness of helical wraps on case, in.

t_θ = Thickness of circumferential wraps on case, in.

t_c = Composite case thickness, in.

t_n = Thickness of nth layer of RFG, in.

t_{g_t} = Total grain thickness, in.

R, r = Radius, in.

R_o = Radius of polar dome opening, in.

D_b = Diameter of boss, in.

D_w = Diameter of wire, in.

α = Filament wound plastic case and wire wound grain helical wrap angle (Angle between the wrap direction and longitudinal centerline of motor, degrees)

α_n = Wrap angle of nth layer of RFG, degrees

N_w = Number of wires

LOADS AND SAFETY FACTOR

P_i = Internal pressure, psi

P_1 = Ultimate design maximum pressure. Equal to the initial maximum hot operating pressure (including an assumed deviation from nominal) multiplied by the appropriate safety factor, psi.

P_2 = Ultimate design pressure just prior to motor burnout. Equal to the maximum hot operating pressure just prior to burnout (including an assumed deviation from nominal) multiplied by the appropriate safety factor, psi.

F_z = Longitudinal load applied to a particular motor cross-section due to flight acceleration, lb

M_F = Moment applied to a particular motor cross-section due to flight or handling loads, in.-lb

S_F = Safety factor

S_{F_u} = Ultimate safety factor

Glass Filament Wound Case

μ_{c_θ} = Poisson's ratio in circumferential direction

E_{c_α} = Composite tensile modulus of case along the direction of the fiber, psi

E_{c_θ} = Composite circumferential tensile modulus of case, psi

E_{c_z} = Composite longiudinal compressive modulus of case, psi

C_{cr} = Critical buckling coefficient for axial compression loading

$\overline{\sigma}_{\alpha_\theta}$ = Allowable tensile strength of case along direction of filament for circumferential (near 90°) wound thickness, psi

$\overline{\sigma}_{\alpha_z}$ = Allowable tensile strength of case along direction of filament for longitudinal (low helical angle) wound thickness, psi

$\bar{\sigma}_{c_\theta}$ = Allowable composite circumferential strength, psi

$\bar{\sigma}_{c_z}$ = Allowable composite longitudinal strength, psi

$\bar{\sigma}_{cr}$ = Critical buckling stress for the case from any loading condition of interest based on the composite thickness of the case, psi

Wire Reinforced Grain

μ_{g_θ} = Poisson's ratio of RFG in circumferential direction

E_{g_θ} = Composite circumferential tensile modulus of RFG, psi

E_{g_z} = Composite longitudinal tensile or compressive modulus of RFG, psi

$\bar{\sigma}_{g_\theta}$ = Maximum tangential tensile stress allowable in composite RFG, psi

σ_{g_z} = Longitudinal grain stress, psi

$\bar{\epsilon}_{g_\theta}$ = Maximum tangential tensile strain allowable in composite RFG

f_w = Volume fraction of wire

$\bar{\sigma}_w$ = Allowable tensile stress of wire, psi

$\bar{\sigma}_{w_s}$ = Allowable shear stress of wire, psi

CALCULATIONS

P' = Pressure between case and RFG, psi

N_{z_T} = Total longitudinal tensile load in case from pressure, axial compression and bending, lb/in.

N_{θ_T} = Total circumferential tensile load in case from pressure, psi

σ_{c_θ} = Composite circumferential stress in case, psi

σ_{c_z} = Composite longitudinal tensile or compressive stress in case, psi

σ_{g_θ} = Maximum induced tensile stress in grain during pressurization (at inside radius in circumferential direction), psi

(3) Core Grain

While the core grain is not primarily a structural member, certain loads are imposed and the structural integrity influences the motors' ballistic performance. The imposed loads are due in part to motor cool-down after cure, thermal cycling, and ignition pressurization. The core-grain stress analysis serves to determine structural reliability under these loading conditions. Analysis of the core grain is limited to a two-dimensional axisymmetric configuration with elastic, isotropic material properties. Since the actual motor does not fit this description, certain assumptions about the geometry and mechanical properties are required.

The Motor A requirements do not include a temperature cycling capability, so thermal loading results only from motor cool-down after cure. In this section the motor geometries are described, and the methods and results of the analyses are presented. The analyses are discussed in terms of motor performance; conclusions about the analyses and motor design are drawn. A general description of the motor characteristics is presented. This is followed by the method of analysis, and is concluded by the calculated results.

(a) General Description

(C) Motor A is a five-pointed star configuration in the core grain with a wire-wound, RFG external to the core; the RFG is encased in a glass filament wound case. The first restriction on the analysis is that of a two-dimensional capability. This is accounted for by analyzing a grain cross-section assumed to be in plane strain. While plane strain can exist only in a grain of infinite length, the length of the reinforced grain motor makes it applicable and, in fact, slightly conservative.

The cross section analyzed is shown in Fig. 24. Since the exact solution for this stress-analysis method applies to a simple cylindrical grain, the star-point design was accounted for through the use of a stress-concentration factor. This involves an experimental determination of the factor by which local stresses are increased at the internal bore due to the addition of the star point. For the present analysis, the stress concentration factors were determined from the data presented by M. E. Fourney and R. R. Parmerter.(5) In addition, photoelastic tests on grain models were performed to verify these values.

(5) Fourney, M. E. and Parmerter, R. R.: Stress Concentration Data for Internally Perforated Star Grains, NOTS TP2728, NAVWEPS 7758, December 1961.

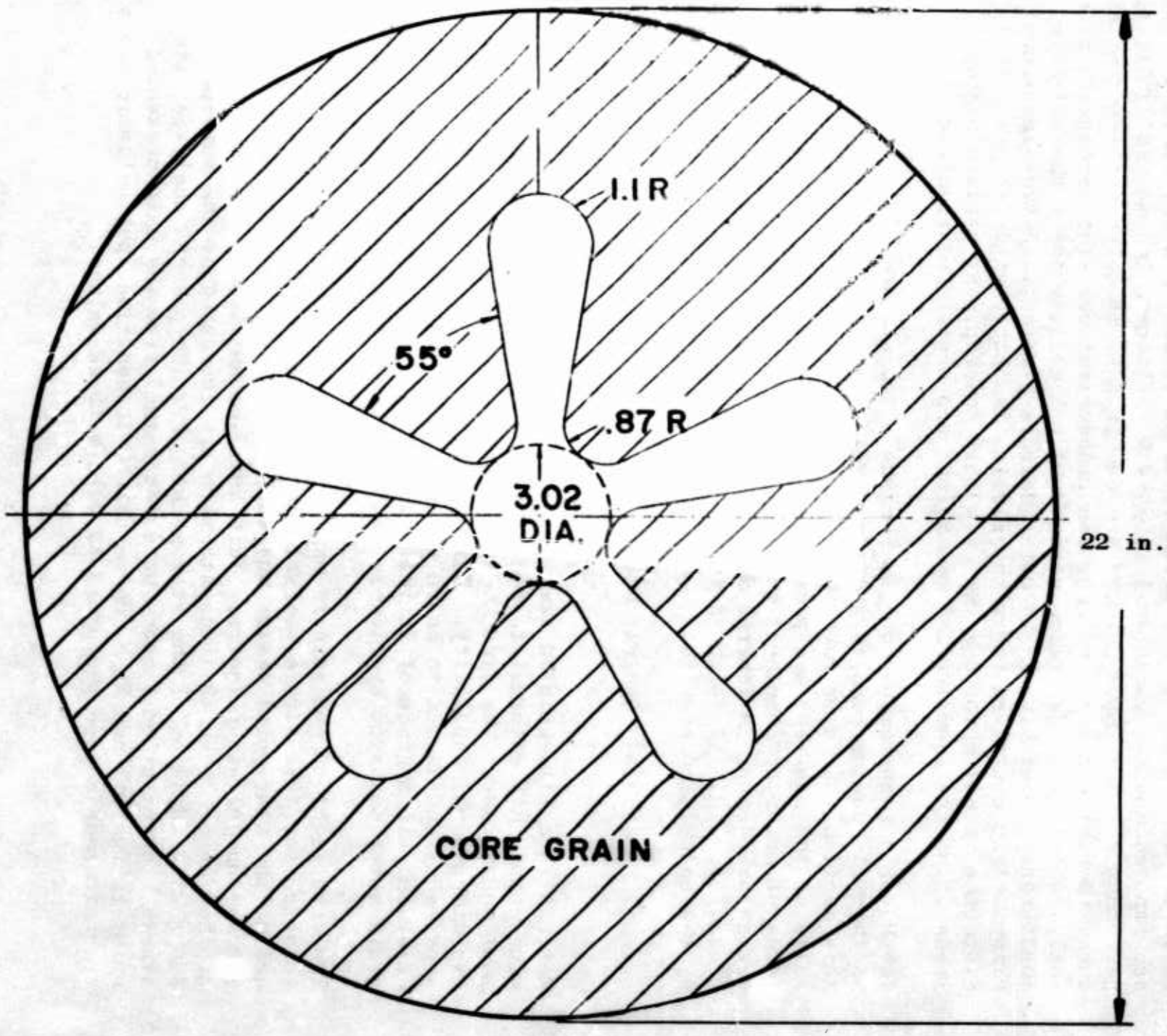


Figure 24. Motor A Core Grain Configuration

CONFIDENTIAL

The nature of solid propellant is such that the material properties are dependent on applied loadings. The existing stress solutions are for simple isotropic elastic materials. Therefore, the propellant is of necessity represented as an isotropic elastic material; the analysis is performed for a specified rate or strain over a narrow range of temperatures, with the effect of these several small changes being accumulated to give the result of the total temperature change.

The material properties are given in Fig. 25, plotted as function of reduced strain rate. The strain capabilities are displayed numerically with the calculated strains as a function of temperature for the strain rate (3×10^{-5} in./in./min) used in the thermal analysis.

(b) Method of Analysis

The equations used in the analysis of the grain cross sections are documented by J. D. Burton.(6) These were programmed into a high-speed digital computer to perform the analysis efficiently. The primary engineering effort involved making the necessary assumptions to utilize the analysis.

The following conditions are requisite to implementation of the analysis:

Plane strain
Homogeneous, isotropic, elastic material properties
Simple cylindrical configuration
For the thermal analysis, a single grain with a thin-walled case
No allowance for stress relaxation in the propellant

Quite obviously the actual motor does not satisfy these conditions. As mentioned before, the assumption of plane strain is applicable and conservative. The homogeneous, isotropic requirements are fairly easy for the core propellant but are not applicable for the reinforced grain even though the analysis required this assumption. The elastic property requirement is satisfied by analyzing the grain for small temperature increments, using the properties at the indicated strain rate and temperature representative of each increment. The resultant stresses and strains are summed over the entire range of analysis to give a fairly accurate representation of the viscoelastic propellant in an elastic analysis.

(6) Burton, J. D.: DDM 63-38, "Ignition Stress Analysis of Core Grain Motor A."

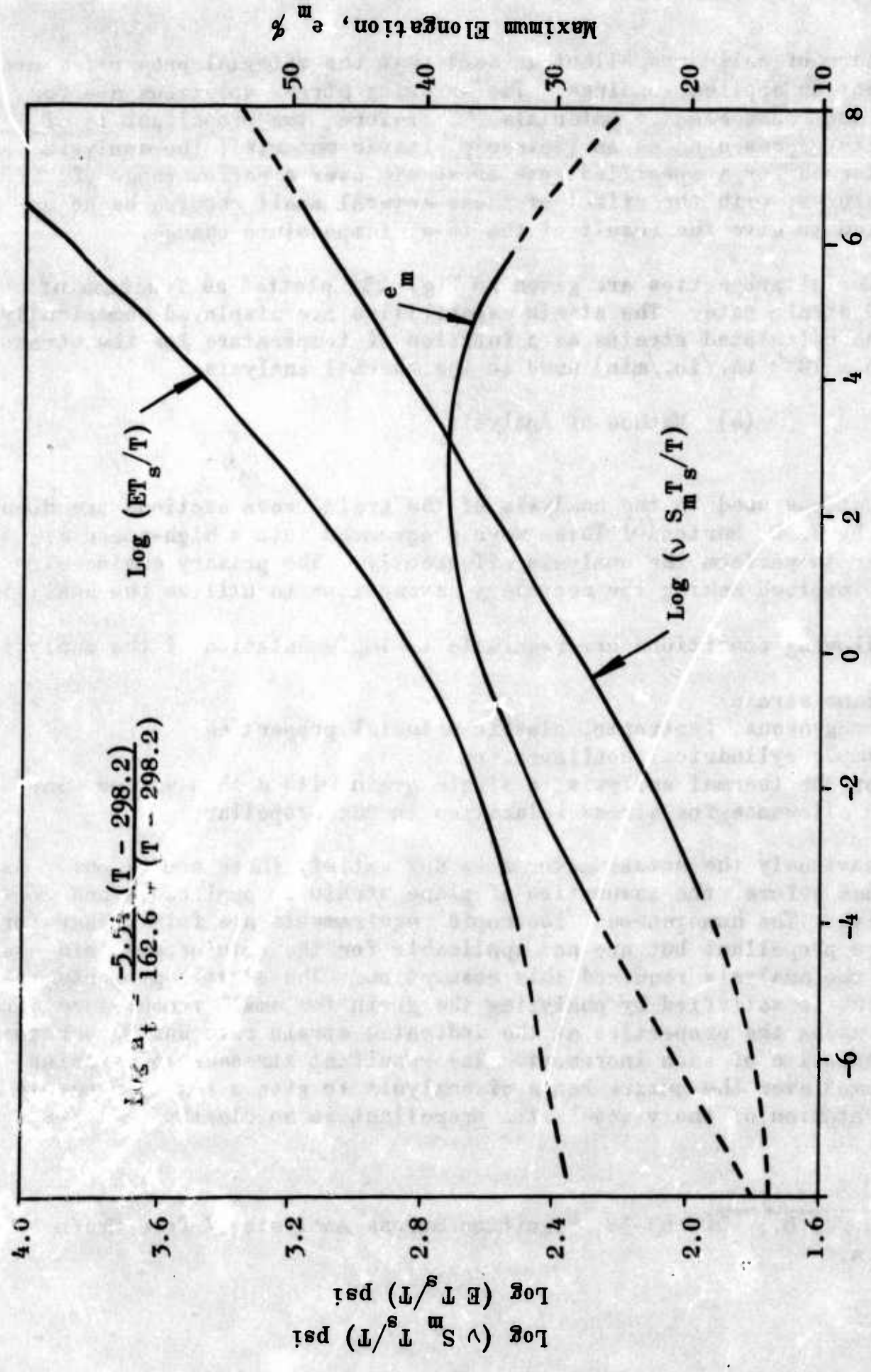


Figure 25. Propellant Spectrum, RDS-526

The simple cylindrical configuration is accounted for through the use of the stress concentration factor described previously. Thus, the analysis is made for a simple cylinder of the same web as the actual motor and the results are increased by an amount equal to this factor. For the thermal analysis, it was necessary to treat the part of the motor external to the core grain as a thin-walled case. The assumption was made that the reinforced grain would be the main load carrier during thermal cycling. Thus, the glass case was ignored in this part of the analysis. The pressurization analysis is slightly more generalized; the RFG and glass case were both included, though represented as homogeneous, isotropic elastic entities. The relaxation of stresses in the propellant with time were not accounted for, so strain was used as the criterion for failure. This is the generally accepted failure mode for internal bore loadings, e.g., pressurization or temperature cycling.

(c) Calculations

The calculated strains are presented in Table IX below.

TABLE IX

RESULTS OF IGNITION PRESSURIZATION STRESS ANALYSIS

FOR MOTOR A CORE GRAIN

Type of Loading	Calculated Strain, in./in.	Allowable Strain, in./in.	MOS, %
Pressurization	0.083	0.374	349
Thermal	0.037	0.259	601
Combined Loads	--	--	174

(C) Examination of these data reveals a 174% margin-of-safety for Motor A at 60 F.

c. Components

The remaining components that were developed for the motor are discussed next. The discussion is arranged as follows: polar boss, load rings, nozzle, igniter, and restrictors. Within each component discussion, the design and development of the individual component is presented.

(1) Polar Bosses

The forward and aft polar bosses are composite metal-plastic structures (see Fig. 26) fitted into the end openings of RFG motors.

These bosses are composite constructed components consisting of 6Al 4V titanium ring closures, silica phenolic internal insulators, and glass phenolic load ring supports.

The forward and aft titanium ring closures are utilized as the primary structural components in the polar boss assemblies. The components support the hoop tension loads and retain the load ring support structures. Additionally, the forward ring supports the igniter closure and the aft ring is used to retain the nozzle.

Internal insulator components are fabricated from MX-2646 silica phenolic molding compound. The insulator on the forward polar boss is used primarily as insulation for the titanium ring closure. Additionally, this insulator is designed to maintain a positive interlock with the igniter closure. The insulator on the aft polar boss provides the entrance and interface control for the nozzle, and also serves as the insulation for the aft titanium ring. This component also provides a sufficient area on which to cast the core grain.

The load ring supports are utilized as structural components in the design of the polar boss. These supports are used to position the load ring during grain winding and to react the longitudinal loads applied through the polar boss into the load rings during motor firing. In addition to the structural features indicated, this part functions as an external insulator for the titanium ring closures. The material for these components is MX-4600, a phenolic glass tape.

Prior to component testing, a requirement establishing a percentage of the total load for each load ring step was assumed as follows. Completion of the component tests indicated that each assumed load could be met or exceeded.

Load Ring	Load, %
1st	30
2nd	20
3rd	20
4th	20
5th	20
6th	12
7th	12
8th	12
9th	12

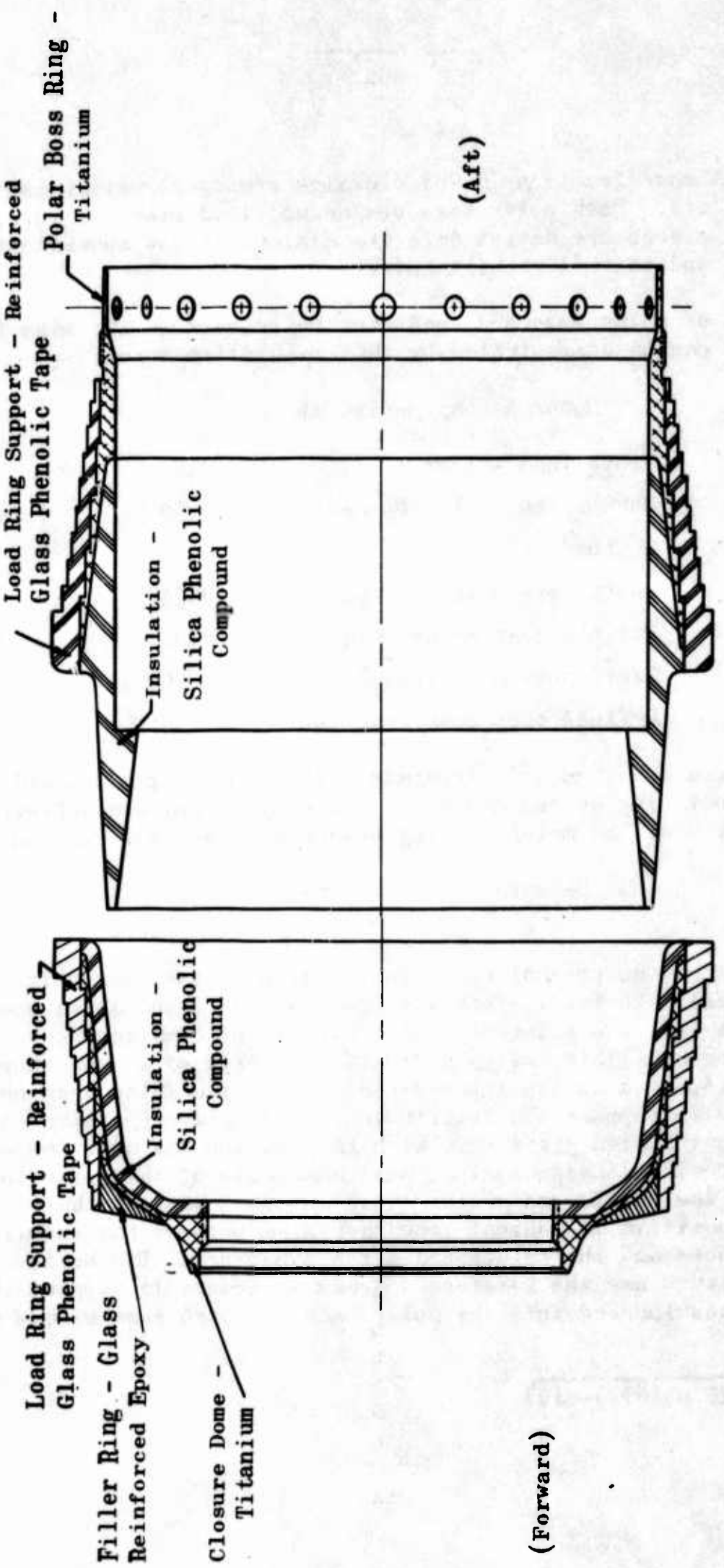


Figure 26. Forward and Aft Polar Bosses

(C) The Motor A mass fraction (0.96) dictates stringent weight control for all components. Each polar boss component, load ring, closure, and all insulation pieces are designed to the minimum weight consistent with structural and thermal requirements.

(C) The effect of polar boss and load ring refinement on the mass fraction of a motor can be demonstrated by the computation below:

Motor A Components, lb

Propellant weight	2483
Heavyweight polar bosses	55
Refined polar bosses	33
Heavy boss motor weight	2614
Refined boss motor weight	2592
Heavy boss mass fraction	0.951
Refined boss mass fraction	0.958

The significance, then, of performing stringent weight control in polar boss and load ring design can be observed by noting the difference in mass fraction of the motors having bosses of heavy and refined weights.

(a) Background

The concept of the present polar boss design evolved directly from the testing results in the 10-inch and 20-inch reinforced grain programs.(7) The initial use of a polar boss as a structural component was on the 20-inch program. This design depicted the usage of a cone-shaped structure, and depended on the tapered surfaces of the polar boss and the wound grain to support the longitudinal loading during motor operation. A 20-inch reinforced grain unit with this design was hydrotested and the results revealed longitudinal outward movements of the polar boss with respect to the reinforced grain. This movement was attributed to the lack of a positive mechanical locking system between the interfaces of the polar boss and the reinforced grain structure. The design solution for this was to use the reinforced grain structure to support the longitudinal loads induced into the polar boss, through some method which

(7) Contract AF 04(611)-8193

The so-called random oriented fibrous materials will normally have fibers oriented in one direction; that direction will be dependent upon the manufacturing processes. Most important in this process is the method of applying mold pressure.

The thermal properties are also especially important because aluminum load ring and RFG heating on the back side of the boss must be maintained at a low level. This requirement generally dictates the use of plastic materials rather than metallics. In addition, the inside melting and erosion must be maintained at a lower rate than provided by most metals.

A polar boss design with the initial load ring integral was attempted on the first 20-inch RFG polar boss and is depicted in Fig. 29 to illustrate the problems with molded plastic polar bosses.

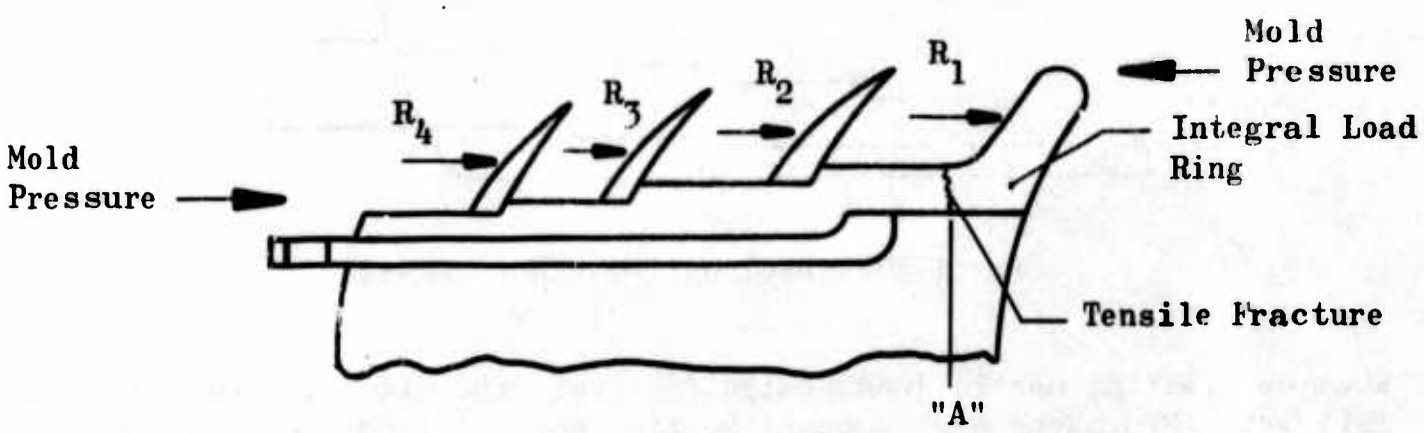


Figure 29. Polar Boss Design with Integral Load Ring

The mold pressure was applied as shown per Fig. 29 causing a fiber orientation normal to the mold pressure direction, or essentially in the hoop (circumferential) direction. The integral load ring had the rotaticnal strength necessary to support the R_1 load, but the tension strength across Plane "A" was less than required to support R_1 load. Fracture occurred at Plane "A" under a load considerably less than required.

Subsequent polar bosses were fabricated from a crossplied glass cloth, to be assured that tension strength in the longitudinal direction was adequate. The flange could not be integrally fabricated using a cloth wrap technique; thus, a ring seating surface was fabricated for an additional ring to be installed at the location, as shown in Fig. 30.

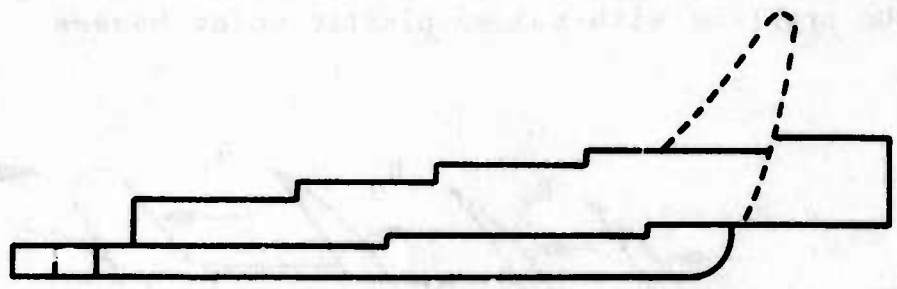


Figure 30. Revised Polar Boss Design

When considering nozzle load design features, the aft polar boss on each full scale RFG motor must support nozzle inertial loads, and in some cases, vectoring loads. This requirement effects the following design areas:

Vectoring Loads. The moments produced by nozzle inertial and vectoring loads caused increased polar boss loads and stresses. These are superimposed forces. Since nozzle moment loading produces compression on one side of the boss assembly and tension on the other side. These compression and tension stresses are in addition to those stresses caused by chamber pressure loading.

Rotational Stiffness ans Sealing. The moment loading, imposed by the nozzle assembly causes rotational deflection and creates difficulty with some sealing methods. One of the prime advantages of the polar boss is in its ability to support rotational

The so-called random oriented fibrous materials will normally have fibers oriented in one direction; that direction will be dependent upon the manufacturing processes. Most important in this process is the method of applying mold pressure.

The thermal properties are also especially important because aluminum load ring and RFG heating on the back side of the boss must be maintained at a low level. This requirement generally dictates the use of plastic materials rather than metallics. In addition, the inside melting and erosion must be maintained at a lower rate than provided by most metals.

A polar boss design with the initial load ring integral was attempted on the first 20-inch RFG polar boss and is depicted in Fig. 29 to illustrate the problems with molded plastic polar bosses.

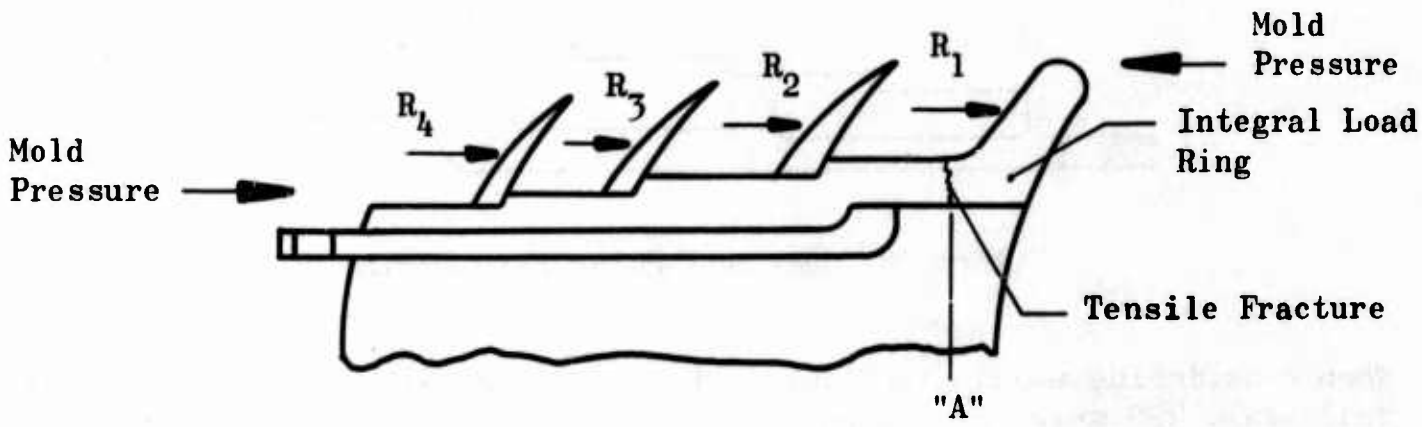


Figure 29. Polar Boss Design with Integral Load Ring

The mold pressure was applied as shown per Fig. 29 causing a fiber orientation normal to the mold pressure direction, or essentially in the hoop (circumferential) direction. The integral load ring had the rotational strength necessary to support the R_1 load, but the tension strength across Plane "A" was less than required to support R_1 load. Fracture occurred at Plane "A" under a load considerably less than required.

Subsequent polar bosses were fabricated from a crossplied glass cloth, to be assured that tension strength in the longitudinal direction was adequate. The flange could not be integrally fabricated using a cloth wrap technique; thus, a ring seating surface was fabricated for an additional ring to be installed at the location, as shown in Fig. 30.

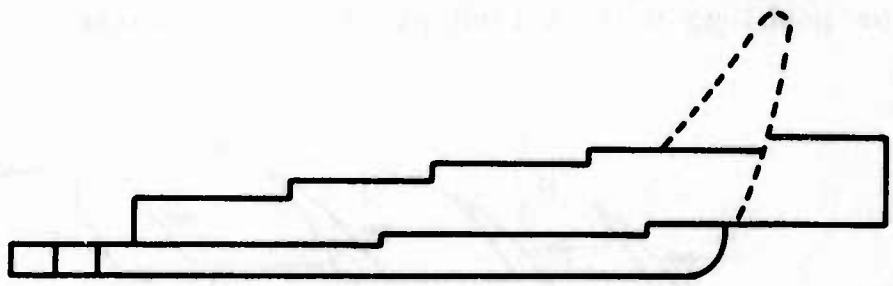


Figure 30. Revised Polar Boss Design

When considering nozzle load design features, the aft polar boss on each full scale RFG motor must support nozzle inertial loads, and in some cases, vectoring loads. This requirement effects the following design areas:

Vectoring Loads. The moments produced by nozzle inertial and vectoring loads caused increased polar boss loads and stresses. These are superimposed forces. Since nozzle moment loading produces compression on one side of the boss assembly and tension on the other side. These compression and tension stresses are in addition to those stresses caused by chamber pressure loading.

Rotational Stiffness ans Sealing. The moment loading, imposed by the nozzle assembly causes rotational deflection and creates difficulty with some sealing methods. One of the prime advantages of the polar boss is in its ability to support rotational

loads with small rotational deflections. It must be realized, though, that the boss assembly deteriorates during motor burning; the rotational strength diminishes until finally, at burnout, the rotational support is afforded only by the glass case attachment.

(c) Composite Plastic Evaluation

Since the initial evaluation indicated that a composite metallic and plastic boss would be required and that the plastic would be required as a thermal protection and a load carrying member, Rocketdyne proceeded to evaluate candidate plastic materials. The area of composite plastic components presents several problems, as outlined below:

Random Fiber Orientation. The "random" fiber orientation is something of a misnomer; any fabricated component is characterized by a particular orientation of fibers. This orientation depends primarily upon the pressure used in fabricating the component and the method and direction of applying the pressure.

Machining of Polar Assemblies. The machining of component assemblies which are fabricated from various plastic and metal materials can be a significant problem. The optimum machine speed and feed may vary considerably for the different materials, and a plan is required which will compromise but not cause damage to any of the materials.

Thermal Treatment Problems. The thermal expansion characteristics of different materials in the make-up of a polar boss assembly may vary significantly. There can, therefore, be problems of unbonding, delamination, and/or fracture of materials during thermal curing processes if the design does not allow for the associated shrinkage and expansion.

Test Coupon Fabrication. The technique for fabricating plastic test coupons must be carefully worked out for each component design. Experience has demonstrated significant problems in fabricating test coupons which accurately represent the structural quality of the component part. Generally, the molding pressure, method of applying pressure, geometry, and curing cycles must be equivalent for test coupons and components if coupon test results are to be meaningful.

⊙ Coupon Tests

A series of coupon tests was performed to define structural capabilities of boss component parts fabricated from various high-strength glass-impregnated phenolic resins.

Each of the materials tested having fill yarns parallel to the part centerline was wrapped on the mandrel, held between centers of a lathe, and heated to a maximum of 170 F. During the wrapping cycle, a roller was used to apply pressure, ensuring a live load sufficient to prevent any wrinkling or wadding of the material. After the part was wrapped, it was then rubber-bagged and placed into a hydroclave and allowed to cure at 325 F for 3 hours under a pressure of 750 psi. After the part was cured, it was lightly sandblasted to facilitate the removal of volatiles during postcure. The part was postcured for 16 $\pm$ 1 hour at 300 $\pm$ 25 F.

Tensile, compressive, and interlaminar shear tests were performed by the fabricator and the Rocketdyne Engineering Test Facility. The specimen tests performed by the fabricator were in accordance with Federal Test Method Standard No. L-P-406. The specimens which were tested by Rocketdyne were removed from a component blank part. Data derived from these tests were then used to determine design features for polar bosses used in the reinforced grain program.

The structural plastic materials which were considered and tested for polar bosses are as follows:

Fiberite MX-4600 with 181-E Glass. This material is a product of the Fiberite Corp. (a Division of Universal Manufacturing Co.). The fabric used in this product is Style 181, Type E glass, which has 57 yarns in the weave direction and 52 yarns in the fill direction. The resin used is a high temperature, modified, polymide, phenolic resin. The properties of the uncured materials have resin content of 17--22% and volatile content of 2--5%.

Fiberite MX-4600 with 181-S Glass. This material is not a catalogued item with the Fiberite Corp. The basic difference between this material and the MX-4600 is the 181, Type S glass. The Type S glass fabric has the same number of yarns in the weave and fill direction as Type E, but is processed in a different manner. The uncured properties of this material have the same values as those of MX-4600.

Conalon 506. This is a product of the NARMCO Resin and Coating Co., and is a modified high temperature phenolic resin impregnated on 181 Type E glass fabric. The properties of the uncured material are resin content of 33--37% (by weight), and volatile content of 6--8%.

Scotchply 1400. This material is a product of Minnesota Mining and Manufacturing Co. The Scotchply 1400 is a preimpregnated tape made from a high temperature phenolic resin reinforced with continuous nonwoven E glass filaments. The properties of this uncured material are resin content of 32--38% (by weight), and volatile content 3.5--5%.

The tensile specimens for which the fabricator reported tensile properties were in accordance with Federal Test Method Standard No. L-P-406, Method 1011. The parts were cured and postcured in the same manner as discussed above. Following the cure cycle, the parts were machined to the configuration shown in Fig. 31. The part was then tested to failure. The tensile properties reported by the fabricator for the various materials are as shown in Table X.

The compressive specimens (per L-P-401, Method 1021) tested by the fabricator were tested parallel to the plane of the fabric, as shown in Fig. 32. The compressive specimen was cured and postcured in the same manner as mentioned in the fabrication method. Upon completion of the cure cycle, the ends of this specimen were machined parallel to each other and perpendicular to the adjacent faces. It was then placed into the compressive jig and tested to failure. The results which the fabricator reported for this specimen are as listed in Table XI.

The method the fabricator employed for the interlaminar shear test, per L-P-406, Method 1042, was a side-supporting steel plate to inhibit peel effects and cause a bond failure between piles of the glass reinforcement. This specimen was cured and postcured in the same manner as described in the fabrication method. Upon completion of the cure cycle, two parallel cuts, one on each opposite face of the specimen and 0.50 inch apart were made across the width of the specimen. The incisions were of sufficient depth to sever the center lamina located mid-way between the two faces of the specimen. See Fig. 33 for specimen configuration.

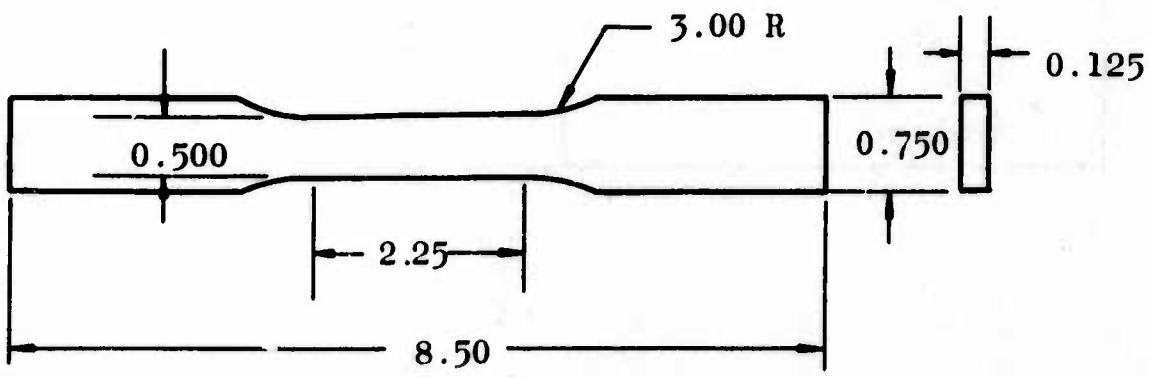


Figure 31. Tensile Test Specimen

TABLE X

TENSILE PROPERTIES, FTMS L-P-406

Material	Specimen	Tensile Strength, psi
Fiberite MX4600 with 181-E Glass	1	50,754
	2	45,903
	3	42,885
	4	46,667
	5	46,885
	6	45,246
Average		46,390
Fiberite MX4600 with 181-S Glass	1	65,574
	2	71,721
	3	77,500
Average		72,265
Conalon 506	1	21,774
	2	26,230
	3	21,311
Average		23,105
Scotchply 1400	1	29,851
	2	28,358
	3	29,104
Average		29,104

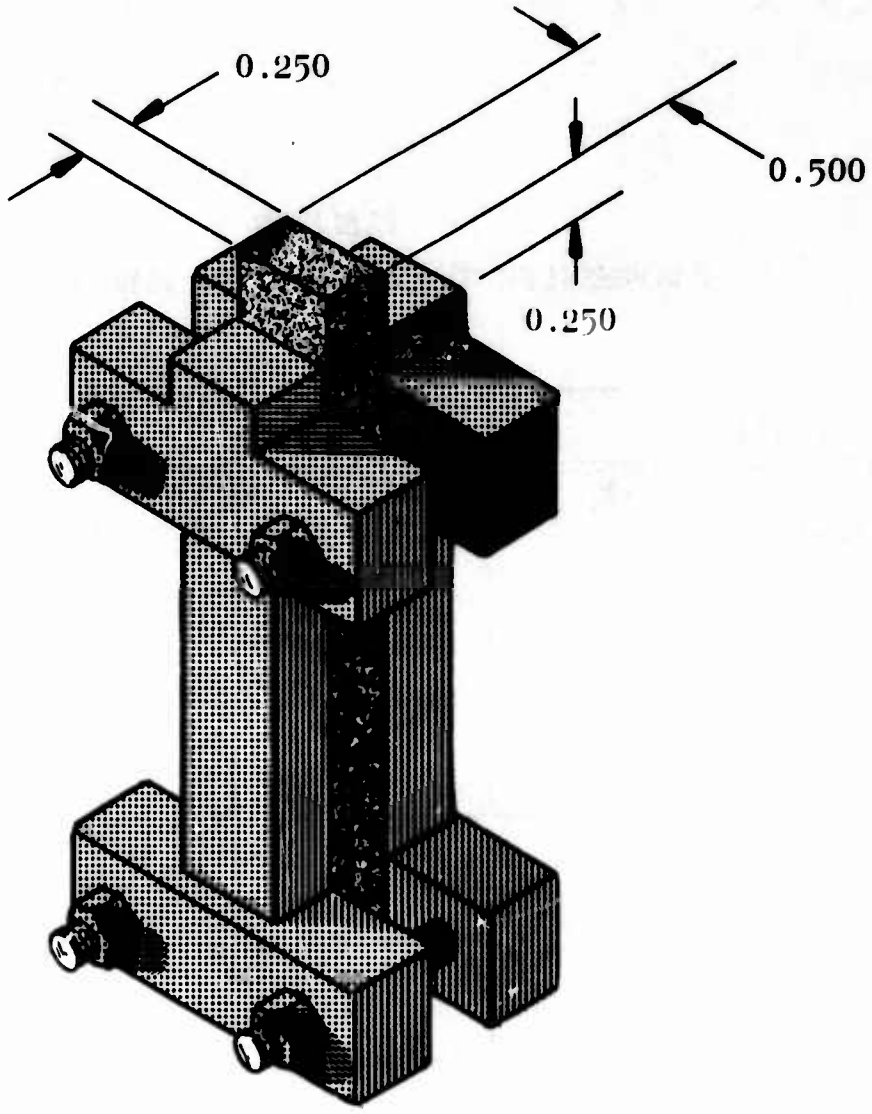


Figure 32. Compressive Test Specimen and Fixture

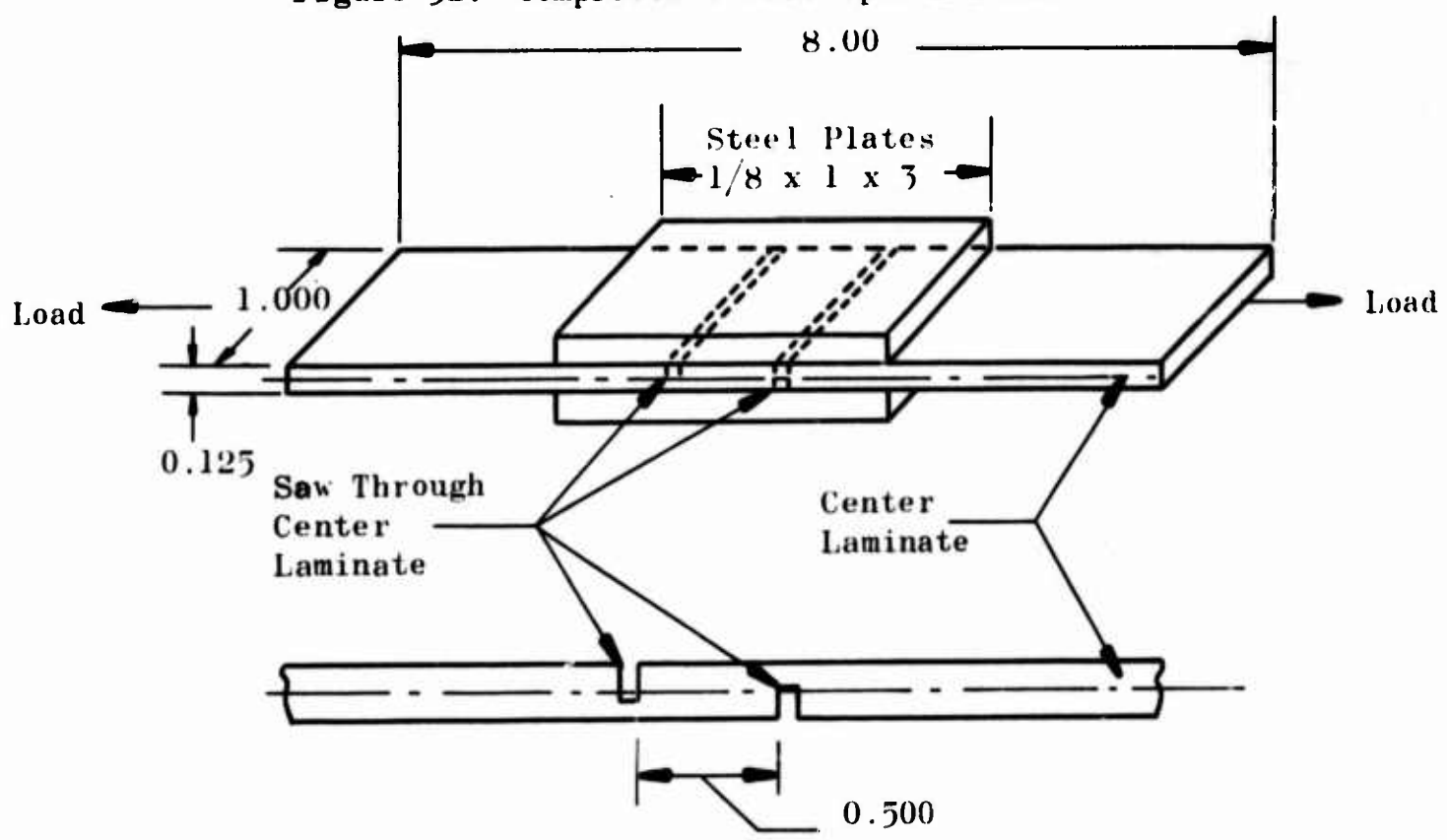


Figure 33. Interlaminar Shear Specimen

TABLE XI

COMPRESSIVE PROPERTIES, PER FTMS L-P-406

Material	Specimen	Tensile Strength, psi
Fiberite MX 4600 with 181-E Glass	1	59,231
	2	68,077
	3	55,385
	4	74,074
	5	72,685
	6	65,278
Average		65,788
Fiberite MX 4600 with 181-S Glass	1	36,538
	2	39,313
	3	41,221
Average		39,024
Conalon 506	1	42,929
	2	39,899
	3	45,500
Average		42,776
Scotchply 1400	1	37,984
	2	48,450
	3	39,922
Average		42,118

The side supporting steel plates were held snugly against the faces of the specimen by means of two small "C" clamps located 2.50 inches centerline to centerline and fastened with the steel plates; the specimen was then tested until the rupture occurred. The interlaminar shear values reported by the fabricator are as listed in Table XII.

TABLE XII

INTERLAMINAR SHEAR PROPERTIES, FTMS L-P-406

Material	Specimen	Interlaminar Shear, psi
Fiberite MX4600 with 181-E Glass	1	6,774
	2	5,645
	3	4,878
	4	3,724
	5	3,802
	6	3,858
Average		4,780
Fiberite MX4600 with 181-S Glass	1	3,805
	2	3,008
	3	3,532
Average		3,448
Conalon 506	1	3,455
	2	3,659
	3	4,605
Average		3,906
Scotchply 1400	1	4,198
	2	4,038
	3	3,409
Average		3,881

- Full-Scale Component Specimen Test

To further evaluate the candidate materials and to eliminate the variable of test specimen fabrication technique, Rocketdyne designed component specimens tests (specimens were obtained from full-scale blank billets).

Destructive tests were performed on tensile, compressive, and interlaminar shear specimens on all the materials previously mentioned except Conalon E-506. Because the values reported by the fabricator were considerably lower on this material than on the three other materials tested, it was agreed that this material should be eliminated as a possible candidate for fabrication of polar bosses.

The tensile specimens (see Fig. 34) were segments removed from a ring of reinforced glass 11.50 OD x 9.00 ID x 5.75 long. The results of the tensile tests are as shown in Table XIII.

The interlaminar shear specimens, Fig. 34, were "hat" shaped sections removed from a reinforced glass ring. These specimens were placed between two flat platens and loaded until failure occurred. Results of these tests are presented in Table XIV.

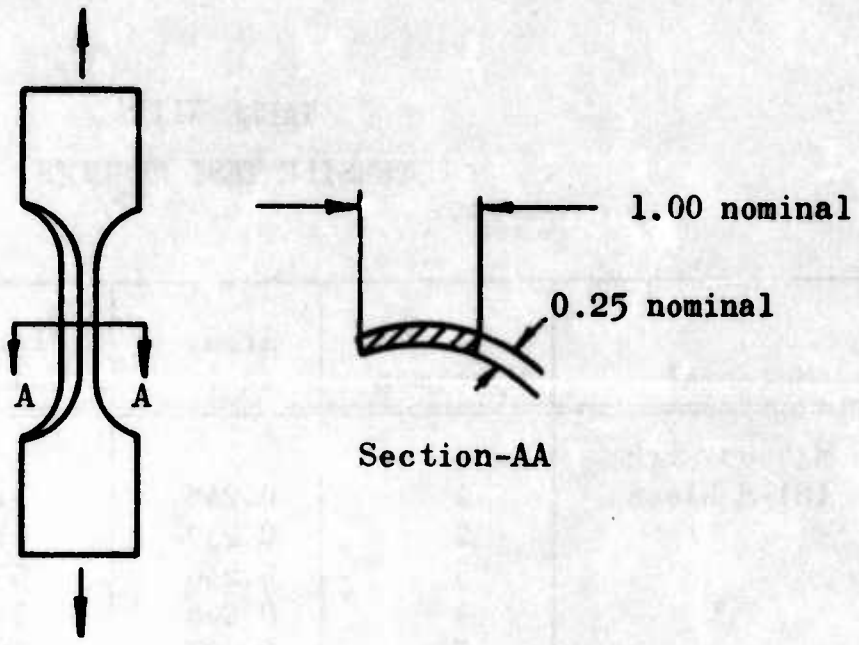
The compressive specimens, Fig. 34, were "T" shaped segments removed from a reinforced glass ring. These specimens were placed between two flat platens and loaded until failure occurred. Results of these tests are presented in Table XV.

- Polar Boss Bench Test

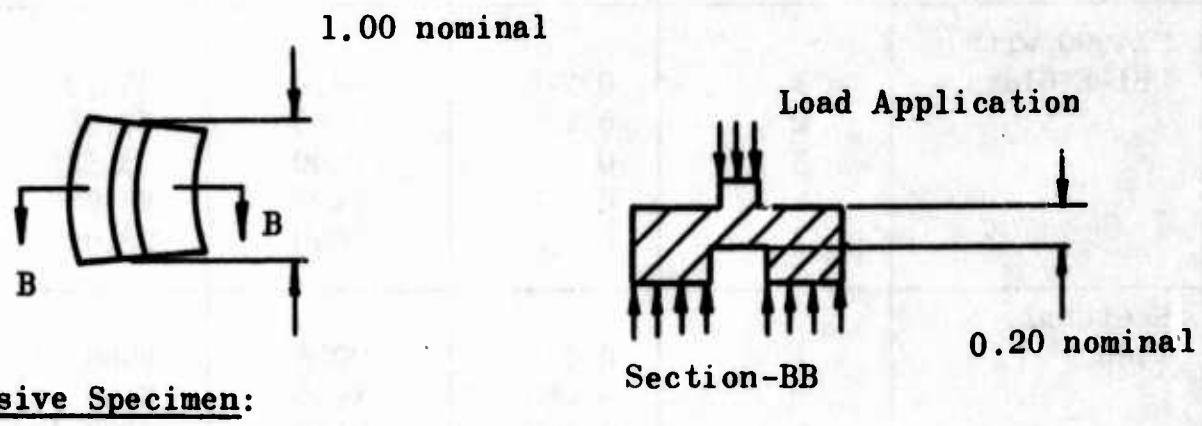
The results of the previous tests indicated that MX-4600 with E glass would be the superior material. The remaining two tests, polar boss static load test and hydrotest, were the final test requirements to assure design requirements could be attained.

The forward and aft polar bosses, using MX-4600 as the structural plastic component, were static load tested at four load ring locations (see Fig. 35). At each of the ring locations, the boss was loaded to the design load requirement and if no failure occurred it was further loaded until failure occurred. The results and mode of failure are tabulated in Table XVI. Results indicated that the design requirements were exceeded on each polar boss step.

Tensile Specimen:



Shear Specimen:



Compressive Specimen:

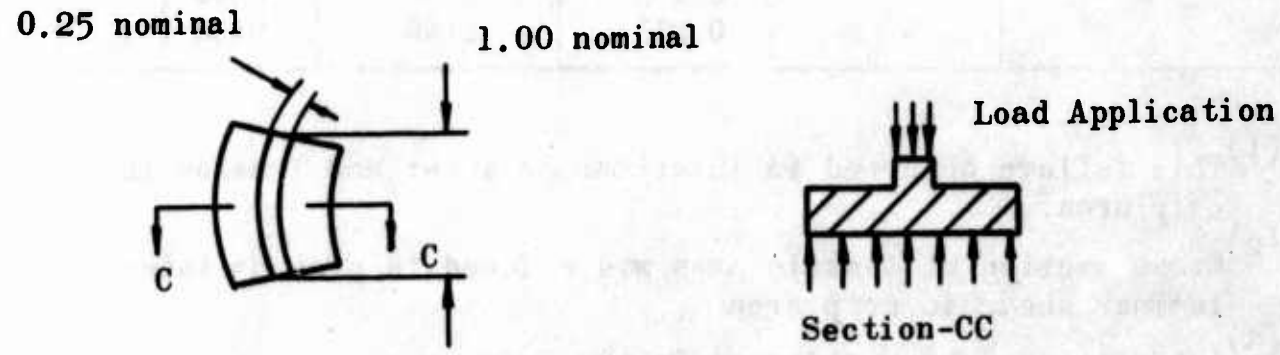


Figure 34. Polar Boss Tensile, Shear, and Compression Tests

TABLE XIII

TENSILE TEST RESULTS

Material	Specimen	Area, sq in.	Ultimate Load, lb	Tensile Strength, psi
MX4600 with 181-S Glass	1	0.245	7100	29,000
	2	0.250	6100	24,100 (1)
	3	0.246	5750	23,300 (1)
	4	0.246	5150	21,000 (1)
	5	0.123	3600	29,200 (2)
	6	0.123	3925	32,000 (2)
	7	0.122	3825	30,700 (2)
	8	0.245	6320	25,796 (1)
	9	0.242	5210	21,529 (1)
MX4600 with 181-E Glass	1	0.246	8970	35,702
	2	0.257	9590	37,242
	3	0.255	7290	28,588
	4	0.256	7420	28,984
	5	0.257	7440	28,949
Scotchply 1400	1	0.248	2000	8060 (3)
	2	0.250	1440	5750 (3)
	3	0.253	2150	8500 (3)
	4	0.253	2140	8450 (3)

(1) This failure occurred in interlaminar shear and tension in grip area.

(2) Cross section of tensile area was reduced to prevent interlaminar shear in grip area

(3) Interlaminar shear occurred in the grip area.

TABLE XIV

INTERLAMINAR SHEAR TEST RESULTS

Material	Specimen	Area, sq in.	Ultimate Load, lb	Shear Strength, psi
MX4660 with 181-S Glass	1	0.415	1700	4096
	2	0.417	1720	4124
	3	0.418	2500	5980
	4	0.418	1240	2966
	5	0.416	1540	3701
MX4600 with 181-E Glass	1	0.388	1315	3389
	2	0.393	1380	3511
	3	0.297	1590	4007
	4	0.400	2158	5395
	5	0.400	1924	4810
Scotchply 1400	1	0.416	80	192
	2	0.418	115	275
	3	0.415	415	493
	4	0.417	(1)	
	5	0.418	(1)	

(1) Specimen failed when initial load was applied

TABLE XV

COMPRESSIVE TEST RESULTS

Material	Specimen	Area, sq in.	Ultimate Load, lb	Compressive Strength, psi
MX4600 w/181 S Glass	1	0.258	8,400	32,945
	2	0.264	9,420	35,681
	3	0.258	9,520	36,900
	4	0.259	10,240	39,536
	5	0.260	10,240	39,384
MX4600 w/181 E Glass	1	0.251	8,134	32,406
	2	0.252	12,088	47,968
	3	0.249	10,597	42,544
	4	0.250	12,288	49,152
	5	0.250	10,294	41,176
Scotchply 1400	1	0.266	4,440	16,691
	2	0.264	5,220	19,772
	3	0.270	4,300	15,925
	4	0.264	5,000	18,940
	5	0.266	4,240	15,940

CONFIDENTIAL

TABLE XVI

STATIC LOAD TEST RESULTS ON MOTOR A
POLAR BOSSES AND LOAD RINGS

Part No.	Design Requirement		Test Results		Margin of Safety	Mode of Failure
	Applied Load, lb	Equivalent Pressure, psi	Applied Load, lb	Equivalent Pressure, psi		
Fwd Polar Boss (802378)						
Ring (802365)	10,500	140	22,700	278	0.98	Load ring failed
Ring (802367)	10.500	140	22,400	274	0.96	Load ring failed
Ring (802371)	19,185	234	59,700	730	2.11(1)	Boss failed in bearing
Ring (802357)	28,788	351	55,000	673	0.91	Boss failed in inter-laminar shear
Aft Polar Boss (802376)						
Ring (802365)	8,500	140	20,800	254	0.82	Load ring failed
Ring (802367)	8,500	140	20,700	253	0.82	Load ring failed
Ring (802371)	14,297	234	65,700	804	2.43(1)	Boss failed in bearing
Ring (802357)	21,446	351	75,101	919	1.62+	Load cell capacity not large enough to carry ring or boss to failure

(1) Margin of safety determined for ring at polar boss failure load

CONFIDENTIAL

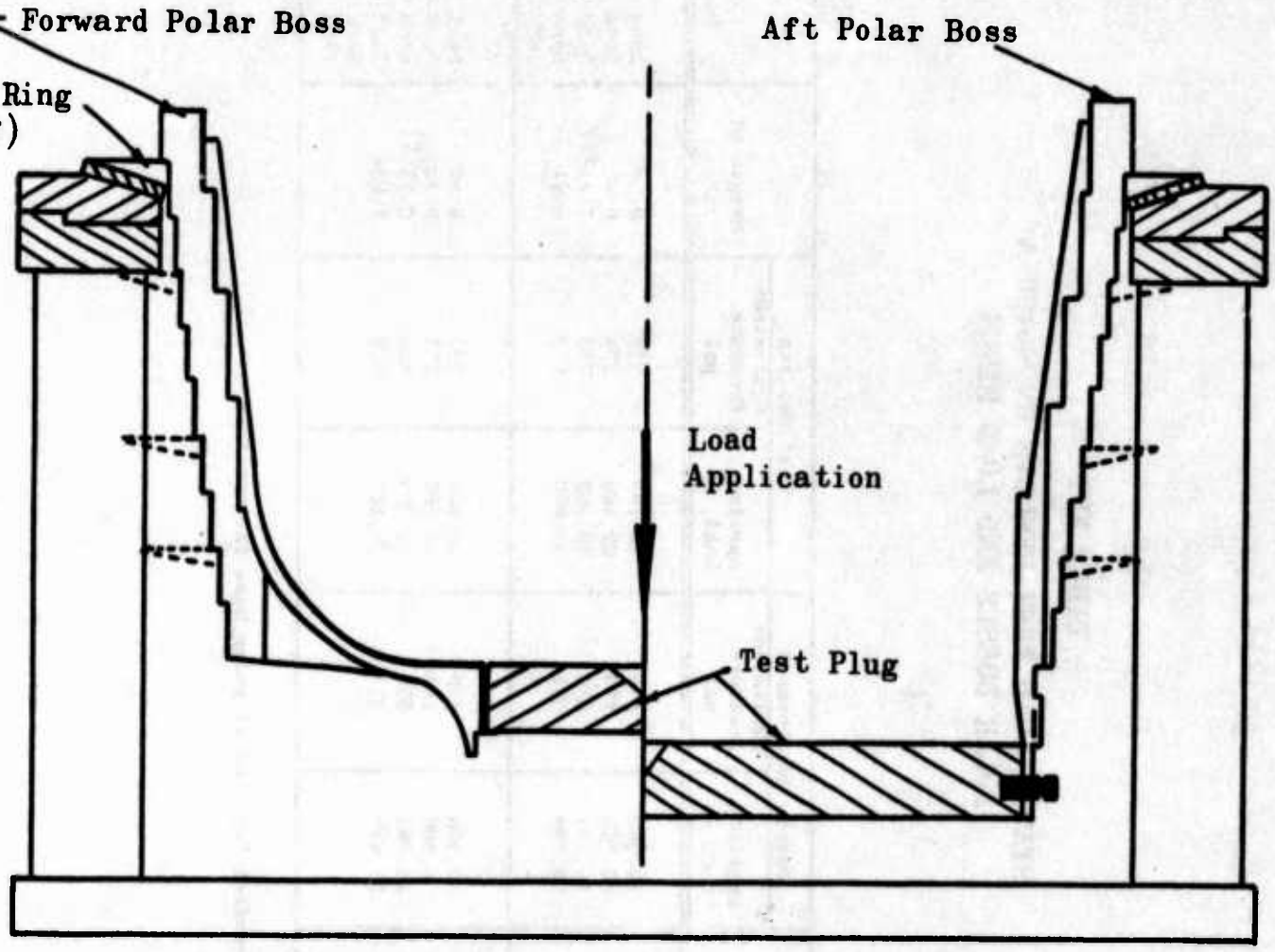


Figure 35. Polar Boss Static Load Test

The forward and aft polar bosses, using MX-4600 E glass, as the structural plastic component for load ring support, assembled with their respective test components (see Fig. 36), simulated a conventional pressure vessel. These test components were designed to withstand approximately 5 times the ultimate design load, ensuring a polar boss failure.

(C) The forward Motor A polar boss was hydrotested to a pressure of 1525 psi before failure occurred. The failure occurred when the titanium dome expanded in the hoop direction, causing a hoop failure in the plastic component which propagated down the longitudinal axis, resulting in an interlaminar shear failure. The wall thickness of the titanium dome was 0.030 under the required design thickness, because of a machining error. However, it was felt that the part would still have the capability of meeting the ultimate design pressure. Compared to the design pressure of 1170 psi, the fail pressure of 1525 psi indicates a margin of safety of 0.3 for the forward boss, where the margin of safety is defined as:

$$\left[\frac{\text{allowable pressure}}{\text{design pressure}} - 1\right] 100 = \text{MOS}$$

$$\left[\frac{1525}{1170} - 1\right] 100 = 0.3$$

(C) The aft Motor A polar boss was hydrotested to a pressure of 2187 psi. At this pressure the closure retainer pins failed in shear and the pressure dropped. Comparing this pressure to the design pressure of 1170 psi, the fail pressure of 2187 psi indicated a margin of safety of 0.87 for the aft polar boss.

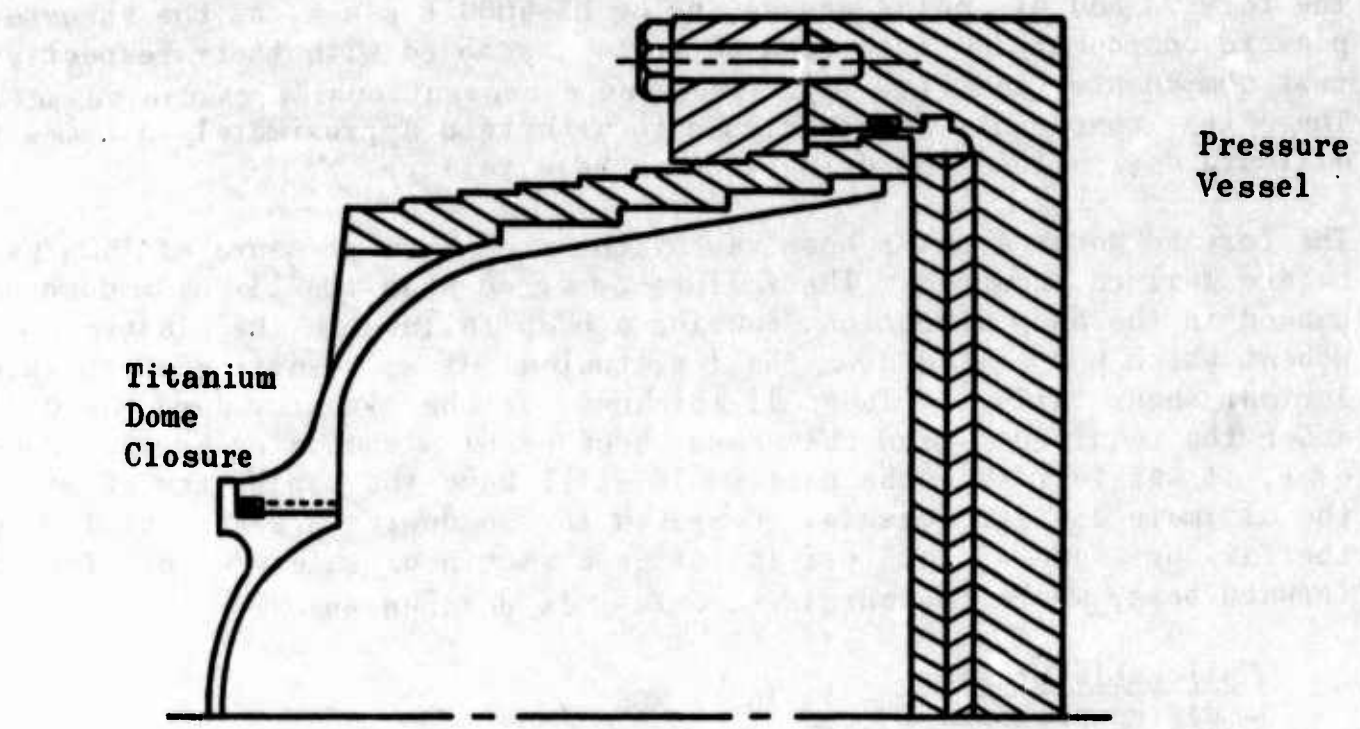


Figure 36. Polar Boss Hydrotest

(d) Insulation

The material used for interior insulation of the polar boss assemblies of Motor A was a phenolic/silica fabric molding compound, MX-2646, supplied by the Fiberite Corp., Winona, Minnesota. Table XVII contains a listing of some of the more pertinent physical and mechanical properties of this material. The insulation components were compression molded in billet form, postcured and then machined to drawing dimensions. Initially, only minor processing and machining problems were encountered with this component. As the program progressed, two problems related to the material became apparent. The first difficulty was shrinkage of the MX-2646 component during motor cure operations. The shrinkage caused stresses between the insulator and titanium structure of the boss assembly that resulted in unbond. In an effort to correct this condition, postcure duration was extended from 16 hours at 300 F to 72 hours at 350 F. Although dimensional stability was improved, a second problem, thermal cracking during postcure, was encounted. Investigation revealed that circumferential cracks were initiating in the unreinforced resin matrix that exists between the highly oriented reinforcement material. Inasmuch as existing tooling and processes could not effectively provide random reinforcement orientation, it was decided to attempt to eliminate the cracking tendency by reducing the thermal shock experienced by the material during postcure. A stepwise postcure was initiated as one means of coping with the crack problem. In addition, the cross section of the part was reduced to a practical minimum prior to postcure, to lower the thermal gradient. The effectiveness of these measures was still in the process of being verified at the time the program was halted.

To provide accurate thermal coefficient of expansion data for design analysis purposes, tests were conducted on two MX-2646 billets molded by different suppliers. The results of these tests are contained in Tables XVIII and XIX. Eventually the material supplied by Lone Star was selected because of their ability to remove the billet from the mold and place it in postcure without cooling the billet down from the cure temperature.

The bonding capability of MX-2646 to the core propellant (RDS-526) was verified by a series of tests. Results of these tests are contained in Table XX. Since phenolic resins are known to produce reaction products at elevated temperatures that are detrimental to solid propellants, suitable cure and postcure cycles were developed. Propellant physical properties were not affected significantly during 4 weeks of aging at 170 F with MX-2646 that had been postcured a minimum of 48 hours at 300 F.

TABLE XVII

PHYSICAL AND MECHANICAL PROPERTIES
MX-2646 MOLDING COMPOUND

Specific gravity, ±0.02		1.79
Compressive strength, psi		36,000
Flexural strength, psi		20,000
Tensile strength, psi		13,000
Izod impact ft lb/in. notch (side)		2.0
Modulus in flexure, 10^6 psi		2.5
Shear strength, psi		13,000
Thermal conductivity	@ 300 F	2.40
BTU/hr (ft^2) (deg F/ft)	@ 500 F	2.15
Specific heat @ 150 F		0.24
Barcol hardness		68-72
Molded shrinkage, linear, in./in.		0.0007
Linear thermal expansion (80 to 500 F) x 10^{-6}	Normal	5.1
in./in./deg F	Parallel	4.9

TABLE XVIII

CALCULATED LINEAR COEFFICIENTS OF EXPANSION FOR MX-2646*

Inside Radius			
Point	Δ/deg F/in./in. -75 F to 75 F	Room Temp R = 2.30 in. 75 F to 225 F	225 F to 340 F
1	46×10^{-6}	29×10^{-6}	15×10^{-6}
2	26×10^{-6}	11×10^{-6}	38×10^{-6}
3	40×10^{-6}	11×10^{-6}	19×10^{-6}
4	17×10^{-6}	6×10^{-6}	
Avg	32×10^{-6}	14×10^{-6}	18×10^{-6}
Outside Diameter			
Point	Δ/deg F/in./in. -75 F to 75 F	Room Temp D = 7.563 in. 75 F to 225 F	225 F to 340 F
1	25×10^{-6}	---	No Change
2	---	25×10^{-6}	No Change
3	---	---	No Change
4	---	---	No Change
Avg	6×10^{-6}	6×10^{-6}	No Change
Thickness			
Point	Δ/deg F/in./in. -75 F to 75 F	Room Temp T = 1.90 in. 75 F to 225 F	225 F to 340 F
1	14×10^{-6}	84×10^{-6}	33×10^{-6}
2	13×10^{-6}	63×10^{-6}	7×10^{-6}
3	13×10^{-6}	70×10^{-6}	7×10^{-6}
4	13×10^{-6}	63×10^{-6}	7×10^{-6}
Avg	13×10^{-6}	70×10^{-6}	14×10^{-6}
	Overall Average - 19×10^{-6}		

*Hollow cylinder; billet supplied by Lone Star Plastics

TABLE XIX

CALCULATED LINEAR COEFFICIENTS OF EXPANSION FOR MX-2646*

Inside Radius			
Point	Δ/deg F/in./in. -75 F to 75 F	Room Temp R = 1.6475 in. 75 F to 225 F	340 F to 225 F
1	12×10^{-6}	23×10^{-7}	53×10^{-7}
2	12×10^{-6}	23×10^{-7}	53×10^{-7}
3	7×10^{-6}	45×10^{-7}	53×10^{-7}
4	12×10^{-6}	12×10^{-7}	16×10^{-6}
Avg	11×10^{-6}	25×10^{-7}	79×10^{-7}
Outside Diameter			
Δ/deg F/in./in.		Room Temp D - 11.625 in.	
No Changes Noted			
Thickness			
Point	Δ/deg F/in./in. -75 F to 75 F	Room Temp T = 1.390 in. 75 F to 225 F	340 F to 225 F
1	24×10^{-6}	11×10^{-6}	12×10^{-6}
2	83×10^{-7}	8×10^{-6}	12×10^{-6}
3	83×10^{-7}	11×10^{-6}	12×10^{-6}
4	No Change	No Change	1x a 10^{-6}
Avg	63×10^{-6}	10×10^{-6}	12×10^{-6}
		OVERALL AVERAGE - 28×10^{-6}	

*Hollow cylinder; billet supplied by Cincinnati Testing Laboratories

TABLE XX

EFFECT OF AGING PROPELLANT RDS-526 WITH FIBERITE MX-2646

PROPELLANT MECHANICAL PROPERTIES

	Aged One Week at 170 F Tensile Specimen Number								Aged Four Weeks at 170 F Tensile Specimen Number					
	Control	1	2	3	4	5	6	7	1	2	3	4	5	6
Propellant RDS-526														
e_r, %	40	44	46	46	46	48	44	43	25	43	37	40	44	26
S_r, psi	180	179	177	188	192	187	177	186	194	179	184	191	188	195
E, psi	715	640	615	650	675	645	615	675	1020	780	810	815	740	1060
Propellant RDS-526 and Fiberite MX-2646 postcured 24 hr at 300 F														
e_r, %	40	49	39	44	36	39	33	39	60	43*	62	65*	66	56
S_r, psi	180	125	131	152	148	151	122	120	56	41	56	54	52	58
E, psi	715	420	470	530	550	545	470	420	130	110	125	120	115	150
Propellant RDS-526 and Fiberite MX-2646 postcured 48 hr at 300 F														
e_r,%	40	49	48	45	43	38	--	--	33	51	48	**	54	32
S_r, psi	180	165	172	182	180	163	--	--	180	164	170	--	156	178
E, psi	715	605	590	650	650	600	--	--	775	525	560	--	500	785
Propellant RDS-526 and Fiberite MX-2646 postcured 24 hr at 300 F and sealed with Epon 926														
e_r, %	40	--	--	--	--	--	--	--	60	72	74	74	60	--
S_r, psi	180	--	--	--	--	--	--	--	52	45	53	52	49	--
E, psi	715	--	--	--	--	--	--	--	120	90	105	105	105	--

NOTE: Propellant cured 72 hr at 170 F. All insulation dried 3 hr at 225 F.

*Bubbles in uniaxial tensile specimen

**Sample slipped out of Instron grips during testing

CONFIDENTIAL

CONFIDENTIAL

(e) Thermal Analysis

(C) A detailed thermal analysis[8] was performed on each of the bosses. Analysis was carried out in two parts. First with a combustion temperature of 5725 F for 10.5 seconds (corresponding to burning of the core grain) and second with a combustion temperature of 6325 F for 20.5 seconds, corresponding to combustion of the RFG.

○ Aft Polar Boss

Below is a discussion of the thermal analysis performed on the aft polar boss. It includes ablation losses, char depths, and time distribution.

Ablation Losses and Char Depth--The ablation losses vs time and the ablation loss of the aft polar boss at end of firings are shown in Figs. 37 and 38. The forward section of the aft polar boss loses 0.20 inch on the upper surface and 0.15 inch on the lower surface. This section of the aft polar boss is made of MX-2646 and has a char depth of 0.10 inch.

The MX-4600 material protecting the titanium piece of the aft polar boss loses 0.34 inch on the forward end and decreases to negligible loss at the case. The char depth of the material is 0.04 inch throughout the material.

Temperature Distribution--The aft polar boss temperature distribution at the end of firing is shown in Fig. 39. The titanium piece of the aft polar boss, at the end of firing, experiences no temperature rise. For the aft polar boss, as for the forward polar boss, the load rings were assumed to be omitted to determine whether or not sufficient insulation material was available to protect the polar boss.

○ Forward Polar Boss

The results of the analysis of the forward closure and polar boss are presented in Figs. 40, 41, and 42. The following paragraphs discuss the ablation loss and temperature distribution of the forward head obtained from the analysis:

---

[8] The complete analysis technique is presented in Appendix C.

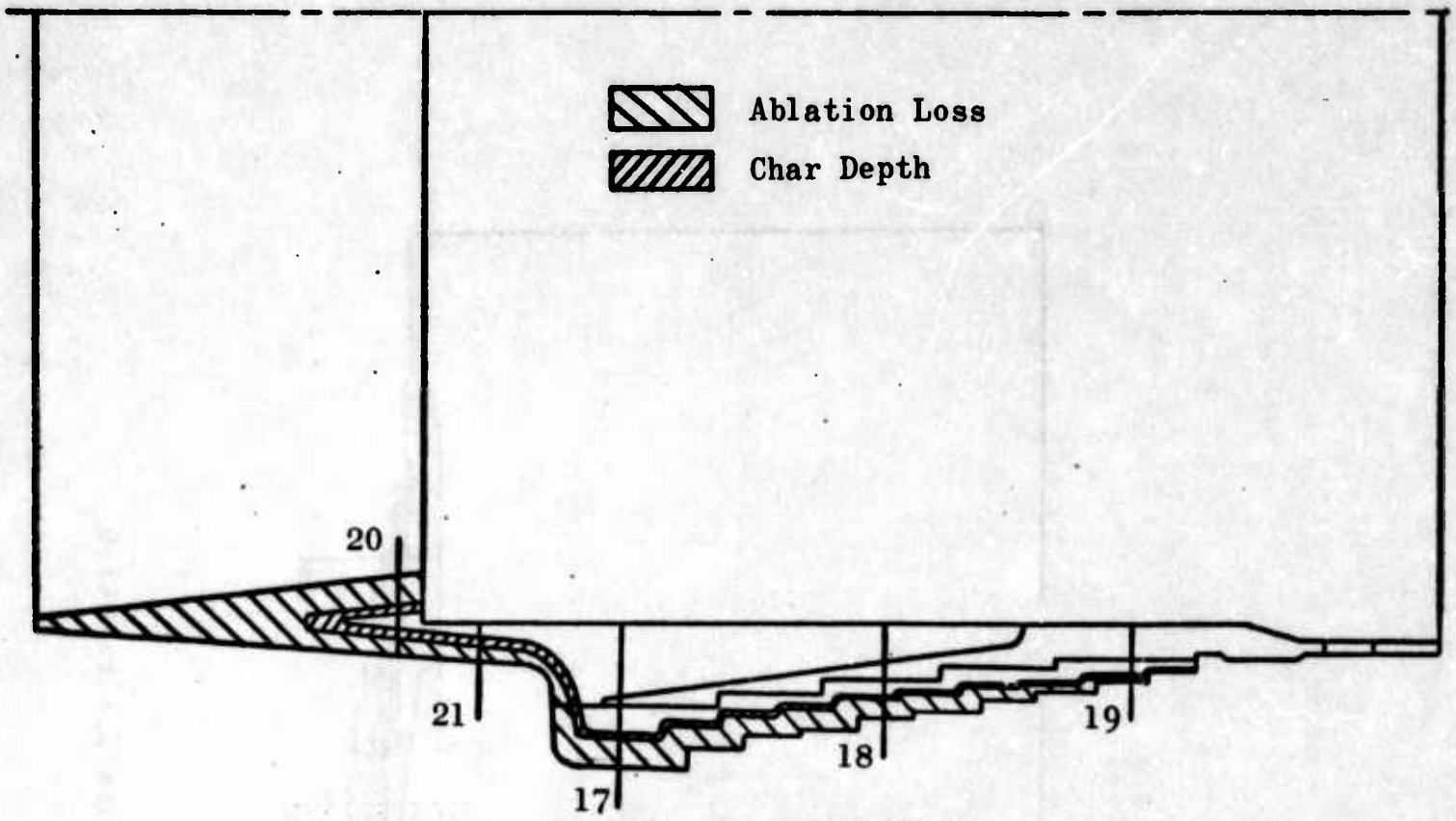


Figure 37. Aft Polar Boss Ablation Loss and Char Depth at End of Firing

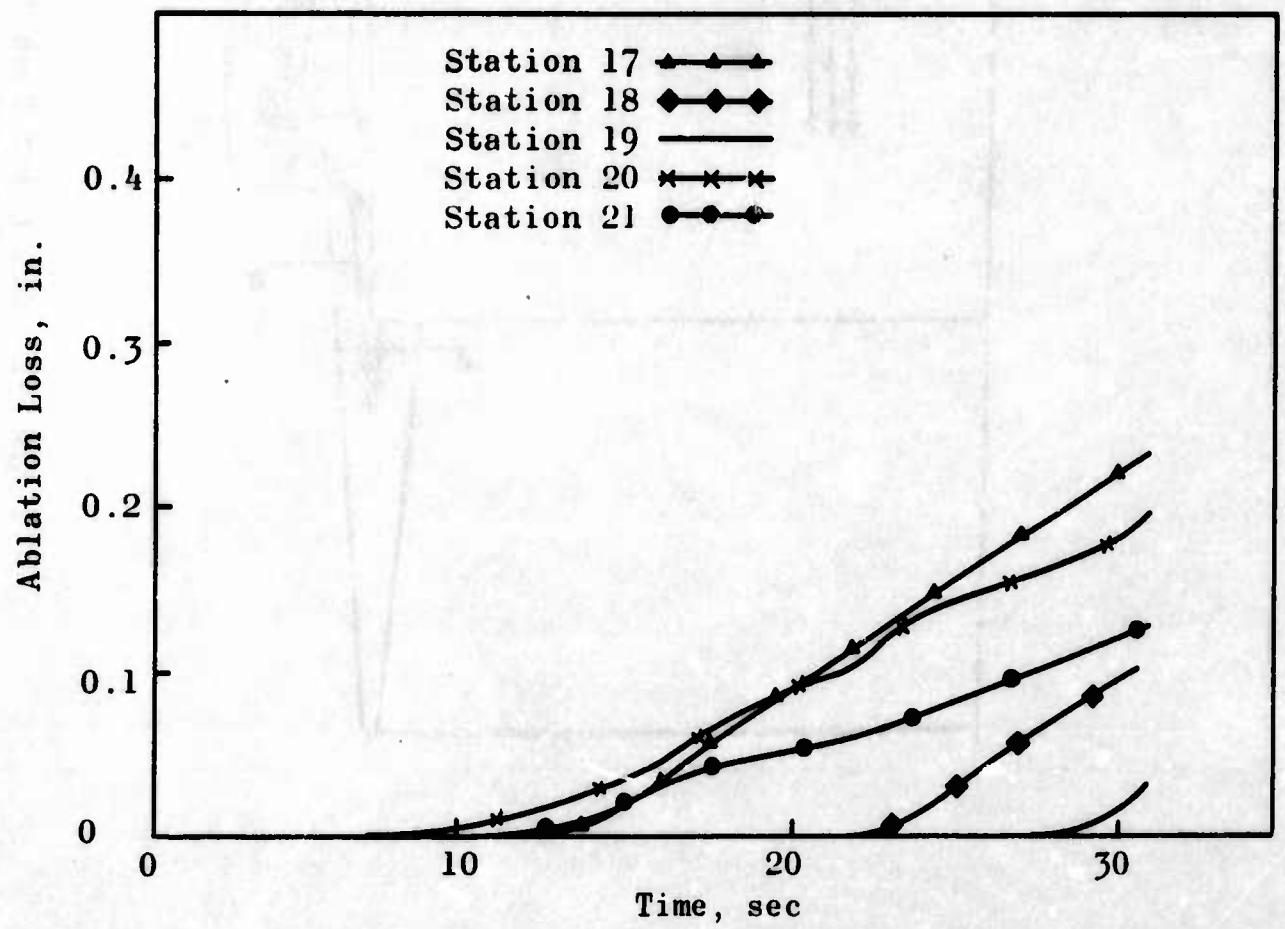


Figure 38. Ablation Loss-vs-Time for Aft Polar Boss Stations

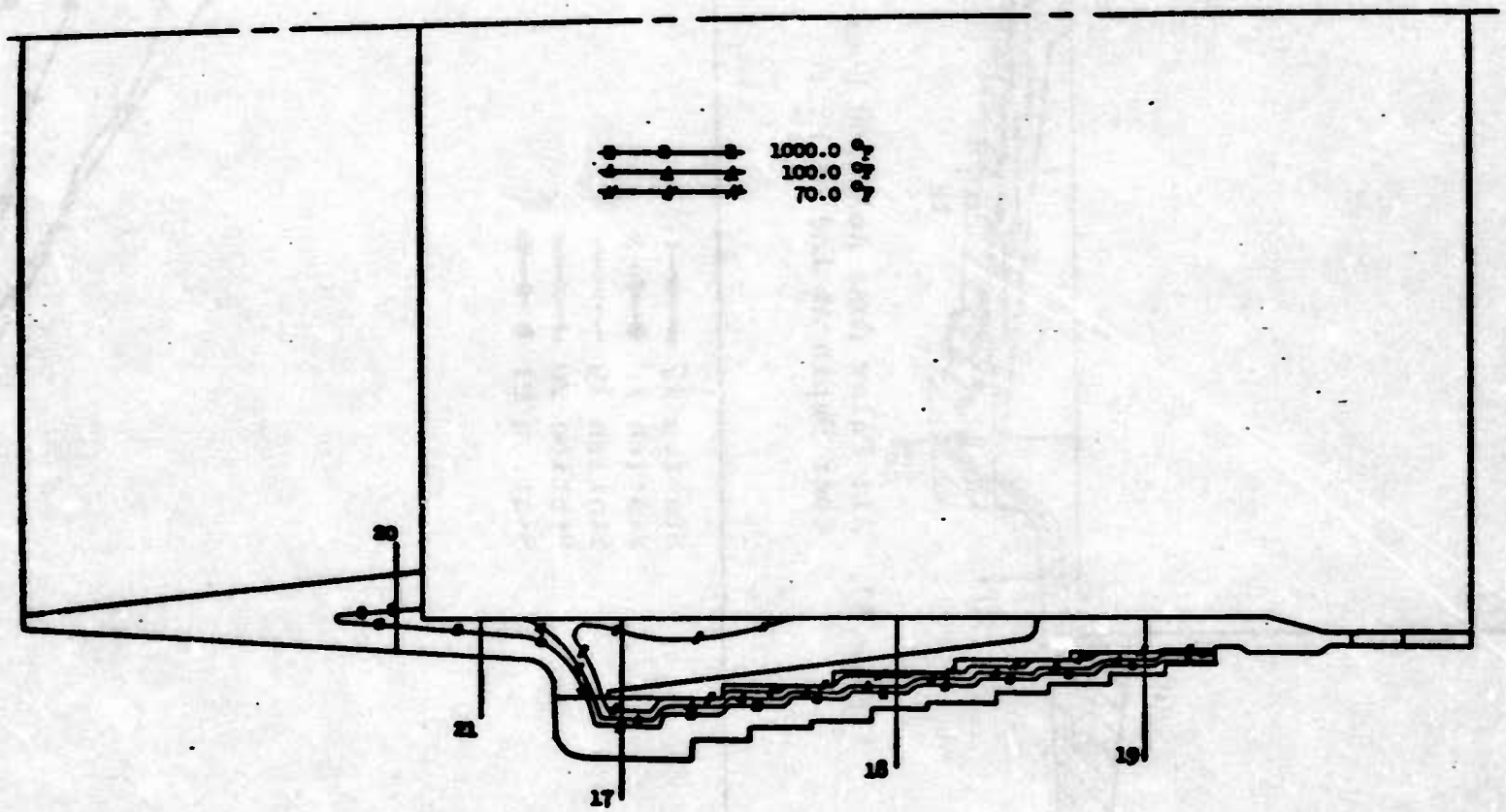


Figure 39. Aft Polar Boss Temperature Distribution at End of Firing

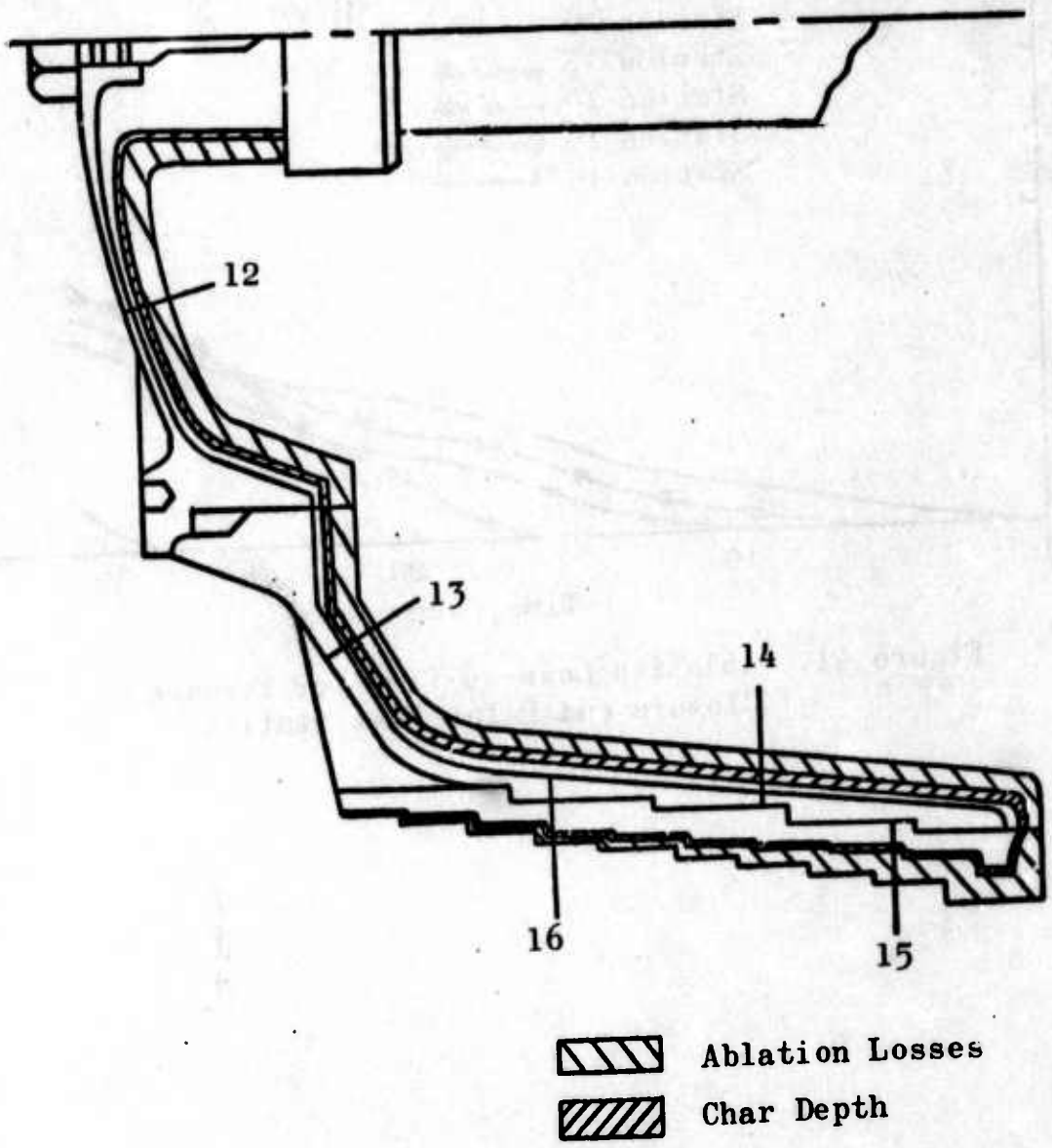


Figure 40. Ablation Losses and Char Depth of Forward Closure and Polar Boss at End of Firing

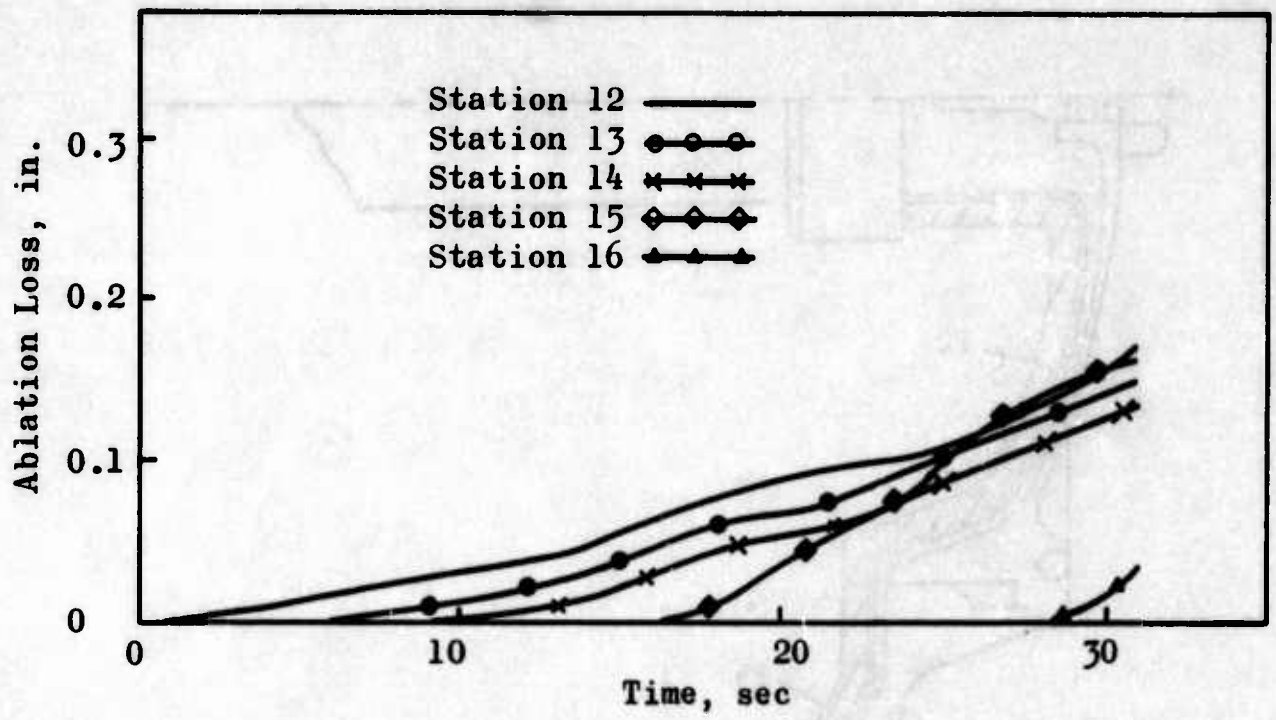


Figure 41. Ablation Loss-vs-Time for Forward Closure and Polar Boss Stations

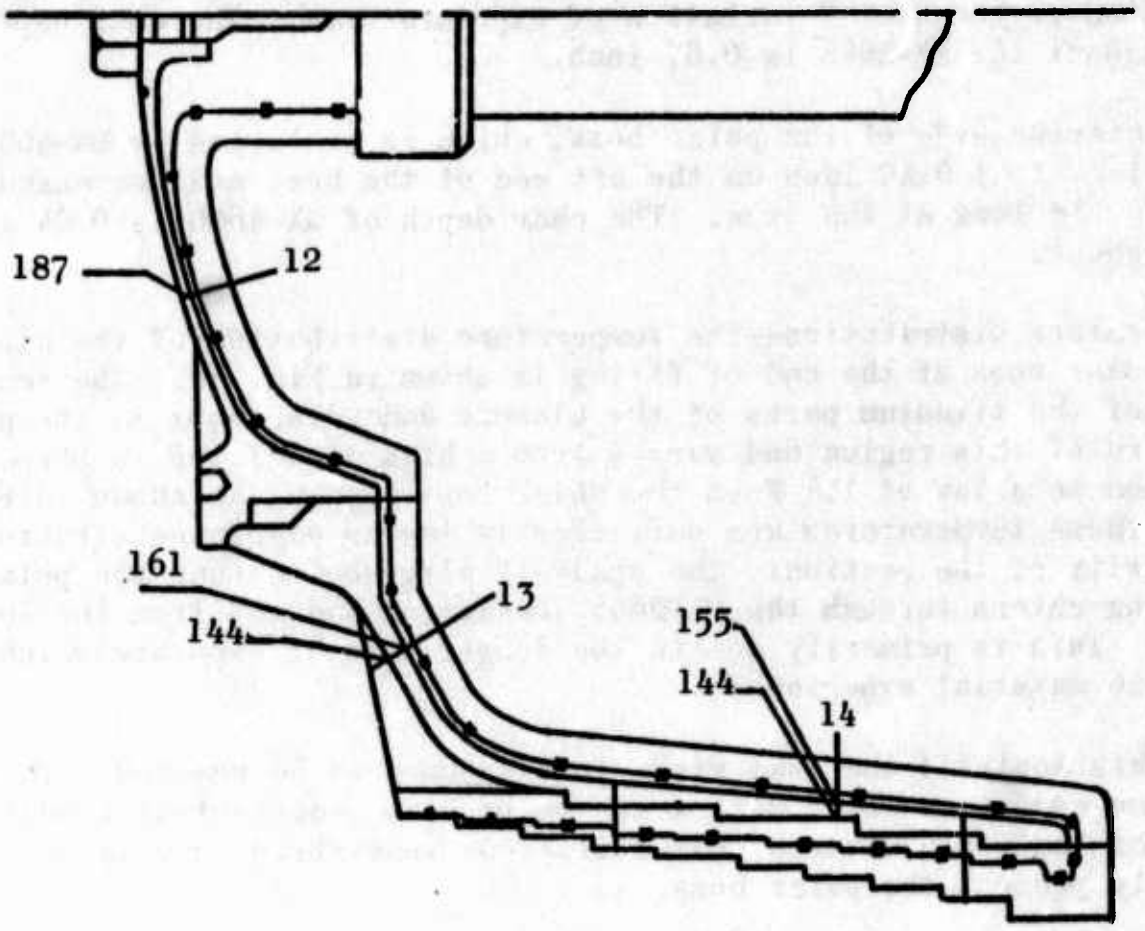


Figure 42. Temperature Distribution of Forward Closure and Polar Boss at End of Firing

Ablation Losses and Char Depth--The ablation loss vs time and the ablation loss and char depth of the forward closure and polar boss at end of firing are shown in Figs. 40 and 41. It can be seen from Fig. 40 that all the parts are still protected by undamaged insulation at the end of firing. The ablation depth of the MX-2646 silica phenolic protecting the forward closure and upper surface of the polar boss was 0.16 inch for the closure and decreased to 0.14 inch on the upper surface of the polar boss. The variation of ablation in the MX-2646 insulation is because of variation of exposure time. The char depth throughout the MX-2646 is 0.07 inch.

The interior side of the polar boss, which is protected by MX-4600 glass phenolic, lost 0.19 inch on the aft end of the boss and decreased to negligible loss at the case. The char depth of MX-4600 is 0.04 inch throughout.

Temperature Distribution--The temperature distribution of the closure and polar boss at the end of firing is shown in Fig. 42. The temperature of the titanium parts of the closure and polar boss is the principal concern of this region and varies from a high of 187.1 F in the closure section to a low of 144 F in the polar boss region, as shown in Fig. 42. These temperatures are sufficiently low to guarantee structural integrity of the section. The analysis also showed that the polar boss heating enters through the MX-2646 insulation and not from the load ring area. This is primarily due to the longer time of exposure which the MX-2646 material experiences.

For this analysis the load rings were assumed to be removed. This is an extreme condition which will never be present under actual conditions, but this approach ensures that sufficient insulation is present to adequately protect the polar boss.

(2) Load Rings

The load-ring concept was initiated after difficulties arose in transferring the polar loads into the RFG, using the original cone-shaped polar bosses. In the load-ring concept, the polar boss transfers its load into the load ring, which is sandwiched between the geodesic-isotensoid RFG layers. In this manner the load rings transfer the polar loads into the RFG structure, utilizing the RFG load-carrying capability to reduce the load requirements of the case. A typical load ring for Motor A is illustrated in Fig. 43.

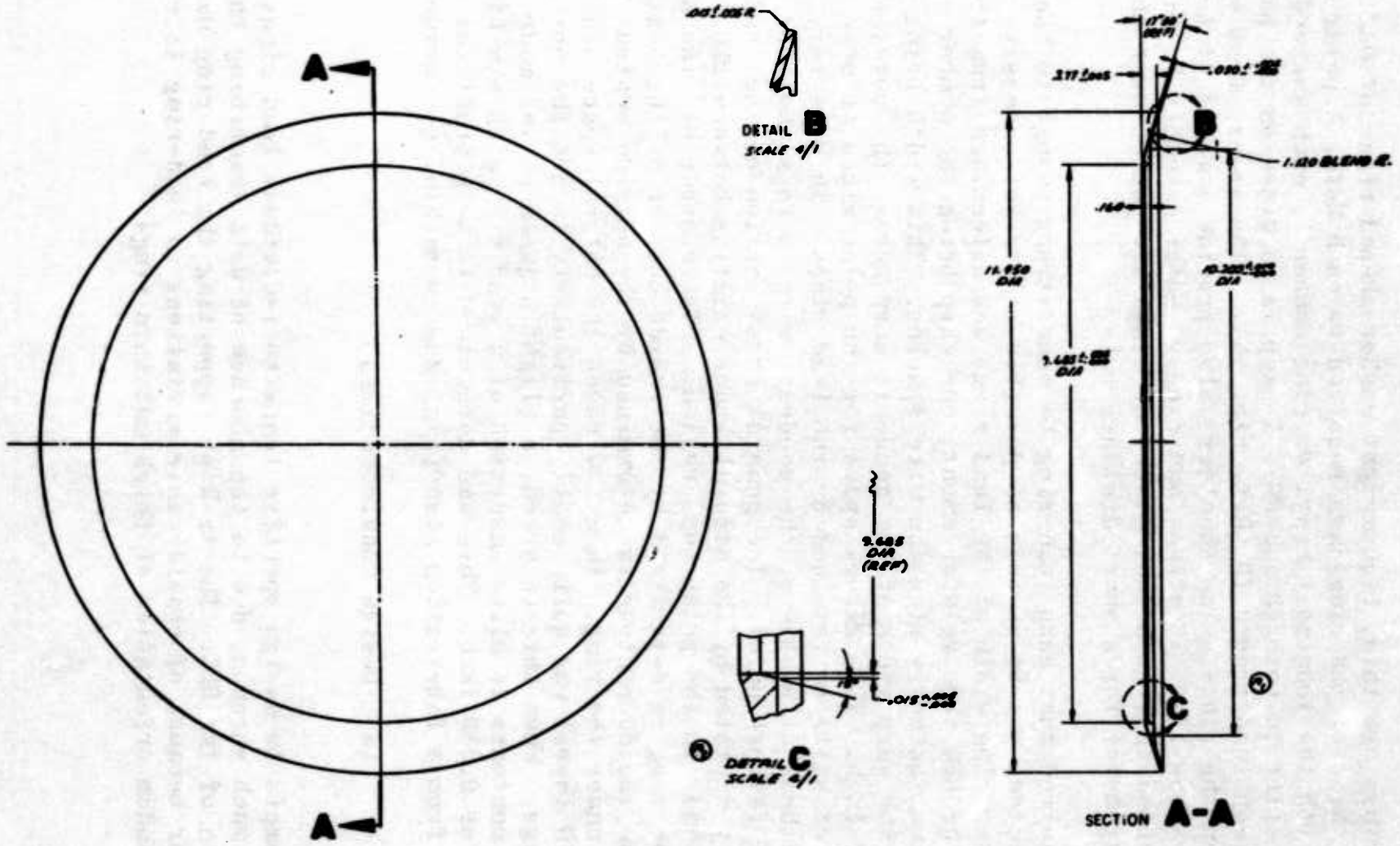


Figure 43. Typical Load Ring Section, Motor A

(C) The load rings are thin, lightweight washer-shaped rings of 6Al 4V titanium. Nine of the rings are required on each Motor A polar boss. Starting with the innermost ring, or ring number 1, each succeeding ring is made smaller in both ID and OD. A step is machined on the polar boss to match each load ring's ID (Ref. Fig. 44). The steps form a stop to position the rings. The shoulders also provide a means of transfer-ring polar-boss loads into the load rings. Motor assembly is made easier by the stepped configuration, since the rings are passed over the close-fit step diameter for a short distance only.

Design required that each load ring be made strong enough to handle the loads expected, yet be as thin as possible to prevent excessive buildup at the boss. The width of the load rings was determined from the warp width of the RFG wire reinforcement, one warp being the number of wires applied simultaneously plus the wire spacing. This width being enough to handle the warp width of the geodesic warp across the pole, plus about 0.25 inch. This allows space for the polar wires to move under pressure yet still be retained by the load rings. This is very important since the shear allowable of the geodesic wires across the load rings is a critical failure point. The general cross section of the load rings was largely dictated by the natural space existing between RFG layers (see Fig. 44) in the polar boss region. The contour of the outside face of the ring is determined by the inside contour of the next RFG layer. The inside contour is determined by the outside contour of the RFG layer under the ring. In a few cases the natural space available between RFG layers was quite small, particularly toward the outer edge of the rings. When this occurred, a slight adjustment was made in the RFG-layer contours to allow insertion of a load ring with a minimum thickness of 0.030 inch. This was determined to be a practical minimum thickness from a fabrication standpoint due to machining considerations.

(a) Design Considerations

Early attempts to assign specific loads to individual load rings did not meet with much success, due to the absence of data describing the load-ing pattern of the RFG. The task of supporting the load ring design was also harder because of considerable variations in load-ring thicknesses and the random orientation of thick and thin rings.

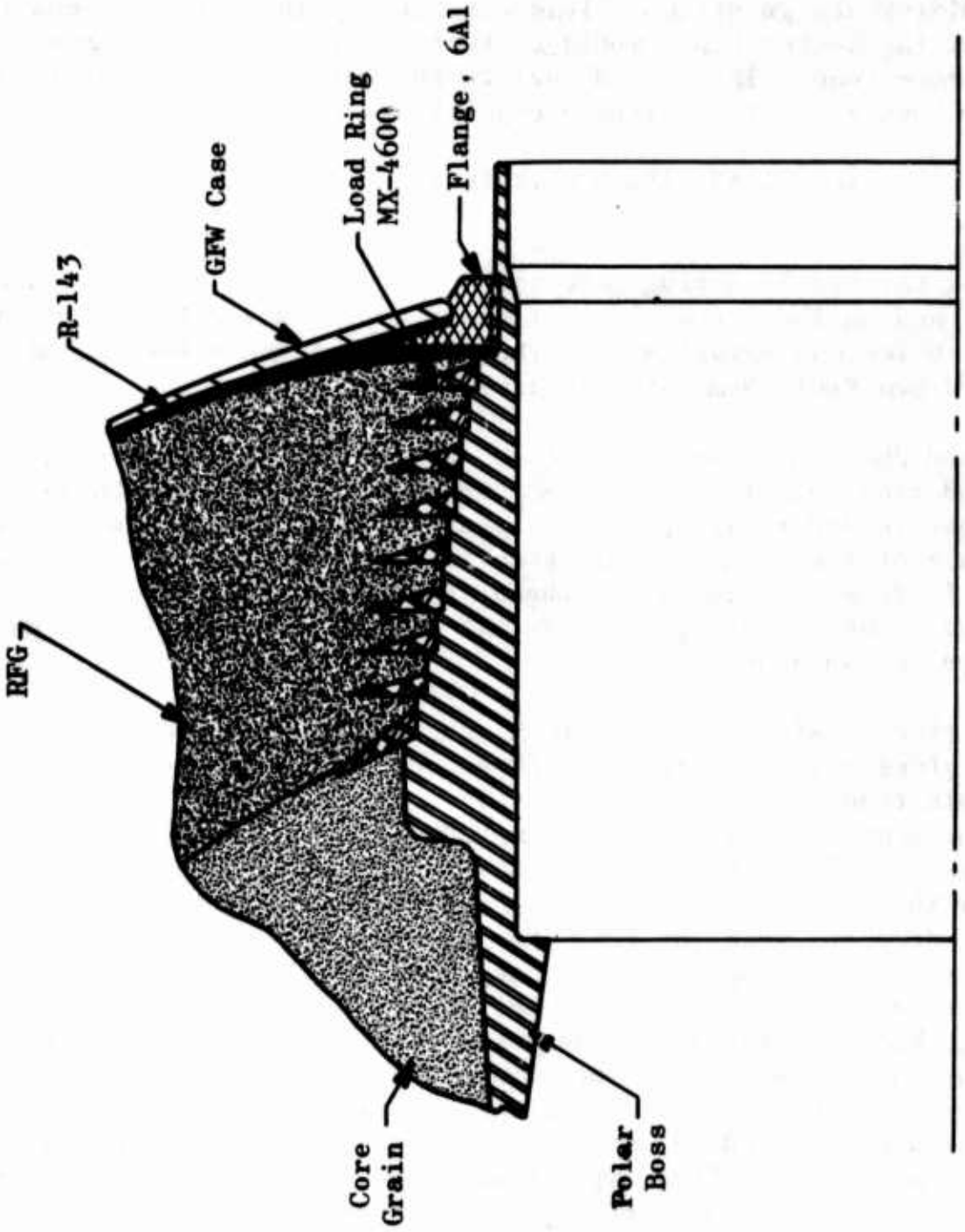


Figure 44. Motor A Aft Polar Boss Area

Eventually an approximation equation was used to determine the theoretical load-carrying capability of each ring. The individual loads were then added to obtain the total load capability of the rings on each boss. This load was then compared with the maximum ultimate load expected during motor operation. When compared, the combined-load-ring strength and the calculated design ultimate load were nearly the same. It was reasoned that the weaker rings would deflect and force the stronger rings to carry more load. This would justify the method used to determine the polar boss load-ring strength capability.

(b) Load Ring Static Tests

By testing various load ring materials on the 10- and 20-inch subscale programs, and on the predevelopment phase of the Motor A program, a material choice was established. The results of these tests, and conclusions drawn from them, are discussed below.

The 10- and 20-inch polar bosses (see Figs. 45 and 46) incorporate the first load ring into the polar boss structure. When these bosses were static load-tested (Ref. Fig. 47), severe material separation occurred at the base of the load ring as shown in Fig. 48. The 20-inch polar boss was fabricated from silica phenolic molding compound and an aluminum sleeve. The 10-inch polar boss was fabricated from MX-4600 phenolic glass tape and an aluminum sleeve.

The load rings tested on the 20-inch program were fabricated from phenolic glass molding compound. These tests revealed severe cracking and delamination at extremely low loads. The load rings tested on the 10-inch program were fabricated from phenolic glass tape. Since the load rings were being bench-tested under relatively high loads, it was initially thought that this material was adequate for load rings for Motor A. However, when the load was relaxed and the load ring was inspected, severe crazing, chipped edges, and ply delamination were noticed. During the development of the 10- and 20-inch load rings and polar bosses, the design had been based on vendor-supplied and industry-reported data concerning the properties of the reinforced plastic materials. Under the test conditions and application of the materials for this program, premature failure occurred (or the failure load was marginal enough to reject the material). This type of material problem plagued development of both the load rings and polar bosses, causing extensive program delay.

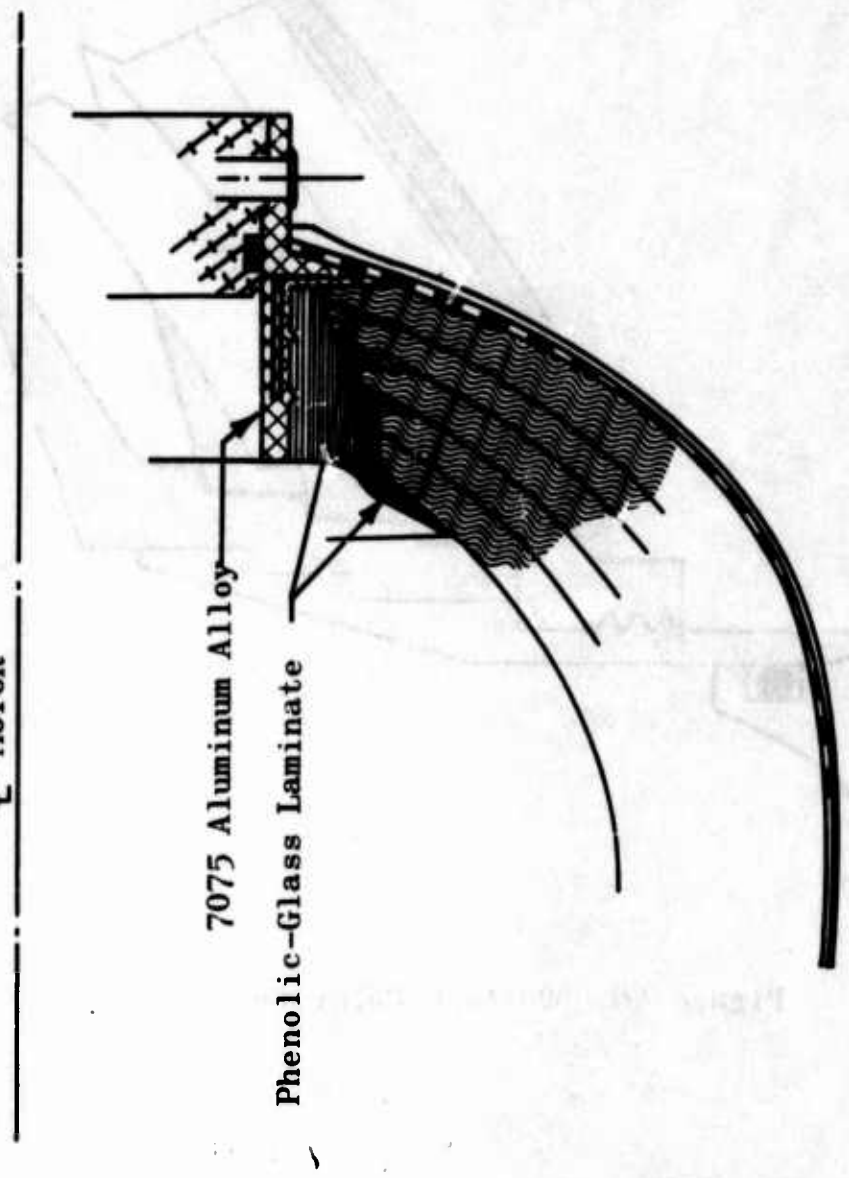


Figure 45. 10-Inch Subscale Polar Boss

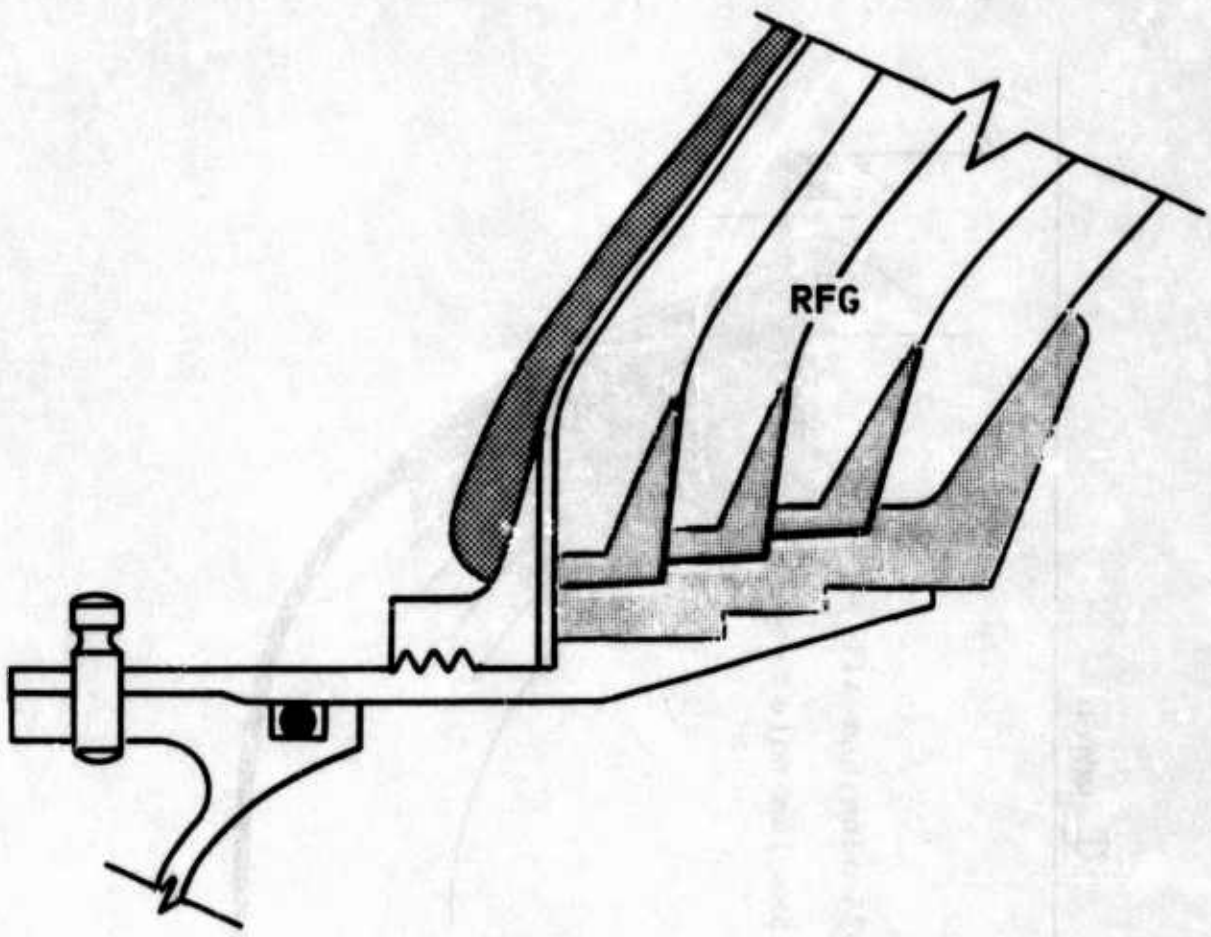


Figure 46. 20-Inch Polar Boss

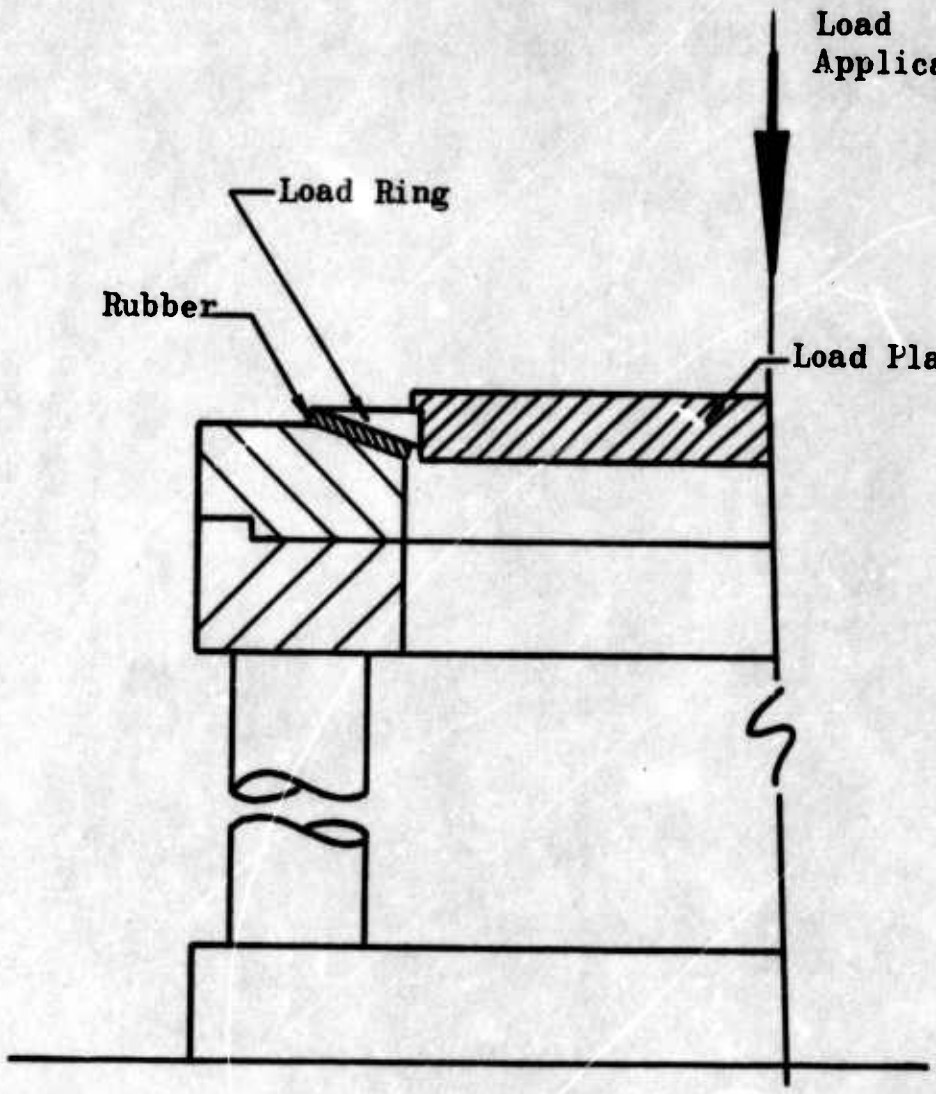
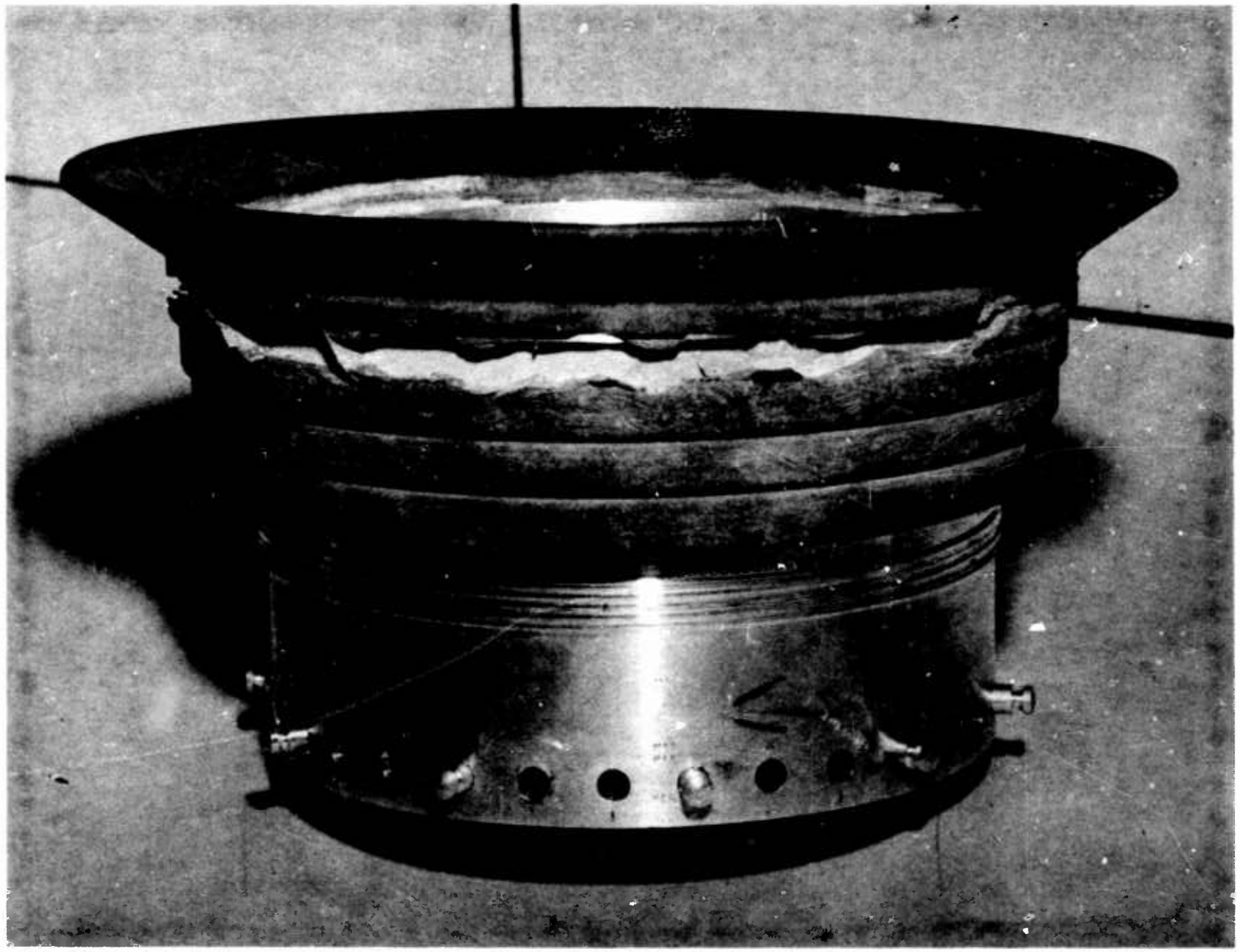


Figure 47. Static Test of Load Ring



2YA25-11 19 63MID

Figure 48. Load Ring Failure Mode

Results of the 10- and 20-inch phenolic load ring tests indicated that these materials were not acceptable for production use in full-scale motors. Three other candidate materials were tested; 6Al 4V titanium, 4130 steel, and 7075-T651 aluminum. Material properties of these three candidates are shown in Table XXI.

TABLE XXI

LOAD RING MATERIAL STUDY

Property	Aluminum (7075-T651)	Titanium (6Al 4V)	Steel (4130)
Density, lb/cu in.	0.101	0.160	0.283
Thermal Conductivity, Btu/hr(ft^2)(deg F/ft)	70	4.3	24.7
Melting Temp, deg F	890--1180	2730--3135	2600--2760
Specific Heat, Btu/lb/deg F	0.23	0.135	0.11
Modulus, psi	10.4×10^6	16×10^6	30×10^6
Ultimate Tensile Stress,psi	83,000	130,000	140,000
Yield Stress, psi	73,000	120,000	120,000
Motor A Load Ring wt, lb	4.85	7.69	13.6
Wt Savings, lb (compared to steel)	8.75	5.91	
Strength Capability	Not adequate on some sections	Adequate	Adequate
Thermal Conductivity (compared to steel)	2.83 greater	5.74 less	----

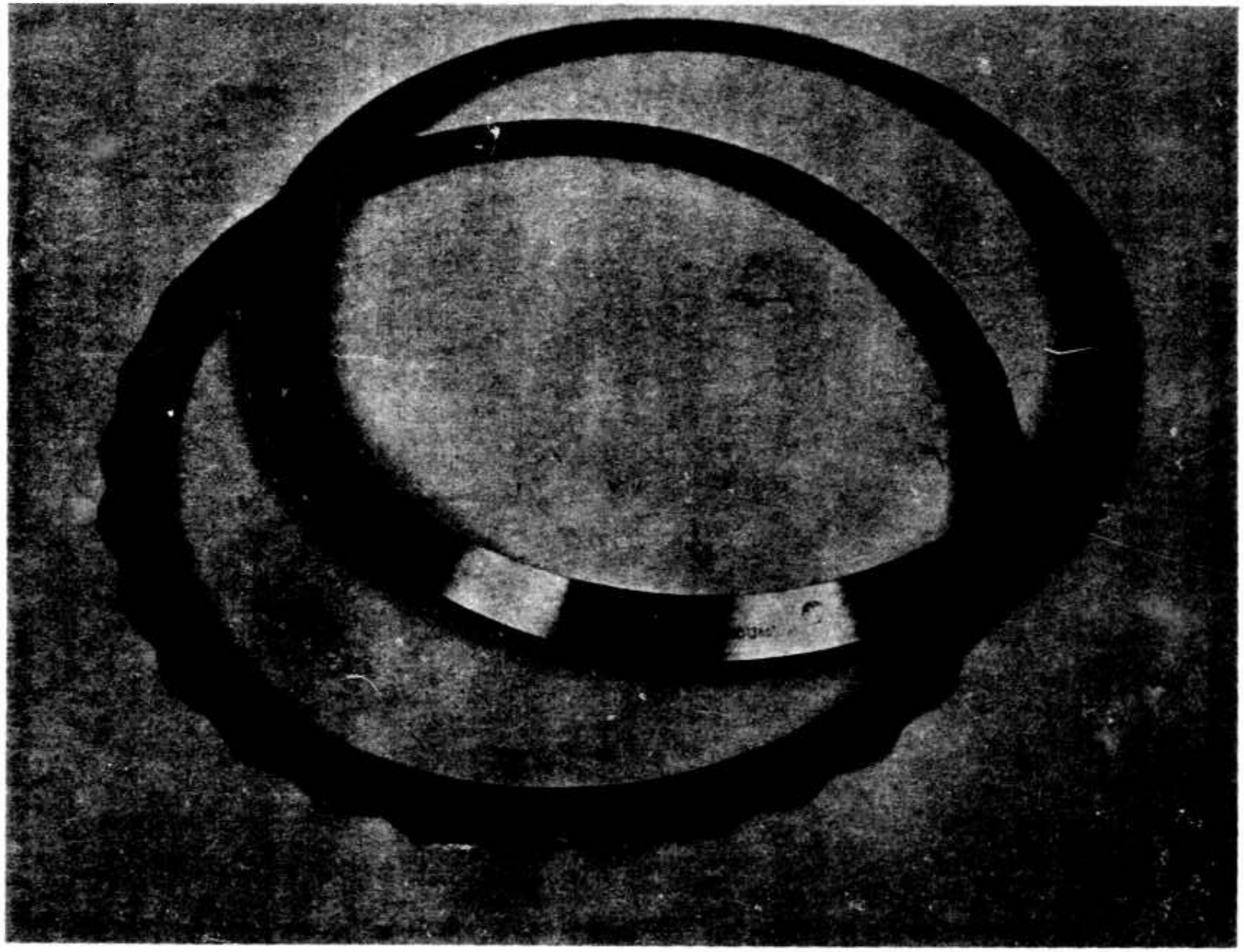
Verification tests were conducted on load rings made from aluminum and steel; the load rings were considered to have failed when the yield strength of the material was exceeded. This was evidenced by pronounced wrinkling around the outer edge of the ring. Figure 49 illustrates ring condition before and after testing. Detailed results of these tests are presented in Table XXII.

Upon completion of the above static tests, load rings fabricated from titanium were tested. However, it was thought that a test utilizing a polar boss/load ring combination would be more applicable to Motor A than the tests previously performed. Detailed results of these tests were presented in the polar boss component section. In a comparison of steel, aluminum, and titanium, the latter proved to be superior.

TABLE XXII

MOTOR A STATIC LOAD RING TESTS

Motor A Part No.	Assumed Load Ring Values, lb	4130 Steel		7079-T651 Aluminum	
		Applied Load, lb	Deflection	Applied Load, lb	Deflection
802357 No. 1	32,300	72,496	0.139	60,036	0.211
802357 No. 2		60,000	0.126		
802365 No. 1	19,400	50,744	0.220	14,067	0.103
802365 No. 2		35,231	0.193		
802367 No. 1	12,100	40,010	0.166	16,156	0.188
802367 No. 2		39,000	0.199	18,970	0.202
802371 No. 1	12,100	42,000	0.139	19,520	0.141
802371 No. 2		42,000	0.153	18,147	0.081



2YA35-1/20/64M1F

Figure 49. Static Load Ring Test, Before and After Test (20 in. Motor Load Ring)

(c) Heat Transfer Analysis

The need for a load-ring material with a low heat-transfer rate was apparent when considering flame front propagation. As the front advances it reaches the inside surface of the load rings first. If the transferred heat is great, there is a possibility of preignition occurring in front of the load rings (ahead of the normal flame front). This could result in premature loosening of the polar boss.

A thermal analysis was conducted concurrent with the static load tests on the three metallic load rings. The analysis was carried out on all three materials for various thicknesses corresponding to the thickness of various sections of the load ring. Temperature histories of the various thicknesses of the three materials are presented in Fig. 50.

The purpose of this analysis was to determine the probability of propellant autoignition after exposure of the load ring to the combustion gases. The failure criteria of the analysis was the propellant/load ring interface (opposite the approaching flame front) attaining a temperature of 1000 F prior to being overtaken by the flame front.

A typical steel load ring was analyzed; it was found that failure was not reached except for sections thinner than 0.18 inch, as shown in Fig. 51. Closer examination of the problem pointed out that the high concentration of wire in the polar boss region lowered the flame temperature in the immediate region, and acted as a heat sink.

The maximum time lag between flame-front contact on the load ring and 1000 F at the interface was 0.32 second for both steel and titanium. Aluminum was eliminated as a load-ring material because the interface temperature rise was more pronounced than that of steel or titanium as shown in Fig. 50.

A considerable weight saving also acted in favor of selecting titanium, after studying the results of the tests run to develop rings for the 10-, 20-, and 30-inch motors. Ultimately, titanium was selected as the load ring material because it is considerably lighter than steel, has a relatively low rate of heat transfer, and stronger than steel or aluminum which has not been heat treated.

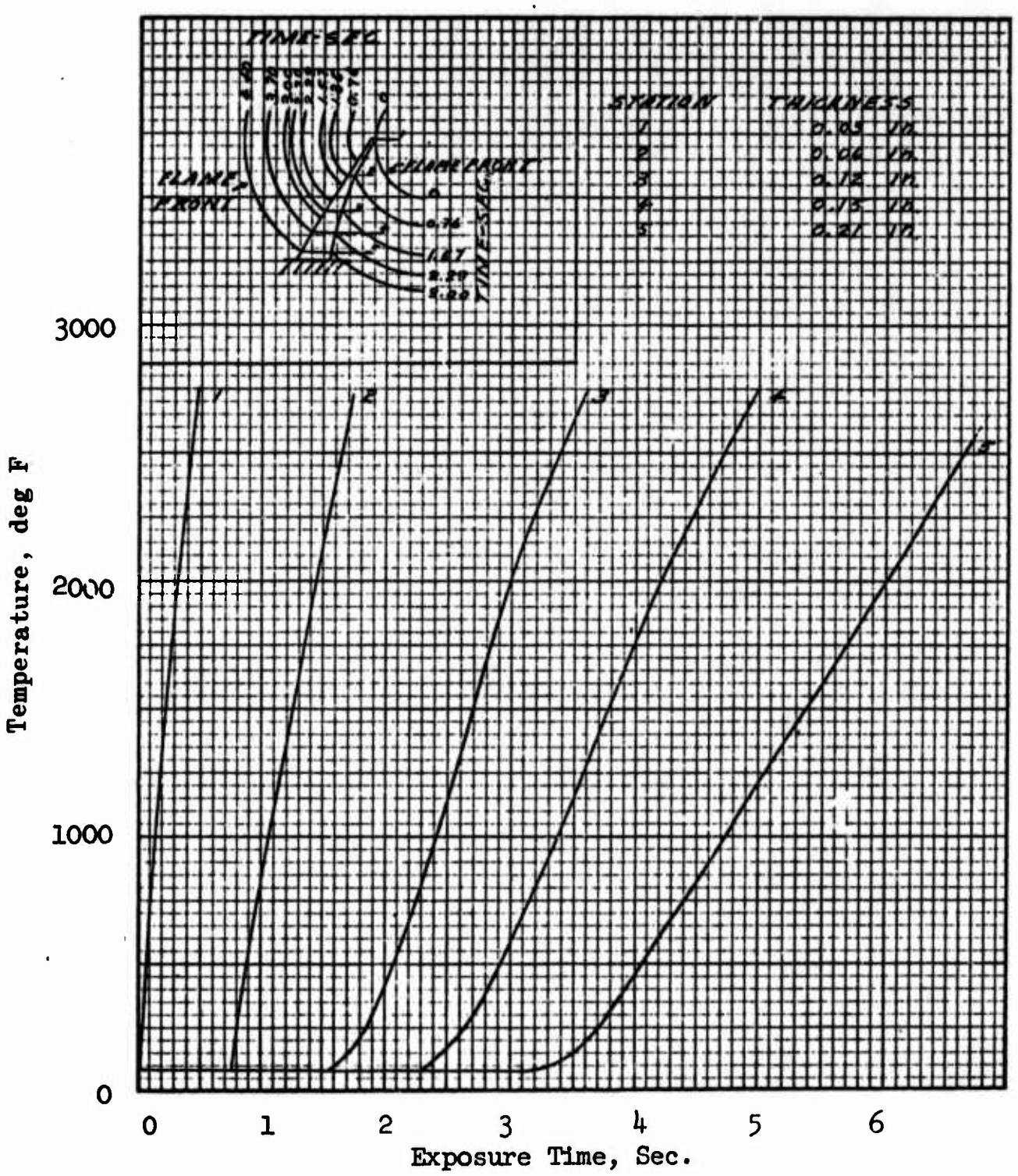
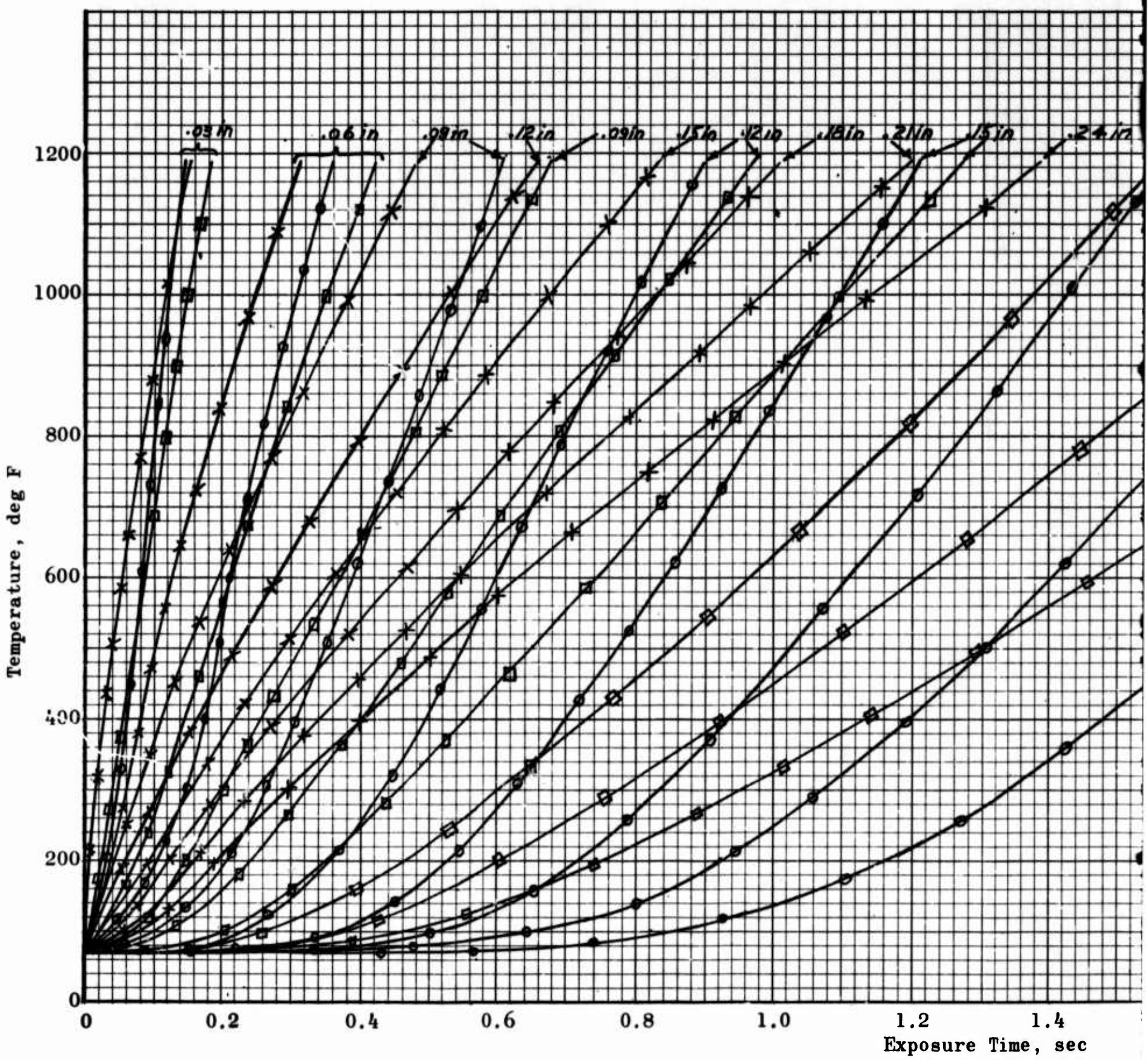


Figure 50. Typical Propellant Load Ring Interface Temperature vs Exposure Time For Various Thicknesses of a Steel Load Ring

CONFIDENTIAL

PREVIOUS PAGE WAS BLANK, THEREFORE WAS NOT FILMED



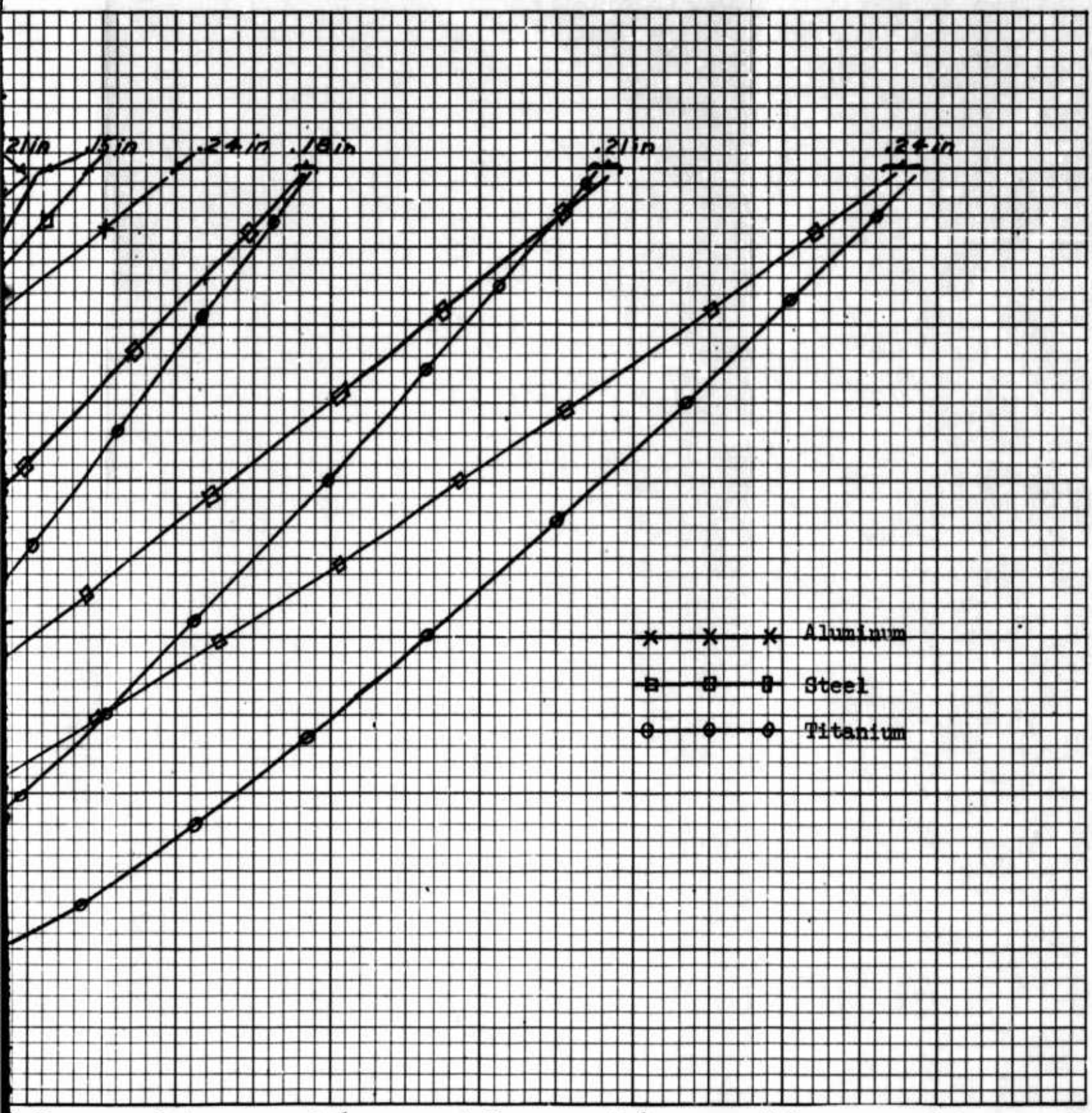


Figure 51. Temperature-vs-Time for Various Thickness of Load Ring Materials

CONFIDENTIAL

PREVIOUS PAGE WAS BLANK, THEREFORE WAS NOT FILMED

(3) Nozzle

Motor A nozzle is an extremely lightweight design, since mass fraction was the major design objective. As a result, each feature of the nozzle received detailed consideration to ensure an optimum design.

(C) The nozzle is an optimized 80% bell contour[9] made up of a Graph-I-Tite-G insert backed with a pyrolytic graphite insert, then wrapped with FM5128 graphite phenolic and FM5067 silica phenolic.

The effects of ablation and corrosion in the nozzle must be considered to determine their effects on the motor ballistic performance. In addition, the temperature distribution must be considered to determine the structural ability of the nozzle to withstand the applied forces.

(a) Ballistic Requirements

(C) The final design for the Motor A nozzle is an 80% bell nozzle. The parabolic contour has a maximum divergence half angle of 25 degrees at the inflection point aft of the throat region. The lip angle at the exit plane is 11.5 degrees. The throat diameter is 5.125 inches, with an exit diameter of 12.55 inches and expansion ratio[10] of 6:1. This final design contour was employed in motors A-1001, A-1002, A-1003, A-1004, and A-1005.

(C) The ballistic performance requirements were stated at 70 F, sea level. Hence, the nozzle was designed for optimum performance at these conditions.

(C) In the preliminary analysis the average pressure over the total action time was estimated to be approximately 600 psia. This pressure was used in the nozzle design studies, and on this basis the expansion ratio of 6:1 was chosen. This ratio results in an optimum theoretical thrust coefficient at 600 psia, sea level conditions. During the duration of core burning, the nozzle is slightly under-expanded, while during burning of the RFG, the nozzle is slightly overexpanded.

---

(9) Length to be 80% of the length of a 15-degree conical nozzle of the same expansion ratio.

(10) The ratio of the exit area with respect to the throat area.

(C) As the mass fraction of the motor was a major parameter influencing design of all components, the nozzle weight was treated with appropriate importance. This was the primary reason for using a shorter, contoured nozzle. Data indicated that an 80% bell nozzle would weigh approximately three pounds less than a 15-degree conical nozzle. In the range of weights encountered in Motor A, three pounds of inert weight would change mass fraction by approximately 0.001. It was not anticipated that the thrust coefficient of the contoured nozzle would be improved over that of a 15-degree conical with the same expansion ratio. In the design analysis it was assumed that the 80% bell nozzle would exhibit the same thrust coefficient as the 15-degree conical nozzle. Test data verified these assumptions.

(C) Nozzle designs were evaluated over the length range from 60 to 80% of the 15-degree conical nozzle length. In particular, thrust coefficients were determined for 62, 72, 76, and 80% of 15-degree conical lengths. For these different lengths, the wall radius was varied and various parabolic contours (differing in maximum and minimum divergence angles) were considered. From these data the 80% length with its optimum contour (with respect to thrust coefficient, mass fraction, and over-all specific impulse of the motor) was selected for optimum performance.

(C) Nozzle throat diameter in Motor A is an implied requirement from total impulse requirements, maximum thrust and pressure limits, duration, grain geometry, and other variables. The parametric studies resulted in the throat diameter of 5.125 inches.

(b) Component Description

Selection of materials for each nozzle component presented the same problems as in every solid propellant nozzle. The entrance section must provide smooth gas transition into the nozzle without material degradation in this turbulent flow area. In this design it was complicated by the design being a light, short submerged nozzle in which the entrance material had the dual function of forming a back side sealing surface and matching with the polar boss component. The throat component must provide good erosion properties at high temperature while retaining adequate strength. In this design the throat material was backed up with a thermal barrier to provide protection to the structural retention member, the skirt. The skirt provides the final expansion of the exhaust gases as well as fulfilling its structural requirements. To prevent extensive erosion and material degradation just aft of the throat insert,

a material was chosen that had high erosion resistance at elevated temperatures. Increased reliability was obtained by including an attachment ring in the skirt to provide a more positive interlock between the nozzle and polar boss.

The materials selected to fulfill these requirements in the Motor A nozzle are high temperature ablative plastics, high density graphite, and an aluminum attachment ring embedded in the plastic material on the periphery of the nozzle. Illustrated in Figs. 52 and 53 are the designs representing a lightweight and heavyweight nozzle configuration. Figure 54 is a design featuring a heavyweight nozzle configuration with a composite throat construction.

The heavyweight nozzle was designed to be used for extrapolating corrosion and char data experienced in the first motor firing. These data were to be used in determining whether or not the flightweight nozzle design had sufficient material thickness in the exit cone region to withstand a 35 second firing duration.

The selection of the materials and their configurations for Motor A nozzle also afforded an excellent opportunity to evaluate materials for subsequent use in Motor B nozzle. A discussion of these materials is presented.

○ Throat

Graph-I-Tite G[11] was selected for the nozzle throat because of its high strength, high temperature, and good erosion properties. Generally, better material erosion resistance and mechanical properties are accompanied by higher density, and due to the fabrication techniques employed in the manufacturing of Graph-I-Tite G, higher mechanical and physical properties are obtained. Graph-I-Tite G is produced by the reimpregnation of an extruded graphite. This process continues until desired properties, tensile strength, compressive strength, and density are reached.

(11)A product of Basic Carbon Corp., Sanborn, New York.

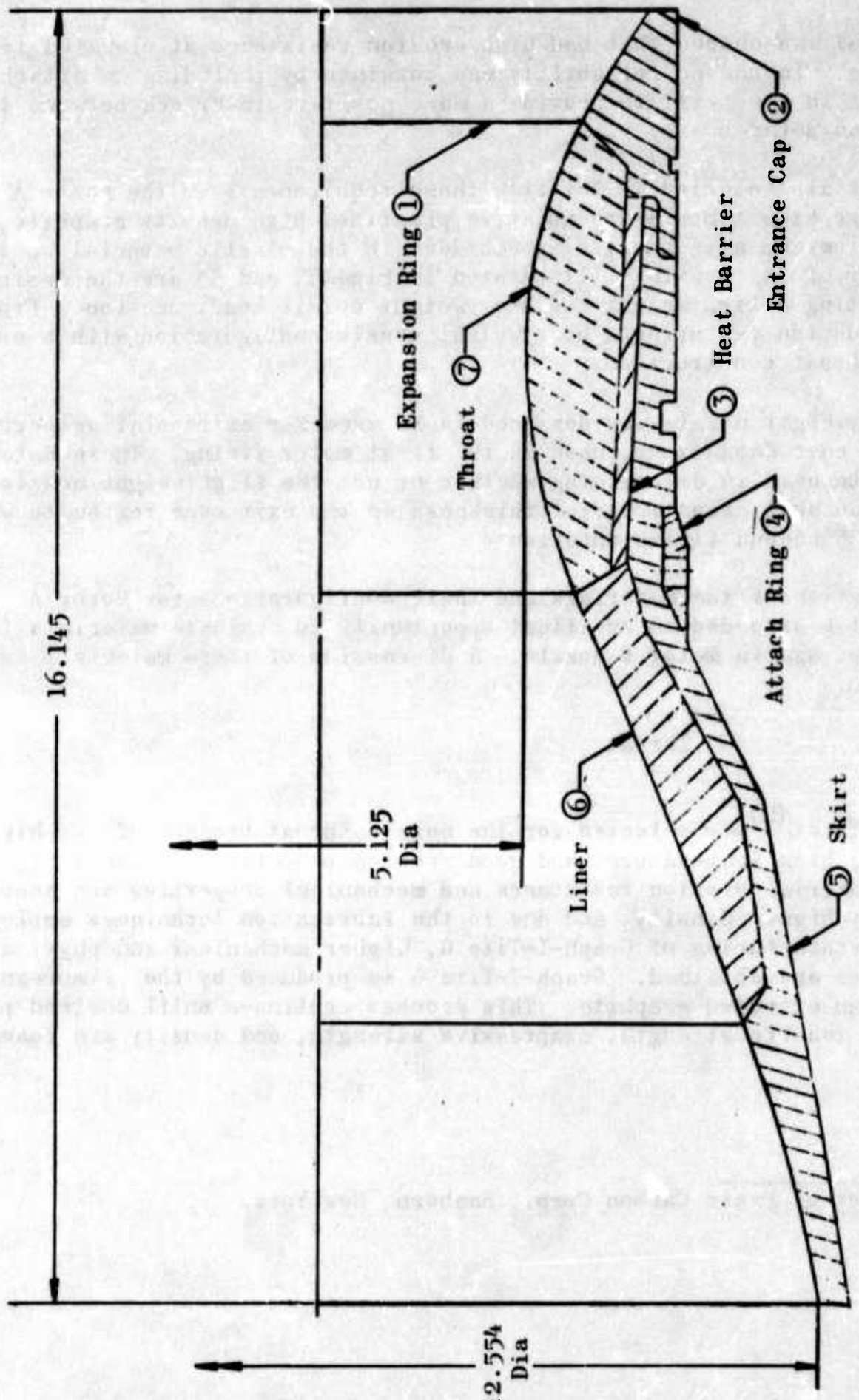


Figure 52. Heavyweight Nozzle Configuration

CONFIDENTIAL

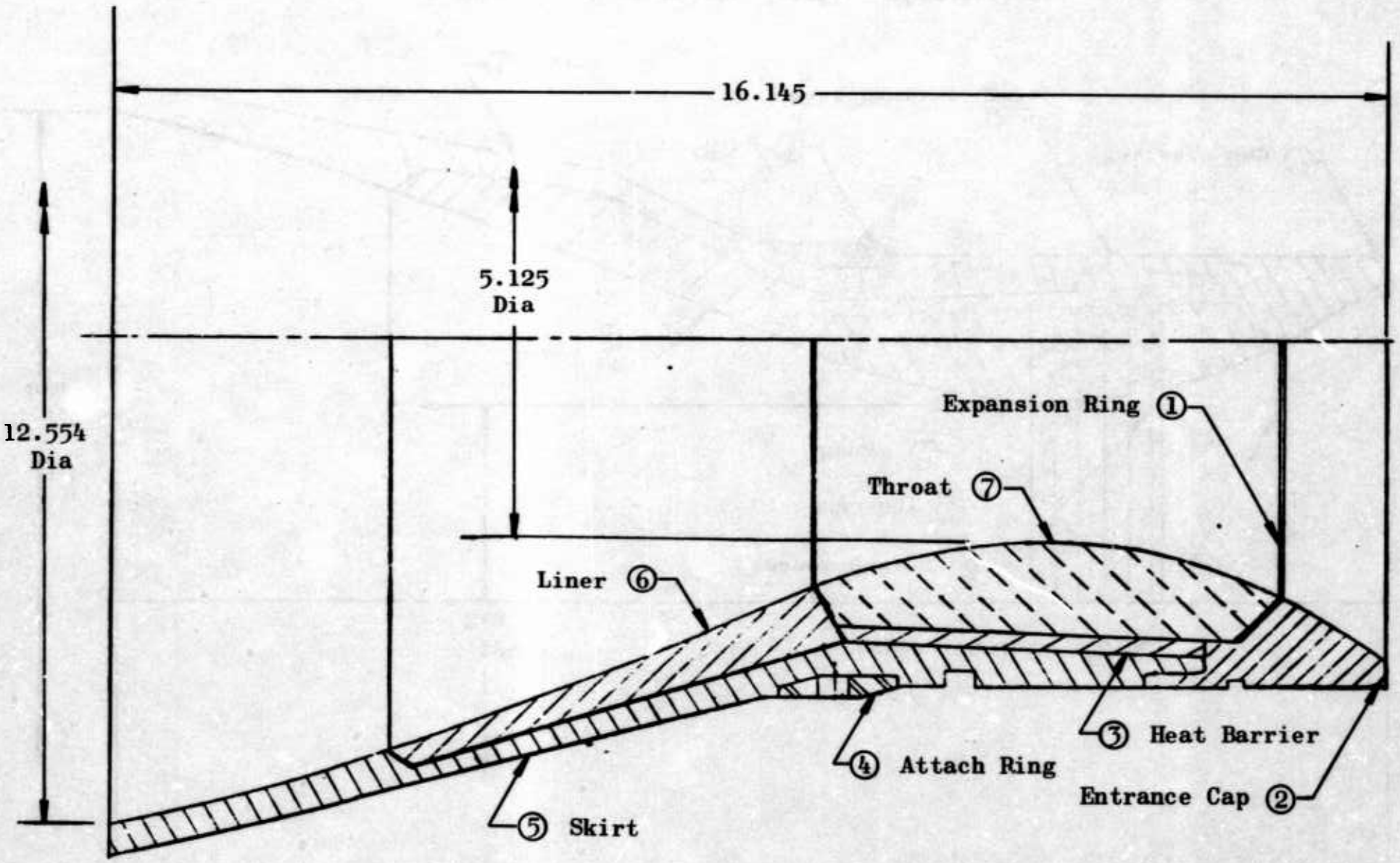


Figure 53. Flightweight Nozzle Configuration

CONFIDENTIAL

CONFIDENTIAL

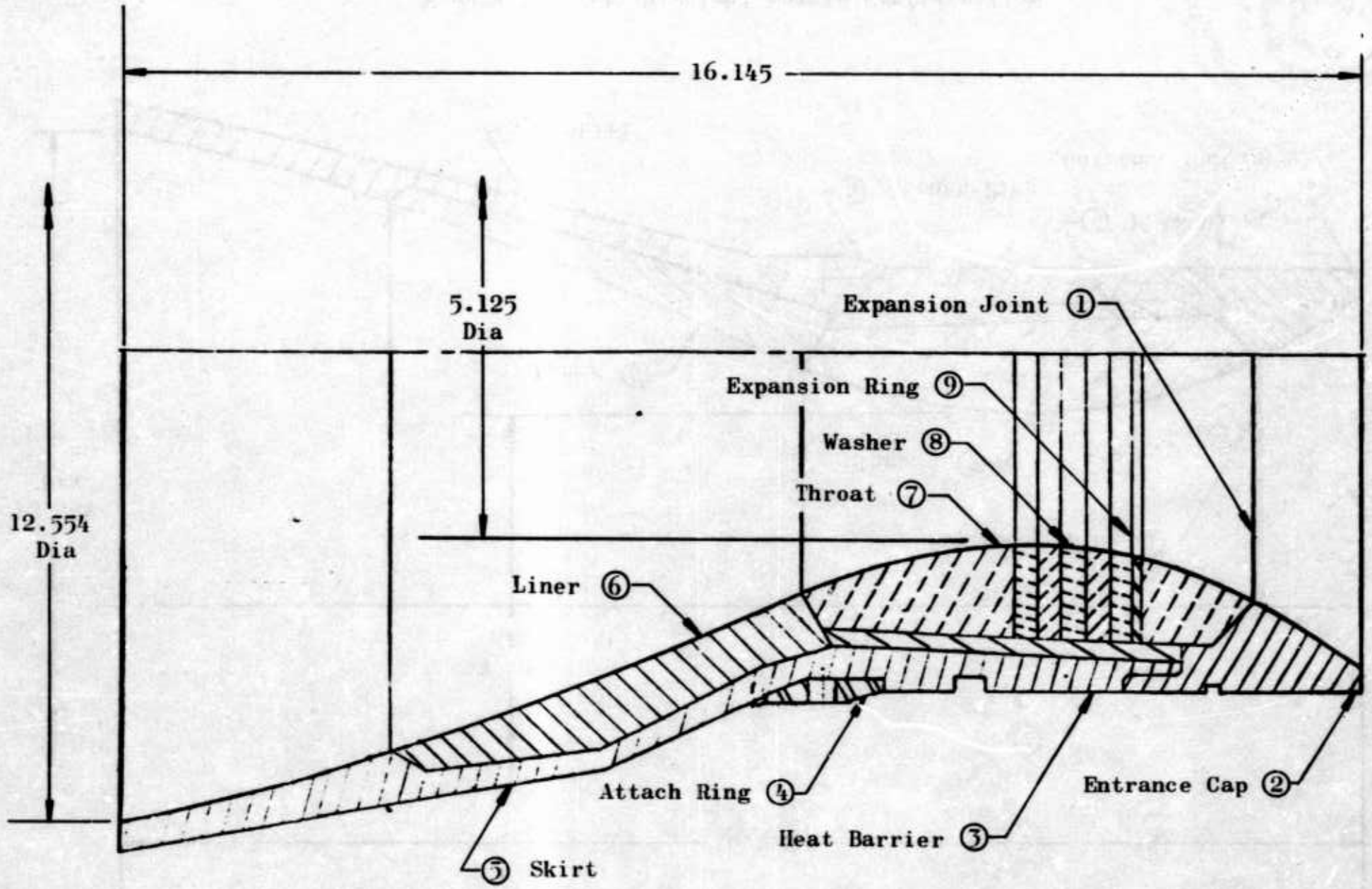


Figure 54. Heavyweight Nozzle Configuration With Composite Throat

CONFIDENTIAL

- Heat Barrier

The heat barrier in Motor A nozzle consists of two telescoping cones made from pyrolytic graphite.[12] It was necessary to fabricate this component from two cones because severe cracking and delamination occurs if the thickness-to-radius ratio is excessive.

The heat barrier's function is to protect the forward portion of the skirt from extreme heat during the latter stages of motor firing and, thereby, reduce its structural capability. Selection of this material was made because of its directional heat transfer properties and its very high mechanical properties at elevated temperatures. By utilizing the low heat transfer directional properties, the heat passing through the throat insert would be directed away from the skirt.

- Expansion Ring

The expansion ring is made from an AMS 3209 silicone rubber. Its function in the design is to prevent high compressive loads from occurring in the graphite throat or the entrance cap (because of thermal expansion during motor firing).

- Entrance Cap

This part transacts the turbulent flowing gases smoothly into the nozzle throat, thereby preventing severe erosion in this area. This component is fabricated from FM5128[13] graphite phenolic cloth, which is wrapped at a 45 degree angle with respect to the nozzle centerline. This provides better erosion resistance.

- Liner Cone

The liner functions as a protective insulator, from high velocity gases, for the nozzle skirt adjacent to the throat exit plane. The material used in this component is identical to that used in the entrance cap, and is wrapped at 30 degrees with respect to the nozzle centerline. Again this angle keeps the material edges perpendicular to the gas flow for better resistance to erosion.

---

[12] The deposition of graphite by the pyrolytic decomposition of carbonacious gases at low pressures on hot surfaces.

[13] A product of U.S. Polymeric Corp., Santa Ana, California.

○ Attachment Ring

The attachment ring is fabricated from 7075-T651 aluminum alloy. This ring contains the attachment pin holes, used for coupling the nozzle to the thrust unit, and allows the load to be evenly distributed into the nozzle skirt. Secondly, it provides additional hoop restraint at the area just aft of the throat section.

○ Nozzle Skirt

The nozzle skirt functions as the main structural component in this nozzle design. It is used to retain the aluminum attachment ring in place, thus transferring all nozzle loads developed in the motor firing. Additionally, it serves as an ablative material in the exit cone aft of the liner. This skirt is fabricated from FM5067[14] a high silica reinforced phenolic tape.

○ Pyrolytic Graphite Washer

The washer illustrated in Fig. 54 (heavyweight nozzle) was selected for use as an erosion resistant throat material, primarily based upon a requirement for evaluation of this material for subsequent use in the Motor B nozzle throat.

○ Material Properties

The mechanical and thermal properties of all materials utilized in the Motor A nozzle are listed in Table XXIII. Stress calculations performed on nozzle components indicate the pin bearing load on the attachment ring represents the stress condition with the lowest margin of safety. A positive margin of 0.64 is the calculated value for this component.

(c) Thermal Analysis

(C) A detailed two-part thermal analysis was performed on the nozzle. First with a combustion temperature of 5725 F for 10.5 seconds (corresponding to burning of the core grain), and second with a combustion temperature of 6325 F for 20.5 seconds (corresponding to combustion of the RFG).

(14) A product of U.S. Polymeric Corp., Santa Ana, California

TABLE XXIII

MATERIAL PROPERTIES

Material	Tensile Strength, psi	Coef Ther Expan 10^{-6} in./in./deg F	Density gm/cm^3
Graph-I-Tite G	2900	0.90	1.87
Pyrolytic Graphite (1)	650 @ 1000 F (c Direction)	10.0 @ 1000 F (c Direction)	2.18
	14,000 @ 1000 F (a Direction)	5.0 @ 1000 F (a Direction)	
FM 5128	8500	6.6	1.48
FM 5067	14,000	3.0	1.76
Alluminum Alloy 7075-T651	83,000	13.1	2.76
AMS 3209 (2)	1700	670.0	1.25

(1) A Direction is Plane of Disposition; c Direction is Normal to Plane of Disposition.

(2) Synthetic Rubber

The results of the analysis as discussed below considered the ablation loss, corrosion loss, and the temperature distribution.

- Ablation Loss and Char Depth

The ablation loss vs time and the ablation loss and char depth of the nozzle materials at the end of firing are shown in Figs. 55 and 56. All ablation of the nozzle occurs in the FM5128, a graphite phenolic material located just forward and aft of the graphite insert. The second aft of the graphite insert loses a maximum of 0.10 inch and decreased to zero loss at a point 3.50 inches downstream of the nozzle insert.

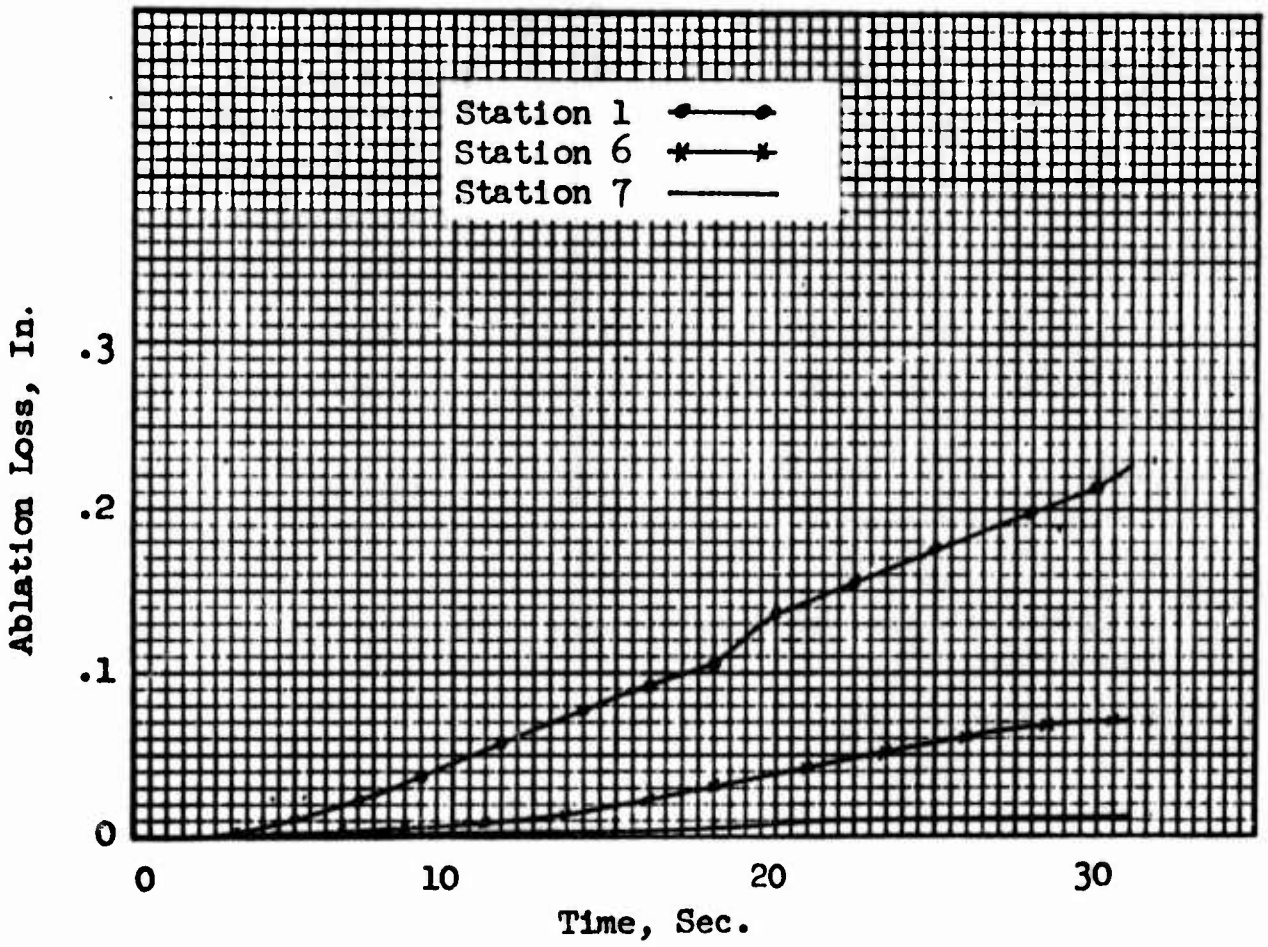
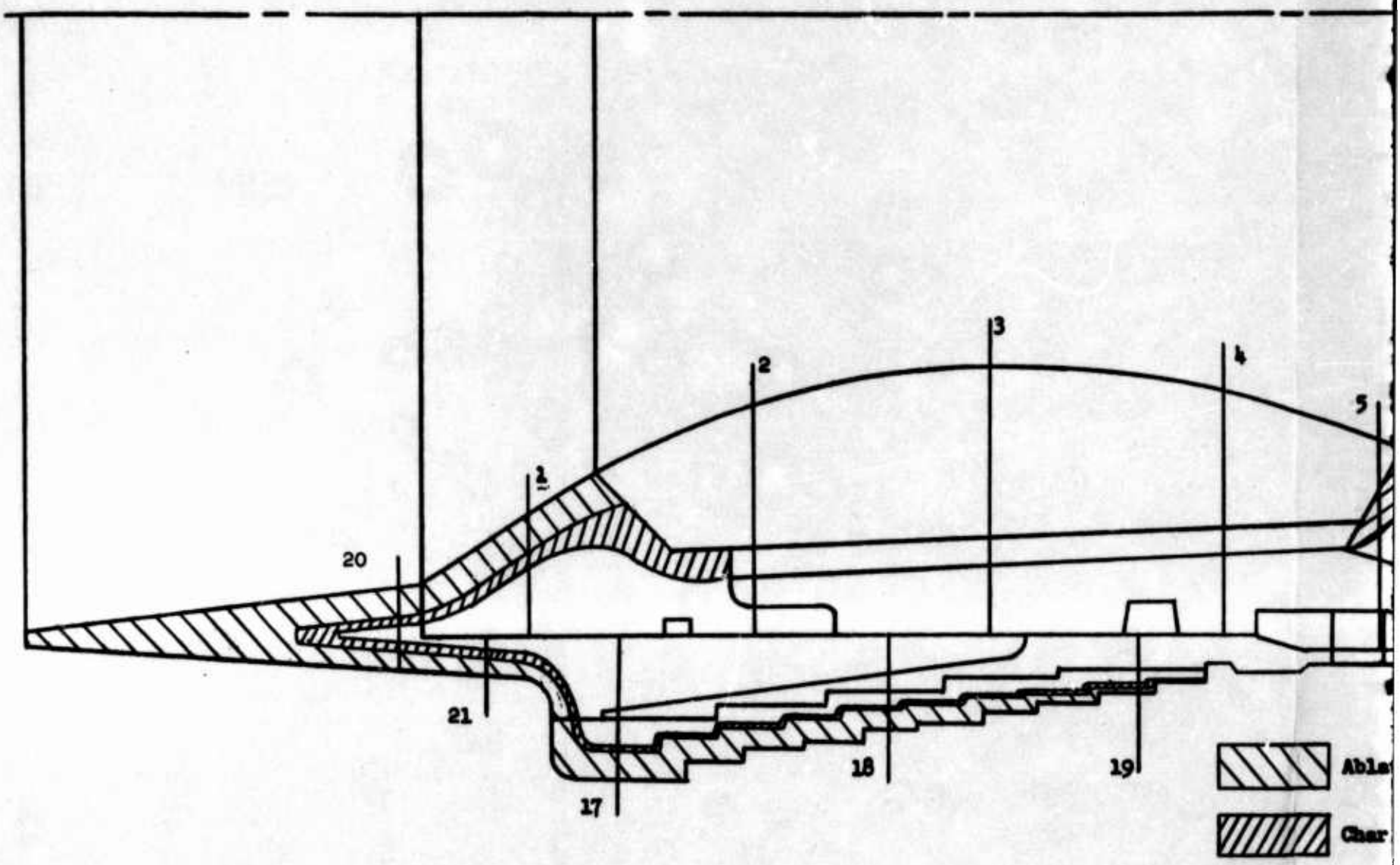


Figure 55. Predicted Ablation Loss vs Time for Nozzle Stations


13
3
4
2
5
1
20
21
18
19
17
Ablat
Char

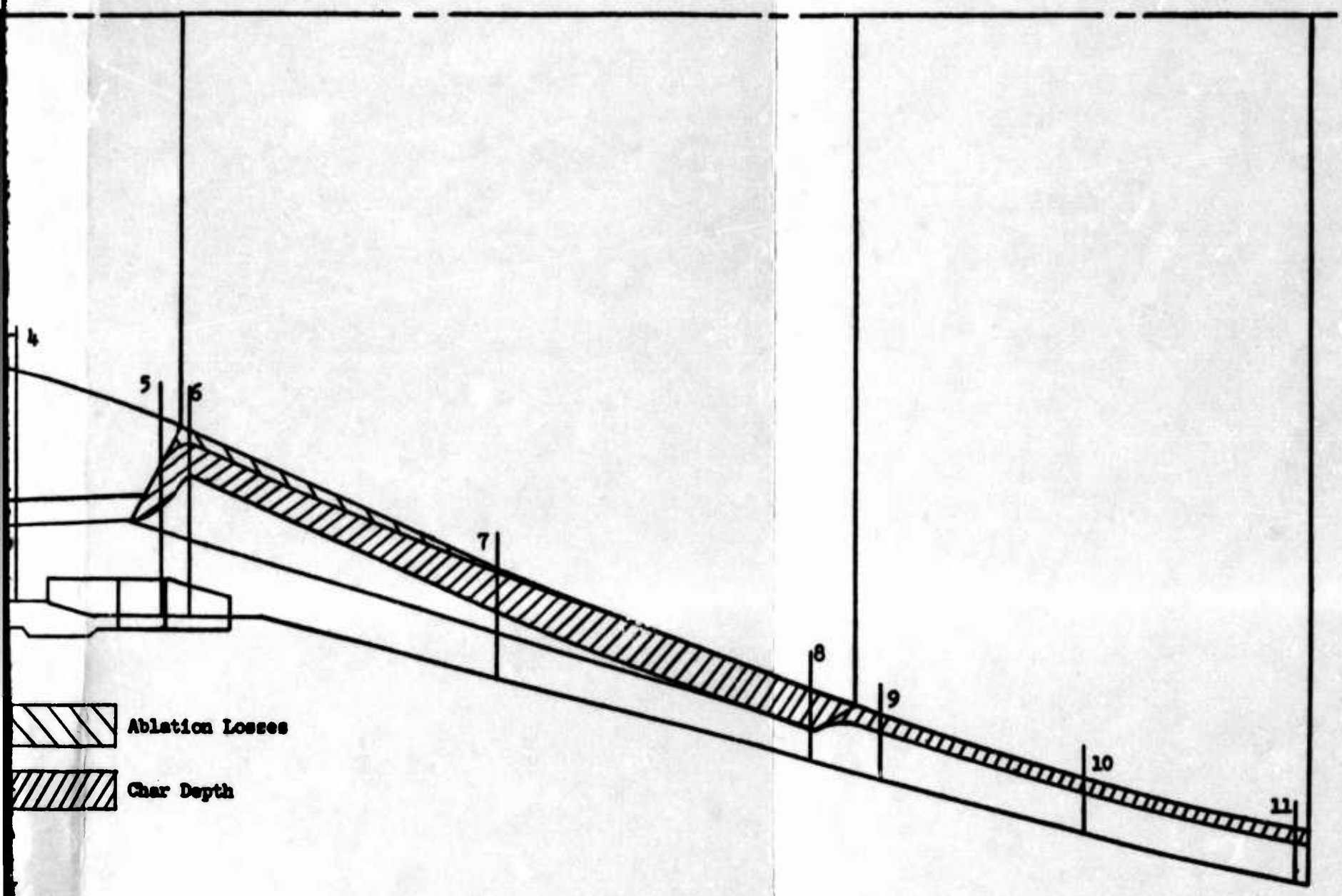


Figure 56. Predicted Ablation Losses and Char Depth of the Aft Polar Boss and Nozzle at the End of Firing

CONFIDENTIAL

PREVIOUS PAGE WAS BLANK, THEREFORE WAS NOT FILMED

The char depth of the FM5128 material in the entrance section is 0.10 inch for three-fourths of the length of the section. The char depth then dips down to a depth of 0.22 inch following the contour of the graphite insert until it intersects the pyrolytic graphite section. In the aft section of this material the char starts at the bottom of the pyrolytic graphite and rises rapidly to a depth of 0.24 inch and increases to a depth of 0.28 inch at the downstream end. The remaining portion of the nozzle, made of FM5067 silica phenolic, has a char depth of 0.10 inch just aft of the FM5128 and decreases to 0.08 inch at the nozzle exit.

○ Temperature Distribution

The nozzle temperature distribution at the end of firing is shown in Figs. 57 through 59. All bonding surfaces are below 1000 F with the exception of the pyrolytic graphite-to-Graph-I-Tite G graphite insert and the Graph-I-Tite G-to-FM5128.

The temperature history of bond surface between the pyrolytic graphite and Graph-I-Tite G graphite at sections 2, 3, and 4 are shown in Fig. 57. Figure 58 shows the bond surface temperature history for the Graph-I-Tite G-graphite-to-FM5128 bond.

It is easily seen from Figs. 57 and 58 that after 5.50 seconds the Graph-I-Tite G graphite insert must have sufficient bearing area on the pyrolytic graphite to withstand its loads. The interface between the nozzle and the aft forward polar boss is 70 F except for the entrance portion which reaches a maximum of 73.2 F.

○ Corrosion Loss

(C) The corrosion loss of the Graph-I-Tite G graphite insert was calculated and found to be very small. The entrance region of the insert will have an increase in diameter of 0.112 inch. The magnitude of the diametrical increase progresses to a maximum of 0.13 inch at the throat, as seen in Fig. 60, and then decreases to 0.088 inch at the exit of the insert. The loss at the throat represents an area increase of 5.14% or 1.16 square inches.

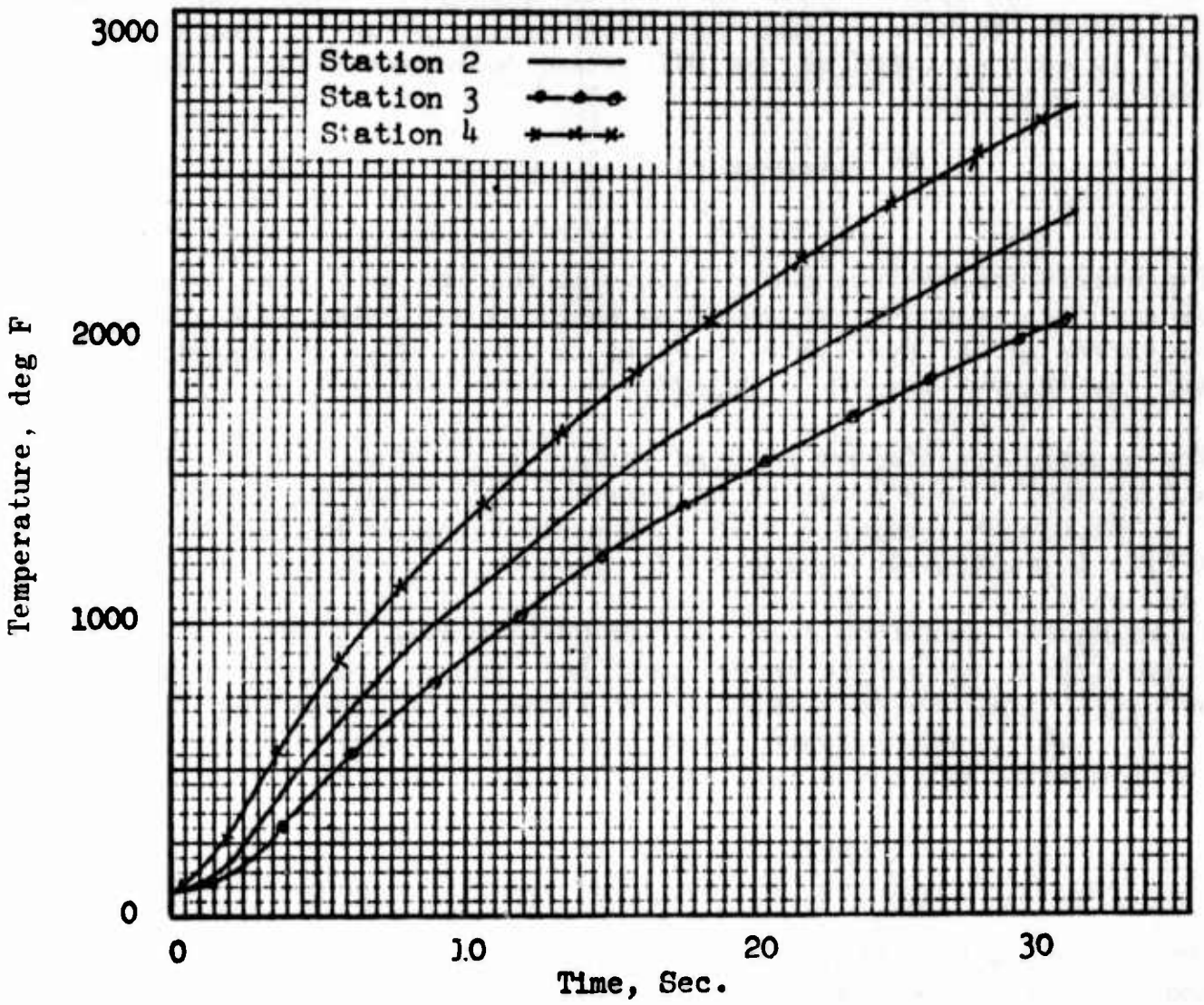


Figure 57. Predicted Bond Line Temperature vs Time Between 101-Graphite and EM5067

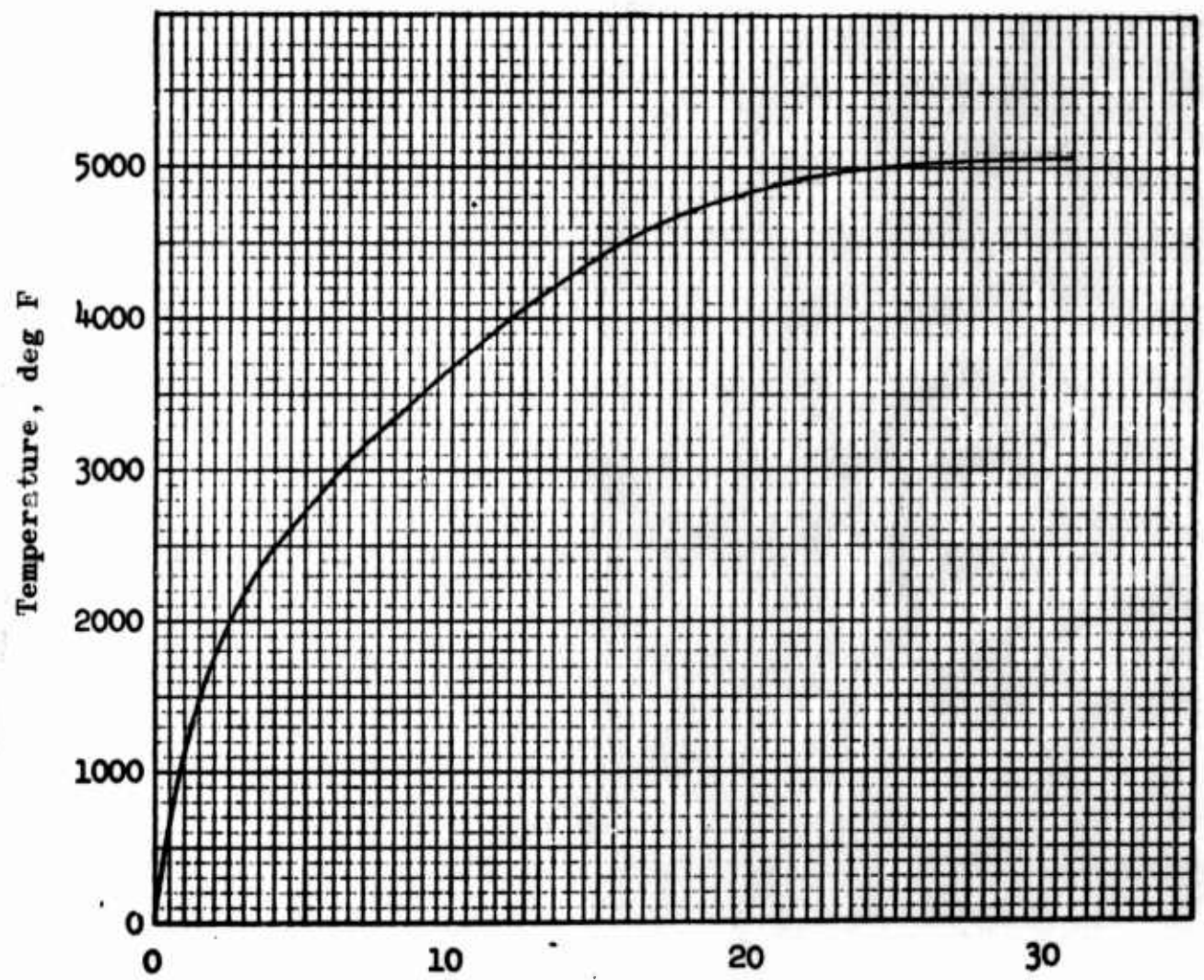
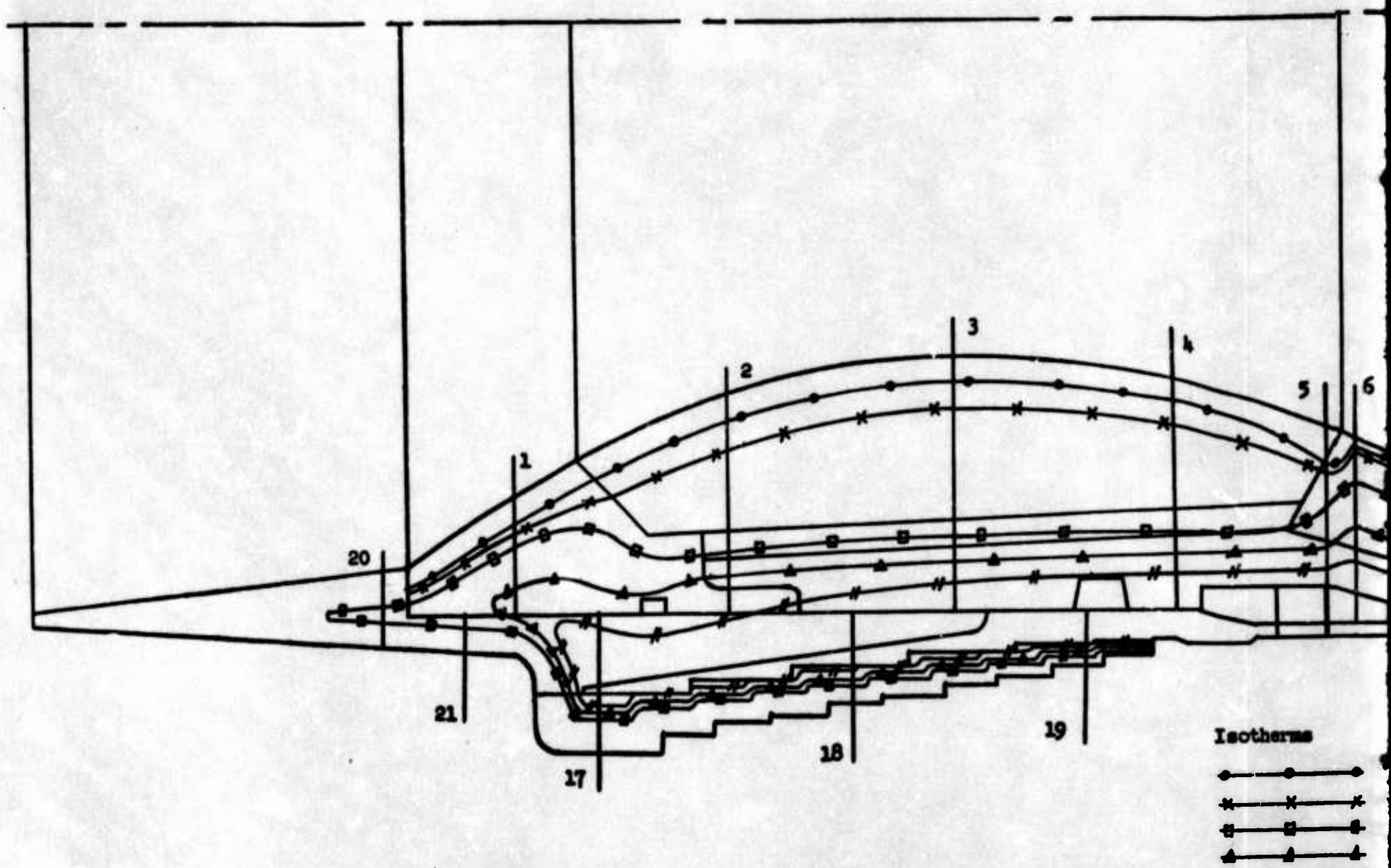


Figure 58. Predicted Bond Line Temperature vs Time at Nozzle Station 5

PREVIOUS PAGE WAS BLANK, THEREFORE WAS NOT FILMED



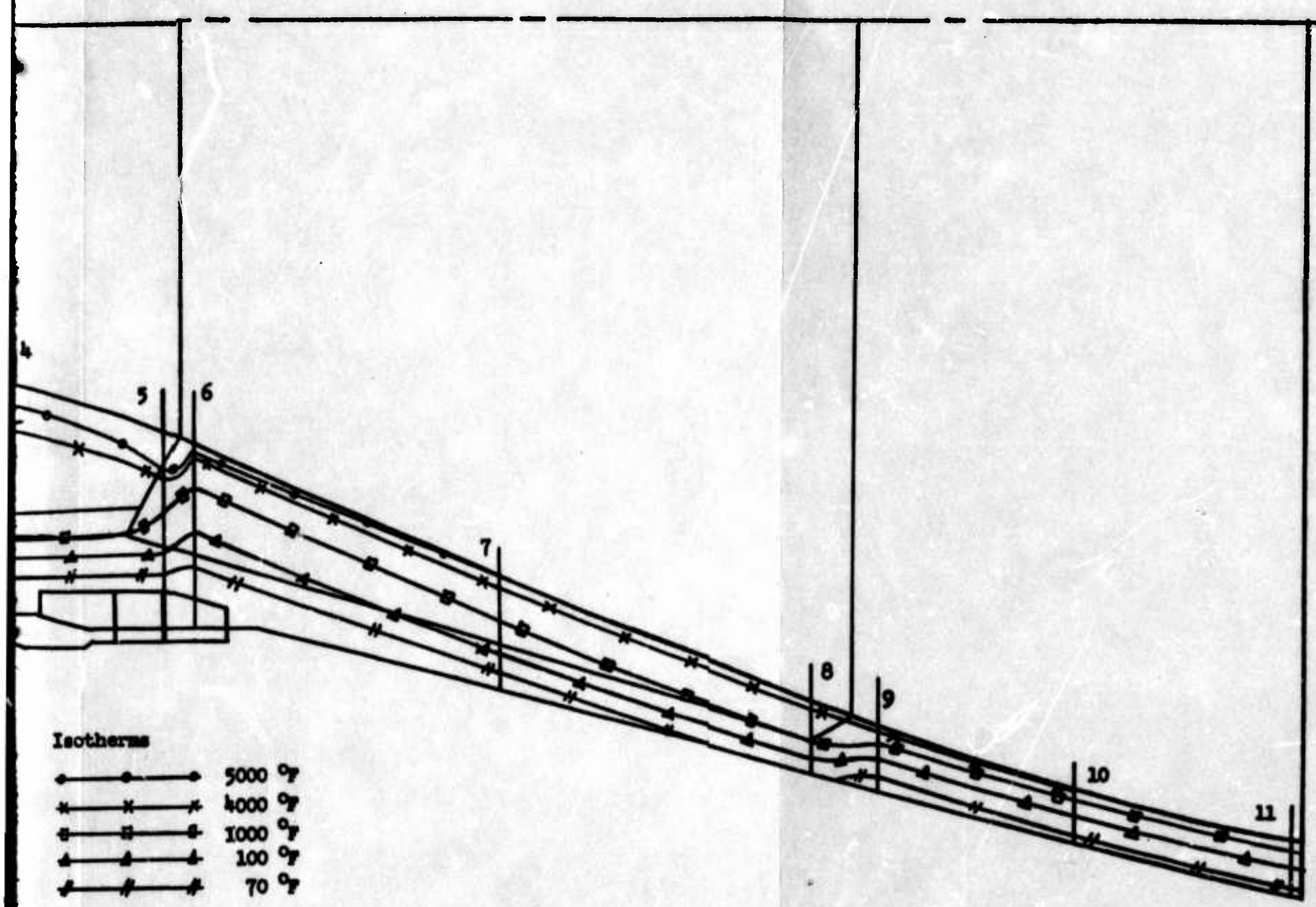


Figure 59. Predicted Aft Polar Boss and Nozzle Temperature Distribution at End of Firing

2

PREVIOUS PAGE WAS BLANK, THEREFORE WAS NOT FILMED

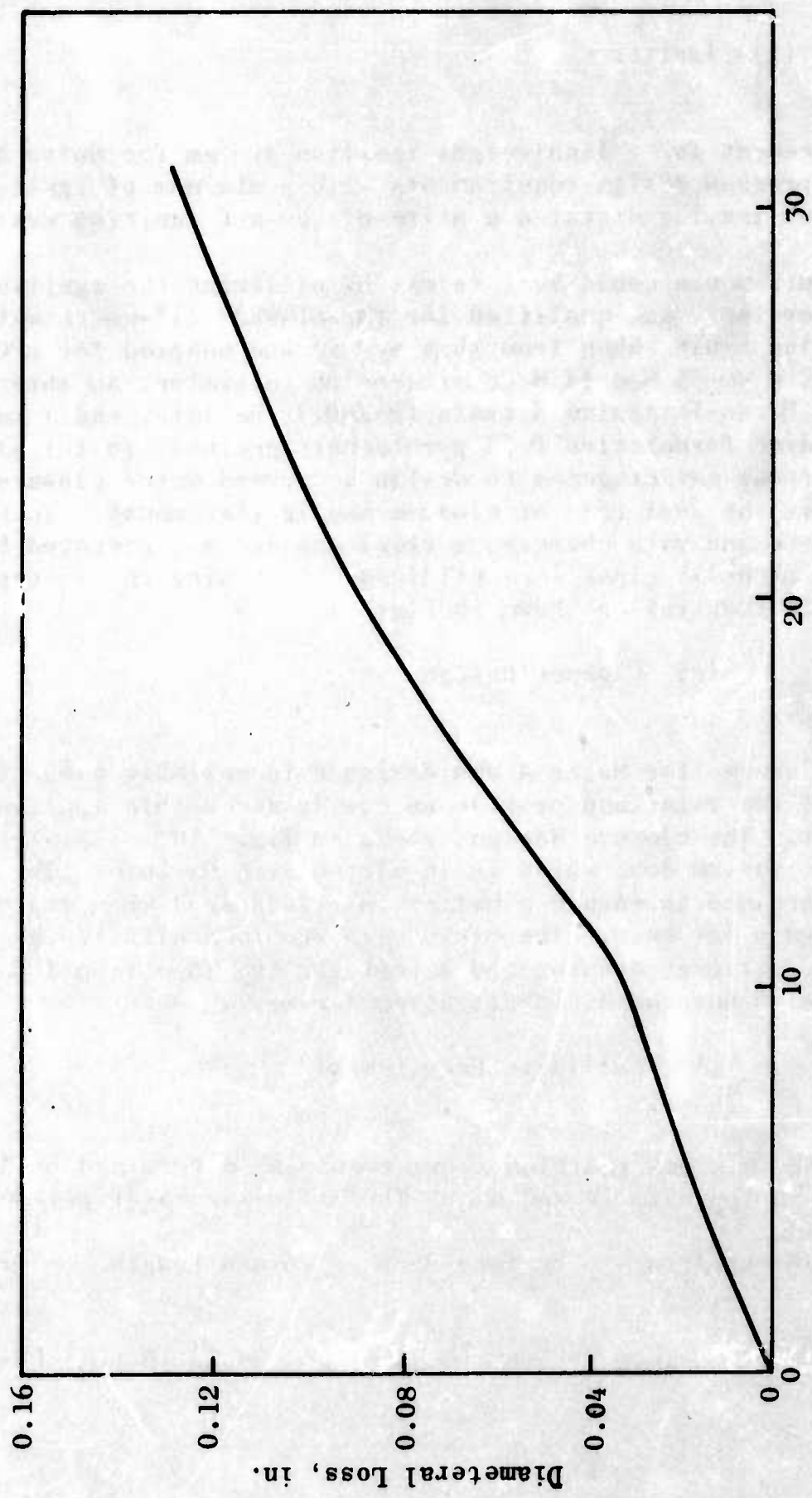


Figure 60. Predicted Corrosion Loss-vs-Time
Nozzle Station 3 (Throat)

(4) Igniter

The requirement for a lightweight ignition system for Motor A which could meet all program design requirements with a minimum of igniter and motor development testing dictated a state-of-the-art ignition system.

These requirements could best be met by utilizing the ignition system concept developed and qualified for the SPARROW III-6b rocket motor. The ignition train taken from this system and adapted for RFG use is made up of a Wm-55 Mod IX McCormick-Selph initiator, an intermediate charge of Boron-Potassium Nitrate (B-KNO_3), pellets, and a main charge of Rocketdyne formulation P-73 pyrotechnic grains. To further minimize weight, it was advantageous to design a forward motor closure which would serve the dual role of closure and igniter mount. To retain the intermediate and main charges, a steel cup and a perforated basket of laminated phenolic glass were utilized. Combining these components resulted in the igniter shown in Fig. 61.

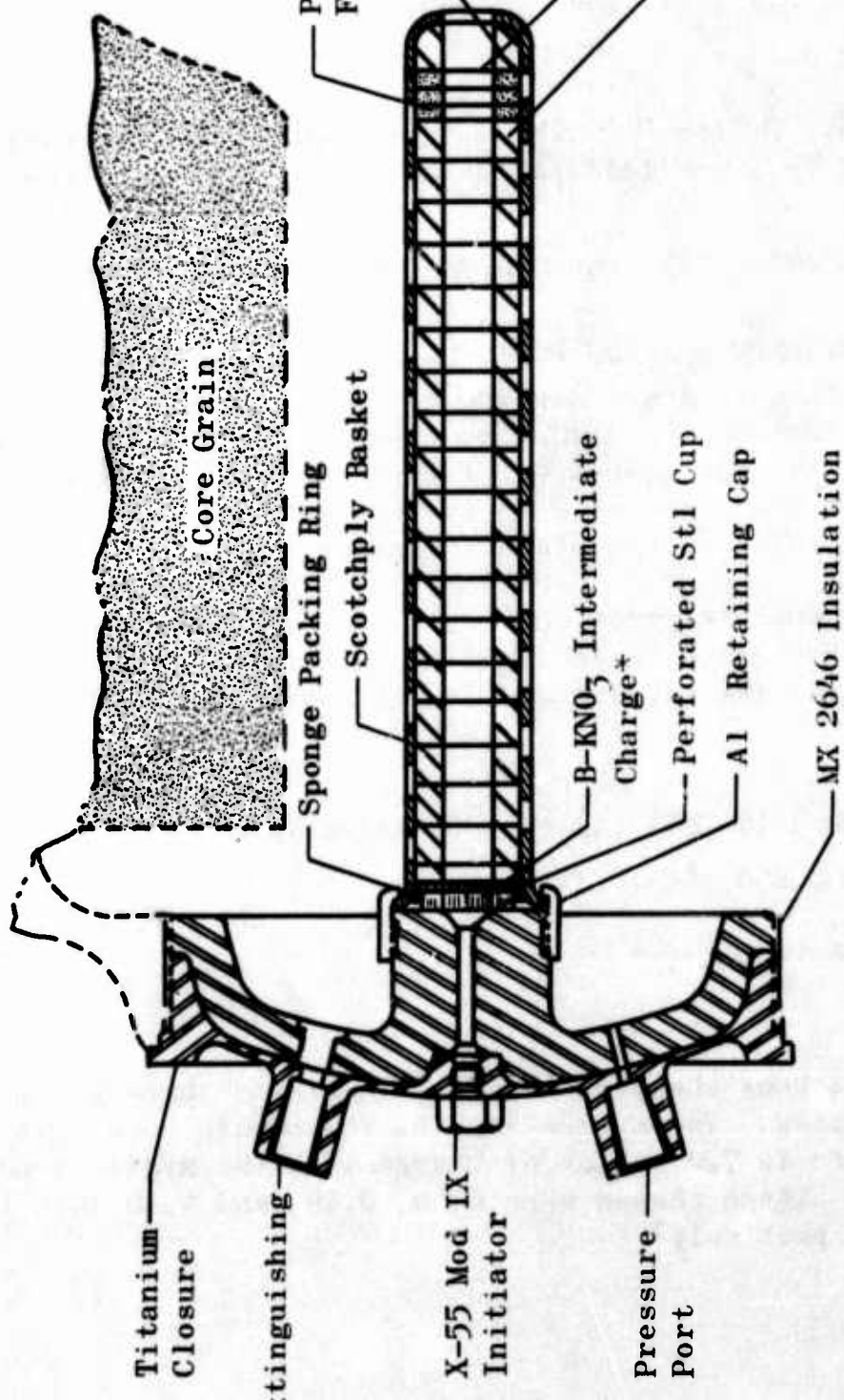
(a) Closure Design

The end closure for Motor A was designed to reliably close the forward opening of the motor and provide an easily accessible ignition attachment point. The closure design, shown in Fig. 10, consists of a threaded titanium dome which is insulated with MX-2646. The insulation is also threaded to ensure a better interface seal when installed in the forward polar boss. The closure is provided with two pressure ports, an initiator opening and a port for CO_2 injection (CO_2 is used to extinguish burning of inerts after firing.).

(b) Ballistic Requirements

(C) Based on the minimum ignition requirements as determined by the method presented in Appendix IV and using the following motor parameters,

Motor	Throat Area, A_t	Surface Area, A_s	Grain Length, L_g	Port Area, A_p
A	20.63 sq in.	3862 sq in.	58.72 in.	51.78 sq in.



*Double row of pellets for motor A-1004
**Material change to silicone for A-1004

Figure 61. Motor A Igniter

(C) The required charge weights were calculated as follows:

$$\text{Motor A: } Q = K\ (A_s)^{0.435}\ (L_g)^{0.625}\ (A_p)^{0.313}$$

$$K(3862)^{0.435}\ (58.72)^{0.625}\ (51.78)^{0.313}$$

$$K(36.7)\ (12.75)\ (3.445)$$

$$K(617)$$

From Fig. 1 of Appendix E, for P-73 the weight required = 210 grams. Thus, if 250 grams of P-73 are used in the igniter, it is seen that:

$$\frac{250 - 210}{210} \times 100 = 19\% \text{ over minimum required for Motor A}$$

It was found in the SPARROW program that the ratio of the igniter basket open area to the pyrotechnic grain surface area, referred to hereafter as K ratio, was very important in ignition shock. Thus, a design study was made to determine the configuration of pyrotechnic charges which would consist of about 250 grams of P-73 and would allow K ratios on the same order as the ratio of the SPARROW igniter.

(C) The dimensions of the annular pyrotechnic grains investigated were 1-inch OD x 0.50-inch ID x grain length. With a density of 0.130 lb/cu in. and these diameters, the total grain length required to obtain 250 grams is:

$$(1.0^2 - 0.50^2)\ (0.785)\ (\ell)\ (0.130)\ \text{lb/cu in.}$$

$$(454)\ \text{gm/lb} \approx 250$$

$$34.7\ \ell = 250$$

$$\ell = 7.2 \text{ in.}$$

To vary the K ratio without changing basket parameters, three grain lengths were investigated. These were lengths that would result in a whole number of pellets in 7.2-inches of charge with the middle length being about 0.5-inch. Those chosen were 0.40, 0.48, and 0.60 inch (18, 15, and 12 grains, respectively).

To obtain a K factor ratio equal to the SPARROW igniter value, the following was examined:

$$\text{SPARROW K factor} = \frac{\text{Basket Open Area}}{\text{Grain Surface Area}}$$

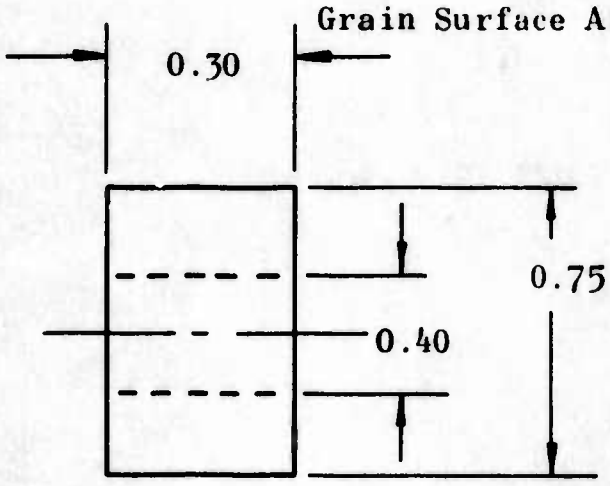
Sixty 0.25-inch diameter holes plus one 0.5-inch diameter hole in a basket provides an open area

$$= 60\ (1/4)^2\ (0.785) + (1/2)^2\ 0.785$$

$$= \{3.75 + 0.25\}\ 0.785$$

$$= \{4\}\ 0.785$$

$$= 3.140 \text{ sq in.}$$



$$\text{Grain Surface Area} = \{0.75\pi + 0.4\pi\}\ 0.3 \times 20 +$$

$$\{0.75^2 - 0.4^2\}\{0.785 \times 2 \times 20\}$$

$$= \{1.15\pi\}\ 6 - \{0.441 - 0.126\}\ 40$$

$$= 6.9\pi + 0.315 \times 40$$

$$= 21.65 + 12.60$$

$$= 34.25 \text{ sq in.}$$

$$K = \frac{3.14}{34.25} = 0.0915$$

To match this K value in the RFG ignition system, the following basket parameters were established:

1. 0.50-inch diameter opening in the aft end of basket
2. 6 rows of perforations down the basket

3. 10 perforations on each row for a total of 60 holes down basket (a)
4. Perforations should be spread out to assure holes over at least the 7.2-inch length of the charge.

Thus, basket open area in equation form is:

$$A = (0.5)^2\ 0.785 + 60\ (d)^2\ 0.785 = 0.196 + 47.1\ d^2$$

Where d is equal to perforation diameter

For the nominal grain length of 0.48 inch, the total grain surface area is:

$$(1^2 - 0.5^2)\ 0.785\ (2) + (\lambda 0.5\pi + 1.0\pi)\ 0.48 = \quad \text{(b)}$$

$$(0.785 - 0.196)2 + (1.5\pi)\ 0.48 =$$

$$(0.589)2 + 2.26 =$$

$$1.178 + 2.26 =$$

$$3.438 \text{ sq in./grain}$$

For 15 grain $A_S = (15)\ (3.438) = 51.5$ sq in.

$$K = 0.0915 = \frac{0.196 + 47.1\ d^2}{51.5}$$

$$d = 0.3097$$

Use d = 0.312

The resulting K value is:

$$K = \frac{0.196 + 47.1\ (0.312)^2}{51.5} = \frac{0.196 + 4.58}{51.5} = \frac{4.776}{51.5} \quad \text{(c)}$$

$$K = 0.0927$$

for 0.48-inch length grains

For 0.4-inch length grains:

$$A_{S\ 1\ grain} = 2(1^2 - 0.5^2)\ 0.785 + (1.0_{\Pi} + 0.5\pi)\ 0.4$$

$$= (0.785 - 0.196)2 + 1.5\pi\ (0.4) = 1.178 + 1.88$$

$$= 3.058 \text{ in./grain}$$

$$A_{S\ Total} = (3.058)\ (18) = 55 \text{ sq in.}$$

$$K = \frac{4.776}{55} = 0.0868$$

for 0.4 inch grains

For 0.6 inch length grains:

$$A_{S\ Total} = 12\ \{1.178 + 1.5\ (0.6)\} = 12\ \{1.178 + 2.835\}$$

$$= 12\ (4.013)$$

$$= 48.1 \text{ sq in.}$$

$$K = \frac{4.776}{48.1} = 0.0993$$

for 0.6 inch grains

(c) Test Program

The proposed igniter development test program consisted of 10 igniters. The first six scheduled tests were to examine the effects of K factor variation on igniter ballistic performance. Of the four remaining igniters, two were scheduled for environmental testing and two were placed in reserve for final design confirmation testing, considering the Motor B' ignition requirements.

The initial six development igniters were fired 13 September 1963. These tests investigated the relative variation in energy release rate which is associated with the variation in pyrotechnic burning surface. This was accomplished by holding the charge weight and perforated basket open area constant and varying the pyrotechnic grain length. Two each of igniters with grain length of 0.40, 0.48, and 0.60 inch were fired. The firings were conducted in Rocketdyne chamber number FF-T-891-102, which has a chamber volume of 2185 cu in. The pressure-time replots of these firings are presented in Figs. 62 through 67 (replots of TO 8001 through TO 8006 firings). Table XXIV is a summary of the prefiring and firing characteristics. These six tests gave confidence in the design to provide the 0.100 second ignition requirement for Motor A by using the 0.6 length pellets. Results of the developed design are presented under the full-scale motor tests.

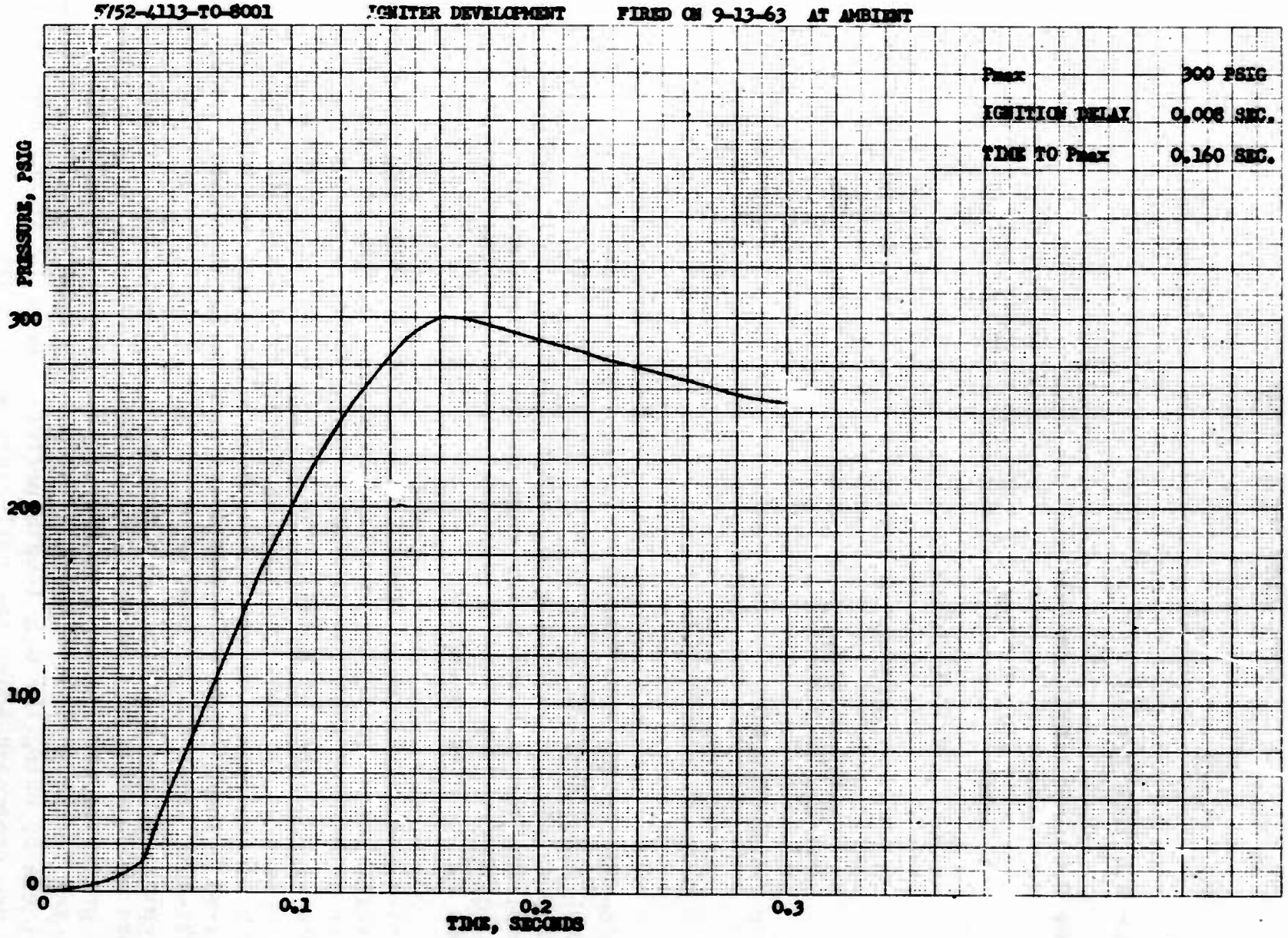


Figure 62. Igniter Development, TO 8001

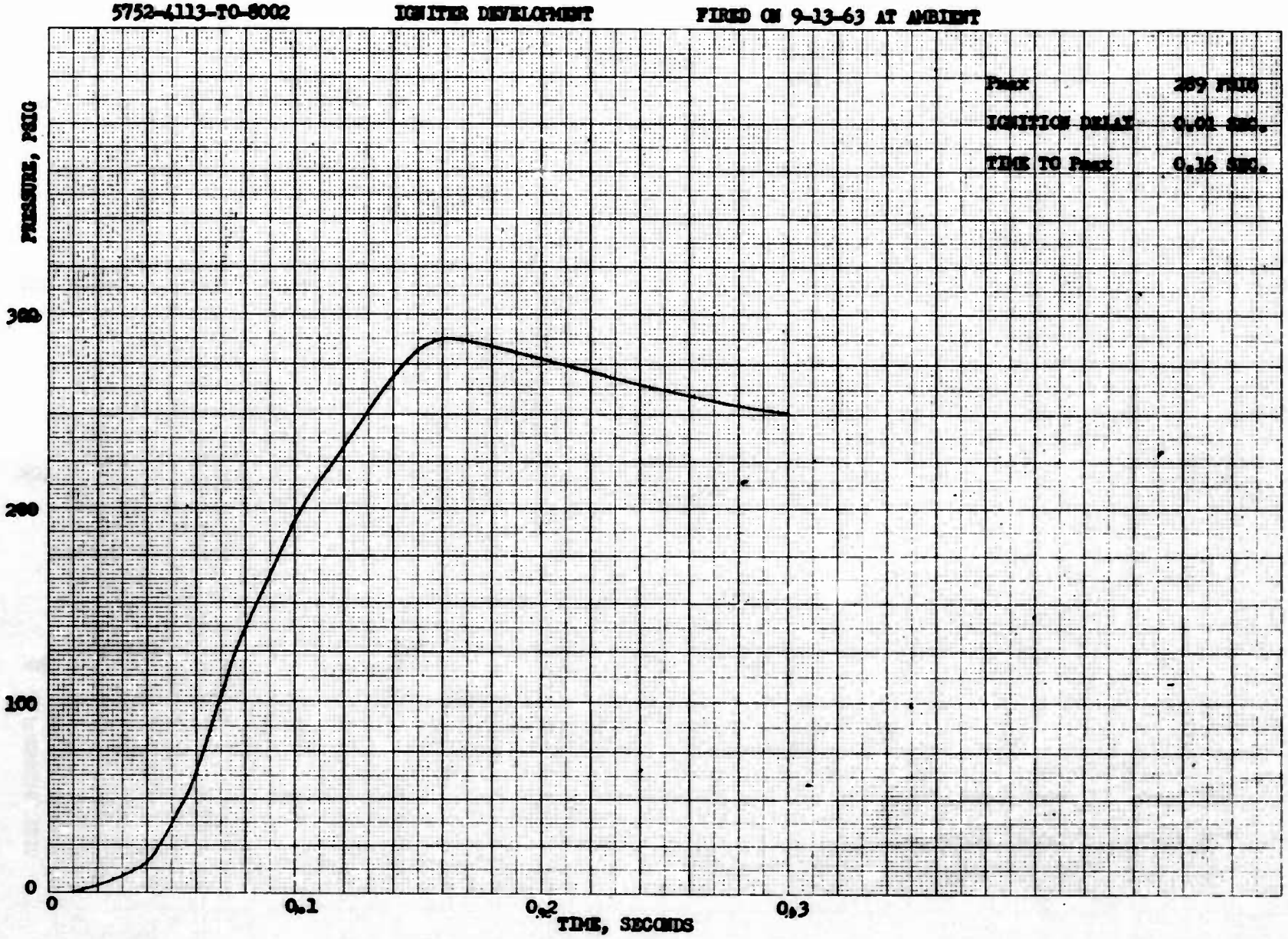


Figure 63. Igniter Development, TO 8002

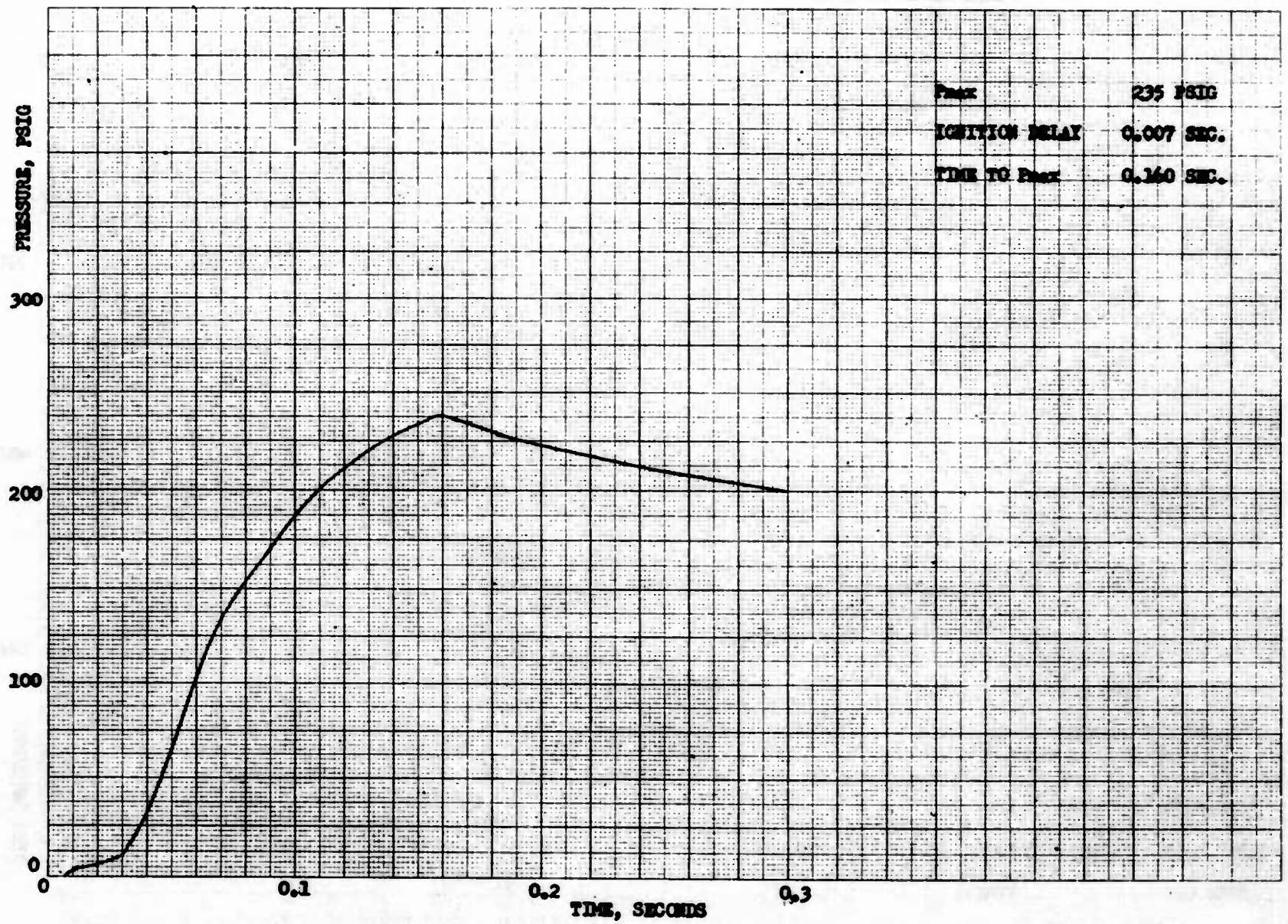


Figure 64. Igniter Development, TO 8003

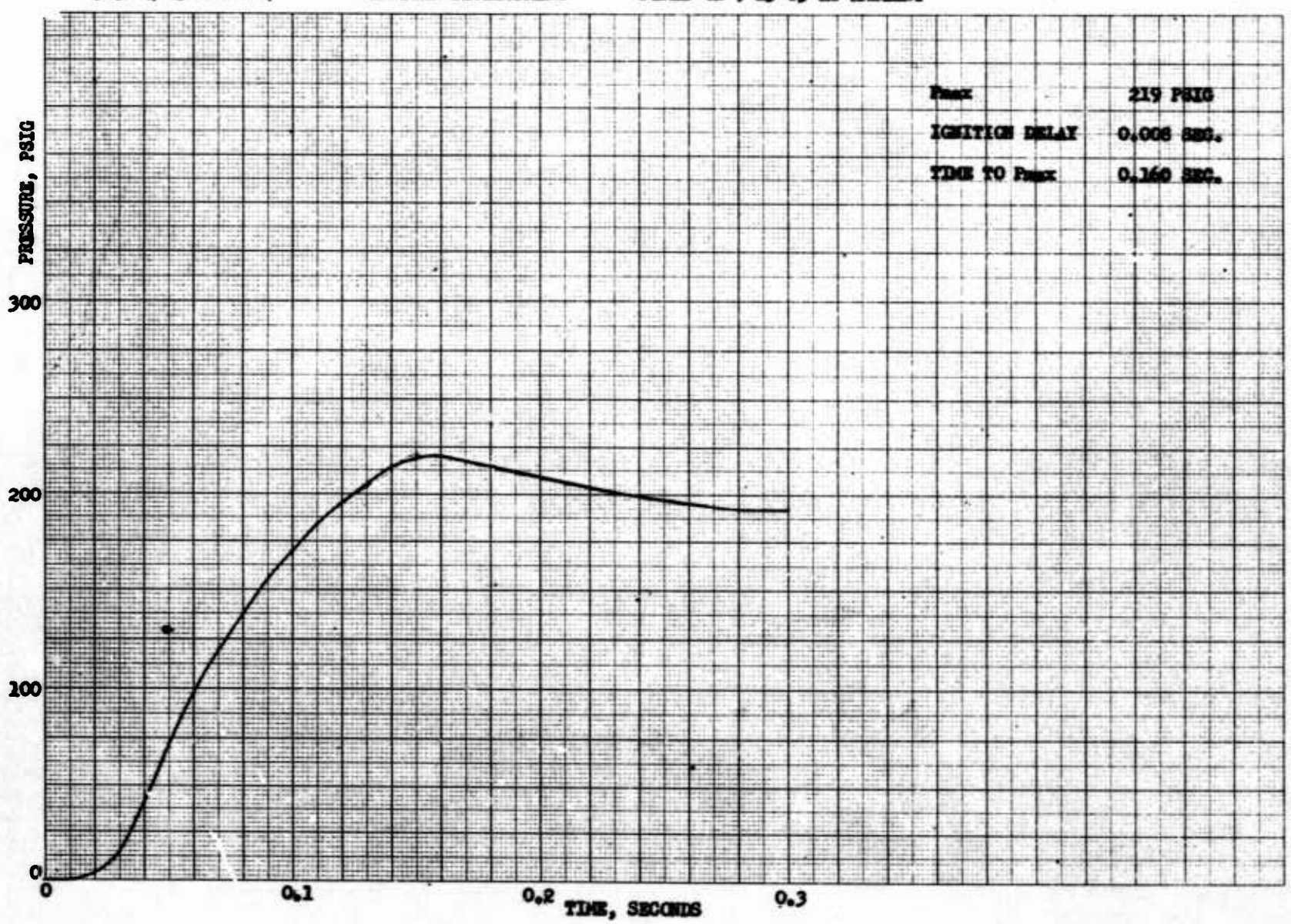


Figure 65. Igniter Development, TO 8004

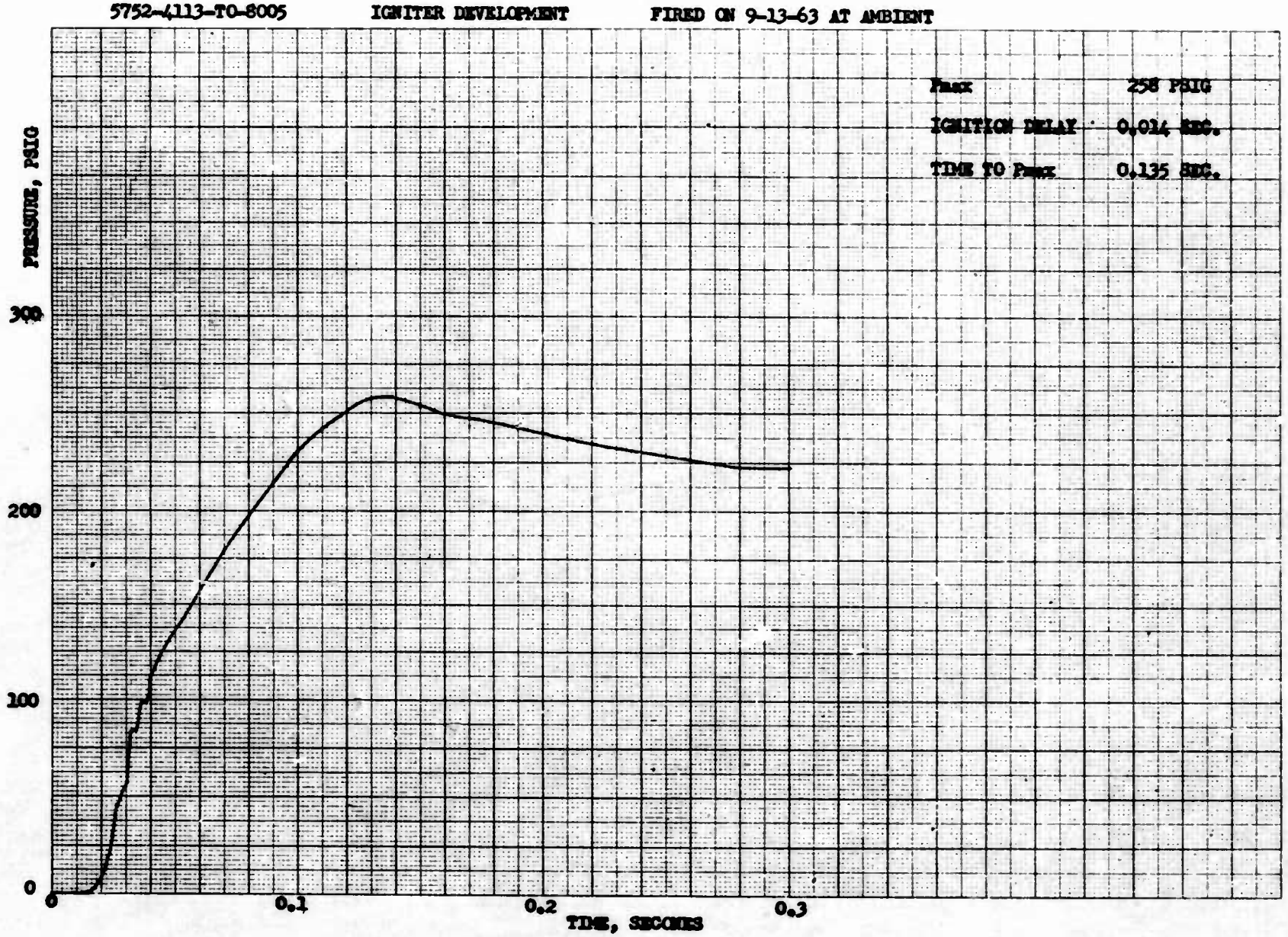


Figure 66. Igniter Development, TO 8005

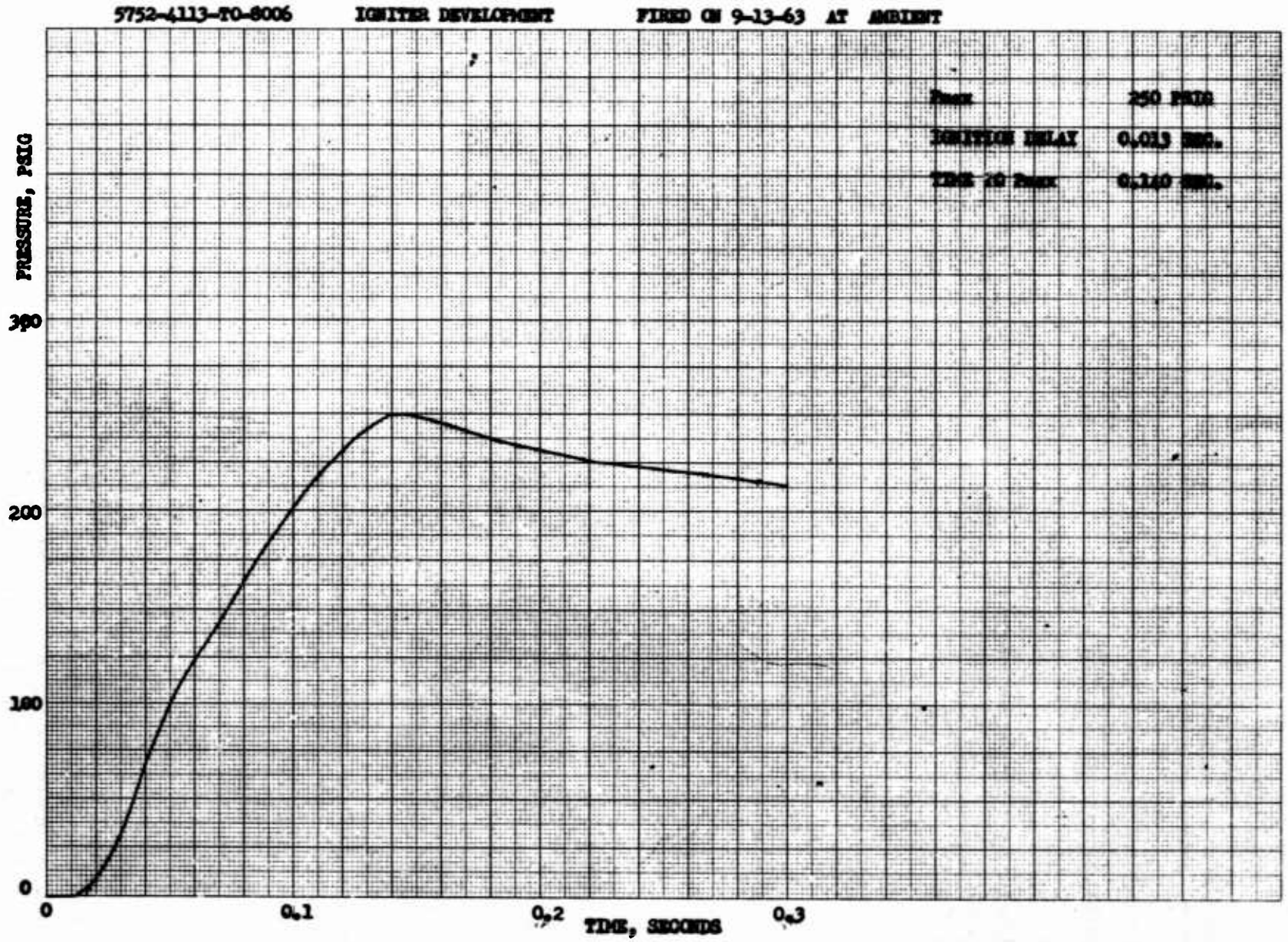


Figure 67. Igniter Development, TO 8006

TABLE XXIV

DEVELOPMENT IGNITER PREFIRING AND FIRING CHARACTERISTICS

Grain Length	0.400 Inch		0.480 Inch		0.600 Inch	
Charge Assembly Drawing	99-802107		99-802107-11		99-802107-21	
Test Order	8003	8004	8005	8006	8001	8002
Calculated Charge Weight Based on Average Densities and Grain Sizes (gms)	245	245	250	250	256	256
Igniter Conditioning Temp, deg F	70	70	70	70	70	70
P_{max}, psig	235	219	258	250	300	289
Time to P_{max}, ms	160	160	135	140	160	160

(5) Restrictors

Early development RFG grains were manually restricted on the outer diameter using R-140 (a Rocketdyne restrictor formulation containing polybutadiene polyme reinforced with carbon black) and loaded into oversize steel cases. When fiberglass case development began, the R-140 surface was found to be too soft and uneven for fiber winding. A new restrictor, R-143, and an improved application technique were developed. This restrictor is thixotropic, viscous enough not to run when applied in thicknesses up to 0.060 inch, yet sufficiently fluid to be stripped onto a rotating grain. It cures to a Shore A Hardness of greater than 50 which is ideal for glass winding. R-143 contains a Butarez base which is compatible with Flexadyne propellant. A smooth surface and controlled thickness is obtained by the use of a restrictor template held stationary while the grain is rotated.

R-143 is similar to R-140 but contains more carbon reinforcement and a trimer acid which almost doubles its carboxy content. A high MAPO (methyl aziridinyl phosphine oxide) content keeps its viscosity in an easily processible range. Good bonds are developed between cured Flexadyne propellants and uncured R-143. Glass reinforced epoxy resins bond well to air-cured surfaces of R-143 provided the surface is thoroughly cleaned with toluene. Normal minimum properties of R-143 are:

Ultimate elongation	150%
Ultimate tensile strength	400 psi
Shore A Hardness	50
Tear strength	25 lb/in.
Density	0.0357 lb/cu in.

(C) The formulation is:

	Wt, %
Butarez CTL, Type II	73.53
Emery Trimer Acid 3162-D	7.35
Acetylene Black	14.71
MAPO	4.41
	100.00

d. Process Development

(1) Reinforced Grain Fabrication Techniques

This section includes a review of the early fabrication efforts and the development of the improved multi-helix angle concept stressing the factors that are important to grain fabrication design. These factors consist of layer thickness, pattern selection, gear ratio determination, weight and volume fractions, and effects of winding variables on build-up. In addition, a summary of the fabrication development for Motor A is presented.

A description of the winding machines used on the program for the 36- and 40-inch machines is presented in Appendix V. A glossary of RFG terms and symbols used in the description of the design and fabrication is presented at the conclusion of this discussion (see page 209), and may be folded out for convenience in reading.

To wind an RFG into an efficient pressure vessel requires a thick-walled cylinder with domed ends and polar bosses or end closures wound integrally with the grain. It also requires the use of longitudinal (low angle) windings for longitudinal strength and hoop (high angle) windings for hoop strength in the cylindrical section. As in glass filament design, the most favorable RFG dome design is a geodesic isotensoid dome.

A geodesic, or stable path, is the shortest path that may be generated on a surface of revolution. A geodesic filament path tends to stay in place since it is the shortest distance on the surface. A geodesic isotensoid dome is one in which the geodesic path on the dome is not only stable but statically remains stable upon application of internal pressure. The filaments in the path are loaded equally and in pure tension. Such a geodesic is applicable to a single filament path in a thin shell (normally defined as a thickness less than 10% of the shell radius) structure.

In a geodesic isotensoid dome, the low angle windings provide the total hoop and longitudinal strength in the domes only. Additional hoop strength is required in the cylindrical section to supplement the low angle winding hoop strength. Since these high angle windings do not extend over the dome, a thickness discontinuity results at the dome and cylinder intersection. This difference in web thickness, as well as the increase in thickness at the polar openings, produces undesirable variations in the dome contours which adversely affect the ballistics and strength of the grain. The conditions are aggravated as the web thickness increases.

Early 10-inch grains were fabricated with alternating layers of polar and high angle helical wraps. In designing 20-inch grains a reasonably constant web and the proper dome contour were obtained by using propellant impregnated wire screen as a filler material. The screen was applied over the domes as an extension of the hoop windings and interspersed between the successive longitudinal layers. This technique was never fully developed due to processing and application problems and ballistic hazards. The probability of void inclusion and layer delamination of the screen precluded a reliable grain.

The method evolved for the design and fabrication of 10-, 20-, 30-, and 36-inch diameter motors under this contract is called the multi-helix angle concept. In this design concept, the number of geodesic isotensoid layers required for longitudinal strength are determined and these layers are distributed through the web. The structural designer, working with the required pressure and the grain envelope, determines the wire layers required, the inner and outer grain contours, and the position and the contour of each geodesic isotensoid layer.

To build the domes to the desired contour for each geodesic isotensoid layer, a method was evolved of winding a series of layers terminating at different diameters along the dome profile, Fig. 68. This method takes advantage of the characteristic polar buildup inherent in filament winding which makes it possible to attain greater web thickness in the dome than in the cylindrical section.

By terminating a series of layers stepwise up the dome and permitting a terminal buildup at the reversing point of each layer to reach a predetermined contour, a fairly smooth profile can be obtained. These series of layers are known as intermediate or filler layers and their number and winding angles can cover a wide range depending on the grain design. The layer winding angle depends on its position on the dome since the stable winding angle (α) is defined (see Fig. 68) by the relationship:

$$\alpha = \sin^{-1} \frac{R_p}{R_c}$$

where

R_p = terminating radius of the layer

R_c = cylindrical radius of the layer

As R_p increases with each successive intermediate layer the corresponding winding angle (α) increases, (Fig. 69), producing a greater hoop component. Thus, the intermediate layers perform two functions:

1. Provide the necessary buildup on the domes to make the correct contour for the succeeding geodesic isotensoid layer.
2. Furnish the necessary hoop strength for the cylindrical section of the grain.

The grain is usually overdesigned in hoop strength so that a considerable latitude is available to add or subtract covers in the layers as required by the grain buildup.

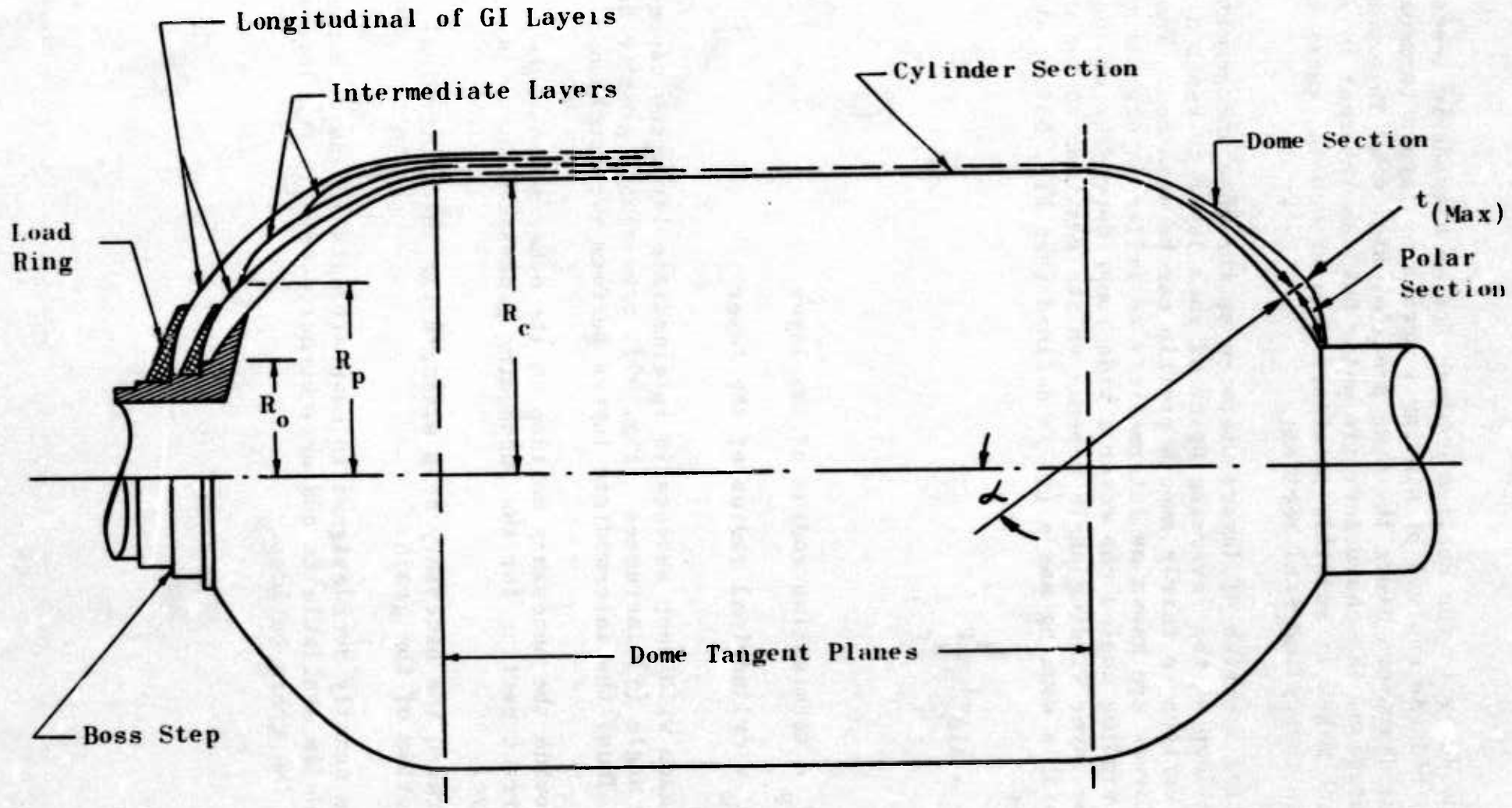
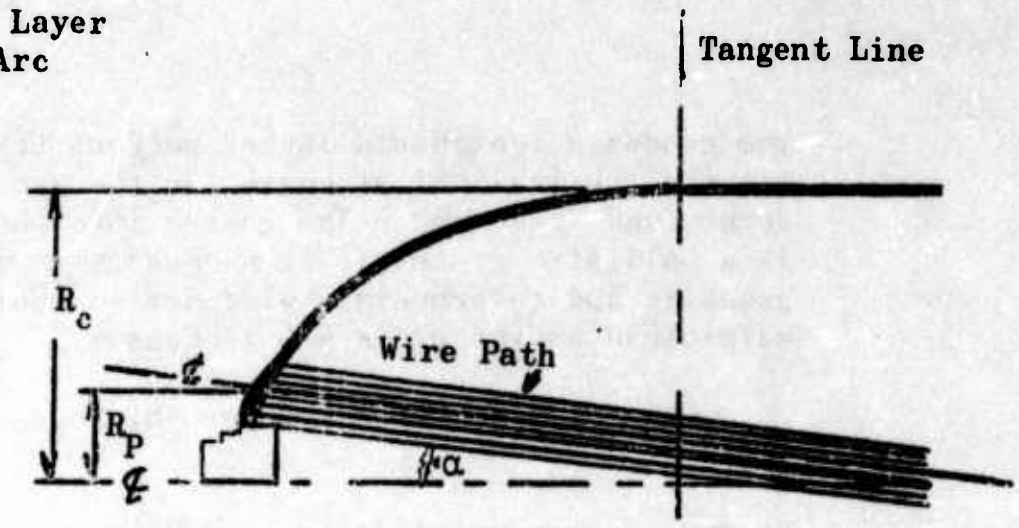
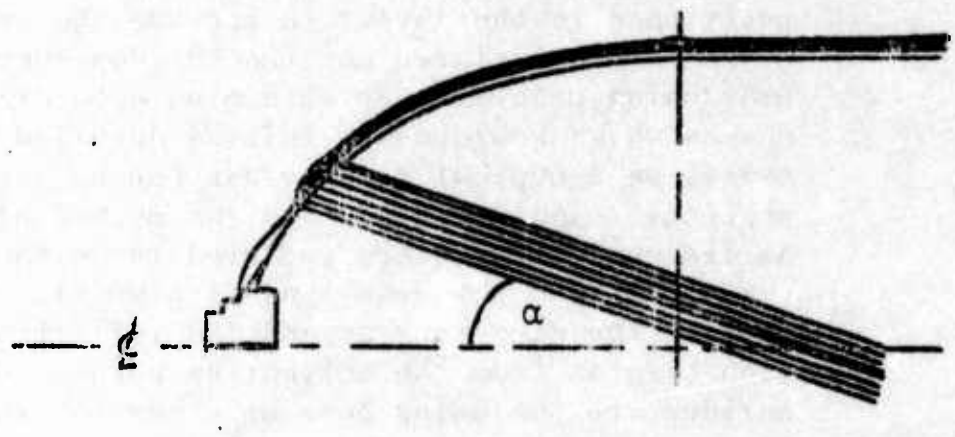


Figure 68. Multi-Helix Angle Concept

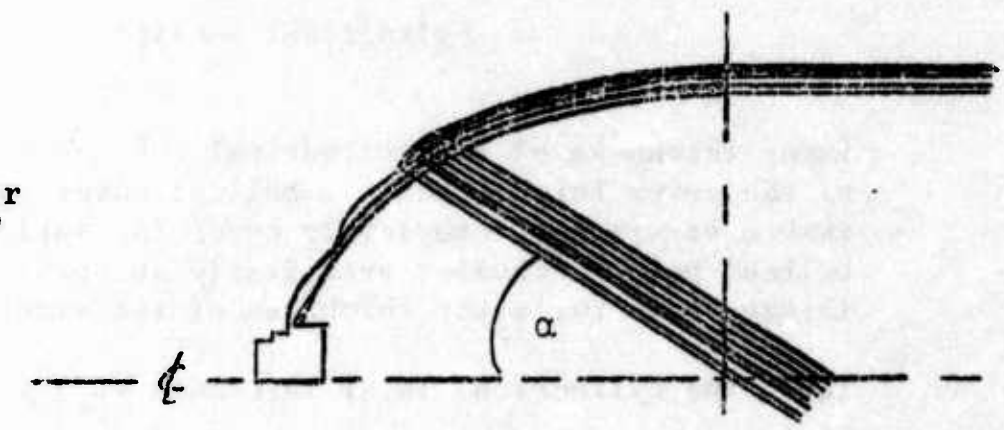
A. Geodesic Isotensoid Layer
Helix Angle = α = Arc sin R_p/R_c = 31.6°



B. Intermediate Layer
Helix Angle = 43°



C. Intermediate Layer
Helix Angle = 54°



D. Intermediate Layer
Helix Angle = 66°

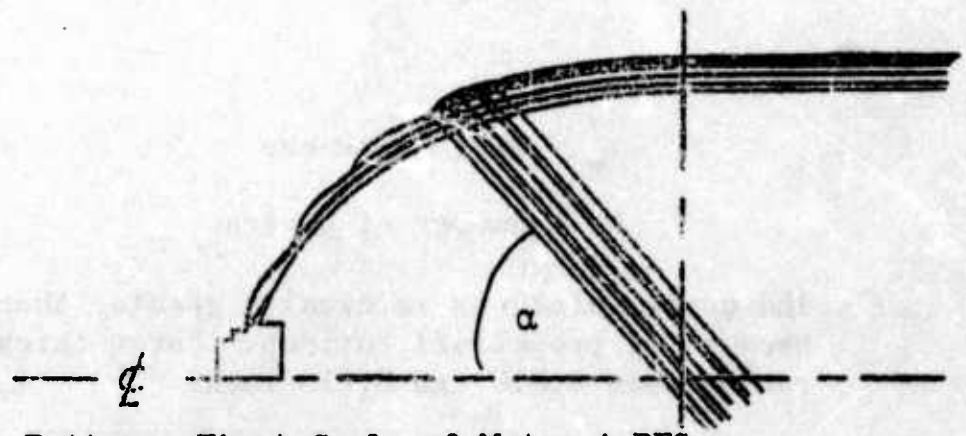


Figure 69. Winding Pattern, First Cycle of Motor A RFG

The geodesic isotensoid layers perform triplicate functions in providing all the longitudinal strength for the grain, the hoop strength for the domes, and tying the polar bosses into the grain. Since the RFG concept is a ballistic grain, it is necessary to divide and intersperse the geodesic and intermediate windings so that the structural balance is maintained as the grain web is consumed.

(a) Grain Layer Thickness Design

Current design practice is to make a layout of the grain beginning with the inner and outer grain contours and positioning of the geodesics for structural and fabrication advantages. The intermediate layers are then positioned in the layout to provide the contours required. Layer thicknesses are calculated and the buildup checked. One of the many early RFG design problems was obtaining accurate calculations of layer thicknesses which would allow initial detailed design layout. Layer thicknesses on a typical domes grain can be separated into three distinct sections, each, with a different method of calculation. These sections, as discussed below, are referred to as the cylindrical section (the region between the dome tangent planes), the dome section (that region between the dome tangent and the inflection point), and the polar section (region from the inflection point, including the point of maximum buildup, to the polar boss or other termination of the layer).

○ Cylindrical Section

Layer thickness of the cylindrical section is determined by addition of the cover thicknesses. A helical cover consists of a sufficient number of wraps to completely cover the surface of the grain. Since a helical pattern crosses over itself in opposite directions, a cover thickness is twice the thickness of the winding filament.

Thus, the cylindrical layer thickness (t_c) is:

$$t_c = 2t_w N$$

where

t_w = wire thickness

N = number of covers

The cover thickness is usually greater than twice the wire diameter because of propellant buildup. Cover thicknesses using 7.5 mil wire run between 0.016 and 0.018 inch.

- Dome Section

The layer thickness at any point (t) on the dome section is defined by:

$$t_t = t_c \sqrt{\frac{R_c^2 - R_p^2}{R_t^2 - R_p^2}}$$

where

R_c = cylindrical radius

R_p = polar radius

R_t = radius at point t

t_c = cylindrical layer thickness

This equation is used in glass filament winding design but is not as accuracte for RFG design since it gives a uniformly thicker layer than actually wound. The equation allows for increasing warp thickness over the dome, increasing to a maximum at the poles. However, the separate filaments do not provide a significant corresponding change in warp thickness. The equation accuracy can be improved by multiplying the calculated thickness (t_t) by the ratio of the warp width at the point on the dome under consideration to the warp width at the cylinder (W_t/W_c).

- Polar Section

Knowledge of the layer buildup at the pole (or at a reversing point) is necessary for accurate grain design. An empirical equation for determining layer thickness in the polar region was developed defining the maximum buildup at the radius $R_p + W_p$ (see Fig. 70). This equation is not completely accurate, although it was used on Motors A and B. W_p was usually obtained by measuring the polar warp width and multiplying by the cosine of the dome angle.

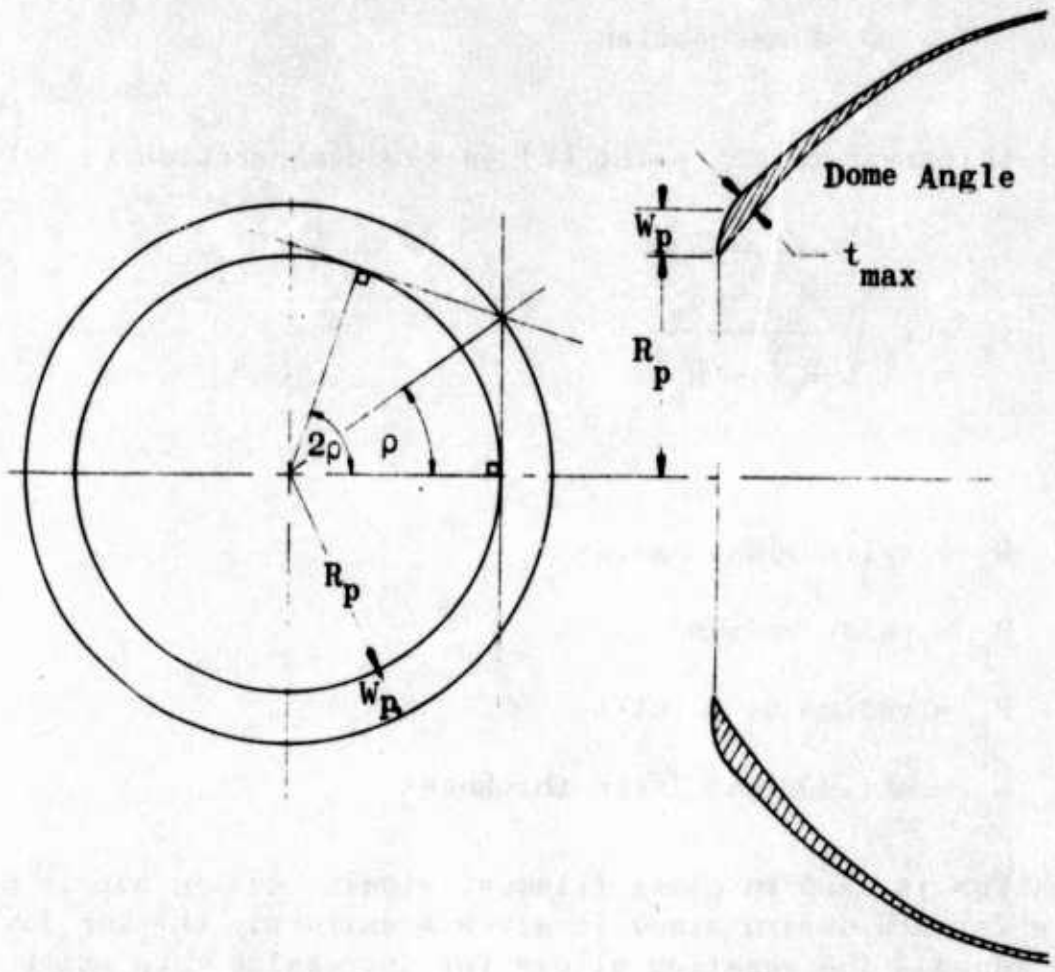


Figure 70. Calculation of Buildup at Pole

For thickness between the maximum buildup (t_{max}) and the polar opening let W_p approach zero. Assume t_x = thickness at any point along the polar region; then

$$t_x = \frac{2\rho \cdot c/c \cdot N \cdot Tw}{360} \text{ and } \rho = \cos^{-1} \frac{R_p}{R_p + W_x}$$

It can be seen that as W_x approaches zero the thickness t_x approaches zero and the contour is defined as in Fig. 71.

$$t_{max} = \frac{2\rho \text{ x } C/C \text{ x } N \text{ x } T_w}{360}$$

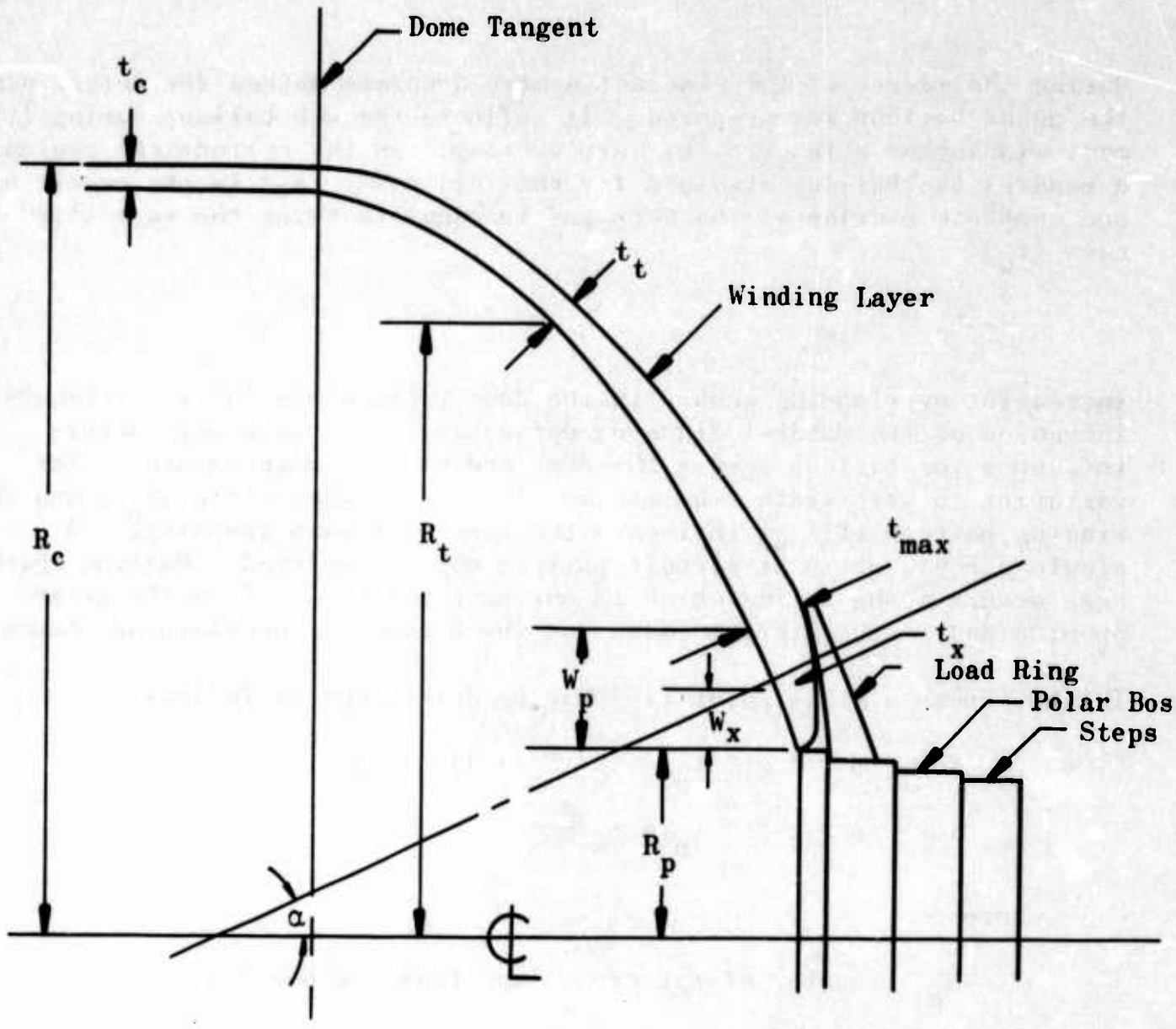


Figure 71. Dome and Pole Layer Thickness

where

$$\rho \quad \cos^{-1} \frac{R_p}{R_p + W_p}$$

C/C = circuits per cover

N = number of covers

T_w = warp thickness on cylinder

W_p = radial warp width

During the course of the contract a more accurate method for determining the polar buildup was prepared. It reflects the web buildup during filament winding as a function of warp overlap. In the cylindrical region of a mandrel the buildup attained for one full cover (t_c) is the result of one complete overlap of the warp and is equal to twice the warp thickness (t_w).

$$t_c = 2\ t_w$$

Increasing overlapping occurs in the dome regions and the web thickness increases as the mandrel diameter decreases. Several other factors influence the buildup across the dome and at the polar opening. The variation in warp width, the minimum (or polar) warp width (W_p), and the winding pattern (T_p/C_p) influence the number of warp crossings. A single circuit or multi-circuit pattern may be employed. Maximum thickness occurs along a line which is one warp width away from the polar opening and is the minimum radius at which complete overlapping occurs.

The thickness at this point (t_p) may be determined as follows:

$$\text{for } \theta/p < 2\ \rho: \quad t_p = t_w\ (N_p + 1)$$

$$\text{for } \theta/p > 2\ \rho: \quad t_p = t_w\ \frac{2\rho}{\gamma}$$

where

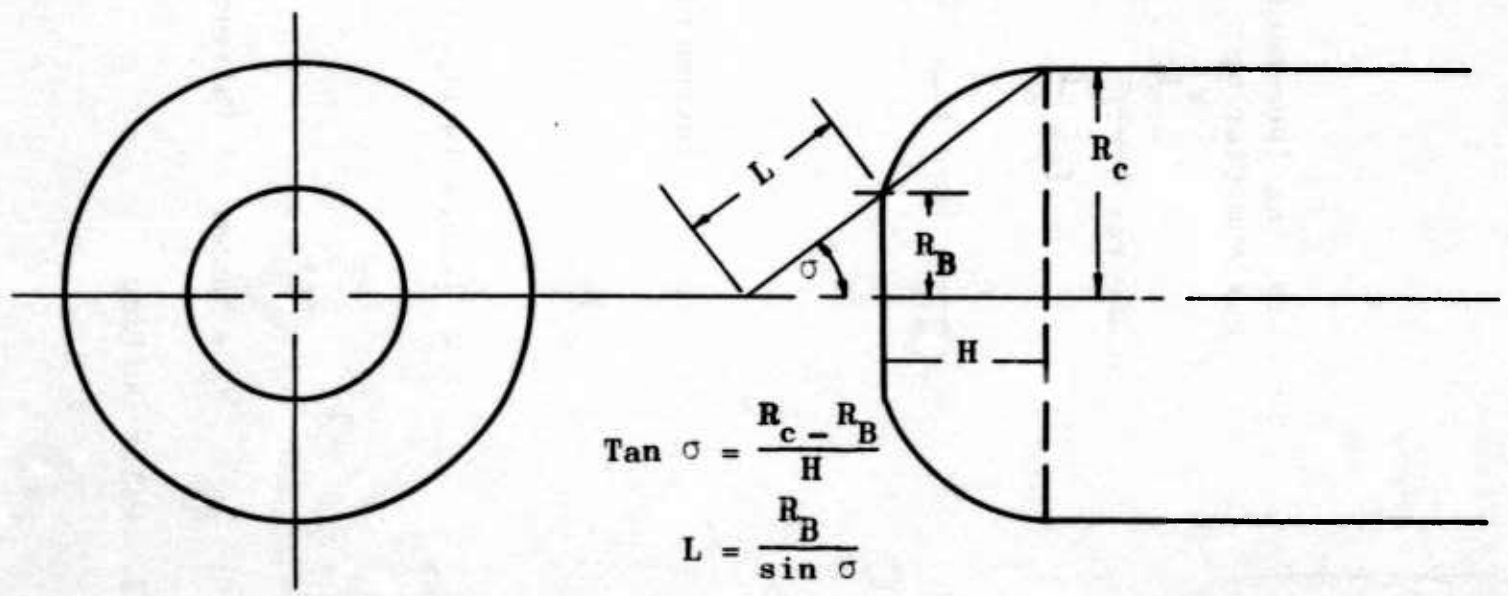
N_p = number of patterns, (see Figs. 72 and 73)

$\theta/p = 360/C_p$

ρ = Arc Cos $(L - \frac{W_p}{2})/(L + \frac{W_p}{2})$

$\gamma = 360/(C/C)$

If a layer consists of multiple covers, the average dimensions should be used in the above equations and the calculated thickness per cover may be multiplied by the number of covers to obtain the layer thickness.



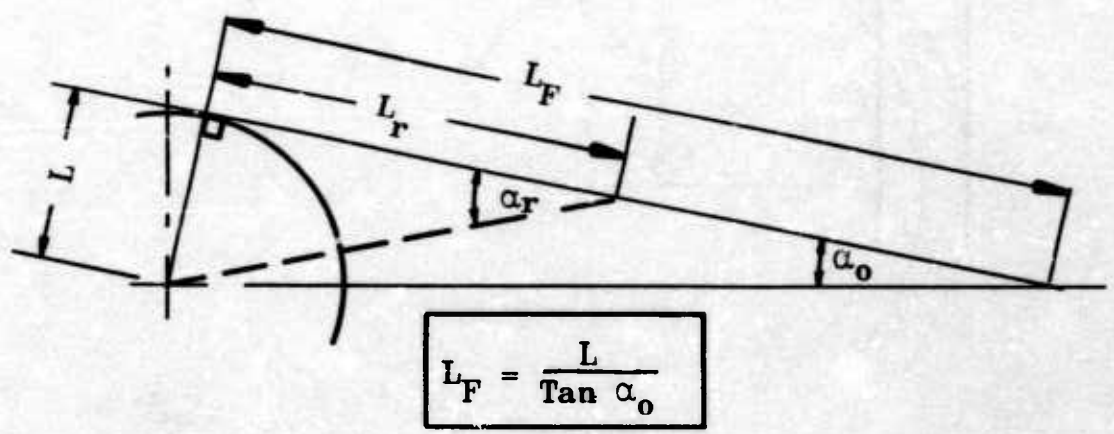
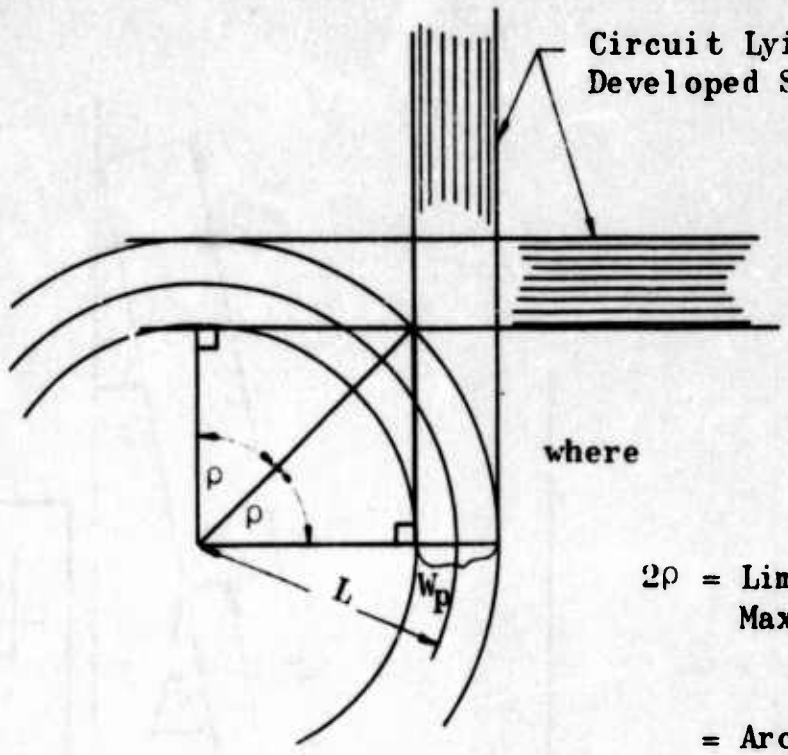


Figure 72. Filament Length on Dome



where

2ρ = Limiting Increment for Maximum Overlap

$$= \text{Arc cos} \frac{L - \frac{W_p}{2}}{L + \frac{W_p}{2}}$$

$$L = \frac{R_B}{\sin \sigma} \text{ (see Fig. 72)}$$

for

$\theta/P < 2\rho$, $t_p = t_w (N + 1)$

$\theta/P > 2\rho$, $t_p = t_w \frac{2\rho}{\gamma}$

t_p = Max Cover Thickness

t_w = Warp Thickness

θ/p = Pattern Increment

$$= \frac{360}{C_p}$$

γ = Circuit Increment

$$= \frac{360}{C/C}$$

N_p = Number of Patterns

Figure 73. Polar Buildup

(b) Pattern Selection

At this point, the grain design is completely laid out. At first this was done before complete pattern selection was made. Usually the approximate winding angle was used for layer thickness and cam design computations and the slight changes later required for the proper pattern were ignored. It is now apparent that careful pattern selections must be made before accurate winding angles, layer thickness, or winding cams can be calculated.

The basic winding ratio (R_W) is the ratio of mandrel rotation to cam rotation (θ_M/θ_C). This ratio is determined by dividing the mandrel rotation during one circuit (θ_T) by one cam revolution (360 degrees). This ratio would yield a single circuit-repeating pattern and must be advanced or retarded to progressively or regressively cover the mandrel. Since the required adjustment is in terms of the mandrel circumference, the ratio (R_W) must be in terms of mandrel turns to cam turns (T_p/C_p) or (turns/pattern ÷ circuits/patterns). The fraction must be composed of integers and a slight shift in R_W is usually required. The corrected winding ratio is determined from the following:

$$R_W = \frac{T_p \pm W_c/\text{Circumference}}{C_p}$$

where

W_c = circumferential warp width = $W_N/\text{Cos}\ \alpha$ <

The number of circuits per cover (C/C) must equal the number of patterns multiplied by the number of circuits per pattern plus or minus the one circuit gained or lost due to the shift in R_W, i.e.:

$$C/C = C_p\ N_p \pm 1$$

where

N_p = number of patterns

In the relationship above, if one circuit must be added to $C_p N_p$, then the winding ratio is retarded and the minus sign is used, i.e.:

$$R_W = \frac{T_p - W_c/C}{C_p}$$

Conversely, if a circuit is lost, the sign in the above equation is plus.

NOTE: There are two exceptions to the above relationships which are

1. If $C/C = C_p$, no advance is required and $R_W = T_p/C_p$
2. If $C_p = 1$, no circuit is lost or gained and $C/C = C_p N_p$

Some amplification of the basic steps covered follows:

1. Once the winding angle (α) an the total mandrel rotation per circuit (θ_t) are determined they must be checked to see if they will result in a suitable winding pattern.

2. A suitable winding pattern is $\frac{\theta_t}{360} \approx \frac{T_p}{C_p}$ and the resultant T_c and C_p must be integers without a common divisor. It is usually necessary to vary θ_t slightly to obtain an integer solution. The amount θ can be changed without affecting the pattern accuracy is difficult to predict. A fair rule of thumb is that if θ_t varies enough to affect the winding angle (α) by one degree then θ_t should be recalculated for the new angle α and a new integer ratio obtained.

3. The next step (previously discussed) is the (N_p) in the equation $C/C = C_p N_p \pm 1$.

   C_p is already determined and the number of circuits per cover (C/C) is obtained by dividing the mean layer circumference by the circumferential warp width (W_c). Thus, the solution for N_p must be an integer also. One is added or subtracted depending on which will most closely approach an integer solution. It is apparent that if an integer result is not obtained the value of W_c must be adjusted (which in effect means changing angle α) or C_p, or both. In any case, it is sometimes necessary to retrace steps 1 and 2 before integers for T_p, C_p, and N_p result.

4. Finally, the winding ratio (R_W) is obtained as shown. This is a ratio between mandrel and cam revolutions that must be built into the winding machine to obtain the required winding pattern.

(c) Gear Ratios

The previously determined winding ratio is converted into the winding machine by the gear train built into the machine with the change gears provided. The gear ratio (GR) for a simple case of direct drive is

$$\frac{1}{R_W} = GR = \frac{A \cdot C}{B \cdot D}$$

A, B, C, D are the order of change gears in the 36-inch and two 40-inch machines. The reciprocal of the winding ratio results from the fact that all winding calculations are based on the mandrel-to-cam ratio while the machine constants are based on cam-to-mandrel ratios.

Early in the RFG studies when there was a limited number of change gears available, gear ratio calculations were done manually. Since this was tedious and inefficient, particularly with five and six decimal place accuracy required, gear ratio values for a large number of gear selections were printed out on the computer. The present method is the use of a gear computer program in which the required gear ratio, accuracy, and range of gear sizes are specified. The program prints out all gear combinations which will meet the specified gear ratio and accuracy tolerances. The program is written for the IBM 7094 and has the code name JWGEAR.

(d) Weight and Volume Fraction

Since design wire percentage is specified in weight percentage, it is necessary to convert this to volume percentage to calculate wire spacing. Volume and weight fractions of a composite material are calculated as follows:

1. $$f_v = \frac{\frac{f_w}{\rho}}{\Sigma \frac{f_w}{\rho}}$$

2. $f_w = \dfrac{f_v \rho}{\Sigma F_v \rho}$

3. ρ Composite $= \Sigma f_v \rho = \dfrac{1}{\Sigma \dfrac{f_w}{\rho}}$

where

f_v = fraction by volume of each constituent

f_w = fraction by weight of each constituent

ρ = density of each constituent

A typical example for finding the aluminum wire volume percentage of a grain with 12% by weight of 7.5-mil wire and a propellant matrix density of 0.062 lb/cu in. is as follows: (Aluminum 5056 wire density in 0.095 lb/cu in.).

	f_w	ρ	f_w/ρ
Aluminum	0.12	0.095	1.26315
Propellant	0.88	0.062	14.19354
	1.00		15.45669

ρ Composite $= 1/15.45669 = 0.06469$

$f_v(Al) = \dfrac{1.26315}{15.45669} = 0.08172$ or 8.17%

Theoretically, wire volume percentage based on wire spacing with wire-to-wire contact between layers assumes

$$F_v = \frac{\pi d}{4D_w}$$

where d is the wire diameter,

D_w is the centerline distance between wires, and is equal to:

$$D_w = \frac{\pi d}{4f_v}$$

In the example above

$$D_w = \frac{(0.0075)}{4\ (0.08172)} = \frac{0.02356}{0.032688} = \underline{0.07207 \text{ in.}}$$

This wire spacing will give 12% aluminum by weight if the spacing remains relatively stable and there is wire-to-wire contact between layers.

Wire spacing combs are made by textile equipment supply companies in standard spacings called dents per inch; therefore, it is necessary to choose the closest spacing available and go back through the calculations to find what weight percentage the standard spacing will give. In the example above, the spacing required is 0.07207. Possible spacings and weight percentage are:

14 dents/in. = 0.07142 spacing - 12.098 wt %

13.5 dents/in. = 0.07407 spacing - 11.683 wt %

Practically speaking, it is often difficult to predict how close the theoretical spacing will be to the resultant wire weight percentage. High angle helix wound cylindrical grains are usually very close (1% or less variation). Dome grains vary more since the warp does foreshorten on the dome, giving high wire content, but wire-to-wire contact between layers is not as readily obtained. Usually the variation is 2 to 3% below the estimated percentage. Wire tension, winding speed, and propellant viscosities affect wire percentage during grain fabrication; however, for the same grain design, the grain-to-grain wire weight percentage variation is very small.

Theoretically, wire percentages up to 25% by weight can be wound before the wire spacing gets too small for good comb design. It is difficult to obtain higher than 22 or 23% because as the wire spacing gets smaller the wire is more difficult to pull through the propellant. Twelve percent wire (by weight) is readily attainable but wide wire spacing results in an intermeshing tendency. At this point, an intentional lack of wire layer contact is necessary to get lower wire percentage.

(e) Effect of Winding Variables on Buildup

In determining the effects of several winding variables on grain buildup, the following tests on fabrication time, wire tension, matrix propellant thickness, mandrel speed, and winding angle were conducted.

The effect of variation in fabrication time on grain buildup was studied. Contrary to expectation the influence of time was greater with high wire tension than with low tension. Therefore, excessive buildup experienced as a result of processing delays--wire breakage, propellant heating, etc.--cannot be eliminated by operating at high wire tension. Fabrication time in minutes per cover was varied from 30 to 66, with the minimum buildup occurring at the low processing time. Presumably the effect of time is a result of the change in propellant viscosity as the propellant cools. With the short time there is a wide spread in buildup for different wire tension values, but at longer time periods this is not the case. These results indicate that with fresh propellant, buildup can be controlled by wire tension while with longer processing times tension appears immaterial and propellant characteristics become the controlling influence. From these data, and using the current techniques, it is apparent that to maintain control over buildup the wire must be wound over freshly applied propellant and that excess propellant remaining on the grain longer than 30 minutes should be scraped off.

The 30 minute time limit probably can be extended when a heated spreader blade becomes available in the mechanized propellant feeding equipment.

Another factor related to processing time and propellant cooling is the thickness of application of propellant. Up to this time application has been an uncontrolled variable dependent upon individual operator technique. Obviously the thinner the application the better as far as obtaining wire-to-wire contact. The new feeding system should alleviate this problem.

As discussed in the preceding paragraphs, wire tension had little effect when processing time was lengthy. On the shorter 30 minute period buildup per cover decreased as wire tension was increased (rapidly in the range of 300 grams tension, then diminishing at higher tension). A tension of 400 grams appears to give the desired wire-to-wire buildup of 0.015 inch per cover. At 500 grams tension a reduction in thickness below the theoretical occurred, indicating interlacing and bending of the wires. This does not seem desirable from optimum wire strength or uniform, reproducible buildup and aluminum content. Also, more wire breakage can be expected at higher tension levels.

The recommended wire tension is 400 grams under normal conditions of propellant viscosity, application, and winding time. This optimum tension value may be altered if changes in these process variables occur. Also, the condition of the wire gathering system, particularly the rollers and combs at the follower head, will effect the actual tension experienced at the grain. It is important that the wire system be kept clean and in good operating condition.

Mandrel speed was considered a significant factor in buildup thickness from earlier work on 10-inch grains (following the reasoning that rapid speed prevented sufficient time for the wires to pull down through propellant to the previous wire surface). The tests on the 27-inch mandrel did not follow this theory. Variation in mandrel speed from 3 to 5 rpm did not appear to effect buildup thickness. One test at 2 rpm was made but the long winding time made it noncomparable to other data. In the faster speeds intentional stopping periods were used to give an over-all constant fabrication time.

Only two tests were made at the low helix angle of 35 degrees. In a comparison of these data with results at an angle of 62 degrees with equivalent tension and fabrication time, no difference in buildup was observed as a result of different winding angles. At low helix angles, the layer buildup was expected to be higher than at higher angles because of the larger radius of the wire path and the resulting lower force from wire tension in the direction toward the mandrel axis. Experience with polar winding on 10-inch grains had supported this theory, however, if the effect exists on the 30-inch grain it is not of sufficient magnitude to be detected.

Propellant RDS-512 was used as the standard for comparing RDS-523 and 514. Two tests with RDS-523 with 6% depressants gave buildups of 0.0148 and 0.0158 in./cover when using 400 grams wire tension. This is essentially equivalent to the cover thickness for RDS-512 at low processing time. One test with RDS-514 with 2% depressants resulted in a buildup of 0.0175 in./cover or about 15% thicker than with RDS-512. This increase is not desirable but may be tolerated for a few layers in the grain.

Buildup thickness is sensitive to other propellant changes besides formulation. Three tests were made with the same mix of RDS-512 as used previously after the cold box had failed, allowing the propellant to thaw. Application of the propellant appeared to be nearly normal but the resulting buildup was too high, as much as 50% above standard.

In general, propellant behavior was found to be the most important single factor in grain buildup, and, in addition, the least controllable variable. The propellant is affected by both the temperature on the grain and the state of cure. Limiting the processing time and application thickness is helpful but incomplete. The heated spreader blade will further aid in keeping the viscosity low on the grain providing the propellant pot life is not exceeded. The degree of curing is the one variable over which little or no control exists. The slow tedious

hand-filling of the propellant tubes results in some propellant remaining in the mix can at casting temperature for several hours. It is possible for much of the pot life of part of a mix to be consumed in tube loading. Added curing occurs in the cartridge oven before application to the grain and this period is variant in time depending on winding requirements. Even though close monitoring is maintained the usage rate is not always predictable. There is no apparent solution to control of this last precuring period (short of rapid induction heating or other innovation), however, tube loading time may be reduced when the new mechanical propellant feeder with its larger, rectangular tubes, becomes operational.

(f) Fabrication Development

Fabrication development ultimately determines design accuracy and is necessary since the present state of winding theory does not allow completely accurate design by calculation and layout. There are enough variables in a new grain wound with the multi-helix angle concept that a fabrication development program is usually essential.

The fabrication development program for multi-helix angle domed grains consisted of a series of windings in which consecutive grain layers were wound 1 to 3 cycles at a time. This allows comparison of total buildup as well as individual layer buildup with predicted buildup. The geodesic layer buildup at the polar boss is a critical design dimension which must be carefully determined. Other design features which are checked during fabrication development winding are:

1. Position of the intermediate layer reversing positions on the domes
2. Buildup of the intermediate layers at the reversing point; this determines the allowable dome distance between geodesic layers for a given cylindrical thickness
3. The best load ring design for each geodesic layer
4. Buildup of the geodesic layers in the dome
5. Required polar boss steps lengths for load rings and geodesic polar windings
6. Dome web thicknesses and internal and external cylindrical lengths
7. Cam design, gear ratios, propellant, and warp widths used

Motor A had a fairly extensive fabrication development program with the first two partial grains RFG-1206 and RFG-1207, to check out cams and grain design helix angles with respect to dome buildup through the first cycle and the second geodesic layer. The partial grains were made with live propellant, which was applied only to one dome in each case. In this way about one-tenth of the propellant required for an entire grain was used with no sacrifice in information obtained.

The winding pattern for both grains consisted of the first geodesic isotensoid (GI) layer of seven covers, a 43 degree helix layer of nine covers, a 54 degree helix layer of nine covers, a 66 degree helix layer of four covers, and a second GI layer of seven covers (Fig. 74).

The two grains differed from each other in the number of wires used in the warp on the GI (24 for RFG-1206, 36 for RFG-1207) and in the reversing point on the intermediate helix fill layers which were all made with a 36-wire warp.

Observation of the winding on RFG-1206 indicated that the cams produced winding patterns precisely according to design, confirming the dependability of the cam design methods. However, study of the measured dome contours indicated that some changes had to be made in the intermediate layer design, the load ring configuration and location, and the location of maximum dome buildup of the GI layer because of the warp width reduction at the pole base. This indicated that the estimated narrowing of the warp width from the 20-inch grain studies was erroneous.

A study was made in an effort to determine the factors affecting this reduction in warp width. Factors considered were dome contour, Z-axis orientation and the distance between the final wire guide and the wire contact point on the mandrel. It is apparent that there would be no reduction in warp width if the final wire guide could be maintained parallel with the dome contour; however, this is not possible with existing equipment.

Since control could be exercised over the distance between follower and grain contact point, the first geodesic isotensoid layer cams were redesigned to produce a follower path with a minimum clearance from the mandrel surface in the polar region.

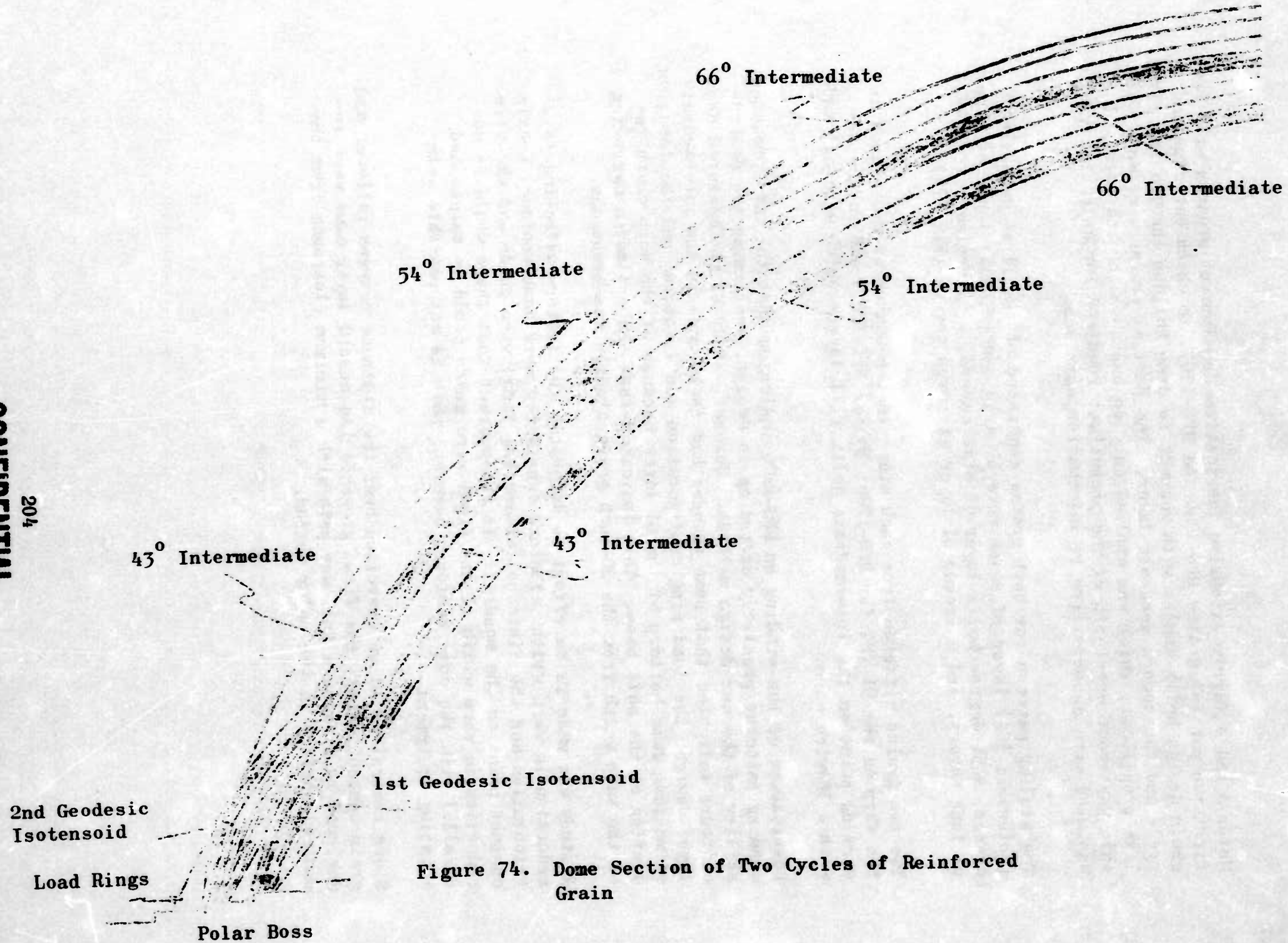


Figure 74. Dome Section of Two Cycles of Reinforced Grain

RFG-1207 was a repeat checkout of contour buildup for the first cycle and second GI layer using the redesigned cams. The first geodesic isotensoid layer was wound using these cams and a 24-wire warp. No appreciable increase in the warp width could be determined; therefore, it was concluded that the clearance did not affect the warp width within the limits investigated. Since the minimum clearance method was no improvement, the first GI cams were returned to the original follower path.

The dome of RFG-1207 was smoother than RFG-1206. This improvement was accomplished by winding each intermediate layer in two portions, one portion being wound slightly lower on the dome than the other. The cylindrical buildup of RFG-1207 was equal to the predicted value of 0.01645 in./cover.

The propellant used in RFG-1206 and RFG-1207 was RDS-512 (58.5% fine AP). This propellant had been previously used in reinforced grains, and processing characteristics were satisfactory.

The next factor studied was the number of wires in the GI layer warp. This was increased from 24 to 36 in an effort to decrease the polar buildup. A lower polar buildup was expected because the wider warp requires fewer circuits per cover thus fewer wire crossovers at the pole. The grain was then rewound and the polar buildup on the first geodesic layer was the same thickness as predicted. However, the polar buildup of the second GI layer was greater than predicted. It was also noted that the warp width of the second GI layer was narrower than the first. This information led to the development of a method for predicting polar warp width which takes into account the increasing size of the grain with successive layers. The method is graphical and is based on the length of the wire path across the dome. As successive layers of the grain are wound, the length of the wire path increases and the warp width decreases. The method was used to successfully predict the polar buildup of the four GI layers of RFG-1208. Thus, the correct warp width is an important factor in calculating predicted layer thickness.

This third partial grain in the Motor A fabrication development phase, RFG-1208, consisted of three full cycles plus the fourth GI layer. Both domes and small portions of the cylindrical section adjacent to the domes were covered with propellant. Special low viscosity propellant was used for about 3/4 inch width adjacent to the polar boss on one end of the grain to determine the effect of propellant viscosity on polar buildup.

The use of low viscosity propellant next to the pole on one end of the grain gave a significant reduction in polar buildup. The buildup at the low viscosity end was approximately equal to design and was very close to buildup predicted by the previously mentioned method. Based on this buildup data it was planned to wind future reinforced grains with low viscosity propellant adjacent to the poles.

Buildup at other points in the domes and in the cylinder was lower than expected. The cylindrical buildup averaged 0.0150 in./cover, which is equal to wire-to-wire contact, compared to 0.01645 in./cover predicted. The low buildup was probably due partially to there being no propellant in the cylindrical section to restrict transmission of wire tension back to the domes and partly because the RDS-512 propellant used in fabrication was a lower viscosity (lower percent fine AP) formulation. It was decided to limit this bare cylinder effect on the next grain by covering a larger portion of the cylinder with propellant. Propellant processibility was satisfactory.

Evaluation of data from this grain revealed new dome buildup and load ring contour information. Based on this information, cams were designed for winding through the seventh GI layer. The polar bosses for the prototype hard mandrel were redesigned to reflect the dome buildup data, and new load rings were designed.

The fourth partial grain, RFG-1209, was wound through the sixth GI layer. Propellant was applied over all of the grain surface except a 12-inch band in the center of the cylinder. Propellant used in the outer layers of this grain, RDS-514 with 6% depressants, had its first trial in a reinforced grain and was not processible.

Fabrication was satisfactory to the fifth GI layer, where use of depressed propellant was started. Processing this propellant resulted in nonuniform buildup because it could not be controlled to obtain a smooth layer, but extruded as uneven lumpy globs. Part of this problem was a reduction in pot life caused by difficulty in potting the propellant into dispensing tubes when it was mixed. Processing this propellant on a large scale was determined not to be feasible and the winding was stopped at the end of the sixth GI.

The propellant processing problem was discussed with the propellant laboratory and new formulations were devised for the next grain, RFG-1211. (There was no RFG-1210 fabricated.)

The fifth partial grain, RFG-1211, was wound on the enlarged reusable mandrel beginning with the sixth GI layer and continuing through the ninth. Propellant was applied to all of the grain except a 12-inch band in the center of the cylinder.

The purpose of RFG-1211 was to check grain and cam design of the outer layers and processing characteristics of three new propellants. The first two were RDS-514 at lower depressant levels than used previously. The third was a new formulation, RDS-523, which has 87% AP vs 88% for RDS-514 and 30 parts per hundred rubber (phr) plasticizer vs 20 phr for RDS-514.

The three propellants used in fabrication of RFG-1211 were prepared with the object of reducing viscosity and therefore improving processibility and reducing buildup. Location and cylindrical buildup obtained were:

Cycle	Propellant	Buildup, in./cover
6th	RDS-514 w/0.5% depressant	0.0157
7th	RDS-514 w/2.5% depressant	0.0163
8th	RDS-523 w/6.0% depressant	0.0200
Average		0.0178

The buildup for the 6th and 7th cycles was on target, while that of the 8th cycle was slightly higher than desirable. The only apparent explanation for the differences obtained is the propellants and a possible difference in application of propellant by operating personnel.

Operation of the winding machine was improved for this grain over that for the previous grain by using the direct gear train with precision gears to eliminate considerable backlash. Also a friction brake was installed on the gear train output shaft to eliminate the effect of backlash through the cam system.

The winding of these five fabrication development grains demonstrated the application of the multi-helix angle grain concept to large motors, and the feasibility of the design and processing techniques. Considerable experience was gained during this winding program with respect to minimizing layer thickness, buildup at the poles, control of polar buildup, predicting warp width and layer thickness, and optimizing cam design.

Particular terms used in grain winding are defined as follows:

1. Helical winding is a general term for any winding on a surface of revolution in which the winding material is laid down at an angle to the rotational axis of the surface being wound. Geodesic isotensoid, polar, and circumferential windings are merely special cases in which the helix winding is further defined.

2. Geodesic-isotensoid winding is a pattern which is stable and in uniform stress throughout its path. Since a geodesic line is the shortest distance between two points on a surface of revolution, it is a stable wind and remains so under pressure. The isotensoid refers to the uniform tensile stress level at any point in the winding path.

3. Polar winding is winding laid down lengthwise on the grain from pole to pole primarily to resist longitudinal loading.

4. Circumferential winding is that around the cylindrical portion of the grain primarily intended to handle hoop loads. In general, high-angle helix winding (75 to 90 degrees) is referred to as circumferential or circ winding.

5. Multi-angle winding is a series of helix windings at different angles used to alleviate polar buildup and obtain uniform dome thickness.

6. Helix angle is defined as the angle between the warp laydown and the longitudinal axis of the grain.

7. A wrap is one complete warp laydown, from dome to dome and back. It is equivalent to one circuit of the machine cams and is also called cam circuit. The warp width, grain diameter, etc., determine the number of wraps per cover. The term wrap angle is sometimes used instead of helix angle.

8. A winding cover consists of sufficient number of wraps to completely cover the surface of the grain. Since a helical pattern crosses over itself in opposite directions, a cover thickness is twice the thickness of the winding material. In circ winding with glass filament, where the helix angle is essentially 90 degrees, a cover is considered a single pass along the cylindrical surface or a single material thickness; however, this ia a special case.

9. A layer is defined as all the winding (a specified number of covers) done at one particular helix angle.

10. The reversal point is the point on the dome where the pattern reverses direction and is described as the radial distance of this point from the grain axis.

GLOSSARY OF SYMBOLS

α = winding or helix angle, the angle the filament makes with a plane through the axis

C_p = control cam revolutions per pattern

D_w = centerline distance between adjacent wires in warp

f_v = volume fraction of wire content in grain

f_w = weight fraction of wire content

N = number of covers

N_p = number of patterns in pattern calculation

R_c = radius of cylindrical section

R_f = wire follower guide height from grain axis

R_p = radius at the pole or distance of winding termination from grain axis

R_t = grain radius at point t

R_W = winding ratio or ratio between mandrel and cam revolutions

ρ = density, also angle of polar rotation in dome buildup calculation

PREVIOUS PAGE WAS BLANK, THEREFORE WAS NOT FILMED

t_c = layer thickness on cylindrical section

T_p = mandrel revolutions per pattern

$t_w(T_w)$ = wire thickness

θ = mandrel rotation

θ_t = total mandrel rotation per circuit

W_c = wire band or warp width on cylinder

W_p = warp width at pole in radial direction

W_t = warp width at a point

(2) Application of Grain Restrictor

Following the grain winding and partial cure, a thin thermal barrier is applied to protect the glass filament wound case from the hot gases during the final burning of the RFG. The major difficulty with restriction operations is thickness uniformity. It develops from problems with the grain dimensions. Variation in grain diameter from end to end, and before and after cure, necessitates variation in restrictor thickness. In addition, variation in eccentricity and lack of accurate measurements contributed to restrictor nonuniformity.

A large factor in measuring the diameter was the use of the periphery tape around the uncured grain. Since the grain was not rigid, the measurement depended on the tension applied. The contour measuring device developed late in the program was a step toward better dimensional control; also, a new optical transit showed promise in this area. Probably the most feasible method of obtaining a thin, uniform restrictor thickness despite grain surface variations is to wind the restrictor on the grain using an inert fiber or wire. This has been done on small cylindrical grains but the extrusion of binder fluids onto the surface of domed grains was a potential problem. Experimental work is required to determine whether or not this would be a problem with a wound-on restrictor.

The restrictor application technique developed for this motor was to apply the R-143[15] to a grain assembly that had been prepared by wiping clean with a toluene-dampened cloth. After cleaning, the grain is oven dried for 1 hour at 170 F and a light coat of MAPO wiped on the propellant surface. The R-143 is applied in three steps. First a thin prime coat is spread and worked into the surface with a plastic spatula. This layer was smoothed and partially cured (16 hours at 170 F). The second (or fill) layer was applied to within 0.030 inch of final dimensions to build up the restrictor thickness and provide a base for a more uniform final coat. Both this fill and the finished layer were applied and smoothed with the contoured template while the grain was revolving. The fill was partially cured and the final layer was cured 48 hours at 170 F. After 24 hours of the final cure period the heating was interrupted and the surface inspected for dimensions, ridges, and depressions. At this point any ridges were sanded down and R-143 added to depressions if necessary. If restrictor was added the unit received a further full 48-hour cure.

---

[15] R-143 is a Rocketdyne prepared restrictor.

(3) Glass Filament Wound Cases

Development of the glass filament wound (GFW) cases was primarily associated with the application of existing materials and processes to the fabrication of Motor A thin-wall cases. Presented in the following discussions is a summary of the GFW process development which was accomplished through the fabrication and test of partial and full-scale GFW case configurations.

(a) Partial Case Fabrication Development

Fabrication development of the GFW case on Motor A was initiated by making two partial full-scale cases for development investigations. The fabrication of these two partial cases (Cases 1406 and 1407) is discussed below.

When GFW Case 1406 was wound on the 40-inch winding machine, several problems were encountered. Since this was the first attempt to wind a complete cover on a mandrel on this machine, adjustment was necessary to get all systems aligned properly. The maximum speed at which the machine could be made to operate stably was approximately one cycle per minute. In addition to this being the first attempt to wind on this machine, this was the first attempt at winding a case with unequal end openings.

In view of the various "firsts" connected with this winding operation, the results appeared good. Winding proceeded without interruption after initial checkout patterns except for two planned stops. One was to change a glass supply spool, and one was to change resin pots and clean the resin system.

Although the pattern lay-down was not perfect, it was sufficiently accurate for a two-cover case. Three main sources of inaccuracy in the pattern were noted:

1. The tracer valves did not always remain exactly on the cam surface. This was not a consistent variation, and as a result, pattern gapping (approximately 1/16-inch) resulted at random intervals in the cylindrical section only.
2. The final glass-feed eye was larger than is desirable for the four-roving band, and at times caused excessive band spread. This resulted in splitting of the band at times.

3. Since this case had unequal end openings, the helix angle was necessarily a compromise between the optimum helix angles for each of the end openings. A very slight amount of band slippage was noted on the domes during the latter phases of winding.

Case 1407 was the second partial case to be wound on the 40-inch winding machine. Prior to winding this case considerable time was spent in "tuning up" the machine and testing various minor variations of the winding pattern to achieve the optimum lay-down with these cams.

The winding speed was appreciably increased over that used for Case 1406. The average winding speed for 1406 was 1.09 rpm, while that for 1407 was 1.60 rpm. Although both speeds are rather slow, this resulted in 30% reduction in winding time.

Once winding was started, no difficulties were encountered. The machine continued to operate smoothly for five hours with no adjustments.

The results of winding 1407 indicate that both the machine and winding pattern design were sufficiently developed to be used for the first hydrotest case with no further changes. There was, of course, always room for improvement, and minor changes were made.

(b) Full-scale Case Fabrication and Test

After completing the partial case fabrication development the first complete full-scale Motor A GFW case fabrication was initiated. Three full-scale cases were fabricated and tested. Below is a discussion on each case.

O GFW Case A-1412 Fabrication

(C) Case A-1412 was the first full-scale Motor A case and was wound for hydrotest purposes. A-1412 was wound so that the circumferential wrap had 1174 ends per inch (instead of 886, as designed for flight load requirements) to balance the case for hydrotest. The helical wrap had 744 ends per inch instead of 716, cue to gear ratio limitations. Following are the principal characteristics of this case:

(C)

Case ID, in.	29.71
Cylinder length, in.	48.20
Case OD, in.	29.83
Type pattern	5/4 Helical
Helical band width, in.	0.258
Helical ends per inch	743.6
Circ band width, in.	0.545
Circ ends per inch	1174
Resin system	DER332/EMI
Glass sytem	S-994 HTS Roving and 143R Glass Cloth

Prior to the winding, difficulty was encountered in obtaining a good restrictor coating on the mandrel. The third attempt at restriction was acceptable. The primary problem lay in obtaining a uniform 0.030-inch thick coating on a mandrel that permits 0.030 inch diameter variation. Considering that a reinforced grain will probably not be as uniform as a molded sand mandrel this problem may be increasingly severe in RFG/GFW combinations.

The helical wrap was wound at a speed of 1.25 rpm and required 10 hours winding time, including one stop to change resin pots.

Approximately 2 hours were required to install the skirt mandrels, and 2.5 hours to wind the eight helical covers. Circ winding speed was 5 rpm and was limited by the ability of the resin pot to pick up the resin. Had variable temperature water (VTW) been available to raise the temperature of the resin slightly, this winding speed could have been increased.

The principal problem encountered was the filling of the skirt-mandrel-case interface area. Further development is required to perfect this technique.

Table XXV presents a summary of the measurement and weight data obtained on GFW Case A-1412 during fabrication.

TABLE XXV

WEIGHTS AND DIMENSIONAL DATA OF GFW CASE A-1412

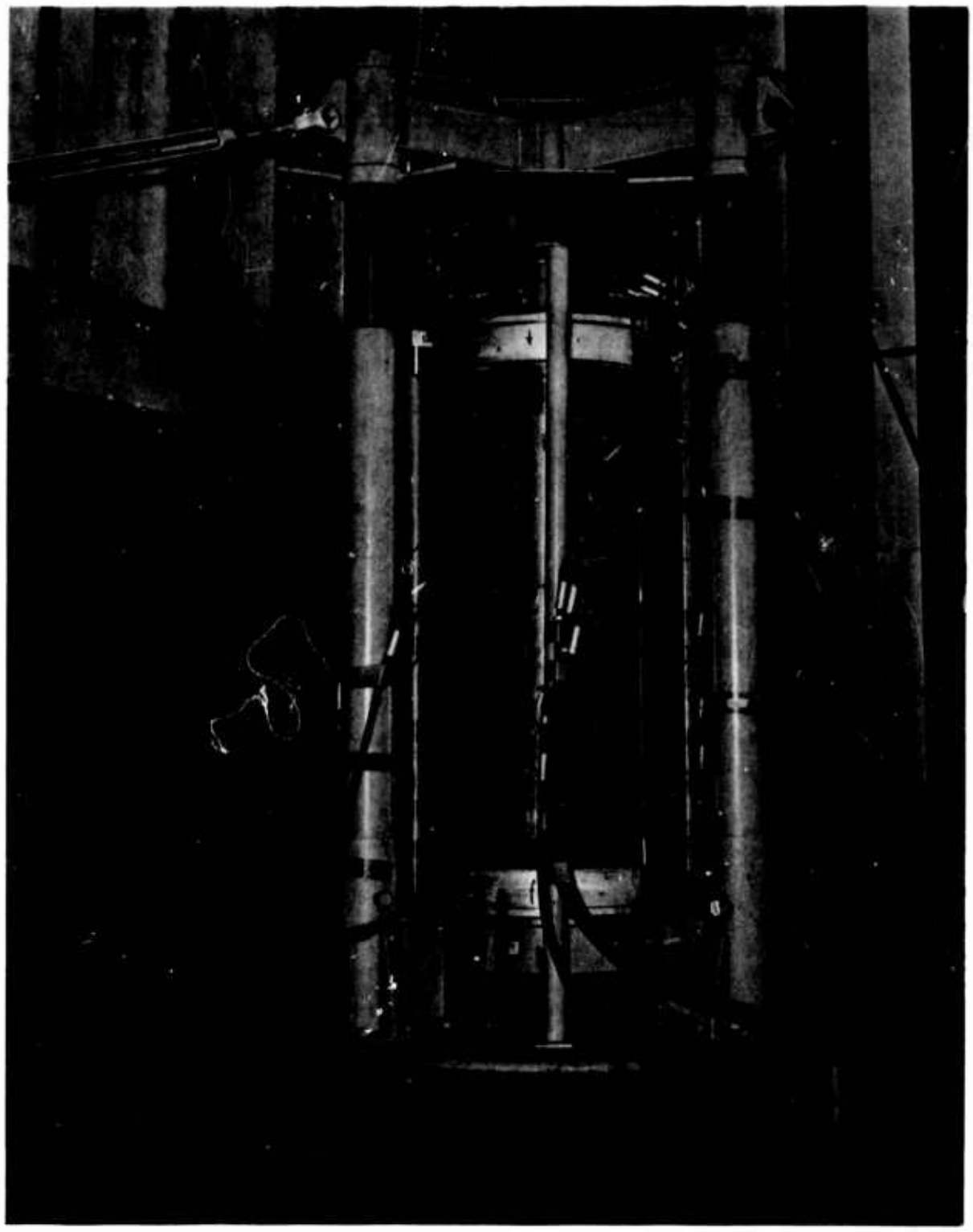
Mandrel Weights, lb	
Flange, aft	2.671
Flange, forward	2.02
Unrestricted mandrel with flanges installed	1679.8
Restricted mandrel	1692.1
Restrictor weight	12.3
Mandrel, case, and skirt rings after cure	1772.1
Case with skirt rings	80.0
Skirt rings	31.9
GFW case only, based on differences of mandrel weights	48.1
Glass Weights, lb	
12-end roving (helix)	11.982
20-end roving (circ)	11.684
Weight of glass fabric in skirts	3.988
Total weight of glass	27.654
Resin content (% by weight)	29.4
Case, based on glass weight and resin content	39.2

TABLE XXV
(Continued)

Diameters (cylinder), in.	Fore	Center	Aft	Average
Mandrel before restriction	29.625	29.650	29.620	29.632
Restricted mandrel	29.715	29.710	29.700	29.708
Average restrictor thickness based on diameters				0.038
Case after cure, before mandrel removal	29.876	29.873	29.863	29.871
Case after mandrel removal	29.860	29.865	29.863	29.863
Shrinkage				0.008
Skirt diameter (average)				29.946
Thickness, in.				
Total wall (cylinder)				0.087
Helical wrap				0.035
Circ wrap				0.052
Skirts at bolt circle				0.155
Lengths, in.				
Inside cylinder length				48.385
Outside skirt-to-skirt length				56.20
Outside boss-to-boss				70.316

○ GFW A-1412 Test

The first hydrotest of a 30-inch diameter GFW case (A-1412) was conducted 10 January 1964, see Fig. 75.



2YA33-1/10/64M1G

Figure 75. Before Hydrotest of Case A-1412

(C) Calculated ultimate pressure for GFW case A-1412 was 770 psig in the hoop direction and 777 psia in the longitudinal direction. Strain measurements were obtained during test by use of strain gages affixed directly to case surface. Typical GFW case instrumentation is illustrated in Fig. 76. Rupture occurred at 538 psig. Failure was a typical hoop failure and approximately 75% of the circ wraps broke, see Fig. 77. The only cylindrical portion which did not fail was a small band approximately 8 inches wide adjacent to the aft tangent plane. Both domes appeared to be in good condition as well as both polar flanges. The forward (lower) skirt was sheared loose from the case but the aft (upper) skirt showed only very slight damage which was limited to one circ roving near the dome-cylinder-skirt junction.

Measurements of the case after hydrotest showed the helical and circ wraps in the cylindrical portion of the case were 0.050 and 0.040 inch thick, respectively. Calculated stress based on these measurements and design stress are given in the following table:

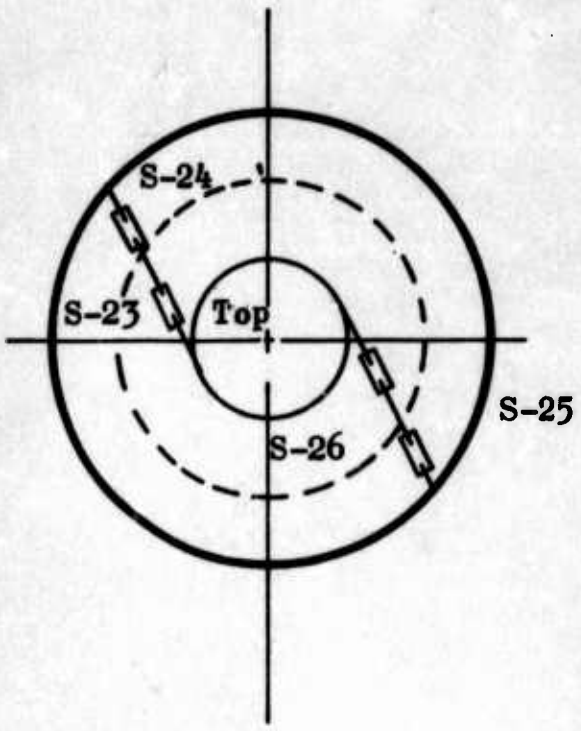
	Stress, psi	
	Calculated	Design
Composite hoop	91,600	---
Helical wraps (direction of fiber)	90,500	230,000
Circ wraps (direction of fiber)	187,500	270,000

The preceding table shows the stress in the GFW case was below design value. Only the stress in the circ wraps in the direction of the fiber is directly comparable because the helical wraps did not fail. Ultimate stress of the circ wraps was only 69.5% of the design value.

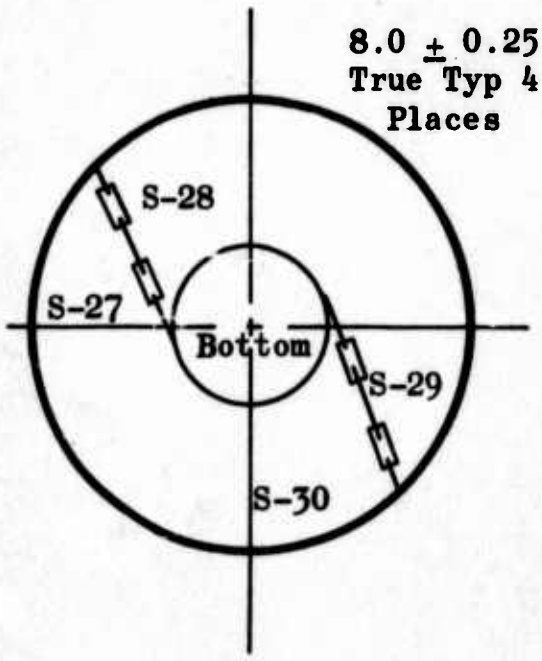
Inspection of the GFW case prior to hydrotest showed an epoxy bulkhead was still inside the case. This bulkhead was formed by the adhesive which the vendor used to bond the sand mandrel halves together. This bulkhead was approximately 2.5 inches wide, and 0.35 and 0.50 inch thick at the outside and inside diameters, respectively. It was decided to leave the bulkhead intact rather than break it out and risk ruining the case.

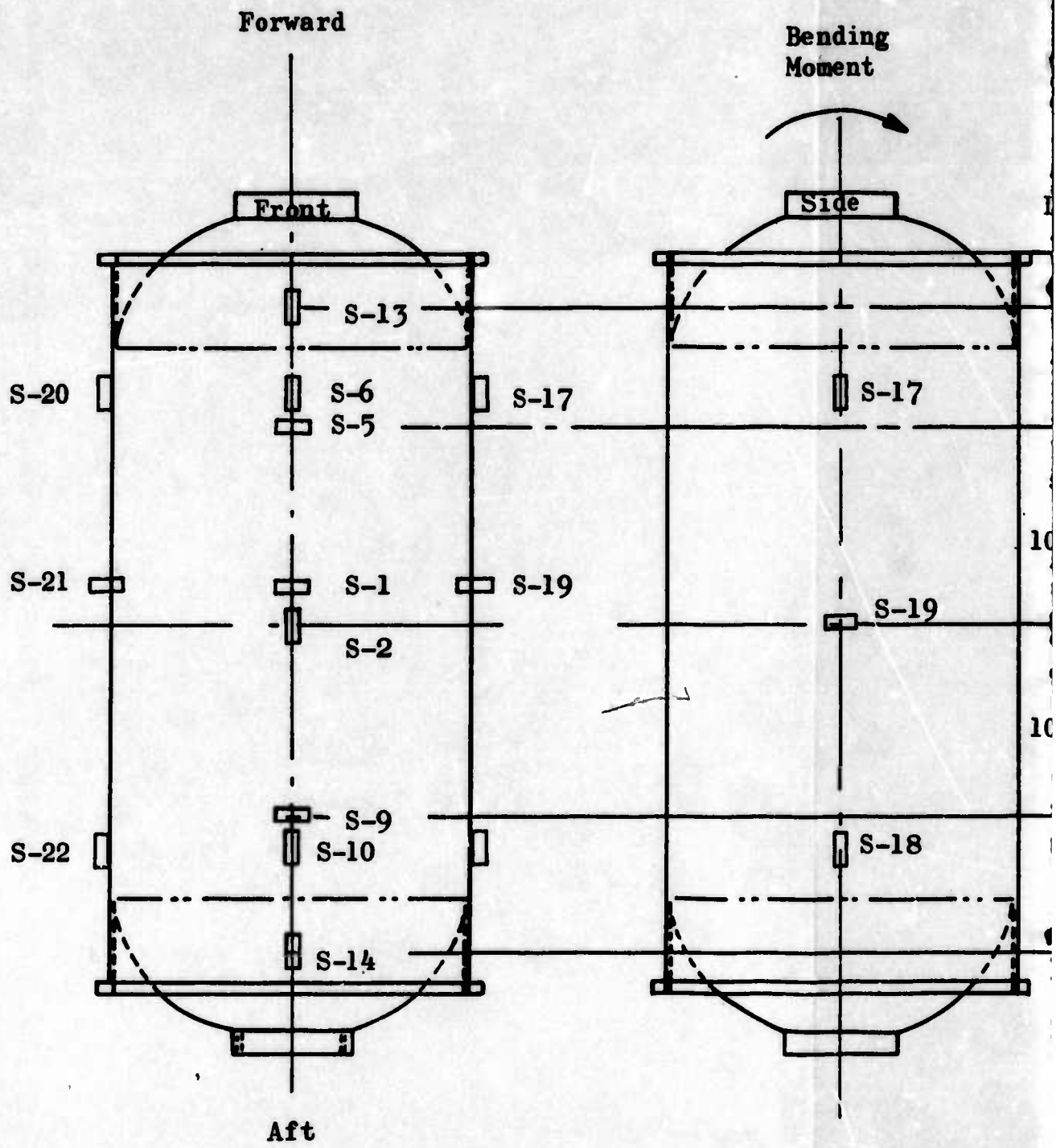
Four additional strain gages were bonded to the GFW case to help determine the magnitude of the stress concentration caused by the bulkhead. One of these gages was not functioning at the start of the test but the other three were satisfactory.

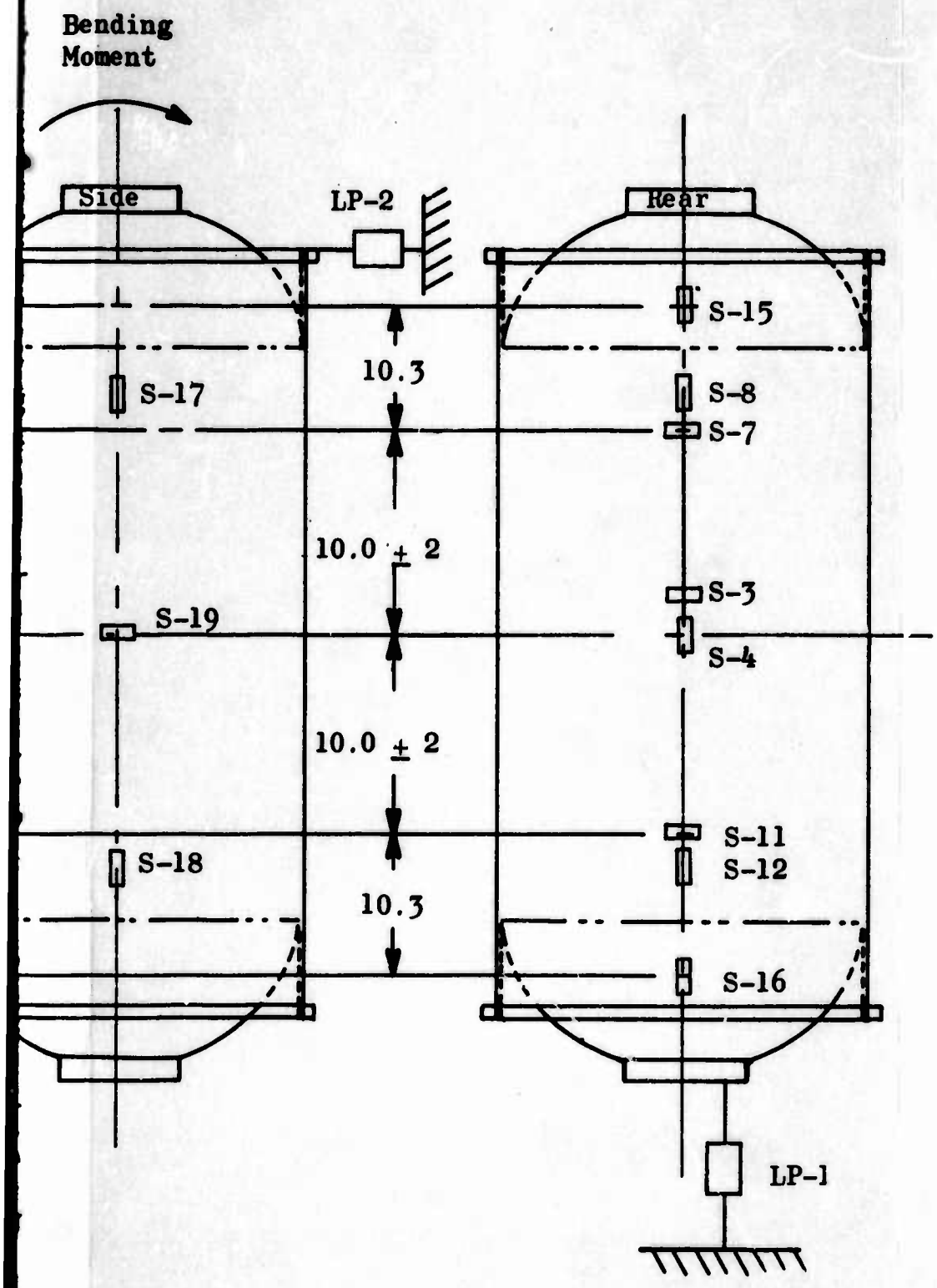
PREVIOUS PAGE WAS BLANK, THEREFORE WAS NOT FILMED



Front







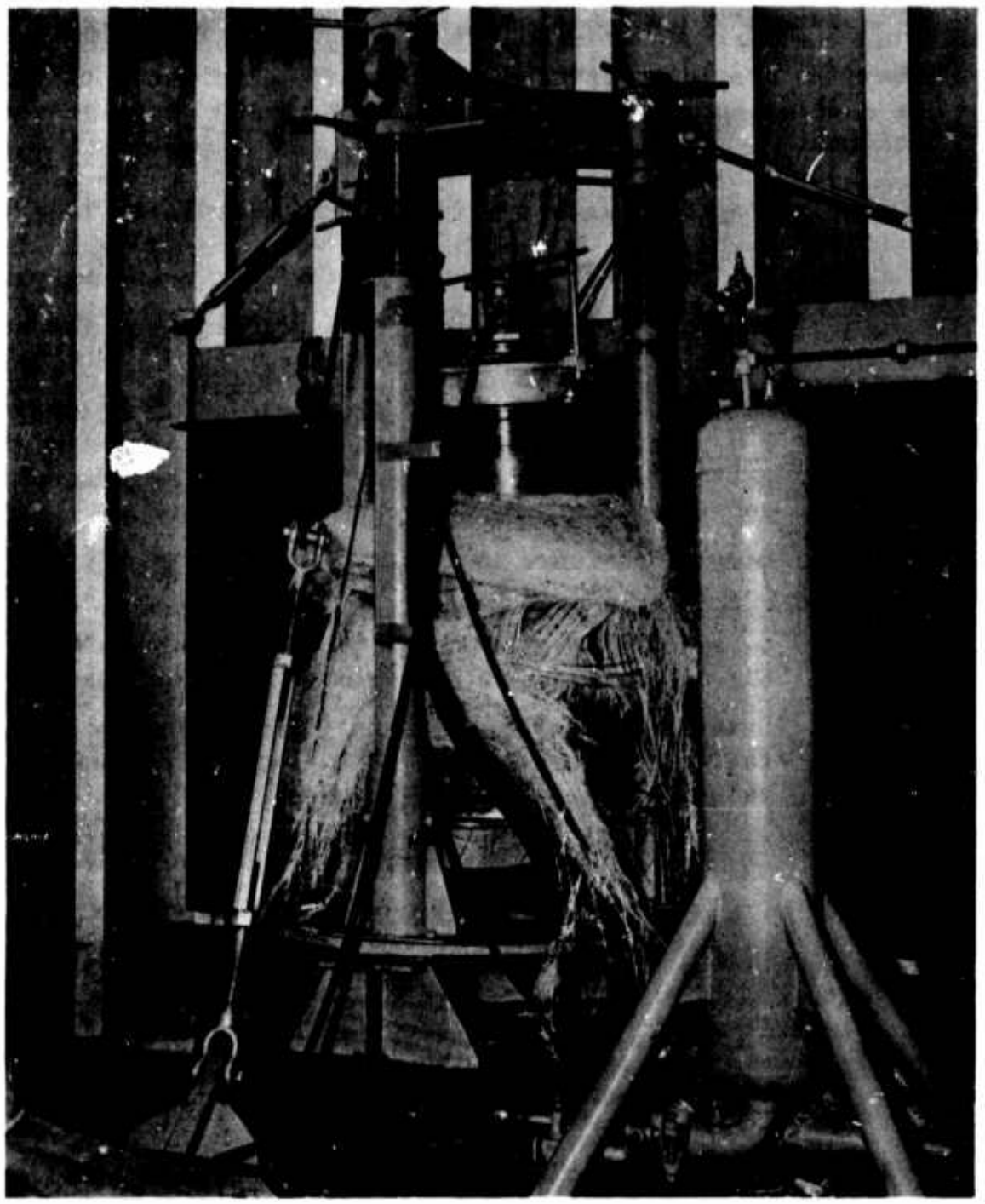
NOTE:

1. Position Case With S-1, 2, 5, 6, 9, 10, 13, and 14 Directly In Line With Tension Cylinder And Toward Front Of Test Cell.
2. Do Not Use PA-7 Strain Gages.
3. Strain Gage Calibration Range ± 35,000 min/in.
4. Locate Gages On Domes In Line With Winding Pattern.
5. LP-1 Must Measure 1.0 Inch Minimum.
6. LP-2 Must Measure 2.0 Inches Minimum.

Figure 76. Typical GFW Case Instrumentation

2

PREVIOUS PAGE WAS BLANK, THEREFORE WAS NOT FILMED



2YA35-1/10/64M1F

Figure 77. After Hydrotest of Case A-1412

Data showed some erratic strain variations in the vicinity of the bulkhead. Four of the six strain gages on the GFW case near the bulkhead were not recording after the pressure reached 485 psig. These data, plug the location of the failure, are not conclusive but do indicate that the case was either damaged near the bulkhead prior to the test or else it caused a stress concentration and resulted in a premature failure.

(C) The following conclusions were made as a result of this test:

1. The hydrotest stand and test setup worked very well.
2. The case liner and LAGZ-coat held 135% of the normal Motor A case operating pressure.
3. Both domes appeared to be capable of withstanding the 770 psig design pressure. This indicated the winding pattern was good and also indicated the unequal dome openings were satisfactory.
4. Rupture pressure was only 70% of design ultimate.
5. Case A-1413 should be designed identically to this case to see if improved fabrication technique would improve the ultimate pressure capability of the case.
6. Data shown in Figs. 78 and 79 indicate the design was fairly well-balanced. Hoop and longitudinal strain values are approximately equal.

- GFW Case A-1413 Fabrication

Case A-1413 was the second full-scale Motor A case, and was wound essentially identical in design to A-1412 except that the skirt length was increased by 1/2-inch on each end. Winding was started on the helical wrap and continued with no serious problems other than a slightly unusual amount of fuzzing of the glass roving.

At this point winding operations were halted and the mandrel was allowed to rotate slowly while heat was applied to the helical wraps to aid in removal of excess resin before the skirt tooling was installed.

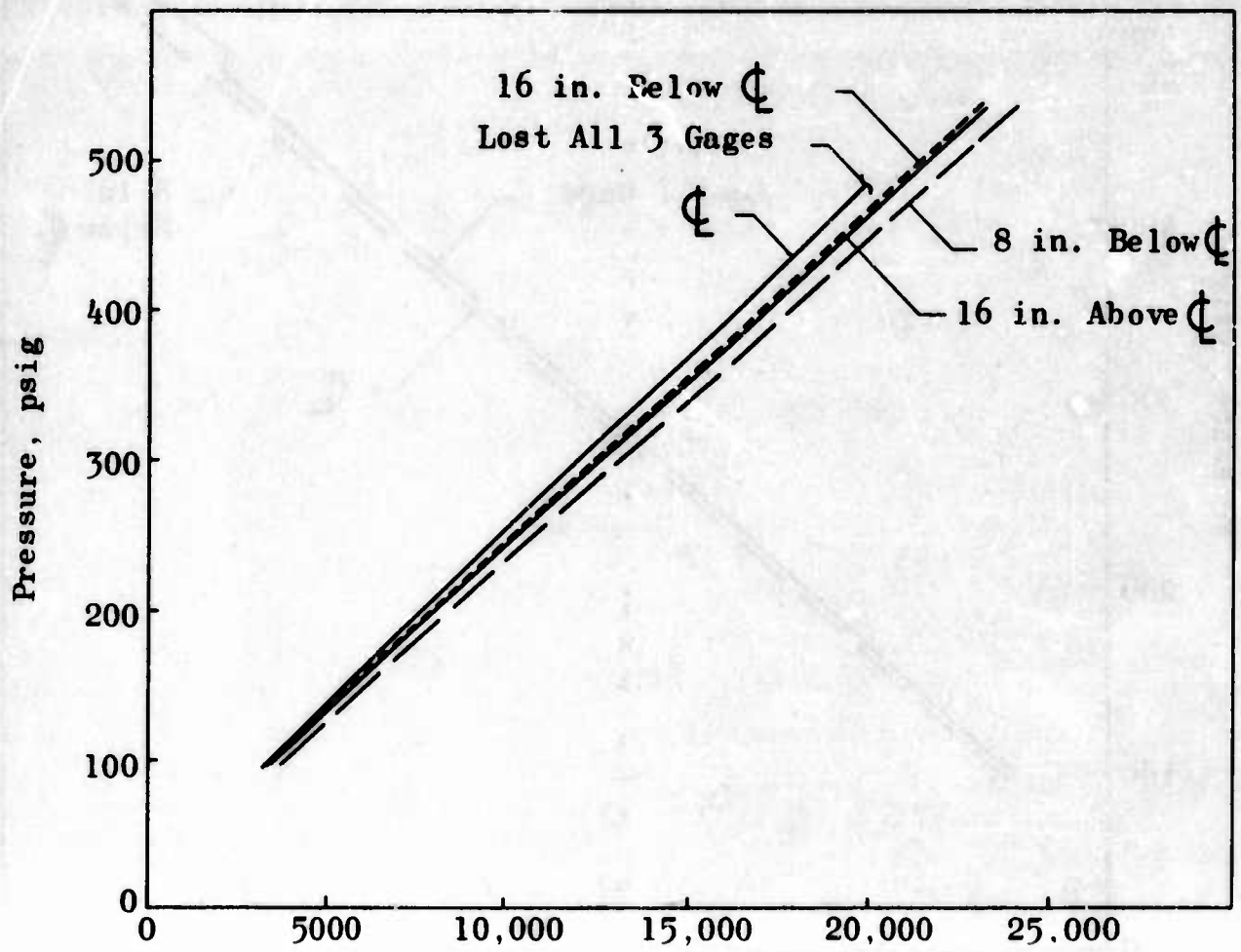


Figure 78. Pressure-vs-Hoop Strain for GFW A-1412

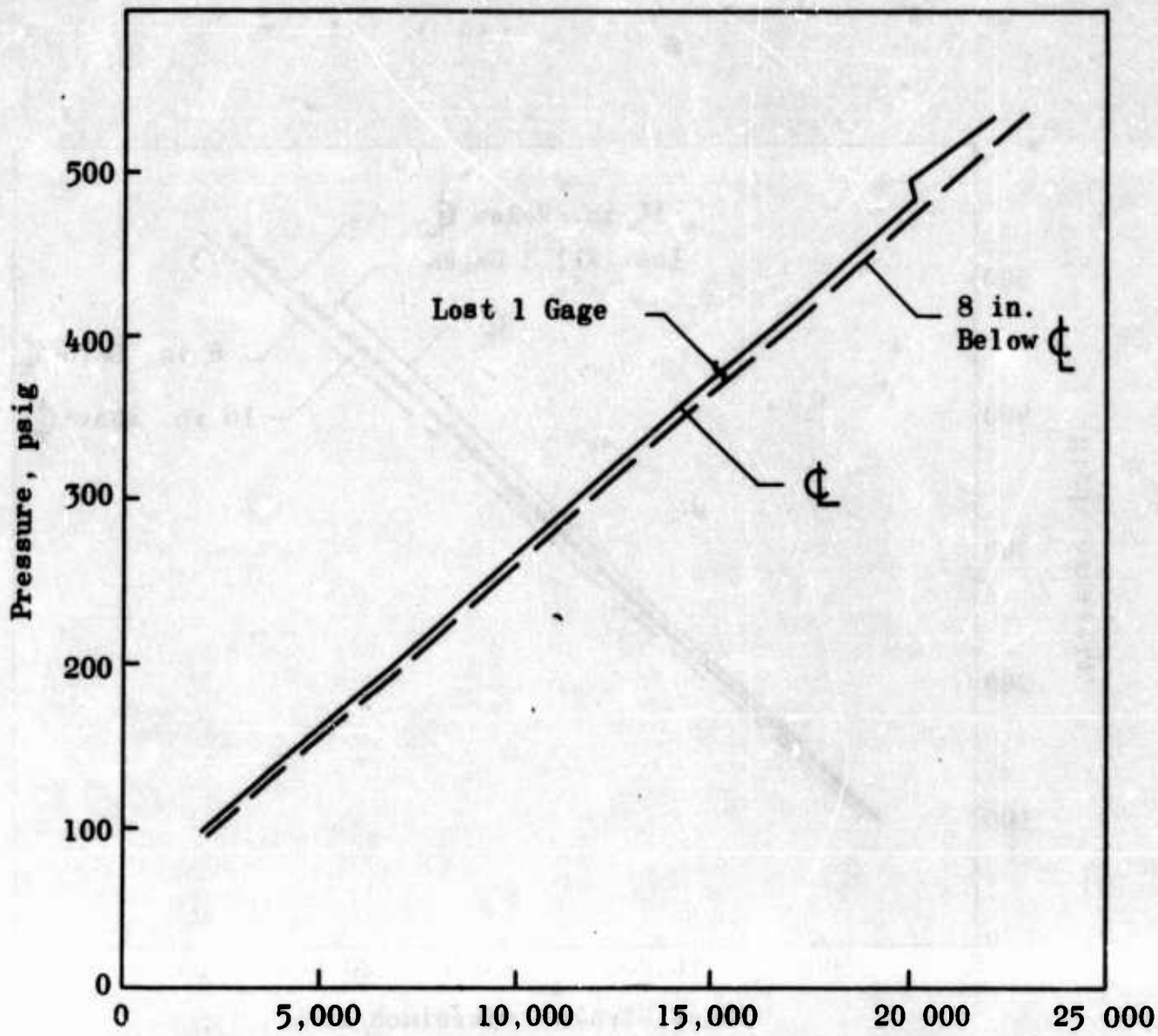


Figure 79. Pressure-vs-Longitudinal Strain for GFW A-1412

Subsequently, the mandrel was removed from the machine and the skirt tooling hung on the spindle. The mandrel was reinstalled and the skirt tooling was worked into position over the domes of the case. At this point it was discovered that the innermost portion of the skirt mandrel support structure was approximately 3/8 inch too long, and the tooling could not be placed in the proper position.

The decision was made to remove the skirt mandrels and send them to the R&D shop for modification. During removal of one of the skirt mandrels it slipped and fell against the aft dome of the helical wraps, cutting approximately a 3-inch gash in the outer layer of rovings. At this point there was no choice but to cut off the entire helical wrap and start over again. It was decided not to start the helical wrap until after the skirt tooling had been modified, placed on the machine, and checked out. This situation was corrected and winding commenced.

During winding, the amount of fuzzing and end breakage was noticeably worse than before and it became apparent that there was entirely too much abrasion of the roving and excessive end breakage. Winding was stopped and the glass was cut from the mandrel.

A modification to the guide pins of the resin pot was made and winding started again. No further fuzzing or end breakage occurred, and the helical layer was completed.

The mandrel was rotated, wiped, and the skirt mandrels were placed in position for circ wraps. Winding of circ wraps commenced and no unusual problems were encountered.

The winding of A-1413 was plagued with a series of unfortunate occurrences, some of which were preventable. It is believed that the final product was not unduly affected by these events. Considerable improvement was made in the smoothness of the joint between the skirt and dome. Also, better control of both tension and resin content was possible with the new resin pot. The actual winding speed of the helical wrap was increased by 40% on this case, largely due to the smoother cam contour used. The winding data are presented in Table XXVI.

(C)

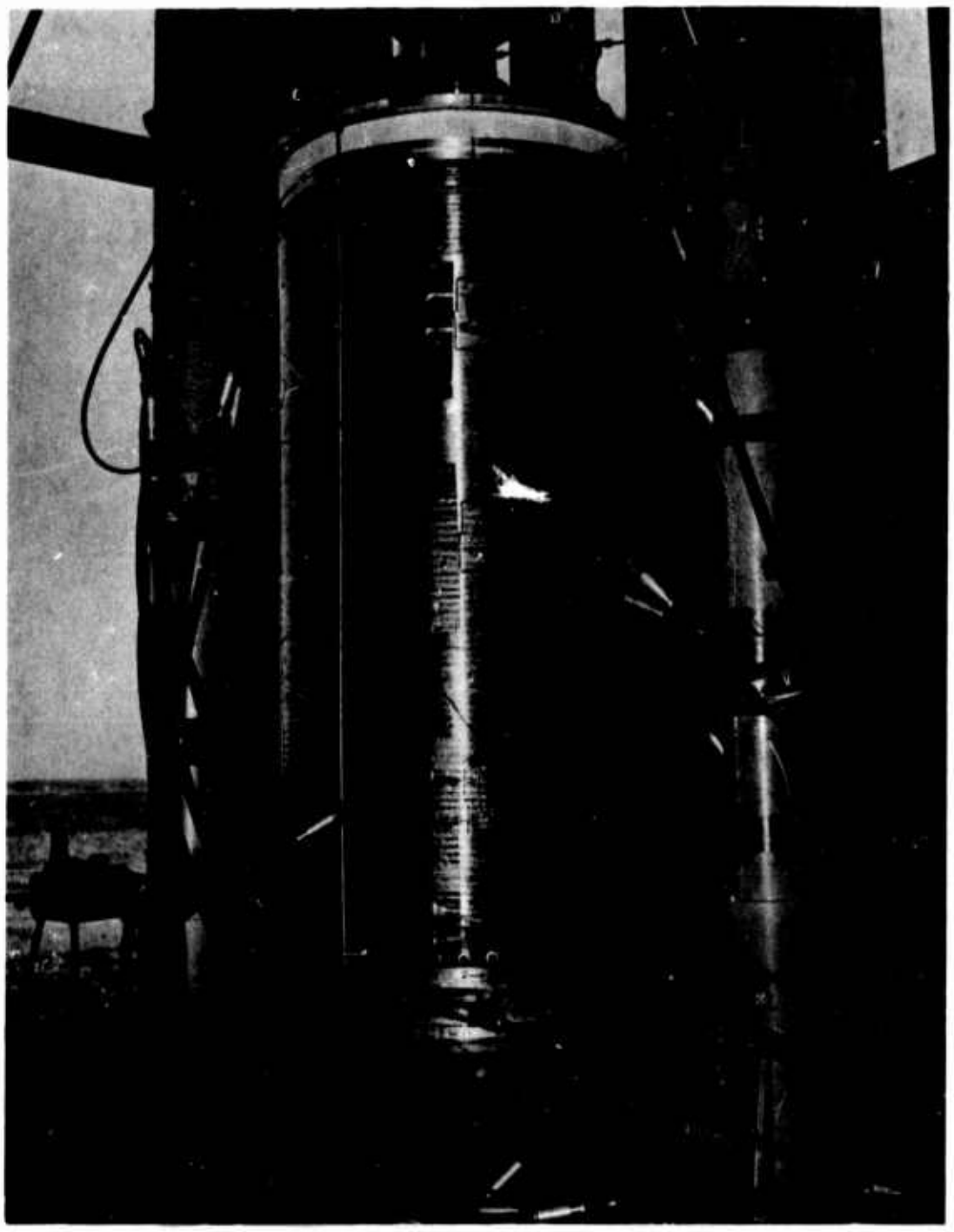
TABLE XXVI

WEIGHTS DATA OF GFW CASE A-1413

Mandrel Weights, lb	
Unrestricted mandrel with flanges installed	1679.6
Restricted mandrel	1697.4
Restrictor	17.8
Cured case, with mandrel, and skirt rings	1780.9
Case with skirt rings	83.5
Skirt rings	32.0
GFW case only, based on differences of mandrel weights	51.5
Glass Weights, lb	
12-end roving (helix)	11.434
20-end roving (circ)	12.430
Estimated weight of glass fabric	4.02
Total glass weight	27.884
Resin content (% by weight)	29.4
GFW case, based on glass weight and resin content	39.5

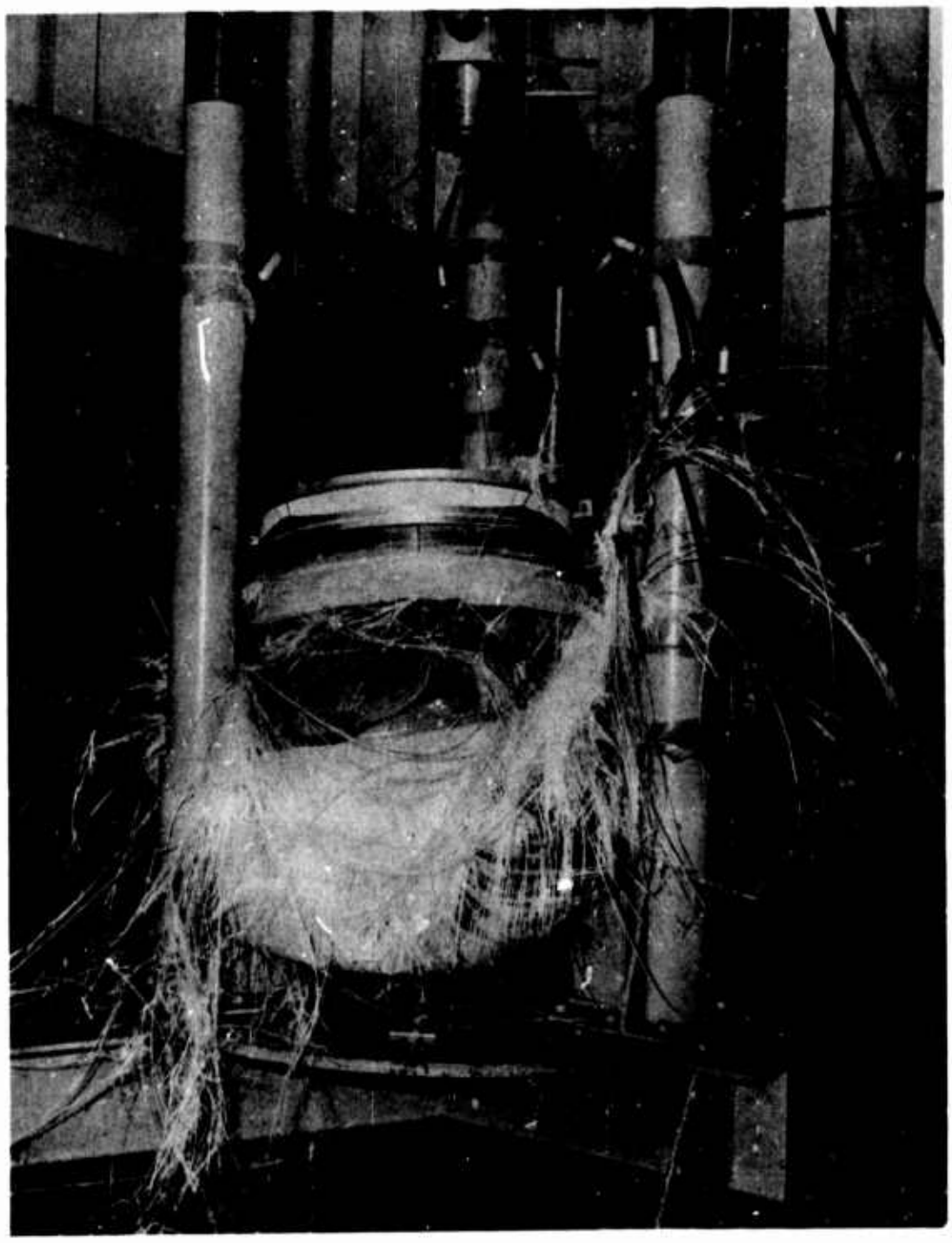
○ GFW Case A-1413 Test

(C) GFW A-1413 was set up to hydrotest 27 January 1964 see Fig. 80. Rupture of the case occurred at approximately 641 psig which is 19% higher than the first case (539 psig), but still 15.5% below the design ultimate pressure of 770 psig, see Fig. 81. The initial failure, as shown by movies, was in the cylindrical section about 2.5 inches forward of the aft tangent plane. A discontinuity, which is caused by ending the skirt glass fabric, exists at this location, and was probably the major reason why the GFW case did not reach the design ultimate pressure. No stress concentration factor was included in the calculated ultimate pressure of 770 psig because previous 10-inch test data indicated only a small stress concentration factor existed at this point.



2YA33-1/27/64MTA

Figure 80. Before Hydrotest of Case A-1413



2YA35-1/27/64M1C

Figure 81. After Hydrotest of Case A-1413

Measurements of the helical wraps after hydrotesting indicated a thickness of 0.033 inch, which was an improvement over the 0.040 inch thickness of the helical wraps on GFW case A-1412. There were not enough circ wraps left intact to give a representative sample for thickness measurements of the circ wraps. From observation prior to testing, however, it appeared that the circ wraps had a great deal of excess resin and were probably thicker than those on GFW case A-1412. No accurate estimate of the resin content could be made, but it was high enough that approximately 70% of the strain gages bonded to circ wraps were lost before the case ruptured. The presence of excess resin will cause premature gage failure due to localized resin crazing (resin cracking) which causes a local stress and premature gage failure. All of the gages bonded to the helical wraps were still functioning properly at the time of rupture.

Deflection data, as measured with linear potentiometers, appeared to be excellent with the exception of the aft dome. This linear potentiometer bottomed out after approximately 0.3 inch deflection. The necessary travel for the manner in which it was mounted was 1.5 inches. Pressure-vs-strain curves (Fig. 82), were almost identical to A-1412 except for the 19% increase in pressure which also increased the helical and circ wrap strain from approximately 2.4% to 2.7%.

Some changes based on this test were made in the fabrication of the GFW case for the RFG/GFW A-1006 composite hydrotest. GFW case A-1414 was fabricated after A-1006 which is discussed under the full-scale motor section. These changes are tabulated here:

1. Wrap a flightweight case as originally designed
2. Use 12-end roving for all wraps instead of 12-end for helical wraps and 20-end for circ wraps (as was done on A-1412 and A-1413)
3. Remove excess resin from the helical wraps, as done on A-1413
4. Remove excess resin from the circ wraps, even if it requires removing the grain and case from the oven once or twice during the cure cycle
5. Modify the skirt design to reduce the discontinuity

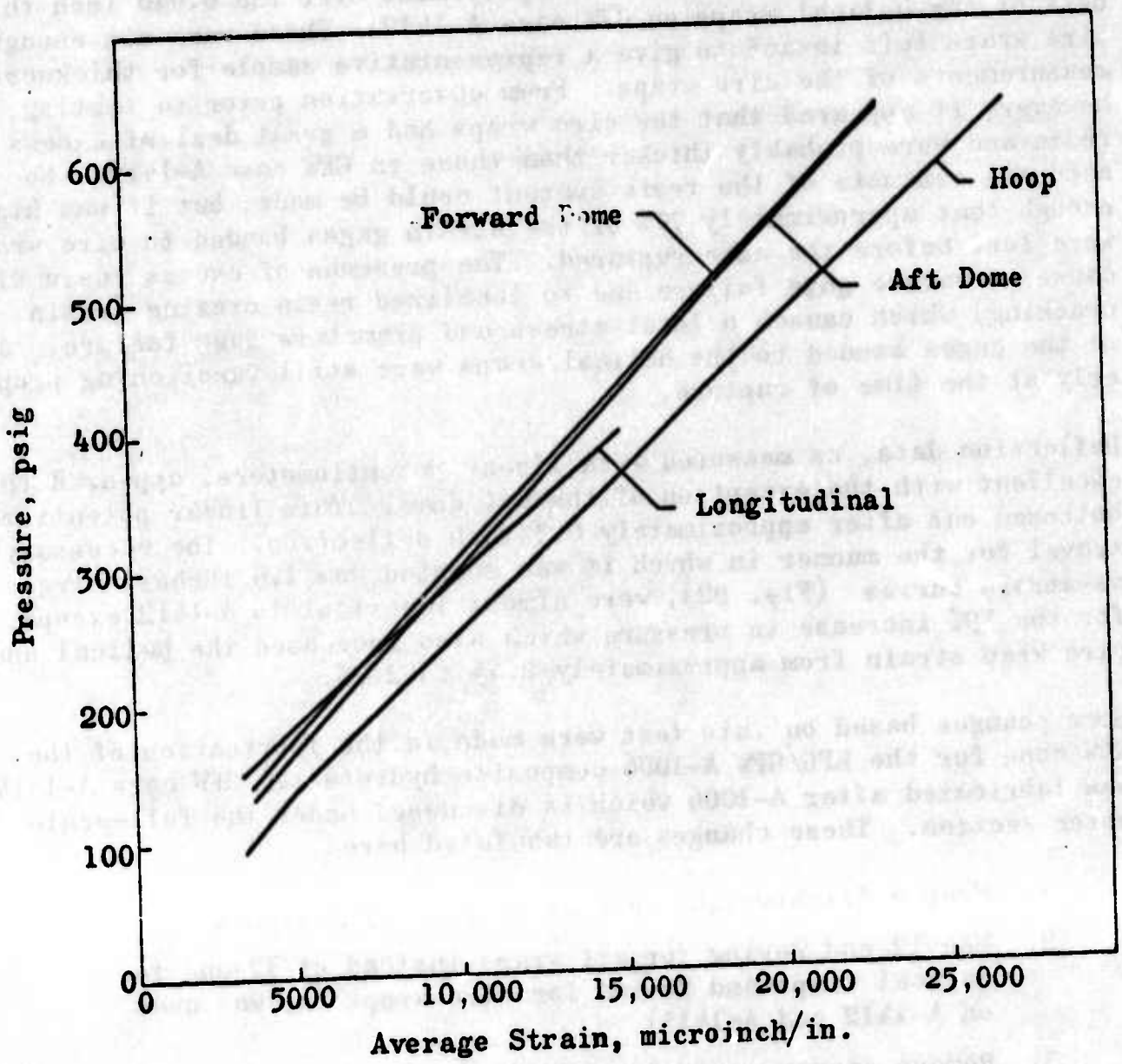


Figure 82. Pressure-vs-Average Strain for GFW A-1413

○ GFW Case A-1414 Fabrication

This was the third and final destructive test of a 30-inch diameter case, but it was the first and only test of a flightweight Motor A case without the RFG. It differed from previous Motor A fabrication development cases in that (due to the bending load to be applied) the straightness of the skirt could not be compromised. Development work undertaken just prior to fabrication indicated that the most readily available method of making the transition fill between case cylinder and skirt ring was nylon cord and room cure rubber, PRC-1201. However, the actual fabrication was unusually difficult and lengthy due to the unpredictability of rubber cure.

Further study was made during actual winding, using the same batch of rubber and curative to be used in the transition area. An excellent fill was eventually made by preheating the rubber to 130 F prior to adding the curative. The material had about 15 minutes working life and cured to good firmness in 3 to 4 hours using hot air blowers. Figure 83 shows how the skirt area was built-up, and the area that was affected by heat.

The problem of filling in the 3-inch gap between the thrust attachment ring and the tangent line was a very difficult one to solve for the following reasons:

1. The fill must be as flat as possible to avoid having built-in corrugations in the skirt
2. The fill must be firm enough to withstand the compressive force of winding tension
3. The fill must be a material that can be applied to the mandrel between the helical and circ wraps, while the case is on the winding machine. If cure is required, it must not involve sufficient heat to be detrimental to either the case or propellant.
4. The fill material must be either completely removable, or partially removable and sufficiently pliable to prevent excessive stress concentrations when the dome expands.

These conditions were not all met within the time and fabrication development allowances of the program. Two alternate approaches are offered, but both require added fabrication development work.

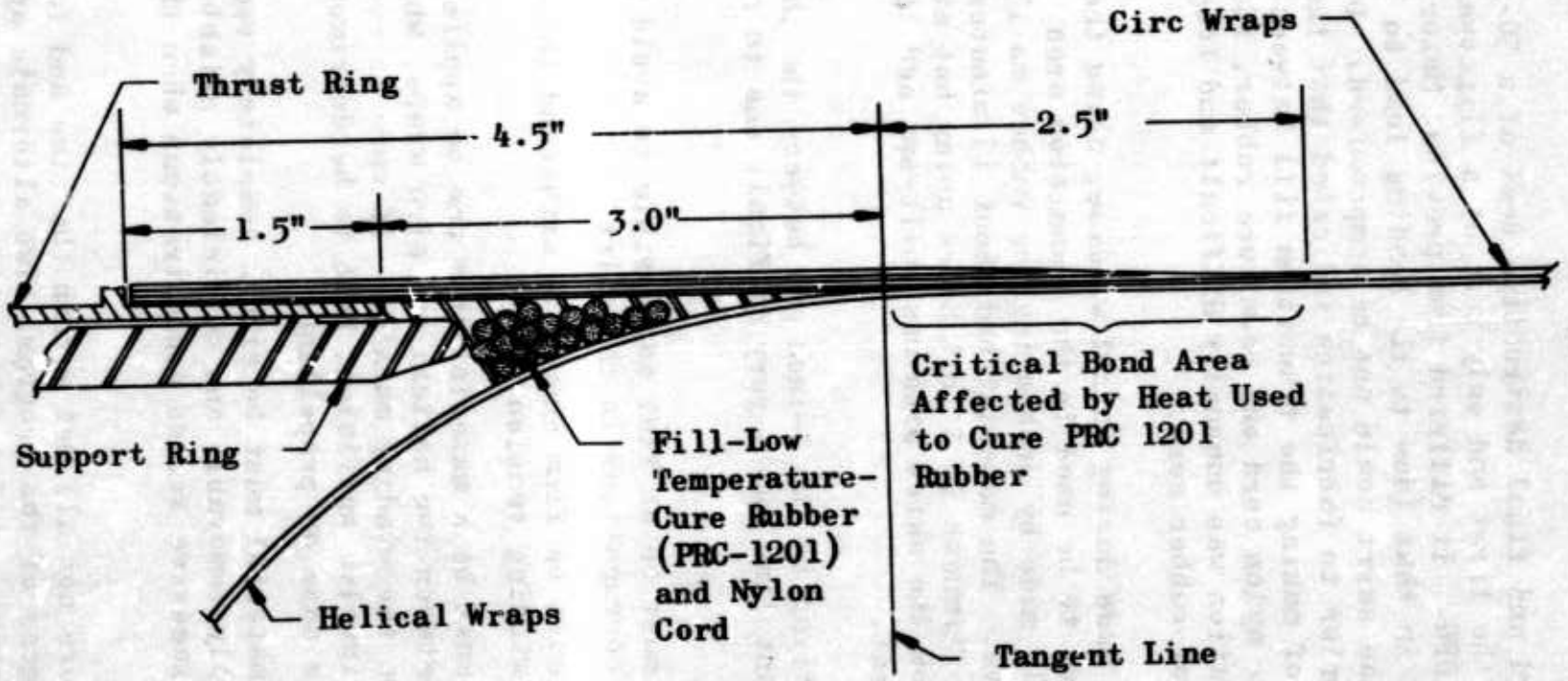


Figure 83 Case/Skirt Buildup on Case A-1414

1. A preformed silastic rubber grommet would be used in the fill area instead of the PRC-1201 now being used. If this grommet fits properly it would simplify the processing problem of making the fill and reduce the time required between helical and circ wrapping. It would also eliminate the requirement for heat. However, it is questionable if this would yield as straight a skirt as desired, and whether or not it would be possible to remove after case cure.

2. Redesign the skirt winding mandrel to the more conventional type that extends all the way in to the case dome and would require only a 1/8- to 1/4-inch fill instead of a 3-inch fill. This mandrel would have to be completely removed after cure. A thrust ring would have to be made to fit the skirt ID and be pressed into the skirt (rather than the built-in thrust ring used).

Either of these methods would require the fabrication and testing of another case to prove the skirt strength. The first method would be the least expensive, and the second would be the most likely to succeed.

After winding was completed, the case was wound in paper toweling and dry glass roving under high tension with a metal strip the length of the case between the toweling and roving. After 10 minutes in the 170 F oven, the roving was cut (using the metal strip for backing) and the paper toweling was removed. This procedure reduced excess resin and gave a much better looking surface to the case.

Some difficulty was experienced in removing the toweling in the skirt area, where resin from the B-staged cloth seeped through. It is planned to use glass cloth under the paper toweling in the skirt areas on the next case.

Due to the unpredictability of cure of PRC-1201, it was suggested, on future cases, to run preheat/cure tests simultaneously with helix winding. It is anticipated that these tests will eliminate skirt winding problems and reduce case processing time to the minimum.

○ GFW Case A-1414 Test

GFW case A-1414 was tested to failure 12 March 1964. The flightweight case was designed to withstand a limit internal pressure and limit

(C) bending moment of 468 psig and 8.0 x 10^5 in.-lb respectively. These loads with a 1.25 load factor are equivalent to an ultimate pressure and ultimate bending moment of 585 psig and 1.0 x 10^6 in.-lb respectively.

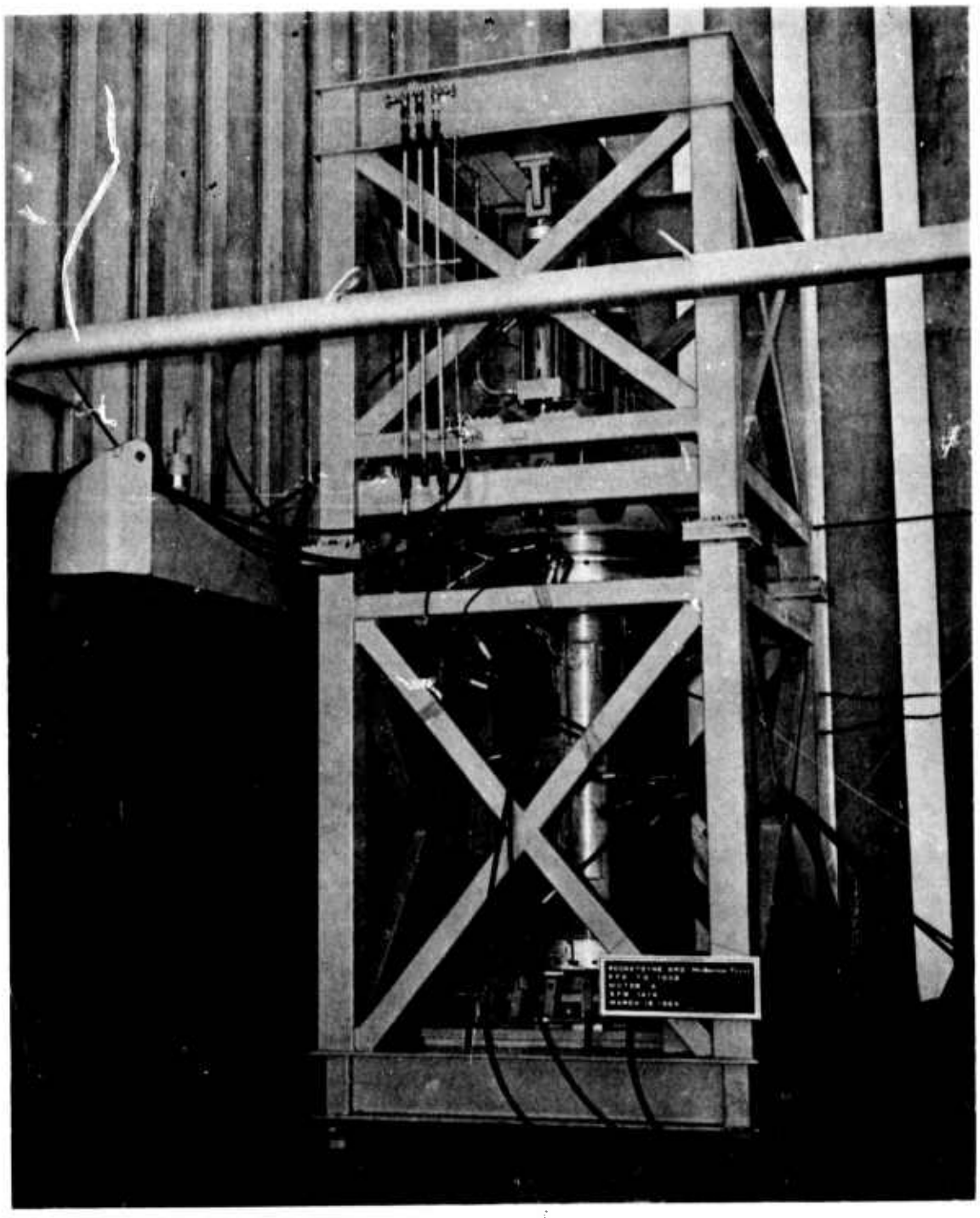
(C) GFW case A-1414 was pressurized to 170 psig in 30 seconds and held approximately constant while the bending moment was applied. The bending moment was applied and reached a value of 8.0 x 10^5 in.-lb at 58 seconds. Pressure was increased from 170 psig at 70 seconds to 497 psig before the case ruptured. The servo valve on the compression cylinder had a tendency to stick and when the pressure was increased from 170 psig, the compressive force increased from 17,000 pounds to 21,000 pounds before the sticky valve freed itself and the force returned to 17,000 pounds. At 80 seconds the bending moment was approximately 9.0 x 10^5 in.-lb and is the maximum bending moment which was applied to the case before failure of the cylinder-skirt bond at 90 seconds.

(C) Movies of the test showed the skirt pulled off of the cylinder and broke some of the circ wraps at a pressure of approximately 295 psig. This damage, however, did not cause failure of the pressure vessel until 30 seconds later when the pressure reached 497 psig.

(C) Damage to the circ wraps, which occurred when the skirt-cylinder joint failed, probably contributed to the slightly low burst pressure but strain gages located on the opposite end of the cylinder indicated the case would have burst below 585 psig without the skirt failure. Longitudinal strains in the cylinder and strains in the domes were very close to the expected values, but hoop strain was approximately 10 to 15% higher than expected.

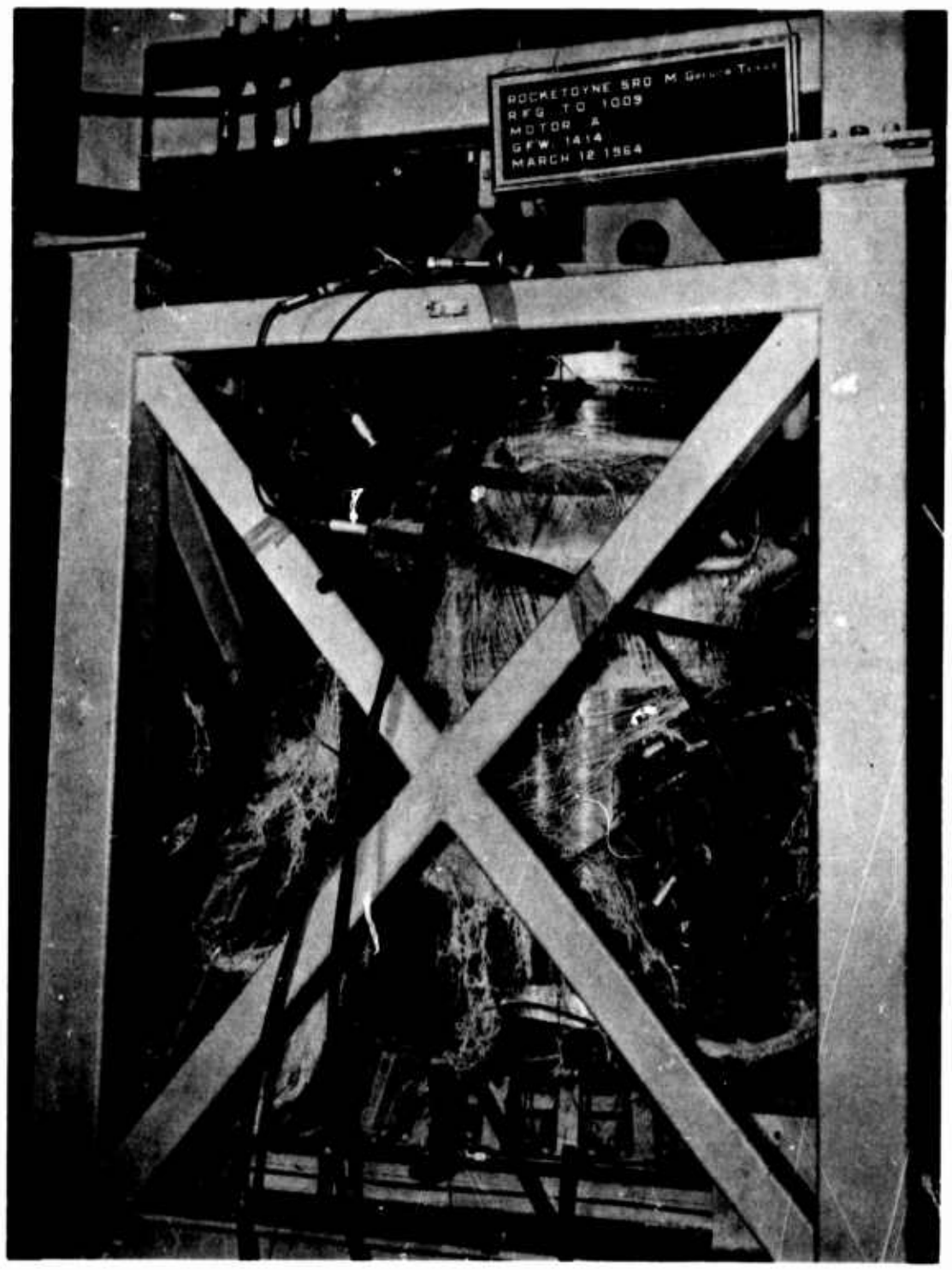
Pictures of this case before and after testing are shown in Figs. 84 and 85. The data relating strain and pressure are presented in Fig. 86.

As a result of this final case test, no change was made in the helical wrap, but the circ wraps were increased approximately 15% to meet the design requirements. Because some fabrication problems were encountered with the skirt on this case and improved fabrication techniques were expected to increase the strength of the joint 10%, no significant design change in the skirt was planned. The resin content of this case was approximately 30% (by weight) and additional work was planned to get the resin content down to the design value of 20%.



2YA43-3/12/64M1B

Figure 84. A-1414 Before Testing



2YA45-3/12/64M1D

Figure 85. A-1414 After Testing

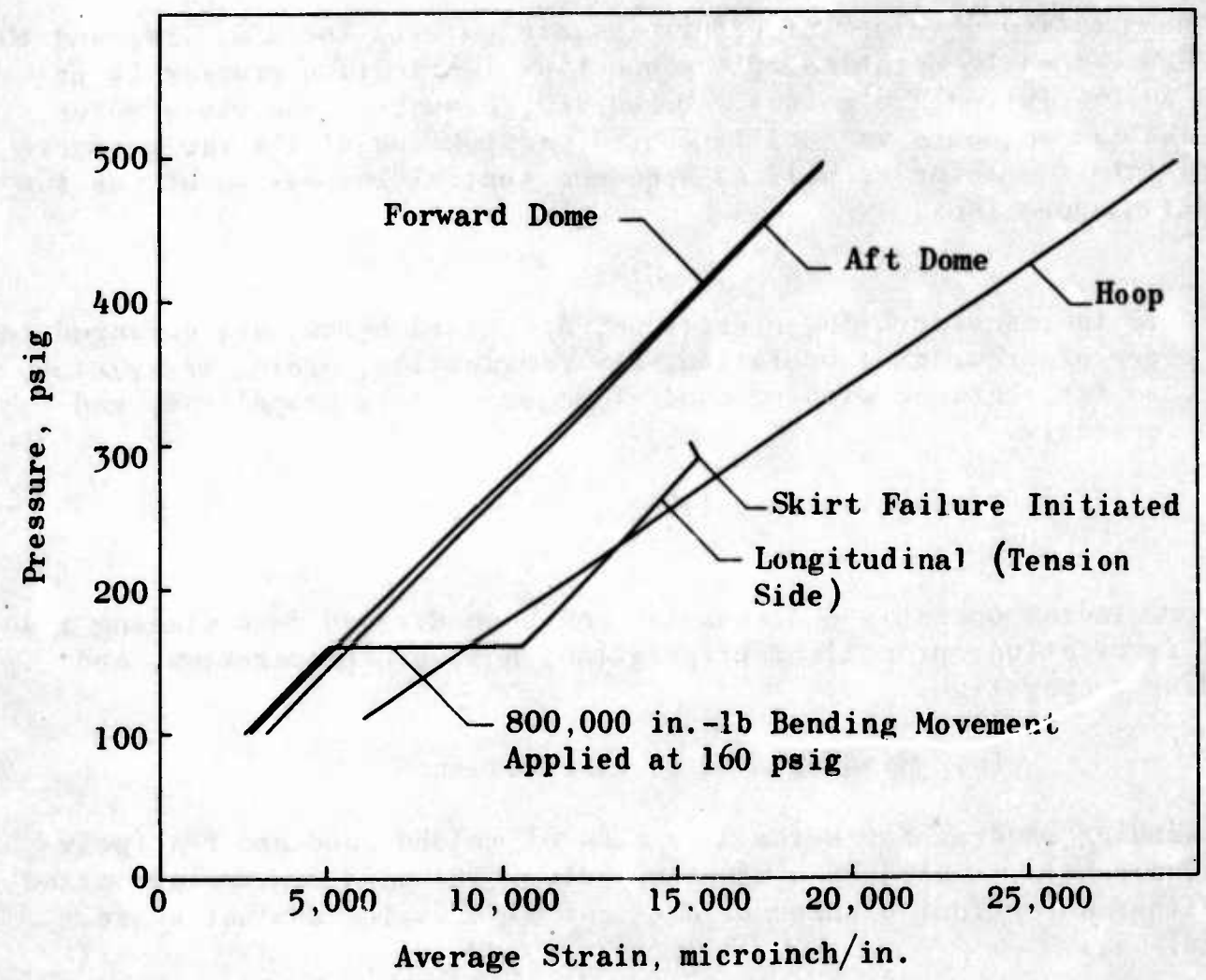


Figure 86. Pressure vs Average Strain for GFW A-1414

e. Processing Procedure

The fabrication development effort associated with the RFG, GFW, and the RFG/GFW composite established a sequential fabrication process to be used on the full-scale motors. Disbursed throughout the whole motor fabrication sequence is quality control inspection of the raw products going into the motor as well as sequence control inspection of the fabrication operations.

The detailed manufacturing operations, discussed below, are arranged in the order of prewinding operation, RFG fabrication, grain, restrictor, GFW case fabrication, winding mandrel removal, core propellant, and motor assembly.

(1) Prewinding Operation

The prewinding operations discussion has been divided into winding mandrel fabrication, propellant preparation, hardware preparation, and winding preparation.

(a) Winding Mandrel Fabrication

The winding mandrel for Motor A is made of molded sand and PVA (polyvinyl alcohol) mounted on a steel spindle. The sand mixture was mixed in either a vertical blender or a cement mixer. The nominal binder formula is:

	Wt, %
Water	70
Polyvinyl alcohol	20
Ethyl alcohol	8
20% Sodium hydroxide	1.8

This binder was mixed 5 parts to 100 parts of sand. The binder was frequently mixed in advance in a Hobart mixer and stored in airtight containers. The mandrels were made in fiberglass molds in two halves which were bonded together with EC-1648. Either the polar bosses or simulated bosses were placed in the molds to shape the sand. The molds were coated liberally with silicone grease as mold release agent. The sand was

packed continually as the mold filled and the mandrel dried in the oven at 190 to 225 F. Dry time varied between 48 and 72 hours depending on use of vacuum. After mandrel removal from the molds the two sections are bonded together and the taper for mold release was worked down to get the cylindrical requirements.

(b) Propellant Preparation

Special propellant development was undertaken for the reinforced grains matrix during the early development phase. One of the advantages of reinforced grain is the ability to process uncastable propellant and achieve a higher total solid loading. Matrix propellants contain either 87 or 88% oxidizer with a bimodal or trimodal blend of oxidizer. In some propellants, some fine oxidizer is replaced with a burning rate modifier. RDS-514 and RDS-523 with large amounts of burning rate modifier are very difficult to process due to high viscosity. Some propellants use 10 micron spherical oxidizer instead of regular 7--11 micron grind to reduce viscosity.

○ Matrix Propellants Burning Rates

The following matrix propellants have been formulated for Motor A reinforced grains. Liquid strand rates multiplied by 1.175 will give motor rate (radial direction).

(C)

Designation	Lab Spec. No.	Mfg. Spec. No.	Lab Adv No.	Liquid Strand (in./sec)	Remarks
RDS-514	RA0119-934	RA0119-935		0.21--0.33 @ 1000 psi	0 to 2.5% depressant
RDS-523	RA0119-948	RA0119-949		0.15--0.21 @ 600 psi	1.0 to 6.0% depressant
RDS-529	RA0119-962	RA0119-963	60	0.112 + 0.030 @ 600 psi	Used at load ring area only
RDS-526	RA0119-958	RA0119-959	53	0.42--0.46 @ 750 psi	25 to 40% grind/ total AP

○ Propellant Storage

(C) Since grains require some time to wind, propellant usage is slower than mixing rate and propellant must be stored after mixing and before use. The heat history (time at elevated temperature) is minimized by moving the propellant to a -70 F cold box as soon as possible (3 hours after curative addition) after casting the mix into tubes. Samples are taken of the mix and results accepted prior to use. In this way all propellant is determined as acceptable before use instead of relying solely on liquid strand burning rates as is done in normal motor casting. Propellant has been stored as long as four months at -70 F with no significant change in physical properties. Prior to use, the propellant is stored at ambient for about an hour, then placed in a 170 F oven for a minimum of 30 minutes. Propellant stored in the oven for two hours becomes too viscous to use, especially for high solids content. If more than 50--60 psi is required to extrude the propellant from the tube at a reasonable rate, it is discarded because the high viscosity will produce off design buildup and increase the possibility of voids.

○ Application

Propellant is applied to reinforced grains with the use of pneumatic propellant feed guns. The guns are filled with cylindrical polyethylene cartridges which are filled with propellant; finally a sealing cup is inserted. The propellant gun is connected to dry air or nitrogen and the propellant is then extruded out the gun nozzle onto the grain. The nozzle is pressed against the grain to make the propellant adhere to the grain. The entire grain is wound with a slight excess of propellant to prevent voids. The propellant layer should not exceed 1/16-inch thickness, to allow the wire to pull down to the previous wire cover.

On grains as large as Motor A it is desirable to add the propellant faster and more uniformly than can be done with the manually operated guns presently used. An automatic propellant feed system was designed and fabricated utilizing larger propellant cartridges. This feed system was designed for the cylindrical grain section only (domes must still be covered manually). The changing curvature of the domes as the grains are wound make the construction of an automatic feeder for the domes too complicated and expensive for the present state of development.

(c) Hardware Preparation

The hardware preparation consists of coating and water-proofing the polar bosses, load ring cleaning, priming and wrapping with plastics for surface protection, cast polar flange coating, and glass case skirt attachments weighing and installing before case winding.

O Polar Bosses

The bosses are fabricated at the machine shop where the load ring steps are machined in the plastic (leaving a porous surface subject to moisture absorption). Therefore, when the bosses arrive at the processing area they are cleaned by wiping with a cloth saturated in methyl ethyl ketone (MEK) then oven dried at 225 F. When cool, each boss is coated by brush or spray with Epon 926 for moisture proofing and cured 2 hours at 190 F. The aft boot is then bonded to the polar boss using EC-1648. The boss and boot are enclosed in polyethylene and polyken tape and/or RTV-60 rubber as additional protection from moisture during mandrel molding and washout. Extreme effort is made to keep the surface clean for subsequent propellant bonding. After coating and preparation the bosses are stored enclosed in polyethylene with desiccant.

O Load Rings

The titanium rings are cleaned by water washing, immersion in nitric acid solution, water washing, tri-sodium phosphate/hydrofluoric acid solution, water washing, then oven drying. The rings are then coated with a bondmaster primer individually wrapped with strips of polyethylene and labeled. The number one load rings are bonded to each boss using EC-1648 adhesive prior to assembly in the mandrel.

O Case Polar Flange

The case flange is cleaned and coated (using the same procedure as used on the load rings) and enclosed in polyethylene for storage.

(d) Winding Preparation

The mandrel preparations prior to winding included installing the polar bosses and coating the mandrel with Tenite[16], RTV[17], and tape[18]. The Tenite is used to seal the sand surface and the give the liner sufficient rigidity to hold it to the grain during sand/PVA washout. The Tenite is applied in seven layers. The RTV (3--5 mils thick desired) is used as a safety liner should the tape layer (applied just before winding) not be waterproof. It is applied by spraying. To form a seal, the inside surface of the bosses were taped radially and coated with RTV and had a 1--2 inch flap of tape extending beyond the number one load ring. This flap overlapped during mandrel taping. The tape layer was overlapped on itself 50% on the cylinder and 66% on the domes. It was stretched only enough to prevent wrinkles and make good contact. The tape acts as a release agent; it does not bond to propellant.

Figures 87, 88, 89, and 90 illustrate the different steps in mandrel preparation, i.e., Tenite coating, RTV coating, boss installation, and taping.

The specified wire guide is installed on the follower to obtain the desired wire spacing. The wire spools are mounted on the tensioner spindles[19], the tensioners are each checked, cleaned, oiled, and adjusted as necessary; and 36 wires are threaded through wire guides to the mandrel. The wire tension is checked on each wire as soon as winding begins. In the background of Fig. 91 the assembled system is shown.

Preparation for winding includes, in addition to mandrel assembly and coating and wire preparation, such things as: preparing data sheets with gear ratios and requirements, arranging cams, designation of propellant, oven adjustments, setting up the contour pantograph (a device to translate the actual measured dome contours being wound to paper for design verification) with prepared mylar tracing of required design contour lines, installing and aligning spreader blade, and setting-up propellant feed guns.

---

(16) Tenite is an Eastmen Kodak acetate product used to seal and coat the mandrel surface.

(17) RTV-30, -60 are G.E. room temperature cure silastic rubbers.

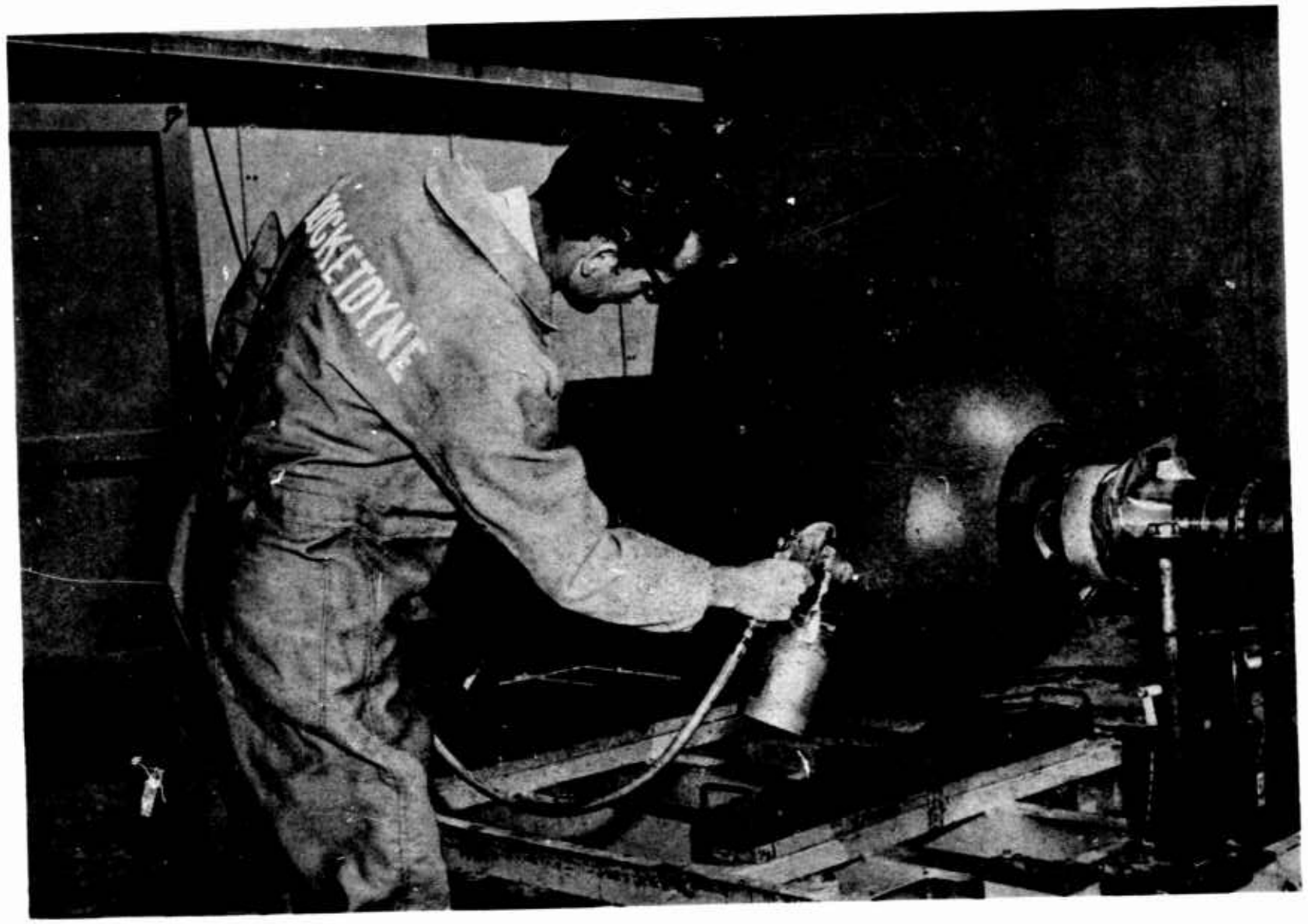
(18) Polyethylene tape was used and the prepared bond was 2-inch wide grey Polyken tape made by Kendall Company.

(19) The wire feed system is discussed in detail in Appendix V.



2YA32-4/13/64M2B

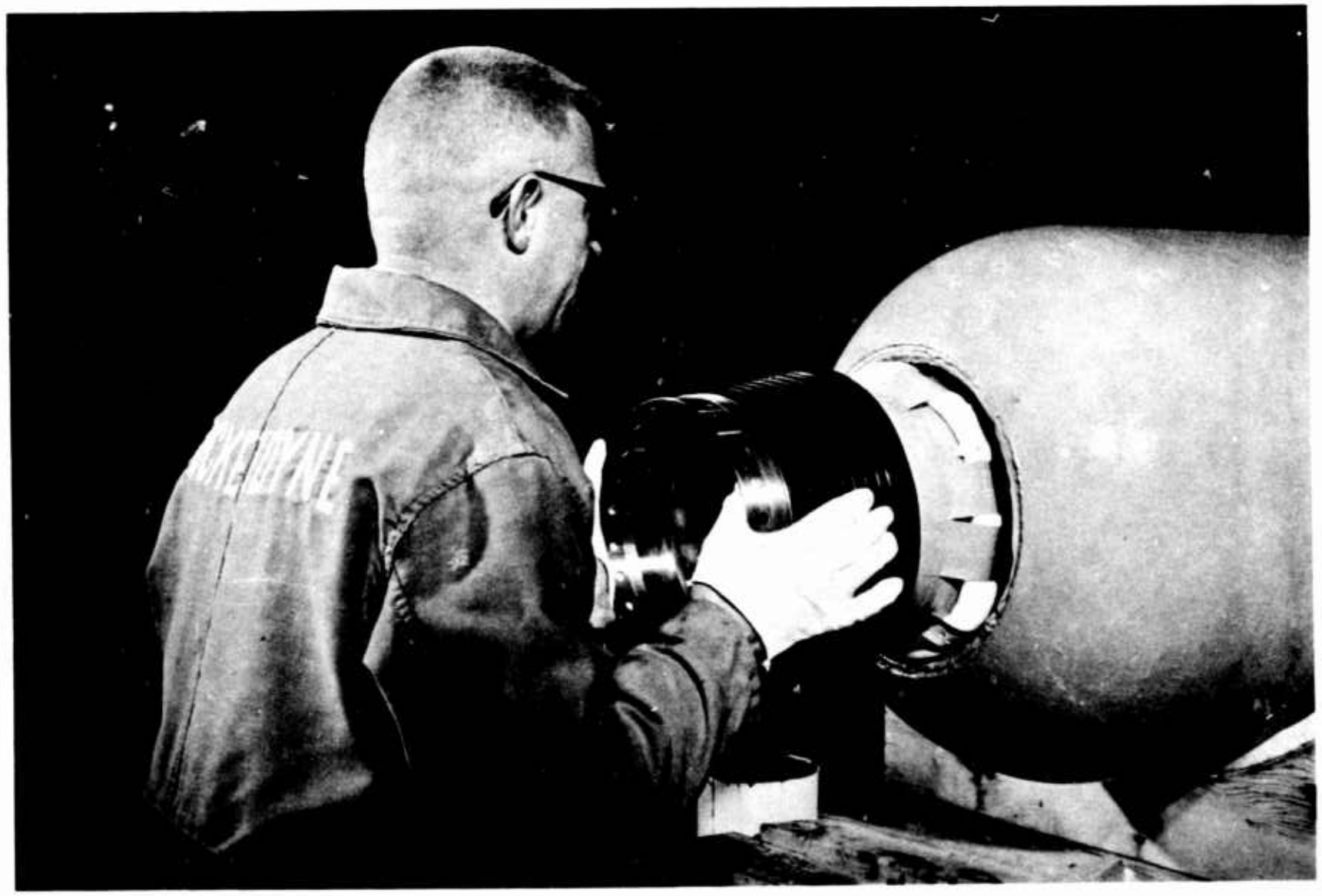
Figure 87. Application of Tenite to Surface of Sand/PVA Mandrel



2YA32-4/13/64M1C

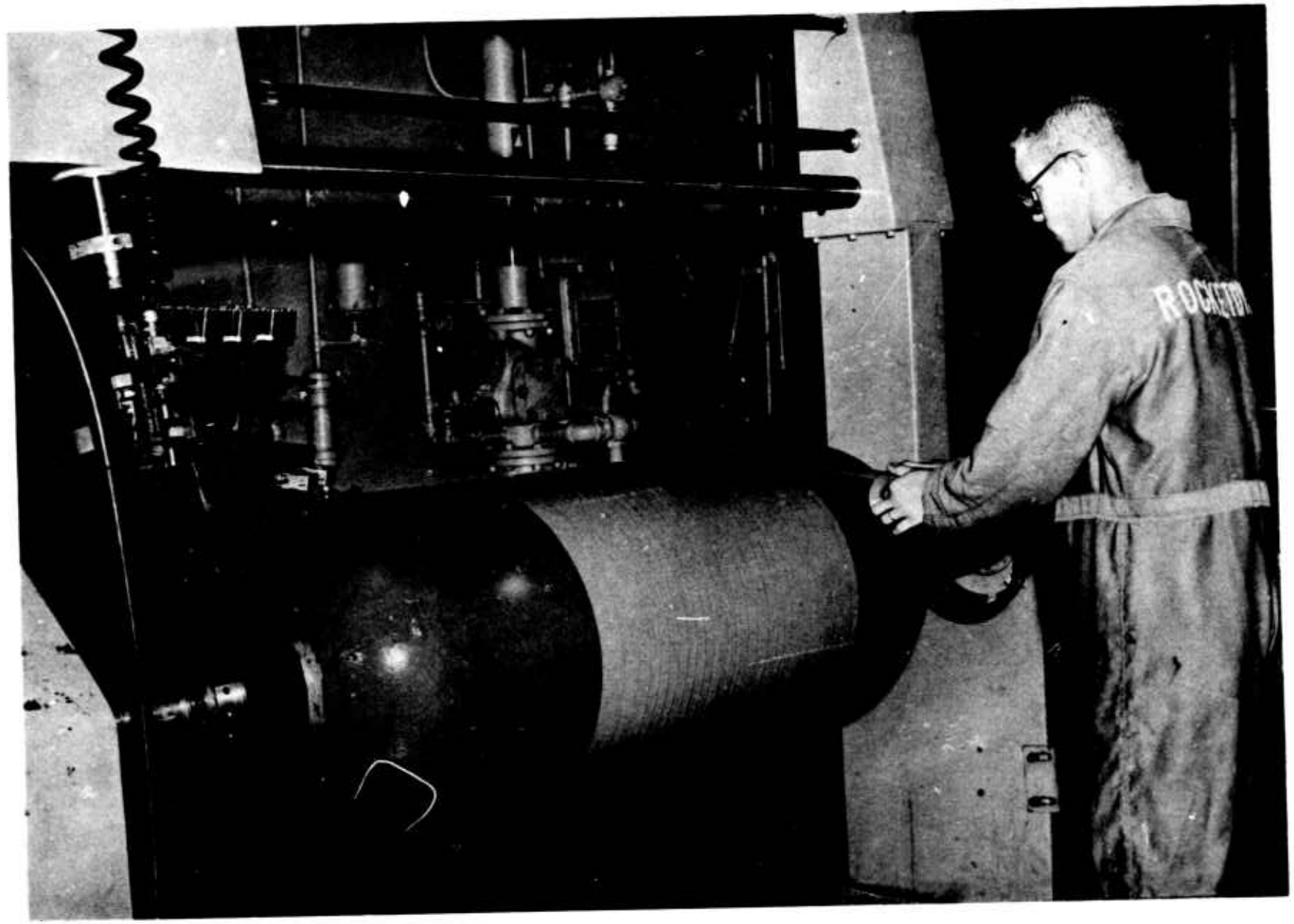
Figure 88. Spraying RTV Over the Tenite Coated Sand/PVA Mandrel

CONFIDENTIAL



12183-5

Figure 89. Installing Aft Polar Into Mandrel Assembly



2YA22-4/17/64M1B

Figure 90. Wrapping Mandrel Assembly With Polykentape



12189-9

Figure 91. Winding of Check-out Pattern on Mandrel Assembly

(2) RFG Winding

Grain winding is started with a checkout pattern to check gear ratios, cams, and wire carriage centering, Fig. 91. A grain is wound in cycles, each cycle consisting of a geodesic isotensoid layer (adjacent to poles) and three to five intermediate layers at increasing helix angles. A load ring is installed at each polar boss between successive geodesic layers. After a layer is completed, the grain is pantographed to compare contour buildup with design and to determine if added winding is necessary. Load rings are checked for proper buildup on the applicable boss step after a geodesic layer is wound. Before winding the next geodesic layer, the load ring is coated with a light layer of R-143 restrictor sufficient to cover the boss step and seal between the ring and step. A complete Motor A reinforced grain consists of eight cycles plus the ninth geodesic layer, and has nine load rings at each polar boss.

After the wire pattern is determined as satisfactory, propellant is applied. Figure 92 shows the winding of a high angle fill layer and Fig. 93 illustrates load ring installation and restricting. At completion of winding the excess propellant is carefully scraped off to the outside wires. The wire ends are secured (until the grain is cured) by wrapping several turns around the mandrel spindle and taping fast.

The reinforced grain is normally cured for 120 hours at 170 F including warm-up time. The grain is slowly rotated for the first 12 hours to prevent eccentricity. The finished grain, ready for restricting, is shown in Fig. 94.



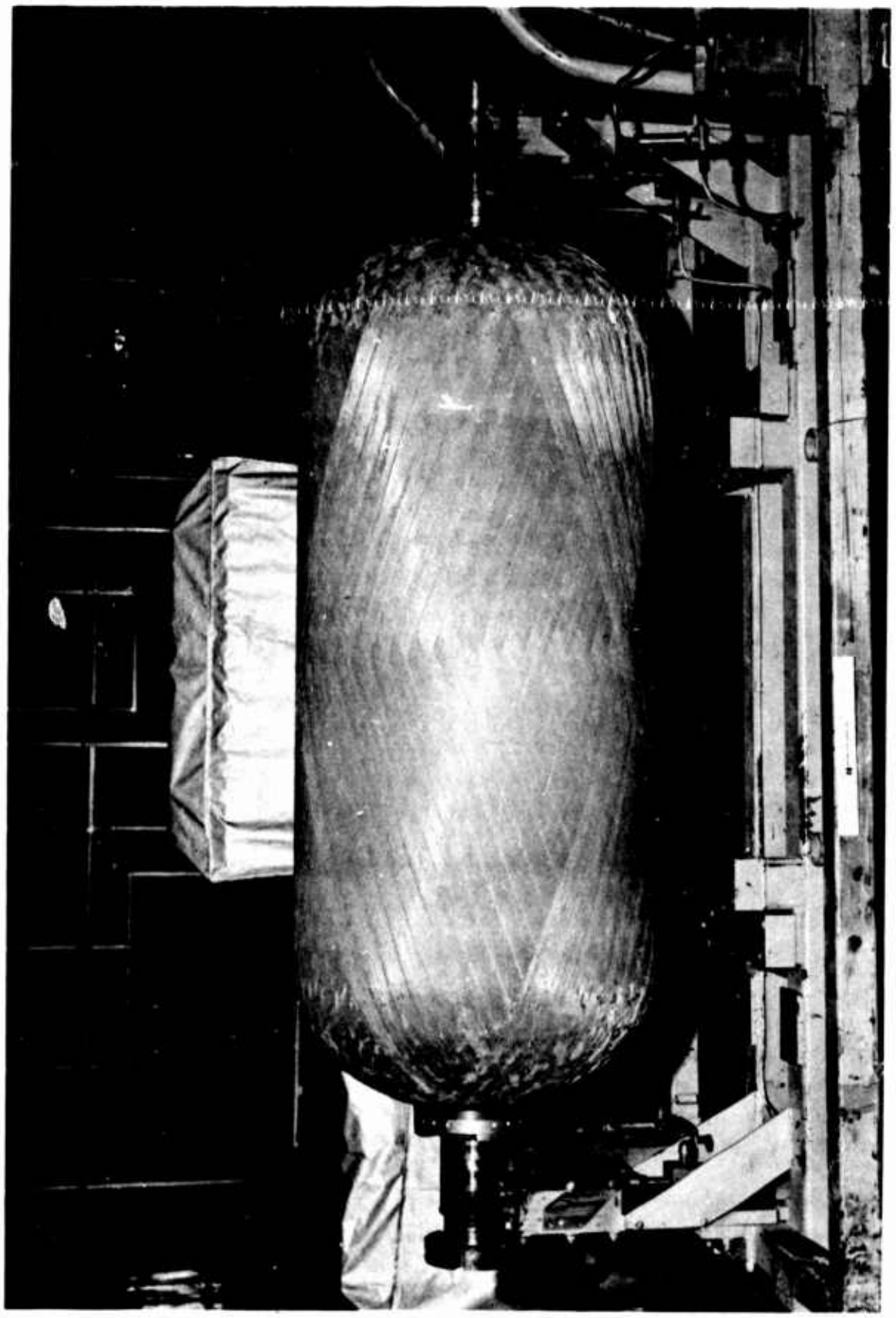
12190-2

Figure 92. RFG For Winding of High Angle Fill Layer



12191-3

Figure 95. Installation of Load Ring During Winding of RFG



2YA32-3/2/64M1B

Figure 94. Reinforced Grain Ready for Restriction

(3) Grain Restriction

Following grain cure, dimensions are measured, the surface is cleaned (using toluene), dried, primed (with MAPO), and the R-143 restrictor applied in two to three steps. The final layer of the R-143 receives 48 hours of cure at 170 F. The finished grain is weighed and the dimensions obtained before winding the glass filament case. A restricted grain set-up ready for glass case winding is shown in Fig. 95.

(4) GFW Case Fabrication

Glass case fabrication consists of (1) winding a helix wrap which is generally longitudinal with the motor axis, and (2) winding a circ wrap which is 90 degrees to the motor axis. Glass cloth for the case skirt reinforcement was integrally wound with the circ wrap.

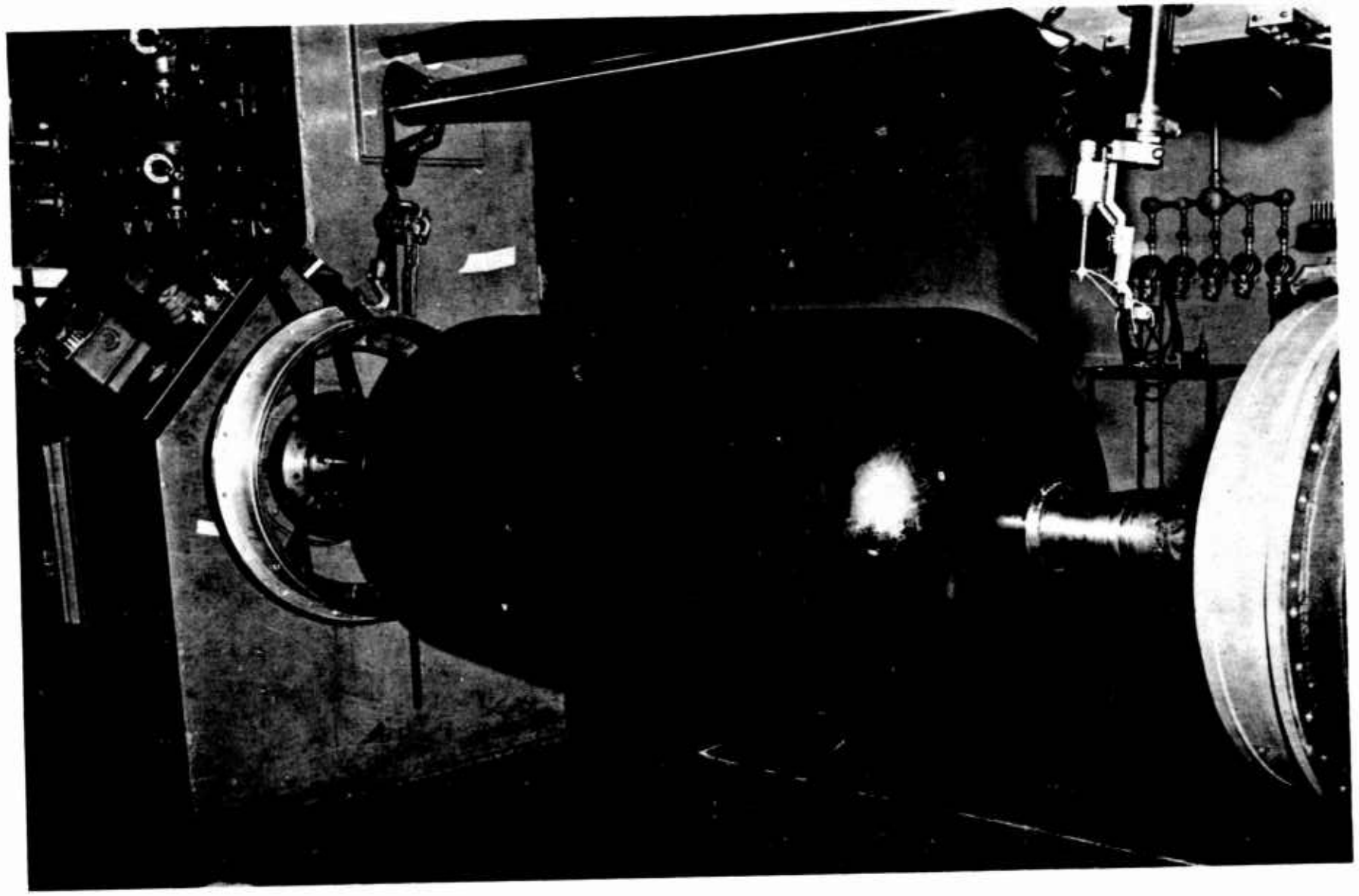
The wet winding process, wherein the dry roving is wetted with liquid resin and the case wound in a continuous operation, was used throughout the program.

For purposes of discussion the processing operation will be divided into three groups: (1) preparation of GFW operations, (2) winding operations, and (3) finishing, or postwinding, operations.

(a) Preparation of GFW Operations

Normally the first step in the case fabrication process was preparation of the glass cloth for the case skirt reinforcement. Cloth preparation consisted of applying a prescribed amount of resin to sufficient cloth for reinforcement for one case, room-temperature curing the resin to a B-stage condition (partial cure), cutting the cloth to the required dimensions, then packaging and storing at 0 F until time for use. The resin/curative system used was the same as that used in case winding.

During the Motor A development program, it was determined that resin content and degree of B-stage were critical in the fabricating of the skirts. It was found that 20-25 weight percent resin in the composite, cured at 70 to 80 F for 24 to 30 hours, gave the best results. This combination yielded skirt material with the following characteristics:



2YA32-10/7/64M1B

Figure 95. Restricted RFG Readied for Winding of GFW Case

1. Reasonably stiff, to facilitate handling and use, but not too cured to prevent resoftening at 125 to 150 F to obtain interblending of the resin with the resin used in winding the case

2. High enough resin content for uniform wetting of the glass, but not so high as to result in extruding excess resin during winding and case cure

Because of the spaces between the woven strands, the resin capacity of the glass cloth was considerably higher than the desired content. Therefore, much technique development was necessary to obtain uniform resin distribution. The desired results were obtained by first preheating the resin to about 110 F to reduce its viscosity, then applying a small amount to the cloth and spreading it rapidly over the surface with a rubber spatula. This very light resin coating was then absorbed into the body of the cloth by interaction with the material added to the surface of the cloth during manufacture.

The next step in the operation was to preassemble the skirt mandrels on the spindle with the restricted reinforced grain and install the assembly in the winding machine. The mandrels were preassembled over the domes to predetermine the position on the spindle which would result in adequate clearance for the helix wrap. This preassembly operation minimizes skirt mandrel handling required after helix winding. After accurate indexing, the mandrels are moved to the ends of the spindle until after helix winding.

Next, some preliminary helix winding was accomplished, using scrap roving without resin. During this winding, the roving tension is set and the machine adjusted to position the pattern adjacent to the polar openings. The final step prior to winding was to remove the scrap roving and clean the restrictor surface with a toluene-dampened cloth.

(b) Winding Operations

With the machine adjusted as described above, helix winding was next. During all winding, roving tension was controlled by CTC (Compensating Tension Controls, Inc.) Model 800C012 tensioners. Tension settings of 0.2 to 0.3 pound per end at the controller resulted in 0.4 to 0.6 pound per end at the case surface. This tension was found to give uniform, firm winding without excessively abrading the glass fibers.

From the tensioners, the glass rovings were drawn through a resin impregnation bath and a series of guide rollers as shown in Fig. 96. The final roving guide, which traversed 0.5 to 1-inch above the restrictor surface, was a partial torus which flattened and spread the strand following impregnation.

Only four spools of 12-end roving were used in the Motor A cases because a greater number did not appear desirable due to the problem of "flattening" the strand to a uniform band on the case surface.

Resin content (from the resin bath) was controlled by the squeegee roller at about 35% (weight) of the composite. This resin content was high enough to ensure thorough wetting and case uniformity, but low enough to minimize excess resin problems on the final case.

Because of erratic winding machine operation during start-up, it was necessary to wind each helix cover (total surface of restrictor covered with glass, with last strand positioned adjacent to the first one) in a continuous operation.

The number of helix covers varied from case to case, depending on design pressure. However, at least two covers were always used to improve uniformity of the case (i.e., any slight gapping in one cover would tend to be covered by the random positioning of the second cover, furnishing a means of transmitting the load from the gap to the adjacent roving). Figure 97 shows a heavyweight case near completion of helix winding.

Resin content in the roving was additionally controlled by means of a water jacket which maintained the resin bath at about 110 F. Also, resin and curative were kept in an oven during the winding operations and mixed and added to the resin bath in small quantities. Mixing and adding the resin in small increments, about 1.5 pounds at a time, also extended the pot life to the 3 to 4 hours required for a helix cover.

During the helix winding operation, excess resin was removed from the case surface by use of soft rubber squeegees and abosrbent toweling.

Following helix winding, the next step was to change winding machine gears and cams to those required to obtain circ wrap winding parameters, and reassemble the skirt mandrels to the predetermined positions. Additional excess resin was then removed from the helix wrap by wrapping the cylindrical section in two or three layers of plain weave glass cloth, winding a circ wrap of scrap roving, heating the unit with a hot air blower, then removing the roving and cloth. It should be emphasized that removing too much resin was not a problem. It was found that extreme effort was required to obtain a resin content as low as 20% weight.

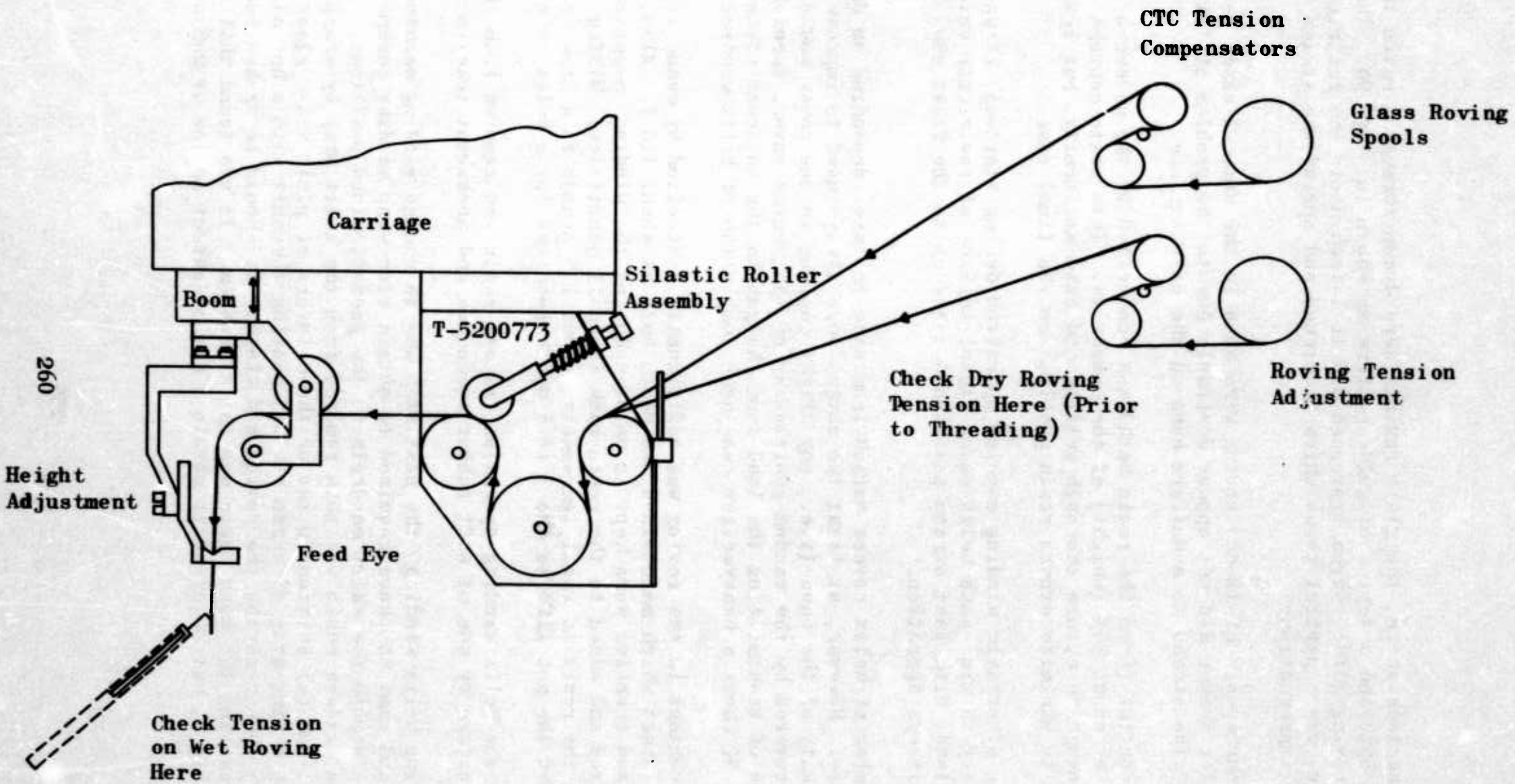
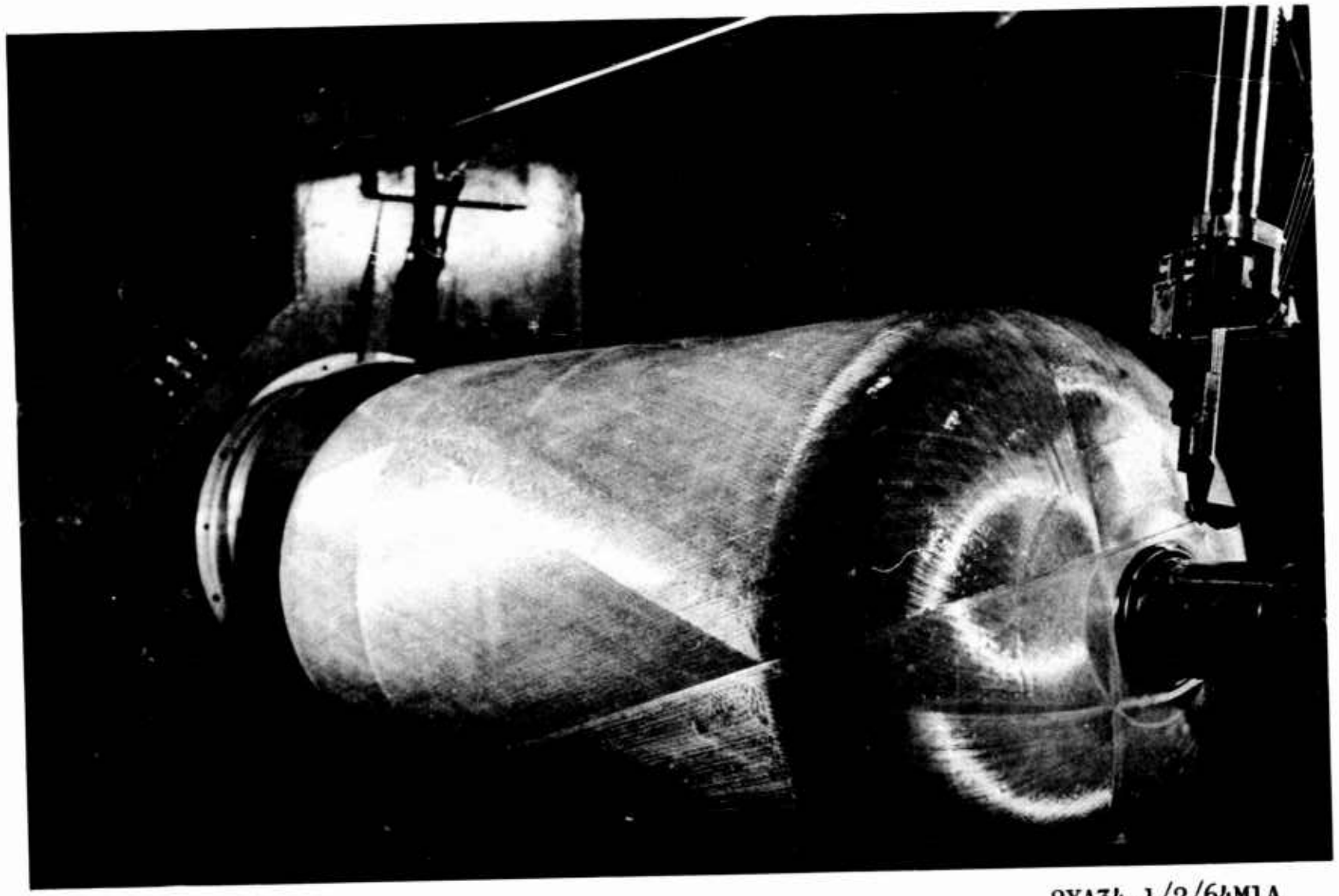


Figure 96. Glass Roving Threading Sequence



2YA34-1/2/64M1A

Figure 97. Helix Winding of a Heavyweight GFW Case

The next step was to fill the area between the cylindrical section of the case and the edge of the skirt mandrel. The purpose of this fill was to obtain a uniform cylindrical configuration from the case proper to the case skirt.

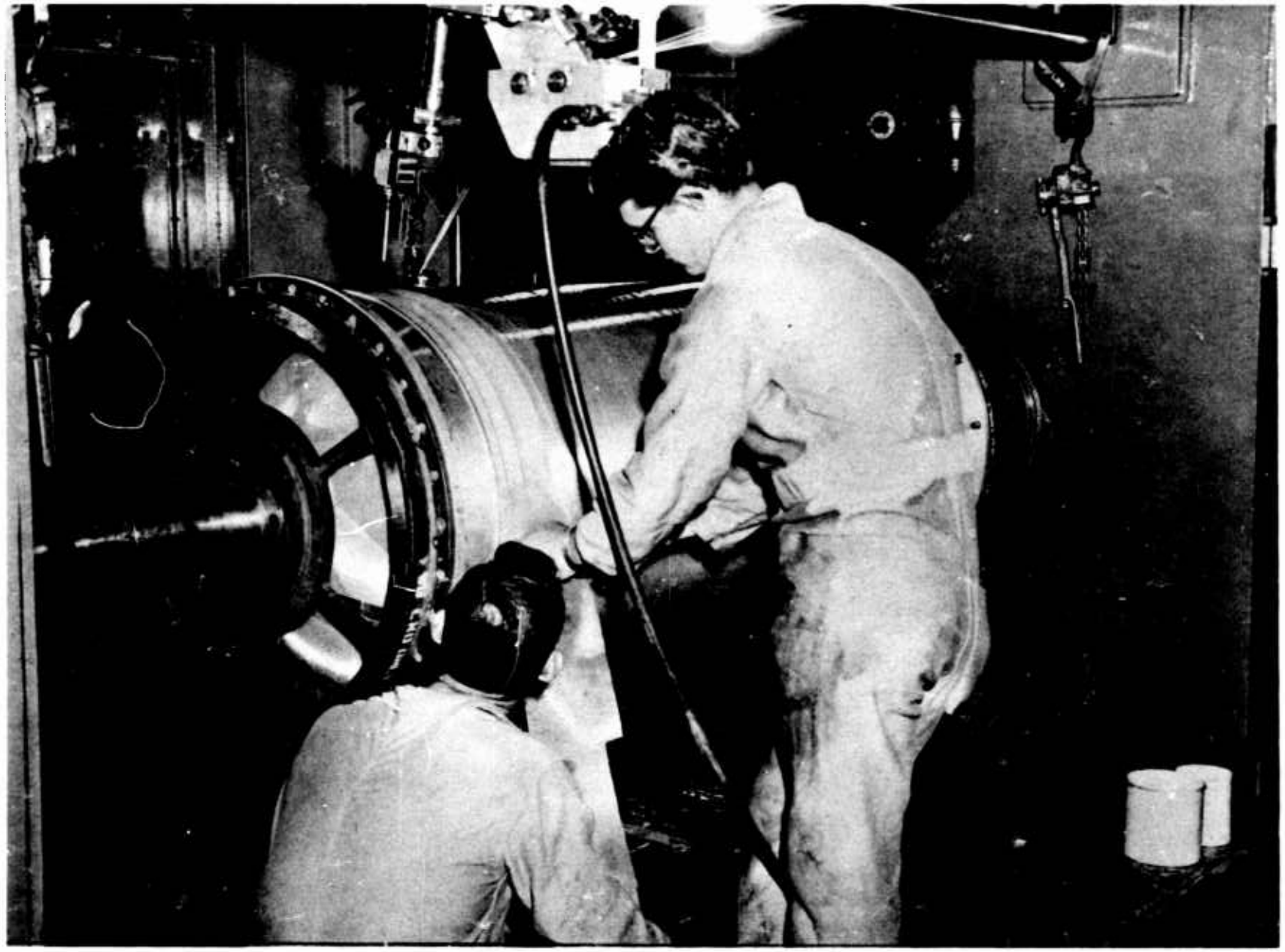
The case is now ready for the first circ cover (movement of the traverse from one end to the other while winding each roving adjacent to the preceding revolution). The skirt cloth reinforcements were added (Fig. 98), and alternately, circ wraps wound until the case was completed as designed. A completed case is shown in Fig. 99. Excess resin was then removed using the same methods described previously, except that the heat source was changed. Instead of using a hot air blower, the case was placed in the 170 F curing oven for approximately 20 minutes prior to removing the scrap roving and glass cloth.

After excess resin removal, the case was cured for 20 hours at 170 F. Following cool down, removal of the skirt mandrels (leaving skirt attachment rings in place), removal of the cord portion of the skirt-to-dome fill, installation of skirt attachment ring bolts, and removal of the spindle in preparation for mandrel washout was accomplished.

(5) Winding Mandrel Removal

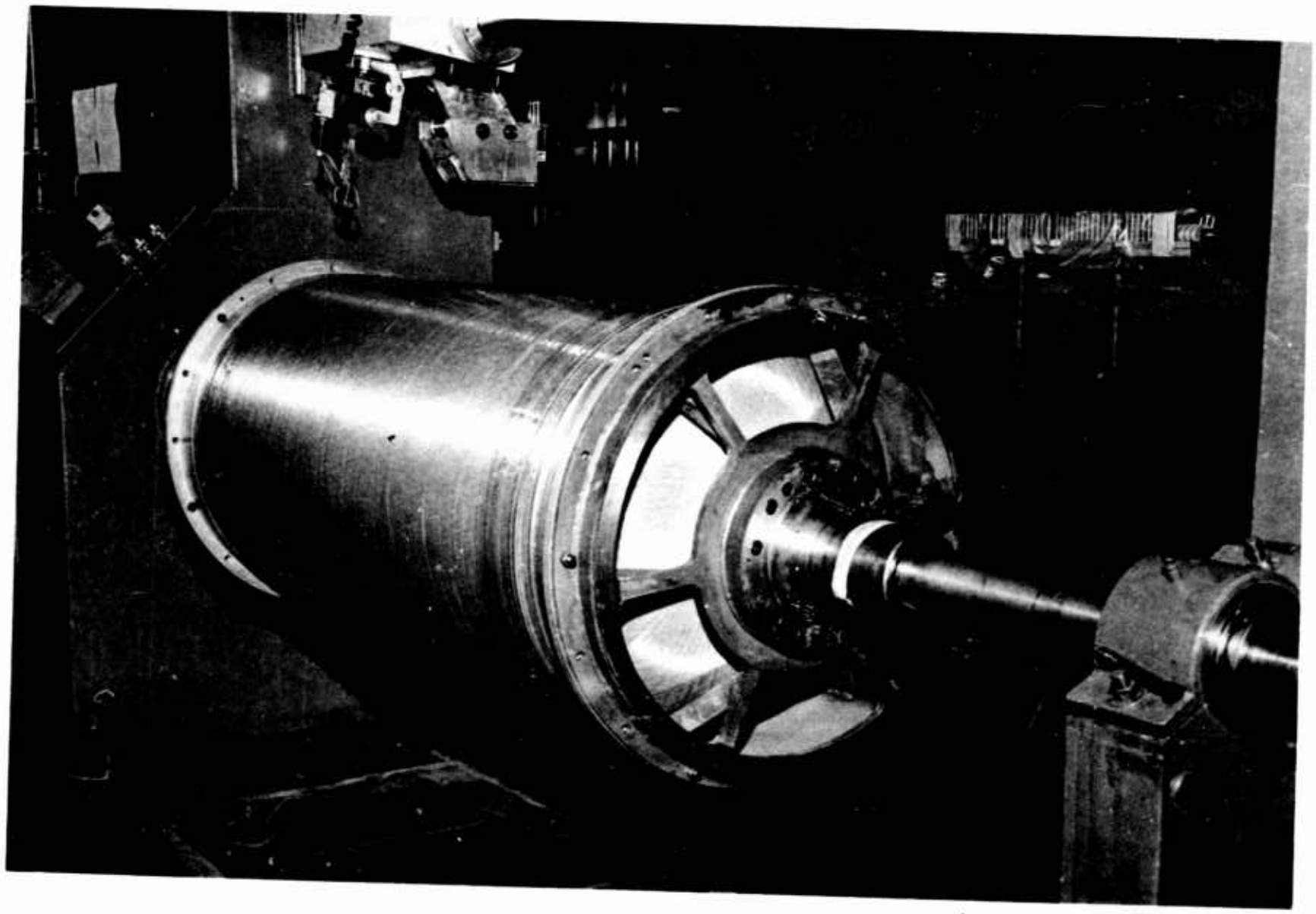
Because of the size, weight, and fragility of the GFW case, a sophisticated handling system during mandrel washout was required. Pneuma-Grips (handling equipment with inflated rubber grips) were purchased to handle the grains during manufacturing operations, and a shed was constructed for mandrel washout. This shed contained two hoists (so that the motor could be up-ended during washout) a water outlet with a mixing valve (for water temperature control, to prevent thermal shock), and a pit to receive the washed-out sand.

The steel mandrel spindle was first removed, then the motor placed in the vertical position, and the lower opening plugged. The cavity left by the spindle was filled with water until absorption was complete, Fig. 100. Large motors required approximately 30 minutes. Water temperature was adjusted to approximately the temperature level of the internal surface of the grain which depended on the cooling time from the cure oven. Washout proceeded as fast as possible to minimize possible propellant/water contact time.



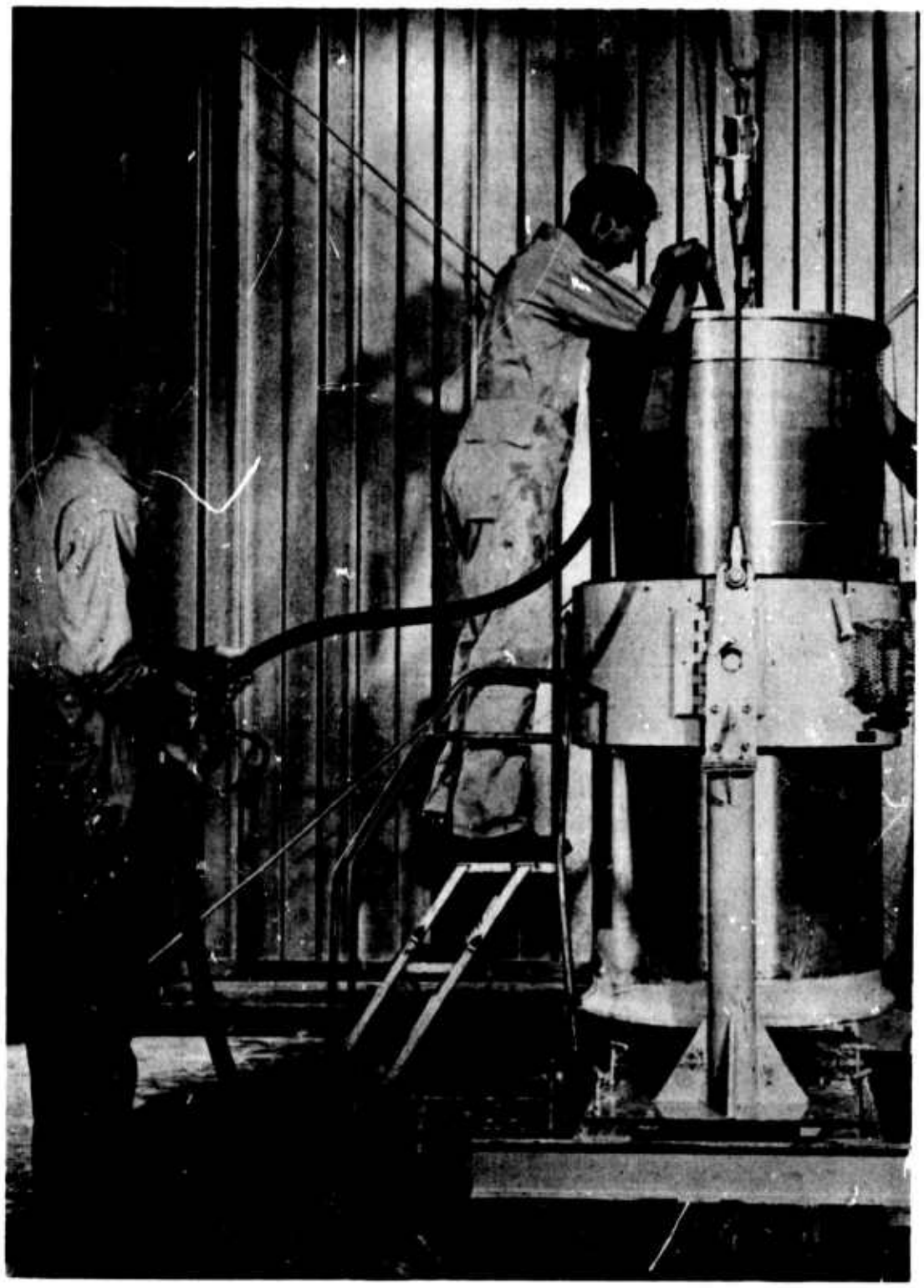
2YA42-5/8/64M1D

Figure 98. Glass Cloth Reinforcement Being Wrapped on GFW Skirt



2/YA22-2/4/64M2G

Figure 99. Completed GFW Case Prior to Removal From Winding Machine



12196-9

Figure 100. Washout of Soluble Mandrel

After the soaking period, the plug was removed to allow the water and sand to drain. Loose sand was flushed out with a stream of water. The lightening tubes (perforated metal cylinders used to reduce the required sand) were removed to prevent liner damage as soon as they were loosened. The inside of the cavity was dried with clean rags and the liner removed immediately; any drops of water were dried with clean rags (Fig. 101), The Tenite, RTV, and tape were normally all removed at once by loosening the liner at one end and pushing it toward the other. In this way, the Tenite/sand surface remained wrapped inside the tape and sand falling to the grain surface was minimized. The grain was placed in an oven, and hot air was blown through the grain to remove any water traces. The motor was dried for two hours at 100 F and two hours at 120 F. If water was noted behind the liner, the grain received an additional two hours at 130 F. The "step-drying" was used to prevent grain thermal shock.

After mandrel removal the motor was ready for casting the core propellant. The following discussion covers the sequence of operations necessary for casting the core propellant into the RFG cavity.

(6) Core Propellant

(C) RDS-526 was used as the core propellant. It has excellent casting characteristics as a result of the low 86% solids loading. Iron oxide (1%) was used to obtain the design burning rate and the 16% aluminum content contributed to both the processibility and performance. The core propellant was mixed in either the 25-gallon or 200-gallon vertical mixers for Motor A.

The core casting operation consisted of preparation of RFG, core mandrel fabrication and assembly in RFG, propellant mixing, casting, curing, and mandrel removal. Following is a discussion of these operations.

(a) Preparation of RFG

Prior to casting the core propellant, the interior surface of the RFG was cleaned by toluene wiping, then coated lightly with MAPO. The junction fillet between the grain and polar bosses was filled with R-140. The R-147 doubler was installed and surface-primed for propellant bonding with Chemlok EXB-500-1.



2YA22-7/9/64M1D

Figure 101. Removal of Liner From RFG/GFW After Mandrel Washout

(b) Core Mandrel Fabrication and Assembly

The casting mandrel was made with a metal core to which foam star points were bonded after insertion inside the RFG. The mandrel assembly also included two foam conicyls which were machined from polyurethane blocks. The star points were formed in molds, using Nopco Lockfoam. Assembly of the mandrel was very tedious. The metal core was sprayed with silicone mold release, except for the attachment slot for the the star points, where adhesive DC-269 was applied. The mandrel core was then inserted into the RFG and the foam star points inserted and attached one at a time. All conicyl foam parts were previously wired for dissection (i.e., loops of wire were placed around the conicyl so that the foam could be cut into removal pieces by pulling the wire loops), and then were coated with RTV-60. The conicyls were made in segments and assembled (using DUCO cement) inside the grain. A preassembled mandrel is shown in Fig. 102. The mixer or cast can in casting position over a motor in the casting pit are shown in Figs. 103 and 104, respectively.

(c) Mixing and Casting

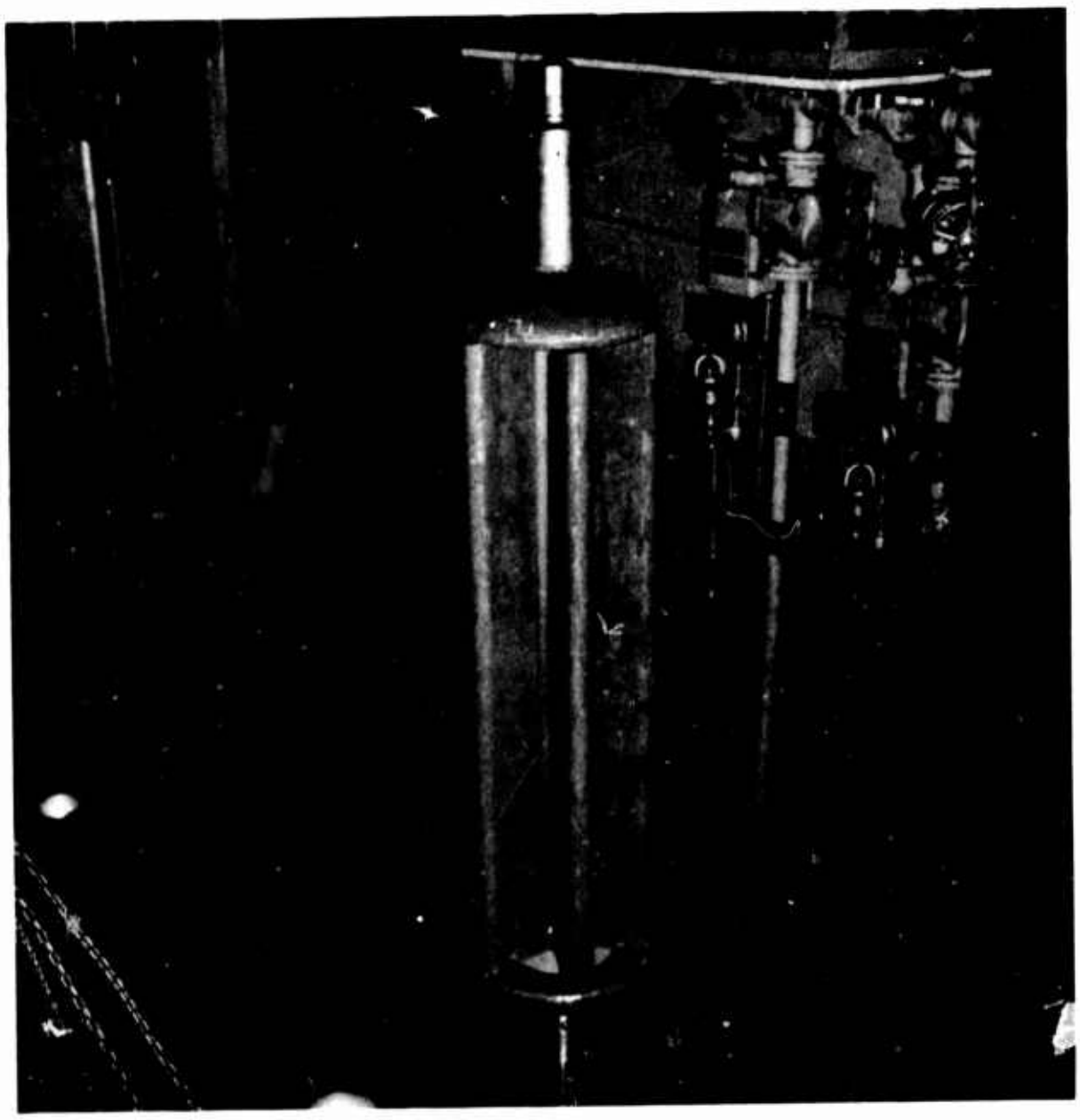
Standard mixing procedures were used and casting was performed using standard vacuum bell procedures with a perforated disc deaeration plate. Prior to casting, the motor was preheated at 170 F for a minimum of 20 hours to bring the reinforced grain to near the casting temperature. During casting the minimum vacuum allowed was 27.5 inches Hg and the mixer temperature was held at 165 F. Vibration was used during casting and for 15 minutes after.

(d) Curing

Curing of core propellant was accomplished in the casting pit using circulating air at 170 F. The standard cure cycle was 72 hours heating, then stepwise cooling at the rate of 5 F every three hours.

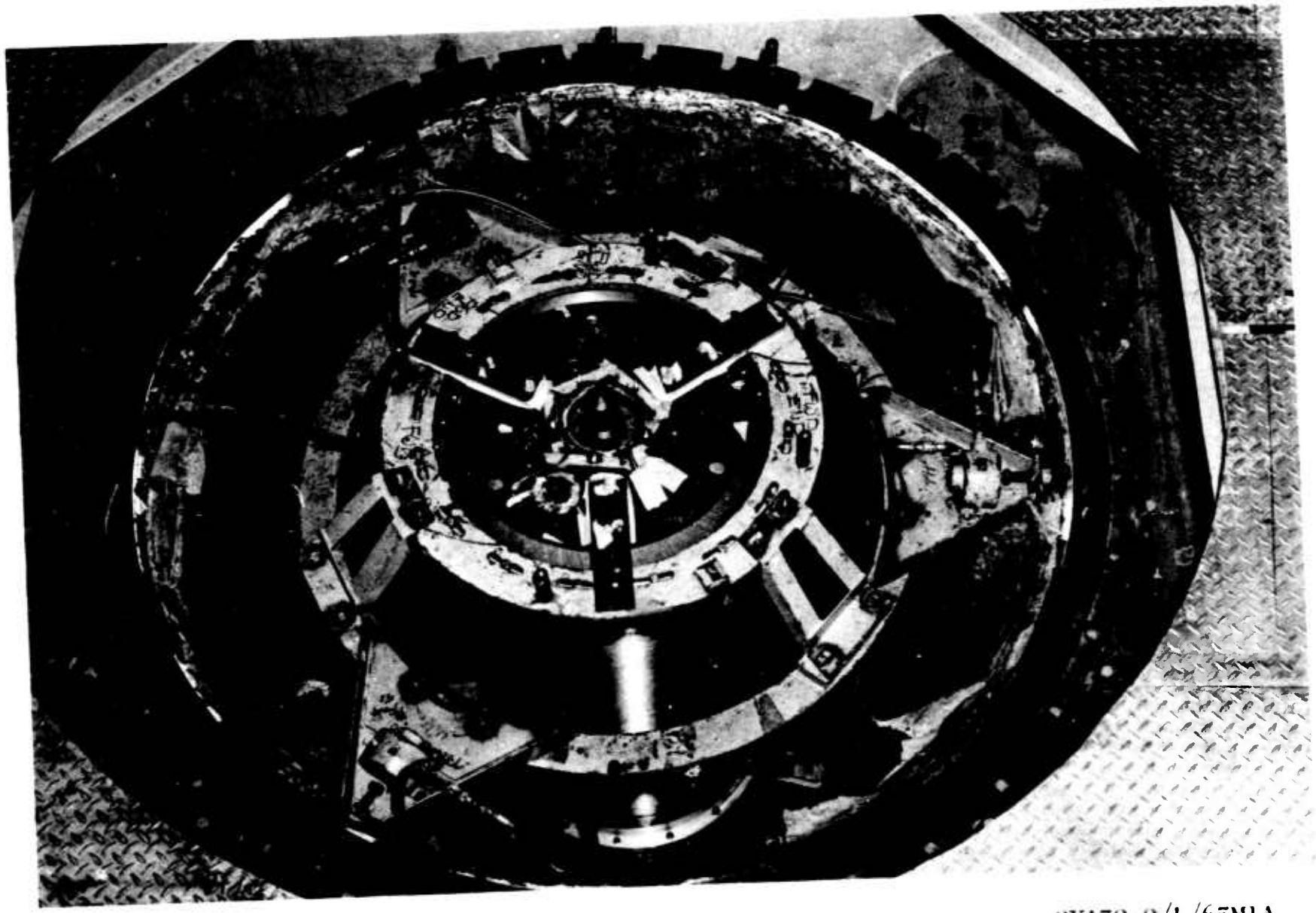
(e) Mandrel Removal

The casting mandrel was removed by breaking down and pulling the metal core. Then, the foam star points and conicyls were manually removed by cutting and breaking the foam.



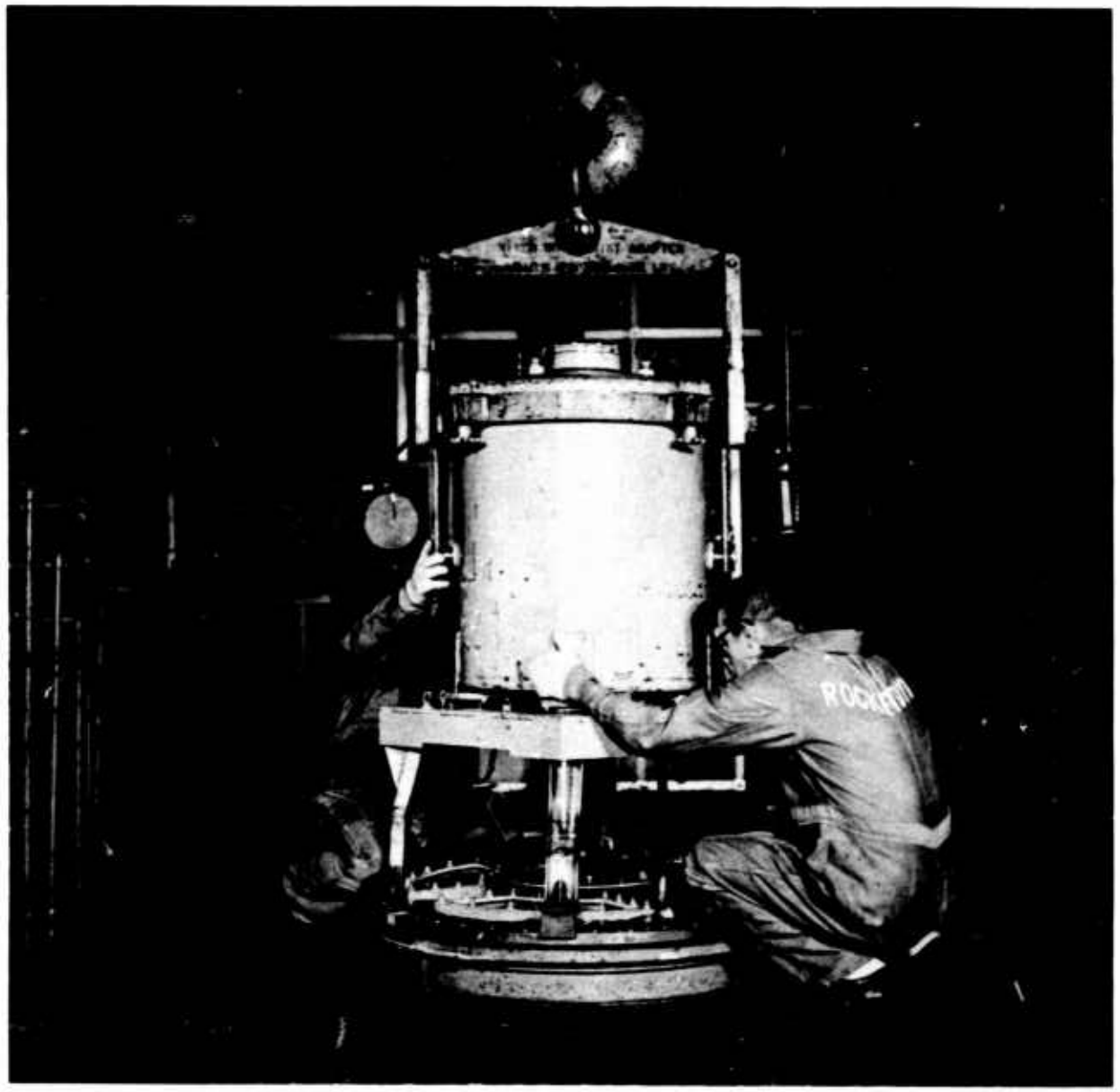
CN12031-6

Figure 102. Core Mandrel Assembly (Mandrel is Assembled Inside of RFG)



2YA32-2/4/65M1A

Figure 103. Motor in Casting Pit Readied for Casting of Core Grain



12199-12

Figure 104. Casting of Core Propellant into RFG

Some difficulty was encountered in removing the foam because of the poor accessibility and the danger of scarring the propellant surface. It is recommended that this procedure and/or design be revised in any future motors. The preferred method is to leave the foam in place if ignition timing is not critical. If the foam must be removed, lower density foam should be used and techniques, such as crushing by pressurization, should be considered.

(f) Final Grain Preparation

After mandrel removal, the level of the core propellant was measured. If the end core surface was below a given point, it was restricted with EC-1949. At the aft end, the space between the boss and the R-142 sleeve, which was filled with nylon cord during casting, was filled approximately two-thirds with a blend of Epon 815 and Versamid 140, then topped with EC-1949 to prevent gas flow from undercutting the nozzle insulation.

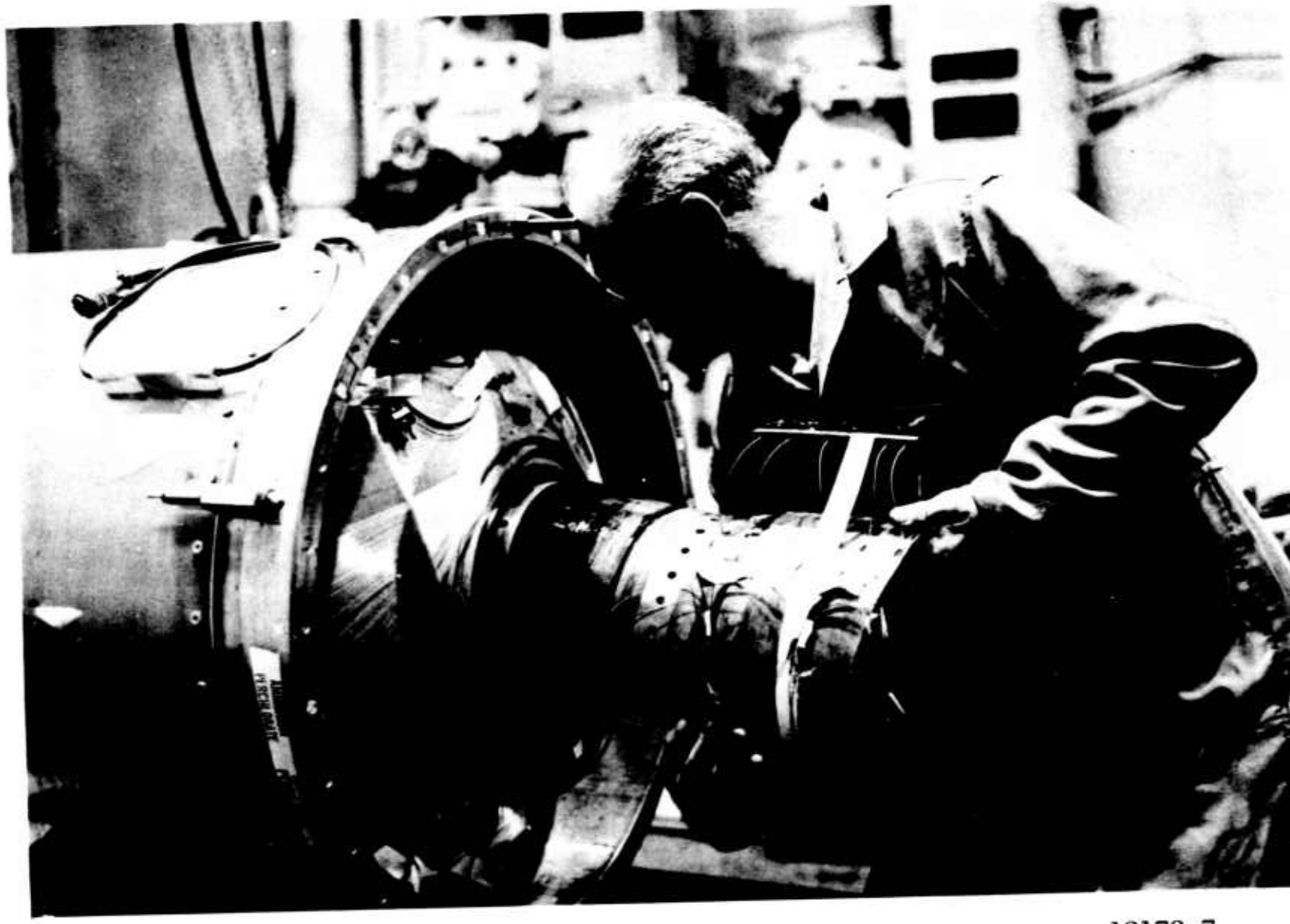
(7) Motor Assembly

Final assembly consisted of installing the nozzle and forward closure and then leak testing. The unit was received from NDT area then weighed, as was each subassembly. The nozzle and polar boss were cleaned, then dry fitted and reworked, as required, to match. The nozzle was installed after applying a bead of RTV-731 to seal at the offset in the insulation by means of an installation fixture. Figure 105 shows beginning of nozzle assembly; the drive pins were inserted with a special pin tool.

The forward closure and polar boss were cleaned and checked for fit (without installation of the igniter). The phenolic threads were sanded, as required, to prevent a force fit. The igniter was installed in the closure and, after being weighed, the closure was installed in the boss with the O-ring lubricated with LB-300-X.

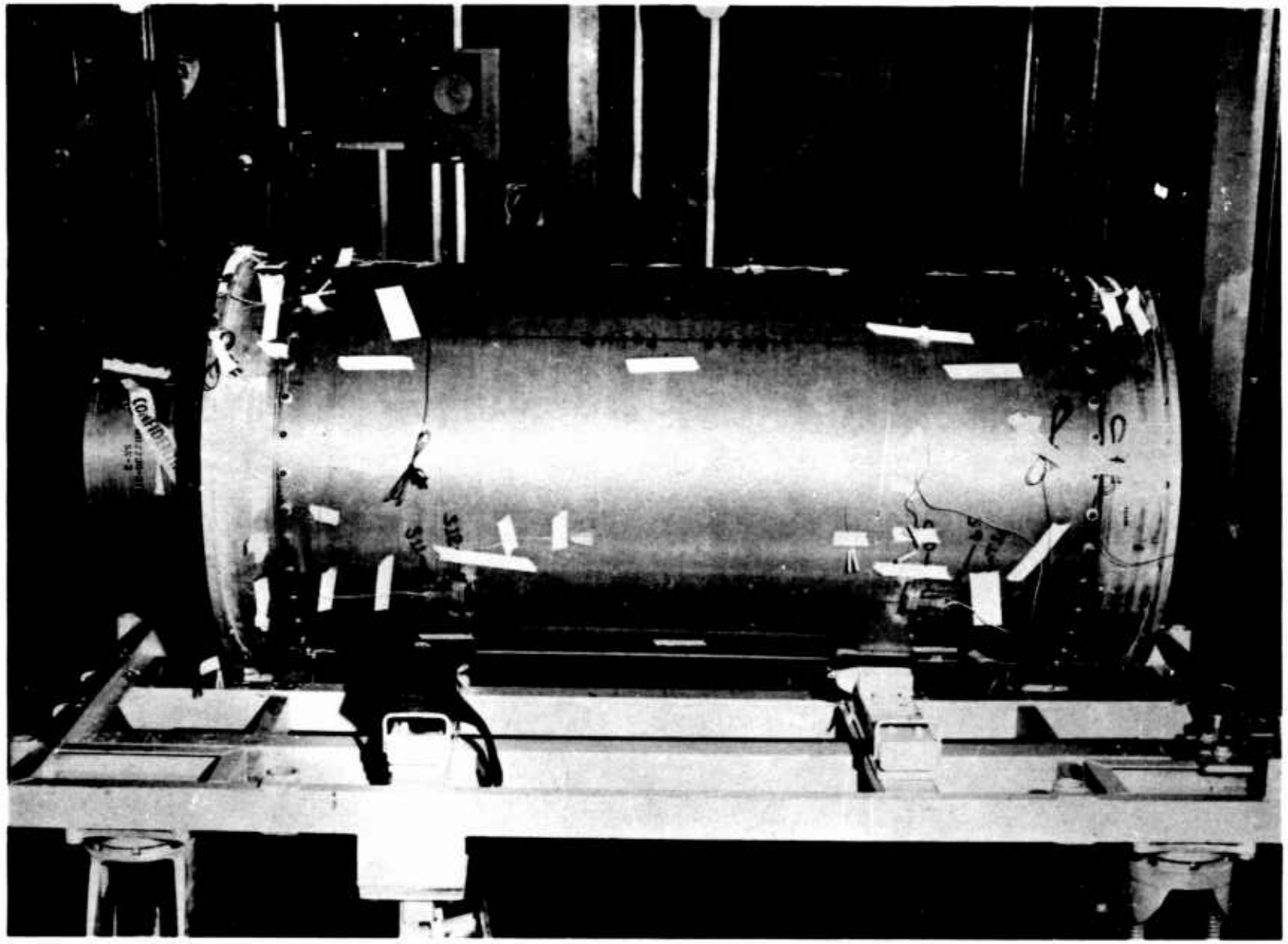
After weighing the motor, the initiator shipping plug, pressure tap plugs, and nozzle test plug were installed. The motor was then leak-tested with 20 psig nitrogen for 5 minutes.

Following successful leak testing, the nozzle plug was removed and the exit cone sealed with sheet plastic and tape. At some convenient time before, during, or after assembly, the case and nozzle were instrumented by bonding on thermocouples with epoxy adhesive. A finished motor is shown in Fig. 106.



12178-7

Figure 105. Installing Nozzle



2YA21-6/4/64M1B

Figure 106. Full Assembled Motor

f. Development of Quality Control and Nondestructive Test Requirements and Techniques

The problems encountered in establishing inspection and test requirements, and the techniques developed by SRD Quality Control to verify design requirements for the RFG rocket motor are described below.

(1) Quality History

The quality history of each unit is maintained on the Quality History Card. The requirements on the card are defined by the Engineering Department in the reinforced grain process order, letters, and the motor process specification. From these requirements, Quality Control developed the Quality History Cards for defining the necessary inspections and recording the results. Basically, the quality history includes raw material inspection, surveillance of propellant sand-PVA mixing, winding the grain fabrication, surveillance of motor processing, and motor weights and measurements. An example of a typical history card is included in Fig. 107.

(2) Process Inspection

These requirements included normal raw material acceptance plus mix ingredient weighout. Propellant physical properties and liquid strand burning rates were used for propellant acceptance. Surveillance of propellant tube loading and storage conditions were also accomplished. On most motors, Quality Control also checked the propellant during the winding operation to ensure that the correct propellant mix was used for each layer.

(3) Motor Weights

Accurate weighing is essential to achieving the required total weight and calculation of accurate mass fraction of each motor. A very accurate weighing unit was employed to handle in-process weighing. In some instances it was necessary to weigh the motor after successive process operations to obtain incremental weights of restrictor, GFW case, and core propellant. It was very important to maintain a calibration of weighing instruments and not recalibrate during processing of a motor, if possible.

QUALITY HISTORY CARD

Reinforced Grain
Grain Cure and Restriction
Motor B

DATE: GO:

Date Issued:	Issued By:	Approved By:	QHC—
9-8-64	N E Sharp	B. Carnahan 9/4/64	598
Date Revised:	**Revised By:**	**Revision Approved By:**	**QHC Serial Number**

CODE	CHARACTERISTIC		Date	Insp
M*701R	Acceptability of Materials	S		
M*702	Foreign Material (Ref. QCM-105)			
M 703R	Grain Cure	M		
M 704R	Weight of polymer deposite	M		
M 705R	Grain Diameter	S M		
M 706R	Weight of grain and spindle W/O harness	M		
M 707	Grain cleaned with toluene			
M 708	Grain wiped with MAPO			
M 709R	Case polar flange weight	M		
M 710R	Restrictor cure	M		
M 711R	Weight of restricted grain & spindle W/O harness	M		
M*712R	Diameter of restricted grain	S M		
M 713	Inspection Status applied	M		

Reference: Supplement to be issued for each motor.

Motor No.

Polar Flange S/N

Grain No.

R-143 Mix Numbers

Wipe	Fill	Final

M 703R Grain Cure

Time In	Date In	Temp.	Time Out	Date Out	Temp.	Insp

M 710R Restrictor Cure

Layer	Time In	Date In	Temp.	Time Out	Date Out	Temp	Insp
Wipe							
Fill							
Final							

Variation Tag Number	Quantity	Characteristic Code	Cause Code	DISPOSITION: Rework	Reject	Use as is	MRB	Insp

MRD NO.
DISPOSITION:

Form 626 A-R (Master) Nov 2.63 New Issue

Figure 107. Quality Control History Card

QEC-598

-Standards-

M*701R Materials must show evidence of prior Q.C. acceptance. Record Mix Numbers of R-143 and identity of polar flange.

M 705R
M*712R Diameter limits will be issued with respective motor supplement.

-Methods-

M 703R
M 710R Verify cure from oven log and record in space provided.

M 704R Record weight of polymer deposits removed from grain surface during cure to nearest .1 lb.

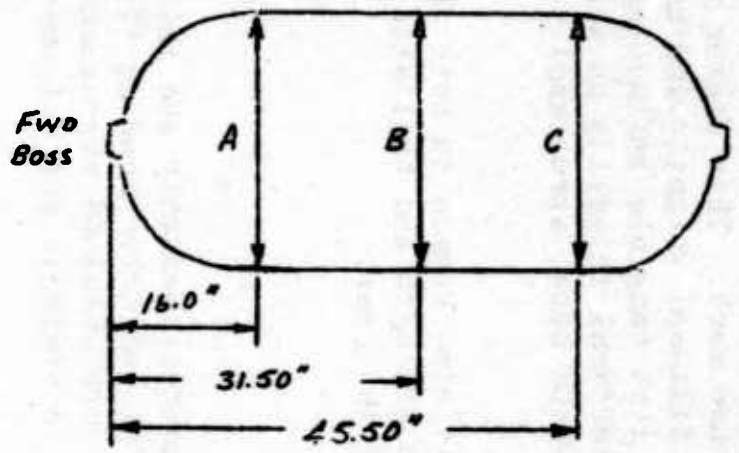
M 705R Measure and record diameter as specified in sketch and record to nearest .001 inch. Measurement to be taken after grain has been cleaned but prior to toluene wipe.

M 706R
M 711R Weigh and record to nearest .1 lb. Assure that drive sprocket has been removed from spindle before weighing. Correct load cell reading as specified in QCM-6.4.25.

M 709R Weigh and record to nearest .1 lb.

M*712R Measure restricted grain after cure, trim, and sanding and record to nearest .001 inch. Measure according to sketch.

M 713 Apply Inspection Stamp to tag or tape attached to assembly indicating acceptance of restricted grain.



Loc.	M 705R Grain			M*712R Restricted Grain		
	Limits	Actual	Insp.	Limits	Actual	Insp
A						
B						
C						

Figure 107
(Continued)

The problem of determining percent of filament by weight is common to reinforced grain and the filament wound case work. This factor is an output of machine settings, gear ratios, filament weight, winding speeds, propellant or resin feed rate, and other less tangible influences. Effect on the propellant grain includes structural integrity as well as ballistic performance. In the filament wound case, structural strength is affected.

The problem of distribution of filament is also common to both the grain and the case, and also affects both strength and ballistic performance in the grain and the strength of the case.

(4) Measurements

Dimensional measurements start with the mandrel assembly and include boss-to-boss length, and diameters on total indicator reading (TIR). These and other dimensional measurements were obtained throughout the grain/case winding process and were used to evaluate and determine necessary changes and/or adjustments.

In a conventional solid rocket motor, web thickness is the difference between a pressure vessel or liner and the core or mandrel (making some allowances for shrinkage, or expansion). In a filament reinforced grain, the web dimension is affected by such things as core or mandrel dimensions, propellant feed rate, filament tension, rotating speed, propellant sag, and shrinkage or expansion which could be inconsistent. Propellant grain web thickness affects total impulse, the ballistic pressure and thrust curve as well as thrust and pressure tail-off. Measurements in these areas were taken to ensure the maximum reproducibility.

(5) Inspection and Test Problems

Many of the fabrication processes used in the reinforced grain program were essentially identical to familiar processes used in the manufacture of conventional rocket motors. These processes presented no new control problems and adequate inspection and test procedures were established early in the program. These processes included chemical raw material preparation, propellant mixing and storage, restrictor and inhibitor preparation and storage, and hardware preparation.

Other fabrication processes were new to the rocket and missile industry and presented new inspection and test problems. The majority of these new problems were associated with the winding operation peculiar to a reinforced propellant grain. The characteristics of greatest concern are discussed below.

(a) Integrity of Bond Lines

The initial approach to bond line inspection was radiography since it would produce a known result. This method proved to be adequate but expensive. In an attempt to reduce inspection cost, and provide, if possible, better bond line definition, the following methods were explored:

1. Radiography
2. Ultrasonics
3. Doppler Radar
4. Microwave
5. Beta-ray Backscatter
6. Eddy Current
7. Infrared
8. Statiflux

Of the above listed methods only three were pursued as a promising means of obtaining useful information. Radiography was used very successfully for various inspection characteristics. Three machines, 300 KV, 400 KV, and 1000 KV were available for use during the program and techniques were developed that were very satisfactory. Until the 13 MEV Linear Accelerator was obtained (during full-scale RFG fabrication) there was no capability for radiographic inspection of assembled motors of larger sizes, except through use of tangential shots. Various tests were performed with both ultrasonic and infrared equipment aimed primarily at obtaining a satisfactory method of evaluating the various interfaces and/or bond lines in the RFG motors.

Using a modified ultrasonic thickness gauge, scans were made of the case-to-insulation and insulation-to-propellant bond lines. Glycerene was used as a couplant between the probe and the motor. Acceptable results were obtained on the case-to-insulation bond line, but definition was very poor on the insulation-to-propellant bond line. Inspection of bond lines and/or other characteristics of greater depth in the motor by various ultrasonic techniques was not possible because of limitations of the equipment and the development of the state-of-the-art.

Since the infrared method also looked promising for bond line inspection it was investigated. Two techniques were pursued. One was soaking the motor to a given temperature prior to scanning and the other was use of a heat lamp being moved ahead of the probe. Both techniques produced results similar to those of ultrasonics (with the same limitations). Infrared inspection was very time consuming; since this method was considerably slower and more expensive than ultrasonics, it was discarded.

(b) Propellant Voids

The method used to determine the presence of this type of discontinuity is radiography. During X-ray inspections, it was noted that at least 95% of all voids visible on the resultant X-ray film were surface voids. They are as prevalent in live propellant as in inert grains. To eliminate false reporting of internal voids, X-ray technicians drew sketckes of each section of the grain covered by a single piece of film and, as accurately as possible, called out all surface voids or imperfections which could cause misinterpretation of these sketches. Otherwise, surface voids made intelligent interpretation difficult.

Cylindrical grains were X-rayed through the single wall and the double wall; the configuration of grains with domed ends limited exposures through the double wall only. This presented a problem in the accurate location of internal voids.

A representative from the nondestructive testing section of the Quality Control Laboratory visted X-ray Products Corporation for the purpose of determining the feasibility and adaptability of fluoroscopy as a nondestructive testing tool for reinforced grains. This concept consists of inserting a 360 degree rod anode X-ray tube into the grain and rotating the grain in front of a fluoroscopic screen. Two factors influenced this approach, which for all practicable purposes can be classified as advantages. An advantage was the maneuverability of the grain during examination, which results in a third dimension perspective which aids in the location of voids. Also, inspection of a single wall (instead of superimposing one wall on another, as in done with the film method) is an advantage.

(1) Conclusions

Conclusions relating to the following controls were reached:

1. Percent of Filament by Weight--This characteristic can be adequately controlled by preweighing of propellant and filament and maintaining accurate constituent weight history. This method can be expected to provide a maximum of a 1% variation, which is adequate for all practical purposes.

2. Distribution of Filament--Processing experience and visual inspection has proved adequate for this inspection characteristic. Since the winding machine malfunction is the primary cause of improper filament distribution, the condition is detectable and correctable at the time it occurs.

3. Grain Web Thickness--To accurately measure the grain web profile, a tool was designed to be used in conjunction with a surface plate. The tool was designed to provide simultaneous measurements of the grain OD and ID. With such a device, variations in grain web thickness can readily be detected.

4. Propellant Voids--Conventional radiographic inspection with techniques developed specifically for reinforced grains proved adequate for this characteristic.

5. Integrity of Bond Lines--Using ultrasonic scanning for the case-to-liner interface (and radiographic inspection for other bond lines), this characteristic can be adequately inspected.

It can be concluded that a solid propellant rocket motor utilizing the reinforced grain concept can be adequately inspected and tested during and after fabricating processes, and that sufficient assurance of rocket motor quality and integrity can be provided.

PREVIOUS PAGE WAS BLANK, THEREFORE WAS NOT FILMED

SECTION V

MOTOR A--FULL-SCALE FABRICATION AND TEST

Development of the Motor A configuration consisted of fabricating and testing six full-scale motors. This development was performed after design and development of full-scale RFG motors with GFW cases. The fabrication of Motor A and tests results are discussed in this section.

1. DEVELOPMENT MOTOR A-1006

The process development effort, which was conducted separately for the RFG and GFW case, culminated in the fabrication of a full-scale RFG/GFW motor assembly. The first full-size, 30-inch RFG/GFW had a two-fold purpose: (1) integrate the process development of glass case and RFG, and (2) evaluate by hydrotest the structural integrity and inter-relationship of case and grain. The motor (less core) was wound as Motor A-1006.[20] The fabrication and configuration represented the latest design and process innovations resulting from the preceding work. The motor was wound as a flightweight unit.

Fabrication of this grain brought together for the first time all of the process sequences involved in fabricating an RFG motor through GFW case winding. This represented the first actual processing of the following:

1. Molding and assembly of full-scale soluble mandrel
2. Winding of full-scale RFG on soluble mandrel
3. Application of liner to full-scale motor
4. Winding of flightweight GFW case over full-scale RFG grain
5. Soluble mandrel and liner removal process with full-scale motor

a. Fabrication

(C) The first full size 30-inch Motor A reinforced grain, A-1212, was wound from 20 to 28 January 1964. Steel load rings were used with flightweight phenolic-titanium polar bosses. Close-to-design weight and dimensions were obtained, thus verifying attainability of the multi-angle helix Motor A design. Final reinforced propellant weight was 1356 pounds with 18.1% aluminum wire. Average final diameter was 29.582 inches with a maximum of 29.625 inches, for an average web of 3.77 inches in the cylindrical section.

---

[20] Frequently referred to as A-1212, which is the RFG number.

(C) Propellants with seven different burning rates approximating ballistic design requirements were used over the 40 winding layers. The grain consisted of eight cycles plus the ninth geodesic layer. Each cycle contained a geodesic layer and three to five intermediate layers, each wound at a higher helix angle than the previous layer.

(1) Equipment

The grain was wound on the 36-inch 3-axis cam-actuated machine. The microtension wire-tensioning system made by Eastern Equipment and Controls Company was used in conjunction with manual propellant application and a pneumatic spreader blade.

The grain was wound over a molded sand/PVA soluble mandrel which was coated with Tenite and Polyken tape.

The GFW case was wound on the 3-axis 40-inch winding machine.

(2) Materials

Prior to winding, the steel load rings were coated with a baked-on film of Chemlok EX-B500-1 as a primer for propellant bonding. The stepped phenolic surface of the bosses was coated with Epon 926 to provide a moisture seal and as a bonding aid. As the load rings were installed during winding, a bead of adhesive, EC-1648, was applied to the edge of the seating step on the boss to serve as a sealant between boss and ring. This adhesive is expected to be replaced with a more pliable material on subsequent units.

Annealed 5056 alloy aluminum wire supplied by Hudson Wire Company was used. This met the current specification for 7.5-mil diameter wire of 5% minimum elongation and 50,000 psi minimum tensile strength. However, most of the spools were found to be in the range of 8 to 10% elongation.

The matrix propellant consisted of three formulations, RDS-512, -514, and -523. The location in the grain and burning rates of the different mixes are shown in Table XXVII. Low-viscosity propellant, LCA-4654, was applied on the domes for an area 1-inch wide around and adjacent to each boss.

TABLE XXVII

PROPELLANT FOR RFG A-1212

Mix No.	RDS No.	Depressant Level, %	Grain Location, Layers	Liquid Strand Burning Rate	
				r, in.	P, psi
K-12-20-M81	512	--	1 GI-2-GI	0.353	760
K-12-20-M82	512	--	2 Hel-3 GI	0.288	680
K-12-26-M82	514	1/2	3 Hel	0.259	625
K-12-31-M81	514	1	4 GI-4 Hel	0.214	550
L-1-6-M81	514	2	5 GI-5 Hel	0.181	490
L-1-8-M81	523	4	5 Hel-6 Hel	0.147	430
L-1-3-M81	523	6	7 GI-7 Hel	0.135	400
K-12-28-M81	523	6	7 Hel	0.130	400
L-1-24-M81	523	6	8 GI	0.132	400
L-1-24-M83	523	6	8 Hel	0.130	400
L-1-9-M81	523	6	8 Hel-9 GI	0.135	400

The case was wound with Owens Corning S-994 12-end roving using the resin system Dow Epoxy Resin 332/8 phr EMI (2-ethyl-4-methyl-imidazole). The skirt laminations were made from 143-reversed glass cloth impregnated with the same resin and B-staged prior to winding.

(3) Processing

(a) Grain Winding and Restriction

(C) The detailed winding data are presented in Table XXVIII. The grain contained nine geodesic-isotensoid layers wrapped over individual load rings to transmit the closure load to the end bosses. Each of these layers was separated by intermediate layers ranging in winding angle from 26 degrees to 80 degrees. Each helical layer was wound to provide designed grain growth as measured by cylindrical diameter and pantograph traces of the head-end dome contour. Thickness of the grain at the polar bosses matched design dimensions of load rings and boss steps very closely. No alterations were required for the next grain.

CONFIDENTIAL

PREVIOUS PAGE WAS BLANK, THEREFORE WAS NOT FILMED

TABLE XXVIII

GRAIN WINDING DATA FOR RG-12

	Cycle 1				Cycle 2					Cycle
	Layer				Layer					
	GI	Intermediate			GI	Intermediate				GI
Winding Parameters										
Winding Angle, deg	31.2	43.7	56.6	71.7	30.1	42.8	58.1	69.9	80.0	28.6
No. Covers	7	9	9	4	7	4	4	7	10	7
Cam Revolutions	250	279	212	52	264	128	92	105	70	280
Mandrel Revolutions	430	594	602	243	430	268	265	434	494	448
Cylinder Build-Up										
Cyl Dia, in. (Mandrel)										
Head 22.030	22.280	0.575	0.855	0.974	23.130	0.245	0.372	0.550	0.925	24.160
Center 22.060	22.284	0.600	0.885	0.985	23.195	0.317	0.425	0.635	0.025	24.215
Aft 22.035	22.259	0.563	0.860	0.968	23.180	0.285	0.386	0.582	0.955	24.185
Layer Depth (av), in.	0.117	0.152	0.127	0.055	0.096	0.057	0.056	0.097	0.189	0.109
Cover Thickness (av), in.	0.0167	0.0169	0.0141	0.0138	0.0137	0.0143	0.0140	0.0139	0.018	0.0156
Misc Data										
Gears Used A	56	55	52	33	55	51	43*	31	33*	56
B	78	84	96	70	82	82	50	76	64	76
C	78	66	65	44	76	74	49	50	39	74
D	95	92	100	98	83	96	59	87	70	78
Winding Speed, rpm	4	5	5	6	4	5.5	5	5.5	5	3
Layer Time, hrs	6.8	2.7	2.3	0.8	5.2	1.8	1.1	1.8	2.3	5.1
Cycle Time, hrs				16					20.5	
Wire Meter Rdg/Layer**	3574	4233	3930	1487	3599	2185	1884	2832	3104	3600

Wire Data

Wire Diameter and Elongation, 7.5 mil, 5% min

Number of Wires in Warp, 36

Wire spacing, in., 0.044

Warp Width, in., 1.620

Wire Tension (nominal), gms, 400

Final Wire Weight, lb, 243.8

*Indirect Gear Train

**This Represents The First Use Of The Wire Meter And Calibration Was Not Complete. The Reading Is Roughly Equivalent To Feet.

ABLE XXVIII

ING DATA FOR RG-1212

Cycle											
		3				4					
Layer											
		GI	Intermediate			GI	Intermediate				
9	80.0	28.6	38.5	48.4	66	26.5	34.9	45.8	58.3	73.3	80.0
	10	7	5	8	9	7	2.3	5	6	3	12
	70	280	251	244	171	297	90	167	150	39	96
	494	448	471	550	456	448	159	486	402	195	1584
550	0.925	24.160	0.285	0.550	0.790	24.990	0.050	0.197	0.350	0.453	0.745
635	0.025	24.215	0.355	0.612	0.860	25.056	0.120	0.278	0.440	0.552	0.815
582	0.955	24.185	0.320	0.558	0.824	25.012	0.075	0.210	0.400	0.473	0.820
097	0.189	0.109	0.067	0.127	0.126	0.097	0.031	0.073	0.084	0.048	0.151
0139	0.018	0.0156	0.0134	0.0159	0.0140	0.0139	0.0135	0.0146	0.0140	0.0160	0.0126
	33*	56	52	53	32*	55	50	52	52	34	30*
	64	76	81	91	54	38	66	72	88	88	63
	39	74	68	73	64	63	64	58	60	50	43
	70	78	82	96	65	67	85	85	95	98	69
5	5	3	4	4	6	3	—	5	7	—	—
8	2.3	5.1	4	4	2.5	8.7	2.0	2.5	1.5	0.5	3.0
	20.5				20.7						24.7
	3104	3600	2535	4155	3779	3700	1406	2745	2886	1312	4487

2

CONFIDENTIAL

CONFIDENTIAL

TABLE XXVI
(Continue

	Cycle									
	5					6				
	Layer									
	GI	Intermediate				GI	Intermediate			
Winding Parameters										
Winding Angle, deg	25.0	32.4	43.7	55.1	66.0	23.7	29.9	40.3	49.3	63.1
No. Covers	7	6	7	5	6	6	3	4	4	10
Cam Revolutions	312	251	252	147	120	280	135	160	134	230
Mandrel Revolutions	451	408	510	432	414	401	210	292	288	710
Cylinder Build-Up										
Cyl Dia, in.										
(Mandrel)										
Head 22.030	26.000	0.139	0.332	0.485	0.670	26.835	0.935	0.060	0.150	0.4
Center 22.060	26.025	0.206	0.420	0.555	0.735	26.900	0.990	0.115	0.225	0.5
Aft 22.035	26.020	0.181	0.370	0.517	0.696	26.860	0.945	0.065	0.180	0.4
Layer Depth (av), in.	0.111	0.080	0.099	0.073	0.091	0.082	0.046	0.062	0.053	0.1
Cover Thickness (av), in.	0.0159	0.0133	0.0141	0.0146	0.0152	0.0137	0.0153	0.0155	0.0133	0.0
Misc Data										
Gears Used A	41*	52	57	51	41	64	50	56	58	38
B	40	59	81	93	96	77	57	71	79	75
C	43	69	68	71	57	79	60	69	59	61
D	31	99	97	98	83	94	82	100	93	94
Winding Speed, rpm	3	4	---	4	5	3	3	4	---	---
Layer Time, hrs	6.4	7.0	3.4	2.0	2.0	4.0	2.3	1.5	1.5	4.3
Cycle Time, hrs					27.8					18.3
Wire Meter Rdg/Layer**	3750	3360	4203	2900	2954	4047	2024	2576	2365	5350

*Indirect Gear Train

**This Represents The First Use Of The Wire Meter And Calibration Was Not Complete. The Reading Is Roughly Equivalent To Feet.

TABLE XXVIII
(Continued)

Cycle		7					8					9
Layer												
ate		GI	Intermediate				GI	Intermediate				GI
49.3	63.1	22.4	32.4	46.1	67.3	80.0	21.5	28.7	37.8	51.2	62.7	20.4
4	10	6	4	4	11	9	5	4	4	5	5	5
34	230	293	180	148	220	81	254	200	177	175	125	264
88	710	405	288	299	632	509	340	300	300	375	360	343
0.150	0.435	27.640	0.808	0.000	0.414	0.671	28.854	0.941	0.090	0.240	0.330	29.537
0.225	0.517	27.765	0.940	0.108	0.460	0.758	28.980	0.045	0.175	0.332	0.456	29.625
0.180	0.460	27.716	0.920	0.034	0.445	0.713	28.890	0.990	0.110	0.289	0.407	29.584
0.053	0.143	0.118	0.091	0.079	0.196	0.137	0.099	0.042	0.067	0.081	0.056	0.092
0.0133	0.0143	0.0197	0.0228	0.0198	0.0178	0.0152	0.0198	0.0105	0.0168	0.0162	0.0112	0.0184
58	38	60	63	54	34	32*	54	68	57	53	32	56
9	75	70	100	75	69	51	64	60	83	78	69	77
9	61	83	93	61	50	35	69	52	78	61	58	94
3	94	98	94	89	84	67	78	89	92	90	77	89
---	---	2	4	5	7	5	2	2	3	5	5	2
1.5	4.3	4.5	2.2	1.3	3.0	4.3	5.8	5.0	2.5	1.5	2.8	4.2
	18.3					22.5					25.5	7.2
5	5350	4281	2750	2857	6703	4574	3000	3068	2910	2830	2800	3212

CONFIDENTIAL

(C) Final grain weight (1356 pounds) was exceptionally close to the design of 1349 pounds. The aluminum content was 18.1%, computed by the recorded weight of wire used and grain weight. This is below the 20% design figure for two reasons. First, the buildup in the cylindrical section was 0.0154 in./cover vs wire-to-wire contact of 0.0150. A buildup of 0.0150 in./cover would have given about 18.8% aluminum. Second, the propellant used had a density of 0.062 lb/cu in. instead of 0.060 lb/cu in. being used when wire spacing was selected early in the program.

It was not planned to make design changes which would increase the aluminum content at this stage of development. The newly fabricated automatic propellant feed system has a heated spreader blade to maintain the propellant in a more fluid condition. A lower buildup per cover is expected and, consequently, a higher aluminum content.

Over-all winding time was 23 shifts of eight hours each, excluding the machine setup period and grain removal and transfer to cure. This time included frequent stoppages. There were two periods for load ring installations on the mandrel, and other delays were related to oven malfunction, electric power failure, and too-frequent wire breakage.

The frequent wire breakage is attributed to numerous factors, principally defective spools, excessive friction in wire guides, a tendency for the wire to climb out of the gathering system, and rough or chattering machine operation. It is believed that much of the breakage and lost time will be eliminated by improvements initiated on the wire system, specifically a restraining bar to prevent wire from working out of the gathering rollers and installation of rollers at the fish-eye guides to eliminate the sharp bend and accompanying frictional drag at the guide eyes. In addition, machine performance has been smoothed by installing a pressure gage in the tracer valve discharge line to enable more accurate tune-up and adjustment of the machine.

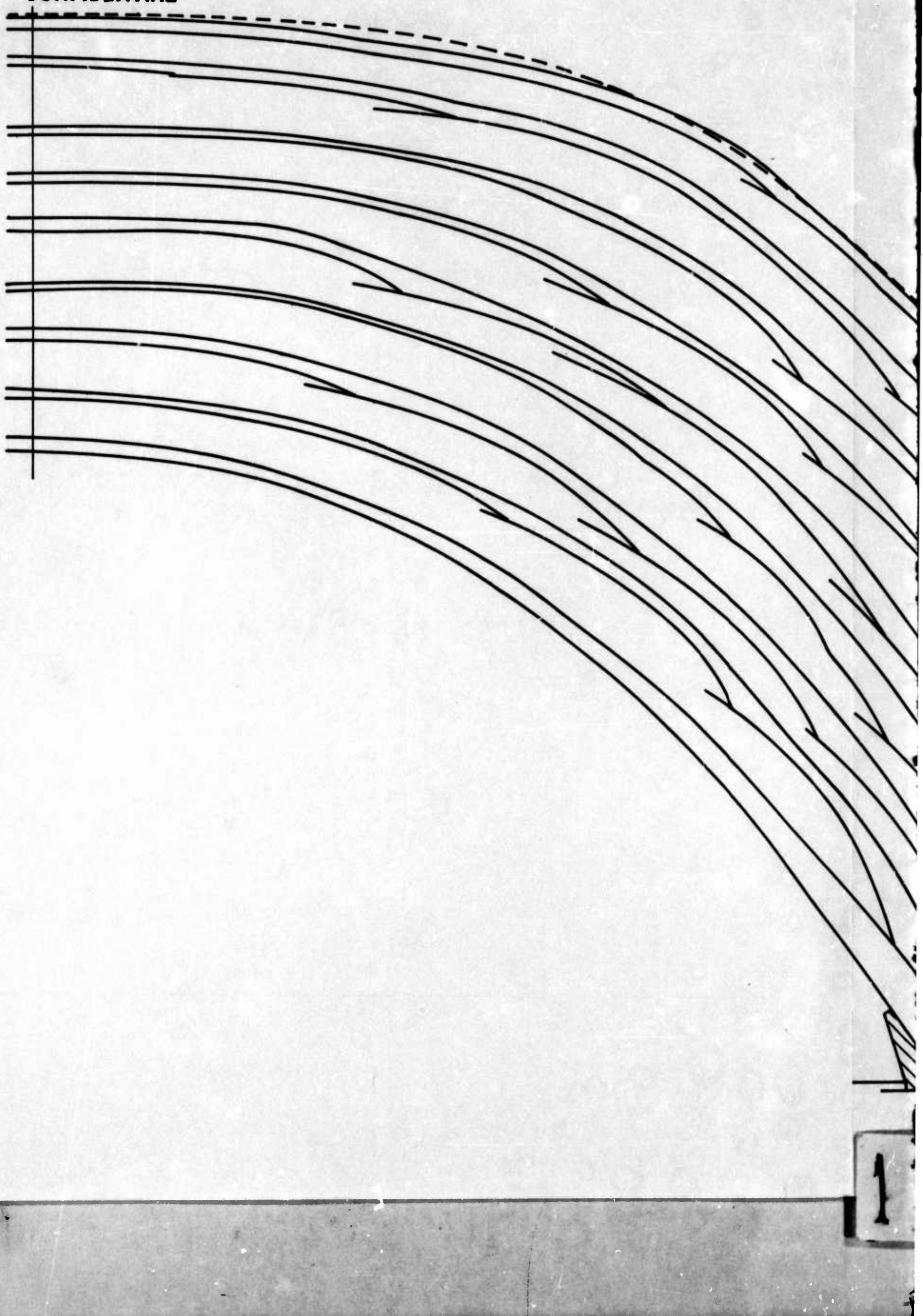
As anticipated, some alteration in the number of covers in certain layers was made during the winding to obtain grain growth conforming to the design contour pattern. A comparison of the initial estimate of layer buildup and the actual construction is shown in Table XXIX. The design contour was closely matched in most respects. The principal deviation occurred near the junction of the domes and in the cylindrical section, where the grain buildup was less than design. This deficiency can be corrected in subsequent grains by increasing the number of covers in the high-angle intermediate layers.

A copy of the pantograph tracing of the aft dome is presented in Fig. 108.

TABLE XXIX

MOTOR A-1006, LAYER CONSTRUCTION FOR RG-1212

Layer	Estimated Covers	Actual Covers	Change
1-GI	7	7	0
1-43	10	9	-1
1-54	9	9	0
1-66	5	4	-1
2-GI	7	7	0
2-43	6	4	-2
2-54	7	4	-3
2-66	8	7	-1
2-80	3	10	+7
3-GI	7	7	0
3-35	7	5	-2
3-45	8	8	0
3-60	9	9	0
4-GI	7	7	0
4-30	5	2.3	-2.7
4-40	5	5	0
4-50	6	6	0
4-65	3	3	0
4-80	3	12	+9
5-GI	7	7	0
5-30	6	6	0
5-38	7	7	0
5-47	6	5	-1
5-60	4	6	+2
6-GI	6	6	0
6-26	4	3	-1
6-32	5	4	-1
6-40	4	4	0
6-56	9	10	+1
7-GI	6	6	0
7-32	4	4	0
7-46	4	4	0
7-67	6	11	+5
7-80	9	9	0
8-GI	5	5	0
8-29	4	4	0
8-38	5	4	-1
8-51	6	5	-1
8-63	5	5	0
9-GI	5	5	0
Total	239	245.3	+6.3



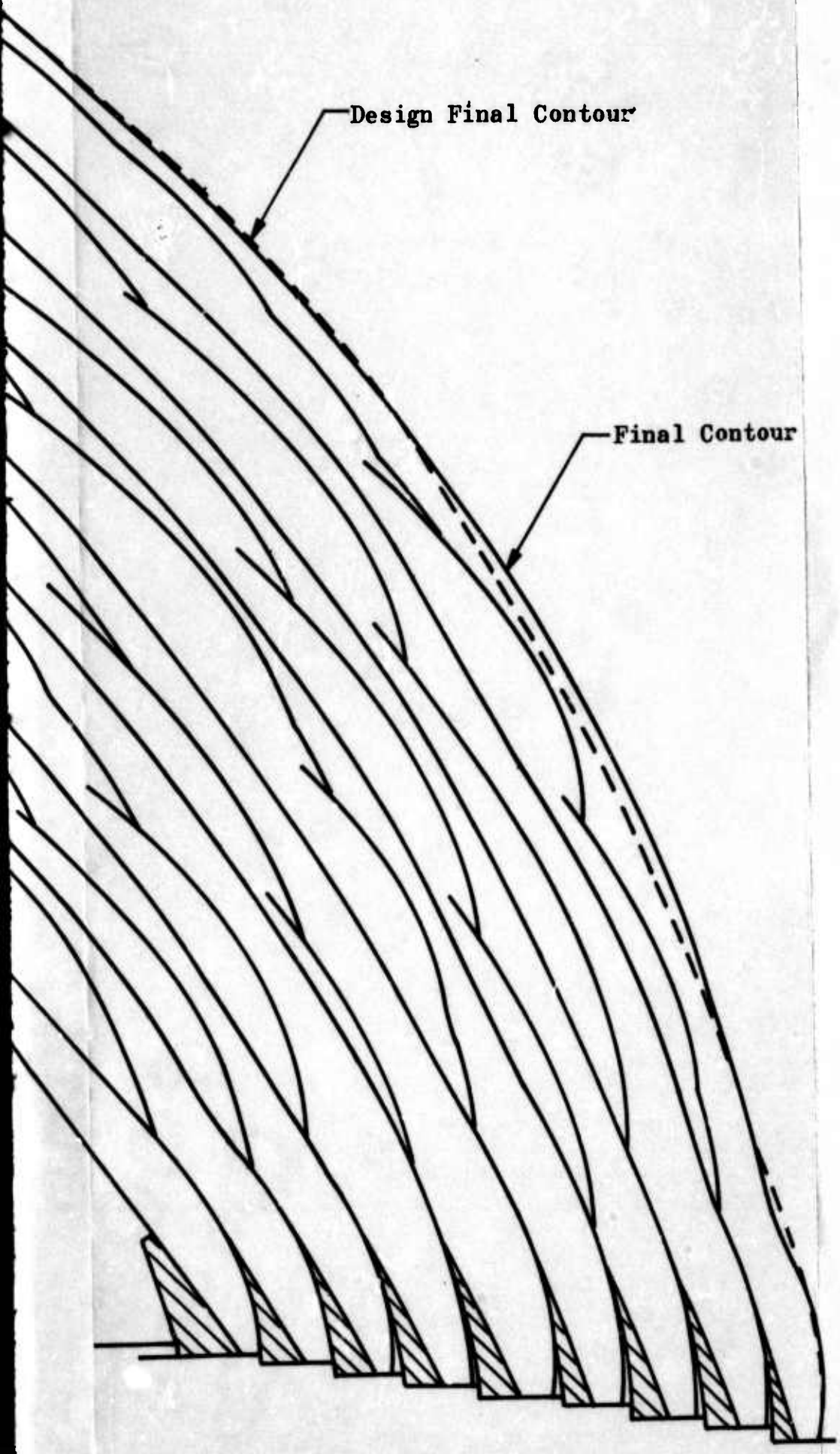


Figure 108. Pantograph Tracing for RFG A-1212 (Motor A-1006)

CONFIDENTIAL

PREVIOUS PAGE WAS BLANK, THEREFORE WAS NOT FILMED

(C) The grain was cured at 170 F for a nominal 48 hours, cooled, then restricted with R-143. Before restriction some time was required to remove globules of extruded binder from the grain surface. These were more numerous and larger than on any previous grain; probably a result of the thick layer of highly plasticized RDS-523 propellant. Restrictor weight was 28.3 pounds and the average cylindrical thickness was 0.099 inch. Restrictor cure was 48 hours at 170 F.

(b) GFW Case

GFW 1415 was the first Motor A case wound over a Motor A grain.

Case winding parameters for helix and circ wraps are shown in Table XXX, a schematic cross-section of skirt lamination is shown in Fig. 109, and weights and dimensions of the completed case are shown in Table XXXI.

The total elapsed time for the case fabrication was 25 hours, excluding cure. The actual helix winding time was 8.5 hours and actual circ winding time was 4.0 hours. Excess resin was removed by wrapping the case in toweling and placing the motor in a 170 F oven for 15 minutes. Cure was at 170 F for 20 hours.

(4) Postwinding Processing

After case cure, the sand-PVA mandrel was washed out, the Tenite-Polyken tape removed, and the grain dried four hours at 170 F.(21) The fillets between the polar bosses and the inner surface of the grain were filled with PR-1201-HT, then the interior of the grain was completely covered with a multiple-layer coating of No. 1 LAGZ rubber material to provide a moisture barrier and permit the grain to be hydrotested without a bladder. The grain was instrumented per testing instructions. A tabulation of significant weights is presented in Table XXXII.

b. Testing

(C) Motor A-1006 was hydrotested on 10 February 1964. The motor was designed to withstand an ultimate internal pressure of 1170 psig applied on a one cycle basis only. The motor was tested by internal pressurization and withstood 1345 psig, exceeding the design ultimate pressure by 14.9%. The pressure vs time curve is shown in Fig. 110.

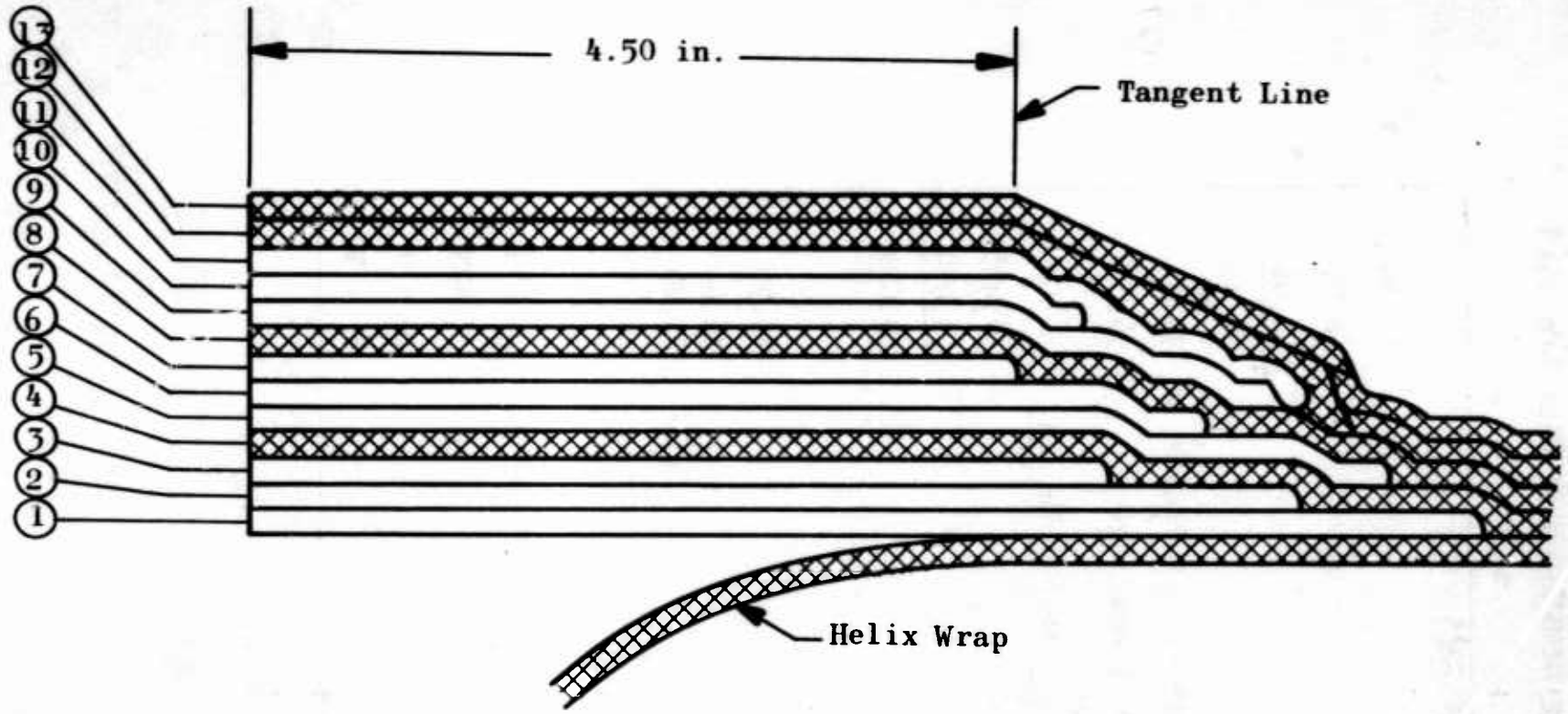
(21) This was a precautionary step to remove any moisture which might have contacted the grain.

TABLE XXX

MOTOR A-1006 WINDING PARAMETERS, GLASS

FILAMENT CASE GFW 1415 ON RG 1212

Helix Wrap	
Pattern, Helical	5/4
Helix Angle, deg	17.2
Helical Band Width, in.	0.261
Helical Band Roving	12-end S-994, 4 Balls
Helical, Ends/in.	735
Circuits Per Cover	341
Number of Covers	2
Roving Tension	
12-end Roving Between Tension Controller and Winding Machine, lb	3 1/4
48-end Band Downstream of Feed Eye, lb	33
Roving Feed Eye, in.	0.30
Circ Wrap	
Pattern Circ, deg	90
Band Width, in.	0.218
Roving	12-end S-994, 4 Balls
Circ, Ends/in.	880
Circ Covers	4
Mandrel Revolutions per Cover (Half Circuit)	266
Roving Tension	
12-end Roving Between Tension Controller and Winding Machine, lb	3 1/4
48-end Band Downstream of Feed Eye, lb	33
Resin System	
Resin D.E.R. 332 w/8 phr EMI hardener was mixed 2.0 pounds/0.16 pounds and added to the resin pot as required.	
Resin pot was maintained at room temperature.	



1. Cloth - 7.0 in. wide
2. Cloth - 6.0 in. wide
3. Cloth - 5.0 in. wide
4. Circ cover - 220 ends/inch, full length of case
5. Cloth - 6.5 in. wide
6. Cloth - 5.5 in. wide
7. Cloth - 4.5 in. wide
8. Circ cover - 220 ends/inch, full length of case
9. Cloth - 5.8 in. wide
10. Cloth - 4.8 in. wide
11. Cloth - 6.2 in. wide
12. Circ cover - 220 ends/inch, full length of case
13. Circ cover - 220 ends/inch, full length of case

Figure 109. GFW-1415 Skirt Buildup

CONFIDENTIAL

TABLE XXXI

MOTOR A-1006, WEIGHTS AND DIMENSION OF CASE GFW 1415

Weight, lb	
Helix Roving	11.39
Circ Roving	8.97
Skirt Cloth (Calc.)	4.06
	24.42
Case Weight at Estimated 29.4% Resin*	34.6
Case Weight by Load Cell Readings	34.5
Thickness, Estimated Based on A-1412, in.	
Helix Wrap	0.035
Circ Wrap	0.039
Total, Cylinder	0.074
Over-all Dimensions, in.	
Tangent	48.9
Skirt to Skirt Outside	58.0-58.06
Diameters	
Forward Skirt	30.000
Cylinder (1)	29.875
(2)	29.895
(3)	29.870
Aft Skirt	29.973

*A-1412 and A-1413 were 29.4% by analysis

TABLE XXXII

PROCESSING WEIGHTS FOR MOTOR A-1006

	lb
Polar Bosses w/Insulation (2)	22.9
Load Rings (18)	13.0
Mandrel, Spindle, Bosses	1311.2
Aluminum Wire	243.8
Propellant With Aluminum	1356.0
Restrictor (R-143) w/Case Flanges	30.3
GF Case (Plastic)	34.5
Case Skirt Rings	39.7
Final Grain w/Case	1493.0

The motor was at ambient temperature (about 60 F) during testing and was oriented in a vertical position. The extensive instrumentation included pressure transducers, four linear potentiometers, and 46 strain gages.

(C) The motor performed satisfactorily during pressurization to 1345 psig. At this point, the pressure dropped to a lower pressure and held awhile. Then the test was terminated. External inspection revealed slight flats in the cylindrical section. Internal observations indicated that two ridges extended from the aft tangent to the forward dome.

The structural performance was near that predicted by theory.

(1) Analysis

(C) Maximum and minimum recorded RFG and GFW case strains are shown in Table XXXIII. The GFW hoop strains are somewhat less than was expected. For the maximum pressure of 1345 psig, maximum hoop strain in the cylindrical portion of the GFW case was 20,200 microinch/inch, as shown in Table XXXIII, and was well below the 30,000 microinch/inch expected strain at rupture. The location of instrumentation is shown in Fig. 111. Maximum strain in the forward dome was 6386 microinch/inch at gage 27 whereas the maximum strain in the aft dome was 24,218

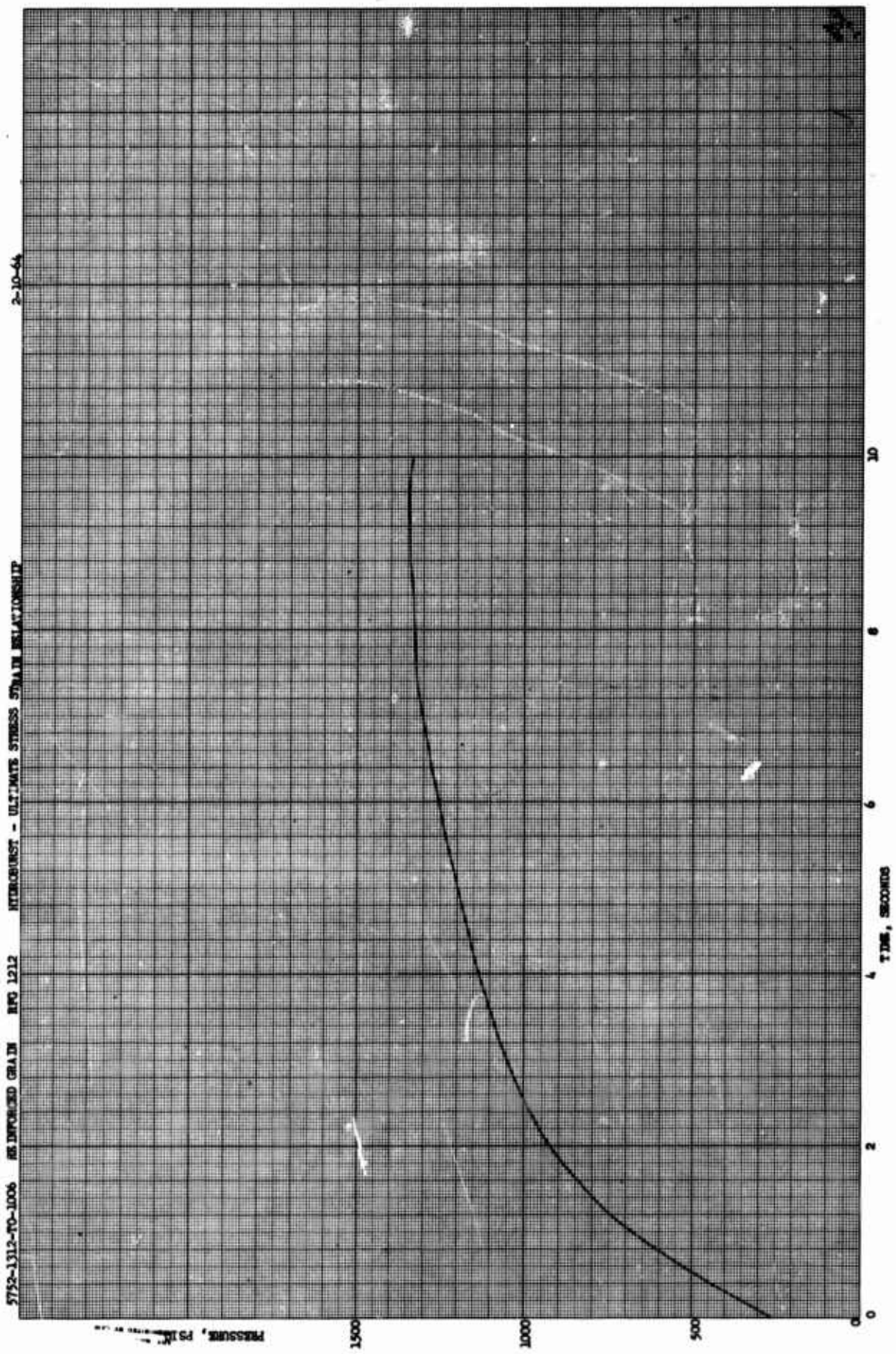


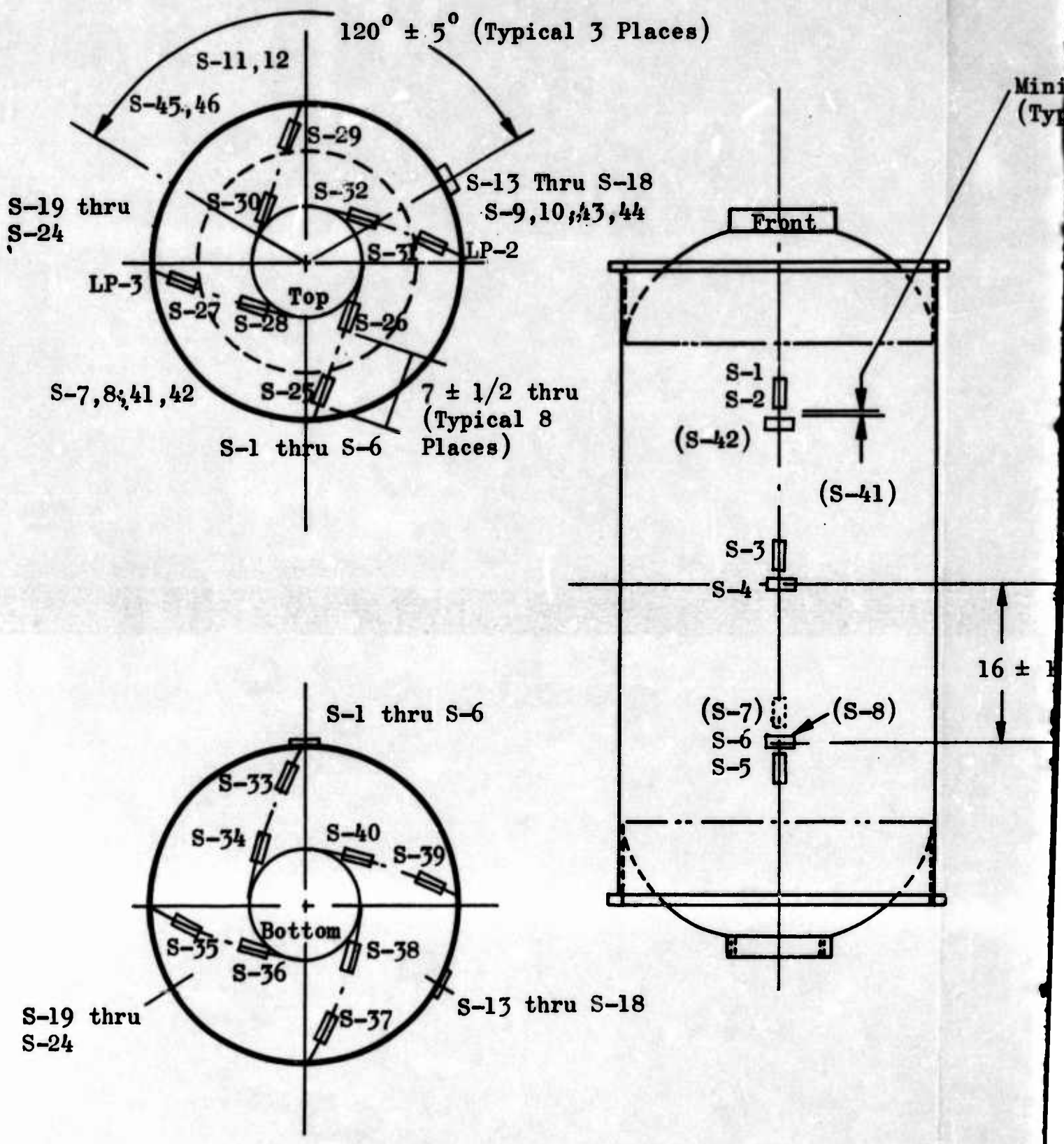
Figure 110. Pressure vs Time for Motor A-1006

TABLE XXXIII

MAXIMUM AND MINIMUM RECORDED RFG AND GFW CASE STRAINS, RFG A-1006

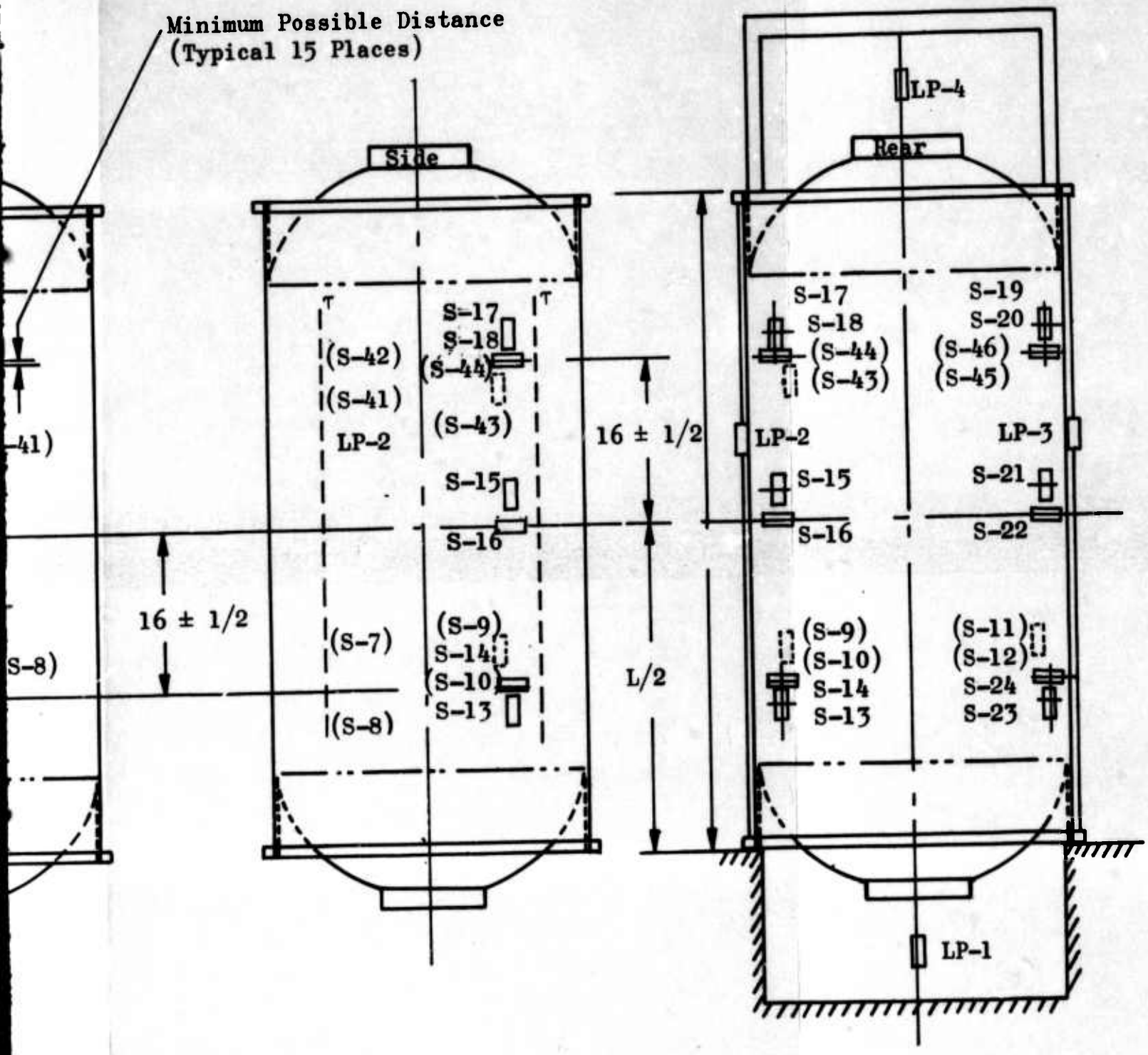
Strain Gage	Pressure, psi	Minimum Strain microinch/in.	Pressure, psi	Maximum Strain microinch/in.
1	260	297	929	6458
2	260	1073	885	28,225
3	260	273	929	6886
4	260	1089	983	30,729
5	266	344	1082	12,694
6	260	1023	1052	25,530
7A	1282	-9232	780	1468
8	260	1642	1258	24,466
9	1052	-6389	766	698
10	260	1840	1332	26,196
11	1307	-6497	816	1049
12	260	2055	1332	31,164
13	260	325	1052	17,232
14	260	1050	1077	24,267
15	260	316	1014	4435
16	260	1092	848	25,120
17	266	326	1345	2551
18	260	1034	1345	16,732
19	266	250	1142	912
20	260	1090	1345	17,046
21	260	284	1009	916
22	260	1066	1345	20,023
23	260	321	1345	6551
24	260	1061	1345	18,076
25	260	635	1345	5309
26	260	486	1345	5575
27	260	787	1345	6386
28	266	412	1345	4508
29	260	639	1345	4858
30	266	553	1345	5743
31	260	543	1345	3845
32	272	218	1345	3890
33	260	803	1345	19,331
34	260	1089	1345	24,218
35	260	766	1345	20,411
36	260	639	1345	22,245
37	266	699	1345	17,133
38	266	1329	1345	24,804
39	266	790	1345	19,581
40	260	1214	1345	24,364
41	954	-22,130	1300	8126
42	260	1324	1345	18,626
43	1345	-3486	505	1516
44	302	950	1284	19,168
45	1345	-4358	505	84
46	260	2053	1345	29,577

PREVIOUS PAGE WAS BLANK, THEREFORE WAS NOT FILMED



NOTES:

1. Do Not Use Type PA-7 Strain Gage.
2. Locations Indicated For LP-1 thru LP-4 and S-25 thru S-40 Are Approximate (Except as Shown by Dimensions). Locate Gages Consistent with Dome Windings and Surface Conditions.
3. Strain Gage Calibration Range: ± 35,000 μ in./in.
4. LP-1,4: 7/16 in. Minimum Deflection.
5. LP-2,3: 1 1/2 in. Minimum Deflection.
6. Measure LP-2 and LP-3 Gage Length to Nearest 1/32 in.
7. (S-X) Denotes Strain Gage on Inside of Grain.
8. Hydroburst Esitmate: 1180 psi allow for 1800 psi Maximum.
9. For Clarity, Instrumentation not Shown in all Views.
10. Dimensions Shown are in inches.



Length to

on Inside

psi allow

on not Shown

nches.

SYMBOLS

S-X Single axis strain gage

LP-X Linear potentiometer

Figure 111. Location of Strain Gages and Linear Potentiometers for Motor A-1212

CONFIDENTIAL

PREVIOUS PAGE WAS BLANK, THEREFORE WAS NOT FILMED

microinch/in. at gage 34. Both of these strains were below the 30,000 microinch/in. The large strain recorded by gage 34 illustrates the localized condition created by the proximity of the polar boss. The maximum internal hoop strain at the internal surface of the grain was 31,200 microinch/in. at gage 22. This strain is also less than the expected wire rupture strain of 50,000 microinch/in.

External inspection revealed slight flats running from the upper to lower tangent in the cylindrical portion of the motor. These flats were approximately diametrically opposite each other. Internal observation indicated that two ridges extended along a straight longitudinal path from the aft tangent to the forward dome. One ridge was more pronounced than the other--it was about 3-inches wide and 1-inch high. The size of the ridge diminished as it continued into the dome. The direction also changed, following a path parallel to the dome wraps. The ridge seemed to have originated at a failure in the RFG web near the forward boss steel load rings.

Replots of reduced data show strain vs pressure only to the point of maximum pressure. The recorded digital data, however, show longitudinal GFW case strain continued to increase even though chamber pressure was decreasing. This increase of GFW case strain and a corresponding decrease in chamber pressure has been observed in all RFG/GFW motor hydrotests when the RFG ruptures without rupturing the GFW case. GFW case strains increase because the chamber pressure acts directly on the case, when the RFG fails, rather than on the composite structure. The increased GFW case strain and resultant increase in volume caused the sudden decrease in chamber pressure.

(C) Extrapolation of the test strain vs pressure curve in Fig. 112 indicates that the GFW case would not have ruptured until the chamber pressure reached approximately 1460 psig if the RFG had not ruptured first. This extrapolated pressure is extremely close to that predicted, 1440 psig.

Two theoretical analyses which were not available when the motor was designed are compared to test results to evaluate both methods of analysis. References 22 and 23 are theoretical methods which have been used to establish separate computer programs. After the descriptive physical characteristics of the materials involved are selected for the computer, it solves the elastic-plastic equations and prints out values of the desired parameters. Therefore, the curves plotted in this report for both references utilize the computer printout for the particular elastic-plastic solution.

(22) Steyer, C. C.: Analysis of Thick-Walled, Layered Anisotropic Elastic Cylinder Subjected to a Radial Pressure Utilizing Three-Dimensional Material Properties, Rocketdyne SRD, Design and Development Section Memo 64-24, July 1964.

(23) Daly, J.M.: Elastic-Plastic Grain and Case Stress Analysis, Rocketdyne SRD, Advanced Design Memo 63-21, December 1963.

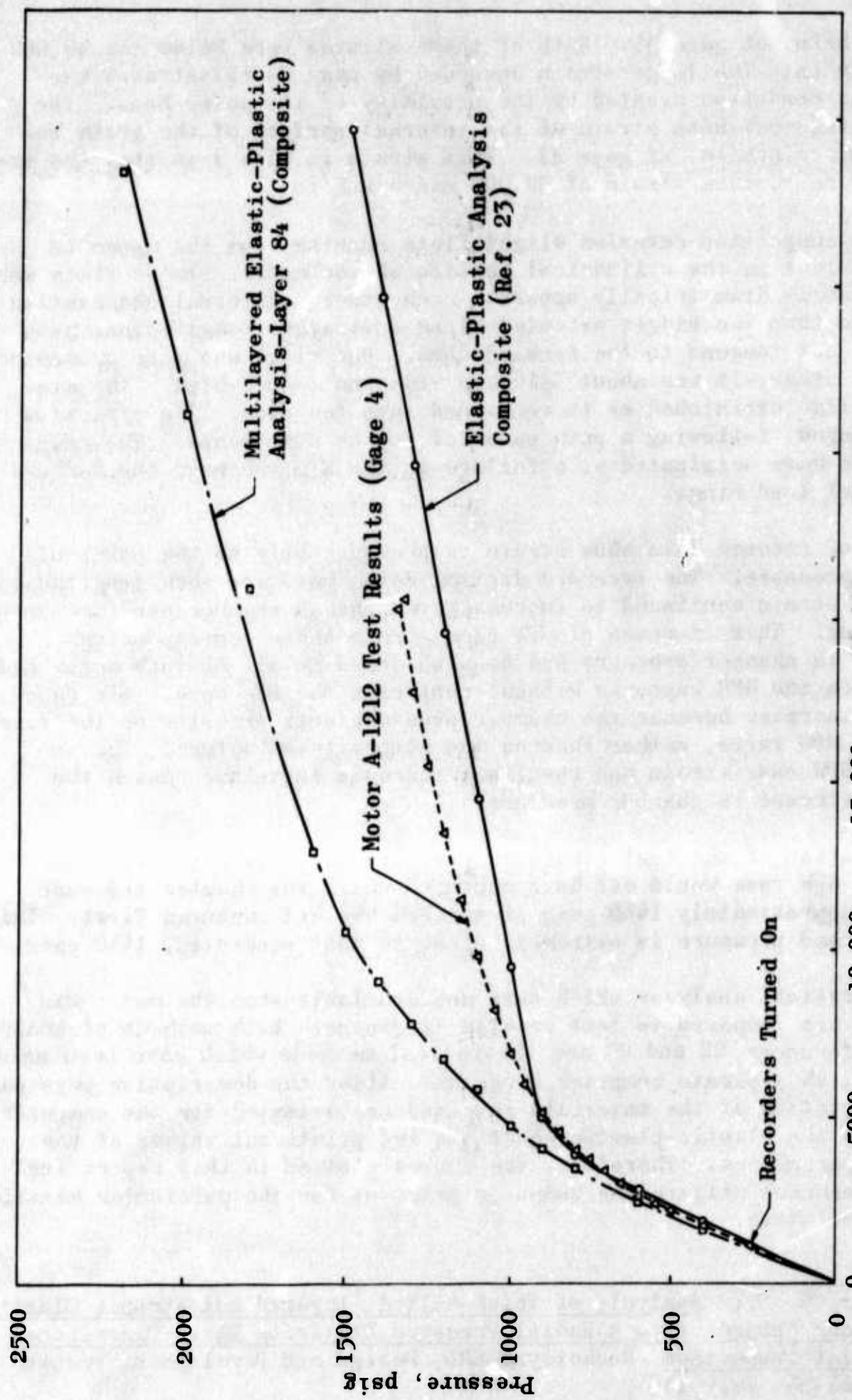


Figure 112. Pressure vs Hoop Strain in GFW Case Motor A-1006

(C) Figure 112 is a plot of internal pressure vs hoop strain in the GFW case. Although both references agree very closely with test results, Ref.22 is more accurate in the elastic region up to a pressure of about 400 psig. From this point onward, Ref. 23 has much better correlation. For an allowable hoop strain in the GFW case of 3.0%, the extrapolated burst pressure for a single pressure cycle from test data would be about 1460 psig. Based on extrapolation of test, Ref.23 tends to be closer than Ref. 22 in predicting burst pressure.

(C) Internal pressure vs hoop strain at the inner surface of the RFG is shown in Fig. 113. In the elastic region, Ref.23 more closely follows test results. If the curve from the test could be extrapolated, the predicted burst pressure would be about 1430 psig based on an allowable strain in the RFG of 5.00%. This would compare very favorably with the predicted burst pressure of about 1370 psig from the Ref. 23 curve whereas Ref. 22 predicts about 1730 psig. Although the strain gage used for comparison was near the skirt, the induced discontinuity strains should have been small.

Figure 114 represents plots of composite hoop stress vs composite hoop strain in the hoop wrap of the GFW case. Both stress and strain were calculated using the theoretical results of the two analyses and show good agreement. Composite hoop stress vs hoop strain for the total GFW case wall is also shown in Fig. 114.

All of the data shown in Figs. 112, 113, and 114 were calculated by a digital computer. An IBM 7094 and 1401 is used for Refs.22 and 23 respectively.

(2) Conclusions and Recommendations

The following conclusions are based on the results of the test and analyses.

Structural performance of Motor A-1006 exceeded design requirements.

Reference 23 theoretical data show better correlation with GFW case test data than Reference 22. A final evaluation of RFG theoretical data may be made only with additional one cycle burst tests.

(C) Figure 112 is a plot of internal pressure vs hoop strain in the GFW case. Although both references agree very closely with test results, Ref.22 is more accurate in the elastic region up to a pressure of about 400 psig. From this point onward, Ref. 23 has much better correlation. For an allowable hoop strain in the GFW case of 3.0%, the extrapolated burst pressure for a single pressure cycle from test data would be about 1460 psig. Based on extrapolation of test, Ref.23 tends to be closer than Ref. 22 in predicting burst pressure.

(C) Internal pressure vs hoop strain at the inner surface of the RFG is shown in Fig. 113. In the elastic region, Ref.23 more closely follows test results. If the curve from the test could be extrapolated, the predicted burst pressure would be about 1430 psig based on an allowable strain in the RFG of 5.00%. This would compare very favorably with the predicted burst pressure of about 1370 psig from the Ref. 23 curve whereas Ref. 22 predicts about 1730 psig. Although the strain gage used for comparison was near the skirt, the induced discontinuity strains should have been small.

Figure 114 represents plots of composite hoop stress vs composite hoop strain in the hoop wrap of the GFW case. Both stress and strain were calculated using the theoretical results of the two analyses and show good agreement. Composite hoop stress vs hoop strain for the total GFW case wall is also shown in Fig. 114.

All of the data shown in Figs. 112, 113, and 114 were calculated by a digital computer. An IBM 7094 and 1401 is used for Refs.22 and 23 respectively.

(2) Conclusions and Recommendations

The following conclusions are based on the results of the test and analyses.

Structural performance of Motor A-1006 exceeded design requirements.

Reference 23 theoretical data show better correlation with GFW case test data than Reference 22. A final evaluation of RFG theoretical data may be made only with additional one cycle burst tests.

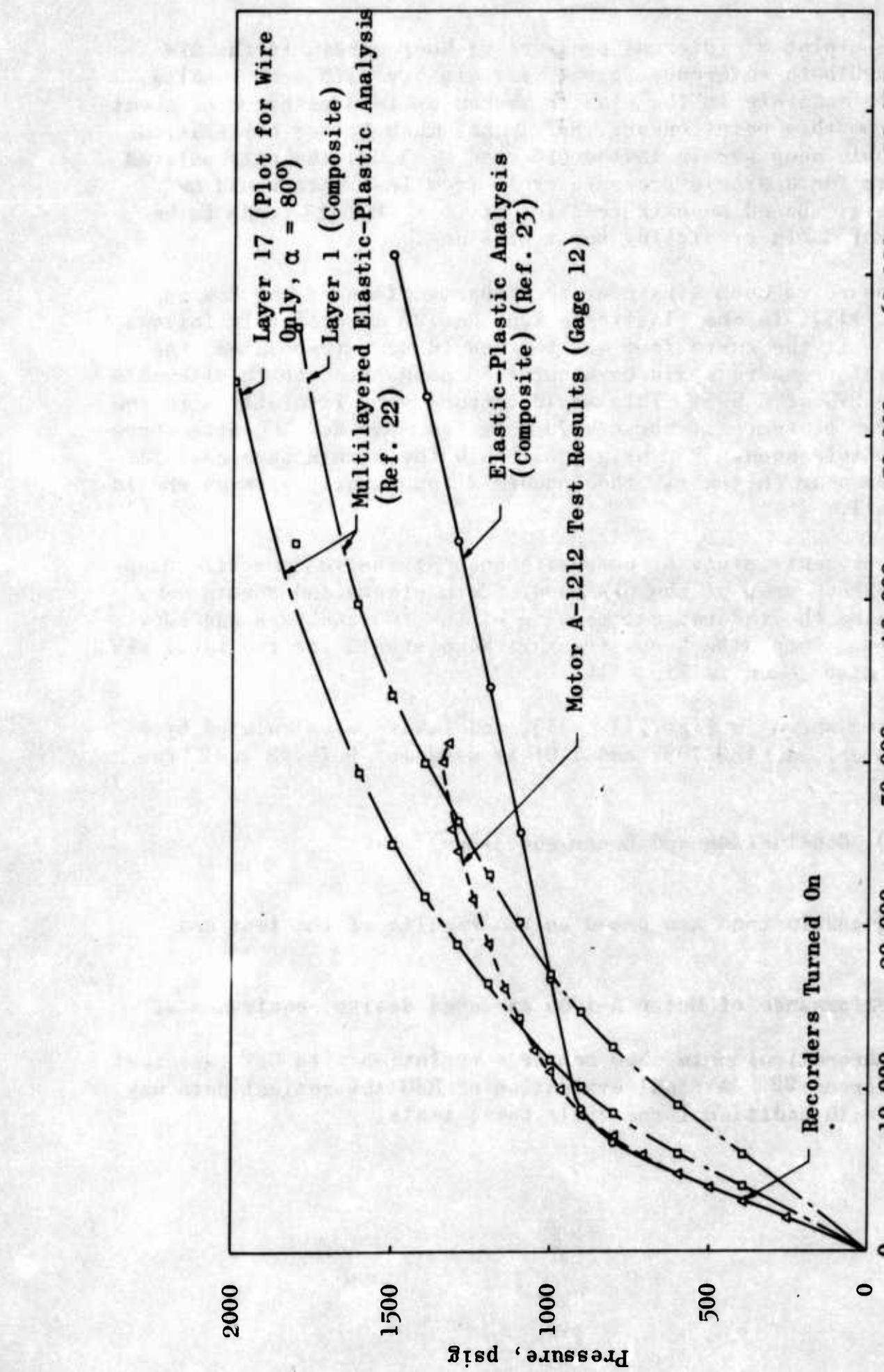


Figure 113. Pressure vs Hoop Strain at Inner Surface of RFG Motor A-1006

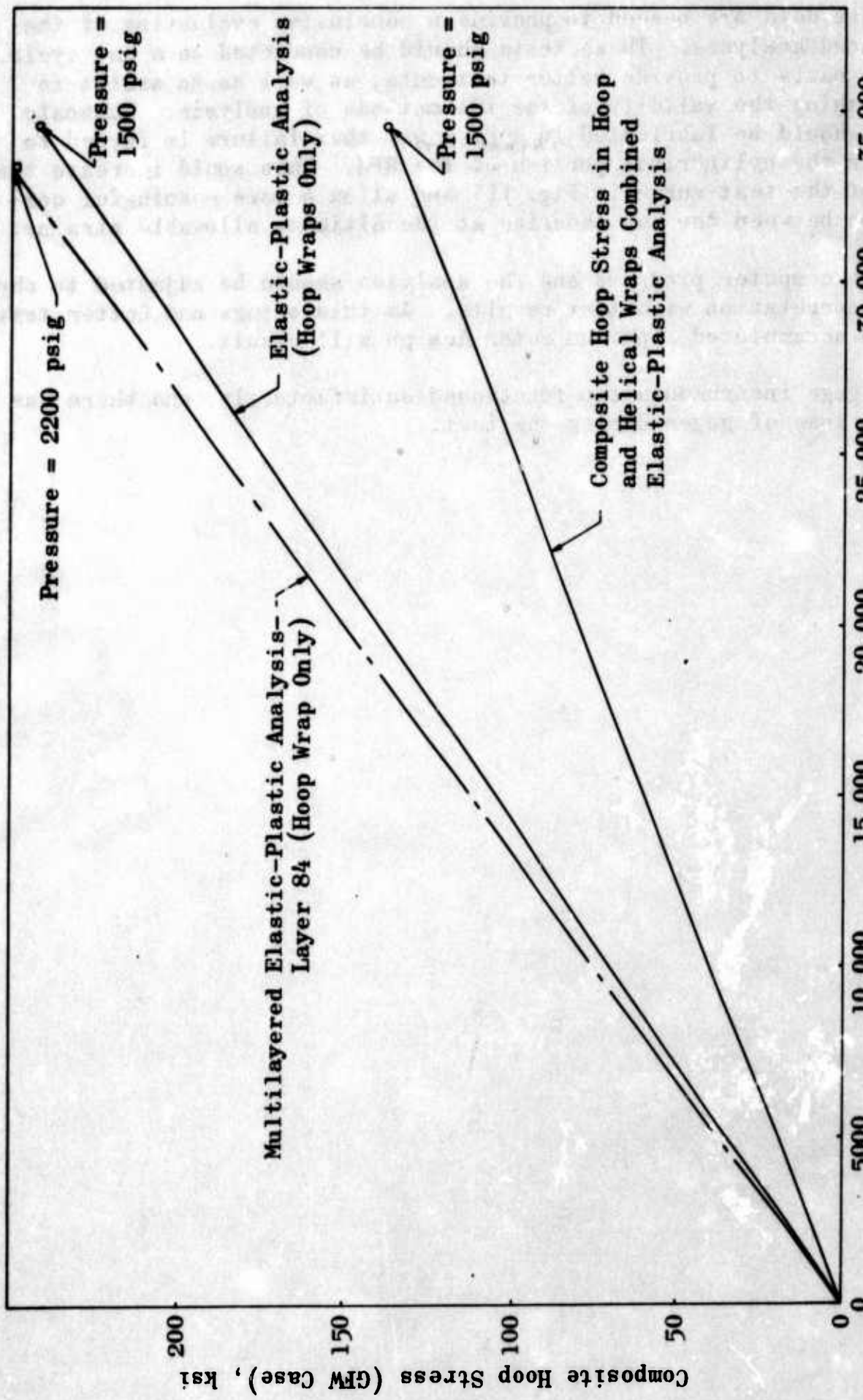


Figure 114. Composite Hoop Stress (GFW Case) vs Composite Hoop Strain (GFW Case) Motor A-1006

More test data are needed to provide a conclusive evaluation of the referenced analyses. These tests should be conducted on a one cycle to rupture basis to provide better test data, as well as to assist in establishing the validity of the two methods of analysis. Subscale models should be fabricated in such a way that failure is forced to occur in the cylindrical portion of the RFG. This would increase the range of the test curve in Fig. 113 and allow a more meaningful correlation between the two theories at the ultimate allowable strains.

Both the computer programs and the analyses should be adjusted to show better correlation with test results. As this occurs and better test data are accumulated, optimum motor design will result.

Strain gage instrumentation functioned satisfactorily, and there was a minimum loss of gages during the test.

2. DEVELOPMENT MOTOR A-1001

This motor represented the first scheduled firing of a fullscale RFG/GFW/ core motor, thus several design modifications were made to the flight-weight design to provide a conservative "heavyweight" motor. The areas of major design modification were concerned with the GFW case and insulation. To provide a considerable margin of safety, the case thickness was increased approximately threefold, and the case insulation thickness was increased approximately tenfold.

(C) The liner was increased to a thickness of 0.3 inch in the cylindrical section. This thickness of liner will provide a margin which will take up to five seconds premature burnthrough. In the domes where the insulator becomes thicker, the protection offered would handle seven to ten seconds of premature burnthrough.

(C) Based on the increased case thickness, the case alone would have a pressure capability of about 2300 psi. This case configuration was derived on the basis of consideration of probable failure pressures of other motor components. In evaluation of the capability of these other areas, the location of minimum strength was associated with the nozzle assembly where a pressure capability of about 2100 psi was indicated.

(C) To accommodate the increased case and insulator thickness, several layers were deleted or reduced in the eighth and ninth cycles. Two of the fill layers in the eighth cycle were eliminated and two were reduced by 50%. Also, the ninth GI layer was reduced from five covers to three.

A new polar GFW flange for the aft polar boss was required to accommodate the heavyweight case. This flange is larger in diameter in order to extend under the extra glass wraps of the heavyweight case design. All load rings for this motor were steel, although the final flightweight design was scheduled for titanium. However, due to availability of materials and the fact that titanium represented primarily a weight savings over steel, steel rings were used.

Also, because of failure of the vendor to provide acceptable forward closures as scheduled, a heavyweight forward closure was designed and fabricated of steel. Insulation of the steel forward closure was accomplished with MX-2646, per flightweight design.

Performance and mass fraction estimates for the flightweight design Motor A and Motor A-1001, utilizing additional insulation and case thickness, are shown in Tables XXXIV and XXXV, respectively. Estimated thrust- and pressure-time curves are shown in Fig. 115.

(C)

TABLE XXXIV

ESTIMATED PERFORMANCE SUMMARY,
A-1001 AND FLIGHTWEIGHT DESIGN

	Flightweight Design	A-1001
Total Impulse, lb-sec	561,600	547,800
Avg Thrust, lb	17,340	18,170
Action Time, sec	32.4	30.1
Avg Pressure, psia	575	600
Core Propellant Weight, lb	1135	1135
RFG Propellant Weight, lb	1349	1249
Total Propellant Weight, lb	2484	2384
I_{sp} @ 1000 psia (composite motor)	241.3	243.6
I_{sp} @ 1000 psia (core propellant)	250.0	250.0
I_{sp} @ 1000 psia (RFG propellant)	234.0	237.8
Delivered I_{sp} @ Motor Conditions (S.L.; ϵ = 6:1)	226.1	229.8
Inert Weight	107.9	254.7
Mass Fraction	0.96	0.90

(C)

TABLE XXXV

ESTIMATED WEIGHT AND MASS FRACTION,
A-1001 AND FLIGHTWEIGHT DESIGN

	A-1001	Flightweight Design
Nozzle Assembly	29.65	26.77
Case	96.00	34.00
Liner	82.06	12.00
Igniter	2.58	2.58
Forward Boss	10.52	10.52
Aft Boss	12.70	12.70
Load Rings*	13.59	6.94
Drive Pins	0.56	0.56
O-rings	0.10	0.10
Flange	6.93	1.71
Total Inerts	254.69	107.88
Igniter Pyrotechnics	0.56	0.56
Core Propellant	1135.00	1135.00
RFG Propellant	1249.00	1349.00
Total Propellant	2384.56	2484.56
Total Motor Weight	2639.25	2592.44
Mass Fraction	0.90	0.96

*Steel for A-1001; Titanium for flightweight design.

(C)

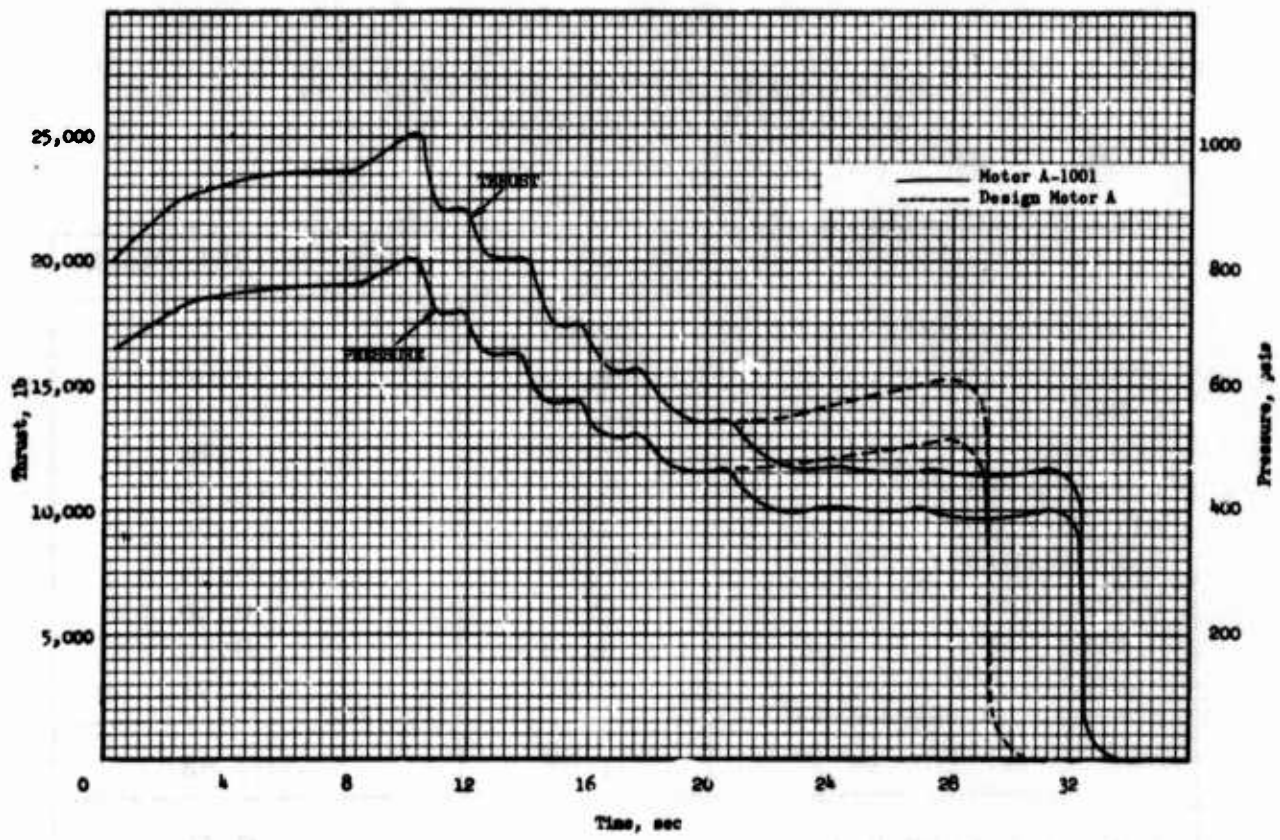


Figure 115. Estimated Thrust and Pressure Time, A-1001 and Flightweight Design

a. Fabrication

(1) Equipment

The grain was wound on the 36-inch, 3-axis, cam-actuated machine. The electric, microtension wire-tensioning system (made by Eastern Equipment and Controls Company) was used with manual propellant application and a spreader blade for distrubution of applied propellant.

A molded sand-polyvinyl alcohol (PNA) mandrel coated with Tenite and polyken tape was used to wind the grain.

(2) Material

(C) The aluminum wire used was 7.5-mil diameter, alloy 5056 heat-treated by the supplier, Hudson Wire Company, to give 5% minimum elongation and 50,000 psi minimum tensile.

The matrix propellant consisted of two formulations, RDS-514 and RDS-523, with various levels of depressant to give tailored ballistic characteristics. Low-viscosity LCA-5249 was used on the dome areas adjacent to the polar bosses.

The restrictor used was R-143, a Flexadyne binder with carbon black filler.

The entire surface of the steel load rings was coated with Chemlok EX-B500-1 and the coating was cured one hour at 170 to 190 F. Each ring was wrapped with 2-inch strips of polyethylene to prevent handling contamination and moisture contact. Strips were removed just prior to installing each load ring in its proper position on the polar boss.

The MX-4600 phenolic polar bosses were cleaned with methyl ethyl ketone (MEK) and dried 24 hours at 350 F. The polar bosses (after drying) were coated with Epon 926 and cured for two hours at 190 F. The Epon 926 acted as a moisture-proof barrier. The polar bosses were wrapped in polyethylene sheets prior to installation on the sand mandrel, to provide additional protection against moisture during mandrel washout.

(3) Processing

(a) Grain Winding and Restriction

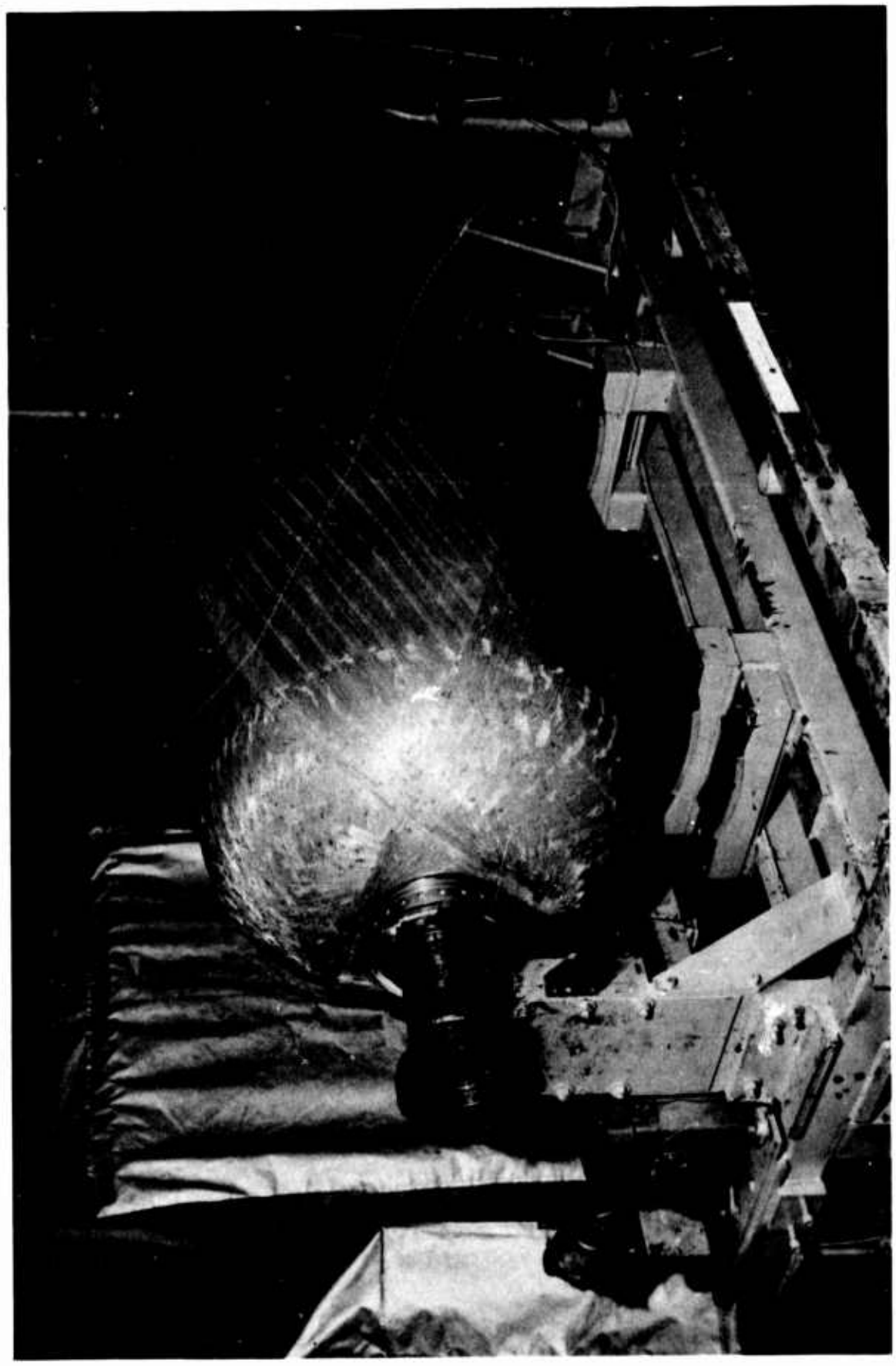
(C) The process targets for the first attempt to wind grain A-1201 were: (1) 350 ± 25 grams tension for aluminum wire to reduce the wire breakage experienced in A-1212, (2) a slightly heavier application of propellant in the dome area to prevent any voids or porosity, and (3) a lower-burning-rate propellant with higher viscosity in the dome area adjacent to the polar boss. The use of lower-burning-rate propellant around the polar boss was considered necessary, to meet ballistic design parameters and prevent the flame front from burning through the dome area before the cylindrical area was spent. The grain winding was stopped when the second load rings did not fit into the polar boss step because of excessive buildup of the first geodesic layer. The pantograph trace of the first geodesic layer appeared to be identical to that of grain A-1212. A check of the load rings showed that the rings met the design specifications. Evidentally, the pantograph accuracy was not sufficient to show variation of 0.050 inch from design. An improved device for checking dome contour was developed.

(C) The second, and successful, attempt to wind A-1201 was completed on 27 February 1964, see Fig. 116. It had modified process targets of 400 ± 25 grams tension for aluminum wire, a slightly lower application of propellant in the dome area, and a lower-viscosity propellant in the dome area adjacent to the polar boss. The propellant in the dome area adjacent to the polar boss for the first attempt was LCA-5249, a plasticized 83% solids-loaded propellant, with 3% strontium carbonate and 3% calcium citrate as burning rate depressants. The propellant for the second attempt was LCA-5281 containing 80% solids-loaded propellant, with 3% strontium carbonate and 3% calcium citrate as burning rate depressants. The lower-total-solids LCA-5281 gave a lower-viscosity propellant, but the 6% depressant content caused the propellant to be very tacky, which made spreading difficult.

In the second attempt, the aluminum wire tension was set at 400 grams and monitored frequently to maintain tension control. Carbolloy eyes used in the wire-tension gathering system were cleaned frequently to remove any accumulation interfering with the tension control of the wires, particularly those coming from the bottom of the tension-control console. Wire breakage for the winding of A-1201 was considerably less than that which occurred when winding A-1212. The reasons for less wire breakage in winding A-1201 were: (1) smoother operation of winding machine, (2) more frequent cleaning of carbolloy eyes for wire-gathering portion of tension control, and (3) better quality of wire. Improvements in the wire-gathering portion of tension control and smoother operation of winding machines will reduce winding time. The winding time for the second attempt was 5-1/2 days, and time for RFG-1212 (A-1006) was 7-1/2 days. A summary of the RFG winding data is in Table XXXVI.

(C) Two wire-weight totalizers were used and they showed excellent agreement with the aluminum-wire weight obtained from Quality Control History Cards. The difference of 1.8 pounds could be the scrap wire discarded in occasional wire breakage. The total weight of aluminum wire used (from totalizers) was 226.1 pounds.

The tension-monitoring transducer equipment for checking aluminum-wire tension gave staisfactory service throughout the grain winding. This device is a satisfactory tool for monitoring wire tension in the grain winding operation.



2YA32-3/2/64-M1A

Figure 116. Reinforced Grain of A-1001

PREVIOUS PAGE WAS BLANK, THEREFORE WAS NOT FILMED

TABLE XXXV

WINDING DAT

Winding Parameters	Mandrel	1-GI	1-43	1-54	1-66	2-GI	2-43	2-54	2-
Winding Angle, deg		31.2	43.7	56.6	71.7	30.1	42.8	58.1	69.
Target No. of Covers		7	7	8	6	7	4	5	8
Actual No. of Covers		7	7	8	5	7	4	5	8
Cam Revolutions		250	217	192	65	266	128	115	120
X-axis Insert		0	0, +2	+1	0, +1	0	+1	+1, +2	0,
Follower Setting		0.9	1.3	1.25	1.5	0.9	0.8, 0.5	1.25	1. 0.
Cylinder Buildup Data									
Cylinder Diameter Aft	22.090	22.345	22.535	22.779	22.923	23.130	23.280	23.388	23.
Cylinder Diameter Center	22.115	22.350	22.585	22.812	22.964	23.193	23.327	23.491	23.
Cylinder Diameter Forward	22.085	22.325	22.557	22.785	22.929	23.160	23.295	23.492	23.
Layer Depth (Avg), in.	--	0.122	0.110	0.117	0.074	0.111	0.070	0.078	0.
Cover Thickness (Avg), in.	--	0.0167	0.0157	0.0146	0.0148	0.0159	0.0175	0.0156	0.
Miscellaneous Data									
Change Gears A		56	55	52	33	55	51	43*	31
Change Gears B		79	84	96	70	82	82	50*	76
Change Gears C		78	66	65	44	76	74	49*	50
Change Gears D		95	92	100	98	83	96	59*	87
Winding Speed, rpm		2 1/4	3 1/2	4	6	4	4	4.5	6
Layer Winding Time, hr		3.4	2.5	3	1.4	3.6	4.3	3	2
Total Elapse Time for Layer, hr		5.7	3.5	4	2.0	6.3	5.5	4.3	2.

Winding Parameters	5-GI	5-30	5-38	5-47	5-60	6-GI	6-26	6-32	6-
Winding Angle, deg	25.0	32.4	43.7	55.1	66.0	23.7	29.9	40.1	49.
Target No. of Covers	7	6	6	6	6	6	3	4	5
Actual No. of Covers	7	2	6	5	6	6	0	4	4
Cam Revolutions	315	84	216	145	120	282	--	160	136
X-axis Insert	+1	0	0, -2	-2, -1	-2, -1	0	--	-1, 0	-2,
Follower Setting	1.45	1.15	1 1/2, 3/8	1.6 1.5	1.5, 0.6	1 1/2	--	1.6, 1.1	0. 1.
Cylinder Buildup Data									
Cylinder Diameter Aft	26.075	26.134	26.390	26.534	26.735	26.962	--	27.117	27.
Cylinder Diameter Center	26.150	26.225	26.485	26.650	26.836	27.065	--	27.216	27.
Cylinder Diameter Forward	26.114	26.225	26.450	26.600	26.785	27.022	--	27.160	27.
Layer Depth (Avg), in.	0.128	0.041	0.124	0.077	0.095	0.116	--	0.074	0.
Cover Thickness (Avg), in.	0.0183	0.0205	0.0207	0.0154	0.0158	0.0193	--	0.0185	0.
Miscellaneous Data									
Change Gears A	56	52	57	51	41	64	--	56	58
Change Gears B	79	59	81	93	96	77		71	79
Change Gears C	78	69	68	71	57	79		69	59
Change Gears D	80	99	97	98	83	94		100	93
Winding Speed, rpm	3	5	4 1/2	5	5	3		6.3	5
Layer Winding Time, hr	3.75	0.75	2 1/2	3	2	4		1 1/2	2.
Total Elapse Time for Layer, hr	4.7	2	4 1/2	3 1/2	2 1/2	5.1		3	2.

*Indirect gear drive

TABLE XXXVI

WINDING DATA

Layer												
2-54	2-66	2-80	3-GI	3-35	3-45	3-60	4-GI	4-30	4-40	4-50	4-65	4-80
58.1	69.9	80.0	28.6	38.5	48.4	66.0	26.5	34.9	45.8	58.3	73.3	80.0
5	8	8	7	6	8	10	7	4	4	6	7	6
5	8	7	7	3	8	12	7	4	4	6	7	6
115	120	49	284	108	248	228	301	156	136	150	91	48
+1, +2	0, +2	+1, +2	0	-1	-1, +1	-2, 0 +, -2	0	-1	-1, +1	-1, +1	-1, +1	-1, +1
1.25	1.5, 0.75	2 1/4, 1 1/4	1 1/8	1	0.8, 1.4	0.5, 1.2	1.1	1.6, 1.1	0.85	0.8, 1.5	1.2, 0.9	1 1/2
23.388	23.700	23.825	24.075	24.145	24.490	24.804	25.038	25.127	25.275	25.455	26,655	25,796
23.491	23.730	23.856	23.856	24.239	24.506	24.850	25.095	25.200	25.315	25.525	25.696	25.885
23.492	23.720	23.896	24.107	24.225	24.510	24.871	25.096	25.187	25.330	25.535	25.700	25.892
0.078	0.132	0.070	0.122	0.101	0.099	0.170	0.118	0.048	0.068	0.099	0.090	0.087
0.0156	0.0165	0.010	0.0174	0.0337	0.0124	0.0142	0.0169	0.0120	0.0170	0.0165	0.0128	0.0145
43*	31	33*	58	52	57*	31	59	50*	52	52	34	29*
50*	76	64*	76	81	40*	80	6	52*	72	88	88	56*
49*	50	39*	74	68	39*	71	61	67*	58	60	50	31*
59*	87	70*	88	82	61*	97	80	55*	85	95	98	59*
4.5	6	6 1/2	3 1/2	6	4 1/2	5-6	3	5	4	5	5	6
3	2	1.5	3 1/2	1.3	4 1/2	4 1/2	3.8	2	2	2	4.2	1.7
4.3	2.5	3.1	5	4.5	5.5	4.8	5.0	8	3.1	3.7	5	3.1
6-32	6-40	6-56	7-GI	7-32	7-46	7-67			8-GI	8-29	8-38	9-GI
40.1	49.3	63.1	22.4	34.2	46.1	67.3	80.0		21.5	28.7	37.8	20.4
4	5	9	6	3	3	7	10		5	3	2	4
4	4	9	6	2	3	5	13		5	3	2	3
160	136	207	294	90	111	100	117		255	147	88	159
-1, 0	-2, 0	-2, +1	0	+1, -1	0	+2, 0, +3	+1, 0, -2, +2		+1	+2	+3	0, -1, 0
1.6, 1.1	0.9 1.0	1 1/2, 0.7	1.25	1 1/2, 2	1.5	1.6	0.5, 1 1/2, 2 1/3, 1 1/8		, 1.5	1	1 1/4	1.6
27.117	27.285	27.525	27.784	27.789	27.821	28.035	28.550		28.855	28.900	28.940	29.062
27.216	27.325	27.650	27.915	27.940	27.987	28.200	28.700		28.984	29.025	20.075	29.200
27.160	27.275	27.610	27.825	27.945	27.976	28.156	28.645		28.874	28.964	29.015	29.108
0.074	0.168	0.048	0.123	0.025	0.019	0.101	0.251		0.136	0.030	0.024	0.057
0.0185	0.0420	0.0053	0.0205	0.0125	0.006	0.0202	0.0193		0.0272	0.010	0.012	0.019
56	58	38	60	63	54	34	30*		54	68	71	91
71	79	75	70	100	75	69	47*		64	60	45	47
69	59	61	83	93	61	50	31*		69	52	44	32
100	93	94	98	94	89	84	70*		78	89	93	83
6.3	5	6-8	2	2	--	5	6		3	2 1/2	3	1.5
1 1/2	2	4	4	2	1	4	5		4	1 3/4	1 1/2	6 1/2
3	2.7	4.2	5.2	3 1/2	1.5	4.2	5 1/2		6	3 1/2	2.2	7.7

PREVIOUS PAGE WAS BLANK, THEREFORE WAS NOT FILMED

(C)

TABLE XXXVI

(Continued)

General		
Winding Parameters		
Cycle	9	Total
Layer	GI	
Winding Angle, deg	20.4	
No. of Covers, dwg 802139	5	245
No. of Covers Revised Design	3	221
Actual No. Covers	4	226
Cam Revolutions	212	
Mandrel Revolutions	276	
X-axis Insert	0	
Follower Setting, in.	1.6	
Cylinder Build-Up Data		
Cylinder Dia, in. Revised Design, Center	29.100	
Cylinder Dia, in., Head	28.995	
Cylinder Dia, in., Center	29.090	
Cylinder Dia, in., Aft	29.050	
Layer Depth (av) in.	0.0510	
Cover Thickness, in.	0.0128	Avg
Miscellaneous Data		
Gears Used A	32	
B	47	
C	91	
D	83	
Winding Speed, Mandrel rpm	4	
Layer Time, hours	2.6	94.0
Total Elapsed Time Complete Cycle, hrs	4.1	132.9
Propellant Type, % depressant	RDS-523(6.0%)	
Propellant Usage, tubes		846
Propellant Usage, wt lbs		1041
Wire Meter Rdg	3192	
Wire Weight, lbs	5.84	226.1
Al % by weight		17.84

Table XXXVII is a tabulation of propellant properties. An attempt was made to calculate the aluminum content of each layer of the reinforced grain. The data are erratic and somewhat inconsistent, because the weight of propellant used per layer was calculated from an average yield of propellant from each polyethylene caulking tube (used for applying propellant).

(C) Two restrictor coats were applied after the grain winding and the second restrictor application resulted in a surface smooth enough for glass filament case winding. The restrictor weight was 89.5 pounds of R-143. The average diameter after restriction was 29.713 inches with a maximum of 29.727 inches. The average restrictor thickness was about 1/2 inch.

(b) GFW Case

(C) This case was wound on March 9 and 10, 1964, using the 40-inch winding machine. Commensurate with other design safety factors for this first Motor A to be fired, the GF case was 300% of Motor A design in the helix wrap and 400% in the circ wrap. The winding configuration was as follows:

	No. Covers	Ends/in./ Cover	Total Ends/in.	Roving
Helix wrap	3	750	2250	4 balls, 12 end
Circ wrap	8	440	3520	4 balls, 20 end

Skirt laminations were made per Motor A design requirements and integrally wound in the first three circ covers. The elapsed total case processing time, excluding cure, was about 48 hours. Operation was continuous and closely followed the predicted processing schedule. Actual winding times were 24.6 hours for the helix and 6.5 hours for the circ wrap.

Winding of the helix layer of the heavyweight case differed from a flightweight case in that the second and third covers were wound at slightly higher helix angles. The purpose of this was to move the second and third layers back from the pole. This was necessary to limit the thickness of the case at the pole. Excessive thickness would interfere with nozzle-attachment drive pin installation. The pattern was adjusted only slightly on the forward pole, and the case was allowed to build up to about 1/4 inch past the flange edge.

TABLE XXXVII

RFG A-1201 PROPELLANT PROPERTIES

Layer	Propellant Formulation	Burning Rate in./sec at psi	Lot Number	Mechanical Properties at 77 F			Number of Tubes
				Elongation, (e_m), %	Tensile (S_m), psi	Modulus, (E), psi	
1-GI	RDS-514 (0.5% depressant	0.269 at 735	L-2-11-M81	17	149	1202	20
	RDS-514 (0.5% depressant)	0.269 at 735	K-12-27-M81	--	--	--	17
	LCA-5281 (6.0%)	0.123 at 715		17	149	1202	3
1-43	RDS-514 (0.5%)	0.269 at 735	K-12-27-M81	17	149	1202	35
1-54	RDS-514 (0.5%)	0.269 at 735	K-12-27-M81	17	149	1202	34
1-66	RDS-514 (0.5%)	0.269 at 735	K-12-27-M81	17	149	1202	21
2-GI	RDS-514 (0.9%)	0.237 at 679	L-2-12-M81	16	174	1442	27
	LCA-5281 (6.0%)	0.123 at 715		--	--	--	2
2-43	RDS-514 (0.9%)	0.237 at 670	L-2-12-M81	16	174	1442	17
2-66	RDS-514 (0.9%)	0.237 at 670	L-2-12-M81	16	174	1442	20
2-66	RDS-514 (0.9%)	0.237 at 670	L-2-12-M81	16	174	1442	27
2-80	RDS-514 (0.9%)	0.237 at 670	L-2-12-M81	16	174	1442	25
3-GI	RDS-514 (1.8%)	0.201 at 600	L-2-12-M82	15	113	902	36
	LCA-5281 (6.0%)	0.123 at 715		--	--	--	2
3-43	RDS-514 (1.8%)	0.201 at 670	L-2-12-M82	16	174	902	25
3-35	RDS-514 (1.8%)	0.201 at 670	L-2-12-M82	16	174	902	25
3-45	RDS-514 (1.8%)	0.201 at 670	L-2-12-M82	16	174	902	34
3-60	RDS-514 (1.8%)	0.201 at 670	L-2-12-M82	16	174	902	32
4-GI	RDS-523 (2.6%)	0.172 at 540	L-2-13-M81	21	102	795	40
	LCA-5281 (6.0%)	0.123 at 715		--	--	--	3
4-30	RDS-523 (2.6%)	0.172 at 540	L-2-13-M81	21	102	795	13
4-40	RDS-523 (2.6%)	0.172 at 540	L-2-13-M81	21	102	795	24
4-50	RDS-523 (2.6%)	0.172 at 540	L-2-13-M81	21	102	795	--
4-65	RDS-523 (2.6%)	0.172 at 540	L-2-13-M81	21	102	795	29
4-80	RDS-523 (2.6%)	0.172 at 540	L-2-13-M81	21	102	795	20
5-GI	RDS-523 (5.5%)	0.140 at 470	L-2-13-M82	16	17	655	35
	LCA-5281 (6.0%)	0.123 at 715		--	--	--	5
5-30	RDS-523 (5.5%)	0.140 at 470	L-2-13-M82	16	17	655	--
5-38	RDS-523 (5.5%)	0.140 at 470	L-2-13-M82	16	17	655	13
5-47	RDS-523 (5.5%)	0.140 at 470	L-2-13-M82	16	17	655	26
5-60	RDS-523 (5.5%)	0.140 at 470	L-2-13-M82	16	17	655	32
6-GI	RDS-523 (6.0%)	0.125 at 400	L-2-14-M81	18	60	539	36
	LCA-5281 (6.0%)	0.123 at 715		--	--	--	8
6-26	RDS-523 (6.0%)	0.126 at 400	L-2-14-M81	18	60	530	27
6-32	RDS-523 (6.0%)	0.126 at 400	L-2-14-M81	18	60	539	20
6-40	RDS-523 (6.0%)	0.126 at 400	L-2-14-M81	18	60	539	29
6-56	RDS-523 (6.0%)	0.126 at 400	L-2-14-M81	18	60	539	36
7-GI	RDS-523 (6.0%)	0.126 at 400	L-2-14-M81	18	60	539	--
	LCA-5281 (6.0%)	0.123 at 715		--	--	--	--
7-32	RDS-523 (6.0%)	0.126 at 400	L-2-14-M81	18	60	529	--
7-46	RDS-523 (6.0%)	0.126 at 400	L-2-14-M81	18	60	529	--
7-67	RDS-523 (6.0%)	0.130 at 400	L-2-14-M82	20	58	491	--
7-80	RDS-523 (6.0%)	0.130 at 400	L-2-14-M82	20	58	491	39
8-GI	RDS-523 (6.0%)	0.130 at 400	L-2-14-M82	20	58	491	36
	LCA-5281 (6.0%)	0.123 at 715		--	--	--	4
8-29	RDS-523 (6.0%)	0.130 at 400	L-2-14-M82	20	58	491	22
8-38	RDS-523 (6.0%)	0.130 at 400	L-2-14-M82	20	58	491	--
9-GI	RDS-523 (6.0%)	0.130 at 400	L-2-14-M82	20	58	491	38
	LCA-5281 (6.0%)	0.123 at 715		--	--	--	2

Dome sections of the finished case are shown in Fig. 117 (Aft) and Fig. 118 (Forward).

Final weights and dimensions for the case are presented below:

(C)

Weights	
Restrictor	89.5 lb
Aft Flange	8.1 lb
Helix Roving	35.5 lb
Circ Roving	36.9 lb
Glass Cloth (Calc)	4.1 lb
Total	76.5 lb
Case Weight at Estimated 29.4% Resin	108.4 lb
Case Weight by Load Cell Readings	106.2 lb
Estimated Thicknesses	
Helix Wrap in Cylinder	0.105 in.
Circ Wrap	0.156 in.
Total	0.261 in.
Average Cylinder Thickness Based on Dia	0.256 in.
Over-all Dimensions	
Inside Tangent Length	48.98 in.
Skirt to Skirt Outside Length	59.20 in.
Diameters	
Forward Skirt	30.410 in.
Cylinder (1)	30.242 in.
(2)	30.215 in.
(3)	30.428 in.
Aft Skirt	30.428 in.

GFW-1412 and GFW-1413 were 29.4% resin by analysis. Weights do not include approximately 8.5 pounds of cord and rubber used in skirt transition filling.

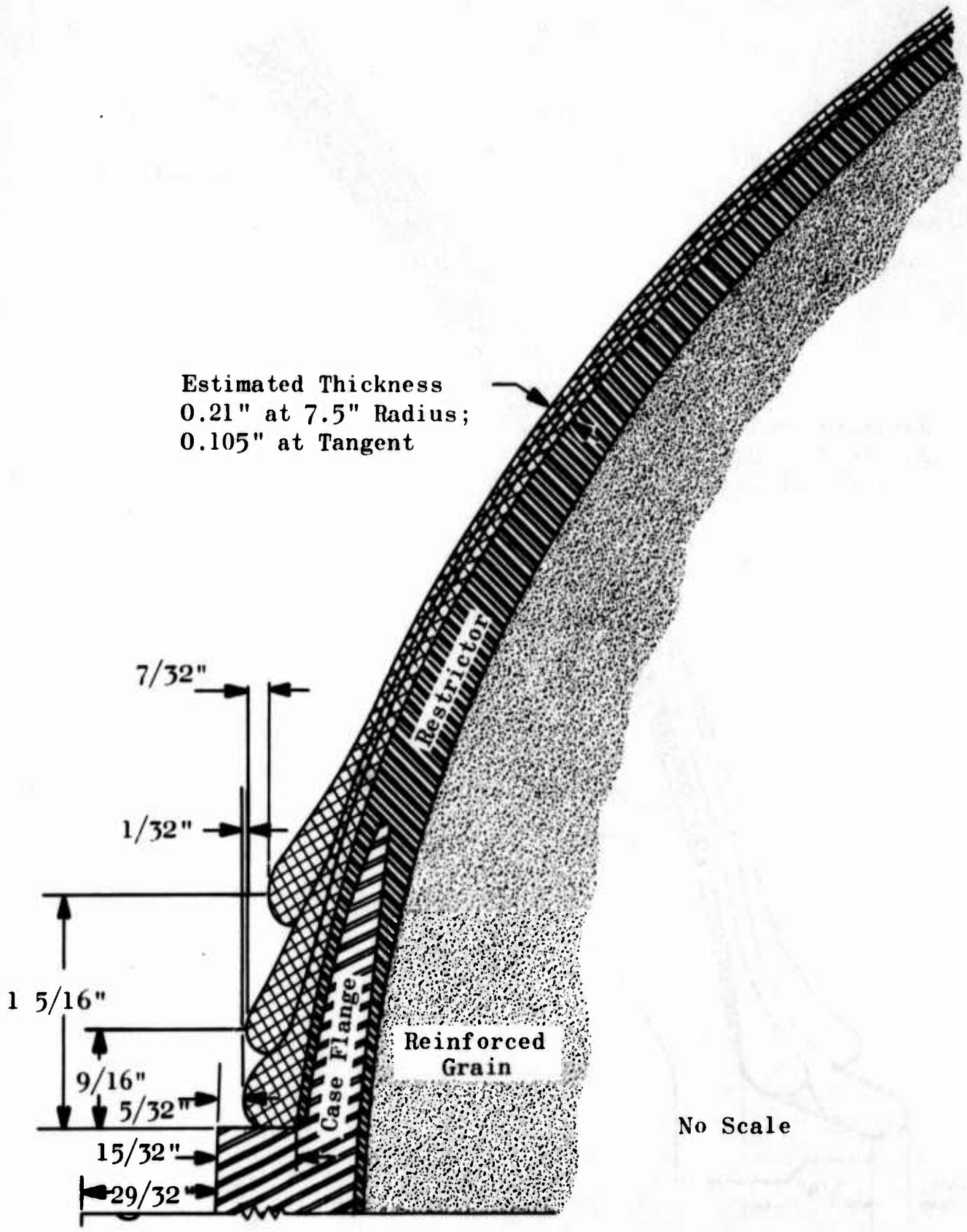


Figure 117 . Motor A-1001 GFW Case Dome Section, Aft End

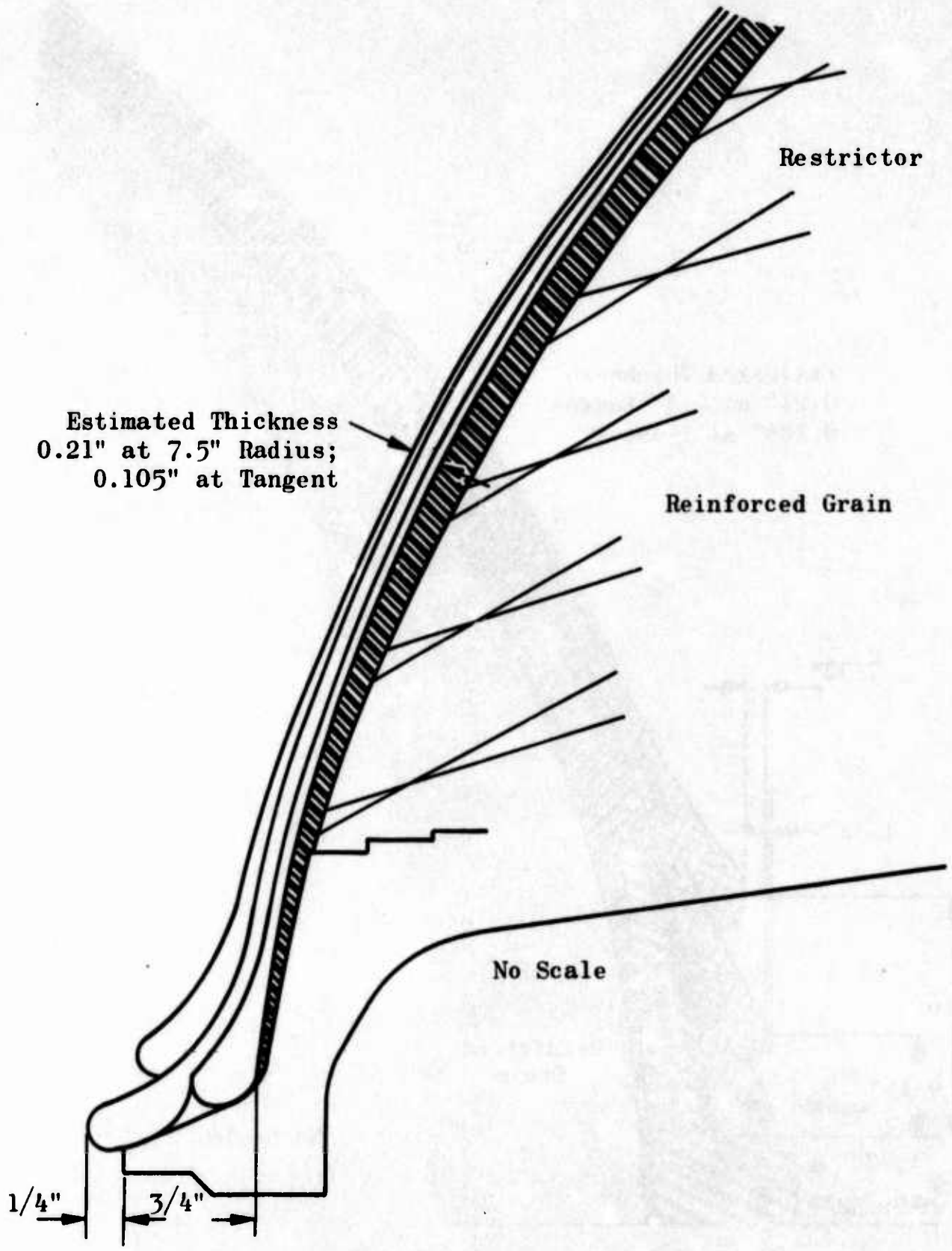


Figure 118 . Motor A-1001 GFW Case Dome Section, Forward End

(4) Postwinding Procedure

Upon completion of glass case cure, the sand mandrel was flushed out with water. Judging from Tenite and phenolic scraps which were found among the sand at a latter date, two discrepancies occurred during washout:

1. A portion of the phenolic ballistic sleeve was broken off, apparently by impact with the spindle or one of the lightening tules.

2. Portions of the Tenite liner came out with the sand. The Tenite coating was thinner than desirable and was also bonded to the epoxy "bulkhead" formed by bonding the two mandrel halves. This bulkhead, or epoxy ring, holds a fair amount of sand and consequently is fairly heavy. When it fell it pulled some of the Tenite with it. A tape liner will be placed over the joint in the future to preclude this from reoccurring. Neither of these discrepancies were noticed until after the drying operation.

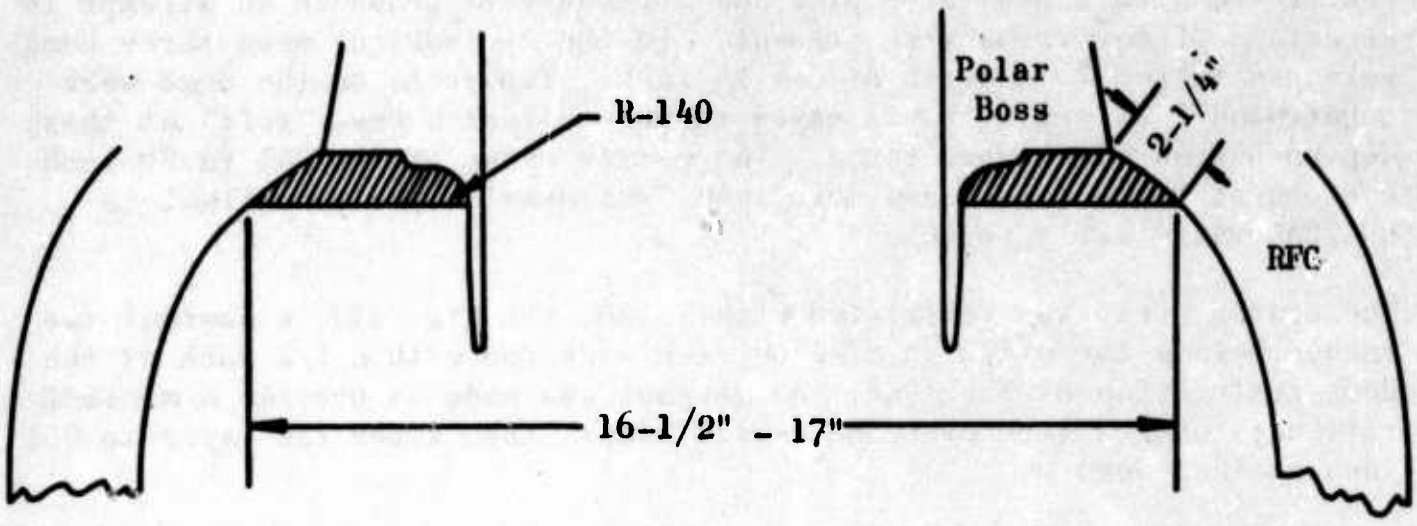
(C) The unit was dried for 12 hours at 170 F, then it was taken from the oven and the tape removed. A leached area (propellant became spongy and parted from the wire) approximately four inches wide (containing many bumps) the full length of the cylindrical section was then apparent, Fig. 119. Additional soft "bulges" were found in both domes. These were scattered. Radiographs were made in an attempt to determine the full extent of the grain damage, but no conclusive results were obtained. The best estimate of damage depth was approximately 1/8 to 1/4 inch.

After consideration of the grain damage it was decided to restrict a limited area of the grain and static test the unit without a core grain. In the Motor A design, the RFG web is reduced near the end bosses, and the total web is maintained by increasing the core thickness in this area. To protect the thin area for firing without a core grain, the ends were restricted with R-140, see Fig. 120, in a band about 2-1/2 inches wide around each port. This was done one end at a time. After the forward dome was cured, the center cylindrical section was noticeably worse. The "bulges" then were 3/4 to 1 inch high, and nearly formed a continuous irregular strip the full length of the cylindrical section. The aft port was then restricted and cured. After this additional temperature cycling, the center strip was slightly worsened.

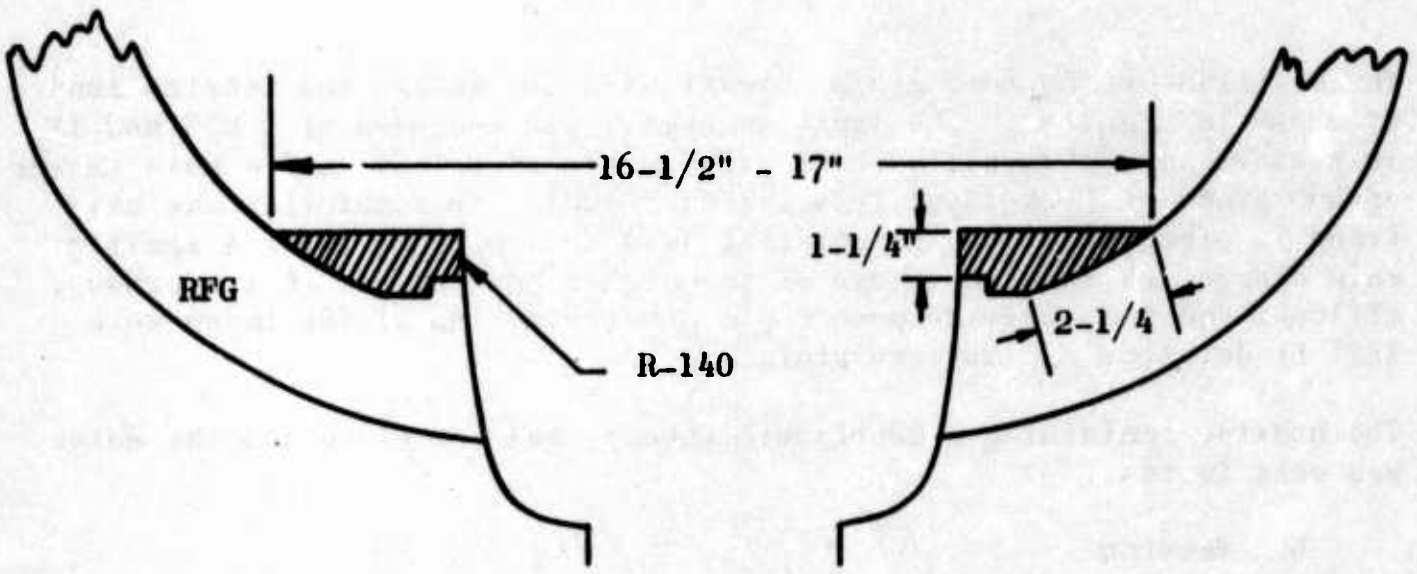


CN12021-10

Figure 119. "Bumps" on RFG of A-1001



AFT DOME



FORWARD DOME

Figure 120. Dome Restrictions of RFG, A-1001

Several of the raised bumps in the center strip and at the aft dome were penetrated with a dentist's pick and a piano-wire probe in an attempt to ascertain if any voids were present. In the cylindrical area three bumps were penetrated to a depth of 2-1/16 inch. Two spots on the dome were penetrated 1/2 inch. In all cases the propellant seemed "soft" at these depths but no voids were found. The wetted areas of RG-7205 (a 20-inch hydroburst grain) also show this same "softness". The propellant in RG-7205 was visibly porous.

The center strip was restricted with R-140, see Fig. 121, a nominal two inches beyond the affected area on each side and within 1/2 inch of the dome restriction at each end. An attempt was made to provide a minimum thickness of 1/2 inch over the raised bumps, then taper the layer to 0.1 inch at the edge.

After the final restrictor cure, the unit was resubmitted to X-ray. No additional information was obtained as to the defect depth. No voids were found and the lower density area could not be seen on the tangential shots through the thick web.

(5) Final Assembly

(C) The deletion of the core grain necessitated the design and fabrication of a special igniter. The ignition system was composed of a M55 Mod IX initiator, an intermediate charge of 3 grams of B/KNO_3, and a main charge of 400 grams of Rocketdyne formulation P-120A. This material was utilized in place of P-73, the material used in the basic Motor A igniter main charge, to take advantage of the higher gas content in its exhaust effluent and thus provide more rapid pressurization of the large void left by deletion of the core grain.

The nozzle, containing a monolithic throat, was installed and the motor was sent to test.

b. Testing

The motor was static fired 3 April 1964. Because of the severe damage to the grain and the anticipation of a malfunction, the motor was tested vertically on a rigid stand (see Fig. 122). The forward skirt was fitted to the lower half of the hydrotest fixture. Pressure, limited strain, and thermocouple measurements were taken, but no thrust measurements. Motion pictures were made. At approximately 670 milliseconds the motor

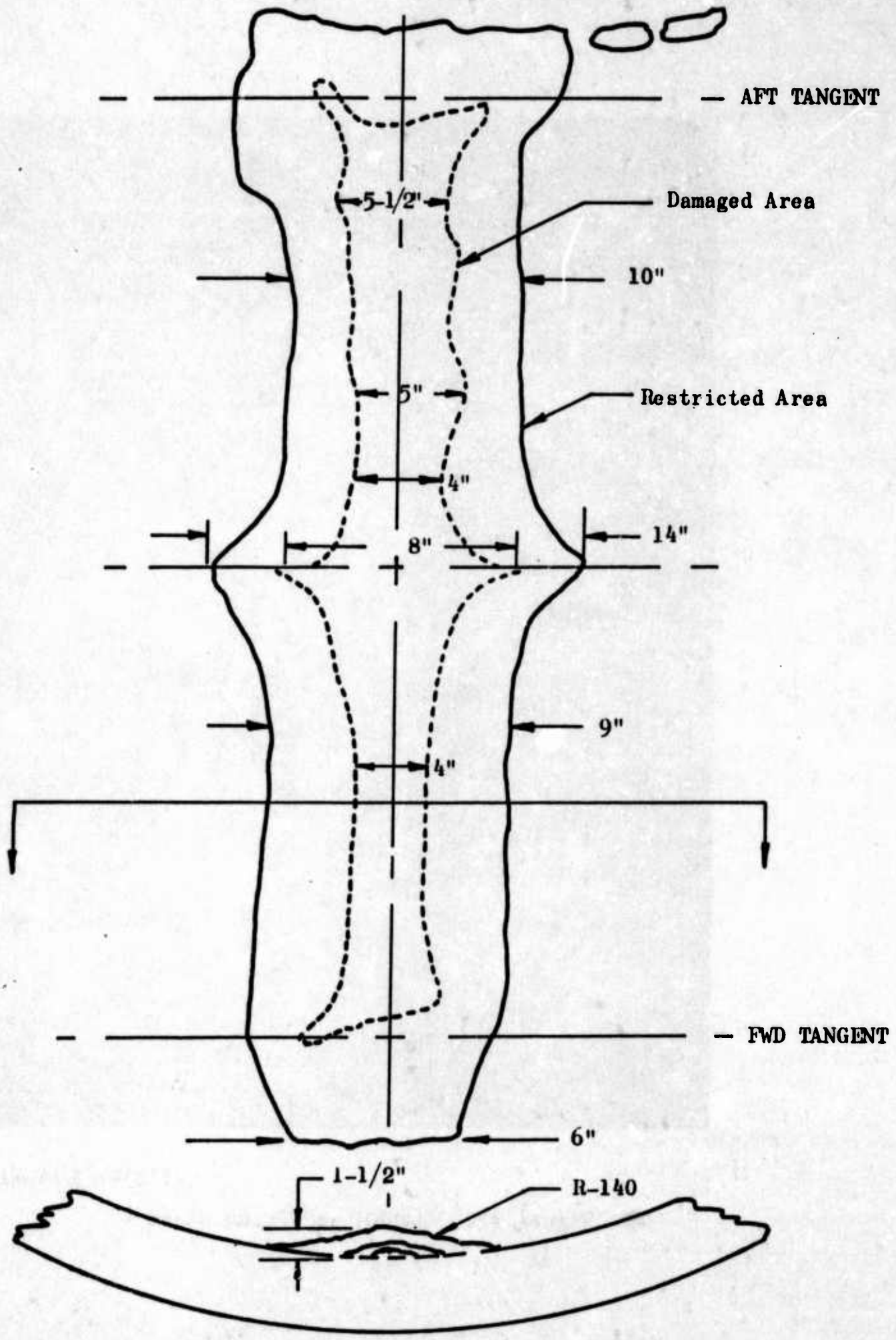
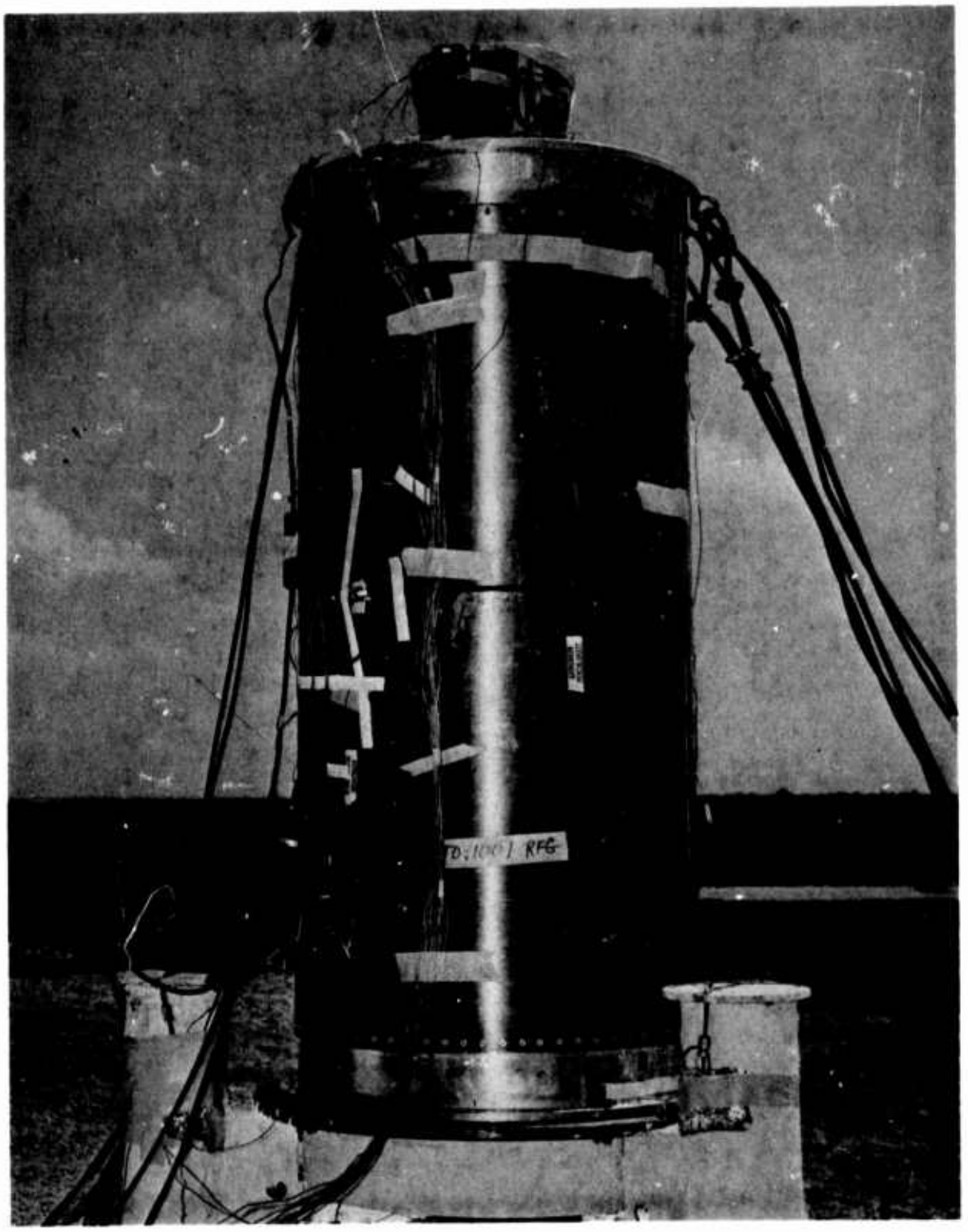


Figure 121. Cylindrical Restriction of A-1001



2YA23-4/3/64-M1A

Figure 122. A-1001 in Firing Stand

ruptured and burned a great deal of propellant and inert material in a widely scattered area. The nozzle, expansion cone, aft polar boss with load rings, parts of the forward polar boss with eight of nine load rings, approximately 130 pounds of unburned propellant, and miscellaneous parts of restrictor and GFW case have been found and examined.

(1) Analysis

Performance predictions, based on the condition of this unit after processing repairs, were made and are presented in Table XXXVIII and Fig. 123. A replot of pressure versus time for Motor A-1001 is shown in Fig.124 .

(C) The first indication of pressure occurred at 140 milliseconds, although pressure did not increase significantly until approximately 300 miliseconds. The ignition transient is similar to that which was expected, with the maximum rate of rise occurring at approximately 370 psi. This value of pressure at inflection of the pressure-time curve appeared normal, considering the initial pressure of 500 psi which had been estimated.

(C) There was an approximate 300-millisecond time span from initiation to the first indication of pressure (see Fig. 124). Between 300 miliseconds and 600 milliseconds the pressure increased in a fairly smooth manner to 760 psig, with the exception of a ringing oscillation of the pressure transducer from 508 milliseconds to 600 milliseconds. Pressure increased from 760 psig at 610 milliseconds to 790 psig at 628 milliseconds. At this time, the pressure began to increase very rapidly to 1835 psig at 662 milliseconds and then decreased to 1280 psig at 665 milliseconds. The pressure record was lost at 666 milliseconds after increasing again to 1375 psig. Only eight strain gages were used for this test because of the heavyweight case and the low strain readings which were expected from a successful firing. The maximum recorded pressure (1835 psig) was 2.3 times the expected maximum pressure (800 psig), and strains in the GFW case reached 22,000 microinches/inch. Based on analysis of the pressure, strain, and motion picture data the following sequence is hypothesized as the most likely to have occurred.

At approximately 533 milliseconds, a large piece or pieces of material, presumably R-140 restrictor, came out of the nozzle. This was followed by another small piece 24 milliseconds later. After the restrictor was torn out of the defective area the spongy RFG started to burn, causing pressure to increase, and concurrently gas pressure leaked to the liner of the case. Strain gages show a slight pressure leak to the liner at

TABLE XXXVIII

ESTIMATED PERFORMANCE RFG MOTOR A-1001

Average Pressure, psia	490
Action Time, sec	19.1
Average Thrust, lb	14,500
Total Impulse, lb-sec	277,000
RFG Propellant Weight, lb	1266
I_{sp}^{o} at 1000 psia, lb-sec/lb	237.0
Del I_{sp} at Motor Conditions, lb-sec/lb	218.5

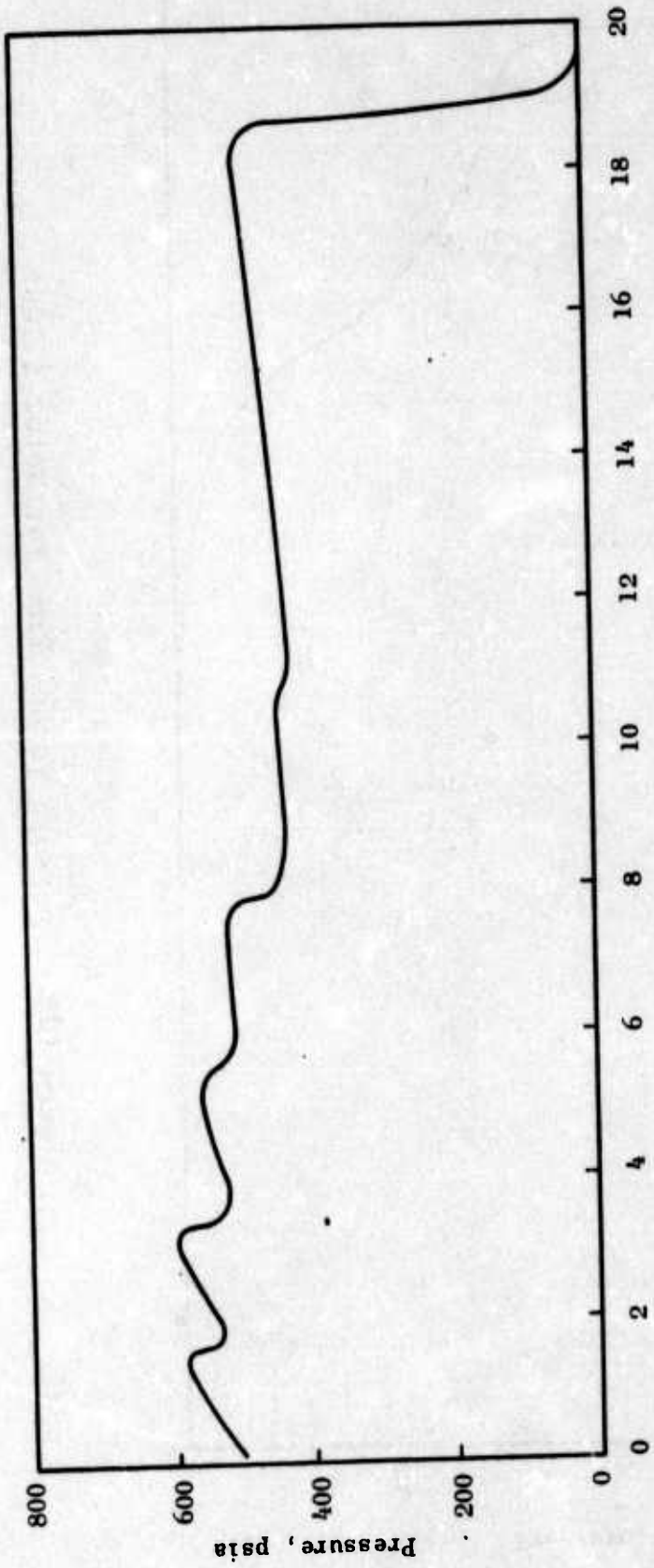


Figure 123. Estimated Pressure-Time, A-1001

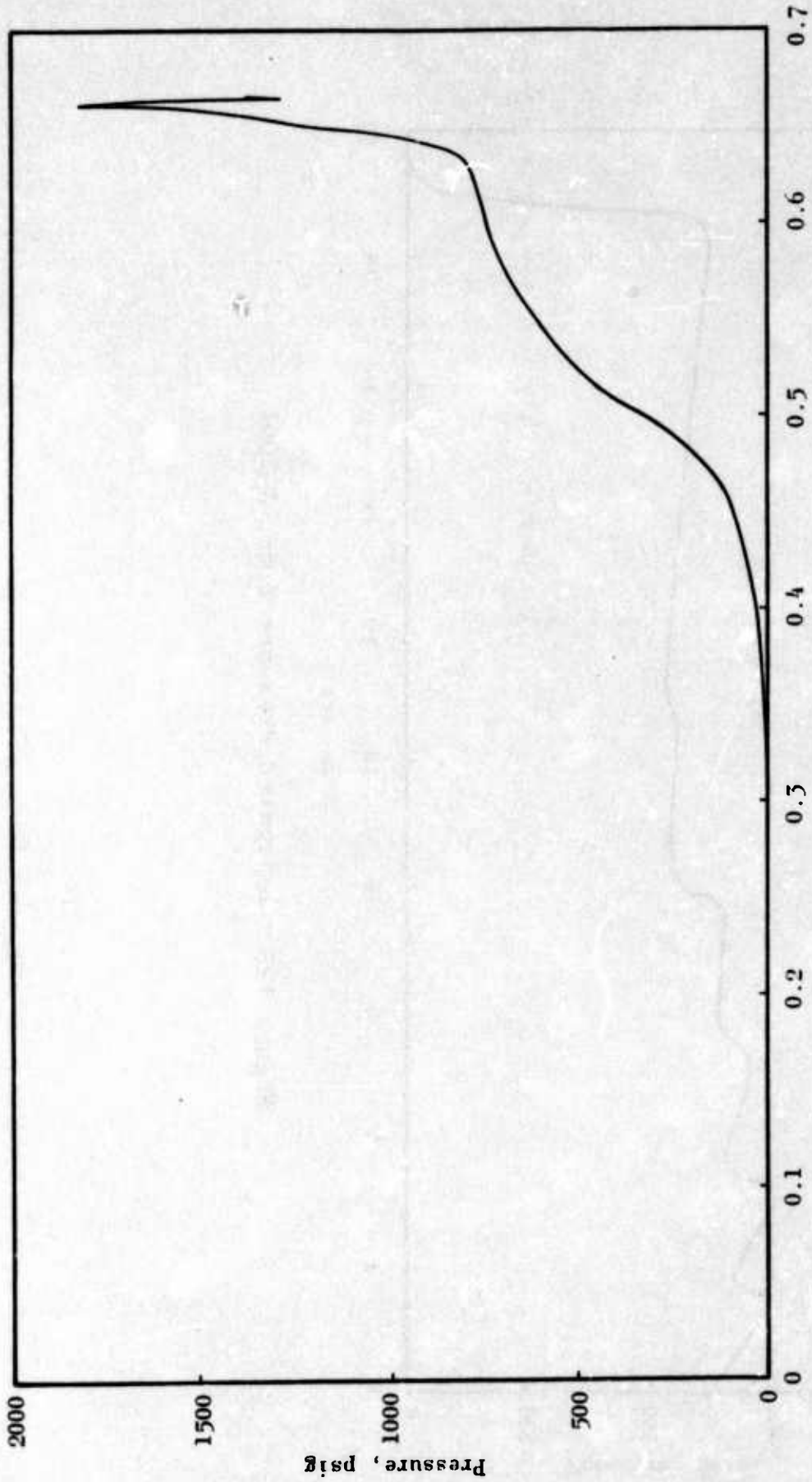


Figure 124. Pressure versus Time for Motor A-1001

(C) about 590 milliseconds, when the pressure was 730 psig. Between 730 psig, pressure begins to increase drastically and is probably caused by interlaminar burning of some form. All strain gages indicate another sudden transfer of load to the case at 1140 psig and 649 milliseconds. One more piece of material went through the nozzle at 651 milliseconds. Pressure continued to increase to 1835 psig at 662 milliseconds. The lower (forward) polar boss can be seen moving downward in the 1000 frame per second motion picture at this time. Flame in the area of the forward polar boss is visible in the next two frames and a hole in the case near the forward skirt-cylinder junction is visible in the third frame. Complete failure occurre one frame later, at approximately 668 milliseconds. This sequence of eve ts may be more clearly followed on the pressure and strain versus time curves presented in Fig. . Only two strain gages, S-5 and S-6 are replotted. These were longitudinal and hoop gages respectively in the cylindrical portion of the motor. These two gages do not show the entire sequence, but are fairly representative.

(2) Conclusions and Recommendations

The following conclusions are based on the fabrication history and analysis of test data.

(C) Failure of motor on firing was due to damage incurred during fabrication and is not indicative of fundamental deficiency in Motor A design.

(C) Strains in case were as expected until pressure increased in an extremely rapid manner.

The reinforced grain performed satisfactorily until the chamber pressure exceeded the design value for this component, therefore no design change is recommended.

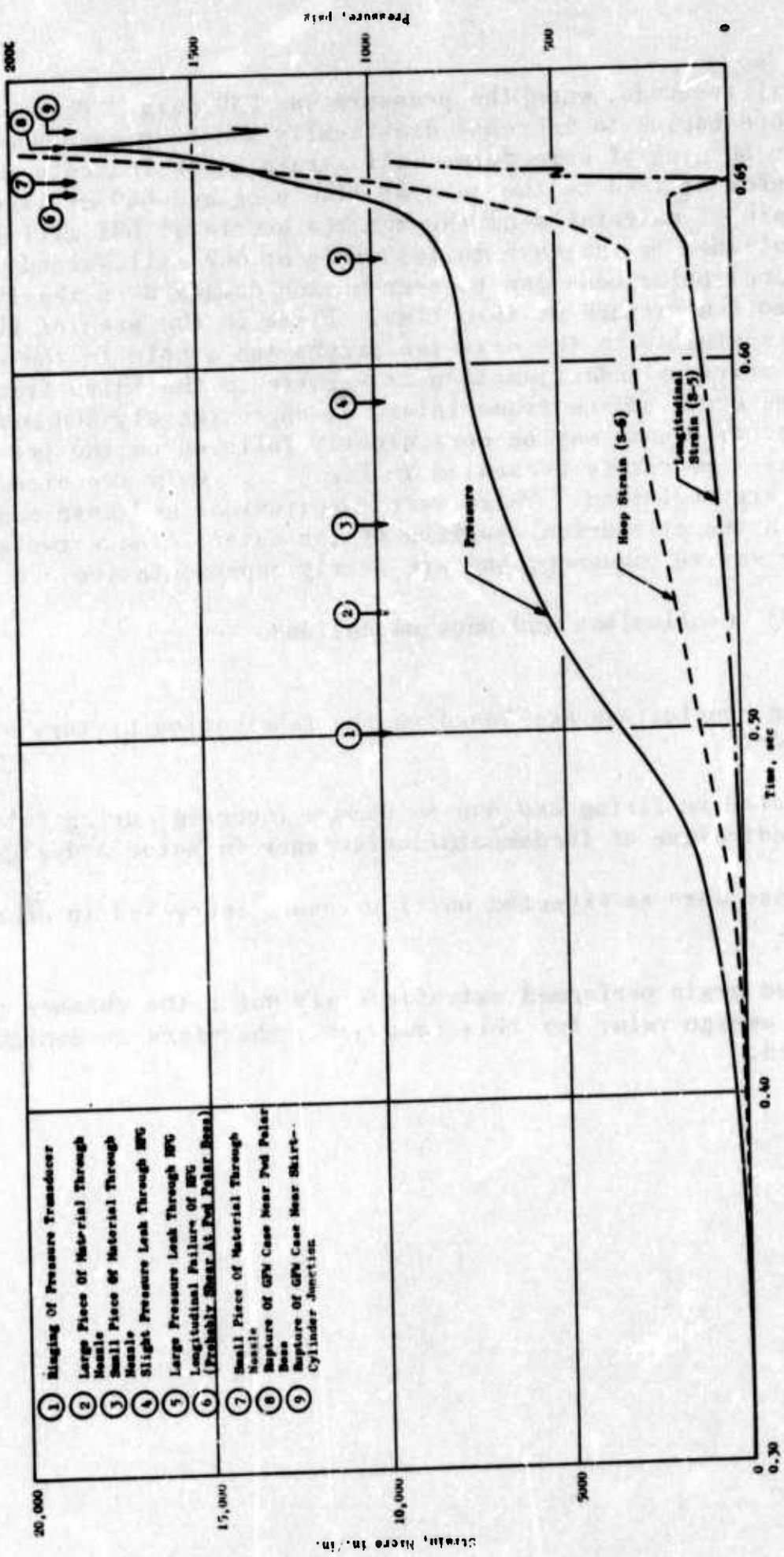


Figure 125. Pressure and Strain vs Time for Motor A-1001

3. DEVELOPMENT MOTOR A-1002

(C) Test of Motor A-1002 was the first static firing of a complete Motor A, which included core grain, reinforced grain, and glass filament wound case. Although this motor was testweight it had a mass fraction of 0.911, which shows that it was much more advanced than a conventional heavyweight motor.

(C) Because of the problems associated with Motor A-1001, only minor design changes were effected for Motor A-1002. The RFG and insulation designs were identical to Motor A-1001, except for the use of titanium load rings, rather than steel. The GFW case thickness was less than that of Motor A-1001, reduced to a scheduled 0.15 inch, with a pressure capability of 1500 psi.

On Motor A-1001, excessive RFG layer buildup was noticed in the polar boss areas and an evaluation concerning this layer buildup was conducted. On motor A-1002, the "steps" on the polar boss on which the RFG layers are wrapped were repositioned to alleviate this problem.

The nozzle for this motor contained a pyrolytic throat, rather than the monolytic throat used in A-1001 and all subsequent A Motors.

The ballistic design was identical to that originally specified for Motor A-1001.

(C) Propellant which yielded a motor burning rate of 0.140 in. per sec at a chamber pressure of 400 psia was not then available for RFG fabrication, consequently the propellant employed yields a burning rate of 0.145 in. per sec and a final RFG burnout pressure of 520 psia (rather than the design of 400 psia).

(C) The restrictor thickness of 0.3 inch included in the cylindrical section provided a margin to accommodate up to 5 seconds premature burnthrough. Restrictor included in the domes offered a protection of 7 to 10 seconds.

The thrust-pressure vs time is shown in Fig. 126 and the resulting performance, estimated from actual strand burning rates for Motor A-1002, is summarized in Table XXXIX. Table XL shows estimated weights and resulting mass fraction of both Motor A-1002 and the ultimate flightweight motor.

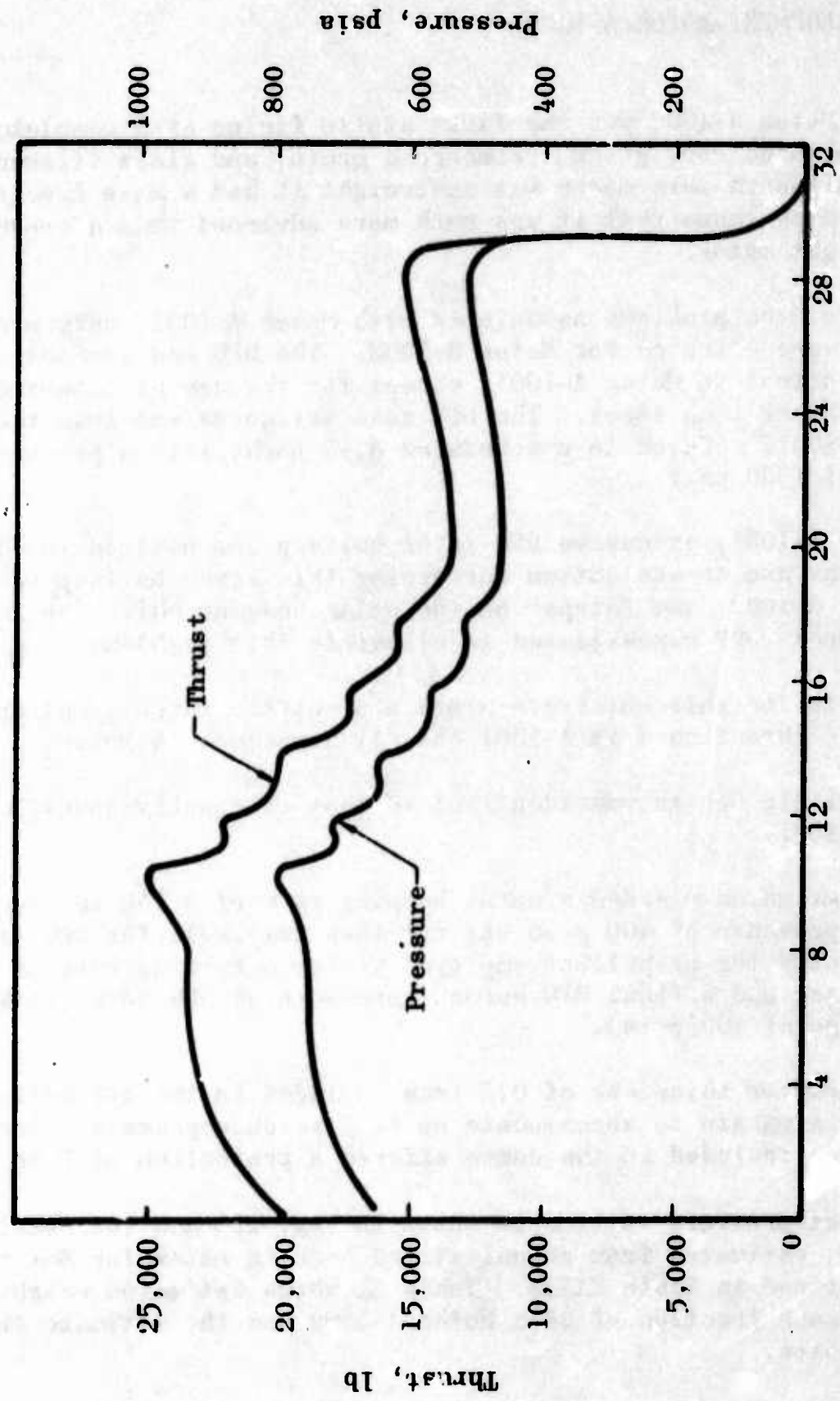


Figure 126. Estimated Thrust and Pressure vs Time, A-1002

TABLE XXXIX

ESTIMATED PERFORMANCE SUMMARY, MOTOR A-1002

Total Impulse, lb-sec	547,800
Average Thrust, lb	18,170
Action Time, sec	30.1
Average Pressure, psia	600
Core Propellant Weight, lb	1135
RFG Propellant Weight, lb	1249
Total Propellant Weight, lb	2384
Isp @ 1000 psia, lb-sec/lb	
Core Propellant	250
RFG Propellant	237.8
Composite Motor	243.6
Delivered Isp @ Motor Conditions, lb-sec/lb	229.8
Inert Weight, lb	223.8
Mass Fraction	0.914

TABLE XL

ESTIMATED WEIGHT AND MASS FRACTION FOR A-1002
AND FLIGHTWEIGHT DESIGN

	Motor A-1002	Flightweight Design
Nozzle Assembly	30.01	26.77
Case	73.00	34.00
Liner	82.06	12.00
Igniter	3.08	3.08
Fwd Boss	10.52	10.52
Aft Boss	12.70	12.70
Load Rings	6.94	6.94
Drive Pins	0.56	0.56
O-rings	0.10	0.10
Flange	5.14	1.71
Total Inerts	224.11	108.38
Core Propellant	1135	1135
RFG Propellant	1249	1349
Total Propellant	2384	2484
Total Motor Weight	2608.11	2592.38
Mass Fraction	0.914	0.958

a. Fabrication

(1) Equipment

The grain was wound on the 36-inch machine, using the spreader blade, manual propellant application, and the electric, microtension wire tensioning system. Because of the water damage to Motor A-1001, special care was taken in the preparation of the mandrel for this motor. The sand mandrel was coated with seven applications of tenite. A spray coat of RTV-60 approximately 0.006-inch thick was applied and allowed to cure. The aft polar boss insulation tube was coated on the ID and OD with polyken tape. The bosses were assembled with a layer of uncured R-143 between the first load ring and the mandrel. The mandrel was taped with polyken tape immediately prior to winding. The tape was overlapped 1/2 its width on the cylindrical section and 2/3 on the domes. The average liner thickness (tenite, RTV, and tape) was 0.037 inch.

(2) Materials

The standard wire was used--5% minimum elongation, 50,000 psi minimum tensile, 7 1/2-mil diameter, 5056 aluminum heat treated.

The propellant burning rates were the same as those used on RG-1201 (A-1001). See Table XLI for propellant properties.

The bosses were prepared the same as those for A-1001. Prior to mandrel assembly it was found that the nozzle would not mate with the aft boss. The aft boss was remachined and processed as follows:

1. Cleaned with MEK
2. Air dried for 30 minutes
3. Dried for 2 hours at 350 F
4. Freshly-machined area coated with Epon 926
5. Cured for 2 hours at 190 F

(3) Processing

(a) Grain Winding and Restriction

Grain winding was completed on 24 April, 1964. It required 152.8 hours or 6-1/2 days winding time, compared to 7-1/2 and 5-1/2 days required for Motors A-1006 and A-1001 respectively. Grain winding was hampered

CONFIDENTIAL

TABLE XLI

PROPELLANT PROPERTIES, MOTOR A-1002

Layer Number	Pressure, psia	Propellant		Liquid Strand B. R. Target	Liquid Strand B. R. Actual
		Type	Mix Number		
1--4 (1st cycle)	735	RDS-514 (0.5%)	L-4-9-M-81	0.260	0.258
5--9 (2nd cycle)	670	RDS-514 (0.9%)	L-4-8-M-82	0.230	0.232
10--13 (3rd cycle)	600	RDS-514 (1.8%)	L-4-7-M-83	0.196	0.198
14--19 (4th cycle)	540	RDS-524 (2.6%)	L-4-8-M-81	0.170	0.167
20--24 (5th cycle)	470	RDS-523 (5.5%)	L-4-7-M-82	0.145	0.140
25--29 (6th cycle)	400	RDS-523 (6.0%)	L-4-7-M-81	0.135	0.130
30--34 (7th cycle)	400	RDS-523 (6.0%)	L-4-6-M-82	0.135	0.131
35 (8th cycle)	400	RDS-523 (6.0%)	L-4-6-M-81	0.135	0.130

Propellant	RG-1202			RG-1201 Corresponding Mixes		
	e_m, %	S_m, psi	E, psi	e_m, %	S_m, psi	E, psi
L-4-9-M-81	18	172	1384	17	149	1202
L-4-8-M-82	16	154	1255	16	174	1442
L-4-7-M-83	15	137	1370	15	113	902
L-4-8-M-81	23	143	944	21	102	795
L-4-7-M-82	19(24)	81(117)	744(772)	16	71	655
L-4-7-M-81	24	117	761	18	60	539
L-4-6-M-82	15(25)	54(119)	501(793)	20	58	491
L-4-6-M-81	21	123	835	18	64	537

CONFIDENTIAL

(C) by wire breakage caused by poor spooling and excessive friction through the guides (rod tips). Some excessive buildup occurred during the fifth and sixth cycles, thus nine covers had to be omitted. A total of 13 covers were omitted during winding of the entire grain. The grain aluminum weight percentage was 17%, 3% less than the target of 20%. The low aluminum content is attributed to the abnormally viscous propellant in the outer layers of the grain. No obvious reason was discovered for the viscous, hard-to-apply propellant. Mixing procedures were the same as for the propellant used in A-1001. Cartridge loading was also handled in the same manner, in that filled propellant tubes were placed in crushed dry ice immediately. Similarity continues in that material lots used were the same as those used in one of the best mixes utilized in A-1001. The average cover thickness obtained in the grain was 0.01649 inch. Table XLII contains the detailed winding data.

The load rings for this grain were titanium, instead of the steel load rings used on Motor A-1001. The load rings were coated with Bondmaster primer and cured before winding, then were coated with R-143 before incorporation into the grain. Some of the eighth intermediate layers were omitted to allow an extra-thick restrictor layer, as was done on RG-1201 for Motor A-1001.

The RFG was cured for 120 hours at 170 F. Previous grains were cured for 48 hours at this point. Based on theoretical heat transfer calculations, about 50 hours would be required for the first geodesic layer to heat up to 160 F. Also, additional time was desired to obtain a more complete state of cure, particularly of the first geodesic layer, which is susceptible to washout and handling damage.

(C) Restriction was normal. A wipe coat, fill coat, and finish coat of R-143 were applied to obtain the finished contour. Thicknesses at 4-inch intervals along the cylindrical section were 0.318 (aft tangent), 0.293, 0.272, 0.232, 0.268, 0.209, 0.220, 0.231, 0.246, 0.245, 0.245, and 0.303 (forward tangent).

Restrictor cure times were 16 hours for the wipe coat, 24 hours for the fill coat, and 48 hours for the final coat. A 170 F cure temperature was used throughout.

(b) GFW Case

The GFW case was fabricated on May 7 and 8, 1964. Despite the many mechanical difficulties during the winding it was the most uniform GFW case wound until that time. Some of the problems encountered included extreme difficulty in obtaining sufficiently smooth machine operation, failure of the Y-valve stylus two times, and a freeze-up of the resin bath due to a malfunctioning VTW system.

TABLE XLII

RFG A-1201 WINDING PARAMETERS AND CYLIN

		1				2					C
	Mandrel										He
Winding Parameters											
Layer		GI	43	54	66	GI	43	54	66	80	G
Winding Angle, deg		31.2	43.7	56.6	71.7	30.1	42.8	58.1	69.9	80.0	
No. of Covers, dwg 802139		7	8	9	5	7	4	5	9	7	
No. of Covers, Revised Design		7	8	9	5	7	4	5	9	5	
Actual No. Covers		7	7	8	6	7	4	5	8	8	
Cam Revolutions		252	217	192	78	266	128	115	120	56	
Mandrel Revolutions		468	460	535	372	424	268	335	567	--(2)	
X-axis Insert		0	0, +2	+1	0, +1, +2	0	0, +3	0, +1	-2, +2	0, +1, +2	
Follower Setting, in.		1.32	1.30	1.25	1.0	0.80	0.75	0.60	1.8 0.75	1.0	
Cylinder Build-Up Data											
Cylinder Dia, in. Revised Design, center	22.075	22.318	22.558	22.828	22.978	23.202	23.322	23.472	23.742	23.892	
Cylinder Dia, in., Head	22.054	22.300	22.532	22.750	22.934	23.125	23.264	23.400	23.610	23.815	
Cylinder Dia, in., Center	22.075	22.338	22.560	22.792	22.962	23.153	23.300	23.475	23.650	23.855	
Cylinder Dia, in., Aft	22.047	22.310	22.525	22.763	22.936	23.127	23.262	23.410	23.640	23.850	
Layer Depth (av) in.		0.1285	0.1115	0.1146	0.0880	0.0955	0.0700	0.0765	0.1025	0.1035	
Cover Thickness, in.		0.0184	0.0159	0.0144	0.0147	0.0137	0.0175	0.0153	0.0128	0.0129	
Miscellaneous Data											
Gears Used A		56	55	52	33	55	51	43(1)	31	33(1)	
B		79	84	96	70	82	82	50(1)	76	64(1)	
C		78	66	65	44	76	74	49(1)	50	39(1)	
D		95	92	100	88	83	96	59(1)	81	70(1)	
Winding Speed, Mandrel rpm		4.5	4.5	4.5	5.0	3.5	5	4	5	5	
Layer Time, hours		3.1	2.0	3.0	1.4	3.7	1.5	2.0	3.0	2.0	
Total Elapsed Time Complete Cycle, hrs		4.3	3.0	3.5	2.1	6.1	2.6	4.1	4.3	2.9	
Propellant Type, % Depressant		RDS-514 (0.5%)	RDS-514 (0.5%)	RDS-514 (0.5%)	RDS-514 (0.5%)	RDS-514 (0.9%)	RDS-514 (0.9%)	RDS-514 (0.9%)	RDS-514 (0.9%)	RDS-514 (0.9%)	RD
Propellant Usage, tubes		20	35	34	20	29	17	20	27	25	
Propellant Usage, wt, lbs		17.28	31.12	30.23	17.78	25.78	15.11	17.78	24.00	22.23	
Wire Meter Reading		3487	3354	3613.5	2313	3765	1979.5	2243	3292	2409.5	40
Wire Weight, lbs		6.38(3)	6.13	6.61	4.23	6.88	3.62	4.10	6.02	4.40	
Al % by weight		27.03	16.46	17.94	19.67	21.07	19.33	18.73	20.05	16.52	
Wire Data											
Wire Diameter and Elongation, 0.075 in., 5%											
Number of Wires in Warp, 36											
Wire Spacing, in. 0.0436											
Warp Width, in. 1.620											
Wire Tension, gms 400 ±25 gm											

(1) Indirect Gear Train

(2) Data Was Not Recorded
Not Wound, 9th GI Was Next And Last Layer

(3) Factor Was 1.828×10^{-3} For 36 Wire Warp

(4) Three Layers Depth, 7-31, 7-46, And 7-67

NOTE: Used LCA-5281 On The Domes Adjacent To Polar Bosses. Follower Setting Was The Distance Between The Wire Distributing Head And The Grain At The Start Of Each Layer To Be Wound.

Tube Average Yield Of Propellant Was 0.889 lbs.

TABLE XLII

PARAMETERS AND CYLINDRICAL BUILDUP

Cycle												
			3				4					
Helical												
	66	80	GI	35	45	60	GI	30	40	50	65	80
1	69.9	80.0	28.6	38.5	48.4	66.0	26.5	34.9	45.8	58.3	73.3	80.0
	9	7	7	5	8	9	7	5	5	6	7	9
	9	5	7	6	8	10	7	4	4	6	7	4
	8	8	7	6	8	10	7	4	4	6	7	6
	120	56	280	216	248	190	301	156	136	150	91	52
	567	--(2)	448	340	552	565	448	156	388	402	455	356
+1	-2, +2	0, +1, +2	0	-1, +1	-1, +1	-2, +1	0	-2, -1	-1, +1	-1, +1	-1, +1	+1, +2
60	1.8 0.75	1.0	1.14	1.0	1.25	0.9 0.7	1.1	1.3 1.6	1.2	0.9 1.2	0.5 0.9	0.3 0.4
472	23.742	23.892	24.116	24.296	24.536	24.836	25.060	25.180	25.300	25.480	25.690	25.810
400	23.610	23.815	24.030	24.230	24.469	24.820	25.000	25.085	25.220	25.390	25.578	25.768
475	23.650	23.855	24.080	24.279	24.532	24.840	25.050	25.145	25.285	25.436	25.635	25.830
410	25.640	23.850	24.065	24.255	24.500	24.832	25.015	25.120	25.230	25.412	25.608	25.792
0765	0.1025	0.1035	0.1092	0.0985	0.1225	0.1155	0.0955	0.0470	0.0645	0.0840	0.0970	0.0950
0153	0.0128	0.0129	0.0156	0.0164	0.0153	0.0116	0.0136	0.0118	0.0161	0.0140	0.0139	0.0158
1)	31	33(1)	58	52	57(1)	31	59	50	52	52	34	30(1)
1)	76	64(1)	76	81	40(1)	80	68	66	72	88	88	63(1)
1)	50	39(1)	74	68	39(1)	71	61	64	58	60	50	43(1)
1)	81	70(1)	88	82	61(1)	97	80	85	85	95	98	69(1)
	5	5	3	4.5	4	3.7	3.7	4	4.8	5.5	6	6
0	3.0	2.0	2.9	2.3	3.0	3.8	3.9	1.8	1.7	2.0	1.4	2.2
1	4.3	2.9	4.9	3.1	4.4	4.4	4.9	2.4	2.9	2.8	2.0	2.7
14 9%)	RDS-514 (0.9%)	RDS-514 (0.9%)	RDS-514 (1.8%)	RDS-514 (1.8%)	RDS-514 (1.8%)	RDS-514 (1.8%)	RDS-523 (2.6%)	RDS-523 (2.6%)	RDS-523 (2.6%)	RDS-523 (2.6%)	RDS-523 (2.6%)	RDS-523 (2.6%)
	27	25	38	25	34	32	43	13	24	--(2)	29	20
78	24.00	22.23	33.78	22.23	30.23	28.45	38.23	11.56	21.36	--(2)	25.78	17.78
	3292	2409.5	4078.5	3291	4255	4603	4297	2363	2240.5	3034	3054.5	2451
10	6.02	4.40	7.46	6.02	7.78	8.41	7.85	4.31	4.10	5.55	5.58	4.48
73	20.05	16.52	18.09	21.31	20.47	22.81	17.04	27.16	16.10	--(2)	17.79	20.12

olar Bosses.
n The Wire
tart Of Each

89 lbs.

2

TABLE XLII
(Continued)

	5					6				
Winding Parameters										
Layer	GI	30	38	47	60	GI	26	32	40	56
Winding Angle, deg	25.0	32.4	43.7	55.1	66.0	23.7	29.9	40.3	49.3	63.1
No. of Covers, dwg 802139	7	6	7	5	6	6	3	4	4	10
No. of Covers Revised Design	7	6	6	5	6	6	3	4	5	10
Actual No. Covers	7	6	6	6	6	6	3	4	5	9
Cam Revolutions	315	252	216	145	120	282	135	160	170	207
Mandrel Revolutions	455	408	438	360	414	402	210	288	360	640
X-axis Insert	0	+1, +2	-1, 0	-2, 0	-2, -1	0	-1	-2, -1	-2, -1	-2,
Follower Setting, in.	1.15	0.78	1.0	1.27	3.25	1.25	1.5	1.4	1.5	0.5 0.7
Cylinder Build-Up Data										
Cylinder Dia, in. Revised Design, center	26.034	26.226	26.418	26.578	26.770	26.962	27.058	27.182	27.342	27.6
Cylinder Dia, in., Head	25.992	26.155	26.335	26.491	26.700	26.910	27.025	27.143	27.325	27.5
Cylinder Dia, in., Center	26.032	26.245	26.390	26.580	26.755	26.990	27.106	27.232	27.410	27.6
Cylinder Dia, in., Aft	25.997	26.215	26.355	26.521	26.732	26.950	27.048	27.175	27.365	27.6
Layer Depth (av) in.	0.1050	0.0990	0.0775	0.0855	0.0990	0.1105	0.0550	0.0615	0.0920	0.1
Cover Thickness, in.	0.0150	0.0165	0.0129	0.0143	0.0165	0.0184	0.0183	0.0154	0.0184	0.0
Miscellaneous Data										
Gears Used A	56	52	57	51	41	64	50	56	58	38
B	79	59	81	93	96	77	57	71	79	75
C	78	69	68	71	57	79	60	69	59	61
D	80	99	97	98	83	94	82	100	93	94
Winding Speed, Mandrel rpm	3	4	4.5	4.5	6	3	3	4	5	5
Layer Time, hours	4.2	3.9	2.2	2.1	2.8	2.8	1.5	2.0	2.0	3.0
Total Elapsed Time Complete Cycle, hrs	5.7	4.5	2.5	5.5	3.7	3.2	2.5	2.7	3.4	3.3
Propellant Type, % depressant	RDS-523 (5.5%)	RDS-523 (5.5%)	RDS-523 (5.5%)	RDS-523 (5.5%)	RDS-523 (5.5%)	RDS-523 (6.0%)	RDS-523 (6.0%)	RDS-523 (6.0%)	RDS-523 (6.0%)	RDS-52 (6.0
Propellant Usage, tubes	40	—(2)	20	26	32	39	27	20	20	36
Propellant Usage, wt, lbs	35.56	—	17.78	23.11	28.45	34.67	24.00	17.78	17.78	32.0
Wire Meter Reading	4554.5	4080	3389	6196.5	—(2)	4102	2055.5	2626.5	3064.5	4883.5
Wire Weight, lbs	8.33	7.46	6.20	11.33	—	7.50	3.76	4.80	5.60	8.9
Al % by weight	18.98	—(2)	25.85	29.99	—	17.79	13.54	21.25	23.95	21.7

See Footnotes Preceding Page

TABLE XLII
(Continued)

Cycle												
6			7					8				
Helical												
	40	56	GI	32	46	67	80	GI	29	38	51	63
3	49.3	63.1	22.4	32.4	46.1	67.3	80.0	21.5	28.7	37.8	51.2	62.7
	4	10	6	4	5	6	9	5	4	4	5	5
	5	10	6	4	5	6	8	5	2	2	0	0
	5	9	6	2	3	10	8	5	3	2	0	0
	170	207	204	90	111	200	72	255	147	88	—(2)	—
	360	640	402	144	225	690	—(2)	340	148	150	—	—
-1	-2, -1	-2, 0	0	+1	0	+1, +3 -2, -1	+3	0	+2	+2	—	—
.4	1.5	0.5 0.7	1.4	0.75	—(2)	0.63	0.5	1.5	1.0	1.3	—	—
.182	27.342	27.662	27.854	27.978	28.138	28.330	28.586	28.746	28.860	28.938	29.222	29.446
.143	27.325	27.570	27.766	—(2)	27.90	28.264	28.505	28.715	28.800	28.905	—(2)	—
.232	27.410	27.670	27.860	—	—	28.335	28.580	28.805	28.875	25.965	—	—
.175	27.365	27.600	27.882	—	—	28.265	28.513	28.735	28.865	28.960	—	—
.0615	0.0920	0.1230	0.1115	—	—	452(4)	0.1225	0.1095	0.0475	0.0480	—	—
.0154	0.0184	0.0136	0.0186	—	—	—(2)	0.0153	0.0219	0.0158	0.0240	—	—
	58	38	60	63	54	34	32(1)	54	68	71	—	—
	79	75	70	100	75	69	51(1)	64	60	45	—	—
	59	61	83	93	61	50	35(1)	69	52	44	—	—
	93	94	98	94	89	84	67(1)	78	89	93	—	—
	5	5	3	4	5	6	5	3	3	4	—	—
.0	2.0	3.0	5.3	0.7	0.4	2.5	2.3	3.8	2.0	1.2	—	—
.7	3.4	3.3	2.9	1.4	2.5	2.9	3.3	6.5	2.6	2.3	—	—
523 .0%)	RDS-523 (6.0%)	RDS-523 (6.0%)	RDS-523 (6.0%)	RDS-523 (6.0%)	RDS-523 (6.0%)	RDS-523 (6.0%)	RDS-523 (6.0%)	RDS-523 (6.0%)	RDS-523 (6.0%)	RDS-523 (6.0%)	—	—
	20	36	—(2)	—	—	—	39	40	22	—(2)	—	—
.78	17.78	32.00	—	—	—	—	34.67	35.56	19.56	—	—	—
.5	3064.5	4883.5	5756	—	7309	—	3380.5	3803	2295	1453	—	—
.80	5.60	8.93	10.52	—	13.36	—	6.18	6.95	4.20	2.66	—	—
.25	23.95	21.79	—(2)	—	—	—	15.13	16.35	17.68	—(2)	—	—

Winding efforts required 32 hours, although actual winding time was only 15 hours. Data obtained during winding are shown in Table XLIII.

(4) Post-winding Procedure

The soluble mandrel was washed out of the reinforced grain on 11 May 1964 with 74 F water (approximate temperature of RFG internal surface). The triple layer moisture barrier was removed immediately after washout. The revisions to mandrel coating were effective, since there was no evidence of moisture on the grain. The unit was subjected to a mold drying of two hours at 120 F, then sealed for shipment to the NDT facility.

The unit was radiographically examined after mandrel washout and 12 radiographs were taken of the grain-to-liner and liner-to-case interfaces. These indicated no separations. Both ports were also radiographed to determine the integrity of the polar boss/load ring/reinforced grain area. Again, no defects were evident.

Following X-ray, the polar boss-load ring area in the domes was restricted. The aft end was coated first and given a partial cure of two hours at 100 F, two hours at 120 F, and three hours at 140 F. The forward load ring was given a six hour incremental heatup period, then ten hours at 170 F.

Casting mandrel assembly was begun May 15 in preparation for core casting, and the core was cast on 18 May.

Prior to casting, R-143 insulation was added to each polar boss. The interior surfaces of the aft boss area which was exposed to core propellant were coated with a film of R-143. A thick fillet was added around the inside surface of the load ring for insulation. This fillet extended above the load ring/grain junction. The restrictor was cured two hours at 100 F, two hours at 120 F, and three hours at 140 F. The grain was then inverted so that the forward boss was at the bottom. A wipe coat of R-143 was applied to the propellant interface surfaces of the forward boss. R-143 was used to fill the area behind the first load ring to prevent a void area during casting. This restrictor was cured two hours at 100 F, two hours at 120 F, two hours at 140 F, and ten hours at 170 F. The inside surface of the grain and R-143 was cleaned with toluene, dried, and MAPO wiped. The core mandrel tooling had to be shortened by 0.27 inch because the boss-to-boss length was shorter than design.

TABLE XLIII

MOTOR A-1002 GFW CASE FABRICATION DATA (GFW 1402)

Dimensions, in.

Restricted Mandrel Diameter

Headstock	Center	Tailstock	Average
29.704	29.675	29.723	29.701

Helical Wrap Diameter

Headstock	Center	Tailstock	Average
29.812	29.788	29.850	29.817

Circ Wrap Daimeter

Headstock	Center	Tailstock	Average
29.970	29.945	30.020	29.978

Thickness

	Headstock	Center	Tailstock	Average
Helical	0.054	0.056	0.063	0.058
Circ	0.079	0.078	0.085	0.081
Total	0.133	0.134	0.148	0.139

Skirts

	Headstock	Tailstock
ID	29.860	29.860
OD	30.185	30.190
Thickness	0.162	0.165

Length

Skirt-to-skirt 56.81

TABLE XLIII
(Continued)

Weights, lb	
Load cell weights	
Weight after case cure	2840.6
Weight of restricted mandrel	2721.5
	119.1
Weight of rubber grommet	3.8
	115.3
Est. skirt ring weight	35.0
	80.3
Class weight	
Helical wrap	23.15
Cric Wrap	28.54
	51.69
Glass cloth	4.10
	55.79
Resin (est)	23.91
	79.70
Tension, lb	
Helical wrap	Start 21 Finish 24
Circ wrap	Start 24 Finish 25
Glass Density	
Helical wrap	1475 ends/in.
Circ wrap	2709 ends/in.

After mandrel assembly the grain was preheated for 33-1/2 hours at 170 F prior to casting. Four mixes of RDS-526 C were required for casting. Core propellant properties are shown in Table XLIV. Casting time (from start of first cast to end of last cast) was 10 hours and 15 minutes. The core cure was interrupted after 12 hours to adjust the propellant level and restrict the top surface with R-143. The grain was cured for a total of 72 hours at 170 F. The grain was cooled by lowering the inlet air temperature 5 F every three hours (down to 95 F).

The casting mandrel removal on May 25 progressed satisfactorily, but was tedious, as the foam star points had to be removed in small pieces. Also, propellant had flowed between sections of the foam and the central core, indicating a need for improving the bonding or installation method.

After core casting, the unit was taken to the X-ray facility for inspection. The unit could not be opened due to the lack of humidity control in the X-ray building, therefore, the film holding fixture could not be used and no single wall radiographs were taken. An attempt to examine the core-reinforced grain interface by tangential inspection failed due to the insufficient power of the 1000 KV unit.

Visual examination of the cast core grain revealed (1) bond failure between the propellant and the phenolic aft boss ballistic sleeve, and (2) one 1/4 inch and one 1/8 inch void at the surface in one of the core configuration valleys. Two of the defects were considered to be insignificant but the 1/8 inch void, which was measured to be 2 to 3-1/4 inches deep, necessitated repair.

Several candidate mixtures of epoxy were tested with laboratory specimens of propellant to establish the most suitable adhesive to repair or fill the separation. Criteria considered were viscosity, pot life, cure time at ambient, bondability, compatibility, availability, and cured flexibility.

A mixture of Epon 815 and Versamid 140 in a 35/65 ratio was selected as the most suitable potting fluid.

The aft boss ballistic sleeve-to-propellant separation was filled using vacuum to help penetrate the gap. A dam was made around the sleeve to hold excess potting fluid then the unit was evacuated. Upon release of vacuum, the fluid was forced into the separation. This procedure was repeated and a final topping applied without vacuum. The material was allowed to cure at ambient for one day before proceeding with final assembly.

TABLE XLIV

CORE PROPELLANT PROPERTIES

Property	L-5-18-M81	L-5-18-M82	L-5-18-M83	L-5-18-M84
Elongation, %, -75 F	40	42	40	45
Tensile, psi	392	414	395	439
Modulus, psi	2107	1993	1834	2238
Elongation, %, 77 F	38	37	39	44
Tensile, psi	160	154	150	165
Modulus, psi	698	652	628	640
Elongation, %, 170 F	37	32	38	39
Tensile	126	125	129	118
Modulus	520	550	517	457
Strand Burn Rate, 1000 psia*	0.476	0.487	0.477	0.487
Strand Burn Rate, 750 psia*	0.423	0.427	0.414	0.422
Position In Grain	Aft Of Center	Aft Dome	Fwd Of Center	Fwd Dome
Density	0.0635	--	--	--
Pit Vacuum, in.-Hg	28.6	28.2	28.2	28.8
Cast Press, psig	12	10-20	12-20	0-5
Casting Started	1314	1122	1724	2122
Casting Completed	1332	1141	1739	2137
Avg Rate, lb/min	15	14	18	18

*The Liquid Strand Burning Rates Compared Favorably With The Previous Pilot Mix, L-3-3-M81, Which Gave 6-inch Motor Burning Rates On Target. Strand Burning Rates For L-3-3-M81 Were 0.427 ips At 750 psia, And 0.487 ips At 1000 psi.

(5) Final Assembly

The heavyweight nozzle (802236-31) using pyrolytic graphite rings in the throat and the 802476 igniter assembly (utilizing heavyweight steel closure) were installed without trouble. Leak testing was completed on 4 June 1964.

Table XLV consists of the weights of components as added to, or subtracted from, the motor during processing, and a sequential total of the assembly weight.

(C)

TABLE XLV

MOTOR WEIGHT HISTORY

Component Weight	Components	Assembly Weight
1372.80	Sand, Spindle, Tenite, RTV	1372.80
7.500	Load Rings	1380.30
13.007	Aft Boss	1392.31
9.82	Forward Boss	1403.13
3.79	Tape	1406.92
210.4	Wire	1617.32
1027.48	Propellant (1025.31 by Tube Weight)	2644.80
5.54	GFW Flange	2650.34
71.20	R-143	2721.54
41.26	Skirt Rings, Bolts	2762.80
80.00	GFW Case	2842.80
-1377.50	Sand, Spindle, Tape, RTV	1465.30
-1.00	Boss Tape, RTV & R-143 at Ring	1464.30
1.00	R-143 Fills	1465.30
1124.00	Core Propellant	2589.30
0.04	Epoxy Fix	2589.70
32.30	Nozzle Assembly with Instrumentation	2622.00
0.53	Drive Pins	2622.53
0.12	"O" Rings	2622.65
9.60	Igniter and Forward Closure Assembly	2632.25
7.65	Strain Gages, Forward Closure Restriction, and Heat Shield	2639.90

b. Testing

Due to the separation which occurred between the aft polar boss and the core grain, and the unsealing of the first load rings, it was decided that Motor A-1002 would be static tested vertically on a rigid test test stand.

It was originally planned to measure pressure, thrust, temperature, at 28 locations, strain at 32 locations, and displacement at 4 locations. But because of the decision to fire on a rigid stand, this instrumentation had to be somewhat reduced since data channels for the rigid firing stand were limited to 2 pressure transducers, 24 thermocouples, 10 strain gages, and 2 linear potentiometers.

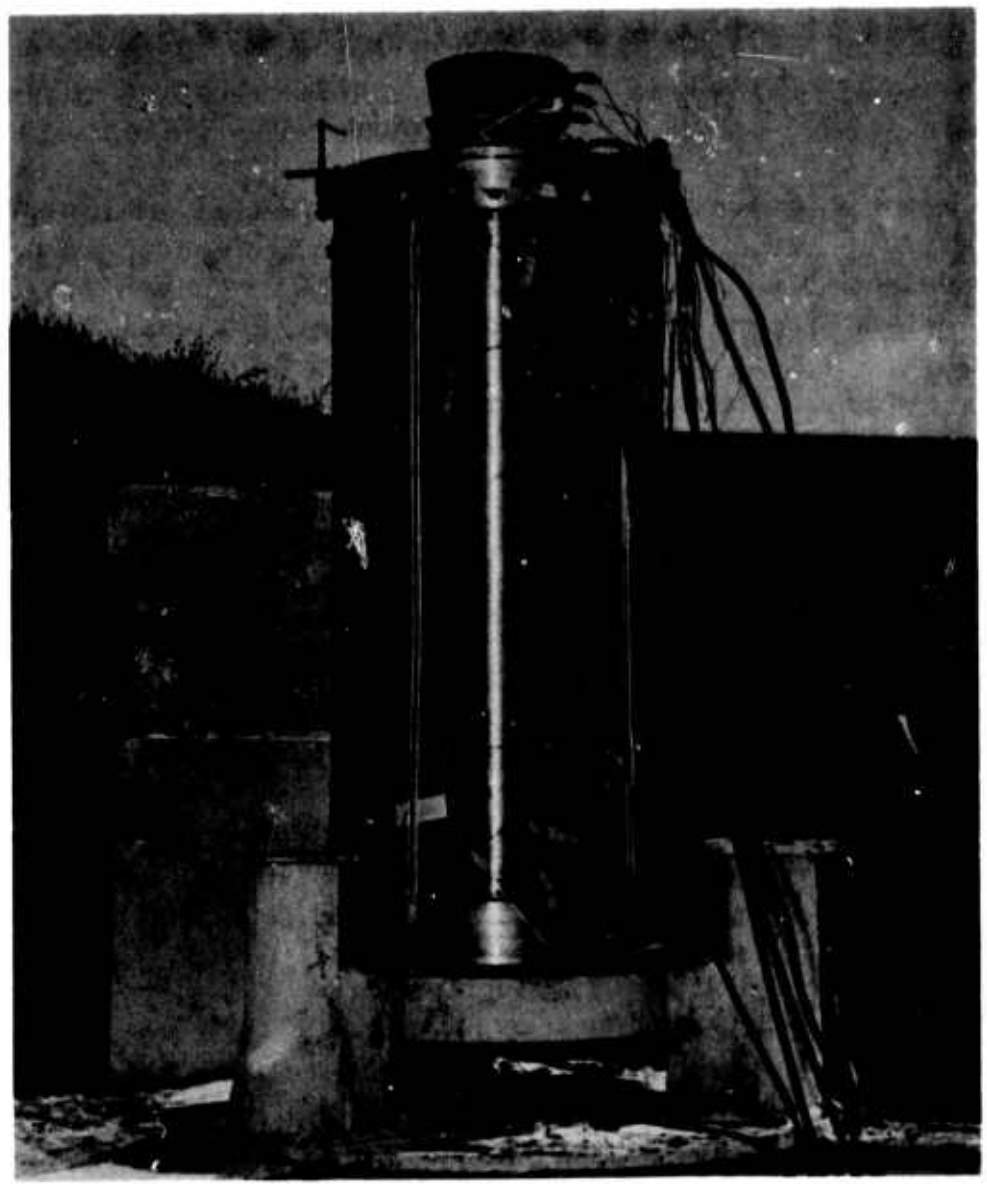
The motor was static fired on 5 June 1964 at ambient temperature, see Figs. 127, 128, and 129. All components functioned properly and the motor burned to completion as predicted. Carbon dioxide was used in an attempt to quench the liner and prevent residual burning after the firings. During tailoff and actuation of the CO_2 quench, there was some evidence that propellant slivers and/or insulation were ejected through the nozzle. The test was considered to be extremely successful in all respects.

(1) Analysis

Ballistic data obtained in the test of Motor A-1002 are presented, with design nominals, in Table XLVI, Performance Summary, Table XLVII, Weight Summary, and Fig. 130, the pressure-vs-time/replot.

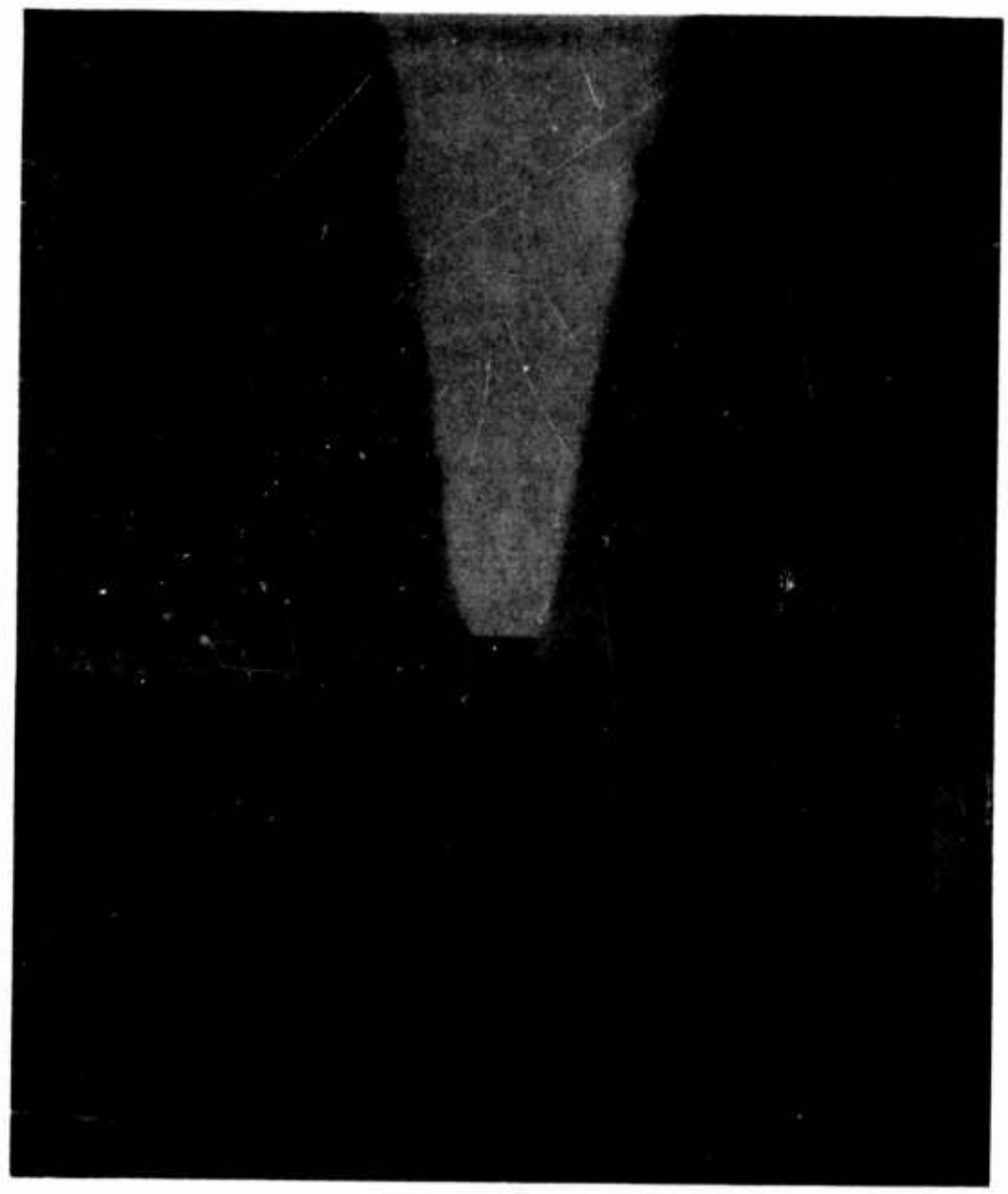
Ballistic design of Motor A-1002 differed from the final flightweight Motor A design primarily in propellant weight of the reinforced grain. The core grain specified and employed in A-1002 was identical to the Motor A flightweight design.

The performance demonstrated by Motor A-1002 was successful in every respect. All design objectives with respect to performance and related propellant characteristics were achieved, and in some cases exceeded. The performance compared most favorably with design estimates for A-1002 and flightweight design where applicable. The pressure demonstrated by this motor during the last portion of the RFG burning did not agree with the predicted pressure, but did compare to the flightweight motor. This is significant in that the burning rates desired in the final motor were obtained in this motor.



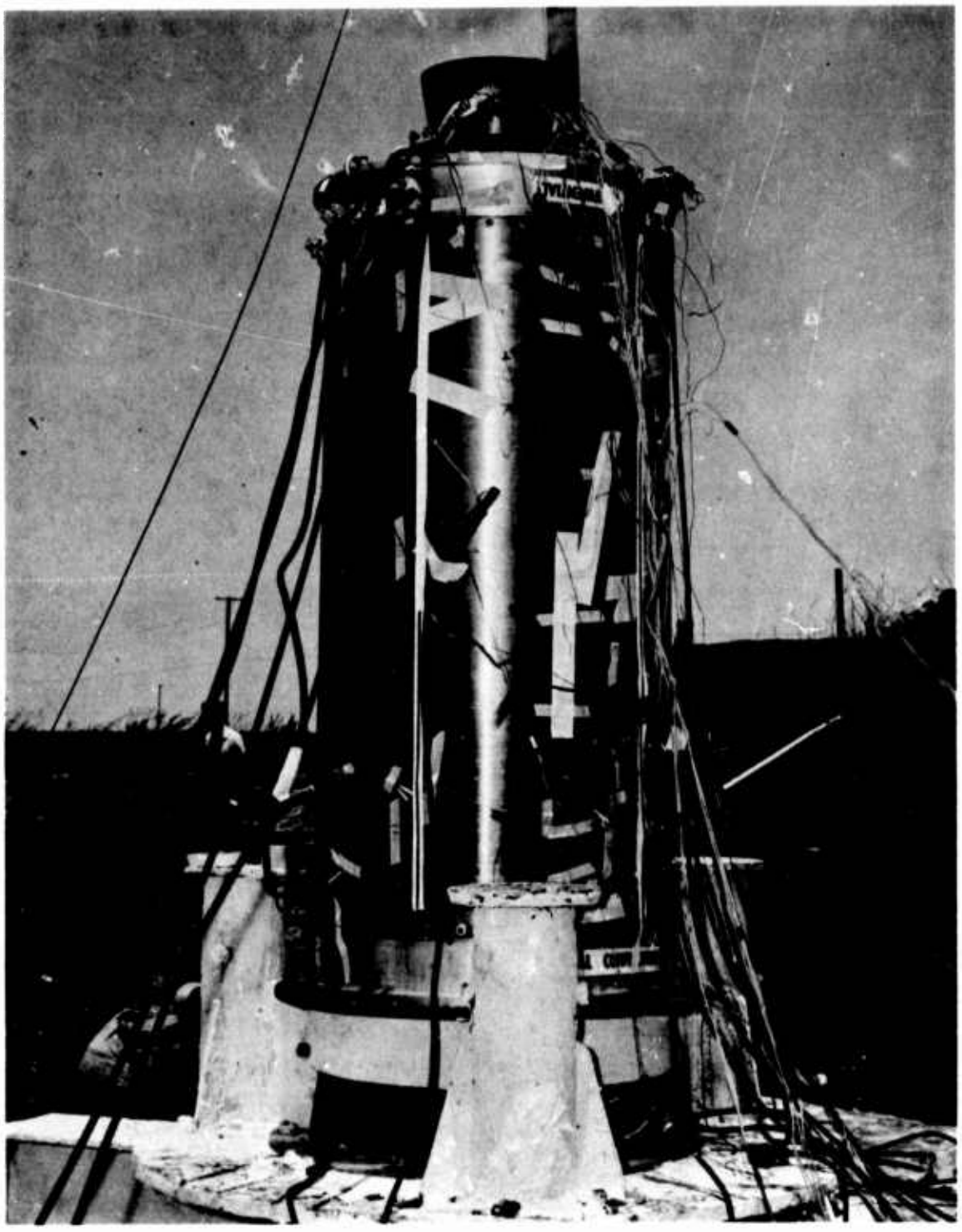
2YA23-6/5/64M1D

Figure 127. A-1002 Before Firing



CN355

Figure 128. A-1002 During Firing



2YA25-6/5/64M1A

Figure 129. A-1002 After Firing

TABLE XLVI

PERFORMANCE SUMMARY FOR A-1002

	Actual Motor A-1002	Design Nominals	
		Motor A-1002	Flightweight Design
Average pressure, psia	560	600	575
Action time, sec	31.44	30.1	32.4
Average thrust, lb	16,970*	18,170	17,340
Total impulse, lb-sec	533,600*	547,800	561,600
Maximum pressure, psia	741	805	805
I_{sp} at motor conditions, lb-sec/lb	225.9*	229.8	226.1
I^{o}_{sp} at 1000 psia, lb-sec/lb	241.4*	243.6	241.3
Impulse to weight ratio	205.8*	210.0	216.6
Core Grain			
Avg pressure, psia	733	750	750
Avg thrust, lb	22,660*	23,690	23,690
Duration (10% to tan), sec	9.81	10.2	10.2
Reinforced Grain			
Avg pressure, psia	482	525	500
Avg thrust, lb	14,400*	15,380	14,410
Duration (tan to 40 psi), sec	21.63	19.9	22.2
Ignition delay, sec	0.095		

*Thrust parameters estimated from pressure

TABLE XLVII

WEIGHT SUMMARY FOR MOTOR A-1002*

	Actual Motor A-1002	Design Nominals	
		Motor A-1002	Flightweight Design
Nozzle Assembly	32.3	30.01	26.77
Case	80.0	73.00	34.00
Liner	72.2	82.06	12.00
Igniter	9.6	3.08	3.08
Fwd Boss		10.52	10.52
Aft Boss	30.33	12.70	12.70
Load Rings		6.94	6.94
Drive Pins	0.53	0.56	0.56
O-rings	0.12	0.10	0.10
Flange	5.54	5.14	1.71
Epoxy	0.4		
Total Inerts	231.02	224.11	108.38
Core Propellant	1124.00	1135.00	1135.00
RFG Propellant	1237.90	1249.00	1349.00
Total Propellant	2361.90	2384.00	2484.00
Total Motor Wt	2592.92	2608.11	2592.38
Mass Fraction	0.911	0.914	0.958

*All weights in pounds

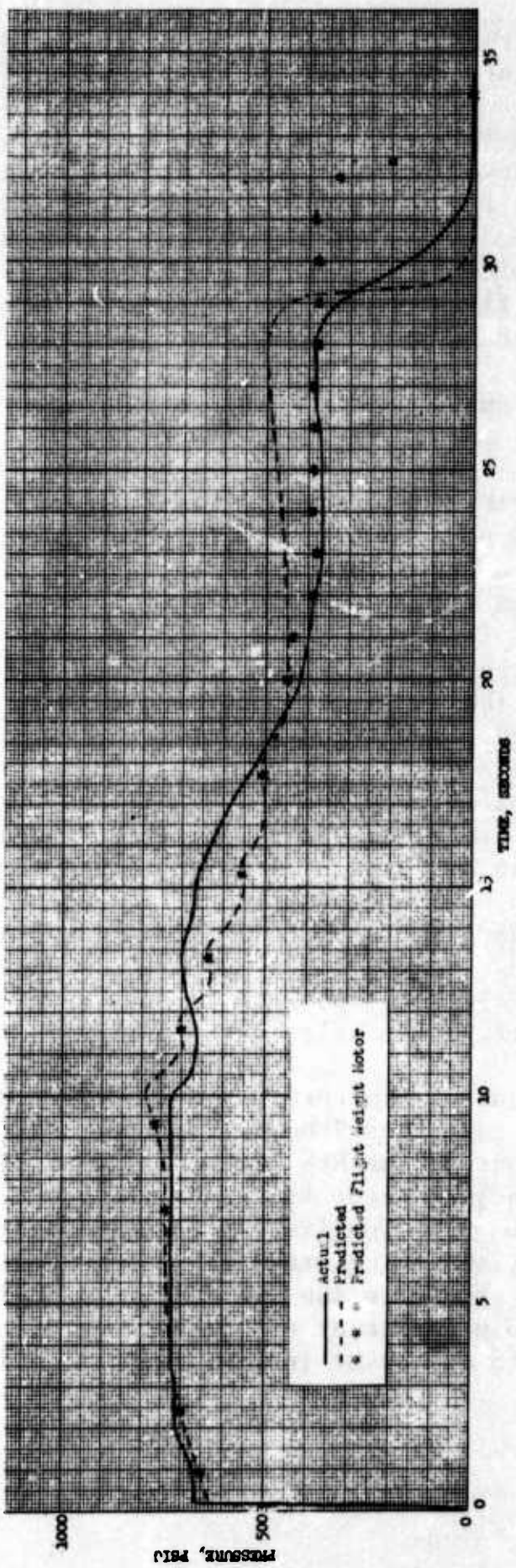


Figure 130. Pressure-vs-Time, A-1002

(C) Since thrust was not measured in the test, it was estimated from pressure data. Estimated specific impulse (I_{sps}) for the motor at reference condition (1000 psia and zero degree half angle) was 241.4 lb-sec/lb compared to 241.3 lb-sec/lb design nominal for the flightweight motor. As the lower burning rates were achieved in the outer layers of RFG, the specific impulse at reference condition demonstrated by Motor A-1002 is comparable to the flightweight estimate rather than the estimate for Motor A-1002. The comparison of specific impulse indicates total impulse for the flightweight motor is well above the required minimum impulse for Motor A.

(C) The percent sliver for the motor, based on percent of total pressure integral in the tailoff, was 3.2%. It is interesting to compare this to the percent sliver of the core cross section, which is 16.2%. However, with greater burning rates in the circumferential direction and ratio of core-to-RFG burning rates, most of the sliver from the core configuration existing at the transition stage is consumed near the end of action time.

(C) The pressure-time performance during the core burning duration was more neutral than predicted, and the maximum pressure was less than had been predicted. This is attributed to a higher degree of erosive burning then had been estimated. The ratio of maximum to average pressure demonstrated by Motor A-1002 will enable operation at an average pressure greater than 750 psia (target for A-1002), with a nominal maximum less than 800 psia. Structural analysis of the GFW case indicated that the strain measurements were close to the expected values. Figure 131 shows the location of all strain gages and linear potentiometers on the GFW case. Strain gages S-5, S-7, and S-24 did not function properly after 22.5. 26.0 and 29.2 seconds respectively. These three gages performed properly early in the firing, but were lost prior to burnout.

At burnout of the core grain (9.9 seconds) hoop strain in the GFW case was approximately 2800 microinches per inch and reached a maximum value at burnout of the RFG (28 seconds) of approximately 6250 microinches per inch just prior to losing the first longitudinal strain gage at 22.5 seconds. Both longitudinal strain gages (S-5 and S-7) were lost before burnout, and therefore the maximum longitudinal strain is not known. Maximum strain in the GFW forward and aft domes was approximately 5200 and 4800 microinches per inch respectively. Strain and deflection vs time data are shown in Figs. 132, 133, 134, and 135.

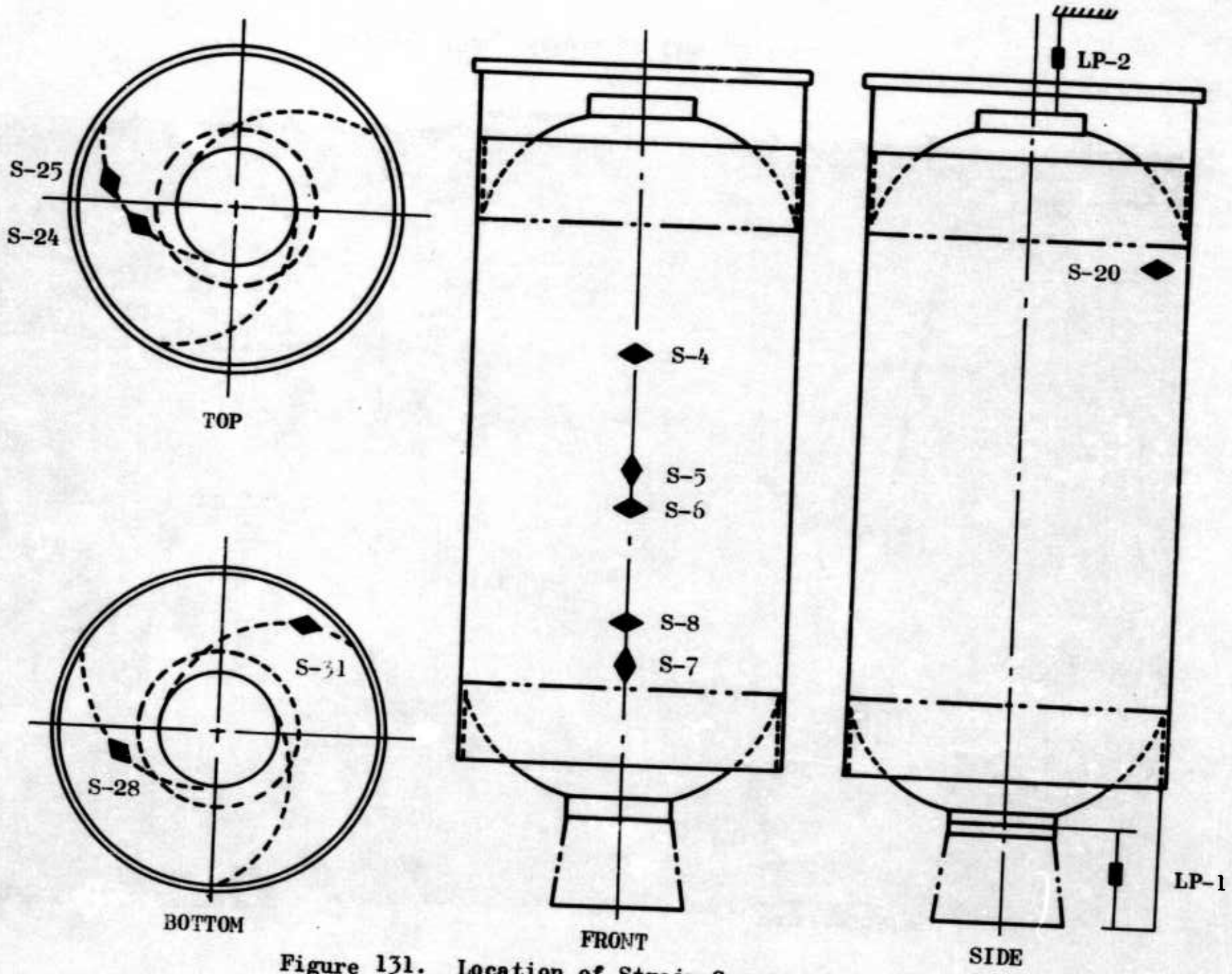


Figure 131. Location of Strain Gages and Linear Potentiometers, A-1002

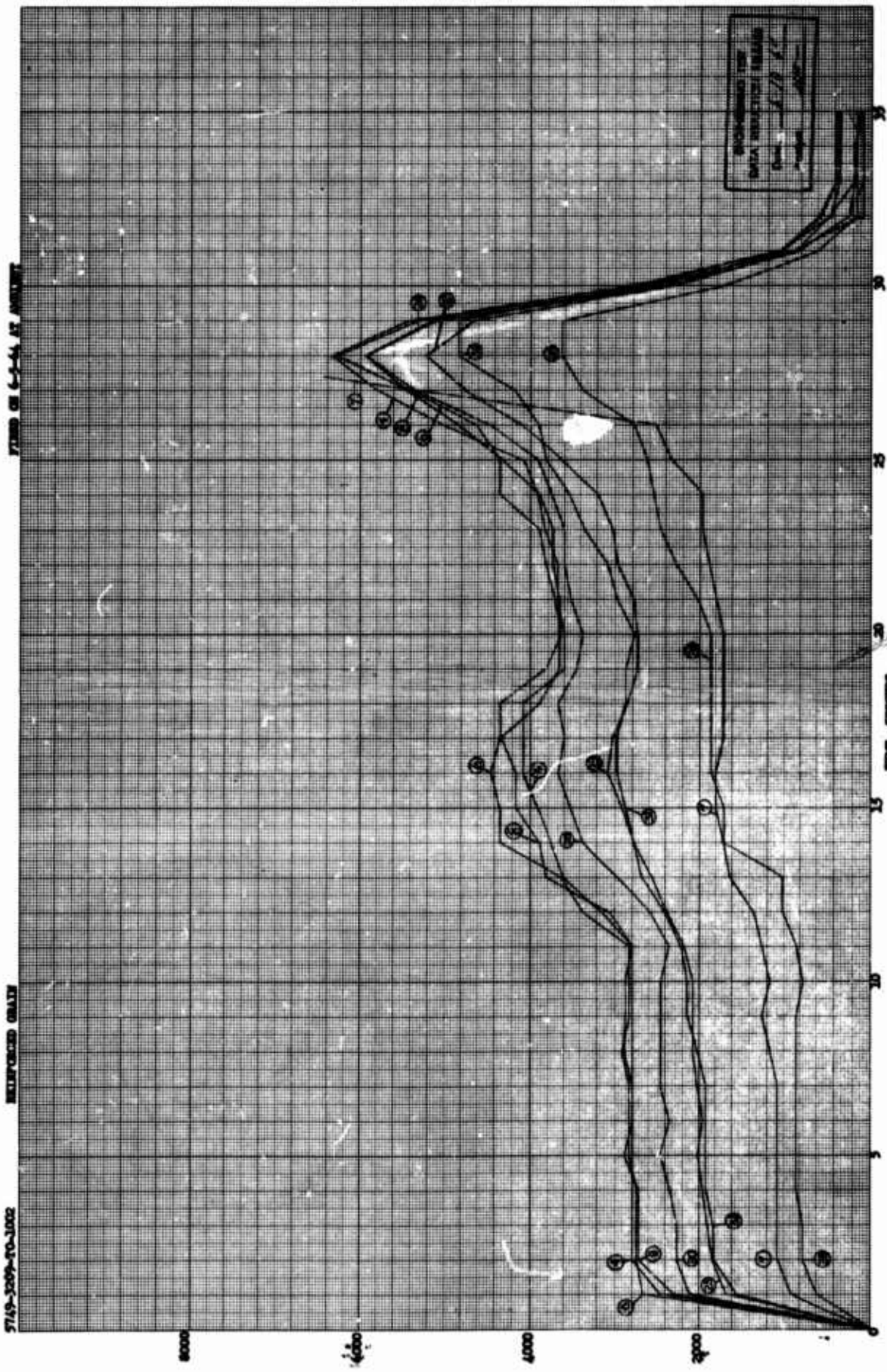


Figure 152. Strain vs Time, A-1002

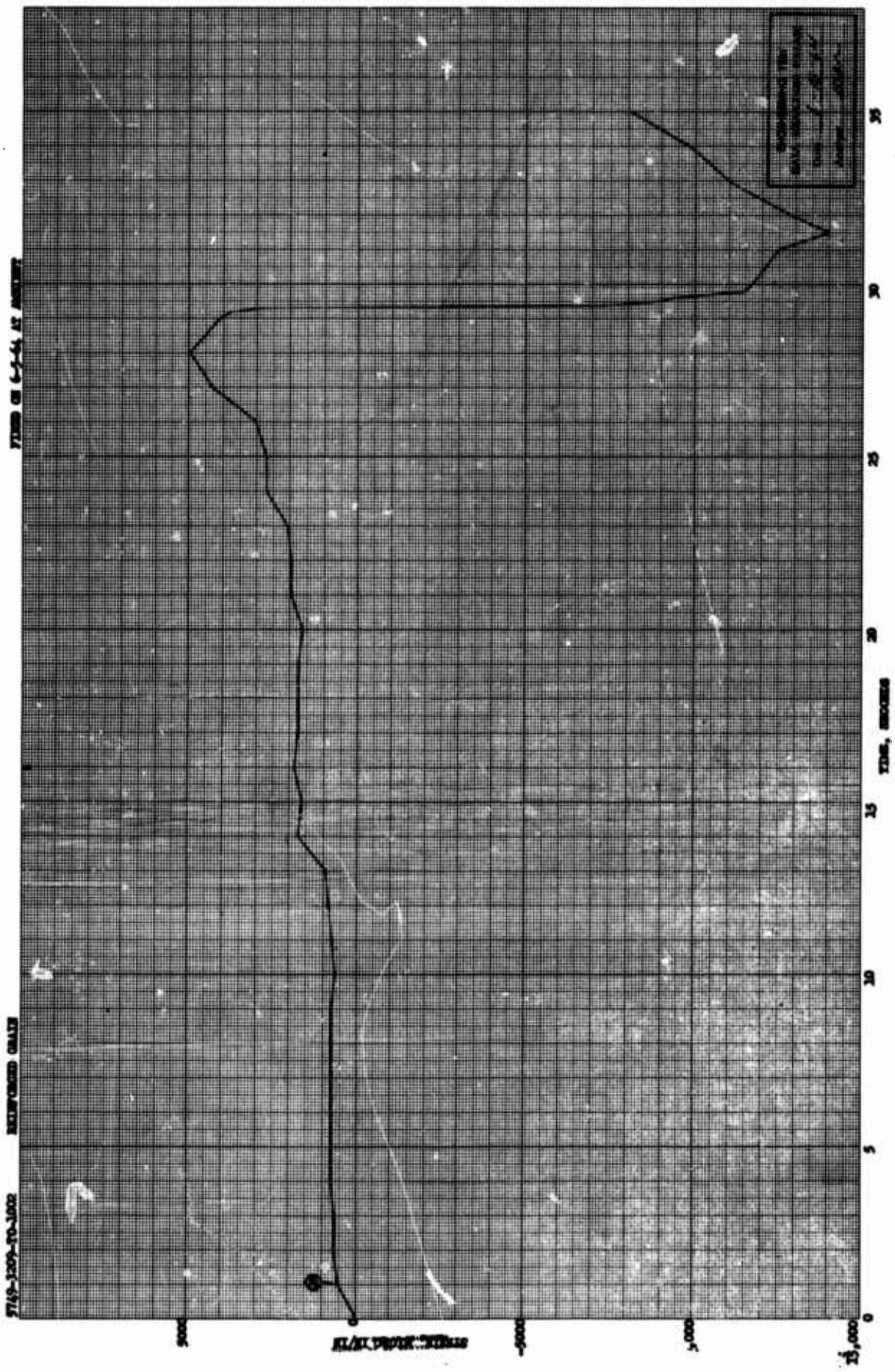


Figure 133. Strain vs Time, A-1002 (Gage 29)

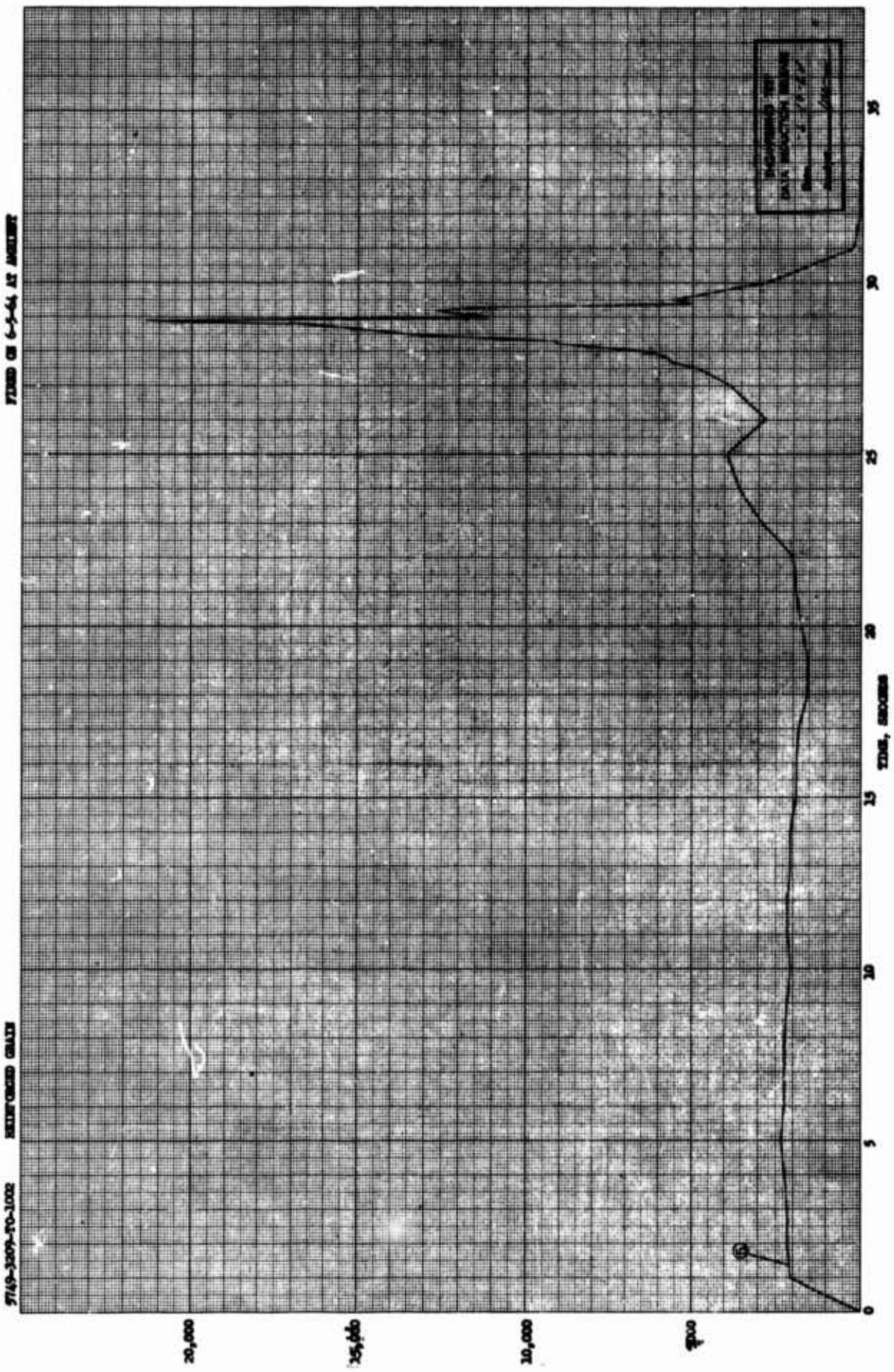


Figure 174. Strain vs Time, A-1002

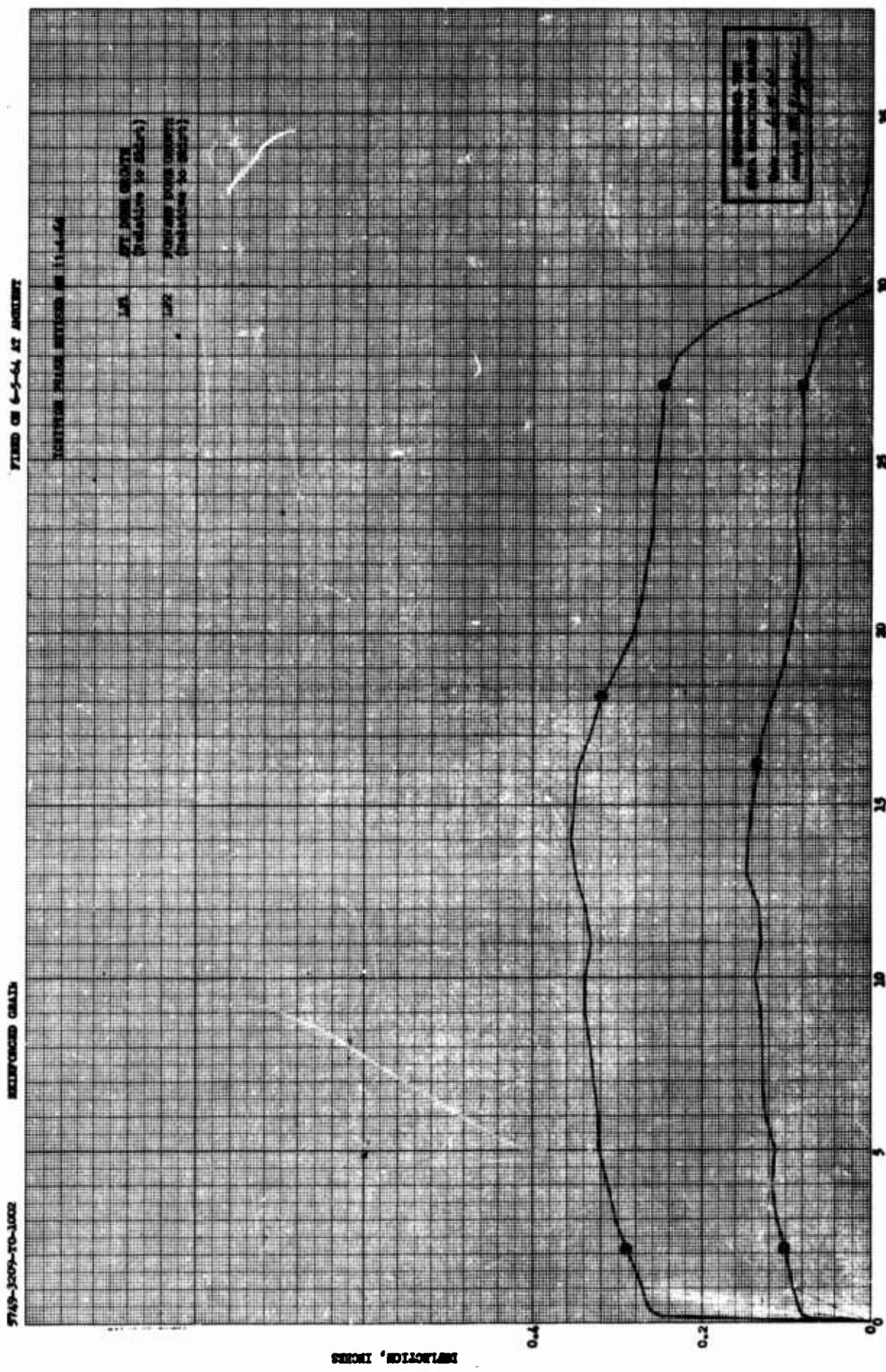


Figure 135. Deflection vs Time, A-1002 (Gages 1 and 2)

(C) GFW case strain vs time curves for this motor are progressive, even though the pressure vs time curve is regressive. The progressive strain-time curve is typical for RFG motors because, as the RFG web is burned, a larger portion of the chamber pressure is resisted by the GFW case. At burnout, the entire pressure must be supported by the GFW case. Figure 136 shows the pressure-time curve for motor A-1002 and hoop strain-time as recorded by strain gage S-4. A curve showing calculated GFW case hoop strain vs time is also shown in Fig. 136. This calculated hoop strain curve is based on the assumption of no support from the RFG. Measured hoop strain during the first 9.9 seconds was only 2800 micro-inches per inch, which shows that the RFG decreased the hoop strain in the GFW case initially by a factor of approximately four. This difference in hoop strain decreases from core grain burnout until the two curves are identical at RFG burnout. The most important thing shown in Fig. 136 is the fact that even with the testweight GFW case, the RFG supported a major portion of the chamber pressure for a large portion of the burn time, and continued to support a portion of the chamber pressure for a large portion of the burn time, and continued to support a portion of the chamber pressure until burnout of the RFG at 28 seconds.

Hoop strain for a flightweight motor at burnout should be approximately three times the strains measured on this test. Dome and longitudinal strains will be approximately doubled. These values of strain will be well within the range of the GFW case capability.

The results of the thermal analysis of Motor A-1002 static firing test data are presented in Figs. 137, 138, and 139. The thermocouple data presented in these figures show graphically the temperature history of the motor case.

The case/restrictor shell remaining after the firing of A-1002 was sectioned for examination, Figs. 140 and 141. The restrictor and case were intact, with relatively light damage except in the forward dome, which faced downward during the vertical firing. The cylindrical section of the case liner had a maximum loss of 0.035 inch at the aft end. The losses at the forward and center section were approximately equal, having values of 0.011 inch. The char depth of the liner had a minimum value of 0.0075 inch at the aft end, increasing to 0.015 inch at the center and 0.012 inch at the forward end.

(C) The maximum loss of liner material in the aft dome was 0.19 inch, which occurred at the tangent point of the dome and cylindrical section of the case. The losses of the aft dome liner material decreased uniformly from that point to a minimum of 0.05 inch at a dome diameter of 21 inches, then increased to 0.15 inch at a diameter of 11 inches.

CONFIDENTIAL

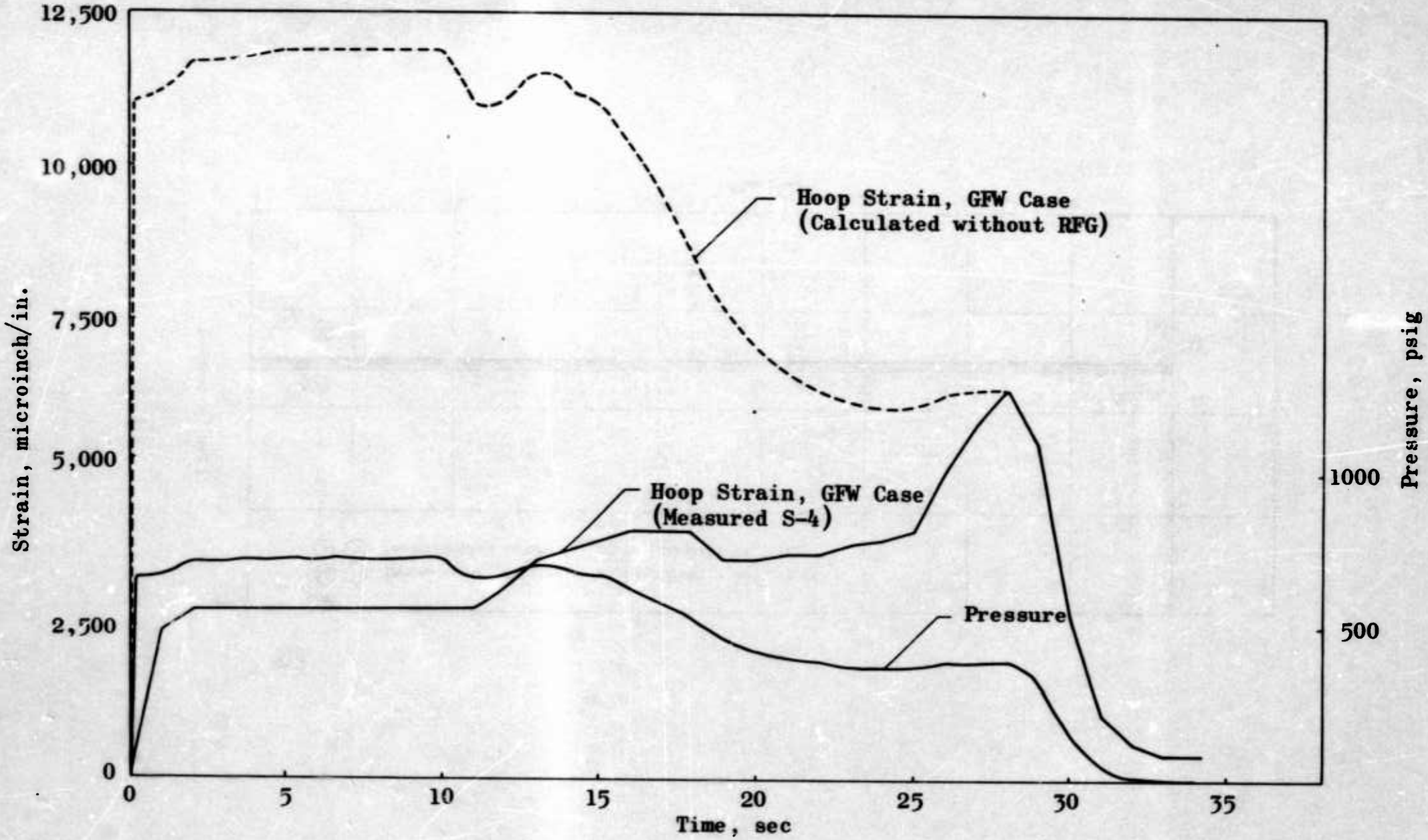


Figure 136. Pressure and Hoop Strain vs Time, A-1002

CONFIDENTIAL

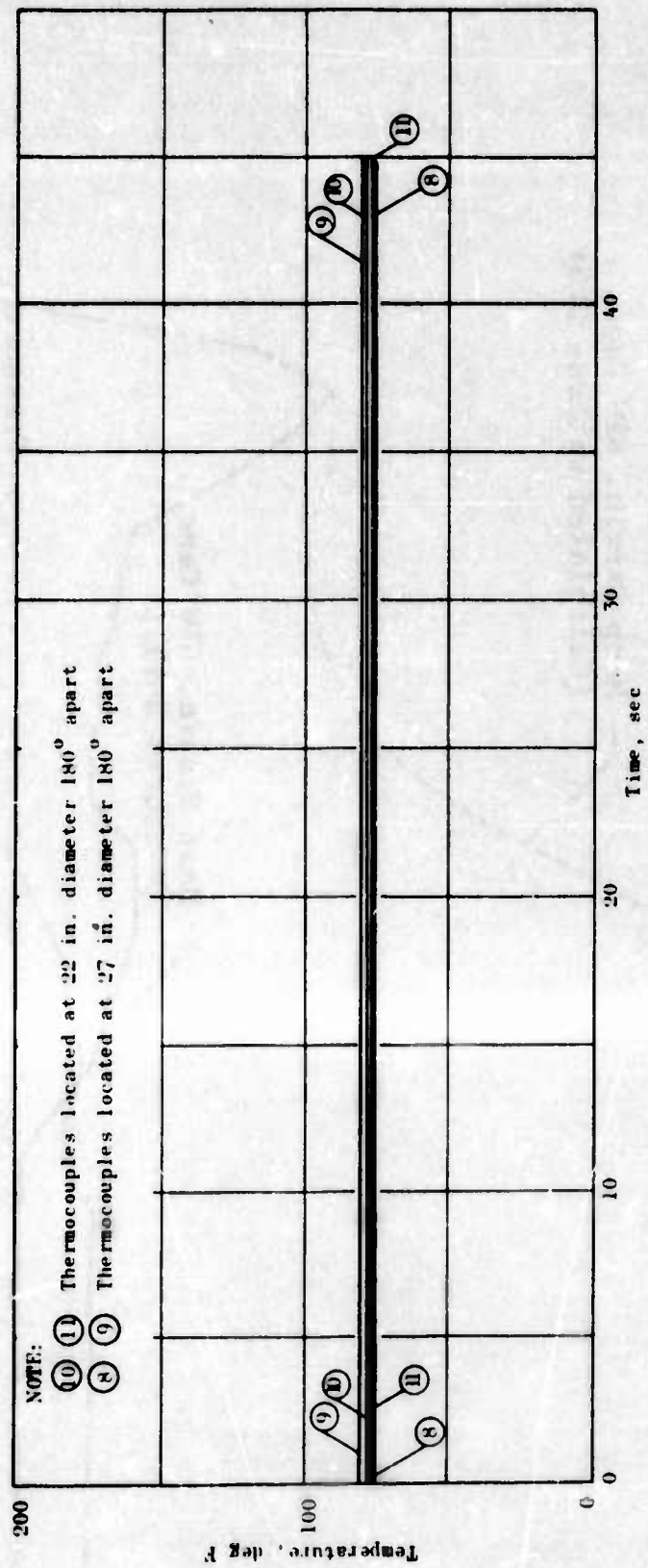


Figure 137. Temperature vs Time from Thermocouples on Motor A-1002 Forward Dome

CONFIDENTIAL

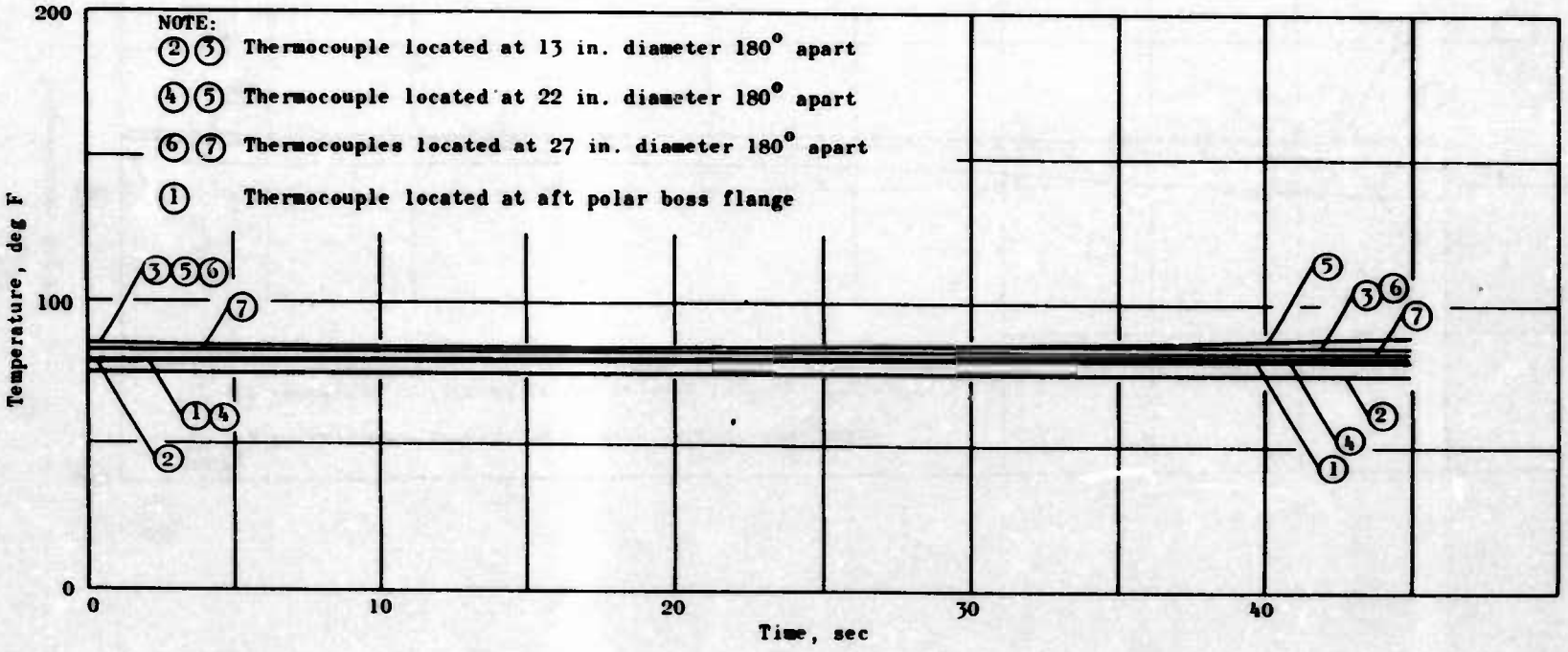


Figure 138. Temperature vs Time for Thermocouples on Motor A-1002 Aft Dome

CONFIDENTIAL

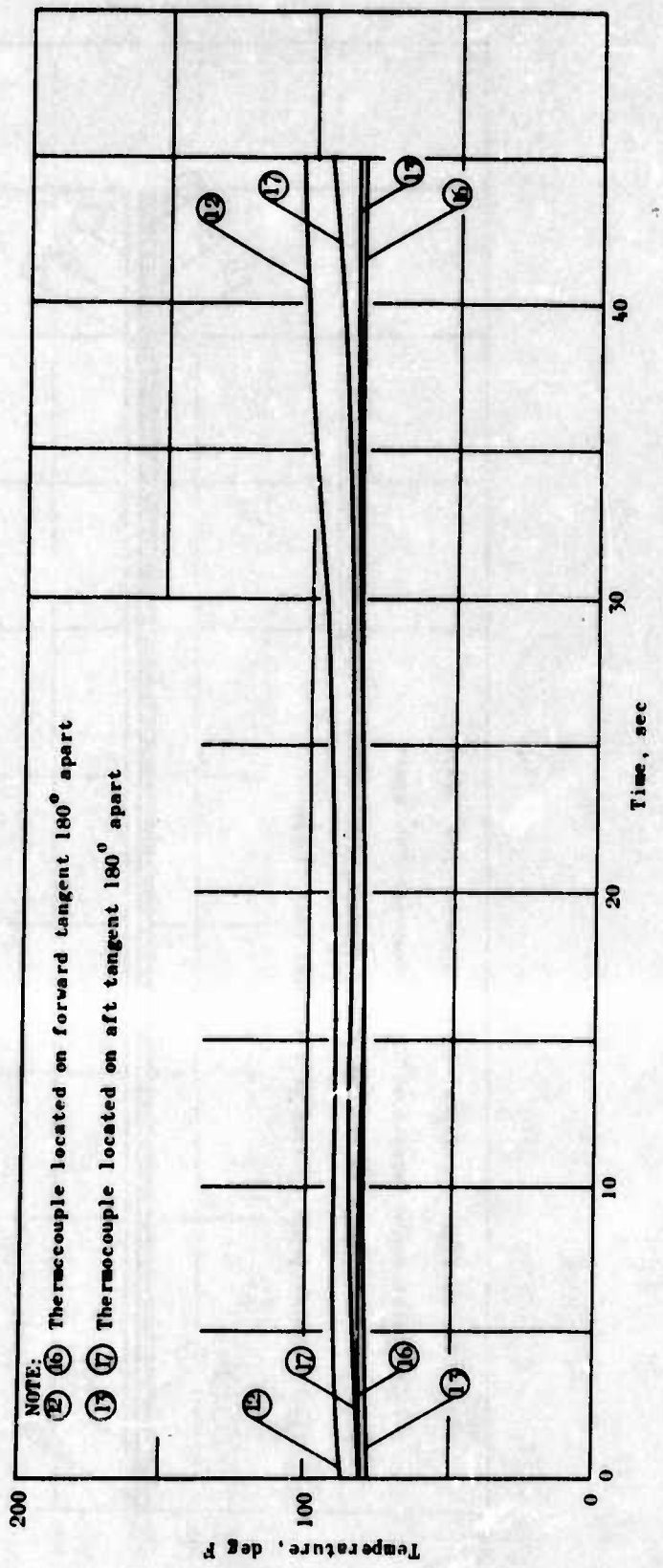
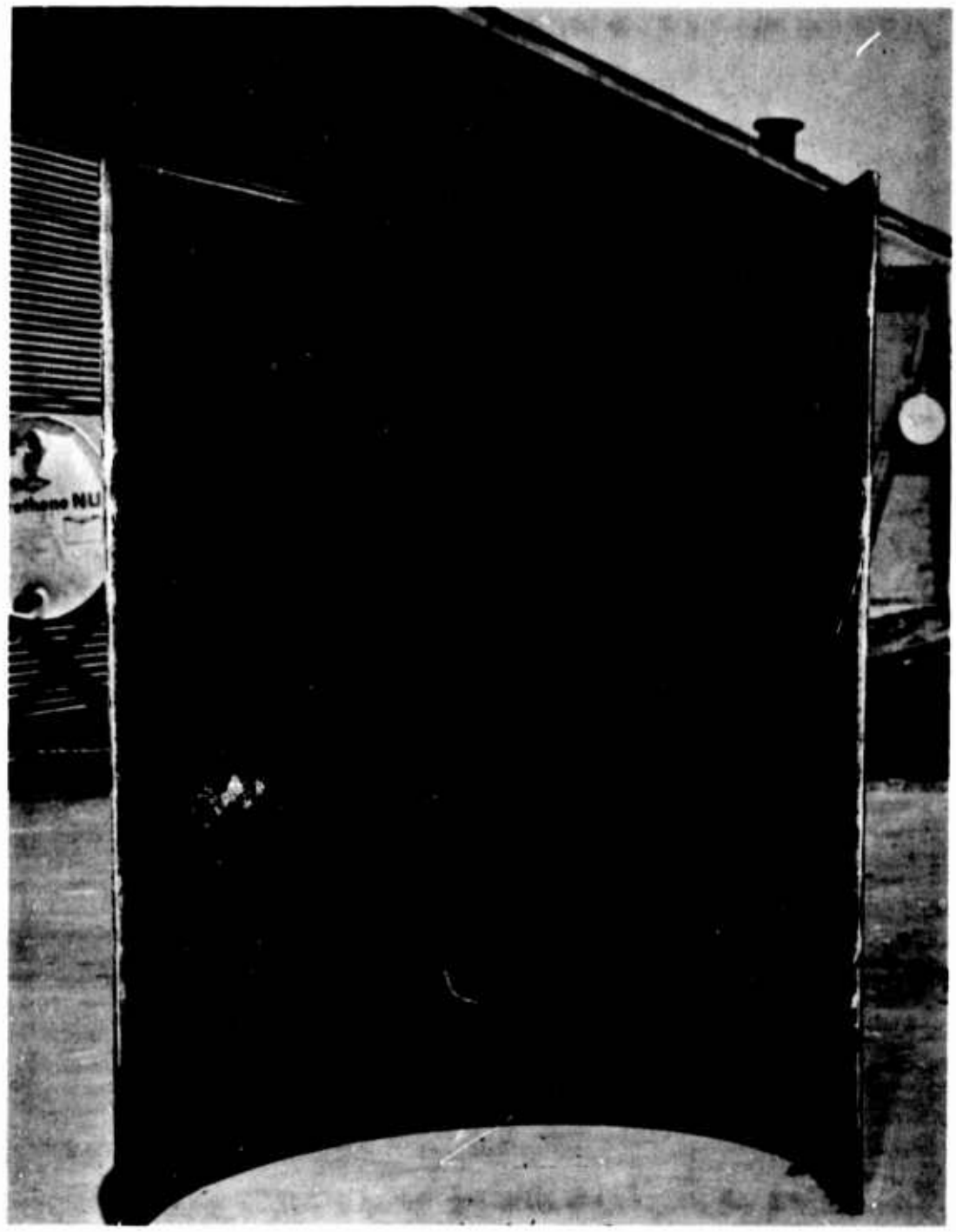
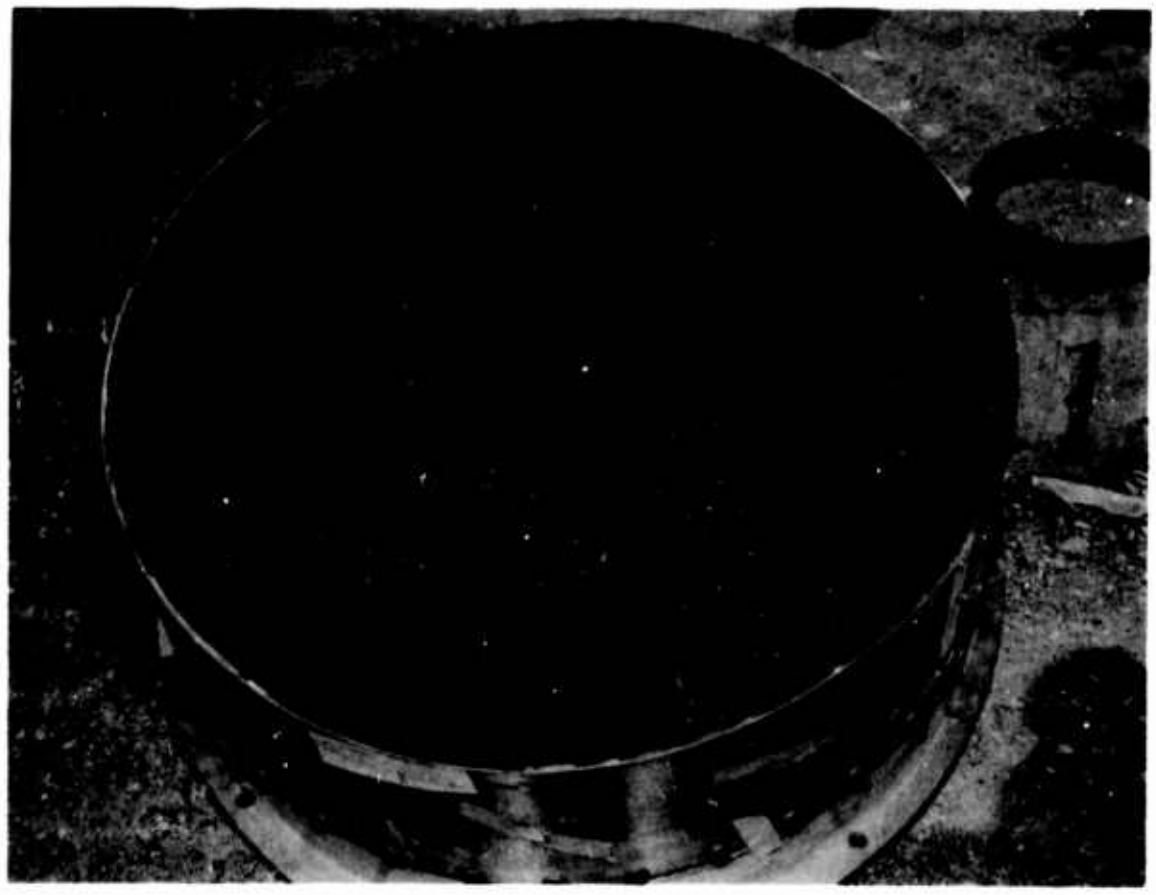


Figure 139. Temperature vs Time from Thermocouples Located at the Forward and Aft Tangent of the Cylindrical Section of Motor A-1002



2YA25-6/8/64M1L

Figure 140. Section GFW Case, A-1002

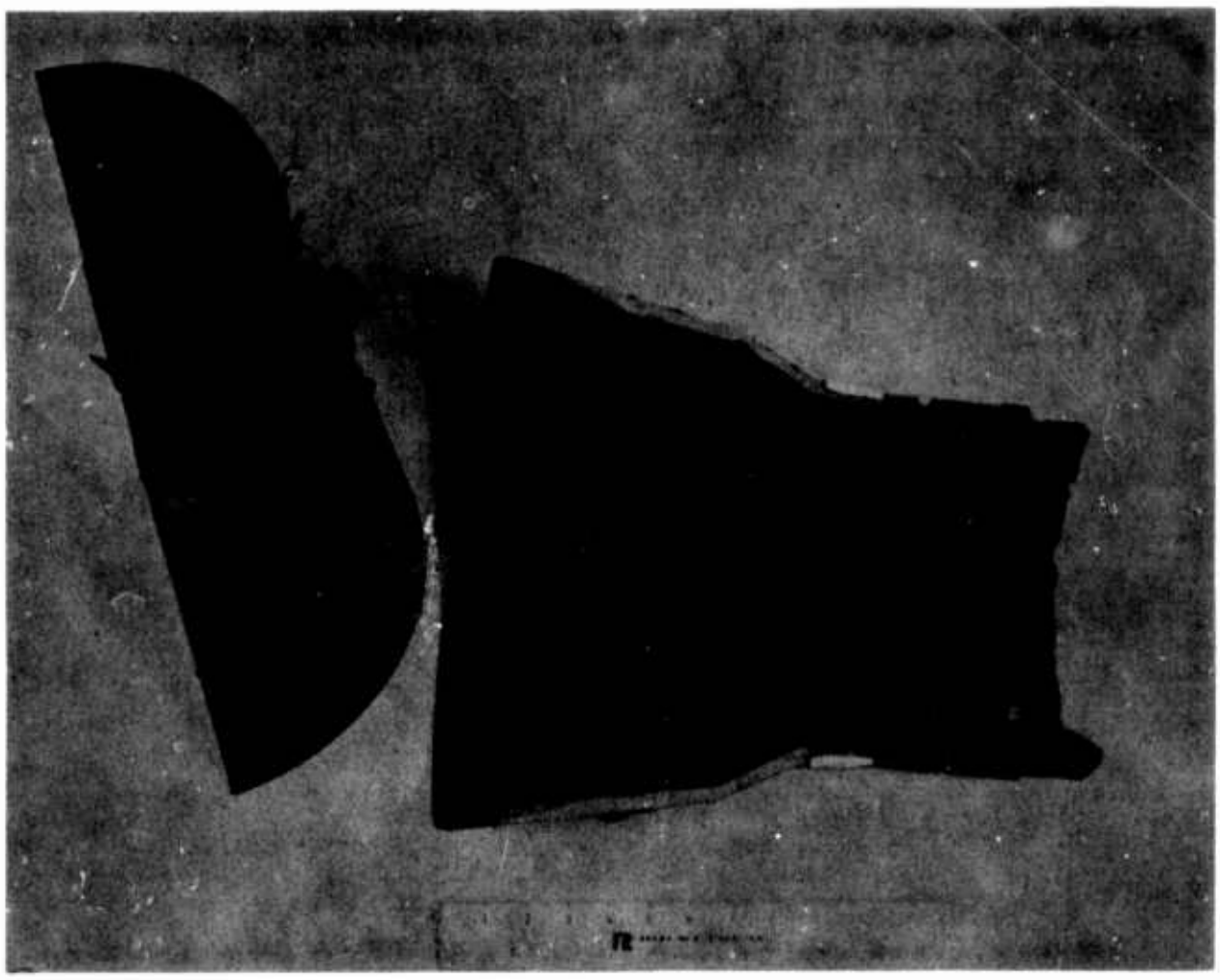


2YA25-6/8/64M1A

Figure 141. Section Forward End of GFW Case, A-1002

(C) The maximum material loss of the aft polar boss was 0.125 inch at the forward section, and decreased to no loss at the fifth load ring step. The char depth was a uniform 0.07 inch. The loss of the complete forward section of the aft polar boss was not anticipated. Examination of the part indicated it had been broken off, rather than consumed thermally. Examination of the high speed films taken of the firing shows that a semi-circular object was ejected at 24.5 seconds after ignition. Although this piece was not recovered, it is believed that the ejected piece was the forward section. The mechanism which caused this failure is not completely known. The forward head itself was of heavyweight design but the protecting insulation was flightweight. The head lost 0.2 inch of insulation uniformly and had a char depth of 0.1 inch. The remaining 0.122 inch of insulation was undamaged. The polar boss was almost charred completely.

(C) The nozzle performed exceedingly well, as shown by Fig. 142. Thermocouples on the exterior of the nozzle exit cone showed no significant increase in temperature, see Figs. 143 and 144. This was expected, since all data taken were on heavyweight sections of the exit cone. The maximum temperature recorded on the embedded thermocouples was 800 F at thermocouple location 23 (see Figs. 144 and 145) and was 200 F lower than was expected.



CN-373

Figure 142. Sectioned Nozzle, A-1002

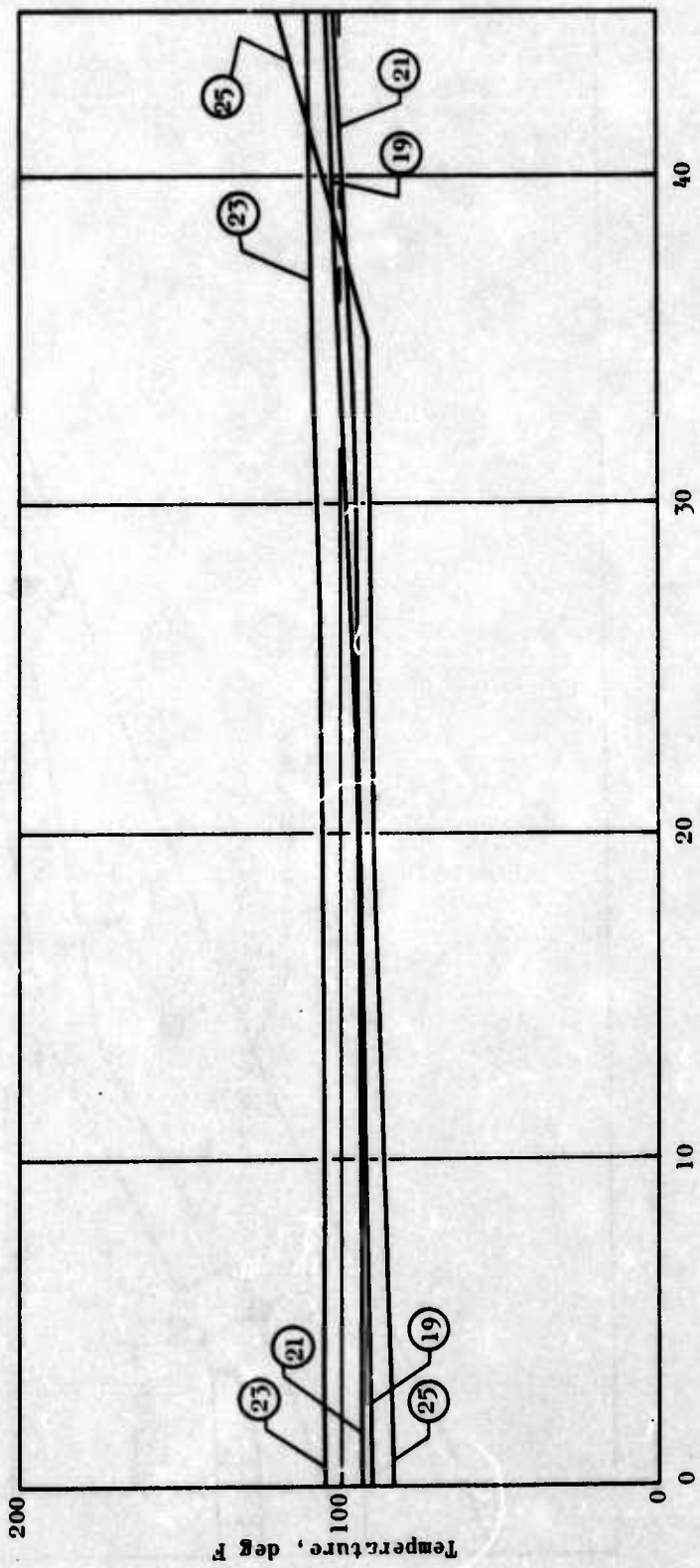


Figure 143. Temperature vs Time from Thermocouples on Motor A-1002 Nozzle Exit Cone

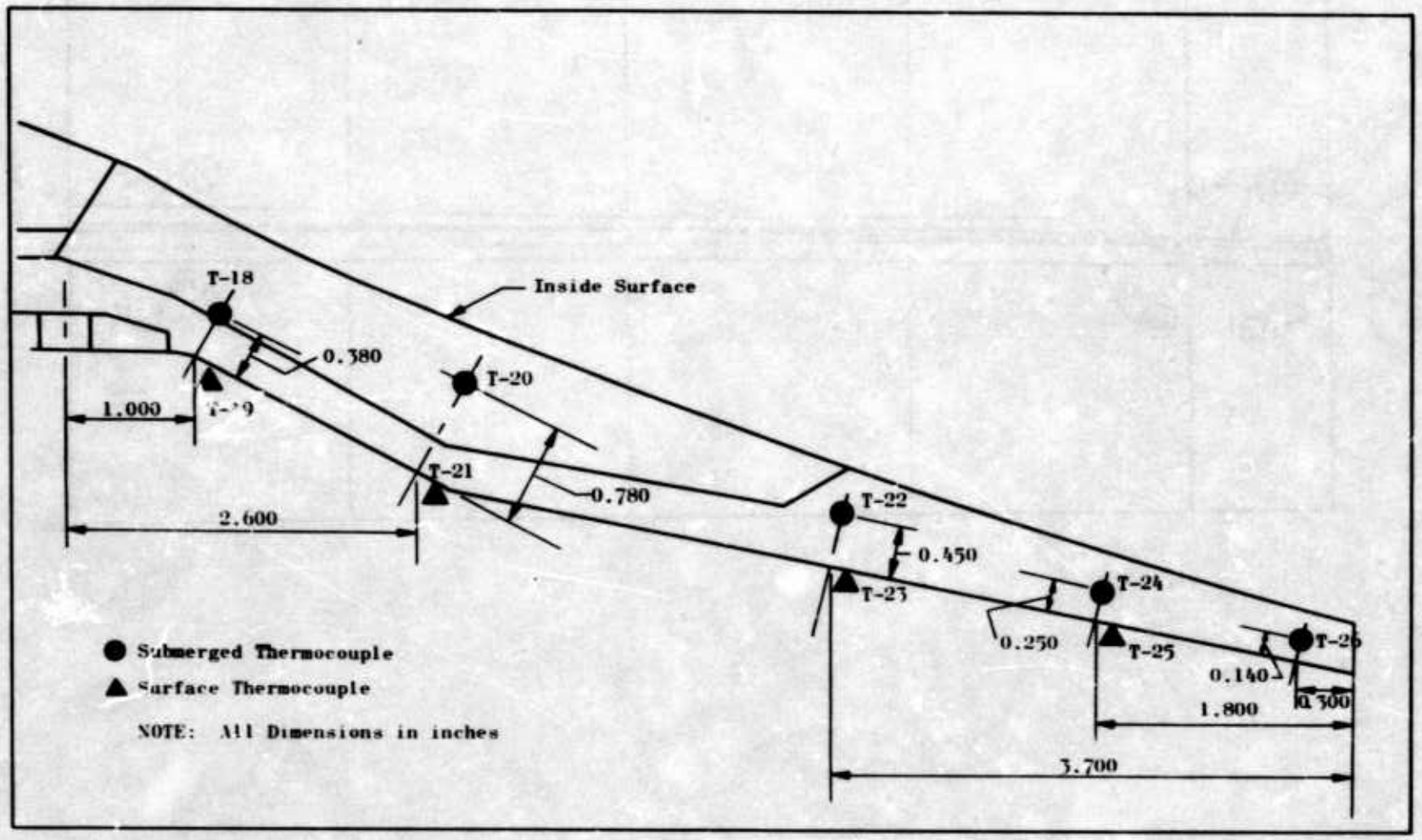


Figure 144. Location of Thermocouples on Motor A-1002 Nozzle Exit Cone

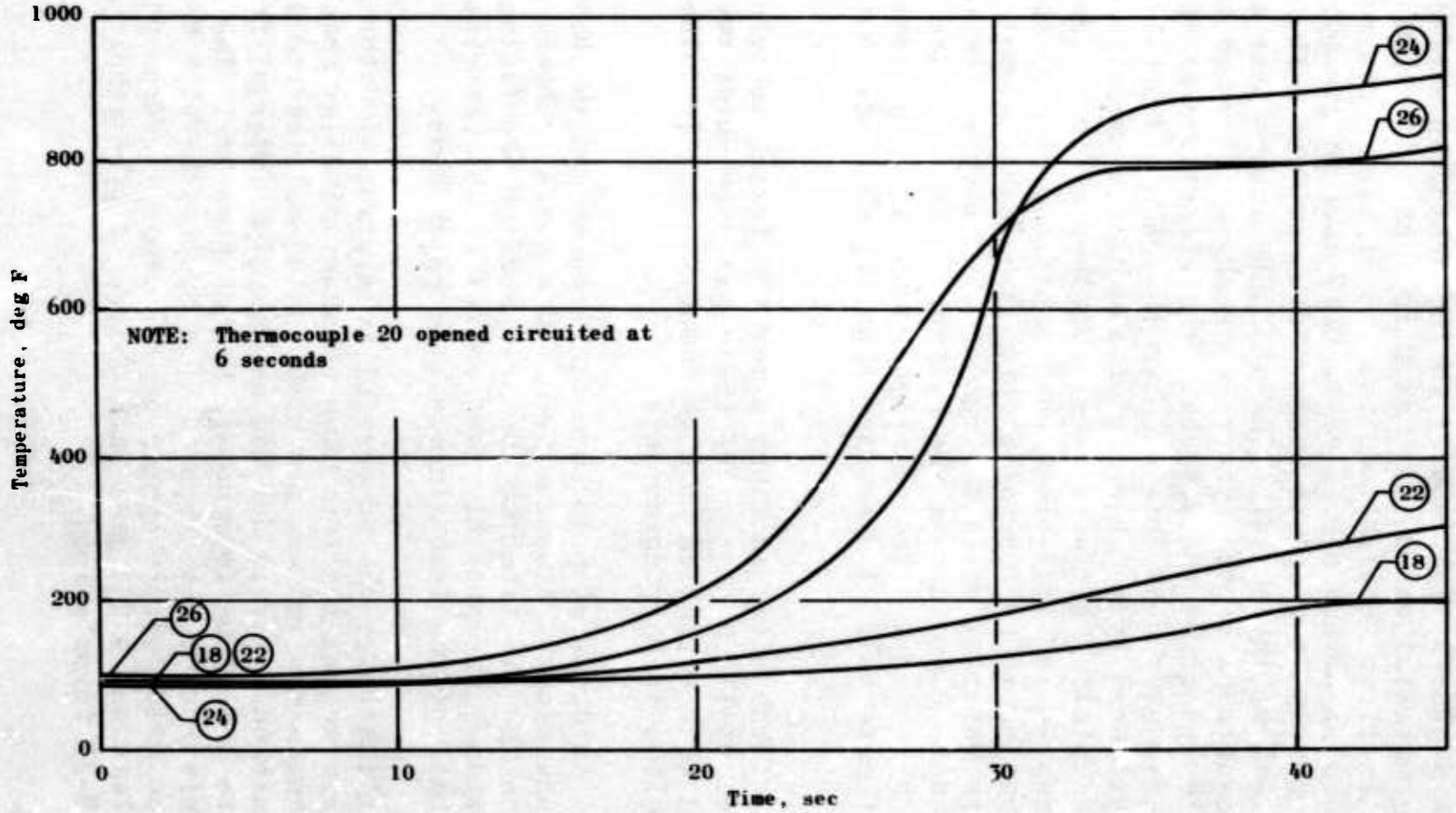


Figure 145. Temperature vs Time from Thermocouples Embedded Motor A-1002 Nozzle Exit Cone

The most severe losses of material in the nozzle occurred in the nozzle entrance region, see Fig. 146, where the graphite phenolic FM5128 lost 0.55 inch measured parallel to the nozzle axis and had a maximum loss of 0.44 inch measured right angles to the contoured surface. The char depth of the material was uniform at 0.10 inch. The AHDG (high density graphite by American Metals Products) insert lost a maximum of 0.40 inch at its forward point and decreased to 0.17 inch at the pyrolytic graphite rings. The pyrolytic graphite rings performed very well, allowing only 0.026 inch loss at the throat. The aft AHDG insert lost a maximum of 0.09 inch downstream of the pyrolytic graphite rings and then decreased to negligible losses at the aft end. The effectiveness of the pyrolytic graphite sleeve as a heat shield under the AHDG and pyrolytic graphite rings was evidenced by no charring of the silica phenolic until heat soak after completion of the firing. Farther along the nozzle, the graphite phenolic (FM5128) cloth lost a maximum of 0.05 inch, with losses decreasing to no loss at a point 3.5 inches downstream. The char depth of this material was a maximum of 0.20 inch at the forward end and decreased to 0.18 inch at the aft end. The remaining section of the nozzle, which is constructed of silica phenolic tape, lost a maximum of 0.20 inch of material. The average char depth of this material was 0.12 inch.

Examination of the aft load rings after the firing revealed that six of the nine were still in place. Of these six, the outer two were undamaged but had been subjected to high temperature. The other four load rings had melted in varying amounts.

There was no evidence of premature ignition around the base of the six remaining load rings. Aluminum wire and a black, rubbery substance was found between the six titanium load rings after the firing. This rubbery substance was probably the remains of the restrictor used to ensure the seal of the load rings to the polar boss.

(C) Figure 147 illustrates the successful initiation of Motor A-1002 with the flightweight igniter. The contractual delay requirement of 100 milliseconds maximum was met with the 95-millisecond delay on A-1002. Ignition delay is defined as the time interval from initiator activation to 10% of maximum motor chamber pressure. The ignition train for this firing was composed of a McCormick-Selph M-55 Mod IX initiator, an intermediate charge of 1.7 grams of boron-potassium nitrate pellets and a 254 gram main charge of pyrotechnic grains (per Rocketdyne P-73 formulation).

TABLE 3-1

ROCKETDYNE GAS GENERATORS

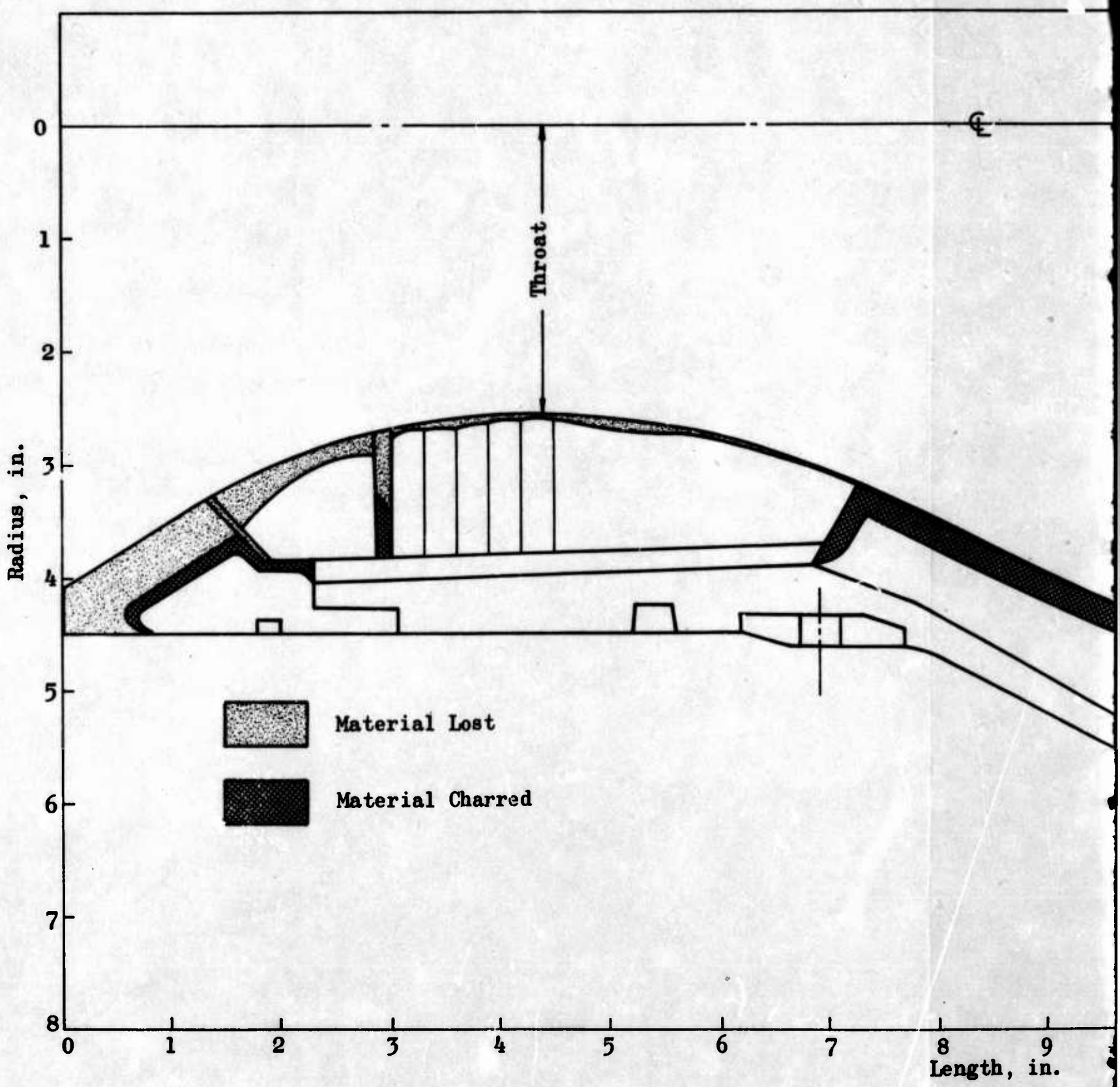


TABLE 3-1

TDYNE GAS GENERATORS

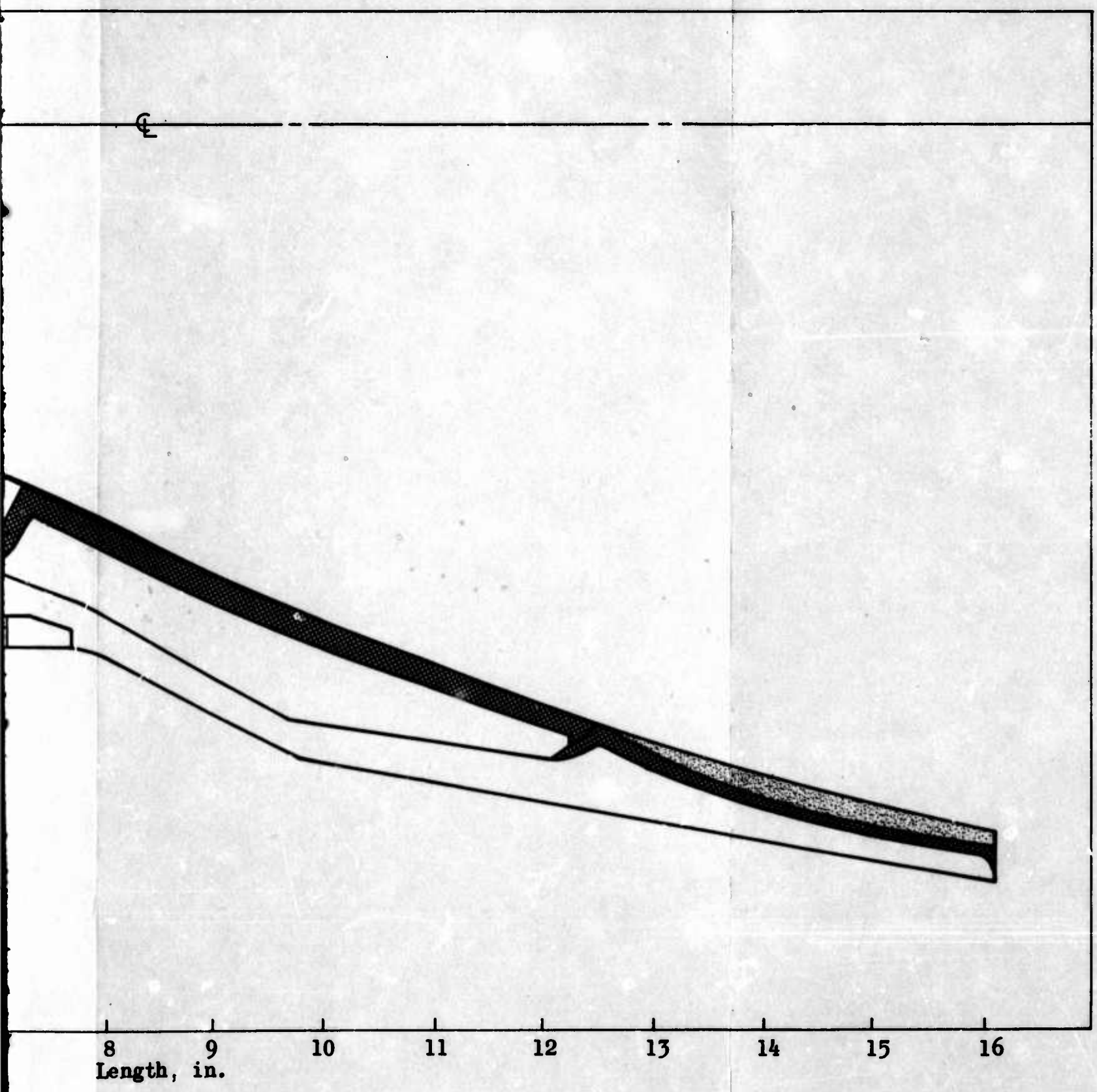


Figure 146. Nozzle Materials Losses and Char Depths after Firing, A-1002

CONFIDENTIAL

PREVIOUS PAGE WAS BLANK, THEREFORE WAS NOT FILMED

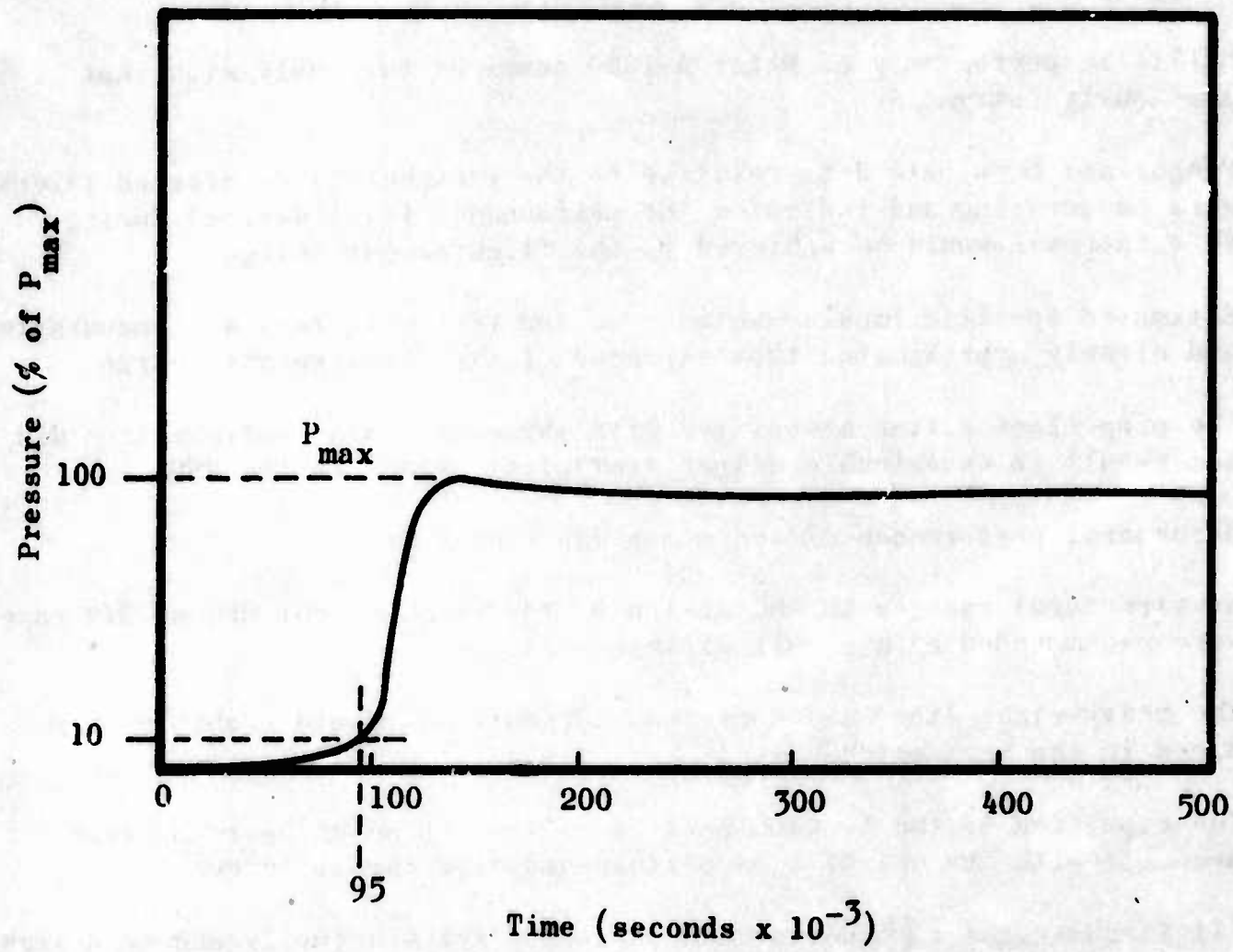


Figure 147. Ignition Transient for Motor A-1002, Utilizing Igniter P/N 802476

(2) Conclusions and Recommendations

The following conclusions were reached, based on the results of the analysis.

Ballistic performance of Motor A-1002 compared favorably with that previously estimated.

Propellant burn rate data relative to the peripheral, reinforced layers were encouraging and indicated the performance level desired during this interval would be achieved in the flightweight design.

Estimated specific impulse which resulted from this test was encouraging and closely approximated that expected of the flightweight design.

The propellant sliver associated with the core grain configuration did not result in undesirable sliver (tailoff impulse) in the RFG.

Structural performance of the motor was excellent.

No structural changes in the design of the flightweight RFG or GFW case were recommended as a result of this test.

The heavyweight liner was more than adequate and could probably be reduced in the next motor.

The expulsion of the forward section of the aft polar boss was less probable with the use of a monolithic-graphite throat insert.

All flightweight components used performed satisfactorily and no design change was anticipated.

The flightweight nozzle should perform satisfactorily, based on the losses and char depth of the heavyweight nozzle. No changes in design of the flightweight nozzle were foreseen.

The use of titanium load rings did not promote premature ignition of propellant.

The expulsion of load rings through the nozzle was improbable, since all post firing evidence indicated the rings were melted in place.

A more effective medium for quenching the motor after firing, such as water, should be considered since the CO_2 failed to adequately quench motor A-1002 after firing.

Motor burning rates of the core and RFG were very close to design nominal. However, the core burning rate and two of the RFG burning rates should be changed for the next motor to bring the pressure closer to nominal requirements.

(C) Because core pressure was more neutral than expected, the average pressure should be raised from 750 psia to 775 psia.

4. DEVELOPMENT MOTOR A-1003

Motor A-1003, the third Motor A for static firing, was fabricated during the period of 14 June to 29 July 1964 and statistically fired on 30 July 1964. Principal components were reinforced grain RG-1203, glass filament case A-1403,and core A-1603.

A fix was designed for A-1003 to prevent recurrence of the propellant separation around the aft ballistic sleeve. A doubler of glass cloth impregnated with R-140 restrictor was bonded between the plastic sleeve and core propellant, Fig. 148. A tapered thickness (0.25 max) of R-142 restrictor was applied to the doubler's outer surface. The aft polar boss, of which the ballistic sleeve is a part, was prepared in advance and installed in the winding mandrel. The doubler and ballistic sleeve was protected during washout by polyethylene and tape.

Another change from A-1002 was a reduction in RDS-514 propellant burning rates in the second and third winding cycles. This results in a viscosity increase in this propellant and an increased layer thickness in this region.

The GFW Case for A-1003 realized further reduction in thickness and strength as compared to A-1002.

(C) Insulation thickness was also reduced to a thickness of 0.14 inch from 0.284 on A-1002 which resulted in an RFG web of 3.71 inches compared to a 3.82-inch target for the flightweight motor.

In addition to the scheduled increase in A-1003 RFG web and weight over that in A-1002, the following changes were incorporated into the ballistic design: (1) the core burning rate was increased by 4%; (2) design propellant weight of the core grain is 1.3 pounds less than the core of A-1002 because of the expansion joint added to the aft polar boss; and (3) RFG burning rates were decreased in the second and third helical layers. Estimated performance for A-1003 reflecting these changes and other characteristics demonstrated by the previous test is shown in Table XLVIII and Fig. 149. A summary of component weights is shown in Table XLIX. Performance estimates for the flightweight design have been updated to reflect changes resulting from A-1002 test, and are included in the tables and figures for comparison.

CONFIDENTIAL

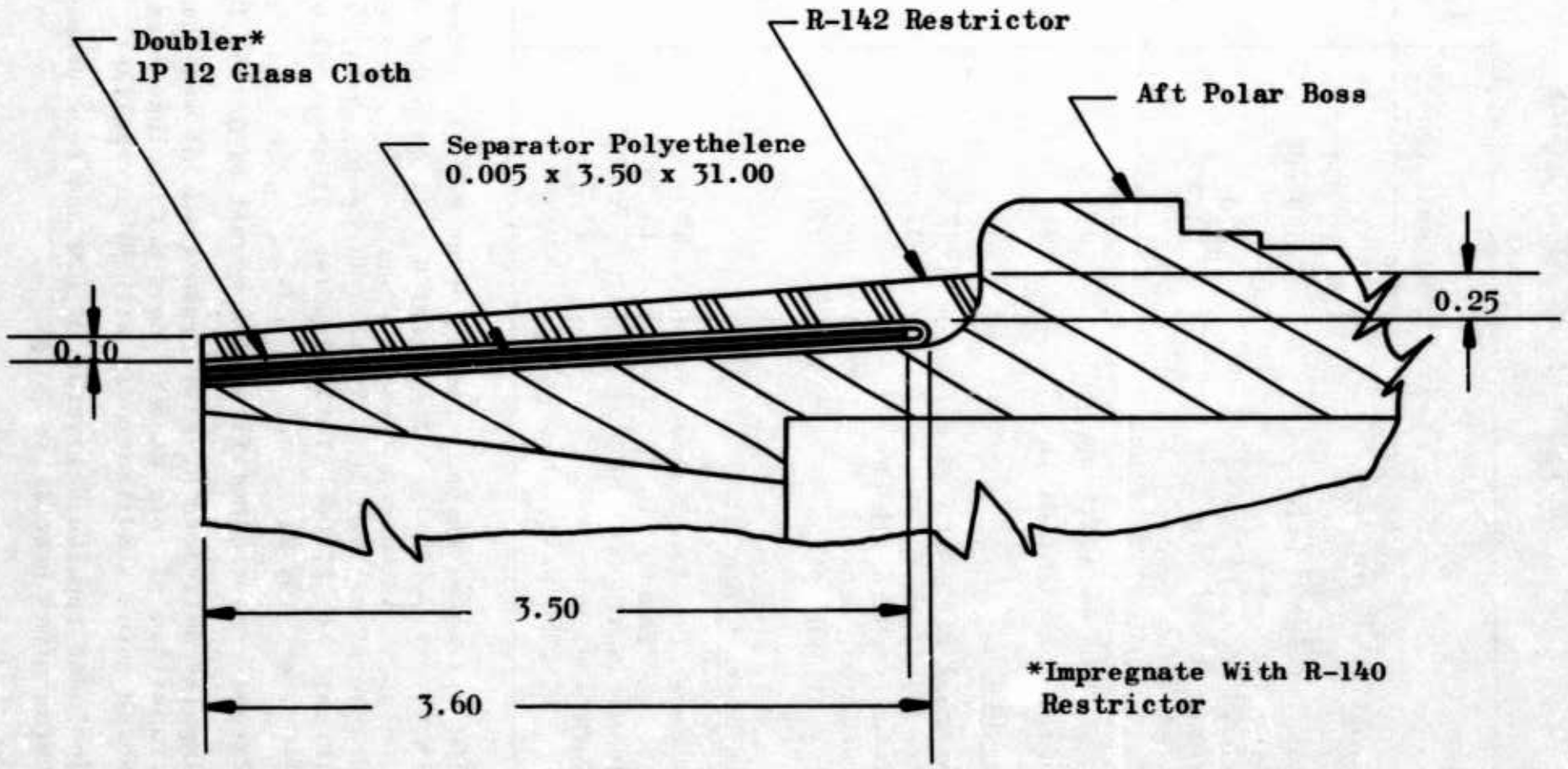


Figure 148. Doubler for A-1003

CONFIDENTIAL

(C)

TABLE XLVIII

ESTIMATED PERFORMANCE SUMMARY MOTOR

A-1003 AND FLIGHTWEIGHT DESIGN

	Motor A-1003(1)	Flightweight Design(2)
Average Pressure, psia	570	565
Average Thrust, lb	17,200	17,040
Total Impulse, lb-sec	549,000	560,700
Action Time, sec	31.9	32.9
Maximum Pressure, psia	800	800
Maximum Thrust, lb	24,800	24,800
I_{sp} at Motor Conditions, lb-sec/lb	226.5	225.9
I_{sp} at 1000 psia, lb-sec/lb	241.5	241.1
Impulse-to-Weight Ratio	212.3	216.3
Core Grain		
Average Pressure, psia	775	775
Average Thrust, lb	23,980	23,980
Total Impulse, lb-sec(3)	225,000	225,000
Duration, sec	9.4	9.4
I_{sp} at 1000 psia, lb-sec/lb	250	250
Reinforced Grain		
Average Pressure, psia	485	480
Average Thrust, lb	14,390	14,280
Total Impulse, lb-sec(4)	324,000	335,700
Duration, sec	22.5	23.5
I_{sp} at 1000 psia, lb-sec/lb	234.0	233.6

(C)

(1) The estimates shown account for no nozzle erosion; however, it is estimated that the erosion will be 0.065 inch (on radius). Average performance for A-1003 allowing for this degree of erosion is: Average Pressure, psia, 555; Average Thrust, lb, 17,000; Total Impulse, lb-sec, 547,600; Action Time, sec, 32.2.

(2) Parameters were modified as a result of A-1006 firing.

(3) Impulse delivered by core grain from 10% maximum pressure to transition of core to RFG; does not include core propellant which burns simultaneously with RFG propellant.

(4) Includes impulse delivered by RFG and core propellant which burns after transition point.

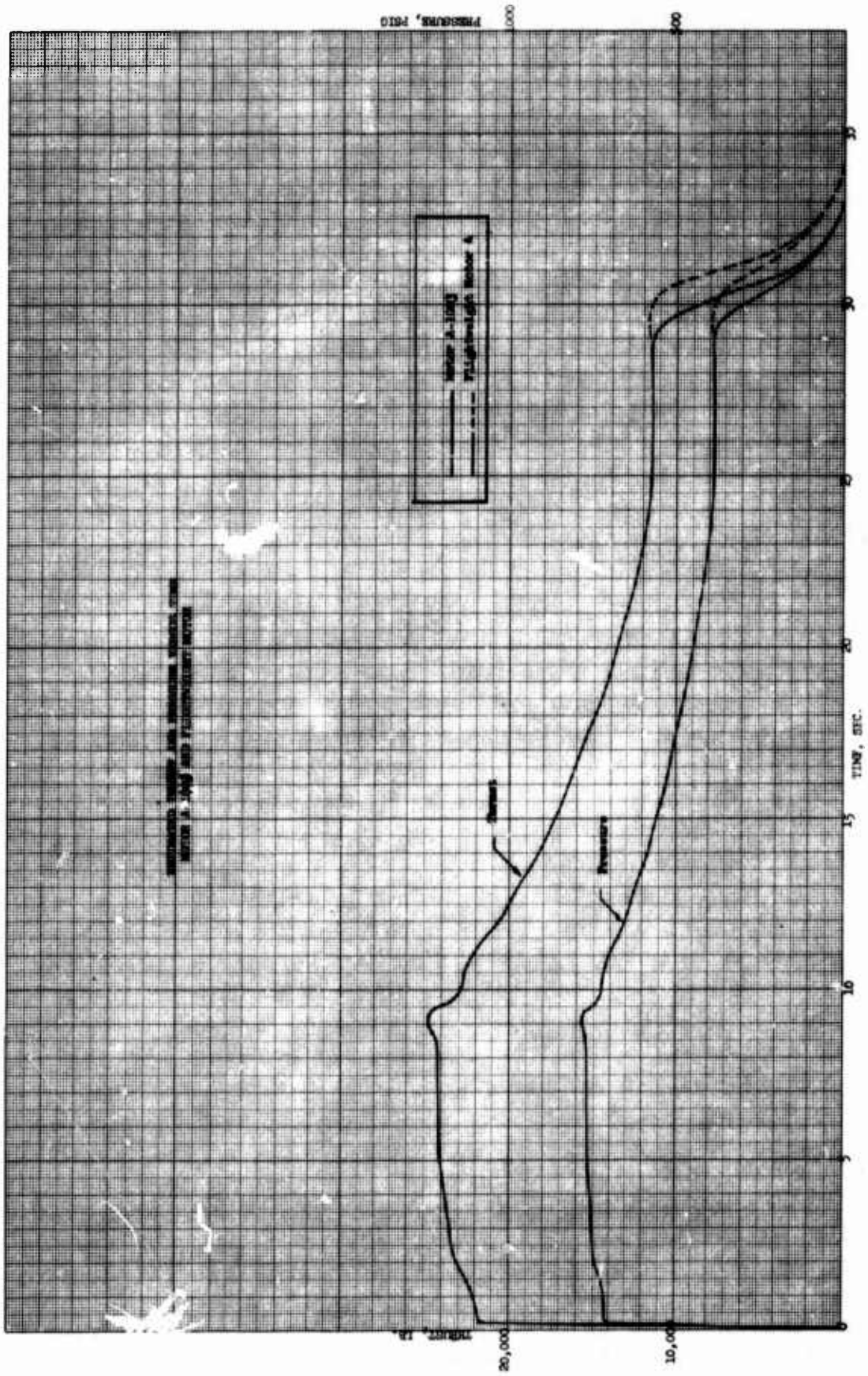


Figure 149. Estimated Thrust and Pressure vs Time for Motor A-1003 and Flightweight Design

(C)

TABLE XLIX

ESTIMATED WEIGHT AND MASS FRACTION MOTOR

A-1003 AND FLIGHTWEIGHT DESIGN*

	Motor A-1003	Flightweight Design
Nozzle Assembly	29.80	26.77
Case	48.00	34.00
Liner	47.30	12.00
Igniter Assembly	3.08	3.08
Forward Boss	10.52	10.52
Aft Boss	13.99	13.99
Load Rings	6.94	6.94
Drive Pins	0.56	0.56
O-rings	0.10	0.10
Flange	1.91	1.91
Total Inerts	162.20	109.87
Core Propellant	1133.00	1133.00
RFG Propellant	1291.00	1349.00
Total Propellant	2424.00	2482.00
Total Motor Weight	2586.20	2591.87
Mass Fraction	0.937	0.958

*All weights are in pounds

(C) Differences noted in previous and current estimates for the flightweight motor are the result primarily of (1) specific impulse (I_{sp} at 1000 psia) associated with the RFG and (2) average pressure over the core duration. Estimate of specific impulse was decreased to reflect the above changes in RFG burning rates. Based on the neutral pressure-time exhibited by A-1002, the design value of average pressure was increased from 750 to 775 psia. Distribution of impulse over core and RFG burning intervals reflects characteristics of A-1002 performance.

a. Fabrication

(1) Equipment

The grain was wound on the 36-inch machine, using the spreader blade, manual propellant application, and electric wire tension system. A mold sand PVA mandrel was used to wind the grain. Mandrel preparation was the same as used on A-1002.

(2) Materials

The standard 5% elongation, 50,000 psi tensile, 5056 aluminum wire was used.

The polar bosses and load rings for A-1003 were of flightweight design and were fabricated to the same specifications as for A-1002, except for the doubler on the aft boss insulation sleeve. A tapered thickness (maximum 0.25 inch nearest aft end of motor) of R-142 restrictor was applied to the doubler's outer surface. The doubler and sleeve were protected during mandrel assembly and later washout of the soluble mandrel by polyethylene sheeting, RTV rubber, and tape.

The forward closure assembly and aft glass case flange were flightweight as opposed to the special designs used in A-1001 and A-1002.

The nozzle for A-1003 was the same as A-1002 except for the graphite insert. The insert for the A-1003 nozzle was solid Graph-I-Tite "G" whereas the insert for A-1002 was made of AHDG graphite and contained five pyrolytic graphite rings in the throat area.

(3) Processing

(a) Grain Winding and Restriction

Winding was started 15 June and completed 21 June 1964. Preparation for this unit differed from the preceding grain in that the first load ring of each boss was bonded to the boss with EC-1648 adhesive and metal spacers were inserted between the bosses and sand mandrel to position the bosses more positively.

After winding the first GI and part of the intermediate layers the aft boss was observed to be slightly canted. An indicator gage placed near the end of the boss disclosed a 0.140-inch eccentricity; the forward boss, 0.010 inch. The grain was unwound and additional shims installed behind the aft boss to realign it. Winding was restarted after a delay of nearly three shifts. Throughout grain winding, the concentricity of the aft boss was checked before and after geodesic layers.

Layer construction of the reinforced grain for A-1003 varied slightly from previous grains due to lowered propellant burning rates (increased depressant levels) in the second and third cycles. Propellants used are described in Table L, which shows RFG construction by propellant layers.

(C) Table LI shows RFG construction by wire layers. Total number of covers was 233 compared to 231 predicted. Average cylindrical cover thickness was 0.0157 inch. Average grain ID was 22.058 inches and average OD was 29.359 inches for an average web thickness of 3.651 inches.

(C) Total propellant weight of the reinforced grain was 1310.3 pounds, of which 229.8 pounds was aluminum wire, resulting in a satisfactory aluminum content of 17.5% by weight.

The "wipe-on" primer coat of R-143 was applied 29 June and cured 16 hours. The buildup layer was applied and cured 24 hours. The finishing coat applied 2 July received a 48-hour cure at 170 F.

The total three stage restrictor layer between the RFG and glass case weighed 52.7 pounds and had the following dimensions:

(C)

	Cylindrical Thickness, in.	Outside Diameter, in.
Forward	0.208	29.760
Center	0.184	29.730
Aft	0.165	29.700
Over-all Avg	0.186	29.730
Cylinder Length	49.07 in.	

TABLE L

CONSTRUCTION OF MOTOR A-1003, BY PROPELLANT LAYERS

Cycle	P_b, psia	Matrix Propellant	Depressant Level, %	Burning Rates at P_b				Web Thickness, in.
				Liquid Strand		Motor		
				Design	Actual	Design	Actual	
1	735	RDS-514	0.5	0.260	0.249	0.305	0.293	0.419
2	670	RDS-514	1.1	0.220	0.219	0.258	0.257	0.416
3	600	RDS-514	2.5	0.179	0.171	0.210	0.201	0.403
4	540	RDS-523	2.6	0.170	0.169	0.200	0.199	0.514
5	470	RDS-523	5.5	0.145	0.139	0.170	0.163	0.489
6,7,8,9	400	RDS-523	6.0	0.132	0.128	0.155	0.150	1.340
								3.651

CONFIDENTIAL

CONFIDENTIAL

TABLE LI

CONSTRUCTION OF MOTOR A-1003, BY WIRE LAYERS

Layer Designation	Dwg Det 802139	No. Covers		OD Average, in.	Layer Thickness, Average, in.	Cover Thickness, Average for Layer, in.	Cover Thickness, Average for Cycle, in.
		Predicted	Actual				
Mandrel				22.058			
1-GI	-99	7	7	22.333	0.138	0.0197	
1-43	-103	7	7	22.550	0.109	0.0156	
1-54	-105	8	7	22.742	0.096	0.0137	
1-66	-107	6	6	22.895	0.077	0.0128	0.0155
2-GI	-109	7	7	23.115	0.110	0.0157	
2-43	-113	4	4	23.230	0.078	0.0195	
2-54	-115	5	5	23.383	0.077	0.0154	
2-66	-117	8	8	23.600	0.109	0.0136	
2-80	-119	8	9	23.868	0.134	0.0149	0.0148
3-GI	-123	7	7	24.083	0.108	0.0154	
3-35	-125	6	5	24.307	0.112	0.0224	
3-45	-127	8	4	24.413	0.053	0.0133	
3-60	-129	10	10	24.673	0.130	0.0130	0.0155
4-GI	-133	7	7	24.893	0.110	0.0157	
4-30	-135	4	2	24.960	0.034	0.0170	
4-40	-137	4	3	25.043	0.042	0.0140	
4-50	-139	6	6	25.212	0.085	0.0142	
4-65	-143	7	7	25.412	0.100	0.0143	
4-80	-199	6	9	25.701	0.145	0.0161	0.0151
5-GI	-145	7	7	25.915	0.107	0.0153	
5-30	-147	6	3	26.009	0.047	0.0157	
5-38	-149	6	6	26.193	0.092	0.0153	
5-47	-153	6	6	26.390	0.099	0.0165	
5-60	-155	6	6	26.611	0.111	0.0185	
5-80		0	2	26.679	0.034	0.0170	0.0163
6-GI	-157	6	6	26.895	0.108	0.0180	
6-26	-159	3	3	26.984	0.045	0.0150	
6-32	-163	4	2	27.032	0.024	0.0120	
6-40	-165	5	4	27.145	0.057	0.0143	
6-56	-167	9	8	27.390	0.123	0.0154	
6-80		0	7	27.635	0.123	0.0176	0.0160
7-GI	-169	6	6	27.892	0.129	0.0215	
7-32	-173	3	2	28.112	0.110	0.0157	
7-46	-175	3	5				
7-67	-177	7	9	28.349	0.119	0.0132	
7-80	-179	10	6	28.600	0.126	0.0210	0.0173
8-GI	-183	5	5	28.794	0.097	0.0194	
8-29	-185	3	3	28.867	0.037	0.0123	
8-38	-187	2	3	28.949	0.041	0.0137	
8-51	-189	2	2	29.011	0.031	0.0155	
8-63	-193	2	7	29.201	0.095	0.0136	0.0151
9-GI	-195	5	5	29.383*	0.091	0.0182	0.0182
		231	233		Over-all Average	0.0157	

*Before Grain Was Cured And Surface Scraped.

(b) GFW Case

(C) The GFW case for A-1003 was a heavyweight case designed for 1000 psi. The helical wrap had a glass density of 965 ends per inch and was wound in two covers. The circ wrap of 1837 ends per inch was wound in eight covers. The wall thickness in the cylinder was approximately 0.122 inch and skirt-to-skirt length was 59.05 inches. Pertinent weights of the case assembly are shown below:

Component	Weight, lb
Roving, S-994, 12 end	34.0
Glass Cloth, 143 reversed	4.0
Resin, DER 332 w/8 phr, EMI	9.9
Case Weight	47.9
Skirt Transition Fill	5.4
Skirt Rings and Bolts	34.7
Aft End Glass Case Flange	2.1
Case Assembly Weight	90.1

Resin content was the lowest obtained to date and approched the desired 20% level:

$$\text{Resin Content} = \frac{9.9}{47.9} \times 100 = 20.7 \text{ wt } \%$$

The glass case, A-1403, was wound on 6 and 7 July using the 40-inch winding machine in Cell 1, F-617. Processing times, beginning with a restart which followed accidental wetting of the case with water and a machine failure, were as follows:

Helix Wrap	7.0 hr
Skirt Tooling Installation	4.0 hr
Circ Wrap	5.5 hr
Excess Resin Removal	1.5 hr
	18.0 hr

Excess resin removal was accomplished by wrapping the case with three layers of glass bleeder cloth and one cover of circ winding under high tension, then removing the roving and cloth after 15 minutes in a 170 F oven.

The case was cured for 20 hours at 170 F. Appearance of the case was the best obtained to date.

Following GFW case winding, the soluble mandrel was washed out and the mandrel liner removed without incident. The interior surface of the grain was clean, dry, and in good condition. Dimensions obtained before and after washout indicate a decrease in boss-to-boss length of 0.111 inch and a decrease in diameter of 0.047 after mandrel removal.

The unit was X-rayed after mandrel removal and prepared for core casting. No abnormalities were detected by nondestructive test methods.

(4) Postwinding Procedures

During assembly of core casting tooling, several problems were encountered. A misfit between the aft boss and the aft boss plug of the core tooling caused separation of the aft phenolic (MX-2646) insulation sleeve from the boss assembly. The inside diameter was found to be undersized, the cause of which later was traced to postcure shrinkage of the MX-2646 plastic. The insulation sleeve was rebonded with EC-1648 and hand-sanded to size.

When the core tooling was reassembled it was found that the distance from the conicyl to the forward boss was undersized indicating a mismatch in mandrel parts or a change in boss-to-boss length.

During attempts to determine the cause of the dimension obtained on the core mandrel, it was found that the forward polar boss was loose and displaced inward. The boss was moved into the grain to facilitate cleaning of the surfaces of the grain and the boss, and preparation for subsequent reinstallation of the boss in the grain.

Inside diameter measurements taken of the load rings and the adjacent wound grain indicated an interference fit at the grain surfaces would exist when the boss was reinserted. Consequently wire and propellant were removed (as well as safety considerations would permit) to allow reinstallation.

When the cleaned boss was inserted into the dome in a dry run it "bottomed-out" against the glass case without the boss seating against the load rings. The boss was removed and the glass case interior surface was cleaned to allow the boss to be pulled back as far as possible. R-140 restrictor was then spread over the surfaces of both the boss and the grain adjacent to it. The boss was manually inserted and forced against the grain or case by use of 30 ft-lb of torque on a 3/8 inch - NF bolt. This load was held during cure.

Measurements taken after cure indicated that the boss lacked approximately 0.150 inch of seating against the load rings. Sufficient R-140 was applied to fill the space between the boss steps.

(C) The core casting mandrel was reassembled in the grain and the core cast, using four mixes of RDS-526. Properties of the four mixes are shown below in the order of their casting into the motor. Total core weight was 1116.6 pounds.

Burning Rate, Liquid Strand, ips	L-7-16-M81	L-7-16-M82	L-7-21-M81	L-7-21-M82
(C) 750 psia (Target 0.438)	0.426	0.426	0.428	0.432
1000 psia	0.484	0.487	0.485	0.494
Mechanical Properties at 77 F				
Elongation, %	38	35	40	34
Tensile, psi	176	173	183	173
Modulus, psi	770	825	741	857
Density, lb/cu in.	0.0636			

When the pit was opened (after 8 hours of curing) to examine and restrict the exposed forward surface of the core grain, the propellant level was found to have dropped to a level varying from 1/2 to 2 inches below the planned level. This was not detrimental except in reducing propellant weight. This cavity was filled with R-140 to the desired level. Following a 72-hour cure period at 170 F the unit was incrementally cooled to ambient.

(5) Final Assembly

Addition of the nozzle and forward closure on 28 and 29 July completed motor fabrication. The aft end heat shield (Seal-Fast and aluminum foil) and miscellaneous instrumentation were also applied during this period.

Component weights are listed in Table LII.

TABLE LII

WEIGHT SUMMARY FOR A-1003

AND FLIGHTWEIGHT DESIGN

	Component Weight, lb		
		Design Nominals	
	A-1003	A-1003	Flightweight Design
Nozzle Assembly	31.10	29.80	26.77
Case	47.90	48.00	34.00
Liner	52.70	47.30	12.00
Igniter	2.58	3.08	3.08
Forward Boss	9.80	10.52	10.52
Aft Boss	14.20	13.99	13.99
Load Rings	7.40	6.94	6.94
Drive Pins	0.54	0.56	0.56
O-rings	0.12	0.10	0.10
Flange	2.10	1.91	1.91
Adhesives	7.00	--	--
Total Inerts	175.44	162.20	109.87
Igniter Combustibles	0.55		
Core Propellant	1116.60	1133.00	1133.00
RFG Propellant	1310.30	1291.00	1349.00
Total Propellant	2427.45	2424.00	2482.00
Total Motor Weight	2602.86	2586.20	2591.87
Mass Fraction*	0.933	0.937	0.958

*Ratio of propellant weight to motor weight.

The boss-to-boss length of A-1003 at various stages in processing is given below. The first figure is given as a range because the measurements were made externally using the dome contour measuring device prior to its rework to remove slack in the bearings. All other measurements were taken through the cavity of the motor using an accurate measuring device.

Stage of Processing	Boss-to-Boss Length, in.
During RFG winding (reference only)	70.7--70.8
After case cure, before mandrel washout, cold	70.705
After mandrel washout, cold	70.594
After potting in and curing dome fillets, hot	70.574
After forward boss reinstallation and cure, before casting, warm	70.429
After core casting and cure, cold	70.375

b. Testing

(C) Motor A-1003 was the second static firing test of a complete Motor A and was the first test which measured thrust, Fig. 150. The motor had a mass fraction of 0.933 (compared to 0.911 for A-1002).

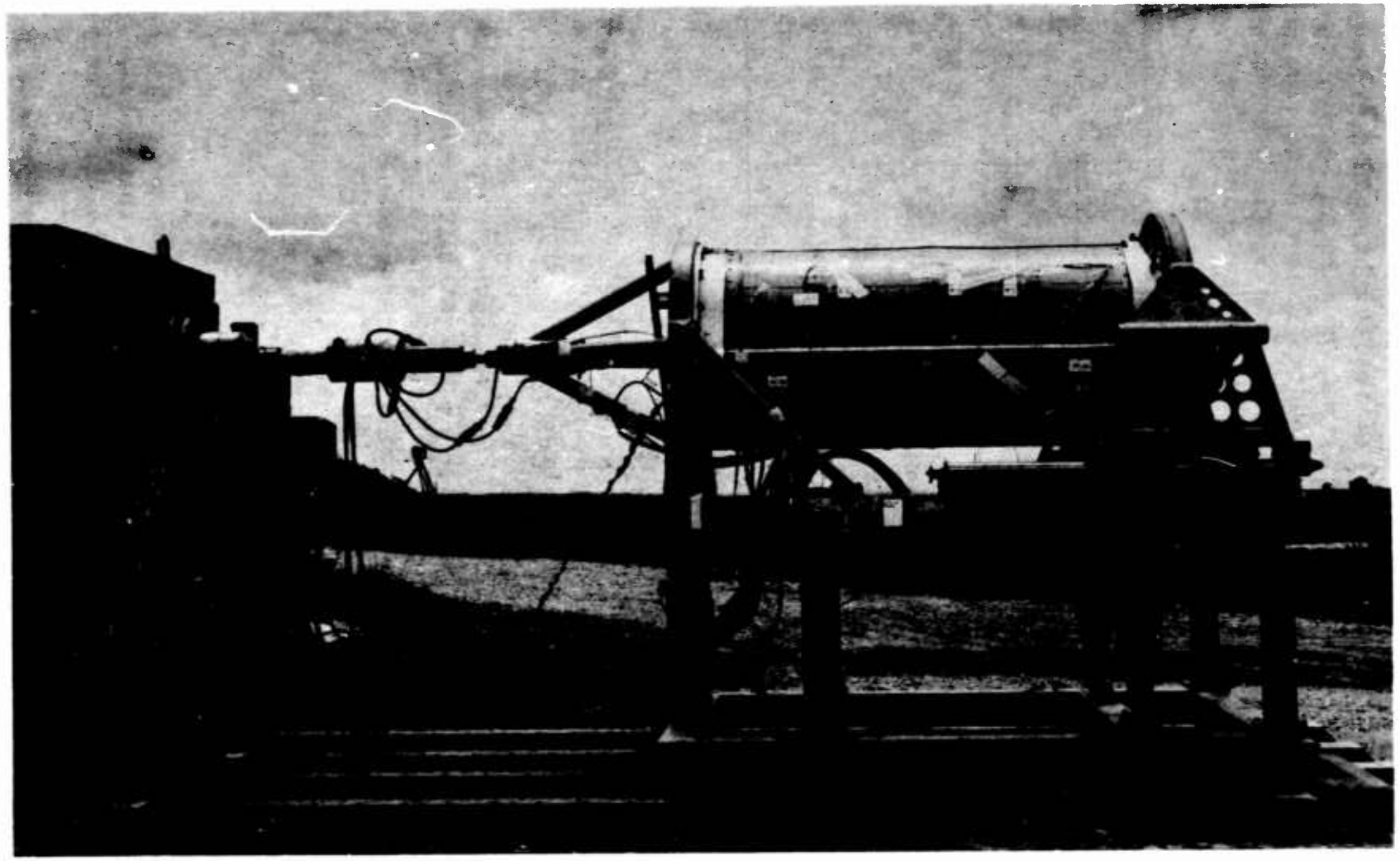
(C) The motor ignited normally, and all data channels recorded properly until the motor pressure reached 1610 psig at 3.388 seconds. At that time the GFW case ruptured on the aft dome, and large pieces of burning propellant as well as inert components were scattered over a wide area.

The most likely modes of failure appeared to be associated with either the forward polar boss and closure, or the doubler on the aft polar boss. In either case, data indicated bond failure between RFG and core grain resulted, causing case overpressurization.

Measured data included two pressure and thrust channels, 24 thermocouples, 24 strain gages, and two linear potentiometers. Thrust-to-pressure relationships during normal operation indicate the design nozzle efficiency of 0.96 would have been achieved.

(1) Analysis

Replots of thrust- and pressure-vs-time for A-1003 and design predictions are shown in Fig. 151.



2YA23-7/30/64M1A

Figure 150. A-1003 on Firing Stand

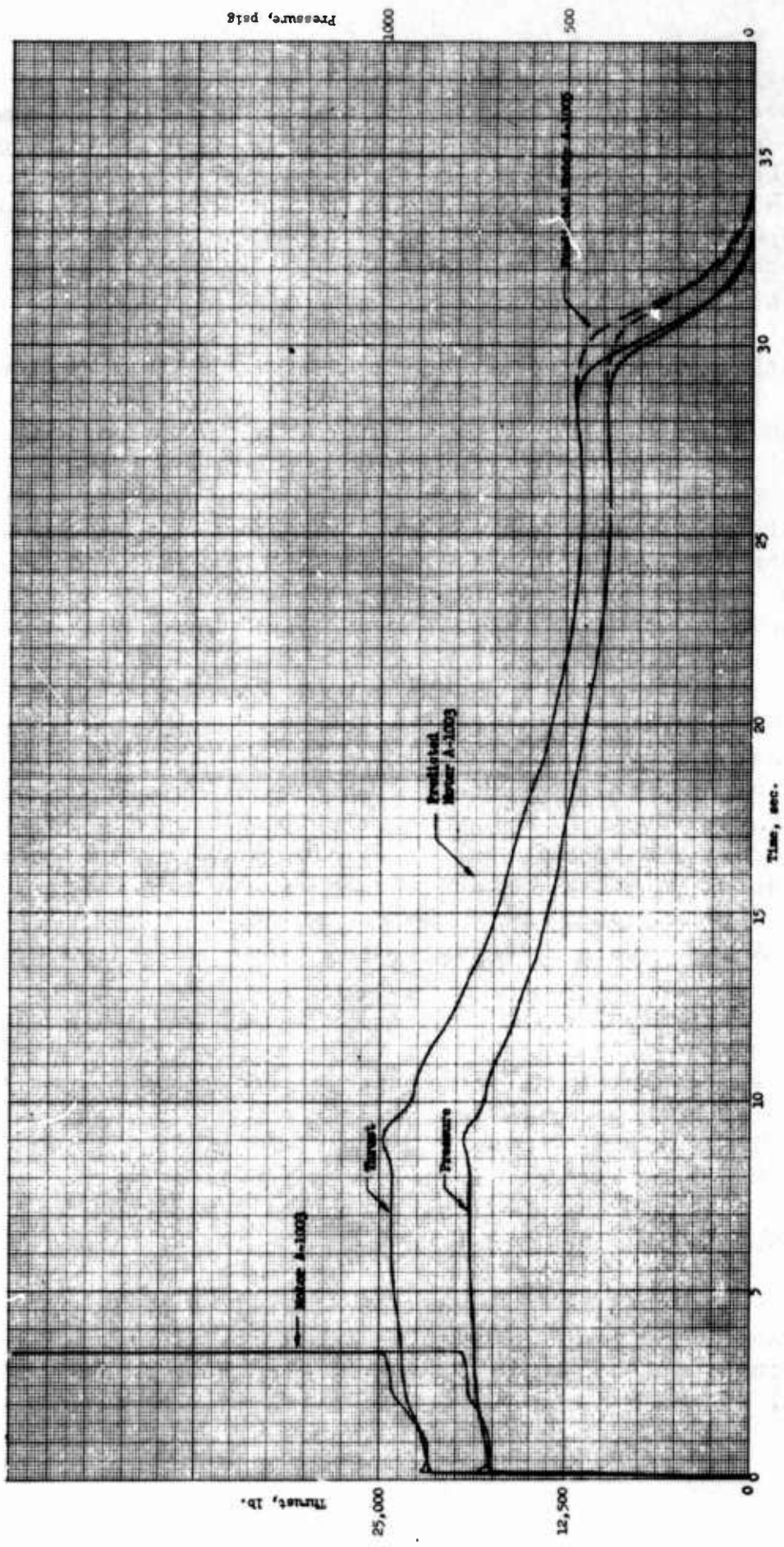


Figure 151. Thrust and Pressure-vs-Time, A-1003

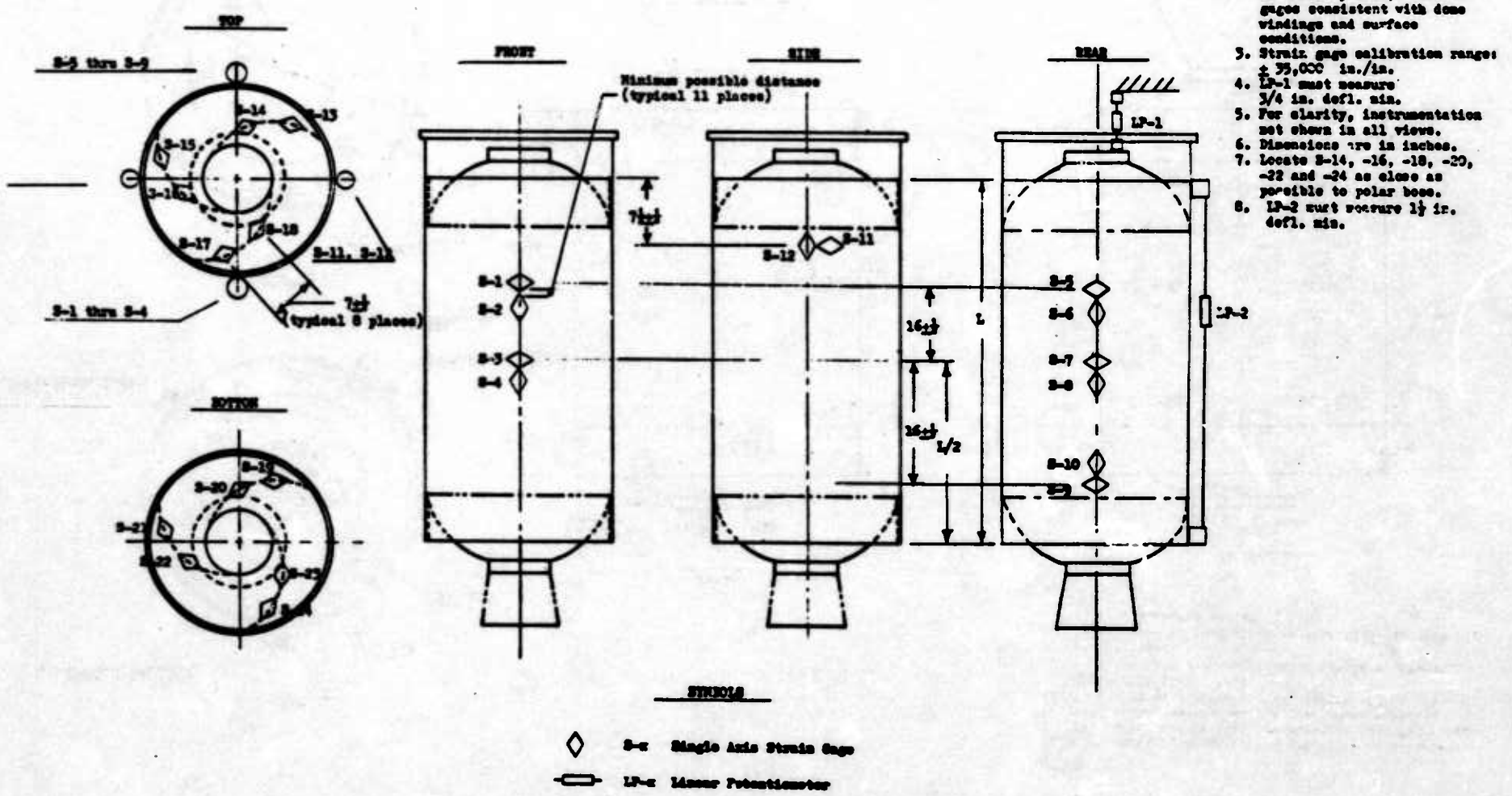
(C) As previously stated, during the first 3.3 seconds of normal operation, the motor performed very close to estimates. It appears from the level of pressure at 3 seconds that the average pressure over the core duration would have been approximately 2.5% greater than estimated, well within the normal band of reproducibility. The design average pressure over the core duration for A-1003 was 775 psia compared to 733 psia average for A-1002. The increase was accomplished by raising the target motor rate by 4% over A-1002.

Characteristics of pressure-time up to time of failure were very similar to A-1002. The only difference was in the initial pressure, which peaked higher than did A-1002. This is attributed to normal variation in flow channel geometry, initial surface, and other variables resulting from manufacturing tolerances. Pressure for both motors progressed for approximately 2 seconds, then operated with neutral pressure-time for the remainder of core duration. The progressive portion correlates with the burning surface geometry which increases until the rounded star-tips burn to a point.

(C) The thrust-to-pressure relationship compared favorably with design nominal. The ratio of actual to theoretical thrust coefficient estimated for design nominal is 0.96. Point-by-point nozzle efficiency for A-1003 was computed for comparison. The average ratio for the first second was 0.94, and the ratio increased to 0.96 at 2.4 seconds. The increase in point values of nozzle efficiency during the early phase of burning is normal, and it appears the average nozzle efficiency of 0.96 would have been achieved. With the design nozzle efficiency, total impulse for A-1003 would essentially coincide with design nominal.

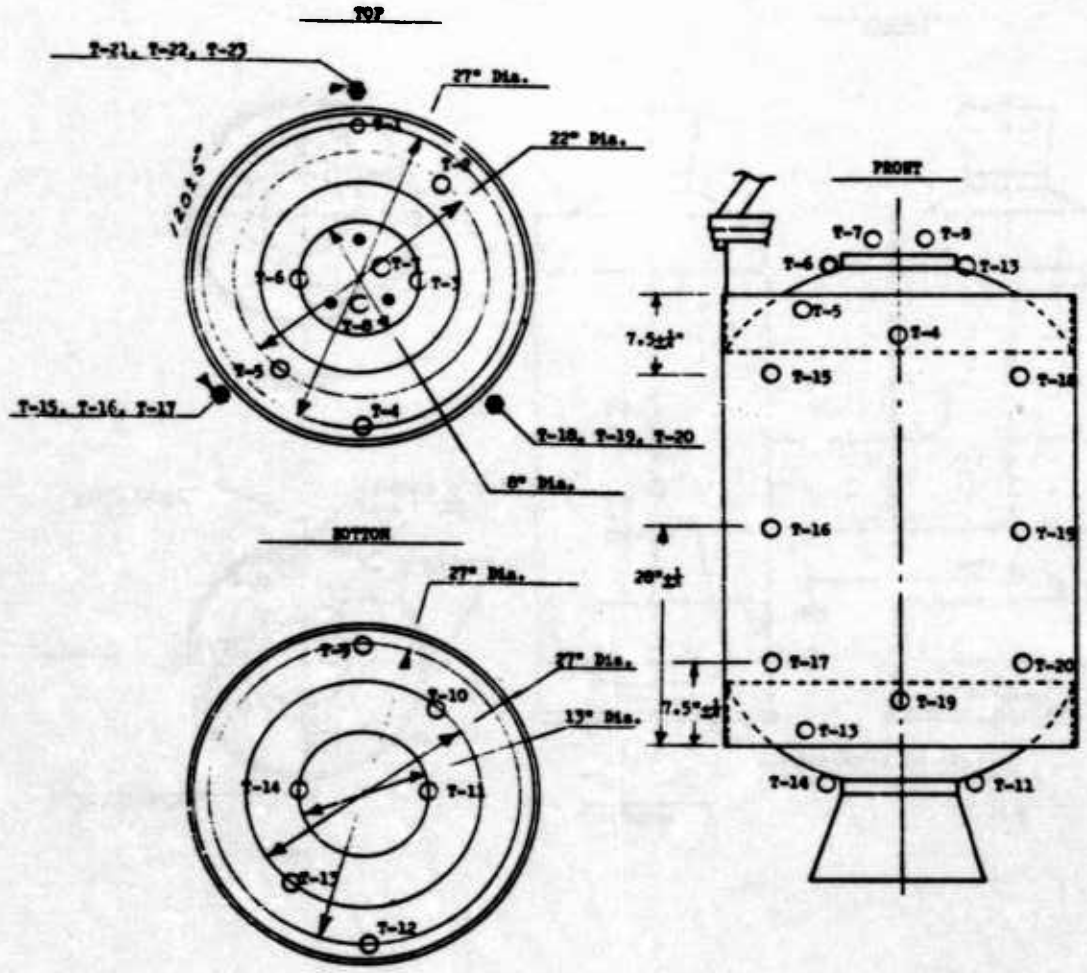
(C) Actual total propellant weight for A-1003 was 2427.5 pounds as compared to 2424.0 design nominal. However, the core was approximately 1.5% less and the RFG approximately 1.5% greater in propellant weight than anticipated. A breakdown of propellant weight and inert component weight is included in Table XXVIII. Mass fraction achieved for A-1003, was 0.933 compared to 0.937 estimated. Target mass fraction for the flightweight design motor is 0.958. Propellant weight of A-1003 was 54.5 pounds less than flightweight design nominal, due to the thicker liner used.

Measured data included two pressure and thrust channels, 24 thermocouples, 24 strain gages, and two linear potentiometers. Thermocouple, strain gage, and linear potentiometer locations are shown in Figs. 152 and 153. Normal and high speed movies of the firing are also available.



NOTES:
1. Do not use Type FA-7 Strain Gage.
2. Locations indicated for LP-1 and LP-2, and S-13 through S-24 are approximate (except as shown by dim.). Locate gages consistent with dome windings and surface conditions.
3. Strain gage calibration range: ± 35,000 in./in.
4. LP-1 must measure 3/4 in. defl. min.
5. For clarity, instrumentation not shown in all views.
6. Dimensions are in inches.
7. Locate S-14, -16, -18, -20, -22 and -24 as close as possible to polar boss.
8. LP-2 must measure 1½ in. defl. min.

Figure 152. Location of Strain Gages and Linear Potentiometers for Motor A-1003



NOTES:

1. For clarity, all gages are not shown on all views.
2. T-7 is located between pressure plug and CO_2 plug.
3. T-8 is located between the two pressure plugs.
4. T-24 will be located on the surface of the aft heat deflection shield.
5. Total of 24 thermocouples will be placed on motor and nozzle.
6. Place motor in test stand so that thermocouples 15, 16 and 17 are on bottom.

Figure 153. Location of Thermocouples for Motor A-1003

GFW case strains and deflection, as shown in Figs. 154 through 159, for the first 3.3 seconds of the firing were very close to expected values and are in good agreement with data from A-1002 except for the forward dome. Strains and deflection of the forward dome were approximately 20 to 30% greater than those measured for A-1002. These strain and displacement values of the GFW case were expected to increase because the forward polar boss after reworking was bearing directly on the GFW case and was still approximately 0.150 inch clear of the load rings in the RFG. The initial axial motion of the boss was resisted primarily by the GFW case and afterwards by the RFG-GFW composite. Maximum strain of the forward dome during the first 3.3 seconds was 6480 microinch/in. which is well below the 30,000 microinch/in. expected strain at rupture. Actually, the 7480 microinch/in. strain occurred at a point very close to the polar boss and, as shown by the other five strain gages, was a highly localized condition. This high value is attributed to some resin surface irregularities on the inside of the GFW case which caused some variation in the liner thickness between the boss and GFW case after the boss was reworked.

Strains in the cylindrical section and aft dome of the GFW case were almost identical to those measured for A-1002. This was expected even though the GFW case for A-1003 was 40% lighter than the case on A-1002. The good agreement is further proof that the RFG supports the major portion of the chamber pressure during core grain burning and the GFW case is not loaded to any appreciable extent until late in the burning of the RFG.

(C) Movies of the firing show ultimate failure of the motor occurred at the aft dome. Strain gages on the aft GFW dome also show a drastic increase in strain at 3.388 seconds which precedes the ultimate failure by 5 milliseconds. This drastic increase in case strain was caused by shear of the RFG in the area of the polar boss at a pressure of 1610 psig. When the RFG sheared, chamber pressure was resisted by the GFW case only which was designed for an ultimate pressure of 1000 psig and rupture occurred. Rupture pressure (1610 psig) was 83% higher than design maximum operating pressure (880 psig) and 37.6% higher than design ultimate pressure (1170 psig).

Presented in Fig. 160 are the thermocouple data obtained during the firing duration. The three thermocouples shown are the only ones of the 24 thermocouples attached to the motor which experienced an increase in temperature.

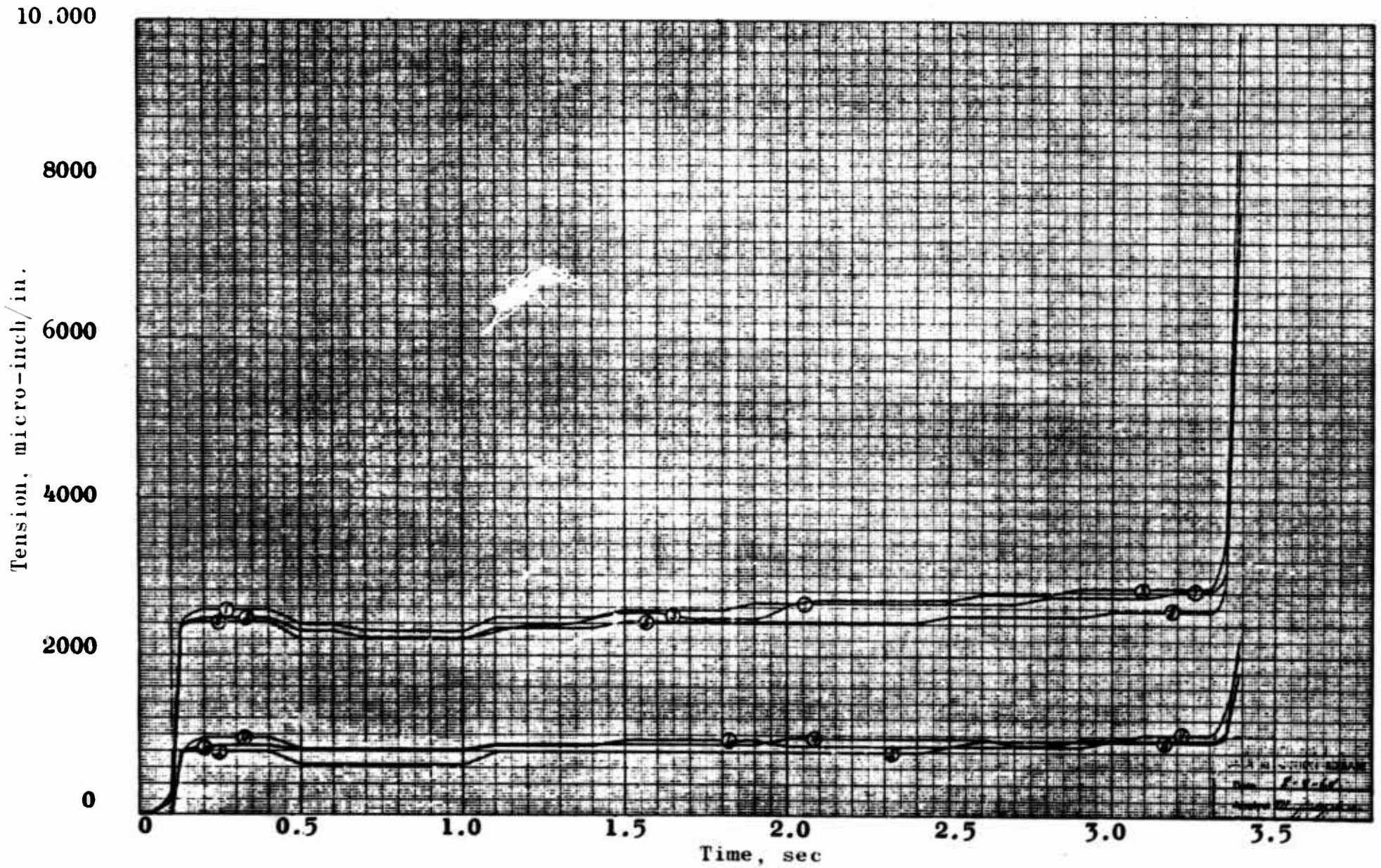


Figure 154. Strain-vs-Time in Cylindrical Section for Strain Gages 1 Through 6 for Motor A-1003

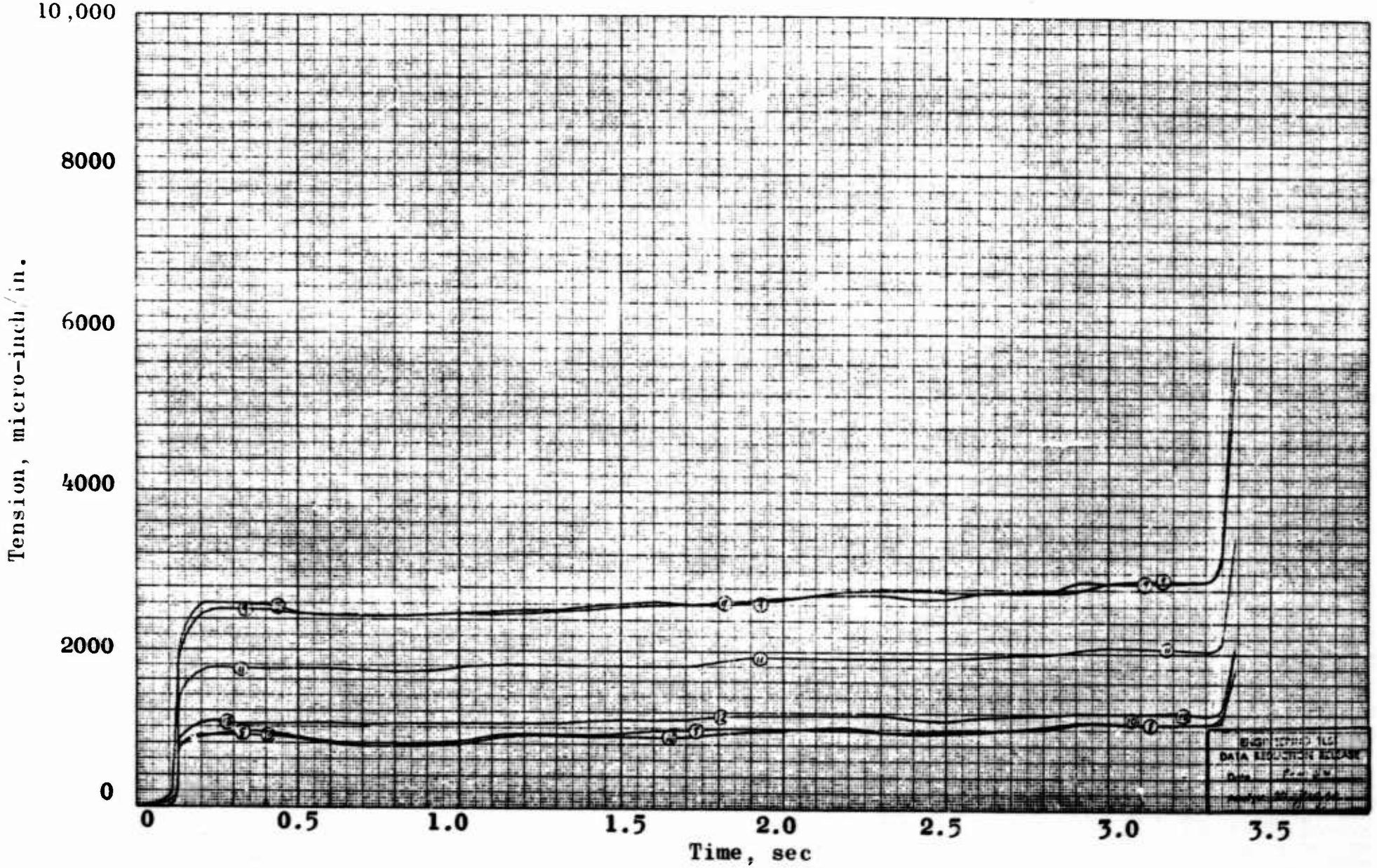


Figure 155. Strain-vs-Time in Cylindrical Section for Strain Gages 7 through 12 for Motor A-1003

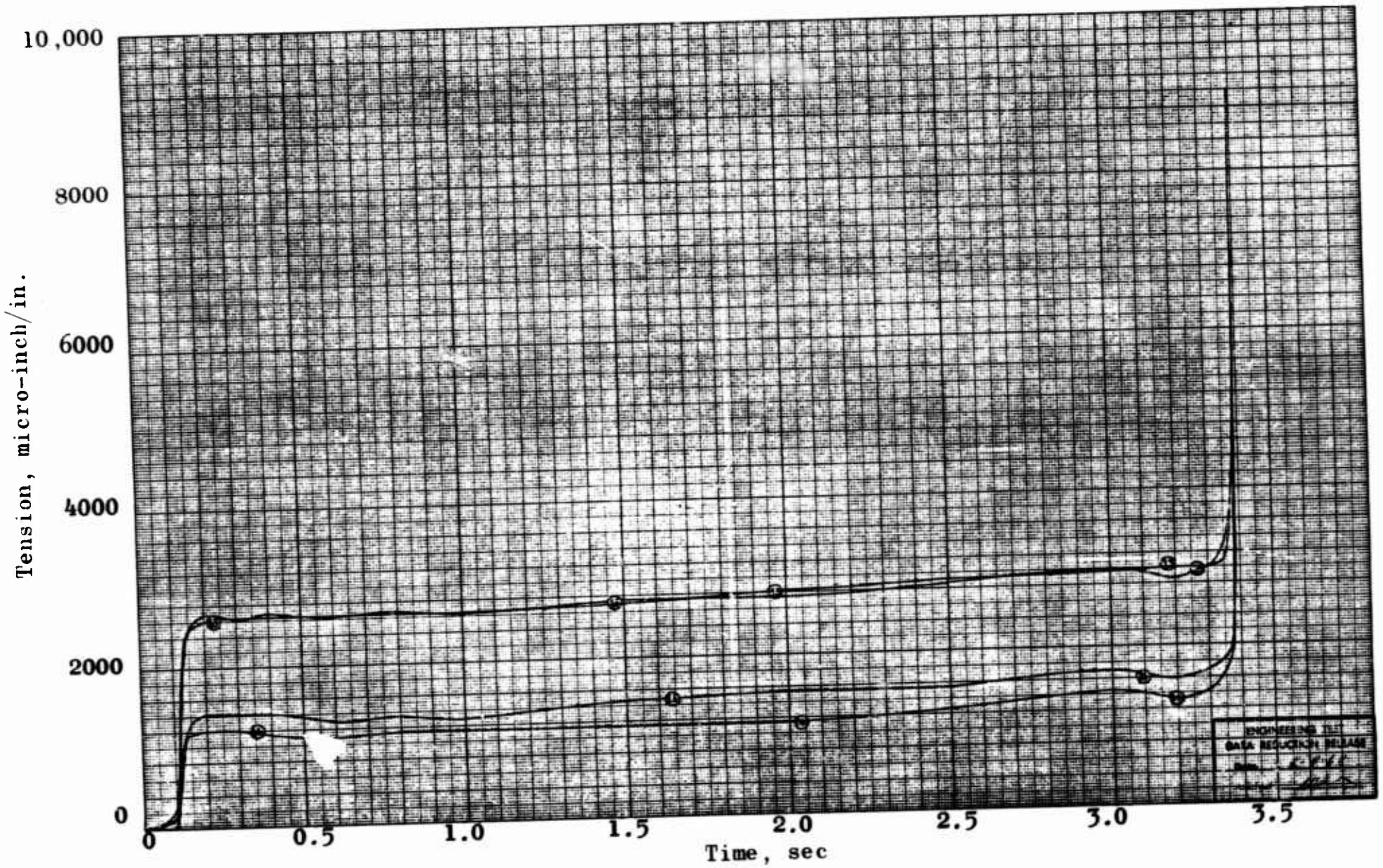


Figure 156. Strain-vs-Time in Forward Dome for Strain Gages 13 through 16 for Motor A-1003

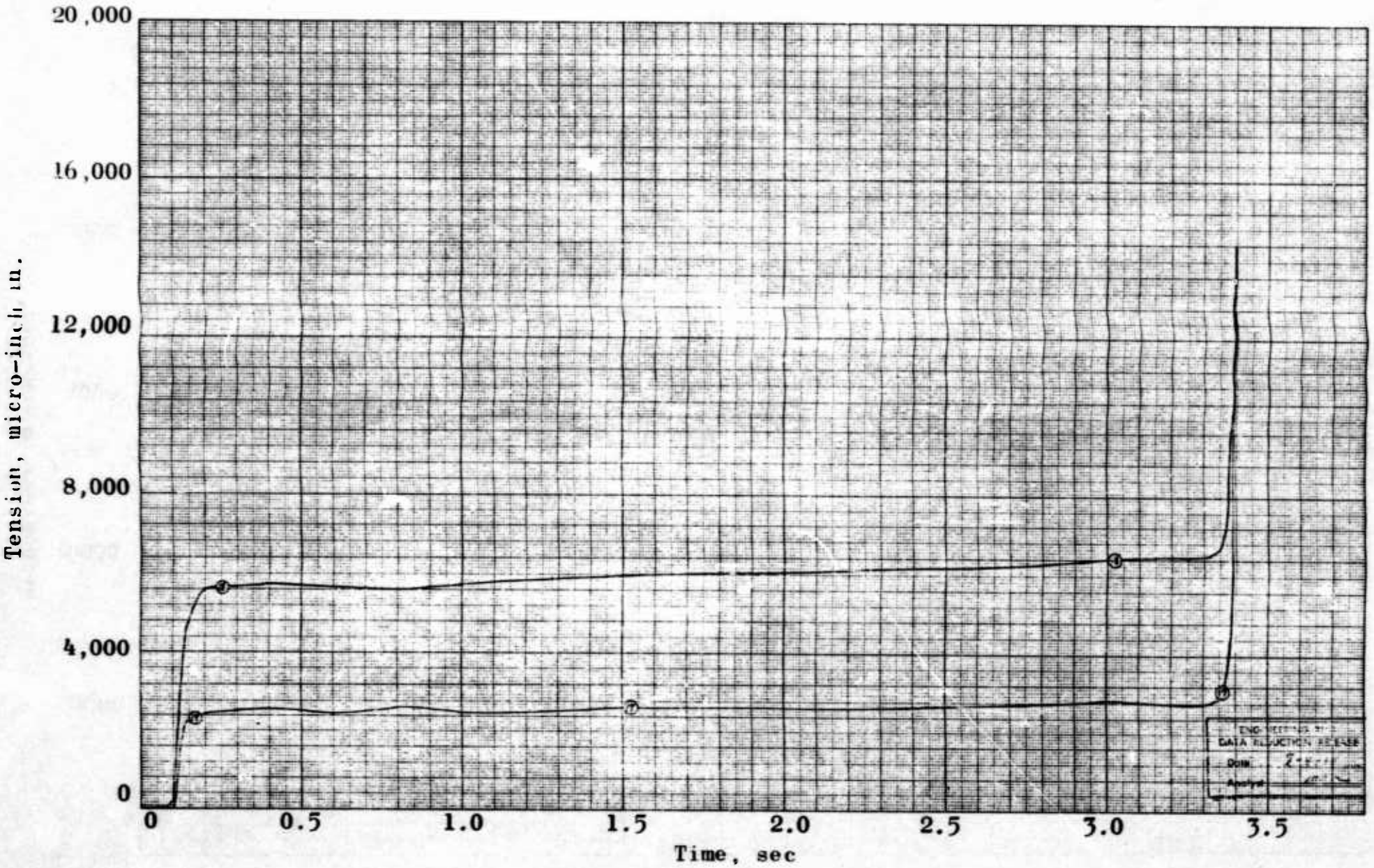


Figure 157. Strain-vs-Time in Forward Dome for Strain Gages 17 and 18 for Motor A-1003

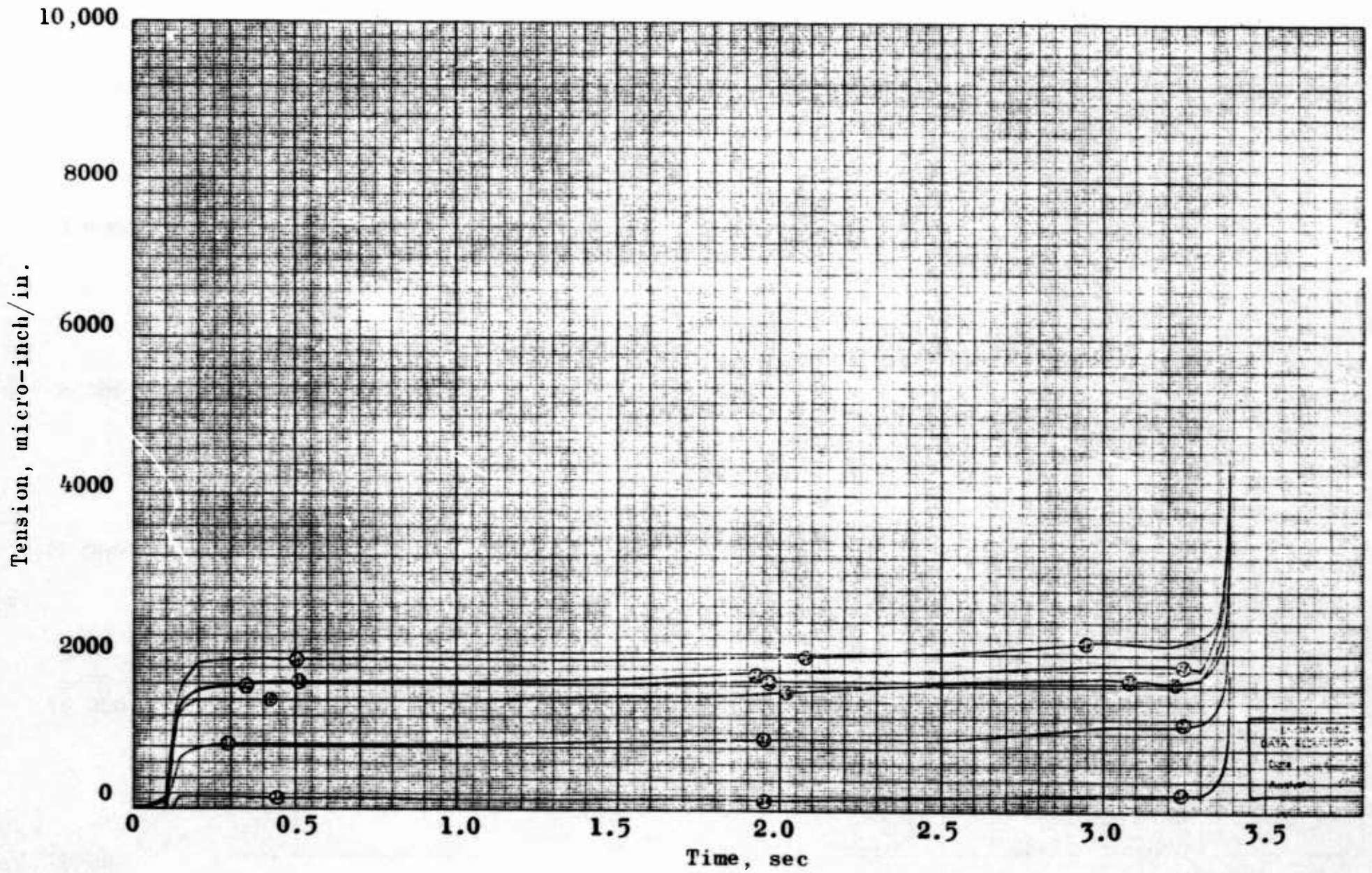


Figure 158. Strain-vs-Time in Aft Dome for Motor A-1003

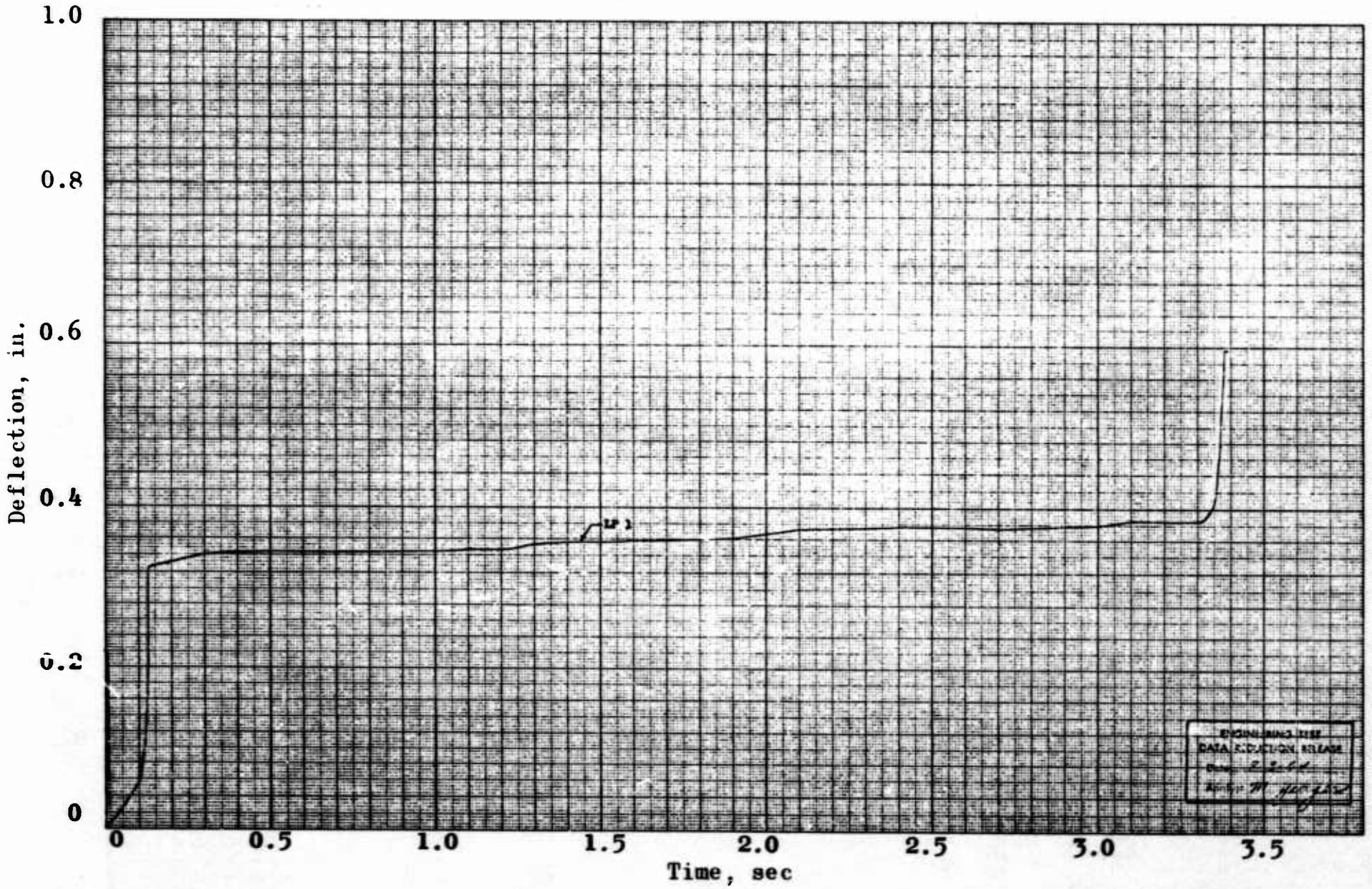


Figure 159. Deflection-vs-Time for Motor A-1003

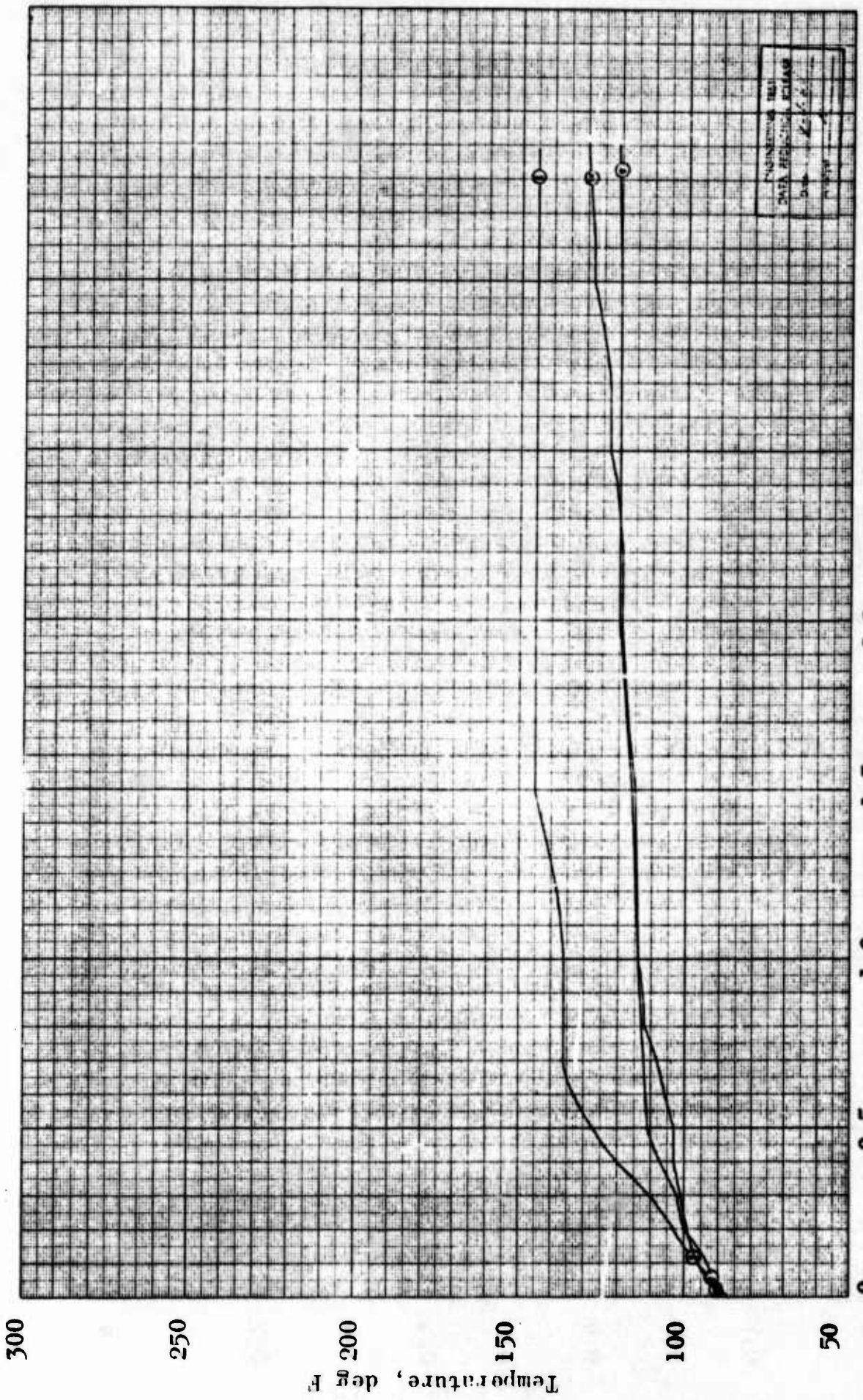


Figure 160. Temperature-vs-Time for Motor A-1003

Thermocouple 24, located on the outer surface of the aft dome insulation to determine the amount of base heating from the exhaust plume, attained a temperature of 130 F which represents a 40 F temperature rise in 3.4 seconds.

Thermocouples 7 and 8, located on the outer surface of the forward closure, indicated an unexpected temperature rise since the closure is protected by 0.4 inch of MX-2646 silica phenolic insulation. Thermocouple 8, located between the two pressure ports, rose rapidly from ignition to 136 F in 0.7 second, then stabilized for 0.3 second and increased to 145 F at 1.5 seconds and remained constant for the remaining duration of the firing. Thermocouple 7, located between the pressure port and CO_2 port, rose to 111 F during the first 0.5 second of the firing then continued to rise slowly to 120 F at two seconds duration and remained constant for the remaining duration of the firing. Since the forward closure is protected by 0.4 inch of insulation the only way for the titanium to increase in temperature at the beginning of the firing is for combustion gas to get between the insulation and the titanium closure. Either of two conditions could explain why the temperature of the closure did not continue to increase after two seconds: (1) flow of gas into localized voids in the bond, or (2) flow of gas between the insulation and titanium which could have been separated on ignition and later closed allowing no further flow.

Examination of pieces of the forward section of the aft polar boss where the doubler was attached shows that the doubler side of the boss experienced approximately the same heating conditions as the nozzle entrance side. Three conditions could have precipitated this result: (1) an unbond of the doubler and polar boss allowing ignition of the core grain at the aft end of the doubler, (2) an unbond of the core grain and doubler, allowing the core to ignite behind the doubler, resulting in removal of the doubler, and (3) a defect in the doubler such as a hole, thin spot, or void allowing premature ignition of the core grain behind the doubler, resulting in removal of the doubler.

(C) Motor A-1003 exhibited an ignition delay interval of about 95 milliseconds (approximately equal to that exhibited by A-1002), Fig. 161.

(C) As in A-1002, the ignition train was composed of a McCormick-Selph M-55 Mod IX initiator, an intermediate charge of 1.70 grams of boron-potassium nitrate pellets, and a 254-gram main charge of pyrotechnic grains, per P-73 formulation.

(C)

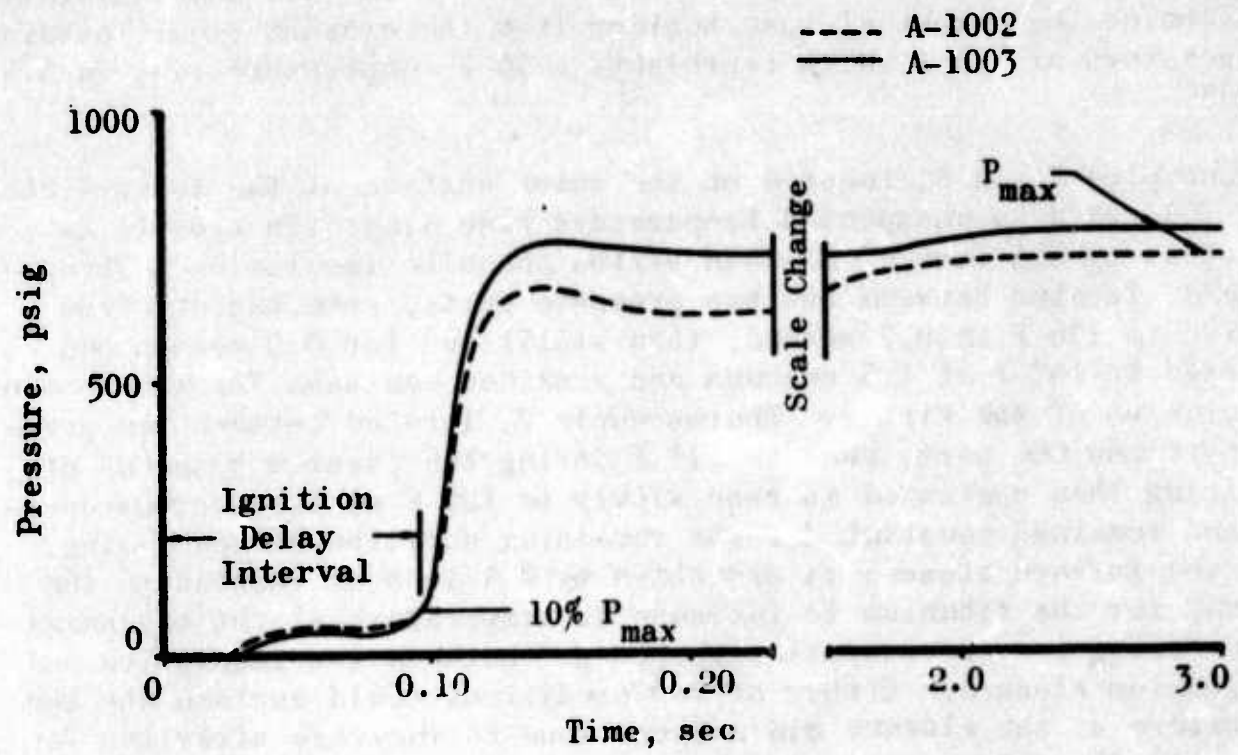


Figure 161 . A-1003 Ignition. Pressure-vs-Time

(2) Conclusions and Recommendations

Several possible modes of failure were considered. Voids, cracks, and other deformities in the core grain could result in pressure greater than normal. However it was concluded, based on performance up to the point of malfunction and prefiring examination of the motor, that cracks or voids of the magnitude required would have been detected otherwise. Increased burning surface of 2600 sq in. (or more) is indicated by the abnormal pressure recorded.

The most likely modes of failure appeared to be associated with either the forward polar boss and closure or the doubler on the aft polar boss. Based on the results of the analysis the following conclusions were drawn:

(C) Performance for the first 3.3 seconds was normal, and thrust-to-pressure relationships during this interval indicated the design nozzle efficiency of 0.96 would be achieved on subsequent motors.

Initial failure began at the forward polar boss or doubler at the aft polar boss, but ultimate failure was probably caused by an inadequate bond of the RFG-core grain. Reworking of both bosses inside the RFG was difficult and, no doubt, contributed to RFG-core grain interface contamination promoting an inadequate bond.

The RFG and GFW case structural response was satisfactory and was very similar to A-1002. Neither the RFG-GFW case nor the liner was responsible for the malfunction.

Base heating measurements indicated that continued use of insulation on the aft dome would be required to prevent over heating the case from the exhaust gases during static tests.

(C) To increase the margin between the contractual ignition delay requirement (100 millisecond maximum) and the 95 milliseconds experienced on A-1002 and A-1003, the intermediate boron-potassium nitrate charge for A-1004 will be increased from 1.70 to 2.55 grams. This slight modification to the ignition train reduces the time interval between initiator actuation and main charge ignition (and reduces the motor ignition delay interval).

5. DEVELOPMENT MOTOR A-1004

This motor was statically tested at ambient condition on 13 November 1964 in a horizontal position. Fabrication of A-1004 was halted pending design and process changes, as deemed necessary by evaluation of A-1003 test data.

One change was to redesign the forward boss to prevent movement of the boss with respect to the reinforced grain. At the aft boss, the doubler was replaced by a single boot spaced 1/8-inch from the insulation sleeve.

At the forward boss, the end restrictor (which had been applied to the core propellant before completion of cure) was omitted to allow visual inspection of the propellant-to-boss bond. An ambient-cure restrictor may be applied after inspection if the propellant level is low enough to affect ballistic design.

The GFW case for A-1004 will be the first flightweight Motor A case. The skirt length was shortened from 5.0 to 4.5 inches (the length originally estimated) and the aluminum skirt ring design was modified to reflect these changes.

(C) The burning rate requirements of the RFG are essentially the same as those of A-1003, differing only in amount of propellant in the outer layer. The burning rate required for the core propellant is defined by an uncured strand rate of 0.438 in./sec at 750 psi and 77 F, (same as A-1003).

(C) Motor component weights and mass fraction, which are based on a liner thickness of 0.06 inch and RFG outside diameter of 29.80 inches, are listed in Table LIII.

TABLE LIII

ESTIMATED WEIGHT AND MASS FRACTION
A-1004 FLIGHTWEIGHT MOTOR*

	Design Estimate
Nozzle Assembly	26.77
Case	34.00
Liner	29.20
Igniter Assembly	2.53
Forward Boss	11.02
Aft Boss	17.20
Load Rings	6.94
Drive Pins	0.56
O-rings	0.10
Flange	1.91
Adhesives	7.00
Aft Boss Repair	
Total Inerts	137.23
Igniter Combustibles	0.55
Core Propellant	1129.00
RFG Propellant	1337.00
Total Propellant	2466.55
Total Motor Weight	2603.78
Mass Fraction	0.947

*All weights are in pounds

(C) The only item varying from earlier estimates is the core propellant weight, which is 1129 pounds. This decrease is due to a modification of the aft boss and does not significantly alter the design mass fraction of 0.947. The predicted performance of the motor is presented in Table LIV and Fig. 162.

TABLE LIV

ESTIMATED PERFORMANCE SUMMARY A-1004

Average Pressure, psia	565
Average Thrust, lb	17,040
Total Impulse, lb-sec	557,350
Action Time, sec	32.70
Maximum Pressure, psia	800
Maximum Thrust, lb	24,800
I_{sp} at Motor Conditions, lb-sec/lb	226.0
I_{sp} at 1000 psia, lb-sec/lb	241.2
Impulse-to-weight Ratio	214.1
Core Grain	
Average Pressure, psia*	775
Average Thrust, lb*	23,970
Total Impulse, lb*	224,090
Duration, sec	9.35
I_{sp} at 1000 psia, lb-sec/lb	250
Reinforced Grain	
Average Pressure, psia**	485
Average Thrust, lb**	14,270
Total Impulse, lb-sec**	333,260
Duration, sec	23.35
I_{sp} at 1000 psia, lb-sec/lb	233.7

*Impulse delivered by core grain from 10% maximum pressure to transition of core to RFG; does not include core propellant which burns simultaneously with RFG propellant.

**Includes impulse delivered by RFG and core propellant which burns after transition point.

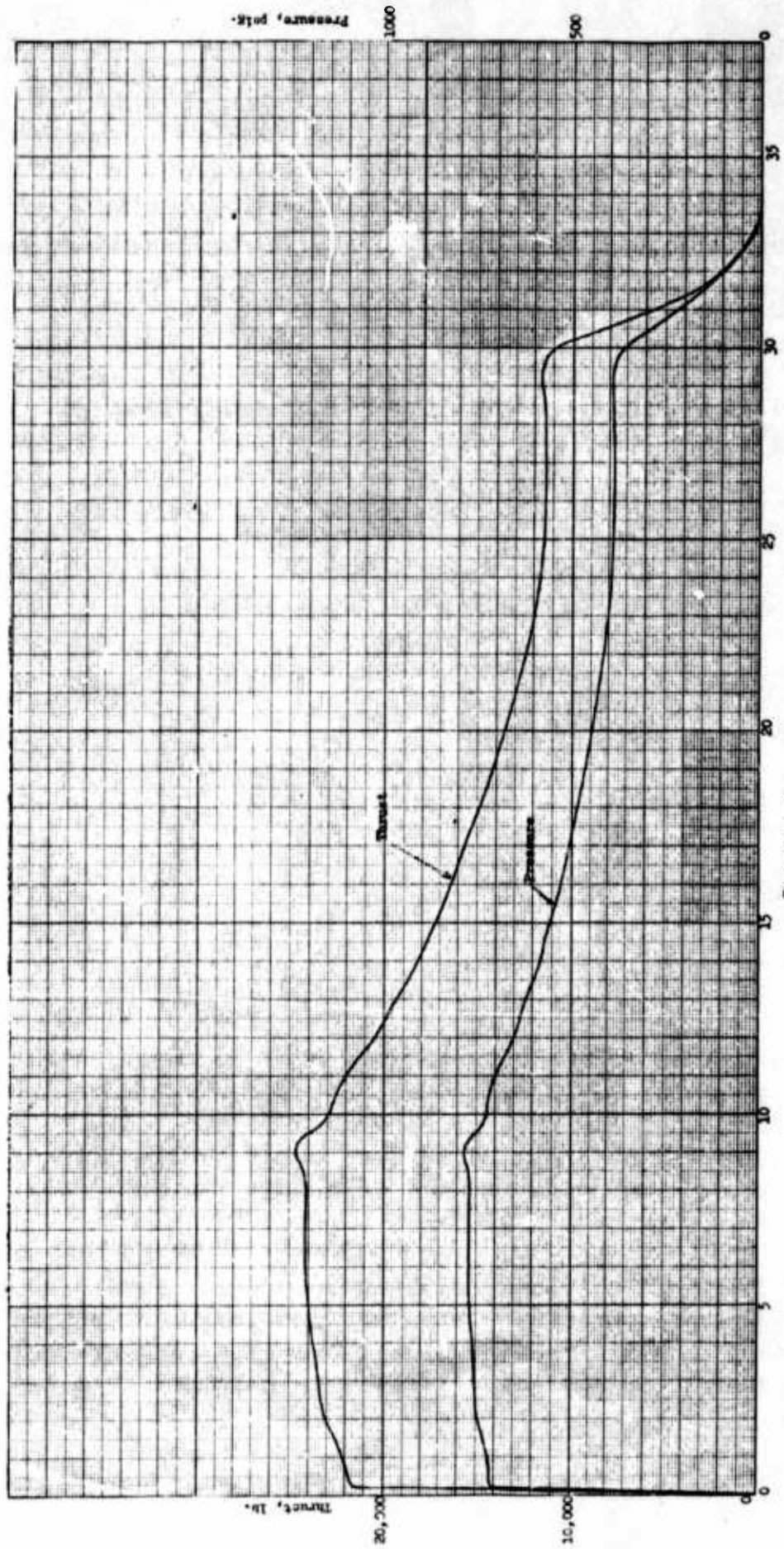


Figure 162. Estimated Thrust-and Pressure-vs-Time Motor A-1004

a. Fabrication

(1) Equipment

The same equipment used on A-1003 was used to make this motor.

(2) Materials

The materials were the same except for the design changes.

(3) Processing

(a) Grain Winding and Restriction

(C) The grain winding was completed in 6 days. It consisted of 229 covers of wire with an average buildup per cover of 0.0165 inch. The aluminum content was 16.7% and the average grain diameter was 29.652 inches. Tabulations of propellant properties and winding data are presented in Tables LV and LVI. Presented in Table LVII are the actual strand rates of the propellants, compared to those of the design. Examination of these data reveals that desired rates were provided with exceedingly small variations. Data for A-1002 are also presented to illustrate the designed rate reduction of layers 2 and 3, to reduce the motor pressure in this interval and bring it closer to the design nominal.

Several design and process changes were made on components for this motor. The polar bosses were molded into the sand mandrel rather than installing them in polar recesses provided in the finished sand mandrel. This method, while exposing the bosses to the possibility of water contamination during sand molding, did eliminate the problem of boss movement during winding operations.

The forward boss, which was redesigned to prevent inward separation from the grain, presented no processing problems. A lock ring was installed between the 8th and 9th load rings (Fig. 163) to hold them against the boss step and prevent relative movement from external loads on the boss.

TABLE LV

A-1004 PROPELLANT BURNING RATES AND AMBIENT MECHANICAL PROPERTIES

Cycle	Type	Mix No.	Strand Rate, in./sec at psi	e_m, %	S_m, psi	E, psi
1	514	L-7-31-M-81	0.261 at 735	17	180	1436
2	514	L-8-3-M-82	0.222 at 670	20	160	1276
3	514	L-8-3-M-83	0.181 at 600	15	104	1030
4	523	L-8-4-M-81	0.170 at 540	24	111	700
5	523	L-8-4-M-82	0.139 at 470	24	121	752
6	523	L-8-4-M-83	0.128 at 400	17	88	771
7	523	L-8-5-M-81	0.128 at 400	26	123	777
8,9	523	L-9-8-M-82	0.128 at 400	22	120	991
Core	526	L-10-30-M-81	0.427 at 750	34	148	692
		L-10-30-M-82	0.433 at 750	32	166	821
		L-10-31-M-81	0.434 at 750	40	168	726
		L-10-31-M-82	0.432 at 750	38	166	683

CONFIDENTIAL

TABLE LVI

WINDING DATA, MOTOR A-1004

Layer	Covers		Diameter, in.			Average Cycle Thickness, in.	Average Cover Thickness, in.
	Design	Actual	Aft	Center	Fwd		
1GI	7	7	22.077*	22.082*	22.075*		
1-43	6	6					
1-54	6	5					
1-66	6	10					
1-80	3	0	22.895	22.925	22.940	0.42	0.0151
2GI	7	7					
2-43	3	3					
2-54	4	5					
2-66	7	7					
2-80	10	11	23.878	23.895	23.882	0.483	0.0146
3GI	7	7					
3-35	4	3					
3-45	6	6					
3-60	8	8					
3-80	6	5	24.850	24.855	24.864	0.486	0.0167
4GI	7	7					
4-30	3	3					
4-40	3	4					
4-50	6	7					
4-65	6	8					
4-80	8	2	25.725	25.774	25.744	0.446	0.0144
5GI	7	7					
5-30	3	3					
5-38	5	5					
5-47	6	6					

*Mandrel diameter

CONFIDENTIAL

CONFIDENTIAL

TABLE LVI
(Continued)

Layer	Covers		Diameter, in.			Average Cycle Thickness, in.	Average Cover Thickness, in.
	Design	Actual	Aft	Center	Fwd		
5-60	6	6					
5-80	3	2	26.716	26.729	26.725	0.488	0.0168
6GI	6	6					
6-26	3	3					
6-32	2	2					
6-40	4	4					
6-56	7	7					
6-80	8	5	27.645	27.670	27.644	0.465	0.0172
7GI	6	6					
7-32	2	1					
7-46	4	4					
7-67	8	8					
7-80	9	6	28.615	28.620	28.615	0.482	0.0193
8GI	5	5					
8-29	5	2					
8-38	5	4					
8-51	5	5					
8-63	4	6					
8-80	4	0	29.450	29.460	29.460	0.420	0.0191
9GI	5	5	29.595	29.645	29.632	0.084	0.0168
Total	245	229					0.0165

CONFIDENTIAL

(C)

TABLE LVII

BURNING RATE SUMMARY FOR
MOTORS A-1002 AND A-1004

	Reference Pressure, psia	Design Strand Rate* A-1004	Actual Strand Rate*	
			A-1004	A-1002
Core	750	0.438	0.432	0.422
Layer No., Helical				
1	735	0.260	0.261	0.258
2	670	0.220	0.222	0.232
3	600	0.179	0.181	0.198
4	540	0.170	0.170	0.167
5	470	0.145	0.139	0.140
6--9	400	0.132	0.128	0.130

*At reference pressure

The previous aft boss doubler was replaced by a molded boot (Fig. 164). The boot, molded of R-142, will be bonded at one end to the boss. Core propellant will be cast against the boot and after propellant cure, the spacer between the boot and insulator will be removed and the gap filled with a potting compound. A fluid Epon/Versamid mixture, used to fill a similar space in A-1002 will be used in most of the gap in conjunction with a 1-inch topping of EC-1949 (which is more heat-resistant than Epon).

As a result of the A-1003 test analysis, which indicated probable bond failure between MX-2646 insulation and titanium in the aft boss, a test was performed on the aft boss of A-1004 to determine if the bond strength was significantly lower than anticipated. A static load of 2000 pounds, sufficient to stress the bond line to 20 psi, was induced into the boss insulation. However, failure did not occur in the bond but rather in the insulation, as shown in Fig. 165.

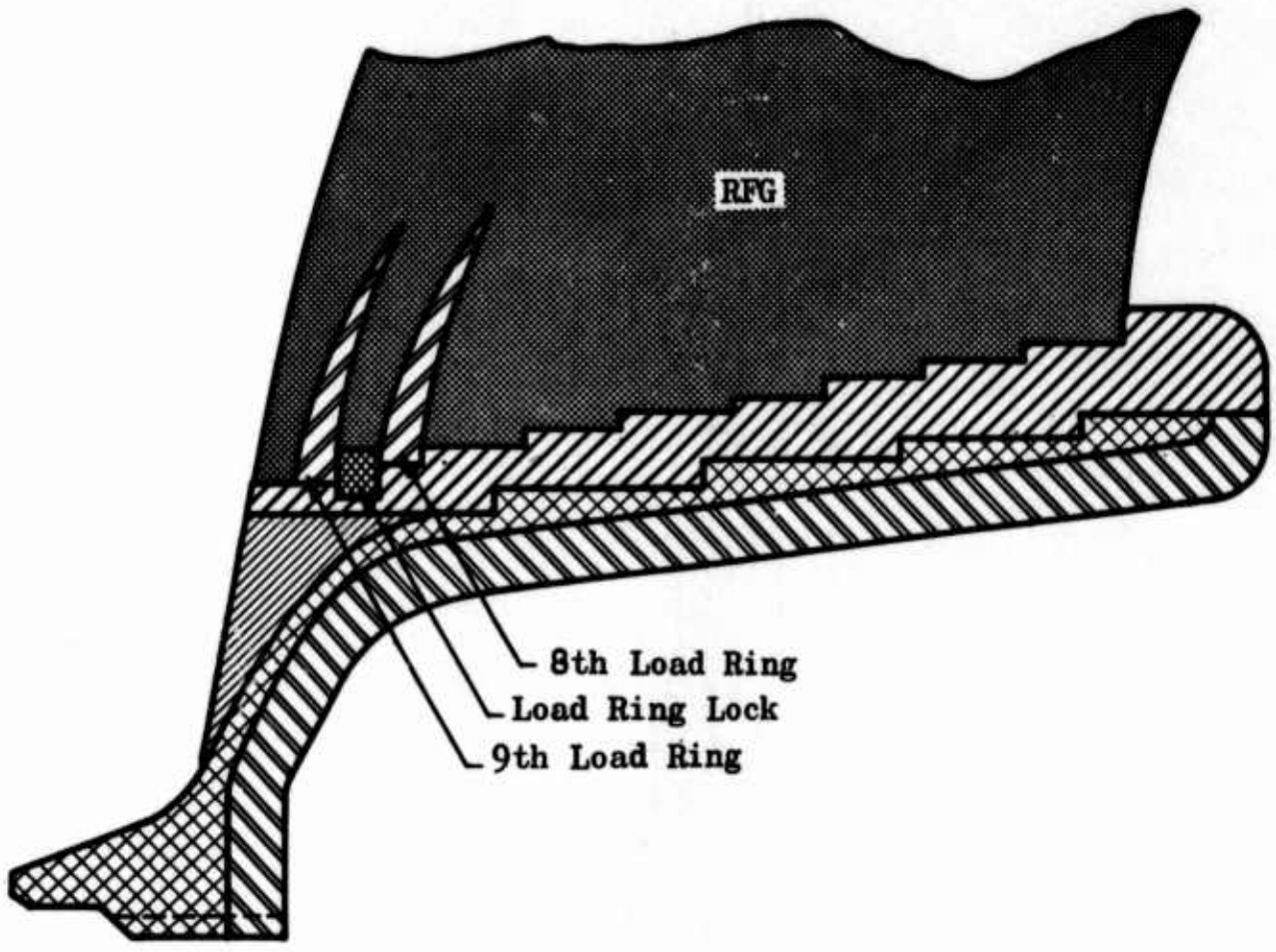


Figure 163. Forward Polar Boss, Showing Added Load Ring Lock

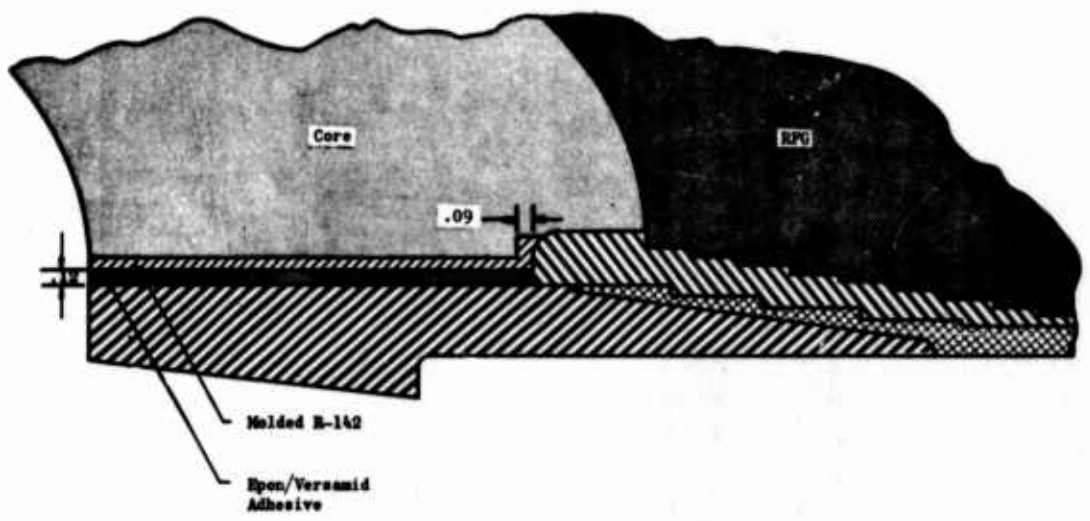


Figure 164. Aft Polar Boss, Showing R-142 "Boot"

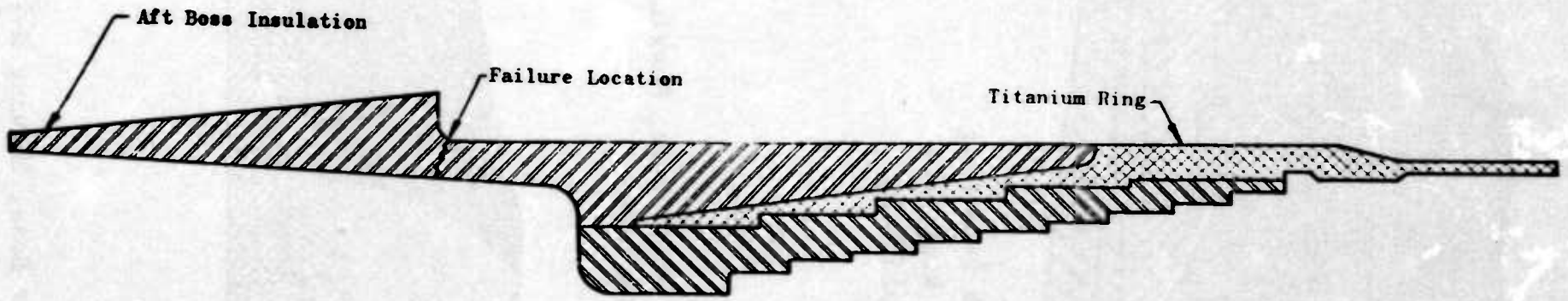


Figure 165. Aft Polar Boss, Showing Test Failure Location

Although the cross-sectional thickness of the insulation "spike" was sufficient to sustain all pressure loads, it was changed to a nontapering insulation configuration to (1) lessen problems connected with the doubler design, fabrication, and installation; (2) increase the insulation's structural and thermal properties; and (3) improve motor reliability.

The revised configuration (Fig. 166) increased the inert weight of the motor very slightly. Obviously, the increased reliability of the aft boss was considered much more significant than the small weight increase.

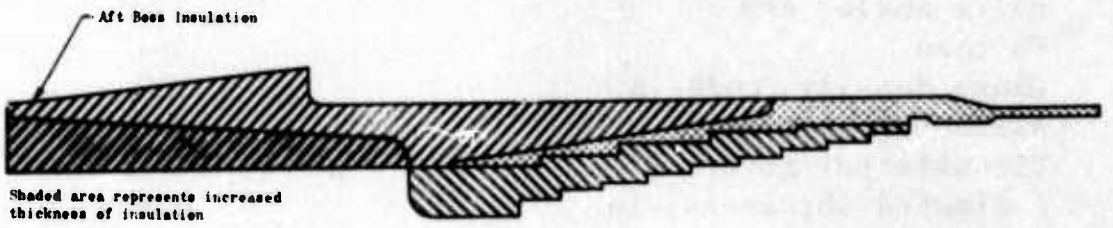


Figure 166. Aft Polar Boss, Showing Increased Boss Insulation

(C) It does not appear that the liner to Motor A can be reduced to the design thickness of 0.030 inch. A more realistic thickness of the liner is of the order of 0.045 to 0.060 inch. This increase in liner thickness is attributed to the tolerances associated with reinforced grain and the application of the liner material. Considerable improvements were planned in this regard; however, it is considered that application thicknesses and tolerances cannot be improved to the extent that a 0.030-inch thickness will be readily obtained. In an effort to improve this situation, additional process care was scheduled to improve the eccentricity of the reinforced grain and to monitor the thickness of the restrictor as it is applied. The restrictor thickness for A-1005 was planned to be of the order of 0.050.

(C) Following a 120-hour cure at 170 F, the grain was given a wipe coat of R-143 restrictor, which was partially cured for 16 hours at 170 F. This was followed by an intermediate and a final coat of R-143. The latter application was made using the restrictor template. After a final cure of 48 hours at 170 F, inspection revealed that the restricted grain diameter exceeded the maximum allowed in several isolated places. This was easily repaired by sanding the restrictor to remove the excess material. Actual cylindrical thickness of the restrictor was 0.091 inch, compared to the specified 0.060-inch thickness. The 0.091 inch is an average of the measurements at three places (the forward tangent plane, center of the cylinder, and aft tangent plane).

(b) GFW Case

Motor A-1004 GFW Case was wound on 8 October. The case was a flight-weight design, of good appearance except for ripples in the skirts. A change will be made in skirt tooling and skirt-to-case fill technique for A-1005 in order to obtain acceptable skirts.

Winding parameters were as follows:

(C) Helix wrap

Helix angle, deg	17.2
Pattern	5/4
Glass density, ends/in.	735
Number of covers	2
Circuits per cover	344
Estimated thickness, in.	0.029

(C) Circ wrap

Pattern, deg sequential	90
Glass density, ends/in.	1009
Number of covers	4
Estimated thickness, in.	0.040

(C) Dimensions and weights of the case are shown in Table LVIII. The case weighed 31.72 pounds excluding skirt-to-case fill, compared to 34 pounds predicted. The lower weight is due to a lower resin content than predicted, 17.7% vs 21--22%. The lower resin content is desirable from a weight standpoint, and is not considered detrimental to strength since the resin content is still considerably greater than the 12--13% theoretical minimum required for bond continuity.

The skirt-to-case fill was again the major processing difficulty, resulting in skirts which would be unacceptable for the bending load requirement of A-1005. It has been decided that Motor A skirt tooling will be modified to obtain a system similar to the Motor B design. The skirt mandrel will extend almost to the case tangent, reducing the required skirt-to-case fill and simplifying the fill technique. Following case cure the skirt mandrels will be removed and skirt attachment rings installed. A side benefit of this method is a reduction in fill weight from about 5.5 pounds to about 1.0 pound.

TABLE LVIII

DIMENSIONS AND WEIGHTS OF MOTOR A-1004 GFW CASE

Dimensions

Restricted motor diameter, in.

Forward	Center	Aft	Average
29.845	29.840	29.815	29.833

Cured case diameter, before washout

Center
30.004

Indicated case thickness

Center
0.082

Skirts

	Forward	Aft
OD (after washout)	30.065	30.075
ID (skirt ring OD)	29.810	29.810
Thickness	0.128	0.132

Lengths

Boss-to-boss

Before mandrel washout	70.57
After mandrel washout	70.49

Skirt-to-skirt

Before mandrel washout	57.85 - 57.99
After mandrel washout	57.92 - 58.01

Weights

Helix roving	11.77 lb
Circ roving	10.57
Skirt cloth	3.77
Total glass	26.11 lb
Resin	5.61
Case weight	31.72 lb
Skirt-to-case fill	5.42
Total	37.14 lb

Resin content = $\frac{5.61}{31.72} \times 100 = 17.7$ wt %

(4) Postwinding Procedure

Washout of the soluble mandrel for A-1004 was initiated following curing and cooling of the glass case. During washout, some difficulty was encountered with removing the mandrel support sleeve. First, adhesive used to bond the two sections of sand together had bonded to the sleeve and prevented its passage through the polar boss. Second, after raising the sleeve to remove the adhesive, the hoist supporting the sleeve failed and allowed the sleeve to strike the aft polar boss. After completion of washout, the ballistic extension of the aft polar boss was observed to be cracked and later two broken pieces were detached, Figs. 167, 168, and 169.

A rework plan was immediately implemented. The rework consisted of bonding the broken pieces in place and then covering the ballistic sleeve with a protective, ablative shield. The shield was made in two components; a split tapered filler ring to build up the sleeve to a cylindrical internal contour, and a one-piece liner which provided a complete, continuous cover for the damaged area (Fig. 170).

The two broken pieces were bonded in place with RPR-2138, an ablation-resistant adhesive, and cured 24 hours at room temperature. The split filler ring was machined from an available billet of MX-2646 phenolic. After machining, the part was dried 12 hours at 170 F. This reduced postcure treatment resulted from definite evidence that previous severe postcure heating was a major cause of past phenolic failures. After drying, the part was X-ray inspected, accepted, and bonded in place with Epon 901/B-1. The filler provided some support to the repaired sleeve during core casting in addition to filling the space between the sleeve and liner. A graphite-plastic material (FM5064) was used for the liner which replaced part of the nozzle assembly. In order to increase the hoop strength of the FM5064, a cover of glass rovings, machined to an approximate 0.06-inch thickness, was wound on the cylinder section of the liner. The normal DER 332/EMI resin system used in the GFW cases was used for this application. The liner was installed after core casting, prior to nozzle assembly. A silicone rubber expansion joint was positioned between the liner and the nozzle. The liner was bonded with Epon 901/B-1 and held in place during cure with a special clamping tool.

The heat transfer analysis of the repaired A-1004 aft polar boss indicated that the repair would adequately protect the damaged part from the thermal environment. Predicted losses, char depth, and the 500 F isotherm of the repaired boss are shown in Fig. 171.

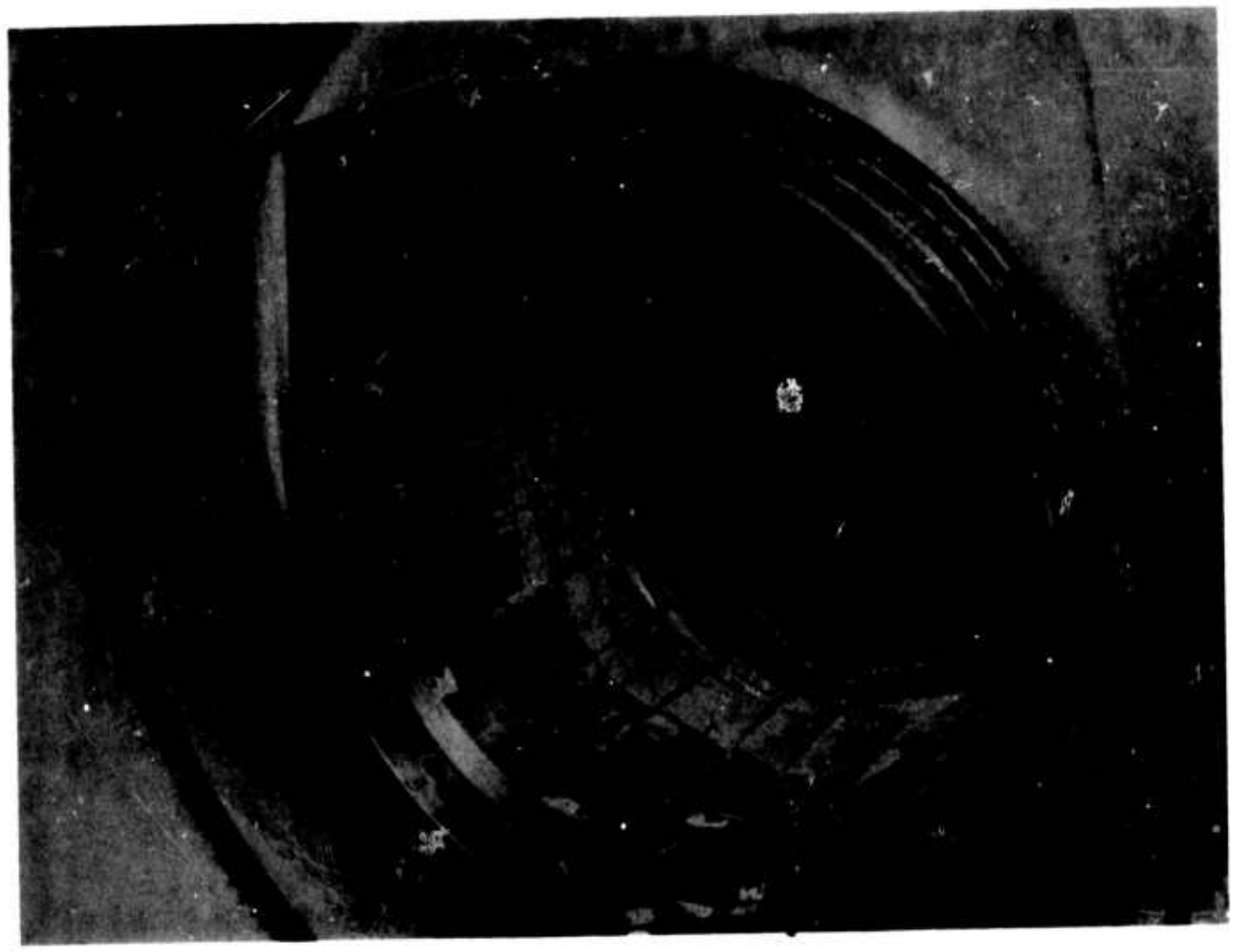


Figure 167 . Cracked Aft Polar Boss of Motor A-1004

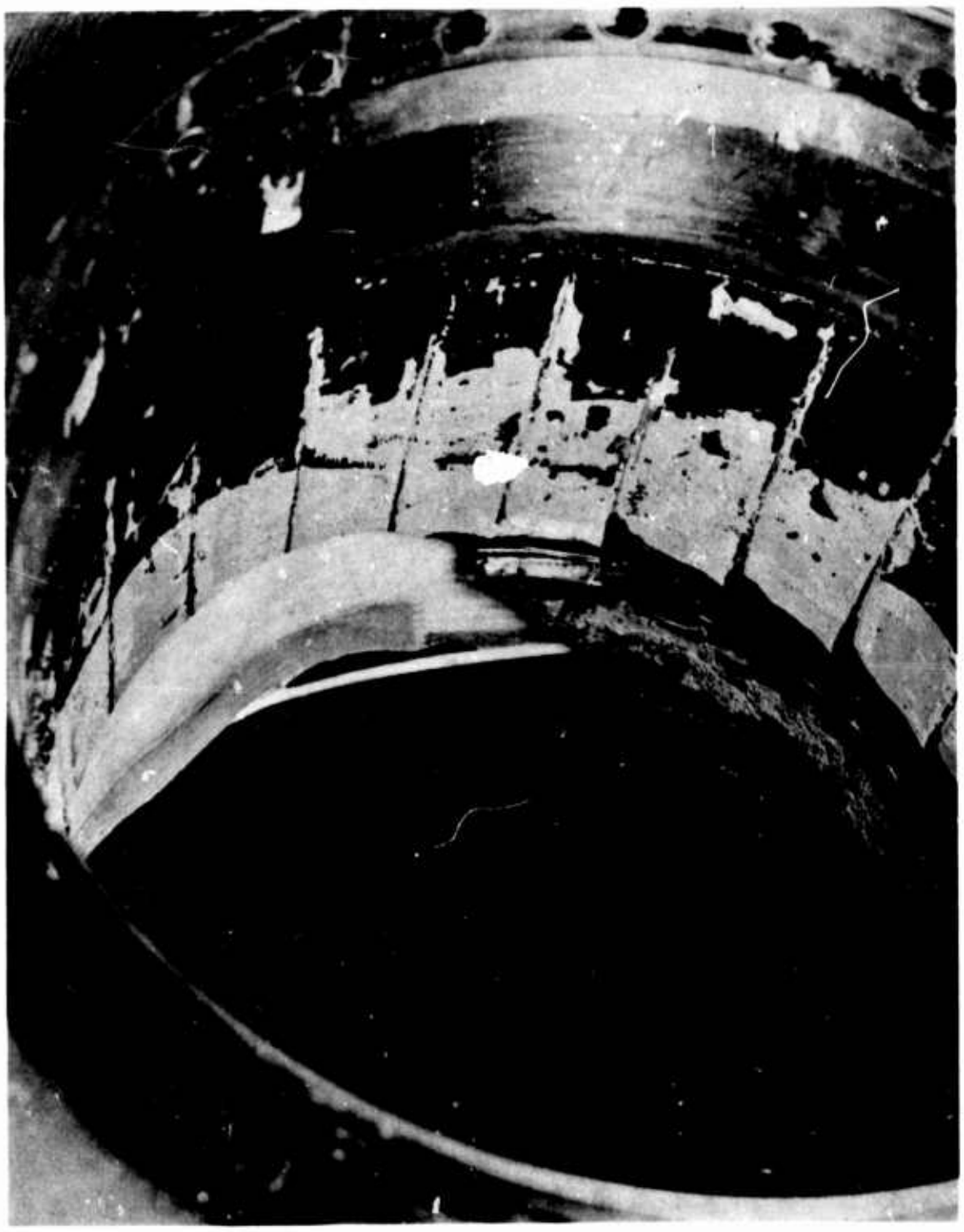


Figure 168. Motor A-1004 Aft Polar Boss After Removal of Cracked Material

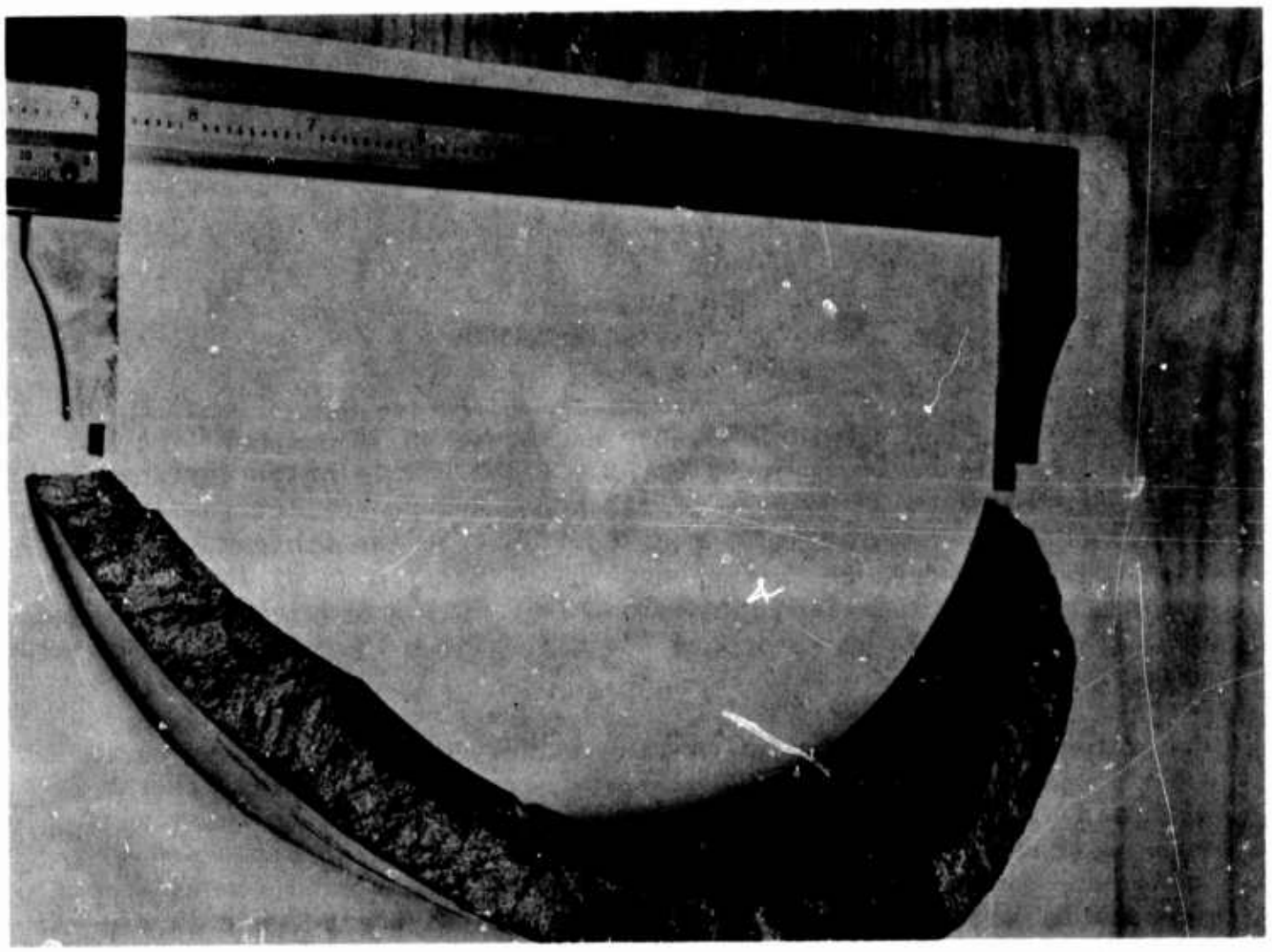


Figure 169. Two Cracked Pieces Removed from Motor A-1004 Aft Polar Boss

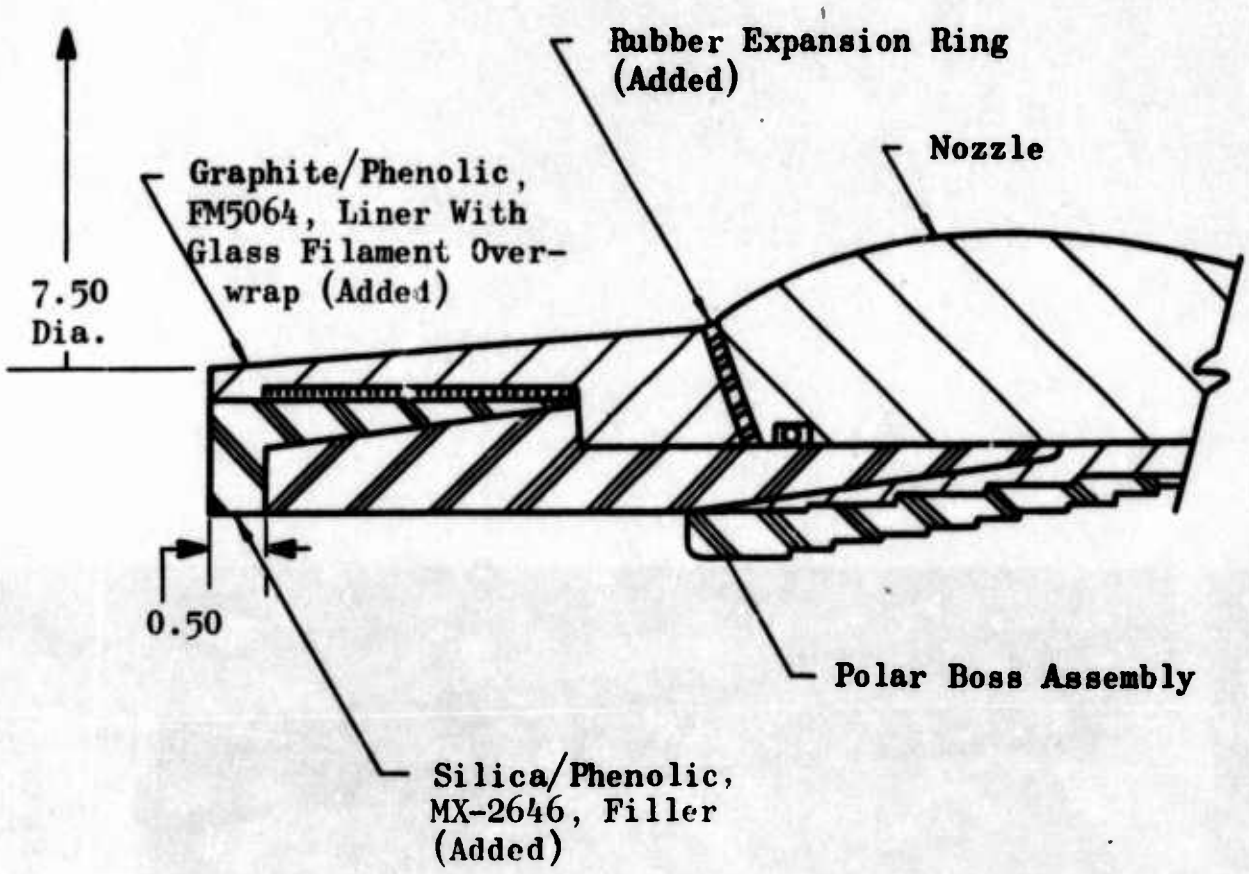


Figure 170. Repaired Aft Polar Boss, Motor A-1004

Casting of the core grain in A-1004 was begun on 30 October 1964 and completed 12 hours later on 31 October. The RFG interior surface had been MAPO-wiped on 26 October or 113 hours before initial casting and 5 days prior to completion of casting. This is the longest known aging time of a MAPO-prepared surface and the effectiveness of the MAPO as a bonding aid was, therefore, questionable. This schedule delay was made to allow review of the motor and its disposition by the Air Force review team.

Concurrent with the delay in casting A-1004 core grain following surface preparation with MAPO, bond tests were started in the laboratory to determine the effect of aging MAPO-treated propellant on subsequent bonding strength. The test procedure simulated pilot plant processing procedures. Cured RDS-514 was MAPO-wiped and then aged for different periods in an air-conditioned laboratory. The samples were then preheated for 10 hours at 150 F before casting RDS-526. After a 72-hour cure at 170 F the samples were tested in the Instron.

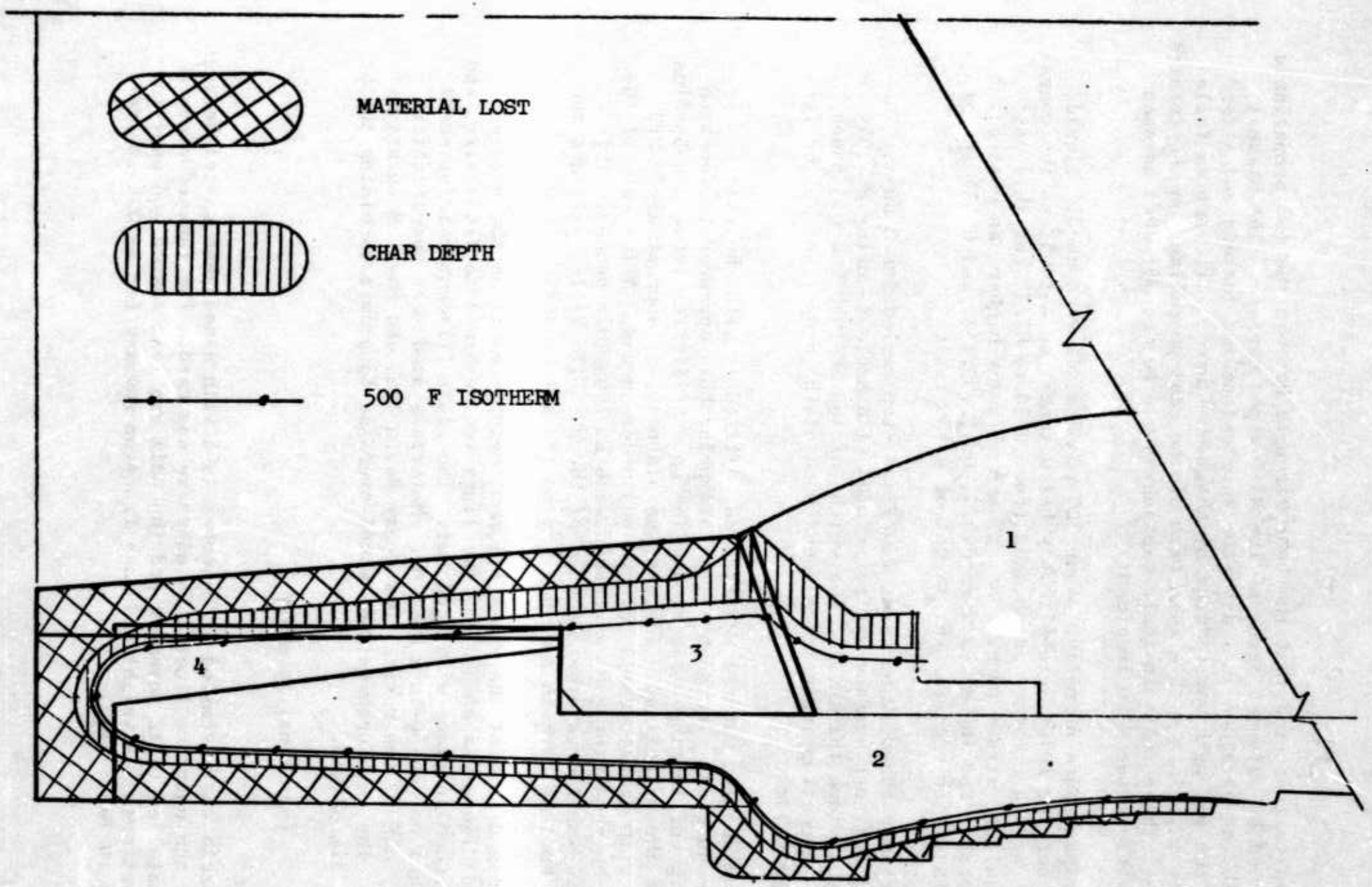


Figure 171. Estimated Material Loss, Char Depth, and 500 F Isotherm for RFG Motor A-1004 Aft Polar Boss

The results indicated that the bond strength between the two propellants is reduced by extended aging of the MAPO-wiped surface. The highest strength was obtained in 1 day (the shortest period tested) and after 5 days the strength was reduced by about one-third. All samples failed near the interface with a thin film of the cast propellant on the treated surface. These tests indicate casting should be accomplished as soon as possible after MAPO treatment.

(C) Casting proceeded normally. Four 325-pound mixes were used. Liquid strand burning rates were slightly below target on A-1003, so the coarse-to-fine oxidizer ratio was changed from 70/30 to 67/33 for this cast and resultant strand burning rates were slightly higher, as desired. The averages for the mixes were 0.427, 0.432, 0.433, and 0.434 ips at 750 psia (which are near the target of 0.438 ips).

The core was cured 72 hours at 170 F and step cooled for 2 days. The forward end core surface was restricted with ambient-curing EC-1949 to a 0.1--0.2 inch thickness. The weight of the EC-1949 was 0.3 pound. Visual inspection indicated a sound bond of the propellant to the forward polar boss.

When the casting mandrel was removed, difficulty with the foam conicyls was encountered. The boot at the aft polar boss appeared to function as designed, leaving a gap around the boss ballistic sleeve and bonding well to the propellant. The gap, as planned, was approximately 2/3 filled with Epon/Versamid (0.9 pound) under vacuum. After cure of the Epon, the remaining gap was capped with EC-1949 (0.8 pound). This adhesive was flared over the edge of the phenolic filler part and the rubber boot to give an over-all cap to the aft expansion joint.

Winding and cure of the glass filament reinforcement on the nozzle entrance liner was completed, the liner was machined to final size, and then bonded in place with Epon 901. The glass filament reinforcement was wound on the 30-inch machine. Materials used were specification quality HTS 12 end roving, Dow Epoxy Resin 332, and Shell M curative (EMI). The reinforcement was wound oversize to permit machining to the proper dimensions.

(5) Final Assembly

The nozzle was assembled 11 November 1964 with a neoprene gasket between it and the entrance liner. No adhesive was used. The forward closure was installed on 12 November and the unit was leak tested and sent to the test area. A weight and mass fraction summary for A-1004 is presented in Table LVIX.

TABLE LVIX

MOTOR A-1004 WEIGHT

AND MASS FRACTION SUMMARY

Component	Weight
Nozzle Assembly	26.02
Case	37.14
Liner	38.91
Igniter Assembly	3.19
Forward Boss	11.24
Aft Boss	17.66
Load Rings	5.92
Drive Pins	0.56
O-rings	0.10
Flange	1.99
Adhesives	2.50
Aft Boss Repair	6.12
Total Inerts	151.35
Igniter Combustibles	0.55
Core Propellant	1125.1
RFG Propellant	1348.70
Total Propellant	2374.35
Total Motor Weight	2625.70
Mass Fraction	0.942

b. Testing

(C) Motor A-1004 was statically fired 13 November 1964, Figs. 172, 173, and 174. The motor performed as predicted for 23.5 seconds, then the chamber pressure increased from 342 psig to 370 psig and appeared to stabilize at 24.5 seconds. Strain gages and one linear potentiometer showed a sudden increase in the GFW case loading in the lower portion of the aft dome at approximately 24.4 seconds. At 25.04 seconds, strain gages and high-speed movies (1000 fps) indicated the upper portion of the aft GFW dome was loaded very suddenly.

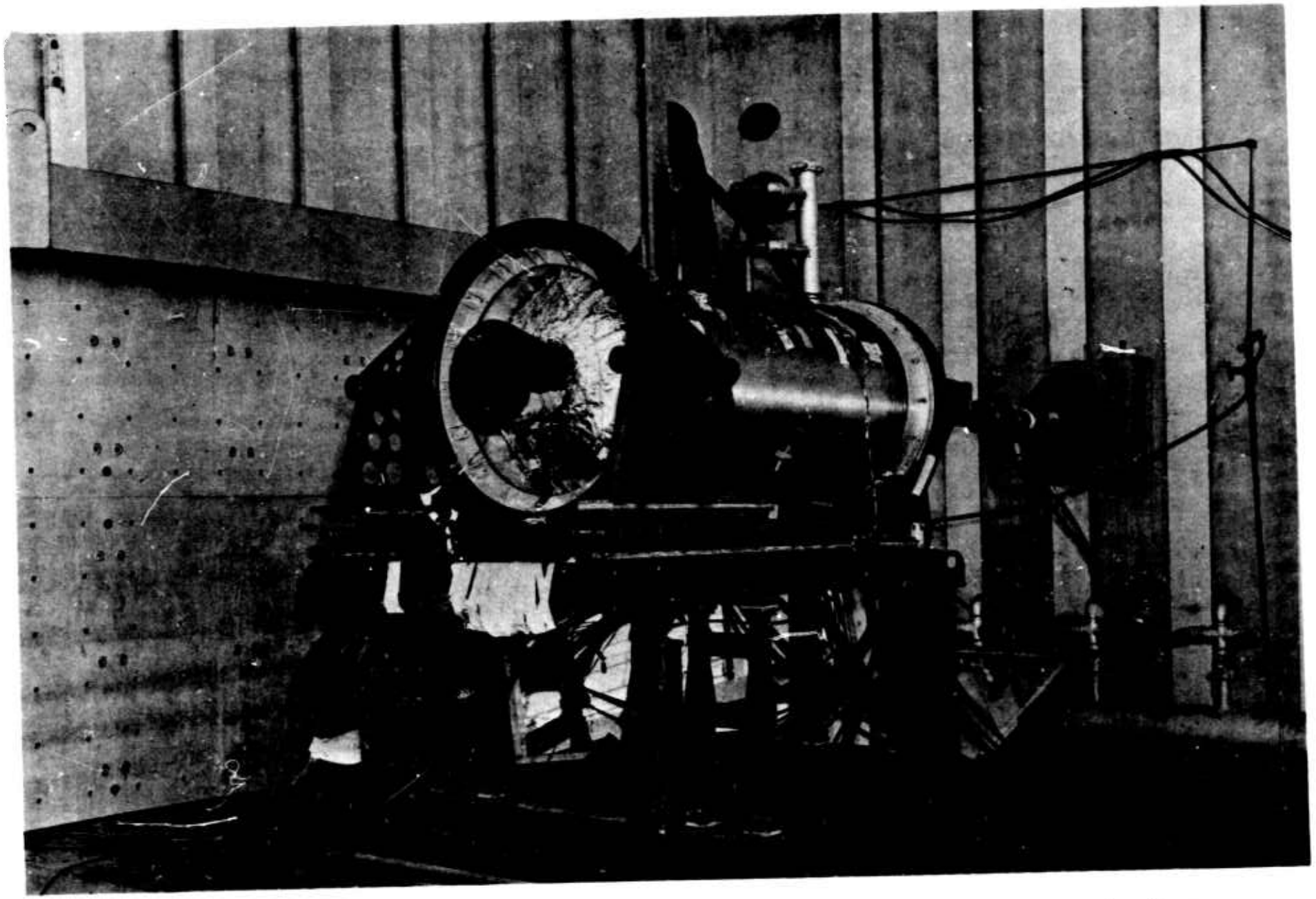
(C) Strain gages in the cylindrical portion of the GFW case indicated the load was transmitted forward in the case until it reached the forward dome. Pressure, as measured by a transducer in the forward end of the motor, increased from 370 psig at 25.060 seconds to 515 psig at approximately 25.107 seconds when the GFW case ruptured in the cylindrical portion near the aft tangent.

(1) Analysis

A summary of ballistic performance of A-1004 is presented in Table LX and Fig. 175. For comparison purposes the estimated and projected performance are included.

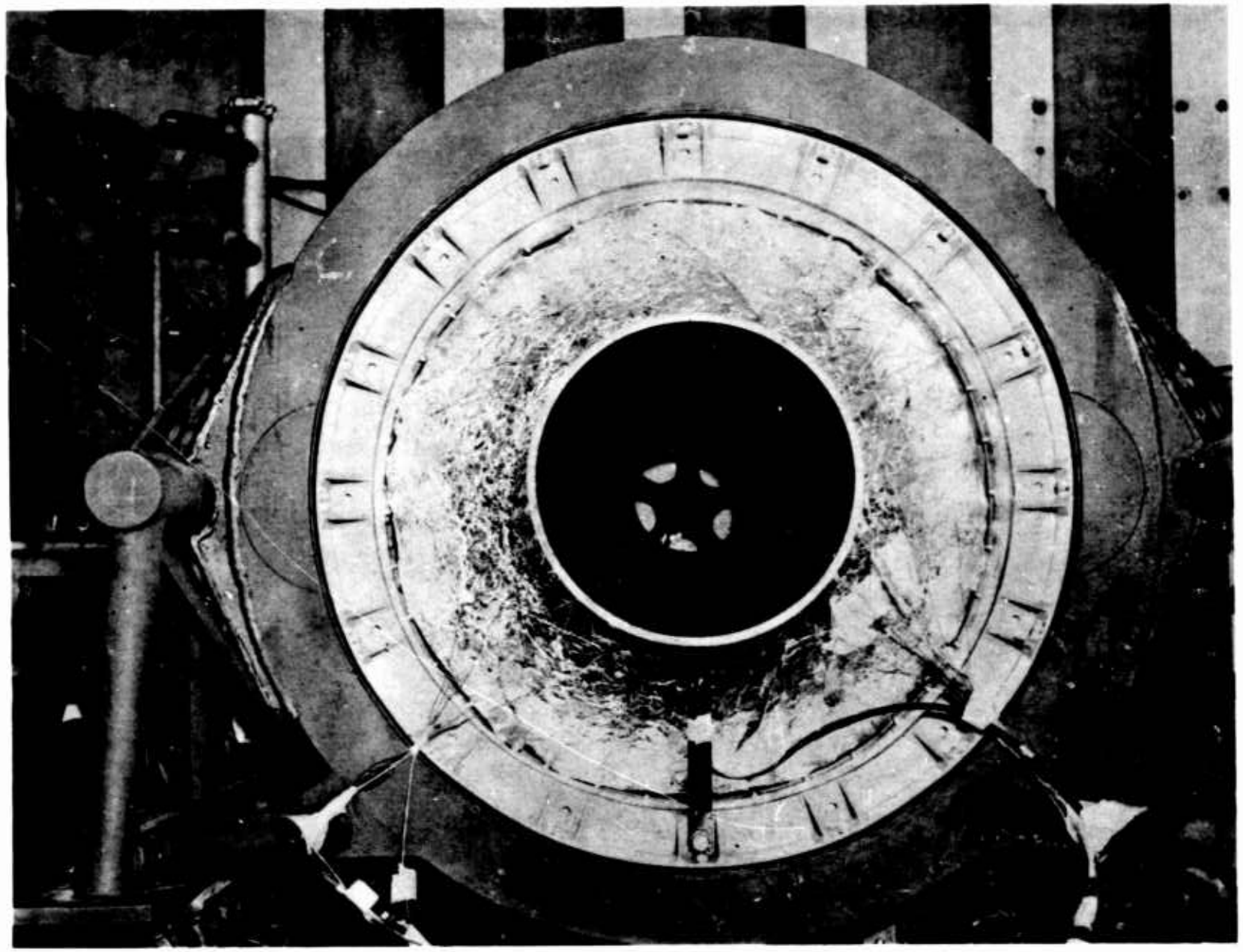
(C) Performance of A-1004, though terminated by motor failure at 25.107 seconds. followed the predicted performance very closely as illustrated in Fig. 176. Average pressure and thrust parameters over the 25.107 seconds duration recorded in Table LX are high as compared to estimated values for the normal duration. This is to be expected since the motor burns regressively during burning of the RFG. Average parameters over the core duration compare very well with design nominals. Average pressure was 779 psia, differing by 0.5% from design nominal of 775 psia, and maximum pressure of 799 psia essentially coincided with design nominal of 800 psia. The average thrust over this interval was 1% greater than nominal.

(C) Since average performance over the 25.107 seconds duration does not lend itself to comparison with the theoretical performance, a projection of full duration performance from actual data obtained was estimated. The projected performance was based on an assumed characteristic velocity of 4650 feet per second for the last two helical layers (original design estimate) and a characteristic velocity for the propellant consumed commensurate with A-1002 data. A calculated propellant weight of



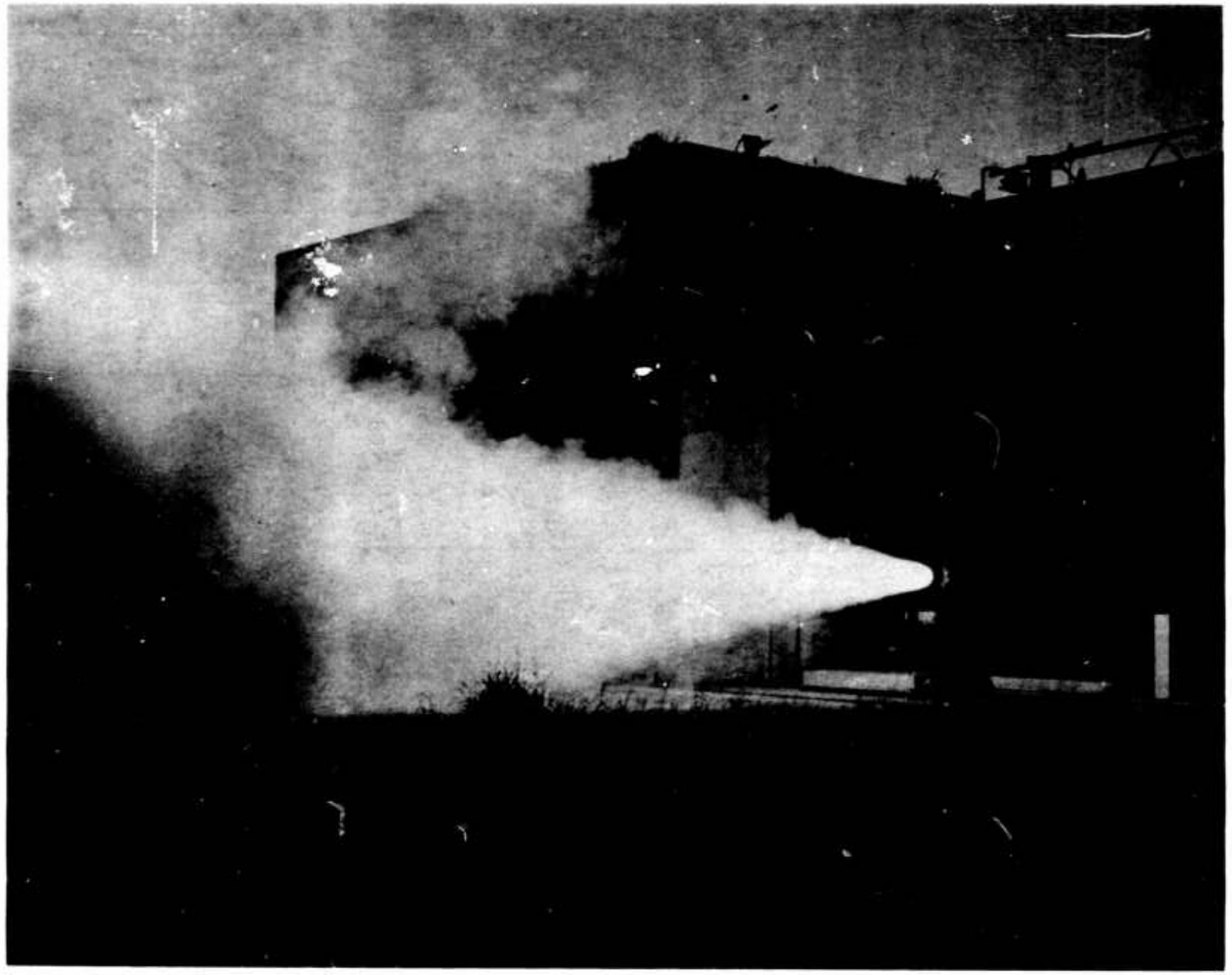
2YA23-11/13/64M1I

Figure 172. Motor A-1004 Before Test



2YA23-11/13/64M1D

Figure 173. Motor A-1004 Before Test, Looking in Nozzle



CN-552

Figure 174. Motor A-1004 Test Firing

TABLE LX

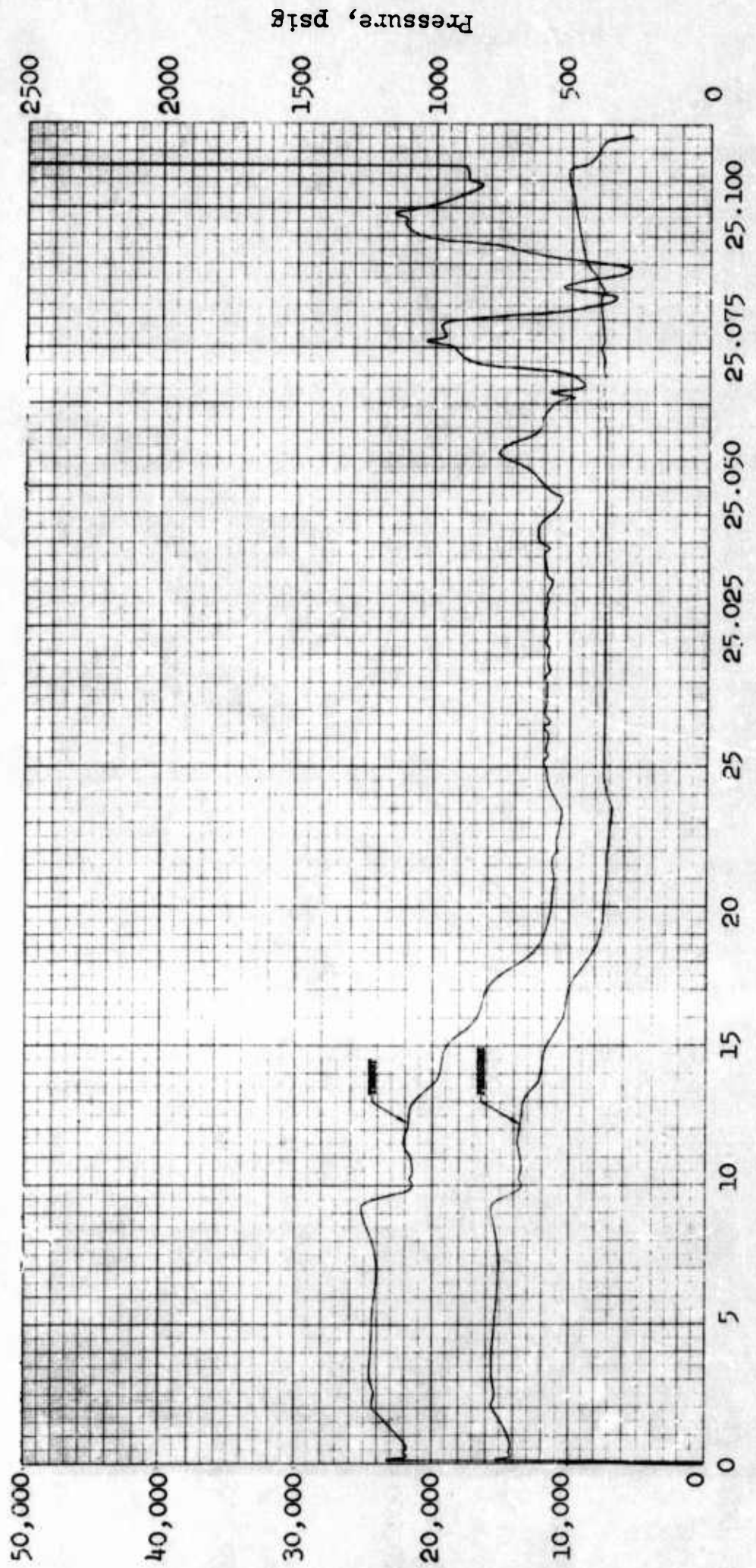
PERFORMANCE SUMMARY FOR MOTOR A-1004

	Actual A-1002	Estimated A-1004	Actual A-1004	Projected A-1004
Average Pressure, psia	560	565	613	537
Average Thrust, lb	16,970 (1)	17,040	19,030	16,570
Total Impulse, lb-sec	533,600 (1)	557,350	475,800	545,100
Action Time, sec	31.44	32.70	25.004	32.9
Maximum Pressure, psia	741	800	799	799
Maximum Thrust, lb	—	24,800	25,271	25,271
I_{spd} at Motor Conditions	225.9 (1)	226.0	225.2	220.3
I_{sps} at 1000 psia	241.4 (1)	241.2	239.4	236.3
Impulse to Weight Ratio	205.8 (1)	214.1	-	207.6
Core Grain				
Average Pressure, (2) psia	733	775	779	779
Average Thrust, lb	22,660 (1)	23,970	24,210	24,210
Total Impulse, lb-sec (2)	222,200 (1)	224,090 (2)	223,700 (2)	223,700 (2)
Duration, sec	9.81	9.35	9.24	9.24
I_{sps} at 1000 psia	--	250.0	--	--
Reinforced Grain				
Average Pressure, psia	482	485	516	443
Average Thrust, lb	14,400 (1)	14,270	15,930	13,580
Total Impulse, lb-sec (3)	311,400 (1)	333,260 (3)	252,100 (3)	321,400 (3)
Duration, sec	21.63	23.35	15.764	23.66
I_{sps} at 1000 psia	--	233.7	230.6	227.3

(1) Thrust parameters estimated from pressure.

(2) Impulse delivered by core grain from 10% maximum pressure to transition of core to RFG; does not include core propellant which burns simultaneously with RFG propellant.

(3) Includes impulse delivered by RFG and core propellant which burns after transition point.



(Scale change at 25 seconds)

Figure 175. Pressure- and Thrust-vs-Time for Motor A-1004

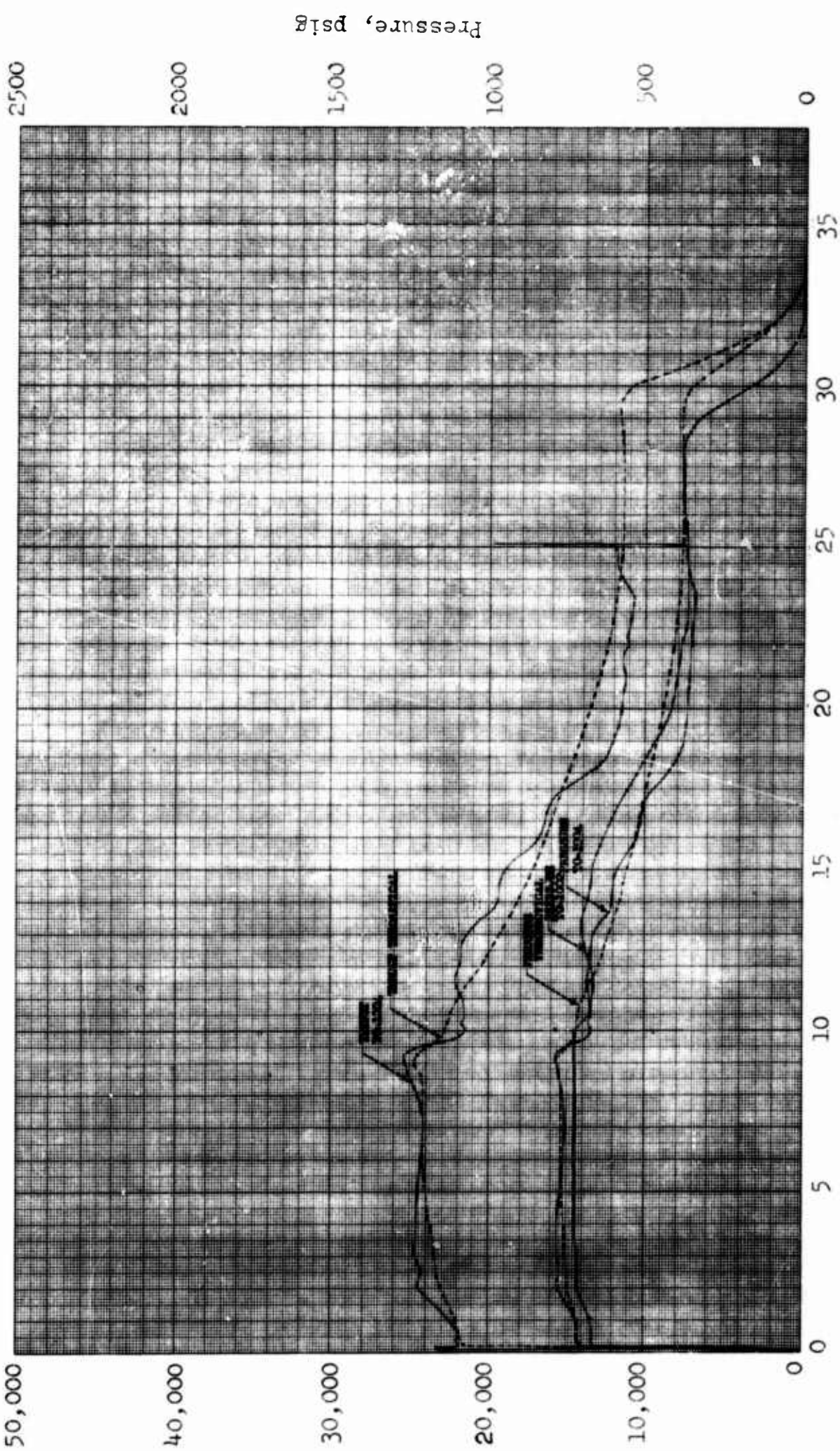


Figure 176. Pressure- and Thrust-vs-Time for Motors A-1002 and A-1004

(C) 371 pounds remained at the time of failure. The pressure- and stress-time curves were extended from a point of time of 23.4 seconds, assuming a nozzle efficiency of 0.931 (ratio of actual to theoretical thrust coefficient) between time of failure (25.107 seconds) to projected duration of 33.40 seconds. The assumed efficiency is an extension of that demonstrated at the point of failure. Comparison of the actual and projected performance with the estimated indicates that the average pressure for A-1004 was lower than anticipated, resulting from the lower pressure over RFG operation. The lower pressure level in the RFG reflects primarily the nozzle throat erosion and lower than nominal burning rates in the fifth to ninth helical layers.

(C) To further facilitate the analysis of the test results, data from A-1002 have been included in the summary of ballistic performance and pressure- and thrust-time curves, Table LX and Fig. 176. The ballistic design modifications of A-1004 were based on A-1002 data, which are useful in the evaluation of the modifications incorporated to tailor the performance. In addition to the basic motor variation (testweight to flightweight) two important modifications to the design were incorporated:

(C) The core pressure was increased by mixing the propellant to a higher liquid strand burning rate of 0.435 in./sec at 750 psia as compared to 0.427 in./sec at 750 psia for A-1002.

The liquid strand burning rates of helical layers 2 and 3 were lowered from 0.230 and 0.190 in./sec to 0.220 and 0.179 in./sec at 670 and 600 psia, respectively, to bring the pressure in this interval closer to nominal.

Results of these changes are shown in the performance of the motor, where the average core pressure was increased, and the pressure over the duration of the 2nd and 3rd helical layers was decreased to the degree desired.

The pressure-time history of A-1004 reveals characteristics of burning in the RFG more pronounced than in A-1002. This marked difference is the distinction of times corresponding to layer interfaces in RFG burning. It had been estimated originally for A-1002 that these times would be noticeable in the RFG pressure-time trace, and A-1002 estimate was very similar to A-1004 actual. However, the actual A-1002 trace was very smooth in this region, and therefore, the A-1004 estimate contained the same smooth feature. Variation in this feature is the result of propellant blending which will vary from motor to motor.

Total propellant weight of the motor was 0.3% over design nominal, which is well within the normal variation expected from manufacturing tolerances. Core propellant was 4 pounds under and RFG propellant was 11 pounds over design nominal.

(C) Ignition of A-1004 was an improvement over that obtained previously, as shown in Fig. 177. Motors A-1002 and A-1003 had ignition delay times of 0.095 and 0.092 second, respectively, which were close to the maximum limit of 0.100 second. Analysis for these data and of igniter test firing data had revealed the need for reduction of the interval between initiation and igniter main charge ignition. This was accomplished by increasing the intermediate charge pellets from 1.6 to 2.4 grams.

(C) The ignition delay of A-1004 was approximately 0.057 second, well below the maximum limit. Ignition occurred smoothly with no indication of any "shocking" or adverse ignition peaks.

(C) Structural performance of this motor was excellent for approximately 23.5 seconds. At that time chamber pressure increased from approximately 340 to 370 psig at 24.5 seconds and then tried to stabilize. Strain gage and linear potentiometer locations and data replots are shown in Figs. 178 through 185. The strain gages and linear potentiometers showed a gradual increase in the GFW case loading beginning at about 23.5 seconds but at 24.4 seconds the aft GFW dome deflection as shown by a linear potentiometer increased from 0.18 to 0.28 inch at 25 seconds. Strain gages S-22, S-23, and S-24 which were located on the lower portion of the aft GFW dome also showed a significant increase in strain at the same time. Strain gages S-19 and S-20 which were located on the upper portion of the aft dome showed only a slight increase in strain prior to 25 seconds, but increased drastically at approximately 25.043 seconds. The high speed movie also showed a sudden bulge in this area of the aft dome at that time. An increase in GFW case loading was shown by strain gages near the aft end of the motor, then near the center, then the forward end of the cylinder and lastly by the strain gages on the forward dome. Chamber pressure increased again from 370 psig at 25.060 seconds to 515 psig at 25.107 seconds when the GFW case, as shown by the high speed movie, ruptured in the cylindrical section near the aft tangent on the bottom side of the motor. No strain gages were located in the immediate vicinity of the case rupture, but the nearest hoop strain gage (S-9) showed 2.4% strain at 25.107 seconds which is 20% below design ultimate strain.

CONFIDENTIAL

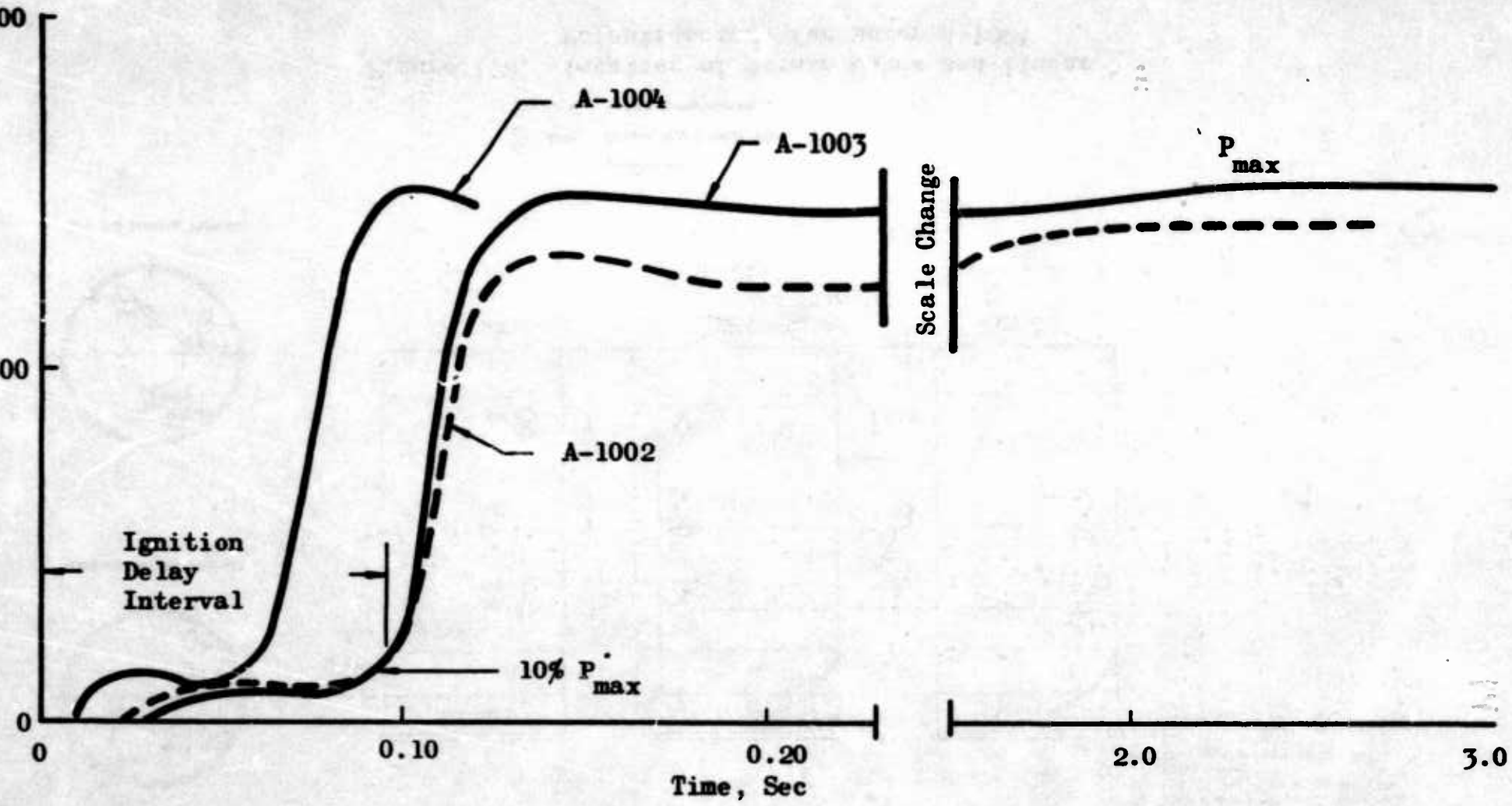
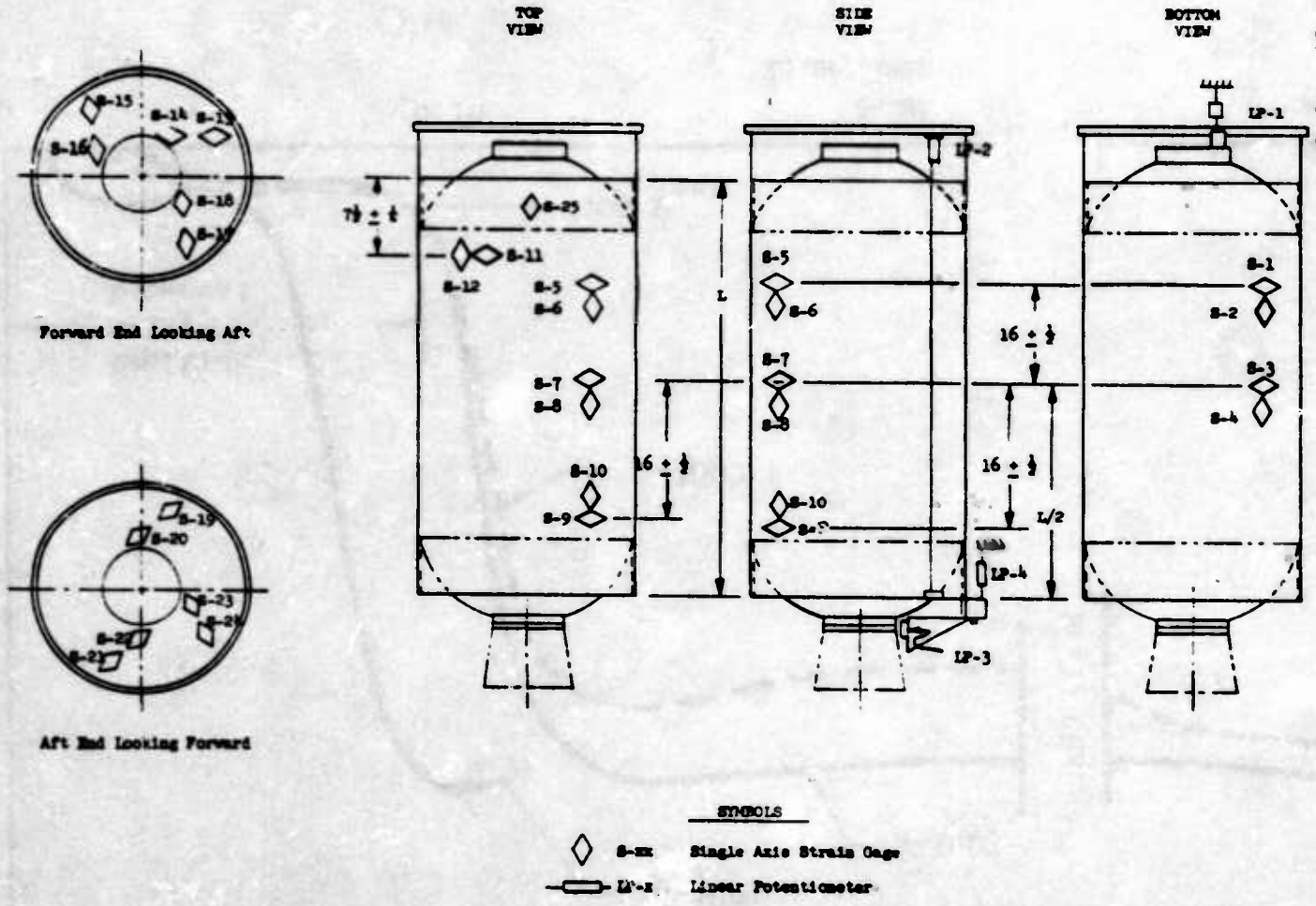


Figure 177. RFG Ignition, Motors A-1002, 1003, and 1004

CONFIDENTIAL



NOTES:

1. Do not use Type PA-7 Strain Gage.
2. Locations indicated for LP-1 and LP-2, and S-13 through S-24 are approximate (except as shown by dim.). Locate gages consistent with dome windings and surface conditions.
3. Strain gage calibration range: ± 35,000 in./in.
4. LP-1 must measure 3/4 in. defl. min.
5. For clarity, instrumentation not shown in all views.
6. Dimensions are in inches.
7. Locate S-14, -16, -18, -20, -22, and -24 as close as possible to polar boss.
8. LP-2 must measure 1½ in. defl. min.
9. LP-3 must measure 2 in. defl. min.

Figure 178. Location of Strain Gages and Linear Potentiometers for Motor A-1004

CONFIDENTIAL

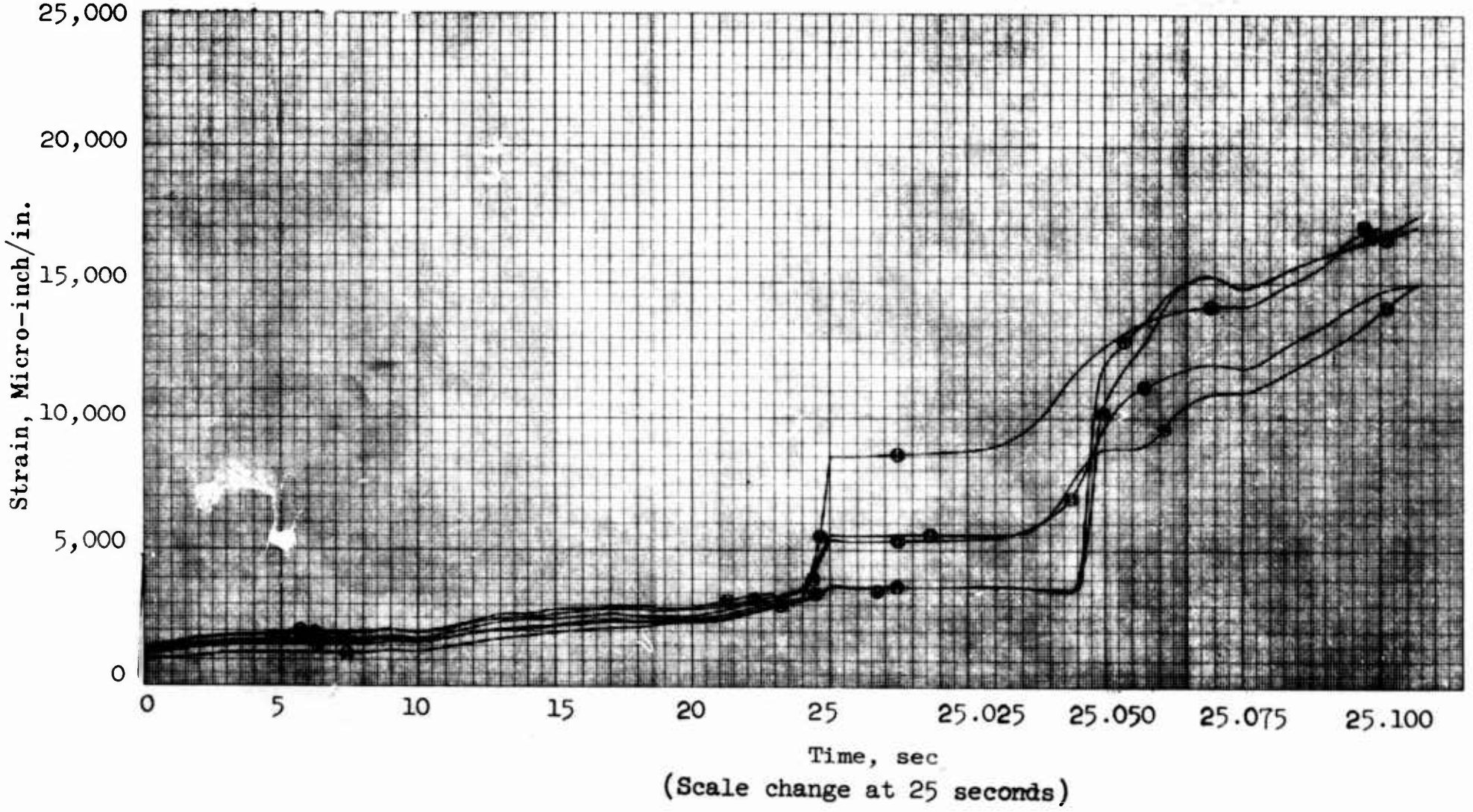


Figure 179. Aft Dome Strain-vs-Time for Motor A-1004

CONFIDENTIAL

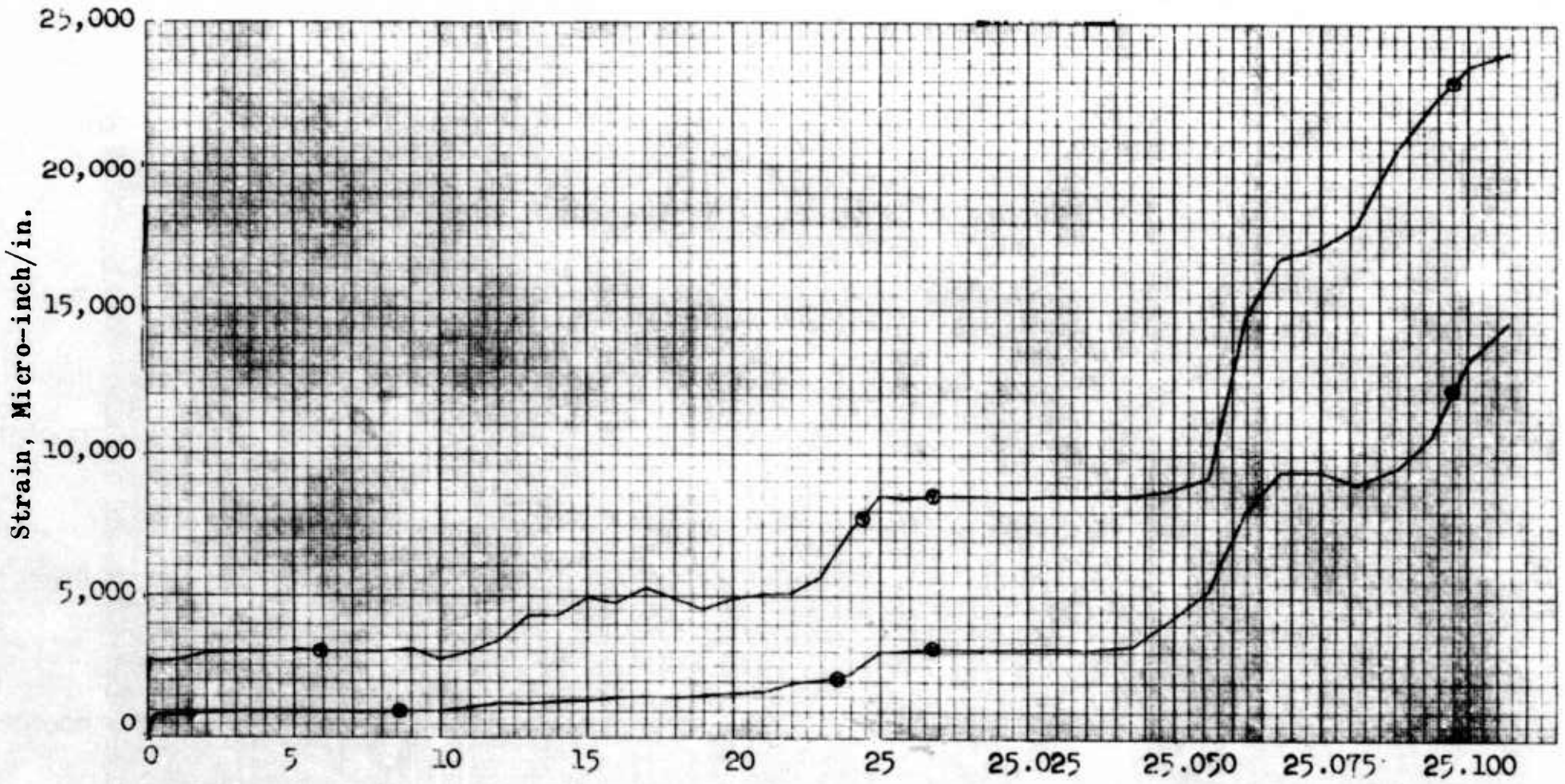
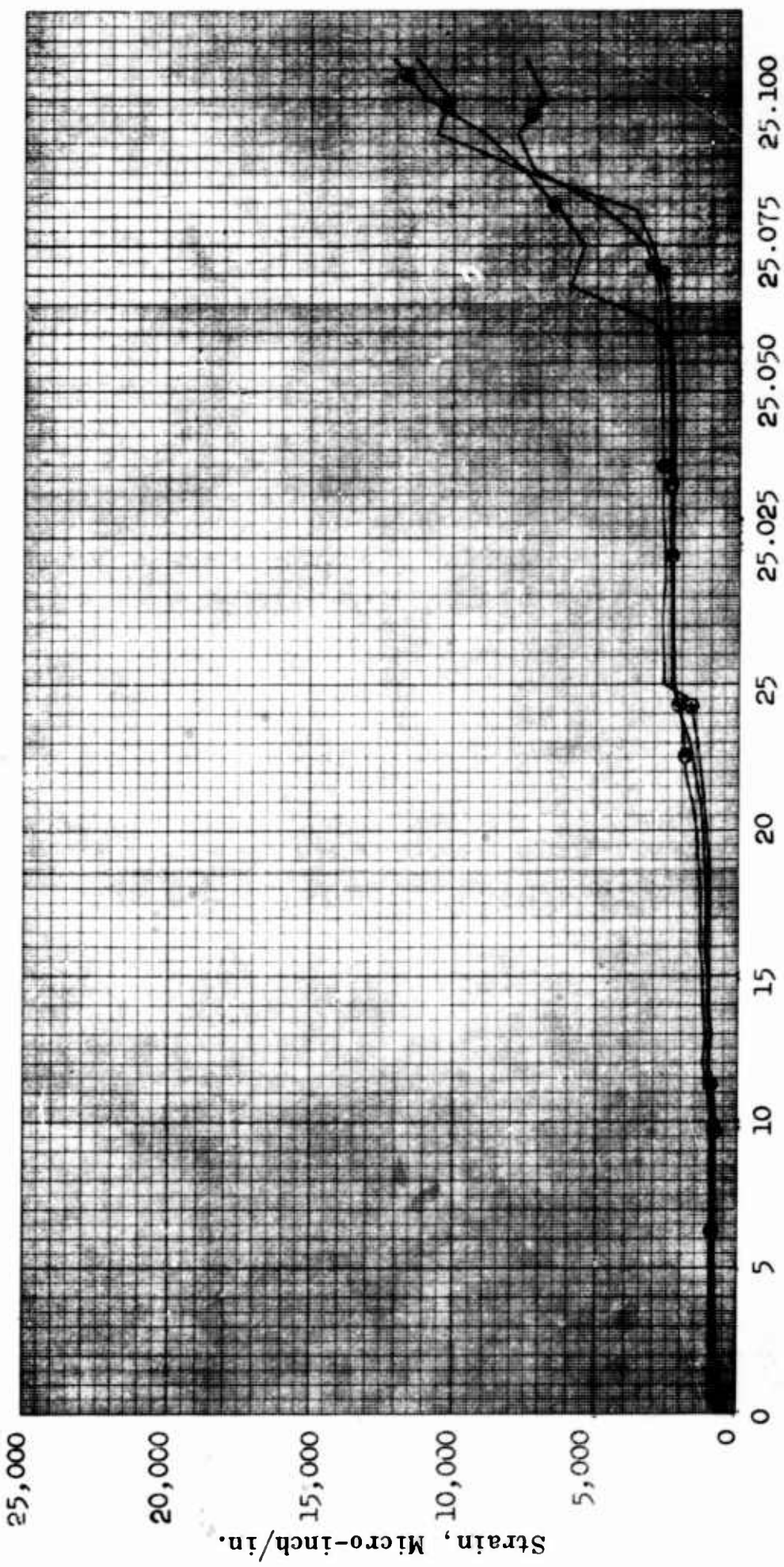


Figure 180. Cylinder Strain-vs-Time for Motor A-1004 (Gages 9 and 10)

CONFIDENTIAL



(Scale change at 25 seconds)

Figure 181. Cylinder Strain-vs-Time for Motor A-1004 (Gages 3, 4, and 8)

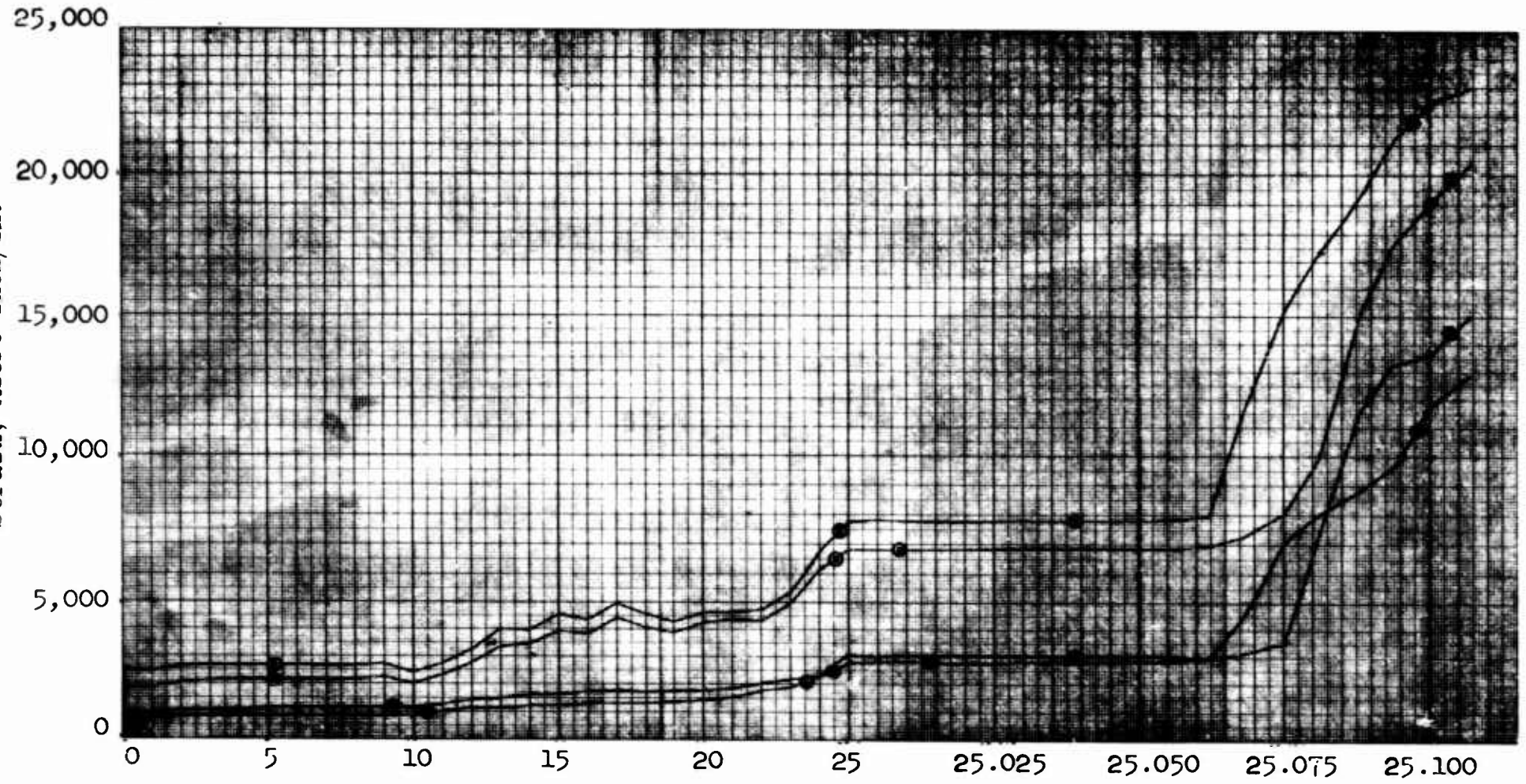


Figure 182. Cylinder Strain-vs-Time for Motor A-1004 (Gages 5, 6, 11, and 12)

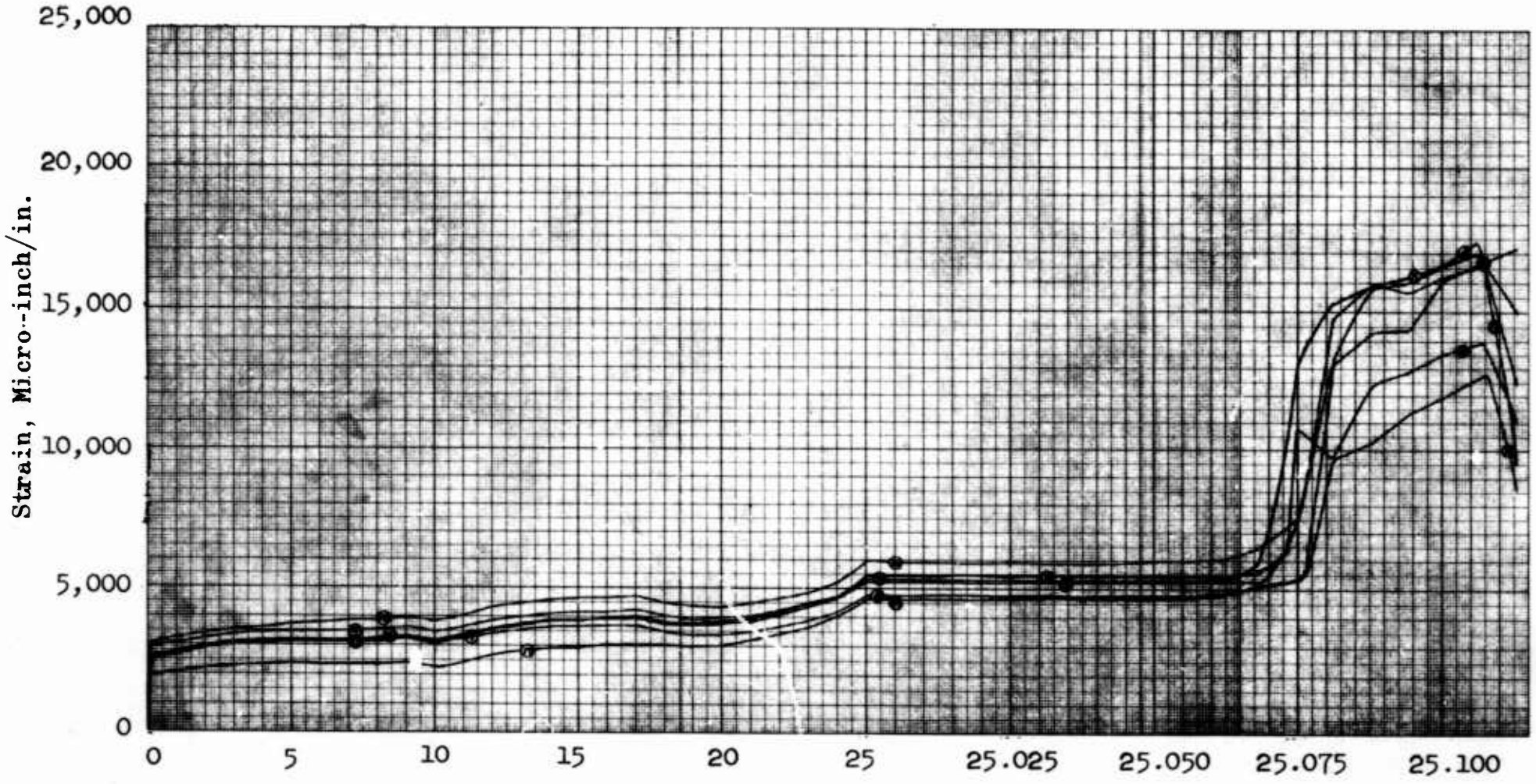


Figure 183. Forward Dome Strain-vs-Time for Motor A-1004

CONFIDENTIAL

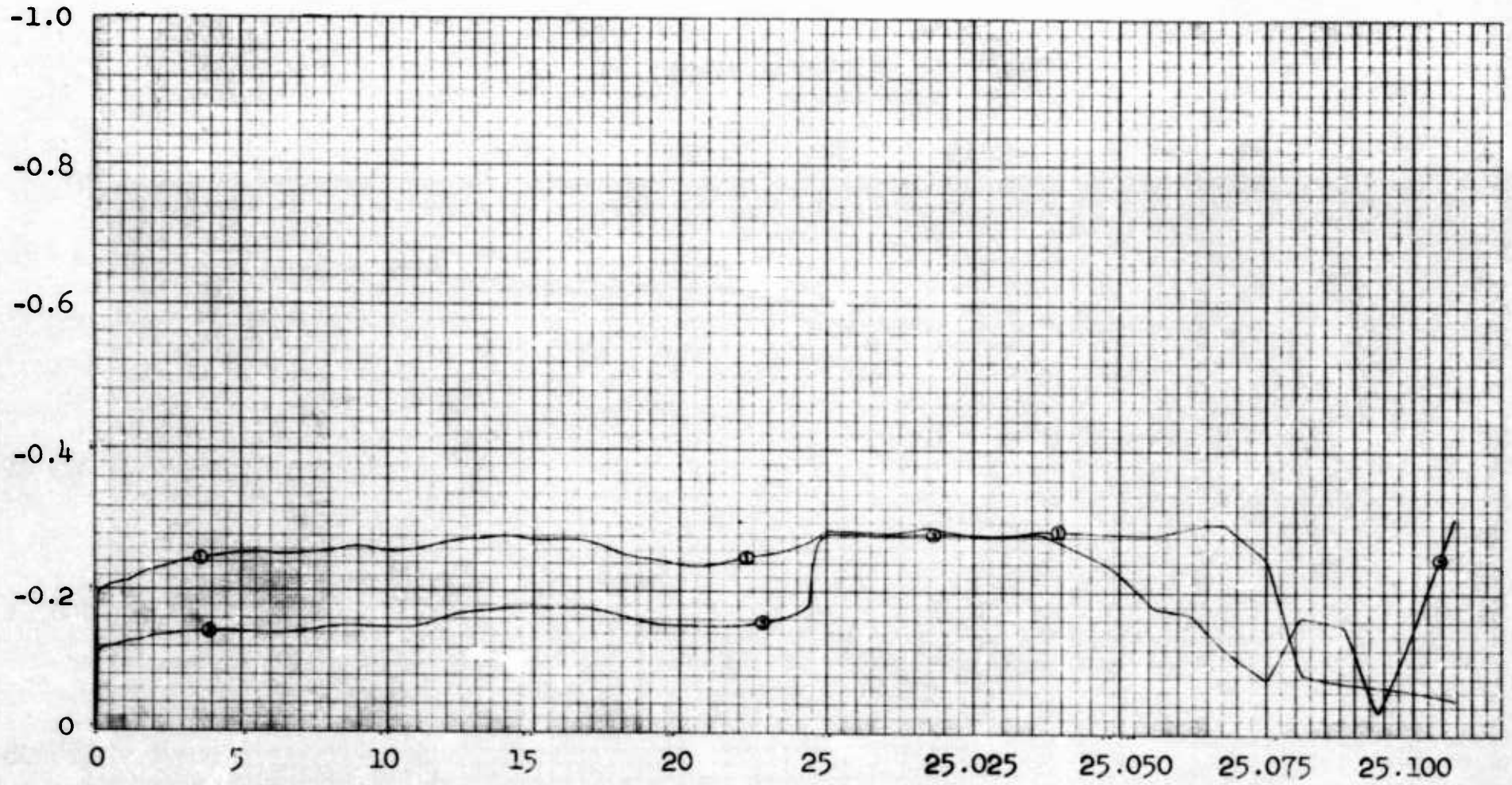


Figure 184. Forward and Aft Dome Deflection-vs-Time for Motor A-1004

CONFIDENTIAL

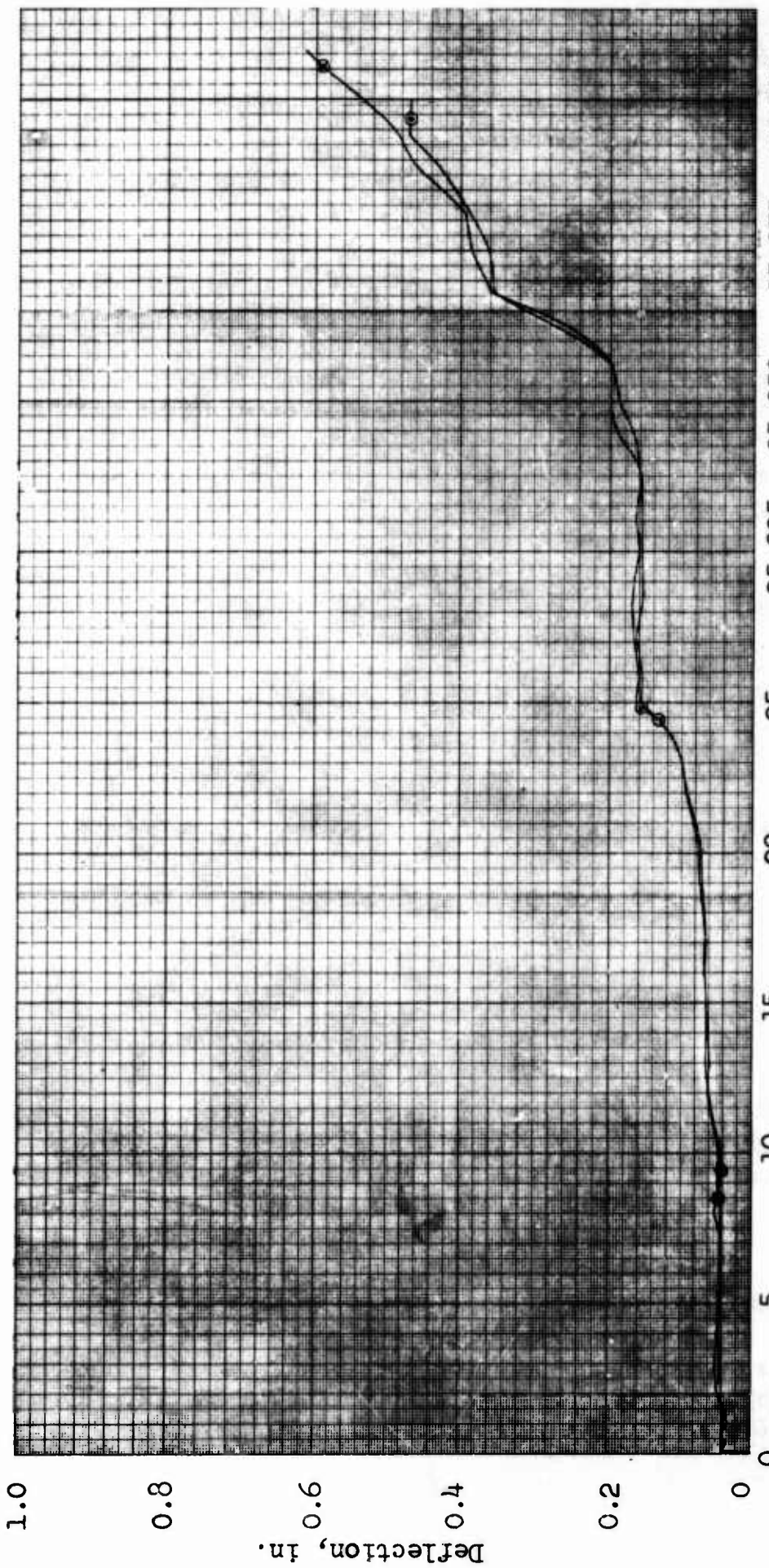


Figure 185. Cylinder Longitudinal Deflection-vs-Time for Motor A-1004

(C) Examination of the inert components which were recovered after the malfunction showed that all of them with the possible exception of the GFW case functioned properly. Rupture of the GFW case occurred at 515 psig which is 70 psig below design ultimate pressure, and was probably caused by the nonuniform load on the case. This nonuniform load was shown by the difference in the time at which various strain gages recorded a significant increase in strain.

The forward and aft polar boss assemblies and two reinforced plastic rings (part of polar boss repair) which were bonded to the aft polar boss after it was damaged were recovered and were in good condition prior to ejection from the motor. Some of these components were broken when they hit the ground but all of the pieces were found and the components were pieced together for study. Observation of the aft polar boss assembly showed much more erosion occurred on the bottom side of the boss and load rings than on the top. Erosion of the forward polar boss assembly was very uniform.

Thermocouple locations are presented in Figs. 186 and 187; Figs. 188, 189, and 190 present the temperature history of the thermocouples on the forward dome. As is easily seen, the forward dome experienced no heating during the firing duration. The maximum temperature attained was 160 F at 1.5 seconds as indicated by thermocouple 8, while thermocouple 7 attains its maximum temperature of 140 F at 6 seconds. Both thermocouples show a gradual decrease to 130 F at the end of the firing duration. The difference of temperature between thermocouples 7 and 8 for this firing is almost identical to that of A-1003 and the maximum temperatures are approximately equal. Since these temperatures are quite low and decrease with time there is no adverse effect.

(C) The thermocouple data for the cylindrical section of the case are presented in Figs. 191, 192, and 193. Thermocouple 18 which was located on the forward tangent was lost prior to the firing. Of the remaining eight thermocouples on the cylindrical section of the case only thermocouples 19 and 20 showed any increase in temperature. Thermocouple 19 indicated the higher temperature of the two and reached a maximum of 106 F at 25 seconds. Thermocouple 20 reached its maximum of 98 F at 25 seconds also. Both thermocouples 19 and 20 started to increase in temperature at 4 seconds. The maximum recorded temperatures of the case were not of sufficient magnitude to be considered as a significant factor in contributing to the malfunction.

Presented in Figs. 194 and 195 are the thermocouple data obtained from the aft dome of the motor. No temperature increase of the aft dome occurred during the firing duration.

NOZZLE THERMOCOUPLE PROCUREMENT

FOR T. O. 1004

NOTES:

1. Locations marked by "◆" are for thermocouples on the surface.
2. Surface thermocouples temperature range is 60-600°F.
3. Surface coordinate dimensions are ± .01 in.
4. Use smallest thermocouples possible.
5. All dimensions are in inches.
6. Surface thermocouples are to be located as near to edge of the drill hole as practical.
7. Total of 5 thermocouples installed in nozzle.

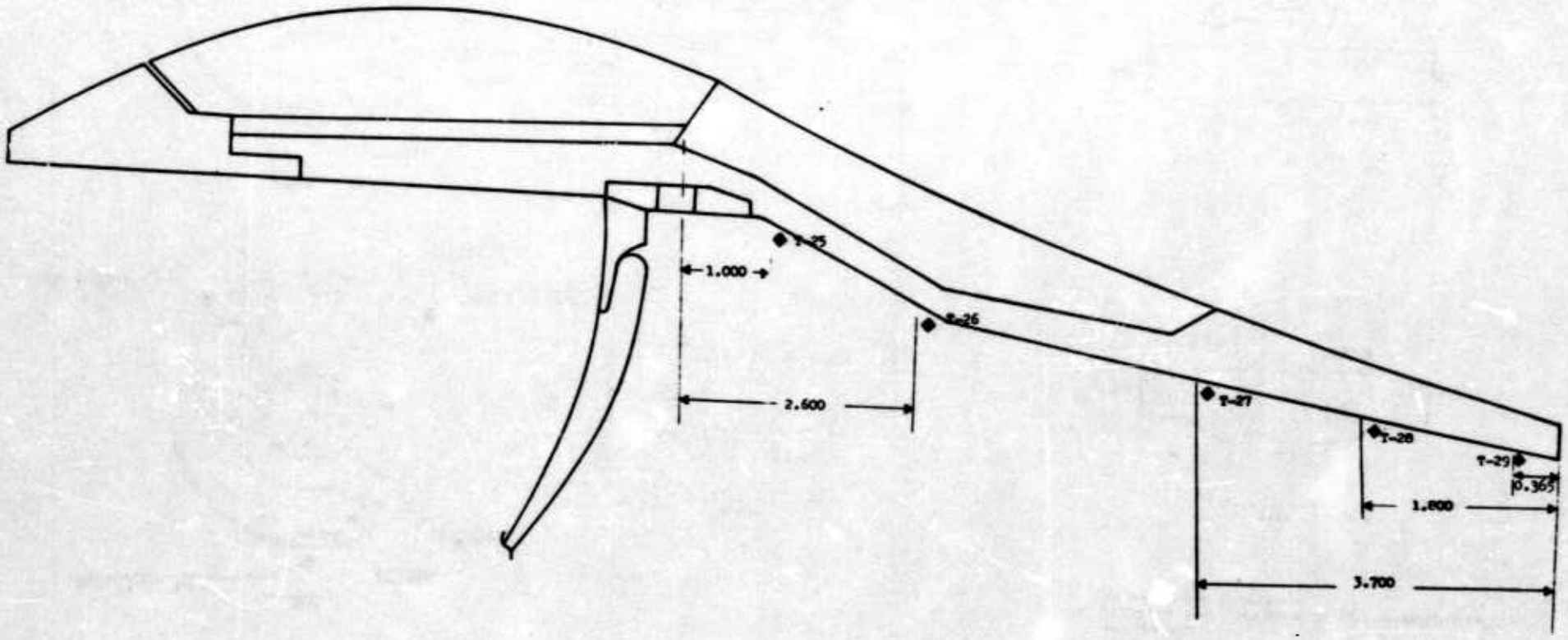
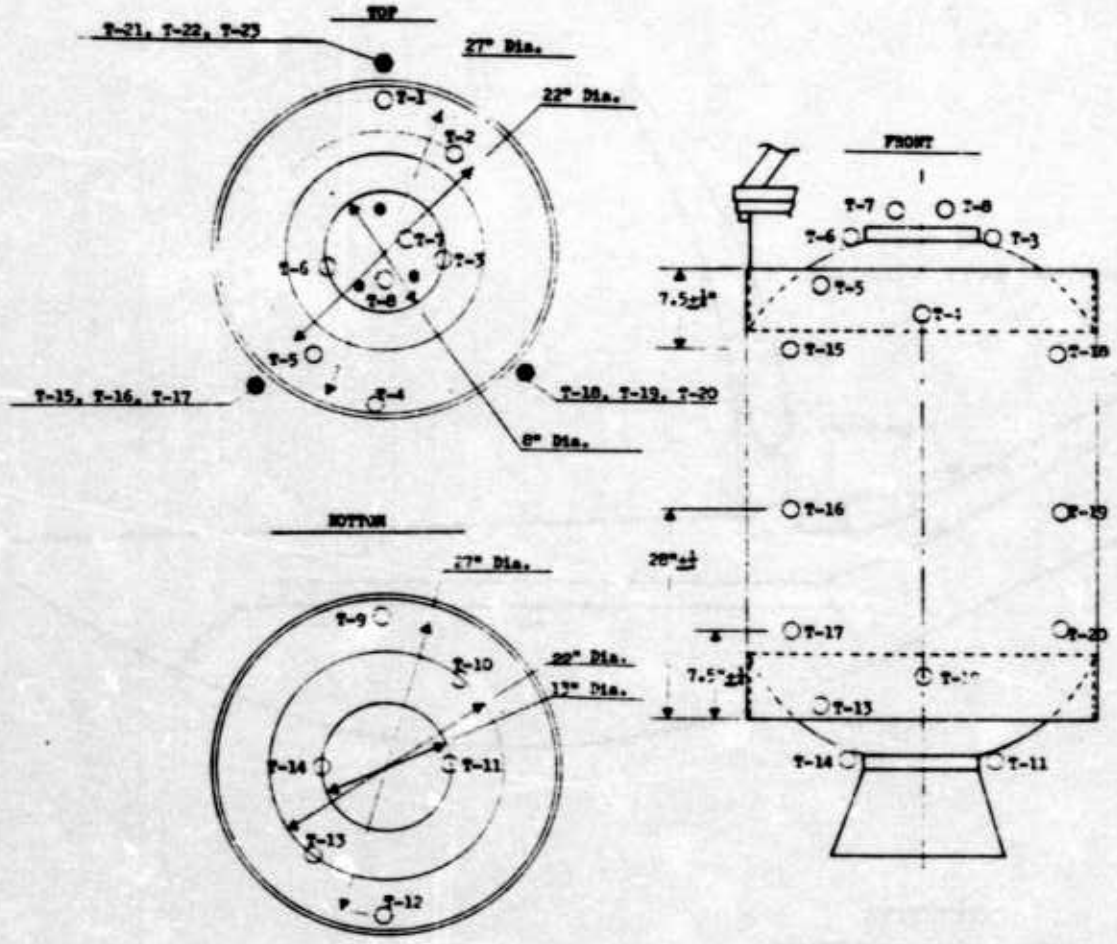


Figure 186. Location of Thermocouples on Nozzle Exit Cone of Motor A-1004



NOTES

1. For clarity, all gages are not shown on all views.
2. T-7 is located between pressure plug and CC plug.
3. T-8 is located between the two pressure plugs.
4. T-24 will be located on the surface of the aft heat deflection shield.
5. Total of 24 thermocouples will be placed on motor and nozzle.
6. Place motor in test stand so that thermocouples 15, 16 and 17 are on bottom.

Figure 187. Location of Thermocouples for Motor A-1004

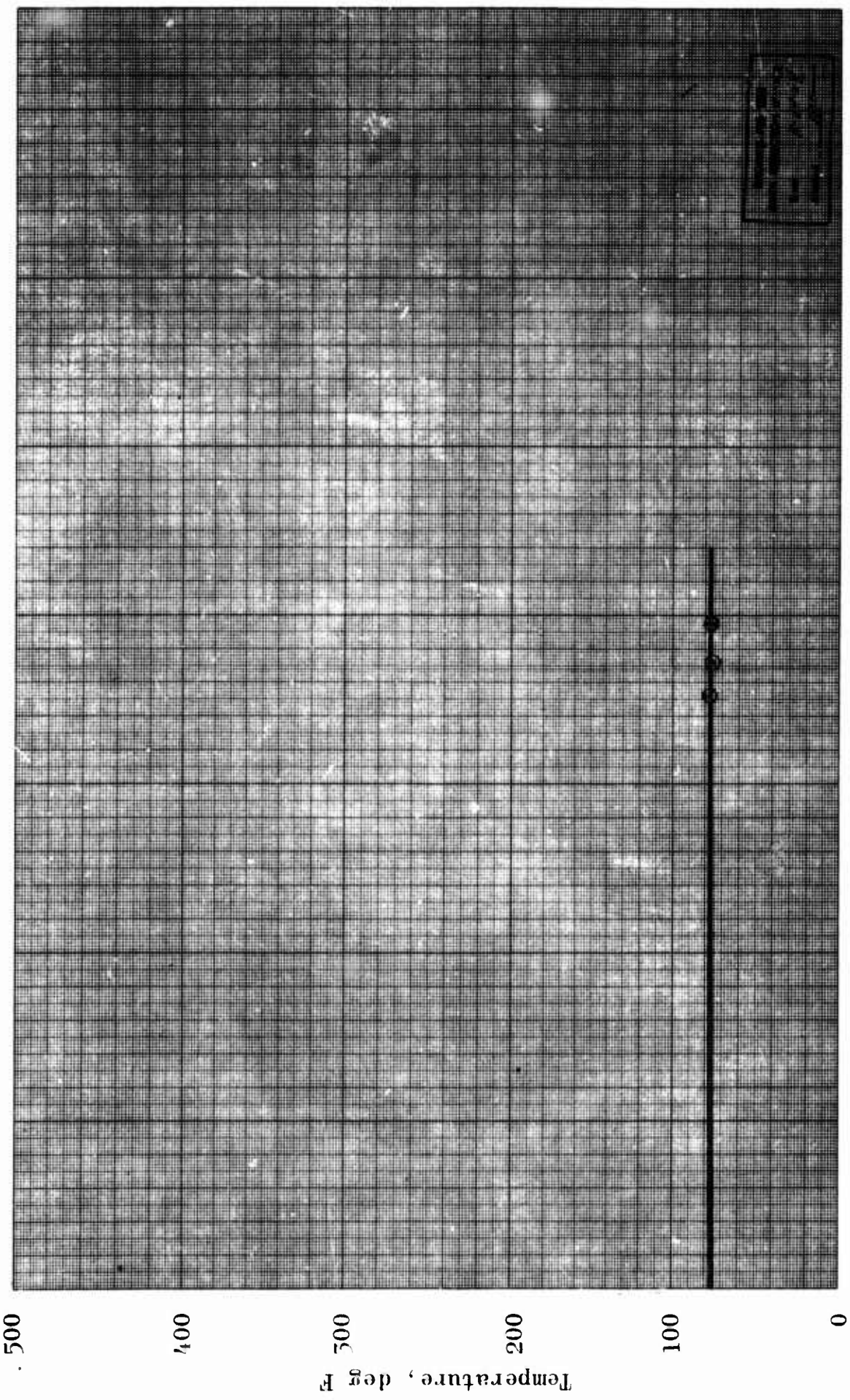


Figure 188. Forward Dome Temperature-vs-Time for Motor A-1004 (Thermocouples 1, 2, and 3)

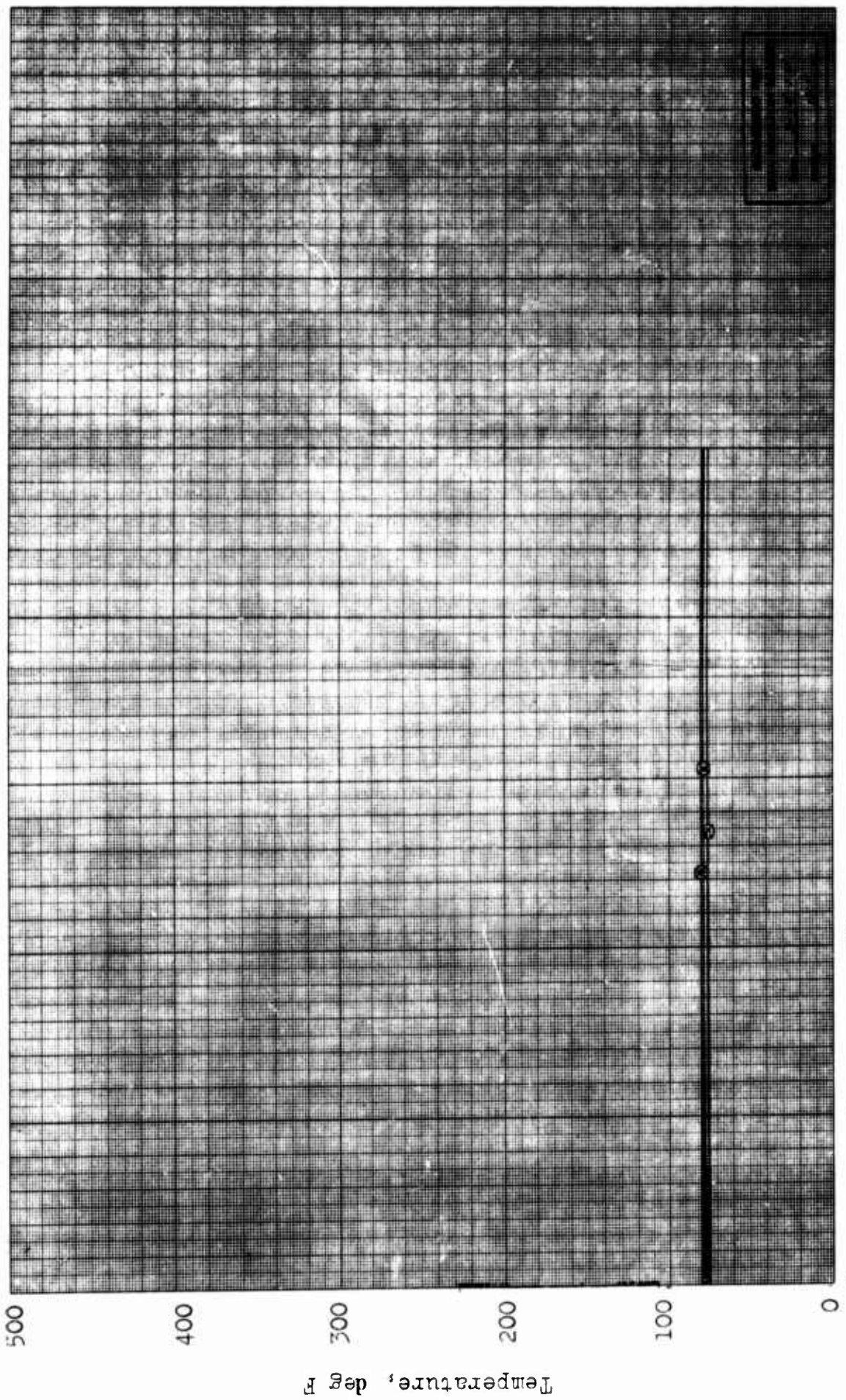


Figure 189. Forward Dome Temperature-vs-Time for Motor A-1004 (Thermocouples 4, 5, and 6)

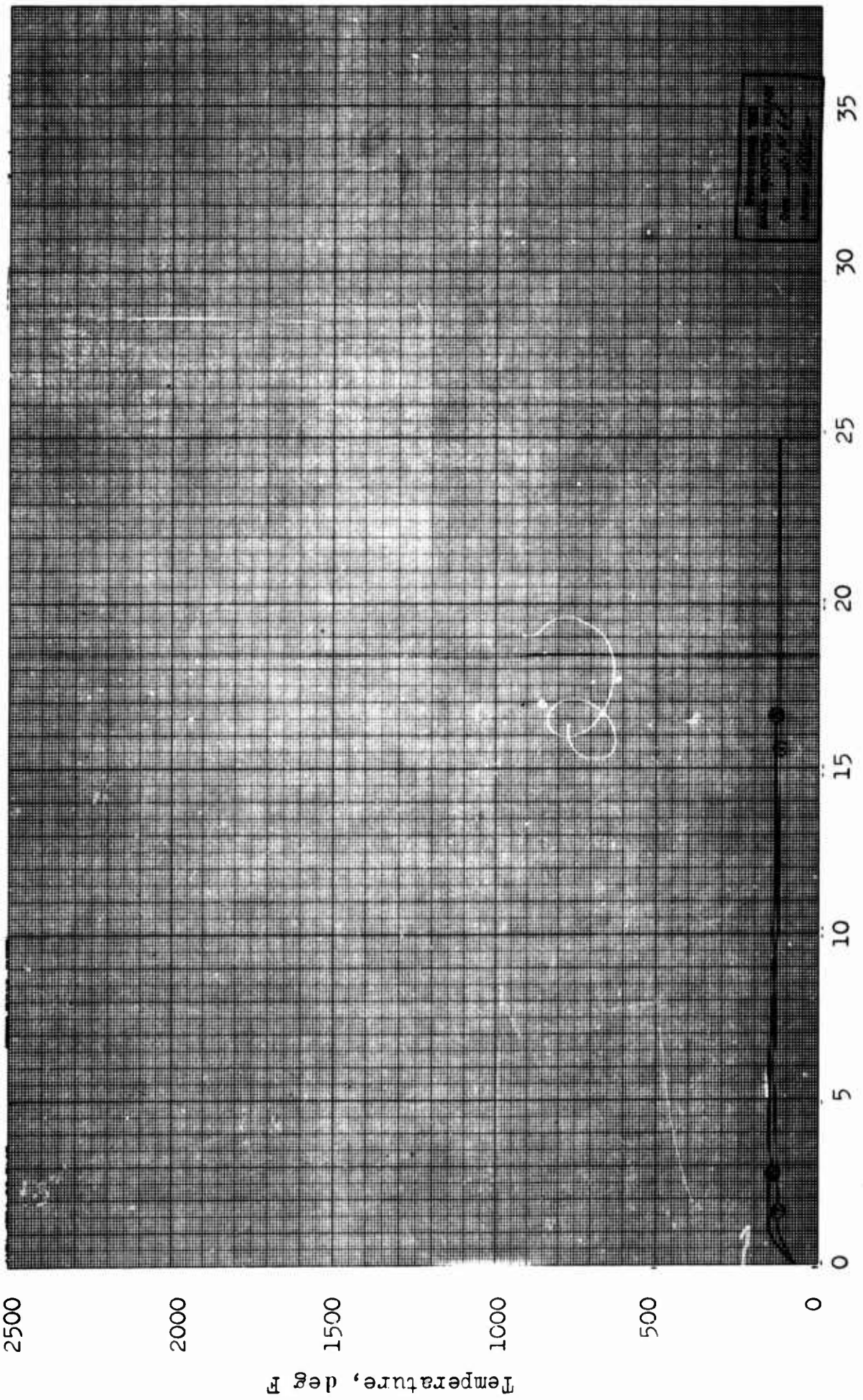


Figure 190. Forward Closure Temperature-vs-Time for Motor A-1004

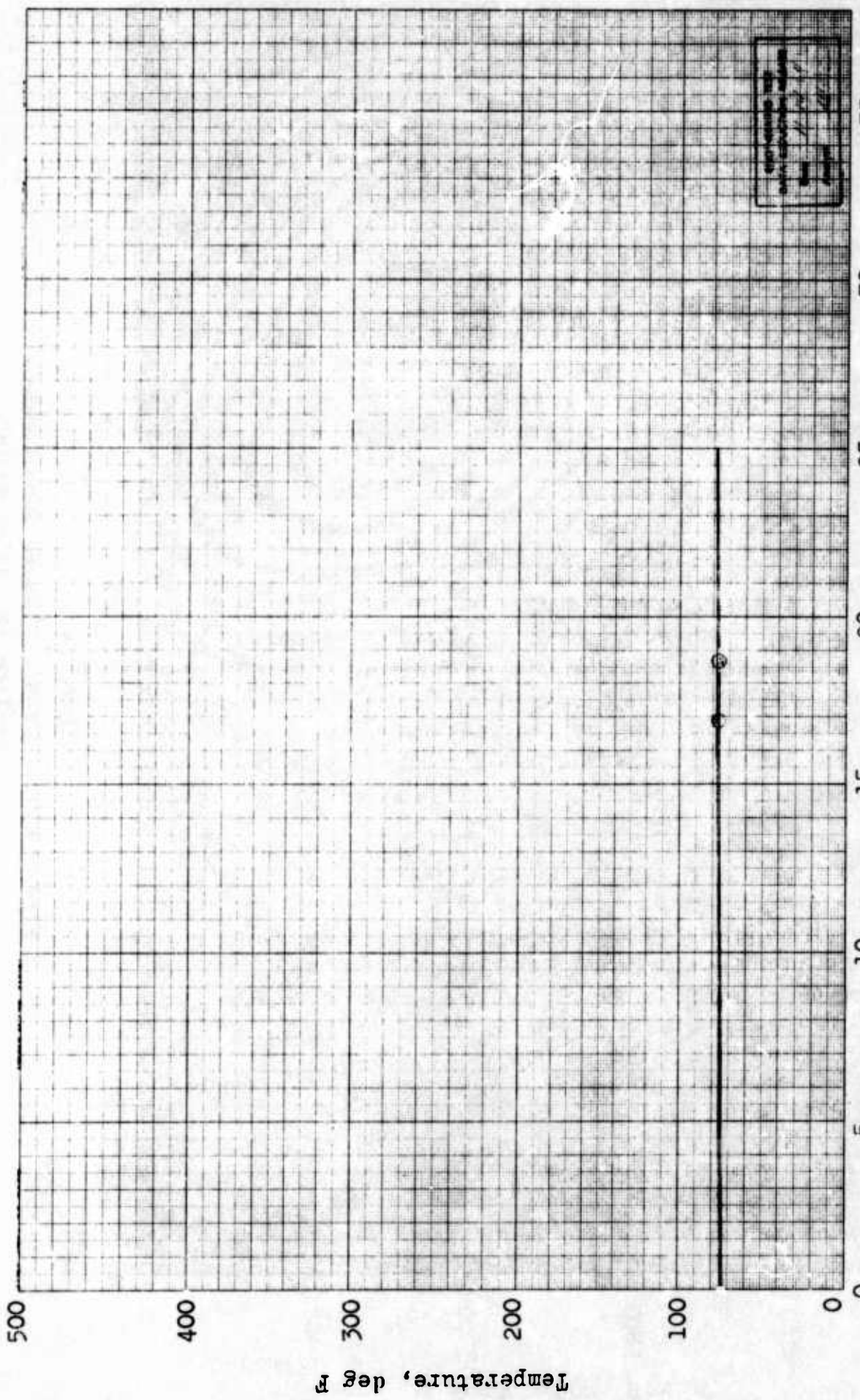


Figure 191. Cylinder Temperature at Forward Tangent Plane-vs-Time for Motor A-1004

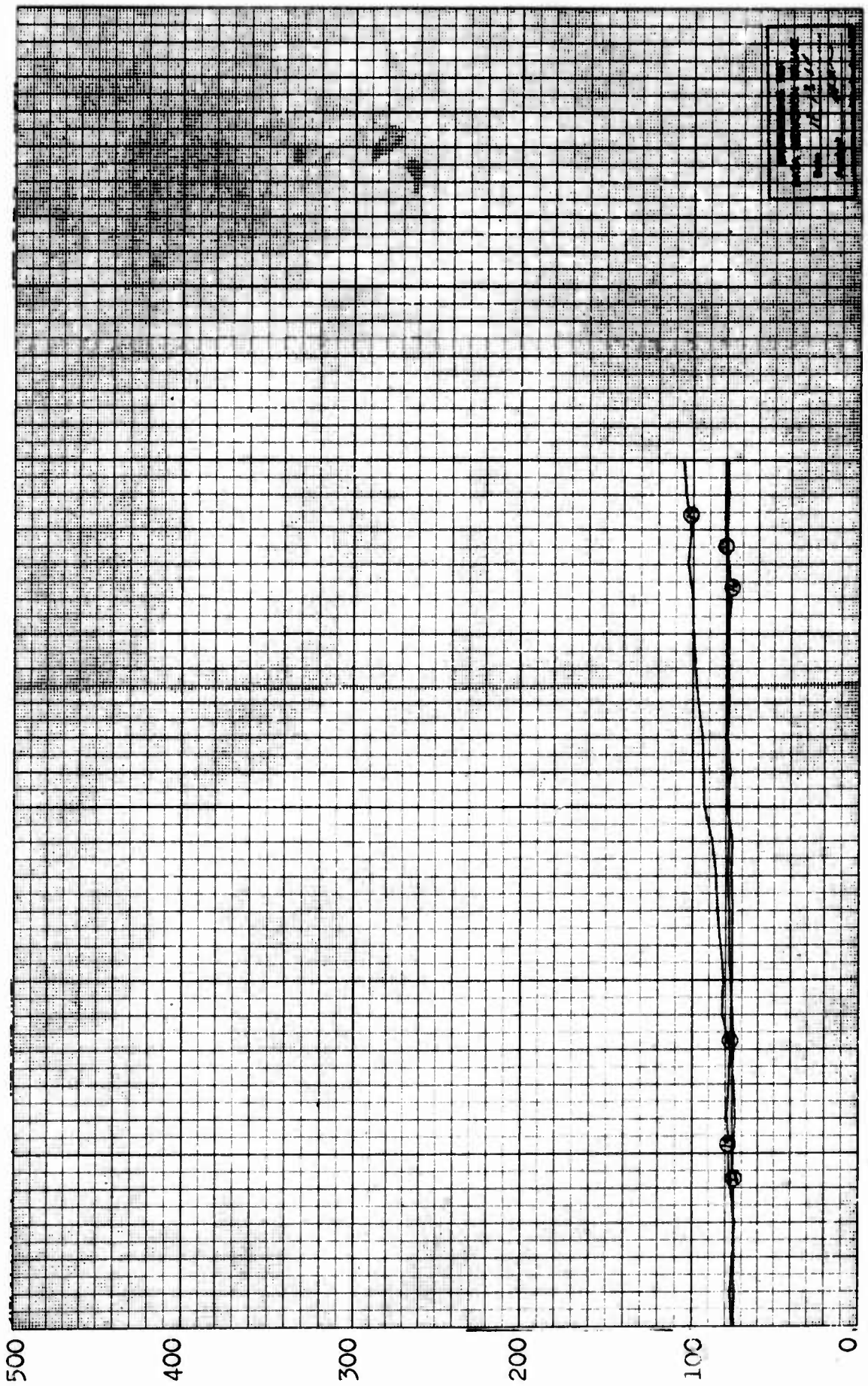


Figure 192. Cylinder Temperature at Center-vs-Time for Motor A-1004

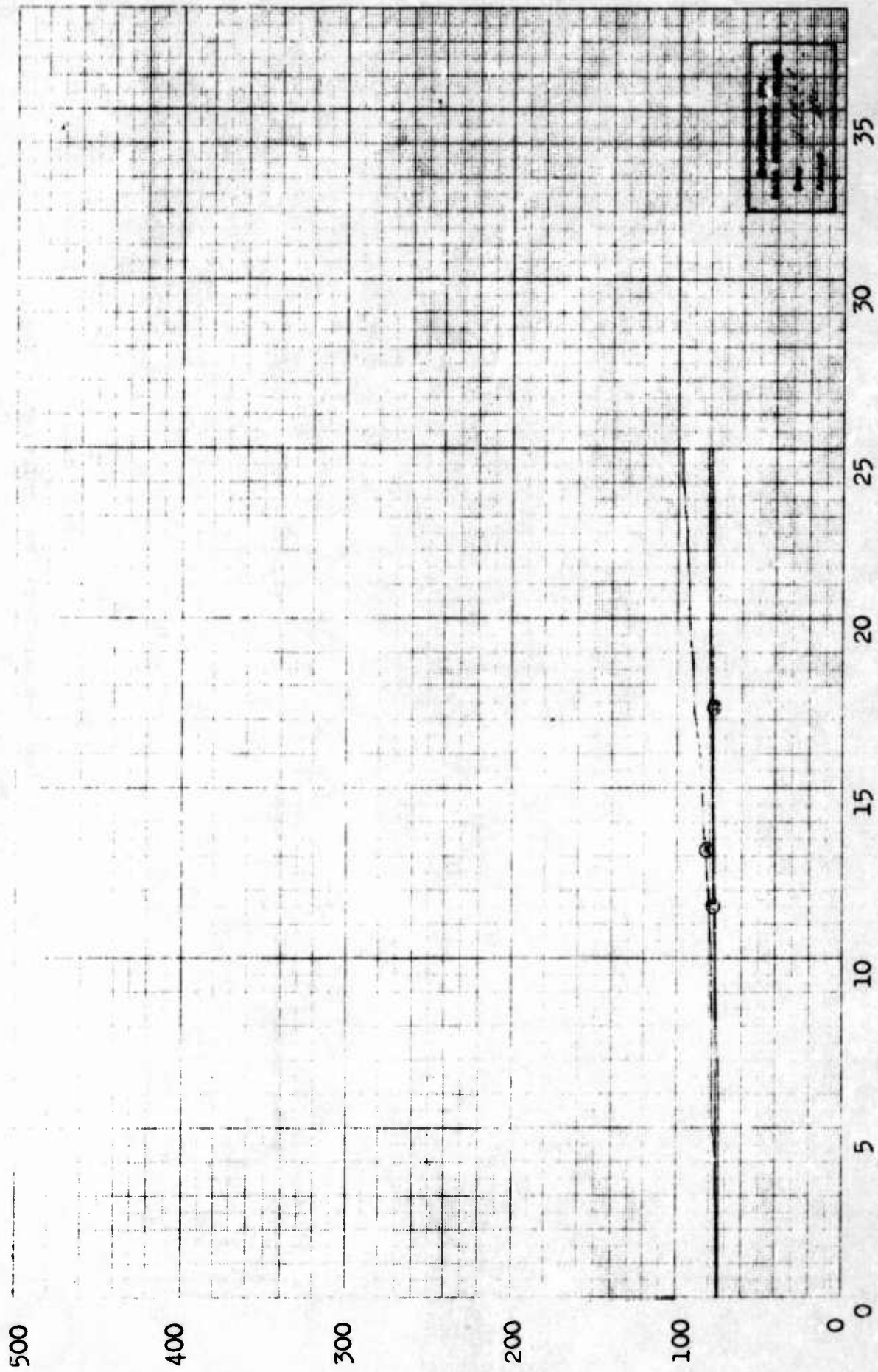


Figure 193. Cylinder Temperature at Aft Tangent Plane-vs-Time for Motor A-1004

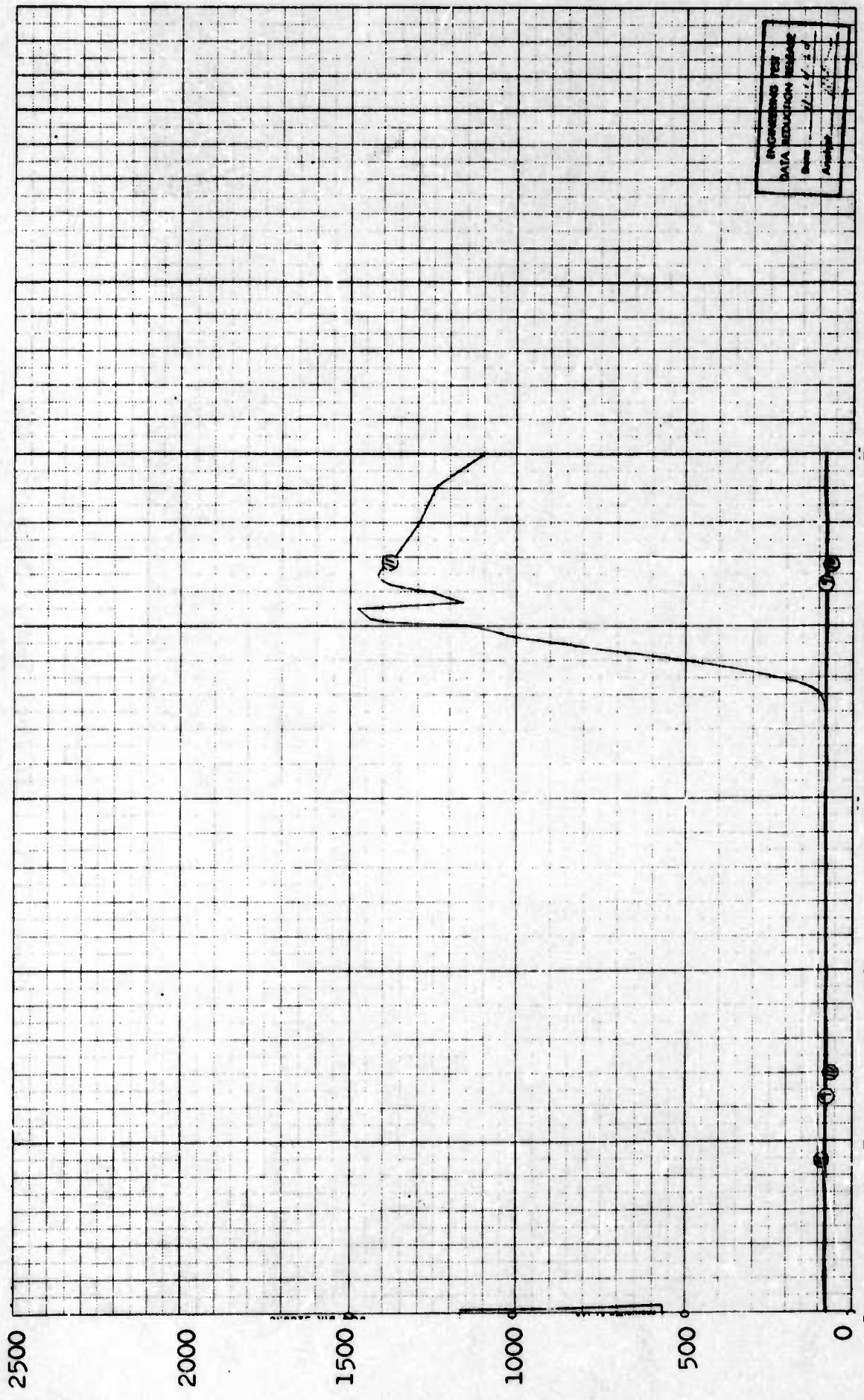


Figure 194. Aft Dome Temperature-vs-Time for Motor A-1004 (Thermocouples 9, 10, and 11)

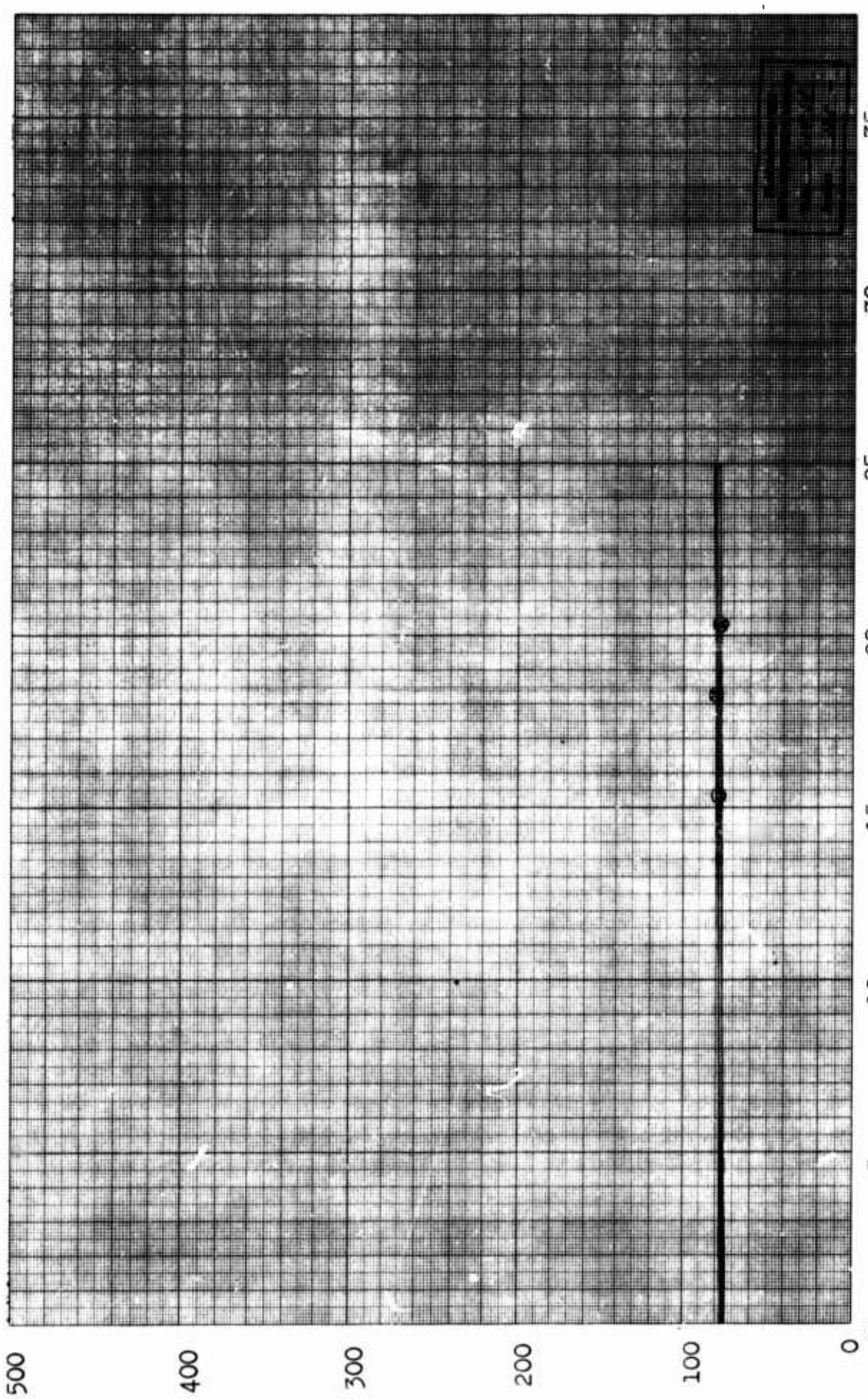


Figure 195. Aft Dome Temperature-vs-Time for Motor A-1004 (Thermocouples 12, 13, and 14)

Thermocouples 11, 25, 26, 27, and 28 were lost after 17.4 seconds of firing due to ignition of the tape securing the instrumentation on the aft end of the motor to the thrust stand. The tape was ignited by radiation from the exhaust plume as was seen in the high speed movie of the firing.

Figure 196 presents the temperature history of thermocouple 24 which was located on the exterior of the aft dome insulation to determine the amount of base heating which would have occurred had the aft dome not been insulated. The maximum temperature recorded was 335 F at the end of the firing duration.

Presented in Fig. 197 is the temperature history of the thermocouples on the exterior of the nozzle exit cone. Thermocouples 25, 26, 27, and 28 were lost as previously mentioned after 17.4 seconds of firing. Thermocouple 29 survived the firing duration and registered a maximum exit cone exterior temperature of 160 F. The fact that the fire which destroyed thermocouples 11, 25, 26, 27, and 28 did occur, places some doubt as to whether or not the temperatures recorded were from internal or external sources. In any event, none of the temperatures recorded were of sufficient magnitude to jeopardize the nozzle.

The forward polar boss and closure, as seen in Fig. 198, lost very little material. Although very little material was actually lost, the char depth was about the expected magnitude and varied from a maximum of 0.15 inch in the MX-2646 of the forward closure to 0.1 inch in the MX-2646 on the upper surface of the polar boss. No char occurred beginning at the third load ring step in the MX-4600. The over-all performance of the forward closure and polar boss was excellent. As can be seen in Fig. 198, the reduction of the forward closure insulation to 0.25 inch could be made without jeopardizing performance of the component in any manner and would reduce the inert weight of the motor.

The material losses and char depth of the modified aft polar boss are presented in Fig. 199. The material losses in the repaired area were slightly greater than that anticipated, but not of sufficient magnitude that, had the firing gone the full duration, there would have been a malfunction. The losses and char depth in the load ring area were very close to that expected. The loss of material under the expansion joint was not expected to be so severe. The appearance of the area was as if a tool had gouged a groove all the way around the boss at the joint of the nozzle and the polar boss. The groove varied in size and depth from about 0.25 inch in diameter to about 0.5 inch in diameter. At its deepest point, but only locally, the material was lost all the way to the titanium reinforcement.

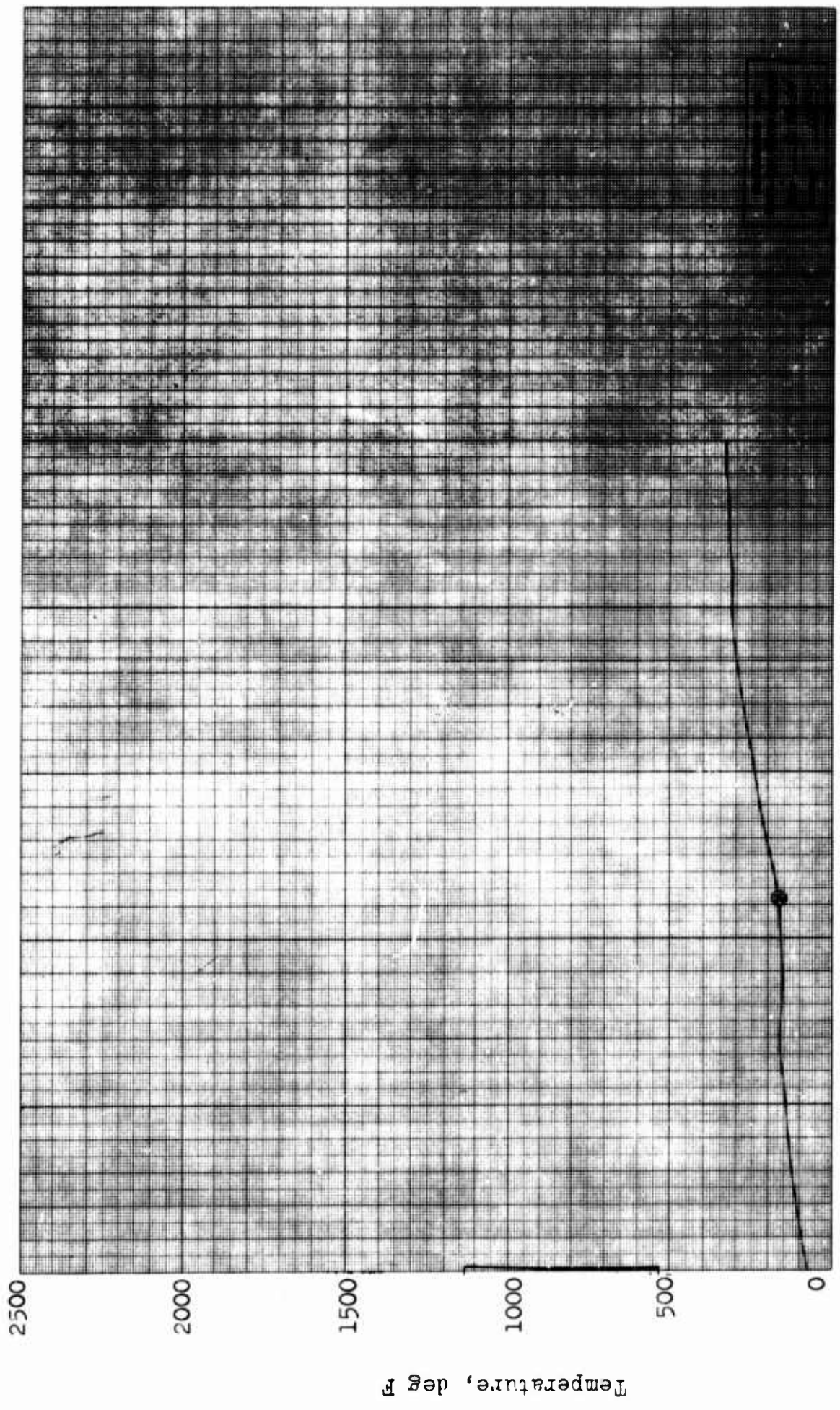


Figure 196. Aft Dome Insulation Exterior Temperature-vs-Time for Motor A-1004

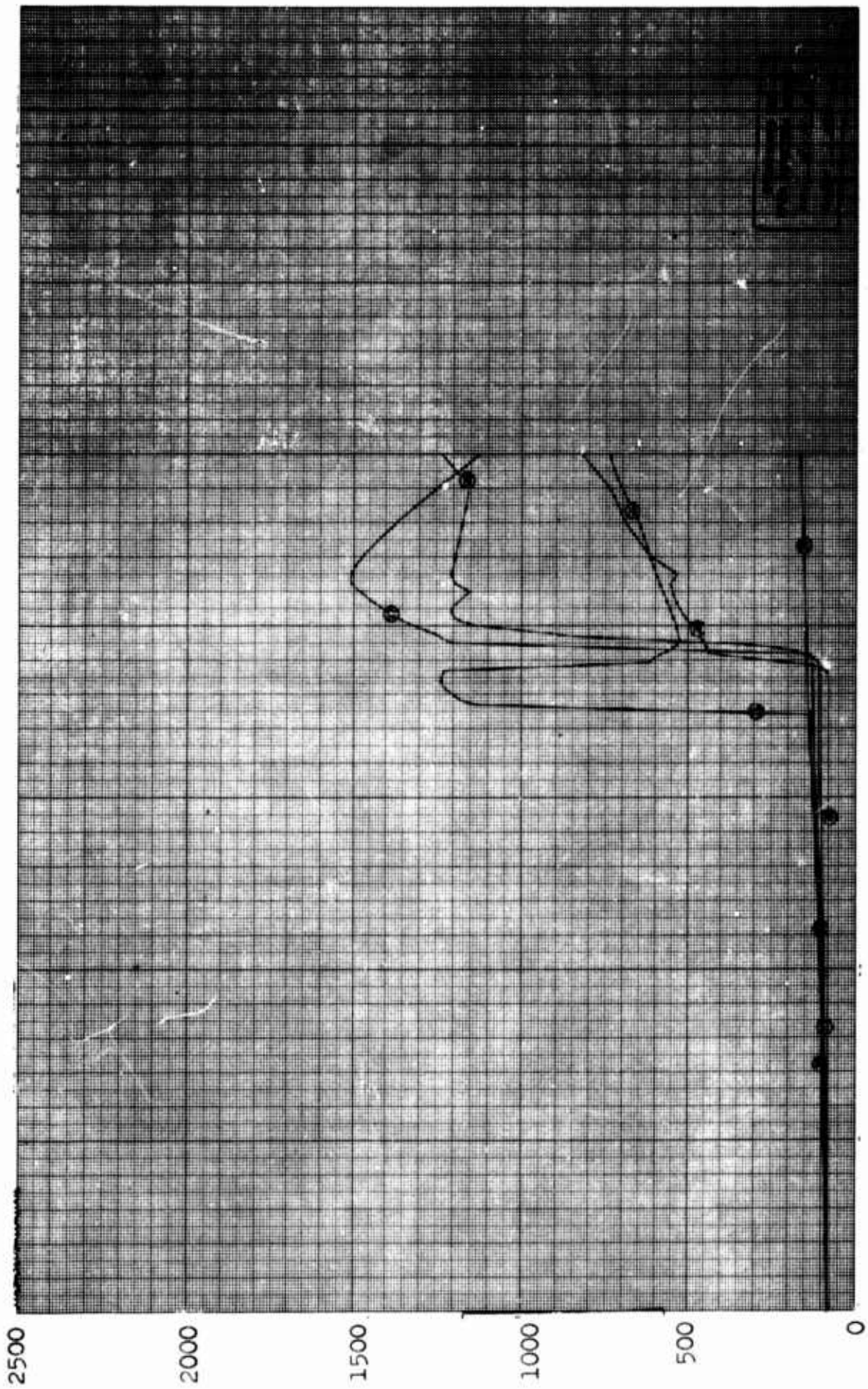


Figure 197. Nozzle Exit Cone Temperature-vs-Time for Motor A-1004

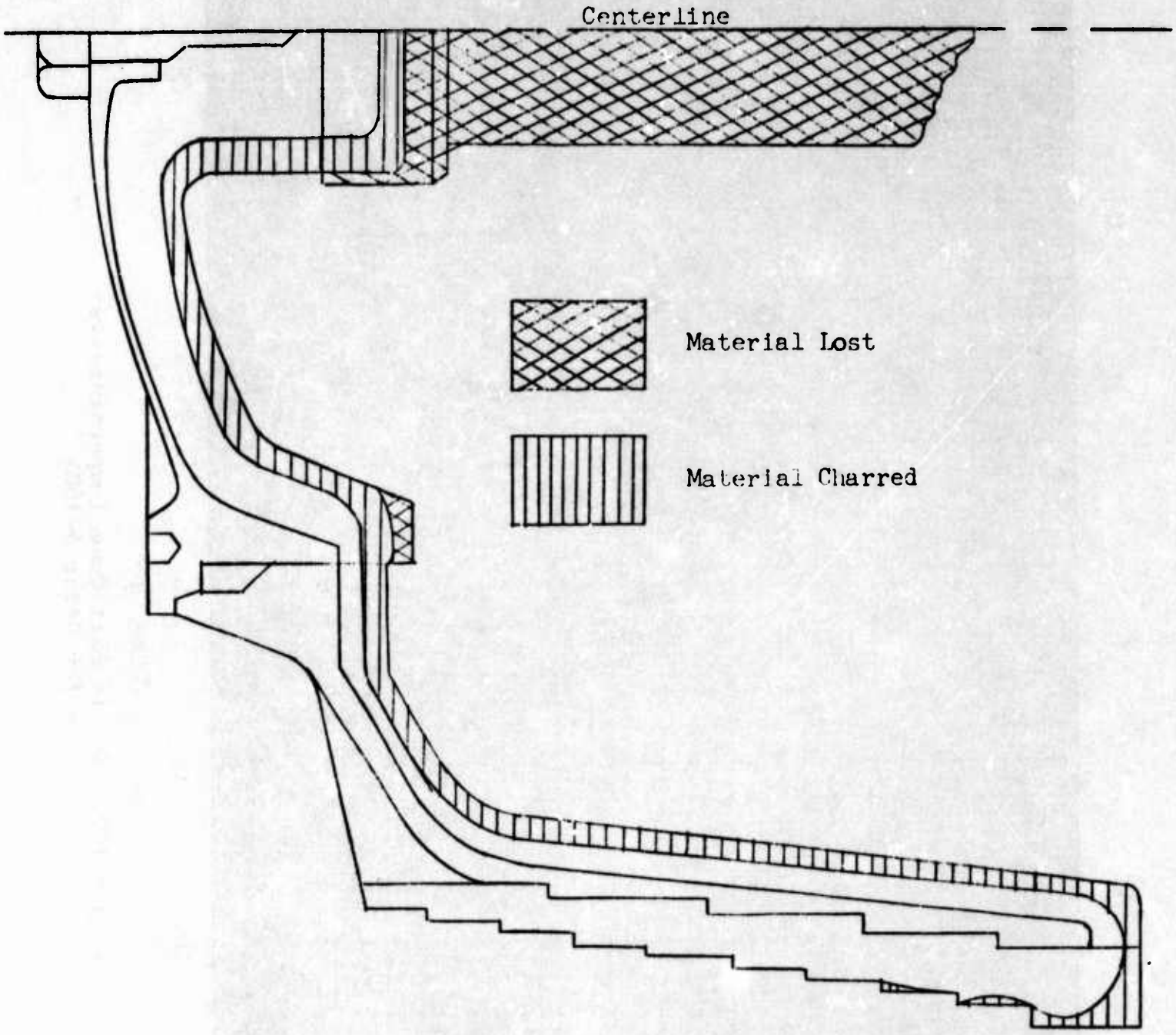


Figure 198. Material Loss and Char Depth of Forward Polar Boss and Closure for Motor A-1004

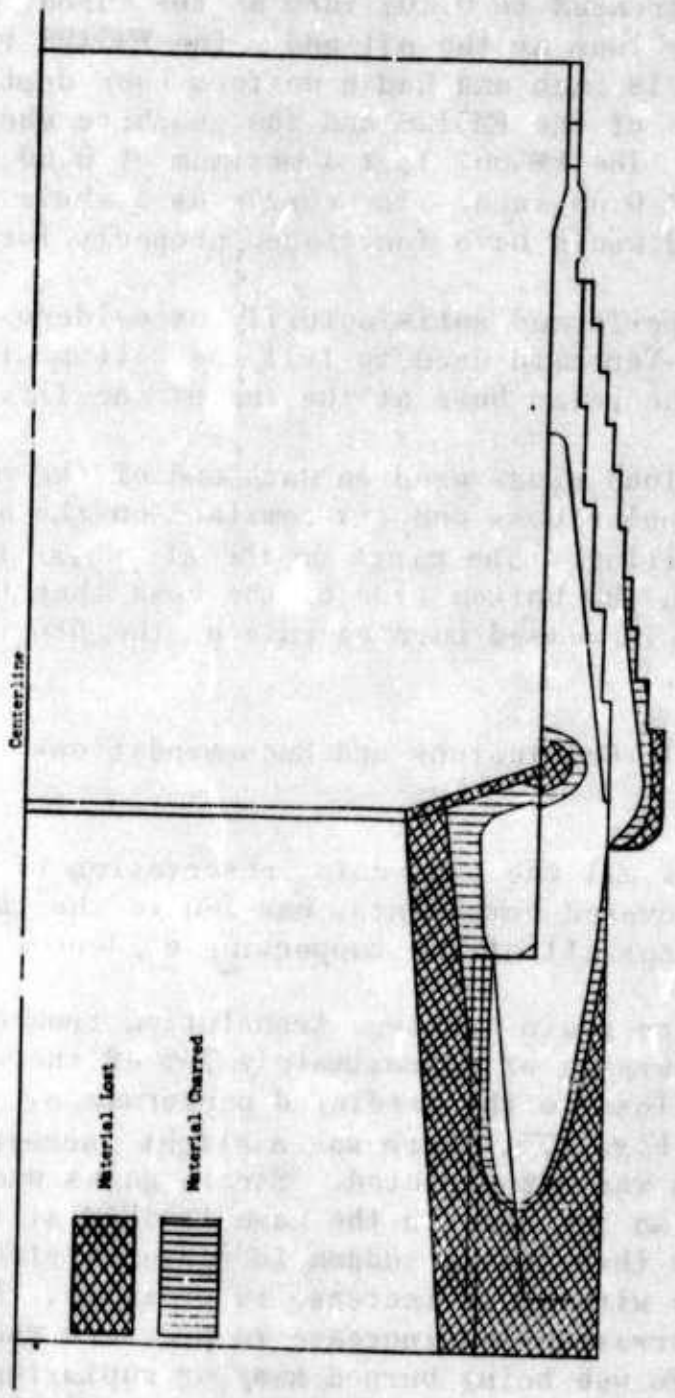


Figure 199. Material Loss and Char Depth of Aft Polar Boss for Motor A-1004

The material losses and char depth of the various materials making up the nozzle are presented in Fig. 200 . The severe loss of the FM5128 in the entrance of the nozzle was not anticipated to be so severe, but was not entirely unexpected since an expansion joint was provided at this point. The char depth in this material was a uniform 0.14 inch. The Graph-I-Tite G insert had a maximum loss of 0.2 inch on the forward end which decreased to 0.107 inch at the throat and continued to decrease to negligible loss at the aft end. The FM5128 in the exit cone lost a maximum of 0.18 inch and had a uniform char depth of 0.14 inch except at the interface of the FM5128 and the graphite where it reached a maximum of 0.5 inch. The FM5067 lost a maximum of 0.20 inch and had a uniform char depth of 0.06 inch. The nozzle as a whole performed very satisfactorily and would have functioned properly for the full firing duration.

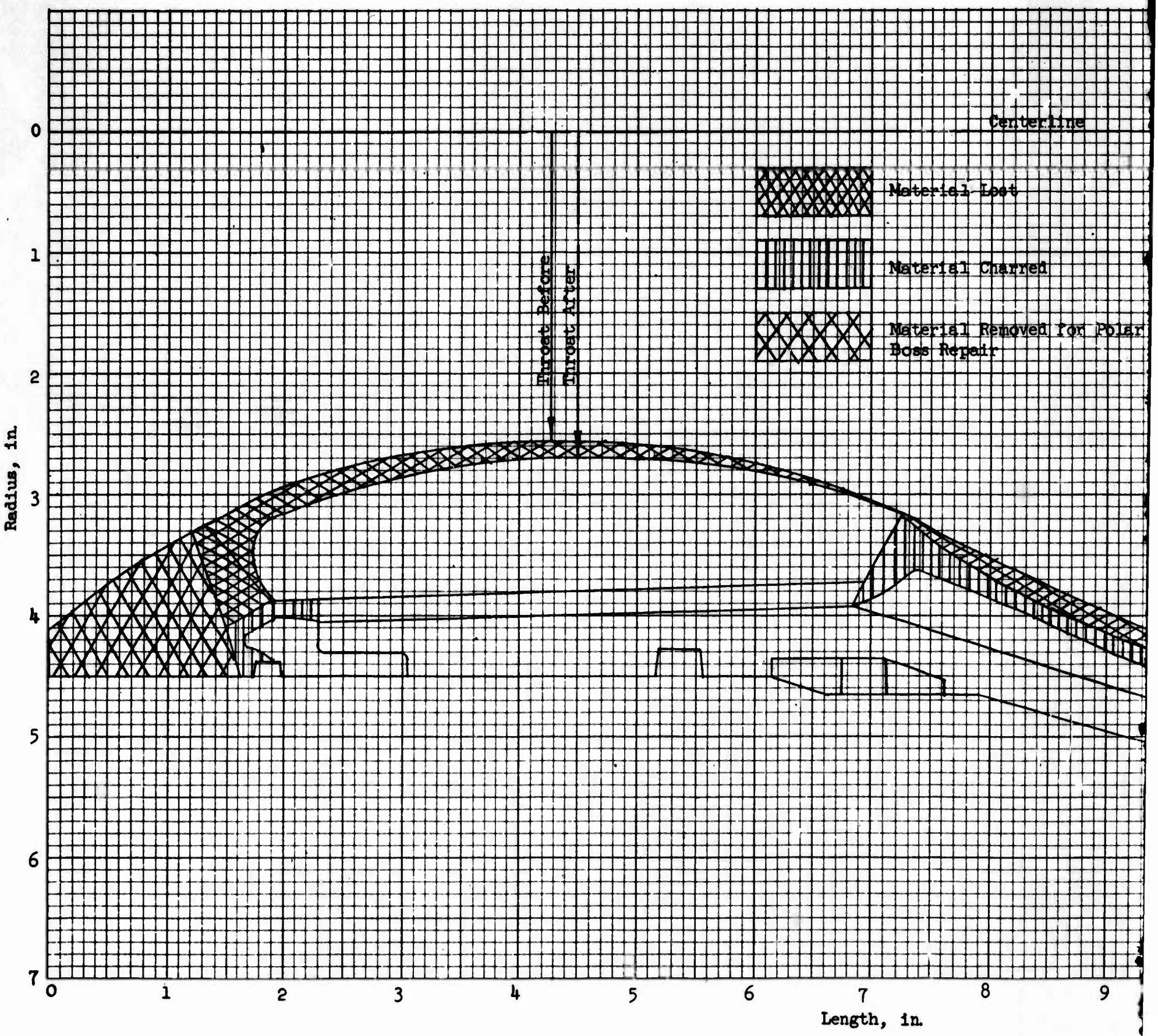
The doubler performed satisfactorily as evidenced by finding portions of the Epon 815-Versimid used to fill the bottom of the doubler still remaining on the polar boss at the end of the firing duration.

Of the nine load rings used on each end of the motor, seven remained on the forward polar boss and six remained on the aft polar boss in various stages of melting. The rings on the aft polar boss showed a greater degree of melting on the bottom side of the boss than the top indicating that there was an increased burning rate of the RFG in the lower portion of the aft dome.

(2) Conclusions and Recommendations

Evaluation of all the test data, observation of the high speed movie, and study of recovered components, has led to the theory of failure which best correlates all of the supporting evidence.

(C) Ignition, core grain burning, translation from core grain to reinforced grain, and burning of approximately 75% of the web of the reinforced grain were close to the predicted performance. However, at 23.5 seconds, as shown in Fig. 175, there was a slight increase in pressure and thrust which was not expected. Strain gages and linear potentiometers also showed an increase in the case loading at that time. However, at 24.4 seconds there was a sudden increase in strain and deflection of the aft GFW dome without an increase in pressure. This increase in strain without a corresponding increase in pressure could only be caused by the remaining RFG web being burned away or rupturing. If the RFG had ruptured, the burning surface and pressure would have increased very rapidly and would have ruptured the GFW case almost immediately. The fact that the case did not rupture until approximately 1.5 seconds after the pressure increase showed that the RFG burning front in the aft dome was


Centerline
Material Lost
Material Charred
Material Removed for Polar Boss Repair
Throat Before
Throat After
Radius, in.
0
1
2
3
4
5
6
7
0
1
2
3
4
5
6
7
8
9
Length, in.

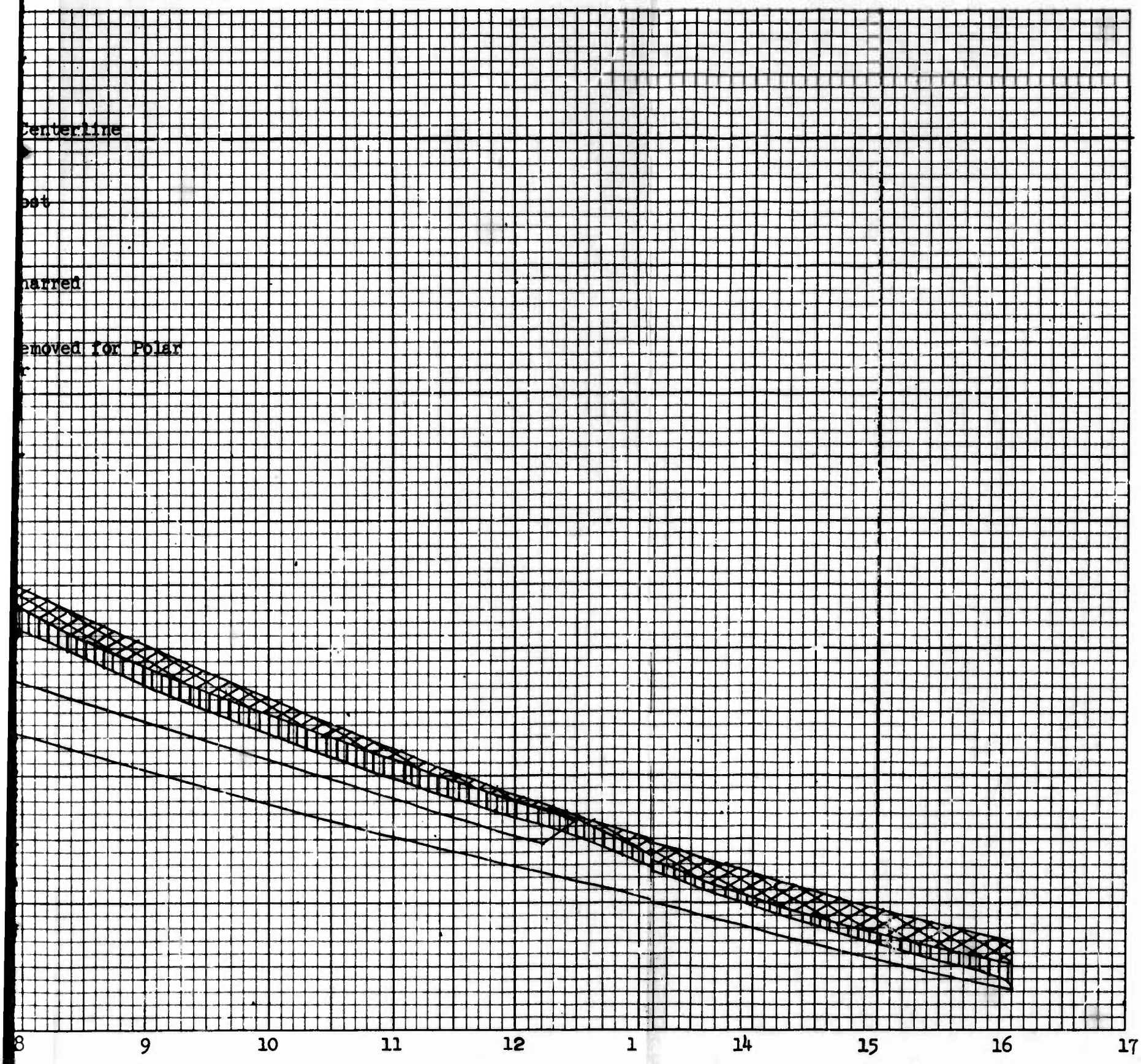


Figure 200. Material Loss and Char Depth of Nozzle Assembly for Motor A-1004

CONFIDENTIAL

PREVIOUS PAGE WAS BLANK, THEREFORE WAS NOT FILMED

(C) ahead of the burning front in the remainder of the motor. Strain gages on the lower portion of the aft dome were the first to show an increase in strain. Subsequently, increased strain was indicated by strain gages on the upper portion of the aft dome at 25.043 seconds which was of enough magnitude that a bulge of the aft dome was shown by the high speed movie. The increase in GFW case loading progressed forward along the cylindrical length of the motor until strain gages on the forward dome also showed an increase in load at approximately 25.062 seconds. At 25.107 seconds chamber pressure reached 515 psig, which is 17% above the design maximum operating pressure at that time, and the GFW case ruptured. Rupture occurred near the aft tangent plane on the bottom side of the motor and was a hoop failure.

(C) Ballistic calculations showed that approximately 0.9 inch of RFG in the cylindrical section was unburned at the time of failure. One large piece of unburned propellant was found, and the web thickness measured 0.8 inch which is in good agreement with the calculated value.

Studies to determine why burning of the aft dome web of the RFG progressed 0.8--0.9 inch ahead of the cylindrical web disclosed the fact that the bottom side of the aft polar boss and load ring assembly was eroded much more severely than the top side. Inspection of the forward polar boss and load ring assembly from this motor as well as the aft boss from A-1002, which was fired successfully, showed uniform erosion around the polar bosses. The forward polar boss from A-1002 was charred severely by an accumulation of molten aluminum/aluminum oxide slag in the forward end of the motor which was in the downward position for a vertical firing.

(C) The accumulation of molten aluminum/aluminum oxide slag in the lower portion of the aft dome and aft dome/cylindrical section junction caused an increase in the burning rate of the RFG in this area. This accumulation of slag in the bottom of this motor (A-1004), which was fired in the horizontal position, is attributed in part at least, to the submerged nozzle used in the Motor A design. The burning front of the RFG reached the liner in the lower portion of the aft dome somewhat prematurely in a localized area and the resulting nonuniform strains and delfections caused the remaining portion of the RFG in the aft dome to delaminate or peel away from the liner. As a result of the increased burning surface, pressure increased to 515 psig and the GFW case ruptured at 25.107 seconds.

(C) The burst pressure of 515 psig is 12% below the design ultimate pressure of 585 psig. In part, this may only be apparent since the pressure transducer was recording forward end pressure and as a result of the delamination or peeling of the RFG-Liner, pressure at the point of

(C) rupture could have been higher than 515 psig, particularly if some of the areas where ignition occurred were essentially confined. Another factor which also could have contributed to the lower burst pressure was the nonuniform distribution of stress and strain previously noted as existing in the GFW case just prior to burst.

Based on the results of the analysis the following conclusions are drawn:

Ballistic performance up to time of malfunction was very good and essentially as predicted. Projection of the performance indicates that the minimum total impulse required would have been exceeded had the motor operated successfully to completion.

Thermal protection features of component designs were entirely adequate.

Structural performance of the motor was close to expected for 23.5 seconds. Strain and deflection of the GFW case after 23.5 seconds probably contributed to case failure at a less than expected ultimate pressure.

The repaired aft polar boss functioned as expected and did not contribute to motor failure.

Motor malfunction was due to pressure failure of the GFW case resulting from the following probable sequence of events:

Localized accelerated burning in the bottom of the aft dome and aft dome/cylindrical section junction caused by washing action of internal flow on an accumulation of molten aluminum and aluminum oxide slag resulted in premature burnthrough of the RFG web.

Loss of structural capability of RFG resulted in modification of load distribution in aft dome-polar boss region and subsequent deflections tending to cause delamination of residual RFG layers.

Ignition of additional exposed burning surface caused chamber pressure to increase to a level exceeding the capability of the GFW case.

6. Development Motor A-1005

(C) Motor A-1005 was to be the fifth and final motor of the A series under Contract AF 04 (611)-9090. The motor was to be of flightweight design. However, upon redirection by the Air Force the case was changed to a heavier case (Fig. 201) and a liner similar to that of A-1002 was used. These changes resulted in a mass fraction of 0.938 instead of the designed 0.951. The RFG was not changed but two different burning rate propellants were used in the core grain to account for the erosive burning which occurred in Motor A-1004. These changes were made to slow the burning in the aft dome and increase case thermal and structural efficiency, particularly in the aft dome.

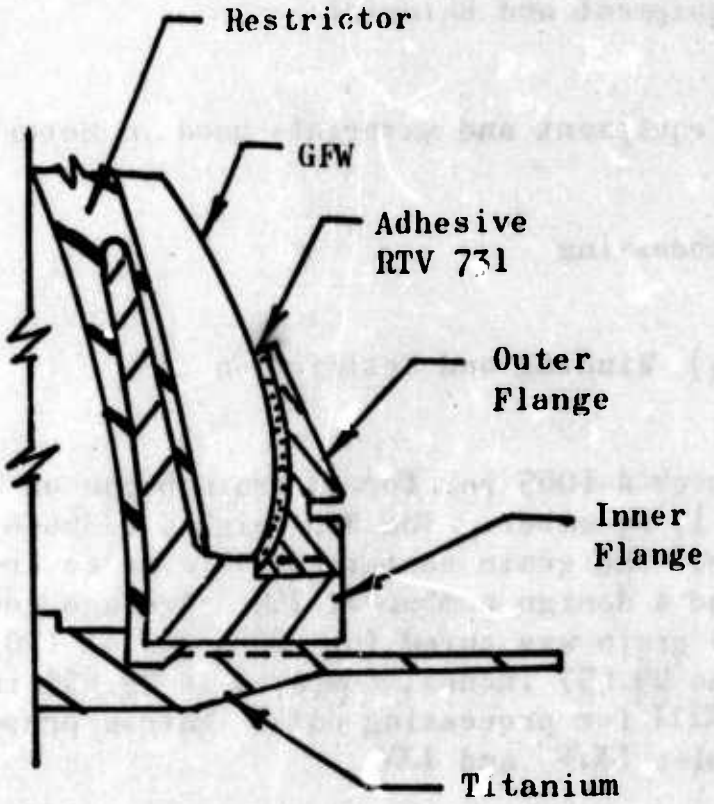


Figure 201. Motor A-1005 Case Change

(C) Restrictor thickness was increased from 0.06 to 0.130 inch (minimum) to provide 9 seconds of tailoff or 1.3 seconds at a chamber pressure of 400 psi. An external polar flange was designed to screw on the aft polar boss and seat against the case. This flange furnished additional stiffness to the aft dome of the case near burnout.

The final Motor A-1005 performance estimate is presented in Table LXI and Fig. 202. Motor A-1004 test data were incorporated where applicable. Low operating pressure and other factors resulting from the nozzle erosion contributed to the decrease of estimated delivered total impulse. This was improved in the final flightweight estimate by increasing the RFG burning rates to compensate for the increasing throat area.

(C) Estimated weight and mass fraction of Motor A-1005 are presented in Table LXII. Total inert weight reflects the heavyweight case and liner design used in this motor. Flightweight mass fraction was expected to increase from 0.939 to 0.951.

a. Fabrication

(1) Equipment and Material

The same type of equipment and materials used in Motor A-1004 were used in A-1005.

(2) Processing

(a) Winding and Restriction

(C) Winding of the Motor A-1005 reinforced grain began on 11 December and was completed on 17 December. The RFG weighed 1,365.6 pounds and contained 17.2% wire. The grain contained 241 wire covers compared to 229 for A-1004 and a design number of 245. Average cover thickness was 0.0157 inch. The grain was cured for 120 hours at 170 F. The average cured diameter was 29.657 inches, compared to 29.655 inches for A-1004. Refer to Table LXIII for processing data. Matrix propellant properties are listed in Tables LXIV and LXV.

Thirty thermocouples, 15 in each dome, were embedded in the base coat of R-143 restrictor to monitor temperature during firing. A testweight titanium polar flange was used in lieu of a flightweight titanium flange to accomodate the heavyweight GFW case.

TABLE LXI

ESTIMATED PERFORMANCE SUMMARY MOTOR A-1005

Average Pressure, psia	505
Average Thrust, lb	15,420
Total Impulse, lb-sec	542,900
Action Time, sec	35.2
Maximum Pressure, psia	790
Maximum Thrust, lb	24,500
I_{sp} @ Motor Cond, lb-sec/lb	220.2
I_{sp} @ 1000 psia, lb-sec/lb	238.1
Impulse-to-Weight Ratio	206.6
Core Grain	
Average Pressure, psia*	770
Average Thrust, lb*	24,050
Total Impulse, lb-sec*	211,900
Duration, sec	8.8
I_{sp} @ 1000 psia, lb-sec/lb	250
Reinforced Grain	
Average Pressure, psia**	415
Average Thrust, lb**	12,540
Total Impulse, lb-sec**	331,000
Duration, sec	26.4
I_{sp} @ 1000 psia, lb-sec/lb	228.6

*Impulse delivered by core grain from 10% maximum pressure to transition of core to RFG; does not include core propellant which burns simultaneously with RFG propellant.

**Includes impulse delivered by RFG and core propellant which burns after transition point.

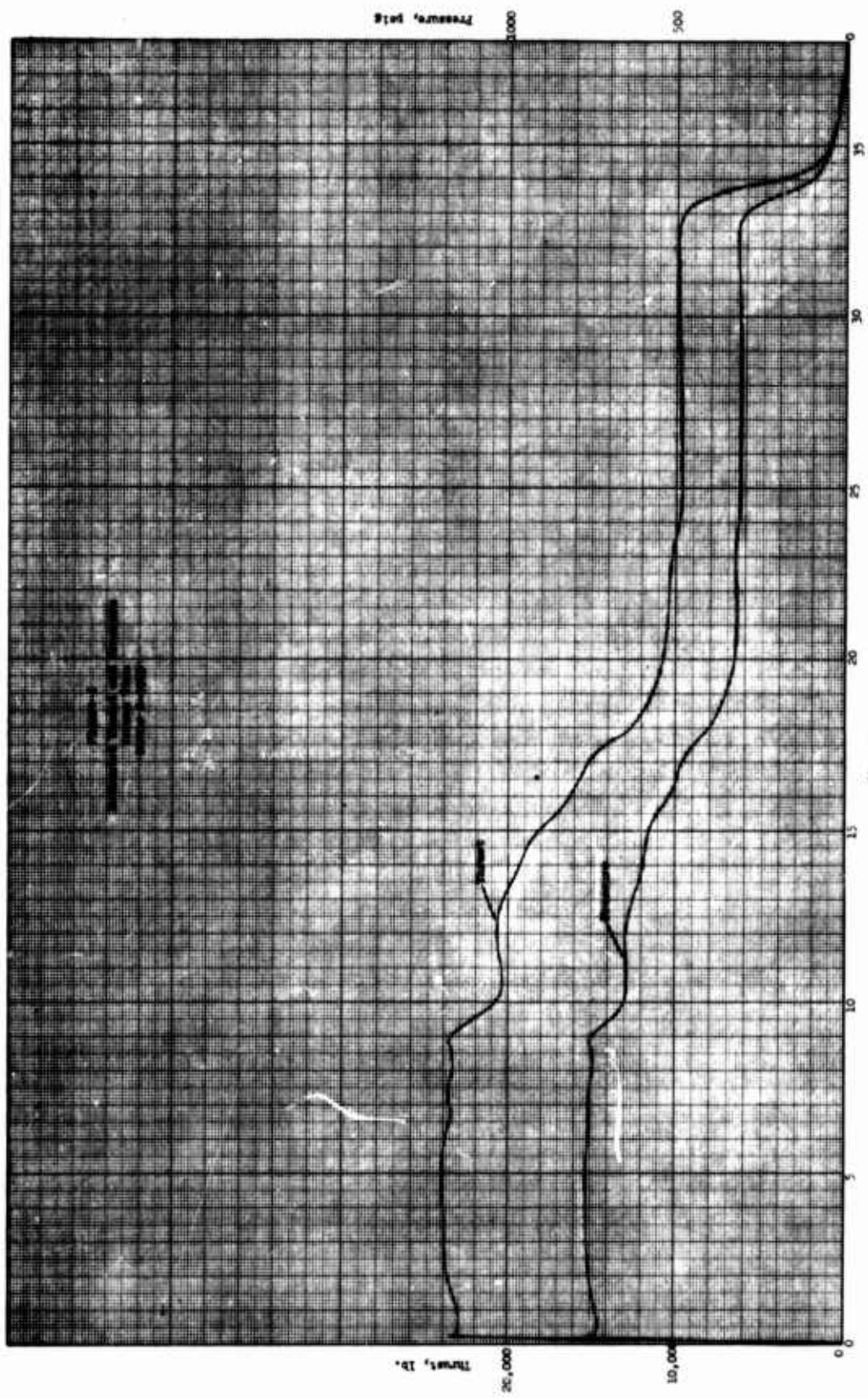


Figure 202. Estimated Thrust and Pressure vs Time
Motor A-1005

TABLE LXII

DESIGN ESTIMATED WEIGHT AND MASS FRACTION,

MOTOR A-1005*

	Design Estimate
Nozzle Assembly	27.77
Case	41.9
Liner	48.0
Igniter Assembly	2.67
Forward Boss	11.02
Aft Boss	17.20
Load Rings	6.94
Drive Pins	0.56
O-rings	0.10
Inner Flange	2.96
Outer Flange	0.5
Adhesives	2.50
Total Inerts	161.12
Igniter Combustibles	0.55
Core Propellant	1129.00
RFG Propellant	1337.00
Total Propellant	2466.55
Total Motor Weight	2627.67
Mass Fraction	0.939

*All weights are in pounds

TABLE LXIII

A-1005 PROCESSING DATA

	A-1002	A-1003	A-1004	A-1005
Boss-to-Boss Dimensional Changes, in.				
Prior to Winding	--	70.90	70.684	70.83
After Winding	--	70.71	70.610	70.74
After Mandrel Washout	--	70.59	70.490	70.60
Total Change	--	0.31	0.194	0.23
Time Temperature, hr/deg F				
After Mandrel Washout	2/100 2/120	2/100 2/120	2/100 2/120 2/130	2/100 2/120 2/130
Time Lapse, hr				
After MAPO Wipe to Start of Preheat	50	10(2nd Wipe)	92	19
Preheat to Cast	35	22	22	31
Between Mixes	[4--6 hours between first two and second two mixes]			1.5 hours between RDS-501 & RDS-526
Casting Time	11.5	10	10	4*

*Core for 1005 was cast with two mixes rather than four

CONFIDENTIAL

CONFIDENTIAL

TABLE LXIV

A-1005 PROPELLANT MECHANICAL PROPERTIES

RDS No.	Mix	Burning Rate, in./sec	Chamber Pressure, psia	Temperature, 77 F		
				Elongation, %	Tensile Strength, psi	Modulus, psi
514	L-10-12-M81	0.266	735	20	189	1511
514	L-10-9-M82	0.214	670	20	186	1497
514	L-10-9-M81	0.176	600	17	166	1536
523	L-10-7-M82	0.164	540	22	129	878
523	L-12-11-M81	0.161	470	29	154	861
523	L-10-7-M81	0.136	470	27	99	632
523	L-10-8-M81	0.129	400	24	83	571
523	L-10-6-M81	0.127	400	18	66	579
523	L-10-6-M82	0.126	400	23	112	809
529	L-10-12-M82	0.124	600	71	64	181
501	M-1-29-M81	0.308	750	43	104	389
526	M-1-29-M201	0.469	750	31	171	879

CONFIDENTIAL

(C)

TABLE LXV

BURNING RATE SUMMARY FOR

MOTORS A-1004 AND A-1005

	Reference Pressure, psia	Design Motor Rate		Design Strand Rate		Actual Strand Rate	
		A-1004	A-1005	A-1004	A-1005	A-1004	A-1005
Core	750			0.438	0.460/0.311	0.432	0.469/0.308
Layer No. (Helical)							
1	735	0.305	0.305	0.260	0.276	0.261	0.266
2	670	0.258	0.258	0.220	0.220	0.222	0.214
3	600	0.210	0.210	0.179	0.179	0.181	0.176
4	540	0.200	0.200	0.170	0.170	0.170	0.164
5	470	0.170	0.170	0.145	0.155	0.139	0.161
6--9	400	0.155	0.155	0.132	0.145*	0.128	0.129

*0.145 in./sec at 410 psia for 6th helical layer.
0.143 in./sec at 400 psia for 7--9th helical layer.

(b) GFW Case

Motor A-1005 was wound on 13 and 14 January 1965, using the 40-inch winding machine. Machine performance was excellent and, except for cloth protrusions in the skirt-to-dome transition areas, the case appearance was good.

The ripples were fewer in number and of less magnitude than experienced on A-1004, but were not expected because of recent modification of the Motor A skirt tooling. This modification consisted of extending the edge of the skirt mandrel near the case tangent line to reduce the skirt-to-case fill. It was expected that the reduction in fill would permit fabrication of a smoother skirt in addition to reducing fill weight. However, there was apparently sufficient spindle deflection during winding to cave relative movement between the skirt mandrels and the grain, thus causing the ripples.

The cloth protrusions had a crazed appearance and there was some doubt that the forward skirt would meet thrust requirements. Therefore, a fix was designed for the forward skirt only. The fix consisted of (1) partial removal of the cloth protrusions, (2) lamination of additional glass cloth and (3) winding of additional circ wraps in the skirt area. Detailed design, in the sequence of fabrication, was as follows:

Item	Length from Edge of Forward Skirt to Termination Point, in.
Glass Cloth	5.0
Glass Cloth	5.5
Circ Wrap, 216 ends per inch	6.25
Glass Cloth	4.75
Glass Cloth	5.25
Circ Wrap, 288 ends per inch	5.75

Materials and processing were the same as used in original case fabrication. The fix weighed approximately 1.7 pounds.

Design and winding parameters for the case were:

(C)

Helix Wrap	
Helix Angle, deg	17.2
Pattern	5/4
Glass Density, ends per inch, total	1110
Number of Covers	3
Circuits per Cover	345
Estimated Thickness, in.	0.039
Circ Wrap	
Pattern	90 deg sequential
Glass Density	1150
Number of Covers	4
Estimated Thickness, in.	0.039

(C) Dimensions and weights of the case are shown in Table LXVI. The case weighed 41.7 pounds prior to adding the forward skirt fix, excluding the skirt-to-dome fill (which was reduced from 5.4 pounds on A-1004 to 1.0 pound on A-1005). Total case weight, including the fill and the skirt fix, was 44.4 pounds; over-all resin content was 19.9% before the fix and 19.8% after.

(3) Postwinding Procedures

Mandrel washout proceeded normally. After liner removal a slick film was noticed in the aft dome, requiring an extra 2 hours of drying at 130 F. The grain surface was inspected after drying and gave no indication of water damage. The grain was now ready for core casting.

Prior to casting the core in Motor A-1005, a method to prevent the erosive burning which occurred in Motor A-1004 was investigated; i.e., the burning of the aft dome web must be delayed sufficiently to cause the instantaneous web burn through with the cylindrical section. Two methods were considered.

1. Cast a propellant having a lower burning rate than the conventional core propellant to a level approximately 2 inches above the interface at the aft conicyl.
2. Shift the aft conicyl approximately 2.5 inches to the inside and lengthen the aft boss spike by 2.8 inches.

The first method was selected as more desirable from the standpoint of protecting the entire dome from effects of localized erosion. The variance in the burn rate of the two propellants provided a 0.9-inch sliver that delayed burning of the aft dome sufficiently to offset the estimated increase in burning rate in the lower section of the dome.

The primary question with the dual propellant casting was whether or not undue intermixing of the two propellants would occur. To evaluate the technique, approximately 10 pounds of RDS-526 propellant (normal core formulation) were cast on top of uncured RDS-501 (a similar but lower burning rate formulation). The casting was performed in a manner simulating the casting of Motor A except it was not cast under vacuum.

TABLE LXVI

A-1005 CASE DIMENSIONS AND WEIGHTS

Dimensions, in.			
Diameters and Thicknesses			
	Forward Skirt	Center	Aft Skirt
OD	30.39 (After Fix)	30.08 (After Washout)	30.29
ID	30.02 (Est)	29.95 (Restr OD)	30.02 (Est)
Thickness	0.185	0.065	0.135
Lengths			
Boss to Boss	70.60		
Cylinder	49.25		
Skirt	4.38		
Skirt to Skirt	58.00		
Weights, lb			

Original Case

	Predicted	Actual	Forward Skirt Fix	Total
Helix Roving	17.55	17.5	---	17.5
Circ Roving	12.18	12.1	0.8 (Calc)	12.9
Skirt Cloth (Calc)	3.77	3.8	0.6 (Calc)	4.4
Total Glass	33.50	33.4	1.4	34.8
Resin	8.38	8.3	0.3	8.6
Glass and Resin	41.88	41.7	1.7	43.4
Skirt-to-Dome Fill		1.0		1.0
Total		42.7	1.7	44.4

Resin Contents: $\frac{8.3}{41.7}$ x 100 = 19.9% by weight before fix

$\frac{8.6}{43.4}$ x 100 = 19.8% by weight including fix

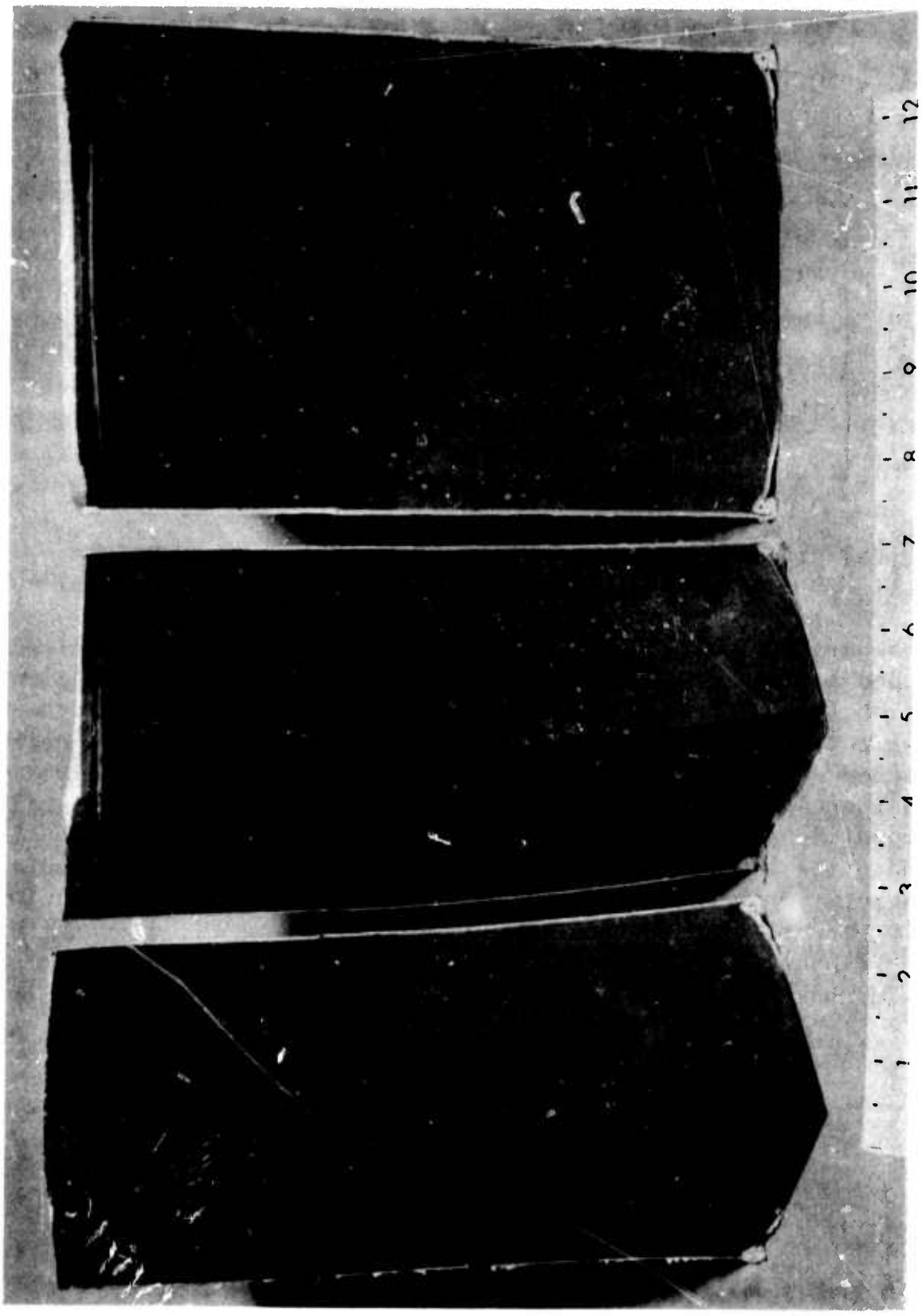
The cured propellant was sectioned for examination of the interface and specimens were cut across the interface for mechanical testing. A clear, sharp interface line indicated no intermixing of the two propellants (see Fig. 203). When testing mechanical properties, all samples broke in the RDS-501 layer, showing a strong bond between the propellants. As a result of this experiment, a dual-propellant core cast for Motor A-1005 was selected.

(C) Motor A-1005 core was cast on 29 January. The 176.6 pounds of RDS-501 cast in the aft end exhibited a strand burning rate of 0.308 ips at 750 psi. After only a 1.5-hour interval, 953 pounds of RDS-526 were cast; its strand rate was 0.469 ips at 750 psi. Physical properties of both core propellants were good. Table LXVII lists the propellant formulations.

During equipment cleanup following casting of RDS-526, it was discovered that the 200-gallon cast can valve contained water. The day before casting, a practice run was made with the can full of water, simulating propellant weight to verify the use of the system. Although the water was drained out, a portion was trapped in the valve's dead space. It was estimated that, due to propellant flow characteristics and volume of water trapped, only a few tablespoons of water entered the propellant stream; however, as much as a pint of water could have been trapped in the valve. How much of this water separated from propellant under 28 inches of vacuum and 150--160 F temperature is difficult to determine. The only reliable method of determining the damage done, if any, would be to duplicate the casting as nearly as possible.

The core was cured for 72 hours at 170 F and step cooled for 42 hours to 96 F. The mandrel was removed on 4 February and the core inspected. While the core contained the usual scuff marks from foam removal, its general appearance was very good. A thin film of uncured propellant remained on the aft-conicyl RTV surface. It has been demonstrated on other motors that RTV sometimes inhibits propellant cure, but the total effect was considered insignificant.

The junction between RDS-526 (red) and RDS-501 (gray) appeared to be excellent.



2YA31-1/11/65MIA

Figure 203. Bi-Propellant Interfaces

(C)

TABLE LXVII

RDS-501 AND RDS-526 FORMULATION

	501	526
Butarez Binder, %	14	14
Ammonium Perchlorate, %	70	69
Ferric Oxide, %	--	1
Aluminum Powder, %	16	16
	100	100

(4) Final Assembly

A slight separation was observed between the titanium and insulation in the threaded portion of the forward boss. The separation prohibited installation of the forward closure. To permit installation of the head, the phenolic threads of the closure were machined off and a 15-degree chamfer added. The forward end of the core was filled with EC-1949 up to the inside edge of the boss threaded area. The EC-1949 was cured at ambient conditions until firm. RPR-2138, an asbestos-loaded phenolic, was added to the boss threaded insulation area. The forward closure and igniter assembly were installed before the RPR-2138 cure to form a joint seal, using the EC-1949 surface to contain the RPR-2138. The nozzle was installed without difficulty and the motor was successfully leak tested. Table LXVIII shows the A-1005 weight and mass fraction summary.

TABLE LXVIII

WEIGHT AND MASS FRACTION SUMMARY

FOR MOTOR A-1005

	Component Weight, lb	
	Design Nominal	Actual
Nozzle Assembly	26.77	27.57
Case	41.90	44.40
Liner	48.00	50.65
Igniter Assembly	2.67	2.64
Forward Boss	11.02	10.32
Aft Boss	17.20	16.96
Load Rings	6.94	5.97
Drive Pins	0.56	0.54
O-Rings	0.10	0.11
Inner Flange	2.96	2.85
Outer Flange	0.50	0.50
Adhesives	2.50	2.60
Total Inerts	161.12	165.11
Igniter Combustibles	0.55	0.56
Core Propellant	1129.00	1129.60
RFG Propellant	1337.00	1365.60
Total Propellant	2466.55	2495.76
Total Motor Weight	2627.67	2660.87
Mass Fraction	0.939	0.938

Motor A-1005 was radiographically inspected 6-7 February. A total of 128 views were obtained, 16 with the 1 MEV unit and 112 with the 13 MEV Linac. A summary of the observations follows:

1. RFG/Liner Case Bondline - The outside interfaces were tangentially radiographed with the 1 MEV unit. Examination indicated a sound bond between RFG, liner, and case.

2. Core and Reinforced Grains - Low density areas were found in the core grain radiographs most of these areas were accounted for during visual inspection when insignificant surface irregularities were found. No surface cracks were seen.

3. Core and Reinforced Grain Interface - Twelve views of the core-RFG interface were obtained in the cylinder. No signs of separation were seen.

4. Polar Areas - Both polar areas were radiographed every 10 degrees. A few small, low-density areas in the reinforced grain were apparent at both ends. At the forward end the low-density area emanated upward from the inside load ring. Several of the forward load rings were not seated against the steps.

b. Testing

Motor A-1005 was placed on the horizontal thrust stand on February 12, 1965. Two independent thrust and pressure measurements were recorded. Three linear potentiometers were used to measure axial displacement of the GFW case, domes, and cylinder. GFW case strain was measured at 30 locations, temperature of the motor was measured at 37 locations and 30 internal thermocouples (on the surface of the RFG in both domes) were recorded. Six movie cameras were used for photographic coverage of the firings. Of the six cameras only two survived the malfunction undamaged. Three sets of film footage were recovered, however; but only one of these (a 1000 frames per second film) showed any significant information.

Motor ignition and core grain burning appeared to proceed as expected. However, at approximately 9.8 seconds the motor malfunctioned. Examination of high-speed movies indicated the failure occurred on the top side at the aft end of the cylindrical portion and then spread counter-clockwise around the motor.

(C) Thermocouple and strain gage data indicated no abnormal conditions prior to the malfunction. Further investigation indicated failure was caused from premature burning of the RFG in the cylindrical part of the motor. As a result of this premature burning, the RFG structure was weakened and interlaminar burning occurred. When the pressure reached 977 psig, the motor ruptured.

(1) Analysis

(C) A summary of average performance and tabulated data for Motor A-1005 are included in Table LXIX with the estimated performance for comparison. Actual and estimated thrust- and pressure-time replots are shown in Fig. 204.

(C) The motor performed normally over the core duration and commenced to burn in the RFG. Burning was normal up to 9.636 seconds after ignition at which time pressure and thrust commenced to increase abnormally. It was determined that burning of the core web had been accomplished at the time of malfunction, and approximately 0.4 inch of RFG web had been consumed at the point of failure. This was estimated from correlation of the pressure-time trace with burning rates in the first layers of the RFG. Core burning was complete (except for core sliver) at 8.711 seconds as indicated by the characteristic drop in thrust and pressure at that time. Difference between that time and the time of malfunction along with the pressure level and burning rate determined the 0.4 inch of RFG web burned.

(C) During the interval of core duration the performance was similar to that estimated. Average pressure for the duration of 8.616 seconds (to core burnout) was 819 psia compared to an estimated 770 psia, or 6.4% greater than estimated. Approximately half of this variation is accounted for in the motor burning rate, in that the strand rate was approximately 2% greater than nominal specified. The significant variation in performance over this interval, however, was in the amount of propellant consumed. This was estimated from the pressure integral delivered over this interval, which was approximately 4% greater than anticipated. Propellant weight corresponding to this deviation is approximately 35 pounds.

TABLE LXIX

PERFORMANCE SUMMARY FOR

MOTORS A-1002, A-1004, AND A-1005

	Motor A-1002	Motor A-1004	Motor A-1005	
			Estimated	Actual
Average Pressure, psia	560	613	505	807
Average Thrust, lb	16,970(1)	19,030	15,420	25,110
Total Impulse, lb-sec	533,600(1)	475,800	542,900	239,580
Action Time, sec	31.44	25.004	35.2	9.541
Maximum Pressure, psia	741	799	790	849
Maximum Thrust, lb	--	25,271	24,500	26,538
I_{sps} at Motor Conditions	225.9(1)	225.2	220.2	--
I_{sps} at 1000 psia	241.4(1)	239.4	238.1	--
Impulse-to-Weight Ratio	205.8(1)	--	204.1	--
Core Grain				
Average Pressure, psia(2)	733	779	770	819
Average Thrust, lb	22,660(1)	24,210	24,050	25,460
Total Impulse, lb-sec(2)	222,200(1)	223,700	211,900	219,400
Duration, sec	9.81	9.24	8.8	8.616
Pressure Impulse, psia/sec	7191	7198	6776	7057
Estimated Propellant Consumed, lb	934	935	881	916
Reinforced Grain				
Average Pressure, psia	482	516	415	
Average Thrust, lb	14,400(1)	15,930	12,540	
Total Impulse, lb-sec(3)	311,400(1)	252,100	331,000	
Duration, sec	21.63	15.764	26.4	
I_{sps} at 1000 psia	--	230.6	228.6	

(1) Thrust parameters estimated from pressure

(2) Impulse delivered by core grain from 10% maximum pressure to transition of core to RFG; does not include core propellant which burns simultaneously with RFG propellant

(3) Includes impulse delivered by RFG and core propellant which burns after transition point

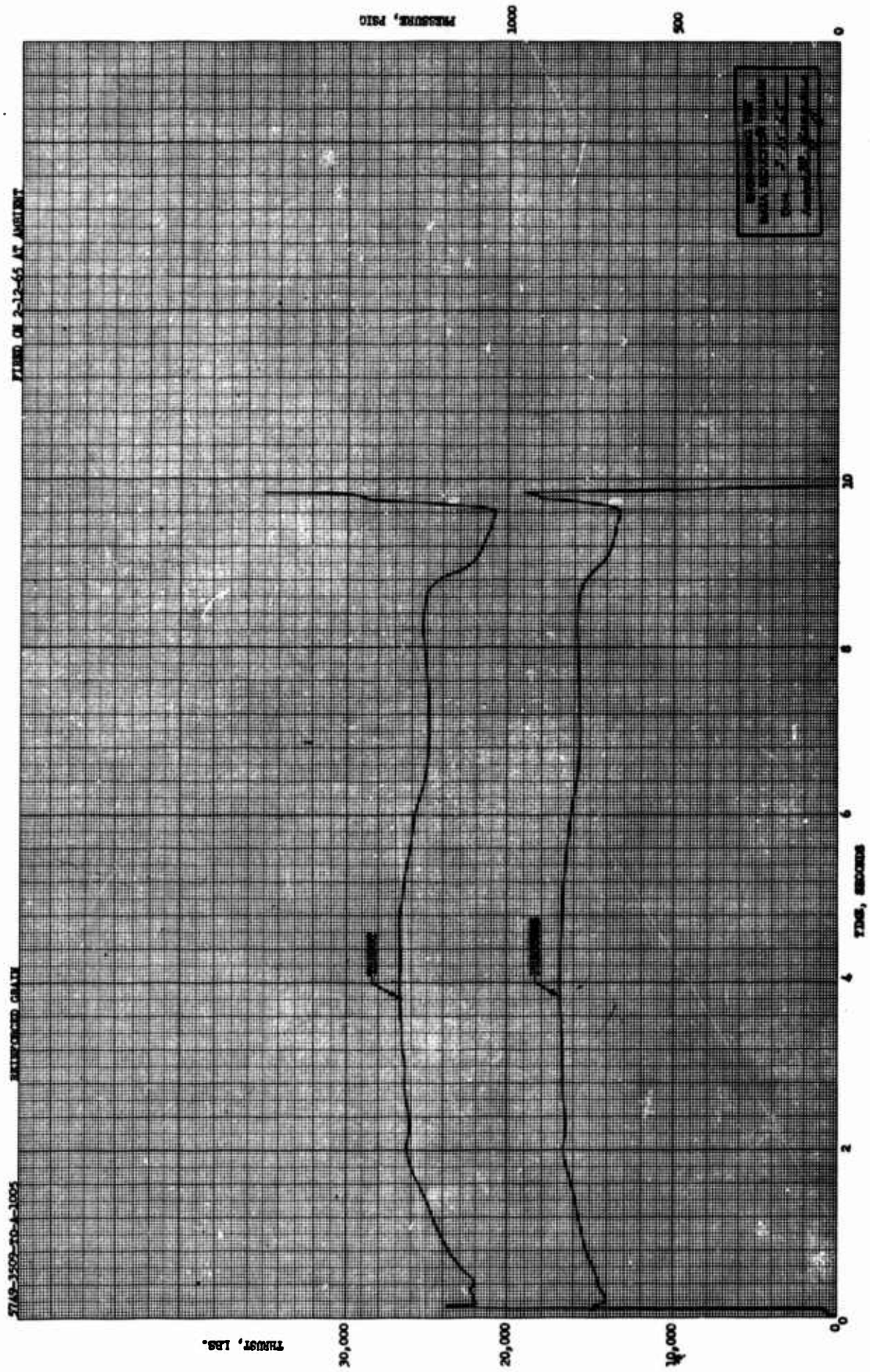


Figure 204. Pressure and Thrust vs Time for Motor A-1005

(C) Normally this parameter is very reproducible. The pressure-time integrals over the same interval for Motors A-1002 and A-1004 were 7191 and 7198 psia-sec respectively, with Motor A-1004 having a core propellant weight 4 pounds greater than that for A-1002. This deviation was found to be significant in determining the failure mode of the motor. The pressure-time trace was more "rainbow" than had been predicted which correlates also with the failure mode.

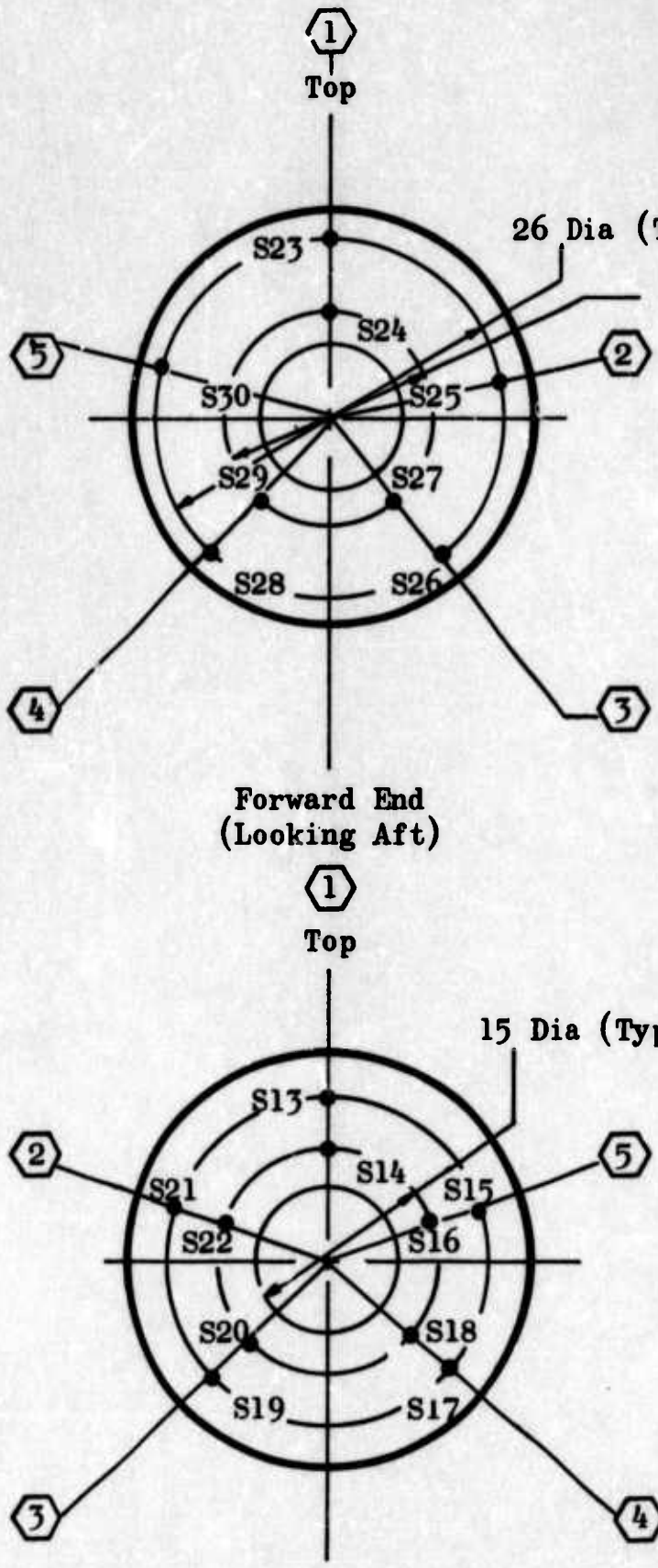
(C) Performance estimated for this motor differed from previous estimates primarily because of the low burning rate propellant. Less propellant was estimated to be consumed over the core duration; hence, the estimated delivered impulse over the core duration was 211,900 lb/sec compared to 223,700 lb-sec actual for A-1004. Actual for Motor A-1005 was 219,400 lb-sec over the core duration.

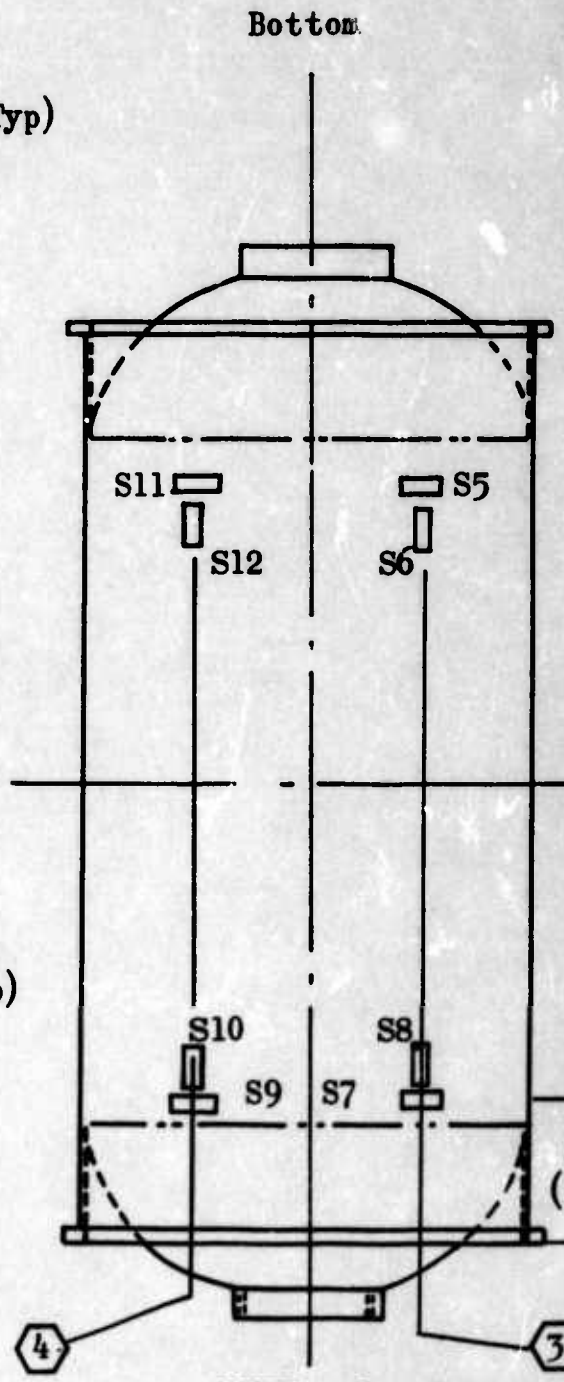
(C) Nozzle efficiency over the core duration was 95.1%. This compares to 96% estimated as design nominal, and was calculated on the basis of average throat area accounting for erosion over this interval.

RFG burning rates specified for this motor were essentially the same as specified for Motor A-1004. Some changes were made, which reflect a compromise between propellant available for Motor A-1005 and that required for optimum performance. However, some of the rates specified in the outer layers were still too low to give the optimum pressure with erosion of the current nozzle.

Strain gage and potentiometer locations and test results are presented in Figs. 205 through 215.

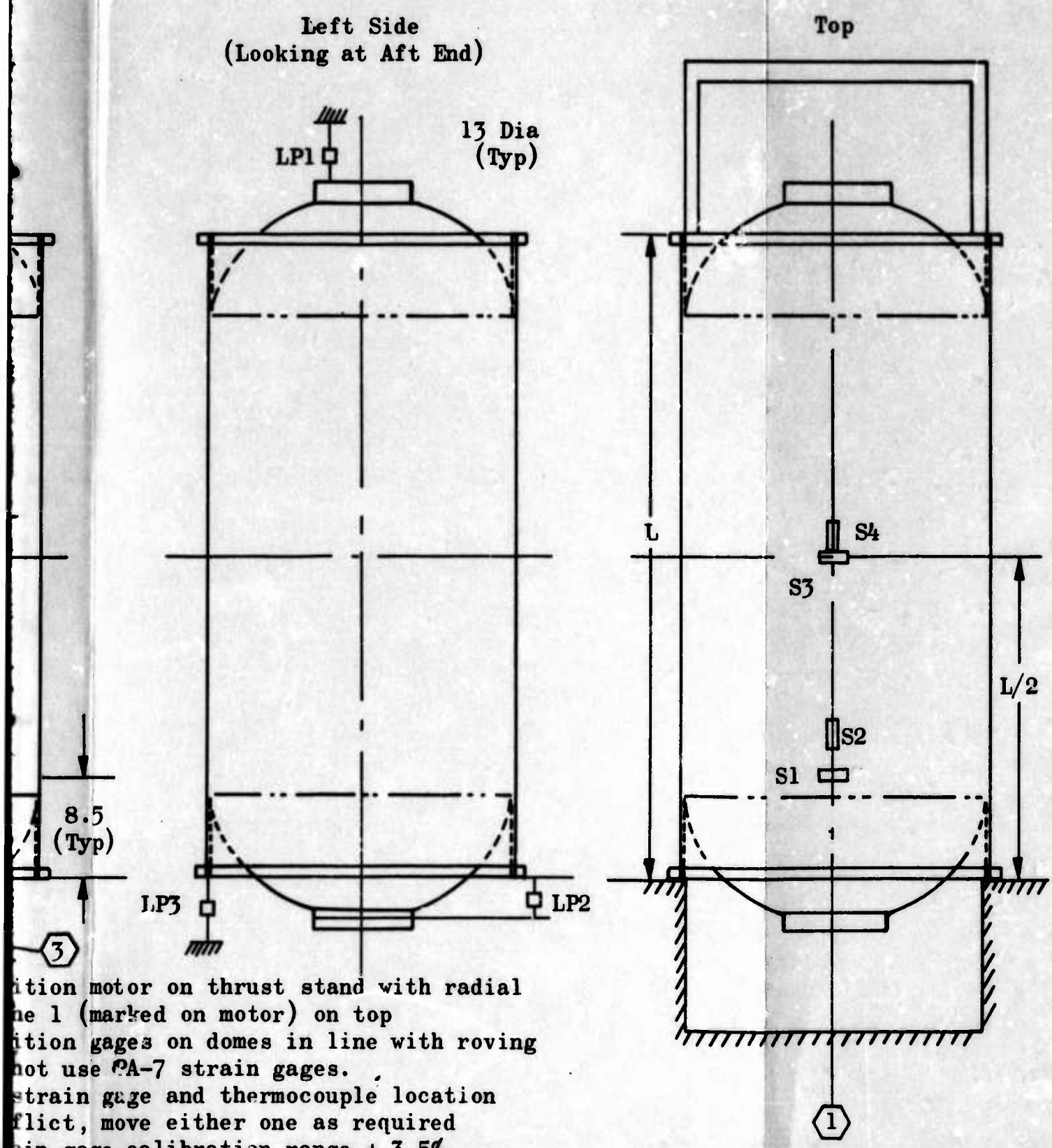
(C) Strains and displacements of the GFW case were close to expected values for approximately 9.6 seconds. Prior to that time, chamber pressure and thrust were slightly higher than predicted but had started to regress after core grain burnout as expected. Maximum recorded chamber pressure was 975 psig which is 28% higher than estimated maximum pressure for this motor. This high pressure however should not have ruptured the motor if it was burning as designed. In areas where the burning front was progressing normally, only 0.4 inch of the RFG web had burned at 9.848 seconds. The remaining RFG web and GFW case were capable of withstanding approximately 1200 psig. Recorded GFW case strains prior to 9.6 seconds reached a maximum value of only 3000 microinches per inch and compare favorably with hydrotest data.







NOTE:
1. Position motor on thrust stand v
plane 1 (marked on motor) on to
2. Position gages on domes in line
3. Do not use PA-7 strain gages.
4. If strain gage and thermocouple
conflict, move either one as re
5. Strain gage calibration range ±
6. LP1 andLP2 must measure 3/4 in.
(minimum)
7. LP3 must measure 2.5 in. deflec
8. Total of 30 strain gages to be



ition motor on thrust stand with radial
ne 1 (marked on motor) on top
ition gages on domes in line with roving
not use EA-7 strain gages.
strain gage and thermocouple location
flict, move either one as required
ain gage calibration range ± 3.5%
andLP2 must measure 3/4 in. deflection
nimum)
must measure 2.5 in. deflection (minimum)
al of 30 strain gages to be installed

Figure 205. Strain Gage and Linear Potentiometer Locations for Motor A-1005

2

PREVIOUS PAGE WAS BLANK, THEREFORE WAS NOT FILMED

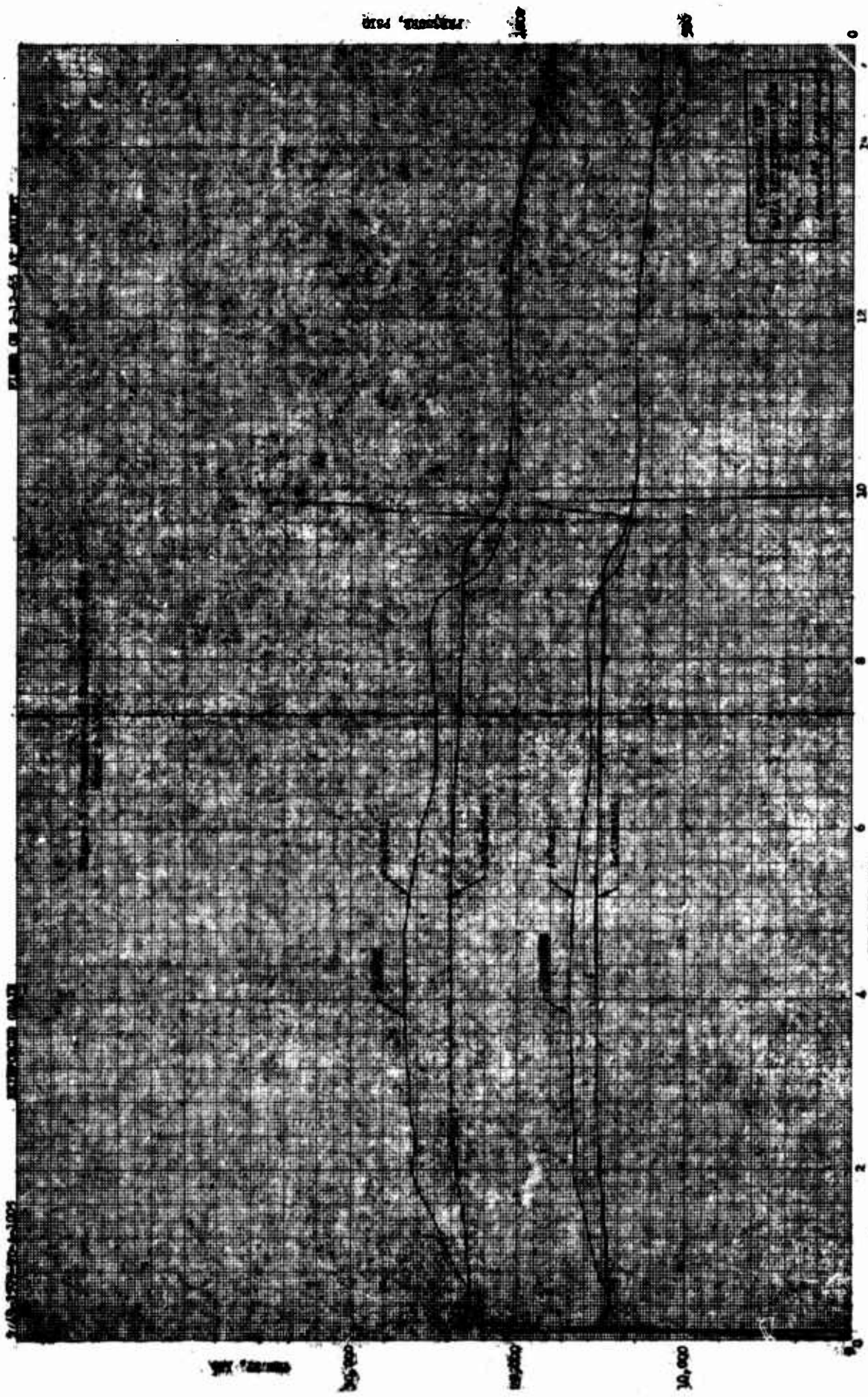


Figure 206. Pressure and Thrust vs Time for Motor A-1005

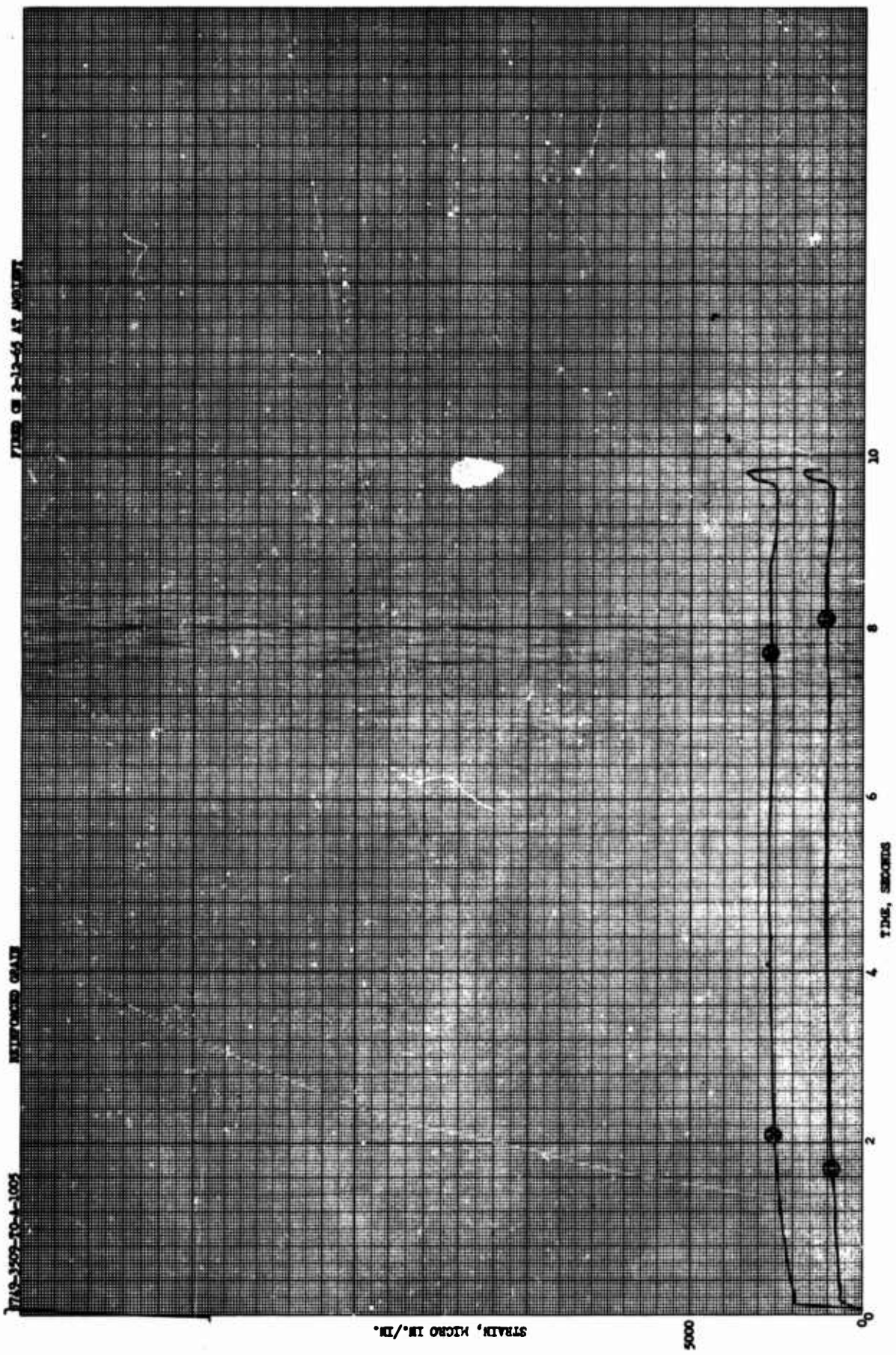


Figure 207. Forward Dome Strain vs Time for Motor A-1005

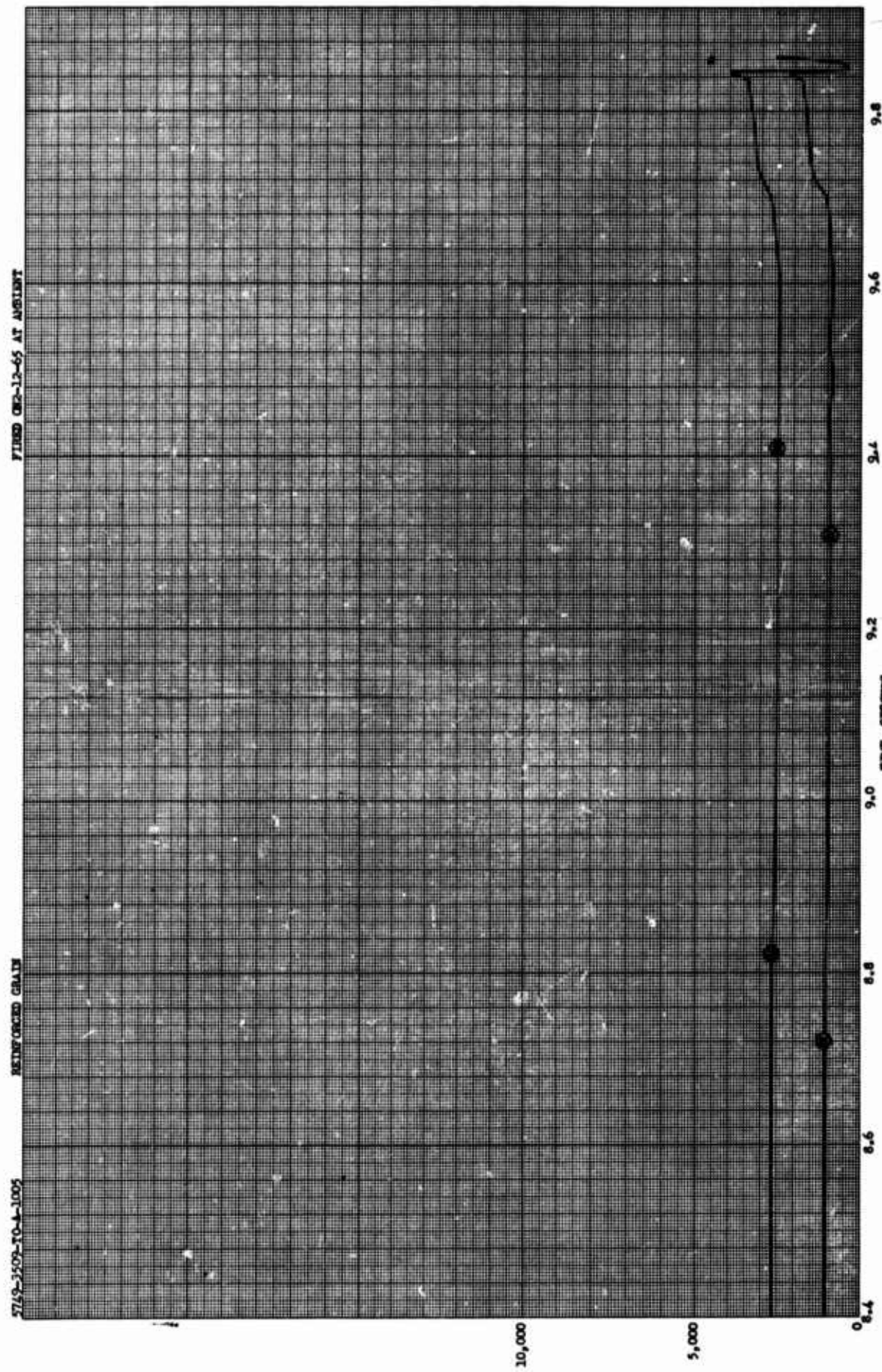


Figure 208. Forward Dome Strain vs Time (Expanded Time Scale) for Motor A-1005

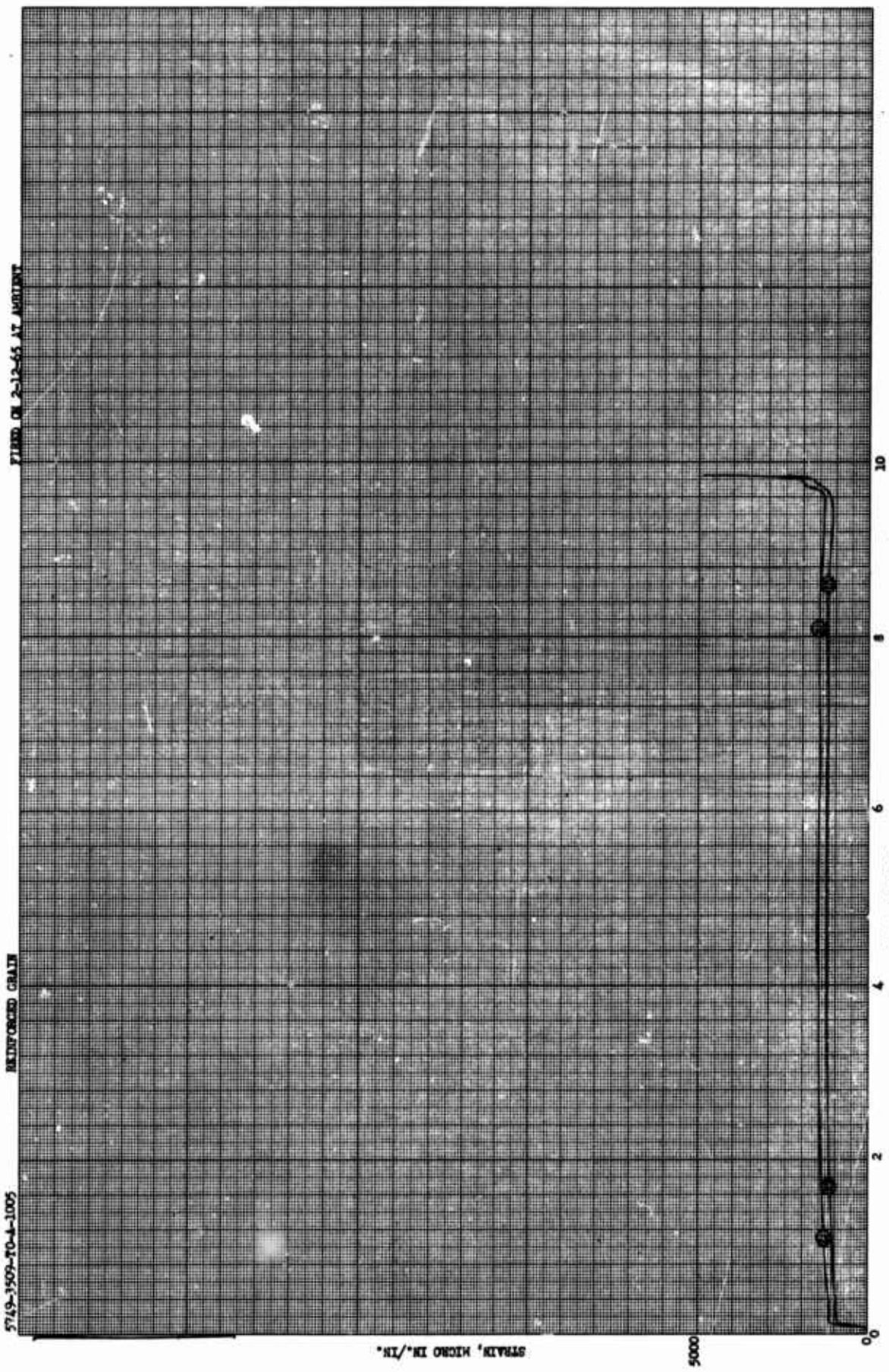


Figure 209. Aft Dome Strain vs Time for Motor A-1005

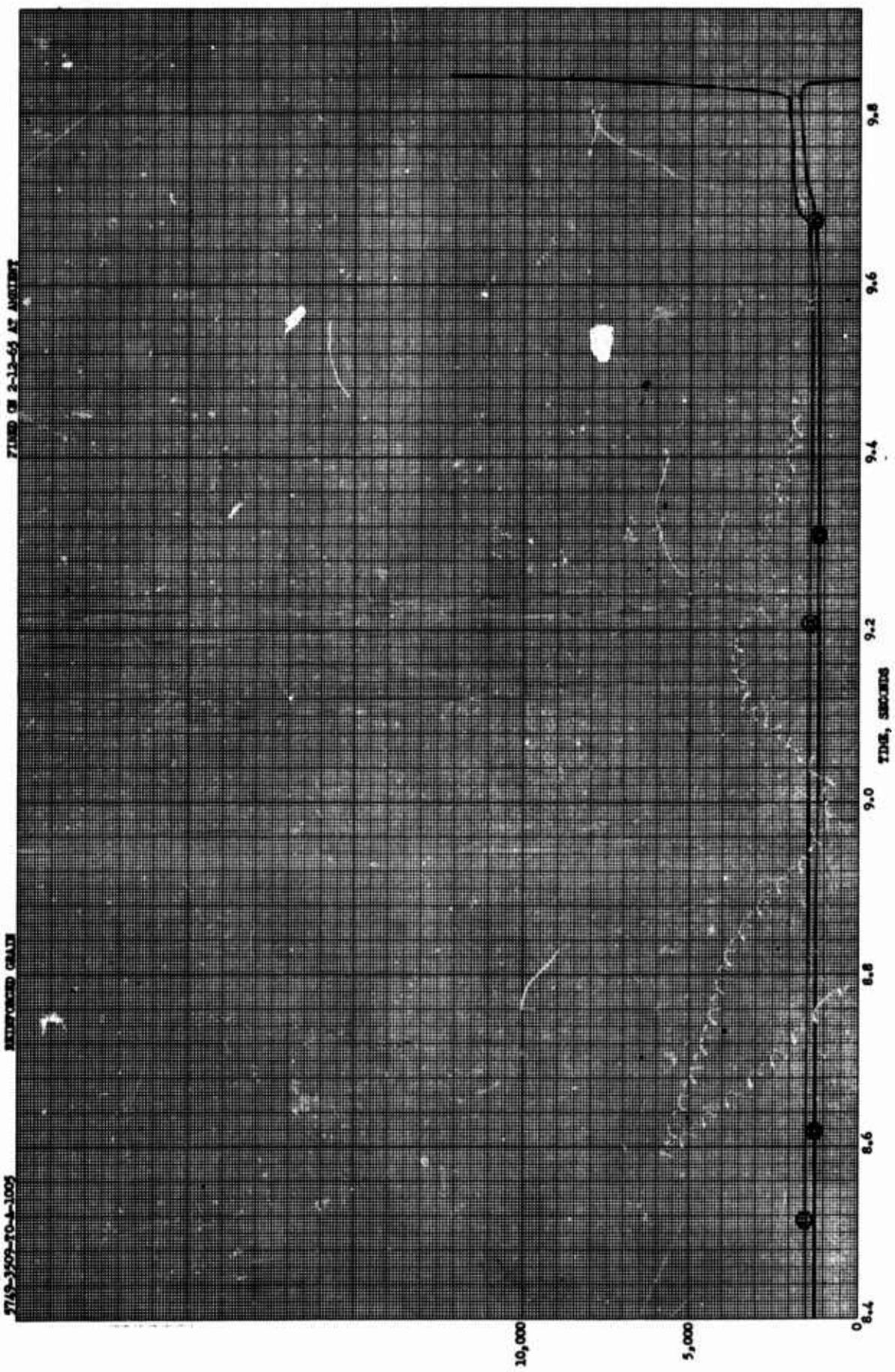


Figure 210. Aft Dome Strain vs Time (Expanded Time Scale) for Motor A-1005

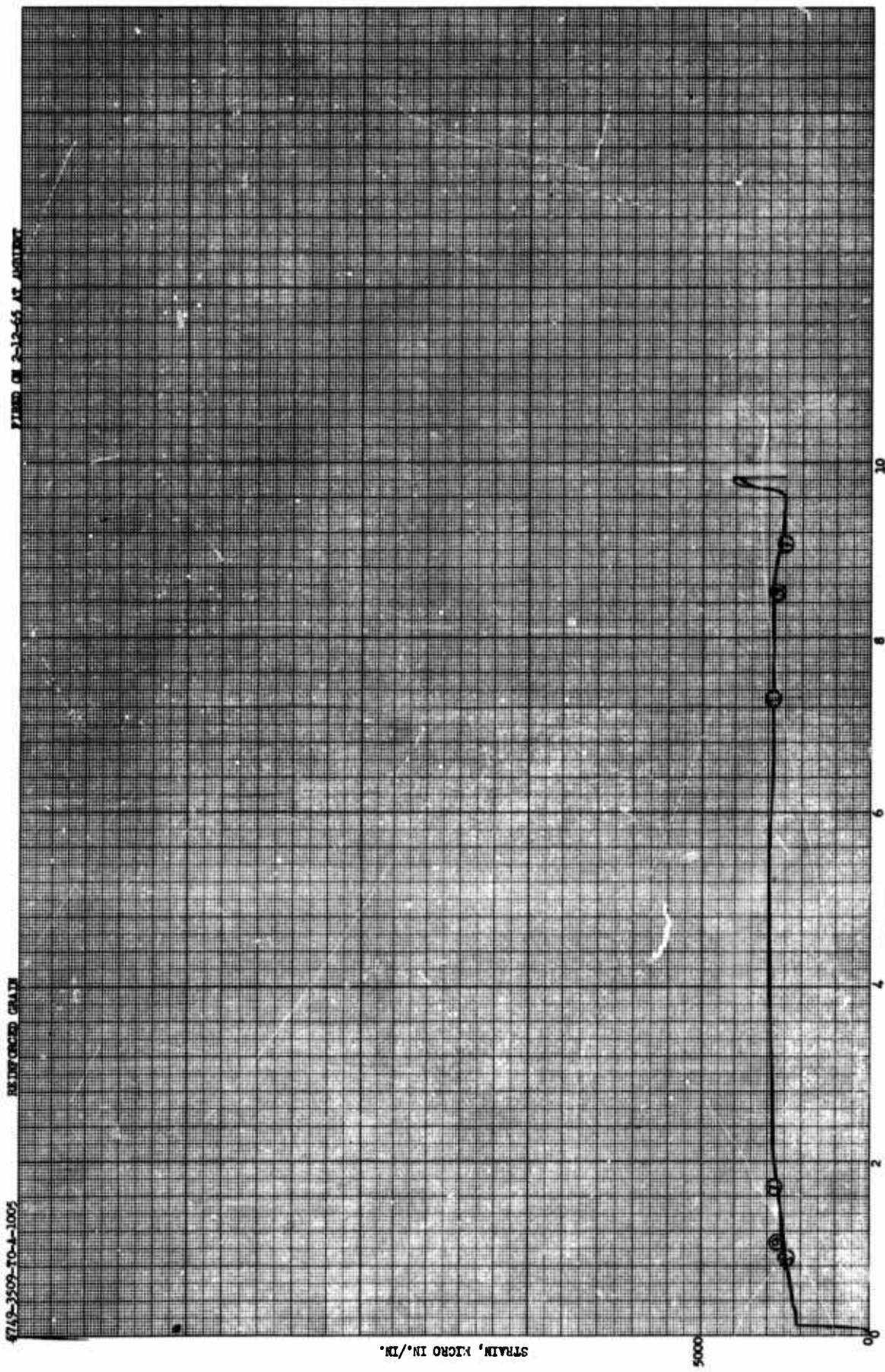


Figure 211. Cylinder Strain vs Time for Motor A-1005

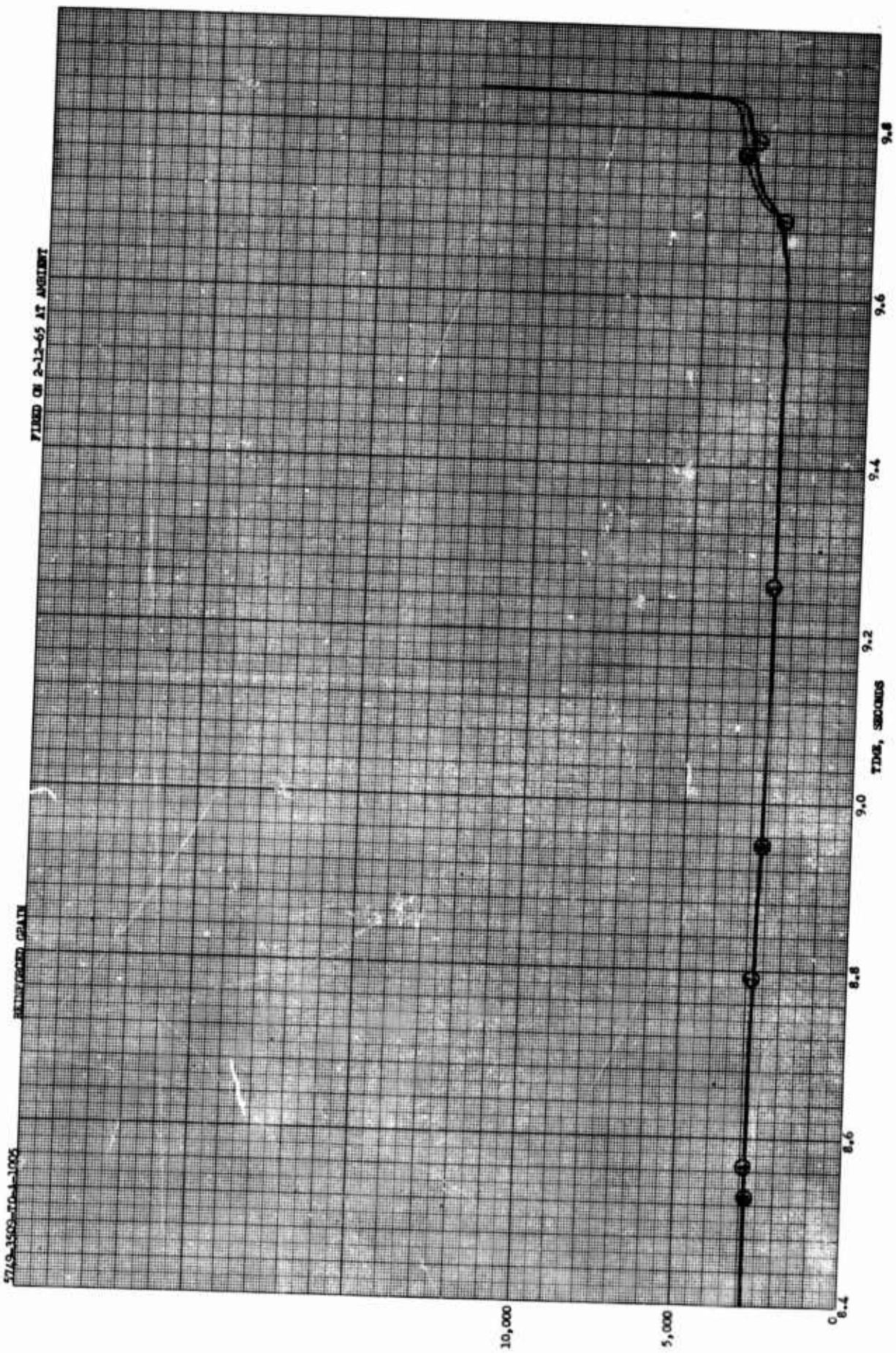


Figure 212. Cylinder Strain vs Time (Expanded Time Scale) for Motor A-1005

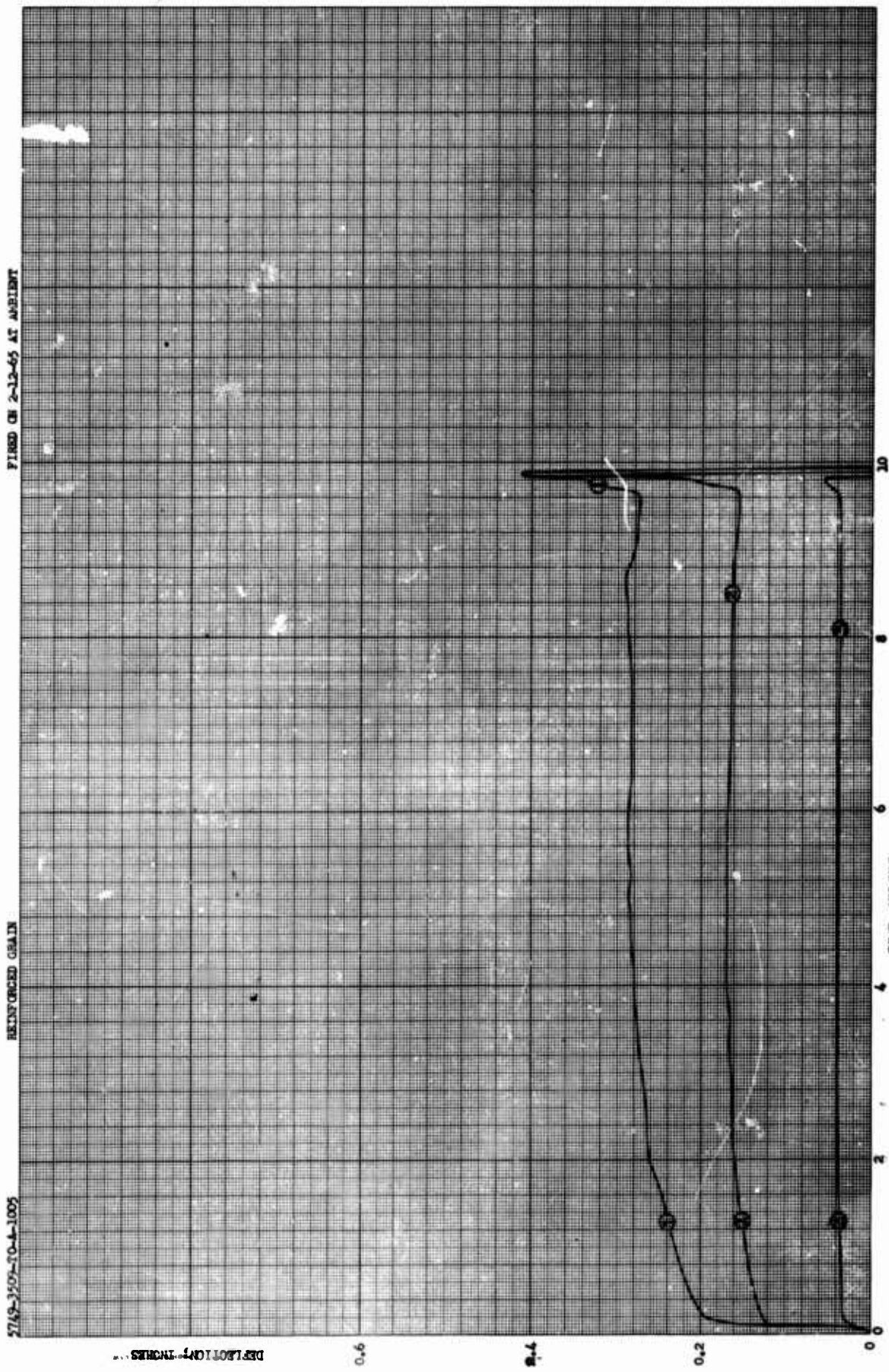


Figure 213. Displacement vs Time for Motor A-1005

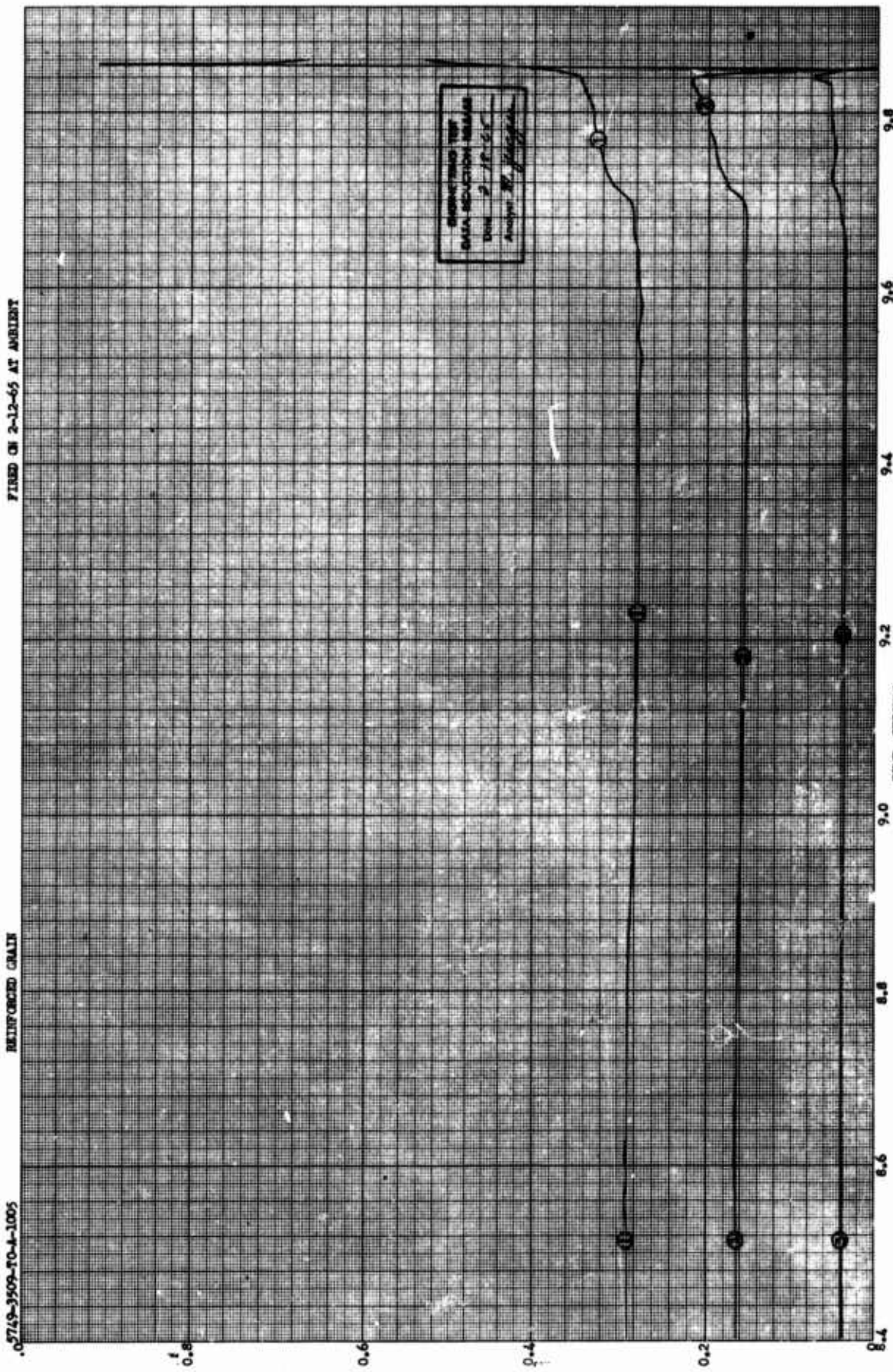


Figure 214. Displacement vs Time (Expanded Time Scale) for Motor A-1005

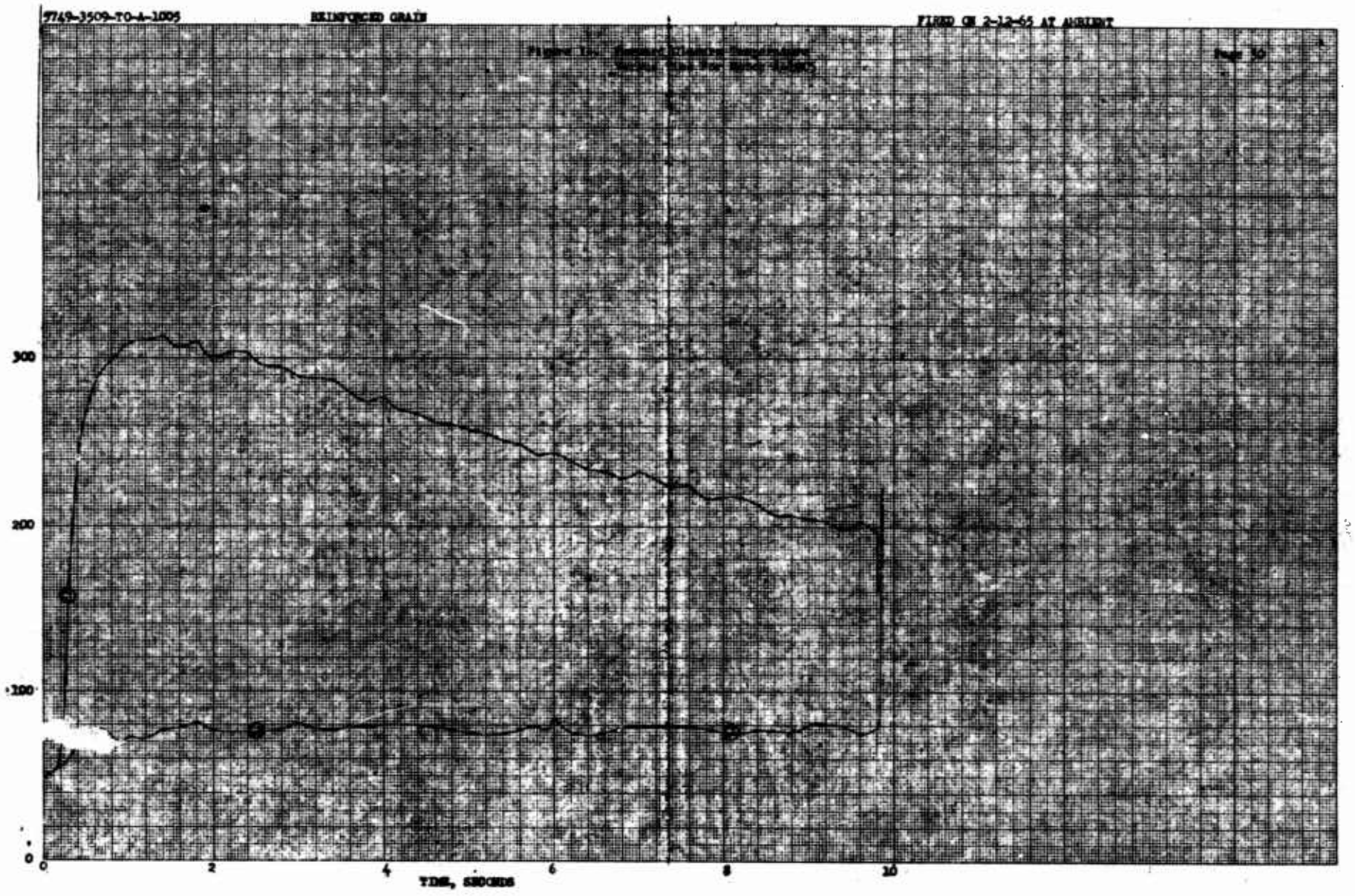


Figure 215. Forward Closure Temperature vs Time for Motor A-1005

The recovered forward dome and a large portion of the GFW case cylinder as well as the high speed movie of the test show the initial failure was near the aft tangent of the motor.

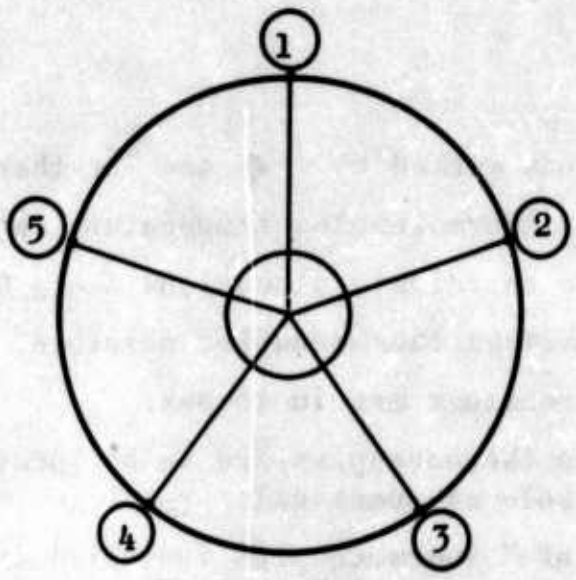
Evidently the core grain separated between the two different propellants near the aft end of the motor at approximately 0.5 second. This started premature burning of the RFG in a localized area which significantly decreased the structural integrity of the motor. Ballistic calculations indicated that approximately 2.23 inches of the RFG web had burned in this area at the time of the malfunction which reduced the remaining RFG web to approximately 1.6 inches rather than the normal 3.4 inches. Calculated rupture pressure for the GFW case and 1.6 inches of RFG was 915 psig which is well below the actual burst pressure of the motor.

Strain gages on the GFW case showed no indication of premature burning of the RFG prior to 9.6 seconds because it was a highly localized condition and no strain gages were positioned on the case in the immediate area of the failure. However, strain gages near the aft end of the cylinder and on the aft dome showed high strain prior to those near the forward end of the motor.

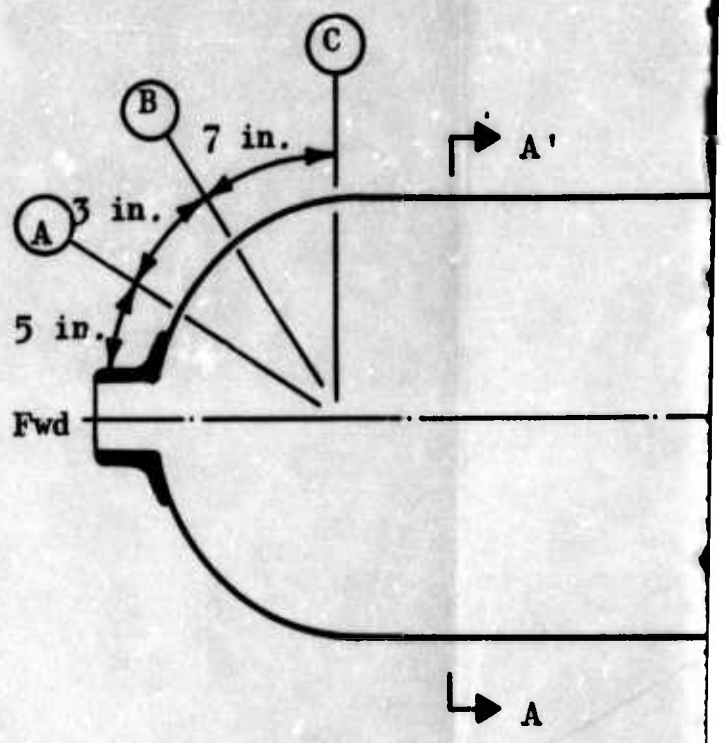
The results obtained from the 30 internal thermocouples (Fig. 216) and 37 external thermocouples (Figs. 217 and 218) indicated that the motor was functioning normally prior to the time of malfunction. Of the 30 internal thermocouples which were to show the burnout pattern of the RFG, only those on the aft end of the motor showed any movement prior to the malfunction. The sequence of indication showed that the flame approached from the cylindrical section rather than the polar boss area. The total time elapsed between the first movement and final movement was 19 milliseconds and the final movement occurred approximately 5 milliseconds after the maximum motor pressure was reached.

Thr remaining thermocouple data, except for the two thermocouples on the forward closure, showed no increase in temperature during the firing duration. As shown in Fig. 219, Thermocouple 61 which was located between the pressure port and CO_2 port reached a maximum temperature of 313 F at 1.4 seconds after ignition and decreased to 200 F at the time of malfunction. Thermocouple 62 located between the two pressure ports rose to 80 F and remained at this temperature for the firing duration. The temperature achieved by Thermocouple 61 was higher than that previously recorded in A-1003 and A-1004 firings, but exhibited the same general characteristic of a fast initial rise and gradual cool down and is associated with the same phenomenon as previously described under Motor A-1004.

PREVIOUS PAGE WAS BLANK, THEREFORE WAS NOT FILMED

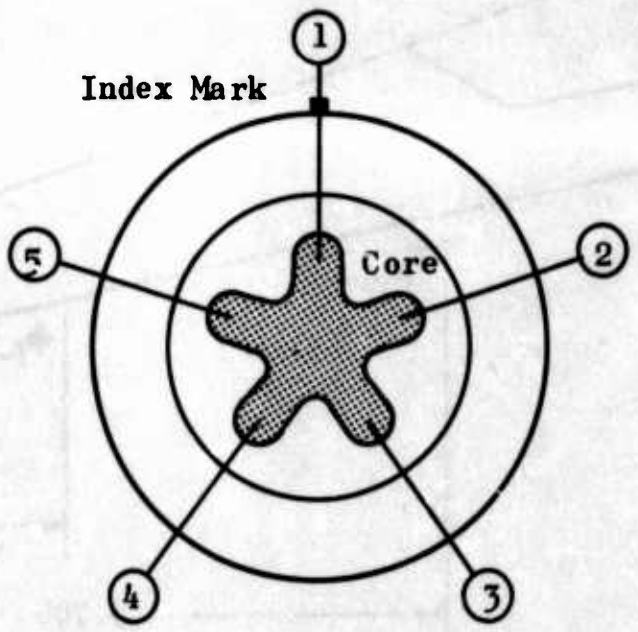


Forward End
(Looking Aft)

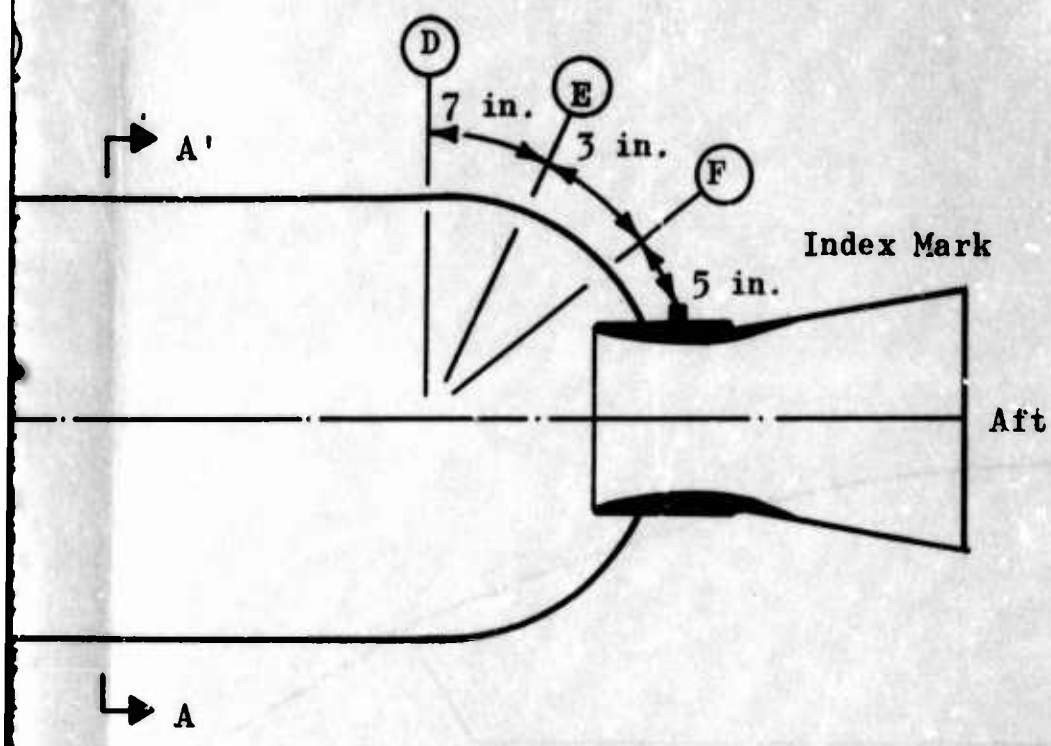


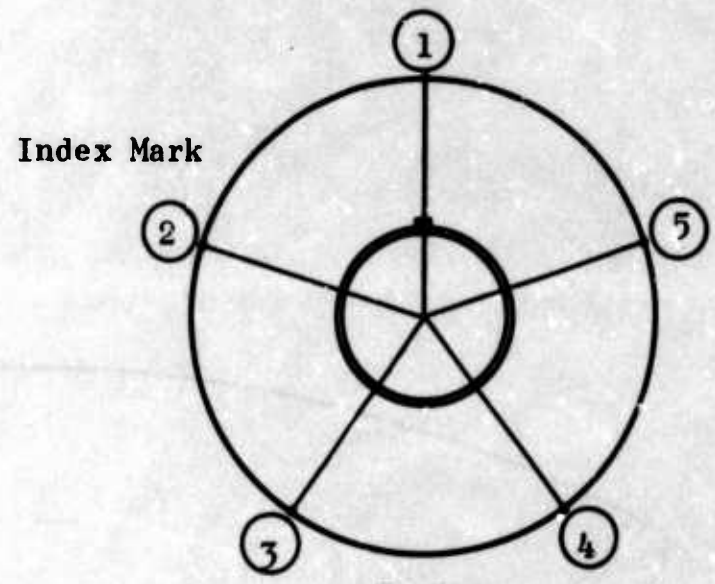
NOTES:

1. There are a total of 30 internal
2. Location of thermocouples is in a location chart below.
3. Motor is located in test stand w position.
4. Index mark on aft boss is in lin
5. Star point valleys are in line w



Location Plane
1
2
3
4
5





bal of 30 internal thermocouples installed.

ermocouples is in accordance with the
below.

ed in test stand with No, 1 plane in up

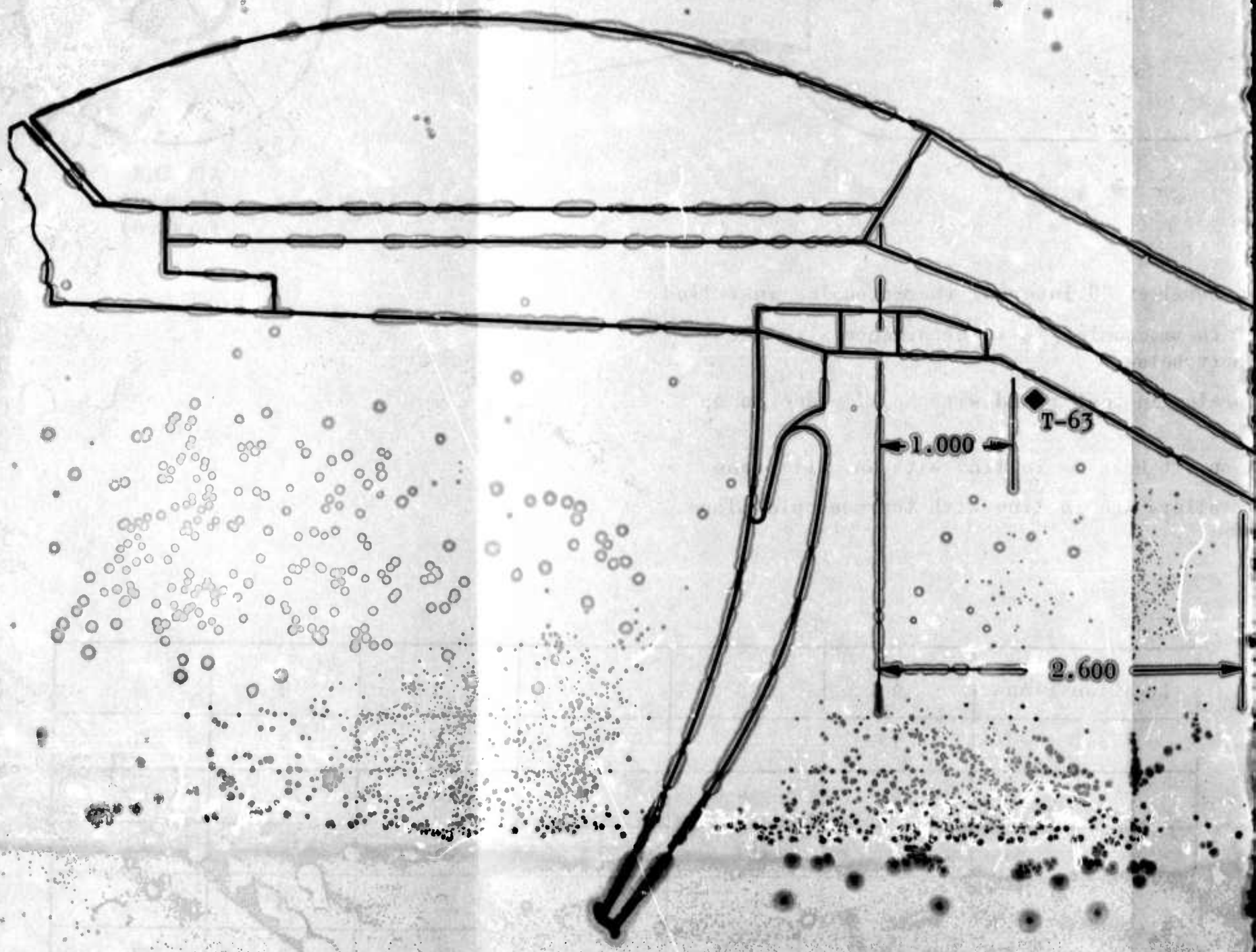
aft boss is in line with No. (1) plane.

leys are in line with thermocouple plane.

Location Plane	A	B	C	D	E	F
1	1	2	3	4	5	6
2	7	8	9	10	11	12
3	13	14	15	16	17	18
4	19	20	21	22	23	24
5	25	26	27	28	29	30

Figure 216. Internal Thermocouple Locations for Motor A-1005

CONFIDENTIAL


T-63
1.000
2.600

NOTES:

1. Locations marked by ◆ are for thermocouples on the surface.
2. Surface thermocouples temperature range is 60—500 F
3. Surface coordinate dimensions are ± 0.01 in.
4. Use smallest thermocouples possible.
5. All dimensions are in inches.
6. Surface thermocouples are to be located as near to edge of the drill hole as practical.
7. Total of 5 thermocouples installed in nozzle.

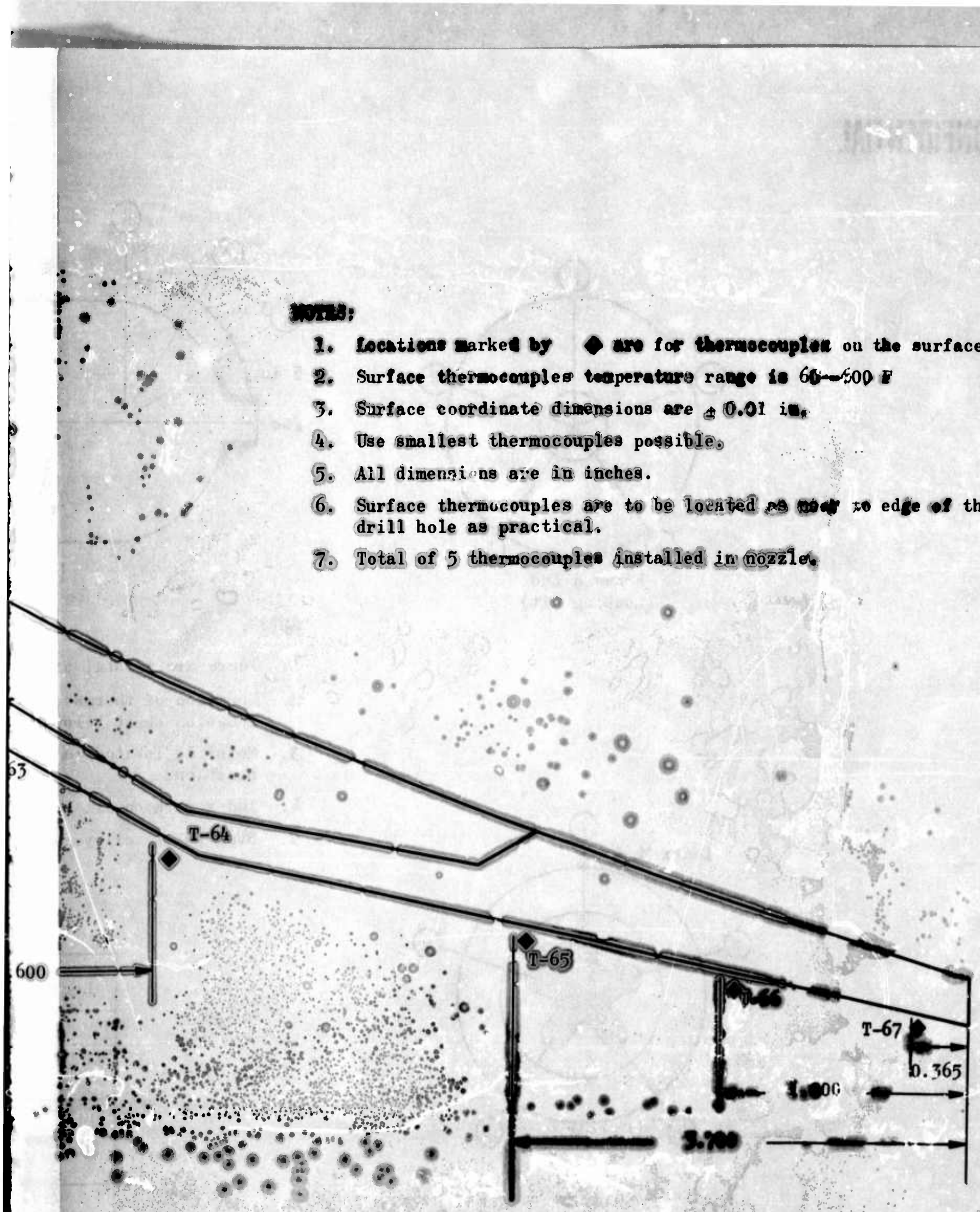
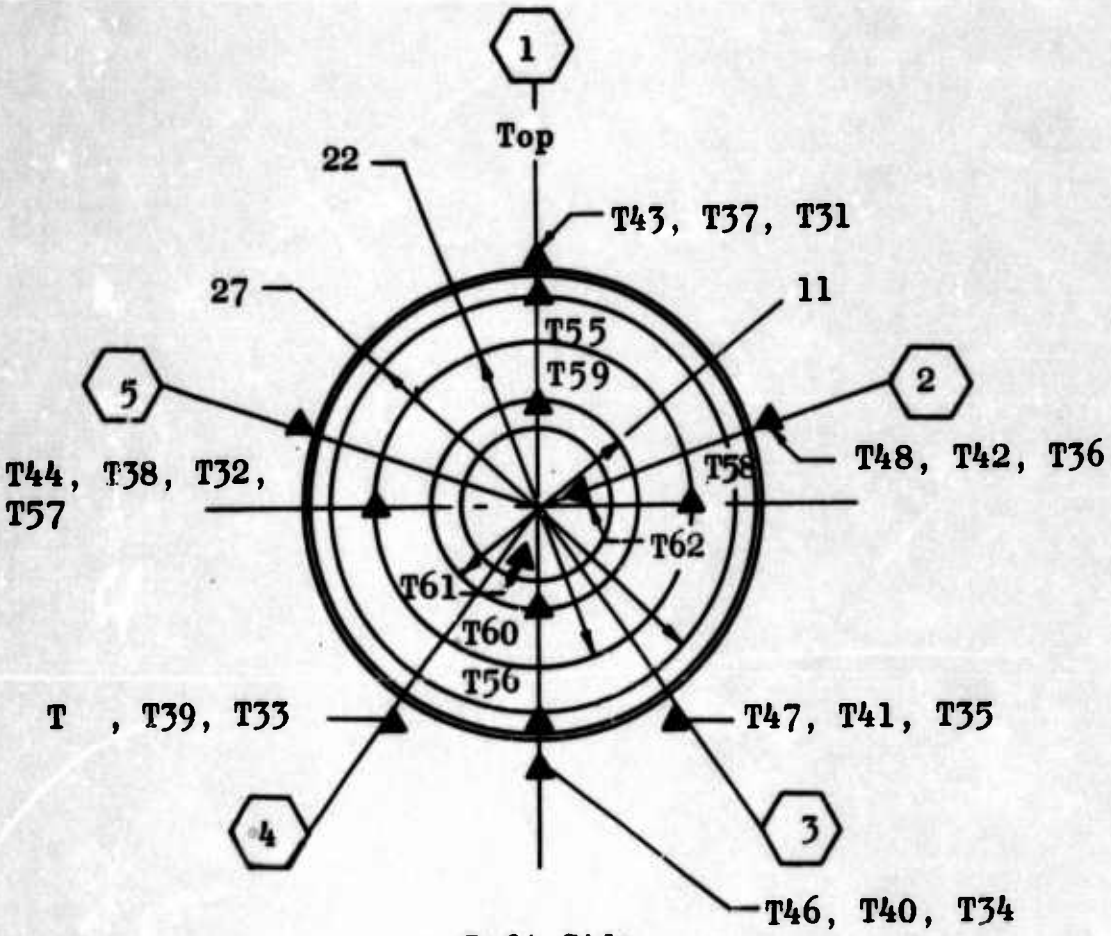
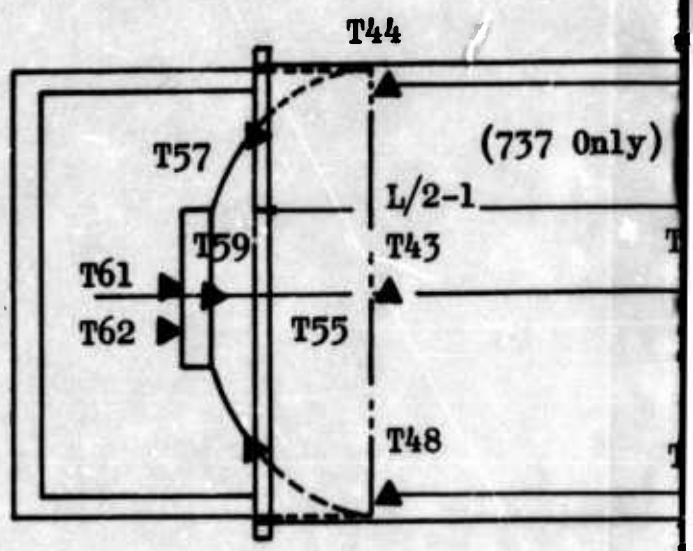
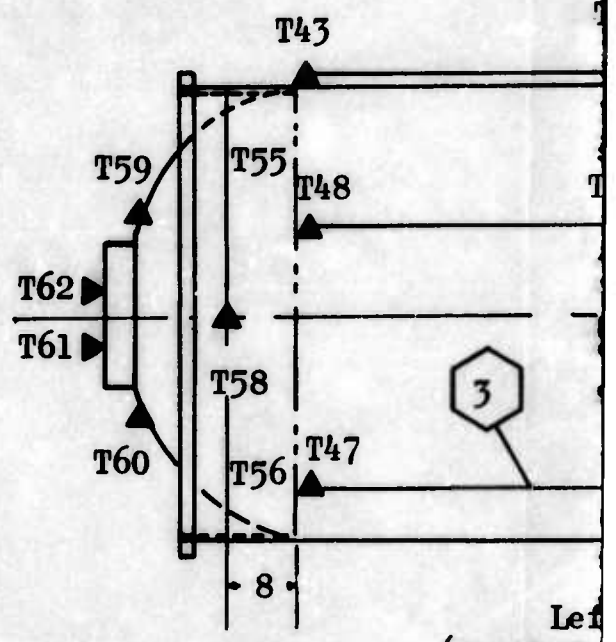


Figure 217. Nozzle Thermocouple Locations for Motor A-1005

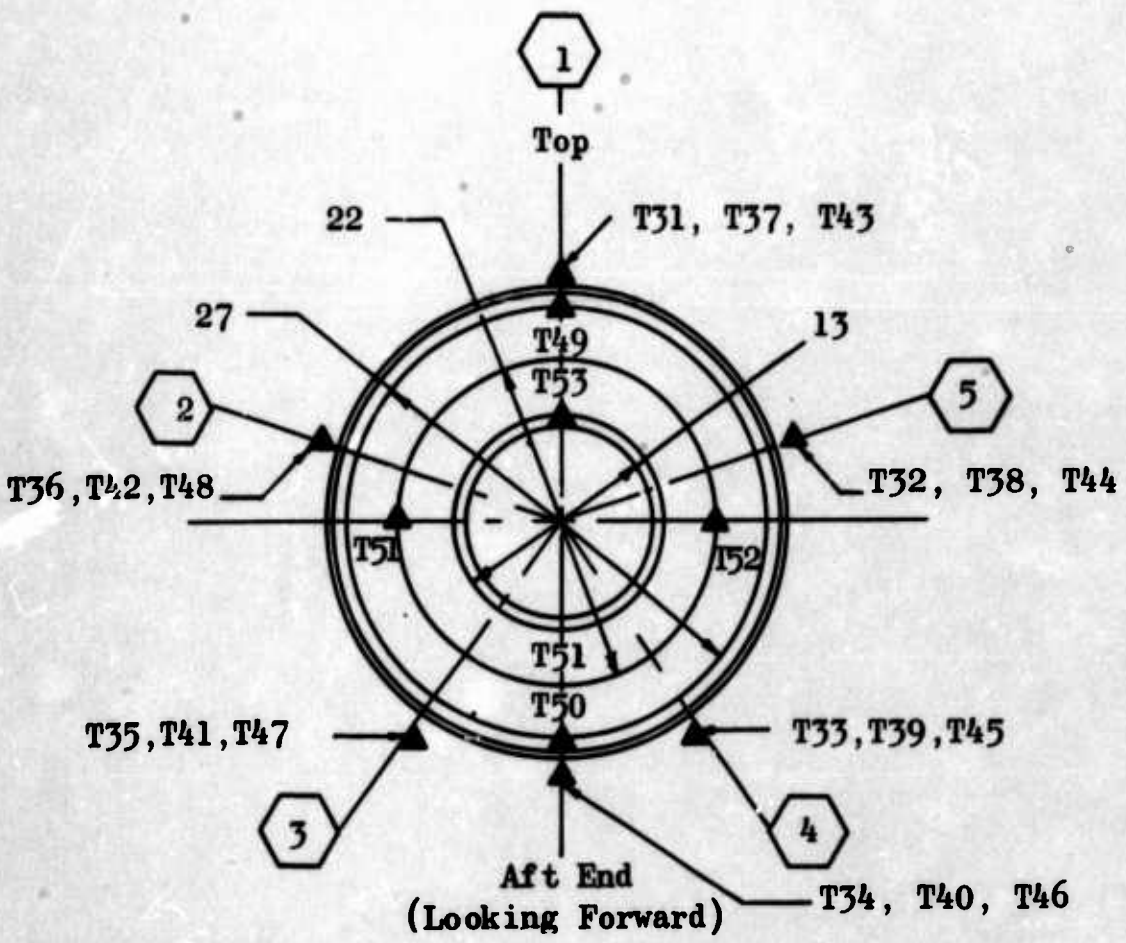


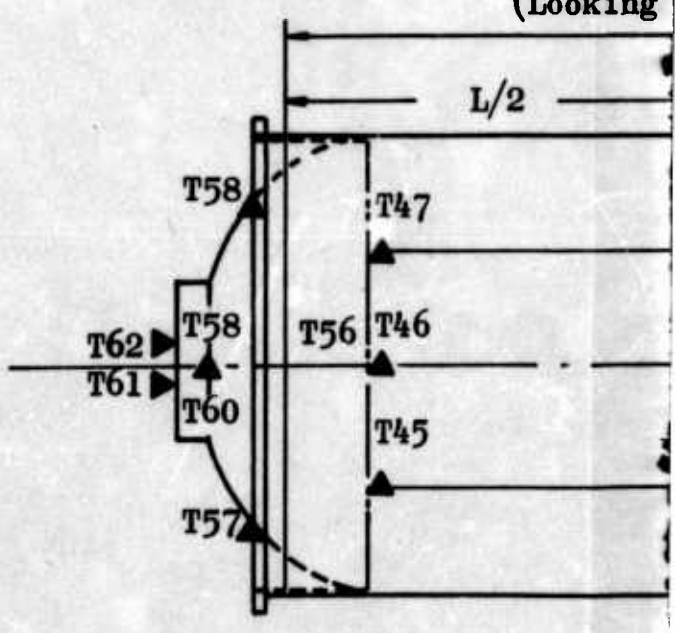
Left Side
(Looking at Aft End)





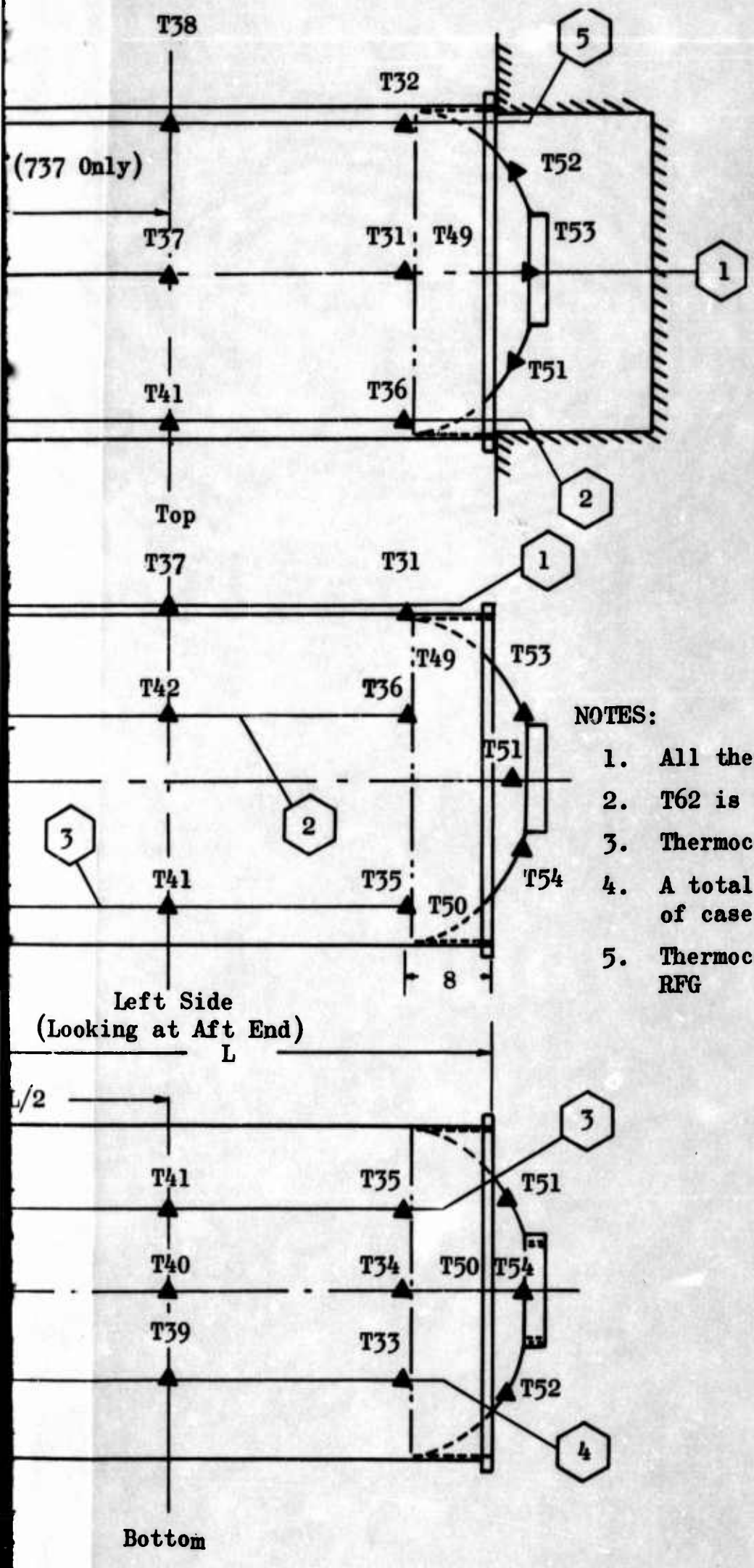
Le
(Looking





Bo

1



NOTES:

1. All thermocouples not shown in all views
2. T62 is to be located between the two pressure ports.
3. Thermocouples to have a range from 60--600 F.
4. A total of 32 thermocouples will be placed on exterior of case.
5. Thermocouples 1--30 are located on the interface of the RFG

Figure 218. Case Thermocouple Locations for Motor A-1005

2

PREVIOUS PAGE WAS BLANK, THEREFORE WAS NOT FILMED

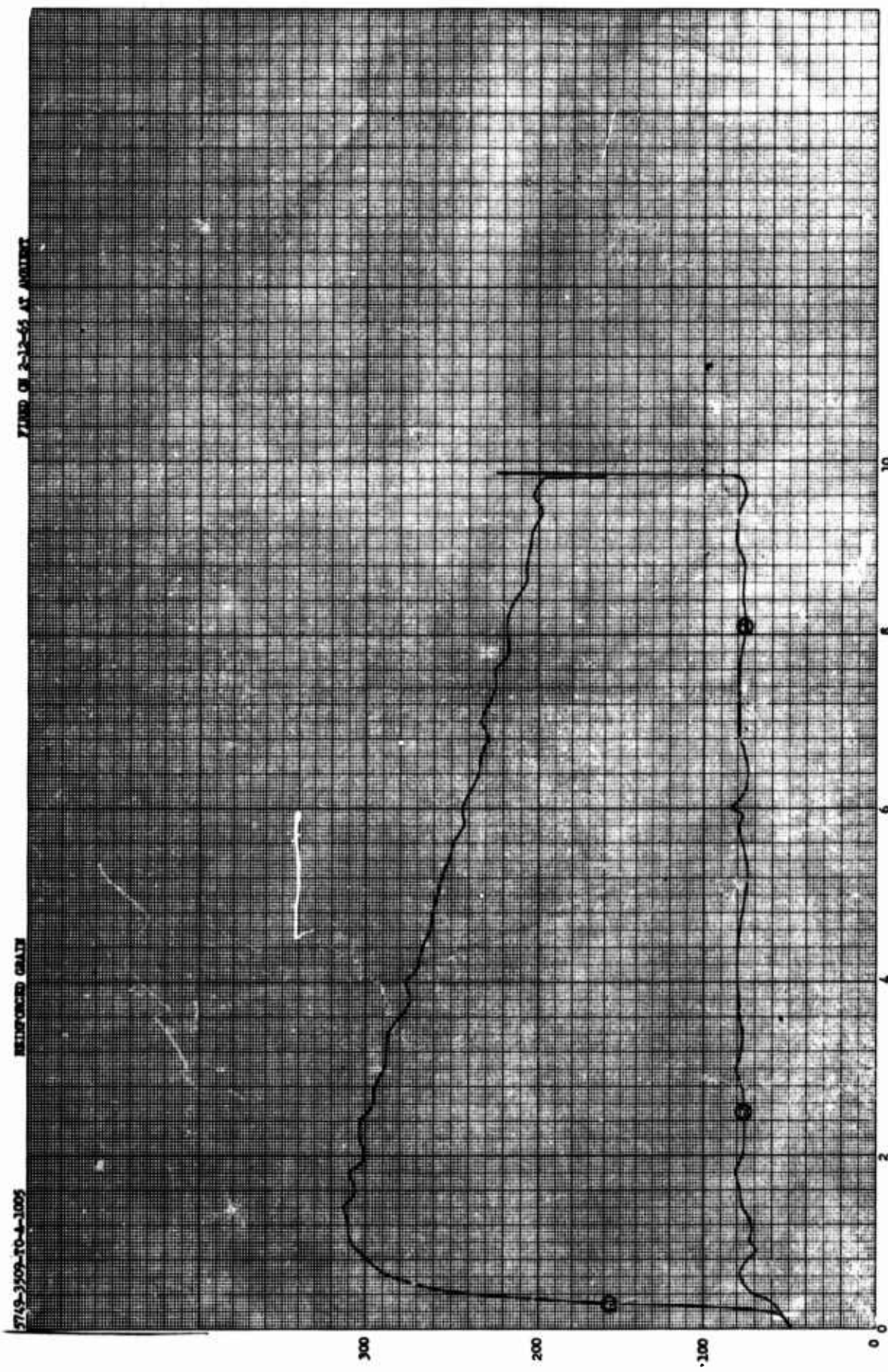


Figure 219. Forward Closure Temperature vs Time
For Motor A-1005

Examination of the sectioned components which were recovered indicates that the thermal protection was adequate. The only unusual area was around the joint between the nozzle and aft polar boss. The appearance of this area was much like that of A-1004. The eroded section was approximately 0.3 inch wide (0.2 inch deeper than the normal erosion) and covered the full circumference. Both the phenomenon in A-1004 and A-1005 were associated with discontinuities of the nozzle wall in the subsonic flow region. The discontinuity causes an interruption in the flow and sets up a vortex which produces a very erosive environment.

(2) Conclusions and Recommendations

Evaluation of test data, observation of the high-speed movies, and study of the recovered components has led to a theory of failure which best correlates all the supporting evidence. Many other possible causes of failure were investigated and proven incorrect.

Ignition and the first 0.5 second of core burning were close to that expected. At approximately 0.5 second the pressure departs from the expected trace and remains high for 8.84 seconds. This additional pressure over this duration represents an increase of 4.1% of core pressure-impulse or the consumption of 35 pounds of propellant above that which was scheduled to burn. The close correlation of the actual and estimated core pressure impulse of previous motors indicated that the additional propellant did not come from core sliver.

Study of the high-speed films and examination of the forward half of the GFW case which was charred but intact after the malfunction indicated that the failure occurred at or near the aft tangent. The increased pressure level and propellant consumption must be accompanied by an associated increase in burning area. The rainbow shape of the pressure-time trace is characteristic of burning where additional surface is slowly being added. Analysis indicated that if the bond between the RDS-501 and RDS-526 had failed at approximately 0.5 second it would not only account for the pressure increase but also the additional 35 pounds of propellant consumed.

Although tests had been conducted on the castibility and bondability of the two propellants prior to casting the motor and the results proved the system to be satisfactory, this area was still questionable since water was found in the casting tooling of the RDS-526 mix after casting was complete. Upon removal of the core mandrel the grain was inspected

very closely for water damage. No visible evidence of damage was observed. However, this does not imply there was no damage whatsoever to the motor. Radiographic inspection of the bond area revealed no abnormalities as would be expected if there were no voids and the grains were in intimate contact. The contamination of the bond line area with water although possibly not of sufficient quantity to be observed visually would result in a weakened if not insufficient bond strength.

(C) The failure of this bond would ignite the RFG locally and over the 9.848-second duration would have consumed approximately 2.23 inches of the 3.79 inches of RFG web. The remaining 1.56-inch RFG/GFW structure was capable of withstanding only about 915 psi which is well below the 975 psi recorded at the time of malfunction. Strain gages on either side of the aft tangent showed little or no increase in strain until just prior to failure, thereby further indicating the extremely localized condition. The 15 thermocouples on the aft dome indicated that the flame approached from the tangent plane rather than the polar boss area which also indicates the failure occurred near the aft tangent.

(C) All evidence indicates that the bond between the RDS-501 and RDS-526 failed at approximately 0.5 second thereby allowing premature ignition of the RFG. The subsequent burning of the RFG accounts for the increase in surface area and propellant burned during the firing duration. The resulting consumption of RFG reduced the structural capability of the RFG/GFW structure to a point at which it was unable to withstand the load and the structure failed at 9.848 seconds at an indicated pressure of 975 psi.

Based on the results of the analysis, the following conclusions are drawn:

1. Thermal protection of the designed components was adequate.
2. Structural performance of the motor was close to that expected for 9.6 seconds.
3. The repaired forward closure functioned as expected and did not contribute to motor failure.
4. The repaired forward skirt performed most satisfactorily and did not contribute to the malfunction.
5. Ballistic performance was higher than that expected for the firing duration and is attributed to the unscheduled burning of 35 pounds of propellant.

6. The water contamination of the bond surfaces between the two propellants was the major contributor to the malfunction.

7. The use of two different propellants did not directly contribute to the malfunction.

8. Motor malfunction was due to failure of the RFG/GFW structure resulting from the following probable sequence of events:

   Failure of the bond between the RDS-501 and RDS-526 due to water contamination during casting resulted in premature ignition of the RFG in a localized area.

   Burning of the RFG for approximately 9.3 seconds reduced the capability of the RFG/GFW structure and resulted in the additional pressure, thrust and consumed propellant.

   Structural capability of the RFG/GFW structure was reduced and the remaining portion was unable to sustain the pressure load.

SECTION VI

MOTOR B

Motor B was a larger diameter motor than Motor A but utilized the RFG in a similar manner. Because of this functional likeness the design and development of Motor B was timed to capitalize on Motor A experience.

The following section has been arranged in an order similar to the section on Motor A. The design and development effort, presented first, includes a general description of the motor, ballistic and structural aspects, and component development. Process development for this larger RFG and GFW case is also included in this discussion. Throughout the section the theoretical approach and background for using a particular limiting load, component design, material, etc., has been omitted because of the similarity to Motor A. However, the results of the various studies, whether theoretical or imperical, have been included here (where appropriate).

Following the design and development section, the fullscale motor sections detail the fabrication, testing, and results of the tests for each motor.

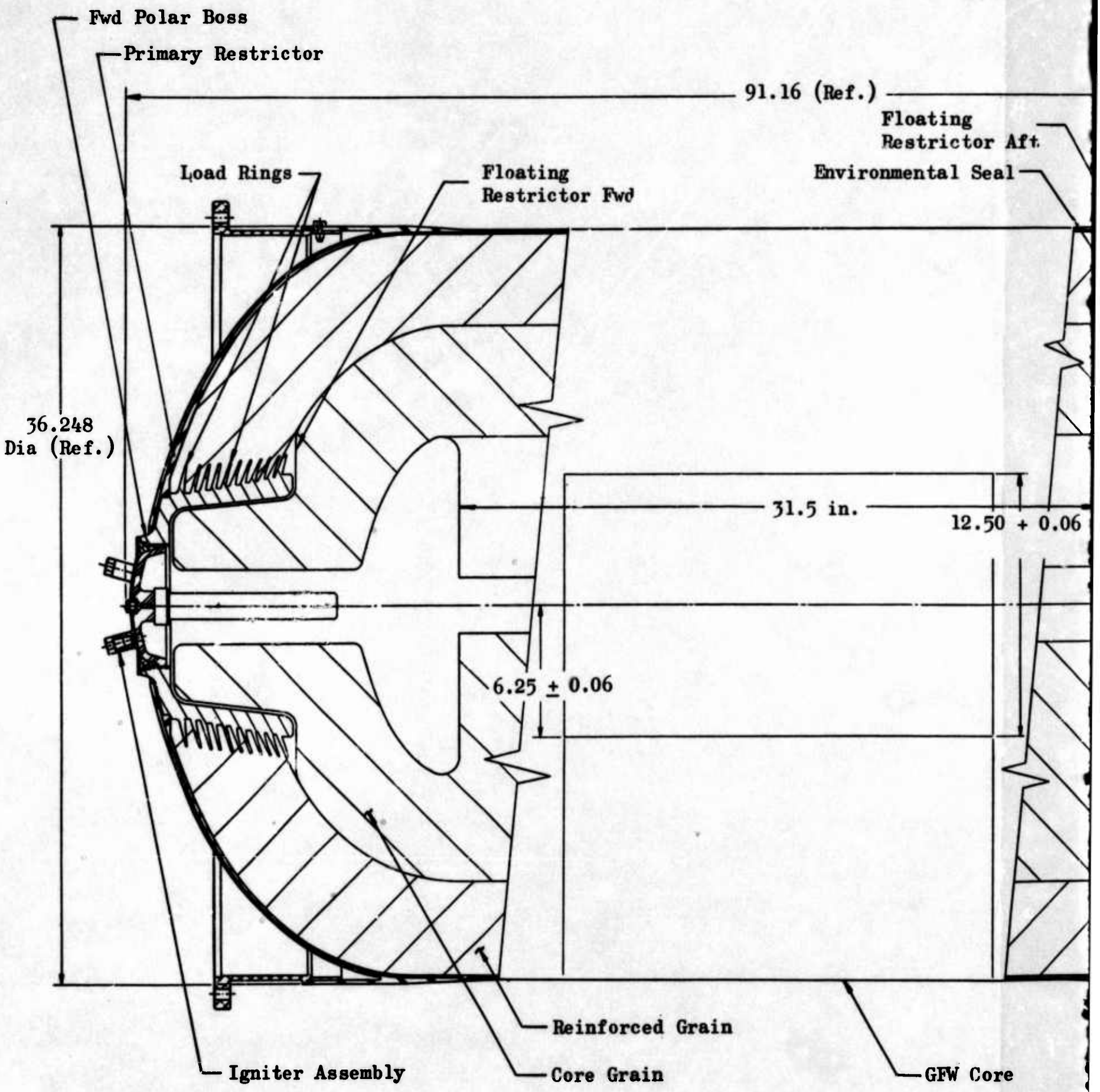
1. DESIGN AND DEVELOPMENT OF MOTOR B

Motor B (see Fig. 220) is a 36-inch diameter cylinder approximately 91 inches long with dome-shaped ends. The GFW case skirt assembly is similar to Motor A with a metal mounting ring provided for interstage coupling and transfer of external loads.

The igniter assembly and forward end is similar to Motor A while the aft end opening must provide additional support for a hydraulically operated thrust vector control (TVC) system.

The grain is a two-section RFG composite construction with the aluminum wire reinforced grain furnishing additional structural strength to the GFW case. Polar bosses and load rings are employed in a manner similar to Motor A. Both ends of the Motor B case grain have stress relief floaters, rather than the end floater used on Motor A.

PREVIOUS PAGE WAS BLANK, THEREFORE WAS NOT FILMED



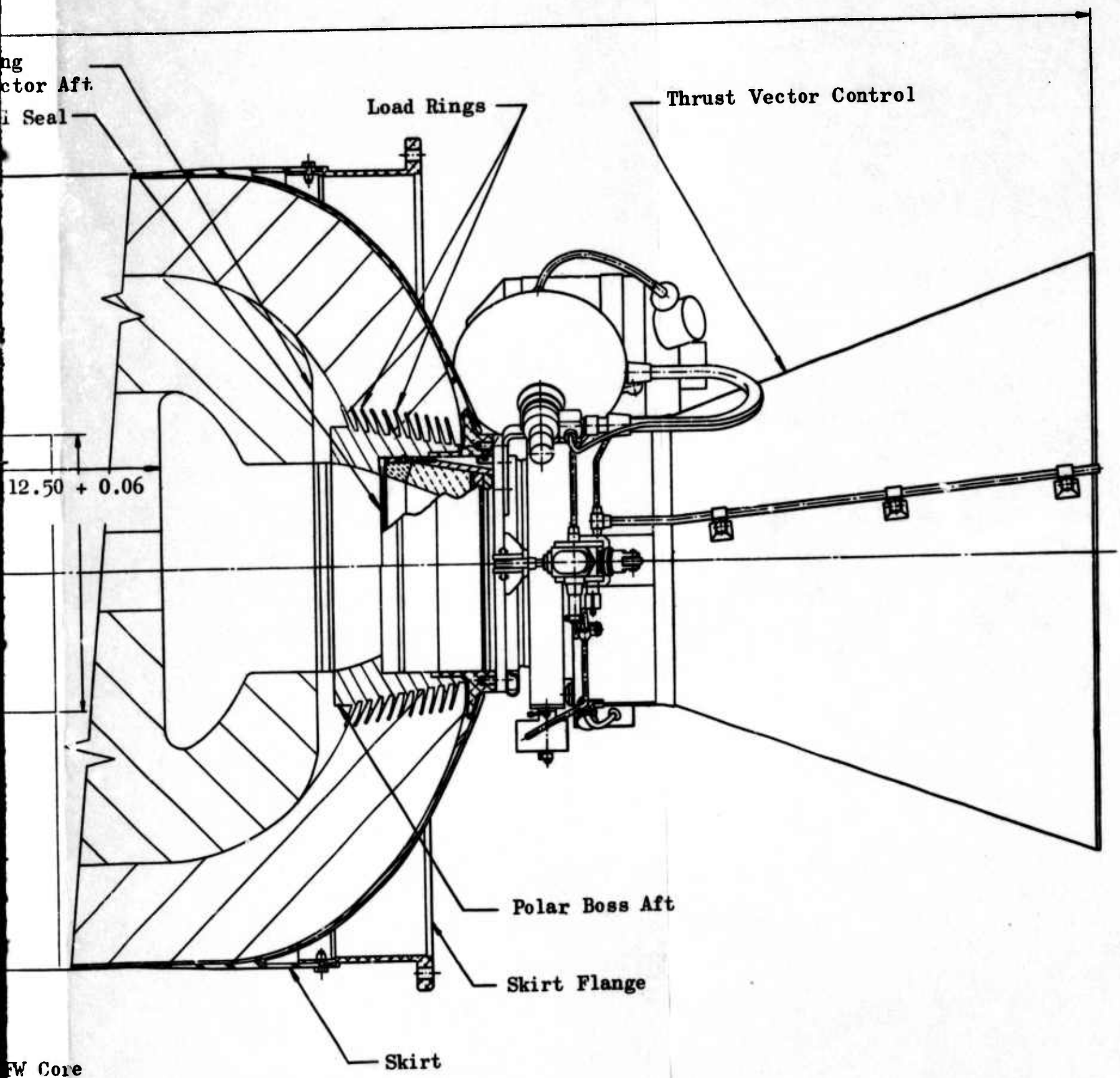


Figure 220. Motor B General Arrangement

CONFIDENTIAL

PREVIOUS PAGE WAS BLANK, THEREFORE WAS NOT FILMED

a. Ballistic Design

(C) There were no explicit ballistic requirements for either the core grain or the RFG, other than those implied in the requirements for the total motor, shown below:

1. The action time total impulse shall be 800,000 lb-sec at 60 F with a 25:1 expansion nozzle at vacuum (altitude) conditions.
2. The design thrust level shall be 21,000 lb average and 30,000 lb maximum at the same motor operating conditions (60 F, 25:1, vacuum).
3. The overall motor shall have the following dimensions: maximum case OD 36 inches, overall maximum length 90 inches including altitude nozzle, and minimum skirt-to-skirt length 40 inches.
4. The total motor weight shall not exceed 3200 lb. Included in the total weight are the altitude nozzle, skirts, igniter assembly, TVC, and thrust reversal.
5. The minimum mass fraction shall be 0.937. Mass fraction will be calculated as total propellant weight, divided by total motor weight, where total motor weight includes: skirts, igniter, thrust reversal system, altitude nozzle, and complete thrust vector control system including gas generator, actuating devices, hydraulic oil, and tank. In the event that a heavyweight gas generator is utilized, the gas generator weight used in calculating mass fraction will be 10.9 pounds.
6. The motor shall demonstrate a delivered specific impulse of 250 lb-sec/lb (corrected to optimum 1000/14.7 expansion).
7. Test firing temperature range shall be from -75 F to 170 F.

(1) Parametric Study

With these requirements a parametric study similar to that for Motor A was conducted, except the study was optimized on the total impulse. Since the analysis was similar to that used on Motor A, only the results are discussed here.

(C) The Motor B analysis was based on the hot (170 F) motor condition, which yielded a 915 psia initial RFG pressure and a web thickness of 4.5 inches. Structural considerations dictate that the motor operating pressure level must decrease as the RFG web is consumed. The permissible motor pressure decreases linearly as a function of web remaining to 500 psia at 1.0 inch of web. (This was established as a minimum pressure level, based on the Motor A tests and propellant capabilities.) The GFW case was designed to contain 500 psia during burnout of the final inch of RFG web.

(2) Propellant Development

The propellant development during the early development of Motor A was directly applicable to the Motor B design.

(3) Ballistic Design, RFG and Core Grain

(C) The decreasing pressure level from 1000 psia to 500 psia during the RFG burning was accomplished by utilizing propellant containing various amount of burning-rate depressant in each of the RFG layers. In contrast to Motor A, which employed depressed propellant (RDS-514) in the first layer, the burning surface-to-throat area (Kn) ratio of Motor B RFG was such that RDS-512, which contains no depressant, could be used. The propellant burning rate and other miscellaneous data for the RFG are shown below:

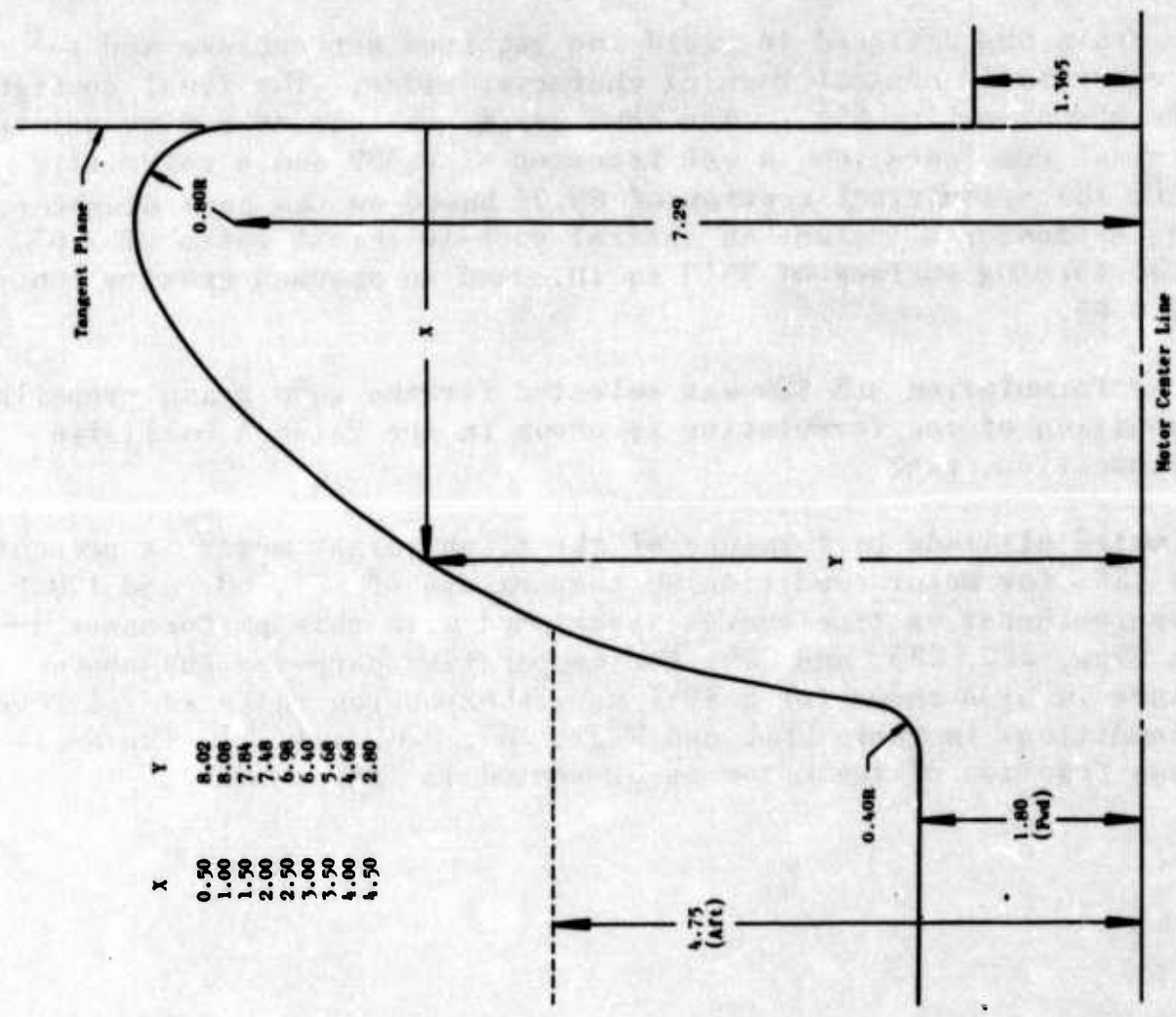
(C)

Helical Layer No.	Uncured Strand Rate At P, in./sec	Estimated Motor Rate At P, in./sec	Propellant Weight, lb	Propellant RDS Number	Percent, Depressant
1	0.336 at 1015	0.337 at 750	130	512	0.00
2	0.261 at 695	0.307 at 695	142	514	0.45
3	0.225 at 645	0.264 at 645	147	514	0.85
4	0.196 at 595	0.231 at 595	156	514	1.70
5	0.173 at 545	0.203 at 545	161	523	2.20
6	0.153 at 495	0.180 at 495	167	523	3.90
7-11	0.130 at 400	0.160 at 400	854	523	6.00

(C) The core grain was designed to yield the required performance and to exhibit essentially neutral burning characteristics. The final configuration is shown in Fig. 221. The core grain consists of a five-pointed star internal configuration, a web fraction of 0.382 and a volumetric loading in the cylindrical section of 89.7% based on the core diameter. Other design features include an initial port-to-throat ratio of 2.63, an initial burning surface of 3515 sq in., and an assumed erosive constant of 0.05.

Rocketdyne Formulation RDS-526 was selected for the core grain propellant. The composition of the formulation is shown in the Motor A ballistic design subsection, page .

(C) The estimated altitude performance of the flightweight motor is presented in Table LXX for motor conditioning temperature of -75, 60, and 170 F. The pressure-thrust vs time curves associated with this performance are shown in Figs. 222, 223, and 224. For comparative purposes the above performance is also shown for a 10:1 nozzle expansion ratio at sea level firing conditions in Table LXXI and Figs. 225, 226, and 227. The estimated mass fraction of the motor is presented in Table LXXII.



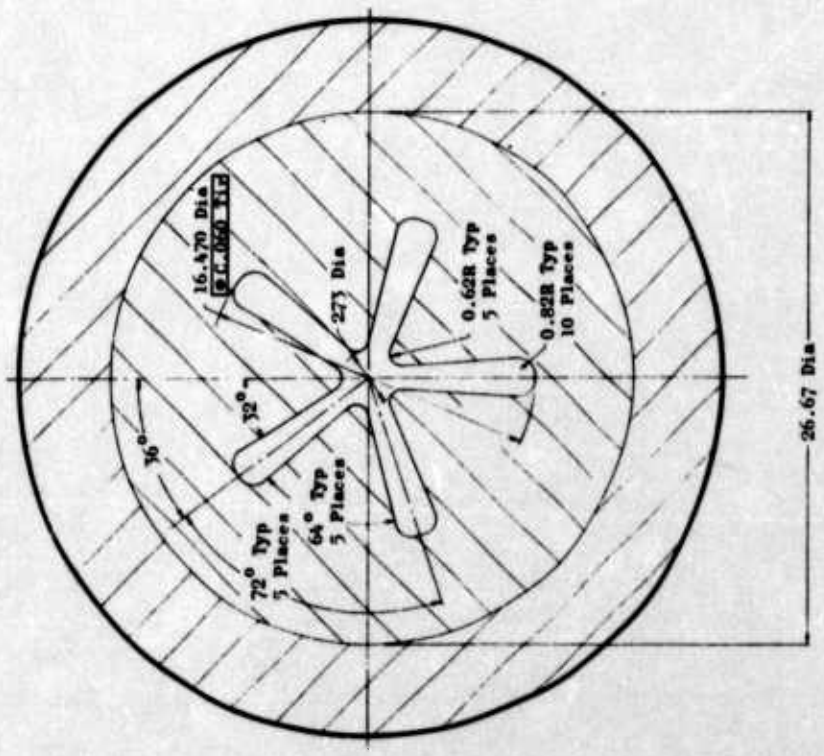


Figure 221. Motor B Core Grain Cross Section and Conicyl Configuration

TABLE LXX

MOTOR B PERFORMANCE ESTIMATE - FLIGHTWEIGHT MOTOR

Nozzle Expansion Ratio: 25:1
Atmospheric Pressure: 0 psia

(c)

	Motor Conditioning Temperature		
	-75 deg F	60 deg F	170 deg F
Motor			
Average Pressure, psia	485	560	645
Average Thrust, lb	19,010	21,900	25,180
Total Impulse, lb-sec	856,800	856,800	856,800
Action Time, sec	45.1	39.1	34.0
Maximum Pressure, psia	680	800	915
Maximum Thrust, lb	26,380	31,070	35,490
I_{sp} @ motor Condition	276.2	276.2	276.2
I_{sps} @ 1000 psia, Sea Level	241.4	241.4	241.4
Impulse to Weight Ratio	255.1	255.1	255.1
Core Grain			
Average Pressure, psia	645	760	870
Average Thrust, lb	25,070	29,530	34,210
Total Impulse, lb-sec	328,900	328,900	328,900
Duration, sec	13.1	11.1	9.6
I_{sps} @ 1000 psia, Sea Level	250.0	250.0	250.0
Reinforced Grain			
Average Pressure, psia	420	480	520
Average thrust, lb	16,520	18,860	21,620
Total Impulse, lb-sec	527,900	527,900	527,900
Duration, sec	32.0	28.0	24.4
I_{sps} @ 1000 psia, Sea Level	234.9	234.9	234.9

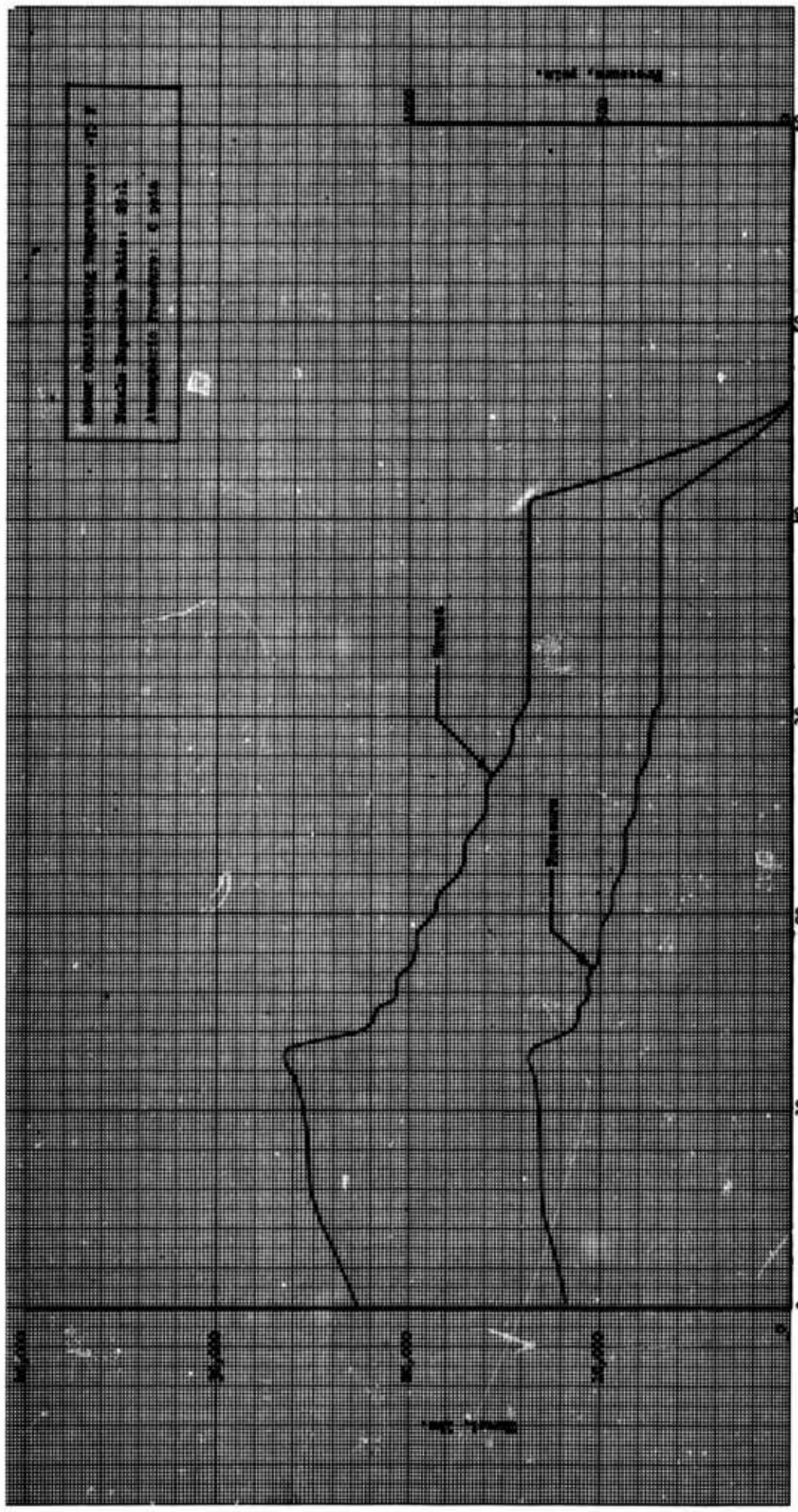


Figure 222. Motor B Estimated Performance - Flightweight Motor (-75 F)

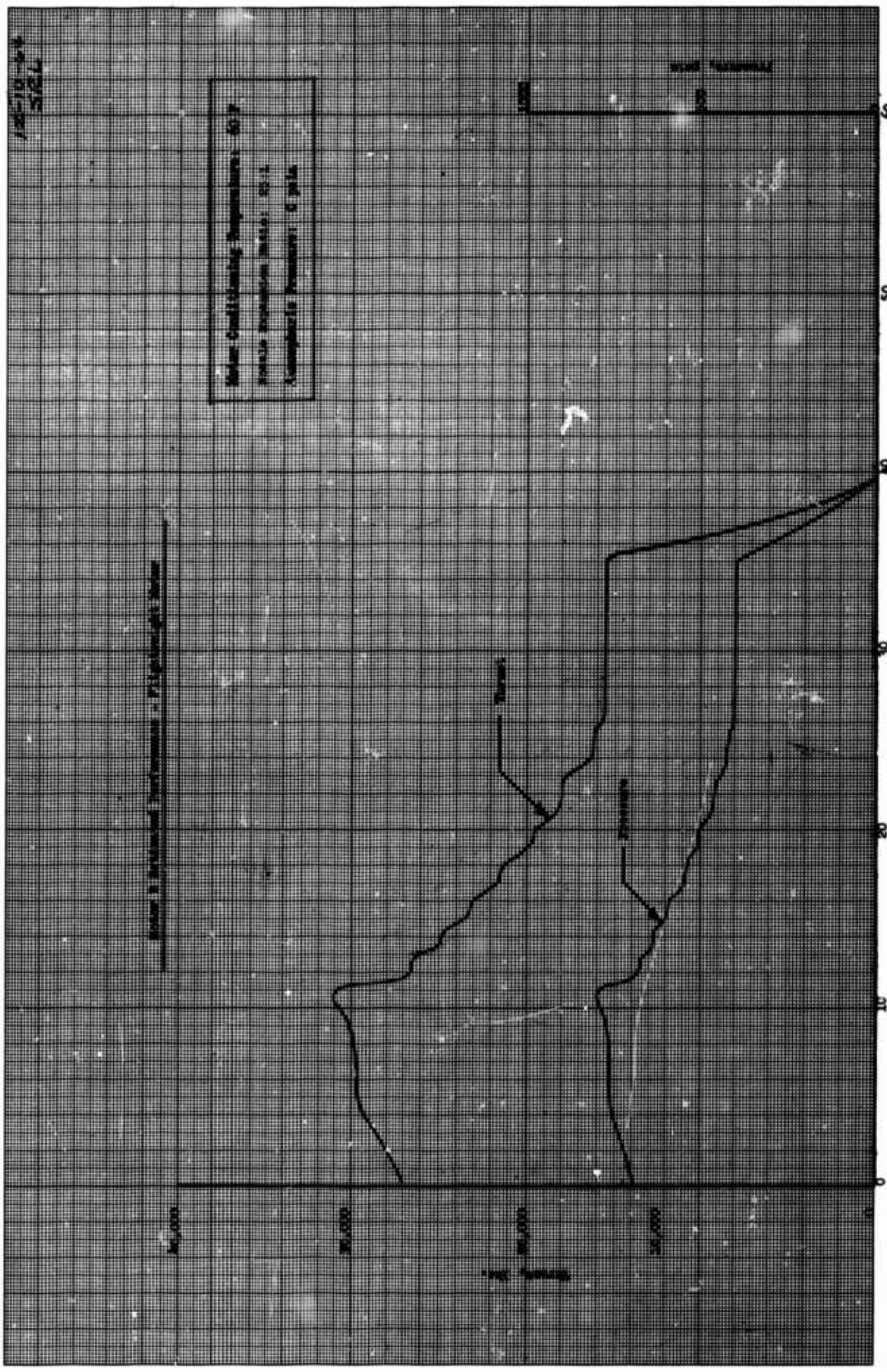


Figure 223. Motor B Estimated Performance - Flightweight Motor (60 F)

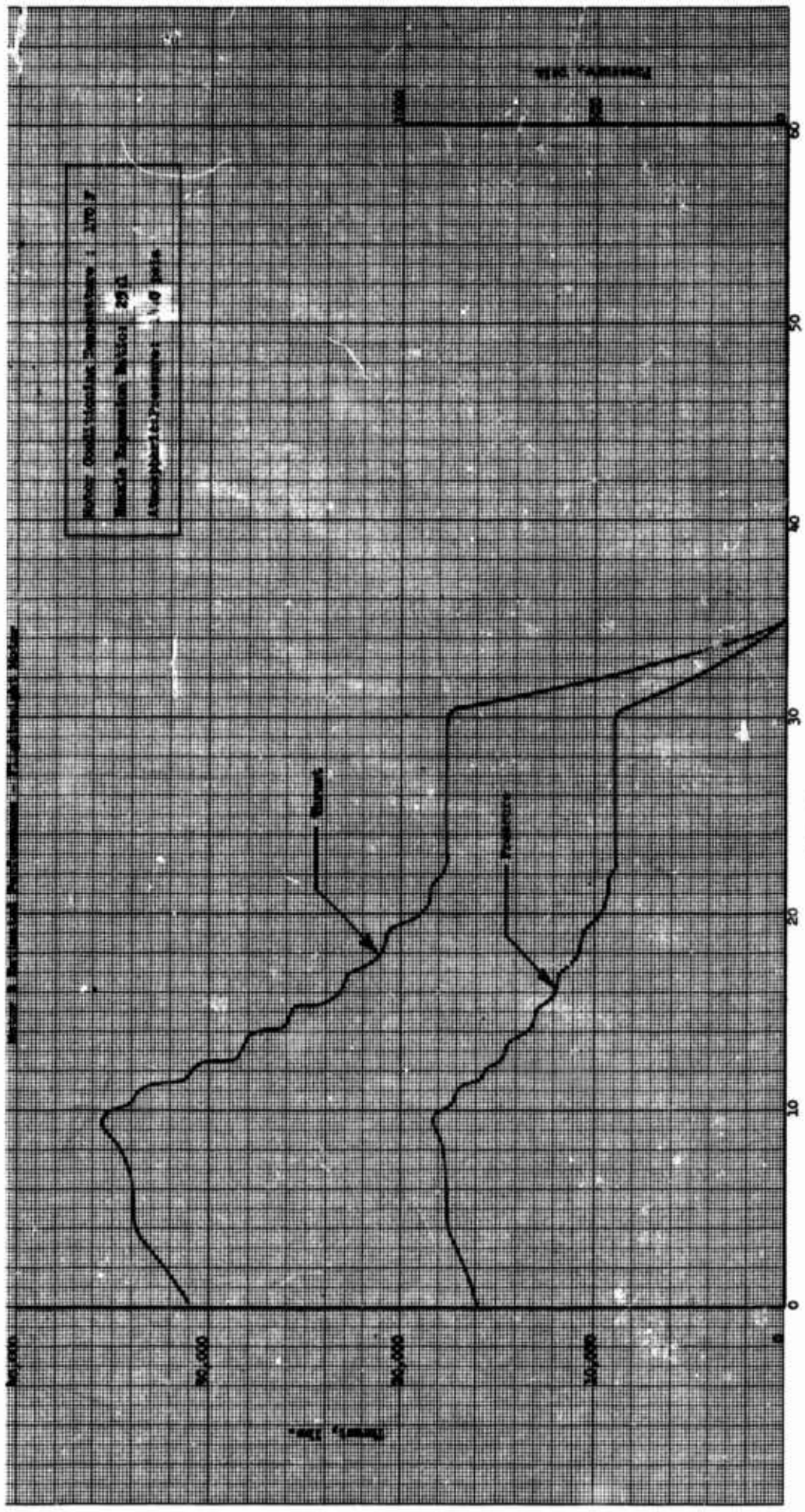


Figure 224. Motor B Estimated Performance - Flightweight Motor (170 F)

TABLE LXXI

MOTOR B PERFORMANCE ESTIMATE - FLIGHTWEIGHT MOTOR

Nozzle Expansion Ratio: 10:1
Atmospheric Pressure: 14.7 psia

	Motor Conditioning Temperature		
	-75 deg F	60 deg F	170 deg F
Motor			
Average Pressure, psia	485	560	645
Average Thrust, lb	14,420	17,070	20,080
Total Impulse, lb-sec	650,000	667,900	683,300
Action Time, Sec	45.1	39.1	34.0
Maximum Pressure, psia	680	800	915
Maximum Thrust, lb	21,240	25,550	29,610
I_{sp} @ Motor Conditions	209.6	215.3	220.3
I_{sp} @ 1000 psia	241.4	241.4	241.4
Impulse to weight Ratio	193.5	198.8	203.4
Core Grain			
Average Pressure, psia	645	760	870
Average Thrust, lb	20,020	24,130	28,400
Total Impulse, lb-sec	262,700	268,800	272,900
Duration, sec	13.1	11.1	9.6
I_{sp} @ 1000 psia	250.0	250.0	250.0
Reinforced Grain			
Average Pressure, psia	420	480	520
Average Thrust, lb	12,120	14,260	16,810
Total Impulse, lb-sec	387,400	399,200	410,400
Duration, sec	32.0	28.0	24.4
I_{sp} @ 1000 psia	234.9	234.9	234.9

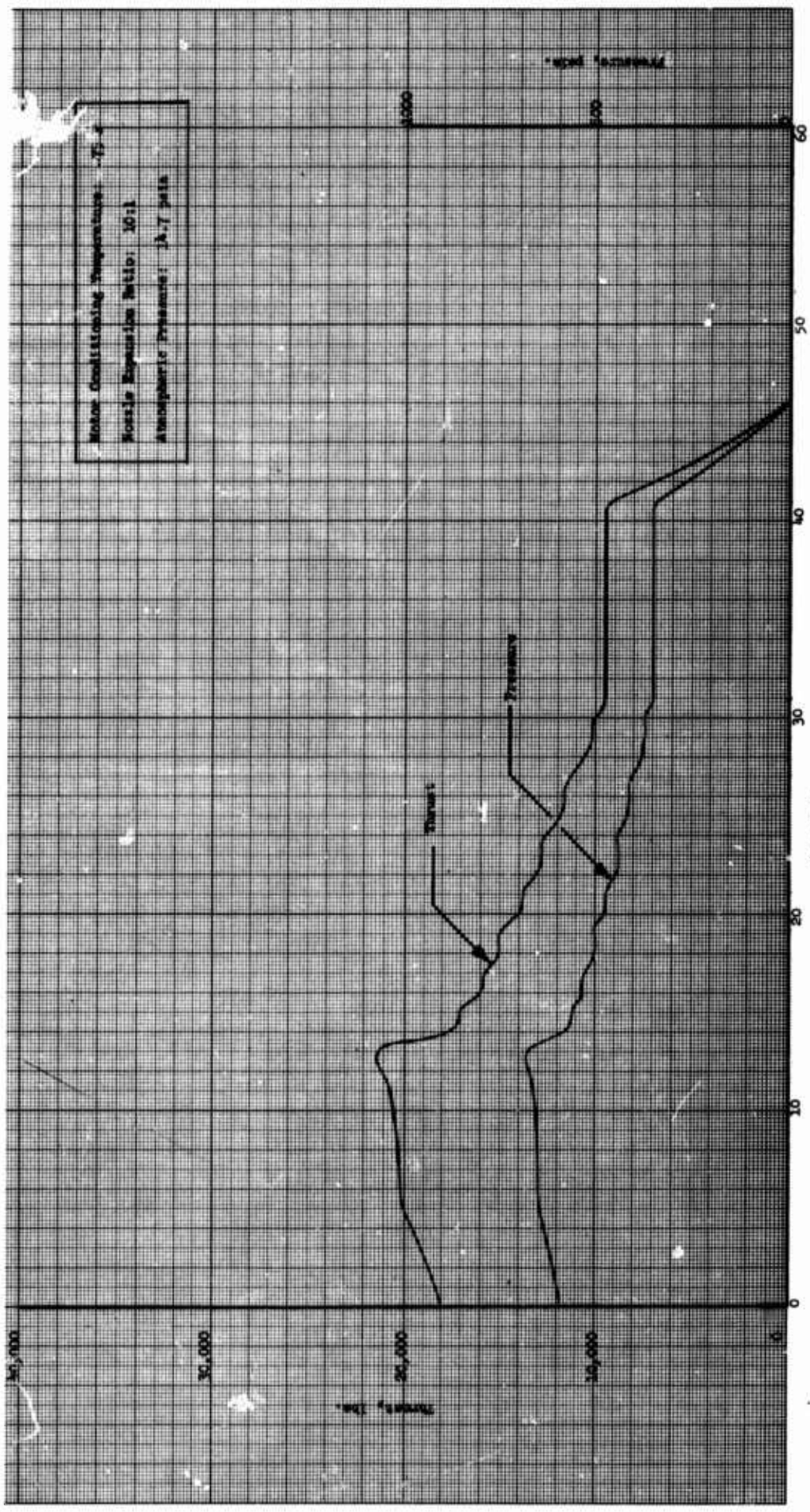


Figure 225. Motor B Estimated Performance - Flightweight Motor, Nozzle Ratio 10:1 (-75 F)

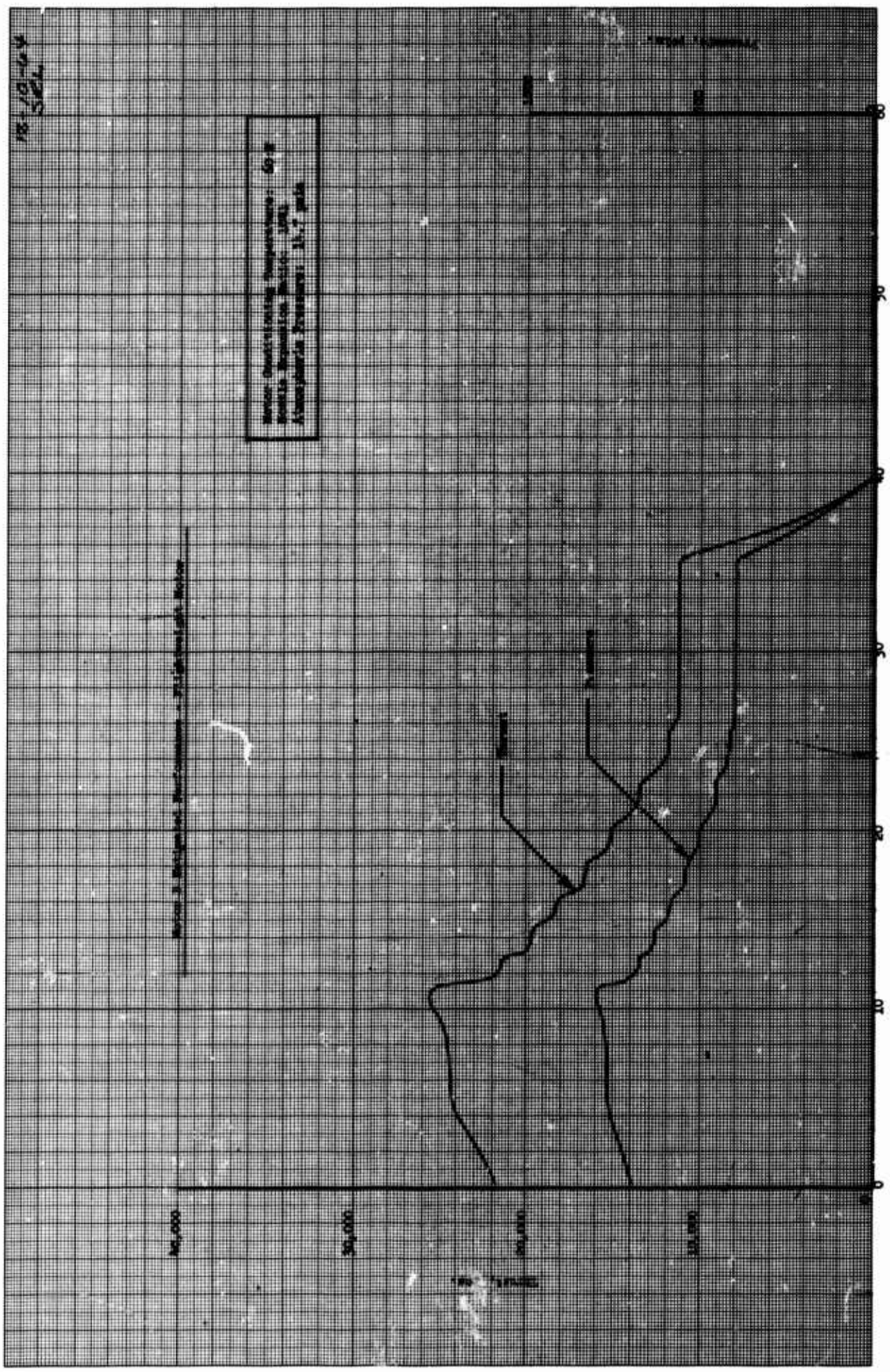


Figure 226. Motor B Estimated Performance - Flightweight Motor, Nozzle Ratio 10:1 (60 F)

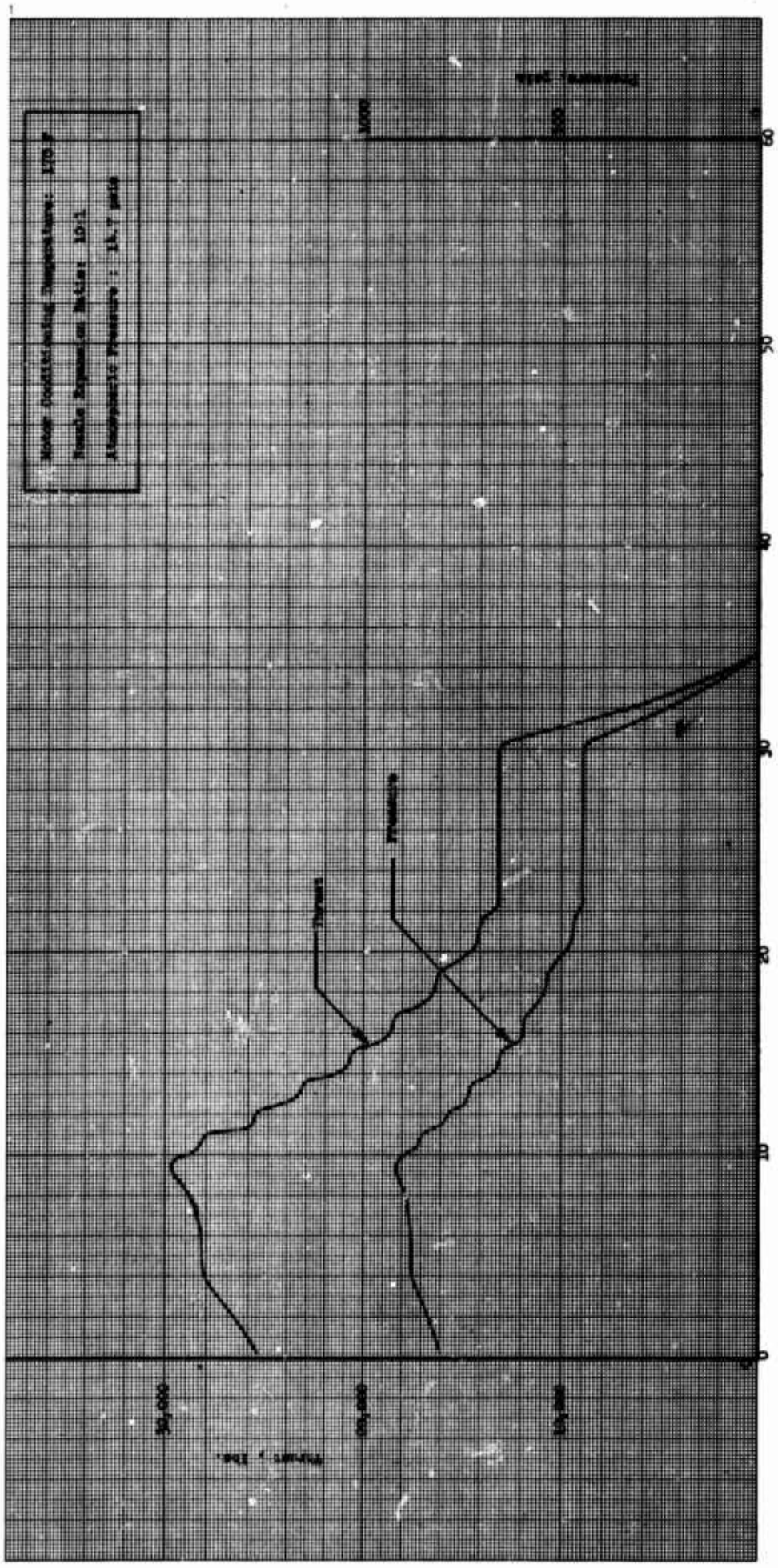


Figure 227. Motor B Estimated Performance - Flightweight Motor, Nozzle Ratio 10:1 (170 F)

TABLE LXXII

MOTOR B DESIGN WEIGHT SUMMARY - FLIGHTWEIGHT MOTOR

Propellant		Weight, lb
a.	Core Grain	1345.00
b.	Reinforced Grain	1757.00
c.	Igniter Combustibles	0.55
	Total Propellant Weight	3102.55
Inert		
a.	Case and Skirts	51.30
b.	Liner	21.44
c.	Nozzle, Gas Generator, and Valve	103.63
d.	Aft Polar Boss, Load Rings, Flange, and Drive Pins	40.85
e.	Forward Polar Boss and Load Rings	28.82
f.	Igniter Assembly	2.63
g.	Forward Floater	3.00
h.	Aft Floater	4.69
	Total Inerts	256.36
Total Motor Weight		3358.91
Mass Fraction		0.924
Mass Fraction Objective		0.937

b. Structural Design

The basic structural design of Motor B was identical to Motor A. Some minor changes were made in the ratio of geodesic isotensoid layers to fill layers to improve the shear strength of the motor near the polar bosses. The preliminary design contained thrust reversal ports, but this requirement was cancelled prior to final Motor B design.

(C) The critical design condition for flightweight Motor A (with the exception of the aft skirt-cylinder) was found to be identical to Motor A. A 1.25 safety factor was applied to the maximum operating pressure at 170 F as well as to the required external loads. This gave the following critical load combination:

	Initial	Burnout
Pressure, psia	1,250	625
Bending moment, in.-lb	375,000	375,000
Shear, lb	3,750	3,750

(C) The GFW case was designed to withstand the loads just prior to burnout and the RFG/GFW composite was designed for the initial loads. Unpressurized buckling of Motor B, just as with Motor A, was not expected to be a problem. However, Motor B had an unpressurized bending moment requirement on the aft skirt and cylinder amounting to 2,469,000 in./lb. Applying a 1.25 safety factor to this value gave a design ultimate bending moment of 3,086,000 in.-lb. This high bending moment was expected to cause some problems at the skirt-cylinder junction based on subscale testing conducted during the motor A effort. These tests had shown conclusively that the quality of the skirt-cylinder junction would have to be improved to meet the required bending moment.

(1) Design Data Acquisition and Design Approach

Because the Motor A program was conducted first, design information on the composite RFG, GFW, aluminum wire, GFE cases, and other components were available when Motor B was being designed and developed. Therefore, the same theoretical approach presented under Motor A was used to design

the RFG and GFW case for Motor B. The proof of these would be verified by actual fabrication and testing. The verification is presented under the Process Development discussion.

(2) Core Grain

Core grain analysis techniques for Motors A and B are the same, with the following exceptions. In addition to the plane strain analysis which is applicable for a major portion of the grain, analysis of plane strain and thermal stress were made for the core grain ends in the Motor B. These analyses were quite preliminary in nature, but the results indicated this portion of the grain to be critical in the over-all determination of grain reliability. The sections analyzed are shown in Figs. 228 and 229.

(a) Method of Analysis

Analysis of the core grain ends in Motor B is even more restricted than that in Motor A. This analysis requires constant material properties throughout the temperature range of interest and again forces neglect of the glass case. The grain was represented as a cylinder with flat ends and the doubler was represented as a square-bottomed notch.

(b) Calculations

The calculated strains are presented in graphical form (along with the allowable strains) as a function of temperature throughout the range of interest for Motor B.

Figure 230 shows the calculated and allowable bore strains for Motor B from thermal cycling; Fig. 231 gives the same information for ignition pressurization. Figure 232 illustrates the margin-of-safety for each condition as a function of temperature, and Fig. 233 shows the margin-of-safety with the combined loadings of temperature cycling and ignition pressurization. Figure 234 shows the configuration analyzed for the forward grain end of Motor B with the calculated longitudinal stresses superimposed, and Fig. 235 presents similar information for the aft end.

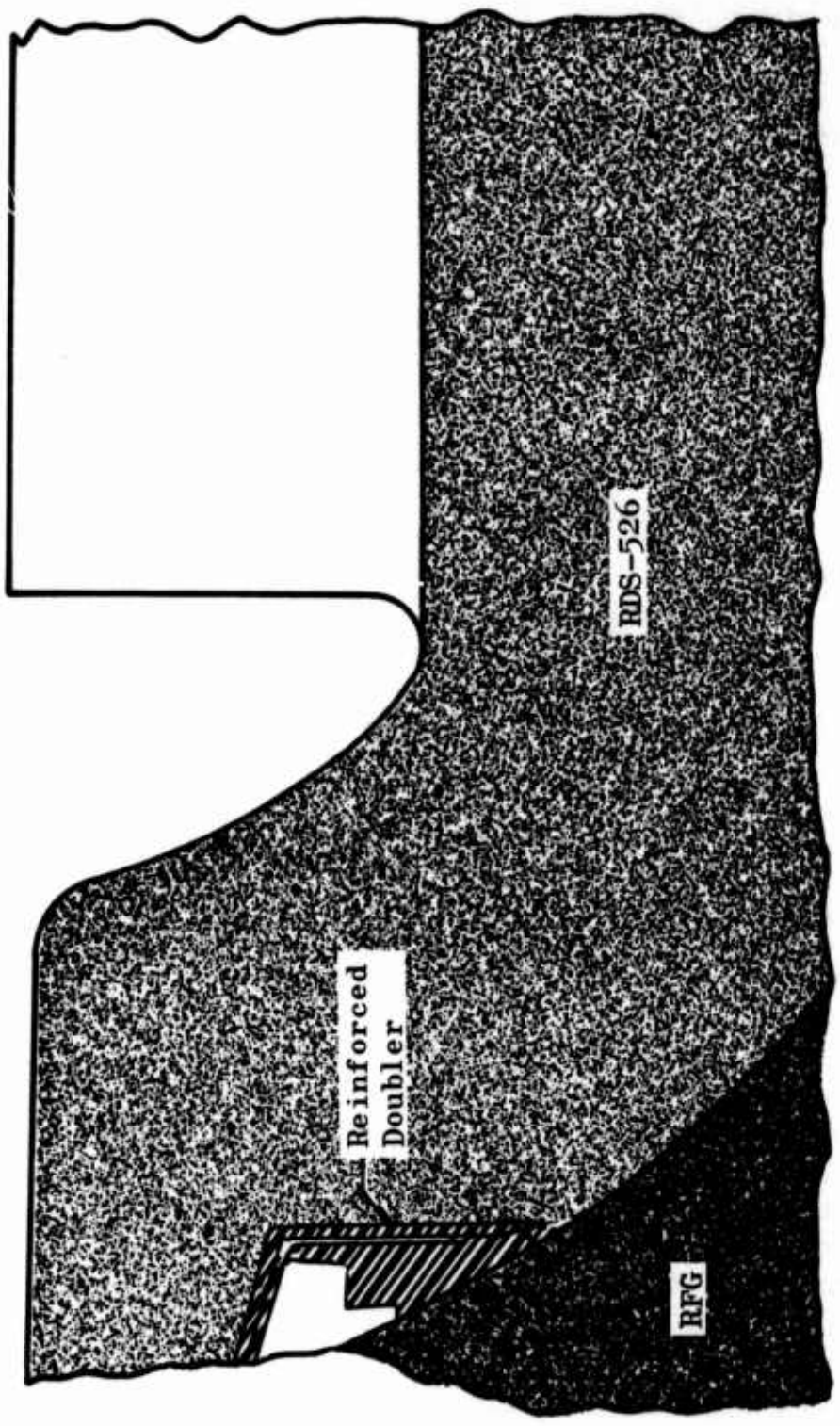


Figure 228. Forward End, Core Grain--Motor B

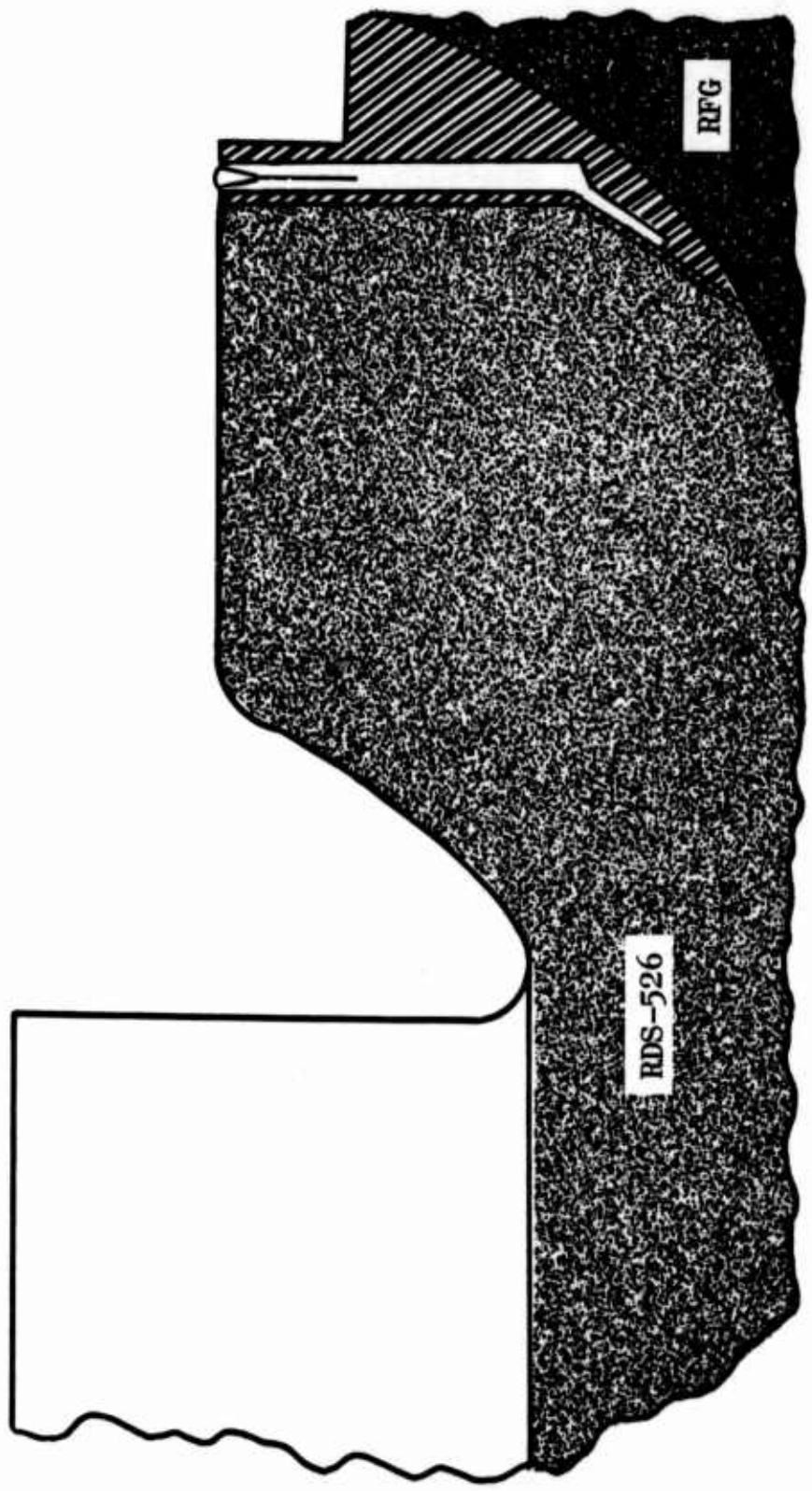


Figure 229. Aft End, Core Grain--Motor B

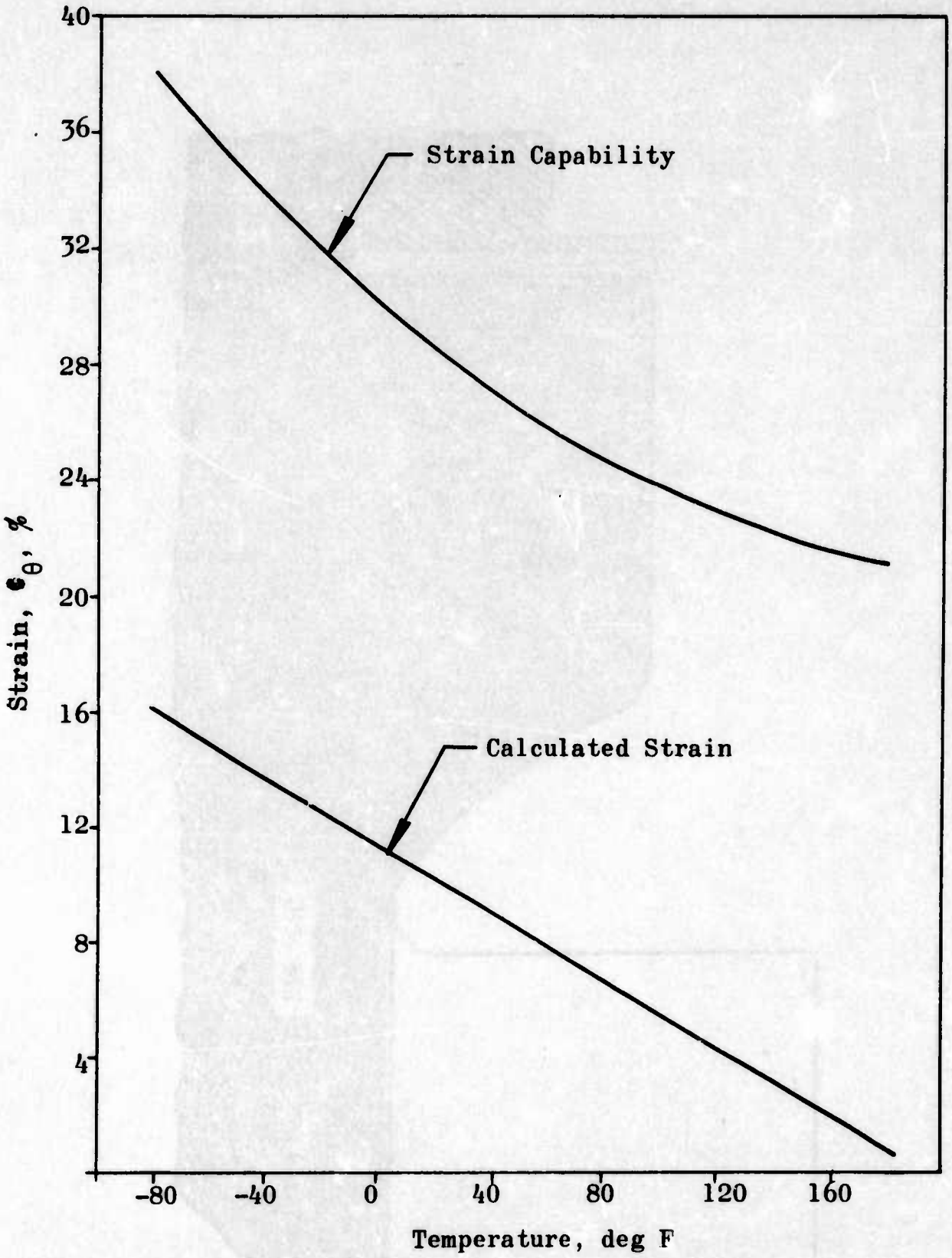


Figure 230. Strain Capability and Thermally Induced Strain vs Temperature

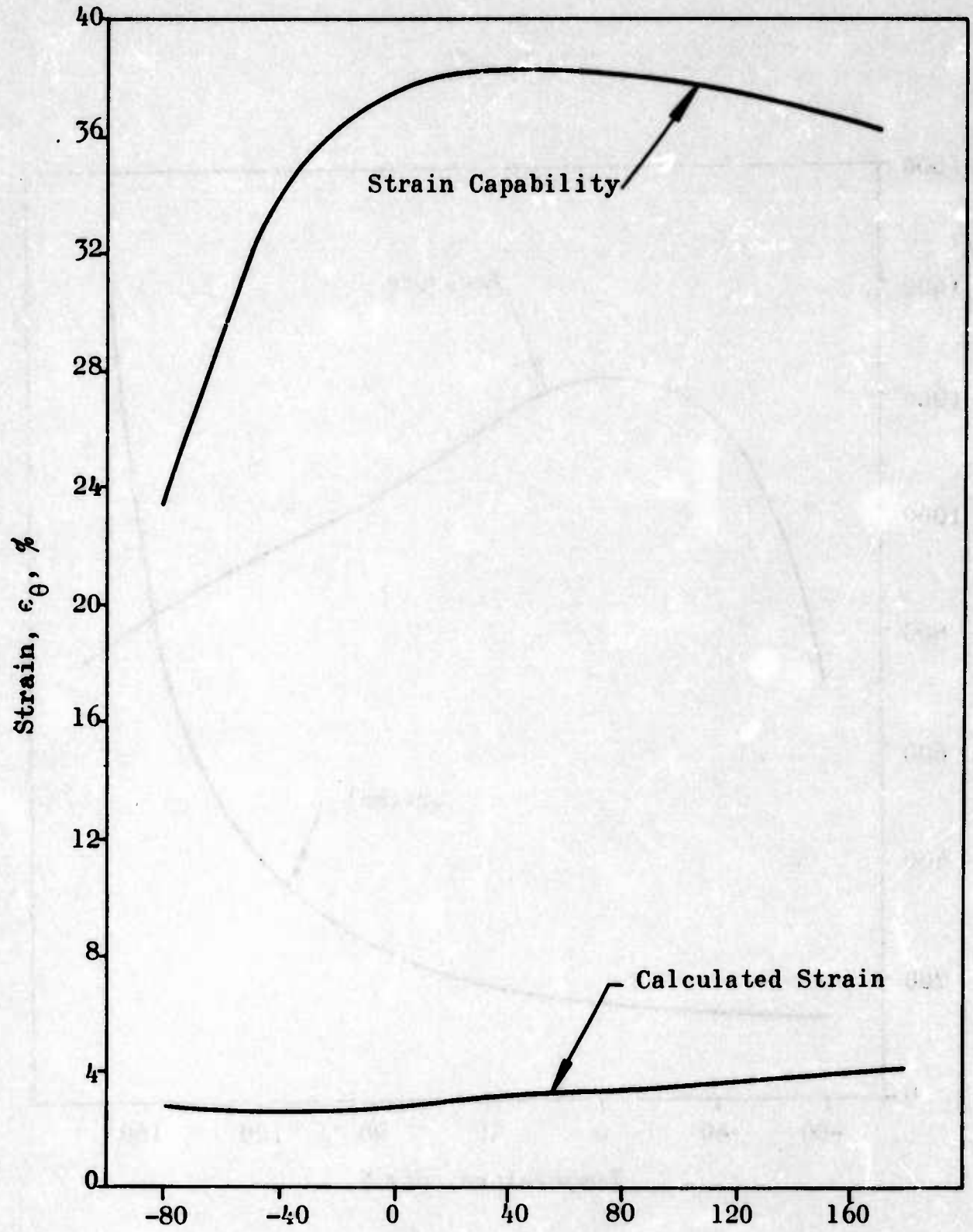


Figure 231. Strain Capability and Pressure - Induced Strain vs Temperature

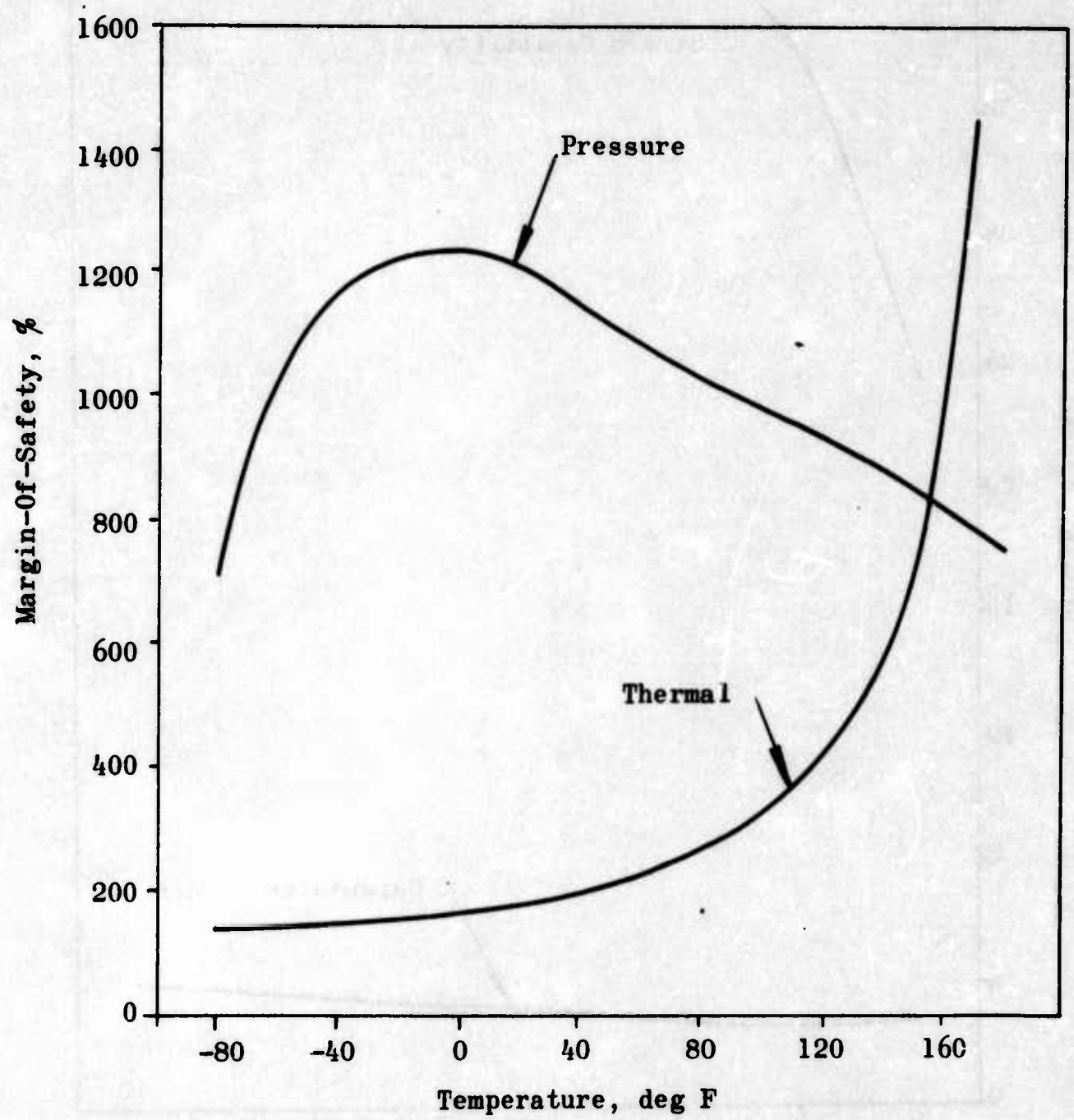


Figure 232. Thermal and Pressure Margin of Safety vs Temperature

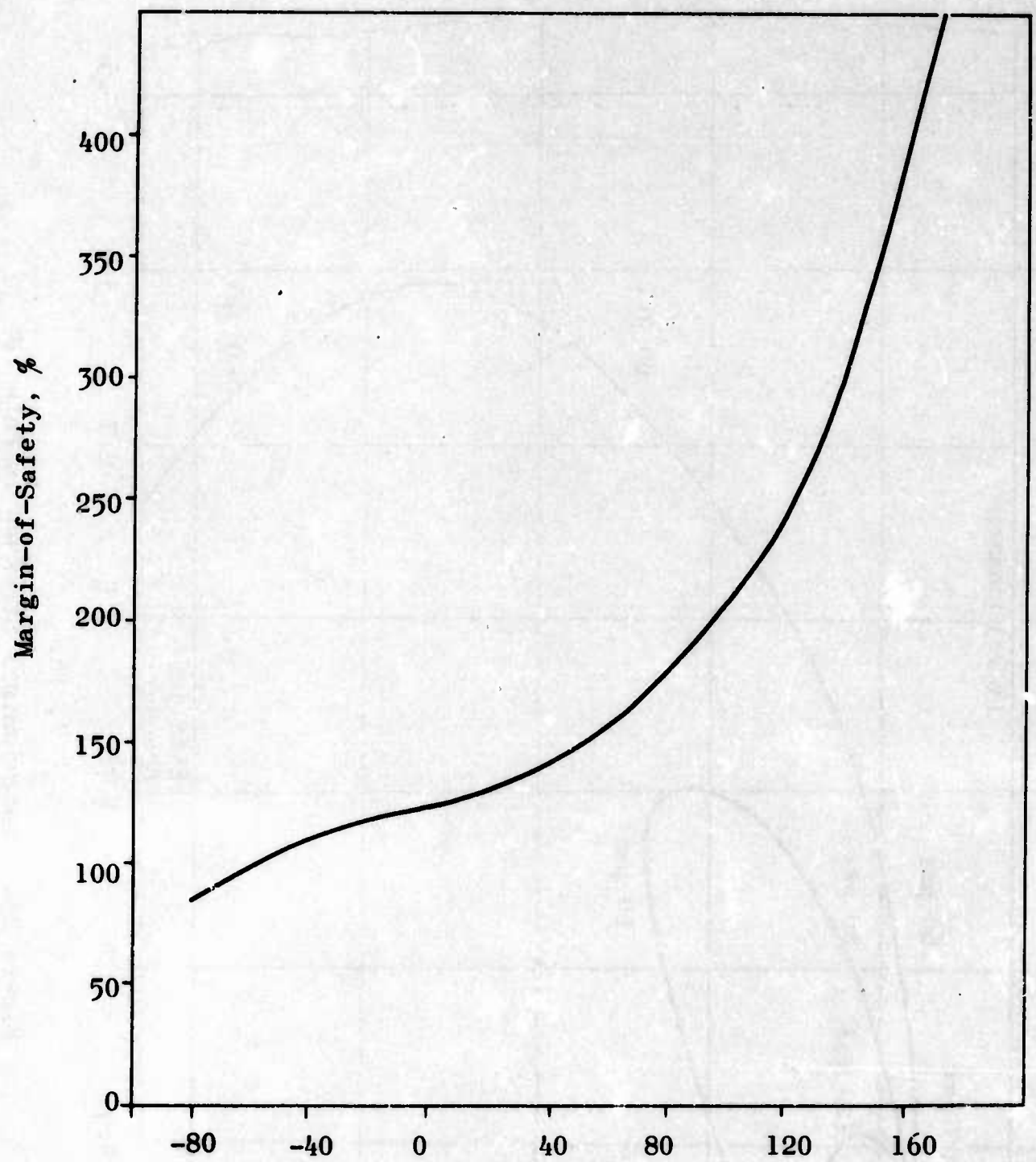


Figure 233. Margin of Safety for Combined Loads vs Temperature

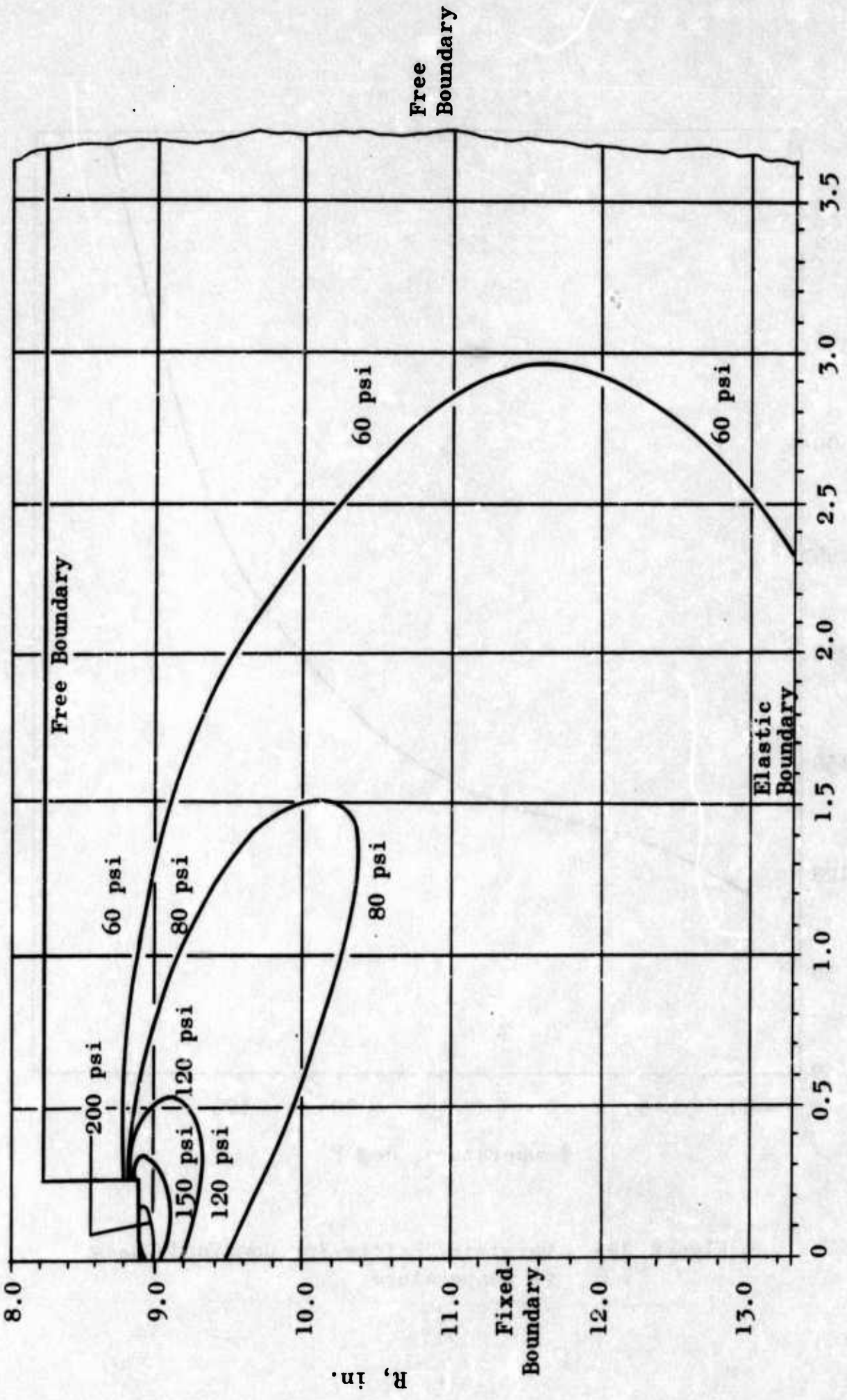


Figure 234. Longitudinal Stresses in Forward End, Model for -75 F

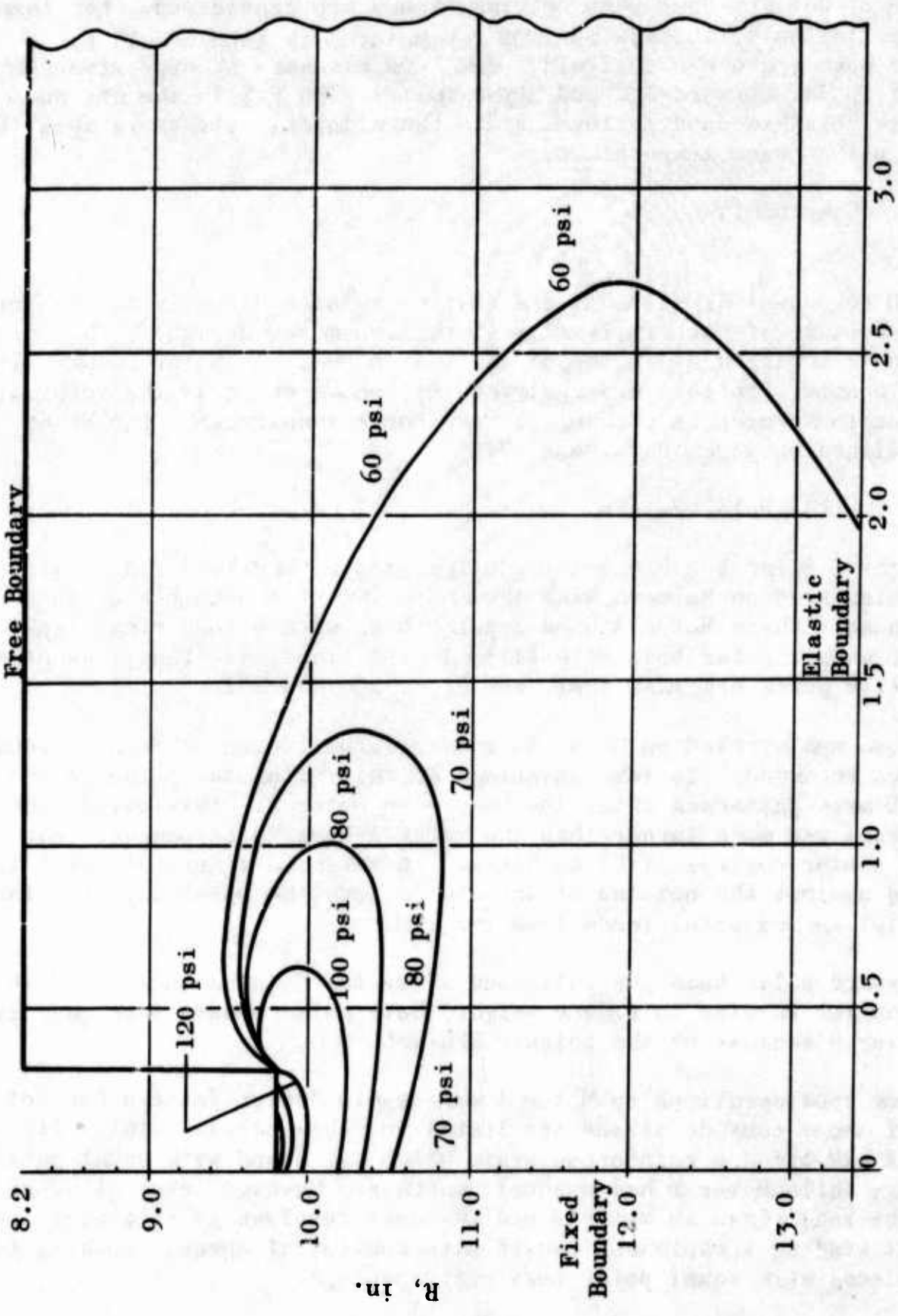


Figure 235. Longitudinal Stresses In Aft End, Model for -75 F

(C) Examination of these data reveals a minimum margin-of-safety (MOS) for Motor B of 90% at -75 F when combined loads are considered. For temperature cycling only, the minimum MOS for Motor B is 140% at -75 F. For the core grain end analysis, peak bond stresses of approximately 250 psi in the forward end and approximately 150 psi in the aft end indicate possible bond failure, since the allowable stress is about 100 to 180 psi at room temperature.

c. Components

Motor B component development and testing related directly to the Motor A effort because of the similiarity of the two motor designs. This discussion is arranged as is the discussion on Motor A (polar bosses, load rings, nozzle, igniter, and restrictors). However, only the information peculiar to Motor B is presented. Air Force requirements for Motor B are outlined on page 10 through 17.

(1) Polar Bosses

(C) The Motor B polar bosses, grain configurations, and load rings parallel the design used on Motor A with the exception of the number of load rings used. Where Motor A used a polar boss with 9 load ring steps, Motor B uses a polar boss with 11 load ring steps; the functions of the respective parts are identical, see Figs. 236 and 237.

When work was started on Motor B, a successful firing of Motor A-1002 had been recorded. To take advantage of this data, the polar bosses for Motor B were patterned after the bosses in Motor A. Physically, the aft polar boss was made larger than the Motor A boss to accommodate the thrust vector control (TVC) mechanism. A threaded flange was also installed against the outside of the RFG to lock the polar boss in place, to resist inward axial loads from the TVC.

The forward polar boss was patterned after the Motor A boss, but was made smaller in size to reduce weight; both polar bosses were made longer for Motor B because of the thicker RFG web.

The same considerations on Motor A were again design factors for Motor B. Some of these considerations are listed in Table LXXIII. Initially, Motor A exhibited a reinforced grain which was wound with equal pola· openings while Motor B had unequal openings. However, wire slippage over the load rings in Motor B and the cost involved in obtaining the correct winding techniques, caused this concept of unequal opening to be replaced with equal polar boss port openings.

CONFIDENTIAL

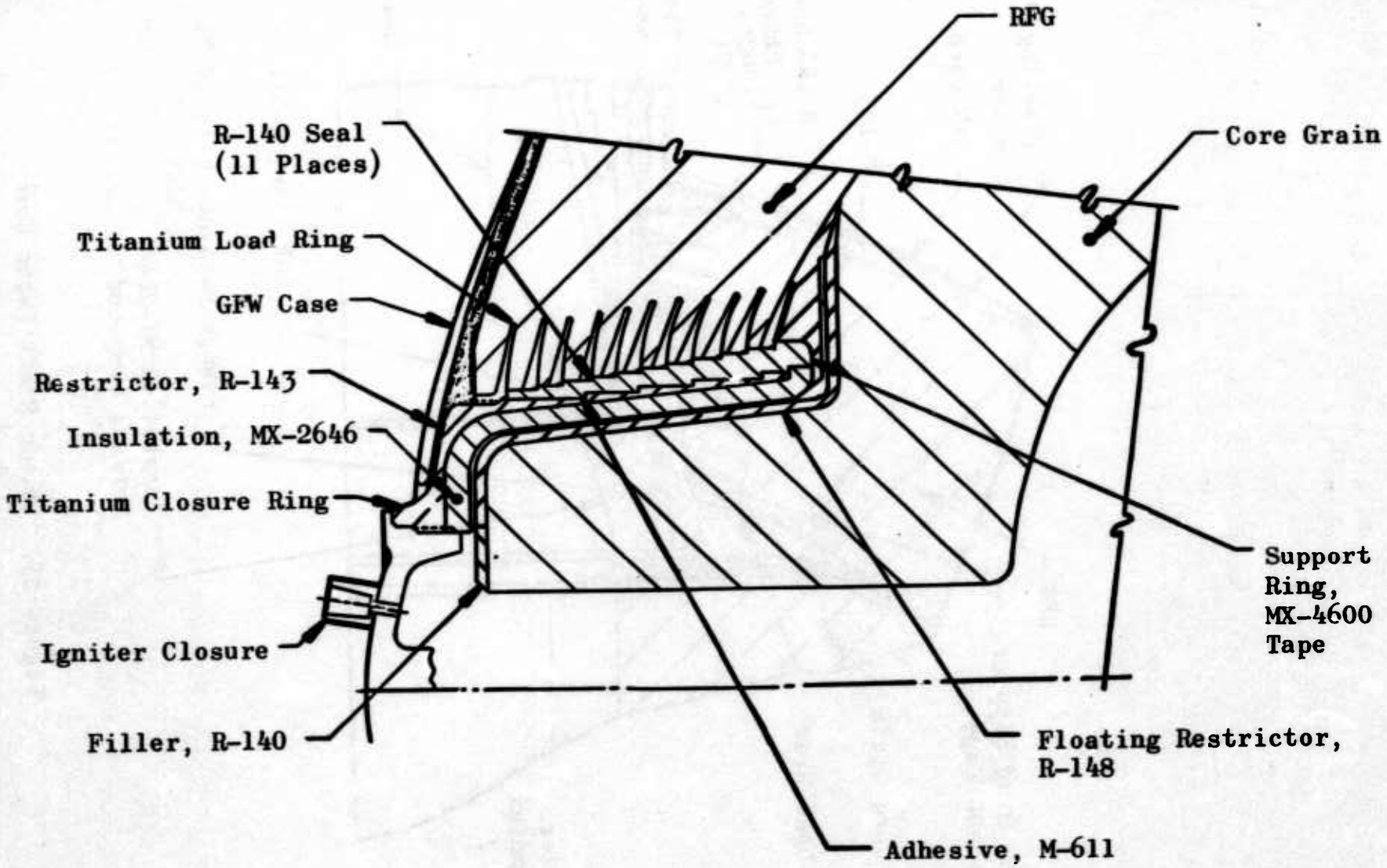


Figure 236. Motor B Forward Polar Boss

CONFIDENTIAL

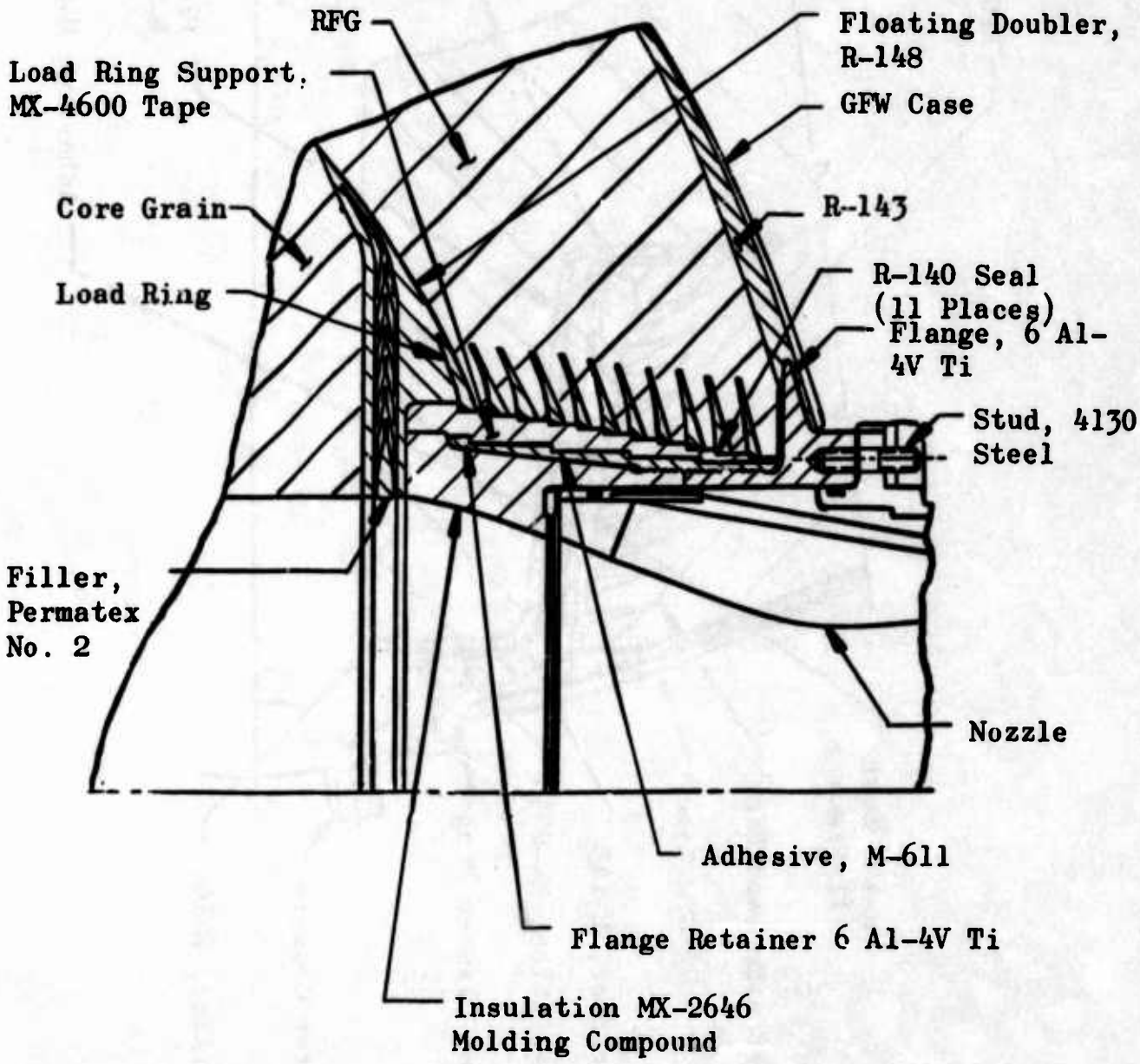


Figure 237. Motor B Aft Polar Boss

TABLE LXXIII

MOTOR B POLAR BOSS DESIGN
AND PROCESS CONSIDERATIONS

Process ——→	Effect On
RFG Layer Build Up	Step Length
RFG Layer Contours	Load Ring Cross Section
Equal vs Unequal Polar Boss Opening	Weight, Strength, Size
Temperature Cycling	Seals, Strength, Bonds
Winding Capability	Size, Assembly Sequence
Tooling Hardware Installation and Removal	Size, Strength, Assembly Sequence

In choosing the materials to use in the design, there was again a heavy reliance on the results of Motor A tests and on the component tests. A list of the major components of the polar bosses is given below with the reason for choosing the material:

1. Load Ring Support. MX-4600 glass tape reinforced phenolic-material, because of high shear and tensile strength and because of its good insulating properties
2. Flange Retainer. 6AL 4V titanium-lightweight, with high strength and permissible costs
3. Polar Flange. 6AL titanium-lightweight, with high strength and permissible costs
4. Closure Ring. 6AL 4V titanium-lightweight, with high strength
5. Insulation. MX-2646 silica phenolic, because of good insulation properties and because of its excellent erosion characteristics

Included in the selection of these materials were the loading requirements and motor dimensional limitations. These considerations are summarized in Tables LXXIV and LXXV.

TABLE LXXIV

MOTOR B POLAR BOSS DESIGN PARAMETERS

(C)

Load Considerations	
Case Pressure	1250 psi
Maximum Operating Pressure	1000 psi
TVC Inertia Loads	15,500 lb-in.
Dimension Considerations	
Min. Casting Mandrel Dimension	3.60 in. dia
Min. Nozzle OD (Inside Motor)	9.75 in.
RFG Webb Thickness (Nom)	4.50 in.
Core Grain Thickness (Nom)	5.10 in.
Wire Warp Width	0.90 in.
Load Distribution (Load Rings*)	
Case Pressure Design Ultimate	1250 psi
Effective Diameter	12.55 in.
Maximum Load (Fwd Polar Boss)	157,000 lb

*Ring No.	Load Assigned, %	Load at Failure-Test, lb	Assigned Load, lb	Margin of Safety
1	30	60,000	48,000	0.25
2	10	No Test	15,700	--
3	13	25,000	20,000	0.25
4	6	No Test	9,400	--
5	4	8,000	6,300	0.27
6	10	No Test	15,700	--
7	5	10,000	7,850	0.27
8	4	No Test	6,300	--
9	10	17,000	15,700	0.13
10	4	No Test	6,300	--
11	4	No Test	6,300	--
Totals	100		157,550	

CONFIDENTIAL

TABLE LXXV

MOTOR B POLAR BOSS STRUCTURE MARGINS

Component	Critical Load Condition	Design Ultimate Load	Ultimate Load Capability	Ultimate Margin of Safety
Forward Boss				
Closure	Combined Stress	P_c = 1,250 psi	>1,480 psi	>+0.16
Ring Support	Interlaminar Shear	Ring Load = 48,000 lb	60,000 lb	+0.25
Dome Insulation	Hoop Strain	P_c = 1,250 psi	>1,480 psi	>+0.16
Load Rings	Torsion Bending	6,300 to 48,000 lb	8,000 to 60,000 lb	+0.25
Aft Boss				
Flange	Bending	P_c = 1,250 psi BM = 15,500 in.-lb	P_c = 1,650 psi BM = 20,100 in.-lb	+0.30
Flange Retainer	Hoop Tension	P_c = 1,250 psi	P_c = 2,360 psi	+0.87
Ring Support	Interlaminar Shear	32,000 lb	96,000 lb	>+2.00
Insulation	Hoop Strain	P_c = 1,250 psi	>1,580 psi	>+0.24
Load Rings	Torsion Bending	4,200 to 32,000 lb	8,000 to 60,000 lb	+0.87

CONFIDENTIAL

To demonstrate the adequacy of the polar boss design, one forward and one aft polar boss was pressure tested to failure, similiar to the Motor A component test. The bosses were complete, except the insulation liner was left out and only the first three load ring steps were machined.

(C) Both bosses exceeded the design ultimate pressure of 1250 psi by a comfortable margin. The forward polar boss failed at 1481 psig and the aft boss at 1580 psig. Both bosses failed in interlaminar shear of the MX-4600 plastic load ring support along the inside diameter of load ring No. 3. Shear values of 2700 psi were obtained, which satisfactorily agree with the 3,100 psi maximum indicated from lab tests of the MX-4600 material.

As a result of Motor A-1003 test firing, the Motor B aft polar boss needed modifications consisting of increasing the longitudinal length by 1.3 inches to protect the titanium component of the boss from the severe erosive environment. Consideration was also given to adding material on the inside diameter, keeping the entrance OD the same, and decreasing the ID at the entrance of the nozzle to 7.45 inches. This modification, however, also required modification of the nozzle and was not effected immediately.

The results of the thermal analysis on the aft polar boss is presented graphically in Figs. 238 through 253. The material loss and char depth at the end of firing for the three firing temperatures are presented in Figs. 238 through 240 for the 8.25 inches nozzle entrance diameter.

The temperature distribution for the 8.25 inches nozzle entrance diameter configuration at the end of the firing for the three firing temperatures are presented graphically in Figs. 241 through 243.

Presented in Figs. 244 through 248 are the material loss vs time for the three firing temperatures and the 7.45 inches and 8.25 inches diameter nozzle entrance at analysis stations 11 through 15. The reduction in diameter would result in a maximum additional loss of 0.05 inch at Station 11 for the 170 F firing and would provide an additional 0.35 inch of material protecting the entrance of the nozzle.

The material loss, or char depth vs time, for the remaining analysis stations are presented in Figs. 249 through 253.

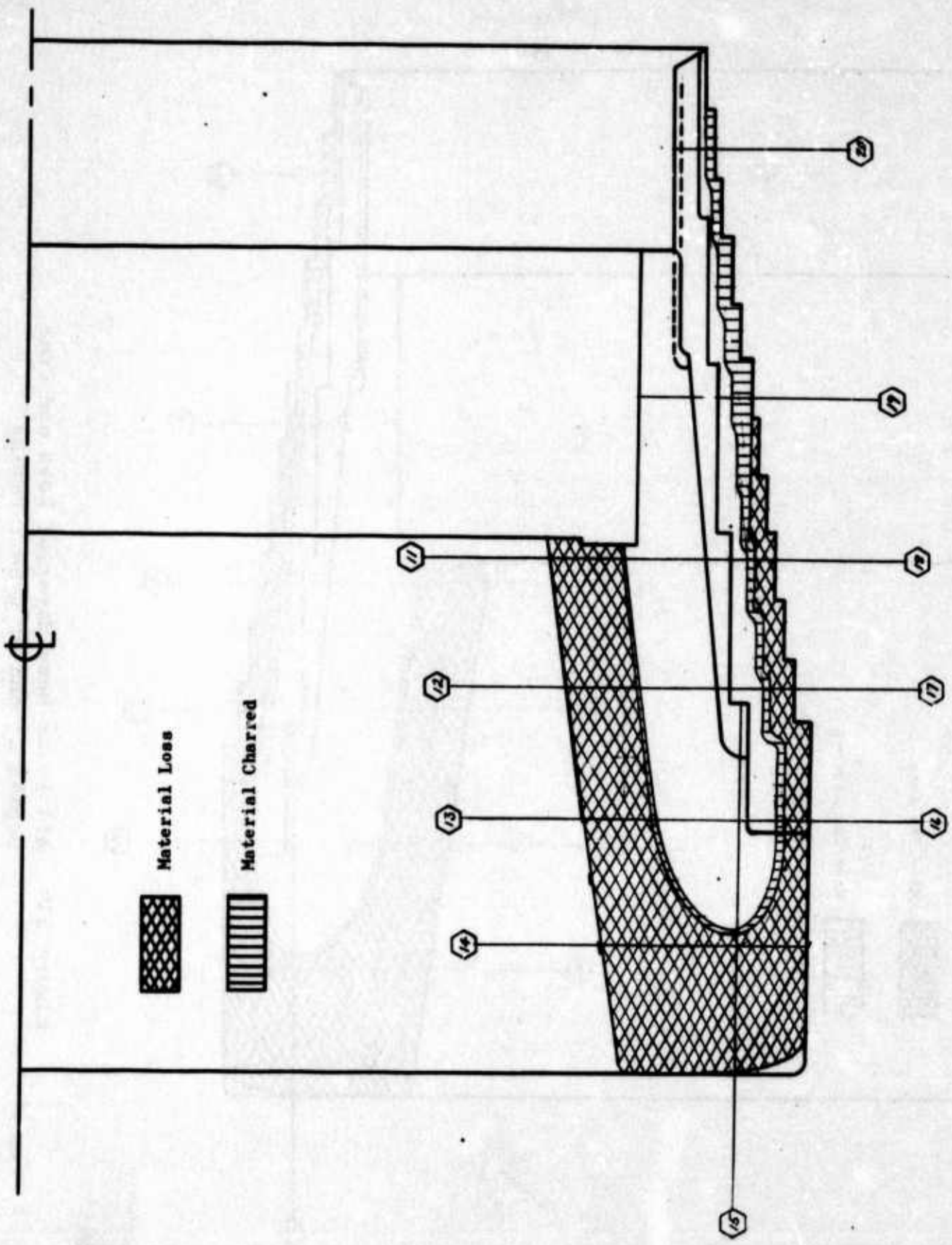


Figure 238. Aft Polar Boss Material Loss and Char Depths at End of a -75 F Firing

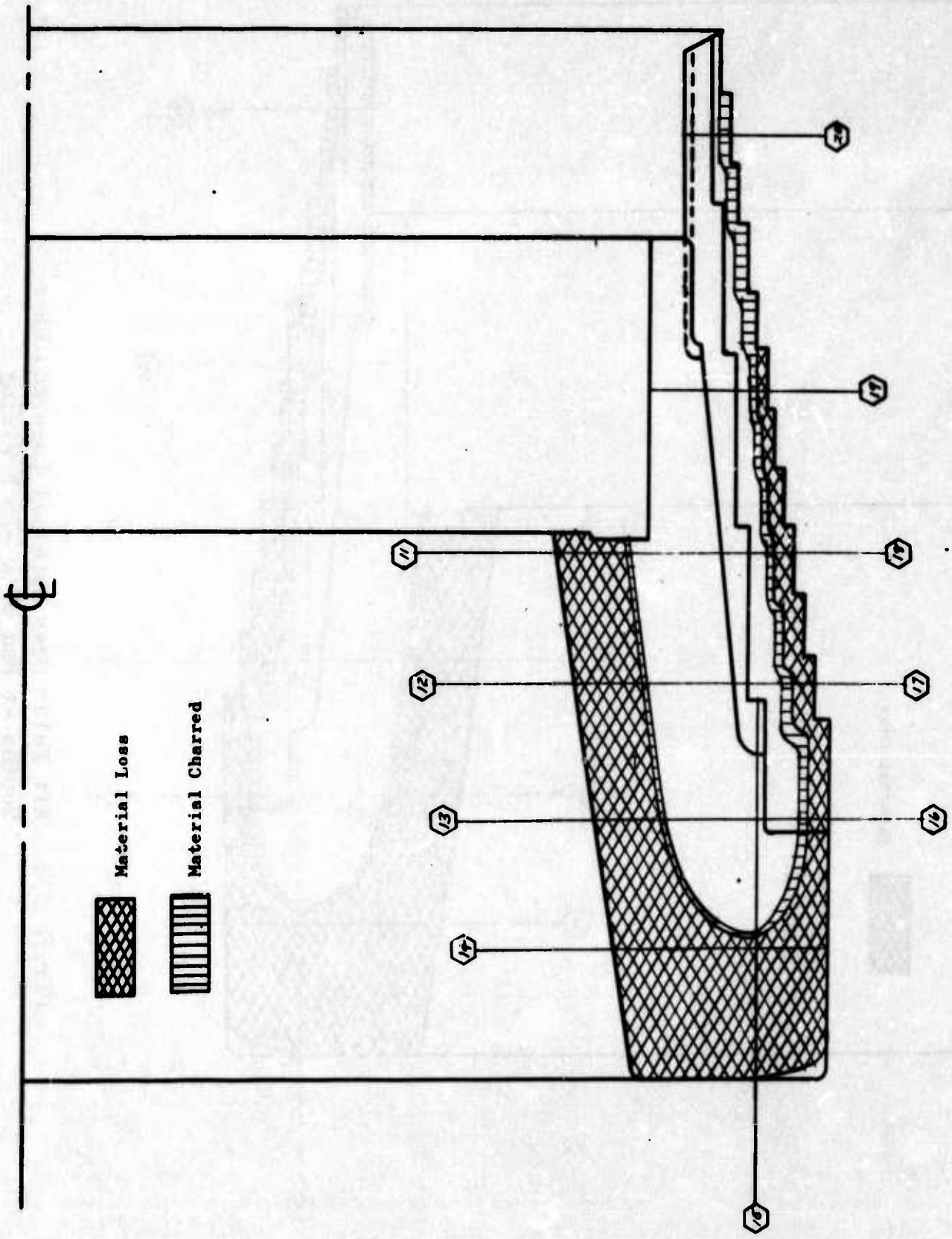


Figure 239. Aft Polar Boss Material Loss and Char Depths at End of a 60 F Firing

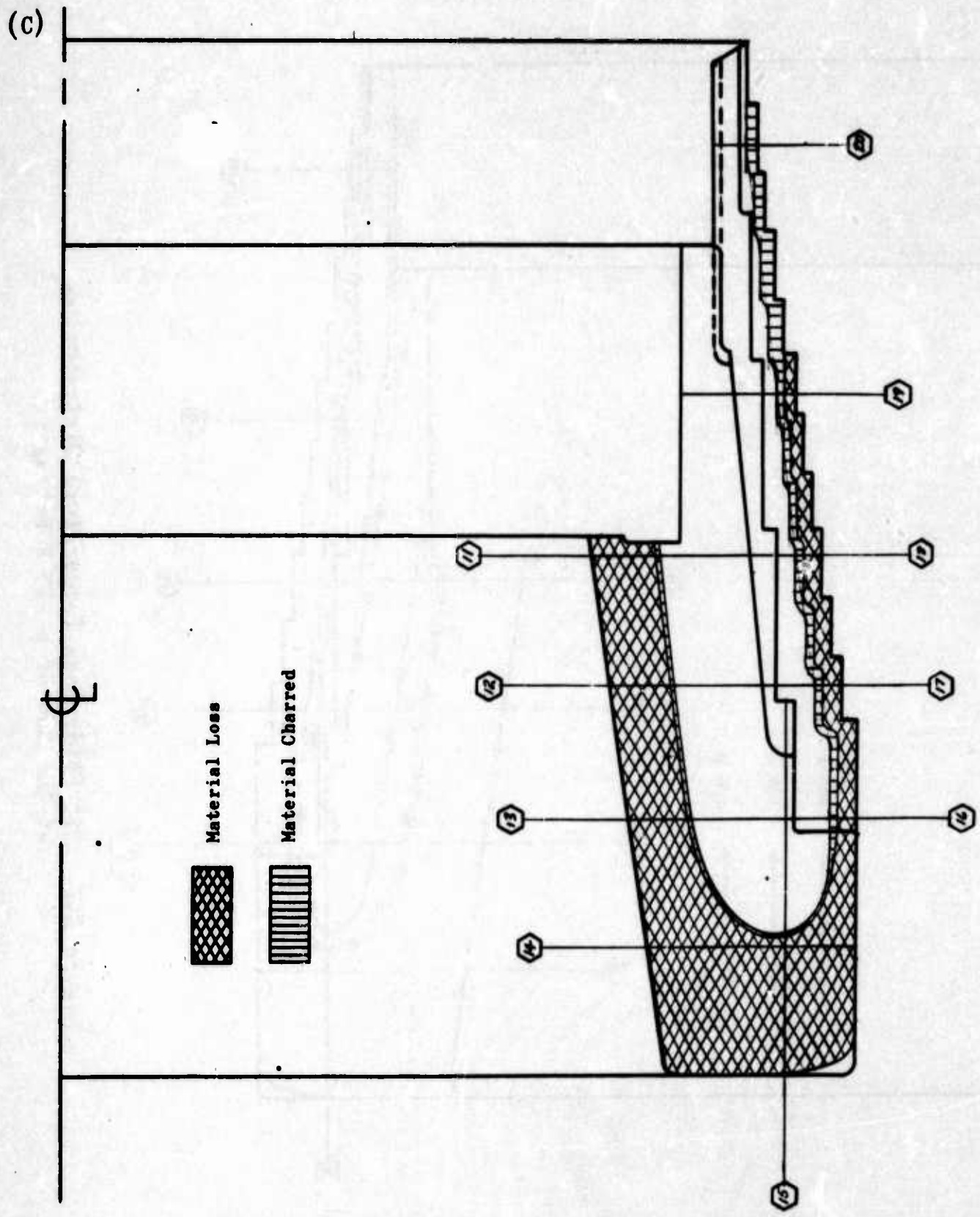


Figure 240. Aft Polar Boss Material Loss and Char Depths at End of a 170 F Firing

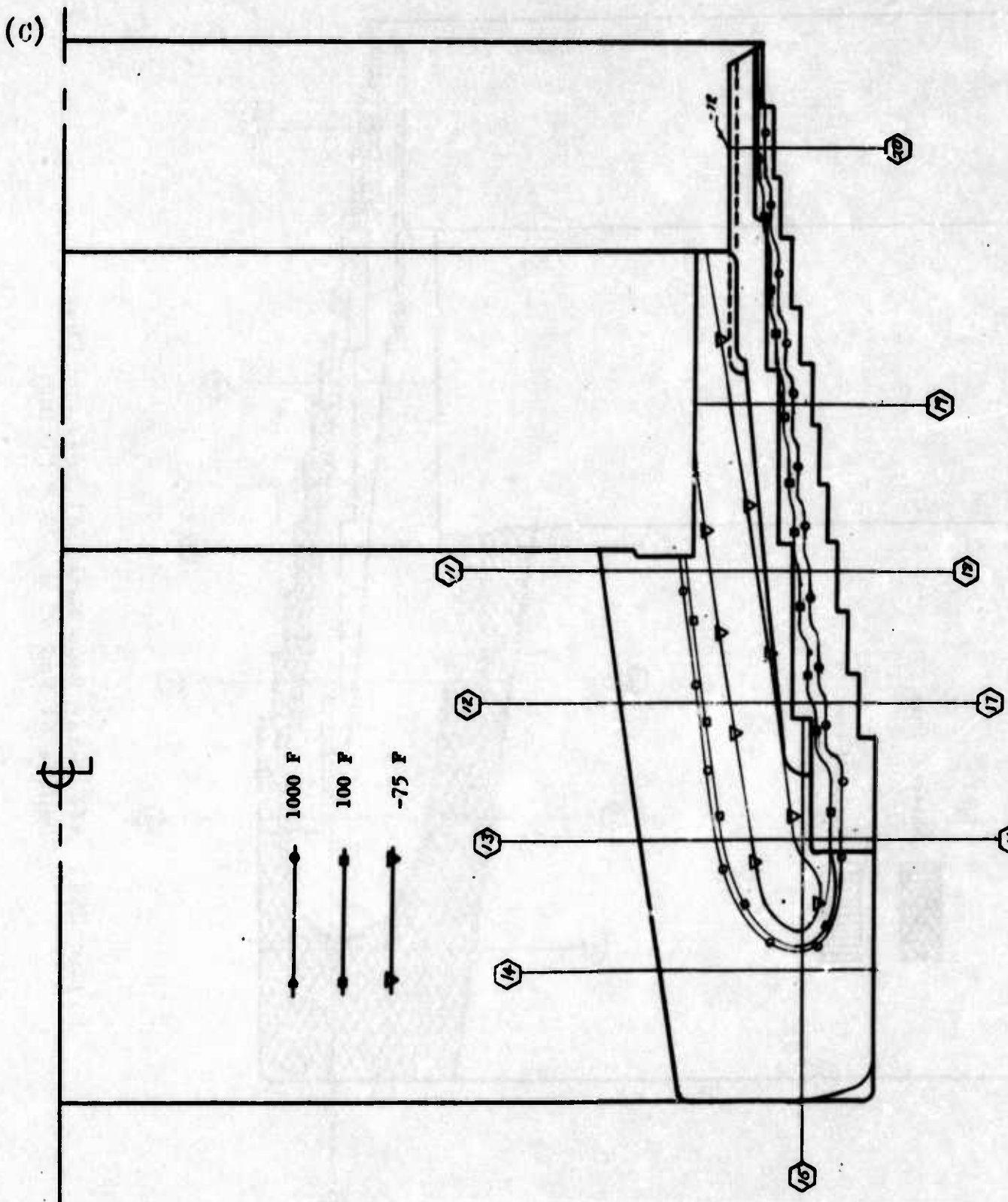


Figure 241. Aft Polar Boss Temperature Distribution at the End of a -75 F Firing

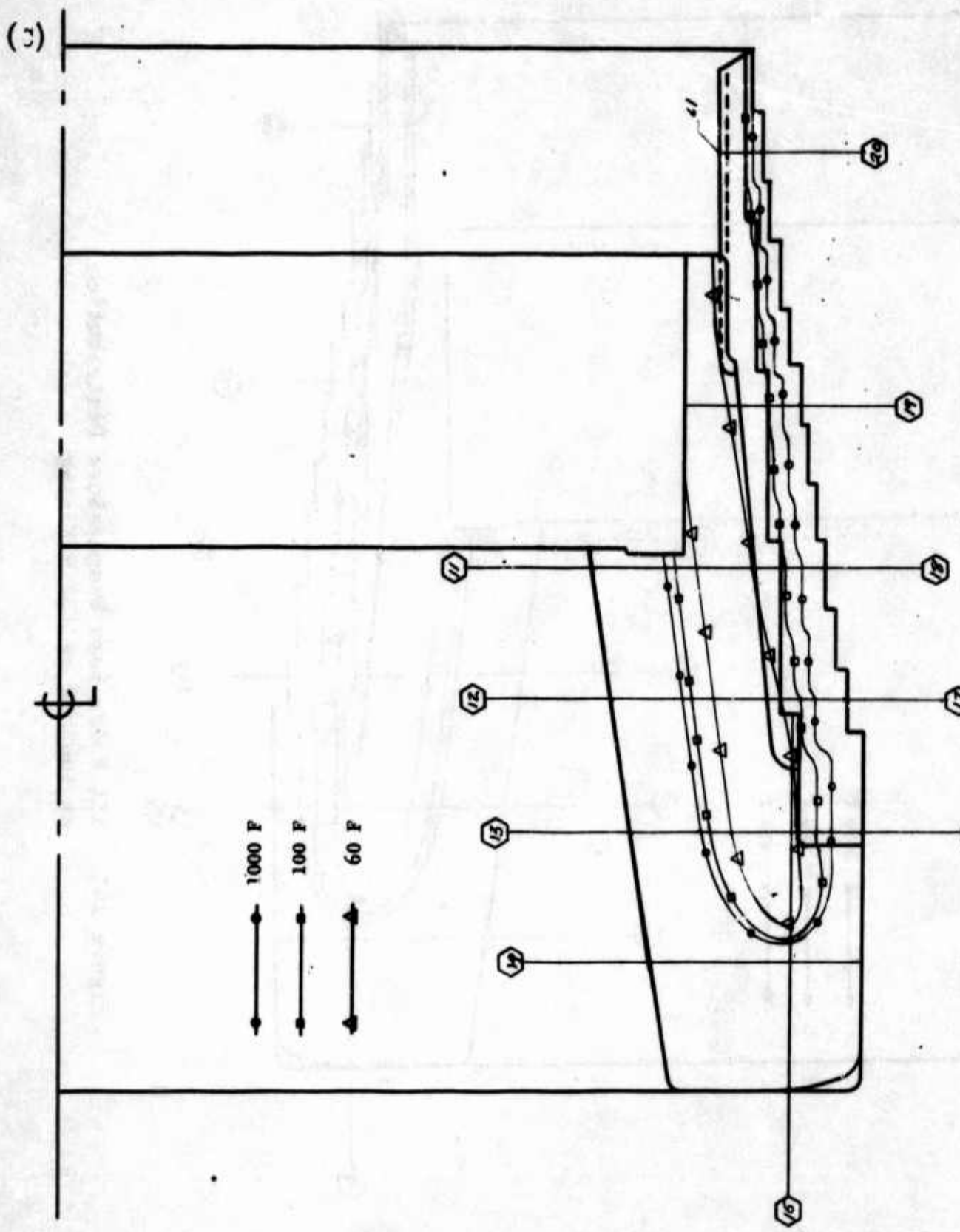


Figure 242. Aft Polar Boss Temperature Distribution at the End of a 60 F Firing

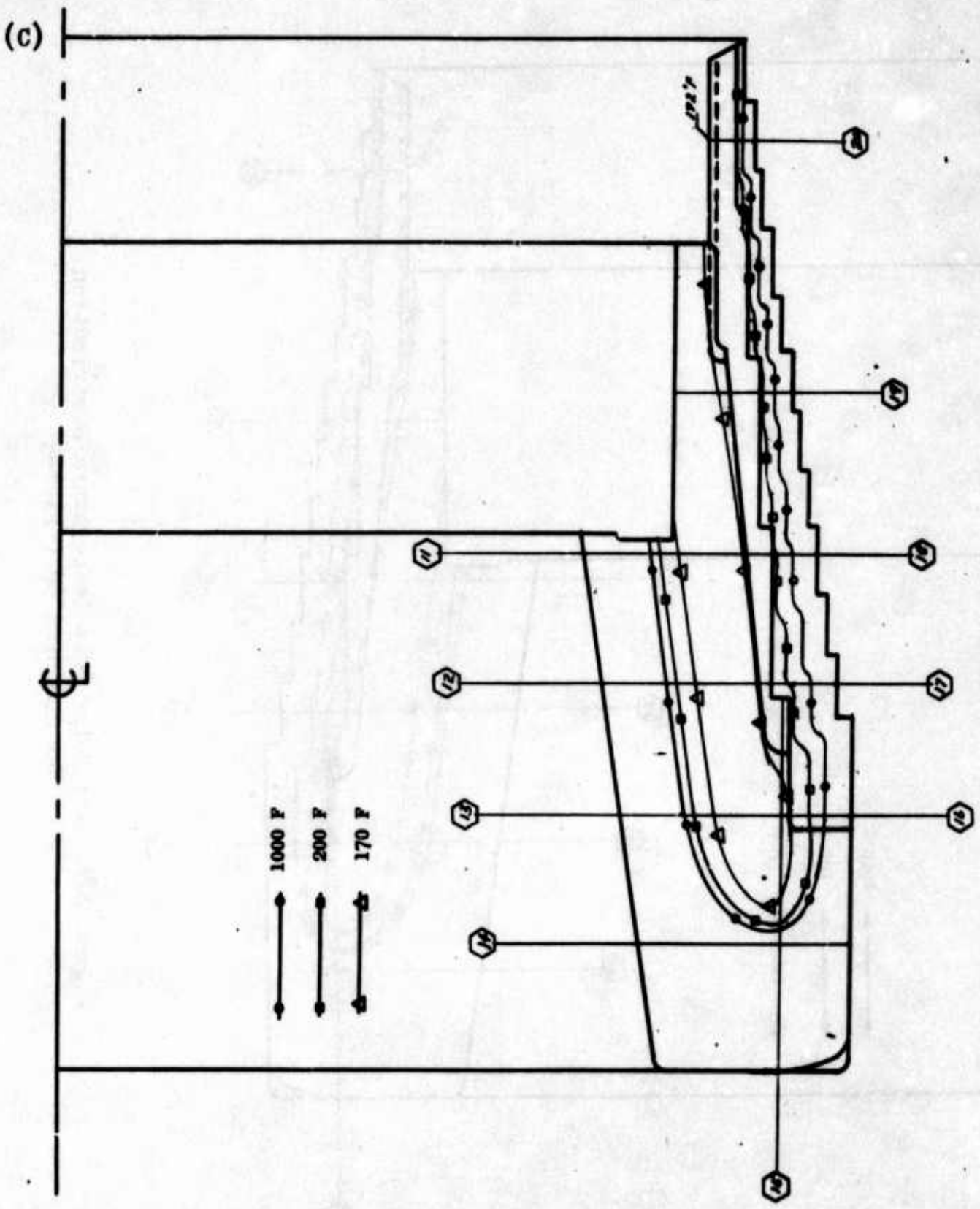


Figure 243. Aft Polar Boss Temperature Distribution at the End of 170 F Firing

(C)

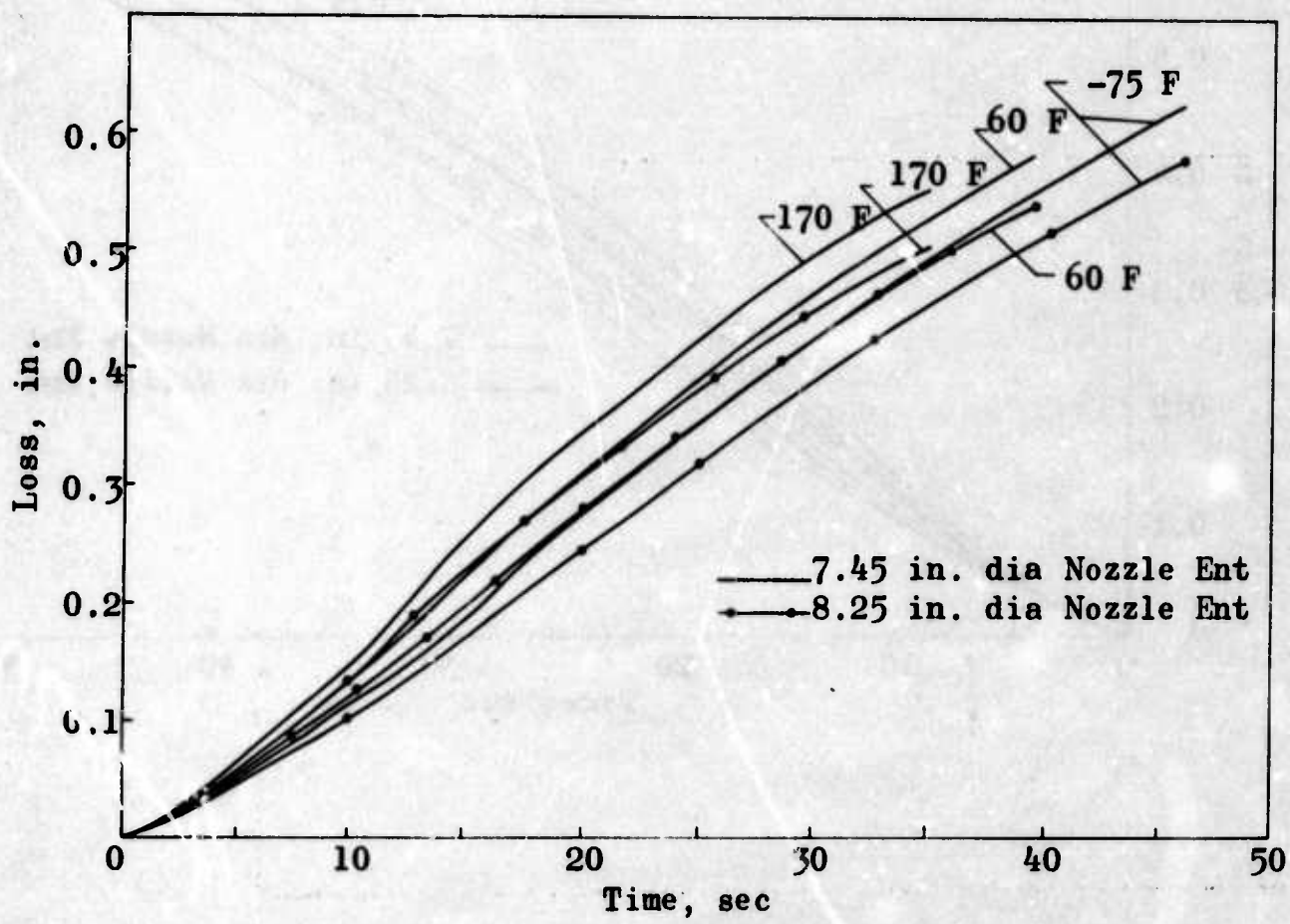


Figure 244. Material Loss vs Time and Various Firing Temperatures and the 7.45 Inch and 8.25 Inch Nozzle Entrance Diameter at Nozzle Station 11

(C)

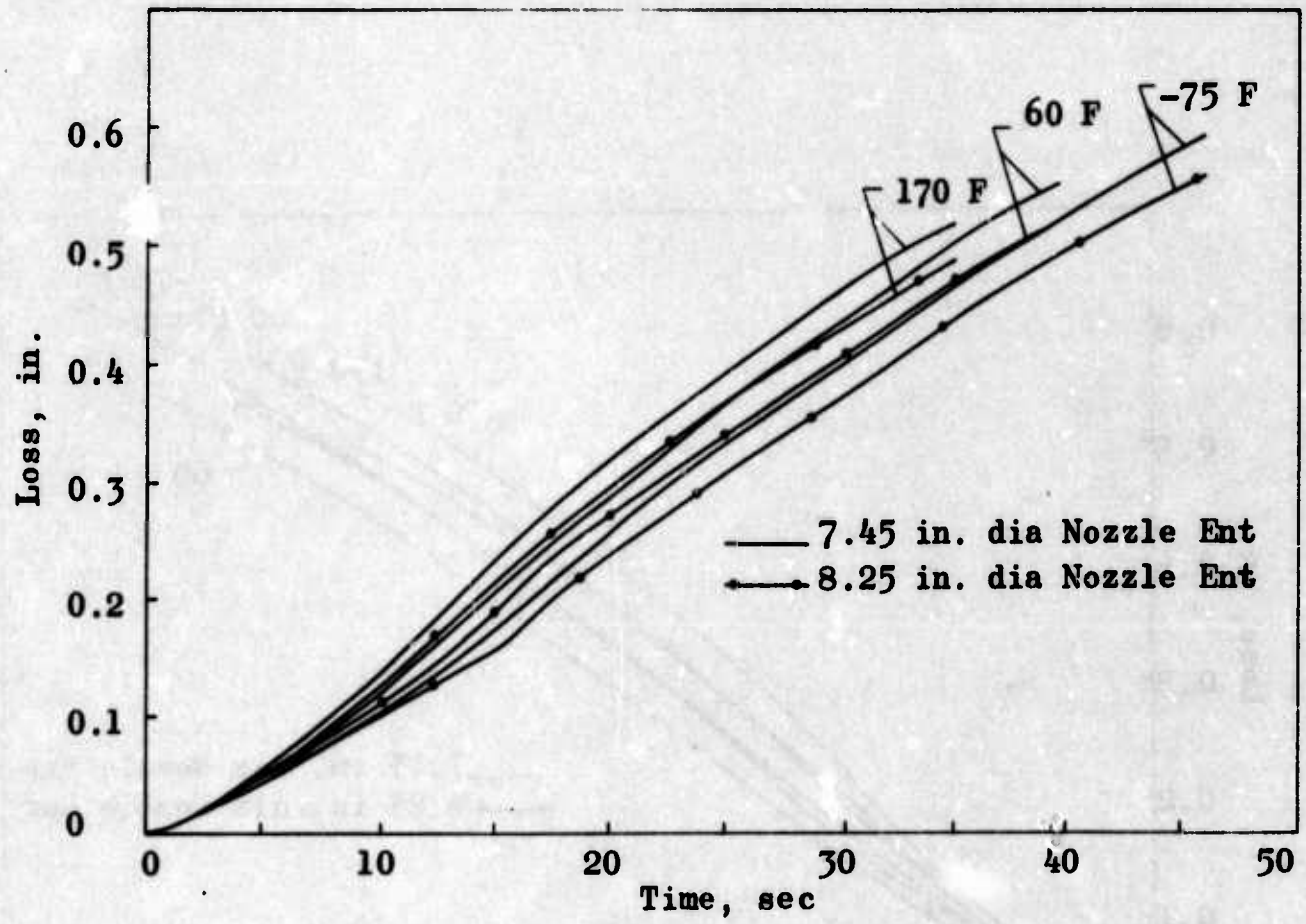


Figure 245. Material Loss vs Time for Various Firing Temperatures for the 7.45 Inch and 8.25 Inch Nozzle Entrance Diameter at Nozzle Station 12

(C)

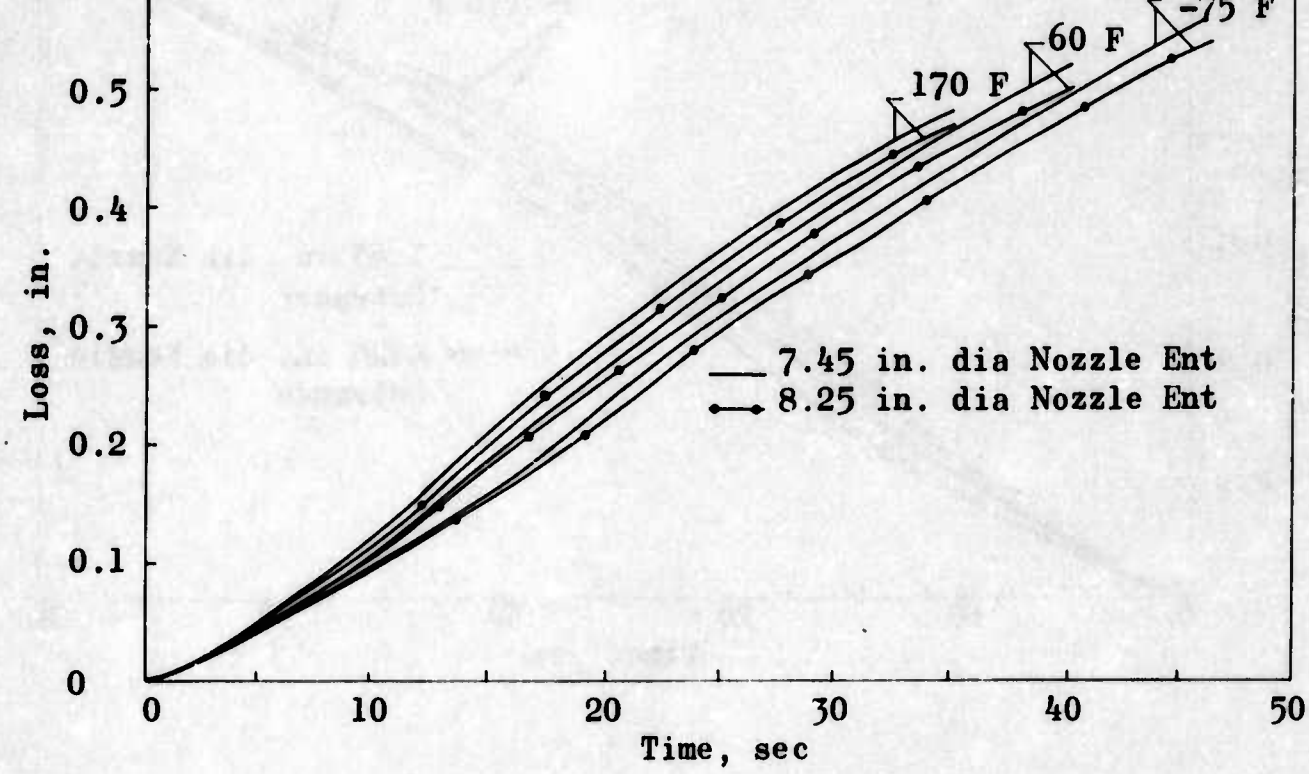


Figure 246. Material Loss vs Time for Various Firing Temperatures for the 7.45 Inch and 8.25 Inch Nozzle Entrance Diameter at Nozzle Station 13

(c)

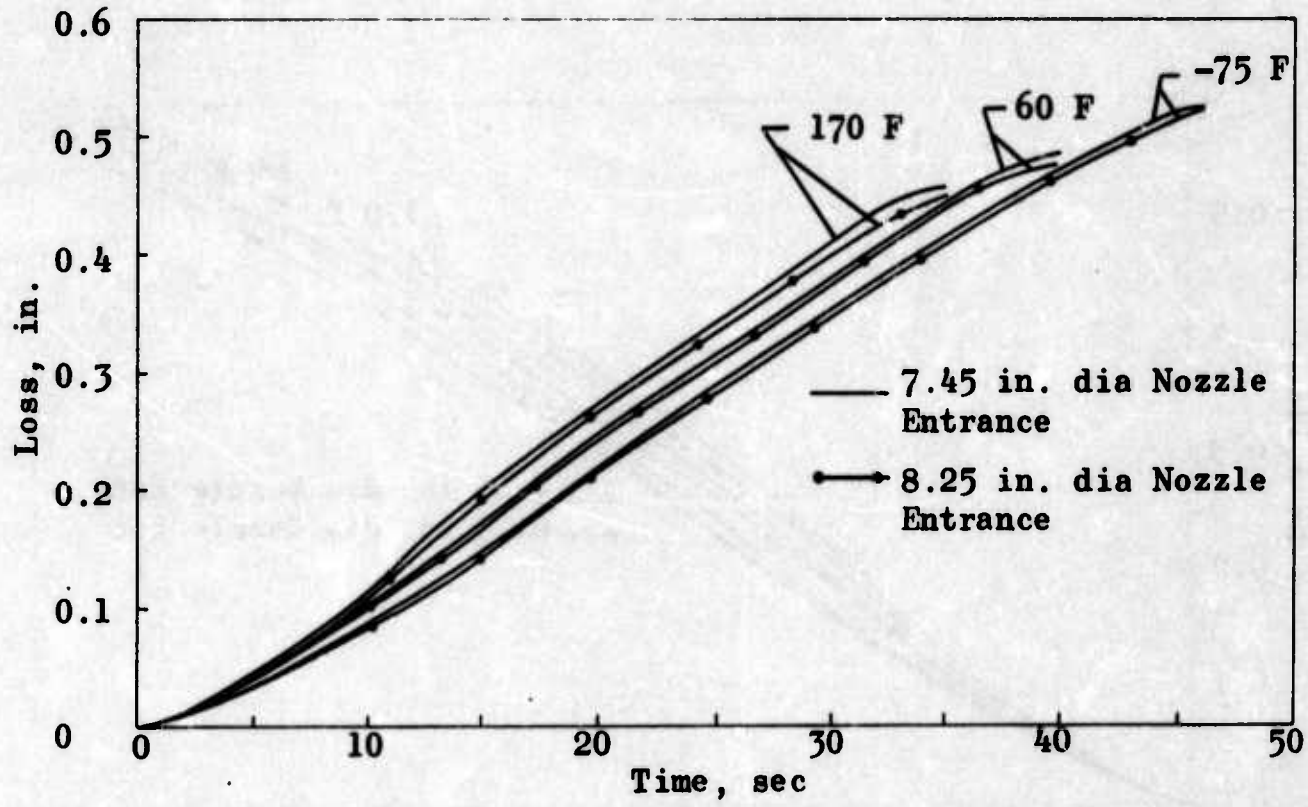


Figure 247. Material Loss vs Time for Various Firing Temperatures for the 7.45 Inch and 8.25 Inch Nozzle Entrance Diameter at Nozzle Station 14

(C)

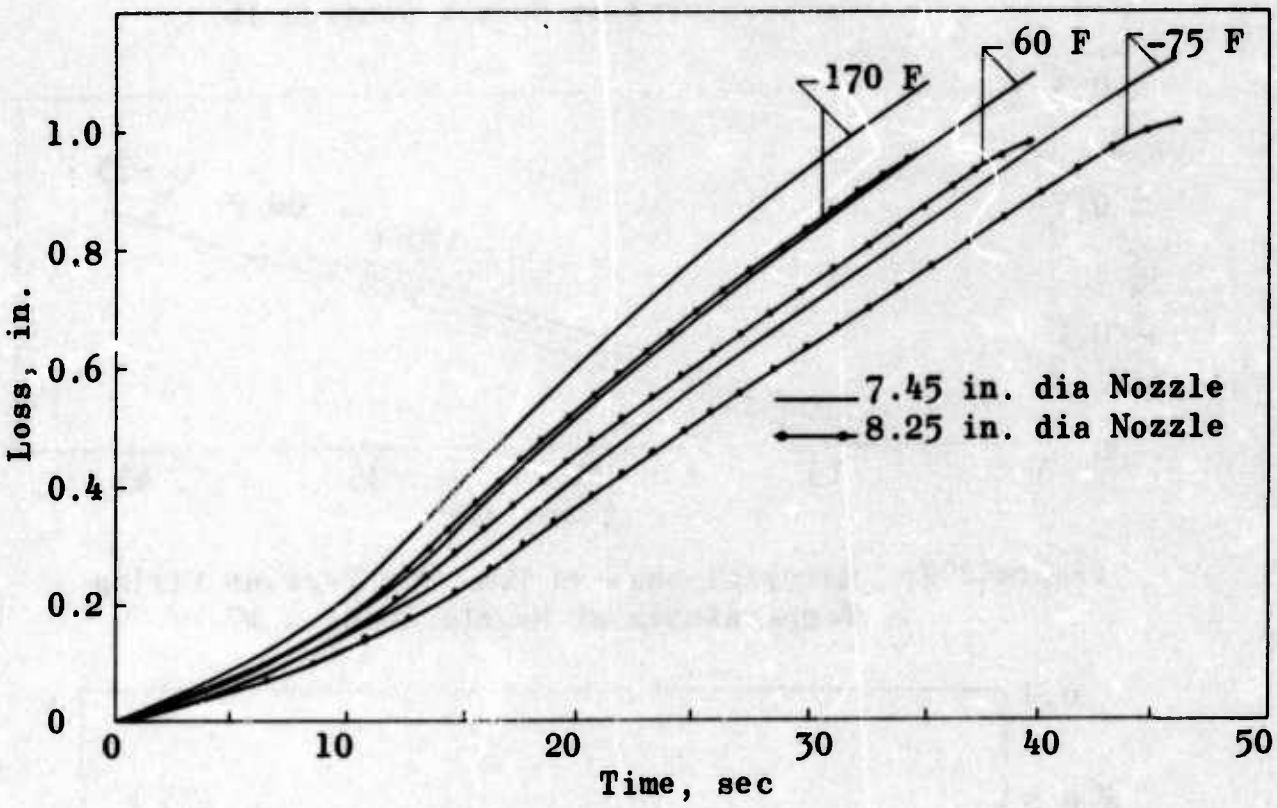


Figure 248. Material Loss vs Time for Various Firing Temperatures for the 7.45 Inch and 8.25 Inch Nozzle Entrance Diameter at Nozzle Station 15

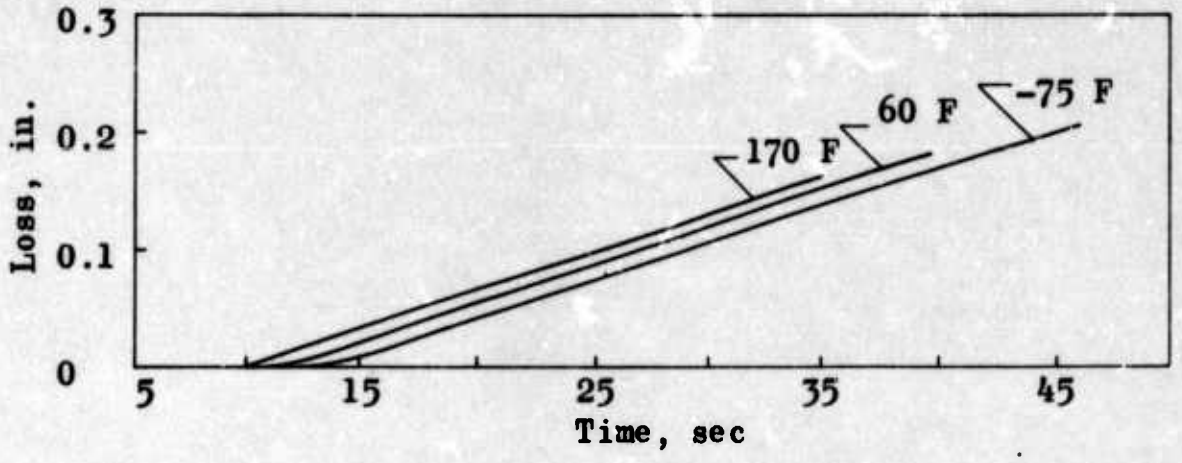


Figure 249. Material Loss vs Time for Various Firing Temperatures at Nozzle Station 16

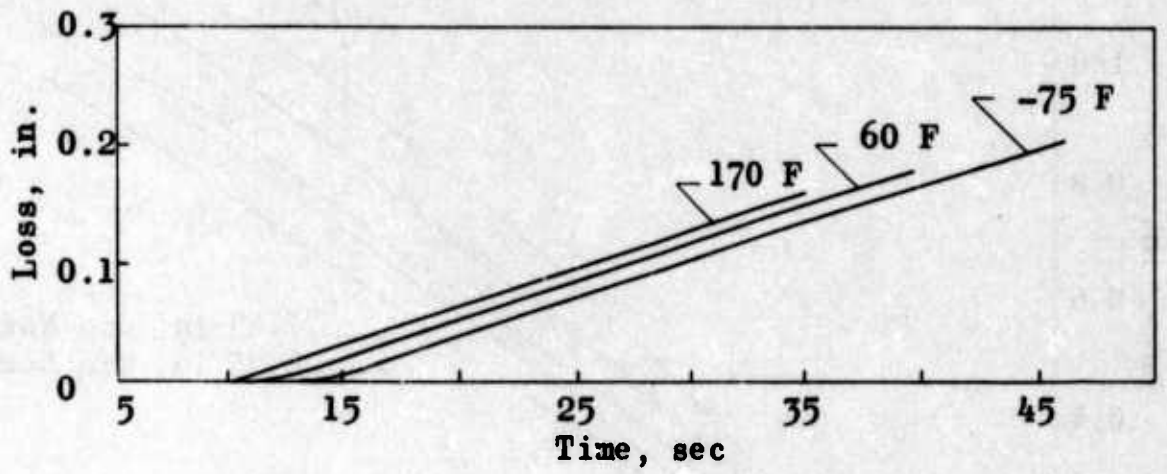


Figure 250. Material Loss vs Time for Various Firing Temperatures at Nozzle Station 17

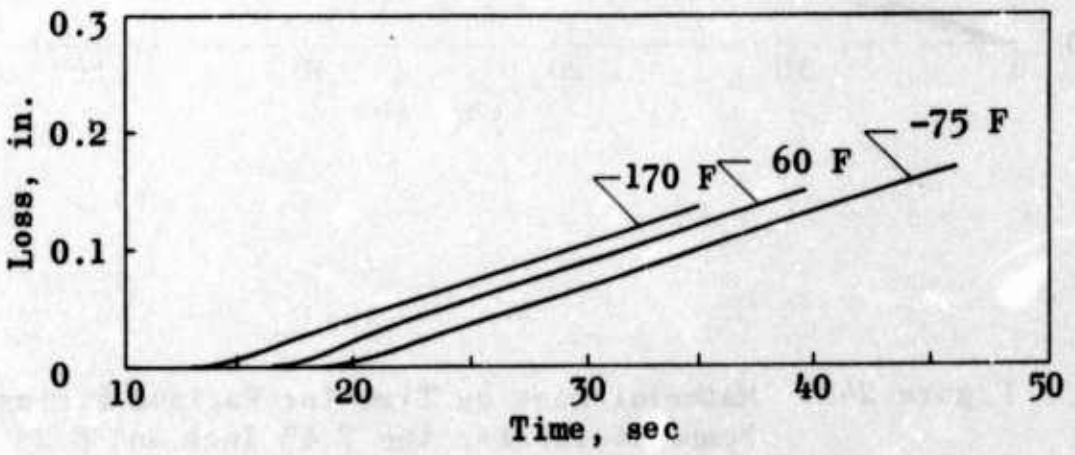


Figure 251. Material Loss vs Time for Various Firing Temperatures at Nozzle Station 18

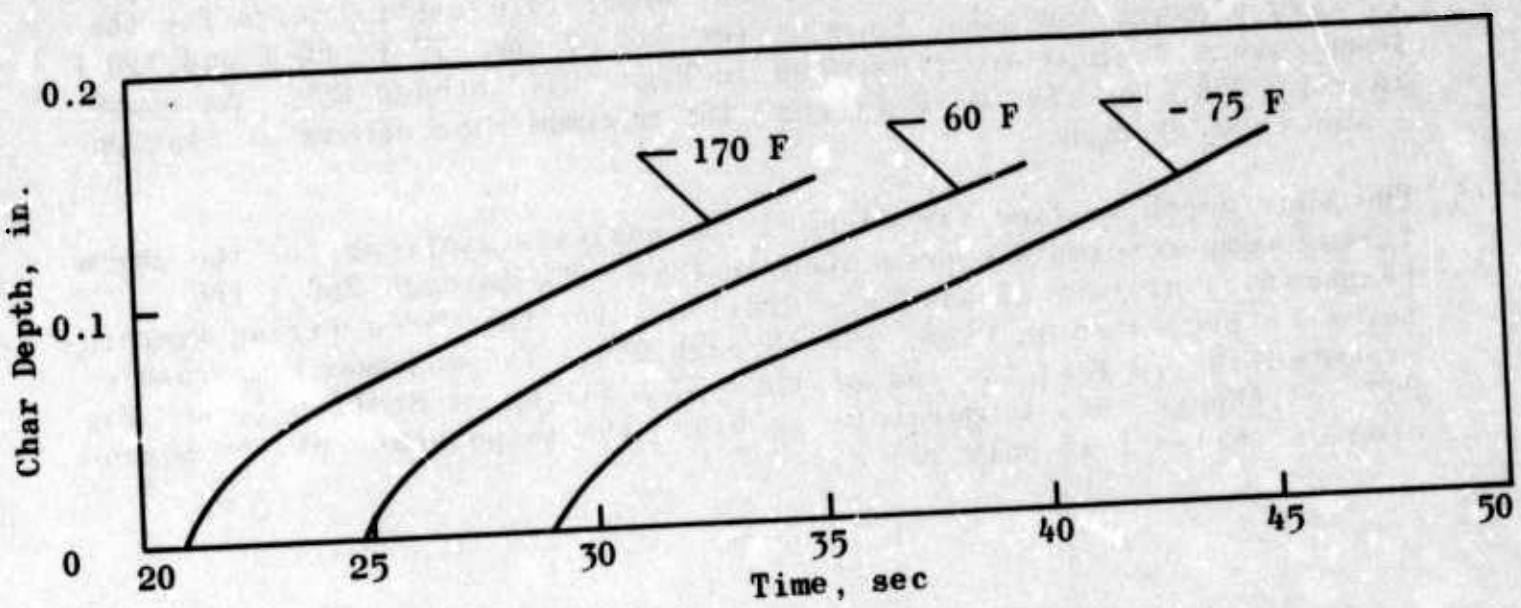


Figure 252. Material Char Depth vs Time for Various Firing Temperatures at Nozzle Station 19

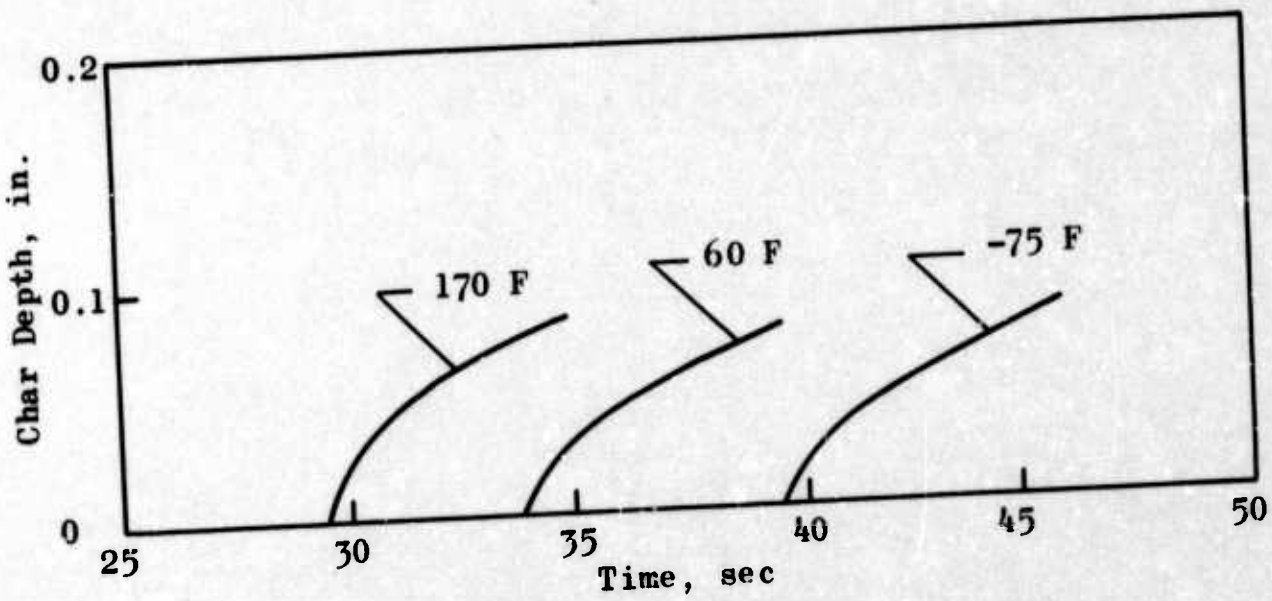


Figure 253. Material Char Depth vs Time for Various Firing Temperatures at Nozzle Station 20

(C) The results of the thermal analysis on the forward polar boss are presented below. The material loss and temperature distribution for the forward closure and polar boss at the end of the -75 F, 60 F and 170 F temperature firings are presented in Figs. 254 through 259. As shown in Fig. 254, for the -75 F firing, the maximum char occurs at Station 1 and is 0.29 inch.

(C) The char depth vs time for each of the analysis stations for the three firing temperatures are presented in Figs. 254 through 256. The temperature history of analysis Station 1 for the three firing temperatures is presented in Figs. 257 through 259. The maximum temperature expected is 770 F at the end of the -75 F firing at Station 1, see Fig. 257. Although this temperature is high, the temperature at the beginning of tail-off is only 205 F.

(C)

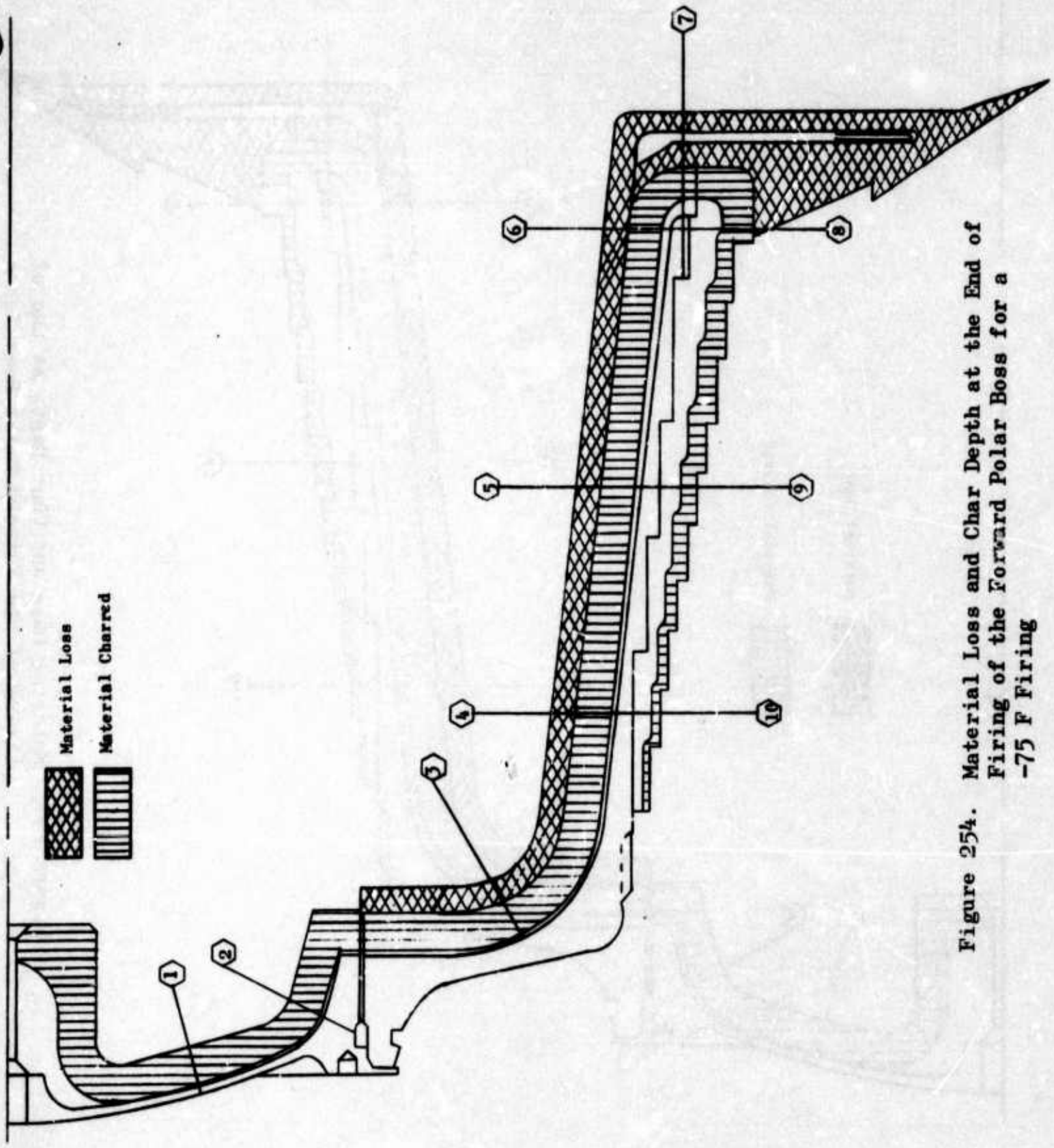


Figure 254. Material Loss and Char Depth at the End of Firing of the Forward Polar Boss for a -75 F Firing

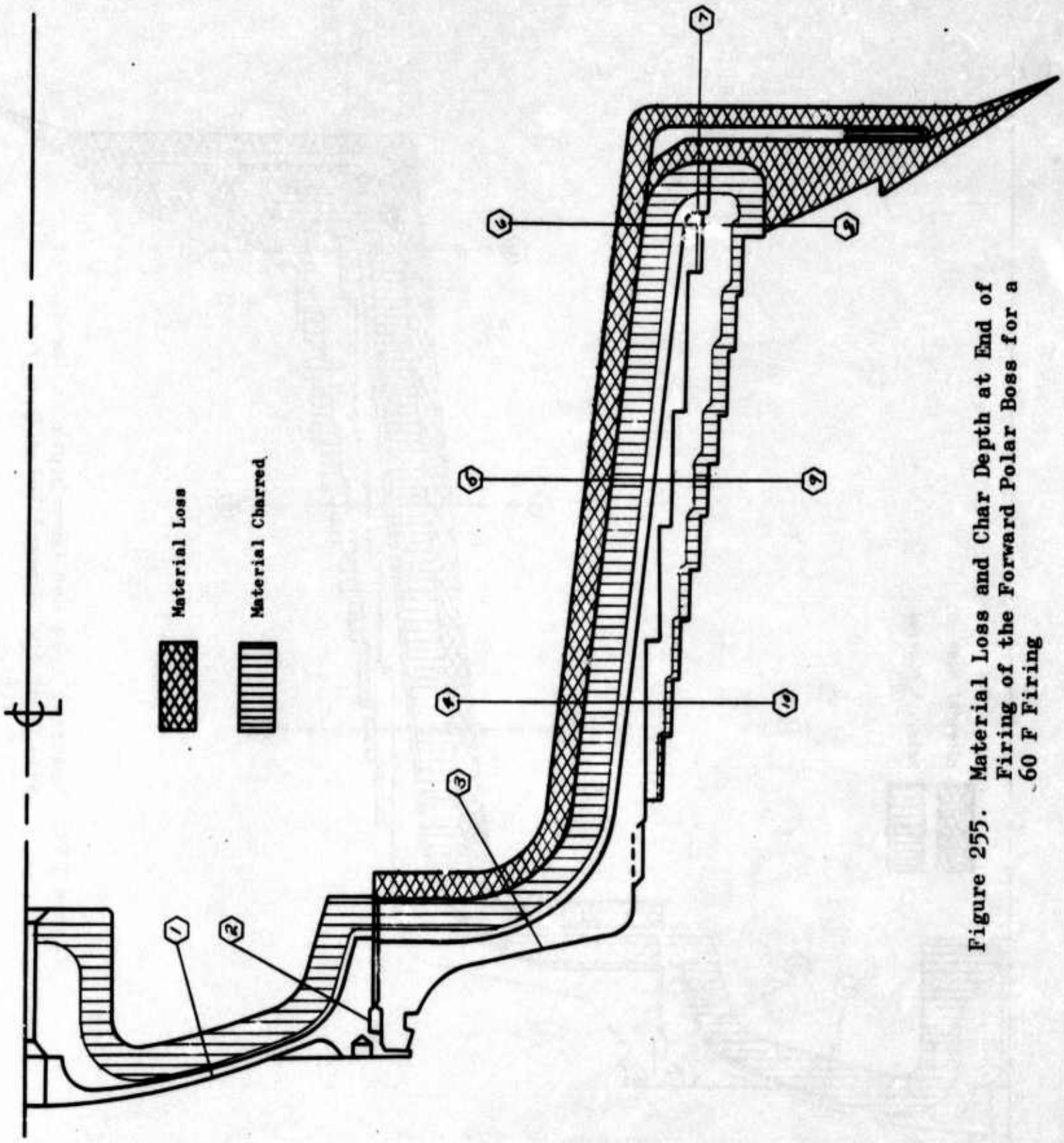


Figure 255. Material Loss and Char Depth at End of Firing of the Forward Polar Boss for a .60 F Firing

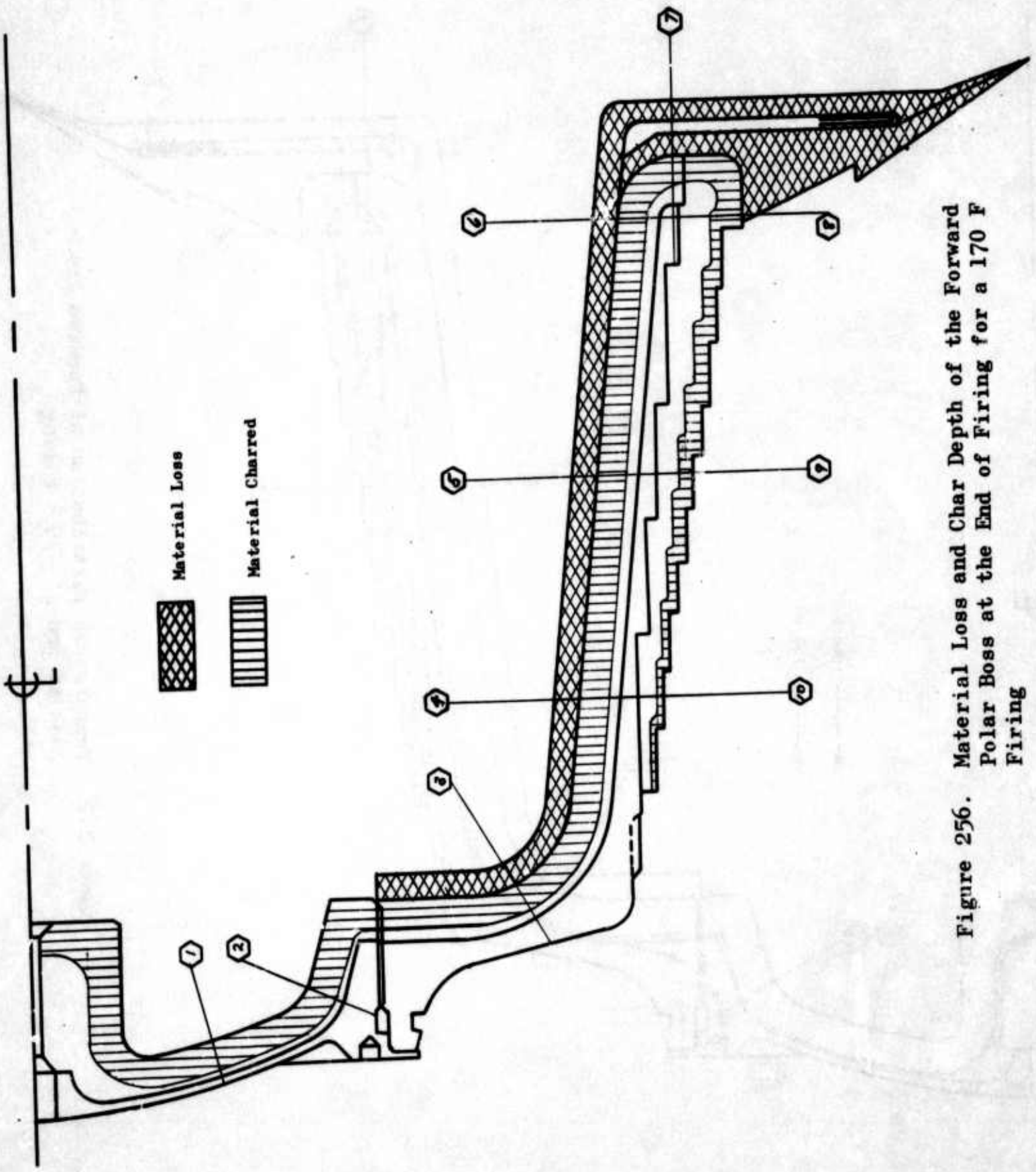


Figure 256. Material Loss and Char Depth of the Forward Polar Boss at the End of Firing for a 170 F Firing

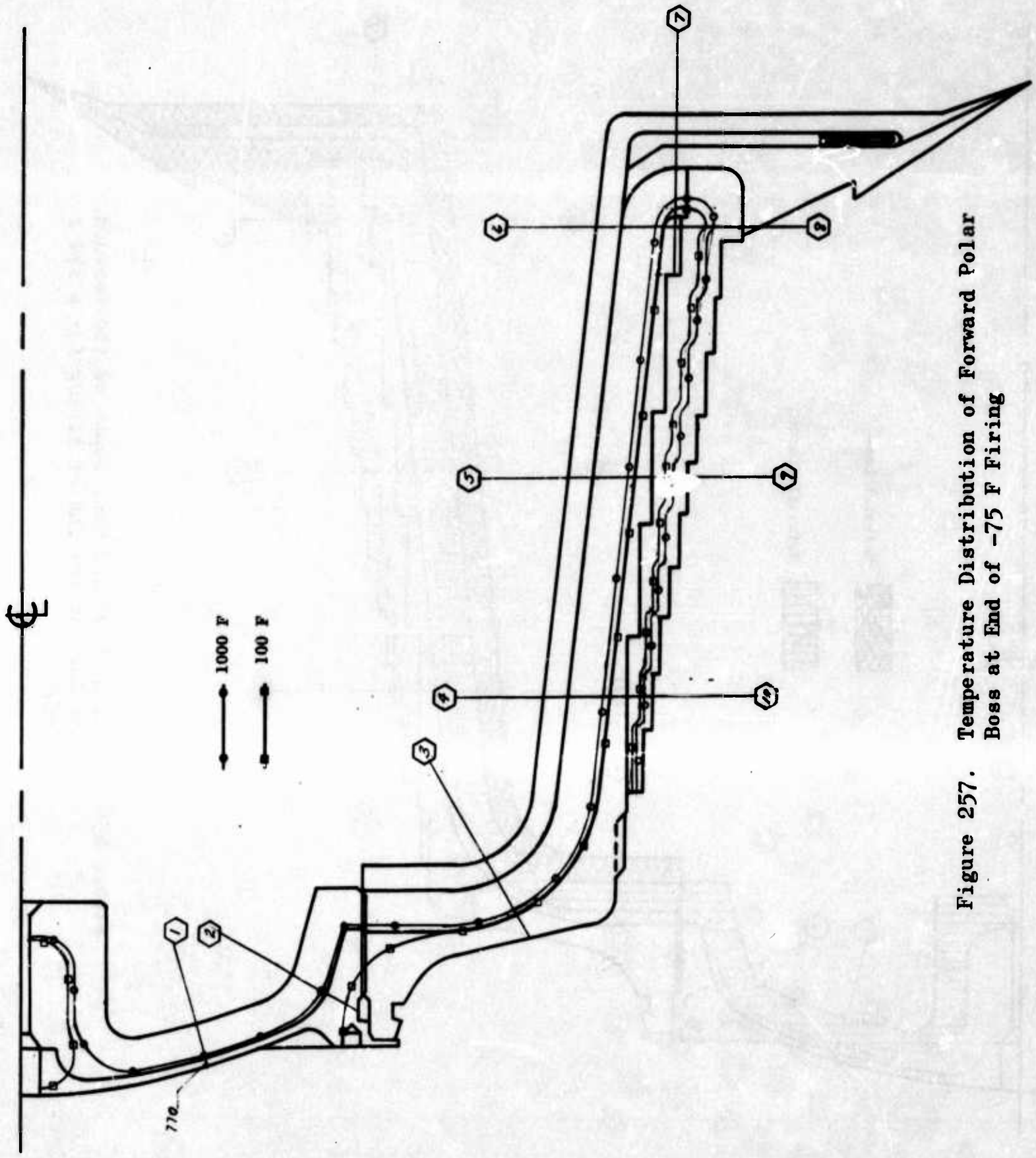


Figure 257. Temperature Distribution of Forward Polar Boss at End of -75 F Firing

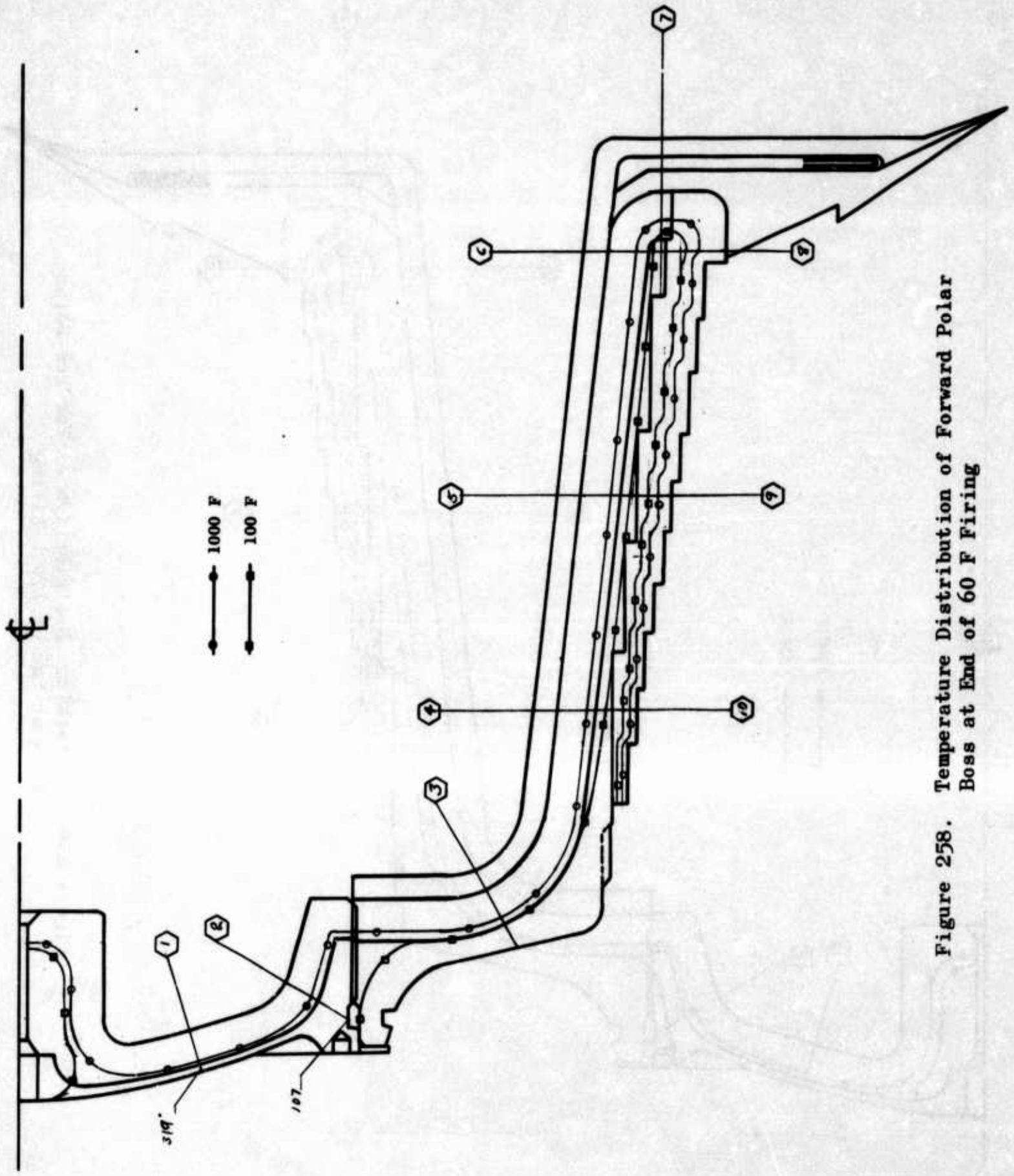


Figure 258. Temperature Distribution of Forward Polar Boss at End of 60 F Firing

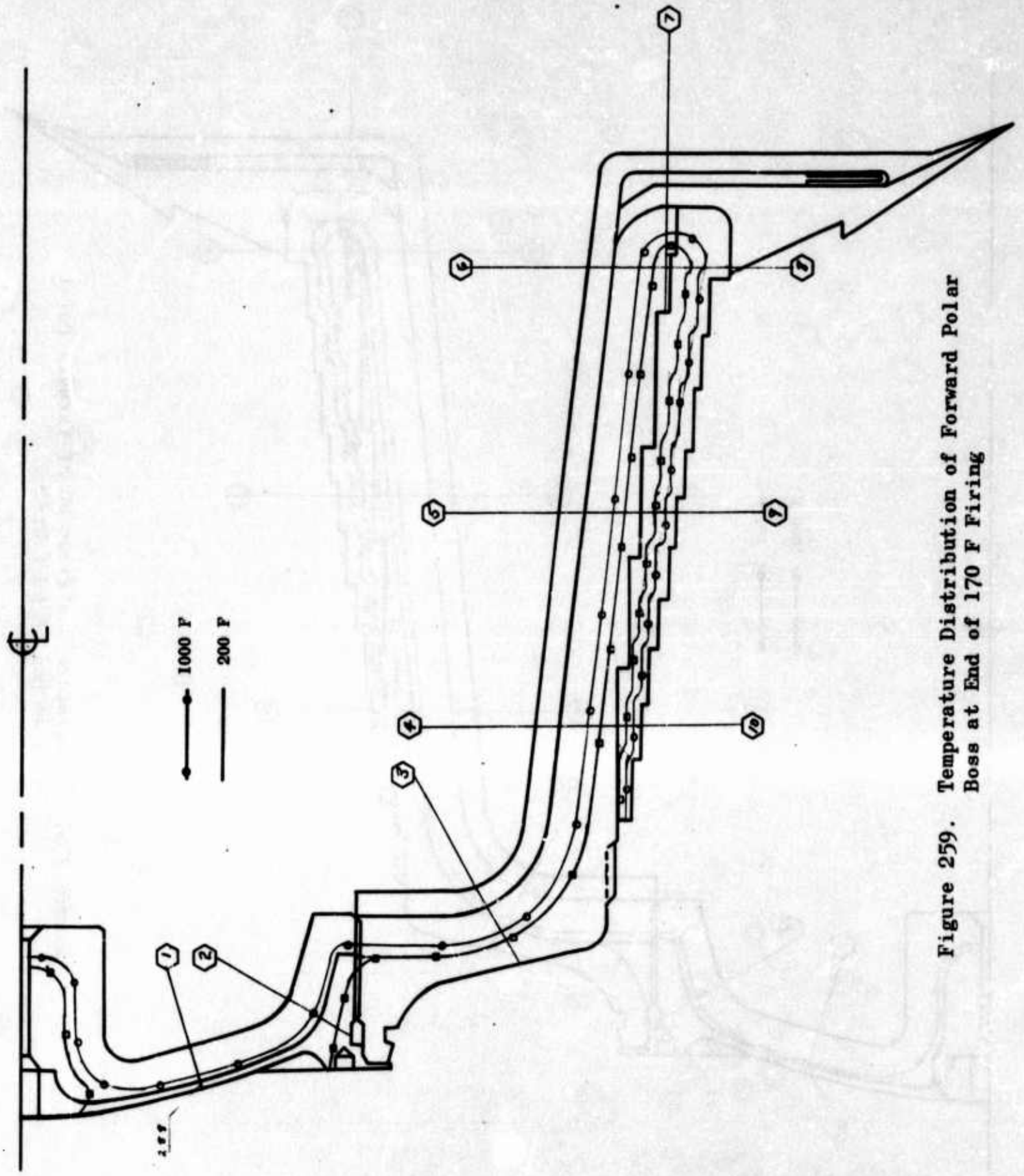


Figure 259. Temperature Distribution of Forward Polar Boss at End of 170 F Firing

(C) The char depth vs time for each of the analysis stations for the three firing temperatures are presented in Figs. 260 through 269. The temperature history of analysis Station 1 for the three firing temperatures is presented in Fig. 270. The maximum temperature expected is 770 F at the end of the -75 F firing at Station 1, see Fig. 270. Although this temperature is high, the temperature at the beginning of tail-off is only 205 F.

(C)

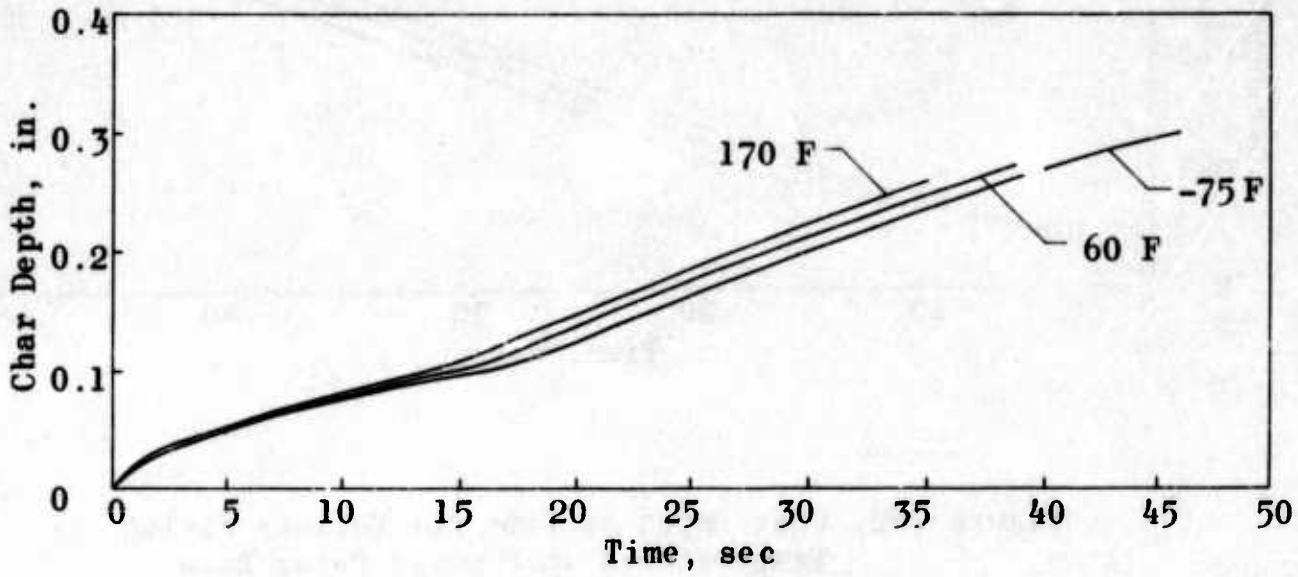


Figure 260. Char Depth vs Time for Various Firing Temperatures, Forward Polar Boss, Station 1

(C)

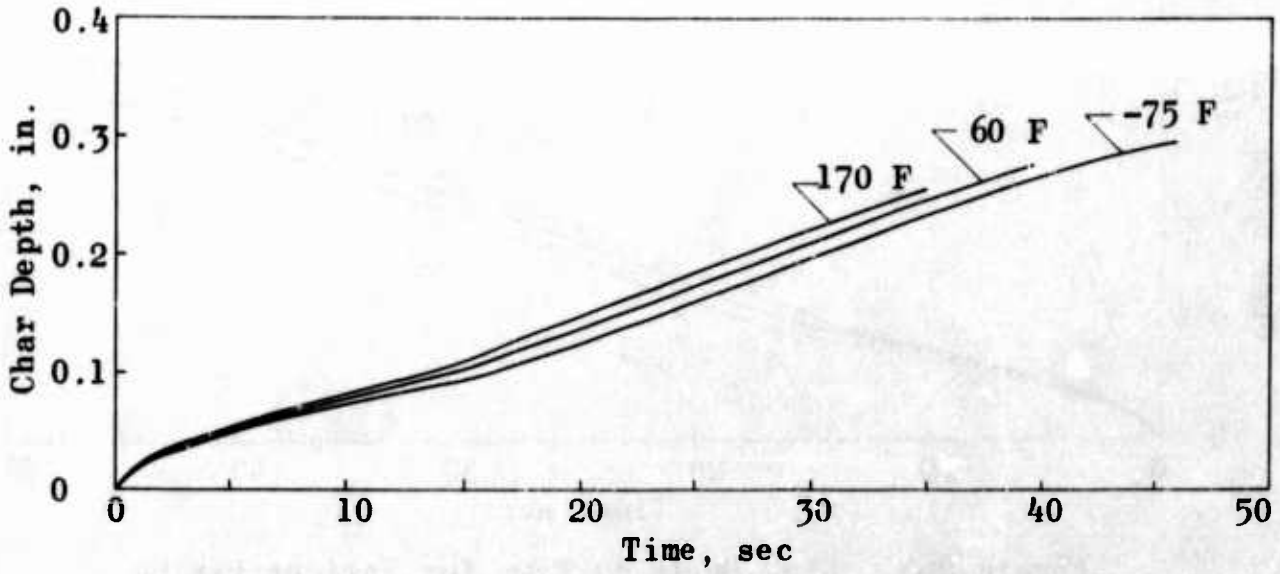


Figure 261. Char Depth vs Time for Various Firing Temperatures at Forward Polar Boss Station 2

(C)

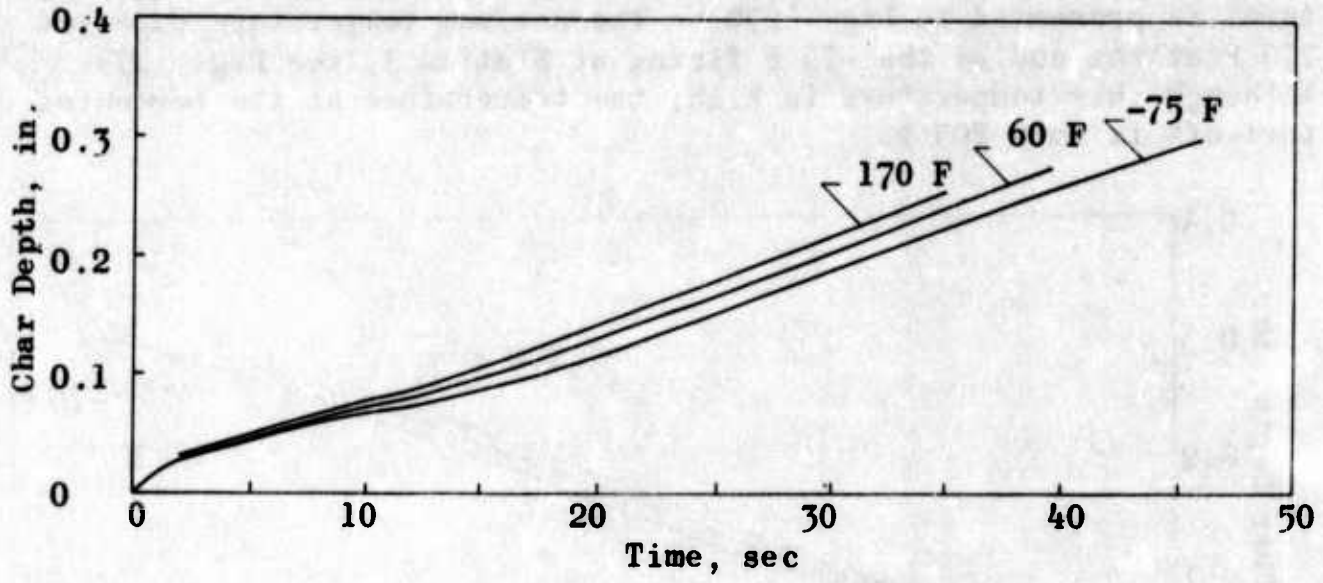


Figure 262. Char Depth vs Time for Various Firing Temperatures at Forward Polar Boss Station 3

(C)

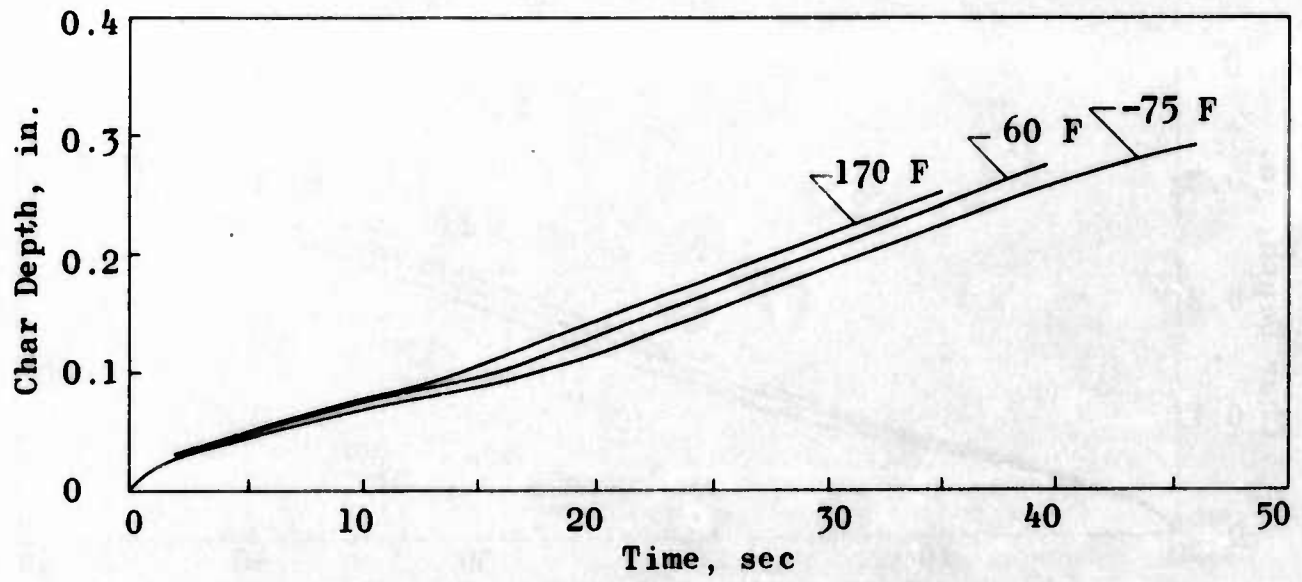


Figure 263. Char Depth vs Time for Various Firing Temperatures at Forward Polar Boss Station 4

(C)

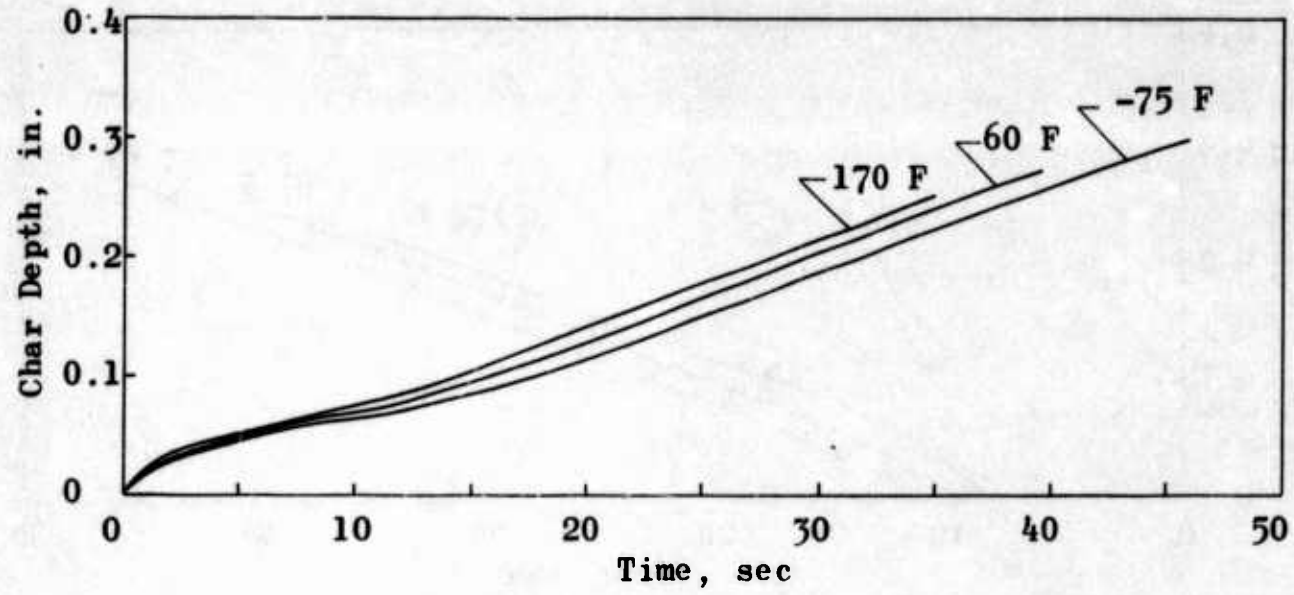


Figure 264. Char Depth vs Time for Various Firing Temperatures at Forward Polar Boss Station 5

(C)

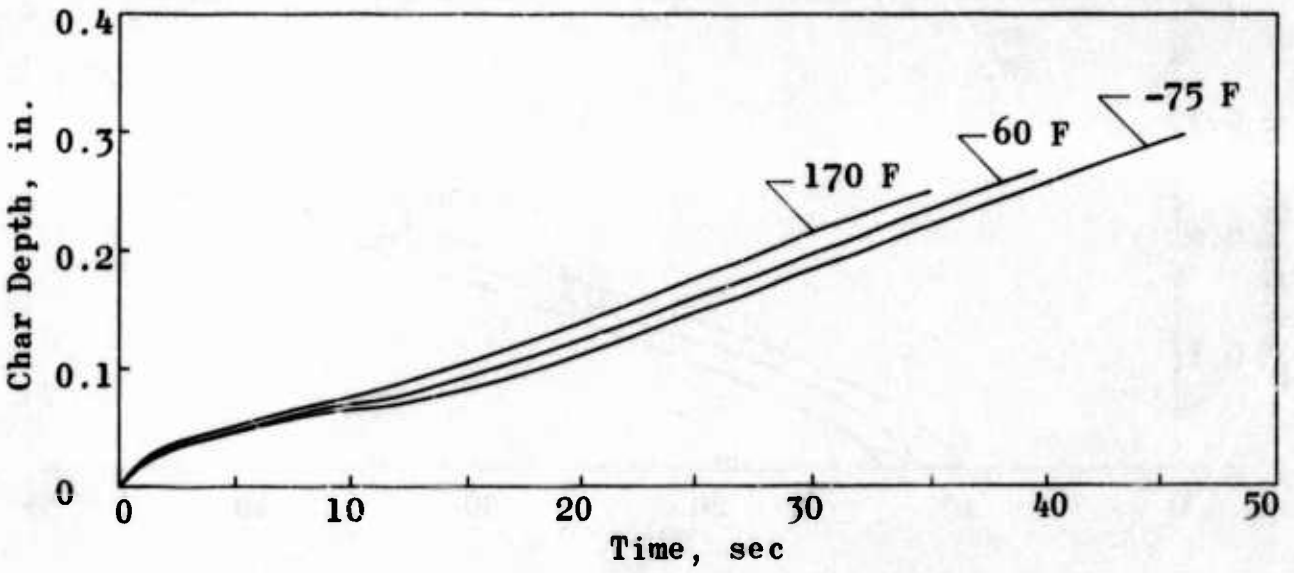


Figure 265. Char Depth vs Time for Various Firing Temperatures at Forward Polar Boss Station 6

(C)

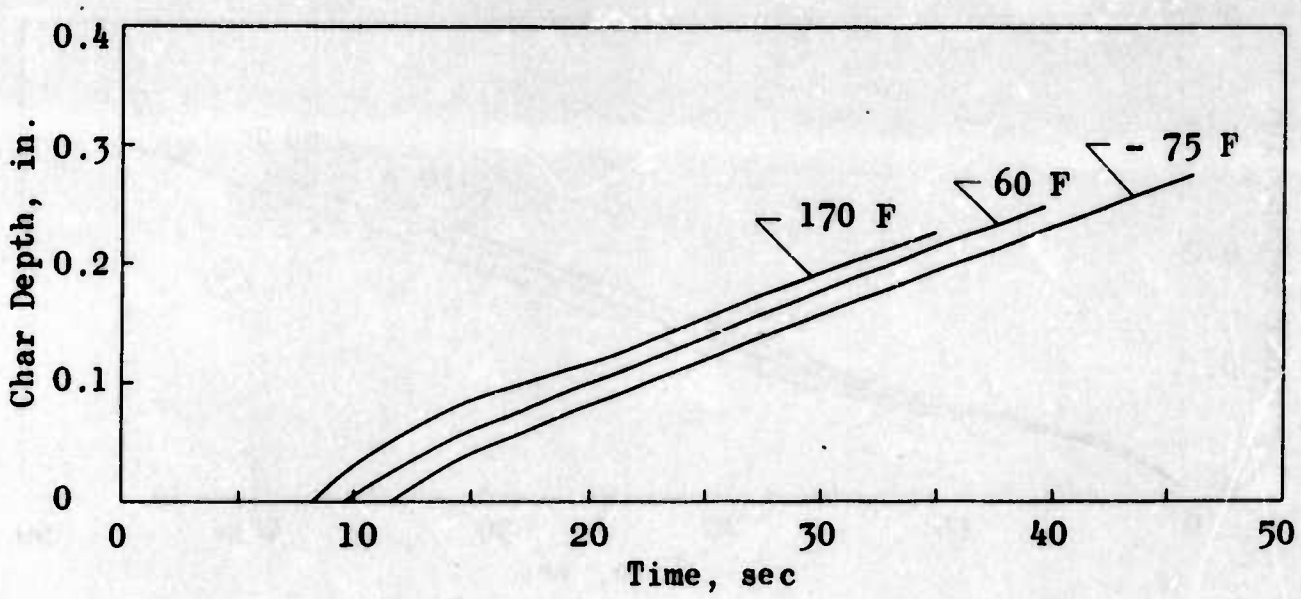


Figure 266. Char Depth vs Time for Various Firing Temperatures at Forward Polar Boss Station 7

(C)

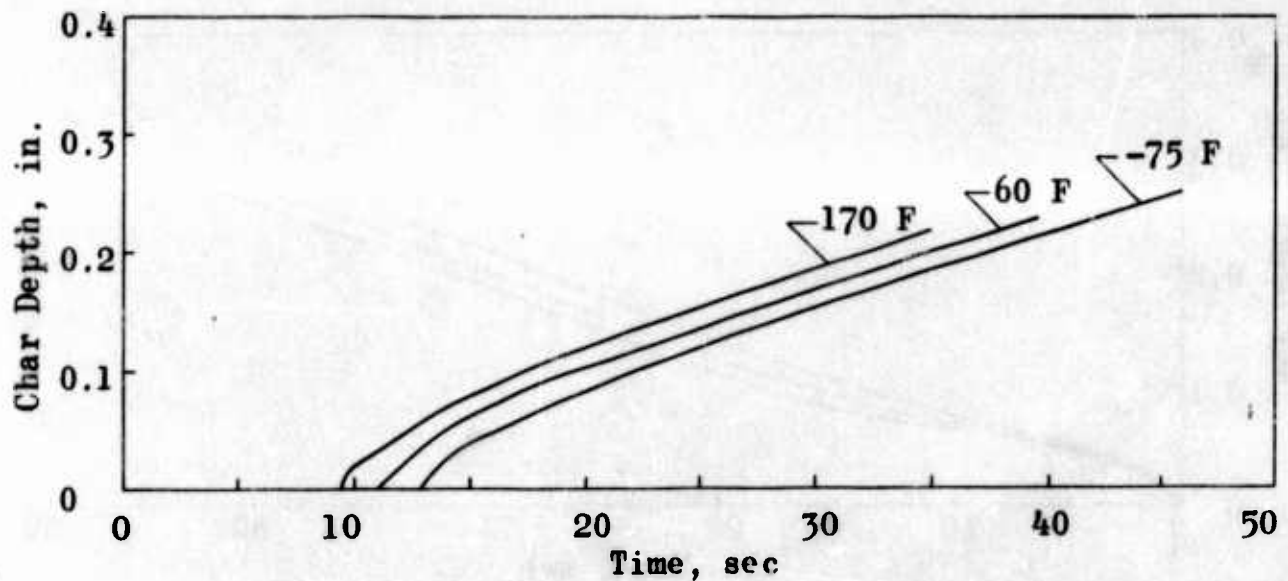


Figure 267. Char Depth vs Time for Various Firing Temperatures at Forward Polar Boss Station 8

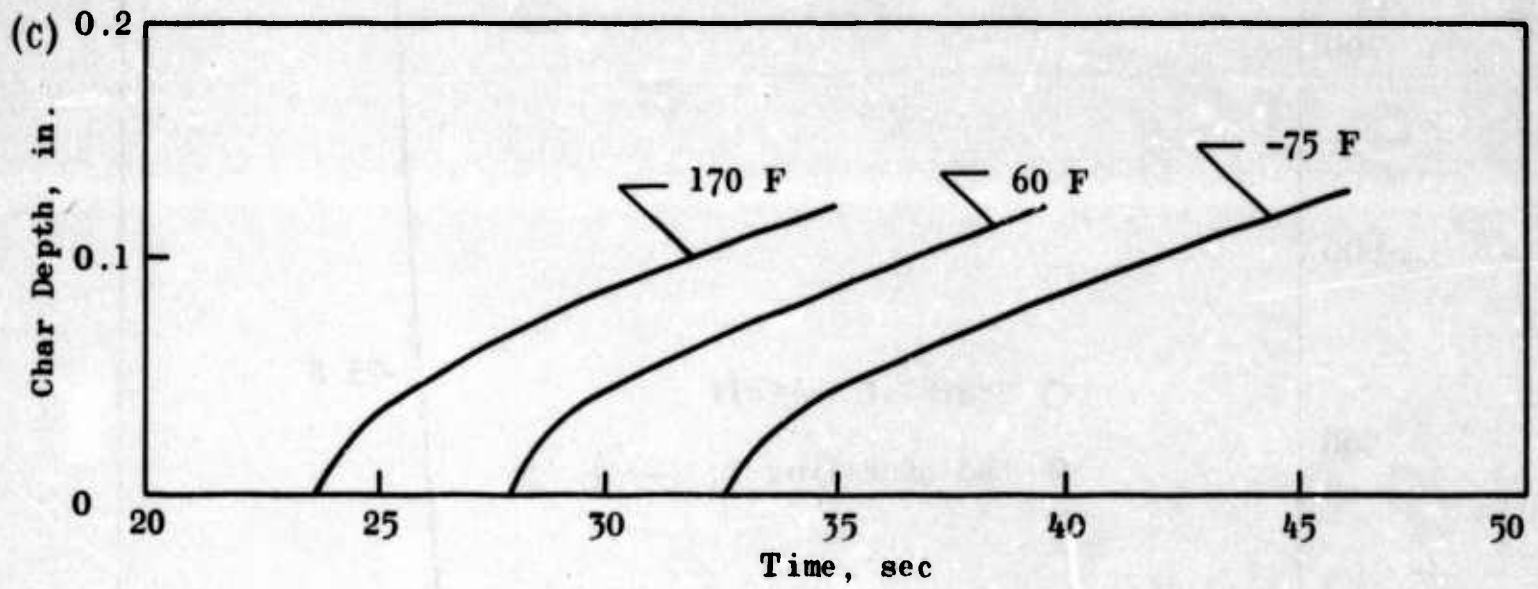


Figure 268. Char Depth vs Time for Various Firing Temperatures at Forward Polar Boss Station 9

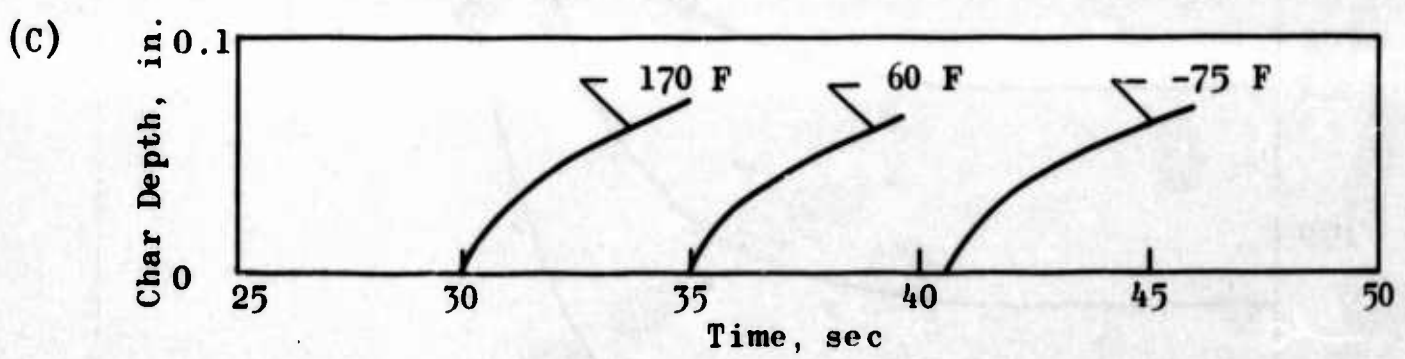


Figure 269. Char Depth vs Time for Various Firing Temperatures at Forward Polar Boss Station 10

(C)

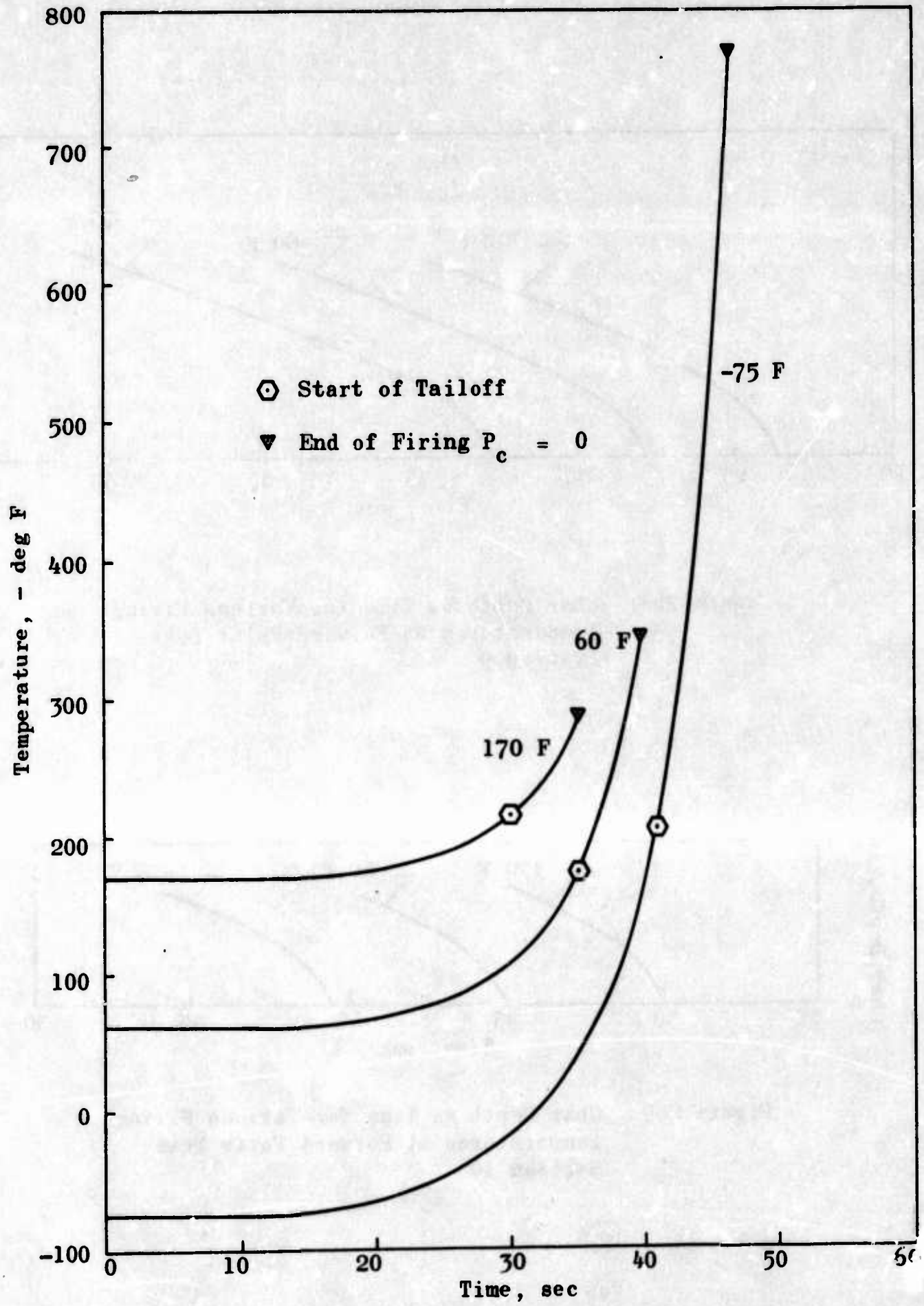


Figure 270. Temperature vs Time for Forward Polar Boss Station 1 for Various Firing Temperatures

(2) Load Rings

The location and general configuration number of load rings used on Motor B is shown in Figs. 271 and 272. The choice of load ring material was based on Motor A and subscale tests. To check the accuracy of the Motor B load ring analytical calculations, tests were conducted on two each of the Motor B load rings number 1, 3, 5, 7, and 9. These rings were selected because they represented a sample of the several weights of load rings.

All rings failed exhibiting the same wrinkling as was experienced in the Motor A ring tests. Maximum loads sustained by the load rings are shown in Table LXXVI. Data in the assigned-load column in (Table LXXVI) was obtained by reducing the test loads of rings number 1, 3, 5, 7, and 9 by 20%, and by assigning reasonable loads to the other rings by cross-section comparison.

TABLE LXXVI

LOAD DISTRIBUTION (LOAD RINGS)

(C)

Case Pressure Design Ultimate	1250 psi
Effective Diameter	12.55 in.
Maximum Load (Fwd Polar Boss)	157,000 lb

Ring No.	Load Assigned, %	Load at Failure-Test, lb	Assigned Load, lb	Margin
1	30	60,000	48,000	0.25
2	10	No Test	15,700	--
3	13	25,000	20,000	0.25
4	6	No Test	9,400	--
5	4	8,000	6,300	0.27
6	10	No Test	15,700	--
7	5	10,000	7,850	0.27
8	4	No Test	6,300	--
9	10	17,000	15,700	0.13
10	4	No Test	6,300	--
11	4	No Test	6,300	--
Totals	100%	140,000*	157,550	

* Total value for one-half the total rings.

(c)

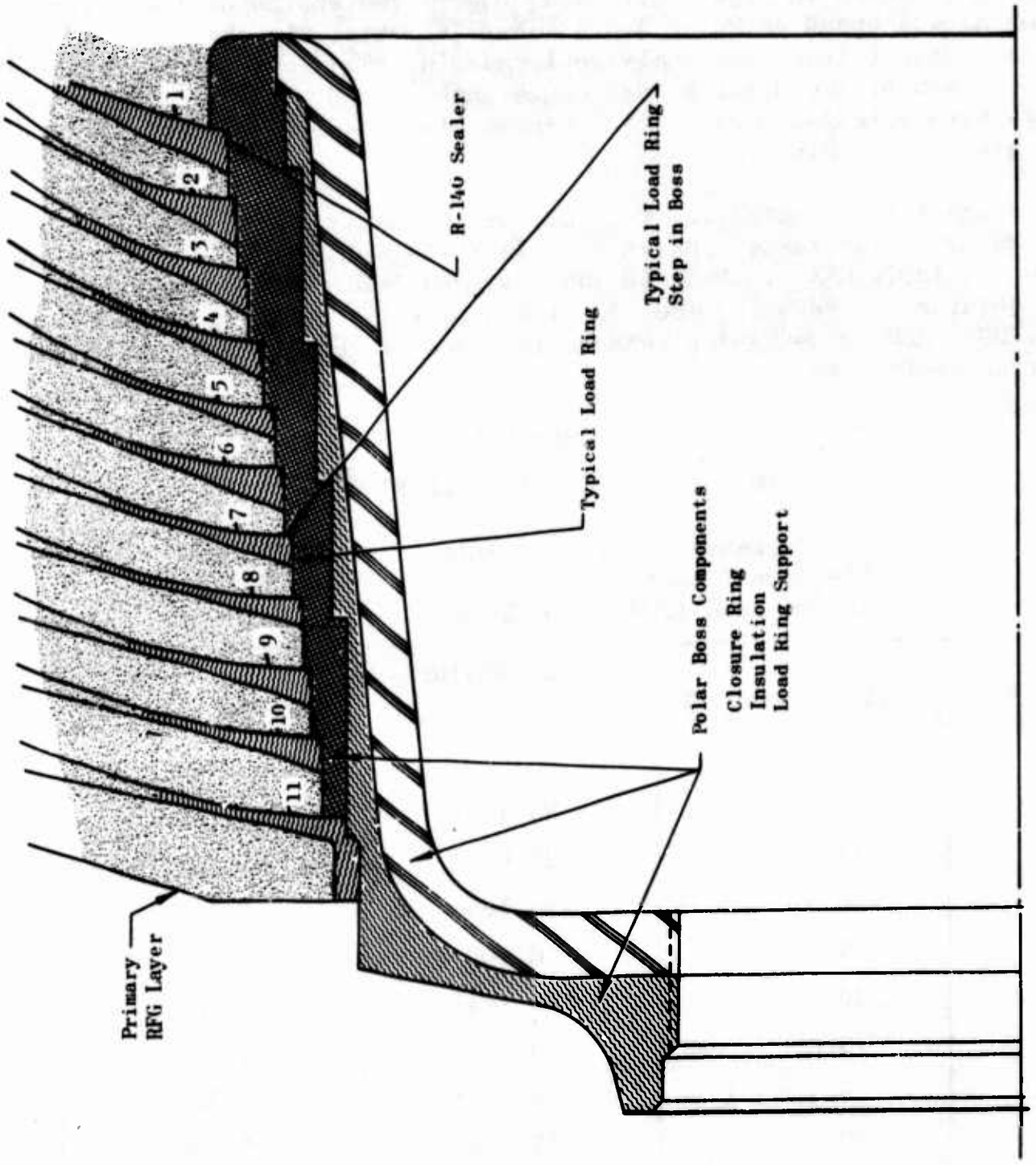


Figure 271. Section View: Forward Polar Boss

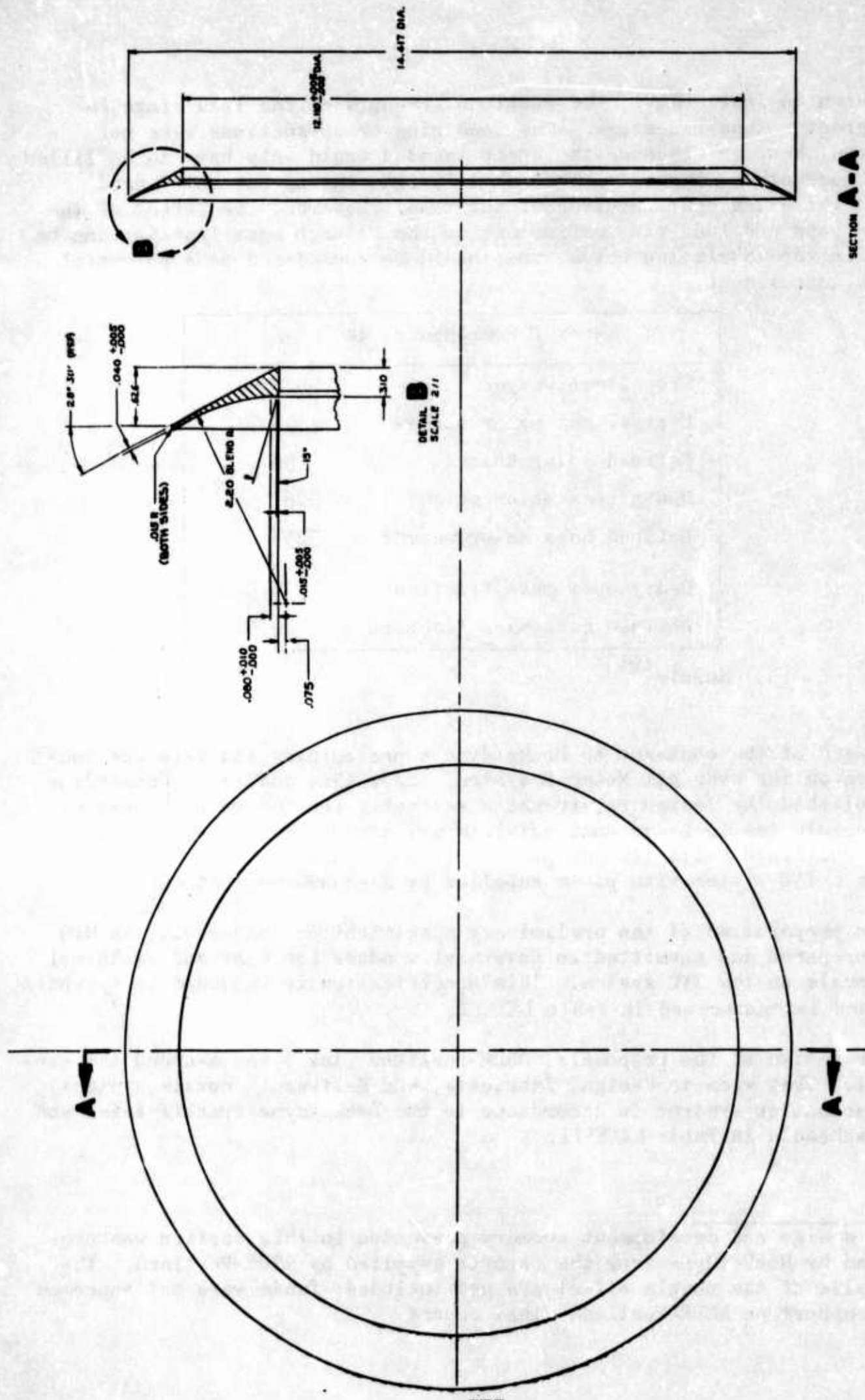


Figure 272. Typical Load Ring Section

As shown in Table LXXVI, the combined strength of the load rings is far greater than necessary. The load ring cross-sections were not reduced, however, because the space vacated would only have to be filled with some other material. This small weight saving was not judged worth the extra cost involved at the time. However, the effect of the polar boss and load ring refinement on the Motor B mass fraction can be seen in the tabulation below, and should be considered as a potential motor improvement.

(C)

Motor B Components, lb	
Propellant weight	3035
Heavyweight polar bosses	78
Refined polar bosses	50
Heavy boss motor weight	3281
Refined boss motor weight	3253
Heavy boss mass fraction	0.925
Refined boss mass fraction	0.933

(3) Nozzle[24]

On award of the contract to Rocketdyne a preliminary analysis was conducted on the over-all Motor B system. From this analysis, Rocketdyne established the design requirements necessary for the Motor B nozzle. The nozzle was to be an omni-axis, thrust vector control (TVC) system, self-contained (with its own power system). This was later changed to be a TVC system with power supplied by a ground support cart.

After preparation of the preliminary specification, NA5-80014, an RFQ was prepared and submitted to potential vendors for cost and technical proposals on the TVC system. This specification is included in Appendix III and is summarized in Table LXXVII.

After review of the proposals, ARDE-Portland, Inc., was awarded the contract. They were to design, fabricate, and deliver 14 nozzle systems and actuation systems in accordance to the Rocketdyne specification and the schedule in Table LXXVIII.

(24) The design and development summary presented in this section was prepared by Rocketdyne from the reports supplied by ARDE-Portland. The details of the nozzle effort are not included; funds were not approved to support an ARDE-Portland final report.

TABLE LXXVII

TVC SYSTEM REQUIREMENTS*

(C)

Thrust vector angle (in any plane), deg	± 4
Maximum duty cycle, frequency of system (at 0.25 degrees deflection), cps	30
Nozzle ballistic performance, %	97.0
Nozzle expansion ratio	
Altitude test	25:1
Ground test	10:1
Initial nozzle throat area, sq in.	21.835
Nozzle divergence geometry, modified bell contour, TVC system max flight weight (25:1 nozzle expansion ratio)	79.9
Operating temperature, deg F	-75 to 170

(C) *Environmental conditions to which nozzle would be subjected are altitude cycling, vibration, acceleration, humidity, fungus, rain, sand and dust, shock, and one-year storage at -75 to 170 F

TABLE LXXVIII

TVC SYSTEM SCHEDULE

(C)

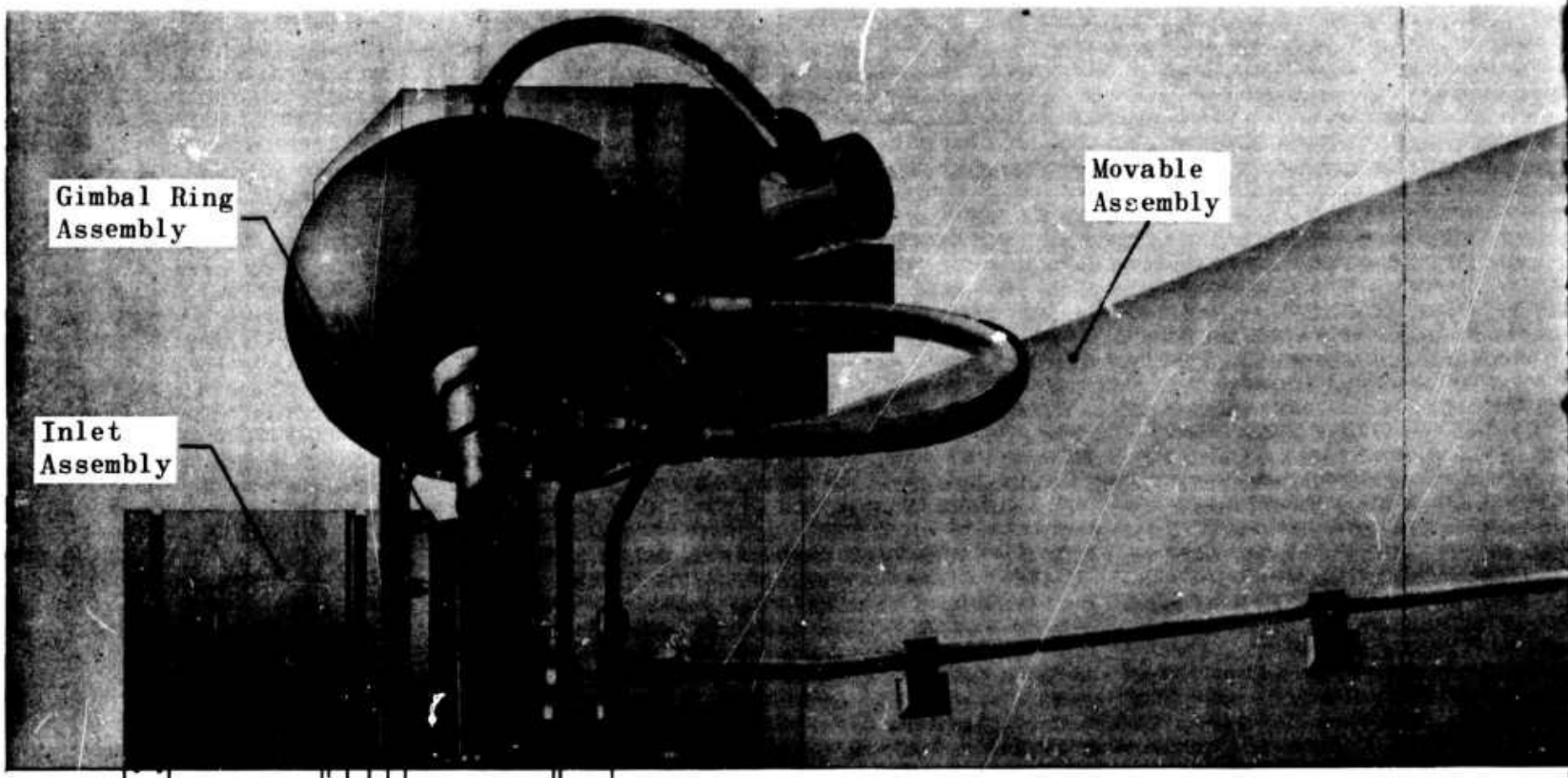
	Area Ratio	Quantity
Nozzles	10:1	10
	25:1	4
Actuation systems		
Fixed link	10:1	7
Actuated	10:1	3
Actuated	25:1	4

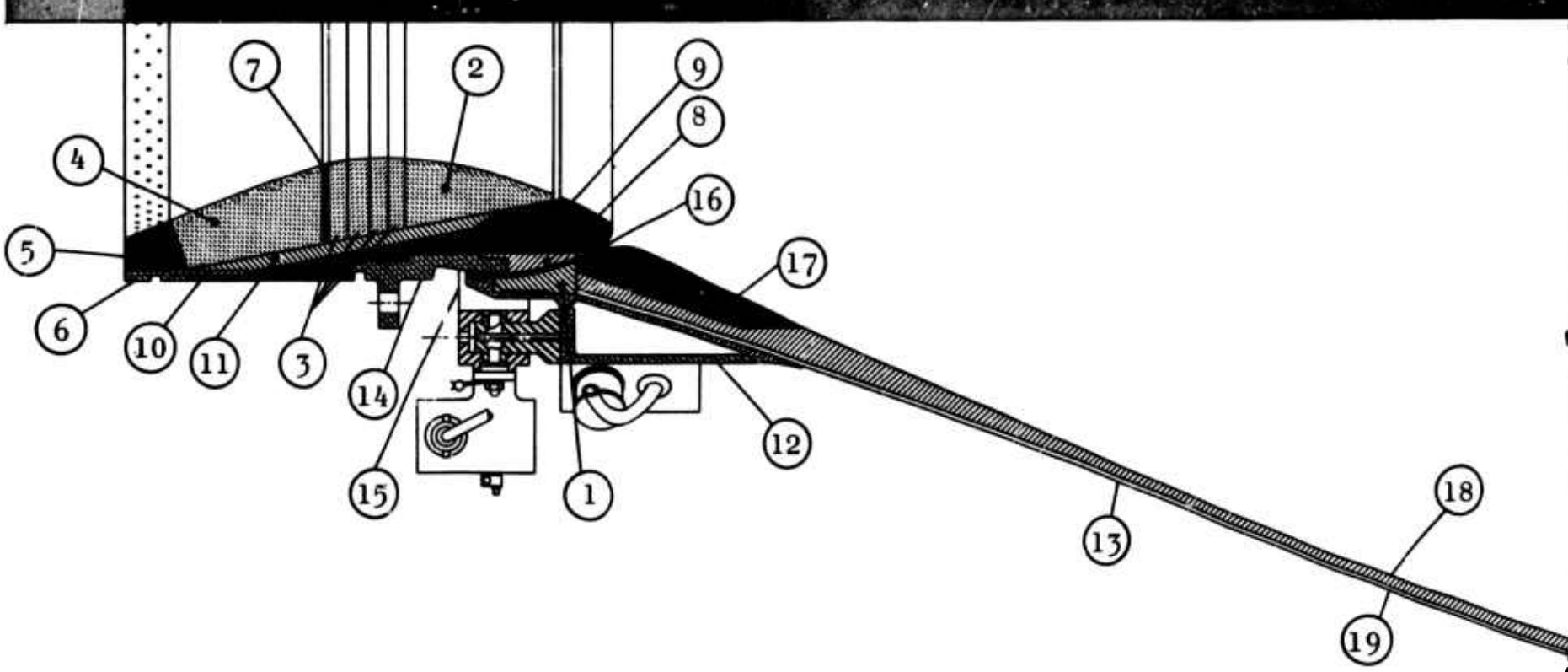
(C) The ten nozzle systems with a 10:1 area ratio were to be static fired on Motors B and C. The four with 25:1 ratio were to be delivered with B and C Motors for testing under altitude simulation conditions. When it became necessary to delete Motor C from the program, the number of TVC systems was reduced to seven, five with 10:1 area ratio and two with 25:1 area ratio. Of the remaining seven TVC units, two were to have fixed links on the 10:1 expansion ratio nozzles (and of these two, the first one was to be fully instrumented). When the program was stopped, ARDE-Portland had finished fabrication and delivery of the first nozzle system to Rocketdyne; the second unit was nearing completion, and the actuation systems were through development testing, but the results had not been prepared in report form. Again, at the direction of RPL, the second nozzle unit and two actuation systems were completed and delivered to RPL for test and evaluation on the char motor. At publication of this report these firings had not been conducted.

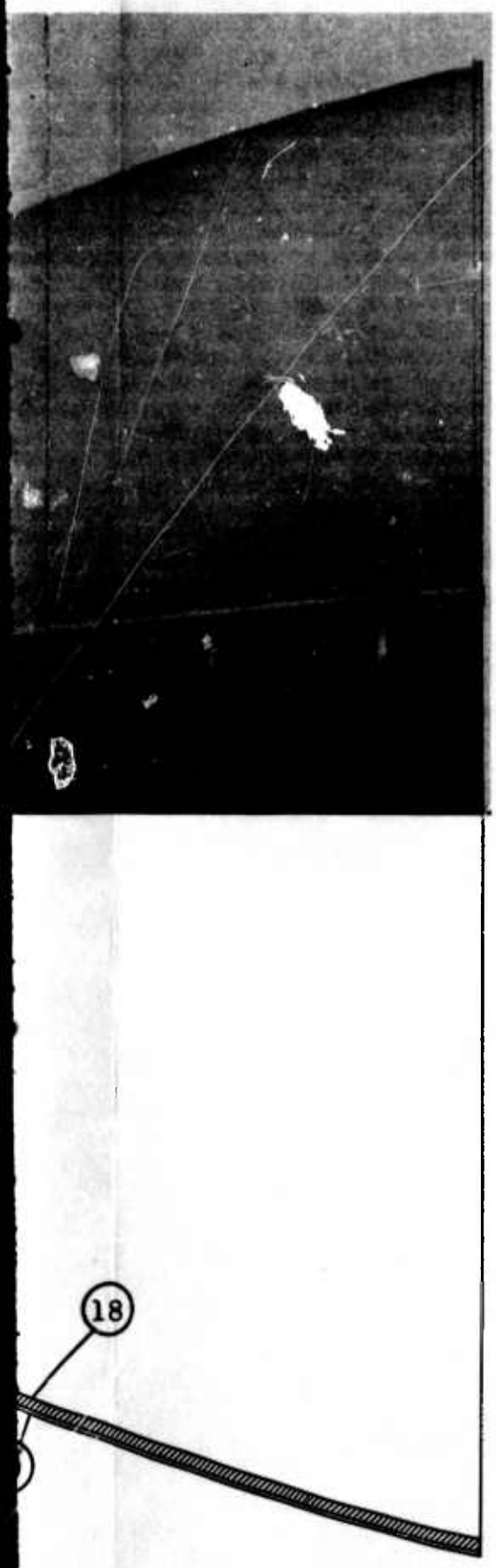
(a) Nozzle Description

As illustrated in Fig. 273, the three-dimensional omni-axis TVC system developed for use on the RFG Motor B consists of three major components: the inlet assembly, the movable assembly, and the gimbaled ring assembly. The location of the split line between the inlet and movable assembly was dictated by the envelope requirements of the TVC system. Design studies indicated that because of the envelope restrictions, location of the split line in the subsonic region would place the O-ring seal in an area where it could not be adequately protected. The split line was, therefore, placed in the supersonic region and its actual location optimized on the basis of seal protection, minimum aerodynamic loss, and minimum weight. The inlet assembly is fixed to the aft closure of the motor and includes the inlet gas passage, nozzle throat, sealing surface, and a support for the gimbal ring. The movable assembly includes the split-line seal, divergent section, and structural support system. The split line between the fixed and movable nozzle members is a ball-in-socket arrangement formed by spherical surfaces on the inlet and movable assemblies. The clearance between the split line is filled with a combination of materials, consisting of silicone rubber, silicone grease, and zinc chromate (which limits the gas circulation and provides lubrication). Gas sealing is effected with an O-ring made of Buna-N rubber.

The nozzle is made omni-axis vectorable by the use of a gimbal. The gimbal ring is mounted on plane bearings and supports the movable assembly from another set of plane bearings displaced 90 degrees. It consists of a hollow ring with a rectangular cross section and bearings at


Gimbal Ring Assembly
Movable Assembly
Inlet Assembly


7
2
9
8
4
16
5
17
6
10
11
3
14
12
15
1
18
13
19



Note	Part No.	Nomenclature	Material
1	B103592	Insert - Movable Housing	Silica Fabric and Phenolic Resin
2	B103599	Insert - Throat, Aft	Graph-I-Tit G
3	B103600	Disc - Throat, 4/Pack	Pyrolytic Graphite
4	B103601	Insert - Throat Inlet	Graph-I-Tite G
5	B103602	Insert - Inlet	Graphite Cloth & Phenolic Resin
6	B103604	Liner - O-Ring, Inlet	Silica Fabric & Phenolic Resin
7	B103605	Ring - Expansion, Inlet	Rubber per MIL-R-3065 Type S, Class 5B, Grade J15
8	B103663	Insert - Nose, Inlet	Silica Fabric & Phenolic Resin
9	B103664	Liner - Nose, Inlet	Graphite Cloth
10	C103603	Liner - Ring, Inlet	
11	D103598	Liner - Insulator, Inlet	Grafoil 101
12	E3056		Aluminum, 6061-T6
13	E3060		
14	E3097		Aluminum
15			4130 Steel
16			Silicone Rubber, Q-2-0103-1/2, Ordance 05-9163
17			Graphite Cloth
18			Silica Cloth
19			Fiberglass & Resin

Figure 273. Motor B Nozzle Assembly

PREVIOUS PAGE WAS BLANK, THEREFORE WAS NOT FILMED

two pivot axes located 90 degrees apart. At one axis the ring is pivoted relative to the stationary inlet assembly, and at the other axis the movable assembly is pivoted relative to the ring. When the nozzle is pivoted about one or the other axis individually, either pitch or yaw correction may be effected. When the nozzle is pivoted about both axes simultaneously, the true motion of the nozzle may be in any desired direction.

- Inlet Assembly

The inlet assembly housing is the primary structural member of the TVC system. It consists of the nozzle attachment flange, which matches the motor case, and a cylindrical member which supports the throat section and insulation materials. It also provides the sealing surface for the O-ring seal. This sealing surface is electroless-nickel plated to provide a hard, smooth surface against which the O-ring seals. Also extending from the attachment flange are two diametrically opposite structural members which support the gimbal ring via thrust pins.

Edge-grain pyrolytic graphite disks form the throat insert to withstand the environmental conditions during firing with minimum erosion. The divergent sections ahead of and behind the throat are made of Graph-I-Tite "G". A neoprene washer is used between the Graph-I-Tite "G" and pyrolytic graphite to take up the axial thermal expansion, to prevent loads being imposed on these relatively brittle materials. Further downstream, graphite cloth is used up to and including the nozzle split line.

Insulating material is required to reduce heat flow to the aluminum housing and the seal area. The use of edge-grain pyrolytic graphite, with its high heat-transfer coefficient in the radial direction, requires a high-temperature insulating material behind the throat section. A sleeve of Grafoil No. 101, a pyrolytic graphite, is used for this purpose. A silica-reinforced material is used as the insulator between the throat back-up section and the aluminum housing. The same material is also used in the split line to protect the aluminum housing and O-ring seal from heat input through the split line.

The nozzle inlet and throat sections are retained by a system of shoulders and ramps that has proven successful in other nozzle programs.

- Movable Assembly

The housing for the movable assembly consists of a cylindrical section flaring out to a conical shell. To this housing is fastened a triangular-cross-section torque box which distributes the actuation loads into the housing. The cylindrical section also carries the O-ring seal. Thrust pins supported from rigid arms anchored in the torque box form the movable-assembly pivot axis, accurately located concentric to the spherical diameter.

Gas and mechanical loads on the movable assembly are uniformly distributed except for minor displacement during vectoring. These loads are reacted by two concentrated loads at the bearing pins. The torque box serves to distribute the effects of the concentrated loads into the movable housing assembly. The actuator bracket for the movable assembly is welded to the housing; it is designed to distribute the actuation loads into the torque box.

The housing is primarily deflection-limited; therefore, 6061-T6 aluminum, a moderate-strength material, was chosen. In a deflection-limited component, there is no weight advantage of aluminum over steel, since the modulus-to-density ratio is the same. However, aluminum is preferred over steel because of its greater thickness, which makes fabrication and handling easier.

The exit cone is primarily silica-phenolic with a fiberglass outer wrap, since little erosion advantage was found for costlier materials. Graphite cloth is used just downstream of the split line since particle impingement would cause excessive erosion of silica in this area during vectoring. The exit cone is bonded into the movable section housing with a large bonding area provided to ensure integrity. The temperature of the bond surface at the end of firing is well below acceptable levels.

- Gimbal Ring Assembly

The gimbal ring assembly consists of a ring and two sets of plane bearings on axes 90 degrees apart. The ring is a weldment in which all openings are reinforced with increased section thickness to compensate for local loss of section properties. It is loaded by two concentrated loads and reacted by two concentrated loads. It is thus subjected to both bending and torsion, of which bending is the major factor. For this reason, the rectangular cross section is placed with the major

dimension in the axial direction, which is the direction of the forces which cause bending. Eccentric loading would exaggerate the torsional effects, so care had been exercised to load the ring through the center of the section. The ring is designed to limit deflections and satisfactorily carry the loads imposed on it. Excessive deflection of the ring, which would move the movable housing upstream, would tend to reduce clearances in the split line and possibly increase friction torque.

There is no superiority of aluminum vs steel on the basis of weight since the gimbal ring is deflection-limited. However, an aluminum gimbal ring with equal weight and deflection would be more bulky and require more space. Hence, 4130 steel in the normalized condition was chosen as the gimbal ring material.

The bearings are all plane journals. The bearing-friction torque is minimized by using the smallest journal diameter consistent with structural requirements. The bearings operate on hardened surfaces and are lubricated by surface treatment and solid lubricants.

The gimbal-ring-bearing thrust pins are fixed in the structural support arm from both the inlet and movable section housings. This support, together with the placement of the bearing surfaces in the gimbal ring (straddle mount) minimizes the bending loads in the thrust pin and assists in controlling deflections in the gimbal ring.

The steel thrust pins are fixed (pinned) to the aluminum structural support arms from both inlet and movable housings, and there is no relative motion during vectoring. The case-hardened thrust pins are supported in the gimbal ring with through-hardened steel bushings which are, in turn, keyed to the steel gimbal ring. Since the materials involved in the bearings are all steel, there is essentially no variation in bearing fit (which might otherwise cause high friction due to temperature differences).

- Split Line and Seal Design

Although supersonic split lines should be easier to protect than subsonic split lines, careful attention was given to the gas between the inlet and the movable assembly. The split-line gaps between the plastic components are based on both Minuteman and Dyna-Soar experience, and are sized to accommodate thermal growth and particle contamination without undue restriction of motion.

In addition, the split line is treated with a combination of fillers which ensure split-line durability and control of actuation torque. The fillers act as a barrier to gas circulation in the split line. Since the gases cannot penetrate, propellant contaminants cannot cause friction drag. Lack of gas flow also alleviates split-line erosion. Heat input into the split line is also minimized, thus controlling thermal growth and heat flow to the seal.

The primary filler is silicone rubber molded into the split line. The silicone rubber meets the following filler objectives:

1. Ablation-resistant
2. High temperature capacity
3. Low thermal conductivity
4. Low spring rate and thus does not affect torque because of swelling
5. Easily applied
6. Does not require any retention device since it is molded to a final shape and cured in place

The secondary filler is zinc chromate which is packed into the recess in the movable-assembly split-line insulation insert.

The third split-line filler is a silicone grease which is packed around the O-ring and into the residual clearance of the entire split line. This material is an excellent high temperature lubricant, it has excellent storage characteristics, and it is chemically compatible with the associated components. The seal design was based on considerations of material, size, location, installation dimension requirements, thermal environment, lubrication, and other factors, all of which have been subjected to extensive analysis and test over several years at ARDE-Portland.

(b) Design, Development, and Fabrication

The Motor B nozzle program was conducted at ARDE-Portland under the over-all technical direction of Rocketdyne. The actual program was divided into three major phases; Design, Development and Fabrication. The program plan schedule is illustrated in Fig. 274.

OVERALL PROGRAM SCHEDULE

7/20/64

DESIGN PHASE	1963 S	O	N	D	1964 J	F	M	A	M	J	J	A	S	O	N	D	1965 J	F	M	A	M	J	J	A	S	O	N	D
Basic Nozzle-Layout & Analysis	X	—	—	—	Δ																							
- Materials & Process Spec	X	—	—	—	Δ																							
- Detail Drawings	X	—	—	—	Δ																							
Actuation - Mechanical Design		X	—	—	—	—	Δ							TANK DESIGN			X	—	—	X								
- Electrical System	X	—	—	—	—	—	Δ																					
- Specifications	X	—	—	—	Δ																							
FABRICATION PHASE																												
Tooling				X	—	—	—	—	—	Δ	-	-	-	-	-	-	-	-	-	-	X								
Procurement				X	—	—	—	—	—	—	—	—	—	—	—	—	—	—	—	—	—	—	—	—	X			
Fabrication & Checkout						X	—	—	—	—	—	—	—	—	—	—	—	—	—	—	—	—	—	—	—	—	—	X
DEVELOPMENT PHASE																												
Actuation System Bench Test											X	—	—	—	X													
Motor Firing Test Analysis														X	—	—	—	—	—	—	—	—	—	—	—	X		
Minor Redesign														X	—	—	—	—	—	—	—	—	—	—	—	X		
REPORTING	X	-	-	-	-	-	-	-	-	-	-	-	-	-	-	-	-	-	-	-	-	-	-	-	-	-	-	X

Δ Completed
X Rescheduled

Figure 274. TVC Program Schedule

CONFIDENTIAL

587

CONFIDENTIAL

○ Design Phase

In initial efforts by ARDE-Portland to define the nozzle shape, a circular contour was fitted to the envelope specified in NA5-80014A. This resulted in too large an exit-plane angle and excessive losses. A modified, circular arc contour with a conicyl section downstream of the throat radius was then used in an attempt to reduce the exit plane angle. On completion of this design, a preliminary weight and gas-dynamic study showed that the design was still too heavy and the performance was still marginal. A third grid layout was prepared (for a Foelsch contour nozzle), which resulted in reduced weight and improved performance. Layouts were again compared against dynamic studies, including the nozzle in a null and in several vectored positions. Oversized layouts of the split line were prepared at several vectors. Although this design represented a weight optimization, it would not meet the requirements of the revised specification. Upon completion of the detailed weight, cg, and moment of inertia calculations for the above contour, a parametric study was made which compared nozzle efficiency to weight for several contours. This data was submitted to Rocketdyne by ARDE-Portland for use in stage optimization and impulse-to-weight studies. In trying to obtain a minimum length nozzle with maximum Cf, it was indicative that a modified Rao nozzle contour should be considered, and, since Rocketdyne already possessed a computer program of this contour, Rocketdyne performed this phase of the study.

(C) Based on the over-all performance characteristic study, using the modified Rao-type contour, a net loss (with lag losses considered) was obtained using an initial nozzle expansion angle of 24.4 degrees. This loss in nozzle thrust coefficient is approximately 4.3%. Based upon the Rao contour, Rocketdyne supplied ARDE-Portland coordinates so that mechanical design could proceed. A new layout drawing was prepared for the semi-optimized Rao contour as follows: initial turning angle, 24.4 degrees; exit angle, 11 degrees; area ratio, 25:1; length from throat, 28.04 inches. Further investigation into gas dynamics indicated that the TVC duty cycle described in the Rocketdyne specification would cause the nozzle to vector in only one plane. At ARDE-Portland's suggestion, this was changed to better demonstrate the omni-axis capability of the nozzle and to obtain a more evenly-distributed erosion.

Having established the nozzle contour, the next major effort was associated with determining the forces and torques acting on the nozzle at the full-vector, four-degree condition. This was accomplished by determining the peripheral pressure distribution on the nozzle contour and integrating this pressure for determining the forces and torques. Only internal forces were considered, which simulated a vacuum condition. The following paragraphs cover the deflection and stress analysis of the gimbaled nozzle.

The methods of analysis used on this nozzle were based, for the most part, on classical stress analysis theory. The solutions for stresses and deflections in such parts of the structure as the exit-cone torque box, the gimbal rings and other ring problems, were derived from minimum-strain-energy theory. Those parts of the structure which are rotationally symmetric and are loaded by axisymmetric loads, were analyzed as beams on elastic foundations using discontinuity concepts at points of change in geometry or loading. Thermal stresses were determined in critical areas assuming plane strain.

Where required, simplifying assumptions were made to facilitate solutions. In all instances, the assumptions made were so that the stresses and deflections determined were conservative.

(C) The following design loads and criteria were used in the stress analysis of this nozzle:

Chamber pressure, psia	P_c = 1015
Vector angle, deg	$\pm$ 4
Side vector force, lb	2852
Actuator stall load, lb	1456

The nozzle structure was treated as a system of three rings connected by two sets of fittings. An interaction analysis was performed to evaluate the redundant forces at the connecting points of the fittings and the rings. These redundants were found for five unit-loading conditions:

1. Net axial pressure load on movable housing
2. Pitch actuator load
3. Yaw actuator load
4. Side vector force, pitch plane
5. Side vector force, yaw plane

The solutions for these unit-loading conditions were multiplied by the corresponding actual loads and combined to give the critical loads for each component of the structure. These loads were then used to determine maximum internal stresses and critical deflections.

The results of stress analysis indicate that this structure will adequately support the imposed loads. The calculated stresses and deflections are all within the limitations of the material strengths and the design criteria, which specify a 1.25 factor of safety on the material ultimate strength.

(C) Concurrent with the gas dynamics and stress analyses, the preliminary thermal analysis was performed on the 24.4-degree initial-angle, truncated Foelsch nozzle configuration. This analysis was later modified for the Rao configuration. The temperature distribution throughout the nozzle is well within the temperature capabilities of the materials used (see Figs. 275, 276, and 277). All of the thermal analyses were conducted by one-dimensional transient heat conduction analysis. The wall geometry, the nature of materials used, and their orientation make the nozzle wall amenable to this type of solution. The sections analyzed are in the most critical areas of nozzle design and are oriented to approximate the heat-flow path through the nozzle wall.

The design analysis and synthesis of the electrohydraulic servo control system for the TVC system is summarized below.

The block diagram of the system is shown in Fig. 278. There are two identical systems per nozzle, one for pitch and one for yaw actuation. Each system consists of an amplifier, a servo actuator, and a position transducer.

The operation sequence is as follows:

1. The amplifier compares the input command signal with the feed-back transducer signal and the difference, or error signal, is fed to the driver portion of the amplifier. The driver amplifier produces a current proportional to and in the direction dictated by the error signal. This current is fed to the servo valve.
2. The servo valve allows hydraulic-fluid flow to the actuator, the magnitude and direction of which is determined by the input current.
3. The actuator drives the nozzle in proportion to the hydraulic fluid flow.
4. The position transducer measures the nozzle position and develops a voltage proportional to position. This voltage is sent to the amplifier.
5. This cycle continues until the transducer signal is equal to the input signal so that the error signal becomes zero.

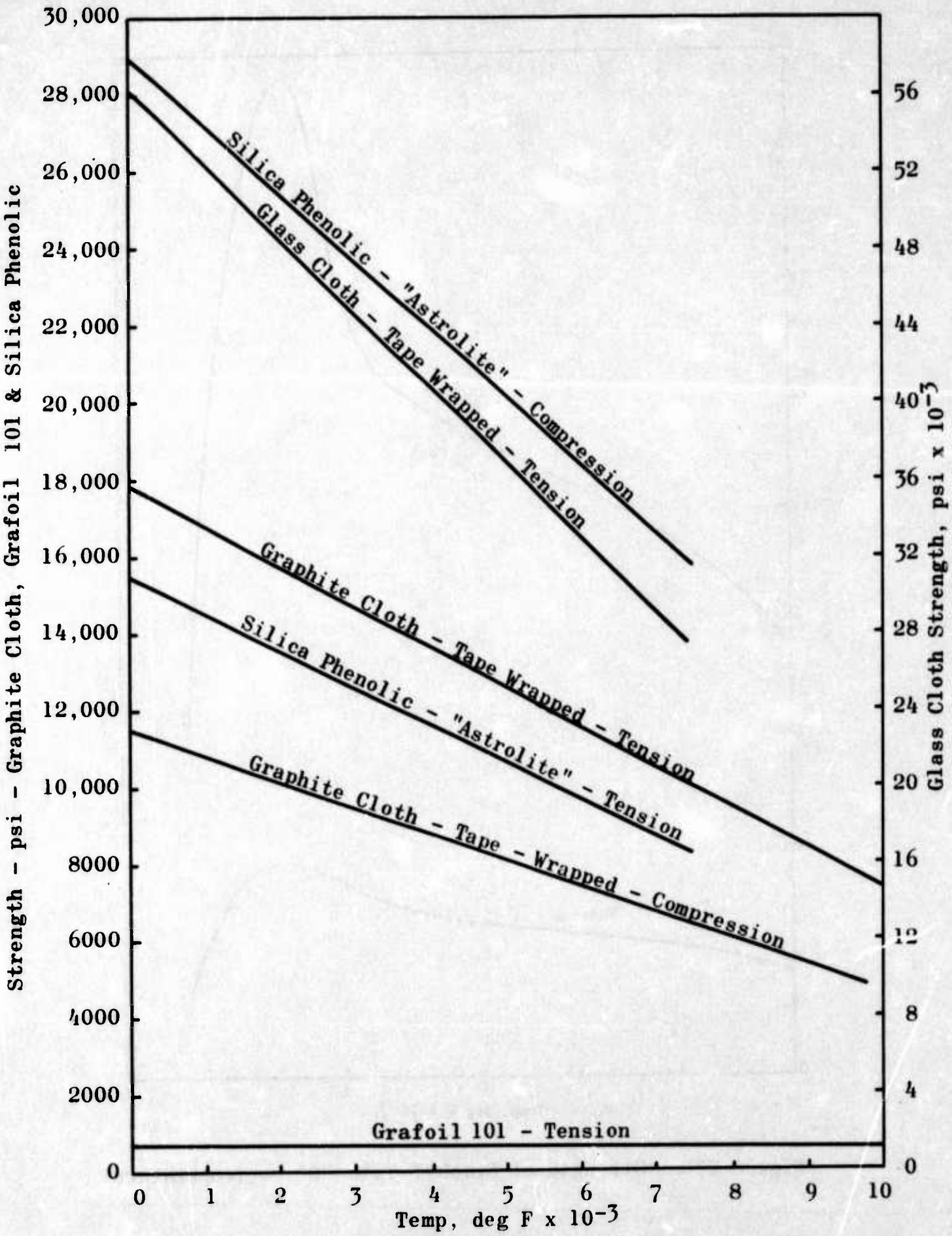


Figure 275 Strengths of Plastics vs Temperature

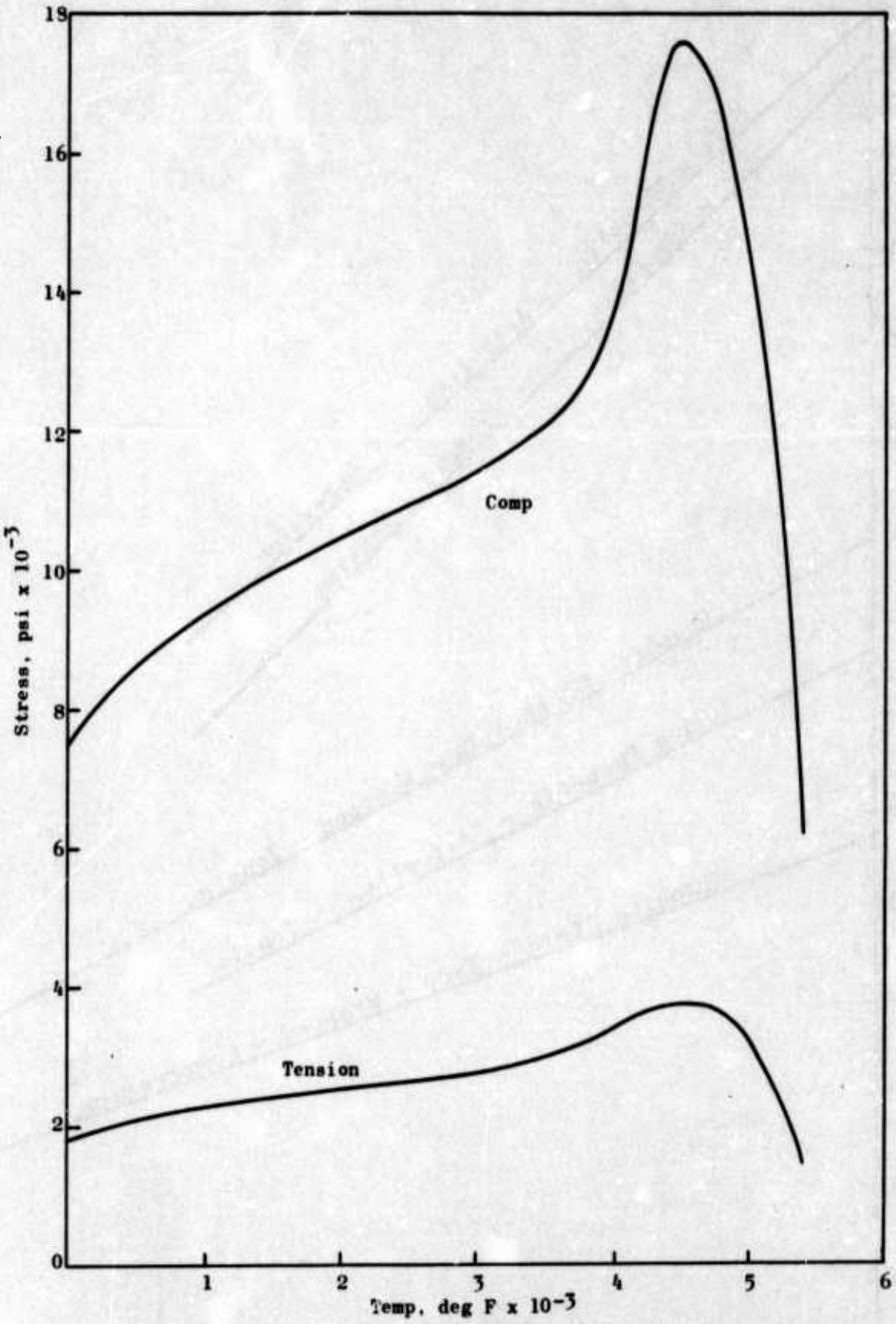


Figure 276. Strength of Graph-I-Tite "G" vs Temperature

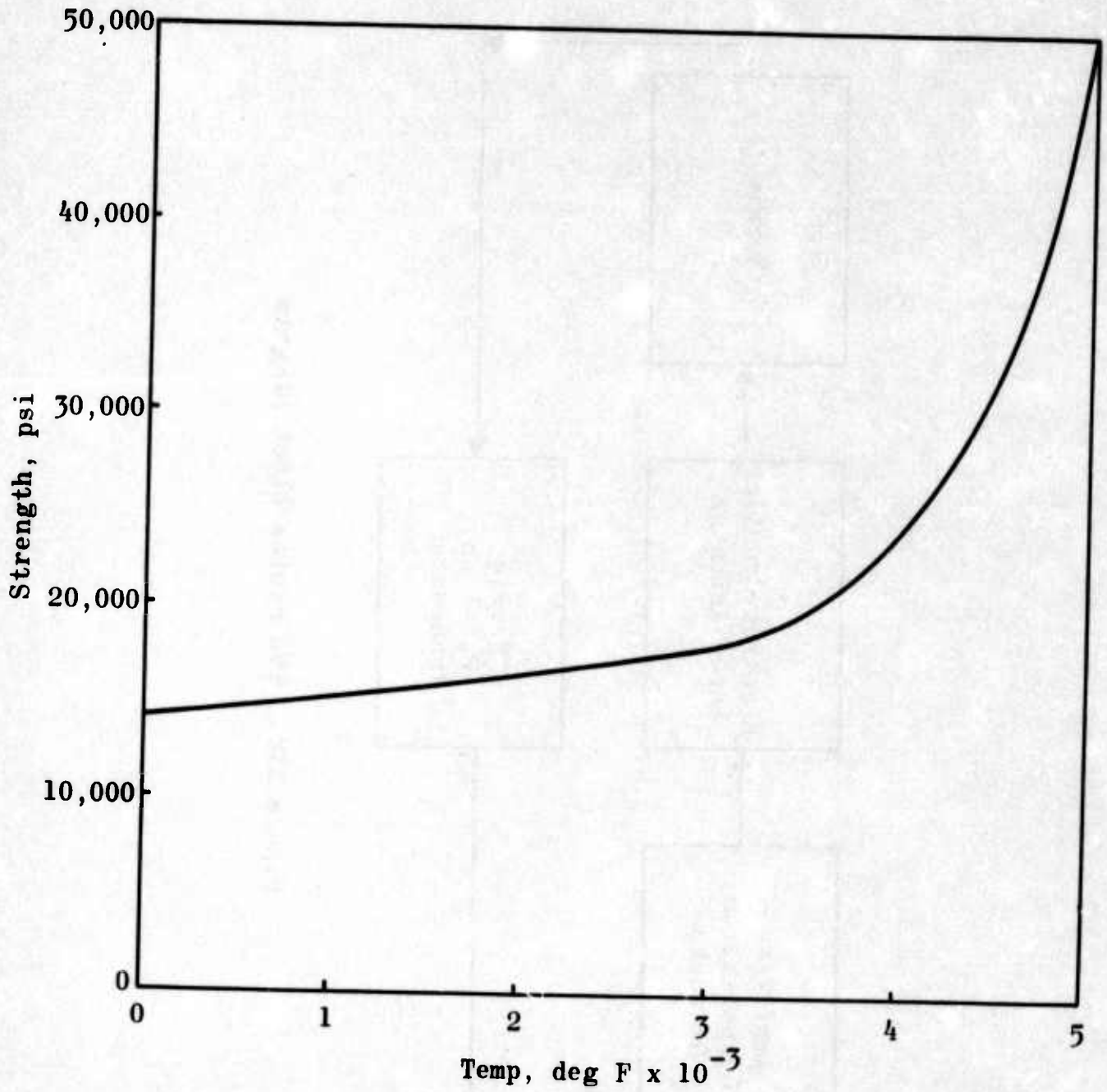


Figure 277. Strength of Pyrolitic Graphite vs Temperature

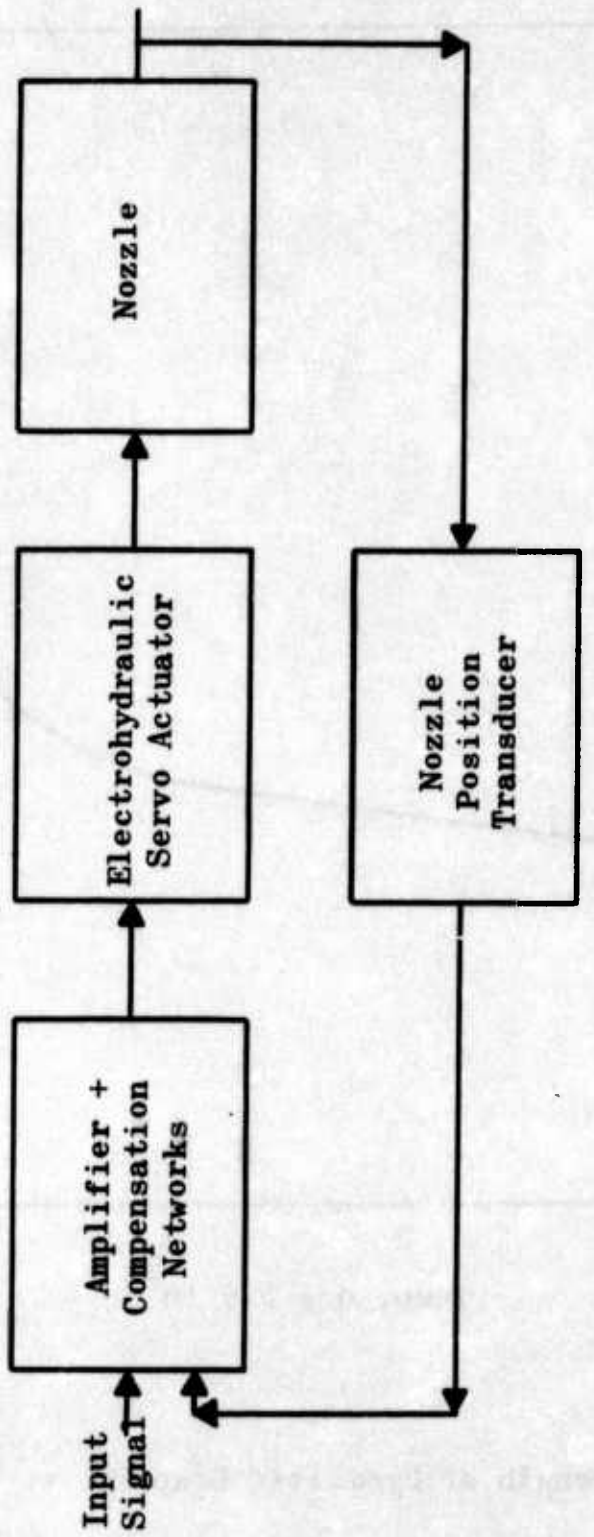


Figure 278. TVC System Block Diagram

The components utilized are well within the state of the art, so that the system as designed is an economical and reliable development.

The amplifier is an all-solid-state unit; it produces a current proportional to the difference between the input signal and the feedback signal. Also included in the amplifier are the compensation networks for the system.

The servo actuator consists of a flow-control servo valve mounted on a linear hydraulic actuator. The servo valve produces a fluid flow proportional to the input current. The fluid is fed to the actuator which produces a velocity proportional to fluid flow rate.

This is a dual-element potentiometric unit. One element is the servo loop, and the other is telemetered to recorders to determine nozzle position.

As determined by the analysis, the system components must meet the requirements shown in Table LXXIX.

○ Development Test Phase

After completion of design of the actuation and control system, it was necessary to test the over-all system. To do this, it was necessary to design and fabricate a nozzle simulator. The design approach used in this simulator was:

1. An air spring was used to simulate the aerodynamic torque; load on the spring is easily adjustable by varying the initial air pressure.
2. Coriolis effect is simulated by oil flow through the orifice; Coulomb friction is simulated by oil flow through the relief valve; the oil is driven by a piston attached to the simulator; the constants may be adjusted by varying the relief-valve setting for Coulomb friction, and the orifice size for Coriolis effect. Inertia is simulated by a weight attached to the nozzle simulator, and is adjustable by moving the weight.

TABLE LXXIX

TVC COMPONENT REQUIREMENTS

Angular Position Transducer:	
Range	$\pm 4^{o}$
Output	1 v/o = 57.3 v/rad
Resistance	7.5 K Ω
Static error band	± 0.9%
Frequency response	± 1% 0 to 30 cps
Amplifier:	
Output	± 10 ma
Load	two 1500 Ω, 7-Henry coils in parallel
Input	± 4 volts
Transconductance gain	20 ma/v DC
Input impedance	100 K Ω min
Transfer-function command signal, input-to-output current	$+20 \text{ ma/v} \times \frac{\frac{S}{(15}+1)}{\frac{(S}{4}+1)} \times \frac{\frac{S}{(30}+1)}{\frac{(S}{2000}+1)}$
Feedback signal input-to-output current	$+20 \text{ ma/v} \times \frac{\frac{S}{(30}+1)}{\frac{(S}{4}+1)} \times \frac{\frac{S}{(30}+1)}{\frac{(S}{2000}+1)}$
Accuracy at null signal	0.010 volts
Gain stability at null	$\frac{+50\%}{-10\%} \times 20 \text{ ma/v}$
Servo Actuator:	
Operating pressure	2000 ± 200 psig
Actuator area	0.73 sq in.
Output	0.94 in./sec/ma
Stroke	1.25 in. total
Rated signal	± 10 ma
Resistance/coil	1500 Ω
Inductance/coil	7 Henries
Hysteresis	3% of rated current maximum

TABLE LXXIX
(Continued)

Resolution	0.5% of rated current maximum
Threshold at null	0.5%
Null shift, temporary	2.5%
Null shift, acceleration	3%/15g
Null shift, PS	1%/10% PS variation
Null shift, back pressure	0.5%/5%
Leakage, external	zero
Leakage, internal	0.10 Gpm
Frequency response	± 3bd 0 to 120 cps
Phase shift	90° maximum at 120 cps
Pressure gain, signal to develop 90% of PS	3%

Test set-up involving the hydraulic power supply and its associated hardware, the electrical power supply, and the monitoring and recording equipment, was completed and testing initiated. Initial development run-through with the full system indicated a low-frequency oscillation approaching 0.038 inch. This appears to have been connected with the looseness of the connecting pins. These were reworked for future testing. During additional testing of the system, the runs incorporated both step function and the program-review cycle in order to give an indication of system transient performance. The computed responses of the electro-hydraulic, omni-axis TVC system presented in the design analysis report closely correspond with the actual results demonstrated under the development testing. Another problem that was found in the development testing was in the program tape, in that it contained spikes at each point where the tape was spliced, and it was spliced at each change in signal; therefore, the tape does contain many spikes. When the program was stopped, ARDE was seeking bids from outside sources for corrections of the spikes in the program tape. In spite of the fact that the reports were not completed on the development testing, it is significant to recognize that all the testing had been completed and that each component had been verified or corrections recommended to correct any problems indicated during the development testing. Therefore, the two systems that were delivered to RPL should have response in accordance with the Rocketdyne specification.

(C) The Motor B final design consisted of a contour of 70% bell (Rao configuration) with the characteristics shown in Table XXC.

TABLE XXC

MOTOR B NOZZLE DESIGN

(C)

Throat area, sq in.	21.846
Exit area ratio	25:1
Length, in.	28.04
Long-to-throat radius ratio	2.0
Initial wall angle, deg	24.4
Exit long angle, deg	11.0
Theoretical thrust coefficient in vacuum	1.867
Half angle correction factor	0.988
Over-all efficiency factor	0.960
Estimated throat erosion rate, in./sec	0.00086

The true test of the Motor B nozzle and actuation system will be under static firing which will be conducted at RPL on the two test-weight nozzle configurations.

(C) A breakdown is available for the flight expansion-ratio system and test expansion-ratio system included in Tables XXCI and XXCII. In Table XXCI the actual weights for nozzle No. 1 are compared to those of design data. The test-weight system's self-contained weight total was 66.201 pounds, and the nonactuated actual weight turned out to be 66.5 pounds fully instrumented. With this indication of design vs actual weight, Rocketdyne feels that the completed 25:1 expansion ratio nozzles would have fallen within the nominal goal of over-all weight.

(4) Igniter

In designing the Motor A igniter, the requirements of Motor B ignition were also considered. Of the original 10 igniter tests, 4 were reserved for design verification. Two of these 4 were for temperature cycling and vibration testing to Motor B specifications.

(C) These two igniters (one each with 0.40 inch and 0.60 inch length grains) were fabricated and subjected to three temperature cycles between -75 F and 170 F and vibrational testing.

TABLE XXCI

WEIGHT BREAKDOWN, TEST CONFIGURATION TVC SYSTEMS

(C)

	J3135 Self-Contained Pressurization	D3116 Nonactuated Actuals
Inlet Assembly		
Pyrolytic Graphite	3.536	3.536
Grafoil	2.009	2.009
Graphite	8.930	8.930
Plastics	7.580	7.580
Elastomer	0.158	0.158
Metal/Aluminum	4.164	4.164
	26.377	26.377
Movable Assembly		
Plastics	15.750	15.750
Elastomers	0.073	0.073
Metal/Aluminum	6.032	6.032
	21.855	21.855
Gimbal Ring Assembly		
Ring/Steel	5.620	10.875
Actuator Bracket/Aluminum	0.115	0.115
Inlet Arms/Steel	1.360	1.360
Inner Arms/Steel	0.724	0.724
	7.819	13.074
Nozzle Total	56.051	61.306
Actuation System		
System Components, Fluid, and Accessories	8.040	---
Disconnect Bracket	2.110	---
Fixed Links	---	1.832
Actuation System Total	10.150	1.832
TVC System Total, lb	66.201	63.138
Instrumentation Nozzle S/N 1		3.36
Actual Total Nozzle S/N 1		66.5

TABLE XXCII

(C) FLIGHT CONFIGURATION TVC SYSTEMS WEIGHT BREAKDOWN

	Self-Contained Pressurization J3190	External Pressurization
Inlet Assembly		
Pyrolytic Graphite	3.536	3.536
Grafoil	2.009	2.009
Graphite	8.930	8.930
Plastics	7.580	7.580
Elastomer	0.158	0.158
Metal/Aluminum	4.164	4.164
	26.377	26.377
Movable Assembly		
Plastics	35.518	35.518
Elastomers	0.073	0.073
Metal/Aluminum	6.032	6.032
	41.623	41.623
Gimbal Ring Assembly		
Ring/Steel	5.620	5.620
Actuator Bracket/Aluminum	0.115	0.115
Inlet Arms/Steel	1.360	1.360
Inner Arms/Steel	0.724	0.724
	7.819	7.819
Nozzle Total	75.819	75.819
Actuation System		
Fluid Tank	1.7	---
Fluid in Tank	4.8	---
Fluid Tank Bracket	1.54	---
Gas Generator Brackets	1.34	---
Relief Valve Brackets	0.15	---
Hot Gas Filter & Lines	1.3	---
Disconnect Bracket	---	2.11
System Components, Fluid and Accessories	8.04	8.04
Actuation System Total	18.87	10.15
TVC System Total, lb	94.689	85.969

Vibrational testing was conducted according to Procedure 1 of MIL-R-25534A with the exception that all testing was at ambient temperatures. The initial portion of this testing was at ambient temperatures. The initial portion of this testing consisted of a resonant frequency survey along the igniter longitudinal axis in the frequency range from 15 to 500 cps. An apparent resonance was found at approximately 20 cps. Thus, according to the specification, 30 hours of endurance testing at this frequency with a 0.1 double amplitude displacement was begun. After approximately three hours of vibration, there was a failure in the test equipment (shaker mount failed). Upon examination of the igniters it was observed that the mylar tape covering the internal surface of the igniter basket containing 0.6 inch grains was torn. An appreciable amount of pyrotechnic powder existed in the plastic bag that had been placed around the igniter. It appeared that the attrition resulted primarily from the movement of the pyrotechnic grain over the edges of the basket perforations which were exposed to the grain movement by the failure of the mylar liner. A design feature to increase the pyrotechnic charge weight, without changing the igniter hardware, inadvertently led to the grain movement and a resulting mylar failure. In this design, the space needed for the additional charge weight was filled with flexible polyurethane spacers, per AMS-3570 During vibration, the spacers compressed and took a permanent set, allowing an excessive amount of freedom for longitudinal grain travel. Disassembly of these igniters showed that of the 12 0.6-inch grains, 7 were cracked; of the 18 0.4-inch grains, 4 were cracked.

To minimize grain travel during vibration, alleviating grain crackage, and reduce attrition, the polyurethane spacers in the igniter aft end were replaced with silicone sponge spacers. In addition, a specified compressive loading was required to be imposed on the grain spacer assembly. This was accomplished by adding sponge spacers to the charge assembly until the required load to seat the intermediate charge retaining cup in the loaded basket was attained. This specified load range was determined theoretically, with the loading magnitude being enough to eliminate any appreciable grain motion during vibrational testing.

Results from these tests, as shown in Fig. 279, indicated that the maximum amplification encountered during longitudinal vibration was 3. This occurred at a double amplitude of -1 and at a frequency of 20 cps. Solving for the g loading it was found that:

$$a = w^2 \chi \sin wt$$

a = maximum value at $\sin wt = 1$

and

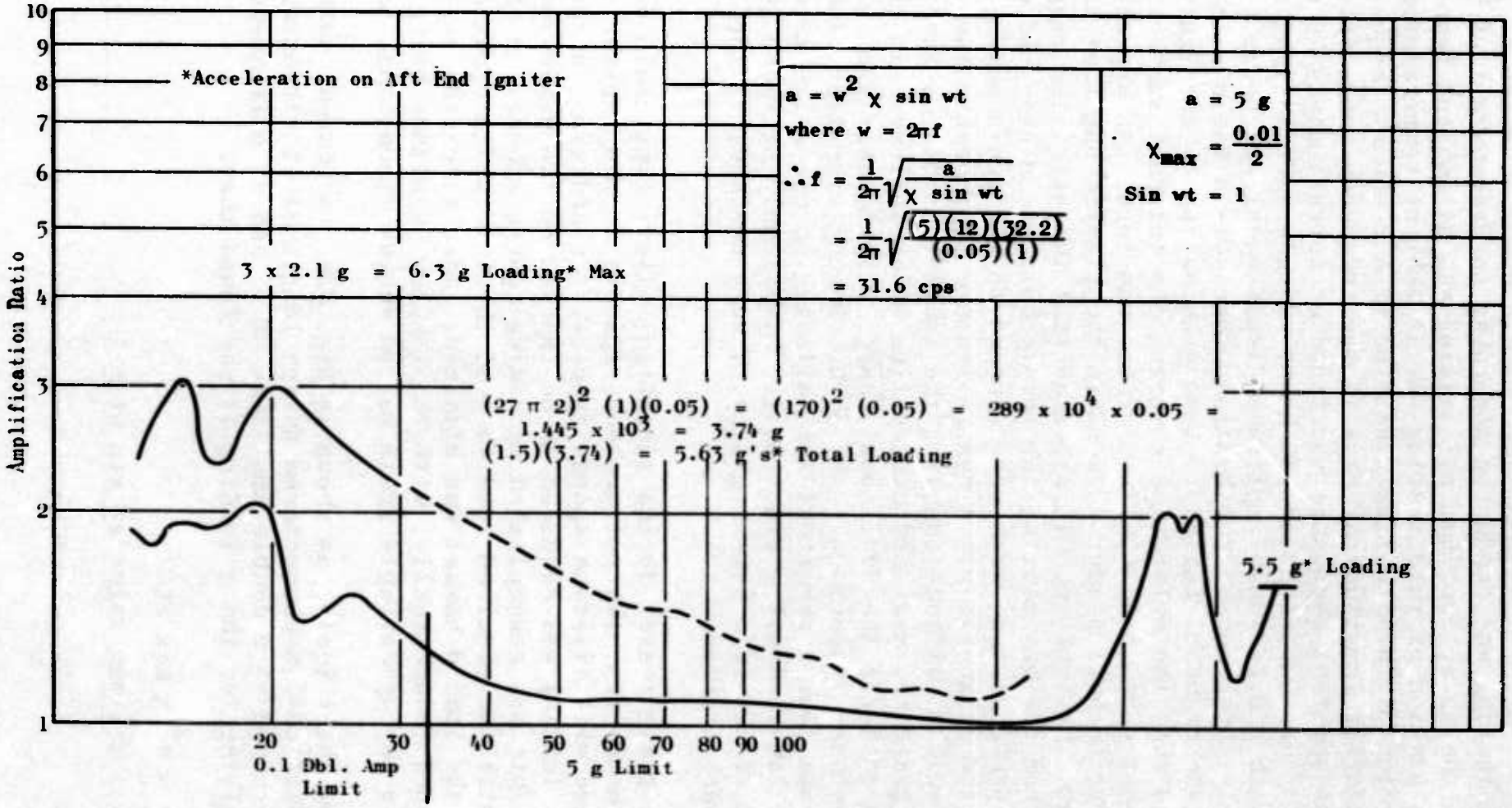


Figure 279. Results of Temperature Cycling and Vibration Tests

$$w = 2\pi f$$
$$= 2\pi 20 = 40\pi$$
$$\chi = \frac{0.1}{2} = 0.05$$

Thus,

$$a = (40\pi)^2 (0.05)(1)$$
$$= 0.795 \times 10^3 \text{ in./sec}^3$$
$$= \frac{0.795 \times 10^3}{12 \times 32.2} = 2.06 \text{ g}$$

The maximum force of the grains on the basket and vice versa, neglecting frictional loses, is:

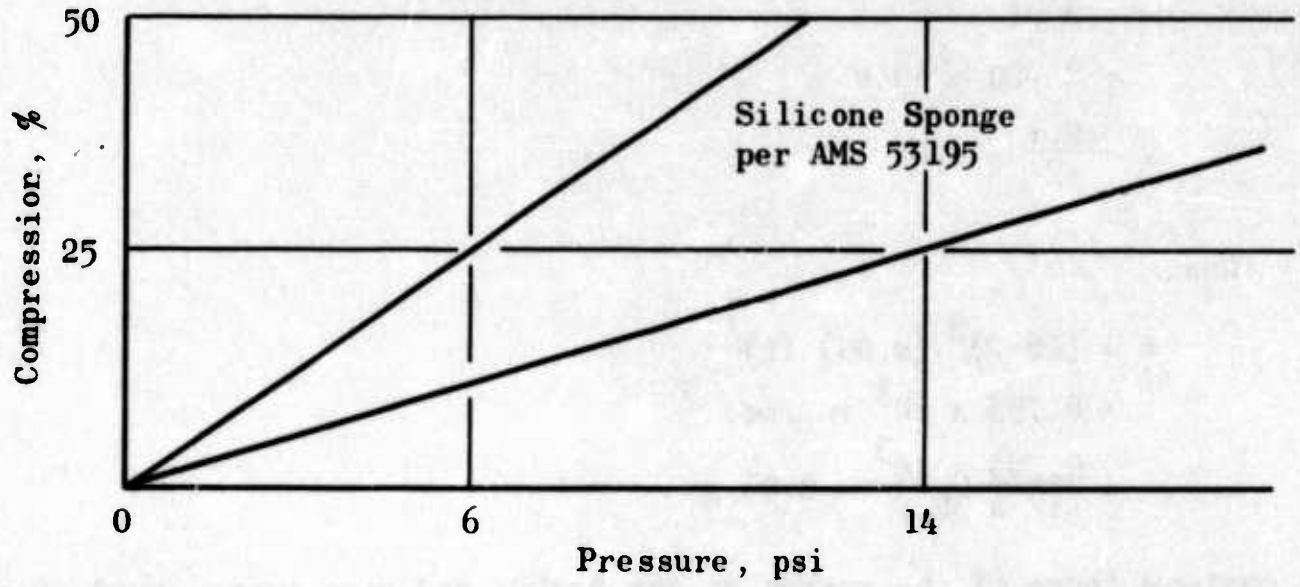
$$F = ma = \left\{\frac{250 \text{ gm}/454 \text{ gm/lb}}{32.2 \text{ ft/sec}^2}\right\} 32.2 \text{ g}$$

$$= 0.551 \text{ g}$$

$$F = 0.551 \, A_{\text{in put}} \left(\frac{A_{AMP}}{A_{\text{in put}}}\right)$$

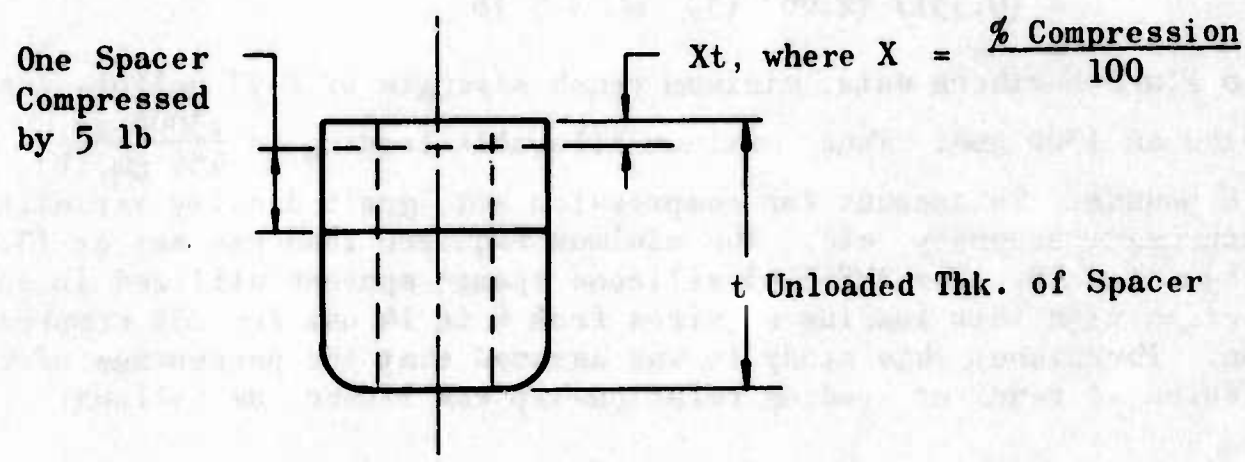
$$= (0.551)(2.06)(3) \approx 3.5 \text{ lb}$$

From Flare-Northern data, minimum crush strength of P-73 pellets was listed as 1300 gms. Thus, maximum allowable loading is $\frac{13000 \text{ gm}}{454 \text{ gm/lb}}$ = 28.6 pounds. To account for compression set, grain density variation, measurement accuracy, etc., the minimum required load was set at $(3.5) \times (1.4) \approx 5.0$ lb. The AMS-3195 silicone sponge spacers utilized in conjunction with this loading requires from 6 to 14 psi for 25% compression. Throughout this study it was assumed that the percentage of compression vs required loading relationship was linear, as follows:



Considering instances of magnitude of the load associated with compression of two, and then three, spacers it was determined what would be upper required load limit.

In the case of 2 spacers, if a load of 5 pounds allows the cup to slightly contact the basket lip when one spacer is installed, the addition of a second spacer should result in the maximum load requirements for two spacers.



The pressure loading associated with 5 pounds on spacers of 1 inch OD x 0.5 inch is 8.5 psi. Thus assuming maximum spacer rigidity, 14 psi for 25% compression:

$$X/8.5 = 25/14$$

$$X = 15.2\%$$

$$Xt = 0.152t$$

Adding a second spacer increases the total sponge spacer thickness to 2 t. This thickness must be compressed to a thickness of t - 0.15 t = 0.85t to seat cup on basket lip. Considering again the most rigid spacers, the required load would be:

$$\frac{(2 - 0.85)\ t}{25} = 0.575 = 57.5\% \text{ compression}$$

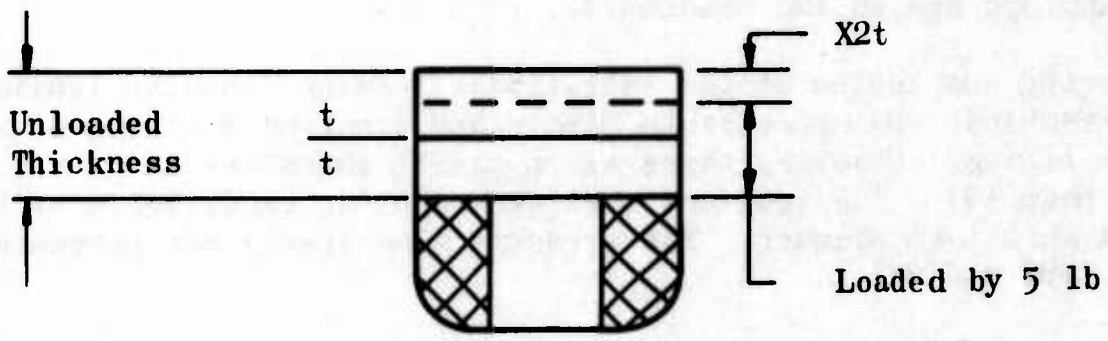
$$L/57.5 = 14/25$$

$$L = 32.2 \text{ psi}$$

$$FL = (32.2)\ (0.589) = 19 \text{ lb},$$

For 0.589 sq in. loading area

For the case of three spacers, the maximum loading occurs when two of the most rigid spacers are compressed by slightly less than 5 pounds and allow the cup to seat on the basket. Thus,



A 5-pound load results in 8.5 psi loading.

Thus

$$X/8.5 = 25/14$$

$$X = 15.2\%$$

Adding a third spacer of rigid material results in an unloaded thickness of 3t which must be compressed to a thickness of 2t - (2t) (0.152) = 1.70t

Thus

$$\frac{(3 - 1.7)t}{3t} = \frac{1.3}{3} \times 100 = 43.3\%$$ compression required. The resulting load is 25/14 = 43.3/L

$$L = 24.3 \text{ psi}$$

and

$$F = (24.3)\ (0.589) = 14.3 \text{ lb}$$

Thus, for the compressive loading, a range from 5 to 19 pounds was specified as required to seat the intermediate charge retaining cup in the loaded basket. To assure that at least two spacers are required for this loading, the length of the phenolic spacer was modified. Two more igniters, one each with 0.40-inch length and 0.60 inch length grains, were fabricated which incorporated this compressive loading requirement. The igniters were subjected to the longitudinal vibrational survey prior to temperature cycling. Following this survey the igniters were subjected to temperature cycling and then once again subjected to vibrational testing. The results of the longitudinal and transverse frequency surveys are shown in Figs. 280 and 281. Resonant frequencies were noted at approximately 370 cps longitudinally and 95, 140 and 350 cps in the transverse.

Following completion of the vibrational testing, the two igniters were disassembled. No appreciable damage had occurred to the grains or mylar lining. However, there was a slight amount of attrition (by weight, less than 1%). The igniters were reassembled, conditioned to 170 F and fired in a test chamber. The pressure-time traces are presented in Figs. 282 and 283.

Checking the development design modification, which requires the compressive loading utilizing the results of the second set of igniter tests, the following minimum load was determined:

$$\frac{A \text{ amplified}}{A \text{ input}} = 2$$

$$A \text{ input} = 5$$

$$F = ma = \left[\frac{(250 \text{ gm}/454 \text{ gm}/1\text{b})}{32.2}\right] 32.2\text{g}$$

$$F = 5.51 \text{ lb}$$

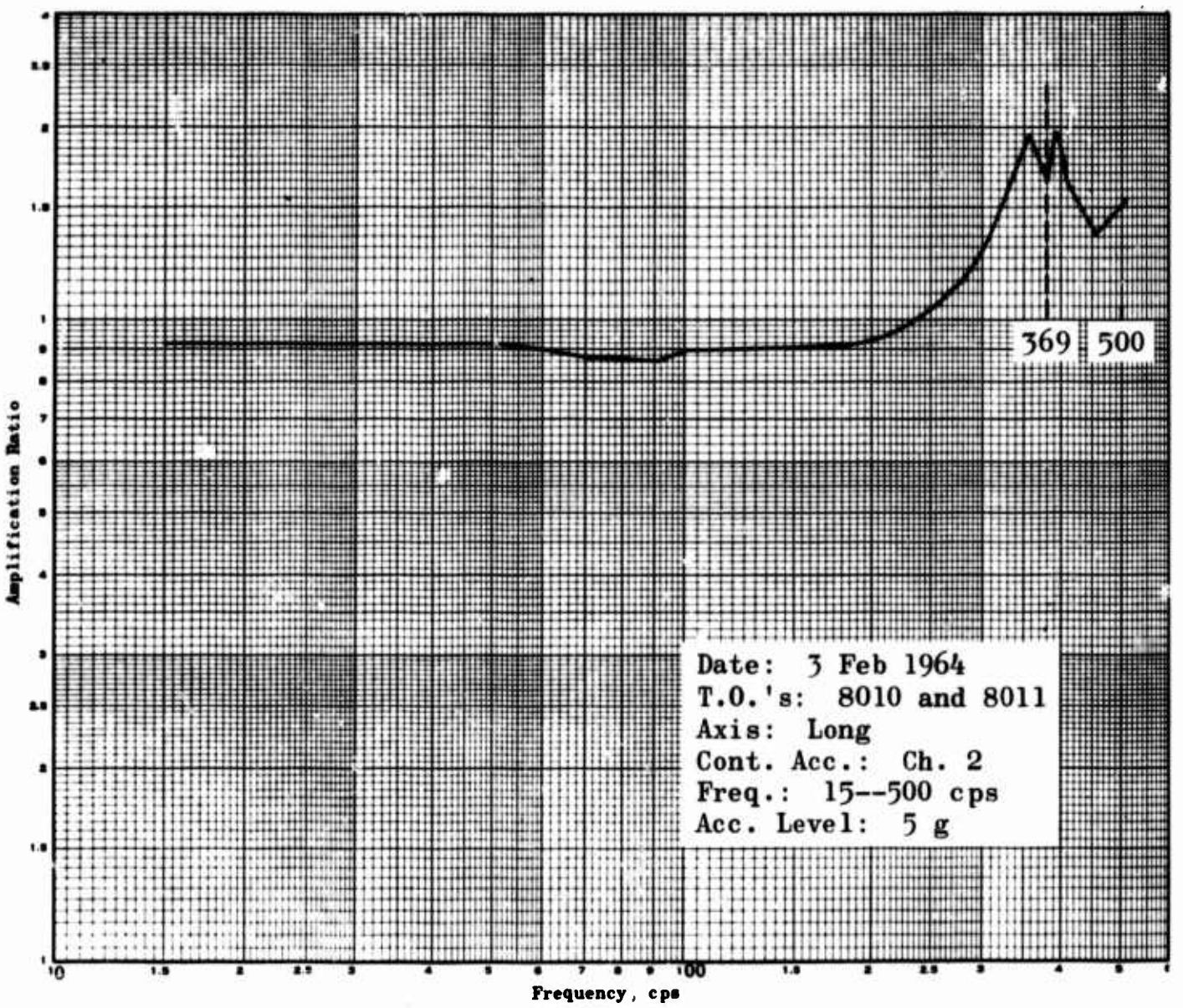


Figure 280. Results of Longitudinal and Transverse Frequency Surveys, Longitudinal Axis

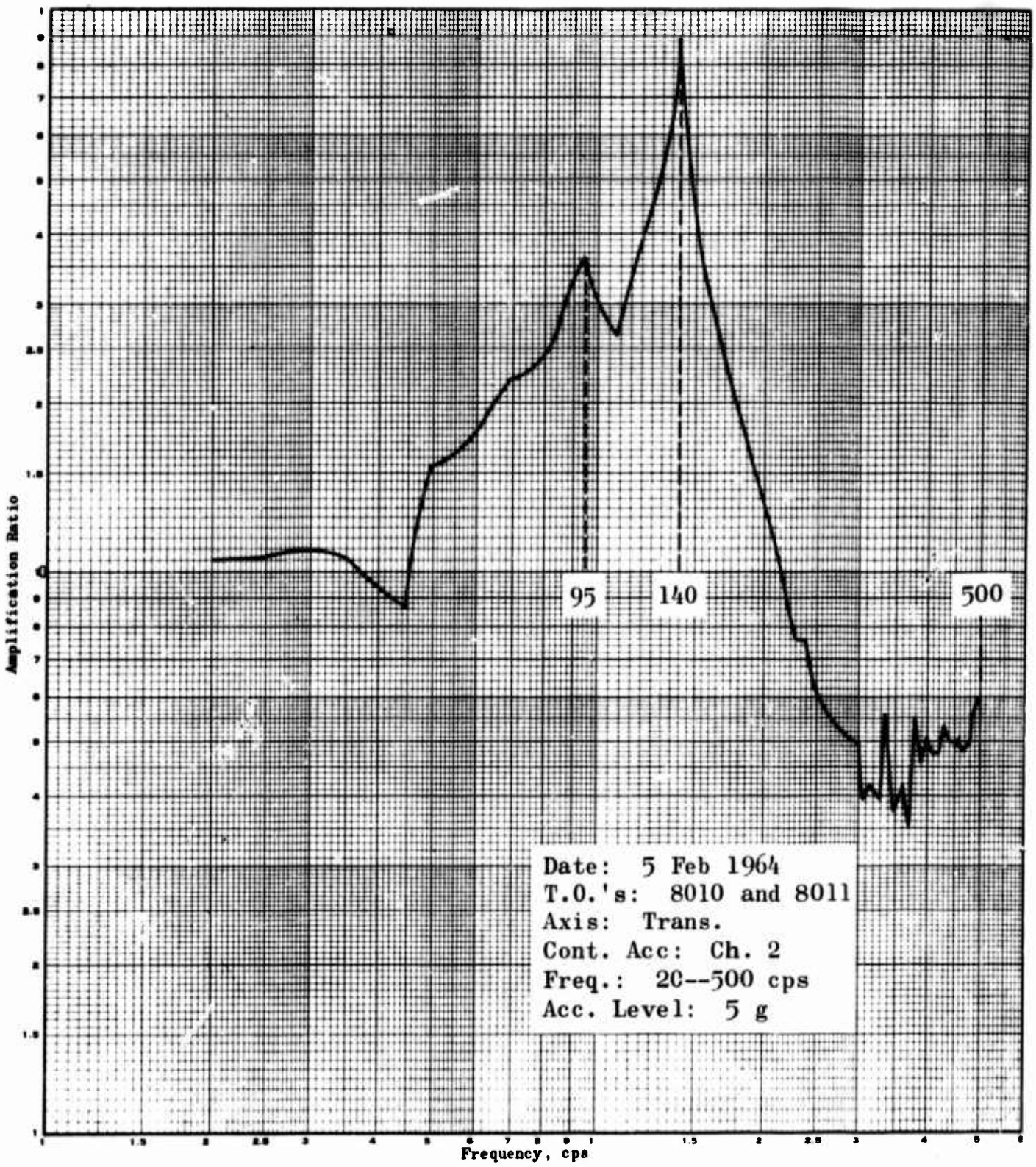


Figure 281. Results of Longitudinal and Transverse Frequency Surveys, Transverse Axis

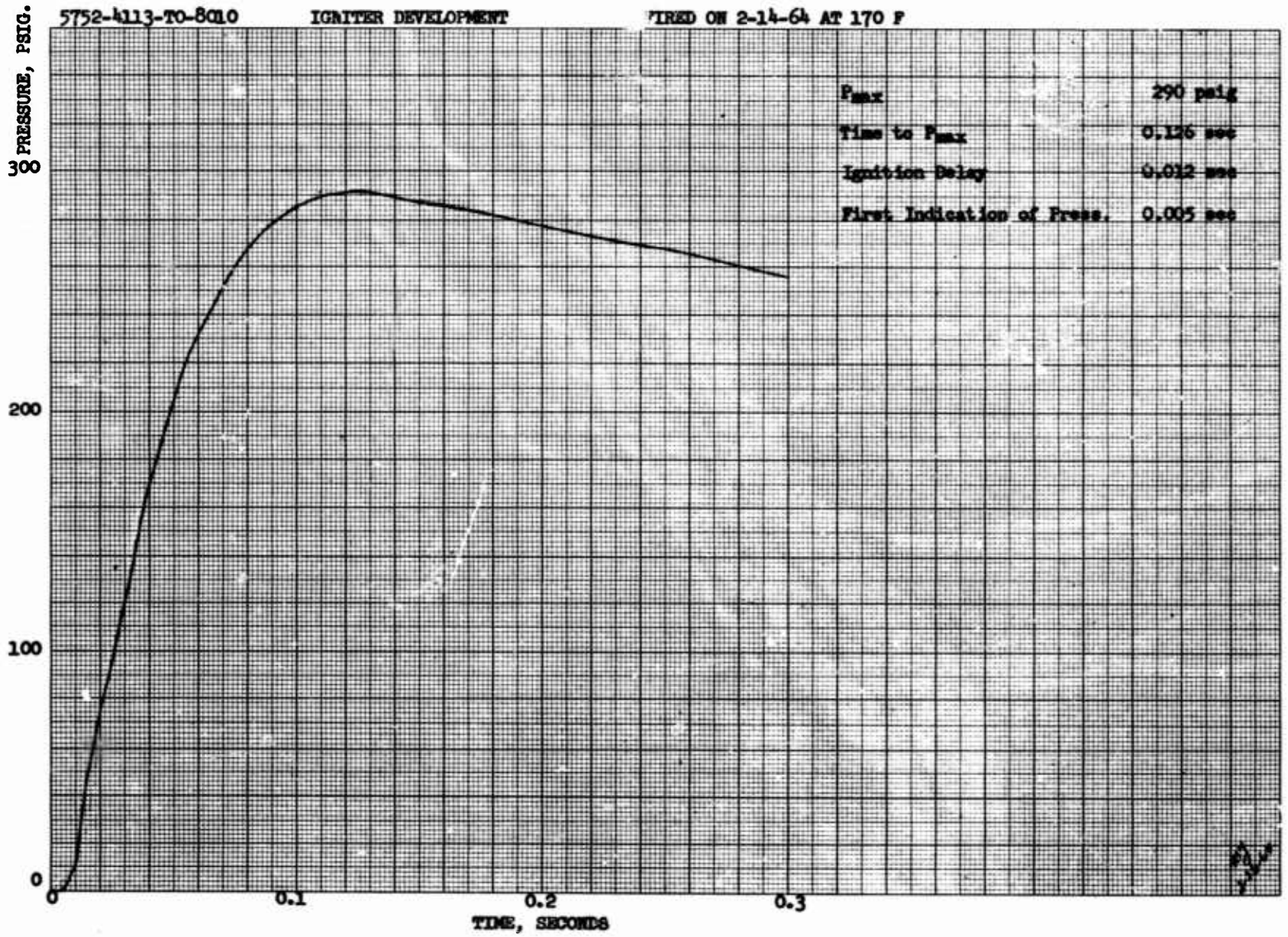


Figure 282. Igniter Development, TO 8010

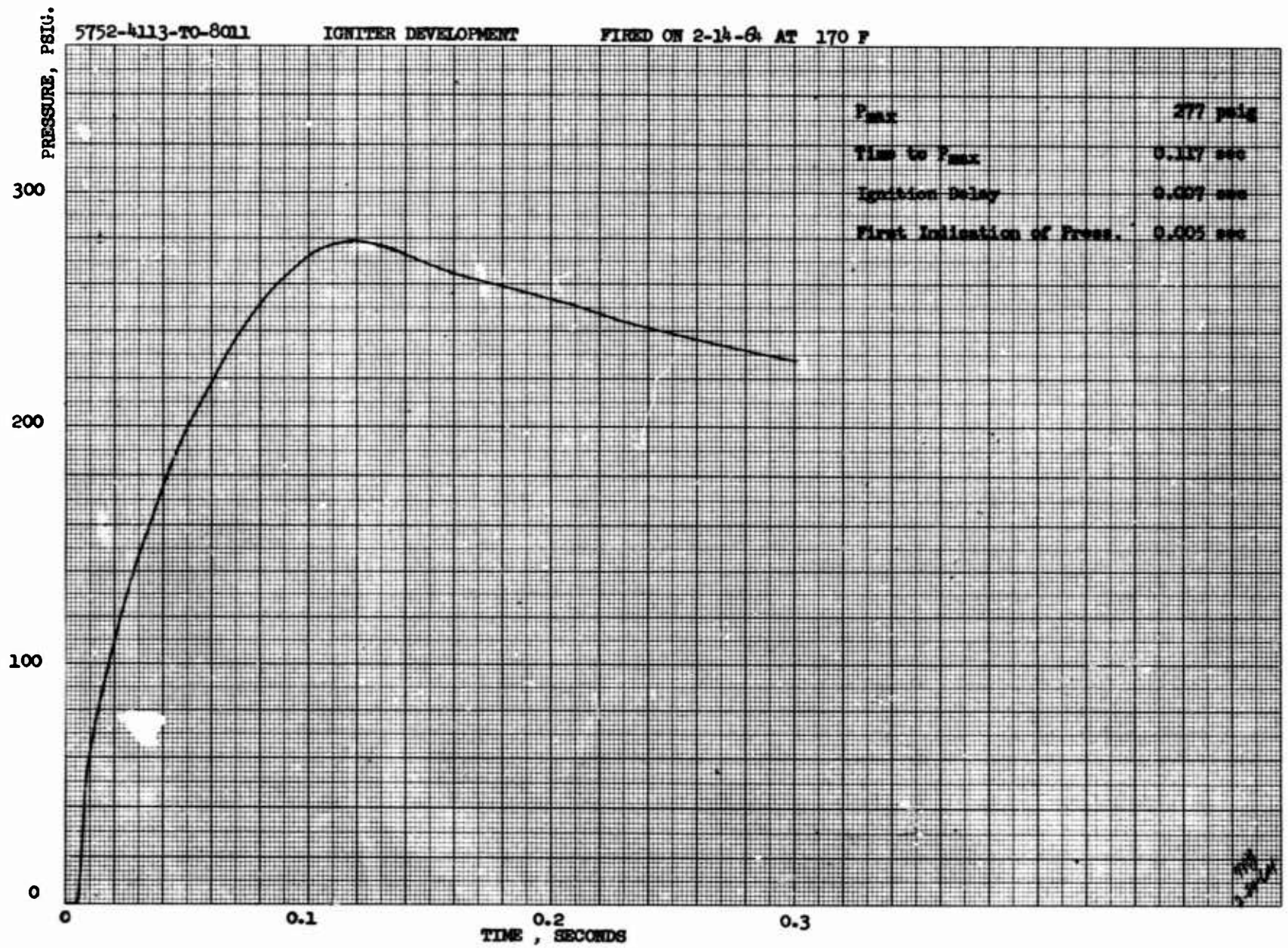


Figure 283. Igniter Development, TO 8011

The loadings applied to these test igniters were about 7 pounds. Thus, the minimum compressive loading should be raised to about 7.5 pounds. This would result in the following possible maximum load. In the case of two spacers:

7.5 lb/0.589 sq in. = 12.75 loading on spacer surface area resulting from 7.5 lb of compressive load.

In this case:

$X/12.75 - 25/14$

$X = 22.8\%$

$Xt = 0.228t$ and the addition of the second spacer results in a load as follows:

$(1 - 0.228)t = 0.772t$

$\frac{(2 - 0.772)t}{2} = \frac{1.228t}{2t} = 61.4\%$ compression required

$L/61.4 = 14/25$

$L = 34.4$ psi

$F_L = (34.4)\ (0.589) = 20.2$ lb

(C) Based on the results of the successful vibration test, the compressive load range was changed from 5--19 pounds to 7--20 pounds. This also gave a maximum confidence in the igniter being able to ignite the motor within the 0.100 sec requirement using the 0.6 inch long pellets. Final proof of the igniter would be demonstrated on the full-scale motor firings.

(5) Restrictors

Motor B and Motor A both had the same processing and restrictor thickness requirements; therefore, the development results of one was applicable to the other. The R-140 and R-143 restrictor formulation were used on both motors.

However, one area of variation in application was in the floating restrictors. From data acquired on the Motor A program, it was apparent (soon after the design of Motor B was started) that some type of stress relief system would be required for both ends of the core grain in the polar boss region. Separation had occurred on several Motor A's, especially around the insulation spike of the aft polar boss. A design change was made to add a doubled rubber sleeve around the spike. A plastic bond relief film was placed between the rubber layers. After the core grain was cured, the plastic was removed and the gap was filled.

Although this was reasonably successful for Motor A, it could not be used for Motor B, because of additional vibration and temperature cycling requirements. It was decided for Motor B that both ends of the core grain adjacent to the polar bosses must be left floating. It was further decided that the "floater" should extend well beyond the outer edge of the load rings, to relieve core grain--RFG interface stresses at the same time.

(C) Several design sketches were made of different ways of solving the problem and from these the following list of design requirements were made:

1. Material of restrictor must bond well to itself, MX-2600 Glass Phenolic, MX-4600 Glass Phenolic, and Flexadyne propellant.
2. Material must have the ability to be molded void-free.
3. Material must be compatible with propellant.
4. Tool requirements must be kept to minimum.
5. The material must maintain a positive seal for inner grain bond line in a temperature range of -75 to 170 F.
6. Material must maintain seal throughout RFG--core grain separations of 0.5-inch (or more) without destroying restrictor-to-grain bond.
7. Component must not impair required ballistics performance.
8. Component must be inspectable.
9. Installation must be easy and positive.

The design finally selected for the forward polar boss, see Fig. 284, consists of a 3/16-inch layer of R-148 restrictor molded to fit the inside contour of the forward polar boss, and extended well along the RFG/core grain interface. A doubler section starts at the polar boss lip and terminates at the extreme outer edge. A cloth tear arrestor is placed in the apex of the doubler opening. Since the liner is not bonded to the inside surface of the polar boss, a built-in expansion seam insulated on both sides is provided. This allows polar boss/core grain separation without exposing the core grain surfaces to the flame.

After much consideration, a unique bellows-type doubler was selected for the aft polar boss, Fig. 285. Since the erosion environment around the nozzle is much more severe than at the forward polar boss, it was necessary to keep the expansion seam filled in the open condition. It was also necessary to provide a pressure seal for the restrictor opening to prevent internal pressure from blowing the RFG and core grains apart. This would allow hot gases between the two and allow additional grain surface to be burned, causing motor failure.

The doubler consisted of two washer-shaped sections of R-148 bonded at the outer edge with a cloth tear arrestor placed over the inside bond seam. Seven "V"-shaped tie rings were bonded between the washers, forming seven separate flame and pressure barriers. This design allows maximum movement of the two restrictor layers with very low bond stresses. It also allowed a weight saving over the Motor A design, and eliminated the ballistic spike cracking problem.

One modification was made to the original aft doubler design just prior to drawing release. Vent holes were placed in the tie rings to equalize pressure across them. This was done to reduce the possibility of the rings being stripped out during sudden pressure changes inside the motor. It was believed that the holes would not in any way reduce the effectiveness of the doubler.

(c)

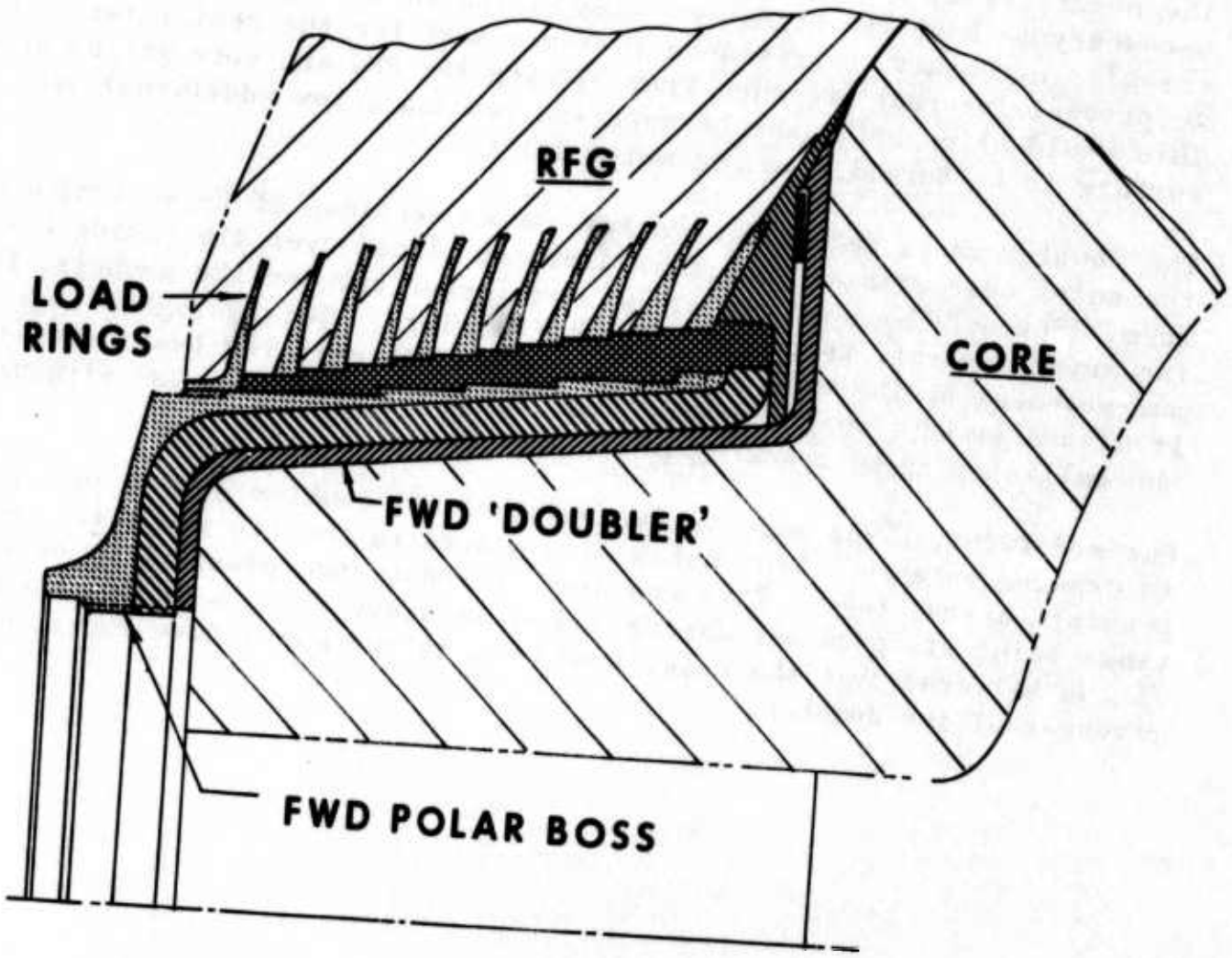


Figure 284. Forward Doubler, Motor B

(c)

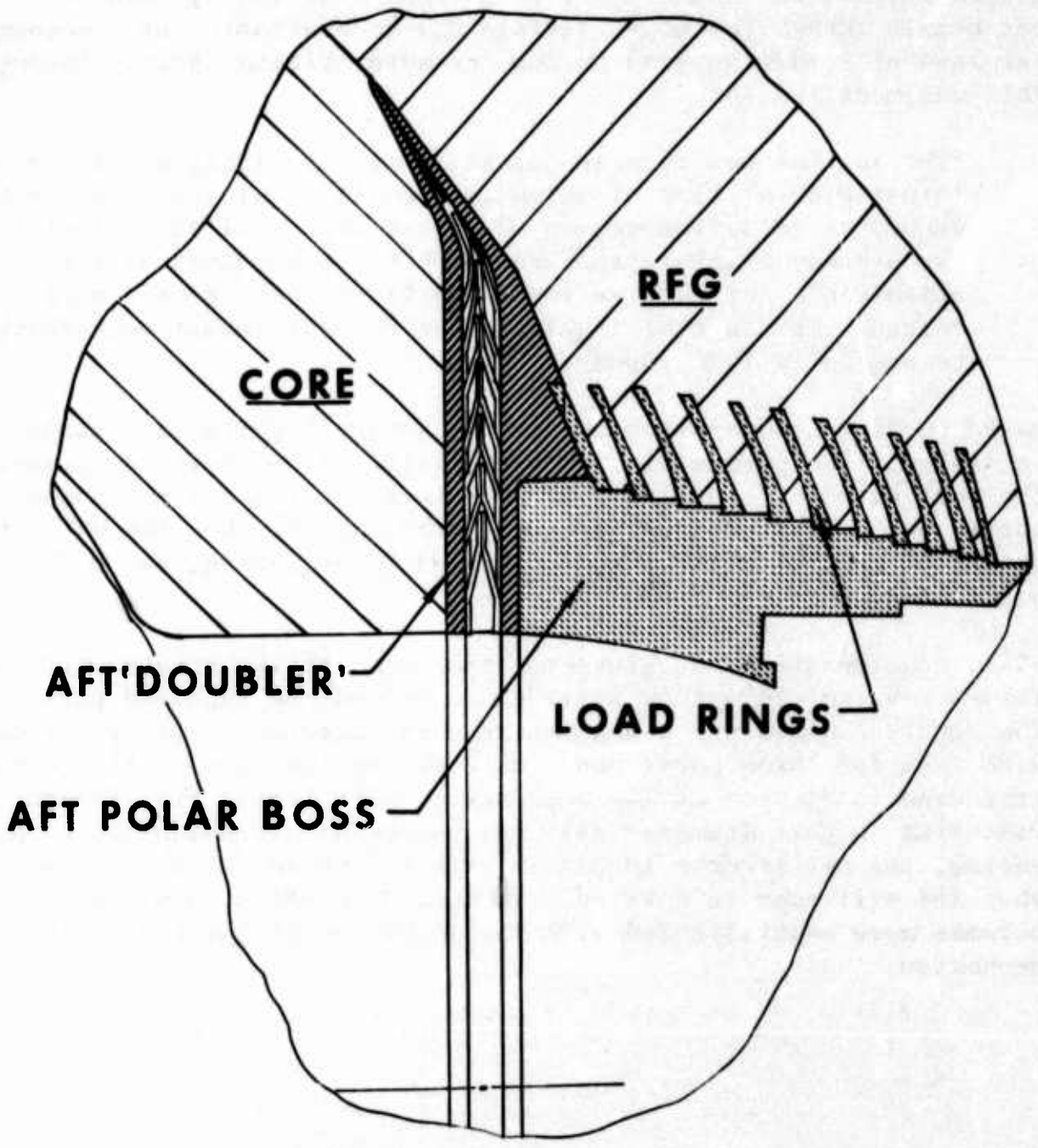


Figure 285. Aft Doubler, Motor B

(6) Thrust Reversal

(C) A thrust reversal requirement was specified by RPL for Motor B to assist in separating the payload from the boost stage. The requirement initially stipulated that a net reverse thrust of 1800 pounds in excess of net nozzle thrust (at 60 F, Average P_c) be available for 7 seconds, regardless of actuation time during the motor firing cycle. Subsequently, this was modified to:

> "The initial net reverse thrust level, excluding any transient thrust peak at time of actuation, shall be at least 200 pounds when port actuation occurs at a pressure level equivalent to the average chamber pressure at 60 F. Subsequent to port actuation a net reverse thrust shall be continuously maintained. The initial transient net reverse thrust peak shall be nominally 1000 pounds."

(C) Based on this new requirement, thrust reversal parametric studies were initiated. The parametric studies considered as variable parameters the port diameter, inclination angle to motor centerline, number of ports, and actuation time. Figures 286 and 287 show the net reverse thrust vs port diameter for 30, 35, and 40 degree angles, with 3 and 4 ports at Average P_c of 632 psi.

Also, consideration was given to separation of the nozzle exit cone upon thrust reversal actuation in order to reduce the required port openings. The studies showed the reduction in port diameter to be approximately 0.80 inch for three ports and 0.60 inch for four ports, if the nozzle exit cone is ejected at the supersonic split line. Even though the reduction in port diameter does not represent a substantial weight saving, the net reverse thrust is almost doubled for a given port size when the exit cone is ejected. It should be noted, however, the system becomes more sophisticated with the inclusion of the additional ejection mechanism.

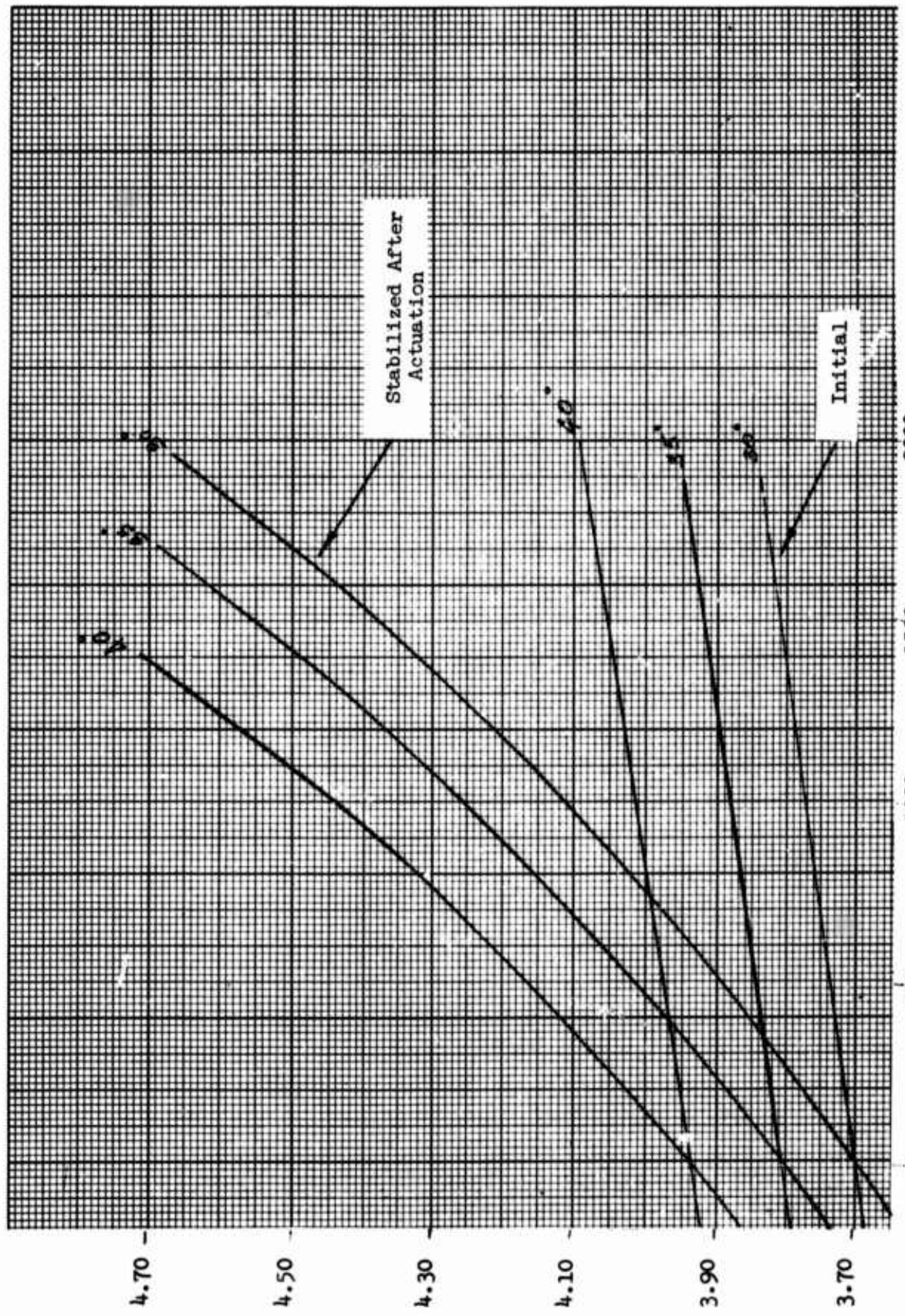


Figure 286. Variation of Flow Port Diameter with Net Reverse Thrust for Four Ports at Angles of 30, 35, and 40 Degrees

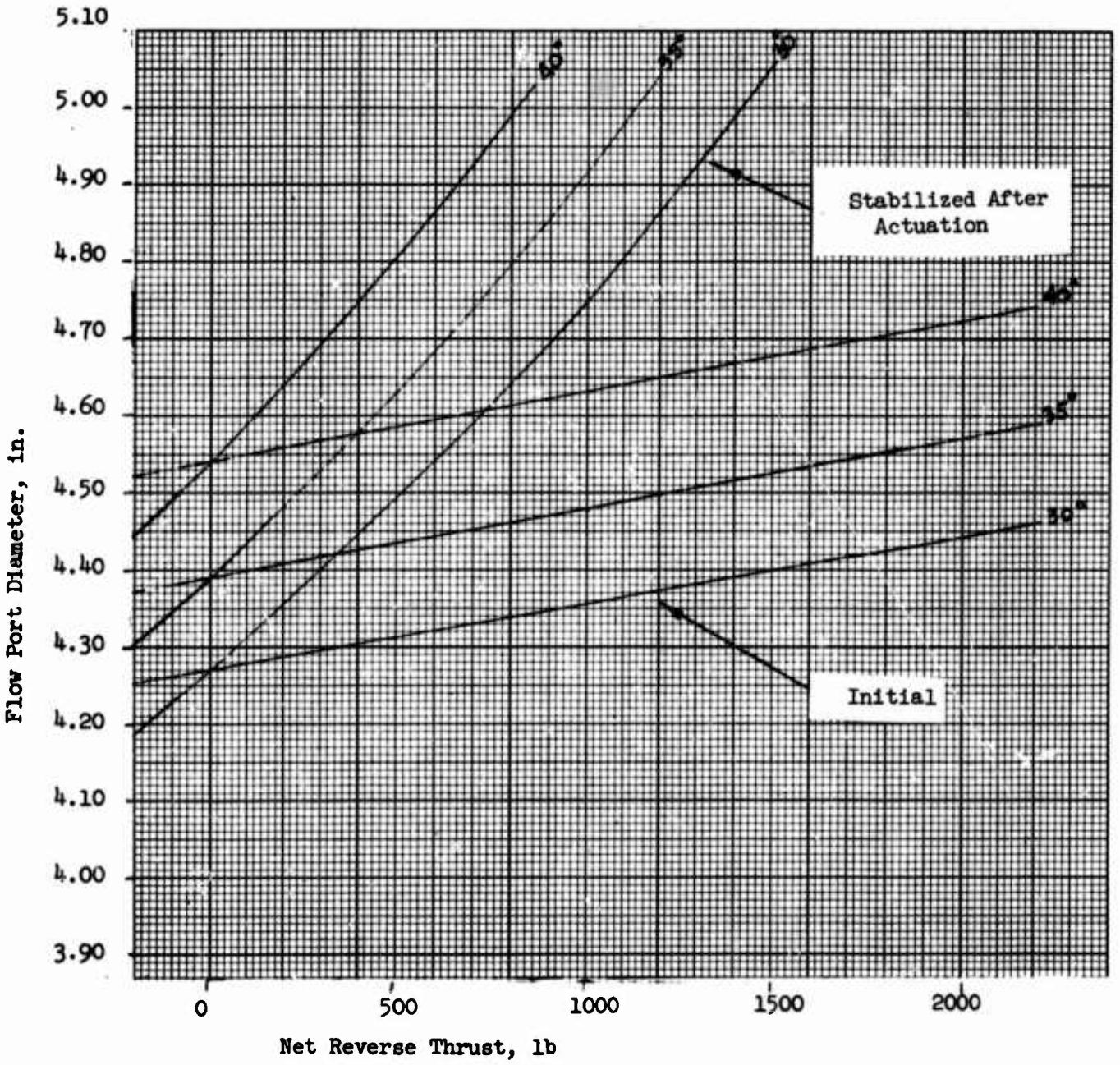


Figure 287. Variation of Flow Port Diameter with Net Reverse Thrust for Three Ports at Inclination Angles of 30, 35, and 40 Degrees

(C) A 3-port system inclined at 35 degrees to the motor axis, along with the previously mentioned modified thrust requirements was selected for design. Rocketdyne initiated a design that consisted of three 4.52-inch diameter ports located in the forward dome and inclined at 35 degrees to the motor centerline.

(C) The net reverse thrust equals

$$F_{Net} = F_{Reverse} - F_{Motor}$$

Where

$$F = P_c A_t \left(C_{f_v} - \frac{A_e}{A_t} \frac{P_a}{P_c} \right)$$

for the reverse or motor thrust, applying the appropriate value for the motor. The net reverse thrust for sea level and altitude conditions (at average chamber pressure and 60 F) are tabulated as follows:

	Net Reverse Thrust	
	Initial, lb	Stablized, lb
Altitude	1535	300
Sea Level	5570	3100

(C) As noted above, the performance level is higher for sea level conditions than for altitude and is primarily attributed to the foreshortened 10:1 expansion sea level nozzle. This is because of the effect of the expansion ratios for the given motor conditions.

Methods of supporting the thrust reversal ports and actuating the ports commenced after the parametric studies. Initial structural studies involved four basic types of thrust reversal ports with the principal difference being the method of supporting the load on the port and closure.

Before finalizing the actuation or support system design, RPL informed Rocketdyne that current studies had indicated the thrust reversal function could be performed better through other means, and that the thrust reversal ports should be deleted. All effort was stopped in this area.

d. Process Development

Because the same design techniques used for Motor A were used in Motor B they will not be elaborated on in this discussion.

(1) Fabrication Development

The original grain design utilized unequal polar openings to take advantage of the inert weight saved in a smaller diameter forward closure design. Based on case winding experience with unequal ports, it was felt that the grain could be wound successfully.

To establish the feasibility of the winding design, five partial web grains were scheduled to be fabricated to develop data to determine layer buildup, load ring design, polar boss lengths, and load ring steps. The results of the grain fabrication are covered below under the individual grains.

The first development grain, RFG-2207 A, consisted of the first geodesic layer only, and was wound primarily to check out the cam design technique and to obtain preliminary geodesic buildup data.

Winding patterns and cam design for the next grains, RFG-2207 B, RFG-2208, and RFG-2209 were based upon averaging the theoretically correct winding angles for each dome. This method will result in an angle that is greater than the correct angle for the small port dome and smaller than the correct angle for the large port dome. Previous experience with glass filament winding indicated that the variation of the average angle from the theoretical winding angle may be as much as 4 degrees without excessive slipping.

Cam operation was good and theoretical buildup data were close to predicted values; therefore, preparations were made to wind RFG-2207 B.

RFG-2207 was wound through the third GI layer. Each cycle consisted of a geodesic layer plus 4 intermediate wraps. Load ring steps were not machined on the polar bosses as it was the purpose of this grain to determine the required step lengths from the buildup at the bosses. simulated load rings were built into the windings using Cab-O-Sil filled EC-1648 adhesive. Slight wire instability was noted on the forward dome during winding, indicating the chosen winding angles were verging upon the practical limit.

Buildup at the polar boss was considerably lower on the second and third geodesic layers than predicted. The reason for this unexpected decrease in buildup was not readily apparent in view of the design correlation of the first geodesic layer. Two variables which could possibly cause this discrepancy were: the winding tension for the first geodesic layer was approximately 50 grams lower than that used on the rest of the grain, and the winding pattern for the first geodesic layer was 9/7 (ratio of mandrel to cam revolutions) compared to a 5/4 for the second and third geodesic layers.

Another possible reason for the buildup variations was an erratic circuit counter. A check of the counter proved it to be consistently high. This raised doubts as to whether the correct number of wire wraps were wound into the layers. In view of these problem areas it was necessary to wind another grain to firmly establish the correct polar boss buildup.

The fabrication of RFG-2208 was identical to RFG-2207 B with two exceptions. Aluminum load rings were used, and the winding pattern for the first geodesic layer was changed to 5/4 to match the second and third geodesic layer. Constant wire winding tension was used throughout the grain. The machine cycle counter was changed and carefully checked to eliminate possibility of error. Evaluation of the dome contour traces and winding data indicated that the second and third geodesic layers did not have the thickness predicted from theoretical calculations and correlating experience obtained on previous motor designs.

To remove any doubt as to the accuracy of the dome buildup, the third geodesic was stripped off and rewound. Rewinding confirmed the previously determined smaller buildup. The change in winding pattern for the first geodesic layer apparently had no affect upon boss buildup.

Since all known variables were eliminated on this grain and the dome buildup continued to vary from design, the actual buildup data obtained were used for predicting buildup for the next fabrication development grain.

Winding patterns and cam design techniques for RFG-2209 were the same as used on the previous partial web grains. RFG-2209 was scheduled to be wound through the sixth geodesic layer. Load rings No. 2, 3, and 4 and the first 3 boss steps were designed based on data obtained on the previous grains. Load rings No. 5 and 6 were to be designed and fabricated as required during winding operations.

Winding had proceeded through the first cycle when it became apparent that the intermediate layers were unstable on the forward dome. The degree of wire instability was greater than on the previous grains and was unacceptable since the buildup would not be repeatable from grain to grain. It was decided to strip the first intermediate layers off, evaluate the possible causes for slippage, and rewind.

The reason for this wire slippage was winding at something other than the stable winding angle for the dome, which is a necessity due to the unequal polar openings. This slippage is aggravated by excessive propellant application. Since both domes were receiving essentially the same quantities of propellant, and the aft dome was stable, the winding angle was changed to something closer to the required stable angle on the forward dome. After this was done, the first intermediate layers were rewound. Some instability was still present on the forward dome, although improvement was evident. The aft dome windings remained satisfactory.

Some instability of this type was noted in previous fabrication development grains; however, it was not as extreme as on RFG-2209 and was not greater than expected for the winding geometry required by the unequal port grain. No apparent reason for the sudden appearance of this instability was available as all fabrication grains were wound as near identical as possible.

Upon completion of the fourth intermediate layer, measurements showed that the design cylindrical diameter had been reached for the fifth geodesic layer but the dome buildups were not sufficient. The insufficient dome buildup is attributed to the accumulative effect of the unstable fill layers in the domes moving from their designed positions.

Since the problem would increase with each layer, it was decided to stop winding and evaluate the winding techniques used on Motor B.

It was recognized when winding design started on unequal port openings that the winding circuit could not be stable over its entirety. The two possible solutions considered feasible were, (1) wind the average of the two dome helix angles and maintain a stable cylindrical section with some instability in the domes, or (2) wind the correct (stable) helix angle for each dome and allow the helix angle variation between the two domes to result in instability along the cylinder section.

Glass filament winding tests showed that the first method was preferable, since winding demonstration of the second method resulted in the glass rovings moving a considerable distance as the pattern was wound. This movement prevented the precise, nongrapping pattern required for a flightweight case. Based on these case tests, Motor B grain and cams were designed by the average winding angle method.

Also based on these tests a maximum of 8 degrees variation between the two dome winding angles was considered the maximum that could be tolerated. Winding development effort showed this arbitrary limit to be too high. Since satisfactory intermediate layers cannot be designed for the grain when restricted to small angle variations, effort was directed towards evaluation of the second winding method.

Cams for the first three geodesic and intermediate layers were designed based on the stable dome, unstable cylinder concept. The method of handling the transition between the different dome winding angles was to split the variation and handle it at each dome knuckle radius. This was done in an effort to minimize expected wire slippage in the cylinder.

RFG-2210, scheduled for 3 cycles, was wound to check the feasibility of the stable dome, unstable cylinder method. The first geodesic layer proved encouraging, as the buildup was much closer to the predicted theoretical buildup than the layers wound by the average angle method. The first and second intermediate layers lay down properly and appeared acceptable. The third and fourth layers were progressively unstable therefore winding was stopped. Inspection of the grain several hours later showed that even the first two intermediate layers on the forward dome had moved down the dome showing they were moving after laydown. The aft dome appeared satisfactory, probably due to the fact that these layers tend to move up the dome and were held in place by the layer on top.

It was apparent from these results that although a stable helix angle was wound on the domes, the effect of slight wire movement going into the cylindrical section was enough to render them unstable. This wire movement is not visible or apparent during winding, and if the wire angle merely borders on instability it is almost impossible to predict the stability of the wire pattern during winding.

As a further check, another X-cam was designed for the third layer of the first intermediate layers. In this case all of the angle transition was made at the center of the grain to minimize the effect on the domes. The third layer was rewound using the new cam. Once again the wire did not visibly slip as expected and again the dome buildup bordered on instability at laydown. Based on these two tries, there was considerable doubt that stable windings could be achieved with unequal port opening domes over the range required.

Another approach under investigation was winding the intermediate layers with equal diameter openings at each end. The forward dome with the smaller port, would have a larger gap between the geodesic layer polar buildup and first intermediate layer buildup. Since the gap would be at the steep angle of the dome it was felt the successive geodesic layer wires would bridge from the high points and (being supported by propellant) only minor contour variations would result.

At this point it was directed that Motor B be converted to equal port openings and work was stopped on unequal port winding studies.

The decision to change the grain to an equal port design required that the forward port diameter be increased to the size of the aft port with concurrent adjustment in the contours of the forward dome. The present Motor B design has identical forward and aft contours.

The plaster mandrel used in the first phase was modified to the new contour by installation of a new dummy polar boss and plaster screeding a new forward dome contour.

Complete fabrication development of the equal port grain required three partial web grains. RFG-2211 was wound through the third geodesic layer. Aluminum load rings and boss steps were designed based on unequal port studies. Good geodesic base-line contours were obtained with the intermediate layers and all layers were stable. Geodesic layer buildup at the polar bosses was slightly lower than the predicted value; however, this was desirable as it provided more space for load rings. The average

cylindrical buildup per cover was higher than expected, 0.0188 inch compared to a predicted buildup, from Motor A, of 0.0165 inch. This increase could have resulted from higher viscosity propellant and winding on a larger mandrel. In general this grain was very successful in establishing buildup data and other information necessary for extrapolating the grain design to the outer layers.

RFG-2212 was wound through the sixth geodesic layer. Load rings No. 2 through 6 (with corresponding boss step lengths) were designed based on information obtained from RFG-2211 and incorporated into the grain. Since this grain was intended to act as the mandrel for the final grain (sixth through the eleventh geodesic layers), the polar boss was undercut past the sixth step to allow installation of a sleeve, which could be machined to the required step lengths when they were established for the seventh through eleventh geodesic layers.

Good wire stability, load ring design, and boss step lengths were evident throughout the grain. The average cylindrical buildup of 0.0177 inch per cover for this grain was slightly less than RFG-2211.

It was decided that this grain was an adequate mandrel for winding RFG-2213. The grain was then cured to give a firm winding base.

RFG-2213 winding started with the first intermediate layer of the sixth cycle. It was wound over RFG-2212 which terminated at the sixth geodesic layer. Step lengths and load rings were designed based upon buildup data obtained during winding of RFG-2211 and RFG-2212.

As in the two previous grains, the grain winding was highly successful in that predicted layer buildups, boss step lengths, and load rings proved adequate. The average cylindrical buildup was 0.018 inch per cover. The complete web, averaging the composite buildup of RFG-2212 and 2213, was 0.0178 inch per cover.

This grain completed fabrication development of the Motor B reinforced grain. Only minor modifications to the load rings and boss step lengths were necessary for the final motor design.

This fabrication development program further demonstrated the applicability of the multiangle helix winding system to large grains, design feasibility, winding, and processing techniques.

The lack of success of unequal port winding in reinforced grains does not necessarily mean the technique is impossible; program schedules prevented exploring many approaches. Possibly further work cound establish winding parameters which would allow winding with sufficient stability.

The speed with which the equal port design was completed, using only 3 partial grains (compared to 5 for Motor A) indicated the usefulness of experience and accumulated data. Correlation of theoretical and actual buildup data were such that design variables for future motors may be predicted with a higher degree of confidence. It is doubtful, however, that a complex motor winding design could be accomplished without a fabrication development effort.

(2) Application of Grain Restrictor

The same techniques developed for Motor A were used on Motor B; therefore, a complete discussion can be found under Motor A.

(3) GFW Case

Nearly all of the Motor A GFW case development work was directly applicable to the Motor B GFW case. The difference in the two was that Motor B included a larger case diameter and initially thrust reversal ports. Work had only been initiated on reinforcing doillies for the thrust reversal ports prior to the cancelation of the requirement; then only case development was required.

(a) Fabrication Development of a Partial Case

As in Motor A, the first Motor B GFW cases were for development of pattern stability and cam design checkout. Winding geometry calculations and cam design for the Motor B GFW case were done by computer program. The design was an eight cycle helical pattern with a helix angle of 15.46 degrees.

Partial GFW case P-2407 was the first of the development cases. The eight-cycle pattern with a helix angle of 15.46 degrees appeared satisfactory except for acceleration and deceleration of the x and y axes. This problem was associated to the particular winding machine and not to the pattern.

A new set of cams was designed for the Motor B helical wrap to reduce the requirements for acceleration and deceleration of the x and y axes. These cams were designed to produce the same pattern laydown, but through the use of a slightly different follower path to improve machine operation.

(C) Further partial case development checked out the new cam's pattern stability and machine operations so that it was planned to start fabrication of the first test case. Then a change in the RFG tangent-to-tangent length from the assumed 35.64 to 36.6 inches occurred. (This length was finalized during the fabrication development of the RFG.) Due to this extra length, additional development effort was required to satisfy the new helical pattern (pattern grapping occurred with the old cams) and check out the pattern stability and cam accuracy.

(b) Fullscale Case Fabrication and Test

After establishing the fabrication process, two Motor B cases were fabricated and tested to evaluate the design and process. The final case was B-2415.

○ GFW Case B-2415 Fabrication

(C) Fabrication GFW Case B-2415 was designed to flightweight requirements of 1004 ends per inch helix wrap, 1480 ends per inch circ wrap, and skirts extending from the cylinder forward and aft integrally wound with the circ.

The forward skirt could not be wound because of the relative movement of the skirt and case mandrels during rotation. This movement was caused by greater-than-expected spindle deflection. The aft end was not affected because the skirt mandrel mounts on the case mandrel sleeve (which extends through the aft port). This sleeve is not subjected to deflection in the same manner as the winding spindle because it is supported on the spindle at only two points.

Winding operations were marked by extremely rough, erratic, inconsistent machine operation. After 18 hours of operation and several restarts because of gapping patterns, machine roughness caused failure of a component and subsequent damage to the mandrel. At this point it was decided to move the mandrel to another machine. After several restarts, winding was completed.

The case which resulted had several small separations in the aft dome, because of an increase in machine roughness during the latter part of the second (of two) helix cover. These gaps were not thought to be of sufficient magnitude to seriously affect results of the case test.

After case cure, the aft skirt mandrel was removed and the skirt ring installed. The skirt diameter shrank about 0.030 inch upon removal of the skirt mandrel; however, the skirt ring had been cooled to -70 F and fit loosely. As the ring warmed to ambient temperature, the ring became tight in the skirt and stretched the skirt by approximately 0.010 inch.

During removal of the mandrel, the case was collapsed slightly by the Pneuma-Grip used in handling. The flexed area returned essentially to normal when pressure was released. This is not considered a general problem in case handling, since normally the case has two skirts and is handled by special tooling attached to the skirt rings.

(C) Weights and dimensions of Case B-2415 are shown in Table XXCIII. The case weighed 44.7 pounds, of which 0.7 pound was the skirt transition fill grommet and tape. Resin content was 24.3 weight %.

(C) Based on the weights and resin content obtained, predicted weight of the Motor B flightweight case is 55.6 pounds. At the target of 20% resin content, predicted case weight is 52.7 pounds.

○ GFW Case B-2415 Test

This case was hydrotested 21 September 1964. The motor was positioned on the aft skirt during the test. Figures 288 and 289 are posttest pictures of the case.

All of the circ wraps and none of the helical wraps broke during the hydrotest. Movies show the initial failure was at the edge of the glass reinforcing cloth in the aft skirt which is near the initial rupture point of two of the Motor A GFW cases.

(C) Rupture occurred at 636 psig and was 20% lower than the calculated burst pressure. Review of the fabrication data indicated the correct quantity of glass roving was used in the helical layer but the circ wraps contained 19% less glass by weight than the design value.

TABLE XXCIII

DIMENSIONS AND WEIGHTS OF GFW CASE B-2415

(C)

Dimensions, in.	Forward	Center	Aft	Avg
Restricted Mandrel Diameter	35.866	35.870	35.876	35.871
Diameter after Helical Wrap	35.975	35.975	35.984	35.978
Diameter after Circ Wrap				
Cured, hot	36.014	36.002	36.027	36.014
Cured, warm	36.002	35.995	36.017	36.004
After washout	35.960	35.965	35.975	35.967
Thicknesses, in.				
Helix	0.054	(Not compressed by circ wrap)		
Circ	0.013	(Low due to compression of helix)		
Total	0.067	(Lower than actual due to compression of restrictor)		
Aft Skirt Dimensions, in.				
OD	36.242	OD w/skirt mandrel		36.242
ID	35.880	OD w/o skirt mandrel		36.211
Thickness	0.181	OD w/skirt ring		36.221
Length	5.0			
Lengths				
Boss to boss				
Before mandrel removal		61.900		
After mandrel removal		61.850		
Cylinder		36.750		

TABLE XXCIII
(Continued)

(C)

Weights, lb	
Helix roving	17.28
Circ roving	10.57
Aft skirt cloth	5.44
Total glass	33.29
Resin*	10.71
Skirt transition fill	0.70
Total Case	44.70

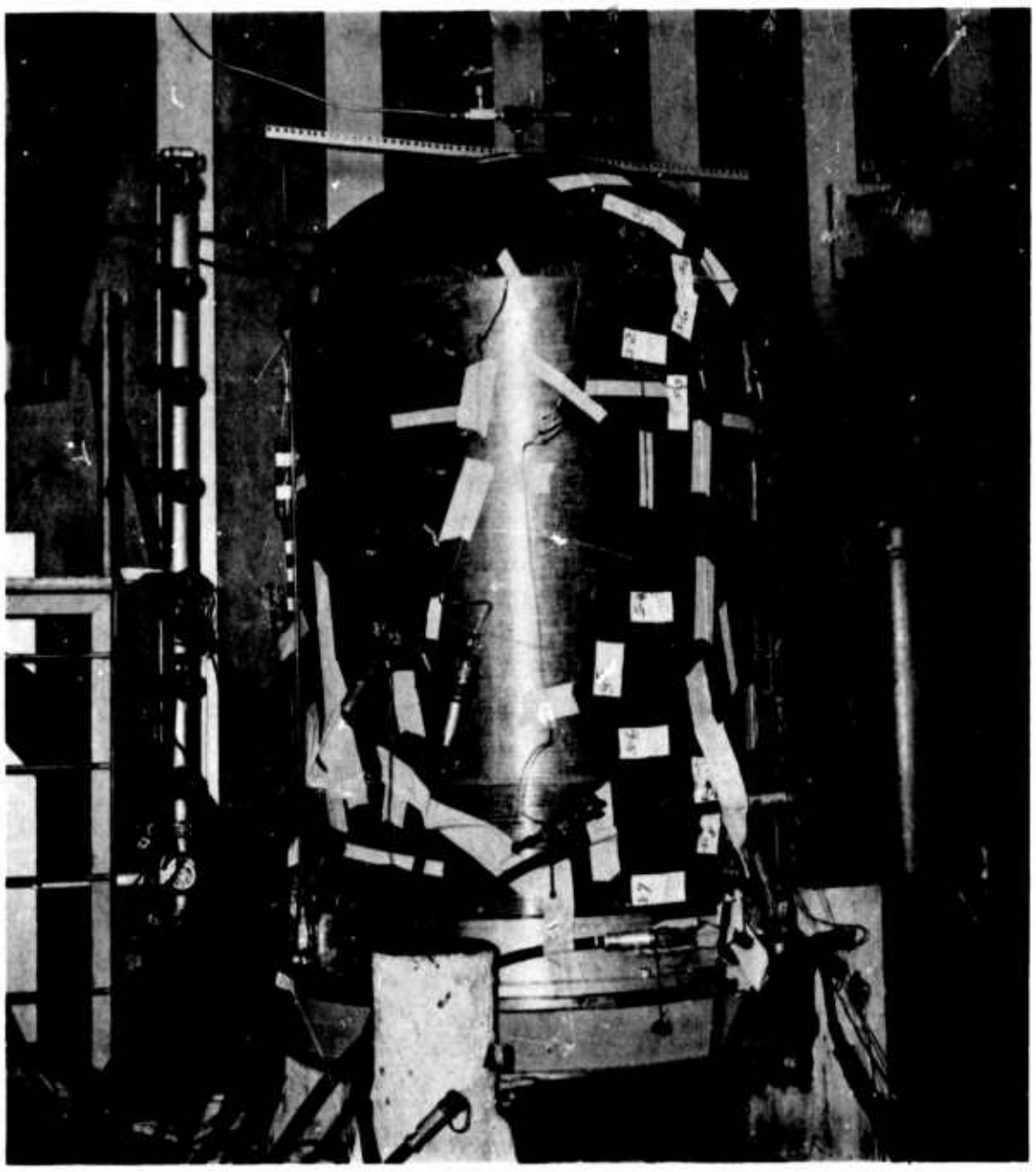
*Resin Content = $\frac{10.71}{44.70}$ - 0.70 = 24.3 weight %

(C) All calculations relative to winding the circ were checked and found to be correct. As an additional check, a partial layer of circs was wound. This partial layer permitted determination of actual boom advance per mandrel revolution and therefore the actual ends per inch. The actual winding was within 3% of the predicted winding, which is within the accuracy of the check method. Using the measured weight of the circ wraps to calculate the burst pressure gives a value of 654 psig, which compares favorably with the actual burst pressure.

Because of the uncertainty in the quantity of glass in the circ wraps, no design changes were made in GFW 2416. Fabrication and test data from GFW 2416 were expected to confirm the fact that the quantity of circ wraps either was or was not 19% below the design value.

○ GFW Case B-2416 Fabrication

GFW Case B-2416 was wound on 9 and 10 November 1964. The case was wound to flightweight design on a restrictor coated sand/rope mandrel. The case was of good appearance (especially the skirts) which contained no ripples or resin-rich areas. There was, however, a slight depression adjacent to the case tangent at each end of the cylinder. This depression was caused by the taper of the skirt-to-case fill grommet, which was designed for Motor A and has a different taper than the Motor B dome. Figure 290 depicts the skirt-to-case fill area.



2YA33-9/21/64M1C

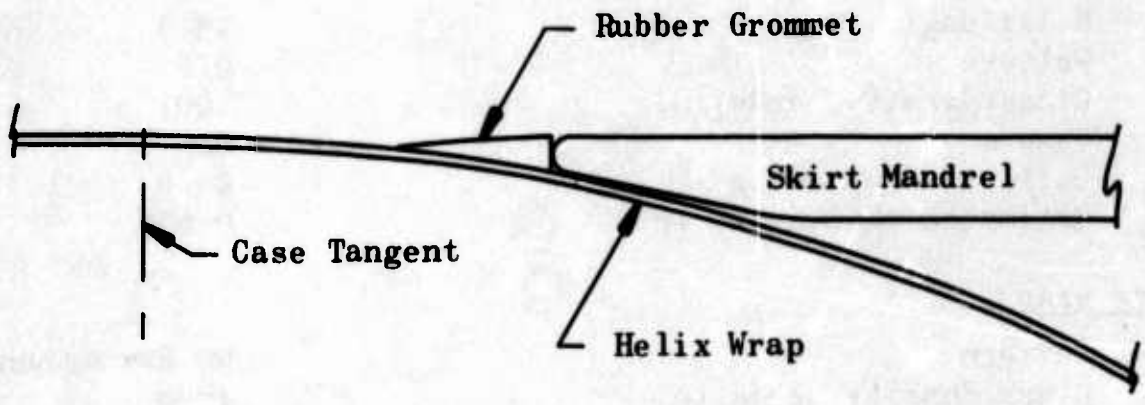
Figure 288. GFW Case B-2415 Before Hydrotest



2YA35-9/21/64M1C

Figure 289. GFW Case B-2415 After Hydrotest

Present Fill



Desirable Fill

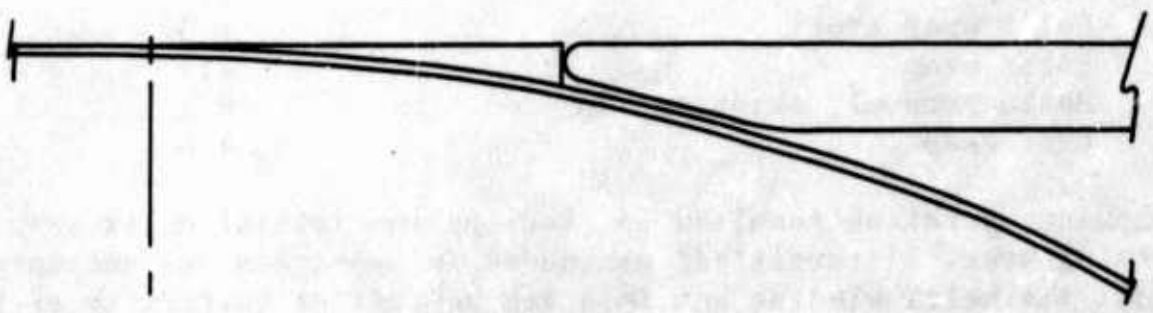


Figure 290. Motor B GFW Skirt-to-Case Fill

(C) Each skirt-to-case fill was made with a strip about 0.75 inch wide, cut from the tapered edge of a Motor A case rubber grommet. The grommet tapers faster than desirable, resulting in a slight depression in the case at the thin edge of the grommet. This depression is considered undesirable since the case is required to withstand a high bending moment. Figure 98 shows a typical glass cloth reinforcement being wrapped on the skirt. Case winding parameters were as follows:

Helix wrap

Helix angle, deg	15.3
Pattern	9/8
Glass density, ends/in.	1001
Covers	2
Balls 12-end roving	6
Estimated thickness, in.	0.035

Circ wrap

Pattern	90 deg sequential
Glass density, ends/in.	1480
Covers	8
Balls 12-end roving	6
Estimated thickness, in.	0.050

The dome speedup mechanism was used moderately during helix winding to prevent possible damage to the mandrel. Base speed was 1.5 rpm and maximum speed over the domes was 2.7 rpm. Winding times were as follows:

Winding times, hr

Set-up	7.5
Helix wrap abort	1.5
Helix wrap	7.7
Resin removal, skirt set-up	8.1
Circ wrap	4.8

Rough machine operation resulted in aborting the initial helix wrap and starting over. Intermittent roughness in operation was encountered throughout the helix winding but this did not affect uniformity of the winding. It is thought that the roughness was caused by inconsistency in the drag brake.

After completing the helix covers, the cylinder was wrapped in three layers of Style 128 glass bleeder cloth and a layer of dry roving. Heat was applied for one hour, using the portable heater hood, and the dry roving and bleeder cloth was then removed. After circ winding, the case cylinder was wrapped in three layers of bleeder cloth and a layer of dry roving, heated in a 170 F oven for 15 minutes, and then the dry roving and cloth was removed.

Excess resin was removed from the domes (using toweling) during helix winding and while applying heat to the cylindrical bleeder wraps following helix winding.

Excess resin removal was not completely successful. When processing future cases it is planned to use toweling to remove a greater amount of the excess resin following circ winding and before applying the bleeder cloth and dry roving wrap. This should make the dry wrap more effective.

(C) Dimensions and weights of B-2416 are shown in Table XXCIV. The case weighed 56.5 pounds and had a resin content of 23.3% by weight. Predicted case weight (with skirt-to-case fill actually used) was 53.05 pounds at 20% (by weight) resin content. Actual roving was about 0.9 pounds heavier than predicted and actual resin was about 2.5 pounds heavier than predicted.

○ GFW Case B-2416 Test

Because of the difficulty experienced with the skirt tooling and the skirt-cylinder-dome junction, it was expected that the inferior skirt would reduce the ultimate bending moment which the case could withstand (but it was hoped that the ultimate pressure load would not be reduced).

(C) The test was programmed to first apply 500 psig pressure and then a 1.5×10^6 in.-lb uniform moment. After this condition was reached, pressure was to be increased to 790 psig and then the bending moment was to be increased to 2×10^6 in.-lb. If the case had not burst at this point, it was planned to increase the pressure until rupture did occur.

(C) The case prior to and after test is shown in Figs. 291 and 292. After applying approximately 500 psig pressure, a 1.52×10^6 in.-lb bending moment was applied. Pressure was then increased to 640 psig and the case ruptured. Strain-vs-pressure data for this test are shown in Figs. 293, 294, and 295. Figures 294 and 295 are included

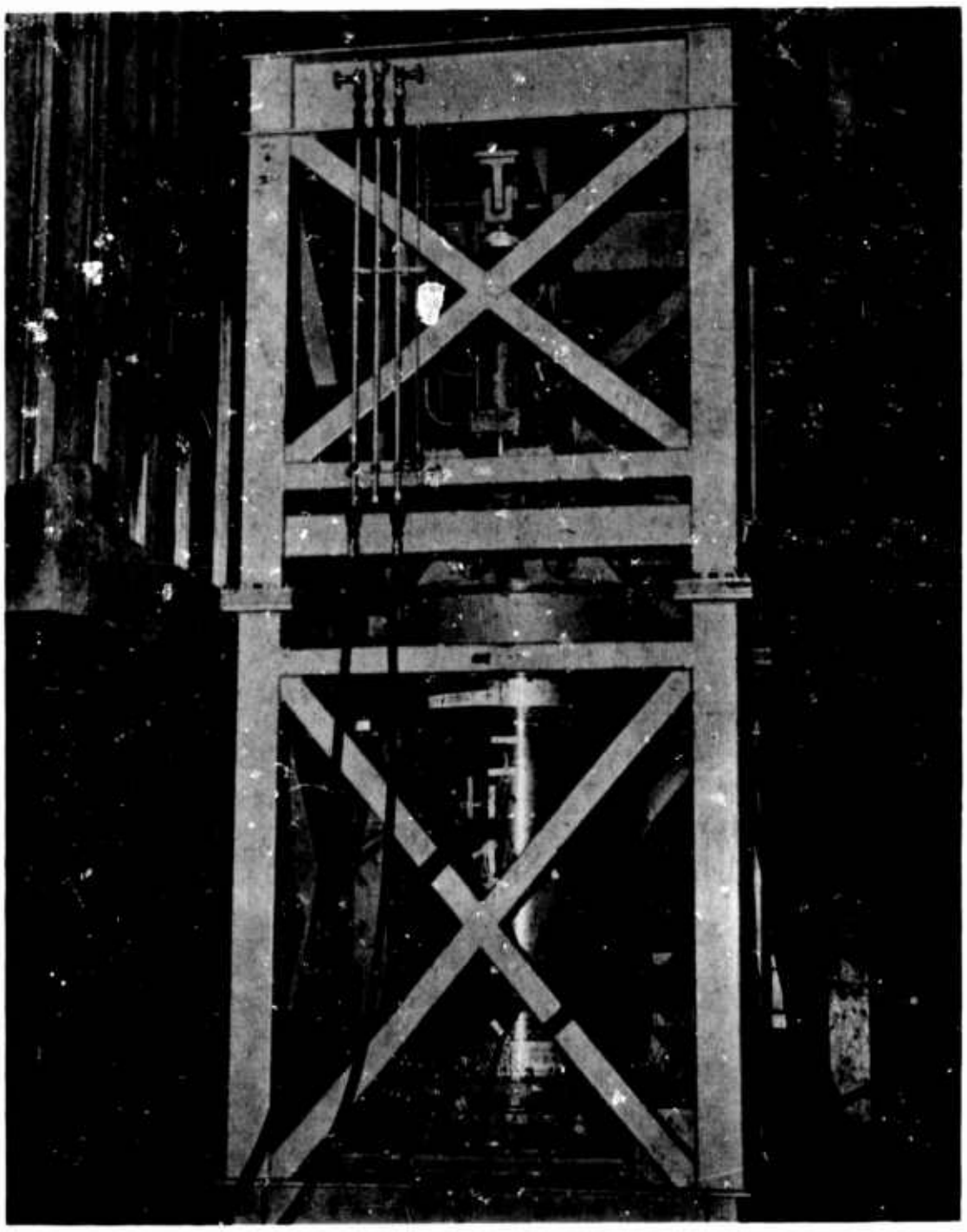
TABLE XXCIV

DIMENSIONS AND WEIGHTS OF GFW CASE B-2416

(C)

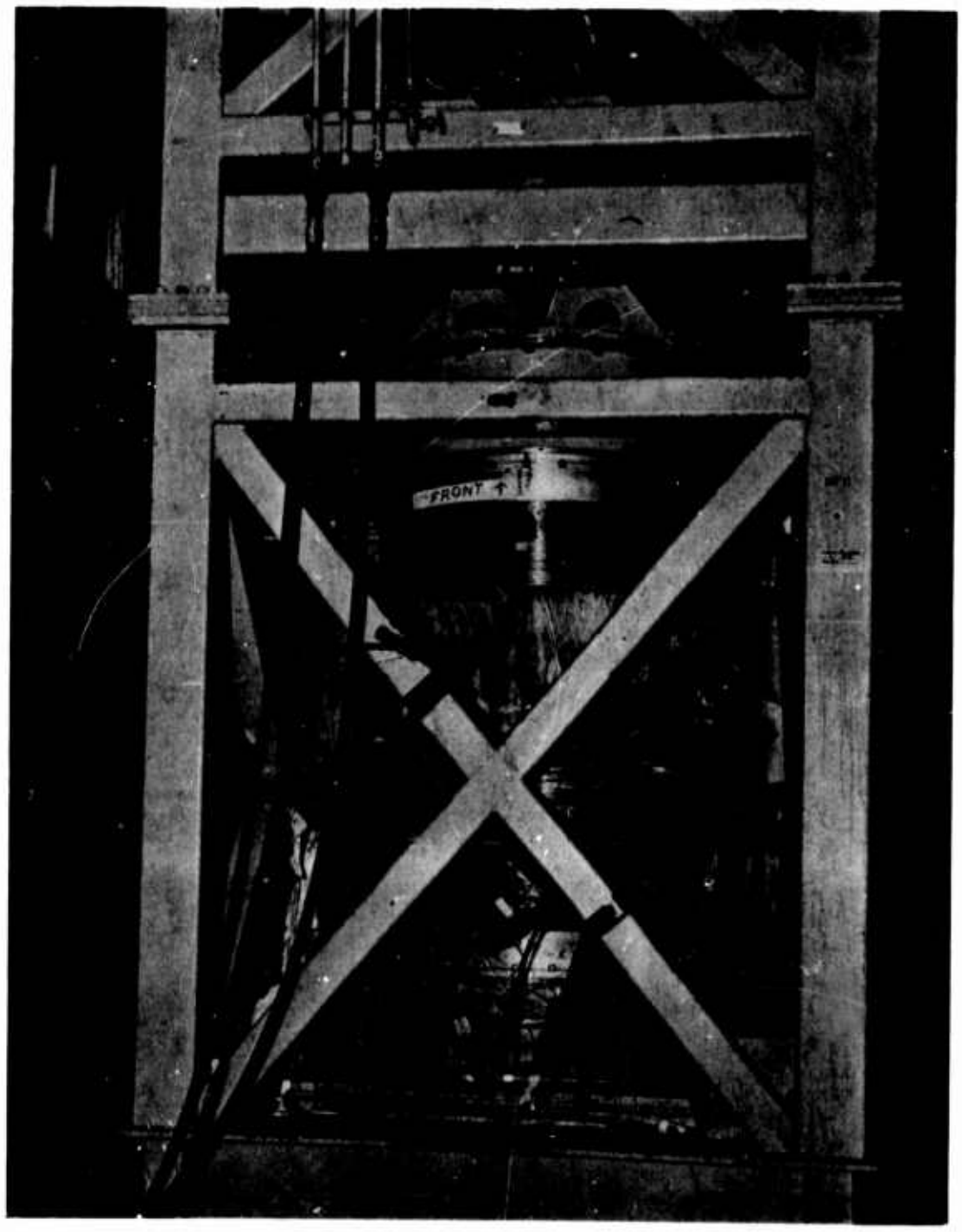
Dimensions, in.	Forward	Center	Aft
Restricted Mandrel Diameters	35.810	35.805	35.828
Case Diameters After Washout	35.884	35.900	35.925
Skirts			
OD	36.143		36.248
ID	35.880		35.880
Thickness	0.132		0.184
Lengths			
Boss to boss			
Before mandrel washout			62.027
After mandrel washout			61.903
Skirt to skirt			
Before mandrel washout			55.89 to 55.98
After mandrel washout			55.86 to 55.95

Weights, lb	Actual	Predicted
Helix roving	18.19	17.64
Circ roving	15.17	14.79
Skirt cloth (calc.)	9.33	9.33
Total glass	42.69	41.76
Resin	12.96	10.44
Case weight	55.65	52.20
Skirt-to-case fill	0.85	0.85
Total	56.50	53.05
Resin content, weight %	23.3	20.0



2YA43-11/20/64M1C

Figure 291. GFW Case B-2416 Before Test



2YA45-11/20/64M1D

Figure 292. GFW Case B-2416 After Test

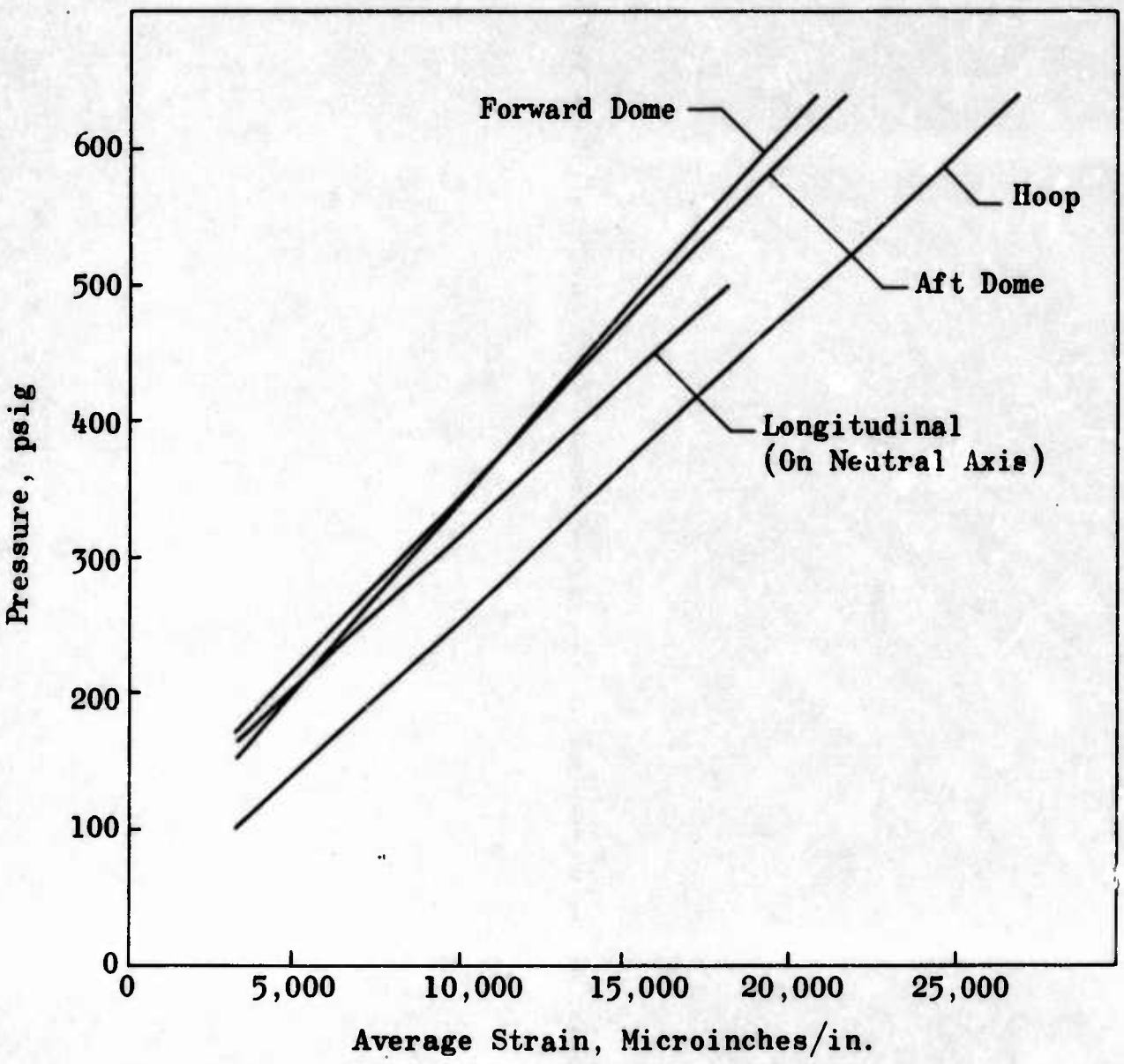
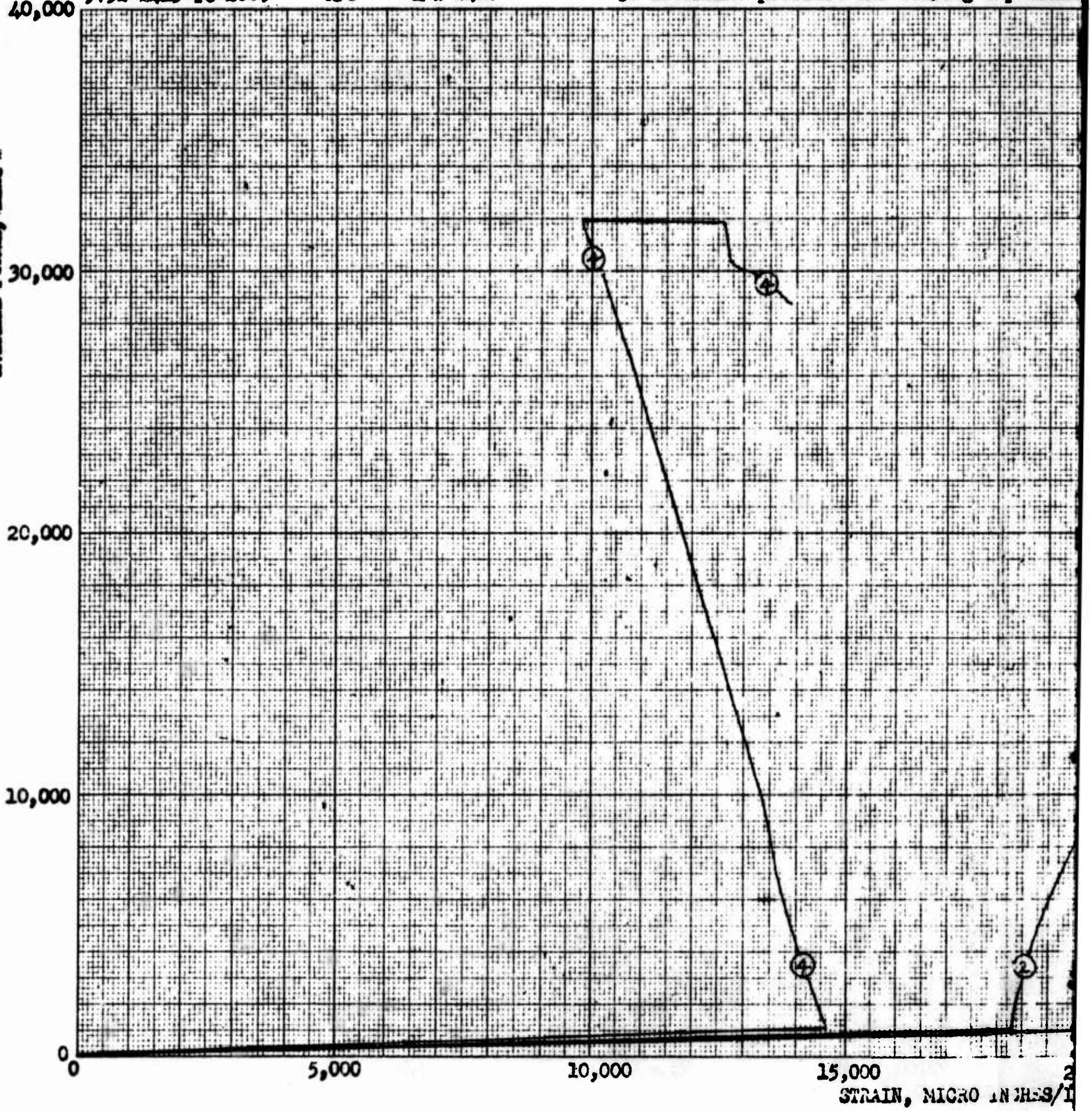


Figure 293. Pressure vs Strain for GFW A-1416

CONFIDENTIAL

PREVIOUS PAGE WAS BLANK, THEREFORE WAS NOT FILMED

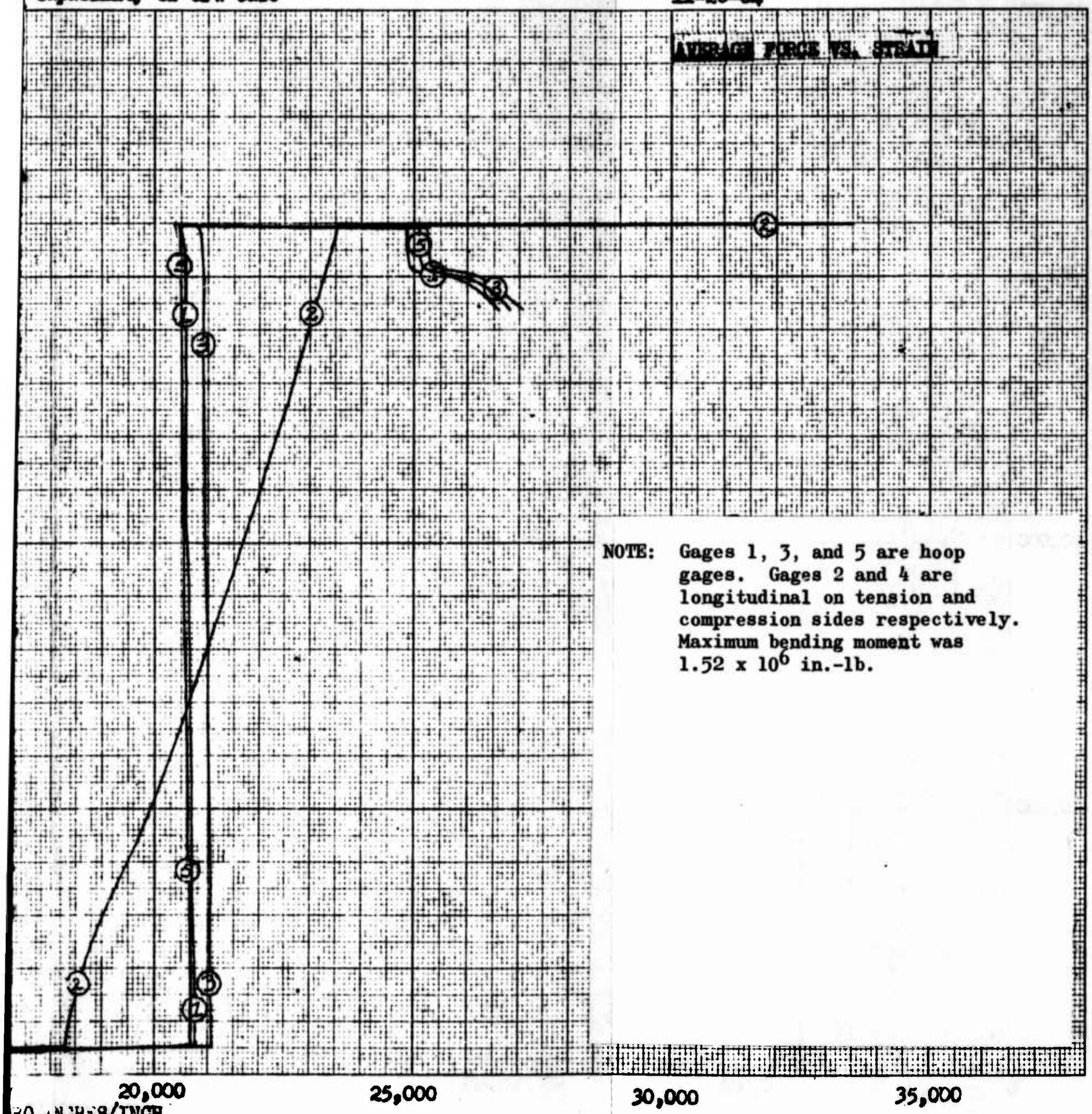
5752-2416-TO-2009 RFC GTW 2416 To determine pressure and bending capabilit



1

capability of GFW case

11-20-64



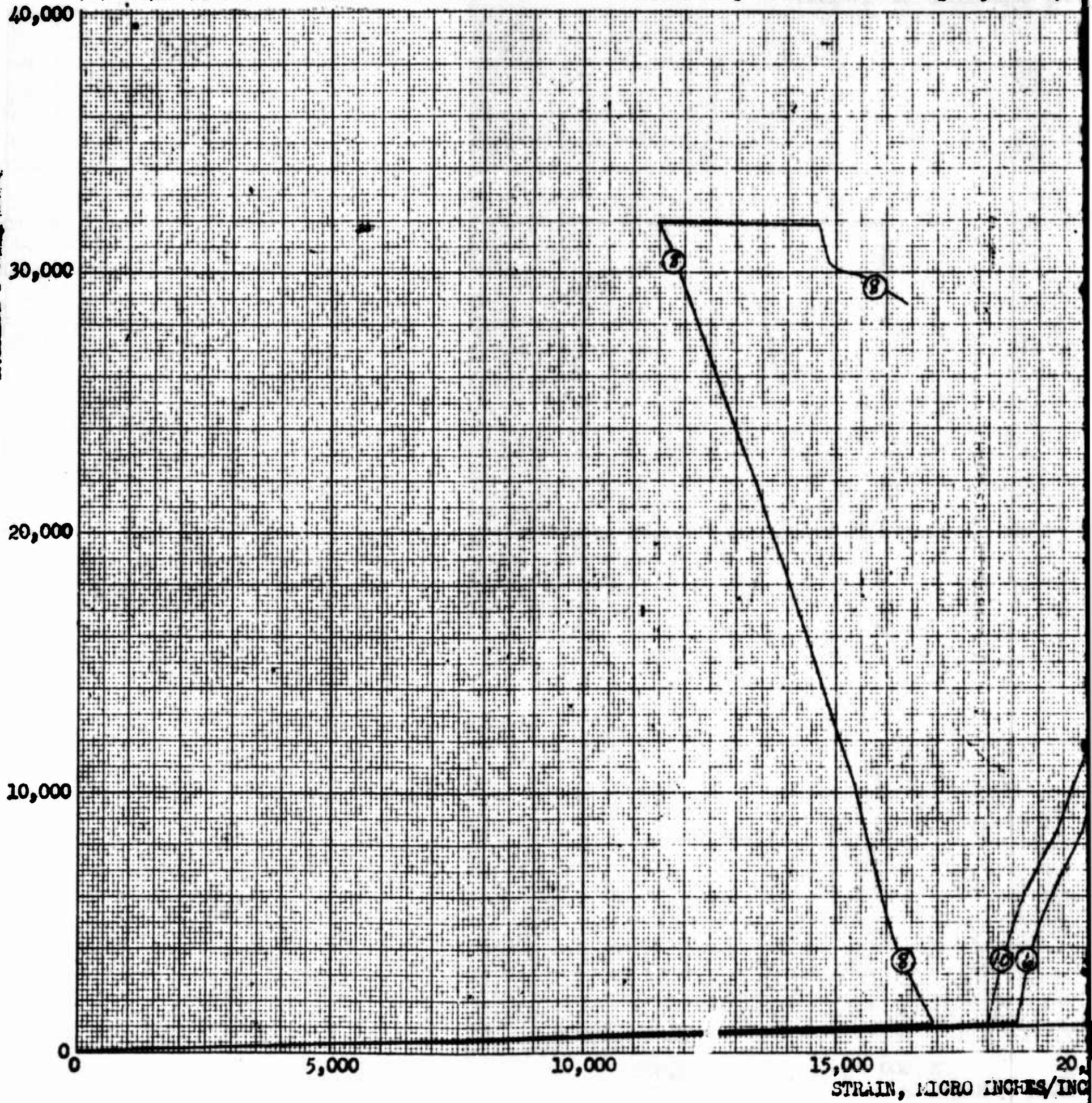
NOTE: Gages 1, 3, and 5 are hoop gages. Gages 2 and 4 are longitudinal on tension and compression sides respectively. Maximum bending moment was 1.52×10^6 in.-lb.

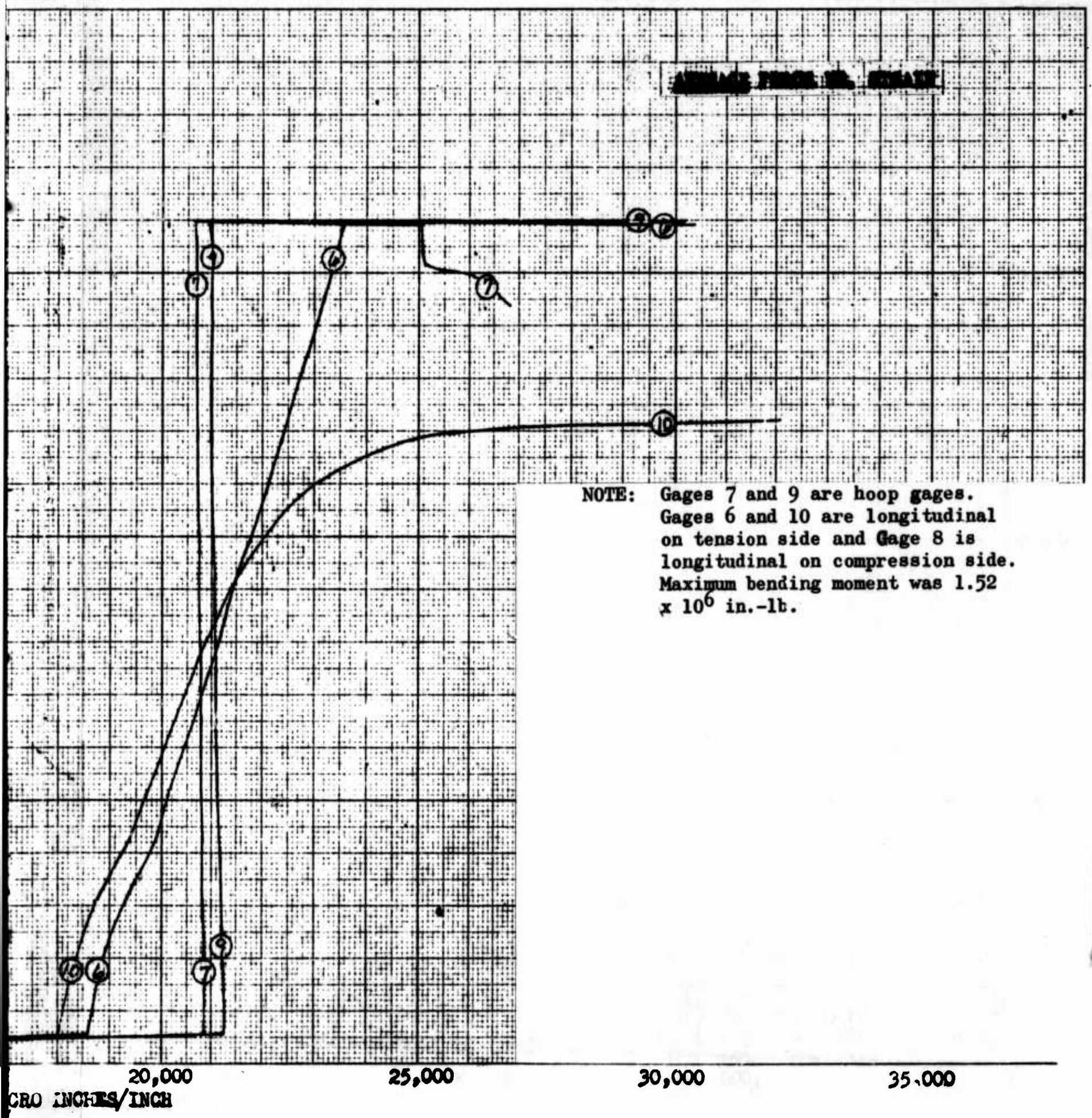
Figure 294. Average Force vs Strain

CONFIDENTIAL

2

5752-2416-TO-2009 RFG GFW 2416 To determine pressure and bending capability





NOTE: Gages 7 and 9 are hoop gages. Gages 6 and 10 are longitudinal on tension side and Gage 8 is longitudinal on compression side. Maximum bending moment was 1.52 x 10^6 in.-lb.

2

Figure 295. Average Force vs Strain

CONFIDENTIAL

(C) here to show the increase and decrease in measured longitudinal strain on the tension and compression sides respectively as the 1.52 x 10^6 in.-lb bending moment was applied. Hoop strain, as shown by gages 1, 3, 5, 7, and 9, remained constant at approximately 21,000 microinch/in. because of the 500 psig internal pressure (which also was held constant during application of the bending moment). Observation of the high speed movies shows that initial rupture occurred in the region of the forward skirt on the tension side of the case, as expected. The skirt was pulled partially off of the cylinder which no doubt weakened the cylinder and contributed to the lower-than-design burst pressure. Although rupture occurred at 640 psig, which was 19% lower than the predicted burst pressure, extrapolation to 3% strain of the hoop strain vs pressure curves indicates the GFW case would have burst at approximately 720 psig, even if the skirt had not torn loose. Longitudinal strains indicate the helical wrap was satisfactory for the planned load combination of 796 psig pressure and 2 x 10^6 in.-lb bending moment. This load combination actually represented an over-test for the GFW case, in that it was intended to withstand the ultimate burnout pressure of Motor B (625 psig) and the ultimate pressurized bending moment of only 3.75 x 10^5 in.-lb. Both of these values were exceeded in this test. The GFW case was designed and tested to the higher condition to make certain that the complete RFG/GFW Case Motor B would withstand the following ultimate unpressurized loads.

Bending moment, in.-lb	3.09 x 10^6
Axial compression, lb	1.54 x 10^3
Transverse shear, lb	3.8 x 10^3

This test showed conclusively that a better skirt-cylinder-dome junction would have to be fabricated to meet the unpressurized load requirements for the Motor B program. Although the case exceeded the required ultimate pressure, it was decided to use a 20% stress concentration factor in the design of the hoop wraps, at least until a better skirt fabrication technique proved it to be unnecessary.

e. Processing Procedure

When fabricating either Motor A or Motor B, the operations are essentially the same; therefore, only those operations that differ from Motor A will be presented here.

(1) Matrix Propellant Burning Rates

The first variation was in the matrix propellants. Some of the matrix propellants are common to both motors. These include RDS-514, -523 and -526. However, RDS-512 was used exclusively on Motor B and its data are presented below.

(C)

Designation	Lab Specification Number	Manufacturing Specification Number	Lab Advisory Number	Liquid Strand Rate (in./sec)	Remarks
RDS-512	RA0119-908	RA0119-909	28	0.34--0.50 at 1000 psi	25 to 45% grind/total AP (used on Motor B)

(2) Core Propellant

The procedure discussed under Motor A was essentially the same for Motor B until the core propellant was mixed. In Motor B, the 25-gallon or 200-gallon mixer was used. Another area of variance was in the preparation of the RFG surface for casting the core grain. For Motor B, the preparation was more extensive. After thoroughly cleaning with toluene-dampened cloths, the aft boss area was filled with R-140 (per motor design) then forward and aft doublers were installed. The doubler surfaces to be bonded to propellant, load rings, or bosses, were primed with Chemlok EXB-500-1, and then bonded in place, using a coating of R-140 adhesive. For core propellant bonding, the RFG surface was MAPO primed, as in Motor A, and the doubler surfaces primed with Chemlok EXB-500-1.

After RFG preparation for core casting, the procedure for both motors was again similar.

f. Aerospace Ground Equipment

In support of both Motor B and Motor C scheduled deliveries, the following AGE items were required by contract:

	Description	Quantity
1.	Container, Shipping Motor	4 ea.
2.	Container, Shipping Igniter	4 ea.
3.	Container, Explosive Ordnance	4 ea.
4.	Transportation Trailer	1 ea.
5.	System, Support Adapter	4 ea.
6.	Adapter Cradle, Transportation	4 ea.
7.	Sling, Hoisting	4 ea.
8.	Protector, Thrust Vector Control System and Expansion Cone	4 ea.
9.	Panels, Protective	4 ea.
10.	Kit, Ordnance Item Servicing	2 ea.
11.	Kit, Ordnance Test	2 ea.
12.	Cover, Nozzle Exit Area	4 ea.
13.	Cover, Propulsion System	4 ea.

Major effort accomplished with respect to AGE was primarily associated with formulating the handling concepts and preliminary design of containers and transportation trailer. Most of the early work was directed toward providing those items which would be used to test Motor C at the NAA Reno Facility. Subsequent deletion of Motor C allowed the AGE effort to be deferred until late in the program.

Prior to resuming work on AGE, a visit was made to AEDC to coordinate the required AGE. This conference led to reductions in the over-all items required. Based on available equipment at AEDC and the deletion of Motor C, the following list of items were required to support the delivery of two Motor B's.

	Description	Quantity
1.	Container, Shipping Motor	2 ea.
2.	Container, Shipping Igniter	2 ea.
3.	Saddle, Horizontal Position	2 ea.
4.	Sling, Hoisting and Handling	1 ea.
5.	Panels, Protective	2 ea.
6.	Support, Vertical Position	1 ea.

Only minor work was undertaken prior to work stoppage.

PREVIOUS PAGE WAS BLANK, THEREFORE WAS NOT FILMED

SECTION VII

MOTOR B FULL-SCALE FABRICATION AND TEST

After RFG and GFW case development was completed and a processing procedure for Motor B was established, the first full-scale Motor B was fabricated. Only two full-scale Motors B were completed; components for the third motor were partially processed. These motors are discussed in the following sections.

1. MOTOR B-2001

(C) Design of Motor B-2001 was flightweight since the motor was scheduled for hydrostatic pressurization to failure. However, by direction of RPL, EAFB, the test was changed from a single pressure excursion to rupture to two pressure cycles from 0--1170 psig followed by pressurization to rupture. The RFG contained all eleven layers while the GFW case and liner were also per flightweight design. (However, the finished liner was slightly thicker due to needed tooling modification.) This motor was not scheduled to have a core grain.

a. Fabrication

(1) Equipment

The same general type of equipment used in the Motor A program was employed under the Motor B program. Since this motor was made for hydrotesting without a core, the internal boss insulation and the ballistic sleeve were not used. The last load ring to go on the forward boss was attached by screws instead of a locking ring as on Motor A.

Mandrel assembly and liner application were similar to Motor A. One exception was the use of split rings between each polar boss and the sand mandrel. The rings were used to allow sand mandrel molding before the bosses were fabricated. After mandrel cure the rings were machined to match the bosses.

(2) Materials

The same materials used for Motor A were used for Motor B with one exception: a No. 322 strippable vinyl coating was used on the inside surfaces of the bosses. This material was being considered for use as a moisture barrier and a protective coating for the internal boss surfaces that were to be bonded to core propellant on future motors. This material still appeared good after mandrel washout.

(3) Processing

(a) Grain Winding and Restriction

(C) Winding began at 1630 on 31 August 1964 and ended at 1100 on 8 September 1964 (7.75 days). Data taken during winding indicated the forward boss Total Indicator Reading (TIR) changed from 0.031 to 0.045 inch and the aft boss TIR changed from 0.016 to 0.040 inch. Initial boss-to-boss length was 61.07 inches decreasing to 60.98 inches at the finish. The design specified 242 covers; 258 covers were used. The 16 extra covers were required as the design cover thickness was 0.0185 inch and the actual obtained was 0.01748 inch. Grain winding data are presented in Tables XXCV and XXCVI.

The propellant used was generally of a higher burning rate than that used in Motor A. However, the propellant planned for Motor B-2002 has lower burning rates than that used on B-2001 and is nearer that used on Motor A. Refer to Tables XXCVII and XXCVIII for propellant data.

(C) The grain was restricted with a wipe coat, fill coat, and final coat of R-143 with a required finished diameter of 35.798 $\pm$ 0.015 inch. A fourth coat was applied to achieve a smoother surface. The final coat was cured for 24 hours rather than 48 hours to expedite processing. The final restrictor diameter was 36.075 (forward), 36.050 (center) and 36.033 (aft) inches resulting in an average restrictor thickness in the cylindrical section of 0.210 inch, rather than the 0.060-inch design thickness.

Four pantograph traces 90 degrees apart were made of the cured grain. After final restriction the grain was pantographed again at the same positions. In the cylindrical section a maximum and minimum thickness of 0.24 and 0.15 inch was noted. On the domes the maximum and minimum thicknesses were 0.32 and 0.08 inch.

CONFIDENTIAL

TABLE XXCV

MOTOR B-2001 GRAIN WINDING DATA*

Layer	Covers		Cycle Dia, in.			Avg Cycle Thickness, in.	Avg Cover Thickness, in.	Cycle Winding Time, hr
	Target	Actual	Aft	Center	Fwd			
1GI	6	6	26.970	26.975	26.970			
1A	2	1						
1B	3	2						
1C	4	3						
1D	4	3						
1E	5	6	27.505	27.550	27.500	0.425	0.0202	15.25
2GI	6	6						
2A	2	2						
2B	3	3						
2C	2	6						
2D	3	4						
2E	8	10	28.460	28.475	28.420	0.4675	0.01508	11.33
3GI	6	6						
3A	3	4						
3B	3	3						
3C	5	5						
3D	7	7						
3E	1	3	29.37	29.412	29.35	0.4625	0.01652	21.66
4GI	6	6						
4A	3	5						
4B	4	4						
4C	4	5						
4D	4	3						
4E	5	3		30.232		0.4100	0.01577	17.33
5GI	6	6						
5A	3	3						
5B	3	3						
5C	4	4						
5D	5	5						
5E	2	4	31.000	31.005	31.005	0.3855	0.01542	15.33
6GI	6	6						

*Mandrel Diameter, in.: Aft, 26.675; Center, 26.665; Fwd, 26.661

CONFIDENTIAL

TABLE XXCV
(Continued)

Layer	Covers		Cycle Dia, in.			Avg Cycle Thickness, in.	Avg Cover Thickness, in.	Cycle Winding Time, hr
	Target	Actual	Aft	Center	Fwd			
6A	4	4						
6B	3	4						
6C	4	4						
6D	4	4						
6E	2	6	31.990	31.910	31.980	0.4785	0.0171	16.33
7GI	6	6						
7A	3	3						
7B	4	4						
7C	4	4						
7D	4	4						
7E	2	4	32.86	32.800	32.80	0.420	0.01680	18.66
8GI	6	6						
8A	4	4						
8B	4	5						
8C	4	4						
8D	4	4						
8E	1	0						
8F	0	4	33.678	33.608	33.636	0.421	0.01559	25.50
9GI	6	6						
9A	2	3						
9B	3	3						
9C	3	4						
9D	4	4	34.525	34.460	34.500	0.427	0.02135	21
9E	2	0						
10GI	6	6						
10A	3	3						
10B	4	4						
10C	5	6						
10D	4	2	35.415	35.390	34.415	0.456	0.0217	26
10E	2	0						
11GI	7	6	35.685	35.685	35.665	0.1355	0.0226	5.75
Total	242	258	35.600	35.672	35.625	N/A	0.01748	7.75 days

CONFIDENTIAL

CONFIDENTIAL

TABLE XXCVI

MOTOR B-2001 DIMENSIONAL CHANGES

	Boss-to-Boss Length, in.	Boss TIR, in.	
		Fwd	Aft
Start of Winding (61.07 + 1.313)*	62.383	0.031	0.016
End of Winding (60.98 + 1.313)*	62.293	0.045	0.040
After Case Winding	62.286		
After Mandrel Washout	62.169		
Before Hydrotest	62.134		

*Correction to include GFW flange length increase of 1.313 inches

TABLE XXCVII

RFG PROPELLANT BURNING RATES

	B-2001			B-2002 (Planned)	
Cycle	Type	Mix No.	Strand Rate, in./sec	Type	Strand Rate, in./sec
1	512	L-8-25-M-82	0.377 at 1015	512	0.336 at 1015
2	514	L-8-25-M-81	0.284 at 745	514	0.261 at 695
3	514	L-8-24-M-82	0.272 at 740	514	0.225 at 645
4	514	L-8-24-M-81	0.264 at 735	514	0.196 at 595
5	514	L-8-21-M-82	0.244 at 710	523	0.173 at 545
6	514	L-8-21-M-81	0.211 at 660	523	0.153 at 495
7	514	L-8-20-M-82	0.187 at 610	523	0.134 at 440
8	523	L-8-20-M-81	0.157 at 475	523	0.130 at 400
9	523	L-8-19-M-82	0.129 at 420	523	0.130 at 400
10	523	L-8-19-M-81	0.129 at 412	523	0.130 at 400
11 GI	523	L-8-19-M-81	0.129 at 412	523	0.130 at 400

TABLE XXCVIII

MOTOR B-2001 AMBIENT PROPELLANT PHYSICALS

Type	Mix	e_m, %	S_m, psi	E, psi
512	L-8-25-M-82	15*	210*	956*
514	L-8-25-M-81	18	194	1543
514	L-8-24-M-82	21	193	1506
514	L-8-24-M-81	19	185	1527
514	L-8-21-M-82	21	163	1224
514	L-8-21-M-81	23	184	1401
514	L-8-20-M-82	17	162	1407
523	L-8-20-M-81	26	132	822
523	L-8-19-M-82	19	91	742
523	L-8-19-M-81	13	62	713

*Samples had bubbles

(b) GFW Case

The GFW case was wound on 12 and 13 October. Winding time (including machine adjustments) for the case was 26 hours. Problems encountered during winding included: (1) difficulty in controlling hydraulic oil temperature and, therefore, machine smoothness, (2) drift of the locked-out Y-axis during circ winding, (3) hangup of the X-axis system during the circ winding, (4) binding in the tailstock machine bearing causing variation in mandrel RPM, and (5) inability of the cure cart to rotate the motor during cure.

During cure, the motor was manually rotated 180 degrees every 10 minutes for 1 hour then at 15-minute intervals for 1 hour.

(C) The case, B-2401, was wound to flightweight requirements of 1004 ends per inch in the helix wrap and 1480 ends per inch in the circ wrap. Five-inch long skirts, extending from the cylinder section forward and aft, were integrally wound with the circ wrap. The helix was wound in two covers and the circ in eight covers.

The helix wrap was more uniform than on the previous development GFW case, B-2415. This uniformity improvement was attributed to shifting the pattern slightly forward during the first cover and slightly aft during the second cover to improve pattern stability.

The circ wrap also was smoother than B-2415. This was accomplished by removing slack from the cam drive system and using a different delivery feed eye to obtain a wider, overlapping pattern.

Both skirts were fabricated, although it was realized that the forward skirt would be structurally inadequate due to excessive skirt tooling deflection. The discontinuity was not expected to affect the case test, and it was desirable to include in this test the effect of the skirt cloth which extends into the cylinder. The aft skirt was not as smooth as desirable due to excess resin in the cloth, insufficient B-staging, and oversized, restricted motor diameter. These problems were corrected on future cases.

(C) Case appearance was also improved by a reduction in surface resin on the cured case, which also indicated a lower resin content than the 24.3 weight percent obtained on B-2415.

(C) Weights and dimensions of B-2401 are shown in Tables XXCIX and XC. As indicated, the weight of the case, 54.6 pounds, is an estimated figure. Actual weight is not available due to a change of spindles during setup for case winding; no subsequent weight was obtained. Therefore, the weight obtained after case winding could not be compared to the weight of the restricted grain to obtain case weight. A case weight which does not require spindle weight was calculated by the use of other weights obtained during processing. A value of 60.2 pounds was obtained. However, this weight does not appear realistic in view of the facts that actual glass weight is known, and resin content is visibly lower than the 24.3 weight percent obtained on B-2415. The 60.2-pound weight would indicate a resin content of 27.5 weight percent.

TABLE XXCIX

DIMENSIONS AND WEIGHTS OF GFW CASE B-2401, MOTOR B-2001

B-2401 Dimensions	
Restricted Mandrel OD, in.	
Forward	36.075
Center	36.050
Aft	36.033
Average	36.053
Cured Case OD, in	
Center	36.217
Indicated Case Thickness, in.	
Center	0.083
Skirt OD (before skirt mandrel removal), in.	
Forward (10 cloth layers)	36.170
Aft (14 cloth layers)	36.268
Skirt ID, in.	
Forward	35.880
Aft	35.880
Skirt Thickness, in.	
Forward (10 cloth layers)	0.145
Aft (14 cloth layers)	0.194
Diameters after Skirt Ring Installation and Mandrel Washout, in.	
Forward Skirt	
π Tape	36.148
Caliphers (2 readings)	36.136
Cylinder	
π Tape	36.187
Calipers (6 readings)	36.155
Aft Skirt	
π Tape	36.183
Calipers (2 readings)	36.237

TABLE XXCIX
(Continued)

Lengths, in.	
Boss to Boss	
After Mandrel Washout	62.169
Prior to Testing	62.134
Cylinder (set by restrictor template)	36.75
Skirt Length	4.91
Skirt to Skirt (set by adjustable skirt stops)	46.57
Skirt Ring to Skirt Ring	55.99
B-2401 Weights, lb	
Helix Roving	17.91
Circ Roving	15.42
Aft Skirt Cloth	5.44
Forward Skirt Cloth	3.89
Total Glass	42.66
Estimated Resin at 20 Wt %	10.67
Glass and Resin	55.33
Skirt Fill Grommets	1.30
Estimated Total Weight	54.63

TABLE XC

MOTOR B-2001 WEIGHT HISTORY AND ALUMINUM PERCENT

Component Weight, lb	Component	Assembly
1580.80	Sand, spindle, tenite, RTV	1580.80
13.17	Load rings	1593.97
2.70 (est)	Threaded load ring	1596.67
10.29	Aft boss	1606.96
13.43	Forward boss	1620.39
18.41	Split rings	1638.80
4.00 (est)	Tape	1642.80
306.44	Wire	1949.24
1441.76	Propellant	3391.00
10.72	GFW flange	3401.72
54.58	Restrictor (R-143)	3456.30
60.20	GFW case	3516.50
46.14	Skirt rings	3562.64
1603.21	Sand, spindle, tape, RTV, and split rings	1959.43

Aluminum Percentage
$\frac{306.44 \text{ lb wire} \times 100}{306.44 \text{ lb wire} + 1441.76 \text{ lb propellant}} = 17.5\%$

(4) Postwinding Procedures

The mandrel was washed out in shorter time than Motor A mandrels. The Motor B mandrel support tube projected out the lower aft end and allowed a better seal of tape and polyethylene to be applied as a cap. This cap held water and allowed soaking, until the support tube slipped downward enough to knock the cap loose. Removal of this support tube caused considerable time delay. The hoist used to lift the motor away from the support tube is not located high enough above the ground to clear the length of the support tube without repositioning the Pneumagrip fixture holding the motor.

After removal of the support tube and lightening tubes, the split rings were removed to avoid the possibility of the rings falling and causing damage to the liner or grain. However, when they were removed, the outside surface stuck to the liner. As a result the liner was pulled away from the grain. This allowed some water to reach the grain surface. After liner removal, the grain surface was dried with rags.

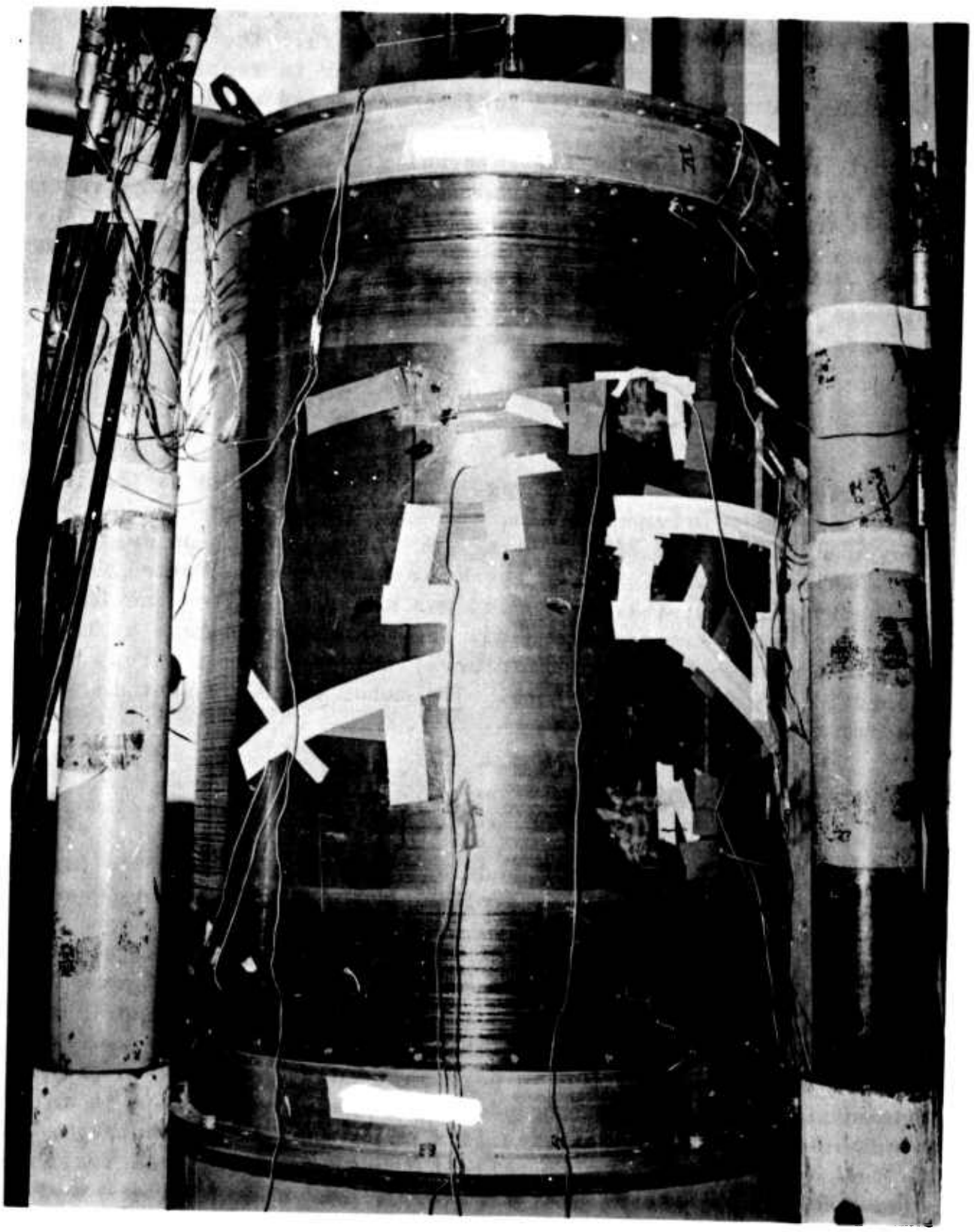
A visual inspection showed the internal grain surface to be in good condition. A 100 F oven was not readily available so the fan was connected and cell air was moved through the grain until the oven was ready. The grain was dried for 2 hours at 100 F, 2 hours at 120 F and 2 hours at 130 F. Time elapsed from the first addition of water until the grain went into the oven was approximately 4.33 hours. Further inspection of the inner surface revealed no water damage.

(5) Final Assembly

After instrumentation (strain gages) had been applied to the interior surface of the reinforced grain, the interior surface was coated with seven applications of LAGZ coating for water protection during hydrotest. While the LAGZ coating operation was being performed, the external instrumentation (strain gages) was applied. After the LAGZ coating dried, the motor was sent to X-ray for tangential X-rays at the liner-to-grain and case-to-liner interfaces; no defect indications were discovered in the tangential shots. The motor was then sent to the test area for testing.

b. Testing

(C) Motor B-2001 was originally scheduled for pressurization to failure to determine the ultimate strength of the Motor B RFG/GFW case composite. However, based on an AF directive from Edwards AFB, the test was rescheduled to include two pressure cycles to 1170 psig followed by pressurization to failure. Subsequently, additional strain gages were added to the external surface of the motor to provide substitute instrumentation in case of damage during the initial pressure cycles. Previous tests of this type resulted in permanent loss of a portion of the instrumentation, therefore, the additional gages were added in an attempt to provide sufficient data even if a major portion of the gages failed. The test plan was changed to reflect the AF directive and testing was initiated on 27 October 1964 (Fig. 296).



2YA32-10/27/64MIA

Figure 296. Closeup of Motor Prior to Testing Cycle 1 (B-2001)

(1) Analysis

(C) Maximum recorded RFG and GFW case strains are shown in Table XCI. The GFW hoop strains were somewhat less than expected. For the Phase 1 maximum pressure of 1150 psig, maximum hoop strain in the cylindrical portion of the GFW case was 0.895% as shown in Table XCI and was well below the 3.0% expected strain at rupture. Maximum strain in the forward dome was 0.597% at Gauge 53 whereas the maximum strain in the aft dome was 1.01% at Gauge 21. (Strain gauge locations are shown in Fig. 297). Both of these strains were also well below 3.0% and occurred at points very close to the polar bosses, illustrating a localized condition. The maximum internal hoop strain at the inner surface of the grain was 1.49% at Gauge 31A. This strain was also less than the expected wire rupture strain of 5%.

(C) The 1150-psig pressure was removed and the motor was visually inspected. No external case damage was detected. Circumferential ridges were found in the forward dome area inside the motor. It could not be definitely concluded whether the ridges were caused by water between layers of LAGZ coating, water between LAGZ coating and grain, ridges of LAGZ coating, or by a buckled RFG layer. Figures 298 and 299 show the motor after the first pressure cycle. Figure 300 shows pressure vs time for the first phase.

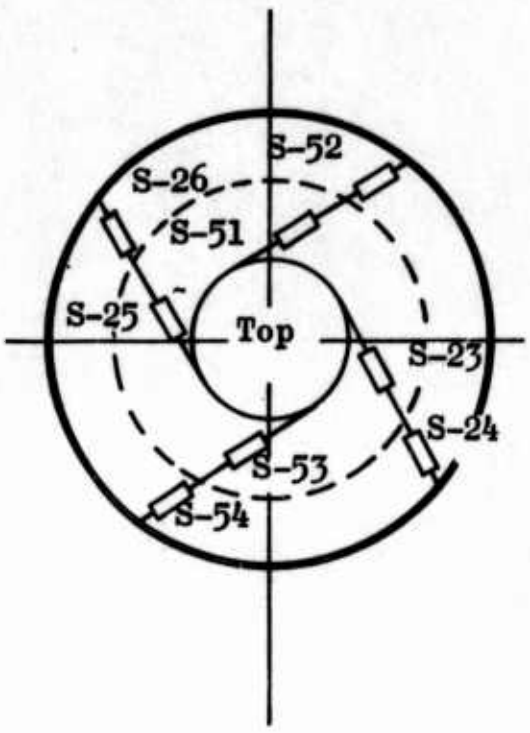
(C) The strain gauges were then zeroed and Phase 2 was initiated. The maximum pressure obtained was approximately 1160 psig. Hoop strains in the cylindrical portion of the GFW case were, in general, 0.2 to 0.3% lower than those recorded during Phase 1. The maximum strain in the forward dome was 0.624% at Gauge 21. Internal hoop strains at the inside surface of the grain were generally 0.6% lower than those found in Phase 1 with the maximum strain in Phase 2 equal to 1.052% recorded at Gauge 31A. The 1160-psig pressure was removed and another visual inspection performed. External observations revealed crazing of the resin due to longitudinal growth of the motor. This was verified by a dimensional check of the unit which showed that the motor had increased in length by about 0.010 inch during Phase 2. Internal inspection revealed the same ridges again in the forward dome region and they were more severe than those noted after Phase 1. The LAGZ coating was torn over one of the ridges to determine the nature of the ridge and it was definitely confirmed that the RFG had buckled when it was depressurized. Figures 301 and 302 show the motor after Phase 2 testing. Pressure vs time for Phase 2 is shown in Fig. 303.

TABLE XCI

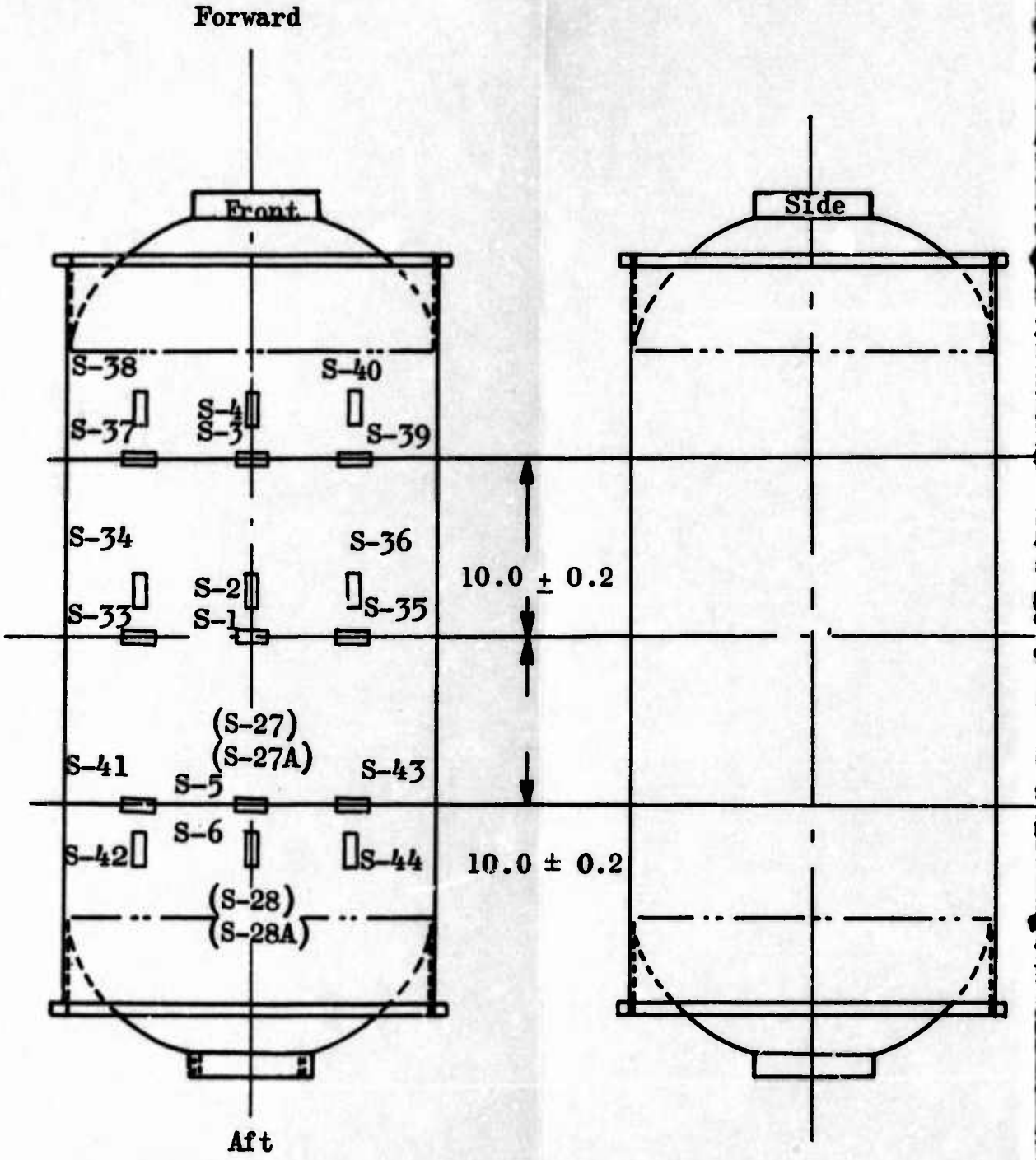
MAXIMUM RECORDED RFG AND GFW CASE STRAINS

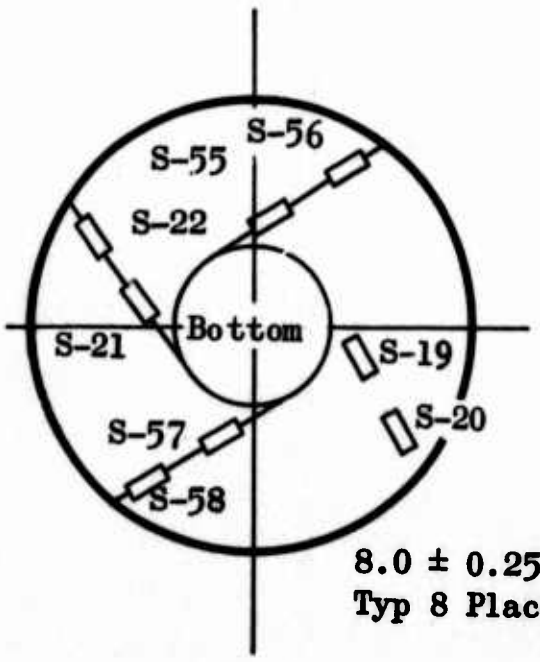
Phase Number	Maximum Pressure, psig	Maximum Strain Micro-in./in.			
		GFW Case			RFG
		Cylinder Hoop	Forward Dome	Aft Dome	Inside Hoop
1	1150	8,950	5,970	10,100	14,900
2	1160	5,850	6,240	8,650	10,520
3 (Hydroburst)	1430	13,250	8,430	10,700	16,980*

*Last recorded strain before losing gauge at 1401 psig



Front





8.0 ± 0.25 True
Typ 8 Places

NOTE: Figures in parenthesis are on inner surface of RFG.

1

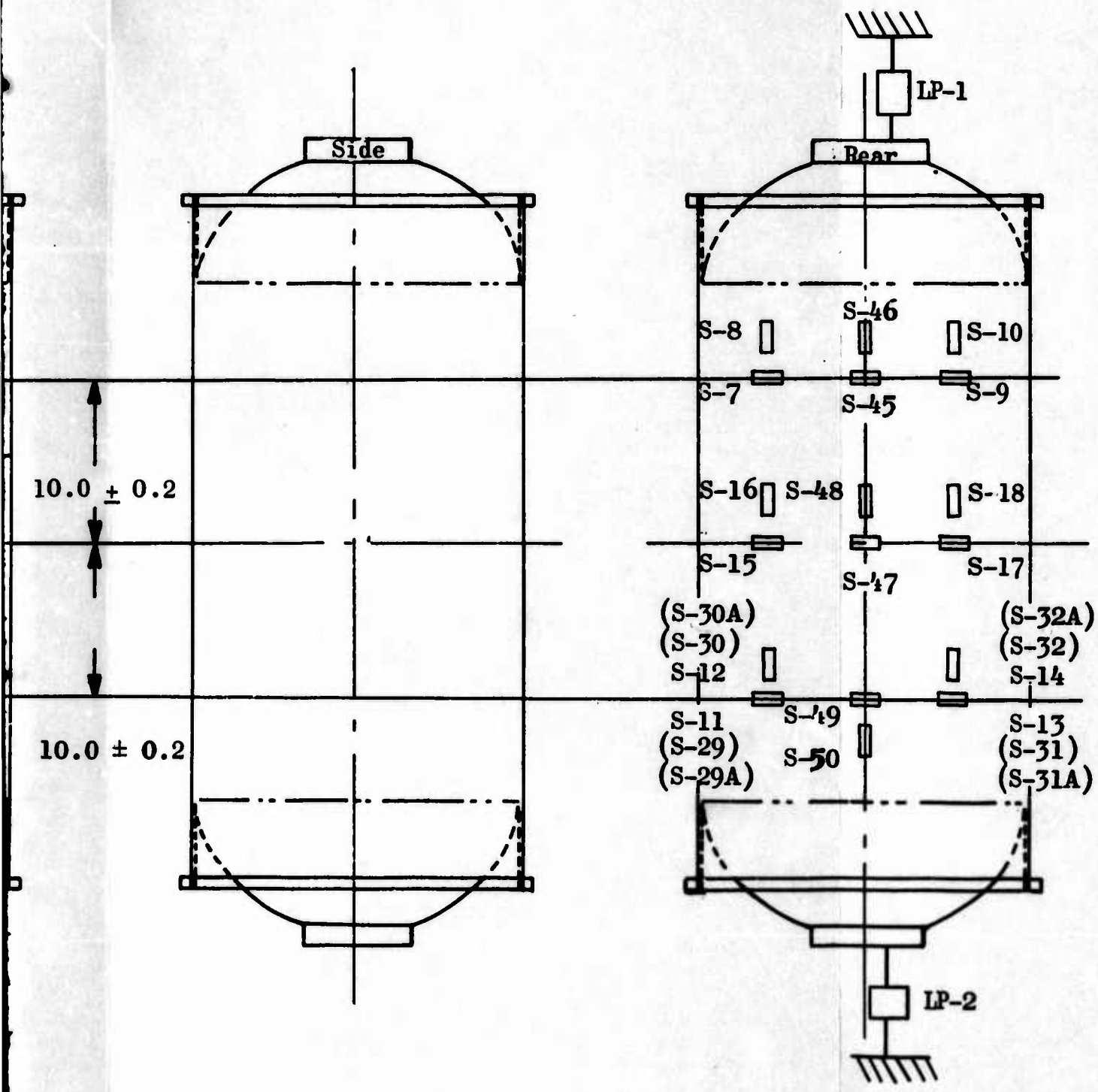


Figure 297. Location of Strain Gauges and Linear Potentiometers for Motor B-2001

2

PREVIOUS PAGE WAS BLANK, THEREFORE WAS NOT FILMED

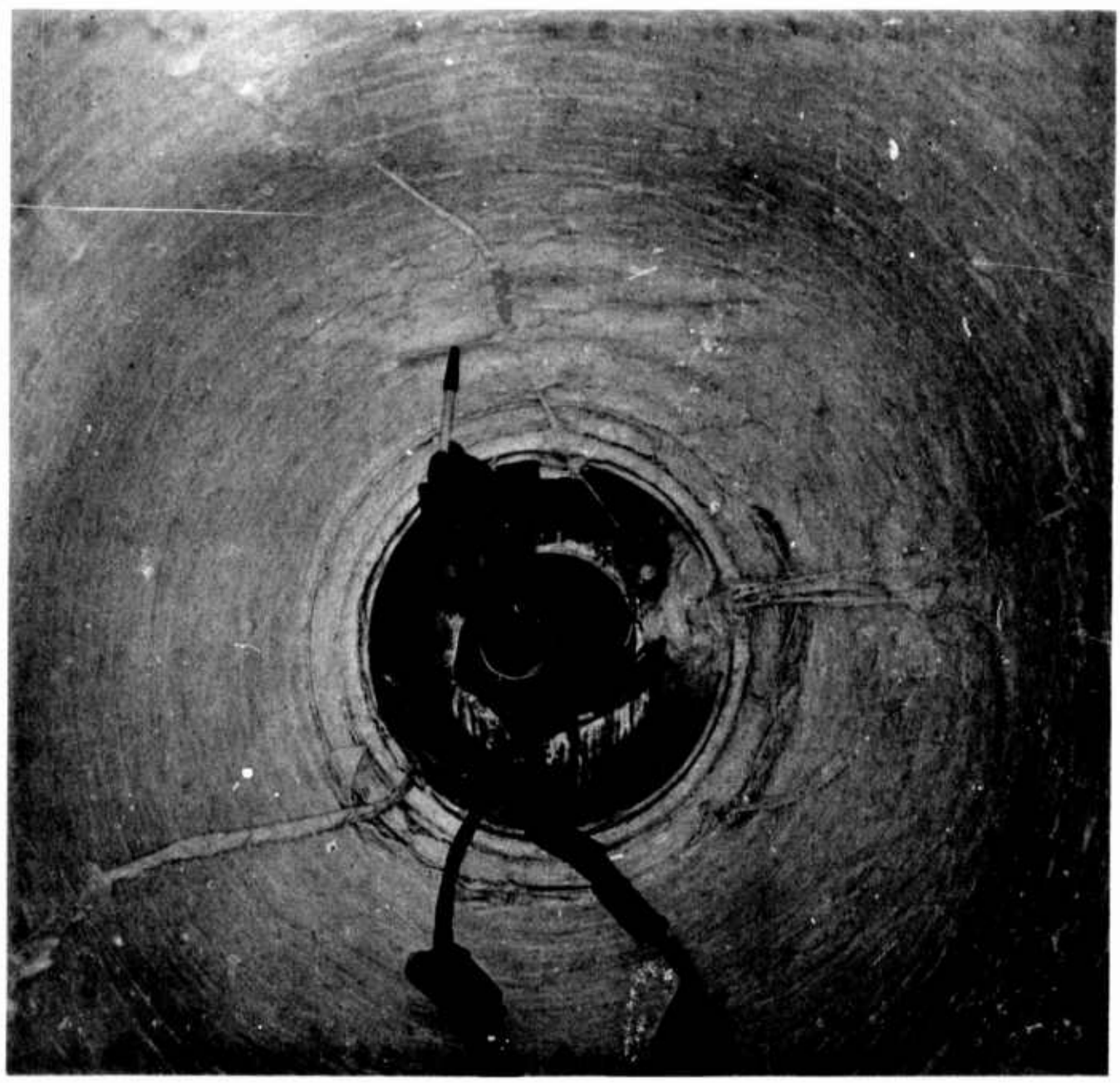


Figure 298. Forward Dome, Internal, After First Pressure Cycle (Note: Buckled grain under LAGZ coating)



Figure 299. Aft Dome, Internal, After First Pressure Cycle

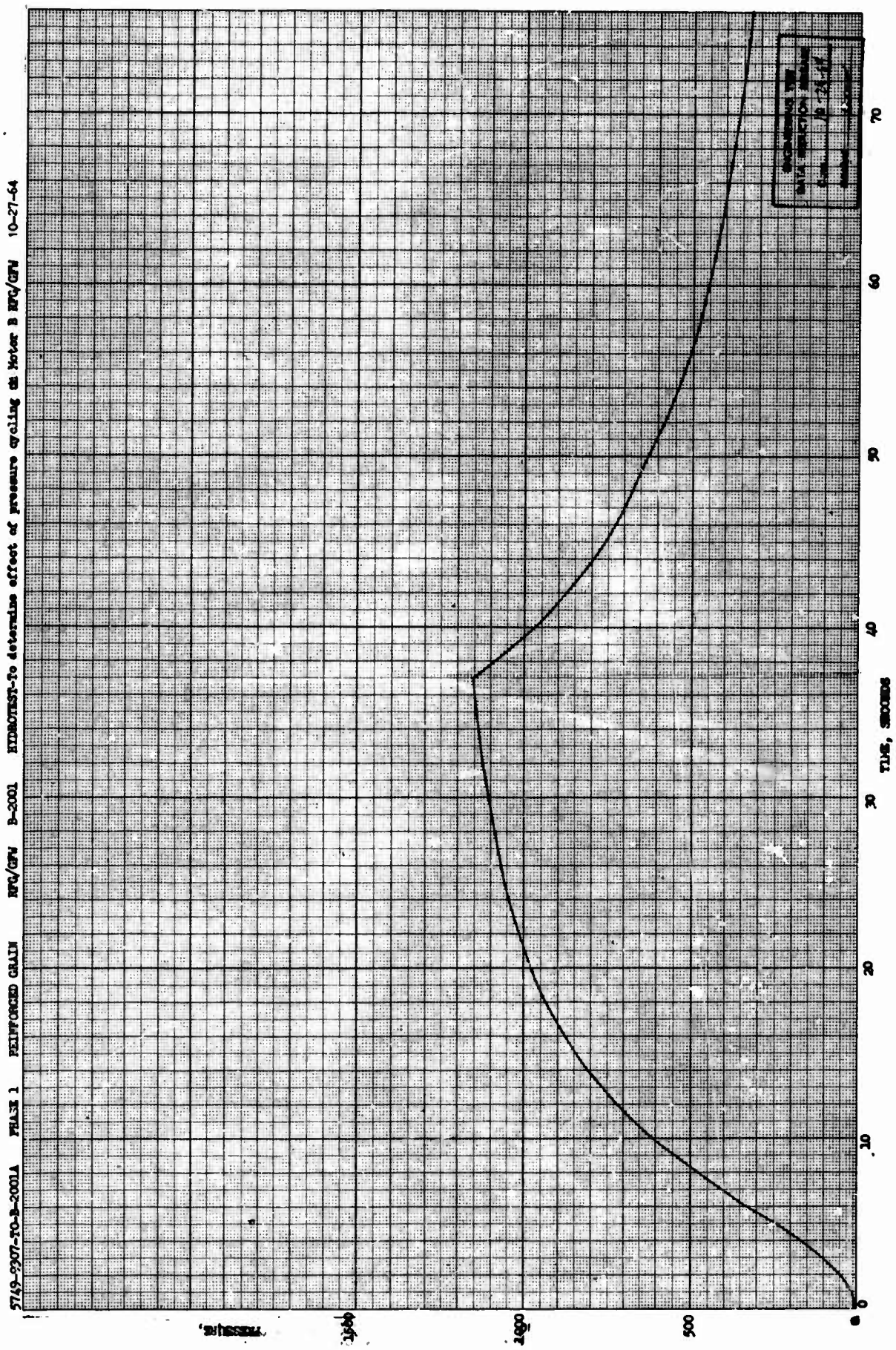


Figure 300. Pressure vs Time for Motor B-2001

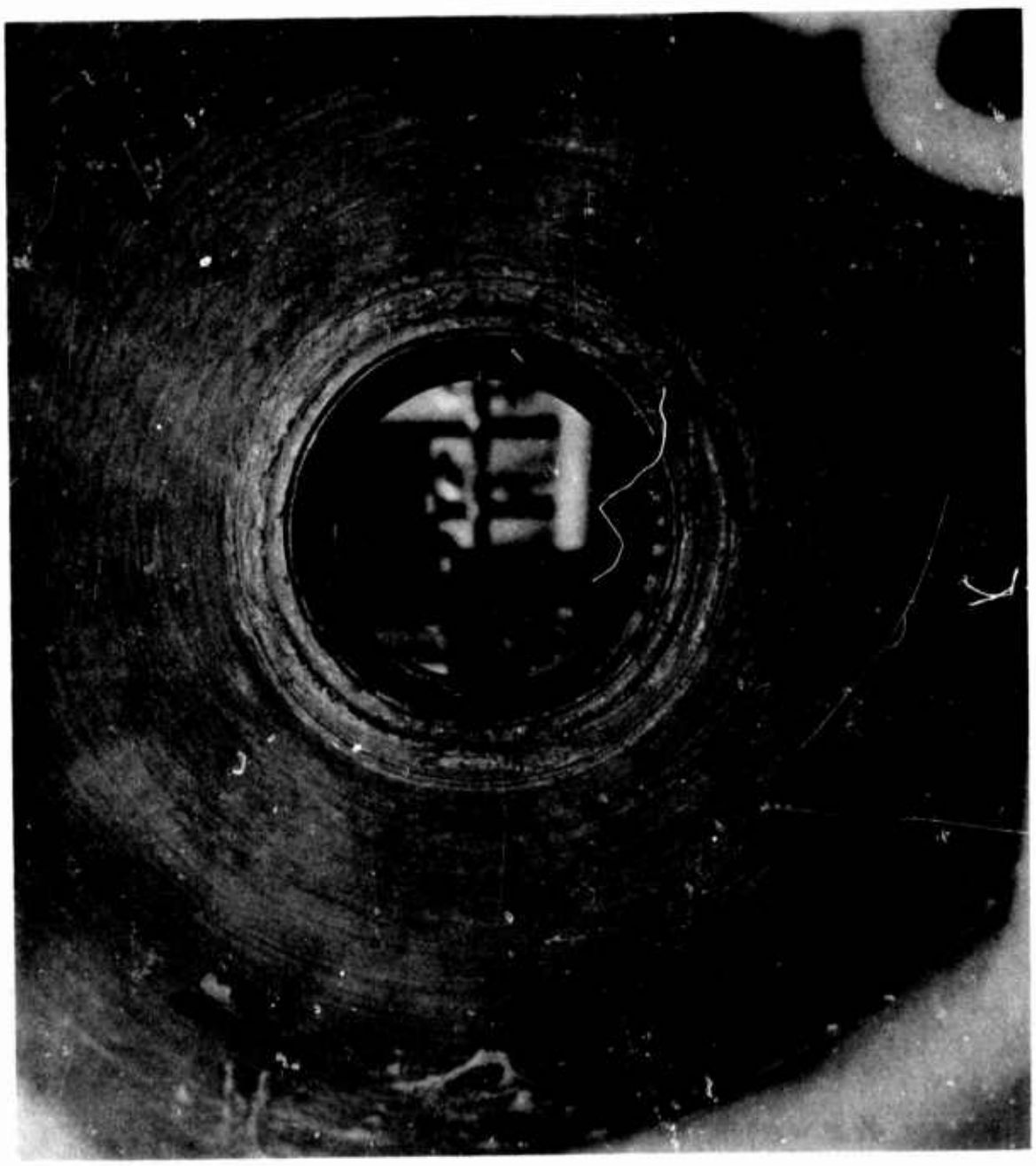


Figure 301. Aft Dome, Internal, After Second Pressure Cycle



2YA35-10/28/64M2A

Figure 302. Forward Dome, Internal, After Second Pressure Cycle (Note: Numerous grain buckles)

CONFIDENTIAL

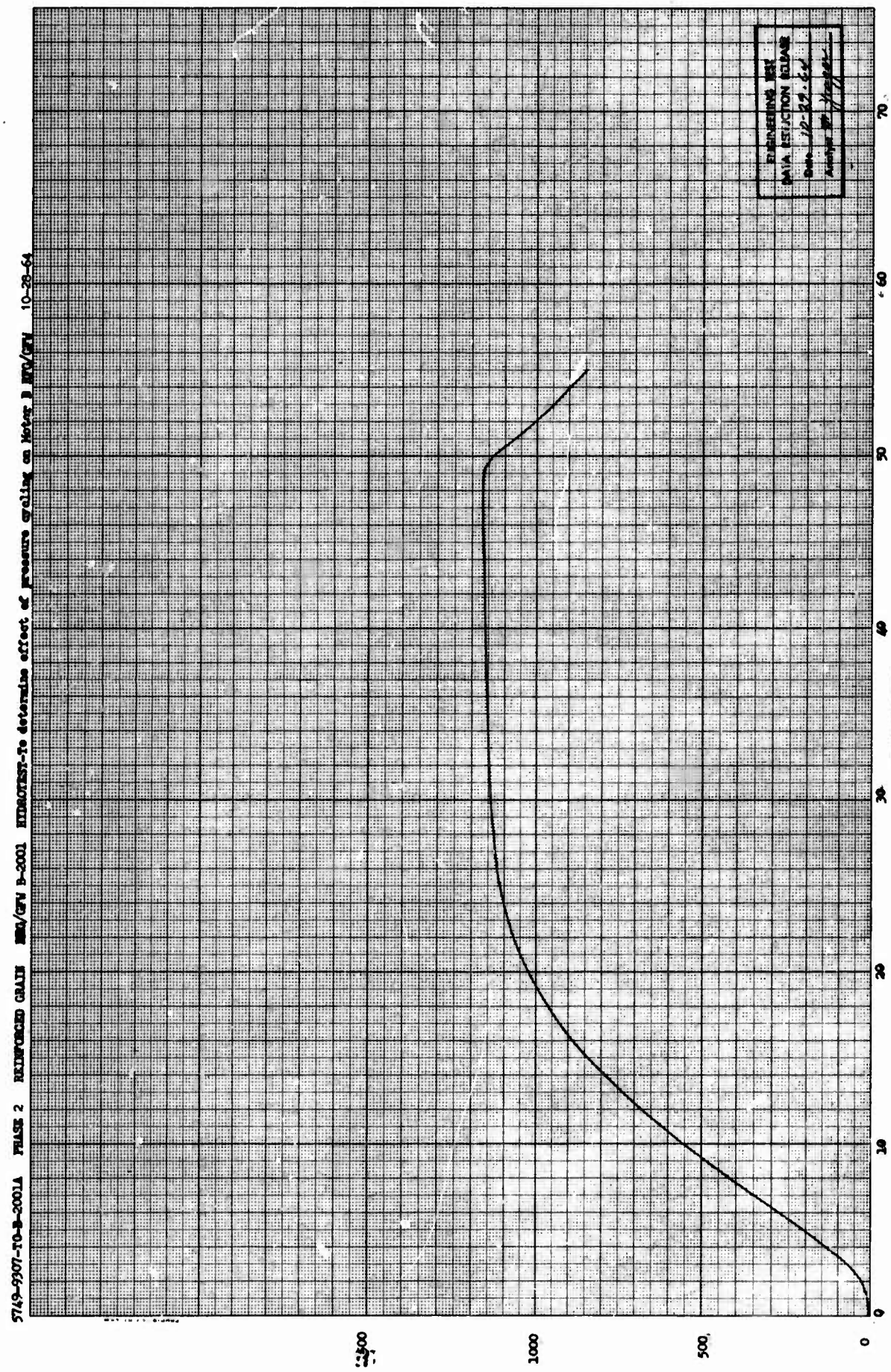


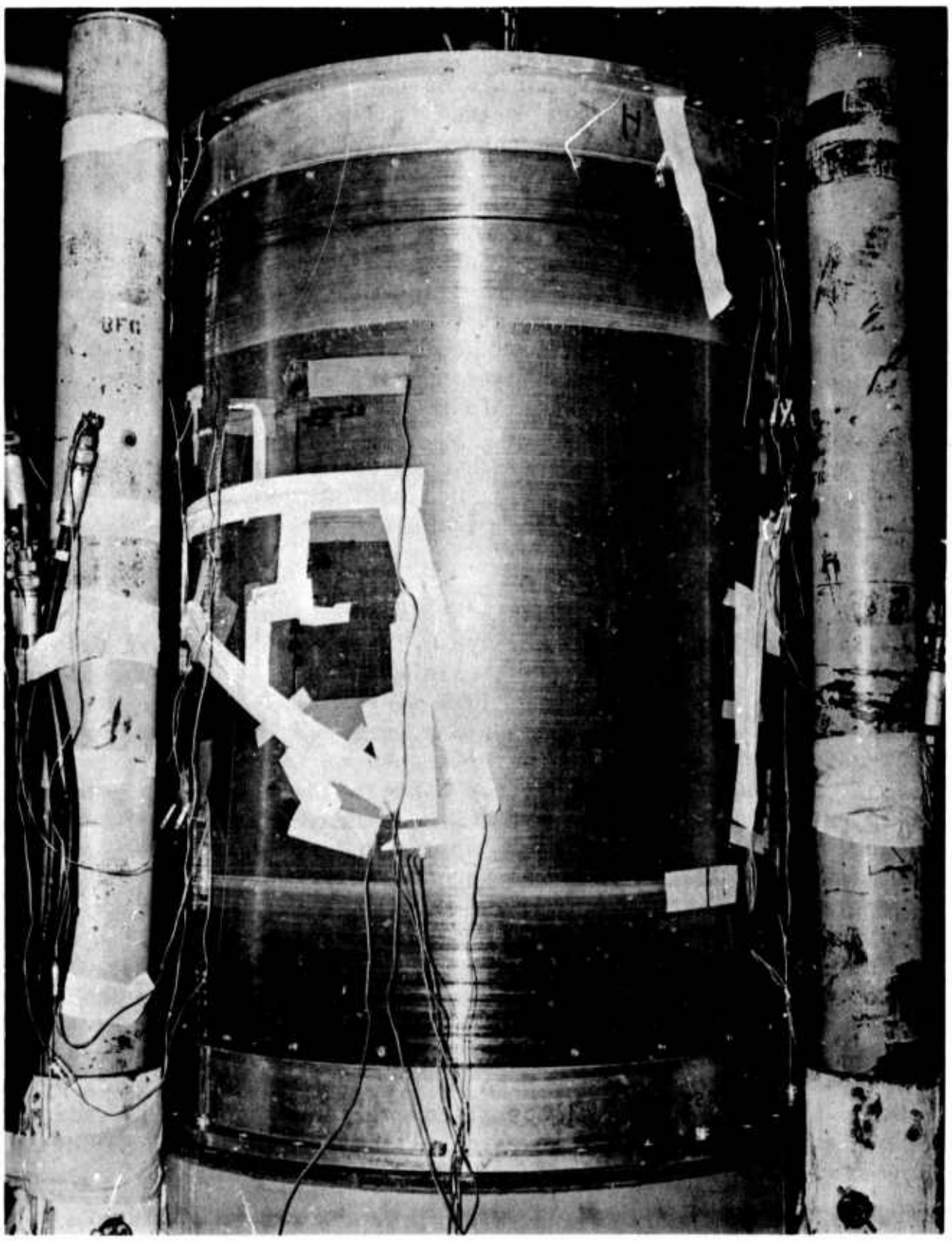
Figure 303. Pressure vs Time for Motor B-2001

(C) The gauges were zeroed again and Phase 3 (hydroburst) commenced. During Phase 3 the motor reached its maximum pressure of 1430 psig. At that time the pressure decreased to about 560 psig and the test was terminated. Maximum hoop strain in the cylindrical portion of the GFW case was 1.325% at Gauge 47. Maximum GFW case strain in the forward dome was 0.843% at Gauge 53 whereas in the aft dome the maximum strain was 1.07% at Gauge 21. The maximum internal hoop strain at the inner surface of the grain occurred at Gauge 29 and was 1.698% for a pressure of 1401 psig.

Visual inspection revealed heavy resin crazing on the cylinder of the GFW case and the forward dome, with light crazing on the aft dome. Two internal longitudinal buckles about 4 inches wide and 3 inches high ran the full length of the cylindrical section. These ridges were about 180 degrees apart. The forward dome buckles that were present at the end of the second cycle increased in size and at the largest place were oval shaped with dimensions about 7 by 5 by 3 inches high. Further inspection revealed that the grain had failed in this buckled region of the forward dome and that the water had passed through or by the LAGZ coating into the grain. Figures 304 through 308 show the motor after Phase 3.

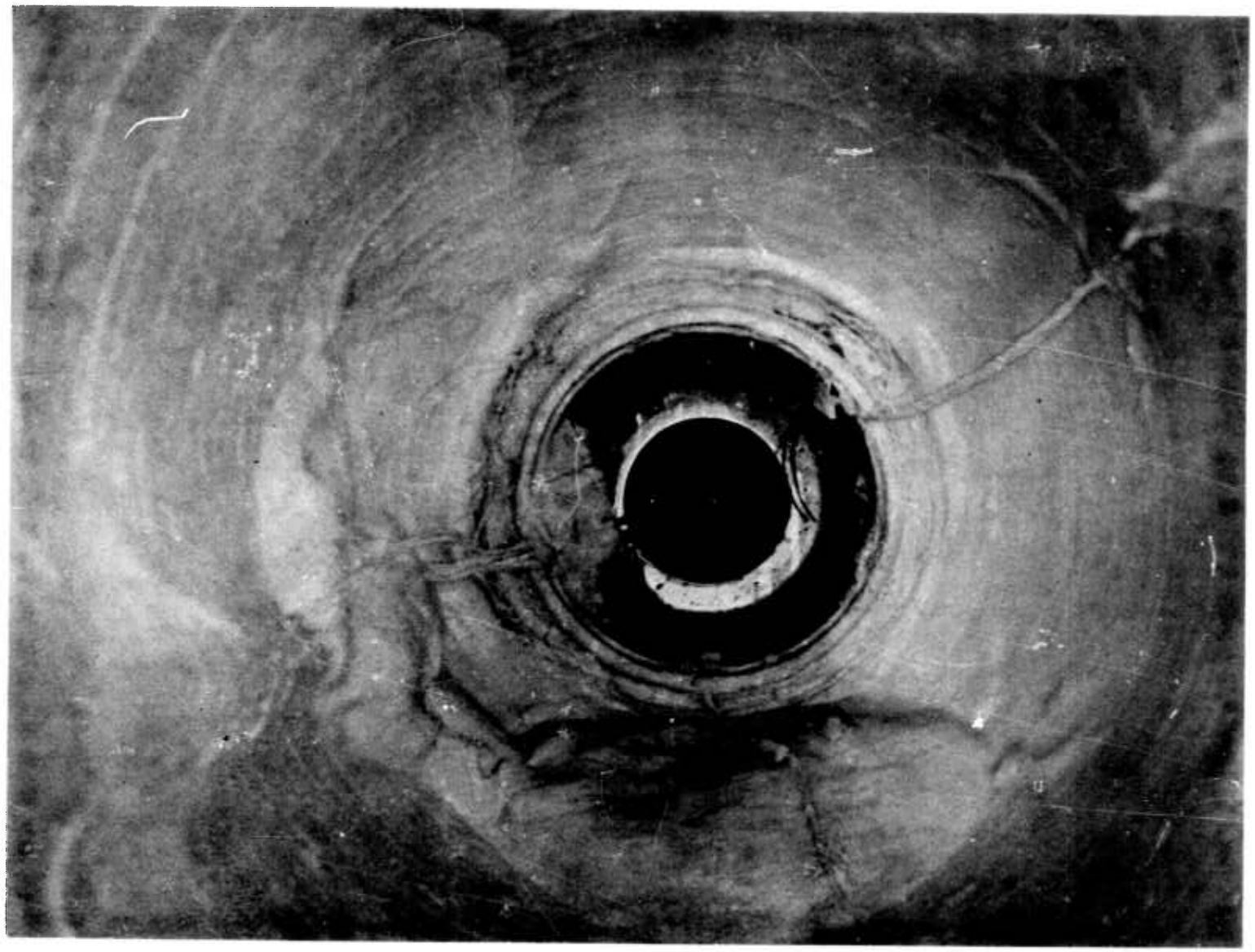
Replots of reduced data for Phase 3, Fig. 309 show strain vs pressure only to the point of maximum pressure. The recorded digital data, however, show longitudinal GFW case strain continued to increase although chamber pressure was decreasing. This increase of GFW case strain and a corresponding decrease in chamber pressure has been observed in all RFG/GFW motor hydrotests when the RFG ruptures without rupturing the GFW case. GFW case strains increase because the chamber pressure acts directly on the case when the RFG fails, rather than on the composite structure. The increased GFW case strain and resultant increase in volume caused the sudden decrease in chamber pressure.

(C) Extrapolation of the test pressure-vs-strain curve, Fig. 310 indicates the GFW case would not have ruptured until the chamber pressure reached approximately 1850 psig if the RFG had not ruptured first. The relatively low burst pressure of the RFG (1430 psig) is attributed to the fact that the aluminum wires on the inside surface of the RFG were loaded beyond the yield point twice before the hydroburst cycle (Phase 3). Even with the cyclical loading, however, the rupture pressure was 14.4% higher than the required design ultimate pressure of 1250 psig.



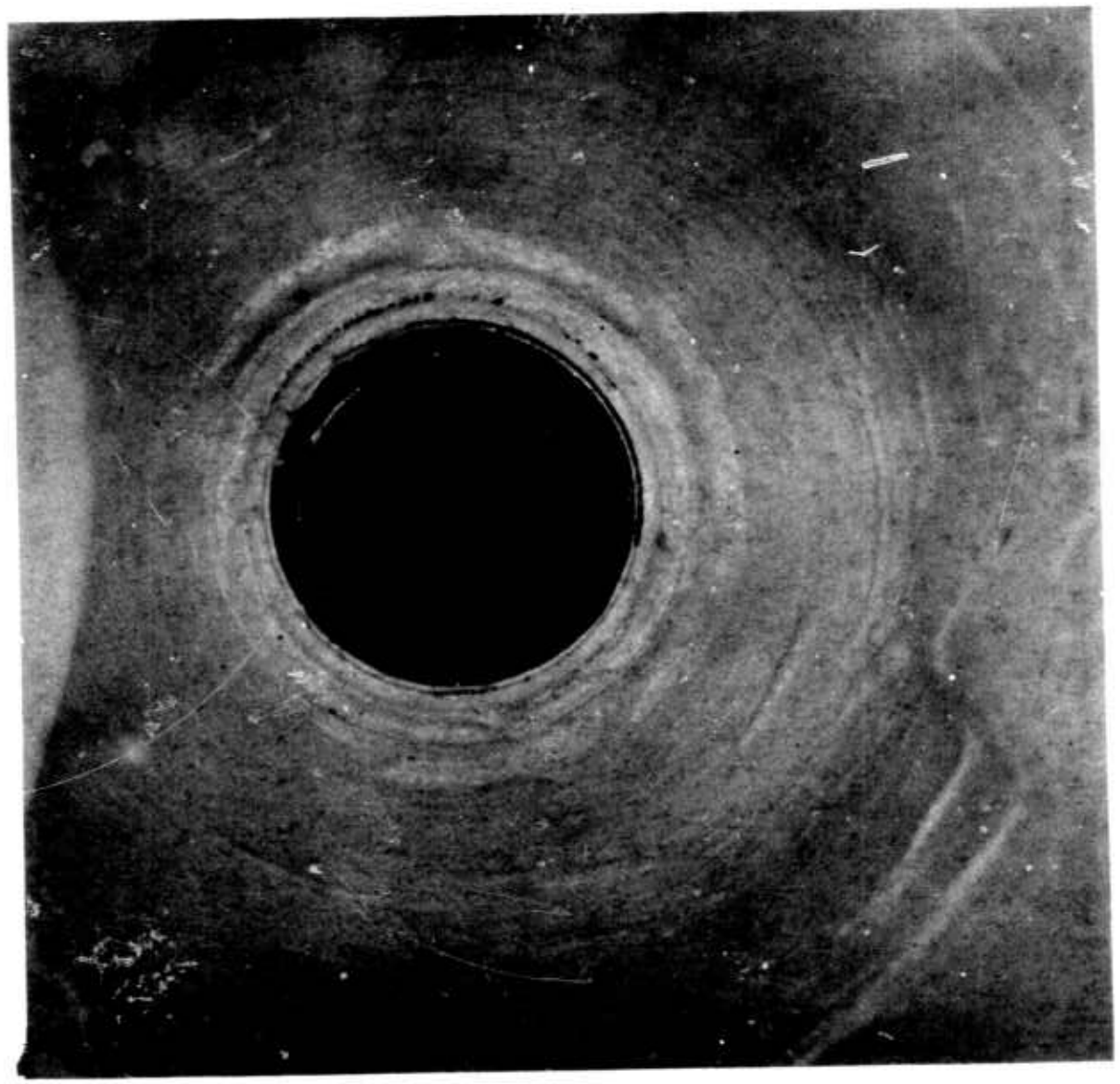
2YA35-10/28/64M3B

Figure 304. External View After Third Pressure Cycle (Note: Water)



2YA35-10/28/64M3D

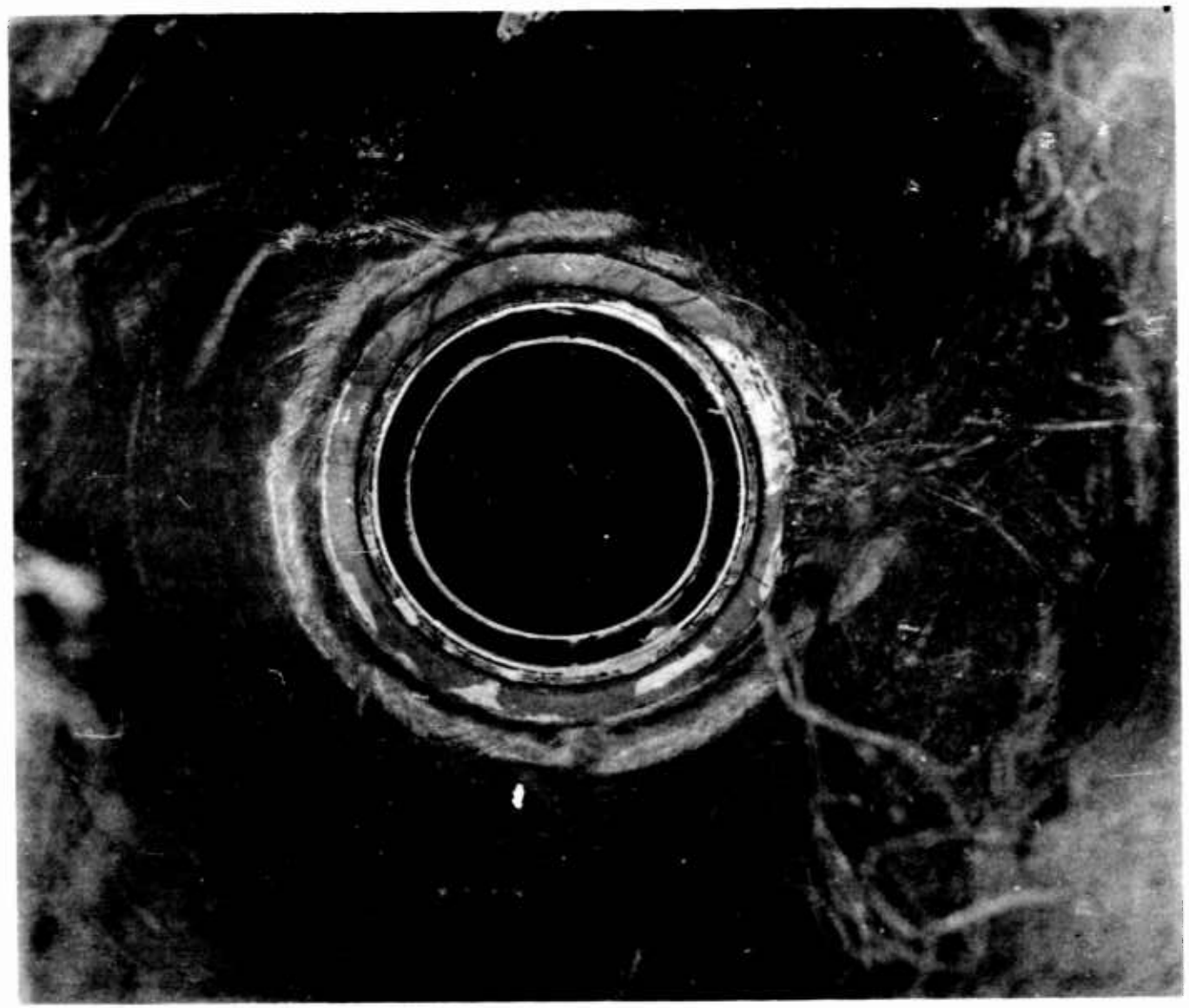
Figure 305. Forward Dome, Internal, After Third Pressure Cycle (Note: Forward dome and two cylinder buckles)



2YA35-10/28/64M3C

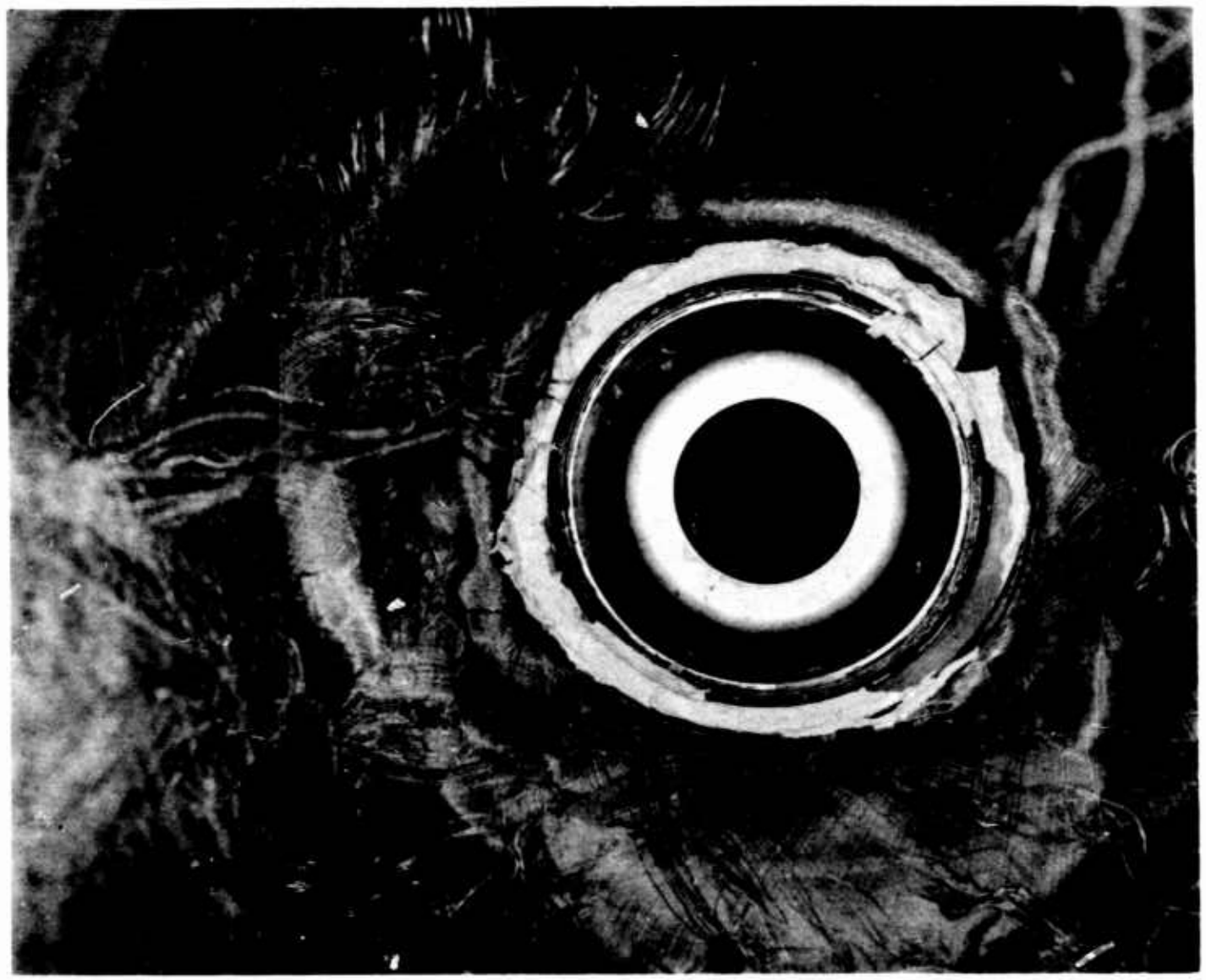
Figure 306. Aft Dome, Internal, After Third Cycle (Note: Buckling around polar opening and down cylinder)

CONFIDENTIAL



2YA35-10/29/64M1C

Figure 307. Aft Dome, Internal, After Third Pressure Cycle With LAGZ Coating Removed (loose wire was pulled free during removal of LAGZ coating liner)



2YA35-10/29/64M1A

Figure 308. Forward Dome, Internal, With LAGZ Liner Removed After Third Pressure Cycle (Note: Tear in forward dome buckle, approximately 8 o'clock)

CONFIDENTIAL

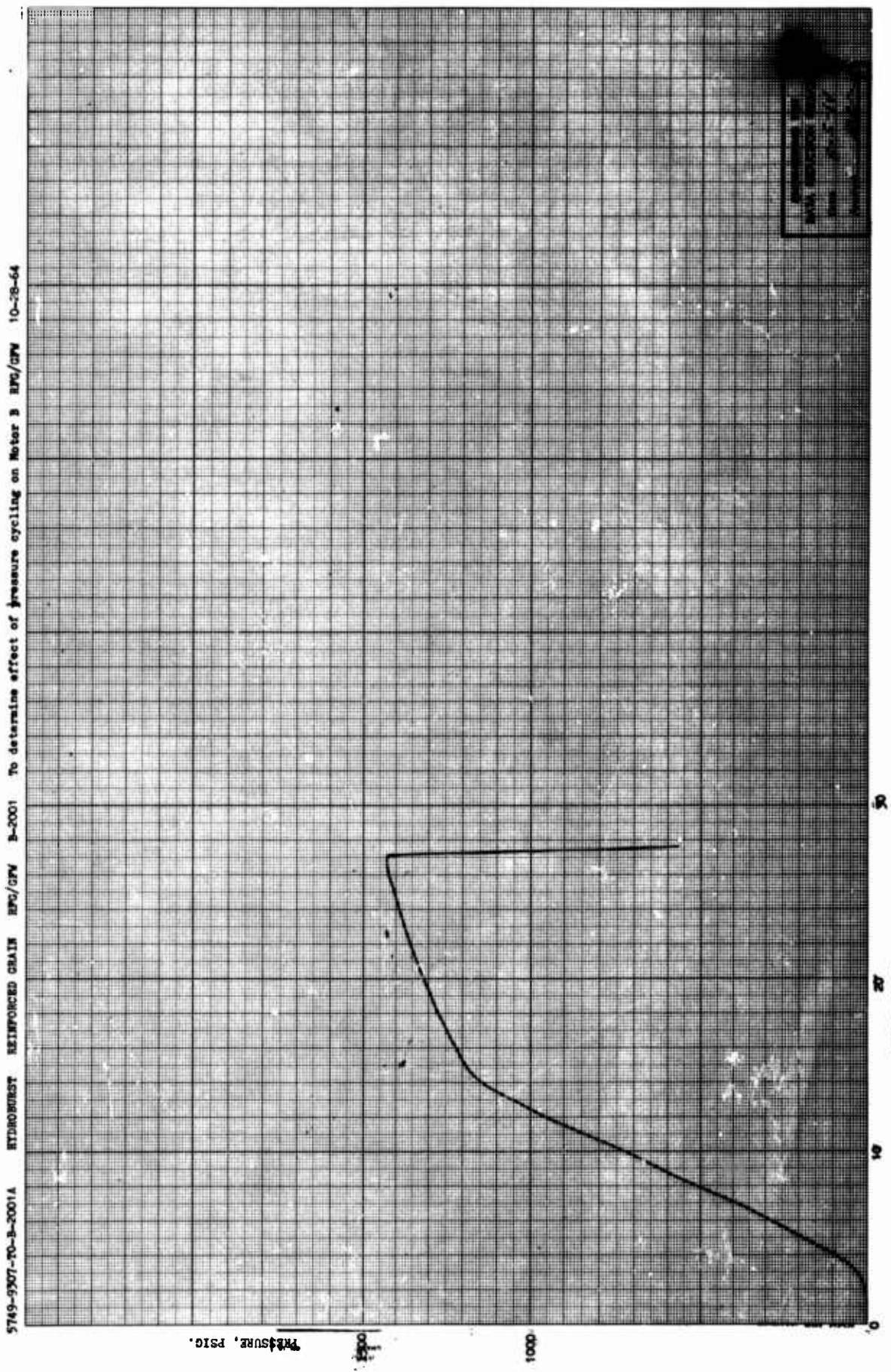


Figure 309. Pressure vs Time for Motor B-2001

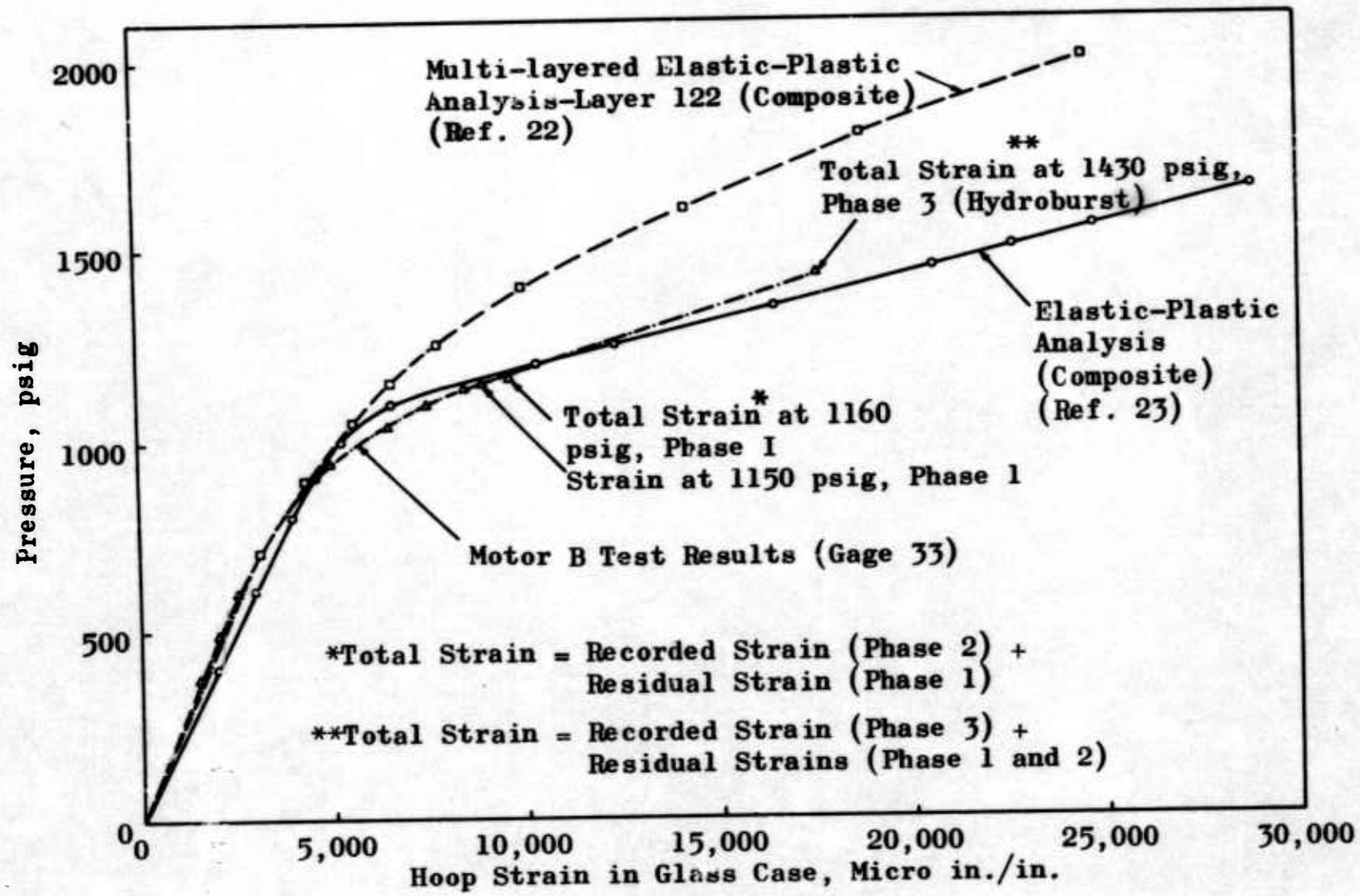


Figure 310. Pressure vs Hoop Strain in Glass Case

(2) Conclusions and Recommendations

Two theoretical analyses, which were not available when the motor was designed, are compared to test results to evaluate both methods of analysis. References 22 and 23 are theoretical methods which have been utilized to establish separate computer programs. After the descriptive physical characteristics of the materials involved are selected for the computer, it solves the elastic-plastic equations and prints out values of the desired parameters. Therefore, the curves plotted in this report for both references utilize the computer print out for the particular elastic-plastic solution.

(C) Figure 310 is a plot of internal pressure vs hoop strain in the glass case. Although both references agree very closely with test results, Ref. 22 is more accurate in the elastic region up to a pressure of about 850 psig. From this point onward, Ref. 23 has much better correlation. It should be noted that the residual hoop strains in the GFW case from test Phases 1 and 2 have been added to the strain obtained in Phase 3. This extends the pressure vs strain curve and allows a broader range for comparison. For an allowable hoop strain in the GFW case of 3.0%, the extrapolated burst pressure for a single pressure cycle from test data would be about 1850 psig. Based on extrapolation of theory, Ref. 2 tends to be closer than Ref. 22 in predicting burst pressure. A better evaluation would have been possible if the motor had been hydrotested to rupture in only one cycle.

(C) Internal pressure vs hoop strain at the inner surface of the RFG is shown in Fig. 311. In the elastic region, Ref. 2 more closely follows test results and the Phase 1 test termination point lies nearly on the Ref. 23 curve. Due to the inelastic strains developed on the inner surface of the RFG, the strains from Phases 1 and 2 cannot be added to Phase 3 strain. Therefore, only Phase 1 strain is plotted. If the motor had been pressurized to failure on a one-cycle basis and the curve from test could be extrapolated, the predicted burst pressure from test would be about 1750 psig based on an allowable strain in the RFG of 5.00%. This would compare very favorably with the predicted burst pressure of about 1800 psig from the Ref. 22 curve (Layer 1) whereas Ref. 23 predicts about 1650 psig. Although the strain gauge was near the skirt, the induced discontinuity strains should have been small. A final evaluation in this region may be made only with additional data from a one-cycle burst test.

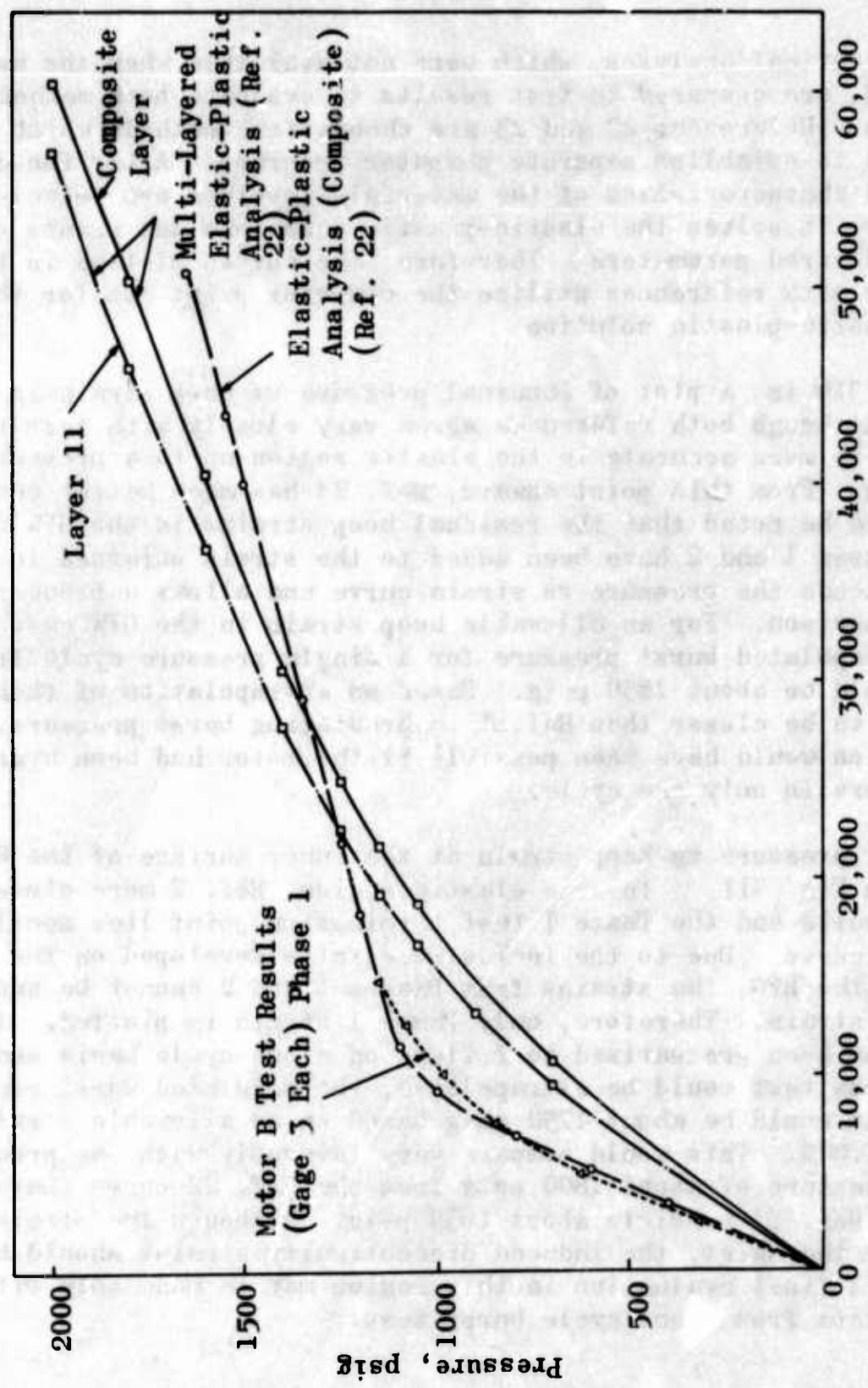


Figure 311. Pressure vs Hoop Strain at Inner Surface of RFG

Figure 312 represents plots of composite hoop stress vs composite hoop strain in the hoop wrap of the GFW case. Both stress and strain were calculated using the theoretical results of the two analyses and show good agreement. Composite hoop stress vs hoop strain for the total GFW case wall is also shown in Fig. 312.

(C) Hoop stress vs hoop strain at the inner surface of the RFG is shown in Fig. 313. The curve was obtained using Ref. 23 analysis and shows a significant decrease in hoop stress after reaching a maximum value of about 2400 psi. This decrease is typical for the maximum shear theory of yielding utilized in Ref. 22.

All of the data shown in Figs. 310 through 313 were calculated by a digital computer. An IBM 7094 and 1401 is used for Ref. 22 and 23 respectively.

Based on the results of the test and analyses, the following conclusions are drawn:

1. Structural performance of Motor B-2001 exceeded design requirements although the motor was subjected to two pressure cycles prior to hydroburst.
2. Reference 23 theoretical data show better correlation with GFW case test data than Ref. 22. A final evaluation of RFG theoretical data may be made only with additional one-cycle burst tests.
3. More test data are needed to provide a conclusive evaluation of the referenced analyses. The tests should be conducted on a one-cycle-to-rupture basis to provide better test data as well as to assist in establishing the validity of the two methods of analysis.
4. Strain gauge instrumentation functioned satisfactorily with a minimum loss of gauges during the three phases of tests.

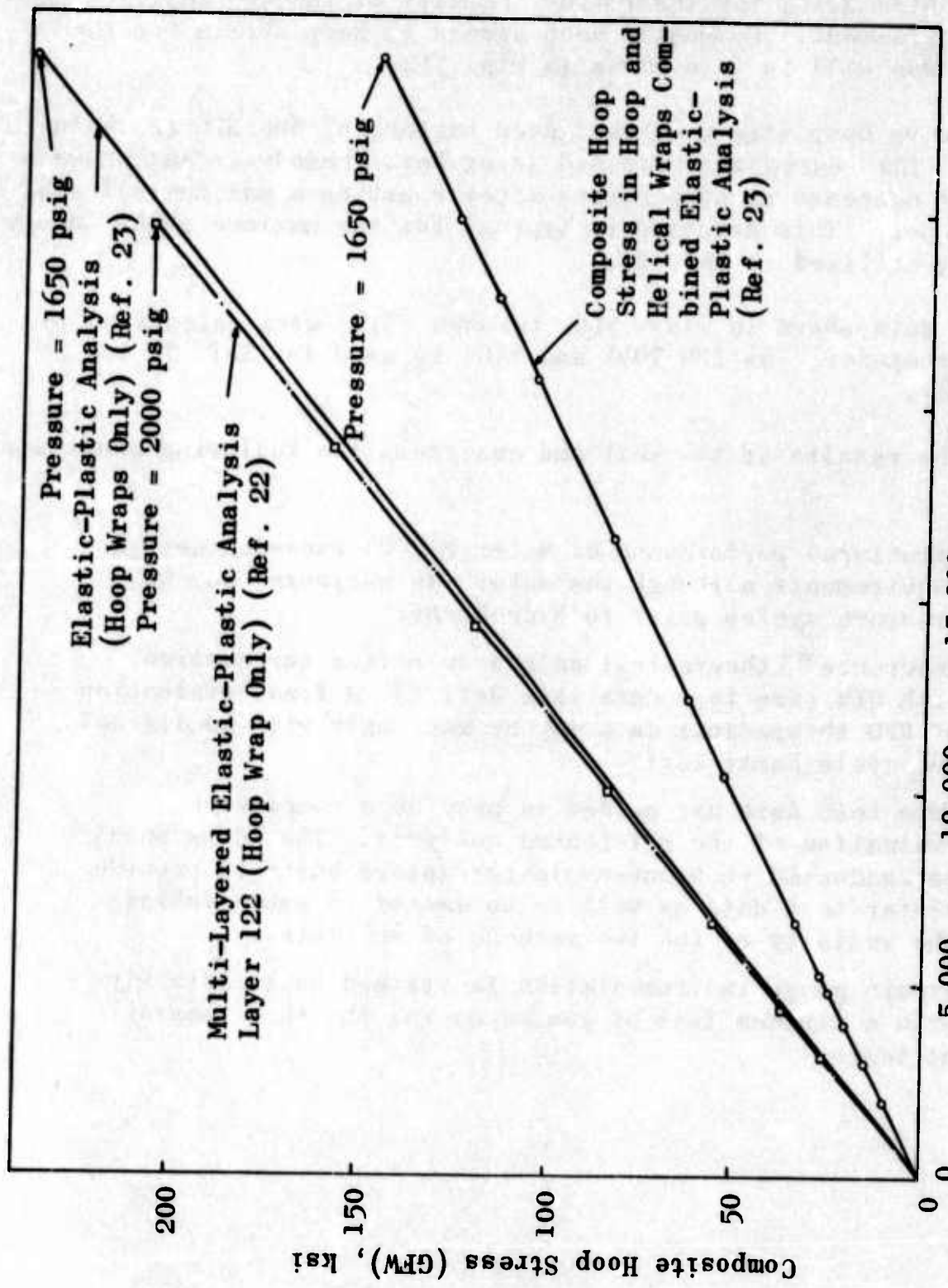


Figure 312. Composite Hoop Stress (GFW) vs Composite Hoop Strain (GFW)

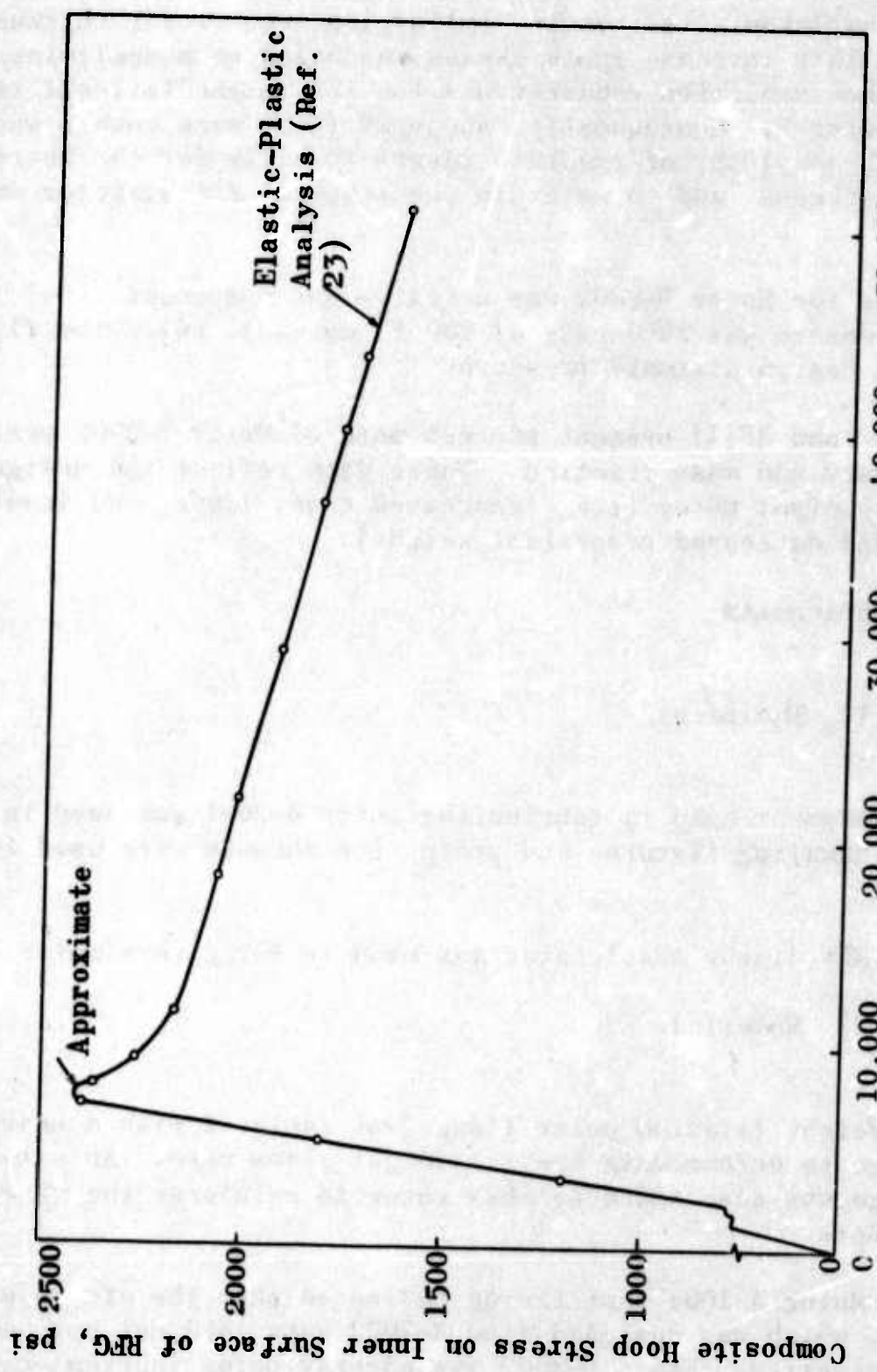


Figure 313. Composite Hoop Stress on Inner Surface of RFG vs Composite Hoop Strain at Inner Surface of RFG

2. MOTOR B-2002

(C) This motor employed a testweight, cylindrical restrictor thickness of 0.38 inch. This increase in thickness was based on a preliminary estimation of the insulation requirements for the longer tail-off time expected in Motor B. Consequently, about 20 to 25 wire covers were omitted from the 9th and 10th intermediate layers to allow for the increased restrictor thickness and to maintain the same outer restrictor contour and diameter.

(C) The GFW case for Motor B-2002 was a testweight component. Calculated ultimate pressure was 1250 psig at 200 F, which is twice the flightweight case design ultimate pressure.

Tables XCII and XCIII present the estimate of Motor B-2002 performance, weight summary, and mass fraction. These data reflect the design changes in the heavyweight motor (i.e., increased case, liner, and insulation thickness and decreased propellant weight).

a. Fabrication

(1) Equipment

The same equipment used in fabricating motor B-2001 was used in B-2002 except new handling fixtures and protection shrouds were used for the first time.

The new 13 MEV linear accelerator was used to X-ray this motor.

(2) Materials

The flightweight titanium polar flange was replaced with a heavyweight steel flange to accommodate the testweight glass case. An external polar flange was also added to this motor to reinforce the case at the aft polar boss.

Input from Motor A-1004 test firing indicated that the aft polar boss of Motor B, which was designed from A-1002 data, did not have adequate thermal protection. Since B-2002 was already being fabricated, a fix was designed for the motor.

TABLE XCII

MOTOR B-2002 ESTIMATED BALLISTIC PERFORMANCE

Nozzle Expansion Ratio: 10:1
Atmospheric Pressure: 14.7 psia
Motor Temperature: 60 F

Motor	
Average pressure, psia	570
Average thrust, lb	17,290
Total impulse, lb-sec	639,800
Action time, sec	37.0
Maximum pressure, psia	800
Maximum thrust, lb	25,550
I_s^o at motor cond, lb-sec/lb	216.5
I_s^o at 1000 psia, lb-sec/lb	242.2
Impulse to weight ratio	193.4
Core Grain	
Average pressure, psia	760
Average thrust, lb	23,900
Total impulse, lb-sec	266,300
Duration, sec	11.1
I_s^o at 1000 psia, lb-sec/lb	250.0
Reinforced Grain	
Average pressure, psia	485
Average thrust, lb	14,420
Total impulse, lb-sec	373,500
Duration, sec	25.9
I_s^o at 1000 psia, lb-sec/lb	235.7

TABLE XCIII

MOTOR B-2002 ESTIMATED WEIGHT SUMMARY

AND MASS FRACTION

	Weight, lb
Propellant	
Core grain	1334.47
Reinforced grain	1619.70
Igniter Combustibles	0.55
Total Propellant Weight	2954.72
Inerts	
Case and skirts	96.00
Liner	95.36
Nozzle and closure	63.33
Aft polar boss, load rings, flanges, studs, and nuts	48.95
Forward polar boss and load rings	28.36
Igniter assembly	2.63
Forward floater	3.00
Aft doubler, plastic ring, and filler	15.03
Total Inert Weight	352.66
Total Motor Weight	3307.38
Mass Fraction	0.893

The fix consisted of a circular ring, machined to fit the entrance cone lip of the existing B-2002 polar boss. The ring was fabricated from a molded fillet of U.S. Polymeric FM 5064 graphite reinforced molding compound.

The ring was fabricated in halves to permit insertion into the motor. A scarf joint was provided at the parting line and the gap held to a minimum by forming the ring into two complete halves.

To provide stress relief for the core grain after cure, a simple doubler was fabricated from two sheets of R-147 restrictor. The ring and doubler were installed as shown in Fig. 314.

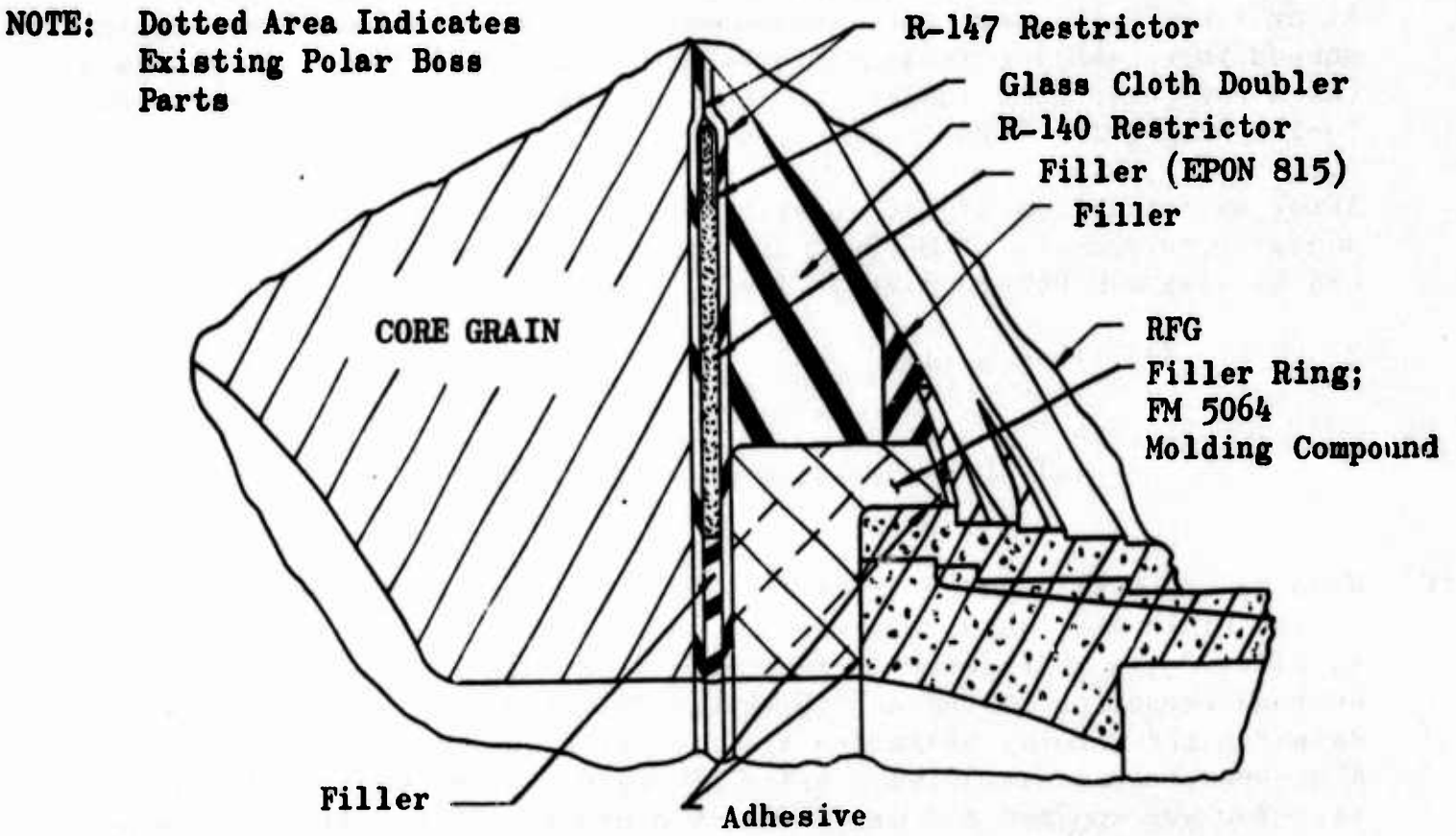


Figure 314. Ring and Doubler Installation; Motor B-2002 Aft Polar Boss Area

The ring was inserted first and bonded in place with RPR 2138 adhesive. Enough excess adhesive was applied to form a fillet which completely covered the first load ring. The remaining space behind the polar boss lip was filled with R-140 restrictor to provide a flat bonding surface for the doubler. The doubler was then bonded in place with R-140 adhesive.

To complete the installation, the doubler gap existing after core grain cure was filled with Epon 815 and EC-1949 adhesive as shown in Fig. 314.

Some trouble was experienced in obtaining sound insulation liners of MX-2646 for both forward and aft polar bosses to be installed in Motor B-2002. Both liners appeared to have numerous cracks after final machining, so they were removed and replaced with liners made from material that had passed careful X-ray and dye-penetrant inspection. After final machining, the replacement forward polar boss liner again showed three small hair-line cracks about 0.25 inch long. A recheck of the X-rays gave some indication that the cracks might have been overlooked during the first inspection.

After an evaluation of the severity of the cracks and of the environmental requirements of B-2002, the liner was repaired by covering the cracks with a 0.060-inch thick layer of RPR-2138.

(3) Processing

(a) Grain Winding and Restriction

(C) Winding was initiated on 4 December, and finished 10 December. Several of the ninth and tenth intermediate layers were omitted on this grain to allow for a restrictor thickness of 0.38 inch. This resulted in an average reduction in the web thickness from 4.5 to 4.14 inches. Detail data for the winding operation are presented in Table XCIV. The aluminum content was 17.4%. After RFG cure, a wipe coat of R-143 restrictor was applied and cured for 16 hours at 170 F. After the wipe coat was cured, 15 thermocouples were attached to each end of the grain as shown in Fig. 315.
bosses.

The testweight (steel) aft case flange was installed and the grain restriction completed. Holes were provided in the case flange to permit exit of the thermocouple leads.

TABLE XCIV

MOTOR B-2002 GRAIN WINDING DATA*

Layer	Covers		Cycle Dia, in.			Avg Cycle Thickness, in.	Avg Cover Thickness, in.	Cycle Winding Time, hr
	Target	Actual	Aft	Center	Fwd			
1G1	6	6	--	--	--	--	--	--
1A	1	0	--	--	--	--	--	--
1B	2	2	--	--	--	--	--	--
1C	3	3	--	--	--	--	--	--
1D	3	3	--	--	--	--	--	--
1E	6	5	27.570	27.585	27.550	0.435	0.229	9.75
2G1	6	6	--	--	--	--	--	--
2A	2	4	--	--	--	--	--	--
2B	3	2	--	--	--	--	--	--
2C	6	4	--	--	--	--	--	--
2D	4	5	--	--	--	--	--	--
2E	10	8	28.419	28.520	28.490	0.454	0.0157	13
3G1	6	6	--	--	--	--	--	--
3A	4	4	--	--	--	--	--	--
3B	3	3	--	--	--	--	--	--
3C	5	5	--	--	--	--	--	--
3D	7	6	--	--	--	--	--	--
3E	3	5	29.404	29.480	29.470	0.488	0.168	11.50
4G1	6	6	--	--	--	--	--	--
4A	5	4	--	--	--	--	--	--
4B	4	4	--	--	--	--	--	--
4C	5	4	--	--	--	--	--	--
4D	3	3	--	--	--	--	--	--
4E	3	3	30.170	30.295	30.265	0.396	0.0165	13.25

*Mandrel Diameter, in.: Aft, 26.675; Center, 26.725; Forward, 26.690

CONFIDENTIAL

TABLE XCIV

(Continued)

Layer	Covers		Cycle Dia, in.			Avg Cycle Thickness, in.	Avg Cover Thickness, in.	Cycle Winding Time, hr
	Target	Actual	Aft	Center	Fwd			
5G1	6	6	--	--	--	--	--	--
5A	3	3	--	--	--	--	--	--
5B	3	3	--	--	--	--	--	--
5C	4	4	--	--	--	--	--	--
5D	5	4	--	--	--	--	--	--
5E	4	4	--	31.080	--	0.419	0.0175	12.33
6G1	6	6	--	--	--	--	--	--
6A	4	4	--	--	--	--	--	--
6B	4	4	--	--	--	--	--	--
6C	4	4	--	--	--	--	--	--
6D	4	4	--	--	--	--	--	--
6E	6	6	31.965	31.985	31.971	0.447	0.0160	19.50
7G1	6	6	--	--	--	--	--	--
7A	3	1	--	--	--	--	--	--
7B	4	3	--	--	--	--	--	--
7C	4	4	--	--	--	--	--	--
7D	4	4	--	--	--	--	--	--
7E	4	4	32.841	32.846	32.805	0.429	0.0195	13.33
8G1	6	6	--	--	--	--	--	--
8A	4	5	--	--	--	--	--	--
8B	5	4	--	--	--	--	--	--
8C	4	4	--	--	--	--	--	--
8D	4	3	--	--	--	--	--	--
8E	1	3	33.740	33.725	33.675	0.441	0.0176	15

CONFIDENTIAL

CONFIDENTIAL

TABLE XCIV
(Continued)

Layer	Covers		Cycle Dia, in.			Avg Cycle Thickness, in.	Avg Cover Thickness, in.	Cycle Winding Time, hr
	Target	Actual	Aft	Center	Fwd			
9G1	6	6	--	--	--	--	--	--
9A	3	2	34.065	33.970	34.000	0.149	0.0186	6.33
10G1	6	6	--	--	--	--	--	--
10A	3	3	--	--	--	--	--	--
10B	4	5	34.635	34.639	34.610	0.308	0.0220	8.75
11G1	6	6	--	--	--	--	--	--
11E	2	3	34.935	35.020	34.980	0.176	0.0196	3
TOTALS	238	231	34.860	35.010	34.950	N/A	0.0178	6.50 days

CONFIDENTIAL

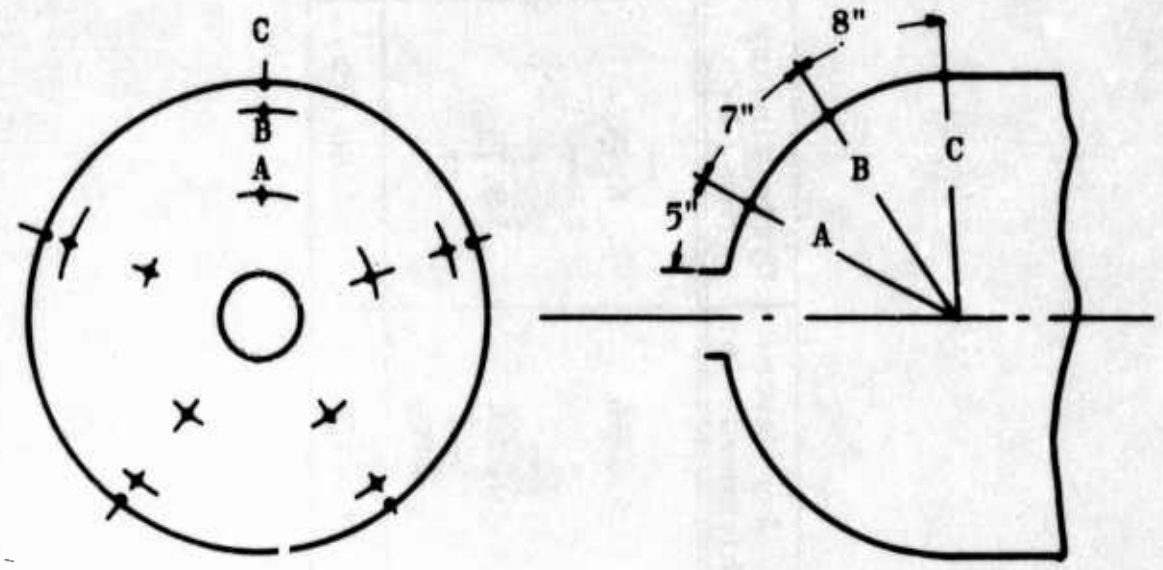


Figure 315. Motor B-2002, Thermocouple Locations (Forward End)

(C) After cure, the restrictor thickness in the cylinder was less than the required minimum thickness (0.38 inch). An additional 0.06-inch layer was applied to obtain the minimum target value and cured for 24 hours at 170 F. The restrictor weighed 124.0 pounds.

Contour traces were made before and after grain restriction at 90-degree intervals. The average minimum restrictor thicknesses were:

(C)

	Forward, in.	Aft, in.
Cylinder	0.401	0.424
Dome	0.401	0.500

Propellant burning rates and ambient mechanical properties are presented in Table XCV.

(b) GFW Case

Motor B-2002 testweight case was wound on 7 and 8 January with a winding time of 27 hours. Helix winding time was about 3.5 hours per cover using the dome speed-up system. Mandrel speed when winding along the cylinder was 1.6 rpm, peak speed in the dome portion of the cycle was 6--7 rpm, and the over-all average speed was 2.4--2.5 rpm.

TABLE XCV

B-2002 RFG PROPELLANT BURNING RATES AND

AMBIENT MECHANICAL PROPERTIES

Cycle	Type	Mix No.	Strand Rate, in./sec at psi	e_m, %	S_m, psi	E, psi
1	512	L-11-13-M81	0.320 at 1015	15	146	1532
2	514	L-11-16-M81	0.254 at 695	17	176	1558
3	514	L-11-16-M82	0.227 at 645	23	167	1191
4	514	L-11-17-M81	0.193 at 595	15	185	1713
5	523	L-11-19-M81	0.169 at 545	23	135	878
6	523	L-11-19-M82	0.149 at 495	24	102	640
7	523	L-10-28-M82	0.132 at 440	24	89	577
8	523	L-10-28-M82	0.128 at 400	24	89	577
9	523	L-11-20-M81	0.127 at 400	26	65	418
10	523	L-10-27-M81	0.127 at 400	19	125	1050
11 (GI)	523	L-10-27-M81	0.127 at 400	19	125	1050
Core	526	M-1-17-M301	0.461 at 760	38	200	837
Core	526	M-1-18-M81	0.469 at 760	35	159	654
Core	526	M-1-18-M82	0.461 at 760	38	196	802

(C) Results showed that use of the dome speed-up system, which increases mandrel rotation speed in the dome portions of the winding cycle, increased average helix winding speed by 50% and decreased winding time by one third. This increase in winding speed is not only desirable, but when processing a heavyweight case the decrease in time is necessary to permit completion of a helix cover within the 4-hour resin pot life.

(C) Emphasis was placed on removal of excess resin from the case in an effort to obtain the target content of 20% by weight. A very favorable

(C) 21.2% was obtained, compared to 24.3% and 23.3% on Fabrication Development Cases B-2415 and B-2416 respectively. The decrease is more significant since this case was of heavier construction, making excess resin removal more difficult. The excess resin removal was accomplished by applying glass bleeder cloth, pressurizing with dry roving, and applying heat to reduce resin viscosity and increase resin migration. Particular attention was given to removing as much surface resin as possible prior to applying the bleeder cloth to make the dry wrap more effective. Resin was removed from the domes by rubber squeegees and absorbent toweling.

Uniformity of the helix winding pattern was good, and the circ wrap was very smooth and flat, as experienced previously on Motor B cases. There were slight tapered depressions in the skirt-to-dome fill area, but roving laydown in these areas was good and there were no sudden discontinuities or protrusion of the cloth. The silastic fill extrusion had been redesigned to more closely match the Motor B dome.

Design and winding parameters of the case as fabricated are shown below:

Helix Wrap

(C)

Helix Angle, degrees	15.3
Pattern	9/8
Glass Density, ends per inch, total	1806
Covers	3
Balls 12-end Roving	6
Estimated Thickness, in.	0.063

Circ Wrap

(C)

Pattern, degrees	90 sequential
Glass Density, ends per inch, total	3400
Covers	8
Balls 12-end Roving	6
Estimated Thickness, in.	0.119

(C) Dimensions of the case winding and weights of the case components are shown in Table XCVI. Total case weight was 1.06 pounds greater than predicted, 98.00 vs 96.94 pounds. The total glass roving weight was 0.64 pound less and the resin weight was 1.26 pounds more than predicted. The skirt-to-dome transition fill was 0.44 pound heavier than predicted because a greater fill width was required.

TABLE XCVI

DIMENSIONS AND WEIGHTS OF MOTOR B-2002 GFW CASE

Dimensions, in.	Fwd Skirt	Center	Aft Skirt
Thicknesses			
Case OD	36.300 (1)	36.150 (2)	36.388 (1)
Case ID	35.880 (3)	35.820 (4)	35.880 (3)
Actual Thickness	0.210	0.165	0.254
Predicted Thickness	0.217	0.182	0.253
Diameters after skirt ring installation and mandrel washout			
Case OD	36.265	36.100	36.365
Lengths			
Boss-to-boss		62.26	
Cylinder		62.27	
Skirt		36.94	
Skirt to skirt		4.84	
Skirt ring to skirt ring		46.62	
		55.88	

Weights, lb	Actual	Predicted
Helix roving	32.35	32.43
Circ roving	34.43	34.99
Aft skirt cloth, calc	5.44	5.44
Forward skirt cloth, calc	3.89	3.89
Total Glass	76.11	76.75
Resin	20.45	19.19
Case weight	96.56	95.94
Skirt-to-dome fill	1.44	1.00
Total	98.00	96.94

Resin content = $\frac{20.45}{96.56}$ = 21.2% (by weight)

Target resin content 20.0% (by weight)

(1) Before skirt mandrel removal

(2) Before washout

(3) Skirt mandrel OD

(4) Restrictor OD, center

(4) Postwinding Procedures

Motor B-2002 mandrel was washed out on 10 January and the new handling fixture and protective shrouds were used for the first time. Approximately 2 hours elapsed between water addition and washout completion. The liner was removed and no water was apparent behind the liner. The motor was dried in the oven for 2 hours at 100 F and 2 hours at 120 F.

After removal from the oven, the aft entrance liner (FM-5064) was installed. RPR-2138 (asbestos-loaded epoxy) was used to bond the liner in place and cover the first load ring. After adhesive cure, 7.2 pounds of R-140 were used to fill and contour the aft section of the RFG around the aft entrance liner. The R-140 was cured for 12 hours at 170 F. The forward and aft doublers (restrictors) were bonded in place under load and the R-140 adhesive cured for 12 hours.

(C) The boss-to-boss dimension was 62.18 inches, (0.26 inch less than the nominal design value). Because of the casting tooling setup, this resulted in a 0.26-inch reduction of the forward web.

(C) To maintain design burnout characteristics, the forward conicyl was modified by removing 0.26 inch of material from the flat side and decreasing the base radius from 0.80 to 0.60 inch. This permitted movement of the conicyl inward, thus maintaining the core grain web at the design value.

(C) The core mandrel was installed in the motor with no difficulties. After a 24-hour preheat period, the pit was evacuated for casting. It was planned to cast the entire core with one 300-gallon mix. However, due to the alignment of the casting plate with the boss, the casting rate was limited and the practical pot life of the propellant expired prior to casting completion. Two additional 25-gallon mixes were required to complete casting. Since no 25-gallon mixes were planned, a time interval of 14.75 hours occurred between the first and second mixes. Previous motors have been cast with four 25-gallon mixes with a maximum of 6 hours between the second and third mixes. However, based on previous tests and experience, no interface bond problems were expected as a result of this delay. Core propellant weight was 1342.2 pounds.

After a 24-hour cure, the forward end of the core was restricted with R-140, which cured concurrently with the core. The core grain was cured for a total of 72 hours at 170 F.

After the core was cured and step cooled (5 F drop every 3 hours) mandrel removal began. The forward conicyl was difficult to remove, primarily due to its inaccessability. Also, some of the aluminum wedges in the star points stuck to the foam. During the star point removal operations, the core was inadvertently cut in about seven places. These cuts were about 1 inch long and up to 0.25 inch deep. The cuts were filled with Epon 815/Versamid 140 under vacuum conditions concurrently with the filling of the aft doubler.

Removal of the core mandrel revealed a misalignment of the core valleys with the thermocouples located in the restrictor. Final torquing of the core mandrel tooling linkage on installation apparently rotated the core mandrel causing the misalignment. This is a blind operation since the star points cannot be seen.

(5) Final Assembly

Motor B-2002 was radiographed 30 January using the 13 MEV linear accelerator (Linac). The inside load ring and doubler integrity, the core grain integrity, and the core grain--reinforced grain interface integrity, all areas impossible to evaluate in the past, were inspected.

Separations at the inside load ring extending up approximately 2.5 inches in the reinforced grain about 0.25 inch away from the doubler were evident at both ends of the grain, showing that both bosses moved inward during grain fabrication, Fig. 316. Measurements of boss-to-boss lengths of all prior motors indicated that this had happened but this was the first time the results of the movement could be evaluated. Upon pressurization the bosses move outward and possibly seal this separation. Since this was the first motor to be radiographed in this area and it had not been fired, a complete evaluation of the effects of these separations could not be made.

At most load rings a low density area was evident, corresponding to the R-143 applied. There was an apparent delamination of the third GI in the aft end of the grain. This started about 0.5 inch from the boss and extended upward about 1 inch. It was apparent in all views around the boss (see Fig. 317).

A tear in the forward doubler interior (at the cloth line) was evident in one view only. It was about 0.75 inch long and extended from the doubled cloth, Fig. 318. It probably did not affect the performance of the doubler in this motor although a cycled motor could be endangered.

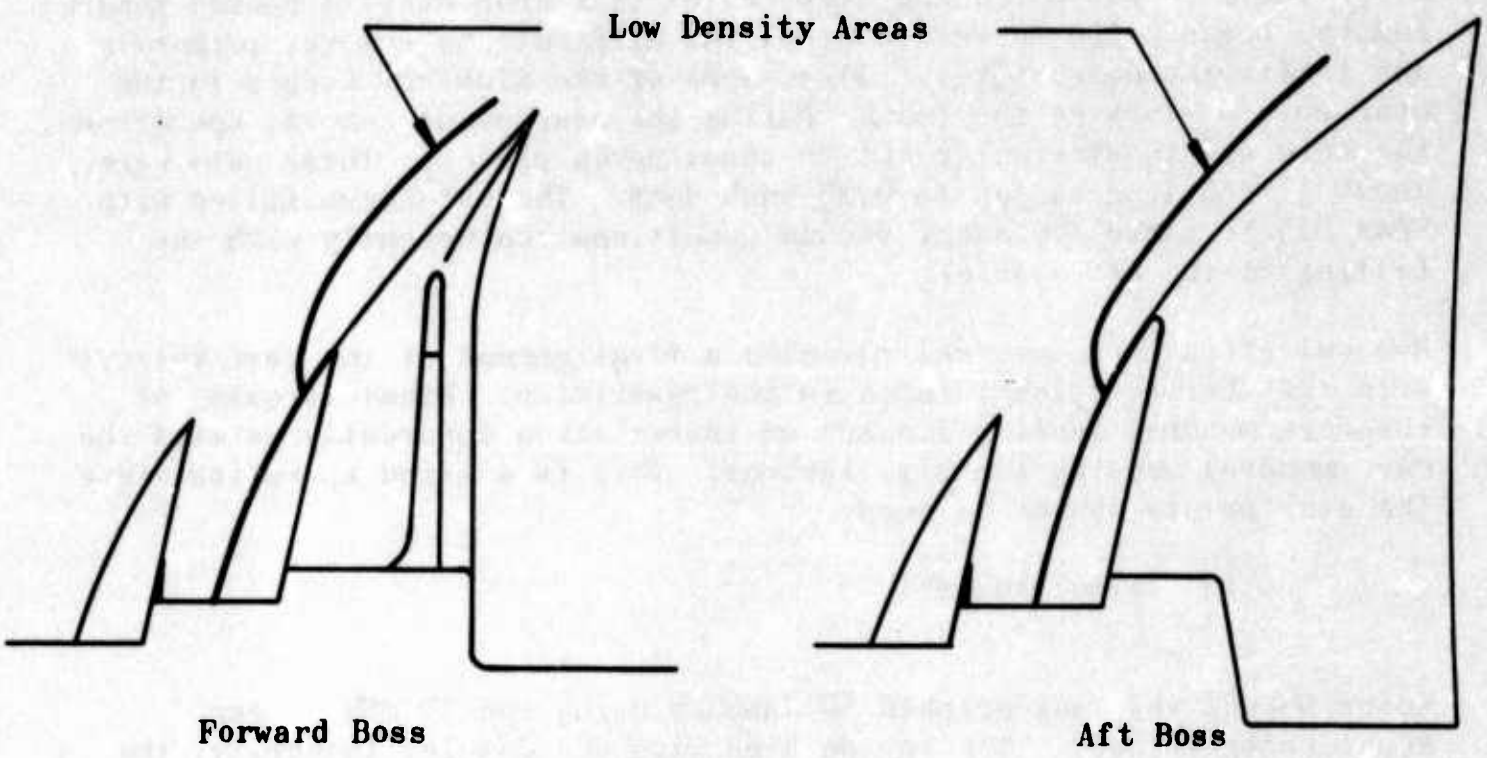


Figure 316. Boss Movement

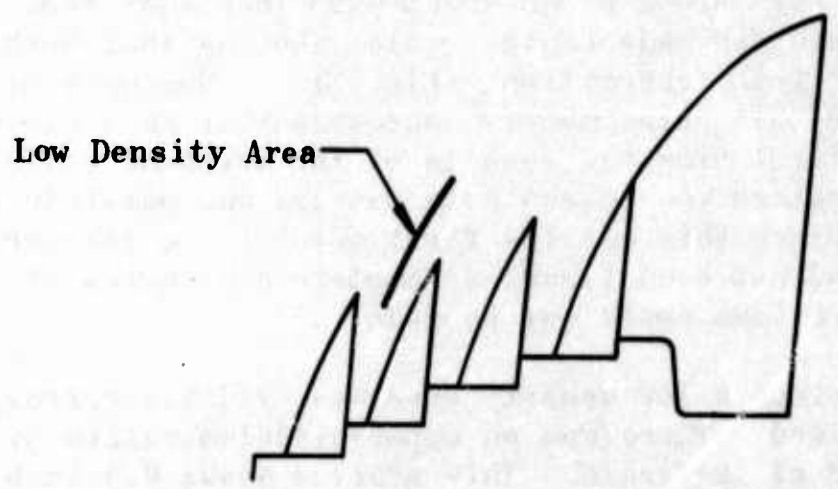


Figure 317 . Low Density Areas Near Bosses

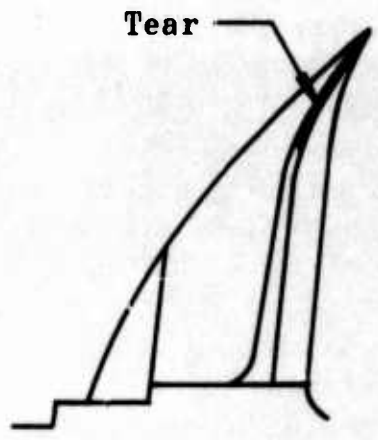


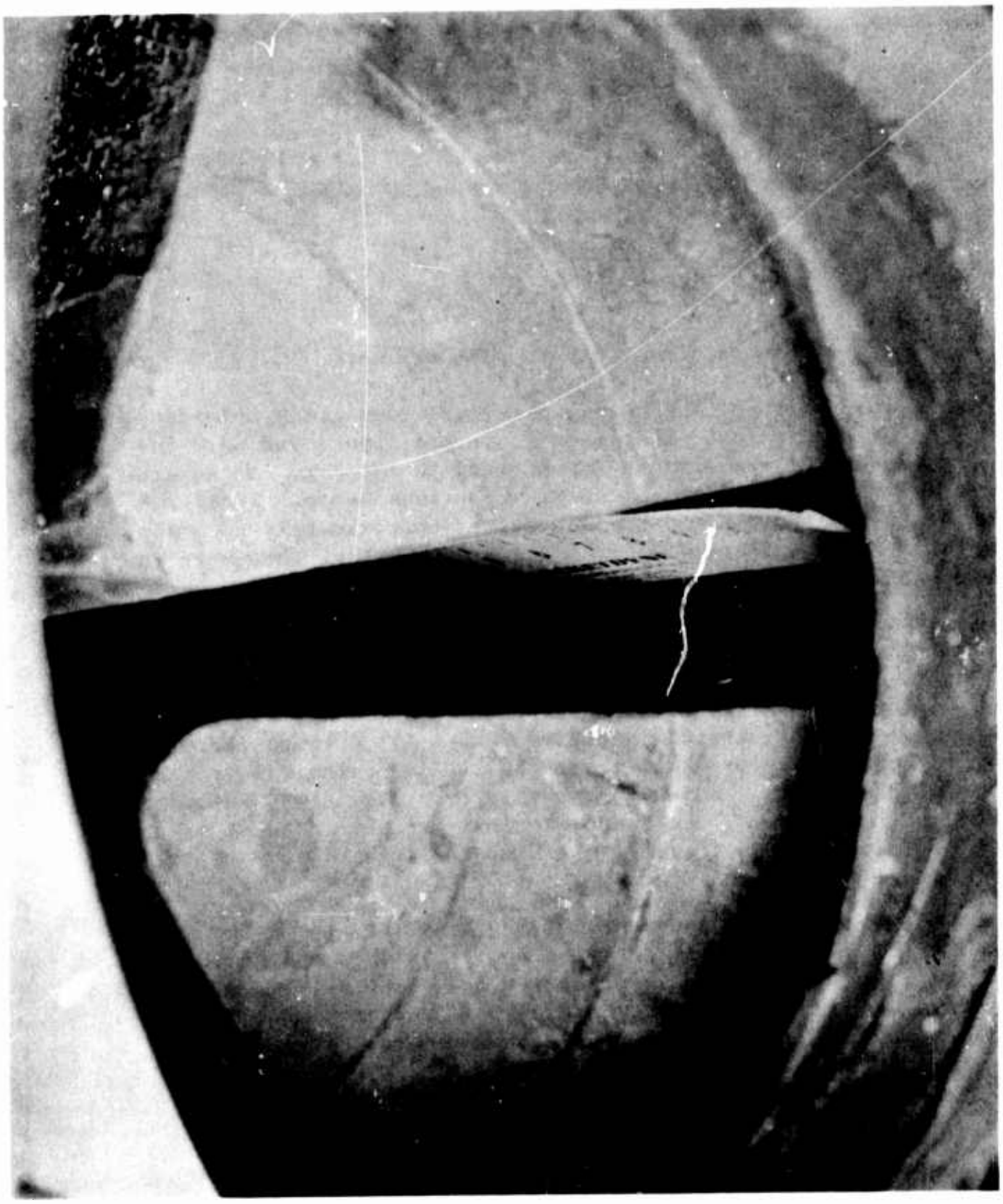
Figure 318. Forward Doubler Tear

Radiographic inspection of the core grain-reinforced grain interface showed signs of separation. The liner-grain and liner-case were inspected by tangential radiographs taken every 90 degrees. No separation or other anomalies were evident at these interfaces. X-ray inspection of the core grain and the RFG showed approximately 25 small, low-density areas (0.125 to 0.75 inch across). Most of them were in the reinforced grain.

One faint shallow crack approximately 1 3/4 inch long by 1/8 inch wide was visible 11 inches forward of the aft conicyl in the core grain. Subsequent visual examination verified that a crack existed in one of the star valleys. This was first observed on 1 February, 14 days after core casting and 9 days after mandrel removal. All work on the motor was stopped and the fissure kept under observation. The fracture grew to about 7 inches x 3/16 inch by 5 February (see Fig. 319). A number of small hairline surface cracks appeared but did not increase in size. Also, a crack or tear was visually noted at the forward edge of the forward conicyl as shown in Fig. 320.

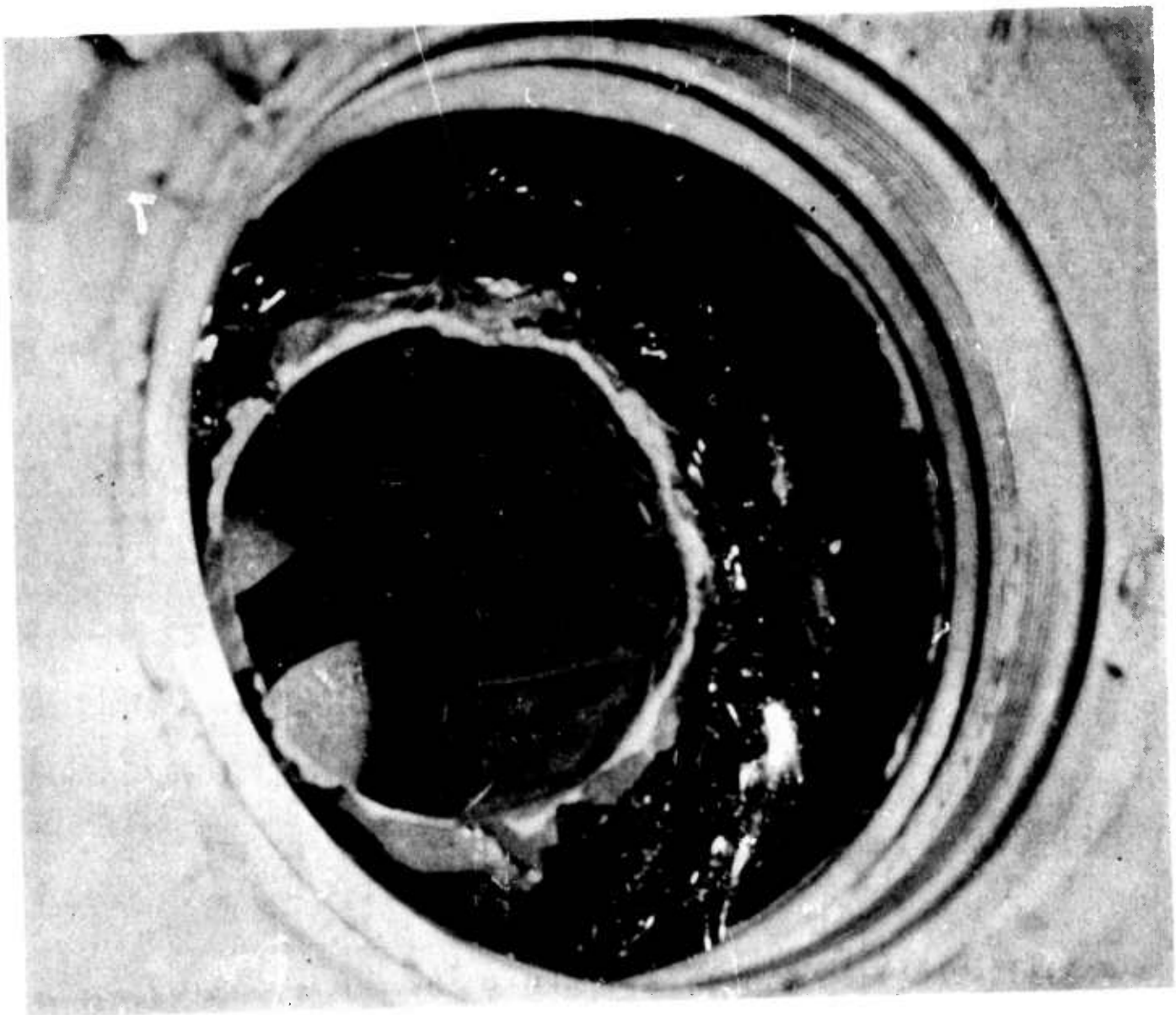
(C) In an attempt to determine the cause of the cracking, the motor processing history was thoroughly examined and all data compared to Motor A processes. This comparison is presented in Table XCVII. Several differences existed; however, none conclusively accounted for the propellant cracking. The principal changes noted were:

1. Use of 300-gallon mixer instead of the 25-gallon mixer
2. Use of the highest-to-date percent (45% of total AP) of fine ground oxidizer in the RDS-526 formulation. To increase the burning rate, this percentage had been increased for each succeeding Motor A.



2YA35-2/20/65M1B

Figure 319. Star Valley Crack in B-2002



2YA32-2/4/65M1

Figure 320. Forward Conicyl Crack in B-2002

TABLE XCVII

CORE PROCESSING DATA, MOTOR B-2002 AND MOTOR A

Item	A-1002	A-1003	A-1004	A-1005	B-2002
Time-Temperature after Mandrel Washout, hr/deg F	2/100 2/120	2/100 2/120	2/100 2/120 2/130	2/100 2/120 2/130	2/100 2/120
Time Lapse					
After MAPO Wipe to Start of Preheat, hr	50	10 (2nd wipe)	92	19	11
Preheat to Cast, hr	35	22	22	31	31
TOTAL	85	32	114	50	42
Casting History					
Method	4 25-gallon mixes with 4- to 6-hour lapse between 1-2 and 3-4	Same as A-1002	Same as A-1002	200-gallon mix for RDS-501; 25-gallon mix for RDS-526	Half of motor with 300-gallon mix; 14.75-hour lapse; one 25-gallon mix; 4-hour lapse to final
Casting Time, hr	11.5	10	10	4	24
Casting Rate, lb/min	16	18	16	21 for RDS-501 8 for RDS-526	17 on 25-gallon mixer
Cure, hr/deg F	72/170	72/170	72/170	72/170	72/170
Cooldown, hr	54 to 96 F	42 to 95 F	42 to 95 F	42 to 95 F Completed 2-4-65	52 to 95 F Completed 1/23/65
Time Lapse from Cooldown to Nozzle Installation, days	10 (6-3-64)	2 (7-28-64)	6 (11-11-64)		
Propellant Properties					
Elongation at 77 F	37 38 39 44	38 35 40 34	32 34 40 38	31	39 35 38
Tensile at 77 F	154 160 150 165	176 173 183 173	166 148 168 166	171	200 159 196
Modulus at 77 F	652 698 628 640	770 825 741 857	621 692 726 683	879	837 654 802
Burn Rate, liquid	0.421 at 750 psia	0.428 at 750 psia	0.431 at 750 psia	0.469 at 750 psia	0.461 0.469 0.461
Durometer--Rex				Pan Sample: RDS-526 Cut 75 Air 77 Polyethylene 83	Pan Sample: 300-gallon Cut 79 25-gallon Cut 75 Air 75 Grain: Aft end On star 85--86 Inside star 80--86 Center star 70--75 Forward end On star 60--75 Inside star 85 Forward Port 65--75
Raw Materials Lot Numbers					
AP					
200 micron	7036-103-1-001	Same	Same	Same	Same
7--11 micron	7031-103-1-001	Same	Same	Same	Same
Coarse-to-Fine Ratio	75:25	70:30	67:33	55:45	55:45
Butarez	7084-039-1-017	Same	Same	Same	Same
MAPO	7324-095-2-010	Same	Same	Same	Same
Al	7026-356-1-007	7026-356-1-008	Same	7026-356-1-007	7026-356-1-008
Iron Oxide	7225-150-3-003	Same	Same	Same	Same
Circo Light Oil	7288-277-4-007	Same	Same	Same	Same
Remarks	RFG wetted during mandrel washout	Boss fell into motor; was replaced Doubler installed	Motor had FM 5064 fix in aft end Doubler installed	Motor cast from 200-gallon mixer	Approx half of motor cast from 300-gallon mixer; remainder from two 25-gallon mixes

3. A new formulation of polyurethane foam was used for the star points of the mandrel.

4. 14-hour delay between casting of the first and second mixes

5. Limited cast rate of 300-gallon mix due to casting plate alignment

The initial two changes were within normal processing alterations and were not expected to cause inferior mechanical properties in the propellant. This is confirmed by the data presented in Table XCVII. Also, the hardness data of Table XCVII negates propellant degradation due to the foam change. Although the 14-hour delay between casting the first and second mixes might be detrimental to bonding at their interface, the crack which developed was completely confined within propellant of the first mix.

Although not conclusive, the excessive time and problems associated with casting the first mix offer the most substantiating evidence. As noted during the core casting discussion, the casting problems prohibited casting all the 300-gallon mix due to the pot life. Pot life is the period of time following mixing in which propellant viscosity remains low enough to permit acceptable casting. As the viscosity increases, casting (particularly deaeration) becomes more difficult. Therefore, it is possible that the propellant viscosity deterred adequate deaeration. Although the total void count as revealed by X-ray was not excessive for a motor of this size, it is possible that the crack originated with a subsurface void. A subsurface void is rationalized since the crack developed after mandrel removal.

Location of the crack relative to the grain geometry plus the re-examination of the stress analysis verified this circumstantial evidence. Utilizing propellant and photoelastic data, stress analysis reconfirmed that the allowable strain was above the most severe condition the propellant would encounter. Review of the crack location and photoelastic data (Fig. 321 and 322) shows that the crack developed in an area surrounded by conditions of much greater stress. A failure affected by propellant overstrain would develop at star valley radii. This latter evidence is hard to refute.

Therefore, based on the data available, it is reasoned that the crack was initiated by a subsurface void or possible damage during mandrel removal.

3. MOTOR B-2003

The redesign, necessary to change the polar boss step lengths and to provide additional thermal protection to the titanium structural components, was completed on Motor B-2003.

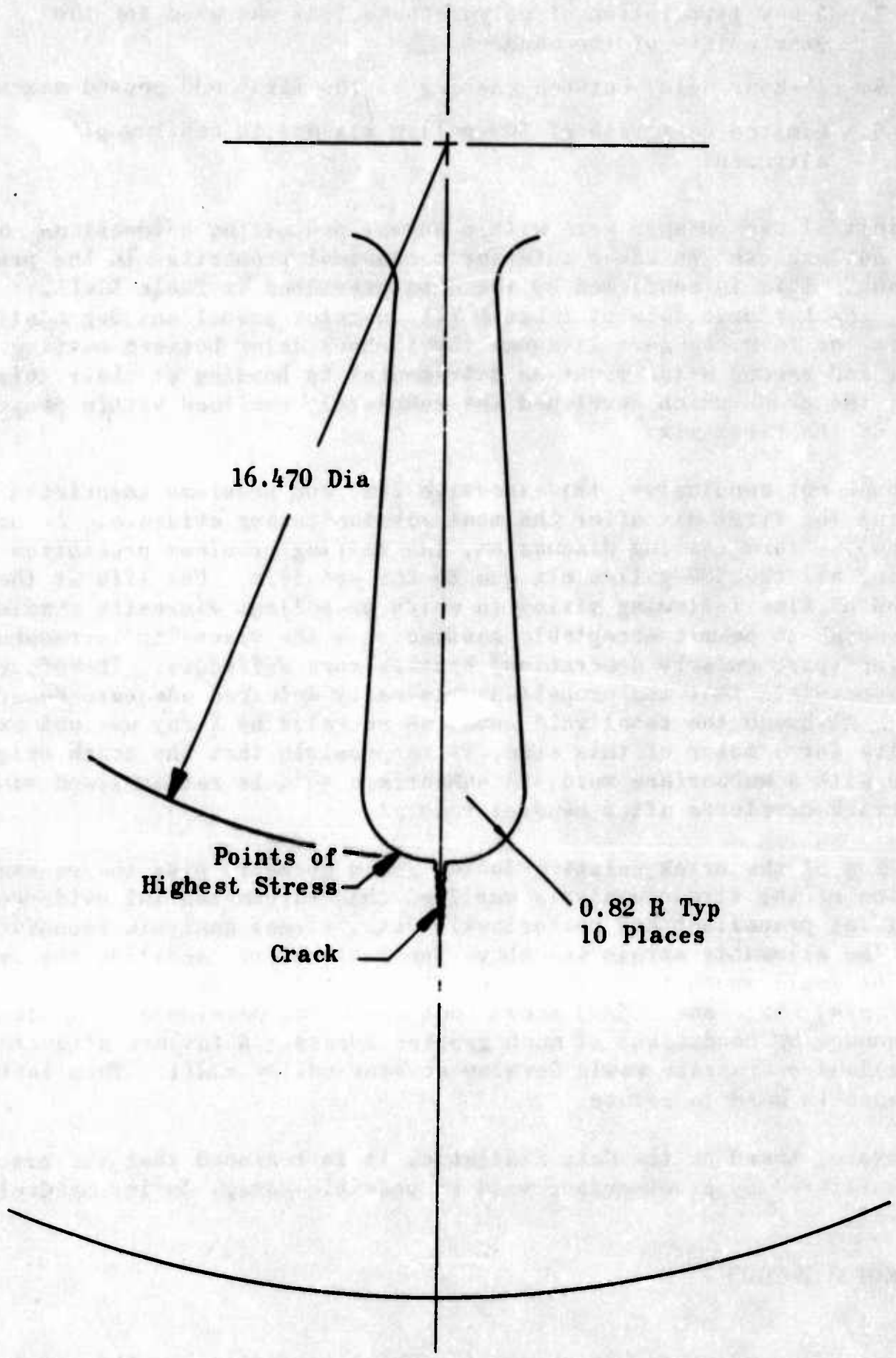


Figure 321. Location of Crack in Star Valley of B-2002 Core

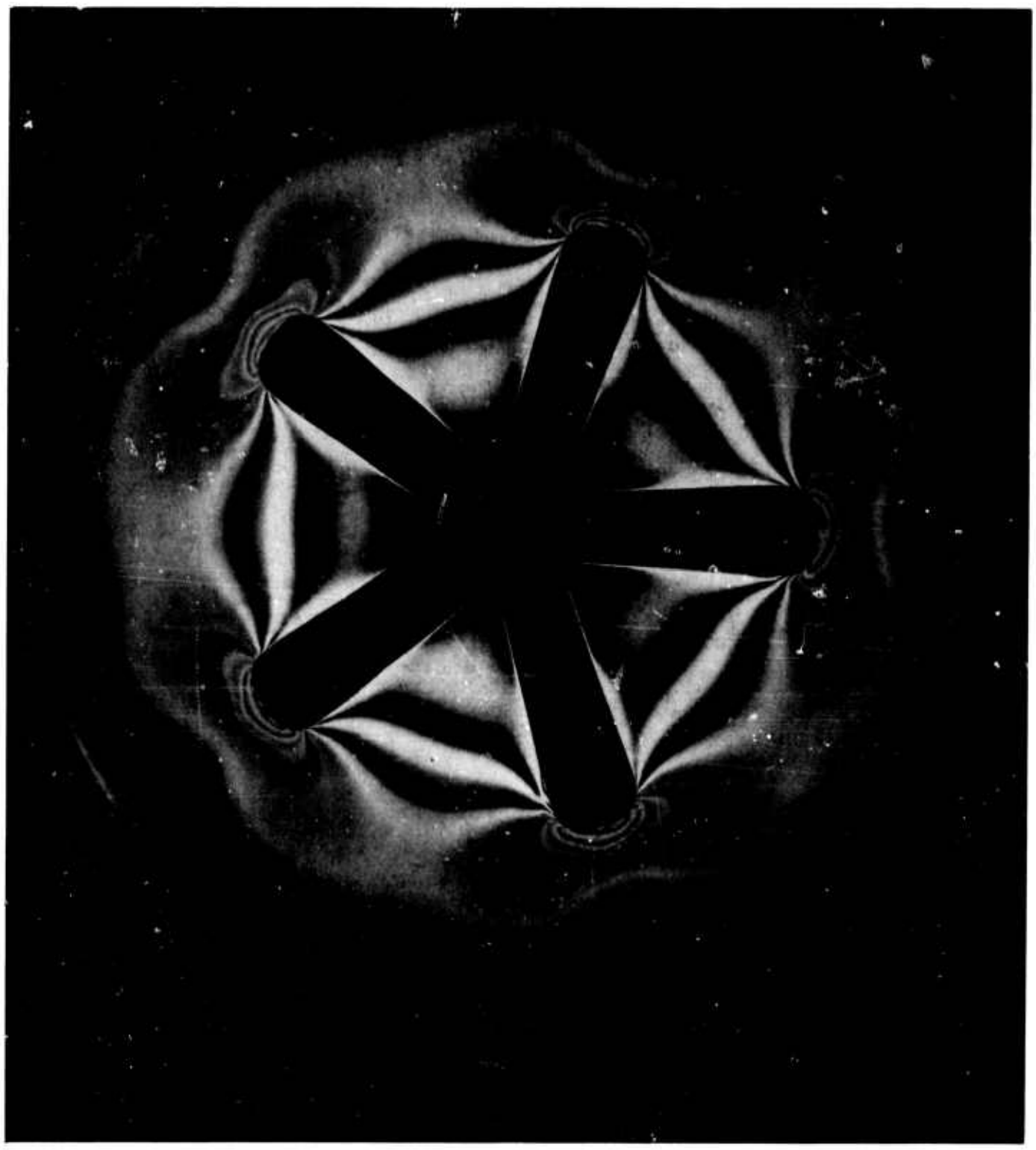


Figure 322. Motor B Photoelastic Study

(C) Motor B-2003 used a modified aft polar boss with the extra insulation thickness and a doubler similar to B-2002. This approach was considered to be more feasible sinch B-2003 was not to be subjected to low temperature and more time would have been available to collect materials test data and information from the Motor B-2002 firing to apply to the design for Motor B-2004 and subsequent motors. Since the function of the aft doubler is complex, it was highly desirable to have as much test data as possible before the final design was released. This would help hold design changes to a minimum and reduce the long lead times required to manufacture the doubler.

A review of the Motor B program was presented during a conference at Edwards Air Force Base, February 23-25, 1965, which resulted in a decision to stop all effort on this motor.

SECTION VIII

MOTOR C

(C) The requirements originally set forth for Motor C specified the use of beryllium in the core propellant and beryllium wire in the reinforced grain. Due to procurement difficulties and cost of beryllium wire, the Motor C effort was terminated in the early part of the program and the design was not finalized. A resumé of activities prior to termination of efforts follows.

(C) 1. BERYLLIUM WIRE TECHNOLOGY

Initial investigations concerning the feasibility of using beryllium wire in reinforced grains were concerned with evaluation of wire-propellant matrix bond strength and with development of winding techniques to overcome the tendency of wire to break in bending. Cleaning of wire sufficiently to obtain adequate bond strength reduced apparent physical properties. However, this should be expected of a material which has less strength in the transverse direction, is notch sensitive, and is dependent upon surface effects for maximum strength.

(C) Small lengths of wire approximately 2 mils, 5 mils, and 8 mils in diameter were obtained, both in annealed condition and as drawn. Variable success was encountered in attempts to wind on small diameter (0.75- to 2-inch) mandrels. Breaking of cleaned wire under stresses imposed by the matrix compacting roller presented the principal problem. Solution of the difficulty was achieved by proper distribution of the compacting force over larger areas of the built-up surface. Use of this technique as well as the avoidance of extreme bending of wire strands led to the winding of small beryllium reinforced composites. Development of acceptable wire-propellant bonds was achieved with bond strength of 200 psi indicated.

(C) The procurement of beryllium wire was the major factor in the termination of Motor C. Wire of usable size, quantity, and physical properties could not be provided within the program schedule and costs. Two firms, Brush Beryllium Corporation and Beryllium Corporation (Berylco), were able to supply some quantity of wire. Also, beryllium aluminum alloy was under consideration at suspension of the beryllium technology development; however, none of the alloy wire had been obtained. At termination of beryllium wire technology, a total of 0.275 pound and 0.385 pound of wire was received from Brush and Berylco, respectively.

2. DESIGN

The original requirements and objectives set forth for Motor C are shown in Table XCVIII. Performance requirements were very similar to those for Motor B, where both were specified for an altitude nozzle (expansion ratio of 25:1) and outside diameter of 36 inches.

(C) The high strength beryllium wire permits a smaller reinforced grain web relative to Motor B. The larger amount of core propellant results in a longer duration at the higher pressure level.

Estimated performance for Motor C based on the preliminary design is shown in Table XCIX.

(C) TABLE XCVIII

DESIGN REQUIREMENTS FOR MOTOR C

(All performance parameters at vacuum conditions)

Minimum action time total impulse, lb-sec	800,000
Average thrust at 60 F, lb	23,000
Maximum thrust at 60 F, lb	31,000
Specific impulse at 1000 psia, lb-sec/lb (vacuum, 25:1 expansion, zero degree divergence angle)	300
Ignition delay, sec	0.100
Outside diameter, in.	36
Over-all length, in.	90
Skirt-to-skirt length, in.	40
Total motor weight, lb (with altitude nozzle, skirts, igniter, TVC, and thrust reversal)	3200
Mass fraction	0.935

(C)

TABLE XCIX

MOTOR C ESTIMATED PERFORMANCE FROM PRELIMINARY DESIGN

	Temperature, deg F		
	-75	60	170
Vacuum Performance (25:1 Nozzle)			
Maximum Thrust, lb	24,600	28,700	33,250
Average Thrust, lb	20,130	23,290	27,260
Maximum Pressure, psia	690	800	930
Action Time, sec	39.8	34.4	29.4
Average Pressure, psia	560	650	760
Total Impulse, lb-sec	801,300	801,300	801,300
Delivered Specific Impulse (I_{spd}) at Motor Conditions, lb-sec/lb		294.6	
Sea Level Performance (10:1 Test Nozzle)			
Maximum Thrust, lb	19,090	22,830	27,150
Average Thrust, lb	15,620	18,530	22,260
Action Time, sec	39.8	34.4	29.4
Maximum Pressure, psia	690	800	930
Average Pressure, psia	560	650	760
Total Impulse, lb-sec	621,900	637,400	654,200
Delivered Specific Impulse, (I_{spd}) at Motor Conditions, lb-sec/lb	228.6	234.3	240.5
Physical Data			
Initial Port Area, sq in.		39.0	
Initial Throat Area, sq in.		19.5	
Propellant Weight lb		2,720	
Prefired Inert Weight, lb		158	
Total Weight, lb		2,878	
Mass Fraction		0.945	

3. HYGIENE AND SAFETY

In support of the Motor C effort, industrial hygiene and safety programs were to be conducted for maintaining the hygienic standards required during the fabrication and testing of Motor C. Preparation of a document outlining all procedures required under this task and the plan of action for implementing the industrial hygiene plan was completed; effort was initiated in accordance with program timing. This detailed plan included such items as procurement of required monitoring meteorological equipment, issuance of detailed safety and operating procedures, and medical examination and history for exposed personnel. A new weather station tower, 198 feet high, was erected at Solid Rocket Division, McGregor, Texas. Also, since Motor C was scheduled to be tested at the North American's Nevada Facility, meteorological data and studies were made concerning this facility.

All effort associated with industrial hygiene was terminated with the deletion of Motor C (and C-1, which is described in the following section).

SECTION IX

MOTOR C-1

1. REQUIREMENTS

(C) During early 1964, effort on Motors C and B was redirected and replaced by a motor designated C-1. Motor C-1 was essentially a Motor B with beryllium powder being utilized in the core rather than aluminum.

Performance requirements for Motor C-1 were similar to those for Motor C, and are shown in Table C.

2. DESIGN

(C) Motor C-1 design differs from Motor B in that beryllium powder was substituted for aluminum in the core propellant. The core grain configuration was the Motor B configuration, a five-point star grain. Preliminary stress analysis indicated that a web fraction modification might be required. Propellant RDS-517 was selected for the core, and a complete spectrum at various strain rates obtained for the RDS-517 propellant formulation. Motor B's web fraction was 0.382, which would yield a core propellant weight for Motor C-1 of 1296 pounds. In conjunction with the stress analysis, web fractions were considered from 0.382 down to 0.274. Webs, weight, and required burning rates for the two web fractions were:

(C)

Web Fraction	Web in.	Volumetric Loading, %	Propellant Weight, lb	Required Burning Rate at 750 psia, in./sec
0.382	5.10	90	1296	0.41
0.274	3.67	88	1240	0.35

(C)

TABLE C

DESIGN REQUIREMENTS FOR MOTOR C-1

(All performance parameters at vacuum conditions)

Minimum action time total impulse, lb-sec	820,000
Average thrust at 60 F, lb	23,000
Maximum thrust at 60 F, lb	31,000
Specific impulse, lb-sec/lb (vacuum at motor pressure and nozzle)	290
Ignition delay, sec	0.100
Outside diameter, in.	36
Over-all length, in.	90
Skirt-to-skirt length, in.	40
Total motor weight, lb (maximum with altitude nozzle, skirts, igniter, TVC)	3200
Mass fraction	0.937

(C) The omission of thrust reversal ports allowed inert weights for Motor C-1 to be reduced to 216.8 pounds. With 2971 pounds (total) of propellant, the motor had a mass fraction of 0.931 and an estimated delivered total impulse at altitude of 847,000 lb-sec. Motor performance is summarized in Table CI. Weight and mass fractions are shown in Table CII.

(C)

TABLE CI

PERFORMANCE SUMMARY FOR MOTOR C-1 AT 60 F IN VACUUM

(ϵ = 25:1)

Pressure, psia	
Motor Average	600
Core Average	740
RFG Range	745--400
Maximum	765
Thrust, lb	
Motor Average	24,200
Core Average	29,900
RFG Range	31,000--15,100
Maximum	31,000
Time, sec	
Action (Total)	35.0
Core	12.9
RFG	22.1
Total Impulse, lb-sec	847,000
Specific Impulse, lb-sec/lb	
I_{sp} 1000/14.7	
Composite	253.2
Core	265.0
RFG	244.0
I_{sp} Delivered, vac, 25:1	
Composite	285.1
Core	298.4
RFG	274.8
Impulse-To-Weight Ratio	265.4

(C)

TABLE CII

WEIGHT AND MASS FRACTION SUMMARY MOTOR C-1

Component	Weight, lb	Load Ring Variations	
		Al	Steel
Core Propellant	1296.0		
RFG Propellant	1675.0		
Total Propellant	2971.0		
Case	40.9		
Skirts	11.3		
Sub-Total	52.2		
Liner	10.0		
Nozzle and TVC	103.4		
Aft Polar Boss	28.9		
Forward Polar Boss	13.3		
Load Rings	8.5	8.7	15.0
Igniter Assembly	2.5		
Total Inerts	218.8	219.0	225.3
Total Motor	3189.8	3190	3196.3
Mass Fraction	0.931	0.931	0.930

SECTION X

MOTOR B'

During the period of program reassessment after completion of the Motor A phase, Rocketdyne, at Air Force request, investigated possibilities for redesign of Motor B. Applying experience and knowledge gained during initial phases of the program, design approaches, aimed at overcoming the difficulties that were encountered on Motors A and B were analyzed. These problems rested primarily in the areas of fabrication complexity and loss of propellant combustion efficiency through addition of burning rate depressants (to achieve regressive burning in the RFG web). This lowered efficiency, in addition to reducing delivered impulse, had a direct effect on the quantity of solid- and liquid-state particles in the exhaust gas. Erosion of propellant and aft inert parts was observed in the horizontal firing of Motor A-1004.

Air Force-Rocketdyne discussions at RPL on 23 and 24 February 1965 resulted in an Air Force request to lay out a program (within remaining program funds) directed at fabricating and testing up to 4 motors of a modified Motor B (termed B') design. The program plan was to design a flightweight version of Motor B' but to test a conservative version to demonstrate attainability by successful firings.

New concepts and principles not recognized or sufficiently demonstrated for inclusion in the ADP Program at its inception received much attention in this reappraisal and design effort. Improved high mass fraction motor designs were being evolved on the basis of Advanced Development Program experience and results of independent research and Navy-funded research programs. Among the applications for which these designs were evolved were the Small ICBM, Mobile Medium Range Ballistic Missile, Third Stage Minuteman, and the Navy Small Ballistic Missile. The key features of Motor B', a slotted RFG design without a cast core, evolved from the studies and are presented in the following discussion.

1. REQUIREMENTS

Ground rules and design objectives agreed to between Rocketdyne and the Air Force for Motor B' were as follows:

(C) 1. General Performance Characteristics:

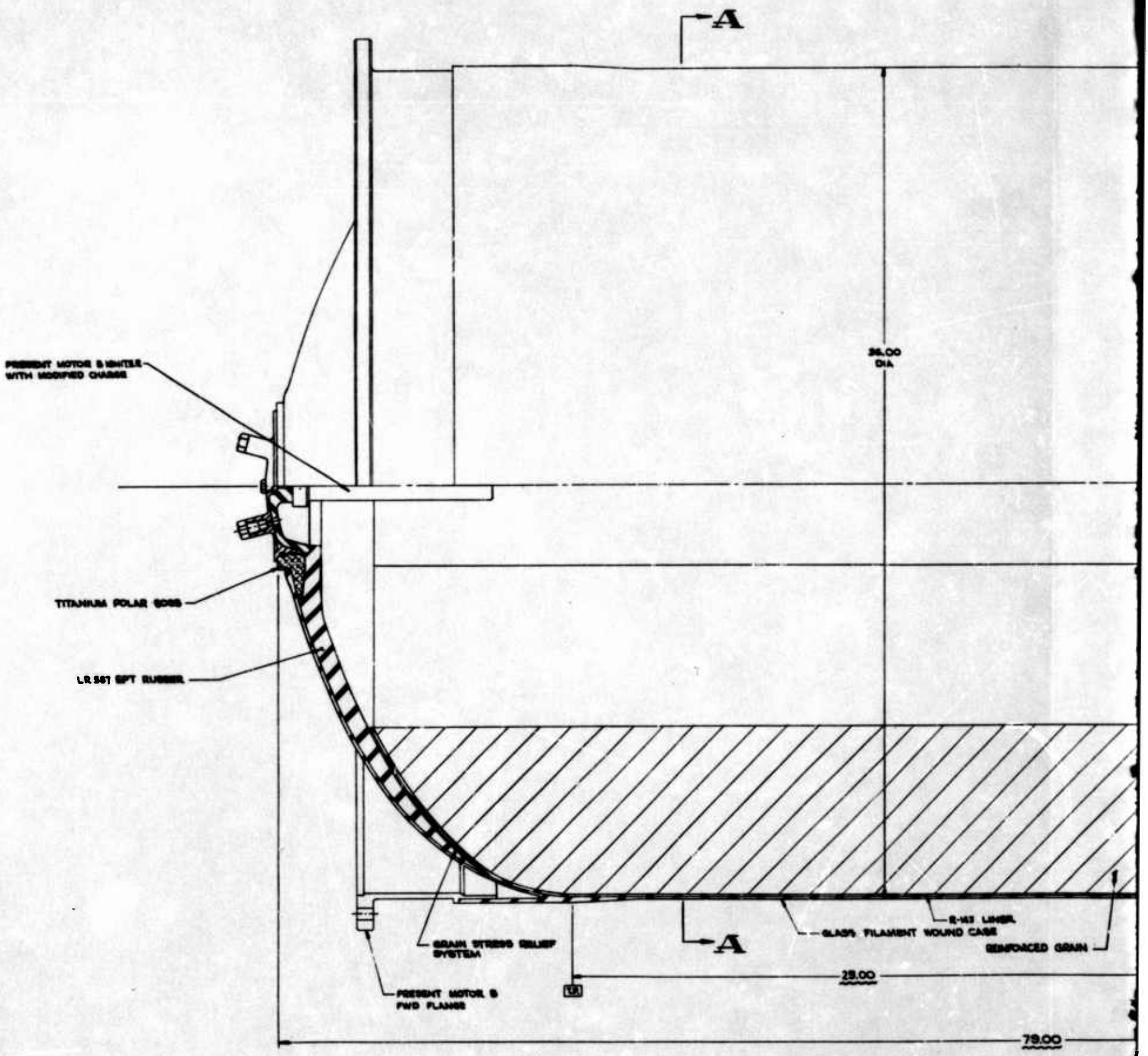
Small ICBM, 3rd Stage
30- to 36-inches diameter
Motor Weight 2200--2800 pounds

2. Use Motor B gimbaled, supersonic, split-line nozzle
3. Tailor motor characteristics to make maximum possible use of Motor B components, tooling, and materials
4. All aluminum wire-reinforced and slotted grain (no cast core)
5. Propellant specific impulse = 250 lb-sec/lb (70 F, sea level, corrected to 0^{o} half angle and 1000 psia)

2. DESIGN APPROACH

(C) Within the framework of these general requirements, the testweight Motor B' design depicted in Fig. 323 was evolved to replace Motor B and proposed for Air Force consideration. The grain was internally slotted, end contoured, and cylindrically (hoop) wound without longitudinal (dome) wraps. The grain shared internal chamber pressure loads with the case in the hoop mode only, but provided stiffness and support to the case in resisting flight loads of compression, bending, shear, and torsion. A restrictor-insulator system of CTL polybutadiene-based rubber covered the outside of the grain. A lightweight glass filament wound case with integral skirts was wound over the restricted grain, with dome end release system provided between the restricted grain and insulated case. Conservative case insulation in the dome areas ensured complete protection for case areas exposed to hot gases or flame during the entire operating time. Motor B nozzle was used without change. A heavy motor aft flange and insulation design was required to accommodate the partially submerged nozzle. Motor B skirt and skirt extensions were employed.

(C) The ballistic design of Motor B' was constrained primarily by the requirement to use the existing Motor B nozzle. In addition, since the RFG was being used to hold chamber pressure in the hoop direction, it was necessary to have a regressive trace just as in the original Motor B. The decision was thus made to design the unit as nearly as possible to the original Motor B performance characteristics, optimizing impulse-to-weight within these constraints. The resulting pressure- and thrust-vs-time curves are shown in Fig. 324.


A
PRESENT MOTOR & NOZZLE WITH MODIFIED CHARGE
TITANIUM POLAR BOSS
LR 567 EPT RUBBER
36.00 DIA
GRAIN STRESS RELIEF SYSTEM
PRESENT MOTOR S FWD FLANGE
A
GLASS FILAMENT WOUND CASE
R-143 LINER
REINFORCED GRAIN
29.00
79.00

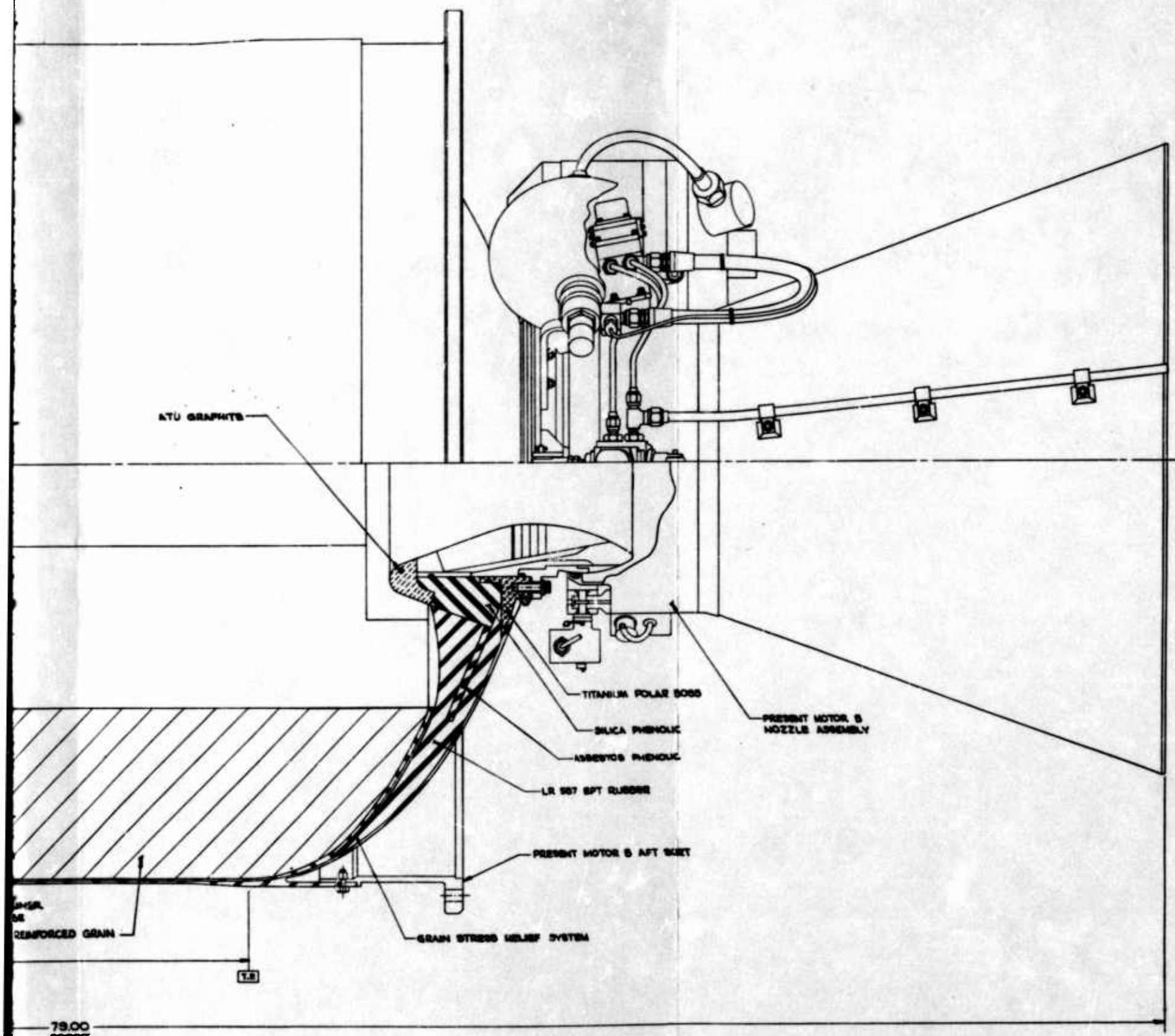
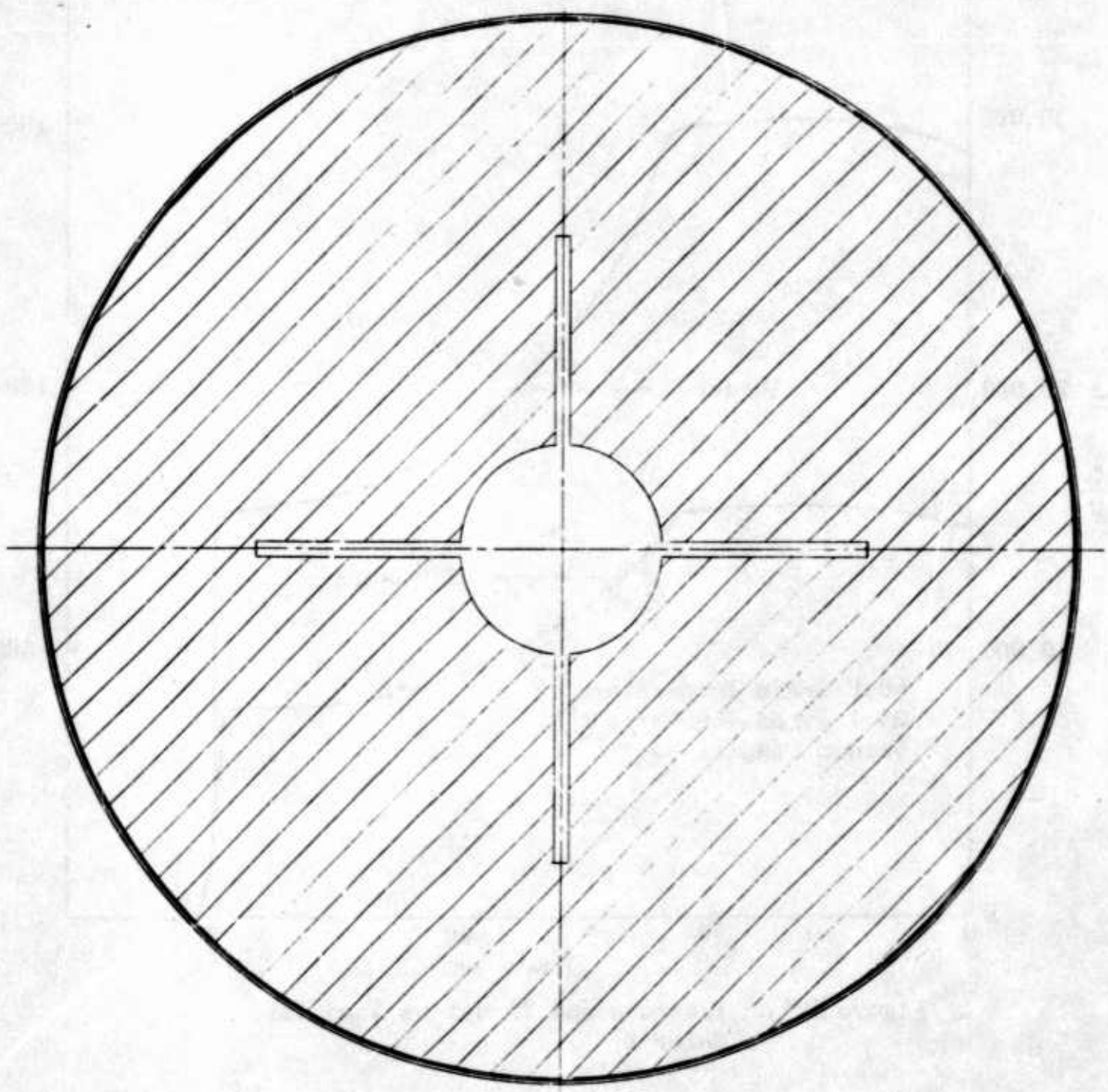


Figure 323. Motor B′ Testweight Design

2

PREVIOUS PAGE WAS BLANK, THEREFORE WAS NOT FILMED



SECTION A-A

Figure 323
(Continued)

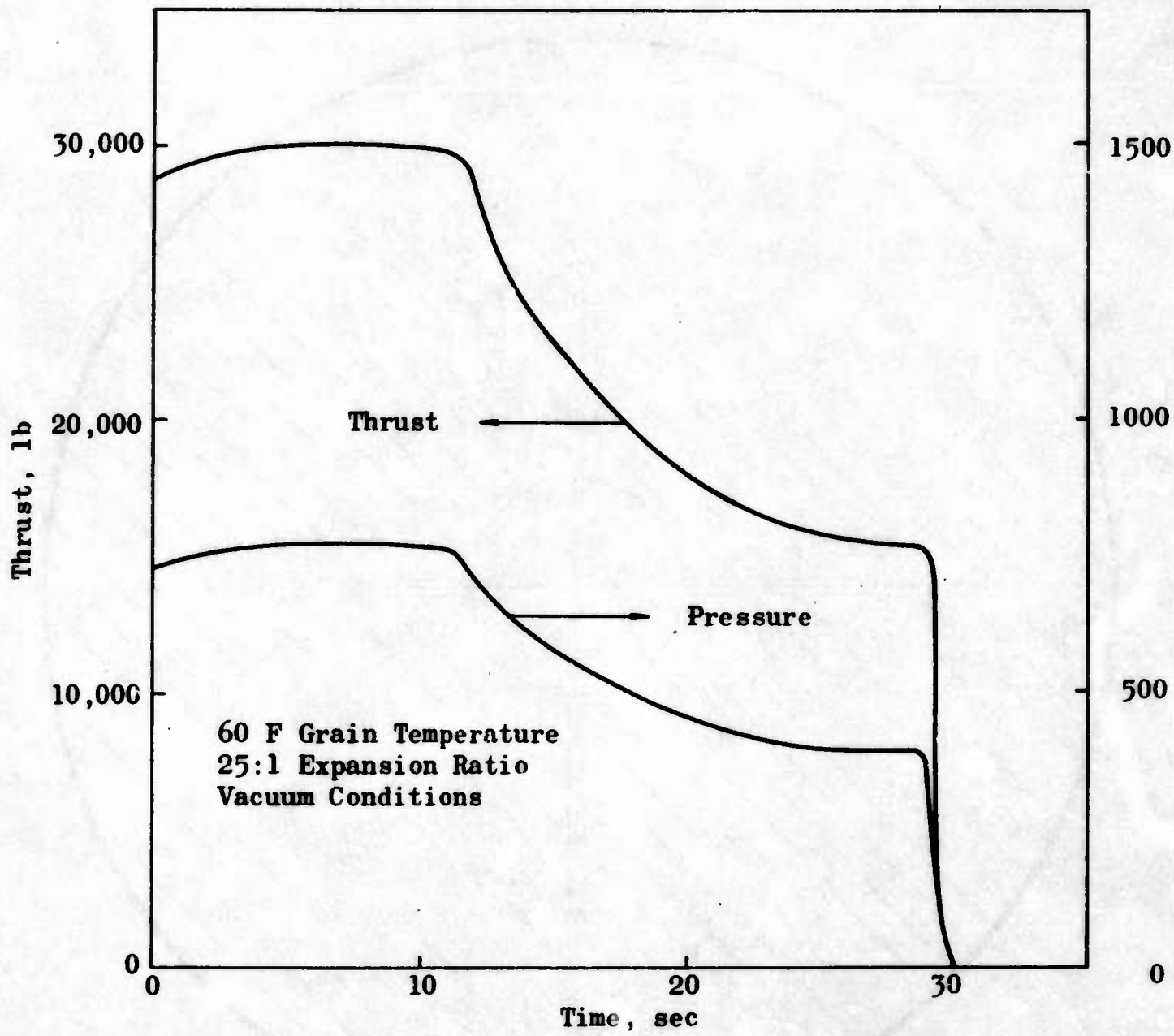


Figure 324. Pressure and Thrust vs Time for Motor B′

There were, however, major differences in the manner by which the regressive trace was achieved in the B and B' units, and it is this difference which resulted in the primary advantage for the B' design.

(C) In Motor B' the regression is achieved by taking advantage of the anisotropic burning characteristic of the RFG propellant in a slotted grain configuration rather than using formulation changes through the grain. The grain, being required to withstand hoop pressure loads only, could be wound at a very high wrap angle. Since the propellant burning rate was increased in the direction of the wire, the propellant exhibited a very high burning rate along the face of a radial slot in the finished grain. This high burning rate resulted in a high initial pressure which remained essentially neutral until the grain between the slots was consumed, after which the grain reduced to an essentially neutral plateau. Figure 325 shows an example of the burning progression in a grain of this type.(24) By controlling number and depth of slots, wrap angle, and basic propellant burning rate, it was possible to achieve almost any desired trace of this general shape without any variation of propellant formulation within the motor. A 4-slot configuration was chosen for Motor B'.

(C)

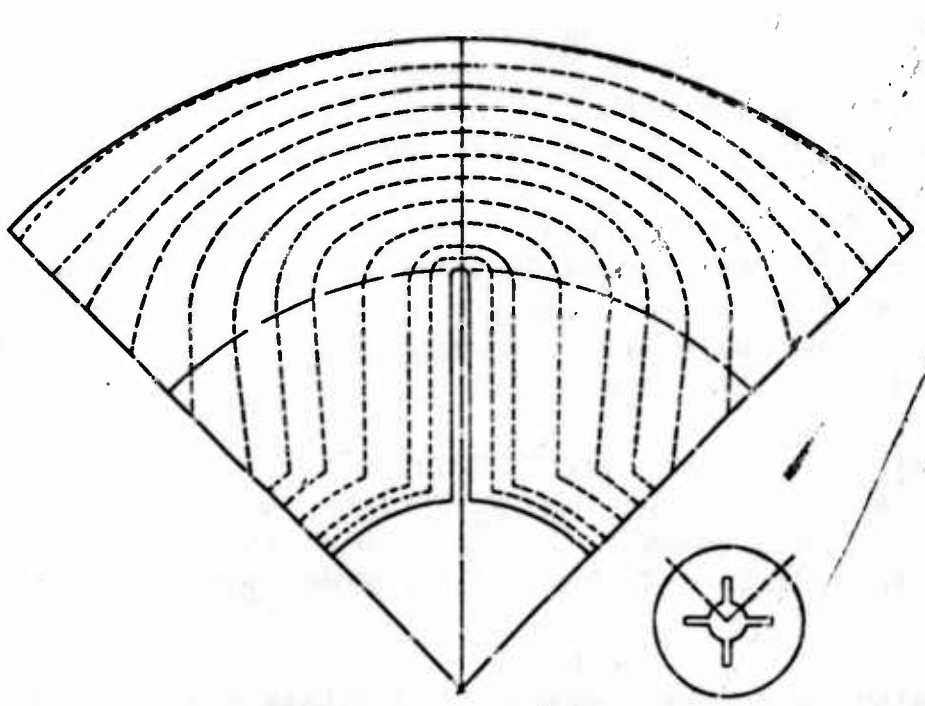


Figure 325. 4-Slot Burning Pattern

(24) Further discussion of the effect of wrap angle on burning rate augmentation is presented in Section XI.

(C) A second significant ballistic advantage of Motor B' over B was the minimum burning rates required were in an easily achievable range. Since only the cylindrical portion of the case, rather than the entire case periphery including the two domes (as with Motor B) formed the final burning surface of Motor B', a higher burning rate could be used without resulting in overpressure of the GFW case near web burnout. The rate required in Motor B' was 0.33 in./sec at 1000 psia, a rate which could be achieved without the use of the depressants similar to those which caused severe slagging problems in the Motor A program.

Feasibility of the slotted RFG approach to achieving regressive thrust-time characteristics was established in independent research experiments and explored in depth on Contract NOw 64-05988d, reported in Rocketdyne Report No. R-6229, Technical Summary Report, Reinforced Propellants for Naval Application, July 1965.

3. FABRICATION

The grain for Motor B' is wound on a steel mandrel, which is cylindrical and without the complexity of the Motor B washout type. Multiple wire wraps are hoop wound in a high angle pattern--a method that is adaptable in production to low-cost, multiple-delivery head, lathe-type winding machines. Since the pattern required only a reciprocating motion, complex cams or tape-controlled devices for dome winding are not required.

After winding and cure, the grains are end contoured by machining to the dome configuration desired, as depicted in Fig. 326, after which the winding mandrel is removed. The grain is internally slotted by mechanical router or saw, both shown schematically in Fig. 327. The slotted and contoured grain is shown in Fig. 328.

External grain restrictor, also serving as case liner, is applied as a viscous liquid and cured on the grain either before or after slotting. The GFW case is then wound as an overwrap on the grain, incorporating the igniter and nozzle attachment flanges and grain end release (doubler) systems.

This fabrication procedure represents a substantially simpler process than for Motor A- and B-type designs, with resultant inherent reliability improvements.

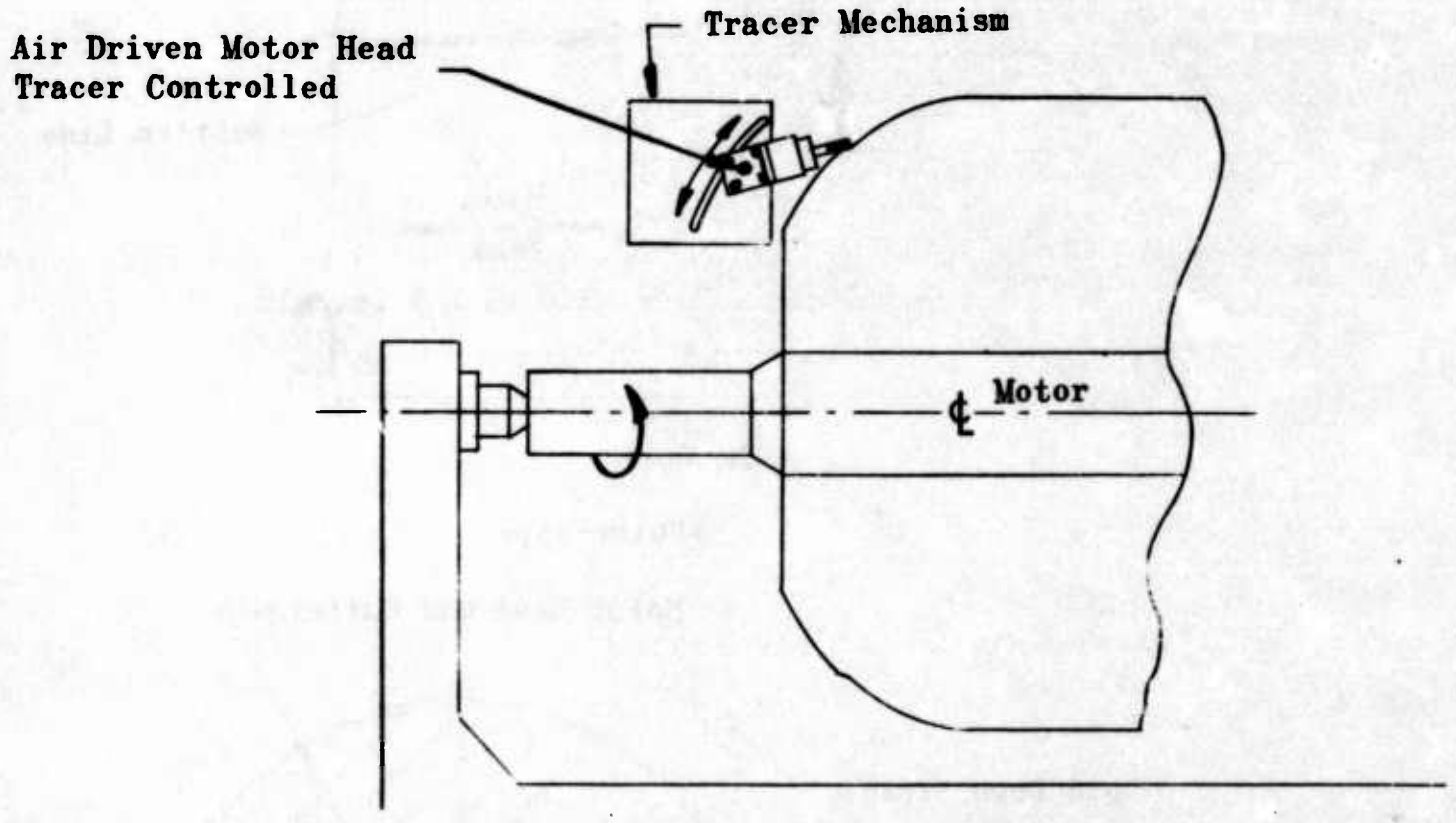
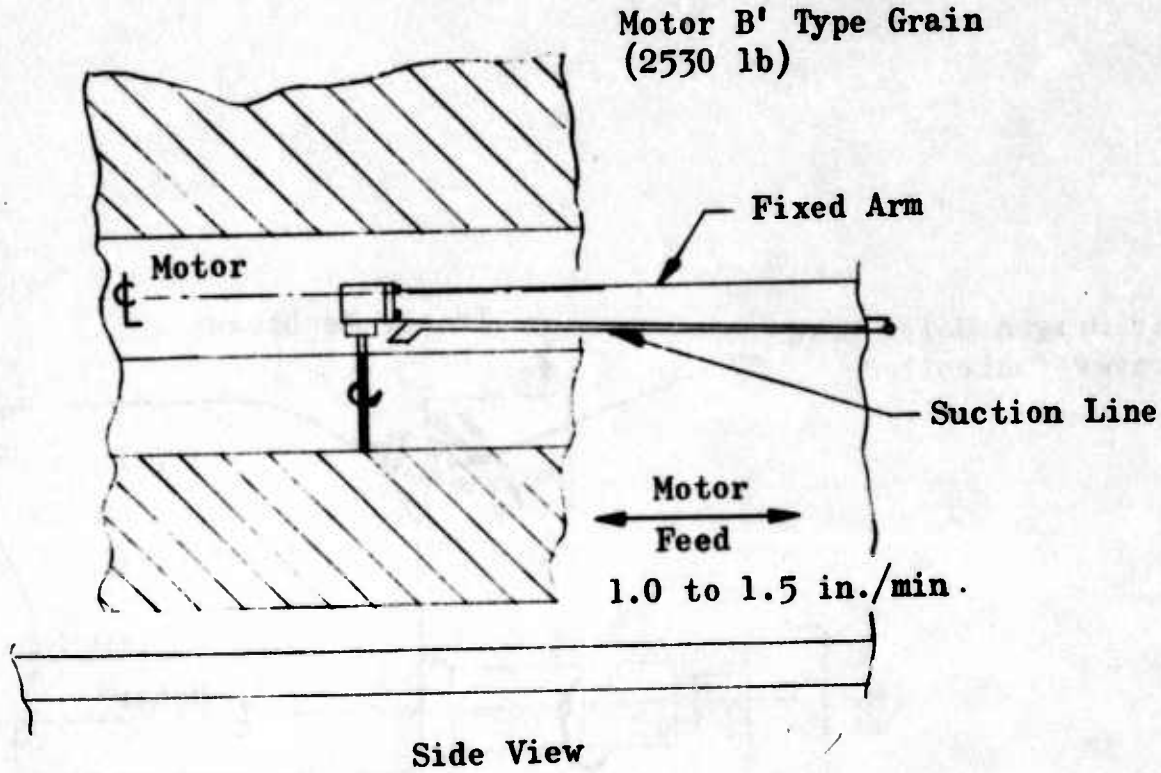
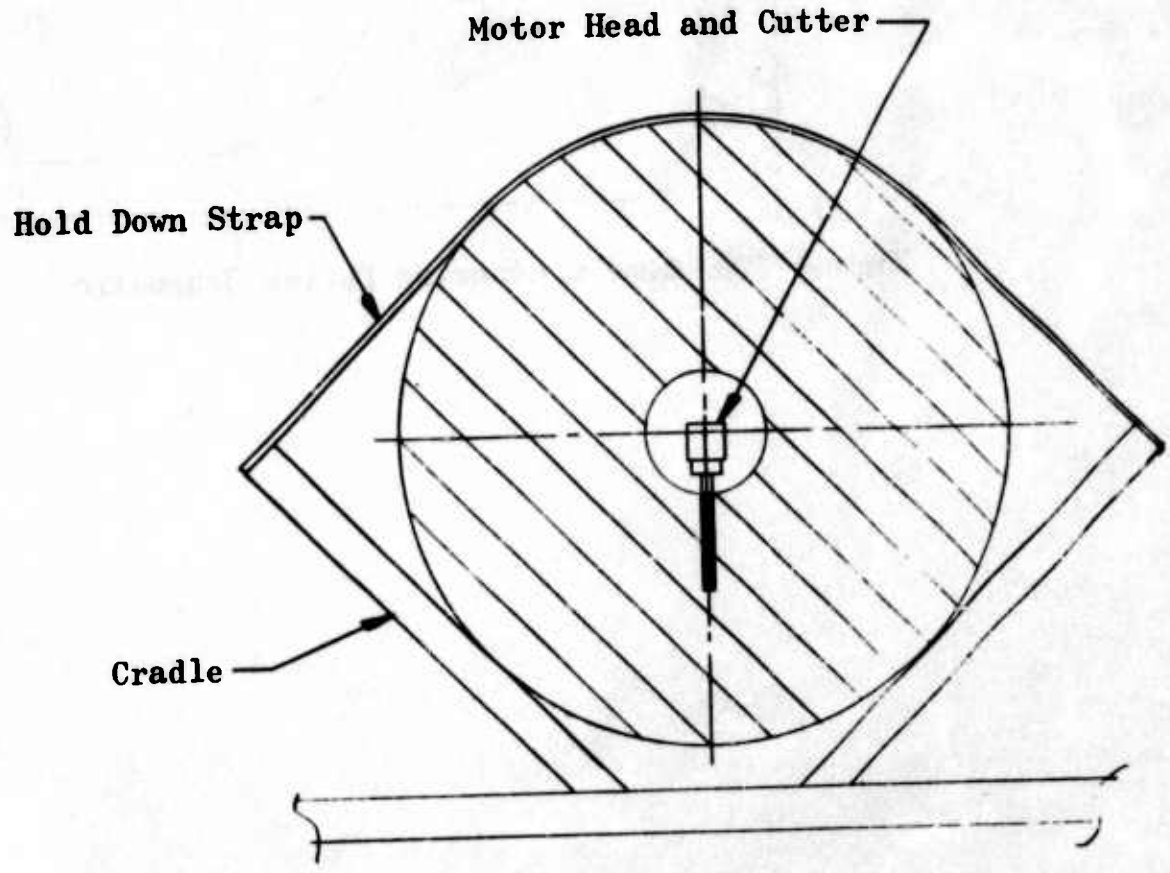


Figure 326. Dome Contouring Device-Schematic



Side View

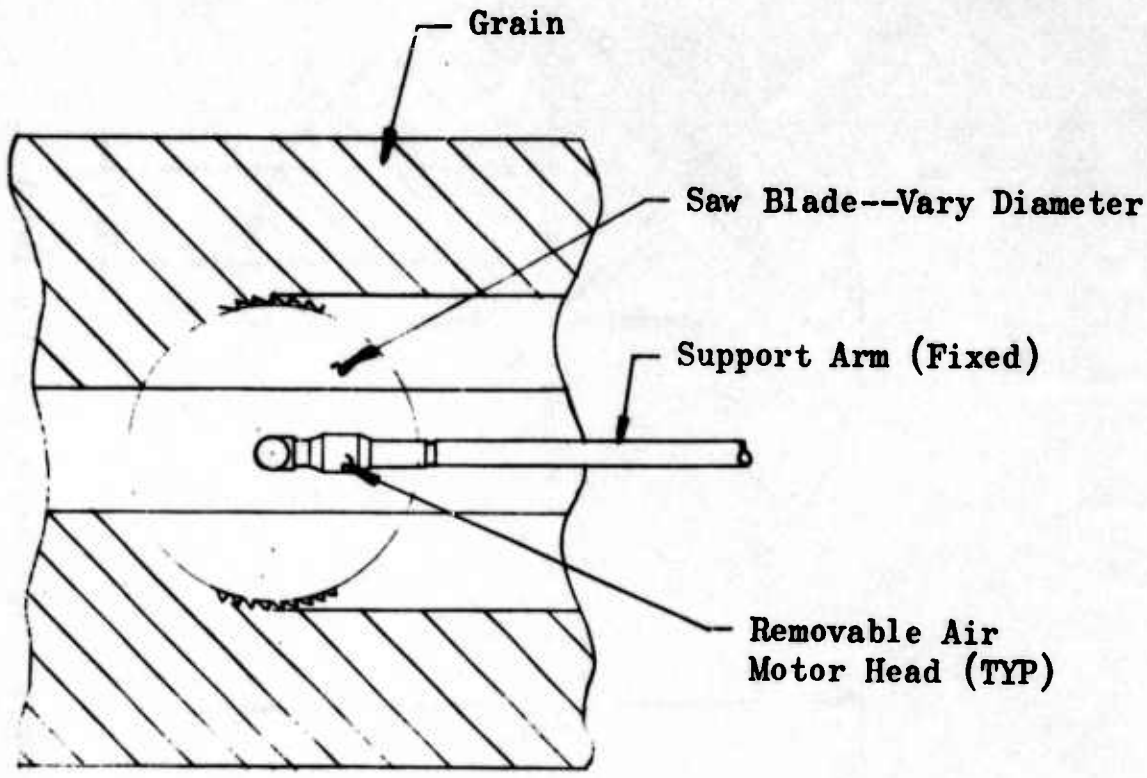
Router-type



End View

Router-type

Figure 327. Slotter



Saw Type

Figure 327
(Continued)

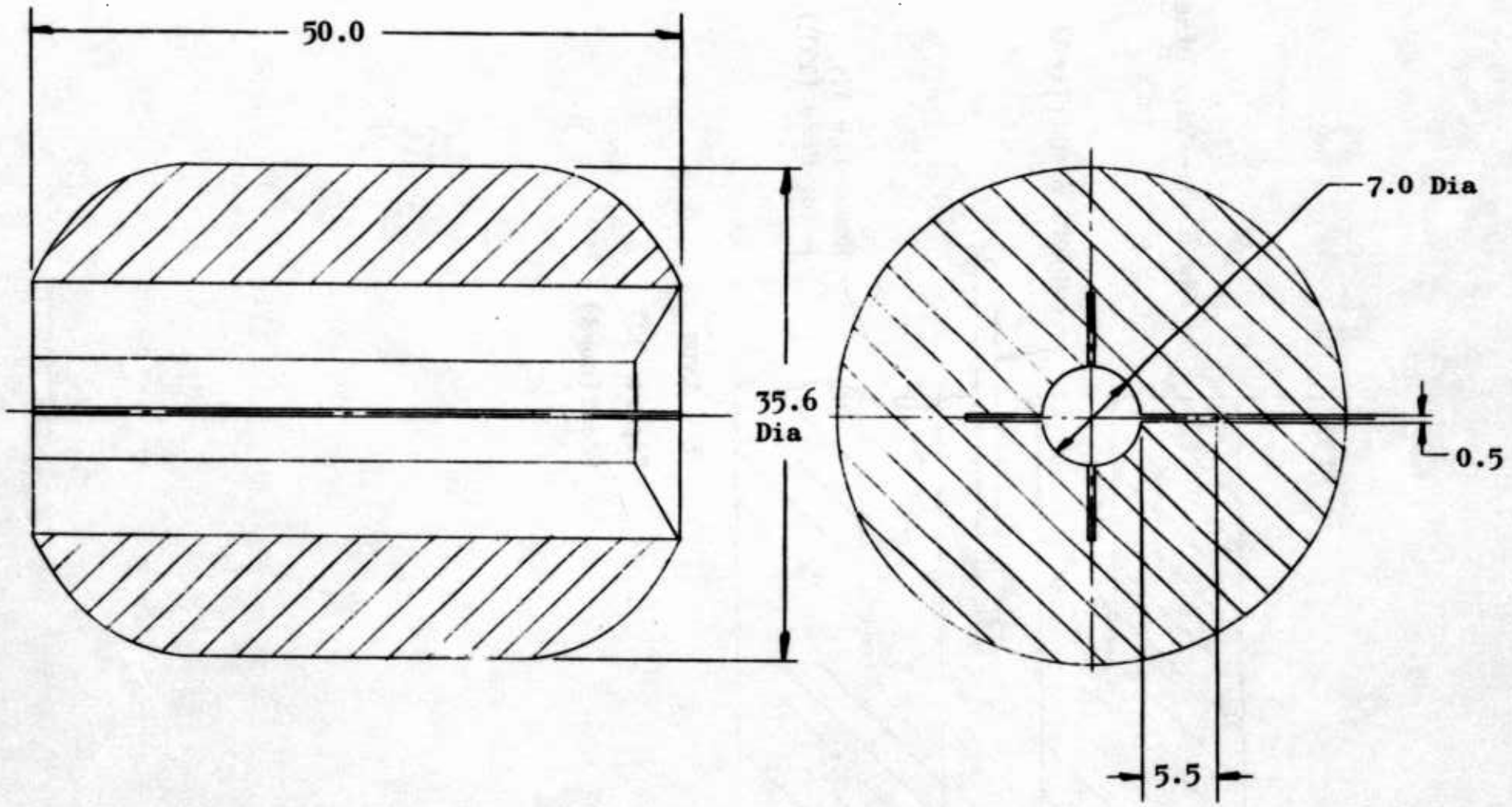


Figure 328. Slotted Motor B′ Type Grain (2530 pounds)

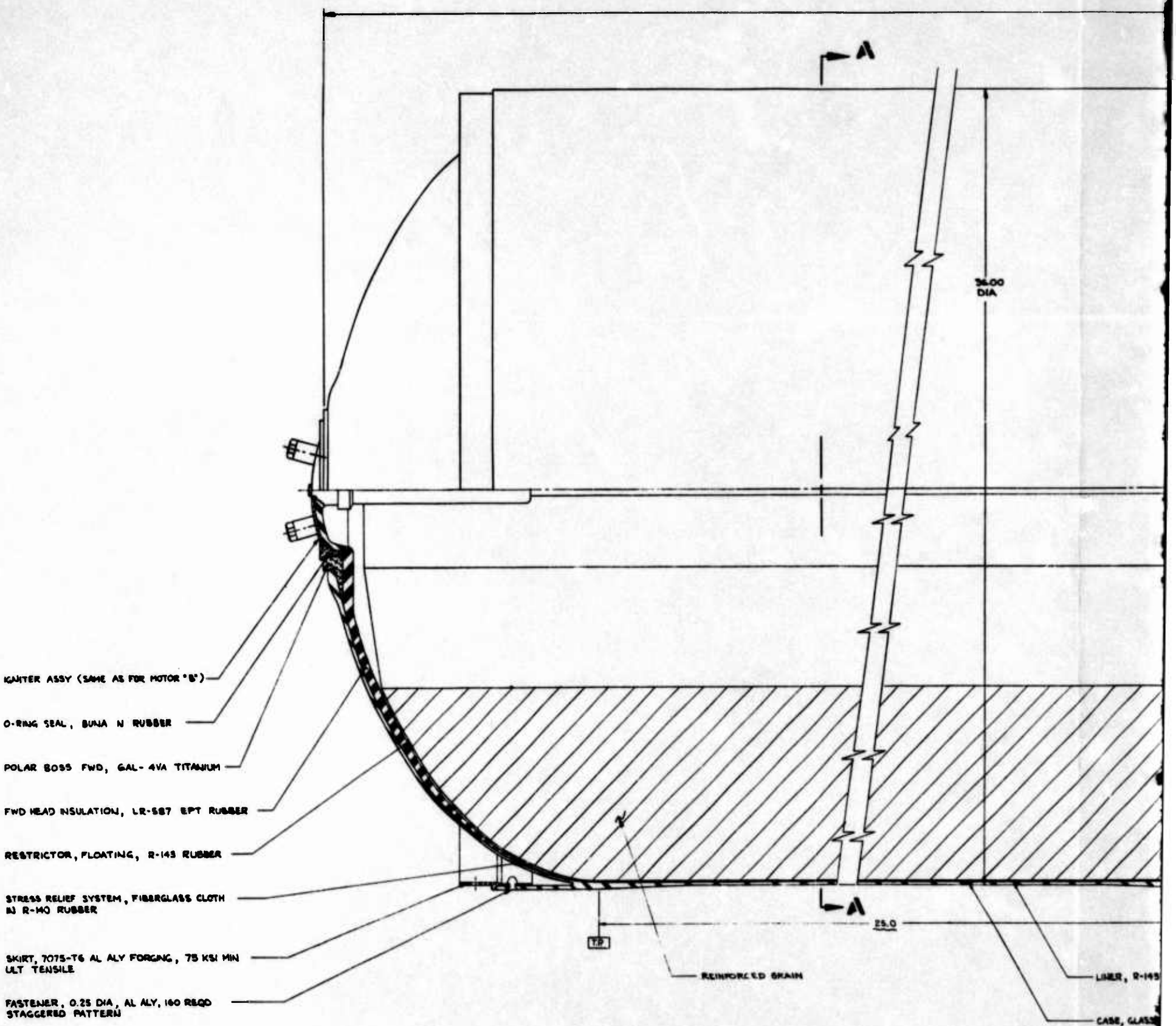
4. FLIGHTWEIGHT DESIGN

A flightweight design, Fig. 329, wherein all components were tailored specifically for this design, was also produced in the course of the studies. Significant reduction in inert weight, as compared with the testweight design, was seen. Specifically, this decrease in weight occurred in the nozzle/motor attachment and case insulation areas. Head insulation was optimized analytically, with adequate but less conservative thicknesses than the testweight version.

(C) Table CIII compares characteristics and altitude performance of Motor B' and flightweight Motor B'. The target motor weight was lower for Motor B' than for Motor B; however, direct comparison could be made between the two designs in delivered impulse, mass fraction, and impulse-to-weight ratio. The Motor B' testweight version was designed for high confidence and, therefore, was targeted at considerably lower mass fraction and impulse-to-weight ratio than Motor B. However, the 0.892 mass fraction with TVC system compares very favorably with advanced motors in service or planned. Motor B' flightweight motor, while not demonstrated, offers a system which has potential for achieving mass fraction in the 0.920 range, including altitude nozzle and TVC accessories.

Although the possibility of pursuing the Motor B' approach was seriously considered, overriding considerations of program risk and remaining program funding resulted in an Air Force decision not to proceed with Motor B' redirection.

PREVIOUS PAGE WAS BLANK, THEREFORE WAS NOT FILMED



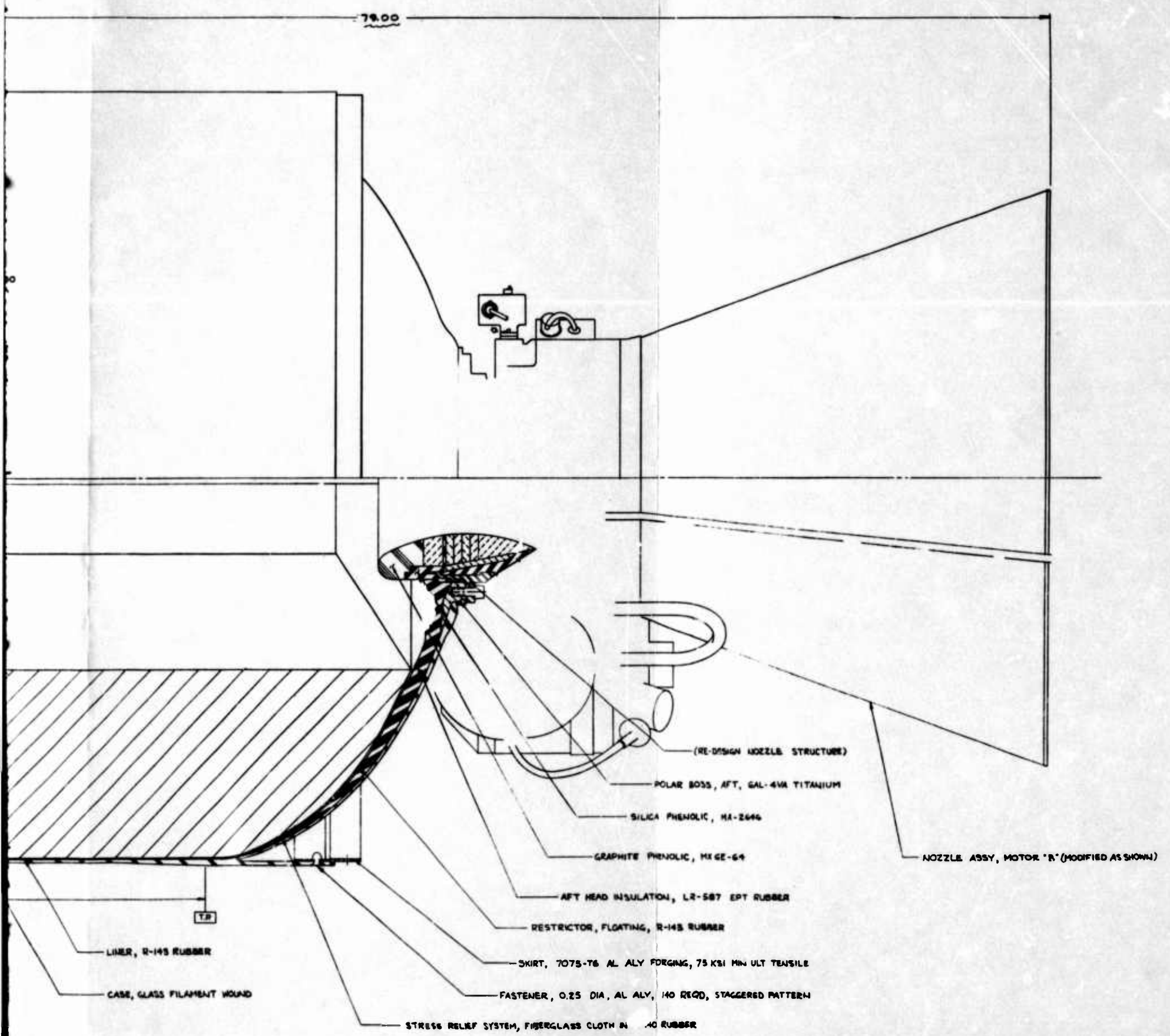
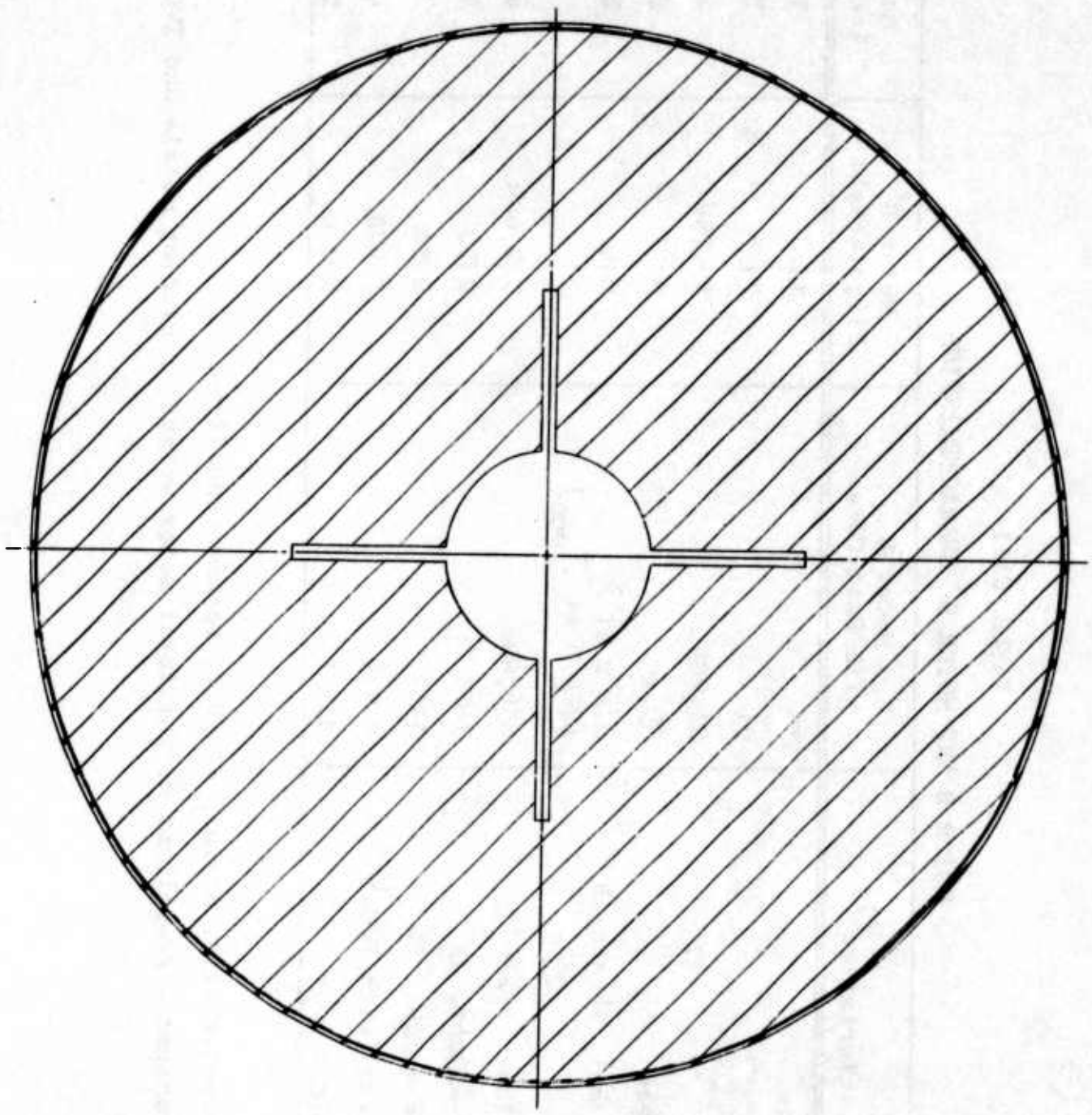


Figure 329. Motor B' Flightweight Design

PREVIOUS PAGE WAS BLANK. THEREFORE WAS NOT FILMED



SECTION A-A

Figure 329
(Continued)

TABLE CIII

MOTOR B AND MOTOR B′ CHARACTERISTICS

Motor Characteristics(1)	Motor B with Cast Core	Motor B′ Flightweight	Motor B′ Testweight
Diameter, in.	36	36	36
Length, in.	91	79	79
Thrust, lb	21,900	24,790	23,700
Duration, sec	39.1	29	29
I_s, vacuum del, lb-sec/lb	276.2 at P_{c_o} (280.0 at I_{1000})	284	284
Total impulse, lb-sec	856,800	719,000	690,000
Propellant weight, lb	3103	2530	2430
Total motor weight, lb	3359	2750	2720
Mass fraction (with TVC)(2)	0.924	0.920	0.892
Impulse/weight, vac.	255.1	261.0	253.0

(1) All characteristics nominal at 70 F, vacuum conditions.

(2) Mass Fraction = Propellant weight/total motor weight, including nozzle and TVC system.

SECTION XI

MOTOR D

In late September 1964, RPL redirected the reinforced grain program to include the feasibility of an air launched propulsion system (ALM) capable of withstanding extreme environments and characterized by stop-restart capabilities in accordance with the design objectives listed in Section I and summarized in Table CIV. The motor, see Fig. 330, was 100 inches long and 15 inches in diameter. Initial problem areas envisioned by Rocketdyne included charge support system, insulation, restart ignition and insulation, materials and materials compatibility, and the grain pressure cycling during boost-restart period. Another obvious problem area was the capability of the nozzle to withstand the thermal stress environment of stop-restart. Since major emphasis was placed on development of the internal charge configuration, costs prevented major development in the nozzle area. The customer and Rocketdyne mutually agreed that the hardware, case, and nozzle would be heavyweight. On completing the major portion of the design, RPL requested a design review meeting at Edwards Air Force Base on 23 March 1965.

(C) Concurrent with the design, bench tests were conducted to verify "suspect" areas. These tests included adhesive systems at all interfaces, support systems, insulation and ignition. Tests were also conducted to demonstrate cartridge loading techniques and environmental capabilities of materials during storage and motor operation. Many of these tests were associated with proving the systems under the extreme environment of 250 F.

The details of each of the above studies are discussed in this section and, although only a feasibility approach was taken in the solution of each of the design confirmation tests, a bench test feasibility approach was achieved prior to initiation of fullscale fabrication on all questionable areas. Thus, the motor design concept presented in this section fulfills all the performance objectives. Work stoppage found the Motor D design in the last detail design stages with materials ordered for all long lead time items. Below is a summary of the status of the various motor components:

Item	Status
1. Detail Component Drawings	Partially complete
2. Motor Assembly Drawings	Partially complete
3. Motor Cases (3)	One case completed fabrication; others in stages of completion

4.	Case Insulation	Started effort on first case only
5.	Nozzle	Contract awarded and tooling effort initiated
6.	Propellant	Propellant tailoring completed
7.	Other Detailed Components	Various stages of procurement action
8.	Wire	All procurement completed
9.	Ignition Materials	All procurement completed

TABLE CIV

(C) SUMMARY OF DESIGN OBJECTIVES FOR MOTOR D

1.	Action time, total impulse, lb-sec (sea level optimum expansion)	155,000
2.	Thrust, average, lb	
	Boost	5,000
	Sustain	1,400
	Restart, minimum	1,400
3.	Outside diameter, in.	15
4.	Over-all length, in.	100
5.	Length, grain, in.	80
6.	Propellant weight, maximum, lb	680
7.	Delivered specific impulse, lb/sec (I_{sp} corrected to optimum 1000/14.7 psi expansion and 0^{o} half angle)	250
8.	Boost grain design suitable for ignition from sea level to 80,000 feet.	
9.	Restart grain design and restart igniter suitable for ignition from sea level to 80,000 feet.	
10.	Action time, sec	
	Boost	12
	Sustain	50
	Restart, minimum	10
11.	Storage, years	5

TABLE CIV

(Continued)

12. Thermal environment demonstration - design considerations

    a. Environment: -75 F to 170 F (storage)
    250 F - 60 Min (captive flight)
    650 F - 2 min (captive flight)

    b. Demonstration: Temperature cycle -75 F to 250 F, 20 times per Military Spec MIL-R-25534A requirement (2 1/2 cycles). End at 250 F, subject to 650 F (hold for 2 min), fire at 650 F amb air temperature.

13. Case structure will be heavyweight

14. Vibration - Design considerations

    a. Capability of withstanding vibration in accordance with Procedure I of MIL-R-25534A.

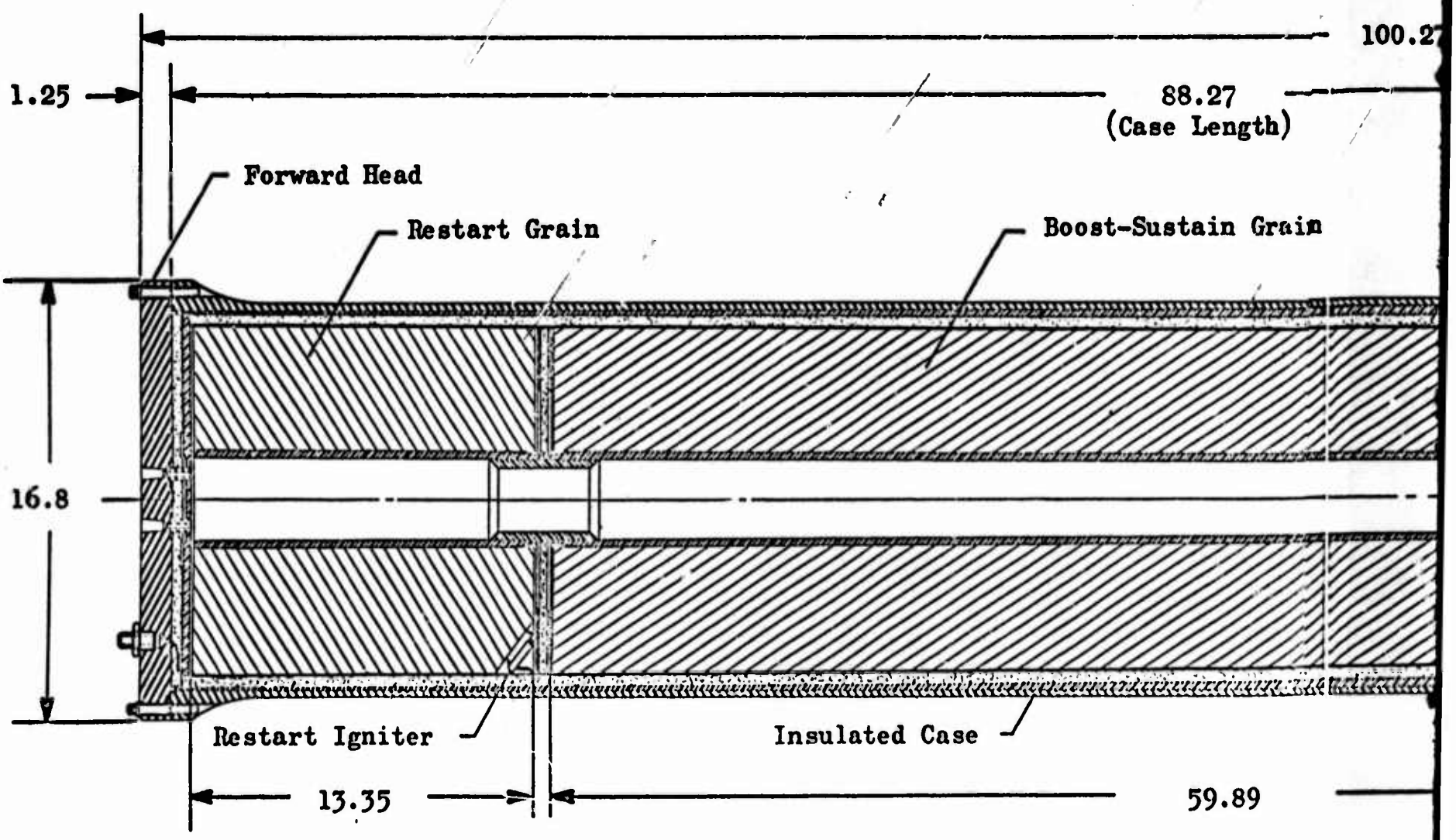
    b. The design shall include the capability of the motors to withstand a $\pm$ 3 g input through 6 log sweeps of 10 minutes each over the frequency range of 30 to 2000 cps; and through 6 log sweeps of 10 minutes, duration over the frequency range of 5 to 28 cps at $\pm$ 4 g input. (A sweep is defined as either increasing frequency of decreasing frequency and shall extend over a 10 minute period). The motor D configuration shall be capable of surviving the above vibration requirements at the following ambient air temperatures: -75 F, 70 F, 170 F, and 250 F.

15. Ignition delay for restart, minimum, 0.100 sec.

16. Ignition delay objective for boost, minimum, 0.100 sec.

CONFIDENTIAL

PREVIOUS PAGE WAS BLANK, THEREFORE WAS NOT FILMED



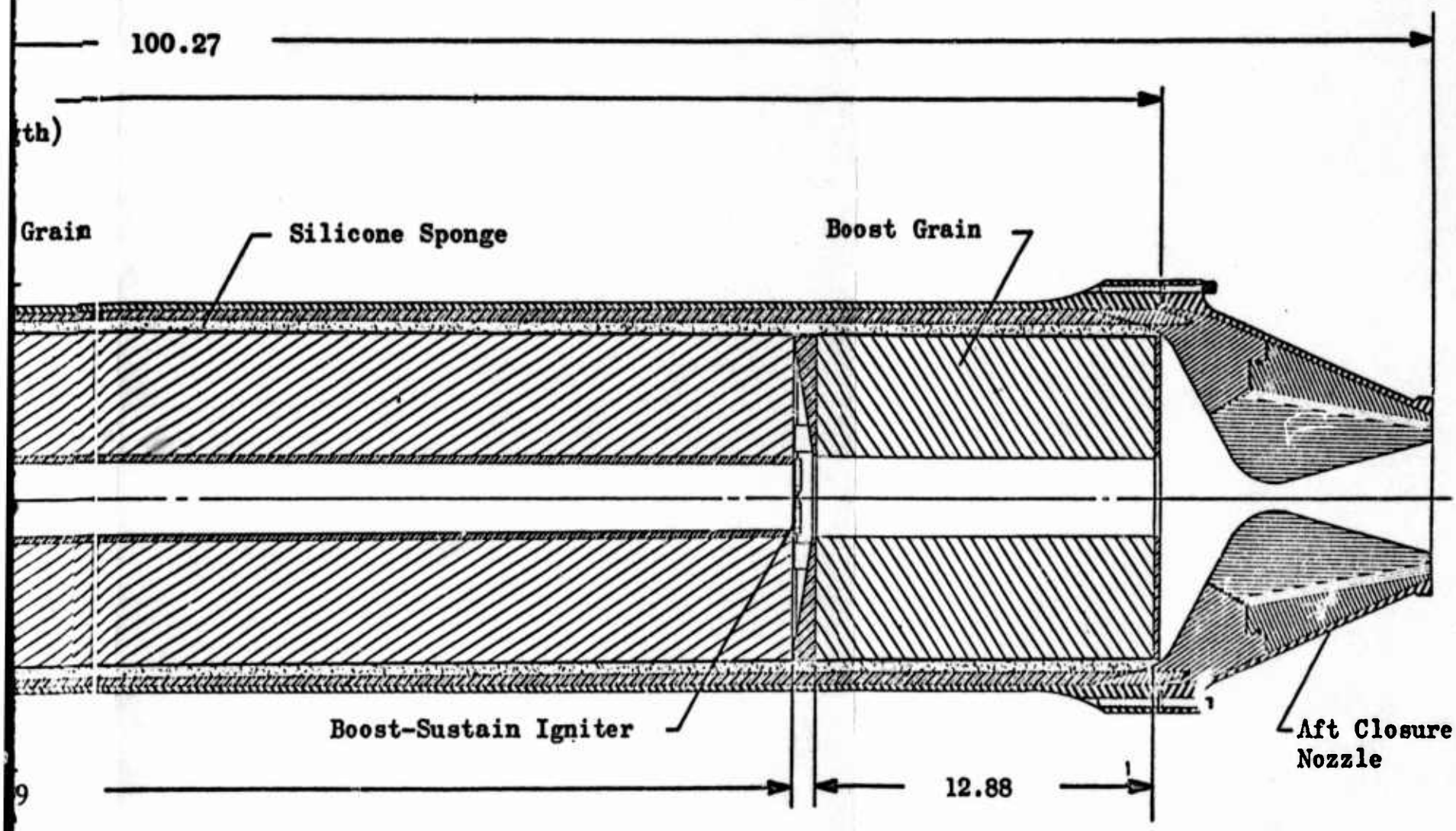


Figure 330. Motor D General Arrangement

CONFIDENTIAL

PREVIOUS PAGE WAS BLANK, THEREFORE WAS NOT FILMED

1. BALLISTIC DESIGN

(C) The design of Motor D presented many unique design challenges, not only stop-restart performance, but also extreme environmental temperature range (-75 to 250 F) and dynamic requirements.

The general design approach taken was an iterative process beginning with the given case design. The next step established the approximate insulation needed to protect the case and grain. Concurrently, a grain support system was considered that allows for grain thermal excursion, yet excludes grain damage during mechanical loading (pressure cycling, vibration, handling, etc.). Also included in this consideration were techniques for inserting the grain into the case/insulation system. Knowing the required total impulse and specific impulse, the total grain weight was determined. Placing this grain weight within the support and insulated case diameter established the over-all grain length.

After establishing the general grain dimensions, the details of the configuration and propellant provided the required performance. Considered in the combination of charge, grain support, and grain structural design is the orientation and quantity of the reinforcing wire in the grains. This is significant in that wire angle and quantity is a burning rate variable as well as the obvious structural support variable. With this last factor the charge design, grain support, fabrication, and loading techniques were interlinked.

It should be noted that no attempt was made in this design to optimize volumetric loading and mass fraction or to maximize delivered impulse. The intent was rather to meet nominal design objectives and demonstrate capability of the key features under specified rigorous environmental conditions.

a. Parametric Study

(C) Performance objectives originally set forth for Motor D were described by a total impulse of 155,000 lb-sec, with a boost-to-sustain thrust ratio of 5:1. Average thrust levels and impulse for each phase were:

(C)

	Average Thrust, lb	Total Impulse, lb-sec
Boost	7500	60,000
Sustain	1400	70,000
Restart	2500	25,000
		155,000

(C) Preliminary estimate of propellant weight was 680 pounds based on a specific impulse (I_{sp}) of 250 lb-sec/lb. (The latter two parameters of thrust level and impulse per phase were included as objectives[25]). With the additional limitation imposed by using existing hardware (which would constrain maximum case pressure and volume), the parametric study began with the maximum pressure allowable at 250 F for the existing case design, 2800 psia. Allowing for reproducibility (10%), temperature coefficients of pressure of 0.18%/F, and estimated ratio of maximum to average pressure (1.07), the average pressure of the boost phase burning at 70 F was 1710 psia.

Pressures in a boost-sustain motor are related by the thrust coefficients, throat areas, and thrust ratio. Either pressure may be shown as a function of the other. The equation defining this function is:

$$P_s = \frac{\frac{F_s}{F_b} \times \frac{A_b}{A_s} \left[P_b C_{F_b} - P_e \epsilon_b\right] + P_e \epsilon_s}{C_{F_s}}$$

where P is pressure, F is thrust, A is throat area, ϵ is expansion ratio, C_F is thrust coefficient (theoretical in vacuum), and P_e is the ambient pressure. Subscripts b and s denote boost and sustain, respectively. The same would apply to a ratio of either the boost or sustain to the restart.

(C) With the thrust ratios known, the equation can be treated as a parametric equation of one pressure as a function of expansion ratio, the other pressure functioning as the parameter. As specific impulse varies with chamber pressure, the propellant weight required for given total impulse is a function of the variables shown above. With these relationships

---

(25) For reasons to be discussed, the final predicted motor performance differed slightly from the above objectives, primarily in total impulse and boost phase thrust. Average thrust levels of the sustain and restart phases are identical to the original objective.

(C) the total propellant weight required for the given impulse can be described as a function of expansion ratio and sustain pressure. This function has a minimum value. The requirements of performance and envelope were such that the nozzle could be optimized on this basis. Hence, the nozzle expansion ratio in the preliminary analysis was determined using minimum propellant weight as criteria. These studies indicated a requirement for approximately 680 pounds of propellant when operating the sustain phase at 300 psia. By the previous equation, this pressure is defined by the pressure in the boost phase.

(C) At this point in the preliminary analysis, the over-all grain was dimensioned for 680 pounds of propellant. Based on insulation requirements, grain taper (0.0112 in./in. on diameter), and other considerations the total charge length was 87.30 inches with an OD at the forward end of 13.43 inches and ID at the aft end of 3.00 inches. With the sustain pressure of 300 psia, estimated performance met with design objectives.

(C) Subsequently, a decision was made to increase the sustained pressure to 400 psia to enhance the combustion efficiency. However, since the boost pressure could not be increased (limited by case strength), the thrust level during boost was dropped from 7500 pounds to 5100 pounds while maintaining the given thrust level in the sustain phase.

The pressure level could be increased in the restart phase, so the original level of restart thrust was maintained by raising the burning rate and pressure in the restart grain. In conjunction with these changes, it was decided to leave the propellant charge weights as originally designed, since tool design and other effort had proceeded on basis of the preliminary grain configurations. Hence, each phase has an estimated total impulse slightly greater than originally planned, primarily because of the higher operating pressures.

During the parametric study, an iterative process was required in order to relate the propellant maximum flow with nozzle erosion. During the operation of the boost phase considerable throat erosion was experienced which necessitated accurate prediction of the nozzle erosion. Therefore, as a result of the sustain pressure increase, the nozzle throat was decreased, thereby necessitating another correlation of weight flow rate vs throat erosion.

(C) Also, with the different pressure levels, the original expansion ratio was no longer optimum; therefore, the nozzle expansion ratio was optimized on the basis of maximum total impulse with fixed propellant weight and specified thrust levels in the sustain and restart phases. Hence, the final estimated total impulse for Motor D was 160,430 lb/sec compared to the original objective of 155,000 lb/sec.

(C) b. Charge Design

At completion of the parametric study, the design of the charge configuration was initiated. Preliminary analysis indicated that the required mass flow rates in the sustain and restart phases could be achieved with end burning grains. However, this could be accomplished only by use of a reinforced grain, since the relatively high burning rates exceeded those available in conventional cast propellant. The reinforced grain, with proper wire orientation, provides the higher burning rates required by the end burning configuration in the sustain and restart phases. From early data acquired in studies conducted by independent research(26), the variation of burning rate with wire wrap angle was established, Fig. 331. The end burning configurations require a burning rate of 0.8 and 1.2 in./sec at 1000 psia for the sustain and restart phases, respectively.

The boost phase thrust level required a mass flow rate greatly exceeding that which was afforded by an end burning grain due to burning rate limitations. Realizing that the most neutral pressure-time program permits the highest average pressure, thereby providing the highest specific impulse, maximum neutrality of pressure was established as an objective of the boost grain design. The incremental application of propellant in fabrication of the reinforced grain enabled this to be accomplished with an internal burning tubular configuration. By increasing the propellant burning rate as the grain is wound resulted in a weight flow rate that maintained a constant pressure. With conventional propellants, the geometry must be suited to a constant burning rate; however, the reinforced grain can vary the burning rate to suit the burning geometry. In addition to the internal burning configuration, a portion of the boost weight flow is provided by the end burning sustain grain. Other configurations were theoretically applicable for the boost grain but were eliminated in favor of the selected design. These others included the slotted cylinder and fluted bore configurations.

Final Motor D grain configuration was composed of three separate tubular charges, see Fig. 332. The center section is the longest and burns during both boost and sustain operations. Approximately 19.3 inches of the center section burns during the boost phase. Sustain and restart grains are both end burning configurations, being restricted on the inner surface. Both the sustain and restart grains utilize Rocketdyne Propellant RDS-531. The burning rate variation is achieved through minor matrix propellant tailoring. The boost grain utilizes propellant RDS-532 at three distinct burning rates to maintain pressure neutrality. Due to the severe erosion of the monilithic throat insert during the high mass flow

(26)Company-initiated IR&D

of the boost phase, the thrust time program is progressive even though the pressure-time program is neutral. Since thrust is directly proportional to throat area, the thrust increases as the nozzle throat becomes larger.

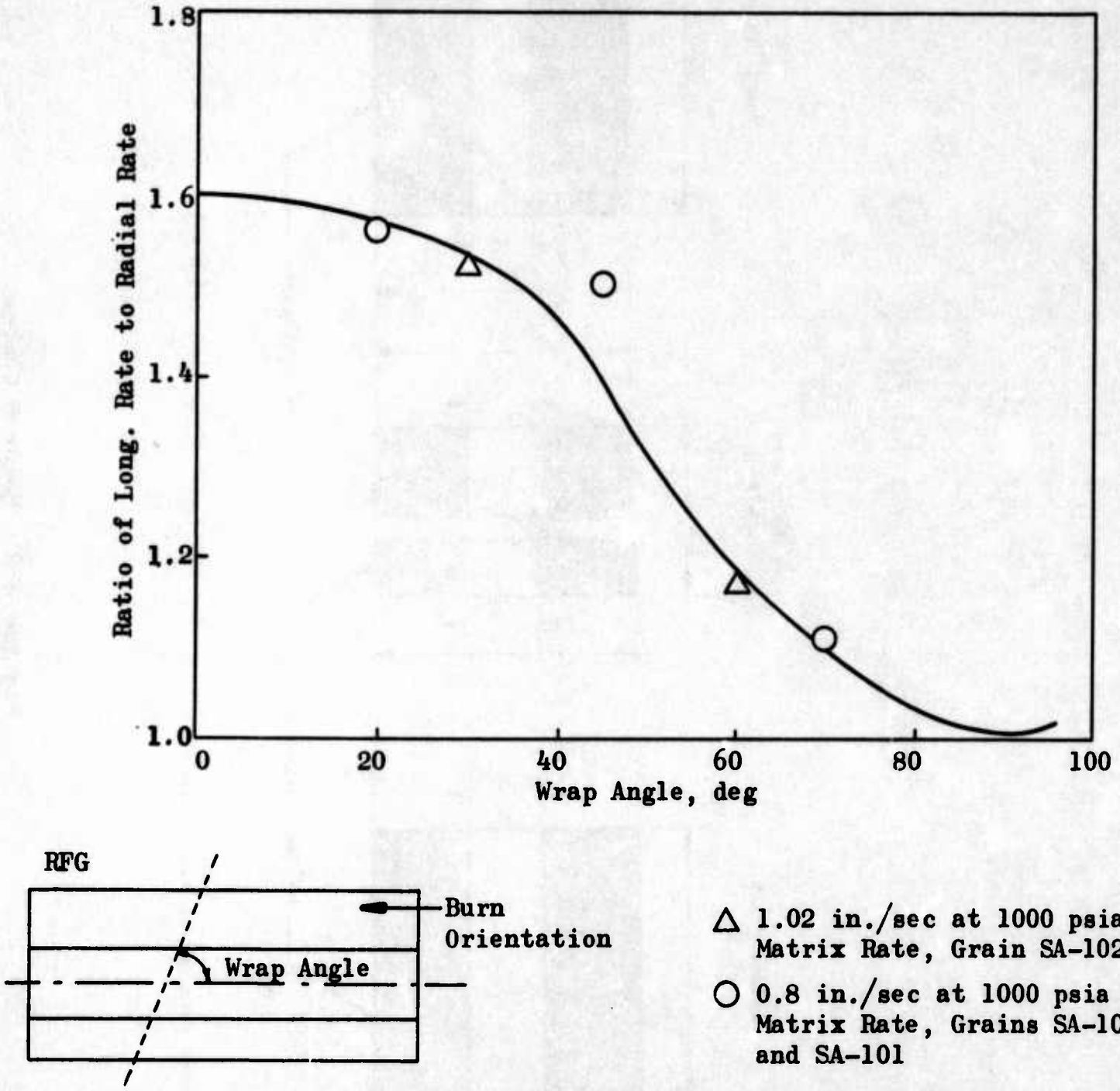
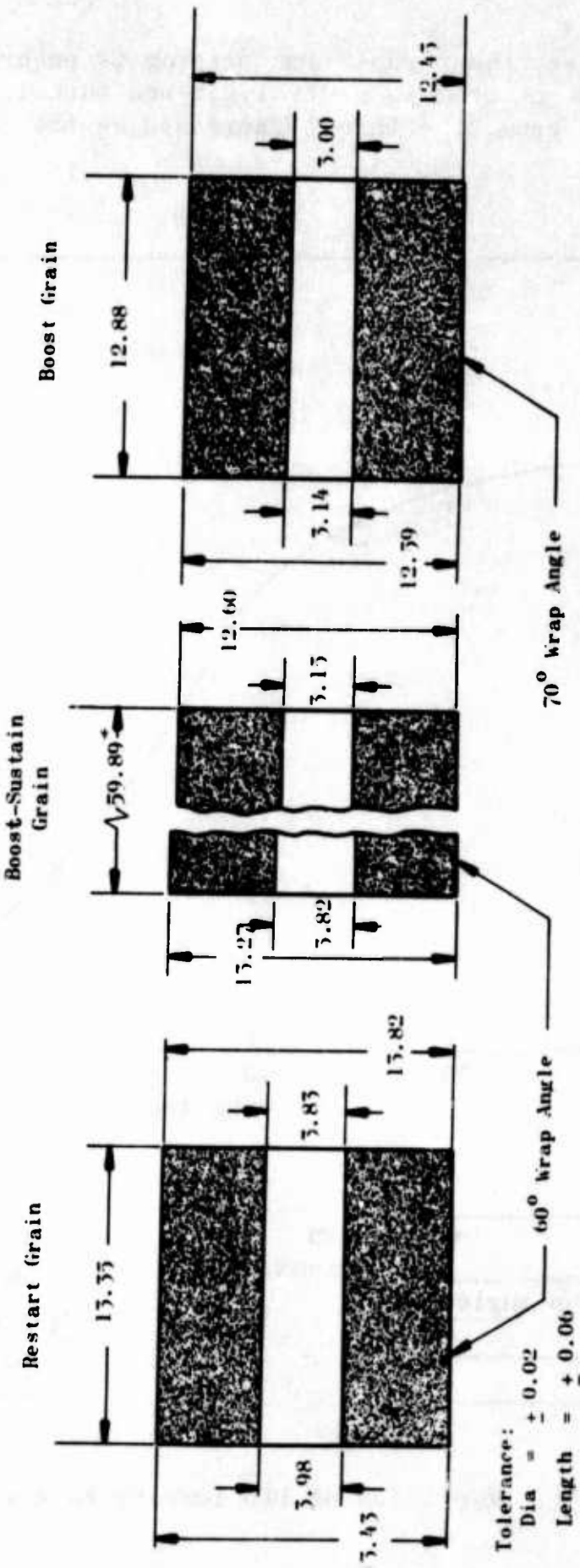


Figure 331. Variation of RFG Burning Rate with Wire Angle



Figures 332. Motor D Grains

(C) A summary of the pertinent dimensions relative to the grain geometry and nozzle are shown in Table CV. Estimated motor performance for the boost, sustain, and restart phases are shown in Table CVI for each of the three temperatures concerned, -75, 70, and 250 F. Estimated thrust and pressure time curves are shown in Fig. 333.

(C)

TABLE CV

MISCELLANEOUS PHYSICAL DATA

Boost Propellant, RDS-514	
Grain Weight, lb	96.9
Propellant Weight, lb(1)	245.5
Wrap Angle, deg	70
Propellant Web, in.	4.725
Sustain Propellant, RDS-531	
Grain Weight, lb	474.5
Propellant Weight, lb(2)	325.9
Wrap Angle, deg	60
Propellant Web, in.	40.6
Restart Propellant, RDS-531	
Propellant Weight, lb	111.1
Wrap Angle, deg	60
Propellant Web, in.	13.35
Total Propellant Weight, lb	682.5
Nozzle	
Throat Diameter, in.	1.352
Exit Diameter, in.	4.382
Expansion Ratio	10.5
Divergence Half Angle, deg	15.0
Initial Burning Surface, sq in.	241.2
Port-to-throat ratio	4.9

(1) Including 19.29 inches of sustain grain which burns during boost phase.

(2) Excludes 19.29 inches of sustain grain which burns during boost phase.

(C)

TABLE CVI

BALLISTIC PERFORMANCE

	-75F	70F	250F
Boost Phase			
Avg Pressure, psia	1,315	1,710	2,365
Avg Thrust, lb	3,855	5,095	7,165
Duration, sec	15.76	12.20	8.87
Total Impulse, lb-sec	60,730	62,140	63,480
Max Pressure, psia	1,390	1,790	2,475
Max Thrust, lb	5,140	6,665	9,290
Avg Throat Area, sq in.		1.895	
Avg Expansion Ratio		7.96	
Sustain Phase			
Avg Pressure, psia	310	400	555
Avg Thrust, lb	1,025	1,400	2,030
Duration, sec	66.69	51.61	37.52
Total Impulse, lb-sec	68,350	72,250	76,020
Max Pressure, psia	315	405	560
Max Thrust, lb	1,065	1,450	2,080
Avg Throat Area, sq in.		2.525	
Avg Expansion Ratio		5.97	
Restart Phase			
Avg Pressure, psia	500	650	900
Avg Thrust, lb	1,870	2,500	3,555
Duration, sec	13.45	10.42	7.57
Total Impulse, lb-sec	25,130	26,040	26,920
Max Pressure, psia	510	660	915
Max Thrust, lb	1,880	2,505	3,545
Avg Throat Area, sq in.		2.615	
Avg Expansion Ratio		5.77	
Total Motor			
Total Impulse, lb-sec	154,210	160,430	166,420
Duration (Excl Stop), sec	95.90	74.23	53.96

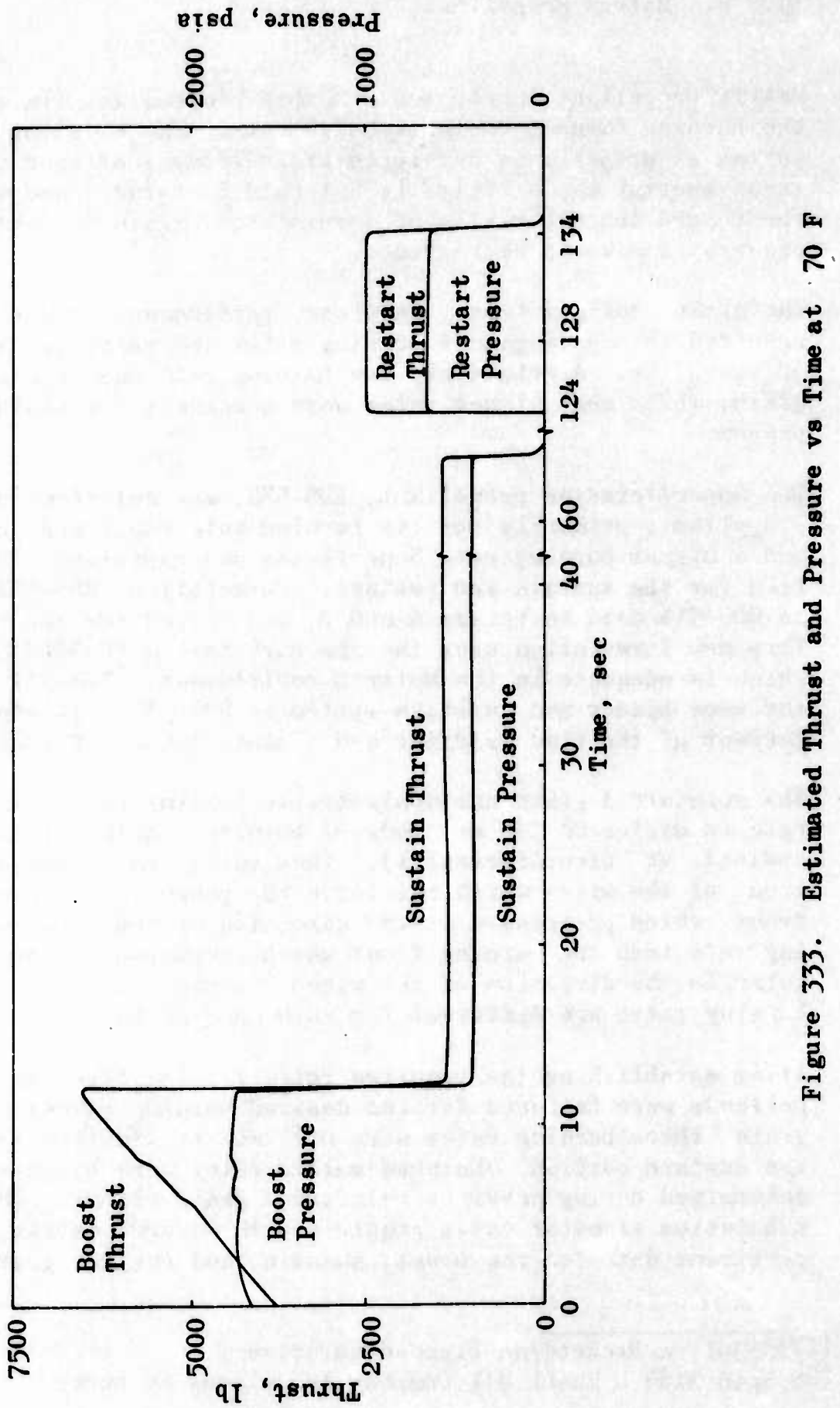


Figure 333. Estimated Thrust and Pressure vs Time at 70 F

c. Matrix Propellant

(C) Matrix propellant development on this program was limited to tailoring the burning rates to motor requirements. The existing Superflexadyne series of propellants developed at Rocketdyne offered the required extreme thermal capabilities (-75 to 250 F storage) and when combined with the rugged characteristic of a reinforced grain the motor mechanical load requirements would be exceeded.

The grain configurations, envelope, performance, and other requirements resulted in two ranges of burning rates necessary for the three phases of operation. A relatively low burning rate was required for the boost grain, while much higher rates were necessary for sustain and restart phases.

The Superflexadyne propellant, RDS-532, was selected for the boost matrix propellant, primarily for its burning rate range and thermal properties, and a higher burning rate Superflexadyne propellant, RDS-531, was specified for the sustain and restart. Formulation, RDS-532, which is similar to RDS-514 used in Motors A and B, was tested for use in the boost grain. This new formulation uses the new cure system (C-301 (27) with Epon 812 (28) which is adequate in the Motor D environment. RDS-531 formulation has the same binder and curative system as RDS-532. It contains a higher percent of the fine oxidizer and a small amount of iron oxide catalyst.

The reinforced grain has nonisotropic burning rates (in that the burning rate is different for any mode of burning, whether it be radial, longitudinal, or circumferential). This variation is because of the orientation of the wires which reinforce the propellant structure. A burning front, which progresses in the direction of the wire, has a higher burning rate than the burning front which progresses along a plane perpendicular to the direction of the wires. Because of this characteristic, the burning rates are different for each mode of burning.

After establishing the required rates for the three grains, the two propellants were tailored for the desired burning rates. For the boost grain, three burning rates were utilized in addition to the rate used in the sustain portion. Uncured matrix rates were based on correlations determined during previous reinforced grain effort. Table CVII is a tabulation of motor rates required with uncured matrix rates and other pertinent data for the boost, sustain, and restart grains.

(27) C-301; a Rocketdyne blended curative
(28) Epon 812; a Shell Oil Company low viscosity epoxy

TABLE CVII

BURNING RATES REQUIRED WITH UNCURED MATRIX RATES

Grain	Aft End Diameter, in.	Motor Rate, in./sec	Matrix Rate at 1000 psia in./sec	Propellant Weight, lb
Boost	3.00 to 7.43	0.372 @ 1710 psia[1]	0.271	30.8
Boost	7.43 to 9.01	0.394 @ 1710 psia[1]	0.284	17.2
Boost	9.01 to 12.45	0.410 @ 1710 psia[1]	0.296	48.9
Sustain		0.787 @ 400 psia[2]	0.83	148.6[3]
Sustain		0.787 @ 400 psia[2]	0.83	325.9[4]
Restart		1.281 @ 650 psia[2]	1.11	111.1

(1) Radial Rate

(2) Longitudinal Rate

(3) Boost Portion

(4) Sustain Portion

(C) Motor D required burning rates were established by the ballistic design and the tailored matrix was verified in subscale test motors. Results of these tests are presented in the Table CVIII. Samples represented wire orientation of both 45 and 70 degree wrap angles. These angles were chosen because the two Motor D grains would have a wire orientation between these two wrap angles.

(C) The burning rates for the boost phase as shown are required at boost pressure of 1710 psia, regardless of the value of pressure exponent. However, as existing data (matrix rates and matrix-to-motor rate correlation) were available only at 600 psia and lower for RDS-532, it was necessary to estimate the motor burning rates at 600 psia and, hence, the pressure exponents. The estimates were made on the basis of Motor A data where the pressure exponent appeared to vary with rate at 1000 psia. Pressure exponents for the three boost propellants were estimated to be 0.29, 0.31, and 0.31, respectively.

(C) TABLE CVIII

MATRIX PROPELLANT DATA (RDS-531)

Wire Angle, degree	Firing Temperature, deg F	Burning Direction	Burning Rate at 1000 psia, in./sec
45	75	Radial	0.90
45	75	Longitudinal	1.35
45	75	Circumferential	1.35
70	75	Radial	0.90
70	75	Longitudinal	1.40
70	75	Circumferential	1.40
45	-75	Radial	0.85
45	250	Radial	1.10

(C) Both the sustain and restart propellant rates were based on a 10-inch motor test whose grain employed a 60 degree wrap angle and 1.02 in./sec at 1000 psia matrix rate and two-inch motor data with 0.8 and 1.02 in./sec rates. These tests were preformed under company-sponsored programs. The formulations of matrix propellants RDS-531 and RDS-532 are as shown in Table CIX. Table CX gives pertinent ballistic and physical characteristics of the reinforced propellants for Motor D.

2. STRUCTURAL DESIGN

(C) The extreme environmental conditions, -75 to 250 F, required a flexible, mechanical support system between the grain and case. This was satisfied by a silicone sponge. Since this flexible system provides little or no external support to the grain during pressurization, the program must be capable of withstanding the internal pressure. The sustain and restart structural capabilities were of particular concern since the grains must remain elastic to prevent plastic deformation when the high pressure boost phase is concluded.

(C)

TABLE CIX

MATRIX PROPELLANTS RDS-531 AND 532

	Weight Percent	
	RDS-531	RDS-532
Ingredient		
Butarez CTL	8.952	8.952
Conoco H-25	2.690	2.690
Epon 812	0.089	0.089
C-301*	0.269	0.269
Strontium Carbonate**		0-2.5
Iron Oxide**	0-2.5	
Ammonium Perchlorate	85.5-88.0	85.5-88.0
Sensitivity		
Autoignition Temperature, F		
5 seconds	640	760
5 minutes	540	620
Impact sensitivity, in.-lb	22	19

*Rocketdyne curative
**Varied to adjust burning rate

(C)

TABLE CX

PERTINENT CHARACTERISTICS OF

REINFORCED PROPELLANTS FOR MOTOR D

	Boost Grain	Sustain/ Restart Grains
Matrix Propellant	RDS-532	RDS-531
Aluminum Wire, %	13	13
Specific Impulse, sec (1000 psia-15° Half Angle)	245.8	243.8
Characteristic Exhaust Velocity (C*), ft/sec	5185	5140
Density, lb/cu in.	0.065	0.065
Ratio of Specific Heats (γ)	1.18	1.18

(C) Since both strength and burning rate are a function of wire orientation and amount, the structural design of the propellant charges was influenced by the ballistic requirements. Coordinated design analysis of the two functions resulted in a 60 degree wrap angle with a wire weight fraction of 13% for the sustain and restart grains. The boost grain is characterized by 70 degree wrap angle and 13% wire.

a. Boost Grain Analysis

(C) Because of the flexible (silicone sponge) grain support system used for this motor, there is little pressure on the outside diameter until the sponge is compressed to its solid thickness (60%). With little initial structural support on the boost grain OD, the grain must deflect until the sponge bottoms out and offers support or the grain must withstand the pressure load within its own structure. Since the boost grain is a radial burning grain, it is obvious that the web will, at some time during the boost burning, become too thin to provide adequate structural strength. Therefore, the grain was designed with high elongation (5%) wire that allowed the grain to expand under pressurization as the grain support system compresses solid and offers back pressure on the grain. Pertinent data for boost grain analysis is presented in Table CXI.

(C) Maximum possible deflection of the RFG occurs when the space between the RFG and steel case is a maximum. This condition was determined to exist for a cold (-75 F) RFG in a pressurized case subjected to aeroheat. Case temperature for a cold motor subjected to aeroheat was not defined, so an ultra-conservative analysis was made. It was assumed that the RFG would remain at the cold temperature (-75 F), and that the cold case would reach the same temperature during the two minutes 650 F aeroheat as it would if it had been conditioned to 250 F prior to aeroheat. This assumption gave a temperature change (ΔF) from fabrication conditions of -145 F degrees (-75 to 70 F) for the RFG and 290 F (360 F--70 F) for the steel case (Nomenclature is presented at the end of this section.)

(C) $$U_r = (1 + \mu)\alpha r \Delta T \quad \text{(Radial deflection)}$$

$$U_{r_c} = (1.3)(6.5 \times 10^{-6})(7.3)(290)$$

$$= 0.018 \text{ in. (case)}$$

TABLE CXI

PERTINENT DATA FOR BOOST GRAIN*

STRUCTURAL ANALYSIS-MOTOR D

Aluminum Wire	
Ultimate Tensile ($\bar{\sigma}_{TU}$), psi	50,000
Elongation ($\bar{\epsilon}_{TU}$), %	5
Modulus (E), psi	88×10^6
Support Sponge	
Thickness (t), in.	0.500
Maximum Compression, %	40
Boost Grain	
Radius, in.	
ID(a)	1.57
OD(b)	6.295
Thermal Coefficient of Expansion (α_G), in./in./F	12×10^{-6}
Poisson Ratio (μ_G)	0.4
Case	
Inside Radius, in.	7.3
Thermal Coefficient of Expansion (α_c), in./in./F	6.5×10^{-6}
Poisson Ratio (μ_c)	0.3

*Materials and Design Data Were Obtained From the Previous Motor A and Subscale Tests

Conversely, since the motor was assembled at 70 F, the cold temperature of the grain causes the grain to contract. Although the grain does warm some during aeroheat, the calculations assume that it has not. The contraction of the grain is determined by

(C) $$U_{r_G} = (1.4)(12 \times 10^{-6})(6.295)(-145) = -0.015 \text{ in. (RFG)}$$

Near burnout, the case will deflect outward from pressure and temperature. The RFG web will be thin and the sponge will be compressed solid.

From pressure,

(C) $$U_{r_c} = \frac{P_c r_c^2}{E_c t_c}\left(1 - \frac{\mu_c}{2}\right) = \frac{2800(1.25)(7.55)^2}{(30 \times 10^6)(0.25)}\left(1 - \frac{0.3}{2}\right) = 0.023 \text{ in.}$$

(C) It is recognized that the 2800 psi chamber pressure will not exist when the grain has been conditioned to -75 F, but in keeping with the initial program philosophy of conservatism it was decided to use the chamber pressure that is commensurate with a 250 F grain temperature. This represents about 4% conservatism on the over-all gap between the grain and case under these conditions.

(C) For assembly, loading criteria were established to provide a compression on the sponge of 13 $\pm$ 5%. Then the maximum installed thickness of the sponge would result under the condition of least compression, 8%, i.e., 0.500 - (0.08)(0.500) = 0.460 inch. Minimum thickness of the sponge under loading is 60% of the original thickness, 0.300 inch. Therefore, upon pressurization, the 0.460-inch sponge thickness would be compressed another 0.160 inch. Accumulating this dimension with those of case deflection (0.018 and 0.023 inch) and grain contraction (0.015 inch) reveals that the maximum radial deflection of the outside radius of the cold grain due to internal pressure is 0.216 inch.

(C) Calculating the hoop strain based on this deflection, it is found to be

(C) $$\epsilon_{G_{\theta_b}} = \frac{0.216}{6.295} = 0.0343 \text{ in./in.}$$

Examination of this value reveals that it is well below the minimum wire strain of 0.05 in./in.

The other possible critical point for this grain is the inside radius when the grain is ignited. For this condition,

(C) $$\epsilon_{G_\theta} = \frac{1 + \mu_G}{E_{G_\theta} (b^2 - a^2)} \left[\left(a^2 P_i - b^2 P_o \right) \left(1 - 2\mu_G \right) + \left(P_i - P_o \right) \frac{a^2 b^2}{r^2} \right]$$

(C) $$E_{G_\theta} = f_{v_w} E_w \sin^4 \alpha$$

(C) $$= (0.082) \ (8.2 \times 10^6) \ (\sin^4 70^\circ)$$

(C) $$= 5.243 \times 10^5 \text{ psi}$$

for values of

(C) $r = a$

$P_o = 0$

$\mu_G = 0.4$

and

(C) $P_i = 3500$

then

(C) $$\epsilon_{G_\theta} = \frac{1.4}{(5.243 \times 10^5)\ (37.16)} \left[(2.25\ P_i - 39.63\ P_o)\ (0.2) + (P_i - P_o)\ (39.63)\right]$$

$$= \frac{1.4}{194.8299 \times 10^5} \left[40.08\ P_i\right]$$

$$= 0.0101 \text{ in./in.}$$

(C) This strain is small when compared with the $\bar{\epsilon}_{TU}$ of 0.05 in./in. minimum.

b. Sustain and Restart Grain Analysis

The sustain and restart grains will be exposed to the boost grain temperature and environment and also be subjected to the high pressure during boost operation. In addition to not rupturing during boost operation, the inner bore of the sustain and restart grains must remain elastic to prevent buckling when the boost or sustain phase is completed. Since the sustain and restart grains have identical wrap angles, wire content, and are fabricated with the same aluminum wire, it is only necessary to check the grain with the larger diameters (restart).

For a thick wall cylinder subjected to internal and external pressure, the maximum hoop stress is given by

$$\sigma_{\theta_a} = \frac{a^2 P_i - b^2 P_o}{b^2 - a^2} + \frac{P_i - P_o}{b^2 - a^2} b^2$$

For the analysis

(C) $a = 1.914$

and

(C) $b = 6.639$ (restart grain dimensions)

Initially P_o is zero. Therefore, during boost phase operation the hoop stress, σ_{θ_a}, using a 1.25 load factor is given by the following:

(C) $$\sigma_{\theta_a} = 2800\ (1.25)\ (1.18) = 4130 \text{ psi}$$

The maximum allowable hoop stress, $\bar{\sigma}_\theta$, is given by Eq. 1.

$$\bar{\sigma}_\theta = f_v\, \bar{\sigma}_{TY} \sin^2 \alpha \qquad (1)$$

The allowable yield stress in the wire $\bar{\sigma}_{TY}$ is used for the sustain and restart grains because they must operate below yield stress during boost phase to make certain that the elastic limit of the wire is not exceeded.

(C) A helix angle of 60 degrees was selected for both sustain and restart grains to provide as much hoop strength as possible without significantly decreasing the longitudinal burning rate.

Two different aluminum wires were available at the preliminary design phase. Ultimate and yield stress of these wires are as follows:

(C)

	σ_{TU}, psi	σ_{TY}, psi
High Elongation Wire (5%)	50,000	47,000
Low Elongation Wire (1%)	70,000	67,000

Solving Eq. 1 for the wire volume fraction, f_v, gives the following:

$$f_v = \frac{\bar{\sigma}_\theta}{\bar{\sigma}_{TY} \sin^2 \alpha}$$

for

$$\bar{\sigma}_\theta = \sigma_{\theta_a}$$

and

$$\alpha = 60 \text{ degrees}$$

(C)
$$f_v = \frac{4130}{\bar{\sigma}_{TY}} \frac{5500}{(0.75)\,\bar{\sigma}_{TY}}$$

The wire volume fraction, f_v, using high or low elongation wire is 0.117 or 0.082, respectively, which corresponds to 18 and 13% weight fractions. Because of the significant difference in wire content the low elongation wire was selected for the sustain and restart grains because it yields more optimum combustion efficiency, less raw materials required, lowers winding time, and provides adequate structural strength.

Prior to finalizing the motor design, high strength aluminum wire was available. This wire is characterized by the following properties:

Ultimate Strength (σ_{TU}), psi	105,000
Yield Strength (σ_{TY}), psi	100,000
Elongation, %	
Ultimate (ε_{TU})	1.88
Yield (ε_{TY})	1.00

A stress-vs-strain curve for this wire is presented in Fig.334.

Using these wire data, and the data in Table CXII, the hoop stress is determined for the restart grain.

(C)

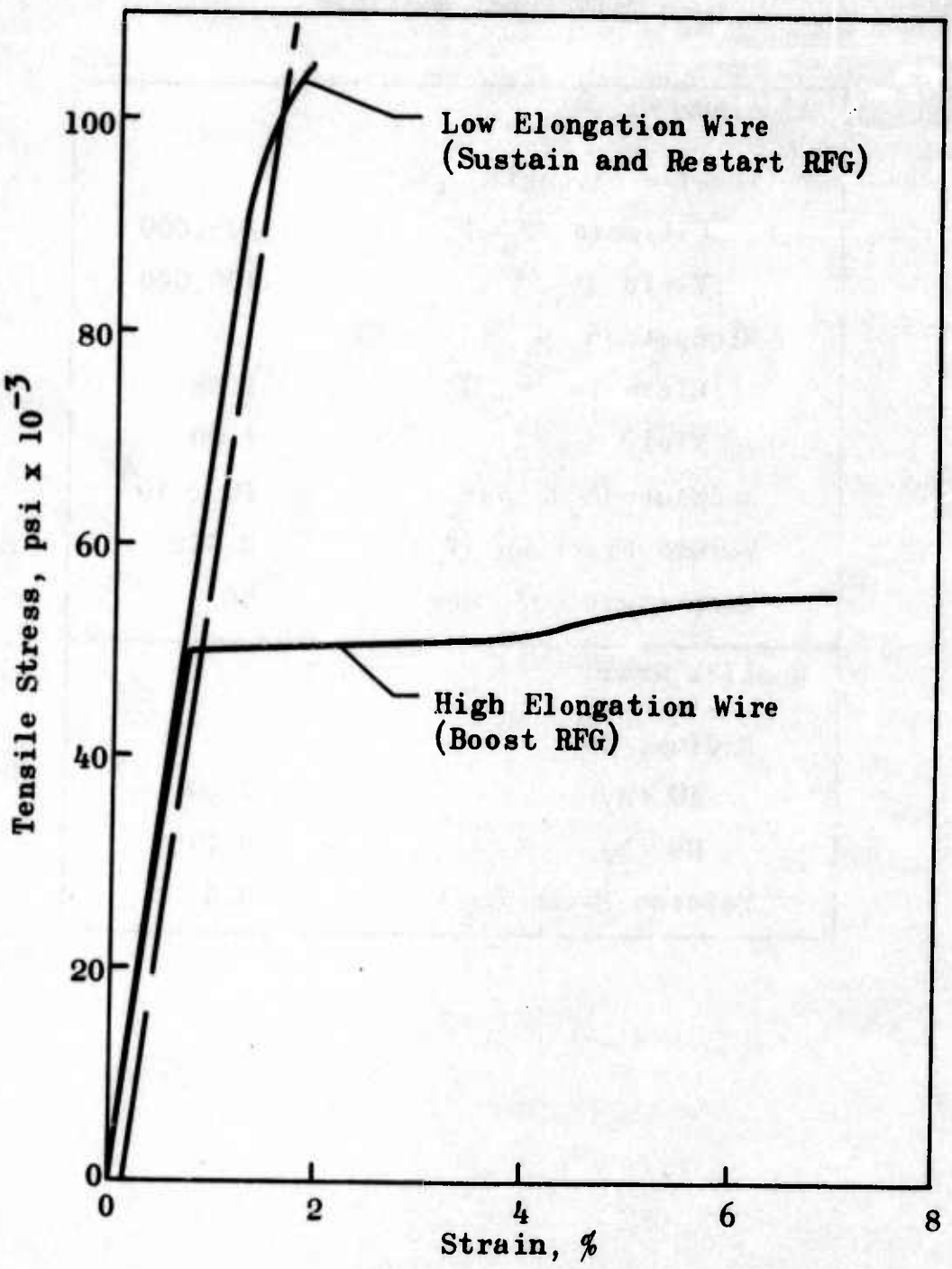


Figure 334. Stress vs Strain for Aluminum Wire in Motor D

(C)

TABLE CXII

PERTINENT DATA FOR RESTART GRAIN

STRUCTURAL ANALYSIS

Aluminum Wire	
Tensile Strength, psi	
Ultimate (σ_{TU})	105,000
Yield (σ_{TY})	100,000
Elongation, %	
Ultimate (ϵ_{TU})	1.88
Yield (ϵ_{TY})	1.00
Modulus (E_w), psi	10×10^6
Volume Fraction (f_v)	0.082
Wrap Angle (α), deg	60
Restart Grain	
Radius, in.	
ID (a)	1.99
OD (b)	6.715
Poisson Ratio (μ_G)	0.4

$$\sigma_{\theta_a} = \frac{a^2 P_i - b^2 P_o}{b^2 - a^2} + \frac{P_i - P_o}{b^2 - a^2} b^2$$

$$= \frac{P_i (a^2 + b^2) - P_o (2b^2)}{b^2 - a^2}$$

$$= \frac{P_i (49.051) - P_o (90.182)}{41.131}$$

for

(C) $P_i = 2800 (1.25) = 3500$ psi

assume

(C) $P_o = 0$ (conservative)

(C) $\sigma_{\theta_a} = \frac{(3500) (49.051)}{41.131}$

(C) $= 4170$ psi

The margin of safety, based on $\bar{\sigma}_{TY}$ of 100,000 psi is:

$$\bar{\sigma}_{\theta_{a_y}} = f_v \, \bar{\sigma}_{TY} \sin^2 \alpha$$

(C) $= 0.082 \; (100{,}000) \; (0.75)$

(C) $= 6150$ psi

(C) $$M.S. = \left[\frac{6150}{4170} - 1\right] 100$$

(C) $= + 47\%$

Checking the strain in the restart grain during boost operation gives:

$$\epsilon_{G_{\theta_a}} = \frac{1 + \mu_G}{E_{G_\theta} \left(b^2 - a^2\right)} \left[\left(a^2 P_i - b^2 P_o\right)\left(1 - 2\mu_G\right) + \left(P_i - P_o\right) b^2\right]$$

$$E_{G_\theta} = E_w \, f_v \sin^4 \alpha$$

(C) $= (10 \times 10^6) \; (0.082) \; (\sin^4 60^\circ)$

(C) $= 461{,}250$ psi

for

(C) $\mu_G = 0.4$

(C) $P_o = 0$

(C) $P_i = 2800\ (1.25)$

(C) $$\epsilon_{G_{\theta_a}} = \frac{1.4}{(4.61 \times 10^5)\ (41.131)} \left[3.96\ P_i\ (0.2) + P_i\ 45.091\right]$$

(C) $= 0.0119$ in./in.

(C) $$M.S._y = \left[\frac{0.015}{0.0119} - 1\right] 100$$

(C) $= + 26\%$

Nomenclature

a = inside radius--subscript denoting a point at the inside radius
b = outside radius--subscript denoting a point at the outside radius
c = subscript denoting case or compression
G = subscript denoting grain
i = subscript denoting inner surface
o = subscript denoting outer surface

t = thickness

P = pressure

E = Young's modulus

w = subscript denoting wire or weight

y = subscript denoting yield

TY = subscript denoting stress or strain at yield

TU = subscripts denoting ultimate tensile

U, Δ = deflection

r = radius--subscript denoting radial

f = fraction

v = subscript denoting volume

ΔT = change in temperature

OD = outside diameter

ID = inside diameter

M.S. = margin of safety

σ = stress

$\overline{\sigma}$ = allowable stress

ϵ = strain

$\overline{\epsilon}$ = allowable strain

α = wrap angle measured from longitudinal axis--thermal coefficient of expansion

θ = subscript denoting hoop direction

ρ = density

μ = Poisson's ratio

3. COMPONENTS

The following subsection discusses the remaining components in the motor. The components have been grouped as case, closure, and nozzle; insulation and grain support system; and igniter.

a. Case, Closure, and Nozzle

In discussing Motor D case, forward closure, and aft closure, it is well to remember that the case design originated with an existing heavyweight design. Because of this, the closures were made as functional parts of this existing case design. Since the case, nozzle, and closure are all exposed to the internal and/or external environments, a thermal analysis and a structural analysis of each were undertaken. A physical, structural, and thermal description of each hardware component is presented in the following discussion.

(1) Case

The case employed for Motor D is a fabricated weldment (see Fig. 335). The center section of this case is 4130 steel, rolled, formed, and welded, with an inside diameter of 14.616 inches and a wall thickness of 0.250 inches. Welded to each end of the center section are 4130 ring forgings machined for attachment of forward and aft closures. After welding and machining, the case assembly is heat treated to an ultimate tensile strength of 160,000--180,000 psi.

(C) Selection of 4130 steel as the case material for Motor D was made because of its high strength, its extensive use in rocket motor cases, and its superior welding and machining properties. Calculations indicate that a hoop tension stress of 127,000 psi (using a design safety factor[29] of 1.5) is the highest stress which occurs during motor operation. The 127,000 psi stress results in a positive margin of safety[30] of 0.25; however, (because of the welds associated with the case assembly), the ultimate tensile strength (160,000 psi) must be reduced by 10%. This, then, indicates a 0.14 positive margin of safety.

(C) The predicted case temperature is presented graphically in Fig. 336. The analysis indicates the case is adequate to withstand the environments to which it is subjected. The aft section of the motor case reaches a maximum of 521 F, which is well within the capability of the case/insulation bond system.

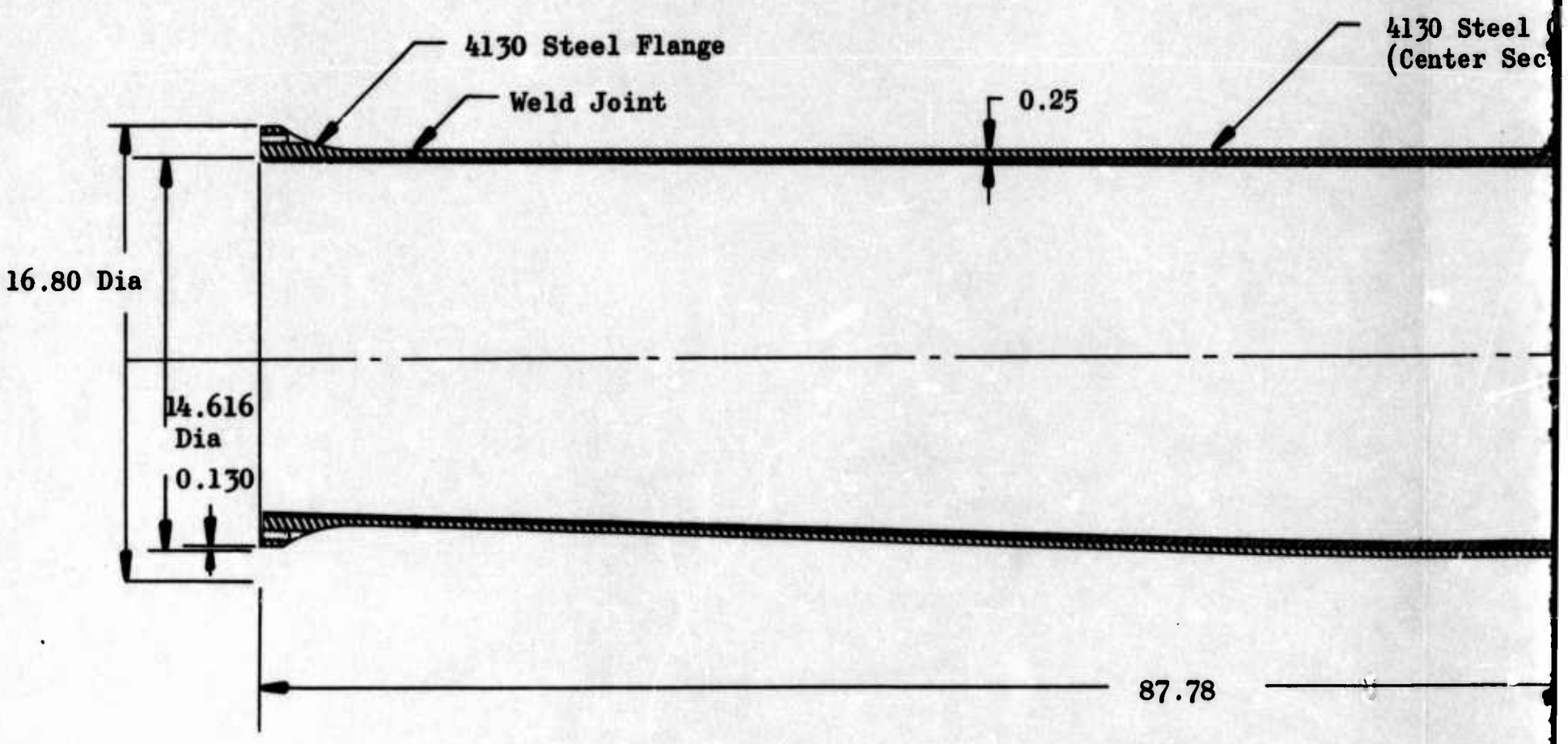
---

(29) Ultimate operating pressure X 1.5

(30) This term refers to the percentage by which the ultimate strength of a member exceeds the design load

CONFIDENTIAL

PREVIOUS PAGE WAS BLANK, THEREFORE WAS NOT FILMED



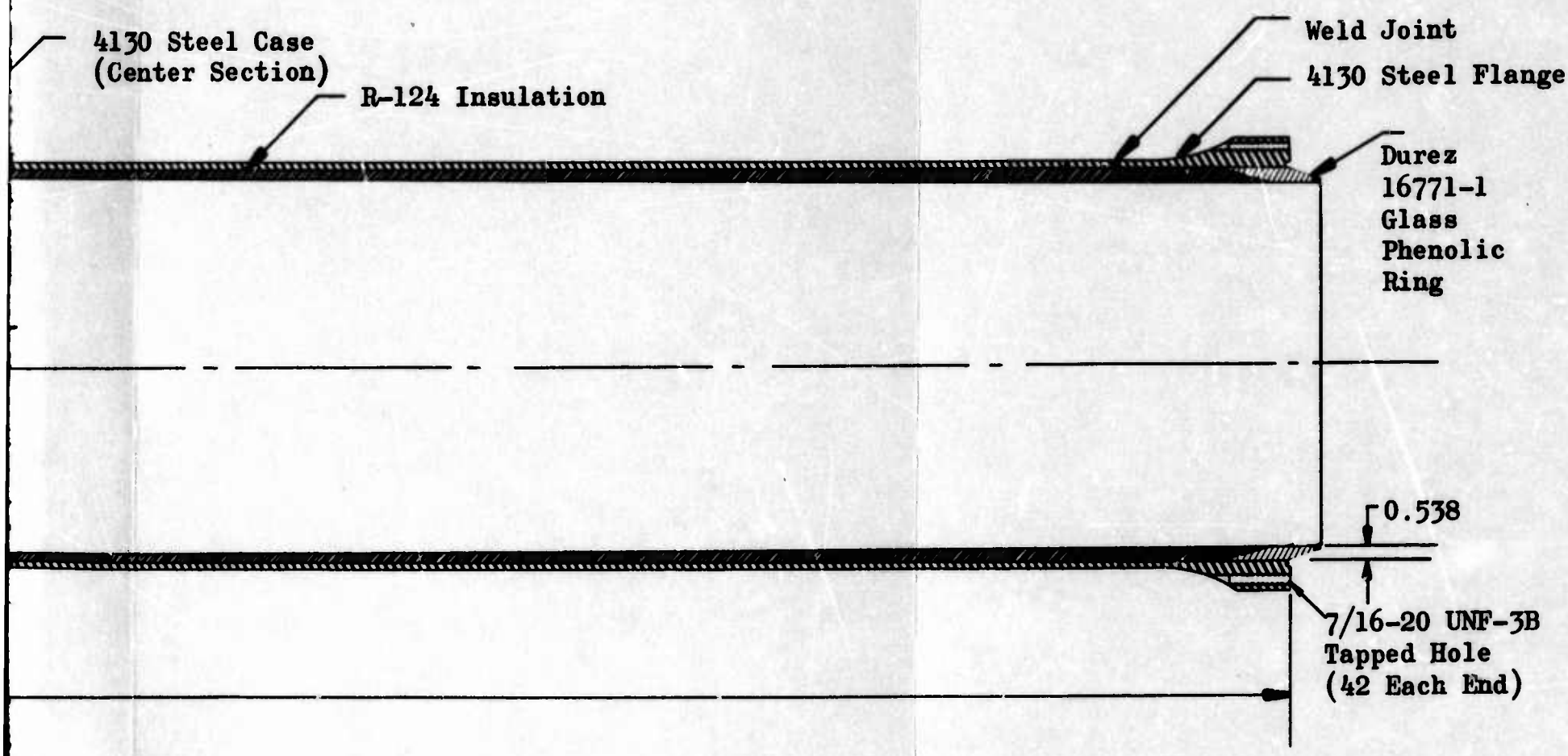


Figure 335. Motor D Insulated Case Assembly

CONFIDENTIAL

PREVIOUS PAGE WAS BLANK, THEREFORE WAS NOT FILMED

(C)

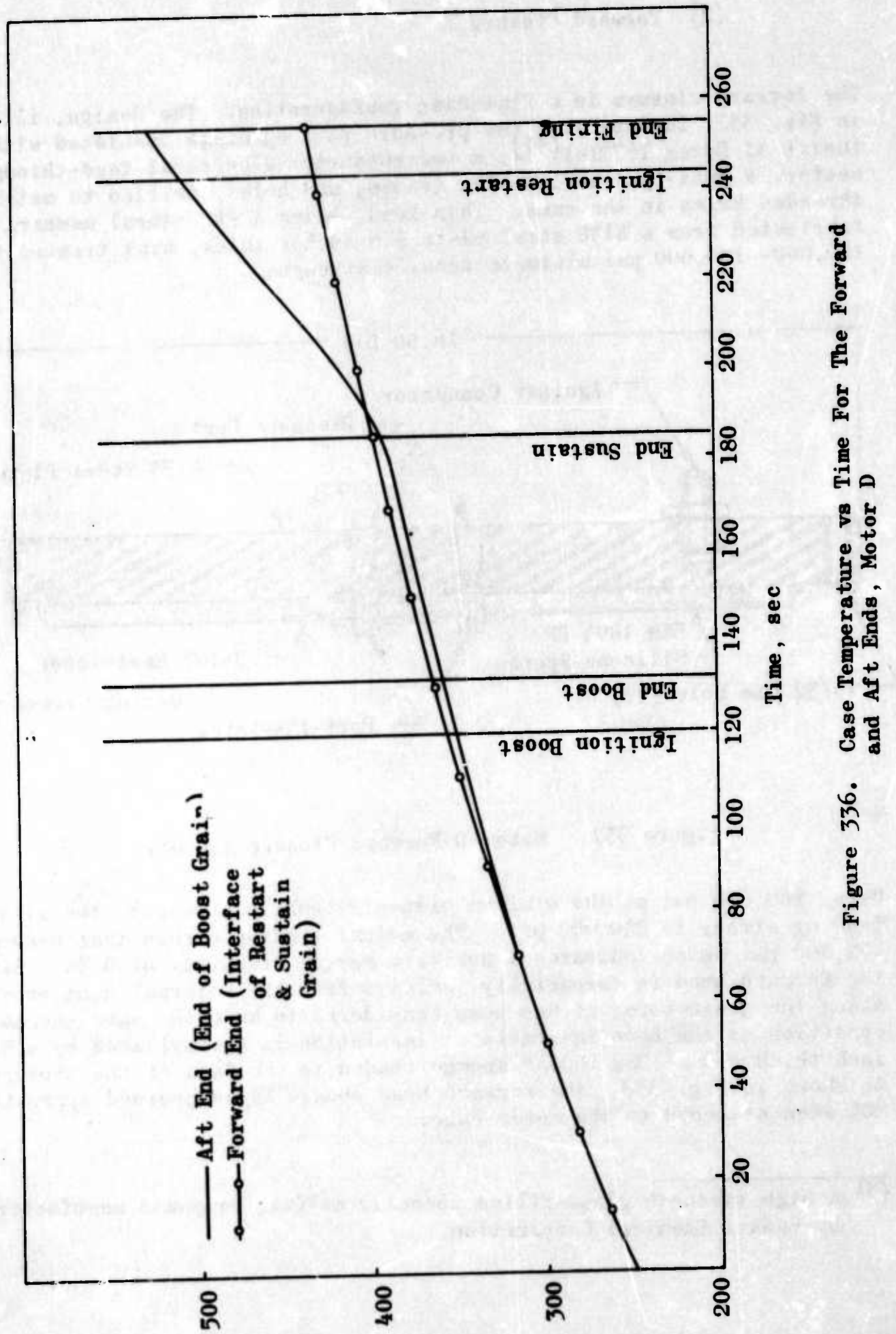


Figure 336. Case Temperature vs Time For The Forward and Aft Ends, Motor D

(2) Forward Closure

The forward closure is a flat disc configuration. The design, illustrated in Fig. 337, incorporates two pressure port openings insulated with an insert of Durez 16771-1[31], a two conductor electrical feed-through connector, a butt-type seal O-ring groove, and holes, drilled to match the threaded holes in the case. This head, being a structural member, is fabricated from a 4130 steel plate 1.5 inches thick, heat treated to 160,000--180,000 psi ultimate tensile strength.

(C)

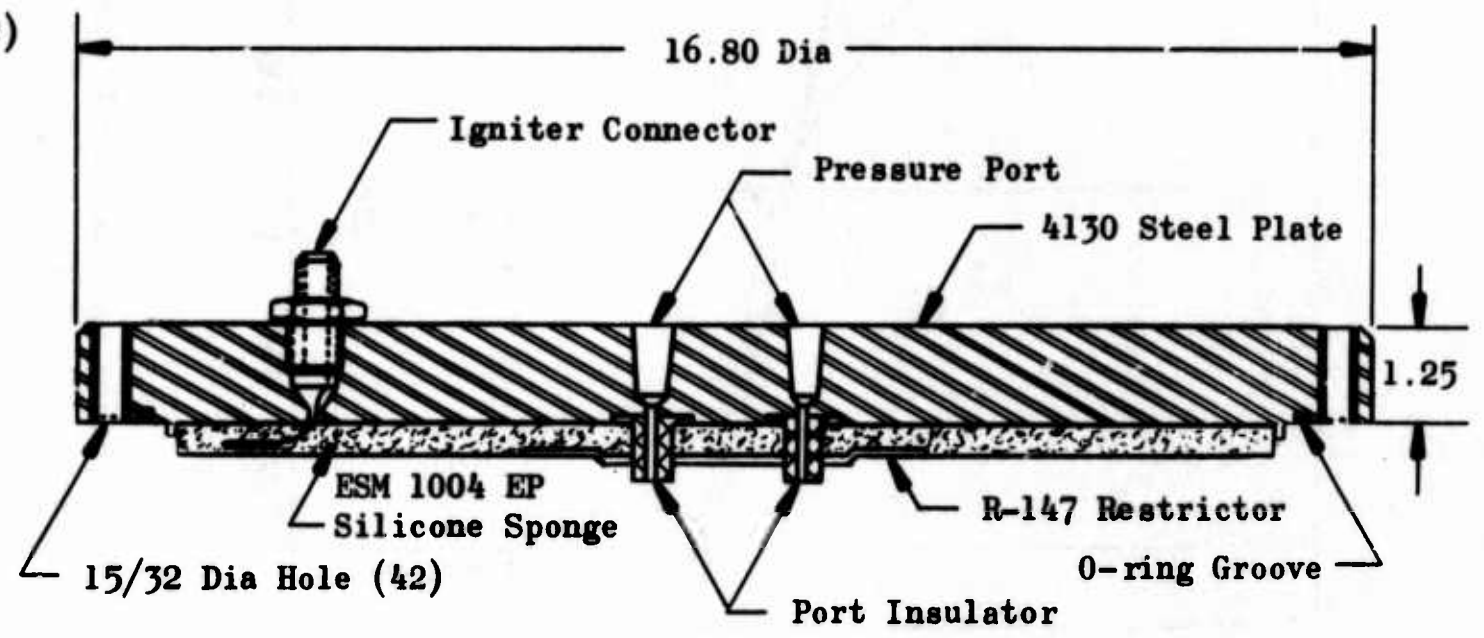


Figure 337. Motor D Forward Closure Assembly

Using 160,000 psi as the minimum ultimate tensile strength, the allowable bending stress is 240,000 psi. The actual bending stress that occurs is 172,000 psi which indicates a positive margin of safety of 0.34. Since the forward head is essentially isolated from the internal heat except along the grain bore, it has been considered to have the same thermal condition as the bore insulation. Insulation is accomplished by a 0.50-inch thickness of ESM 1004AP sponge bonded to the face of the closure. As shown in Fig. 338, the forward head sponge is compressed approximately 20% when attached to the motor case.

(31) A high strength glass-filled phenolic molding compound manufactured by Hooker Chemical Corporation.

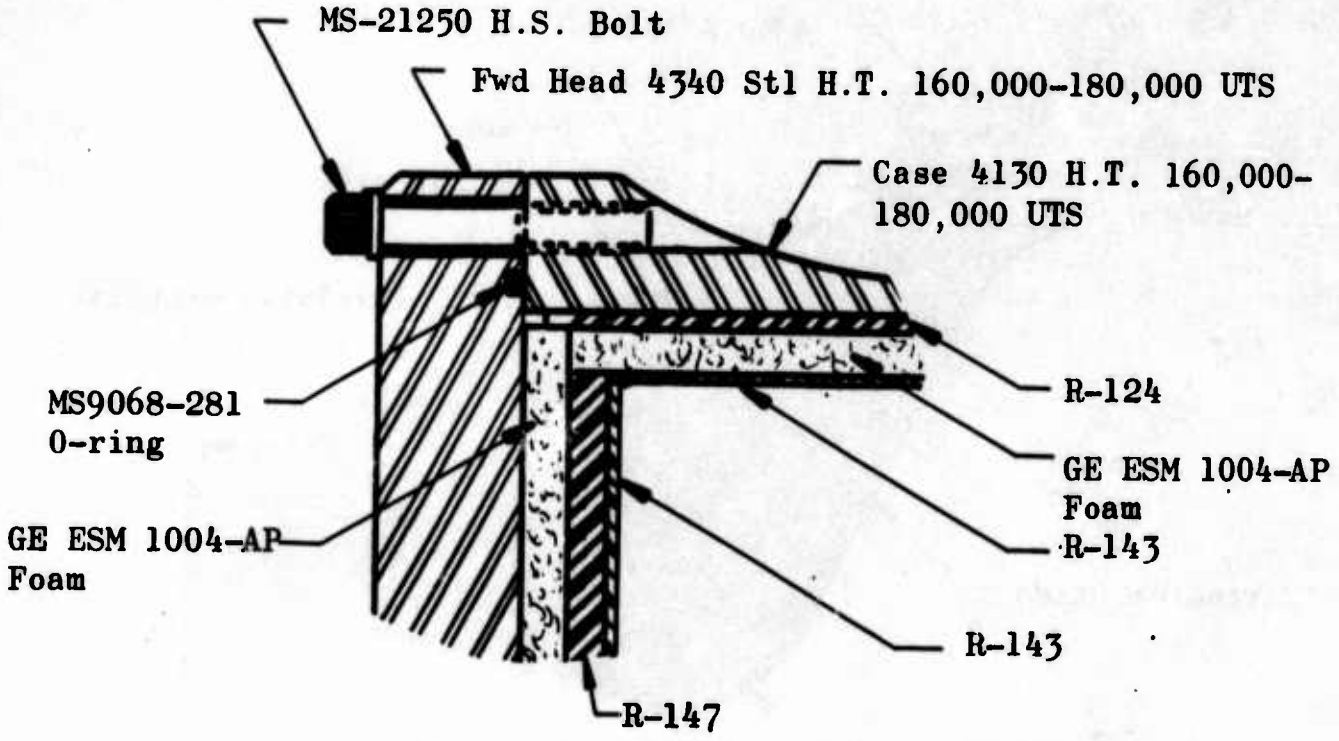


Figure 338. Forward Head/Motor Case Interface Joint

(3) Nozzle

(C) The major design criteria of the nozzle was the 60-second shutdown before restart. The heat soak during shutdown presented several problems. The most severe problem was providing an insulation system to preclude charring during the shutdown duration, thus allowing movement of the graphite insert upon ignition of the restart grain. The nozzle and aft closure design is illustrated in Fig. 339. This nozzle has a throat diameter of 1.352 inches and a 10.5:1 expansion ratio.

(C) The throat and exit cone are fabricated as a single component. The material used is Graph-I-Tite G, a monolithic graphite selected for its high erosion resistance and its good thermal shock properties. In addition to these properties, the tensile and compressive strengths are considerably higher than other graphites (2,900 psi tensile, 10,500 psi compressive). On the back side of the graphite throat and exit cone, a heat barrier of pyrolytic graphite is utilized to transfer heat away from the throat. The pyrolytic graphite barrier consists of three telescoping tubes that are installed on the graphite throat, maintaining a total thickness of 0.300 inch. After the throat and barrier are assembled, the leading edge on the upstream end is flame sprayed with 0.100 inch thickness of zirconium oxide, which is used as an intermediate insulator between the throat and throat entrance insulation.

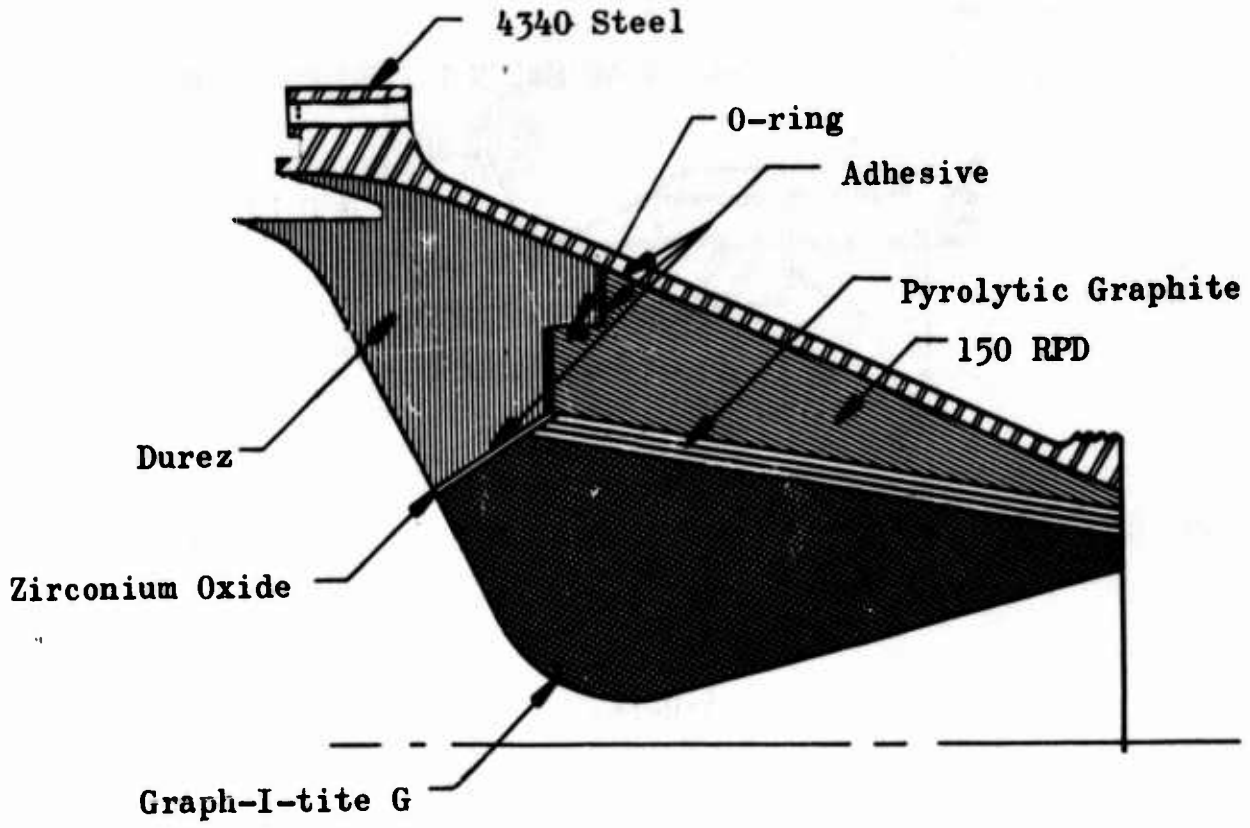


Figure 339. Motor D Nozzle Assembly

(C) The insulation surrounding the heat barrier is molded asbestos phenolic (Raybestos-Manhatten 150 RPD), and is a heat shield for the 4130 steel metal housing. The metal housing, being the main structural component in the design, has a 24 degree taper which provides sufficient bearing area and mechanical interference to maintain all components in their respective positions during motor operation. The insulation used on the upstream end of the nozzle is Durez 16771-1, a molded glass phenolic selected for its good erosion resistance and char properties. In addition to these properties, the thermal coeffieient of expansion (as reported by the supplier) is identical to that of the steel housing. The design tuilizes an O-ring seal between the Durez 16771-1 and the 150 RPD as a redundant sealing technique.

At the case-nozzle assembly point, Fig. 340, the design utilizes two O-ring seals. The primary flange-type seal is located at the case-nozzle interface. The secondary seal is embedded into the nozzle insulation, to provide additional protection for the primary seal.

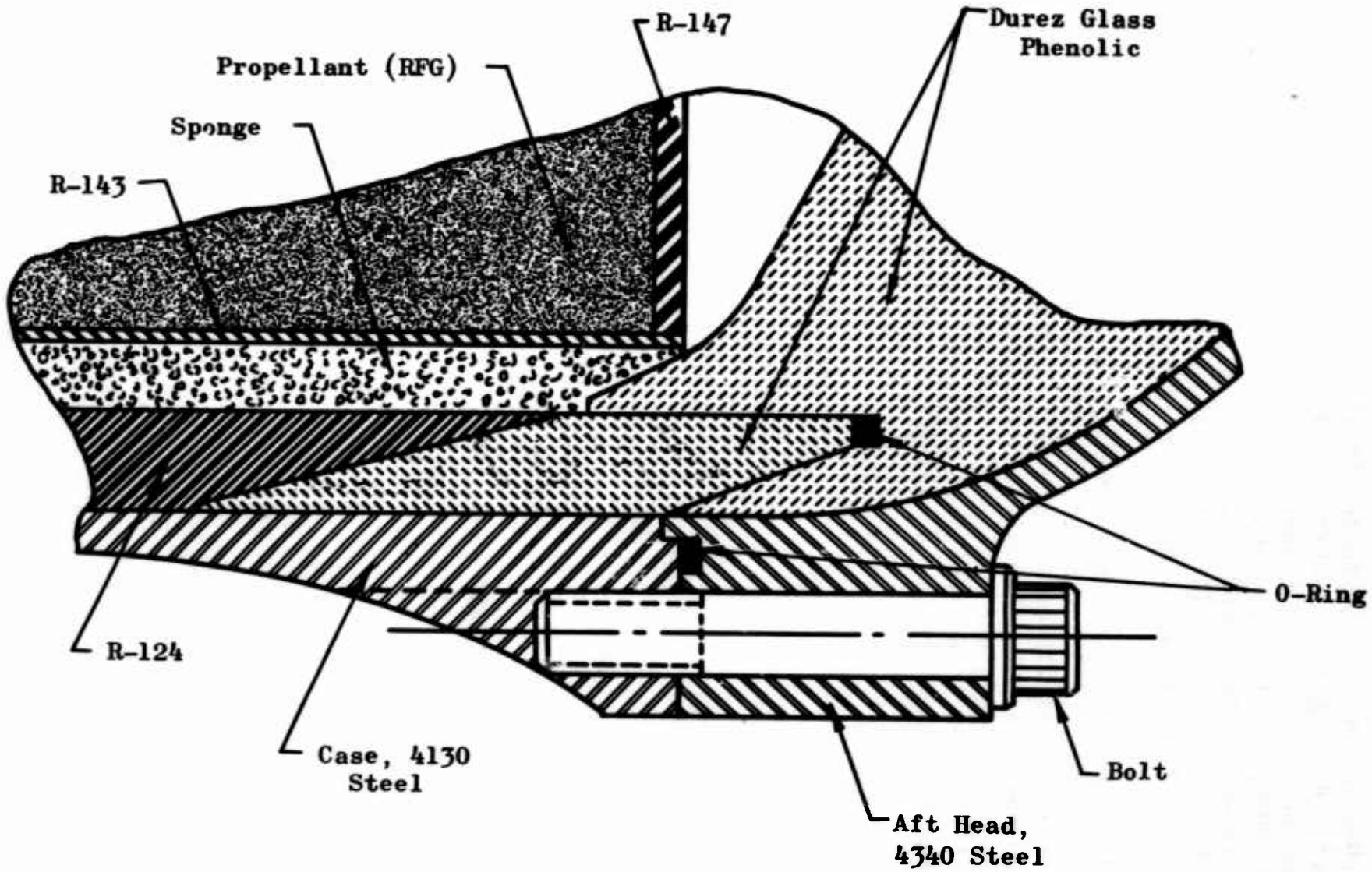


Figure 340. Nozzle/Case Interface Joint

(C) Stress calculations using a 1.5 safety factor were performed for the nozzle housing and the graphite throat insert. The highest stress in the nozzle housing is a combined bending stress of 210,000 psi and occurs near the case attachment flange. When this stress ratio is applied to the 240,000 psi allowable bending stress, a 0.57 positive margin of safety results. The graphite insert's highest stress condition occurs in the hoop direction. This is a hoop compressive stress of 8800 psi and provides a 0.135 positive margin of safety.

Results of the nozzle thermal analysis are presented graphically in Figs. 341 through 343. Figures 344 and 345 represent a preliminary comparison of monolithic and pyrolytic graphite throat inserts. Although the pyrolytic graphite inserts result in a lower throat surface temperature and erosion losses, the monolithic insert was chosen primarily for its lower interface temperatures and cost. The analysis indicated that the selected design was thermally adequate.

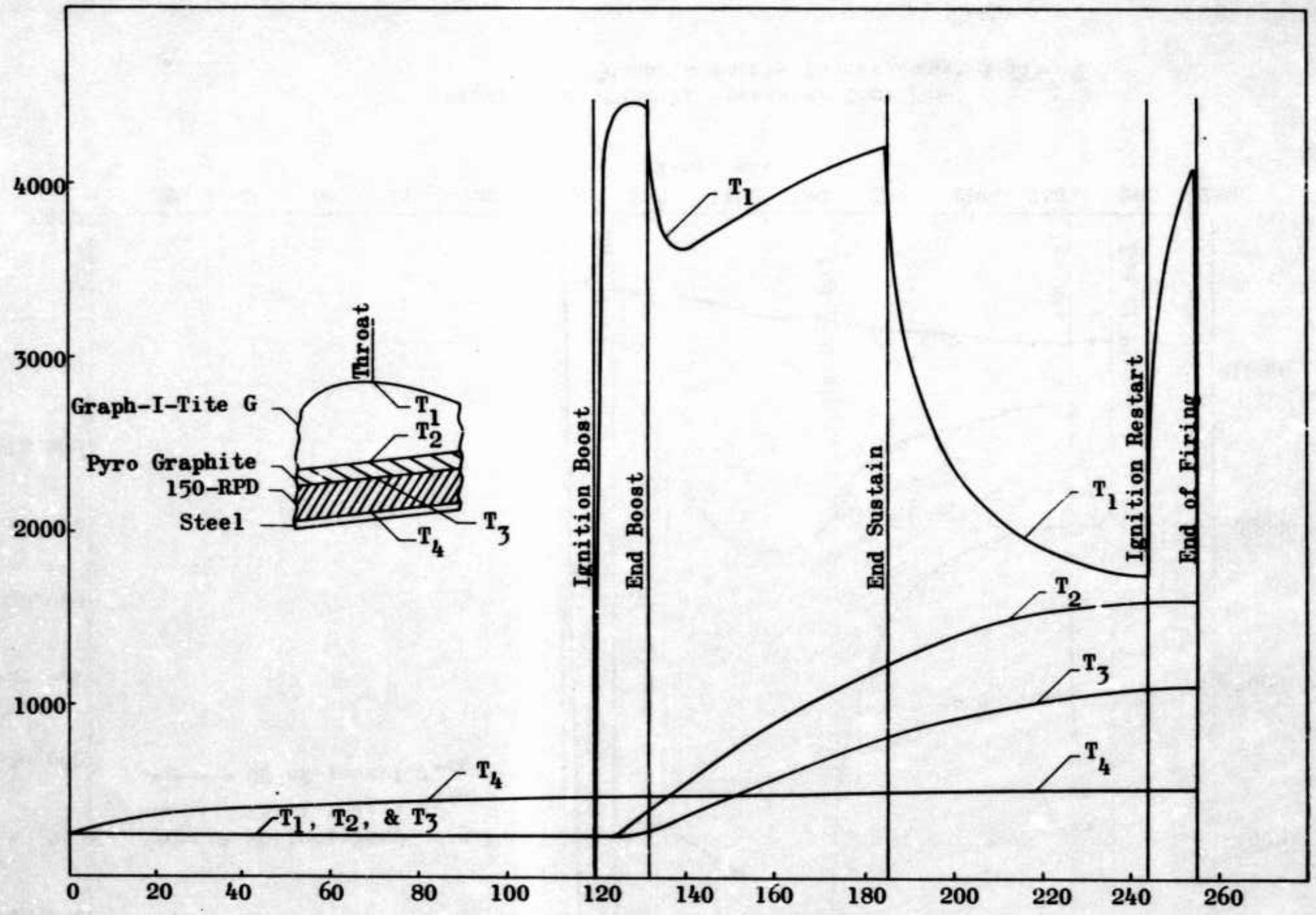


Figure 341. Temperature vs Time, Motor D Nozzle Throat Section

CONFIDENTIAL

CONFIDENTIAL

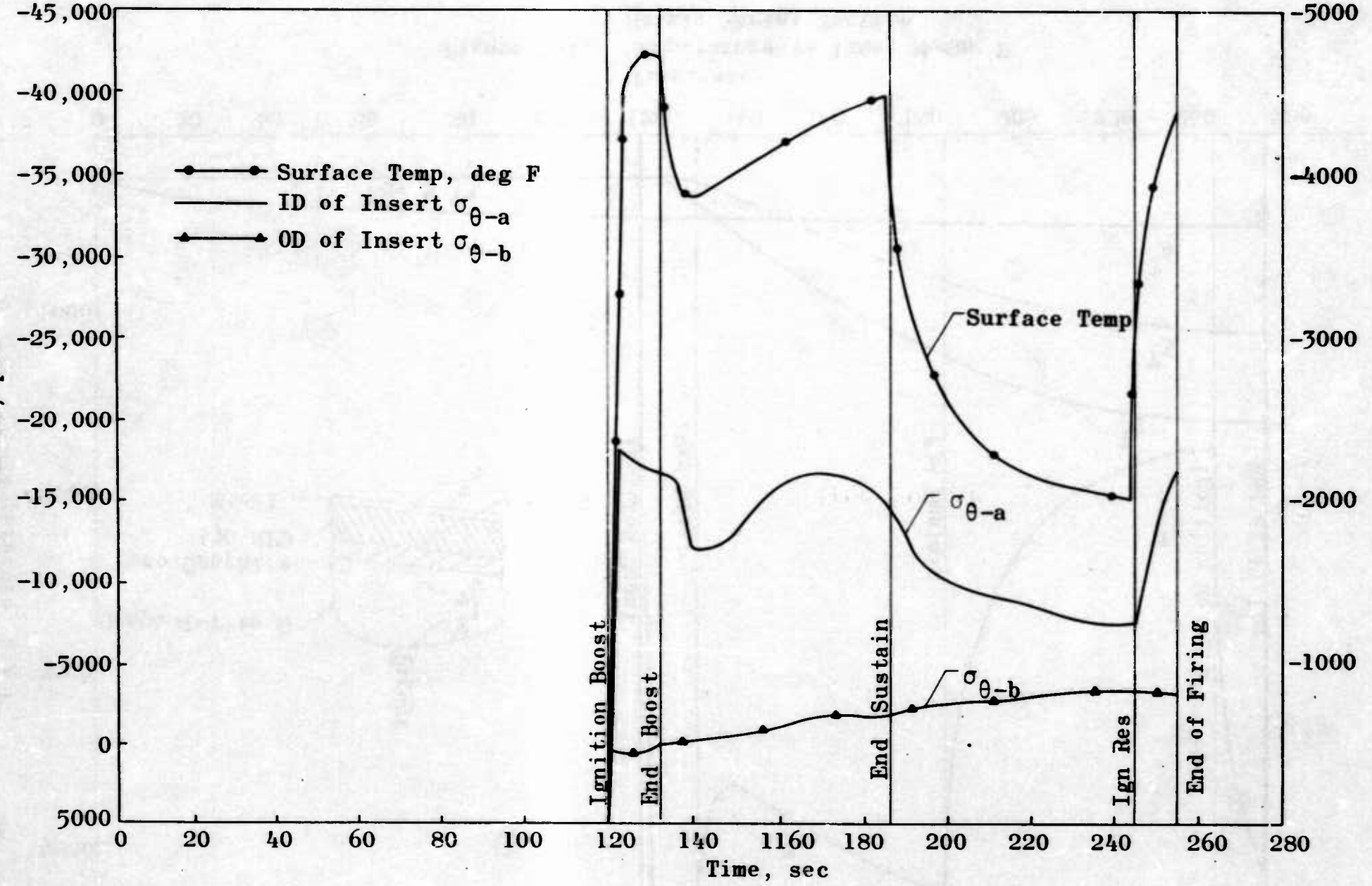


Figure 342. Thermal Stress vs Time For
Motor D Nozzle Insert, Graph-I-Tite G

CONFIDENTIAL

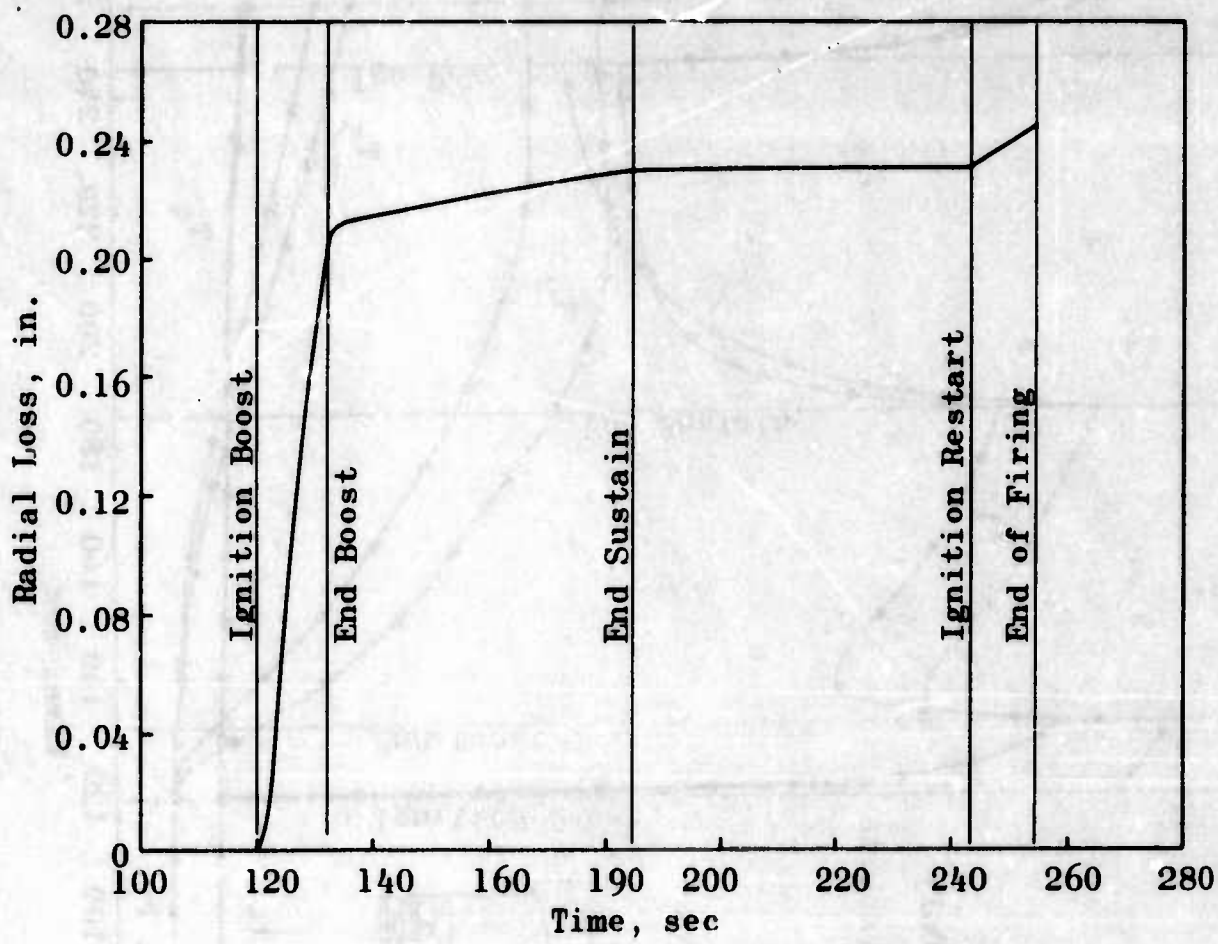


Figure 343. Erosion Loss vs Time for Motor D Nozzle Throat with Graph-I-Tite G Insert

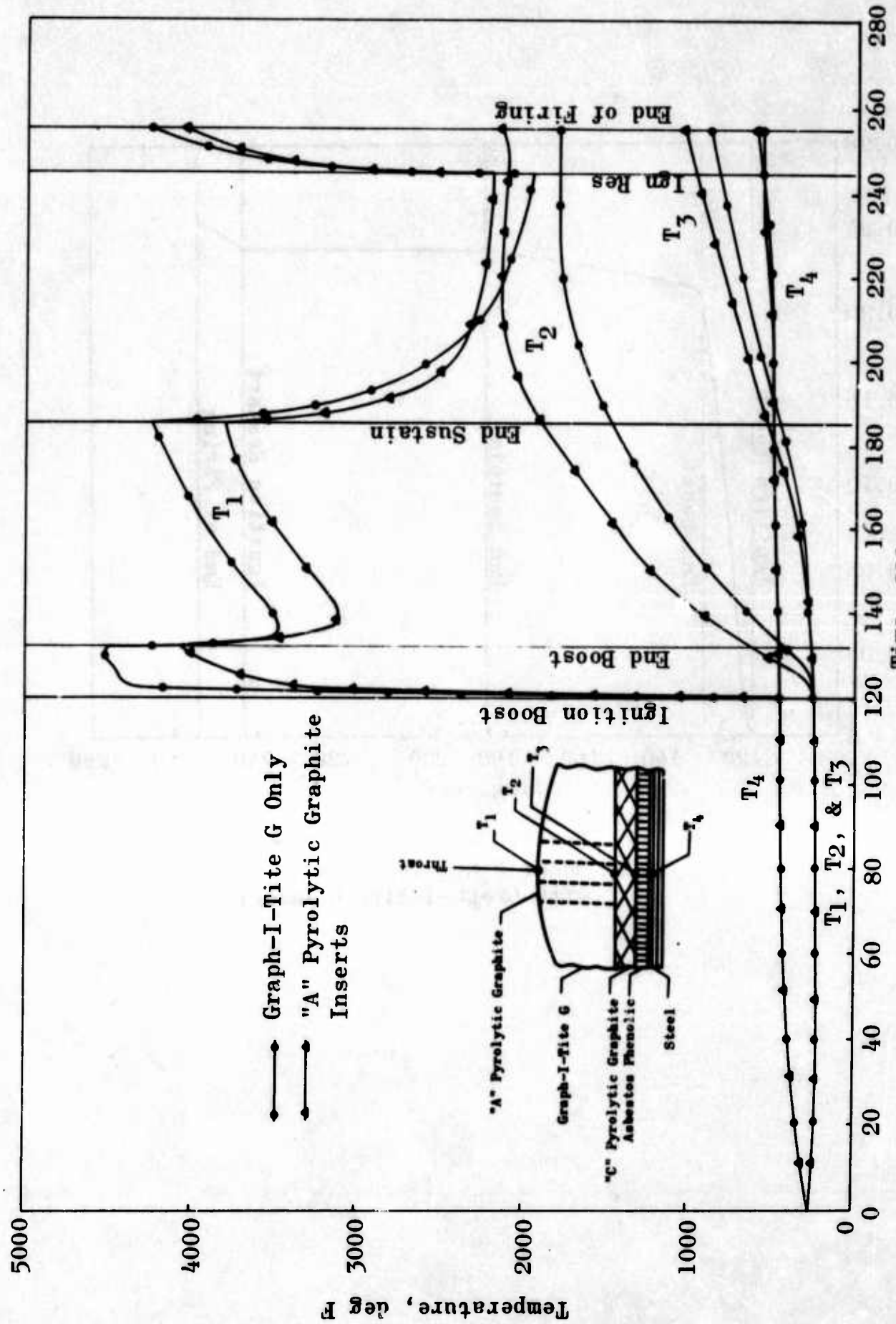


Figure 344. Temperature vs Time Comparison of Pyrolytic and Monolythic Throat Inserts

CONFIDENTIAL

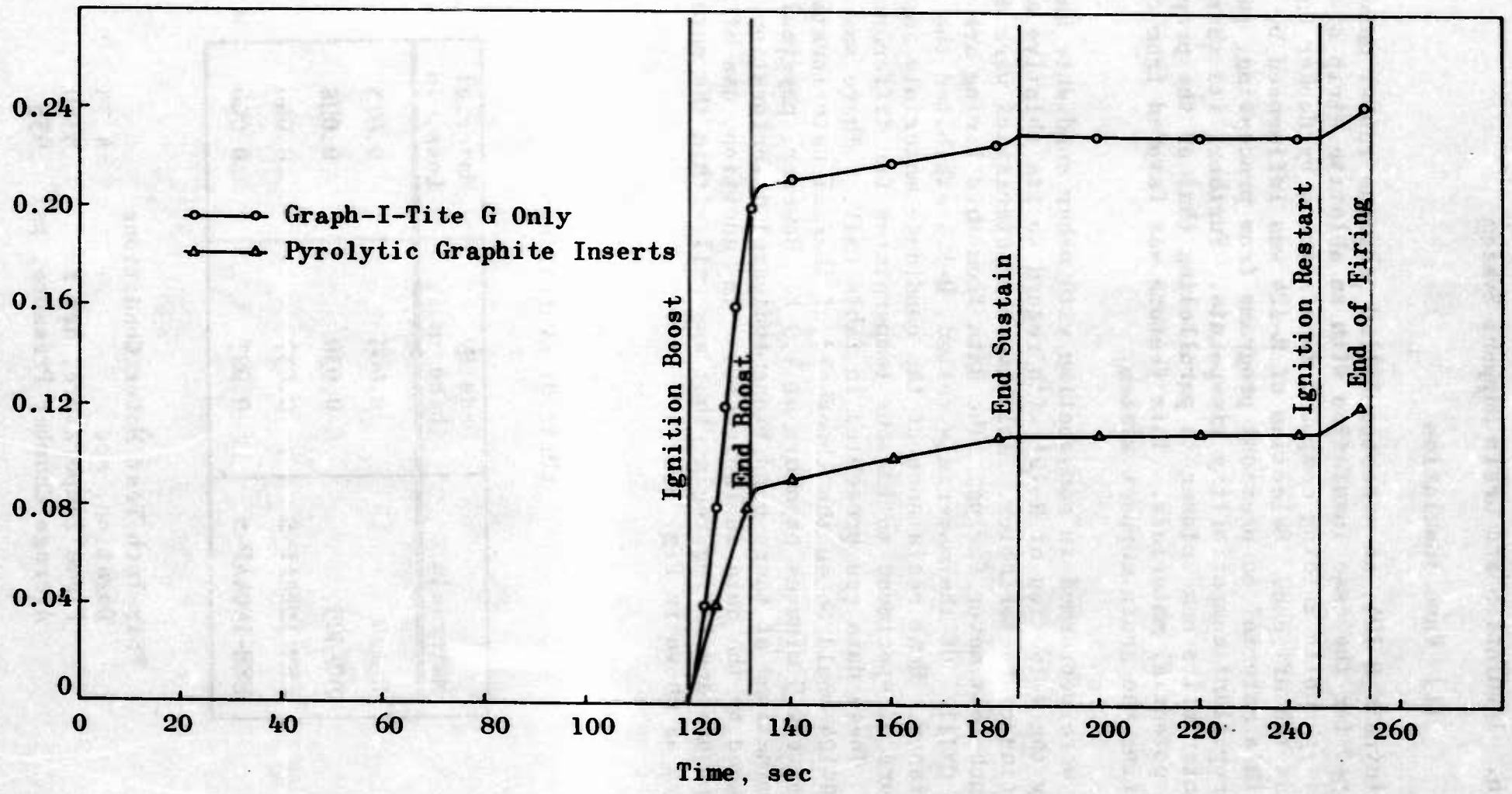


Figure 345. Erosion Loss vs Time Comparison of Pyrolytic and Monolythic Throat Inserts

CONFIDENTIAL

b. Insulation and Grain Support System

(1) Case Insulation

Rocketdyne's R-124, an asbestos-filled neoprene rubber material, was selected for the case insulation with an ablative strip of Durez 16771-1, a glass/phenolic molding compound manufactured by Hooker Chemical Corp., used at the aft end. Selection of R-124 was influenced by experience with this material on previous programs from processing, performance and propellant compatibility viewpoints. Further, its thermal expansion characteristics came closer to paralleling that of the propellant than other potential materials. This feature was favored from considerations affecting the grain support system.

Tests were performed in conjunction with other candidate materials to verify the selection of R-124 with regard to its ablative and heat resisting characteristics. Ablative characteristics were defined by a six-inch test motor firing. The data from this firing are presented in Table CXIII. Of the materials tested, R-124 exhibited the best erosion resistance. Heat resistance of the candidate materials was tested by exposure of specimens to various temperatures for different periods of time. These data are presented in Table CXIV. There was an indication that R-124 would be on the threshold of thermal deterioration after approximately 5 minutes exposure at 450 F. However, physical property determinations at these conditions indicated deterioration was minor as evidenced by the data in Table CXV. In addition, use of R-124 was in an exposure and firing regime that was well within the material's capability, as shown in Fig. 346.

TABLE CXIII

ABLATION EVALUATION*

Material	Density, lb/cu in.	Material Loss, in.
R-124	0.065	0.013
DC-325	0.030	0.028
ESM-1004AP-S	0.037	0.040
ESM-1004AP-S	0.023	0.090

*Six-Inch Test Motor Conditions

Duration, sec	4.75
Flame Temperature, deg F	5350
Average Chamber Pressure, psi	935

TABLE CXIV

HEAT EXPOSURE EVALUATION

Material	Specimen No.	Temp, deg F	Time, min	Remarks
R-124	1	240	120	OK
	2	450	1	OK
		450	5	Started to harden
		450	10	Hardened, cracks
	3	650	1	Blistered, hardened
	4	650	2	Blistered, hardened, cracks
	5	650	3	Blistered, hardened, cracks
DC-325	1	450	10	OK
		650	6	OK
		850	10	Blistered, cracks, crumbles
	2	750	1	No blisters, cracks
	3	750	2	No blisters, cracks
	4	750	5	Blisters, cracks, crazes
	5	650	60	No blisters, cracks, crumbles
	6	850	1	Blisters, cracks, crazes
	7	850	2	Blisters, cracks, crazes
	8	850	10	Blisters, cracks, crumbles
ESM-1004AP-S	1	650	5	OK
	2	650	10	OK

NOTE: 1. Cracks--Defined as Doubling Sample Back Over Itself and Squeezing Down on the Bend with Material Cracking in the Bend.
2. Crazing--Material Cracking without Bending Specimen.
3. Crumbles--Material Breaks when Bent.

TABLE CXV

EFFECTS OF HEAT EXPOSURE ON PHYSICAL PROPERTIES OF R-124[1]

Property	Control	Heated 5 min at 450 F, Exposed[2]	Control	Heated 5 min at 450 F, Sealed[3]
Ultimate elongation, e_m, %	60	45	70	60
Ultimate tensile, S_m, psi	1865	1730	1945	2145
Shore A hardness	87	94	90	93
Weight loss during heat exposure, %	--	0.70	--	0.34

(1) These Data are Relative Since Specimens Did Not Meet Normal R-124 Physical Properties:
110% Elongation
1100 psi Tensile Strength
95 Shore A Hardness
1.8 gram/cc Density

(2) Tensile Specimens Exposed to Air During Heat Treating

(3) Tensile Specimens Sealed in Aluminum Foil During Heat Treating

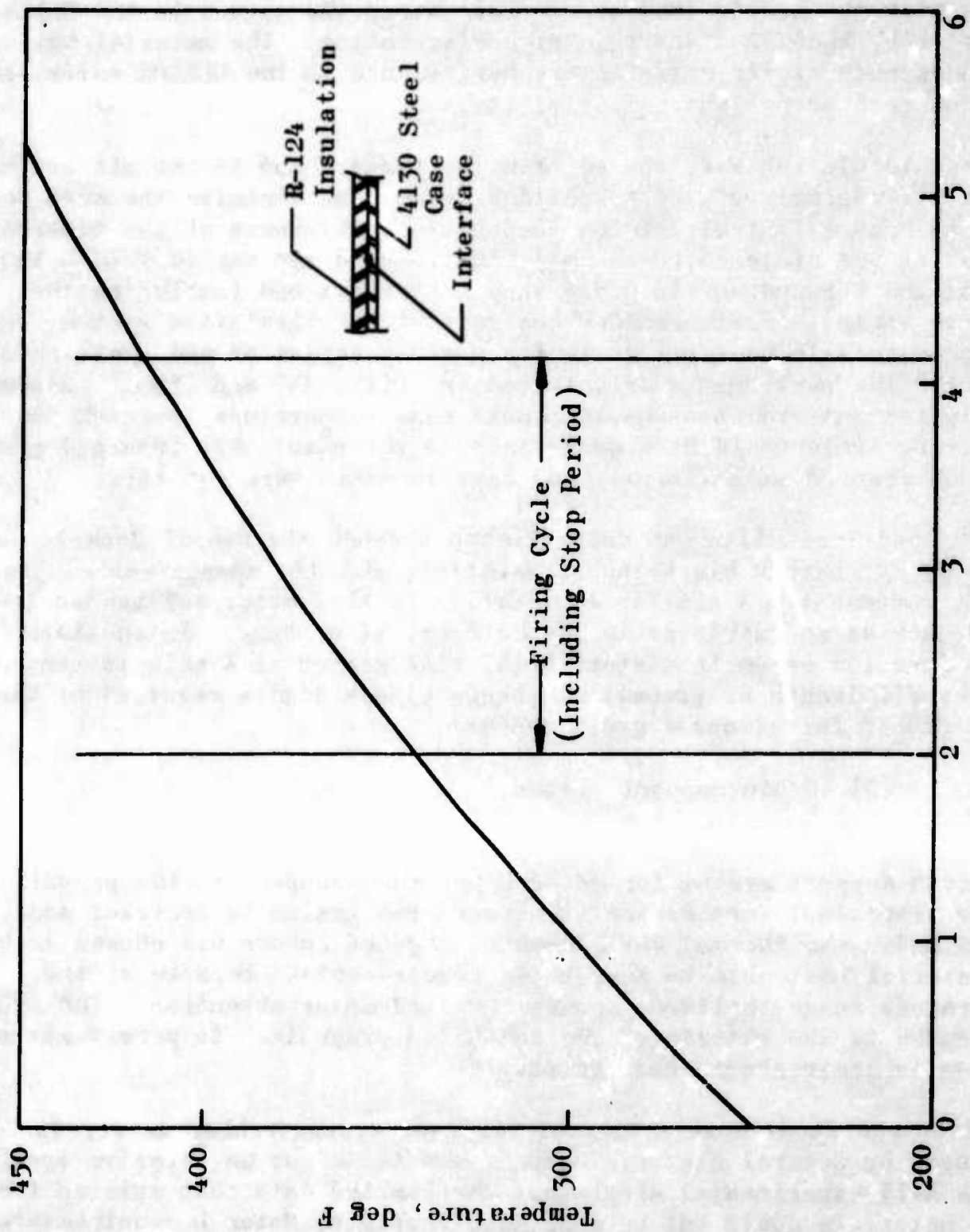


Figure 346. Insulation-to-Case Interface Temperature vs Time When Exposed to 650 F Environment

The Durez 16771-1 ablative strip used at the aft end of the motor assured protection of the case-to-nozzle closure joint against hot gases over the temperature extremes by virtue of similar thermal expansion characteristics with the nozzle insulator. This strip was joined to the R-124 insulator by bonding a scarf joint configuration. The material was chosen because of its satisfactory performance in the ULLAGE motor, low cost and good propellant compatibility.

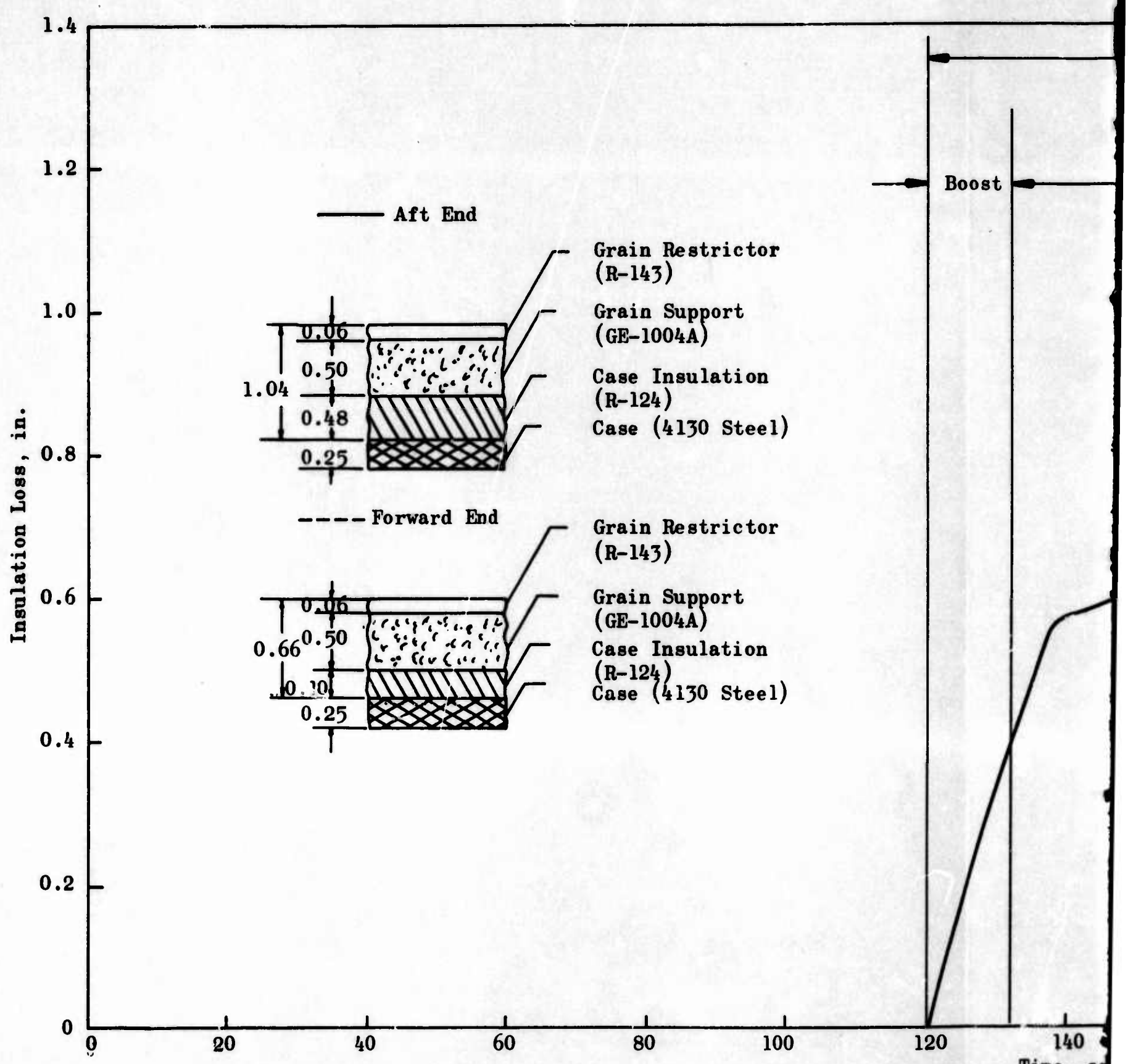
(C) The case insulation was tapered from the forward end to the aft end to facilitate assembly of the propellant grains and minimize the need for close tolerance control between components. Thickness of the tapered insulation was dictated by thermal requirements and varied from 0.130 inch at the forward end to 0.588 inch at the aft end (including the ablative strip). Heat transfer analysis of the insulation system, including materials used primarily for grain restriction and grain support, predicted the performance illustrated in Figs. 347 and 336. Although anticipated material loss would permit case temperature to reach 500 F, the firing cycle would have progressed to the point that internal pressure had reduced significantly and case stresses were not large.

Forward head insulation was accomplished through the use of Rocketdyne's R-147, an EPT carbon black rubber material, and the sponge rubber grain support component. A similar application in this motor influenced its further use as an insulator in the interest of economy. In addition to its function as an insulator, R-147 also served as a shim to control the over-all length of propellant charge within limits required by the sponge rubber for adequate grain support.

(2) Grain Support System

The grain support system for Motor D provided support to the propellant during vibration; furthermore it allowed the grains to contract and expand under the thermal environments. Sponge rubber was chosen to be the material best able to meet these requirements. Because of the temperature range, silicone sponge received major attention. The sponge was bonded to the outside of the inhibited propellant to permit maximum freedom in grain growth and contraction.

(C) Attention was focused on a line of silicone sponge rubber materials developed by General Electric Company and tested as an ablative insulator on the X-15 experimental airplane. The limited data that existed for these materials could not be applied directly to Motor D requirements. So, tests were performed to characterize certain material properties. Of paramount importance to the success of Motor D was the compression characteristics of the sponge, both from a loading and performance standpoint.


Insulation Loss, in.
1.4
1.2
1.0
0.8
0.6
0.4
0.2
0
0
20
40
60
80
100
120
140
Time, se
Boost
Aft End
Grain Restrictor
(R-143)
Grain Support
(GE-1004A)
Case Insulation
(R-124)
Case (4130 Steel)
0.06
0.50
1.04
0.48
0.25
Forward End
Grain Restrictor
(R-143)
Grain Support
(GE-1004A)
Case Insulation
(R-124)
Case (4130 Steel)
0.06
0.66
0.50
0.10
0.25

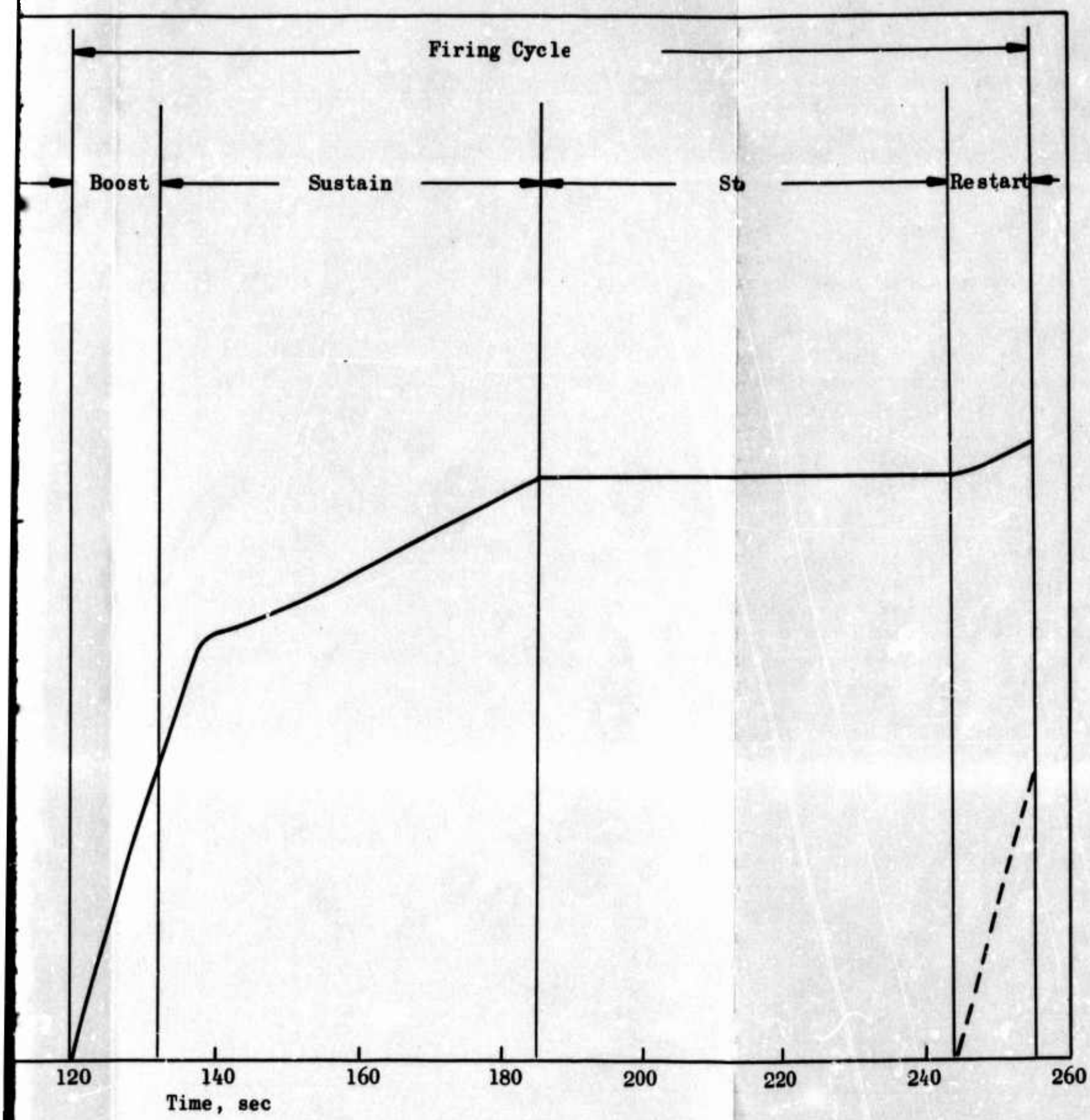


Figure 347. Insulation Material Performance Prediction

CONFIDENTIAL

(C) Support of the propellant grains over the -75 to 200 F temperature range required the support system to be loaded in compression. The loading technique envisioned compressing the sponge by application of gas pressure in the motor chamber. Several tests were conducted to determine loads required to compress various grades of the sponge. The object of these tests was to determine (1) deflection vs pressure, and (2) deflection vs time at constant pressure (to ascertain if pressure equalization occurred). The data are presented in Figs. 348 and 349. Materials used in the tests bracketed the range of compressive modulus that could be selected. Therefore, test results are thought to represent limits of candidate materials. Since 30% compression was initially considered to be optimum for the application, it appeared from Fig. 348 that 32 to 62 psi pressure would be required. Pressure equalization did not occur as evidenced by the curves of Fig. 349 in which the changes in deflection were roughly proportional to the change in pressure for a period up to 30 minutes. The compression load tests were subsequently verified by additional tests in which load was applied by mechanical means. These data presented in Table CXVI not only confirmed previous data but gave additional insight into pressure requirements for deflection greater than 30%. In all, the sponge rubber materials appeared able to meet loading technique requirements.

TABLE CXVI

COMPRESSION DATA FOR GENERAL ELECTRIC CO. SPONGE RUBBER

Percent Compression	Compression Load, psi (1)				
	Specimen (2)(3)				
	(1)		(2)		
	1st Run	2nd Run	1st Run	2nd Run	(3)
10	9.44	11.1	9.44	9.4	10.9
15	16.8	--	16.1	--	--
20	22.8	21.7	21.7	20.5	23.7
25	28.3	--	27.2	--	--
30	34.4	36.7	33.3	33.9	35.8
35	--	43.9	--	40.6	--
40	--	52.2	--	47.8	50.0
45	--	64.4	--	58.3	--
50	--	79.4	--	72.2	73.7
55	--	--	--	94.4	96.2
60	--	--	--	136.1	137.0
65	--	--	--	--	237.0
70	--	--	--	--	442.0
75	--	--	--	--	628.0

(1) Rate of Loading - 0.05 in./min

(2) ESM 1004A-P - 33.8 lb/cu ft

(3) Specimen Size - 3 inches x 3 inches x 0.5-inch thick

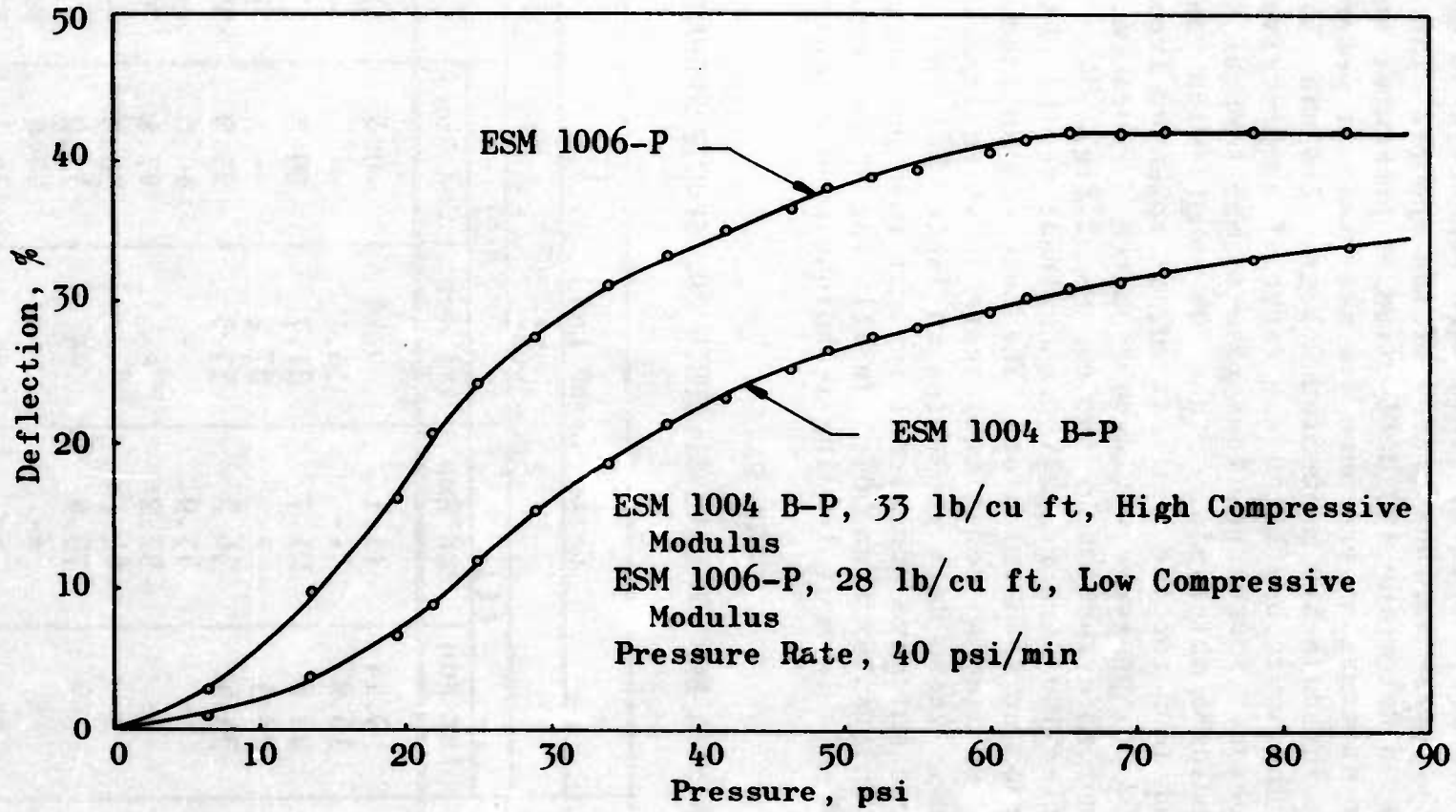


Figure 348. Deflection vs Pressure for General Electric Co. Sponge Rubber

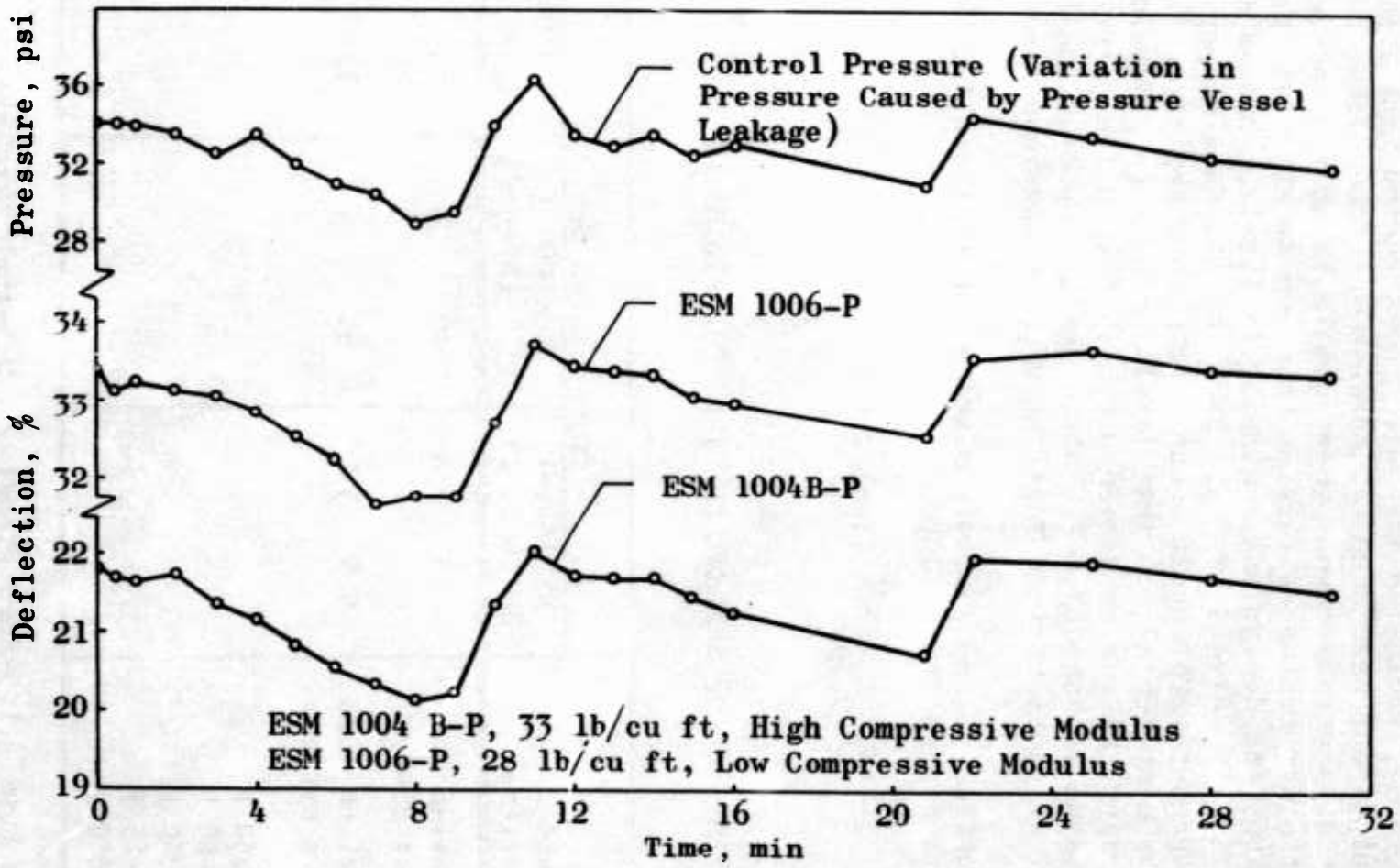


Figure 349. Deflection vs Time at Controlled Pressure for General Electric Co. Sponge Rubber

(C) Whether the sponge rubber would indeed provide support throughout the temperature range prompted an investigation into permanent compression set characteristics. Tests were performed on grades of sponge under thermal conditions approaching those for Motor D. The results, shown in Table CXVII, indicated that all grades tested took a permanent set. The amount of set was found to increase with the higher density materials. The data were somewhat questionable in that a constant deflection over a temperature excursion from -65 to 250 F was not realistic. In addition, the design was beginning to finalize around an initial deflection of 13 ± 5% instead of 30%. However, the data supported the theory that compression set could occur over a long period of time and that it could be detrimental, in that little or no support would be offered to a grain that was conditioned to -75 F when the motor case was exposed to aerodynamic heating. The above design condition maximizes the dimensional distance between restricted grain and insulated case.

Under these considerations, the very maximum set that could be allowed and still maintain support would be

$$\% \text{ set} = \frac{0.500 - 0.493}{0.500} (100) = 1.4\%$$

TABLE CXVII

COMPRESSION SET OF GENERAL ELECTRIC CO. SPONGE RUBBER(1)

Test Conditions	Compression Set, %(2)					
	ESM1006-P 28 lb/cu ft		ESM1001-P 33.5 lb/cu ft		ESM1004B-P 33 lb/cu ft	
30% deflection for 24 hours at 250 F	9.0	2.6	30	20	36	31
30% deflection with temperature cycle as follows: 4 hr @ 250 F 4 hr @ -65 F 4 hr @ 250 F 4 hr @ -65 F 24 hr @ 250 F	4.5	3.9	63	49	53	50

(1) Specimen Size - 1.5-inch Diameter x 0.5-inch thickness

(2) Compression Set - Percent of Total Deflection Remaining in Material 30 Minutes After Releasing Compressive Load

The above information points out the need for additional materials evaluation and basic design philosophy in the grain support system. These facts were recognized and were being pursued at the time of contract termination.

Elsewhere in the motor, sponge rubber was used to provide longitudinal support to the grain and, in addition, provide thermal protection at the sustain grain-to-restart grain interface. At this interface the sponge component was diced to assure breakup into small particle size when the restart grain ignited.

(3) Grain Insulation

Grain insulation throughout Motor D was accomplished by the use of Rocketdyne's R-147, an EPT/carbon black rubber material. Successful use of R-147 in the PHOENIX motor was a significant factor in its selection for this application.

The boost grain was insulated at each end by discs that tapered from the inner bore to the insulated case wall. The taper assured thermal protection to the grain faces over the boost duration and yet permitted the insulator to be consumed as burning progressed. Proximity of the sustain grain and the flow of gases from the burning of this grain required a thicker insulator to be used on the forward end of the boost grain.

Both the sustain and restart grains were designed to burn on their aft ends; consequently, the inner bore of each grain was thermally protected by an 0.30-inch thick tubular section of R-147. Thickness of the insulator was governed by heat transfer considerations at the extreme forward end of the restart grain since this location would be exposed for the longest period of time. Temperature at the insulation-to-propellant interface for a motor conditioned to 250 F is presented graphically in Fig. 350 Temperature rise was predicted to be only 65 F until the last 5 seconds of burning time. Protection afforded the propellant was considered adequate under these conditions.

At the sustain grain-to-restart grain interface an additional sleeve of R-147 was used across the insulation joint to prevent erosive action by the hot gases. The sleeve was bonded only to the sustain grain insulator to allow pressure equalization in the interface region and across the sleeve.

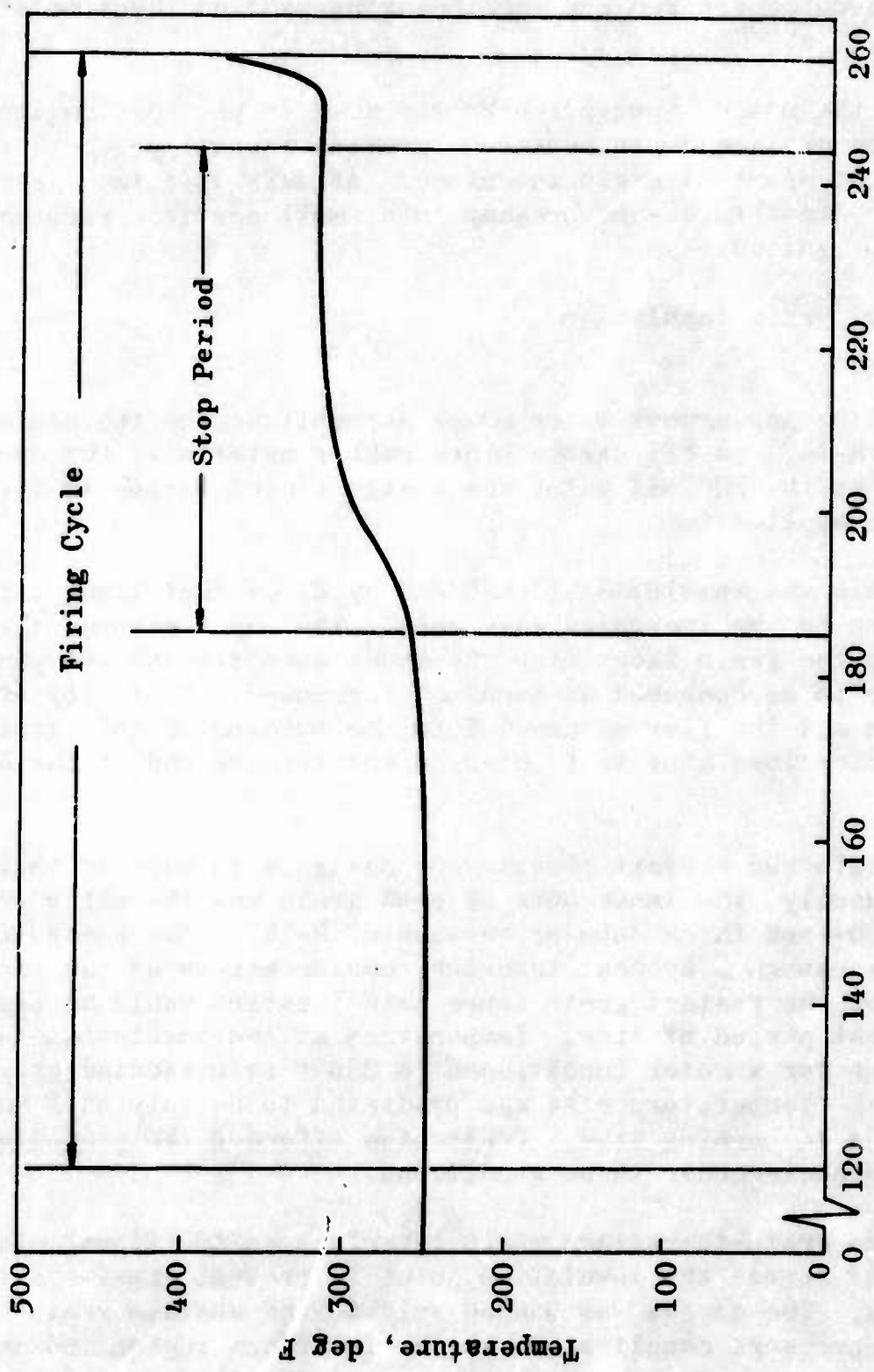


Figure 350. Insulation/Propellant Interface Temperature vs Time at the Restart Grain (Forward End)

c. Igniter

This part covers design, development, and fabrication of the Thermesh igniter to be used in Motor D. The first discussion covers the design and development while the second outlines the proposed igniter fabrication.

(1) Design and Development

Ignition of the boost-sustain and restart grains was to be accomplished with a Thermesh igniter. This ignition system consists of aluminum wire screen coated with a pyrotechnic formulation in a plasticized binder. Initiation is obtained with DuPont 257D primers and 424 Pyrocore. Pyrocore is a small diameter, continuous metal tubing containing (1) a core of PETN, for extremely fast propagation and (2) pyrotechnic material which supplies additional heat energy for ignition. Energy output rate from the igniter is controlled by variations of the screen loading density, screen mesh size, and extent of Pyrocore initiation.

A mixture of $KClO_4$, Boron, and/or ZrNi alloy with either a polyisobutylene or vinyl chloride-acetate copolymer binder performs extremely well in the Thermesh system, producing excellent ignition propagation properties. Heat of explosion determinations have shown available energy to be in the range of 2600 Btu/lb, which is comparable to pyrotechnic formulations currently in use at SRD.

The basic Thermesh concept of ignition system design had been adequately evaluated under IR&D programs to assure its feasibility as a method of solid propellant ignition. This concept has been used very successfully to ignite an 8-inch diameter end burning reinforced grain. The time required from application of current, or zero time, to attainment of maximum pressure was 0.015 second. No nozzle pressure seal was used.

Firings of prototype igniters (consisting of LLP-3 coated aluminum wire mesh held in a rectangular frame as shown in Fig. 351 have been conducted in the open to permit Fastax movie camera coverage. Film review has provided some necessary information as to mode of initiation, flame propagation patterns, and brisance. These films show that the Pyrocore does not rupture the screen mesh, nor even penetrate the coating. Thus, it is desirable to ignite at an edge or on the side adjacent to propellant if fast ignition is required. Otherwise, the coated screen can act as an insulating barrier between the propellant surface and the ignition flame, since it requires a finite time for the pyrotechnic coating to burn through and penetrate itself.

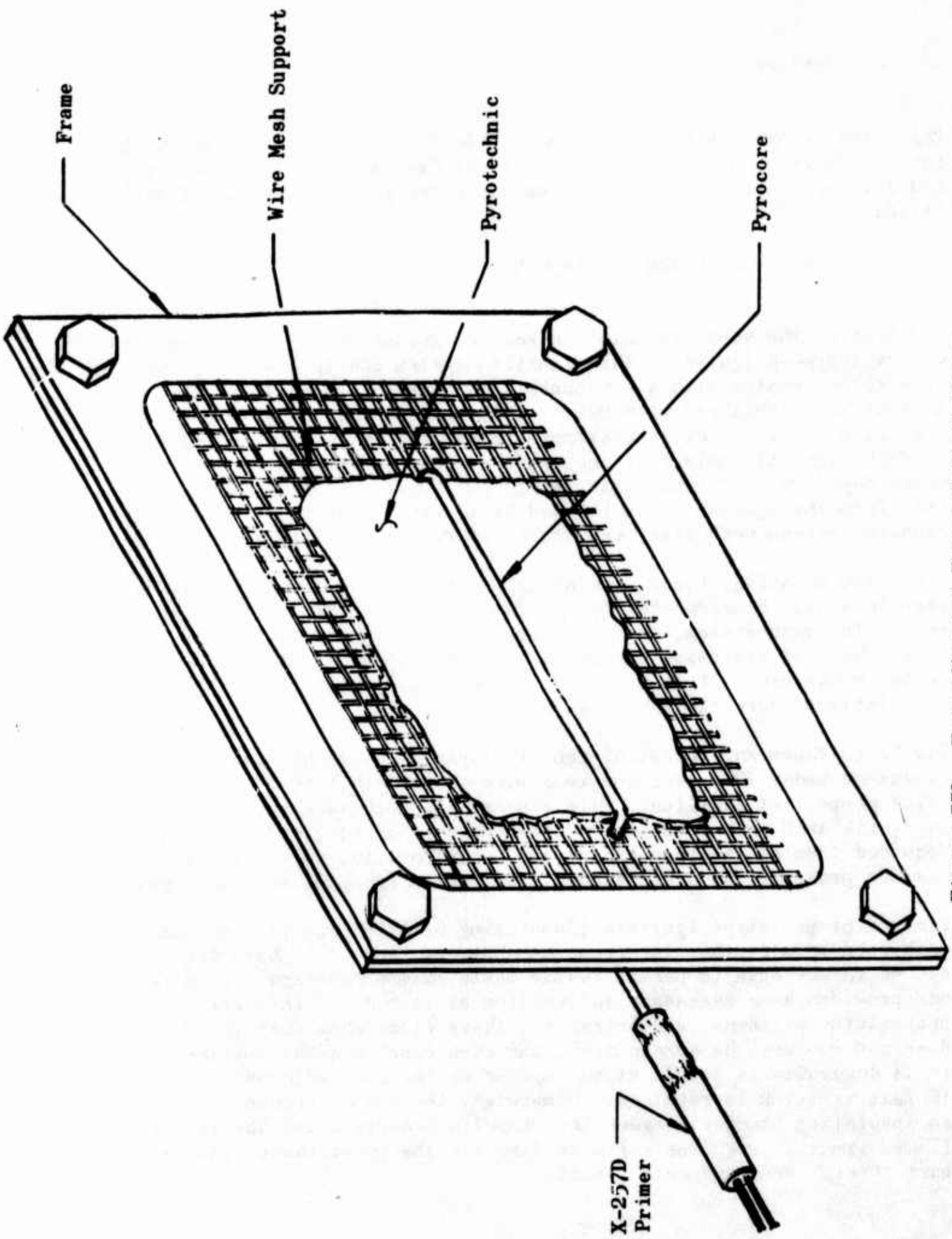


Figure 351. Frame-Mounted Thermesh Test Sample

Optimization of the formulation and determination of the relative effects of loading density (grams pyrotechnic/square inch of screen), loading area, and Pyrocore length were evaluated in 6-inch test motor firings according to the following schedule:

Quantity	Reason	Data Required
3	Optimization of formulation	Pressure-vs-time
9	Evaluation of loading density (Δ) loading area (A), and Pyrocore length (L)	Provide 3 x 3 Latin Square designed experiment according to the following table:

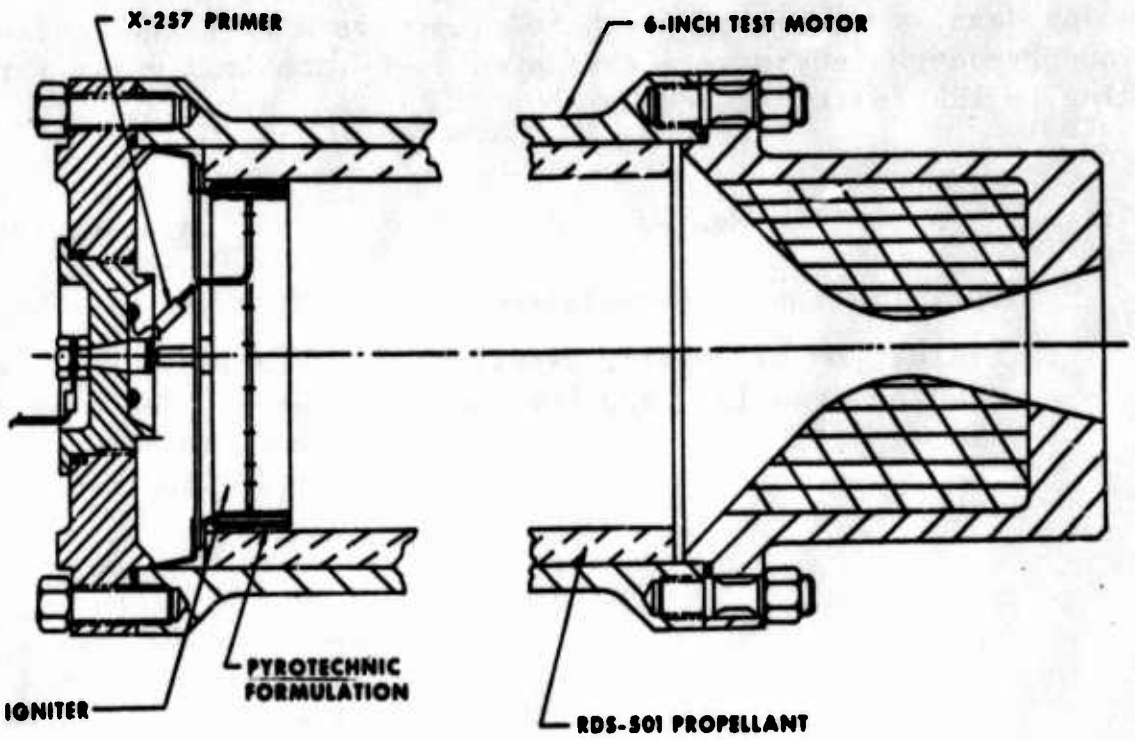
		Load Density		
		Δ_1	Δ_2	Δ_3
Mesh	A_1	L_1	L_3	L_2
Area	A_2	L_3	L_2	L_1
	A_3	L_2	L_1	L_3

(C) The configuration of the igniters for these test motors is shown in Fig. 352. The basic formulation has a heat explosion of 2600 Btu/lb, and has been found to satisfactorily withstand temperatures from -65 to 300 F, with good flexibility and abrasion resistance. Since the binder is held constant, variations in the formulation are not expected to affect these physical properties, but are made to optimize available energy and burning rate.

The formulation of the pyrotechnic coating for the Thermesh ignition was established following analysis of the results of the first three 6-inch motor firings. Three formulations were evaluated as follows:

(C)

Formulation Number	Composition - Percent by Weight			
	Geon 427	$KCLO_4$	Boron	Zr/Ni (50/50)
LLP-1	10	80	10	-
LLP-2	10	80	5	5
LLP-3	10	75	10	5



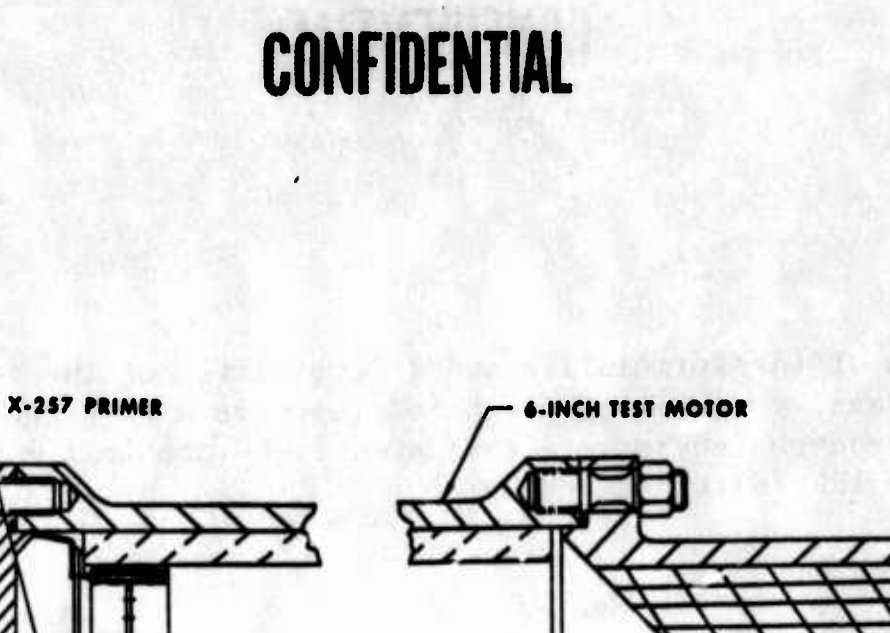


Figure 352. Test Motor and Igniter

The screen was constructed of aluminum wire, 0.028 inch diameter, type 5056 alloy, with 8 x 8 meshes per linear inch, per Federal Specification RR-W-360, type one, class one. The screen loading density was 1.5 grams pyrotechnic per square inch of screen, applied over a total of 10 square inches to provide a net weight of 15 grams of pyrotechnic. The Pyrocore was attached circumferentially around the interior surface of the igniter, with a total length of 17 inches. The energy provided by this quantity of ignition material was estimated to be at the minimum level, since this would provide a more sensitive indication of the relative properties of the formulations being investigated. Results of the firings are provided in the replots shown in Fig. 353.

As indicated by these data, the LLP-1 formulation provided more sustained igniter action, with a lower peak pressure, and faster motor ignition than either LLP-2 or LLP-3. LLP-1 has a further advantage in that it has one less constituent. Consequently, it was the formulation selected for use in the evaluation of other variables involved, which include loading density (Δ) loading area (A), and Pyrocore length (L). Nine 6-inch test motors were fired with igniters in which these factors were varied in accordance with the 3 x 3 Latin Square designed experiment shown below:

Area Coated (sq in.)	Coating Density (GMS/-sq in.) 1.0	1.5	2.0	Pyrocore (in.)
10	12.0	7.0	17.0	
20	17.0	12.0	7.0	
30	7.0	17.0	12.0	

The formulation previously described was modified, however, to include the addition of a plasticizer, dioctyladipate. The exact composition is as follows:

(C)

Component	Weight, %
Boron	9.4
Potassium perchlorate	75.5
Vinylchloride-acetate copolymer	9.4
Dioctyladipate	5.7

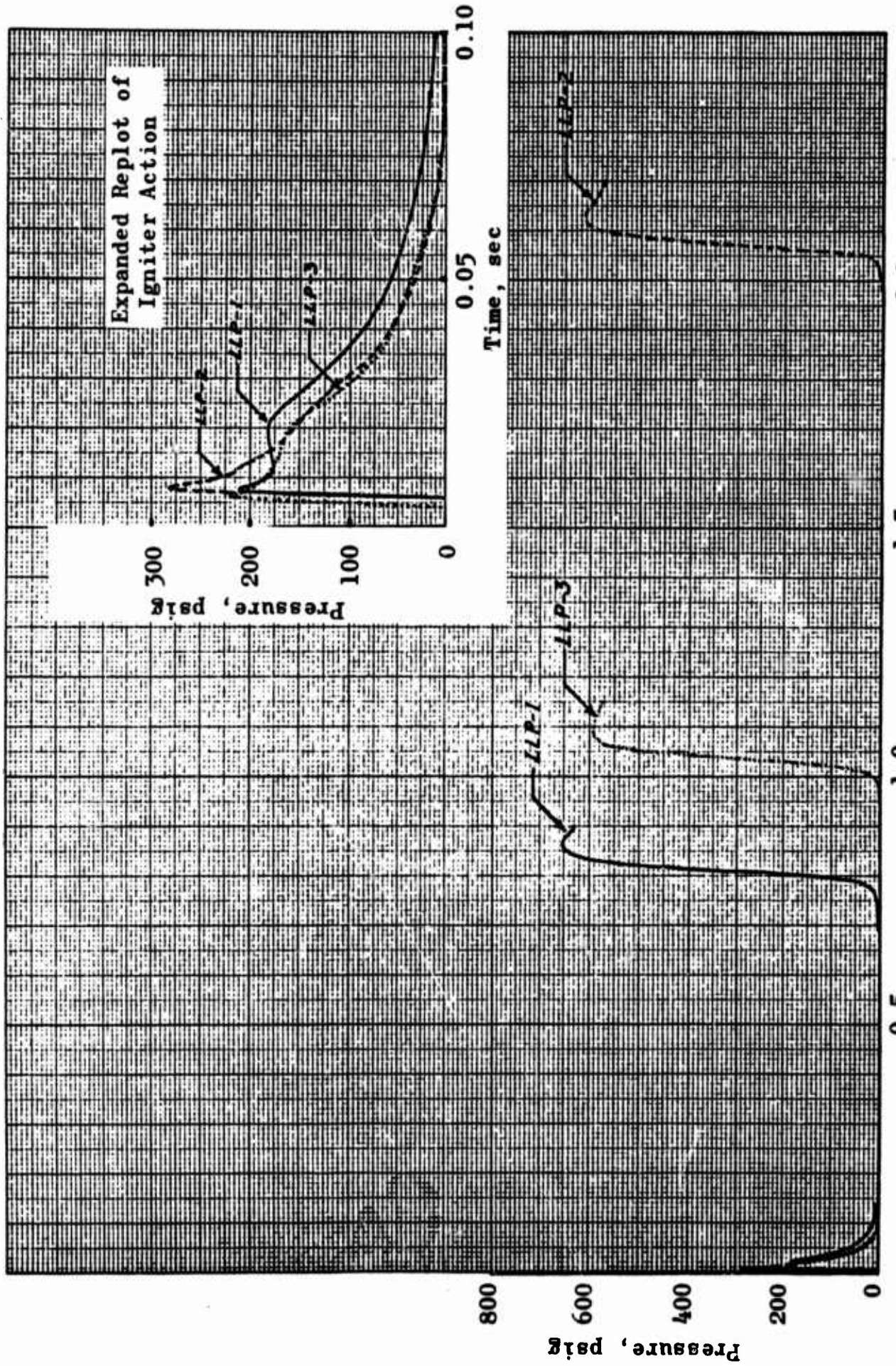


Figure 353. Formulation Optimization Tests, 6-Inch Test Motors, Thermesh Igniters

Nine 6-inch test motor firings were conducted in which loading density, area coated, and Pyrocore length were varied. Figure 354 _ shows the quantities of these three key variables used in each configuration, and the ignition interval obtained. Replots of the pressure-time performance of these motors are provided in Figs. 356 and 357.

Analysis of the above data and motor design parameters indicated the required pyrotechnic loading to be 103 grams for the restart igniter and 50 grams for the boost-sustain igniter. These loads include additional pyrotechnic material to compensate for the differences in relative free volumes and nozzle throat areas. A pyrotechnic load density of 1.5 grams per square inch of screen area was determined to be the optimum and was, therefore, utilized in both igniter designs. The 6-inch test motor firings also indicated an appreciable effect of Pyrocore length on igniter characteristics, the best results being obtained when the Pyrocore completely encircled the igniter. Consequently, the Pyrocore is attached to the restart igniter screen completely around its outer periphery, The Pyrocore is attached to the screen prior to application of the pyrotechnic to ensure igniter action adjacent to the propellant surface. Igniters similiar to the restart and boost-sustain igniter designs for Motor D were prepared under another program and are shown in Figs. 358 and 359 respectively for pictorial clarificiation of the proposal ignition system for Motor D.

Ignition of the boost phase of this motor was achieved very satifactorily, with an ignition delay of 6 milliseconds and an ignition interval of approximately 75 milliseconds. However, motor failure during burning of the boost phase prevented evaluation of the restart igniter.

(2) Fabrication

One of the many advantages of the Thermesh igniter is its flexibility and ease of fabrication. Besides the pyrotechnic used, the Motor D igniter is made of off-the-shelf hardware consisting of aluminum screen wire, aluminum clips, Pyrocore, and an initiator. Assembly of the igniter starts with cutting the screen wire into a washer shape and attaching four elbow clips to the screen. The slips are used to hold the screen wire close to the surface of the grain by sliding the free legs of the attached clips over the inhibited grain outer diameter. Next, the Pyrocore is attached to the screen and the assembly is coated with the pyrotechnic material by either dipping or hand painting. In Fig. 358, the darker outer ring of the ends of the grain is the pyrotechnic coated screen wire. Only the outer edge surface of the wire washer was coated with pyrotechnic for this motor. The four retaining clips are also slightly visible in these end views.

Area Coating (sq in.)	Coating Density (GMS/ sq in.) 1.0		1.5		2.0	
10	12.0	-31	7.0	-41	17.0	-51
		1120		465		159
20	17.0	-61	12.0	-71	7.0	-81
		104		72		152
30	7.0	-91	17.0	-101	12.0	-111
		155		42		70

KEY:

Pyrocore Length (in.)	Igniter Dash No.
	Ignition Interval

Figure 354. Nine Motor Evaluation of Thermesh Design Variables

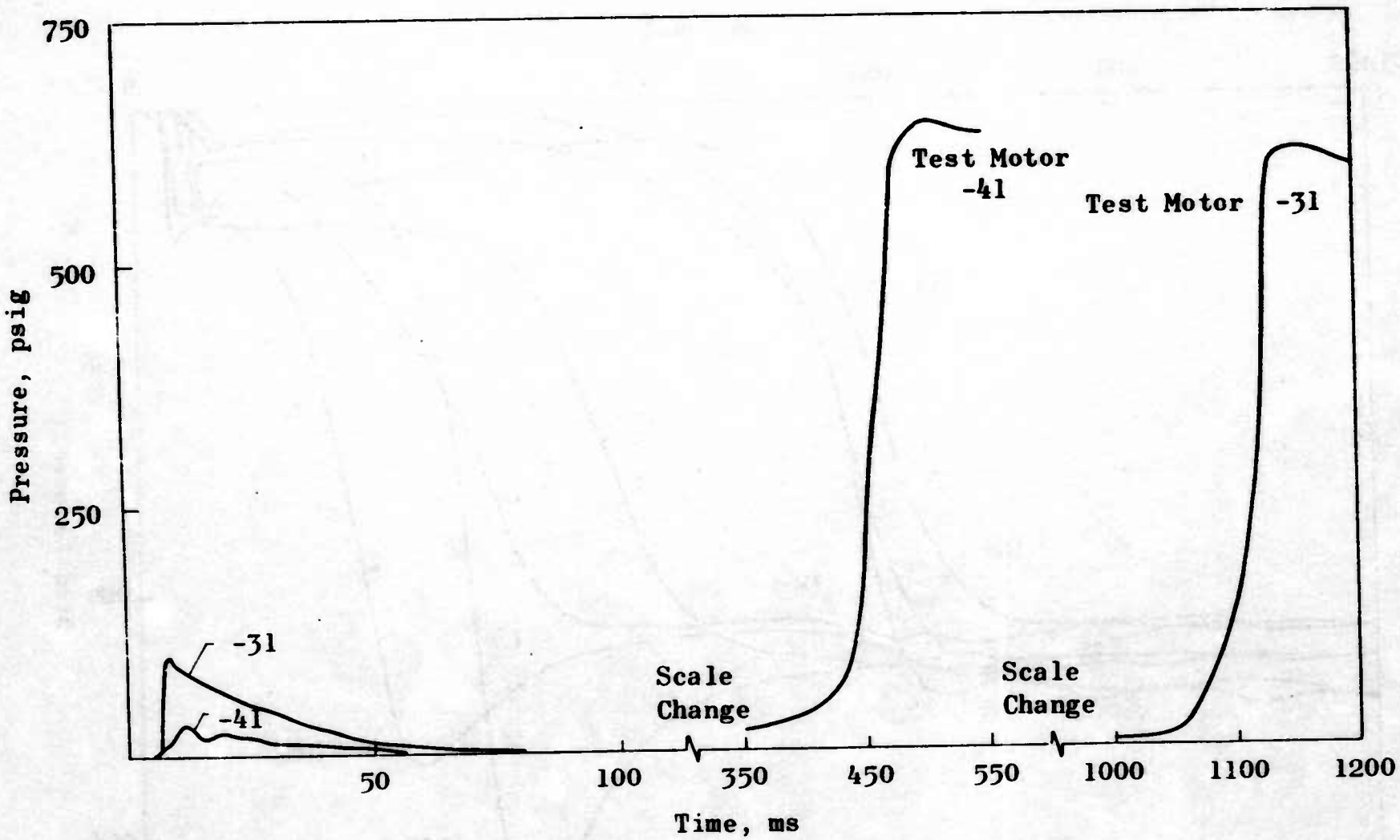


Figure 355. Six-Inch Test Motors, Thermesh Igniter Evaluation; Test Motors -31 and -41

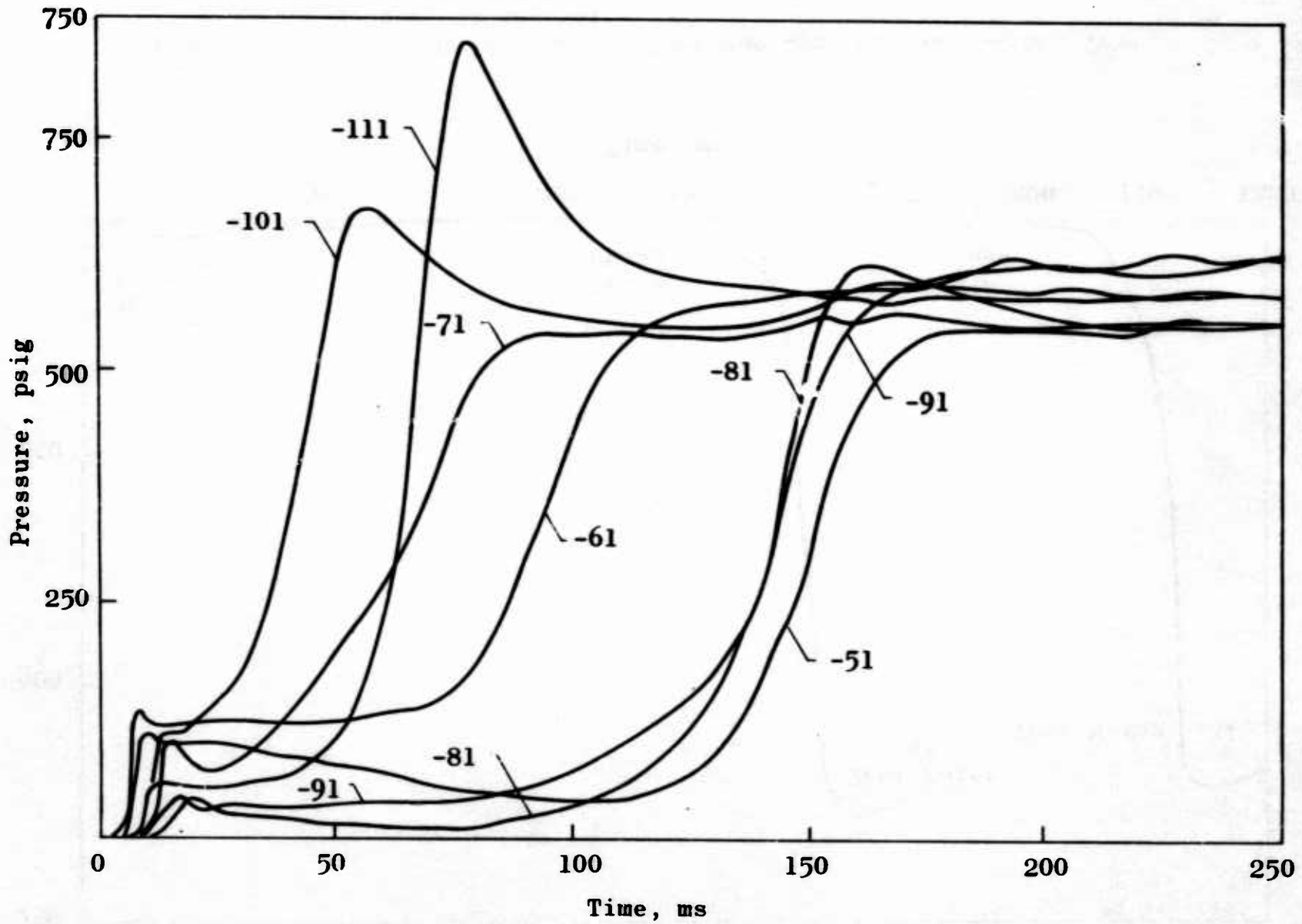


Figure 356. Six-Inch Test Motors, Thermesh Igniter Evaluation



Finished Igniter
Before Installation



Insertion of Igniter
Within Grain

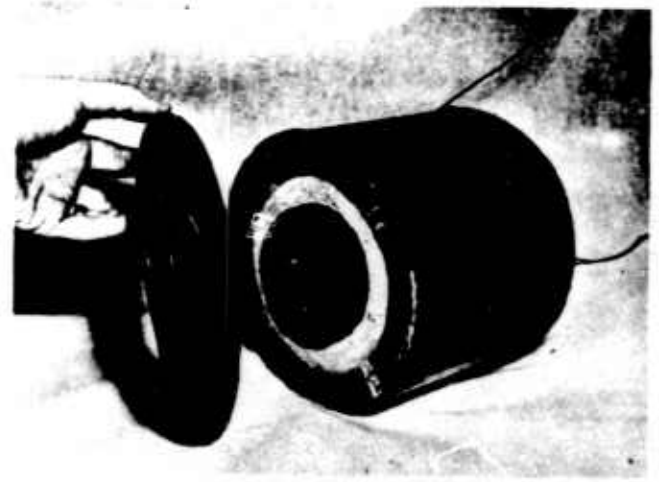


Finished Igniter--Motor
Grain Assembly

Figure 357. Installation of Thermesh Igniter Within a Typical Boost Grain on an Unrelated Program



Restart Grain Showing Internal Disc
Thermesh Igniter, Inhibitor, and Insulation



Restart Grain
In Final Assembly



Assembled Restart Grain

Figure 358. Assembly of Typical Sustain Grain and Integral Thermesh Igniter on an Unrelated Program

After cure of the pyrotechnic, the initiators are attached to the end of the Pyrocore. On the boost phase igniter (Fig. 359) the initiators are attached to the screen but on the restart igniter the pyrocore is trimmed with excess length to allow the initiators to be placed in a slot cut into the restart grain. This allows a thin igniter which can be easily placed between the two grains.

The electrical leads from the restart initiator (Fig. 360) are imbedded in the restrictor along the side of the restart grain as they pass to the initiator connectors in the forward closure. The leads from the boost initiator pass out the nozzle throat.

After installation on the grain, the restart igniter assembly is covered with a thermal barrier insulation. This barrier was designed to break away under restart ignition but still retain the insulation pieces by a series of glass cloth strips partially sandwiched into the thermal barrier. Then the loose ends are bonded to the sides of the restart grain.

The outer edge of the screen wire on the boost grain igniter is compressed between the boost grain and the boost-sustain grain to assist the clips in retaining the igniter. Thus, the end of the boost-sustain grain is ignited and the hot exhaust gases will, in turn, ignite the boost grain ID as they exit.

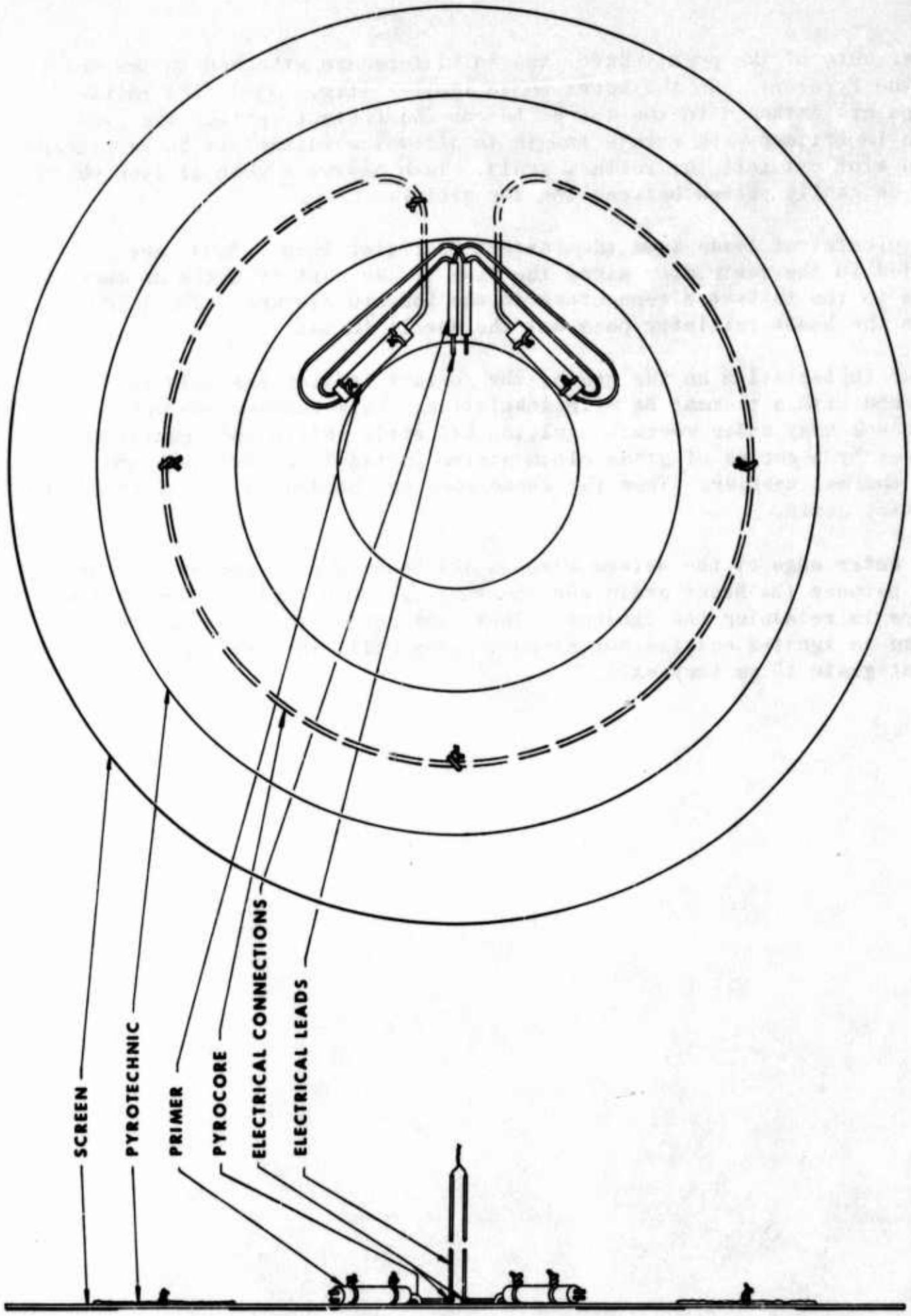


Figure 359. Boost-Sustain Igniter, Motor D

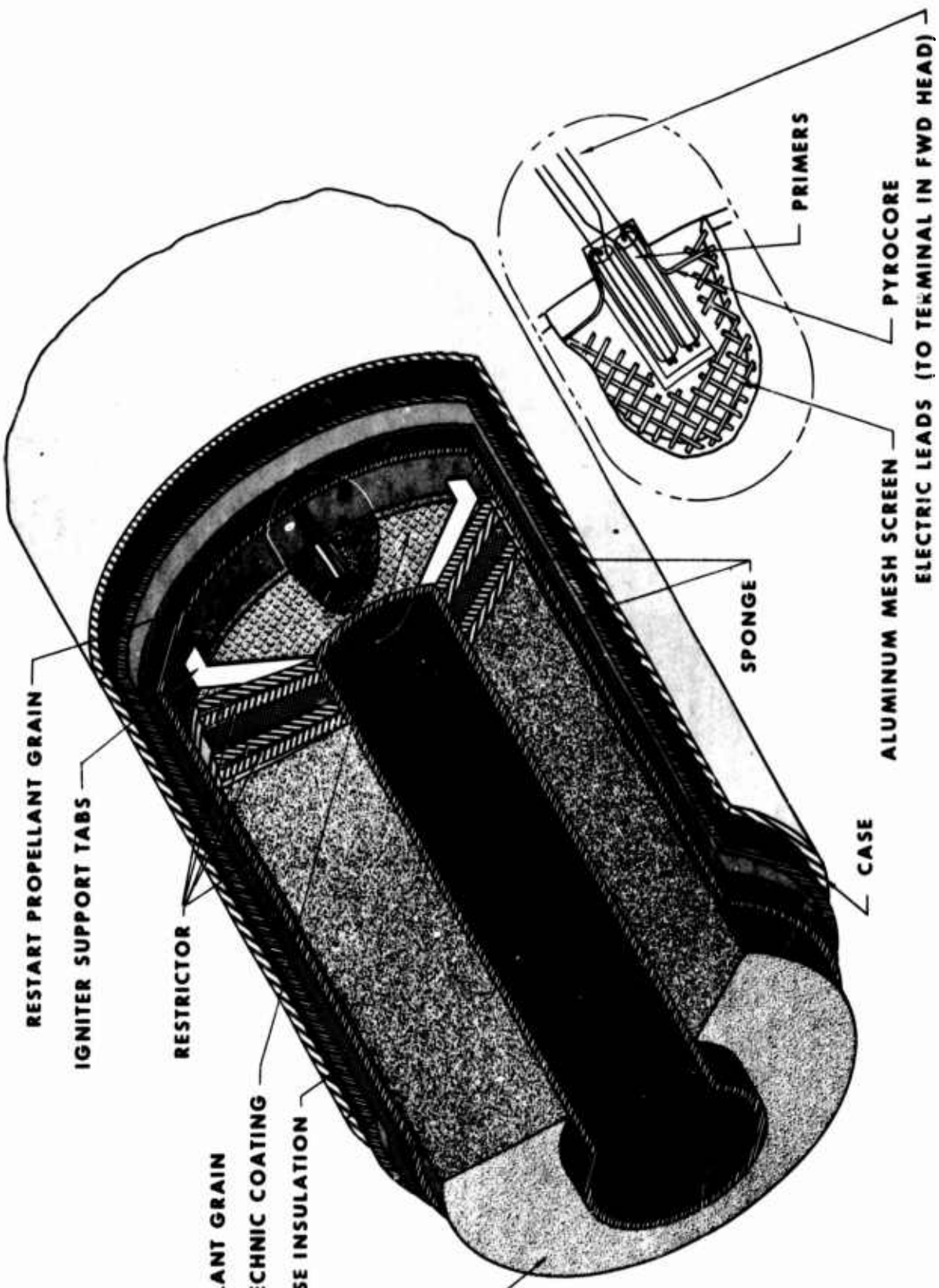


Figure 360. Restart Igniter Concept, Motor D

4. PROCESS DEVELOPMENT

When the reinforced grain program was terminated, all Motor D fabrication procedures were established or under consideration. Preliminary processing procedures were necessitated during the design phase, since process capabilities placed certain restraints on motor design. This was particularly true of the grain support system, which was dependent upon the tolerance buildup between the grain assembly and insulated case and the procedure by which the two assemblies would be joined. This procedure represented the most significant Motor D processing hurdle, since the case and grain would be connected by a sponge support system.

Also, the selection of materials during the design phase required that compatibility of these materials be established with respect to the propellant and adhesive systems. Therefore, considerable effort had been expended in the formulation of processing techniques and associated tests prior to completion of the final design. These items are presented and discussed in the ensuing sections. Presented in Fig. 361 is the preliminary process flow sheet, which represents the steps intended to fabricate and assemble Motor D.

a. Cylindrical Grain Design

Cylindrical grains are simpler and relatively straight-forward to design. Structurally these grains can carry hoop, longitudinal compression, and external pressure loads (but not bending loads, unless a low helix angle is used).

(C) They are usually wound on tapered metal mandrels or on polyurethane foam mandrels. Most grains of this configuration require small internal bores which necessitate winding directly on a metal mandrel, tapered 2 to 3 mils per inch to reduce breakout loads. Small bore grains only allow winding between end plates. This means that the helix angle is limited to a minimum of 60 degrees; below this point, the wires slip at the reversal points. Recommended winding angles are in the 70 to 80 degree range. At the higher angles (above 85 degrees) wire wraps tend to slide and intermesh into the preceding covers because the intersecting angle is so small.

(C) Grains with helical angles below 60 degrees (grains with a 45-degree helix were wound) can be wound if the grain bore is big enough to allow winding a nonstructural dome to prevent wire slippage. This is accomplished by starting with a small dome or cone depending on the size of bore allowed. A tapered end piece (see Fig. 362) is used to prevent the wire and propellant sloughing off. With this type of grain, the resultant domes are cut off to give the desired cylindrical length.

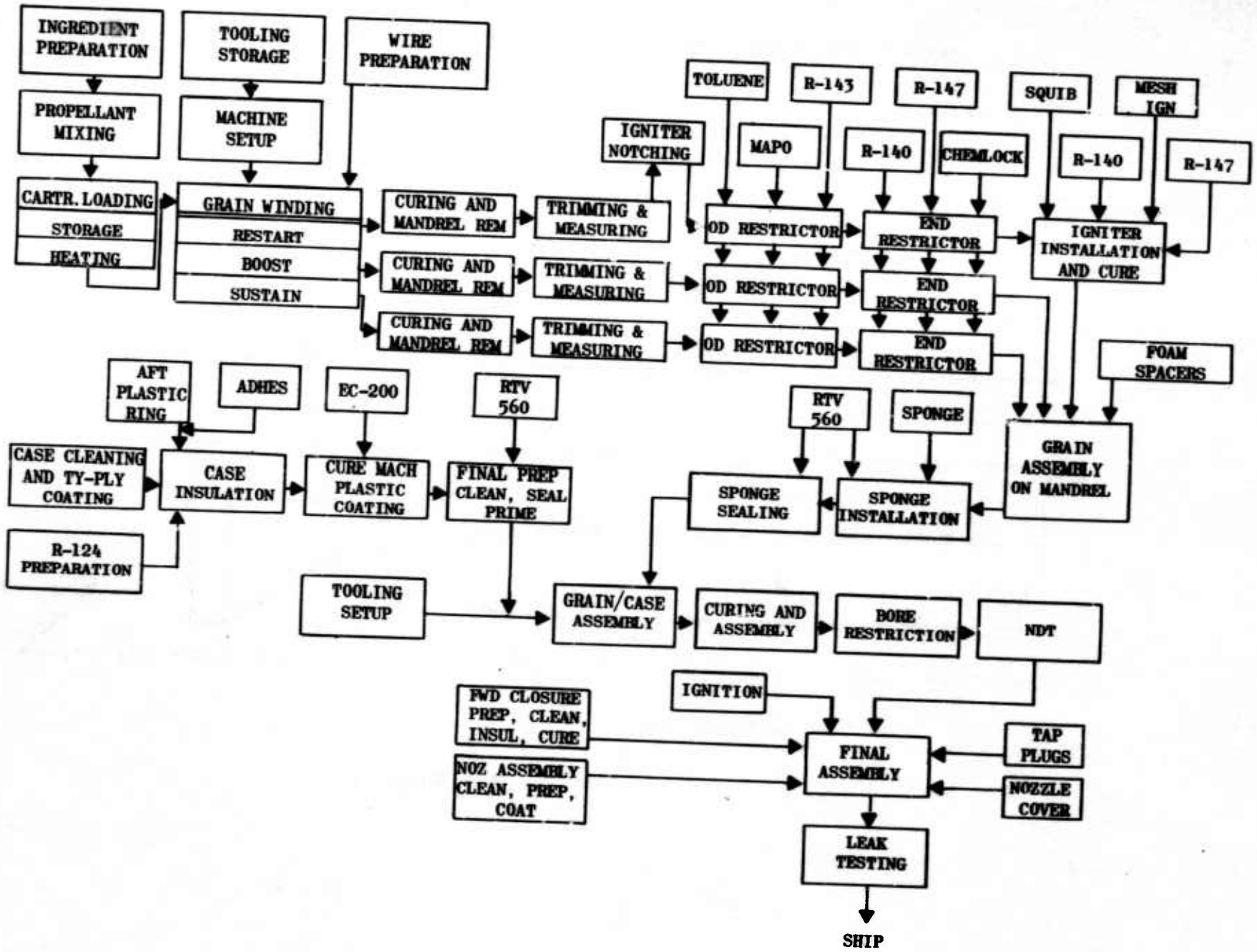


Figure 361. Preliminary Process Flow Sheet for Motor D

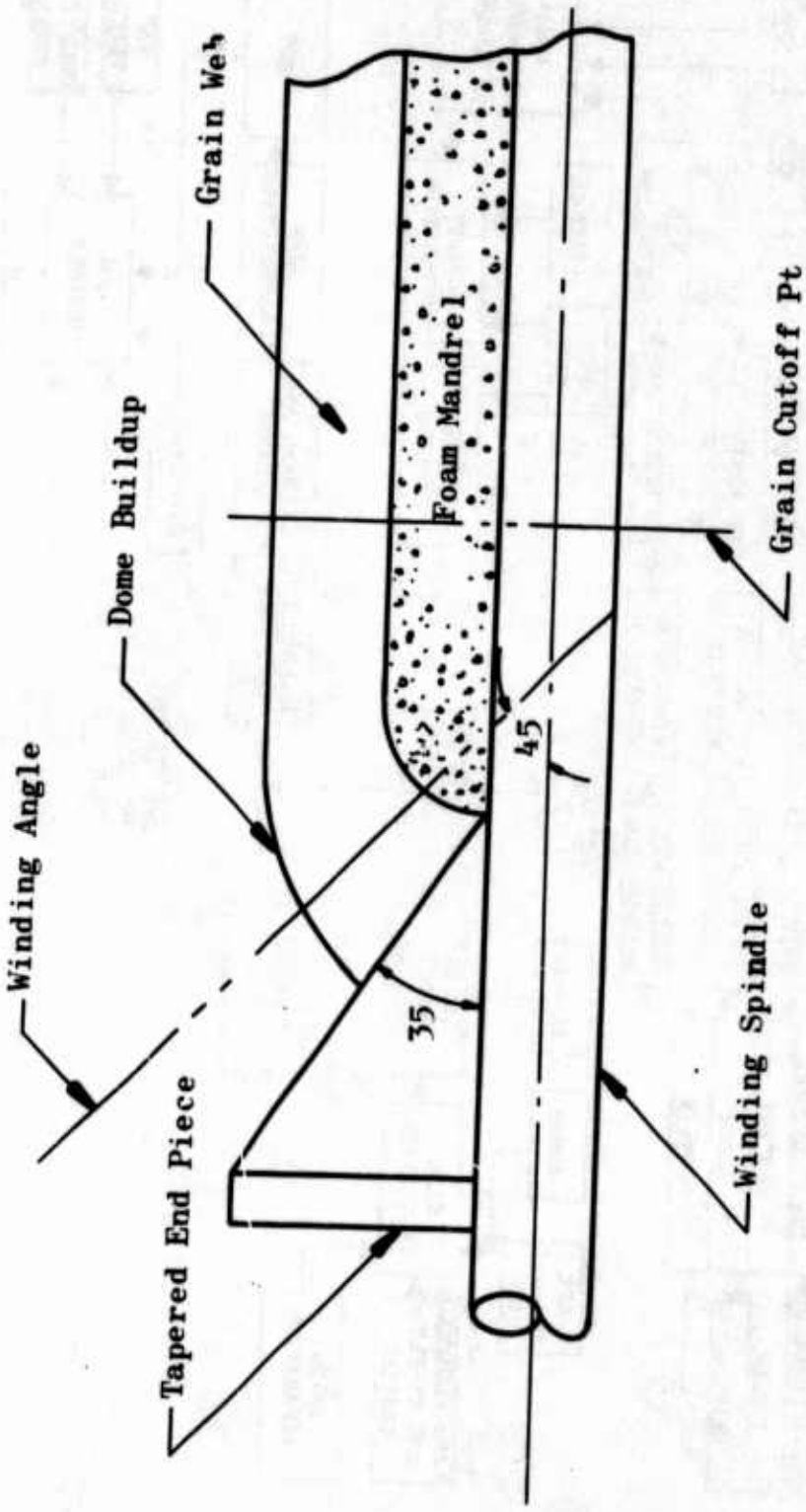


Figure 362. Low-Angle Cylindrical Grain Fab Method

Generally grains are trimmed to final length with a rotary cut-off saw. This allows the removal of the grain ends where the wire pattern and volume differs slightly due to follower reversal. Grain trimming has some disadvantages in that sawing can damage the ends causing stress risers or delamination, the saw coolant forms frost on the trimmed ends and can also cause contamination, the operation is extra and costly, and the resultant aluminum percentage can only be calculated from theoretical wire length (since the total wire weight normally used is useless).

(C) For these reasons the best and easiest method is to fabricate the grain between end plates, set to give the correct length. Some fall-off of the grain at the edges is expected since the last wires of the final warp do not cross each other; however, this fall-off is insignificant on high helix angles (70 degrees up). It also can be corrected on low angle winding by judicious fabrication techniques.

As described under cam design (Motor A Processing), if the web is thick, it will probably be necessary to build the end plates in stacked increments. This allows the wire follower head to stay close to the grain surface. The further the follower is positioned from the grain surface the greater the foreshortening of the wire warp and the more pronounced the affect on angle Z. The condition is most critical for low winding angles and small grain radii. Therefore, if the distance from the grain surface to the follower varies considerably during grain winding, it will be necessary to have more than one Z cam to prevent pattern gapping or overlapping.

(C) In cylindrical grain design the required OD, ID, length, helix angle, wire size, and aluminum content are specified. Wire spacing for the aluminum content is determined as previously described. The next step (see Fig. 363) is layer design. The layer thickness depends on the allowable tolerance in the winding angle. Since the winding angle changes on a grain with increasing diameter, it is necessary to change gear ratios regularly to compensate. An allowable tolerance is specified (depending on the grain); the lower the tolerance, more layers, gear changes, and time is required to fabricate. Usually a $\pm$ 2 degrees is used with the proper angle being wound at the median radius, α -2 degrees at R_1 and α + 2 degrees at R_2. The angle tolerance, the winding angle α, and the initial radius (R_1) determine the layer thickness.

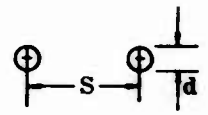
(C) The only other variables are the cover thickness (t), usually considered 0.015 inch for cylindrical grains, and mandrel rotation (θ) at reversal (usually 180 degrees is used). With this information, the appropriate layers are determined for the web required.

GRAIN DESIGN

Given--ID, OD, Length, Helix Angle, Wire Size, Al Content

I. Spacing Analysis

$$S = \frac{\pi d}{4 V_f}$$



S = Wire Spacing, d = Wire Dia, V_f = Vol Fraction, W_f = Weight Fraction

II. Layer Design (Helix Angle Tolerance = $\pm 2^{\circ}$)

Layer Number	R_1 (Mandrel)	R_2 $R_1 \frac{\tan\alpha_2}{\tan\alpha_1}$	R $\frac{R_1 + R_2}{2}$	C $2\pi R$	t $R_2 - R_1$	No. Covers $\frac{t}{0.015}$	θ/in. $\frac{360 \tan\alpha}{2\pi R}$	θ/reversal 180 deg	θ_T θ/in. $(2L - 4W_f) + 360$
1									
2									
3									
4									

GEAR RATIO CALCULATION

Layer Number	R_F Follower	W_F Follower	W_N $\frac{W_F \sin Z}{\sin\alpha}$	W_C $\frac{W_N}{\cos\alpha}$	Tp/Cp $\frac{\theta_T}{360}$	C/C C/W_c and Cp N + 1	R_W $\frac{Tp \pm \frac{W_c}{c}}{Cp}$	W_C Corrected	W_F Corrected	No. Wires $\frac{W_f}{S}$

NOTE: Alter W_c such that C/C = CpN $\pm$ 1 = C/W_c

EXCEPTIONS: (1) If C/C = C_p, R_{1V} = Tp/Cp
(2) If C_p = 1, C/C = C_pN

Figure 363. Layer Design Calculation Chart

Gear ratio calculations are similar to domed grains. The two variables in pattern selection are the follower height, or radius (R_F), and the warp width. If Tp/Cp of N must be changed to obtain integers, you cannot change α as in domed grain pattern selection. The winding angle is already fixed and the only variable to change is the warp width. This is done by adding or reducing the number of wires in the warp to obtain the desired width.

b. Grain Fabrication

The three reinforced grains for Motor D were to be wound on tapered steel spindles with end flanges to contain the grain. The spindles would be Teflon-coated for ease of grain release after cure. The winding machine, wire feed systems, and propellant application methods were those developed under Motors A and B and will not be described further.

(C) The planned procedures for grain fabrication and winding design were based on Motor A processing studies. The boost grain was designed with the 70 degree helix angle with 13% per weight aluminum wire. The sustain and restart grains were to be wound at a 60 degree helix angle, with the same wire percentage.

(C) In grain winding, the appropriate winding spindle is assembled into the winding machine; 36-inch machine for the boost and restart grains and the 40-inch machine for the sustain grain. A liberal bead of RTV-731 is applied to seal the joints between the end flanges and the Teflon-coated spindle. All grains are wound with 7.5 mil aluminum wire. If a wire breaks, no more than three traverses of the feeder head is allowed before the wire is replaced. The weight of the wire wound on each grain is recorded before and after winding. The wire spacing is attained by having the wire pass through a final guide having provisions for 36 wires with an average wire spacing of 0.074 inch. The wire tension is controlled at 300 ± 25 grams and measured with the wire in motion between the gathering guide and the machine forward head. Propellant application is by propellant feed guns as required to maintain a uniform thin coat of propellant on the surface of the grain. Sufficient propellant is applied to prevent formation of voids underneath the wire. Propellant is spread by a pneumatically-powered aluminum spreader blade and non-sparking spatulas. Maximum air pressure on the pneumatic spreader blade is 20 psig. The winding requirements for layers, diameters, number of wires, number of wire covers, and winding circuits for each of the three grains are presented in Table CXVIII.

TABLE CXVIII

MOTOR D WINDING REQUIREMENTS

Layer	Cam Circuits Per Cover	No. Covers	No. Wires	Diameter at Finish (1) (2) HS	C	T.S.
Boost Grain						
1	2	25	28	3.90	3.82	3.75
2	2	31	35	4.83	4.76	4.68
3	3	39	29	5.99	5.91	5.84
4	3	53	36	7.58	7.50	7.43
5	4	52	33	9.15	9.08	9.01
6	5	74	33	11.44	11.37	11.30
7	5	38	36	12.59	12.52	12.45
Sustain Grain						
1	3	20	29	4.43	4.10	3.76
2	3	24	34	5.15	4.81	4.48
3	4	28	30	5.99	5.66	5.32
4	4	33	36	6.99	6.65	6.32
5	5	39	33	8.15	7.81	7.48
6	6	46	33	9.52	9.18	8.85
7	7	53	33	11.13	10.79	10.46
8	8	71	35	13.27	12.93	12.60
Restart Grain						
1	3	23	19	4.67	4.59	4.52
2	3	27	36	5.47	5.39	5.32
3	4	32	34	6.42	6.34	6.27
4	5	37	32	7.53	7.45	7.38
5	5	44	36	8.83	8.76	8.68
6	6	51	32	10.37	10.29	10.22
7	7	60	36	12.17	12.09	12.02
8	9	42	32	13.43	13.35	13.28

(1) Diameters Shall Be Within ± 0.020 inch of the Specified Value on the Final Layer and ± 0.040 inch on Interim Layers.

(2) HS-Head Stock End of Grain; C-Center of Grain; T.S.-Tail Stock End of Grain.

c. Grain Assembly

Following winding of the propellant grains, the grains are cured and trimmed. Cure time was established from Fig. 364. From this operation, the grain OD is given a thin coat of restrictor, the ends restricted, and the igniters applied to the aft face of the restart and sustain grains. Subsequently, the three grains are assembled onto a grain assembly mandrel (Fig. 365) for final restricting, and application of the sponge support system. After grain assembly cure, the grain assembly is ready for insertion into the case assembly.

(1) Restriction

The outside surface of the grain is restricted in a two-step application using R-143[32], similar to Motors A and B, first with a prime coat which is semi-cured and then with a finished layer smoothed with a template. It was planned to apply the finishing coat after all grains are assembled on the loading spindle, to obtain the best possible alignment of all grains. Prior to application of the prime coat, the cure propellant surface is wiped with toluene, air dried, and coated with a film of MAPO.

The grain-end restriction/insulation was accomplished by bonding sheeted or molded discs of R-147[33] to the grain with R-140[34]. During cure of the R-140, 5 psi pressure is maintained on the discs.

---

[32] R-143 is a Rocketdyne thixotropic restrictor containing carbon-filled CTPB.
[33] R-147 is a Rocketdyne EPT rubber formulation.
[34] R-140 is a Rocketdyne low viscosity restrictor made with carbon-filled CTPB.

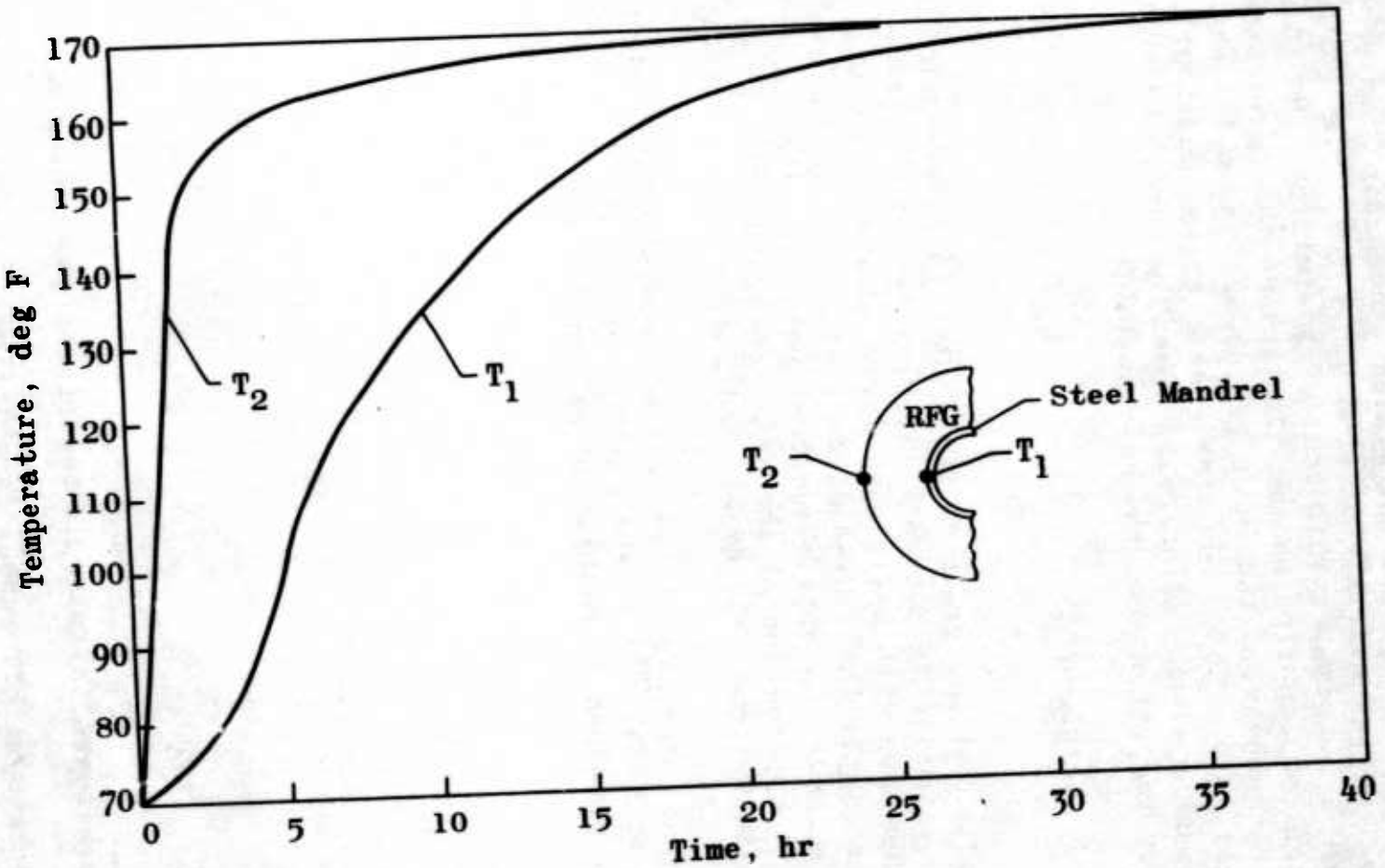


Figure 364. Temperature vs Time for Conditioning Motor D RFG to Cure Temperature

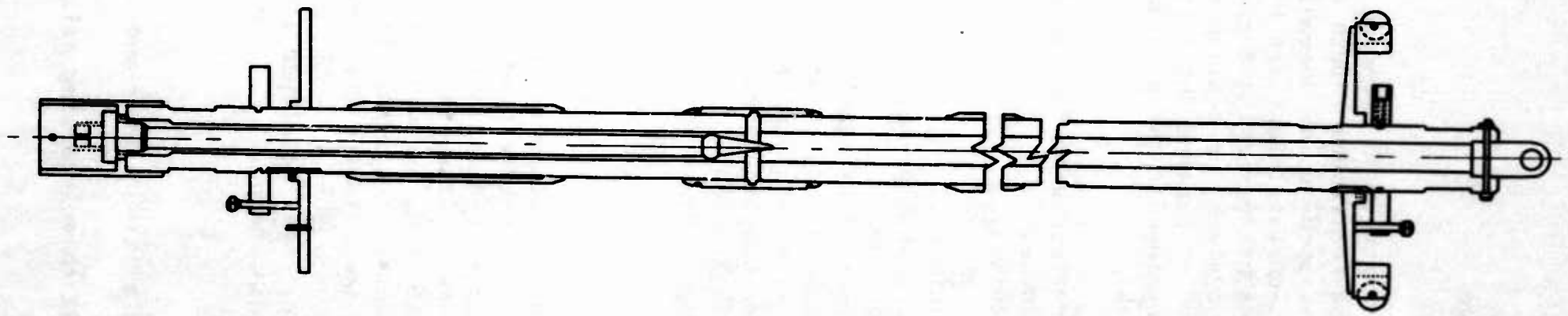


Figure 365. Motor D Grain Assembly and Restrictor Mandrel

(2) Support Sponge

Upon assembly of the three grains on the loading spindle and application of the final OD restrictor, a continuous length of 0.5-inch thick ESM 1004 AP silicon sponge was wrapped on the assembly and bonded to the restricted grains. After extensive laboratory tests, which included tests at extreme temperatures using varying degrees of adhesive and different types of cleaning systems, or sealing systems on the silicone rubber, a satisfactory method of bonding the silicone rubber to R-140 and R-143 restrictors was developed. The procedure for accomplishing the bonding is outlined below:

1. Abrade restrictor surface with fine sandpaper.
2. Wipe clean with toluene.
3. Air dry one hour minimum.
4. Wipe on SS-4056 sealer.(35)
5. Air dry one hour minimum.
6. Apply thin coat of SS-4004 primer.(35)
7. Air dry one hour minimum.
8. Apply 5 to 10 mil coat of RTV-560(36) (catalyzed as required for allowable drying condition).
9. Apply silicone rubber within one hour. The scraping ends of the circular wrapped sponge are scarfed and bonded together with RTV-560.
10. Cure at ambient temperature.

d. Case Insulation

Concurrent with the preceding operation is the insulation of the case with R-124 and Durez. Again, extensive bonding studies were conducted prior to selecting the primer(s) and adhesive(s) for effecting the bond between the insulation and case. After the laboratory had screened many candidate materials, the most promising were critically tested for bond strength, affects of high temperature aging (250 F), and compatibility with other materials. Adhesive selected for testing were Ty-Ply-Q, Ty-Ply-S, Epon 901, SS-4056, SS-4004, RTV-560, RTV-731, and EC-1648. The materials and bonding processes developed from these studies are presented in the following discussion.

(35) SS-4056 and SS-4004 are silicon sealer and primer recommended for bonding with RTV-560.

(36) RTV-560 is room temperature vulcanizing silicone rubber used for bonding silicone foam.

After thorough cleaning and decontamination of the inner case surface, the machined insulation ring of Durez 16771 is prefit and bonded to the steel case with EC-2214. The adhesive is cured for a minimum of one hour at a bond line temperature of 250 F.

Then the case and Durez-scarfed face are primed with a continuous coat of Ty-Ply-Q, which is allowed to air dry for 30 minutes. Uncured R-124, which has been sheeted on the roll mill, is placed over the primed surface with the roll direction parallel to the longitudinal axis of the motor. After obtaining complete and positive R-124-case and R-124-Durez contact, the system is cured under pressure for 10 hours at 325 F. Since the R-124 is uncured, the longitudinal scarf seam is actually vulcanized during cure.

Subsequently, the insulation is machined to the designed taper. The exposed surface of the Durez ring is then coated with a film of EC-200 (Emerson and Cummings) and the entire case sealed to preclude possible contamination of the insulation prior to insertion of the grain assembly.

e. Motor Assembly

(1) Grain-Case Assembly

To compensate for the thermal expansion and contraction of the grain, the silicone-sponge-wrapped grain must be loaded in compression. This causes a complex loading problem and imposes a tolerance limit on the finished grain; in Motor D the tolerance buildup was 0.120 inch. Several insulating systems and loading techniques were evaluated for possible use. This included placing the ablation resistant insulation (R-124) next to the grain with the silicone rubber next to the case. The reverse of this method was also considered. The latter (reverse) design was selected because thermal expansion properties of the R-124 insulation matched more closely with the case than with the grain. With the silicone rubber next to the grain, the grain was free to change with thermal cycling and still be contained during vibration.

Methods of assembling a grain wrapped in compressible insulation were studied with two concepts selected for further consider ion. One design employed a split rigid sleeve as a means of precompressing the silicone rubber before assembly. A clamp would be used for precompression, in much the same way as a piston ring compressor sleeve is used in reciprocating engine repair. The second method of assembly consists

of using elevated pressure to compress the silicone rubber. With this method, the grain would be inserted in a simple pressure chamber, which attaches to the case. The grain would be mounted on a central shaft or mandrel attached to a hydraulic ram. After pressurizing the chambers, the grain would be guided into the case by means of a shaft extension (Fig. 366). Final selection of the latter technique was based on favorable results of the pneumatic compression and friction tests.

Friction tests indicated that the RTV-560 adhesive acts as a lubricant resulting in reduced friction which would probably permit loading by force alone (without pneumatic compression). But, by using the technique of pressure chamber and friction load, the grain can be easily slipped into the insulated case while the sponge surface is under a compressive load. After insertion into the insulated case, the pressure is released and the sponge expands against the adhesive-loaded insulated case surface. Then the adhesive is cured and the motor is prepared for final assembly.

Although detail process procedure was not completed at the time of program termination, tooling for pressure chamber loading of the grain was under design and being fabricated. In actual operation, the three individual grains would be assembled onto the grain assembly spindle, fixed to a relative position, and clamped to the design length before being inserted into the case as a single unit. Again, actual practice might have found that grain loading could have been accomplished by ram force alone, but it appeared prudent to plan for the combined methods of pressure and ram force load.

(2) Bore Insulation

The internal bore insulation/restriction was to be accomplished by bonding a preformed tube of R-147 to the ID of the sustain and restart grains. The R-147 is bonded under pressure using R-140 as the adhesive. When work was ceased, this operation was scheduled to be conducted after the grain assembly had been inserted in the case. However, objection was expressed that inspection and repair would be difficult. Conversely, installation of the R-147 before assembly on the loading spindle would make the R-147/propellant bond susceptible to damage and increase the grain assembly tolerances. Additional analysis of this processing step is required.

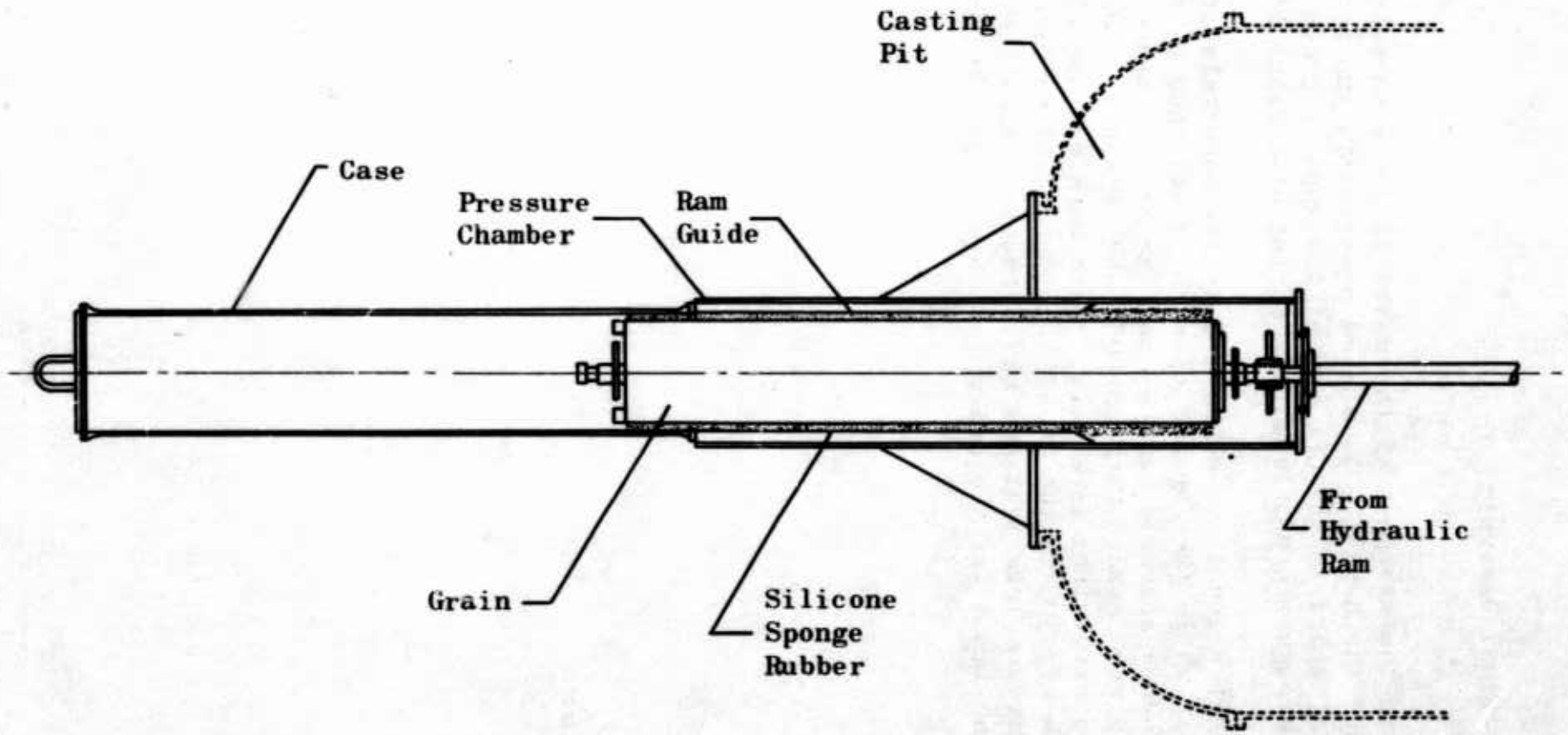


Figure 366. Motor D Loading Pressure Chamber

(3) Final Assembly

The last step in the assembly of the motor is the attachment of the forward closure and the nozzle. As stated previously, the boost igniter (Thermesh) is attached to the aft end of the sustain grain and the leads are extended through the nozzle throat during attachment of the nozzle.

The restart igniter leads are connected to the terminals of the forward closure assembly while the forward closure is attached to the case. The forward closure assembly consists of the steel closure, two Durez bushings (which were sealed with SS-4056 and primed with SS-4004) silicone sponge, and two electrical terminals. Both bushings and silicone sponge are bonded with RTV-560 to the SS-4004-primed steel surface. Finally, the motor receives a leak test and radiographic inspection. To predict the conditioning times for the assembled motor Figs. 367 and 368 were prepared.

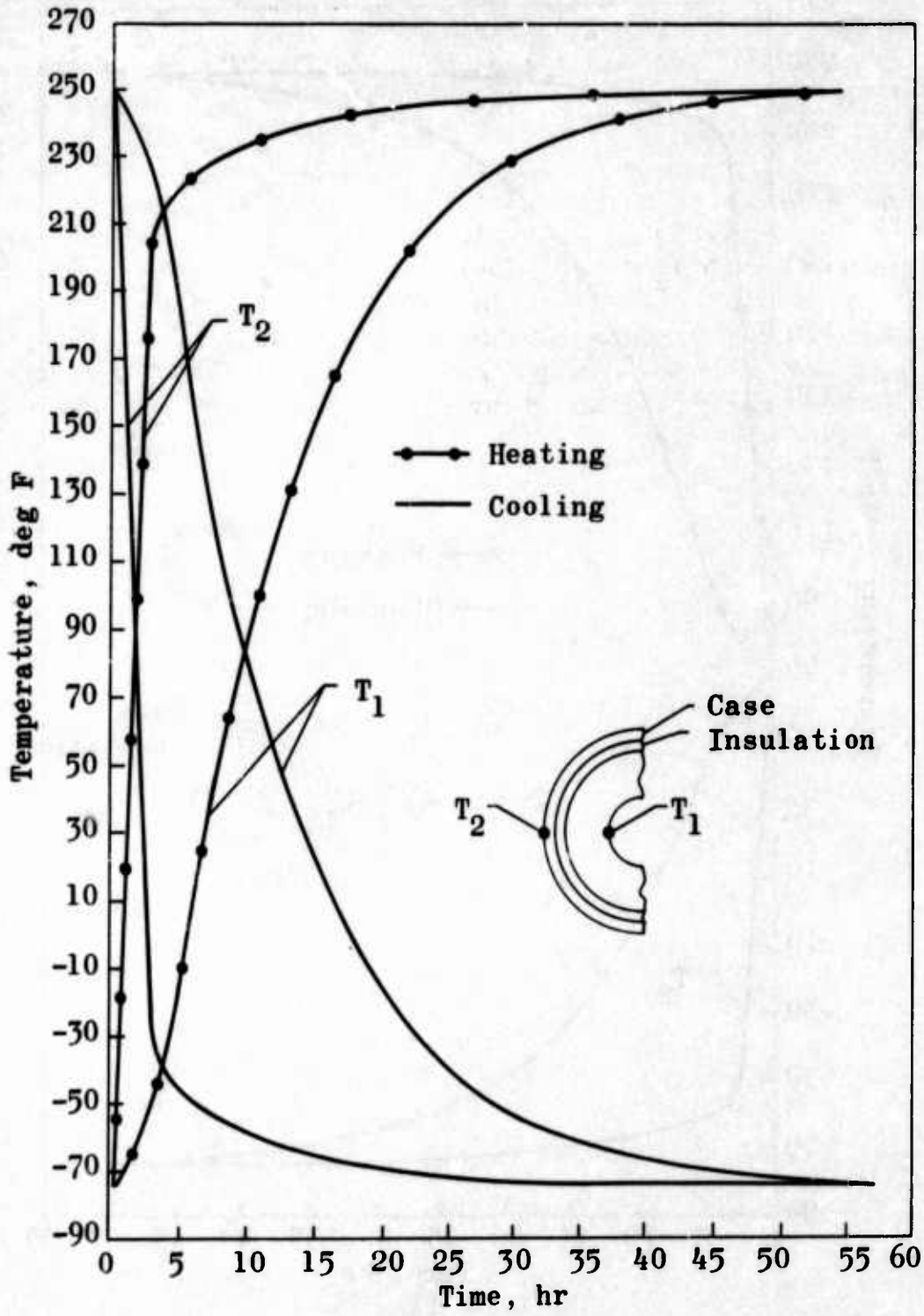


Figure 367. Temperature vs Time for Conditioning Motor D During Temperature Cycling

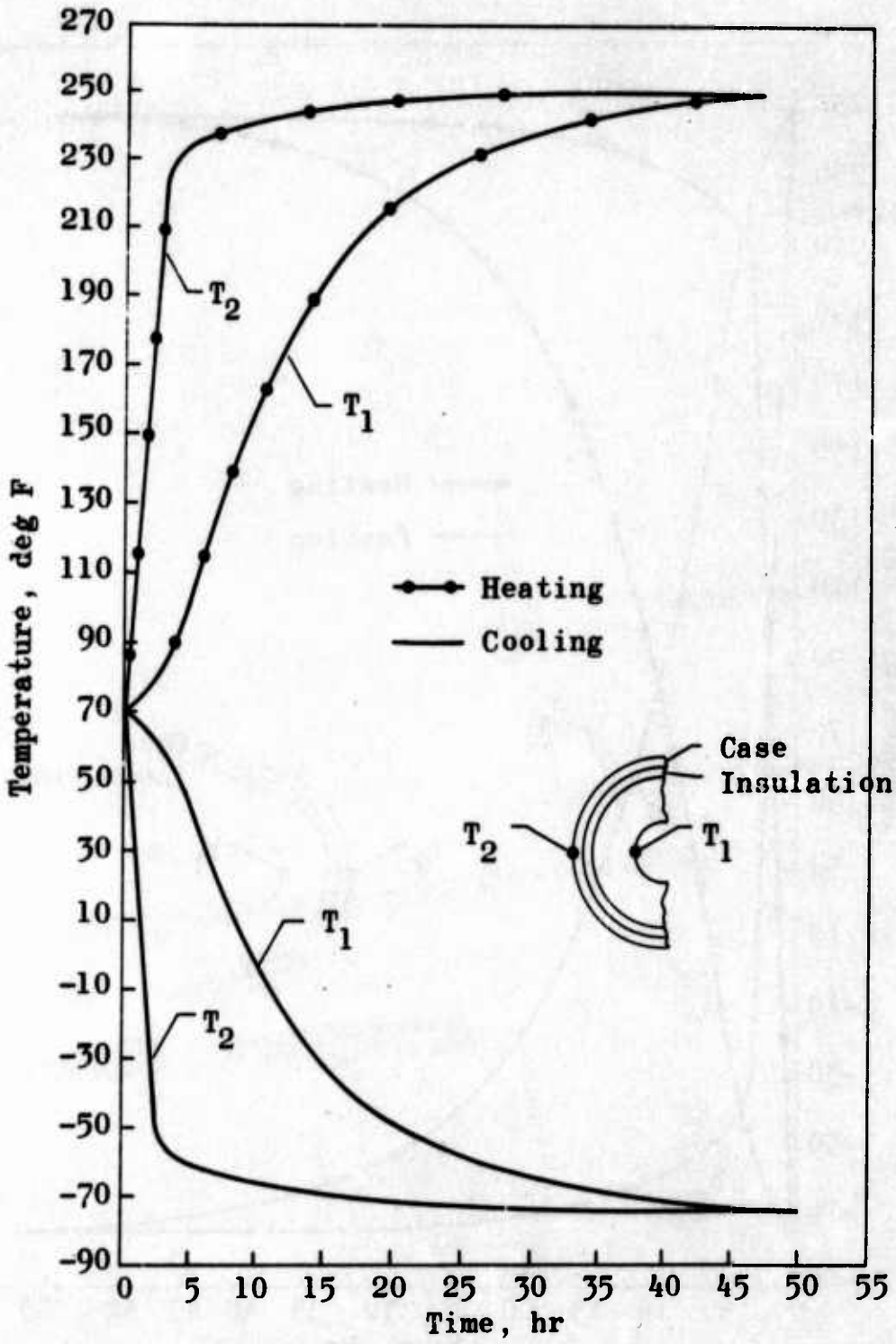


Figure 368. Temperature vs Time for Conditioning Motor D During Temperature Cycling

APPENDIX I

DESIGN AND HYDROTEST OF 20-INCH REINFORCED GRAIN/ FIBERGLASS CASE 7205/7403

PREVIOUS PAGE WAS BLANK, THEREFORE WAS NOT FILMED

APPENDIX I

DESIGN AND HYDROTEST OF 20-INCH REINFORCED GRAIN/FIBERGLASS CASE 7205/7403

SUMMARY

A 20-inch reinforced grain and fiberglass case (RFG/GFW 7205/7403) was designed, fabricated, and hydrotested to prove the structural capability of the motor and to provide strain versus pressure data for use in design of future reinforced grain motors.

(C) Aluminum, rather than plastic, polar bosses and load rings were used in this motor to make certain that either the reinforced grain (RFG) or glass filament wound (GFW) case would fail and therefore provide structural compatibility data for the composite unit. Calculations showed the initial failure should occur between 558 psig, which was the shear out pressure of the RFG only at the polar boss, and 1278 psig, which was the sum of the RFG shear out pressure plus the GFW case ultimate pressure (700 psig). Rupture of the RFG occurred at 1078 psig when the lower polar boss and load rings sheared through the grain. Pressure versus strain data indicate excellent structural compatibility of the composite motor. Initial failure was in the dome of the RFG at 1078 psig but extrapolation of the hoop strain data indicates the GFW case would have failed at an internal pressure on the RFG of 1140 psig if the RFG had not failed first.

INTRODUCTION

(C) The current ATP Reinforced Grain Program originally included the hydrotest of one 20-inch reinforced grain (RFG-7201) and one 20-inch reinforced grain-fiberglass case composite (RFG/GFW 7202/7401). These two tests were intended to provide design information for a multiple helix reinforced grain as well as structural compatibility data for fiberglass cases and reinforced grains containing high (5 percent) elongation aluminum wire. Reinforced grain 7202 was rejected after hydrotest of RFG 7201 and subsequent mechanical tests of the aluminum wire showed it to be below specification requirements. Mechanical tests of the wire showed that only three of twenty-four wire spools used in fabrication of RFG 7201 and 7202 met the minimum requirements of 5 percent elongation and the other twenty-one spools averaged about 2 percent elongation.

RFG/GFW 7204/7402 was added to the ATP program as a replacement for RFG/GFW 7202/7201 which was rejected and tested on a Rocketdyne-sponsored program. The reinforced plastic polar bosses in RFG/GFW 7204/7402 failed prematurely during hydrotest and transferred the pressure load to the GFW case. When the case ruptured the RFG ignited and burned all of the unit except the two polar bosses and a small portion of the GFW case. This hydrotest revealed a polar boss problem but still left evaluation of the structural compatibility of the RFG/GFW composite unaccomplished.

RFG/GFW 7205/7403 was added to the program and was designed and fabricated similar to RFG/GFW 7204/7402 except for the polar bosses and load rings which were made of 6061-T6 aluminum rather than reinforced plastic. This material substitution was made to preclude the possibility of failure of the bosses or load rings and to make certain that the structural compatibility of the RFG/GFW composite would be ascertained.

* Contracts: AF04(611)-8193 and AF04(611)-9090

DESIGN AND FABRICATION

RFG-7205

Fabrication Data

This reinforced grain design was identical to RFG-7204 and is shown in detail on drawing 99-802274. A drawing of the RFG/GFW case assembly is shown in Figure 1. This drawing shows forward and aft skirts which were not made. Grain, case, polar boss, and load ring details, however, are correct. Pertinent details affecting the structural capability of the reinforced grain are included in Table 1. Tables and figures are grouped together at the end of this report.

Design Basis

Considering the RFG as a thick wall isotropic cylinder gives a longitudinal stress σ_{z_G} of,

$$\sigma_{z_G} = \frac{P_i a^2}{b^2 - a^2} \qquad (1)$$

For a series of concentric thin cylinders, the maximum value of σ_{z_G} is given by the following:

$$\sigma_{z_G}(MAX) = \frac{f_w \sigma_w}{t_{TG}} \sum_{n=1}^{n=i} \cos^2 \alpha_n t_n \qquad (2)$$

(C) Near the polar boss, only the four geodesic layers support the longitudinal load and the maximum value of σ_{z_G} from equation (2) is 1242 psi.

$$\sigma_{z_G}(MAX) = \frac{(0.13)(45{,}000)}{1.45} [0.0762 + 0.0684 + 0.0735 + 0.0897]$$

$$= 1242 \text{ psi}$$

(C) The maximum pressure from equation (1) is 578 psig.

$$P_i(MAX) = \frac{1242 (8.325^2 - 6.875^2)}{(6.875)^2}$$

$$= 578 \text{ psig}$$

* Nomenclature is on page 835

(C) Previous tests of reinforced grains have indicated ultimate shear stress values between 17,700 psi and 20,700 psi in the aluminum wires crossing the polar boss and load rings based on the assumption that all wires were uniformly loaded in pure shear. The actual ultimate shear stress of the aluminum wires has not been determined but based on data from Reynolds Metal Company the ultimate shear stress of the wires should be approximately 24,300 psi. Maximum internal pressure based on shear of the wires at the polar boss is given by the following:

$$P_i(MAX) = 2\,\sigma_{s_w}\,N_w\left(\frac{D_w}{D_B}\right)^2$$

$$= 2(20{,}700)(22{,}776)\left(\frac{0.0075}{9.00}\right)^2$$

$$= \underline{653 \text{ psia}}$$

(C) This maximum pressure calculation is based on a shear stress of 20,700 psi which is the highest value from previous RFG tests. A maximum pressure of 558 psig results from using 17,700 psi as the ultimate shear stress of the wire and 766 psig pressure results from using Reynolds Metal Company shear stress of 24,300 psi.

(C) Minimum and maximum values of ultimate pressure based on shear at the polar boss are 558 psig and 766 psig, respectively. This spread of 208 psig is rather large but it is not as important as it appears because the RFG is pressure limited to 578 psig based on wire tension in the geodesic layers near the polar boss.

In the hoop or tangential direction, the stress is a maximum at the inside surface and is given by the following:

$$\sigma_{\theta_G}(MAX) = \frac{P_i(b^2 + a^2)}{b^2 - a^2} \tag{3}$$

The maximum tangential stress which the RFG can withstand is the composite stress which results when all wires are loaded to their ultimate stress and is given by the following:

$$\sigma_{\theta_G}(MAX) = \frac{\sigma_w f_w}{t_{TG}} \sum_{n=1}^{n=i} SIN^2 \alpha_n t_n$$

(C)

$$= \frac{(45000)(0.13)}{1.45} [0.038 + 0.0299 + 0.0254 + 0.0254 + 0.0495 + 0.0664 + 0.1013 + 0.0575 + 0.0665 + 0.0874 + 0.0545 + 0.0774 + 0.0928] \tag{4}$$

$$= \underline{4527 \text{ psi}}$$

(C) From equation (3) the maximum value of P_1 is 856 psig.

$$P_i(MAX) = 4527 \left(\frac{\overline{8.325}^2 - \overline{6.875}^2}{8.325^2 + 6.875^2} \right)$$

$$= \underline{856 \text{ PSIG}}$$

GFW CASE 7403

Fabrication Data

Drawing 99-802231 and Figure 1 show GFW case 7403 in the final assembly with RFG-7205. Table 2 shows the important structural parameters for this case.

Design Basis

(C) In the longitudinal direction

$$P_c = \frac{4N_H \cos^2 \alpha_H F_{EH}}{Di}$$

$$= \frac{4(404)\cos^2 23.85^\circ (8.50)}{16.40} \qquad (5)$$

$$= \underline{700 \text{ PSIG}}$$

(C) In the hoop direction,

$$P_c(MAX) = \frac{2}{Di}\left[N_c F_{Ec} + N_H \sin^2 \alpha_H F_{EH}\right]$$

$$= \frac{2}{16.40}\left[561(9.25) + 404 \sin^2 23.85^\circ (8.50)\right] \qquad (6)$$

$$= \underline{700 \text{ PSIG}}$$

RFG/GFW-7205/7403 COMPOSITE

The preceding sections of this report contain structural information about the individual components. In a composite structure, the load carrying ability of the composite is dependent not only upon the strength of the individual components but also upon the structural compatibility of all of the components.

(C) Calculations in this report show that initial failure of the RFG/GFW should occur between 558 psig and 1278 psig. These values represent the lowest pressure at which the reinforced grain will shear assuming no load is transmitted to the GFW case and the highest value at which the RFG/GFW composite will fail assuming perfect structural compatibility of the grain and case. The 1278 psig is obtained by adding the ultimate pressure of the GFW case (700 psig) to the ultimate shear pressure for the RFG. It has been assumed here that the RFG only will fail in tension or shear, or a combination of tension and shear near the polar boss at 578 psig which is the maximum pressure for the RFG only in the longitudinal direction.

Several analytical methods of calculating the stresses and strains in the composite RFG/GFW structure have been used. To date, these have all been limited to a two dimensional study of the cylindrical portion only. Calculations of ultimate pressure in this report and previous hydrotests of domed reinforced grains have shown the domes to be the critical area. Consequently, one of the principal objectives of the hydrotest of RFG/GFW-7205/7403 was to experimentally determine the structural compatibility of the composite.

HYDROTEST

TEST PROCEDURE

This unit, prior to hydrotest on December 17, 1963, is shown in Figure 2. It was filled with water and pressurized with Nitrogen. Strains in the GFW case were measured with ten low modulus strain gages. Four additional strain gages were located on the inside surface of the RFG and four linear potentiometers were used to measure displacement or longitudinal deflection of the cylindrical portion of the motor and the upper dome. A complete set of reduced data from all gages and a sketch showing the location of the individual gages is included in the appendix.

(C) The motor was pressurized to 1078 psig in approximately 17.7 seconds. Strain gages on the lower dome indicated a failure of the reinforced grain at this pressure. When the reinforced grain ruptured, the pressure load was transferred to the GFW case and as a result of the increased volume, pressure dropped to 475 psig in approximately 7.5 seconds. After the pressure dropped to approximately 450 psig, the circ wraps on the GFW case started breaking, and as can be seen in Figure 3, about 60 percent of the total circ wraps broke before the test was completed.

Figure 4 shows plots of pressure versus average hoop strain, average longitudinal strain, average strain in the direction of the fiber on the domes, and longitudinal displacement of the cylinder.

DISCUSSION OF RESULTS

Strains in the domes were very low as shown on previous tests but longitudinal strains in the cylinder for this test were negative. At first glance this negative strain appears to be impossible. However, with a thick wall cylinder, the longitudinal strain can be positive or negative dependent upon Young's modulus and Poisson's ratio of the material in both the longitudinal and hoop directions. The negative longitudinal strains were not expected in this test because previous tests of reinforced grains as well as the hydrotest of 20-inch RFG/GFW 7204/7402 showed positive longitudinal strains. The plot of pressure versus longitudinal displacement as shown in Figure 4 also casts some doubts on the negative strain measurements because it shows positive displacement. In order for both negative strain and positive displacement data to be correct, the strain would have to change direction toward the ends of the cylindrical portion of the motor and give an average positive strain even though the strain at the center of the cylinder was negative. This condition is hard to visualize and will have to be proved or disproved on future tests.

(C) The most important fact which is shown by the data from this test is the hoop strain in the GFW case. Initial failure of the RFG/GFW composite was in the RFG in the axial direction near the polar boss and was the typical shear or shear-tension combination type of failure. Figure 4 shows, however, that even if the RFG had not sheared at 1078 psig the GFW case was on the verge of failing in the hoop direction. Average strain of the two hoop gages as shown in Figure 4 was 2.54 percent at 1078 psig. Extrapolation of the pressure versus average hoop strain curve, as shown by the dotted portion of the curve in Figure 4, indicates the GFW case would have failed at 1140 psig and 3.0 percent strain if the RFG had not failed previously. This is an increase of only 5.75 percent over the actual burst pressure and indicates a well balanced composite structure.

Another item of importance from the hydrotest of RFG/GFW 7205/7403 was confirmation of the design approach. Preliminary designs of 30 and 36-inch diameter motors had been made prior to this test and were based upon the same design methods as the 20-inch diameter motors. Data from this test indicates the structural design for the 30 and 36-inch diameter motors should be satisfactory for internal pressure loading.

Structural compatibility of the RFG, GFW case and polar bosses was also an important item which was verified. This was the first hydrotest of a reinforced grain motor with rigid (aluminum) polar bosses and load rings. Although the polar bosses and load rings were rigid as compared with the RFG, the structural behavior of the unit was excellent.

CONCLUSIONS

1. Structural compatibility of the reinforced grain and fiberglass case was excellent.

2. The current design method for reinforced grain motors is satisfactory for internal pressure.

3. Polar bosses can be made rigid in relation to the reinforced grain and still function satisfactorily from a structural standpoint.

(C) 4. Ultimate pressure (1078 psig) of RFG/GFW 7205/7403 was 74 percent higher than RFG/GFW 7204/7402 (620 psig) and is attributed to the improved polar bosses.

NOMENCLATURE

σ_{ZG} Longitudinal stress in the reinforced grain.

$\sigma_{\theta G}$ Tangential or hoop stress in the reinforced grain.

σ_w Tensile stress of the aluminum wire.

σ_{sw} Shear stress of the aluminum wire.

f_w Volume fraction of the aluminum wire.

N_w Number of wires crossing the polar boss and load rings.

N_H, N_c Number of ends per inch in the direction of the helical and circ roving respectively.

D_w Diameter of the aluminum wire.

D_B Outside diameter of the polar boss or the outside diameter of the inside load ring.

P_i Internal pressure.

a Inside radius of reinforced grain.

b Outside radius of reinforced grain.

t_n Thickness of the nth layer of reinforced grain.

α_n Wrap angle the wire in the nth layer makes with the longitudinal axis of the motor.

t_{TG} Total thickness of the reinforced grain.

α_H Wrap angle the helical roving makes with the longitudinal axis of the motor.

F_{E_H}, F_{E_c} Break strength of a single helical and circ end respectively.

D_i Inside diameter of the glass filament wound case.

TABLE 1

(C) REINFORCED GRAIN 7205 DESIGN AND FABRICATION DATA

	Design	As Fabricated
Aluminum Wire		
Nominal Diameter, inch	0.0075	0.0075
Minimum Ultimate Strength, psi	50,000	45,000
Minimum Elongation, percent	5.0	5.0
Average Weight Fraction, percent	20.0	18.5
Number of Wires in Warp	24	24
Warp Width, inch	1.080	1.080
Geodesic Isotensoid Layers		
Layer No. 1		
Winding Angle, deg	35.5	35.5
Thickness, inch	0.115	0.115
No. of Covers	7	7
Layer No. 2		
Winding Angle, deg	33.3	33.3
Thickness, inch	0.099	0.107
No. of Covers	6	6
Layer No. 3		
Winding Angle, deg	30.5	30.5
Thickness, inch	0.099	0.083
No. of Covers	6	6
Layer No. 4		
Winding Angle, deg	28.0	28.0
Thickness, inch	0.115	0.0985
No. of Covers	7	7
Fill Layers *		
1-A		
Winding Angle, deg	45.0	45.0
Thickness, inch	0.099	0.0905
No. of Covers	6	6
1-B		
Winding Angle, deg	55.0	55.0
Thickness, inch	0.099	0.0865
No. of Covers	6	6
1-C		
Winding Angle, deg	70.0	70.0
Thickness, inch	0.115	0.0885
No. of Covers	7	7
2-A		
Winding Angle, deg	45.0	45.0
Thickness, inch	0.115	0.1045
No. of Covers	7	7
2-B		
Winding Angle, deg	55.0	55.0
Thickness, inch	0.115	0.099
No. of Covers	7	7
2-C		
Winding Angle, deg	70.0	70.0
Thickness, inch	0.099	0.077
No. of Covers	6	6
3-A		
Winding Angle, deg	40.0	40.0
Thickness, inch	0.138	0.1345
No. of Covers	8	8
3-B		
Winding Angle, deg	50.0	50.0
Thickness, inch	0.138	0.138
No. of Covers	8	8
3-C		
Winding Angle, deg	64.0	64.0
Thickness, inch	0.115	0.115
No. of Covers	7	7
Inside Diameter, inch	13.750	13.750
Outside Diameter, inch	16.65	16.318
Web Thickness, inch	1.45	1.284
Average Buildup Per Cover, inch	0.0165	0.0146
Total Number of Wires Crossing Polar Boss Flange and Load Rings	22,776	22,776

*1-A, 1-B, and 1-C indicates first, second and third fill respectively following geodesic isotensoid layer No. 1

TABLE II

GFW CASE 7403 DESIGN AND FABRICATION DATA

	Design*	As Fabricated
Fiberglass	S-994	S-994
Helical Wraps		
Ends per Roving	12	12
Wrap Angle, deg	23.85	23.85
No. of Ends per inch	404	404
No. of Covers	1	1
Thickness, inch	0.015	0.018
Circ Wraps		
Ends per Roving	20	20
Wrap Angle, deg	90-	90-
No. of Ends per inch	561	561
No. of Covers	2	2
Thickness, inch	0.019	0.017
Resin	DER 332	DER 332
Curative	EMI-8 PPH	EMI-8 PPH
Resin Content, weight percent	20.0	24.2
Inside Diameter, inch	16.40	16.40
Outside Diameter, inch	16.47	16.47
Thickness, inch	0.034	0.035

*Design was changed from drawing 99-802274 to match "as fabricated" RFG 7205.

PREVIOUS PAGE WAS BLANK, THEREFORE WAS NOT FILMED

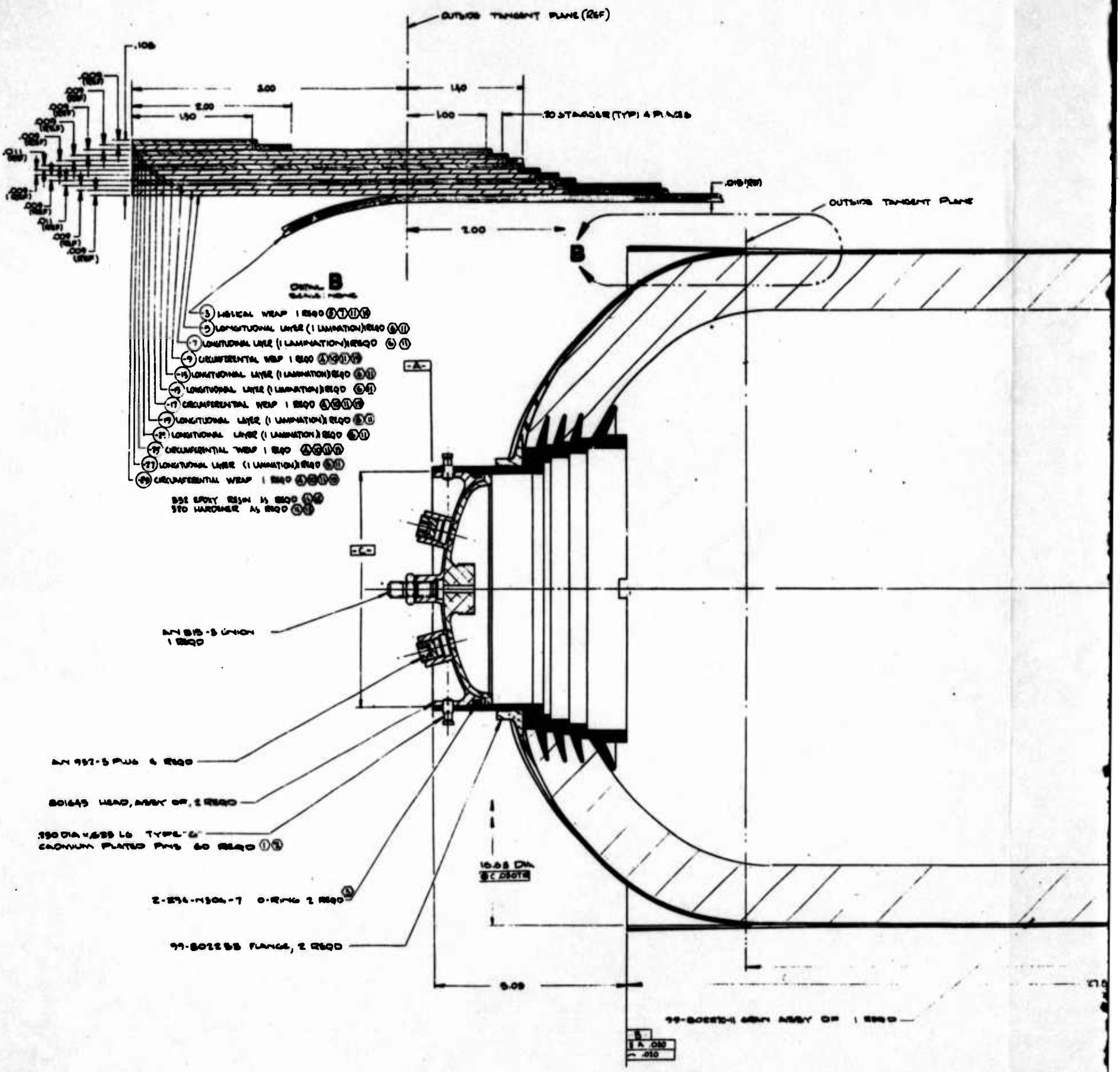
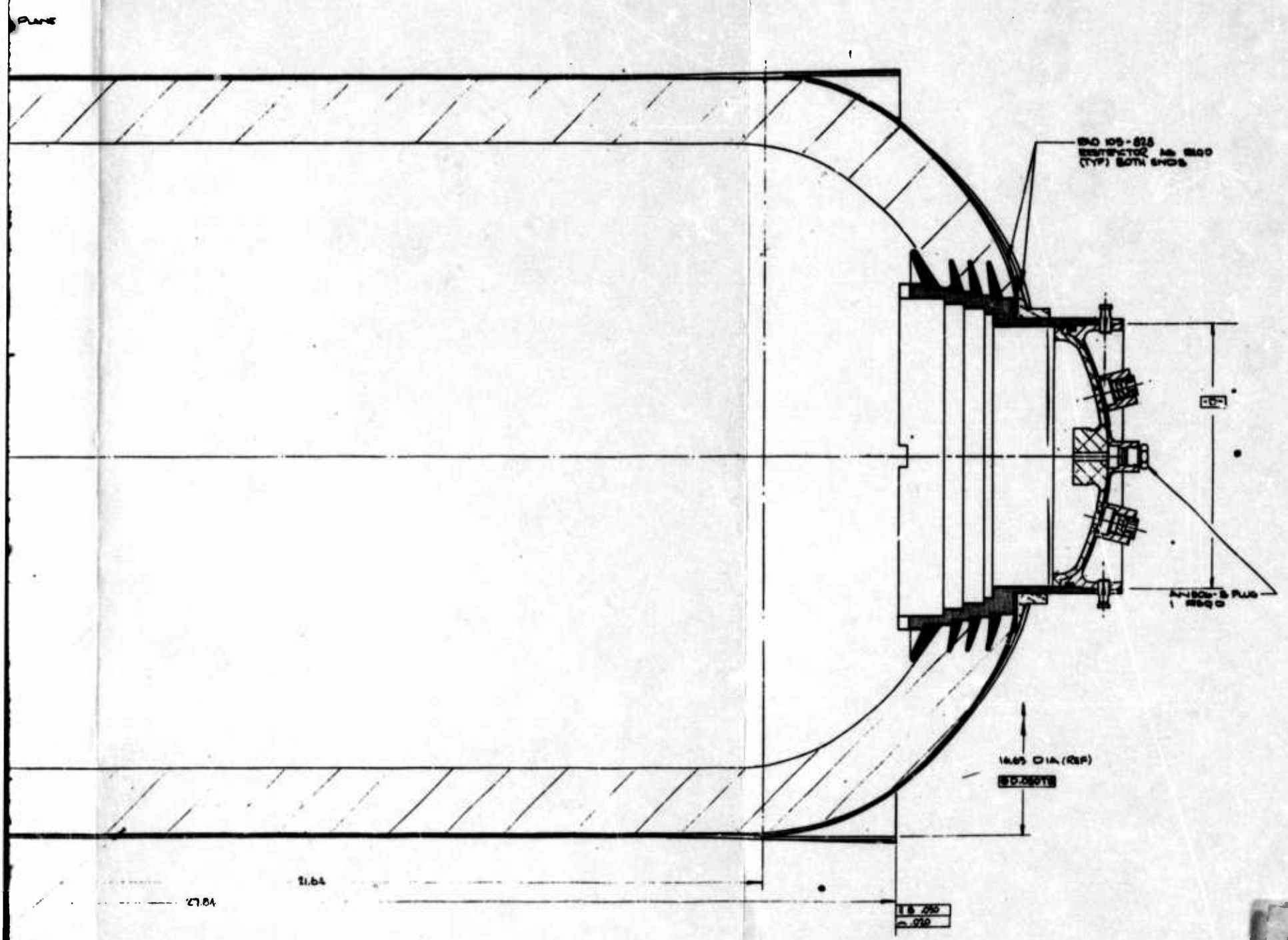


Figure 1. RFG/GFW 7205/7403 Assembly



2

CONFIDENTIAL

PREVIOUS PAGE WAS BLANK, THEREFORE WAS NOT FILMED

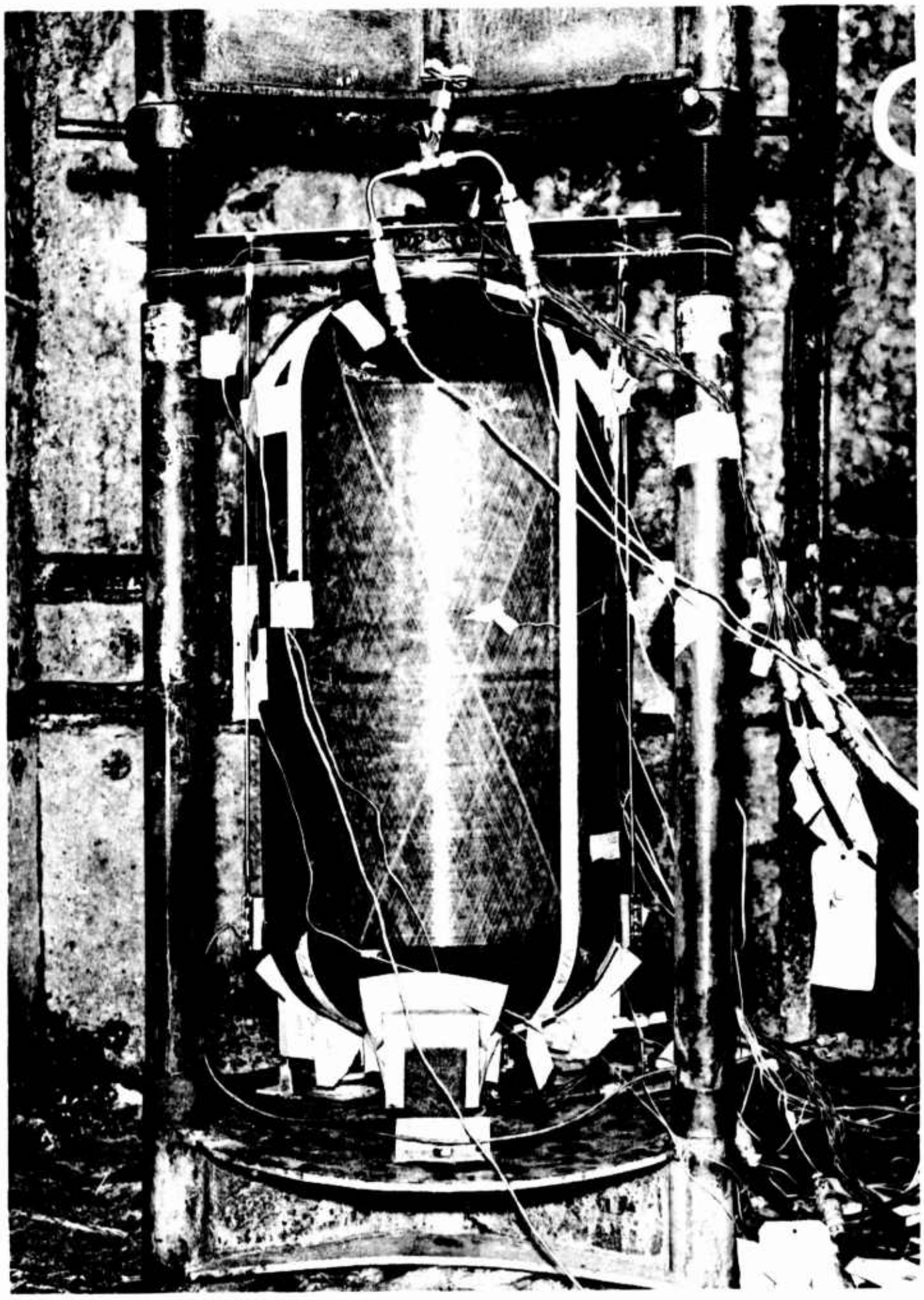


Figure 2. RFG/GFW 7205/7403 Before Hydrotest

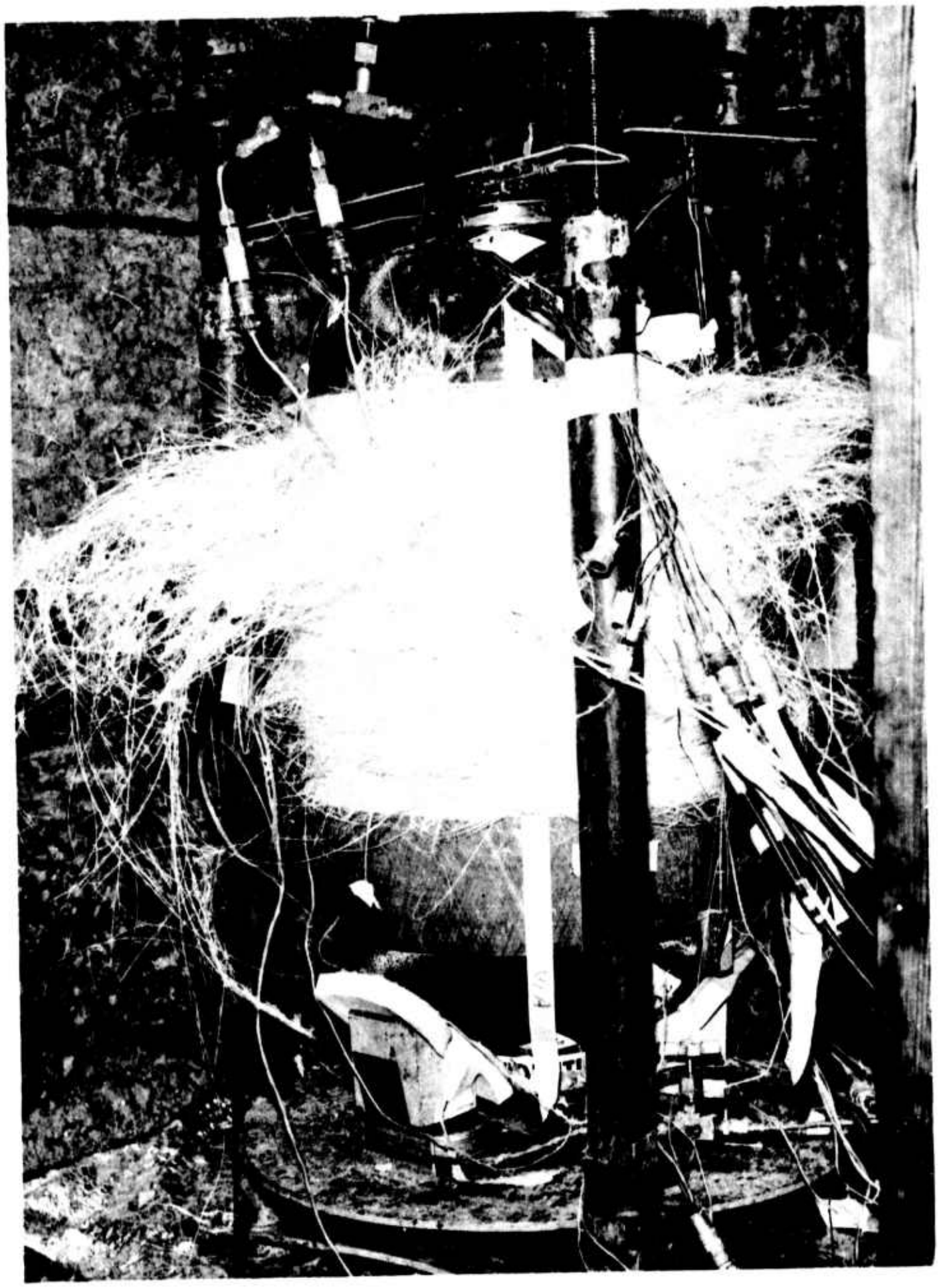


Figure 3. RFG/GFW 7205/7403 After Hydrotest

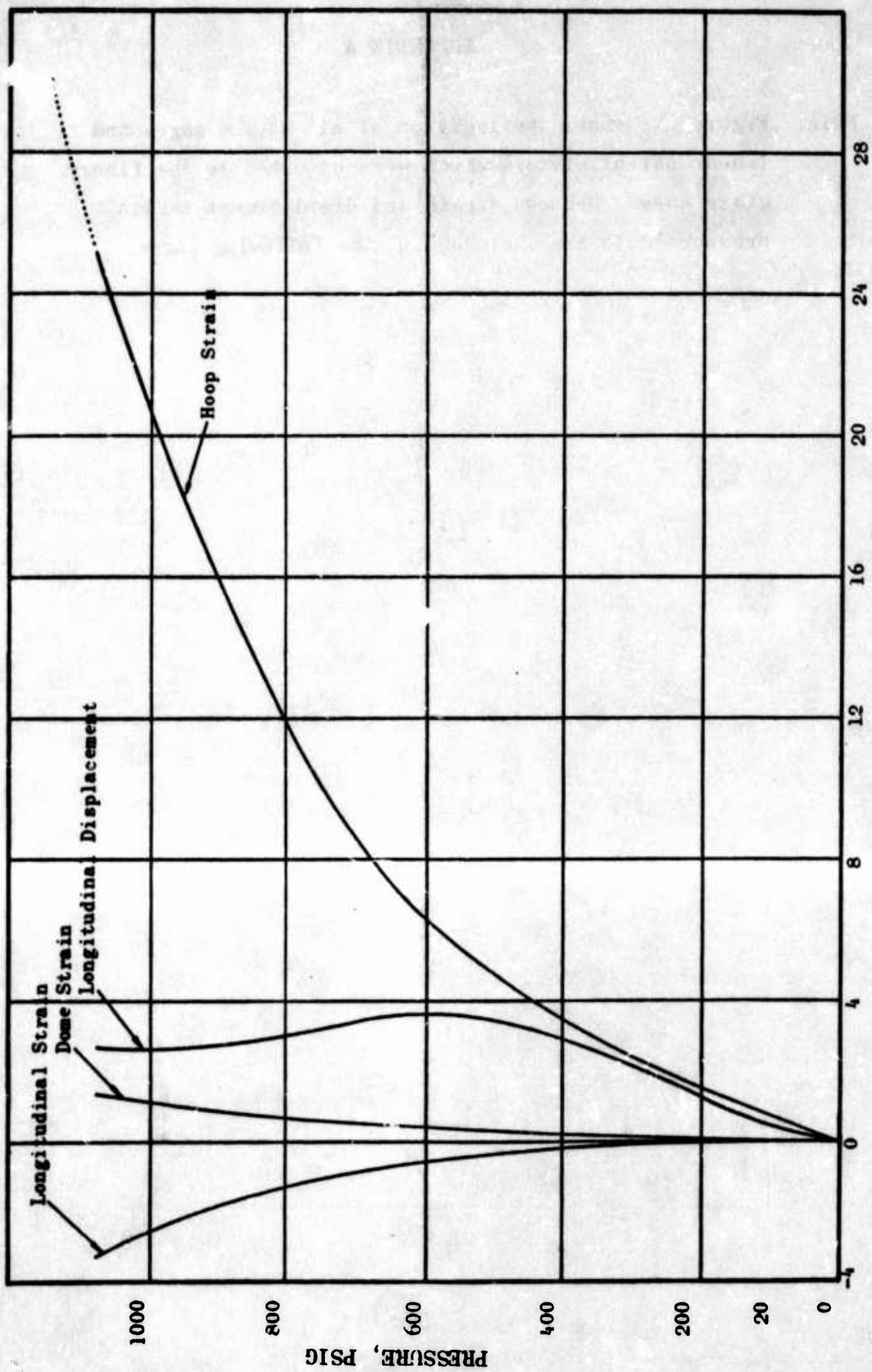
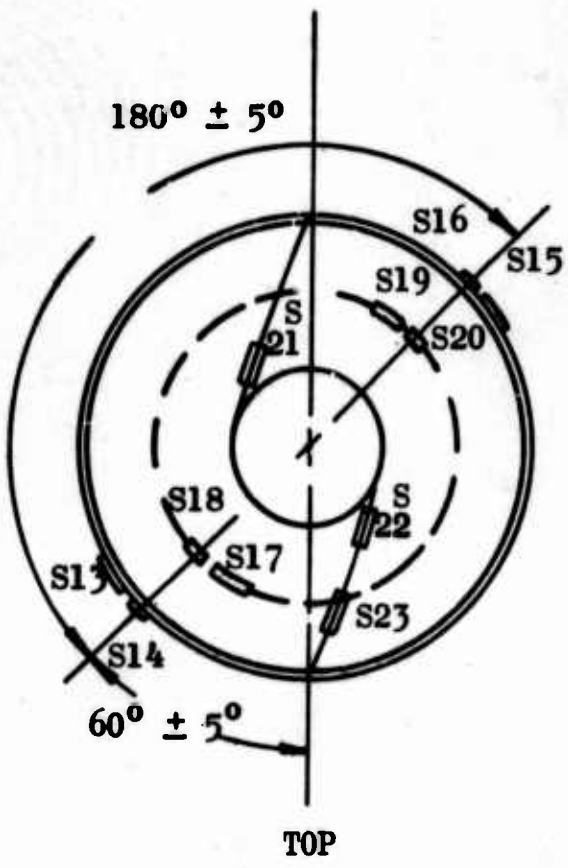


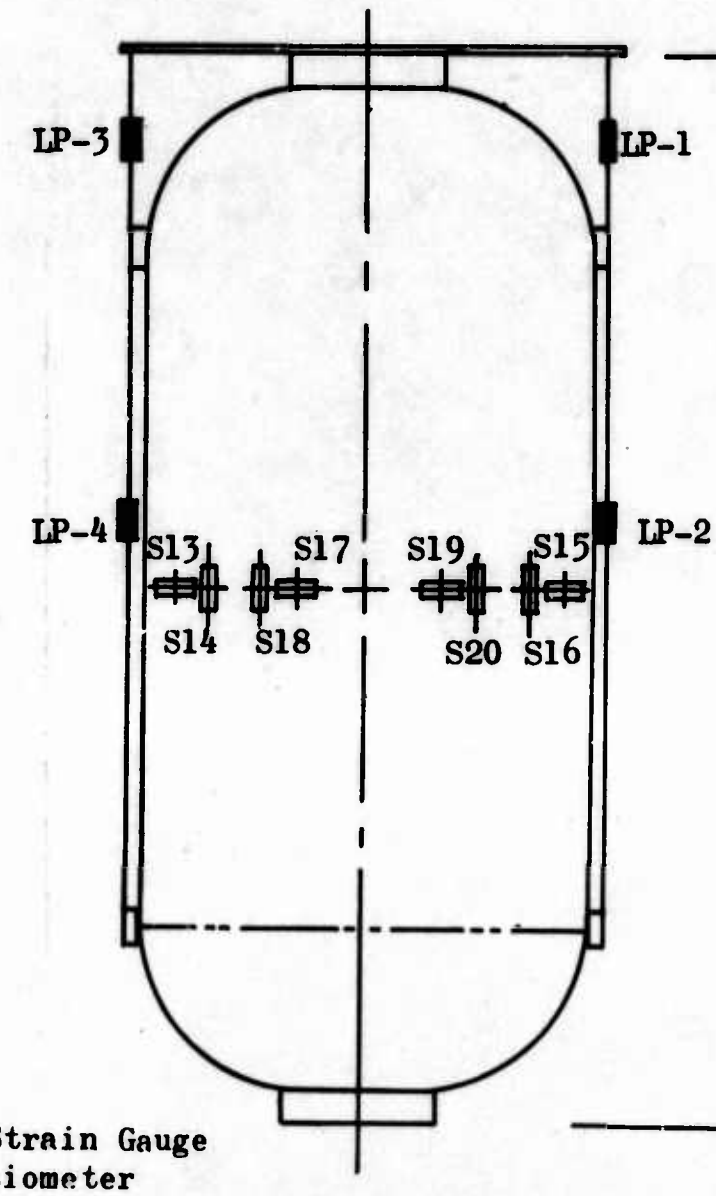
Figure 4. Pressure Versus GFW Case Strain and Deflection

APPENDIX A

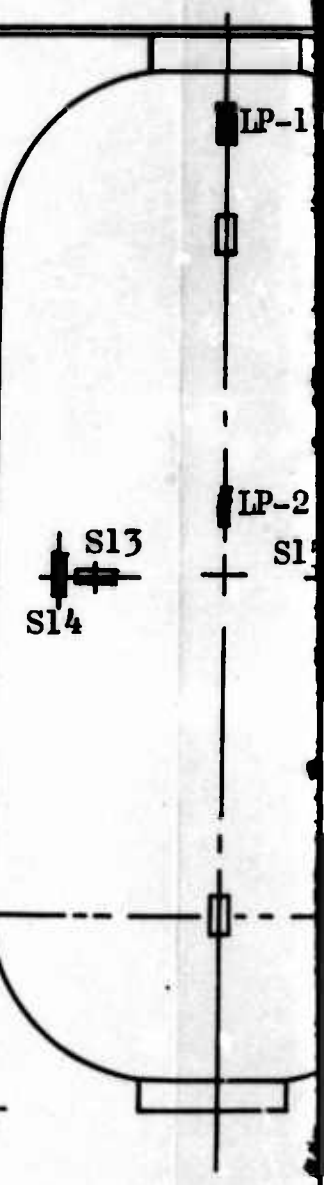
NOTE: Figure 5 shows the location of all strain gages and linear potentiometers which were attached to the fiber-glass case. Reduced strain and displacement versus pressure data are included in the following pages.



TOP



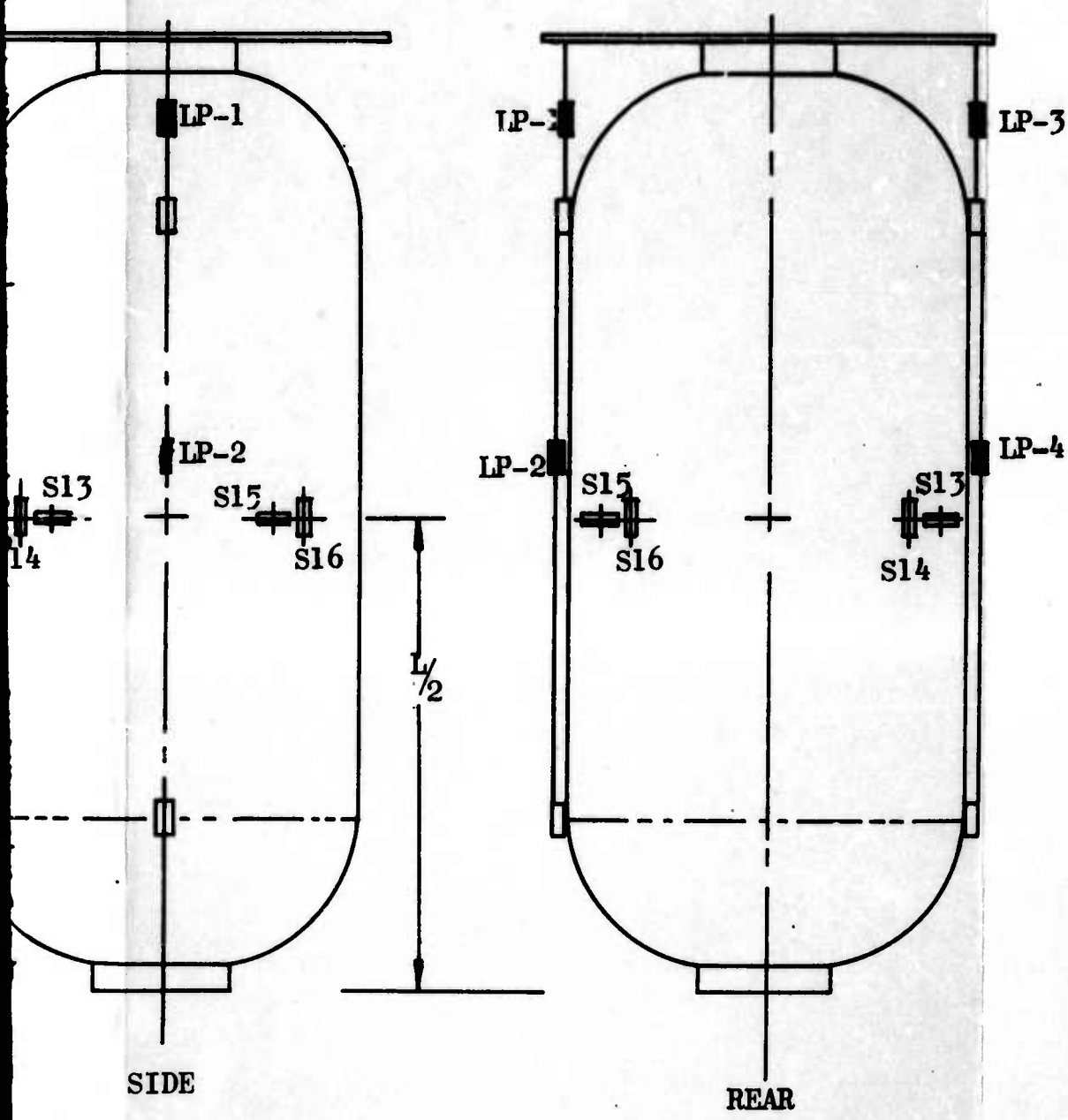
FRONT



SIDE

SYMBOLS:

S-XX Single Axis Strain Gauge
LP-X Linear Potentiometer



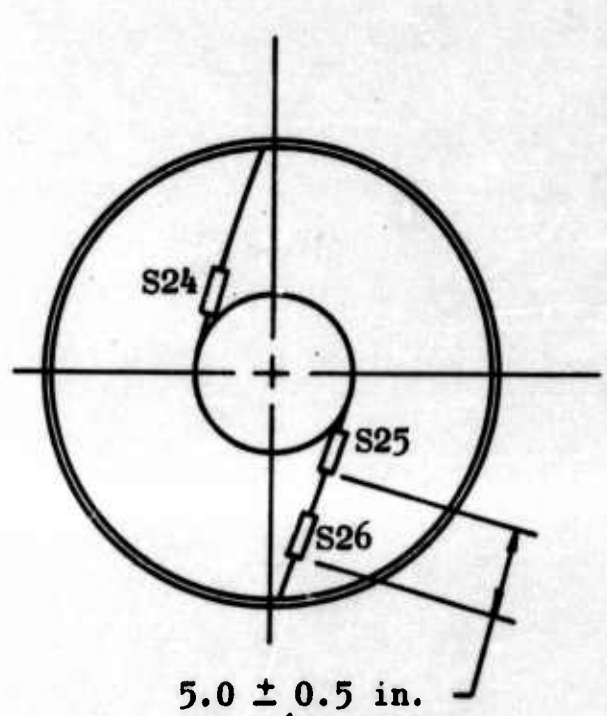


Figure 5. Strain Gage and Linear Potentiometer Location

2

PREVIOUS PAGE WAS BLANK, THEREFORE WAS NOT FILMED

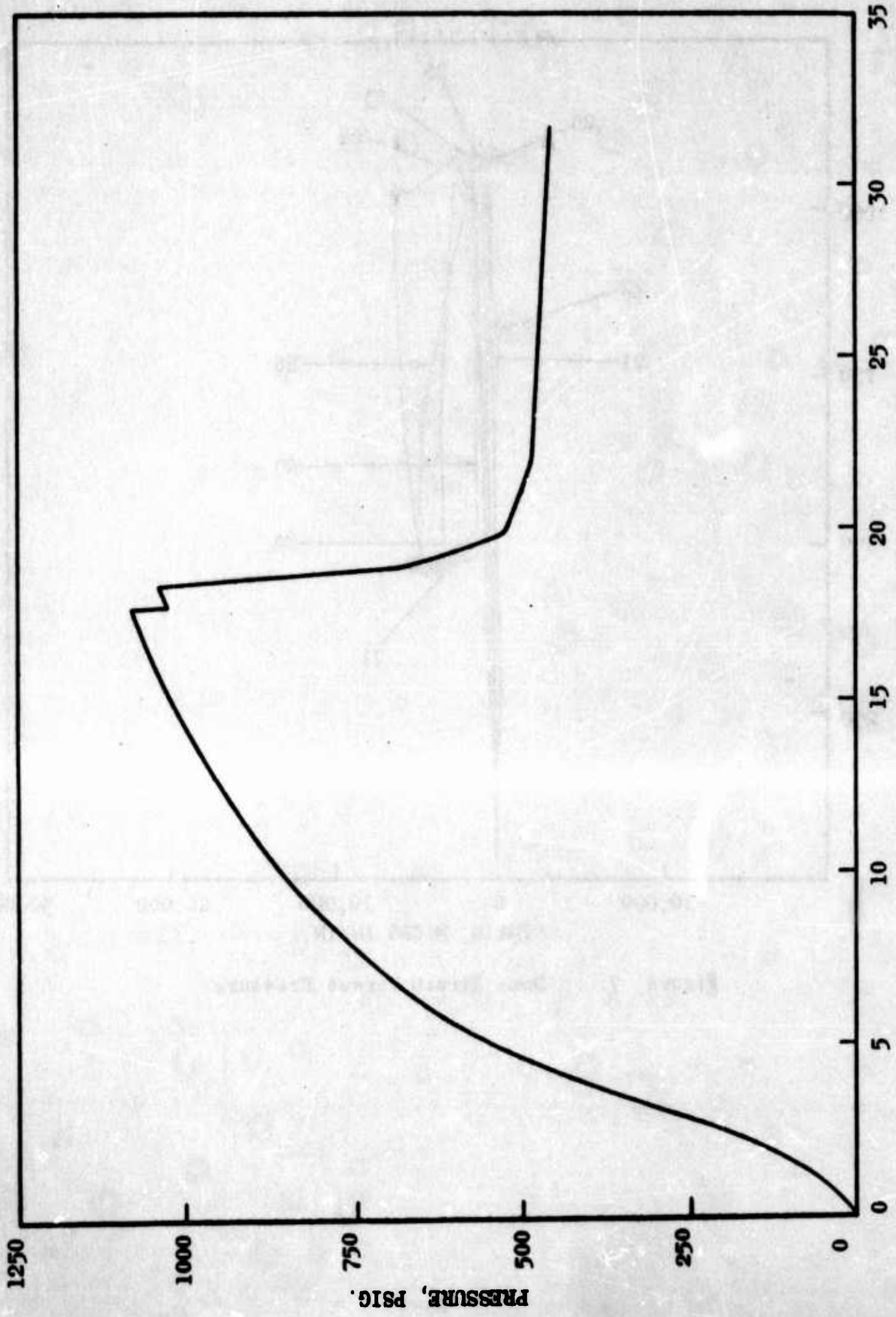


Figure 6. Internal Pressure Versus Time

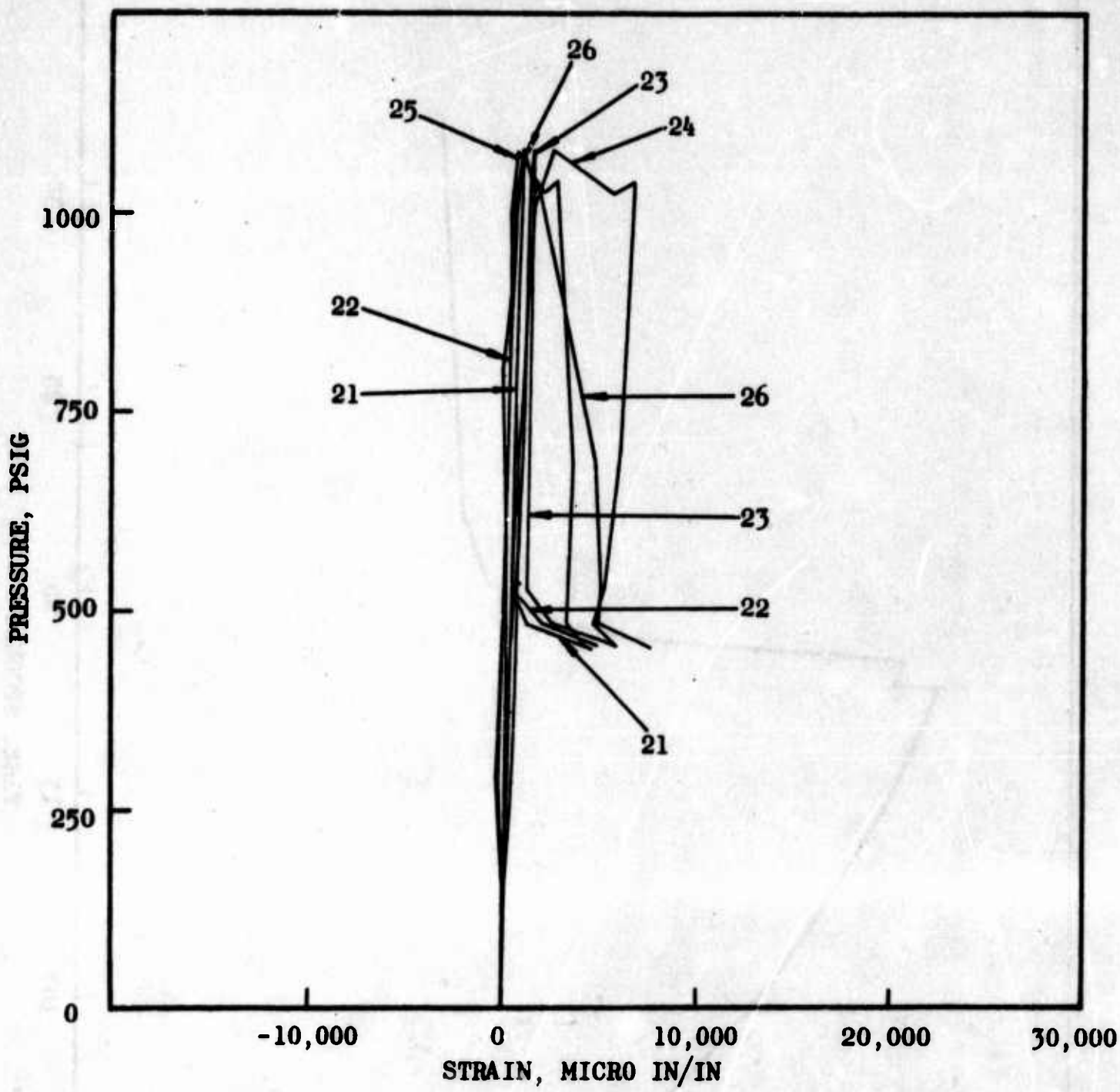


Figure 7. Dome Strain Versus Pressure

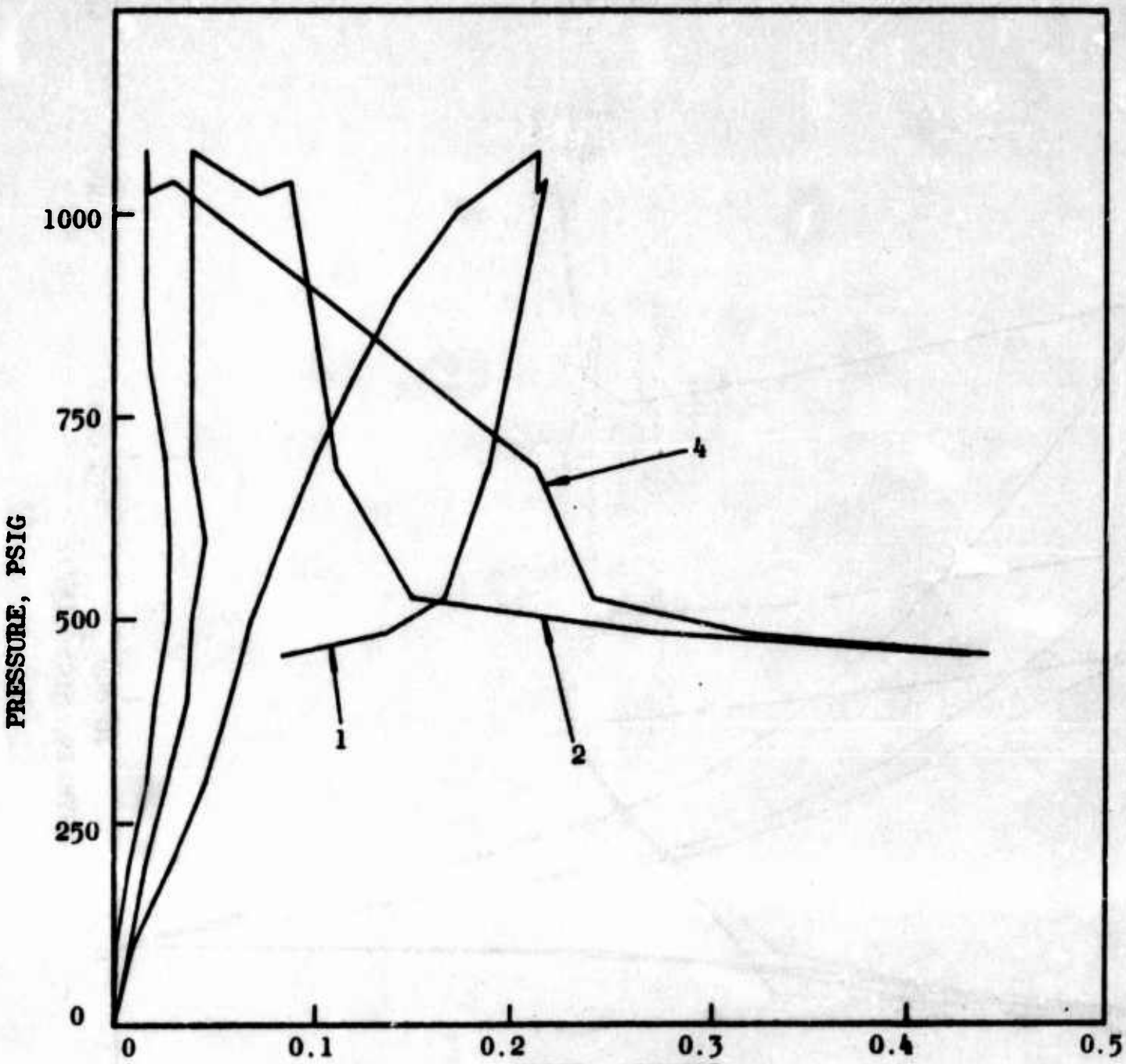


Figure 8. Cylinder and Dome Displacement Versus Pressure

CONFIDENTIAL

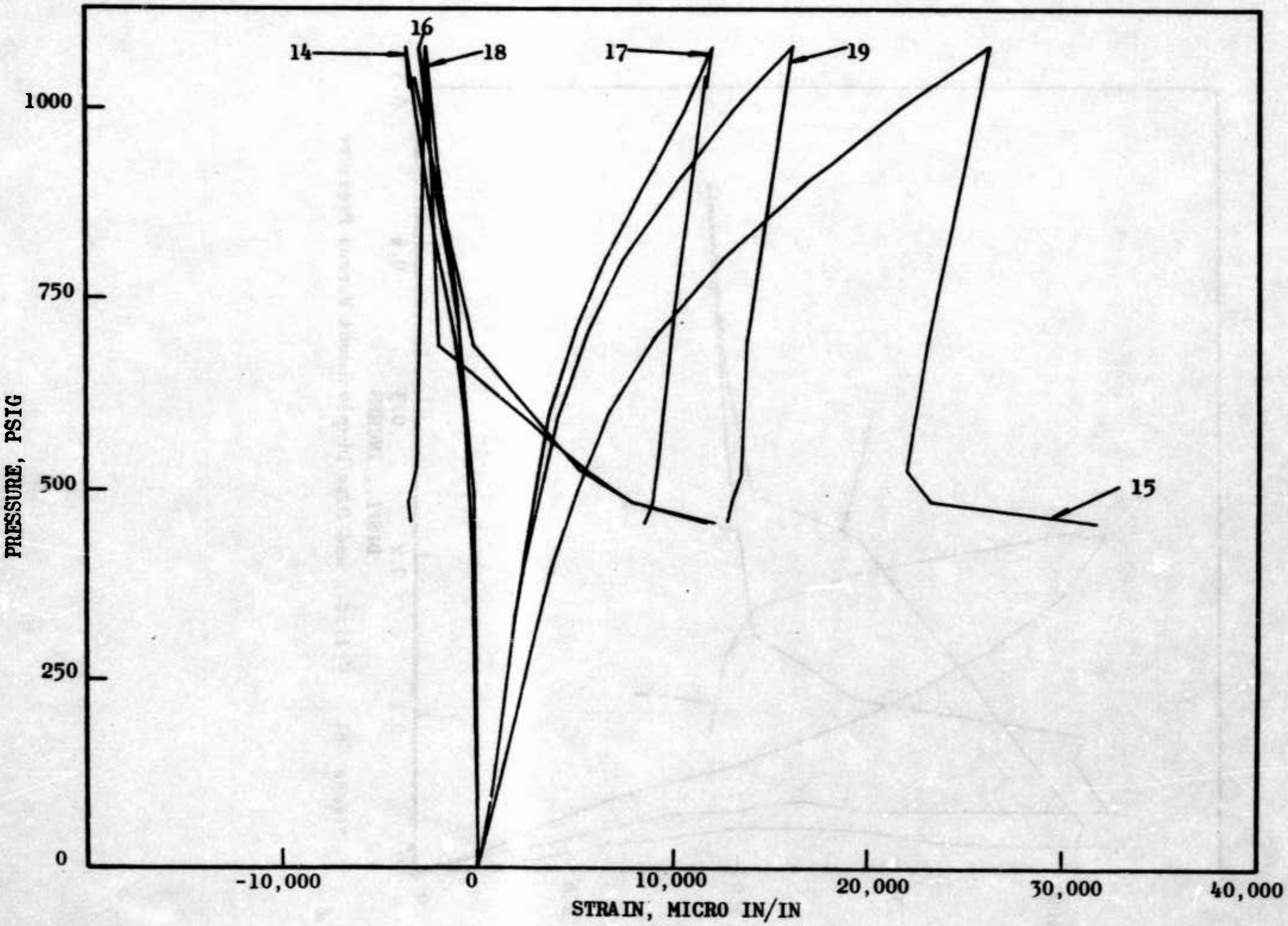


Figure 9. Cylinder Strain Versus Pressure

CONFIDENTIAL

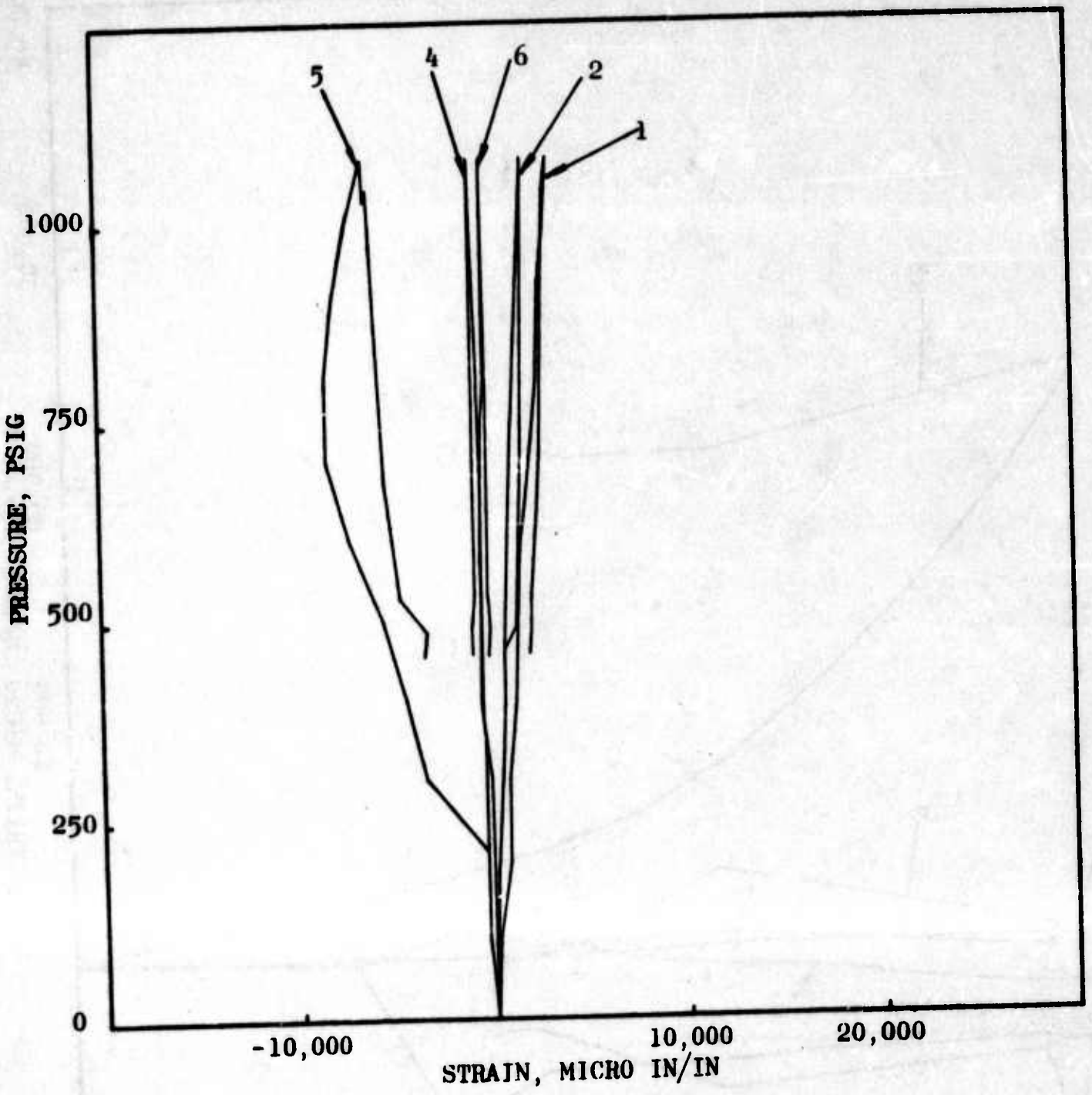


Figure 10. Polar Boss Strain Versus Pressure

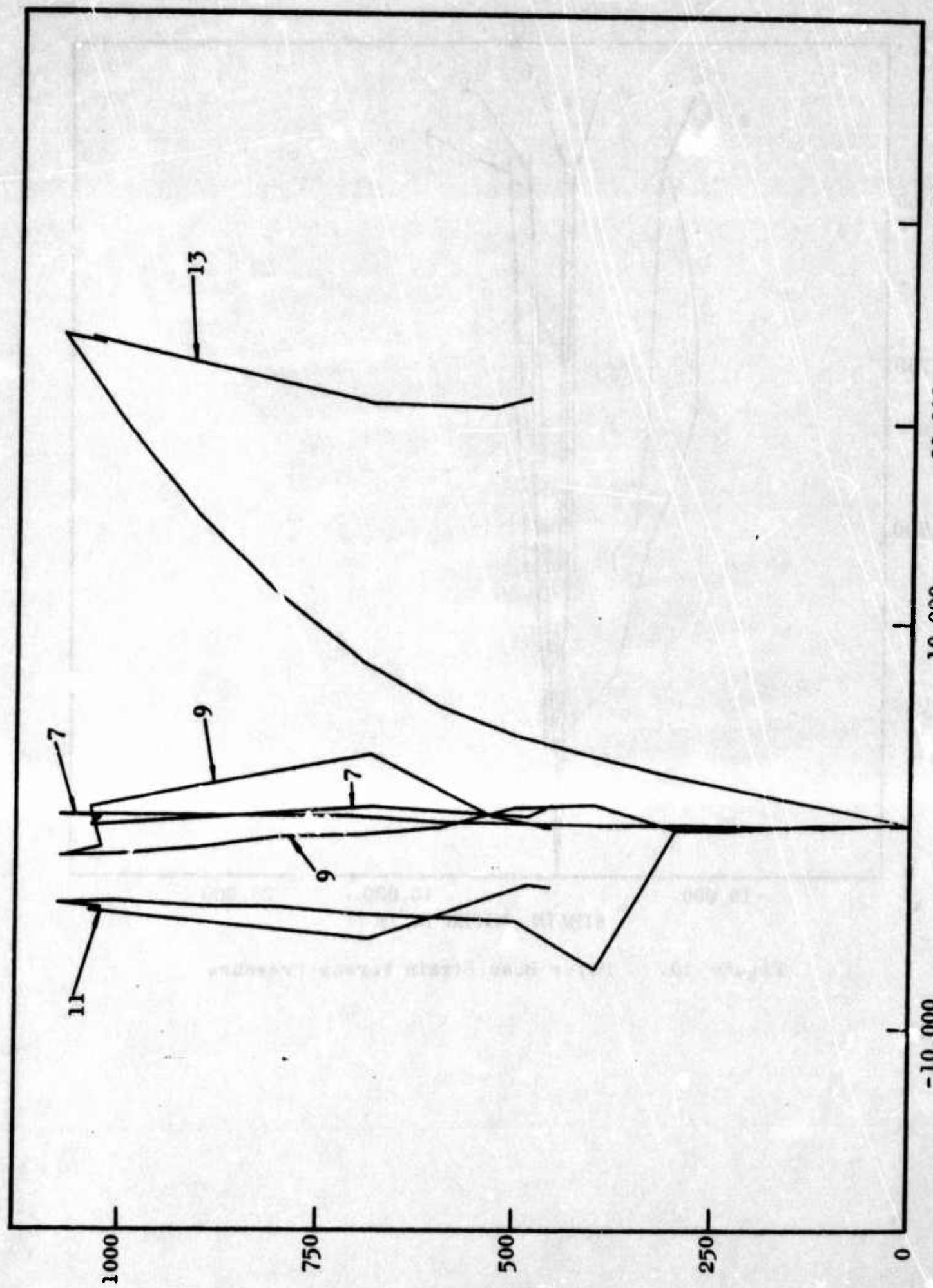


Figure 11. Polar Boss and Gfw Hoop Strain Versus Pressure

APPENDIX II

HEAT TRANSFER METHODS OF ANALYSIS

PREVIOUS PAGE WAS BLANK, THEREFORE WAS NOT FILMED

HEAT TRANSFER METHODS OF ANALYSIS

This heat transfer analysis considers the effects of convection, conduction, and radiation heat transfer in connection with ablation and corrosion losses of applicable components. The prime factors of interest are the depth of material lost due to corrosion and ablation and the temperature distribution at the end of the firing duration.

CONVECTION HEAT TRANSFER

The first mode of heat transfer to be considered is convection. In order to calculate the convective heat transfer the convective heat transfer coefficient must be determined. For this analysis the Bartz equation presented in Reference (1) will be used to determine the convective heat transfer coefficient.

Bartz' equation is:

$$h_c = \left[\frac{0.026}{(D_*)^{.6}}\left(\frac{(\mu)^2 C_p}{(P_r)^{.6}}\right)\left(\frac{P_c g}{c^*}\right)^{.8}\left(\frac{D_*}{D}\right)^{.1}\right]\left(\frac{A_*}{A}\right)^{.9}\sigma' \qquad (1)$$

where

$$\mu = (46.6\times10^{-10})(\bar{m})^{.5}(T_0)^{.6} \tag{2}$$

$$P_r = \frac{4\gamma}{9\gamma-5}. \tag{3}$$

$$\sigma' = \frac{1}{\left[\frac{T_w}{T_0}\left(1+\frac{\gamma-1}{2}M^2\right)+\frac{1}{2}\right]^{(.8-\frac{w}{6})}\left[1+\frac{\gamma-1}{2}M^2\right]}. \tag{4}$$

Thus the rate of convective heat transfer is

$$q_c = h_c(T_R - T_W). \tag{5}$$

The recovery temperature, Tr is given by;

$$T_r = [1+(P_r)^{1/3}(\tfrac{\gamma-1}{2})M^2]T_s. \tag{6}$$

The convective heat transfer is a major contributor to the heat load in regions of high velocity flow. Thus the main heat loading in the nozzle will be due to convective heat transfer.

RADIATION HEAT TRANSFER

The second mode is that of radiation heat transfer. The heat transferred to the surface due to radiation from the combustion gases is:

$$q_r = h_r(T_s - T_w). \tag{7}$$

where h_r is given by;

$$h_r = \frac{(0.174)\times10^{-8}\epsilon_g(T_s^4 - T_w^4)}{(T_s - T_w)}. \tag{8}$$

Radiation heat transfer is the major mode of heat transfer in regions of low velocity gas flow. Thus the major heat loading of parts in the forward and aft head will be due to radiation.

CONDUCTION HEAT TRANSFER

The third and final mode of heat transfer is conduction. Assuming one dimensional heat flow, the Fourier heat conduction equation is:

$$\frac{\partial^2 T}{\partial x^2} = \frac{1}{\alpha} \frac{\partial T}{\partial \tau} . \tag{9}$$

where, for the present analysis, the boundary conditions are given by:

$$T(0, \tau) = T_w . \tag{10}$$

$$\frac{\partial}{\partial x}(T(L, \tau) = 0. \tag{11}$$

$$T(x, 0) = T_i . \tag{12}$$

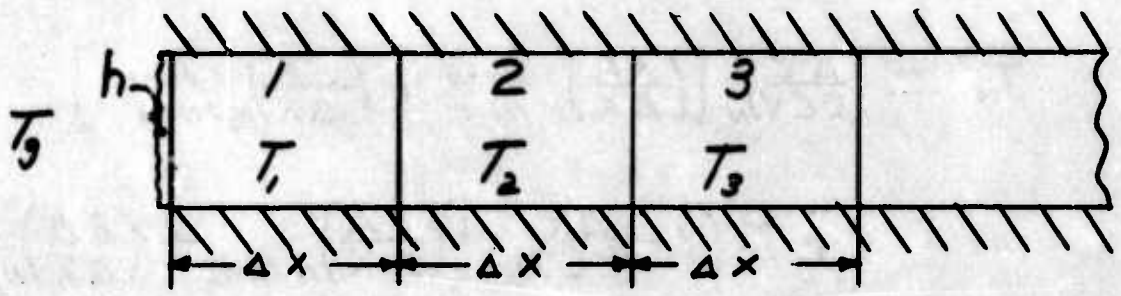
and T_w is determined from Equations (5) and (7).

Difficulties associated with evaluation of the boundary condition described by Equation (10) have prevented a rigorous solution of Equation (9). Thus a numerical means of determining the heat transfer due to conduction was employed. The method chosen is that of finite difference and for small increments of time and distance gives very good results.

The analysis proceeds as follows: First divide the material(s) into a finite number of small nodes. Then write a heat balance for each node using:

$$q_{IN} - q_{OUT} + q_{STORED} = 0. \tag{13}$$

Looking at three nodes for example, as shown below.



Nodes for Finite Difference Analysis

the heat flow into Node 2 over the time increment $\Delta\tau$ is

$$q_{IN} = \left(\frac{KA}{\Delta X}\right)_{1,2}(T_1 - T_2)\,\Delta\tau \tag{14}$$

The heat flowing out of Node 2 is

$$q_{OUT} = \left(\frac{KA}{\Delta X}\right)_{2,3}(T_2 - T_3)\,\Delta\tau. \tag{15}$$

The heat stored by Node 2 over the same time increment is

$$q_{STORED} = [\rho CV]_2(T_2' - T_2). \tag{16}$$

where T_2^1 is the new temperature of Node 2 at time $(\tau + \Delta\tau)$.

Substituting Equations 14, 15, and 16 into 13 and simplifying yields:

$$T_2' = \frac{\Delta\tau}{(\rho CV)_2}\left[\left(\frac{KA}{\Delta X}\right)_{1,2}T_1 + \left(\frac{KA}{\Delta X}\right)_{2,3}T_3\right] + T_2\left(1 - \frac{\Delta\tau}{(\rho CV)_2}\left[\left(\frac{KA}{\Delta X}\right)_{1,2} + \left(\frac{KA}{\Delta X}\right)_{2,3}\right]\right). \tag{17}$$

From Equation 17 one can easily see that the general form of the conduction equation for internal nodes is:

$$T_N' = \frac{\Delta\tau}{(\rho CV)_N}\left[\left(\frac{KA}{\Delta X}\right)_{N,(N-1)}T_{(N-1)} + \left(\frac{KA}{\Delta X}\right)_{N,(N+1)}T_{(N+1)}\right] + T_N\left(1 - \frac{\Delta\tau}{(\rho CV)_N}\left[\left(\frac{KA}{\Delta X}\right)_{N,(N-1)} + \left(\frac{KA}{\Delta X}\right)_{N,(N+1)}\right]\right). \tag{18}$$

Applying Equation 13 in the same manner to the surface Node 1 yields:

$$T_1' = \frac{\Delta\tau}{(\rho CV)_1}\left[hA_1 T_g + \left(\frac{KA}{\Delta X}\right)_{1,2} T_2\right]$$

$$+ T_1\left(1 - \frac{\Delta\tau}{(\rho CV)_1}\left[hA_1 + \left(\frac{KA}{\Delta X}\right)_{1,2}\right]\right). \qquad (19)$$

which is the conduction equation for a node with finite surface resistance. Conduction heat transfer is the means by which the heat loads brought to the wall material by convection and radiation are absorbed and transmitted through the wall materials. It is from this mode of heat transfer that the ablation and temperature distribution are determined.

TEMPERATURE DISTRIBUTION

The prime interest of any heat transfer analysis is to determine the temperature distribution in the wall material(s). The temperature distribution of the material(s) can be calculated by using Equations (5), (7), and (19) simultaneously. Equations (5), (7), and (19) have been programmed on an IBM7094 high speed digital computer to facilitate solution of applicable heat transfer problems. These computer programs were used in this analysis.

ABLATION

Ablation is defined as the degradation and removal of material due to heating. In this analysis the ablation of material is computed by checking each nodal temperature against the temperature of ablation of

the material, (Ta). When the ablation temperature is reached the node is held at this temperature until sufficient heat flows into the node to be equivalent to the heat capacity of the node (H_{eff}) and the node then is eliminated. This procedure is repeated in conjunction with Equations (5), (7), and (19) for the duration of the firing.

The ablative capacity of the node is given by:

$$q_{ABLATION} = \rho V H_{eff.} \tag{20}$$

where

ρ = density of material.

V = volume of node.

H_{eff} = effective heat of ablation obtained from test data.

Although material is lost due to ablation, this sacrifice of material is justified by the amount of heat consumed to remove this material. The heat consumed in this process eliminates heat which would normally be absorbed and transmitted by the remaining material(s). Thus ablation losses are justified by the reduction of heat loading.

CORROSION

The increase in nozzle throat diameter during firing can seriously affect the efficiency of the motor if the losses are large and not compensated for in the ballistic design. Since many nozzles, including the Motor A nozzle, are designed with throat regions of graphite, or graphite based materials, a means of determining the loss of graphite during firing was

sought. The method by which these losses may be predicted is given here briefly*, and is based on approaches found in Reference 2.

The loss of graphite in inches per second is given by:

$$\dot{R} = \frac{h B^* \phi}{\rho C_p} . \qquad (21)$$

where:

h_c = Convection heat transfer coefficient.

B^* = Reactivity constant which is a function of temperature and concentration of the various gas species composing the combustion gas.

ρ = Density of the graphite.

C_p = Specific heat at constant pressure of the combustion gas.

ϕ = An empirical function of temperature and pressure to compensate for the non-equilibrium conditions in a nozzle.

The reacitivity constant B* is given by:

$$B^* = B_1 M_1 + B_2 M_2 + B_3 M_3 + \cdots B_N M_N . \qquad (22)$$

where:

B_1, B_2, B_3, etc. = The reactivity constant for each gas specie in the combustion gas.

The empirical relations for ϕ are presented in the following tabulation.

---

* A complete presentation of the corrosion analysis is to be presented in a forthcoming Design and Development Section Memo.

Empirical Relations for ϕ

(C)

T_{wall}	Chamber Pressure	ϕ
> 4221 F	< 870 psi	$0.0878(1-e^{-(P\times10^{-2})})+2P\times10^{-6}$
> 4221 F	> 870 psi	$(1.146)P(e^{(P\times10^{-4})}-1)\times10^{-3}$
< 4221 F	> 870 psi	$(1.146)P(e^{(P\times10^{-4})}-1)\times10^{-3}$
< 4221 F	< 870 psi	$0.0878(1-e^{-(P\times10^{-2})})+2P\times10^{-6}$

The ϕ presented in the above listing should be used only for the regions indicated by the chamber pressure and wall temperature. As the pressure and wall temperature change during the firing duration, the corresponding ϕ is selected.

SUMMARY OF METHOD OF ANALYSIS

The method used in this analysis was to combine Equations (5), (7), (19), (20), and (21) in finite difference equations. These equations were programmed for use with a high speed digital computer. The program was set up so that the following conditions could be taken into account: variable material properties, up to a maximum of three different materials, internal temperature distribution in the materials, and convective heating of the materials taking into account the pressure change during firing.

The output of the program gives the ablation depth, corrosion losses, convective heat transfer coefficient, radiation heat transfer coefficient, and the temperature at each node for each increment of time.

RESULTS

The preceding method of analysis was applied to the various sections of Motor A shown in Figures 4, 5, and 6. The analysis was carried out in two parts. First with a combustion temperature of 5725 F for 10.5 seconds corresponding to burning of the core grain and second with a combustion temperature of 6325 F for 20.5 seconds corresponding to combustion of the RFG.

FORWARD CLOSURE AND POLAR BOSS

The results of the analysis of the forward closure and polar boss are presented in Figures 7 through 14. The following paragraphs discuss the ablation losses and temperature distribution of the forward head obtained from the analysis.

Ablation Losses and Char Depth

The ablation losses versus time and the ablation loss and char depth of the forward closure and polar boss at end of firing are shown in Figures 7 and 8. It can be seen from Figure 7 that all the parts are still protected by undamaged insulation at the end of firing. The ablation depth of the MX2646 silica phenolic protecting the forward closure and upper surface of the polar boss was 0.16 inch for the closure and decreased to 0.14 inch on the upper surface of the polar boss. The variation of ablation in the MX2646 insulation is due to variation of exposure time. The char depth throughout the MX2646 is 0.07 inch.

PREVIOUS PAGE WAS BLANK, THEREFORE WAS NOT FILMED

APPENDIX III

THRUST VECTOR CONTROL SYSTEM

PREVIOUS PAGE WAS BLANK, THEREFORE WAS NOT FILMED

WRITTEN BY: [signature]
APPROVED BY: B. J. C.
[signature]

ROCKETDYNE
A DIVISION OF NORTH AMERICAN AVIATION, INC.
SOLID ROCKET DIVISION
MCGREGOR, TEXAS

SPEC. NO. NAS-80014D
ORIG. DATE 16 May 1963
REV. DATE 2 December 1964
PAGE 1 OF 21

EQUIPMENT SPECIFICATION

TITLE: THRUST VECTOR CONTROL SYSTEM

OMNI-AXIS GIMBALLED SKIRT TYPE NOZZLE, SOLID PROPELLANT ROCKET MOTOR

BASIC SPECIFICATION

NOTE: This revision incorporates all previous amendments issued against this specification and supersedes all other issues.

LIST OF CONTENTS

Paragraph

1. SCOPE
2. APPLICABLE DOCUMENTS
3. REQUIREMENTS
4. QUALITY ASSURANCE PROVISIONS
5. PREPARATION FOR DELIVERY
6. NOTES

ø Indicates a change from the previous issue of this specification.

EQUIPMENT SPECIFICATION

1. SCOPE - This specification covers the requirements for the complete thrust vector control (TVC) system for a solid propellant rocket motor. This system includes a fixed throat-gimballed skirt nozzle assembly, hydraulic actuation system, and electro-hydraulic control system. It does not include the primary hot gas pressure source, but does include the source mounting structure, pressure lines, and interfaces.

2. APPLICABLE DOCUMENTS

2.1 Equipment Specification - This Basic Specification covers the minimum requirements for the design, performance, manufacture, testing and packaging of the TVC system. Separate Specific Specification will be issued to designate the supplier whose product has been approved for procurement under this Basic Specification. The specific Specification may provide supplemental requirements applicable only to the supplier's particular product.

2.2 Documents - The following documents shall form a part of this Specification to the extent specified herein. If the requirements of this Specification and the documents listed below differ, the requirements of this Specification shall govern. Unless stated otherwise herein, the applicable issue of the following documents shall be the issue in effect on the date of issue of this Specification.

MILITARY SPECIFICATIONS

MIL-E-5272	Environmental Testing, Aeronautical and Associated Equipment, General Specification for
MIL-S-7742	Screw Threads, Standard, Optimum Selected Series, General Specification for
MIL-P-8564	Pneumatic System Components, Aeronautical, General Specification for
MIL-H-8775	Hydraulic System Components, Aircraft and Missiles General Specification for
MIL-E-25366	Electric and Electronic Equipment and Systems, Guided Missiles, Installation of, General Specification for
MIL-H-25475	Hydraulic Systems, Missile, Design, Installation, Tests, and Data Requirements, General Specification for
MIL-E-25534A	Engines, Rocket, Aeronautical, Qualification Test for
MIL-R-27542	Reliability Program Requirements for Aerospace System, Subsystems and Equipment
MIL-D-70327	Drawings, Engineering, and Associated Lists

EQUIPMENT SPECIFICATION

MILITARY STANDARDS

MIL-STD-143	Specifications and Standards, Order of Precedence
MIL-STD-130	Identification Marking of U.S. Military Property

MILITARY STANDARD DRAWINGS

MS-33586	Metals, Definition of Dissimilar

3. REQUIREMENTS

3.1 General Requirements

3.1.1 Selection of Specifications and Standards - Specifications and standards for all materials, processes, and parts which are not specifically designated in this Rocketdyne Specification, but which are necessary for compliance with the requirements of this specification, shall be selected in accordance with MIL-STD-143.

3.1.2 Materials and Processes - Materials and processes used in the manufacture of TVC system components shall conform to the applicable drawings and specifications designated herein. The materials used in the manufacture of the TVC system shall be of the highest quality and functionally suitable for the application. The use of critical or strategic materials shall be kept to an absolute minimum consistent with the performance and service required.

3.1.3 Interchangeability - All parts having the same part number shall be directly and completely interchangeable with respect to installation and performance. Changes in any manufacturer's part numbers after the specific specification has been issued shall require Rocketdyne approval and shall be governed by the drawing number requirements of MIL-D-70327.

3.1.4 Threaded Parts - All threaded parts shall be made of corrosion resisting material or shall be suitably protected against corrosion. Screw threads shall conform to MIL-S-7742. All threaded parts shall be positively locked or secured by safety wiring or by other approved methods.

3.1.5 Finish - All materials used in the TVC system shall be treated to resist corrosion, if not inherently corrosion resistant. Dissimilar metals, as defined by MS-33586, shall not be used in intimate contact with each other unless suitably protected against electrolytic corrosion. No pits, scratches, corrosion or other defects shall be present which are detrimental to the finish or function of the TVC system. The TVC system shall be free of all foreign matter during and after assembly.

3.1.6 Special Tools - Components shall be designed so that special tools are not required for assembly, disassembly, or installation of the TVC system or the components.

3.1.7 Marking - The TVC system and major components shall be marked in conformance with MIL-STD-130. All electrical terminals, pressure ports, and hydraulic fill and bleed ports shall be clearly identified.

3.1.7.1 Nameplate - Nameplates shall be used for the gimballed nozzle assembly and for the major components of the actuation system. The following minimum identification shall be permanently stamped on the nameplates.

Part Name
Electrical Input (where applicable)
Rocketdyne Specification Number
Manufacturer's Part Number
Manufacturer's Serial Number
Manufacturer's Name or Trademark
System Pressure (where applicable)
Date of Manufacture

Change letters shall not be applied as part of the Specification or Manufacturer's part numbers.

3.1.8 Qualification and Acceptance - The qualification and acceptance of the TVC system shall be in accordance with the tests specified in Section 4 of this Specification.

3.2 Design Requirements

ø 3.2.1 System Design - The TVC system shall provide control for a solid rocket motor in the pitch and yaw axes. The nozzle design shall utilize a single fixed throat with an omni-axially gimballed nozzle skirt. Actuation of the nozzle shall be by hydraulic means with provisions for connecting hydraulic supply and return lines to an external power source. When specified by Purchase Order, hydraulic components shall be replaced by rigid adjustable support links for a non-actuated TVC system.

(C) ø 3.2.2 Nozzle Performance - The TVC system shall be used with rocket motors containing either of two basic types of propellant. The nozzle contour design shall yield the most efficient performance when used with propellant B. Increase in throat area during firing shall not exceed 1.90 sq. in.

(C) 3.2.2.1 Requirements of TVC System

(a)	Thrust Vector Angle, θ, deg	±4 (in any plane)
(b)	Maximum Duty Cycle Frequency of System, cps	30 (at .25 degree deflection) (See Table I)
(c)	Nozzle Ballistic Performance, percent	97.0 (See Para 3.2.4)
(d)	Nozzle Expansion Ratio	Altitude Test 25:1 Ground Test 10:1 (See Para 3.2.2.3)
(e)	Initial Nozzle Throat Area, sq. in.	21.835
(f)	Nozzle Attachment Bolt Circle (see Fig. 1)	10.625 Basic

	(g)	Nozzle Attachment Diameter, in. (See Fig. 1)	9.747 $^{+.000}_{-.004}$
	(h)	Number of Attachment Bolt Holes	18
	(i)	Nozzle Divergent Geometry	Modified Bell Contour (See Para 3.2.4)
ø	(j)	TVC System Maximum Weight, lb (25:1 nozzle expansion ratio)	79.9 (See Para 3.2.5)

(C) ø 3.2.2.2 Design Parameters

(a)	Duty Cycle	See Table I
(b)	Ambient Pressure, psi	14.7 (maximum) Vacuum @ 100,000 ft_{alt} (minimum)
(c)	Motor Chamber Pressure	See Fig. 3 & Para 3.2.14.1

(C) PROPELLANT CHARACTERISTICS

		A	B
(d)	Weight percent of fuel in propellant	16	20
(e)	Combustion temp. (1000 psi), deg. F	5725	6325
(f)	Exhaust temp. (14.697 psi) deg. F	3295	3950
(g)	Total Motor Burn Time	Fig. 3	Fig. 3
(h)	Specific Heat ratio (chamber)	1.194	1.176
(i)	Specific Heat ratio (exhaust)	1.204	1.169
(j)	Molecular weight of combustion products (chamber)	25.55	27.93
(k)	Molecular weight of combustion products (exhaust)		
	1. Gas phase	19.71	20.31
	2. Condensed phase	101.94	101.94
	3. Mean effective	28.22	32.62

$$\frac{\text{(Total wt. of reaction products)}}{\text{No. of moles of gas}}$$

(C) ø 3.2.2.2 Design Parameters (Cont'd)

	A	B
(1) Exhaust gas composition, moles/100 gm (14.696 psi)		
H_2O	0.461	0.522
H_2	1.189	0.904
CO	0.918	0.646
CO_2	0.074	0.063
N_2	0.300	0.300
OH		0.004
H	0.006	0.033
HCL	0.593	0.576
Cl	0.002	0.016
$AlCl_2$		0.002
$Al_2O_3(s)$	0.296	0.370
Total Moles	3.839	3.436
Moles gas	3.543	3.066

(C) 3.2.2.3 Nozzle Expansion Ratio - A flightweight nozzle shall be designed with a 25:1 expansion ratio for altitude operation. A foreshortened version of this nozzle having a 10:1 expansion ratio shall be provided for sea level operation. The supplier shall furnish estimated nozzle performance losses for these two nozzle configurations in the null and deflected positions.

ø 3.2.3 Dimensional Requirements - The nozzle TVC system shall be maintained within the space envelope shown in Figure 1.

(C) ø 3.2.4 Nozzle Geometry and Ballistic Performance - The nozzle divergent geometry shall be a modified bell contour giving an overall nozzle efficiency over the burn time of at least 97.0% (for a 25:1 expansion ratio) in the null position. Nozzle efficiency is calculated by the following expression:.

$$\text{Nozzle Efficiency } (\%) = \frac{C_{f_{test}}}{C_{f_{theo(frozen)}}} (100)$$

where: $C_{f_{theo\ (frozen)}}$ is 1.857 for A and B propellants (25:1 expansion ratio nozzle), and $C_{f_{test}}$ is defined and calculated from measured altitude test data as follows:

$$C_{f_{test}} = \frac{\bar{F}_b}{\bar{P}_{c_b} \bar{A}_t}$$

where:

$$\bar{F}_b = \frac{\int F_{del}\, dt_b + \int \bar{P}_{cell} A_E\, dt_b}{t_b}$$

$$\bar{P}_{c_b} = \frac{\int P_c\, dt_b}{t_b} \quad \text{and} \quad \bar{A}_t = \frac{A_{t_i} + A_{t_f}}{2}$$

Modifications to the nozzle contour to improve performance characteristics and reduce erosion shall be compatible with the nozzle space envelope and weight limitations.

(C) ø 3.2.5 TVC System Weight - The altitude (25:1 expansion ratio) nozzle TVC system shall be designed for minimum weight consistent with TVC performance requirements but shall not exceed 79.9 pounds. This weight includes system fluid, components and internal connections as shown in Figure 2 but does not include the lines, fittings, and brackets necessary to connect to the external power source. (i.e. test hardware) This weight does not include attachments for monitoring pressure and other performance featuers.

ø 3.2.6 Actuation System - The TVC actuation system shall be similar to that shown by the schematic in Figure 2. All major items of the actuation system shall be supplied as directed by the Purchase Order. The entire actuation system must be mounted on the nozzle so that no loads will be imposed upon the motor grain and case except through the nozzle mounting flange.

ø 3.2.6.1 Hydraulics - The hydraulic system shall be a closed-loop type designed to operate from an external hydraulic power source. The hydraulic oil shall be compatible with the operating and storage temperature requirements of paragraph 3.2.16.

ø 3.2.6.1.1 Hydraulic System Contamination - The external power source will supply hydraulic fluid which has been continuously filtered through at least a 10-micron absolute standard element. There shall be no system response degradation during static firing due to contamination.

ø 3.2.6.1.2 Hydraulic System Pressure - The hydraulic system shall be designed for a 2000 ± 50 psi supply pressure which is provided by an external power source. This unit will be provided by Rocketdyne.

ø 3.2.6.1.3 Hydraulic System Leakage - The maximum internal leakage of the servo control valves shall not exceed 0.1 gpm total leakage under full system pressure with the nozzle in any position (static) required by the duty cycle. Total external leakage for all components during vibration tests or static firing shall not exceed 0.05 gpm under full system pressure with the nozzle in any position (static) required by the duty cycle

3.2.7 Auxiliary Hydraulic Ground Power - The supplier will furnish his own hydraulic source for any development tests deemed necessary.

3.2.8 Electrohydraulic Servo System Performance Criteria

(a) Closed loop gain	One degree thrust axis movement per volt from programmer (1^{o}/volt)
(b) Minimum input impedance to command signal	100,000 ohm
(c) Minimum resolution	0^{o} -1' arc
(d) Maximum phase shift	15^{o} from 0-8 cps 34^{o} at 16 cps 83^{o} at 30 cps
(e) Maximum dead band	0^{o} -3' arc
(f) Steady state amplitude accuracy including hysteresis and linearity errors	0^{o} -6' arc (Maximum error)
(g) Dynamic Frequency Response	± 3% from 0-8 cps + 30% at 16 cps + 70% at 30 cps

3.2.9 Nozzle Position Feedback - An electrical output signal shall be available from the servo system that can be used to monitor and record nozzle position versus time. The feedback transducer shall be located so that a minimum of nozzle position error is introduced. The relationship between true nozzle position and feedback reading shall be provided by the supplier.

3.2.10 Electrical Power - The TVC system shall utilize a 28 volt dc power source. Power requirements for the TVC system shall be kept to a minimum.

3.2.11 Test Programmer - The supplier will furnish his own programmer for any tests he deems necessary. Manual null shift provisions shall be incorporated into the control system.

3.2.12 Nozzle Axis/Thrust Vector Relationship - In the event the nozzle geometric axis and the nozzle thrust axis are not coincident, the relationship shall be defined.

3.2.13 Non-Actuated TVC System - Non-actuated TVC systems as specified by the purchase order shall be complete insofar as nozzle ballistic, thermal, structural, and dynamic characteristics are concerned. Actuators, and other non-operable precision components shall be replaced by adjustable links or struts or similar devices having dynamic characteristics similar to the replaced item. Commercial material shall be utilized where feasible.

3.2.14 Design Loads - The following loads criteria shall be used in the design of the TVC system.

(C) 3.2.14.1 Structural Loads - The limit operating chamber pressure (3 sigma) for design purposes shall be 1015 psia. All structures shall be designed with an ultimate design load factor of 1.25.

(C) 3.2.14.2 Acceleration Loads - All TVC system components shall be capable of functioning during and following exposure to the acceleration loadings shown below. Forward acceleration loads act through the C.G. of the TVC system along an axis parallel to the motor centerline and side loads act through the C.G. of the TVC system normal to the motor centerline. All acceleration loads shall be considered as ultimate for design purposes.

(a) Non-operating (nozzle in null position)

Forward - 15 g

Side - 15 g

(b) Operating (nozzle in any position)

Forward - 15 g

Side - 3 g

Induced - See Figure 5 for magnitude, direction and point of application.

3.2.14.3 Vibration Loads - All components shall be capable of normal functioning prior to, during, and after exposure to vibration loads listed below when attached to the rocket motor in the normal flight configuration.

3.2.14.3.1 Vibration Test - The rocket motor, including the TVC system, shall be vibrated in accordance with Procedure I of MIL-R-25534A except that all vibration survey and endurance testing shall be conducted at ambient temperatures.

3.2.15 Altitude - The TVC system shall be capable of normal duty cycle operation at altitudes from sea level to vacuum conditions.

3.2.16 Temperature

(C) 3.2.16.1 Storage Temperature - The TVC system and its components shall be capable of storage in the ready service condition for a period of one year at temperatures between -75 and 170 F without degradation of components or performance.

(C) 3.2.16.2 Operating Temperature - The TVC system and its components shall perform in accordance with the requirements of this specification when conditioned to equilibrium temperatures from -75 to 170 F.

(C) 3.2.16.2.1 Nozzle Flange Operating Temperature - The nozzle shall be designed so that the nozzle mounting flange (see Fig. 1) shall not exceed 250 F during the motor firing.

ø 3.2.17 Check-Out - The electrical components shall have adequate provisions for performing a check-out of all circuits prior to firing the rocket motor. A ground hydraulic cart with at least a 10-micron filter capability will be used for sea level system checkout. A service port shall be provided in the hydraulic system (see Fig. 2, Item 8). Pressure ports shall be provided as indicated for hydraulic system check-out and monitoring before and during firing for both 10:1 and 25:1 expansion ratio nozzles (Items 4 and 9, Fig. 2).

3.3 Performance Evaluation Criteria - Compliance of the TVC system design with this specification may be evaulated by performance of the tests listed below. Performance of these tests by the supplier will be required when specified by the purchase order.

3.3.1 Environmental Tests - Prior to each test, the TVC system shall be operated under prevailing room conditions and a record made of all data necessary to demonstrate that the TVC system conforms to the actuation performance requirements of this specification. After each test, the TVC system shall again be operated and a similar data record compiled to show that TVC system performance has not been affected by the test.

(C) 3.3.1.1 High Temperature - The TVC system shall be subjected to the conditions of paragraph 4.1.2 of MIL-E-5272, Procedure II, except temperature shall be 170 F.

(C) 3.3.1.2 Low Temperature - The TVC system shall be subjected to the conditions of paragraph 4.2.1 of MIL-E-5272, Procedure I, except temperature shall be -75 F.

(C) 3.3.1.3 Humidity - The TVC system shall be subjected to the conditions of paragraph 4.4.1 of MIL-E-5272 except high temperature shall be 170 F.

3.3.1.4 Vibration - The TVC system, while mounted by its normal means, shall be tested in accordance with Procedure I of Specification MIL-H-25534A at room temperature (see paragraph 3.2.14.3.1).

3.3.1.5 Fungus - The TVC system shall be subjected to the conditions of paragraph 4.8.1 of MIL-E-5272.

3.3.1.6 Rain - The TVC system shall be subjected to the conditions of paragraph 4.10.2 of MIL-E-5272. A protective cap may be in place over the electrical connectors on the TVC system during this test.

(C) 3.3.1.7 Sand and Dust - The TVC system shall be subjected to the conditions of paragraph 4.11.1 of MIL-E-5272 except high temperatures shall be 170 F.

3.3.1.8 Shock - The TVC system shall be subjected to the conditions of paragraph 4.15.3 of MIL-E-5272.

3.3.2 Dielectric Strength Test - The dielectric strength of the TVC system electrical circuits shall be tested by applying the following voltages between the current carrying parts and the mounting provisions of the TVC system for 60 seconds:

(a) 28 volt circuits: 600 volts rms, 60 ± 1 cps
(b) 115 volt circuits: 1500 volts rms, 60 ± 1 cps

No damage, arcing, or breakdown shall occur as a result of this test. Leakage current shall not exceed 1.0 milliampere. The TVC system shall then be subjected to the test of paragraph 3.3.3.

3.3.3 Insulation Resistance Test - The insulation resistance of the TVC system shall be measured with a 500 volt insulation tester and shall be determined immediately after the dielectric strength test of paragraph 3.3.2. The resistance shall be a minimum 100 megohms between the current carrying parts of the TVC system and the mounting provisions when the 500 volts dc is applied for 60 seconds.

3.3.4 Sub-Systems and Components Tests

3.3.4.1 Electrical System

3.3.4.1.1 Components - Electrical system components shall be subjected to tests specified in MIL-E-25366 and other applicable military specifications for the component.

3.3.4.2 Hydraulic System - The complete hydraulic system shall be subjected to tests specified in MIL-H-25475, except proof pressure shall be 150% minimum of operating pressure and burst pressure shall be 200% minimum of operating pressure.

3.3.4.2.1 Components - Hydraulic system components shall be subjected to tests specified in MIL-H-8755 and other applicable military specifications for the component except proof pressure shall be 150% minimum of operating pressure and burst pressure shall be 200% minimum of operating pressure.

3.3.4.3 Pneumatic System

3.3.4.3.1 Components - Pneumatic system components shall be subjected to tests specified in MIL-P-8564 and other applicable military specifications for the component.

3.3.5 Static Firing Tests - The nozzle and actuation system shall perform according to the system performance requirements of this specification throughout the imposed conditioning prior to firing and the subsequent static firing without malfunction.

4. QUALITY ASSURANCE PROVISIONS

4.1 Acceptance Tests - Acceptance tests shall be performed on each TVC system prior to acceptance by Rocketdyne. Acceptance tests shall consist of the following:

(a) Product examination per paragraph 4.1.2, including use of suitable non-destructive test techniques to assure compliance with design.

(b) Performance tests per paragraph 4.1.3.

4.1.1 Rejection and Rework - Failure of one component in a given TVC system to pass the tests of this specification shall be cause for rejection of the entire TVC system. The rejected system may be reworked by the manufacturer to correct defects and resubmitted for acceptance. The manufacturer shall provide the Rocketdyne Inspector with full particulars concerning the previous rejection and the action taken to correct the defects when the TVC systems are resubmitted for Rocketdyne inspection. A second rework shall not be permitted without written approval from Rocketdyne.

4.1.2 Product Examination - The TVC system shall be examined for conformance to the workmanship, dimensions, threaded parts, finish and marking requirements of this specification. The package containing the system shall be examined for the proper marking.

4.1.3 Performance Tests - The TVC system shall be mounted in a test stand simulating motor installation, connected to a command signal programmer and a ground checkout hydraulic system, and operated to determine proper functioning of all components.

4.2 Reliability

4.2.1 The Design Reliability Goal for the TVC system will be 99.8%. Demonstration of the reliability attained will be predicted on a synthesis of all testing done on total systems and on subsystems and components. Where possible, proof of reliability on functional components will be shown by life-cycle, MTBF, results of over-testing and/or prior history of performance and tests on similar or identical model hardware. MIL-R-27542 will be used as a guide plus any provisions explicitly agreed to in the purchase contract.

4.2.2 For the purpose of this program, MIL-R-27542 will be applicable as a guide and explicitly to the extent of:

(a) Design Review - Furnishing necessary data and drawings, technical descriptions and analytical treatments to assess the inherent reliability of the system, sub-systems, and components. Schedule of tests will be shown and will be subject to review and approval.

(b) Testing - Conducting environmental tests as referenced herein and other destructive and life testing by the supplier to verify safety margins or give assurance on design features or materials use.

(c) Failure Reporting - Failure Reporting and Analysis of cause and corrective action on any TVC system or component.

(d) Estimates of Reliability Demonstration levels for sub-systems and components will be shown as part of scheduled tests with an associated confidence number.

5. PREPARATION FOR DELIVERY

5.1 General - The TVC systems shall be delivered, assembled, and packaged individually. The provisions specified herein govern preparation for delivery to Rocketdyne. In addition, the supplier shall perform preservation, packaging or packing necessary to ensure the protection of the TVC system during transportation, handling and storage.

5.2 Protection - The supplier shall develop and use methods of preservation, packaging, and packing which will adequately protect the TVC system against corrosion, contamination, physical damage or other deterioration during transport to Rocketdyne and during subsequent indoor storage for 90 days.

5.3 Marking for Shipment - Containers shall be durably marked in a legible manner in such a way that the marking shall not become damaged when the containers are opened. The markings shall provide at least the following information:

1. Manufacturer's Part Number
2. Manufacturer's Serial Number
3. Manufacturer's Name and Address
4. Rocketdyne Specification Number
5. Name of Equipment in Package
6. Purchase Order Number

6. NOTES

6.1 Engineering Data and Approval - The supplier shall submit the following engineering data for Design Review and approval by Rocketdyne prior to delivery of any TVC system:

1. Performance records and test results demonstrating TVC system conformance with these requirements.
2. Drawings of the TVC system and its components showing mounting provisions, electrical connections and component operation.
3. Electrical wiring diagrams identifying terminals used.
4. Schematics of pneumatic and hydraulic systems.
5. Procedures for servicing and operating the TVC system.

6.2 Qualification Approval Data - If the manufacturer has obtained Qualification approval from any government agency for the system and/or components covered by this specification, or has performed tests similar to those required by this specification, such tests may fulfill requirements of this specification. Supporting data shall be submitted for Rocketdyne evaluation.

6.3 Data on Production Changes - After the specific specification has been released, the supplier shall make no changes to the TVC system without first obtaining written approval from Rocketdyne. Within 30 days after receipt of a specification change, the supplier shall submit written notification to Rocketdyne of all changes in the TVC system design, dimensions, materials, processes or performance. The suppliers approval request for any change shall demonstrate that the proposed changes will not adversely affect the quality or performance of the TVC system and that the modified TVC system and/or component shall be interchangeable in all respects with systems or components previously received by Rocketdyne. If test results will be affected, a test program shall be submitted to retest the system or component that the proposed change will affect.

6.4 Deviations from Specification - If the supplier finds it necessary to deviate from the requirements herein, he shall reference by paragraph number of this specification the proposed deviation and state the reasons for non-compliance. Rocketdyne will evaluate all such proposals and determine whether the product can be granted deviations to this specification.

6.5 Definition of Terms

6.5.1 General Definitions

ø 6.5.1.1 TVC System - The term "TVC system" shall mean the gimballed skirt nozzle employed for omni-axial thrust vector deflection, together with all sub-systems and components required for nozzle actuation and position indication, excluding the external power source.

6.5.1.2 Component - The term "component" shall mean a control valve, actuating cylinder, or similar element.

6.5.2 Ballistic Definitions (see Figure 4)

6.5.2.1 Burn Time, t_b - Burn time is the interval from the point on the pressure trace which represents 10 percent of the maximum chamber pressure to the point on the trace which represents 75 percent of the aft tangent pressure (sec). Aft tangent pressure is determined by drawing tangents to the final regressive portion of the pressure-time curve and drawing a line from the intersection of these tangent lines bisecting the area enclosed between the tangent lines. The intersection of this bisecter line with the pressure-time curve represents the aft tangent pressure.

6.5.2.2 Average Thrust, $\overline{F}_b$ - Average thrust is the burn time total impulse divided by the burn time, corrected to vacuum conditions (lb_f).

6.5.2.3 Delivered Thrust, F_{del} - Measured value of delivered thrust at any time during rocket motor firing, (lb_f).

6.5.2.4 Burn Time Total Impulse, I_b - Burn time total impulse is the area under the thrust-time curve between the points defined in 6.5.2.1 (lb-sec).

6.5.2.5 Average Chamber Pressure, $\overline{P}_{c_b}$ - The average chamber pressure is the area under the pressure-time curve between the points defined in 6.5.2.1 divided by the burn time, (psia).

6.5.2.6 Average Cell Pressure, $\overline{P}_{cell}$ - Average pressure existing in test cell during rocket motor firing, (psia).

6.5.2.7 Nozzle Exit Area, A_e - The exit area of the exhaust cone determined before firing ($in.^2$).

6.5.2.8 Initial Nozzle Throat Area, A_{t_i} - The area of the nozzle throat determined before firing ($in.^2$).

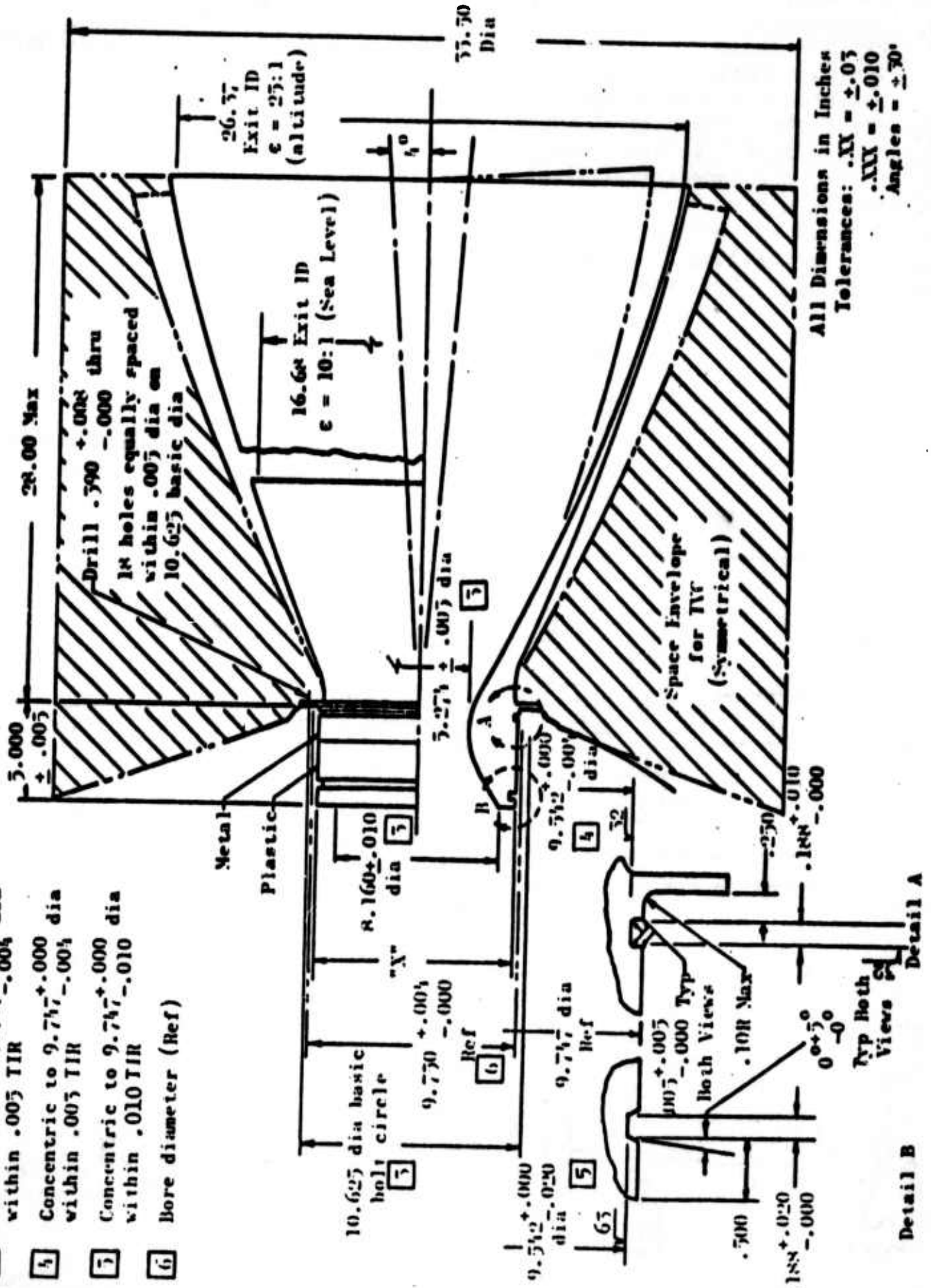
6.5.2.9 Final Nozzle Throat Area, A_{t_f} - The area of the nozzle throat determined after firing and cleaned of deposits ($in.^2$).

6.5.2.10 Chamber Pressure, P_c - Chamber pressure at any time during rocket motor firing, (psia).

TABLE I

THRUST VECTOR CONTROL ACTUATION PROGRAM

Duty Cycle Time Requirement (sec) Ignition = 0	Pitch Amplitude (Deg. about center line)	Yaw Amplitude (Deg. about center line)	Phase Shift in Pitch Plane (Degrees)	Cycling Frequency (cycles/sec)	Actuatory Cycles Completed Pitch	Yaw
0-0.5	0	0	0	0	0.	0
0.5-2.5	±4	±4	+90	0.5	1.	1.
2.5-3.5	±3.5	±3.5	+90	1	1.	1.
3.5-4.5	±3.5	±3.5	+90	2	2.	2.
4.5-5.0	0	0	0	0	0.	0.
5.0-6.0	±3.25	±3.25	-90	2.5	2.5	2.5
6.0-7.0	+3.25	+3.25	-90	3	3.	3.
7.0-7.5	0	0	0	0	0.	0
7.5-8.5	±3	±3	+90	3	3.	3.
8.5-9.0	0	0	0	0	0.	0.
9.0-10.0	±3	±3	-90	1	1.	1.
10.0-10.5	0	0	0	0	0.	0.
10.5-11.5	±2.5	±2.5	+90	3	3.	3.
11.5-12.0	0	0	0	0	0.	0.
12.0-13.0	0	±2	0	1	0.	1.
13.0-13.5	0	0	0	0	0.	0.
13.5-14-5	±2	±2	180	3	3.	3.
14.5-15.0	0	0	0	0	0.	0.
15.0-16.0	±2	±2	0	4.5	4.5	4.5
16.0-16.5	0	0	0	0	0.	0.
16.5-17.5	±1.5	0	0	2	2.	0.
17.5-18.0	0	0	0	0	0.	0.
18.0-19.0	±1.5	±1.5	180	4	4.	4.
19.0-19.5	0	0	0	0	0.	0.
19.5-20.5	±1.5	±1.5	0	6.	6.	6.
20.5-21.0	0	0	0	0	0.	0.
21.0-22.0	0	±1	0	4	0.	4.
22.0-22.5	0	0	0	0	0.	0.
22.5-23.5	+1	0	0	6	6.	0.
23.5-24.0	0	0	0	0	0.	0.
24.0-25.0	±1	±1	+90	8	8.	8.
25.0-25.5	0	0	0	0	0.	0.
25.5-26.5	±0.5	±0.5	180	4	4.	4.
26.5-27.0	0	0	0	0	0.	0.
27.0-28.0	±0.5	±0.5	0	8	8.	8.
28.0-28.5	0	0	0	0	0.	0.
28.5-29.5	0	±0.5	0	16	0.	16
29.5-30.0	0	0	0	0	0.	0.
30.0-31.0	±0.25	0	0	16	16.	16.
31.0-31.5	0	0	0	0	0.	0.
31.5-32.5	±0.25	±0.25	-90	30	30.	30.
32.5-33.0	0	0	0	0	0.	0.
33.0-35.0	±0.25	±0.25	+90	30	60.	60.
35.0-Tailoff	0.	0.	0	0	0	0.



1. Dim "X" is 9.747 +.000 -.004 for metal parts
2. Dim "X" is 9.747 +.000 -.010 for plastic parts

3. Concentric to 9.747 +.000 -.004 dia within .005 TIR
4. Concentric to 9.747 +.000 -.004 dia within .005 TIR
5. Concentric to 9.747 +.000 -.010 dia within .010 TIR
6. Bore diameter (Ref)

Figure 1. Space Envelope for Thrust Vector Control

1. Servo Valves
2. Yaw Actuator
3. Pitch Actuator
** 4. Manifold Pressure Port
5. Position Feedback Transducer
6. Nozzle Position Control Amplifier
* 7. Ground Cart (See Para 3.2.17)
8. System Disconnect (w/filter)
** 9. Pressure Port
*10. Filter
*11. Nozzle Position Instrumentation
*12. Programer (See Para 3.2.12)

* Furnished by Rocketdyne for test firings.

** For Ground Test Units Only.

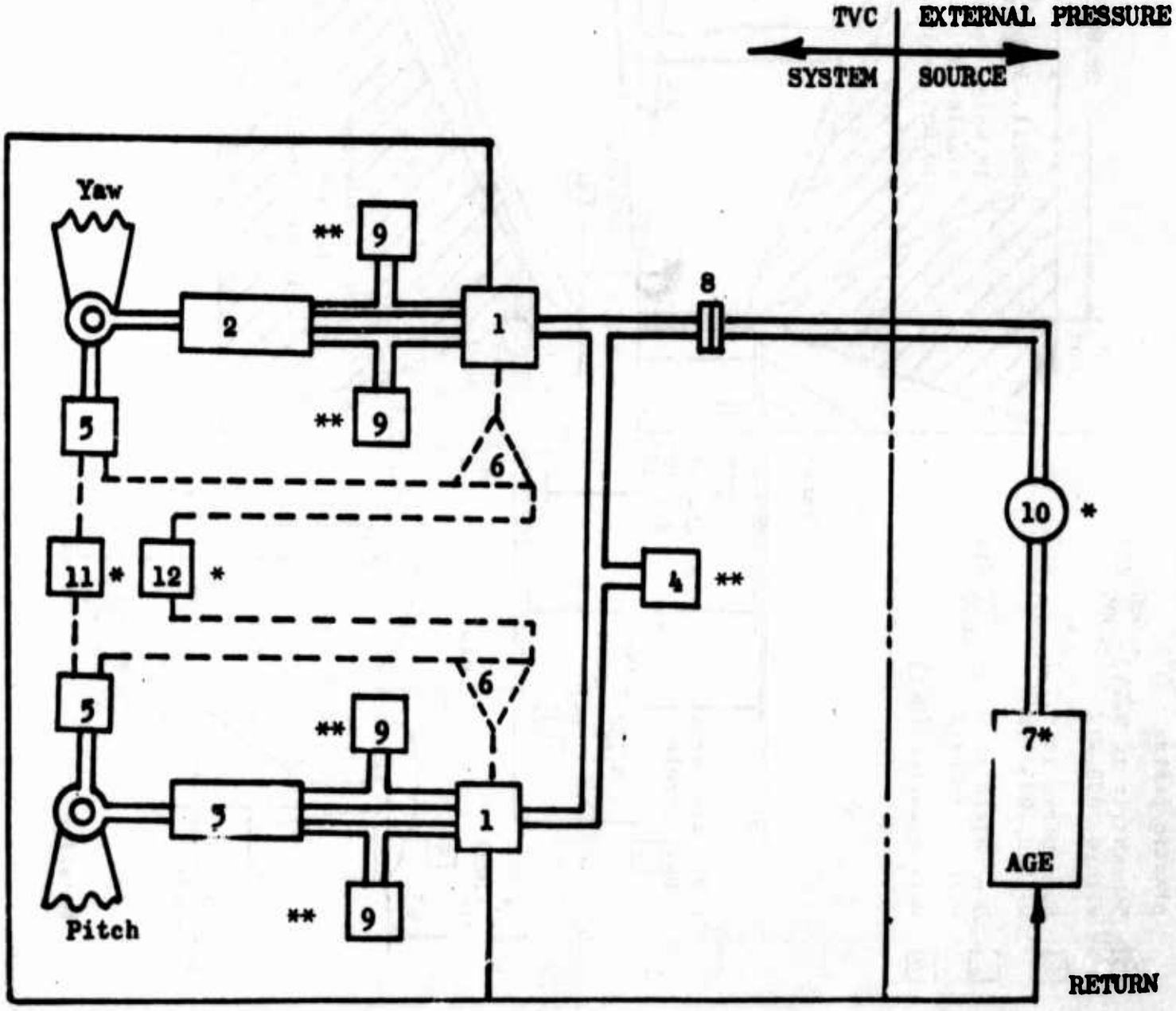


Figure 2. Typical Gimballed Nozzle Actuation System Schematic

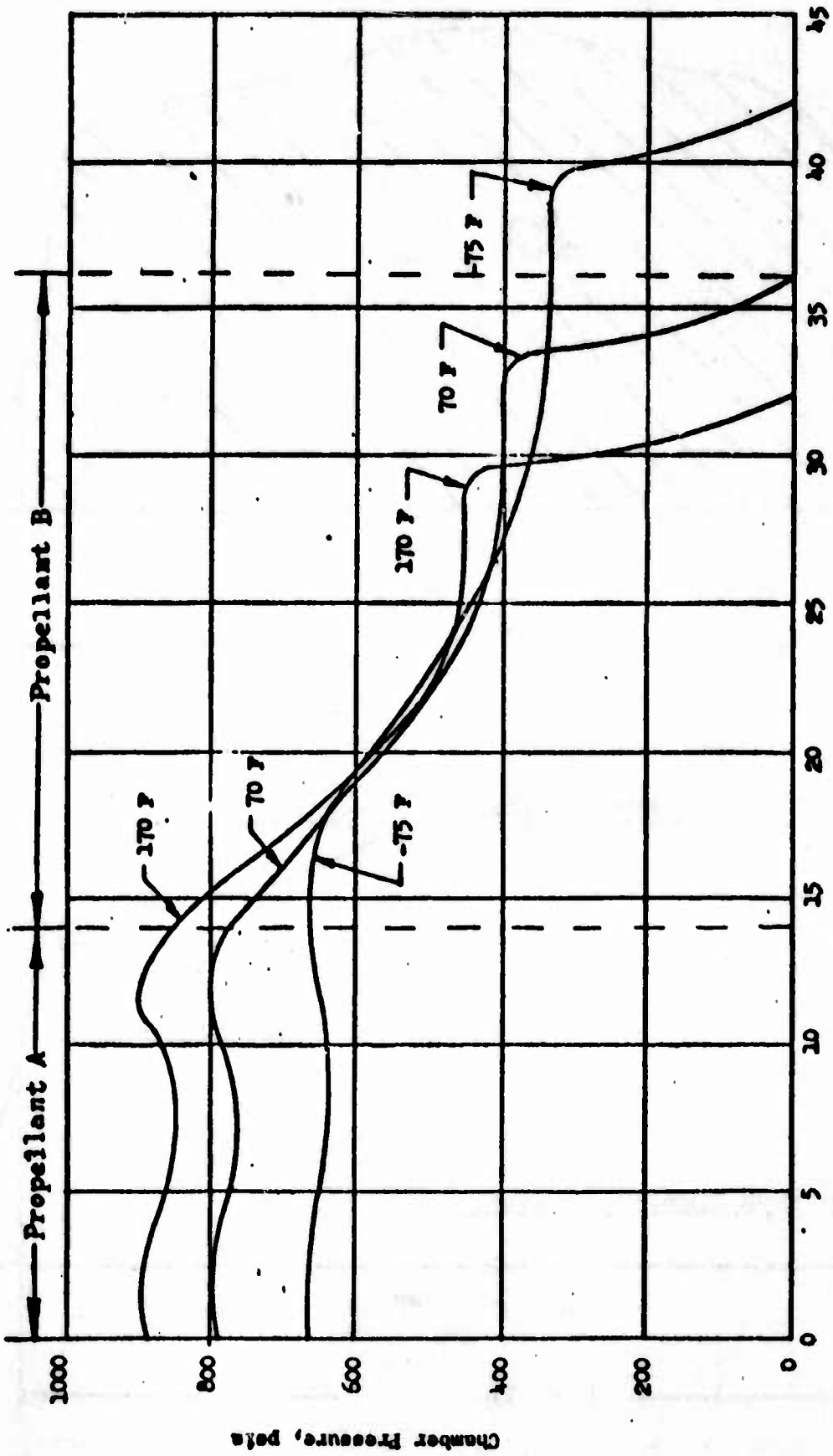
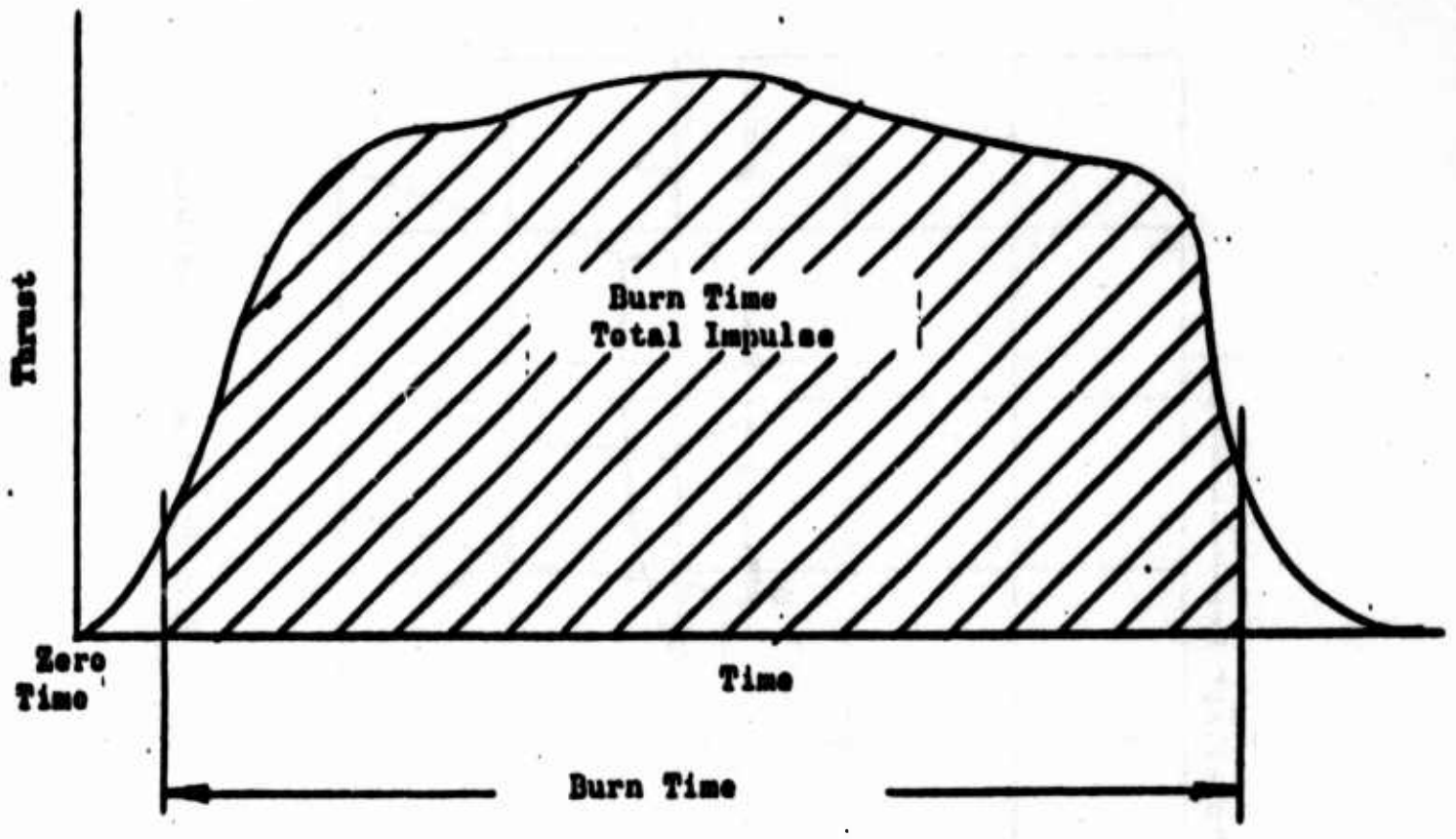


Figure 3. Nominal Motor Chamber Pressure versus Time for Type I Propellant (A and B) with Typical Propellant Distribution at 70 F...



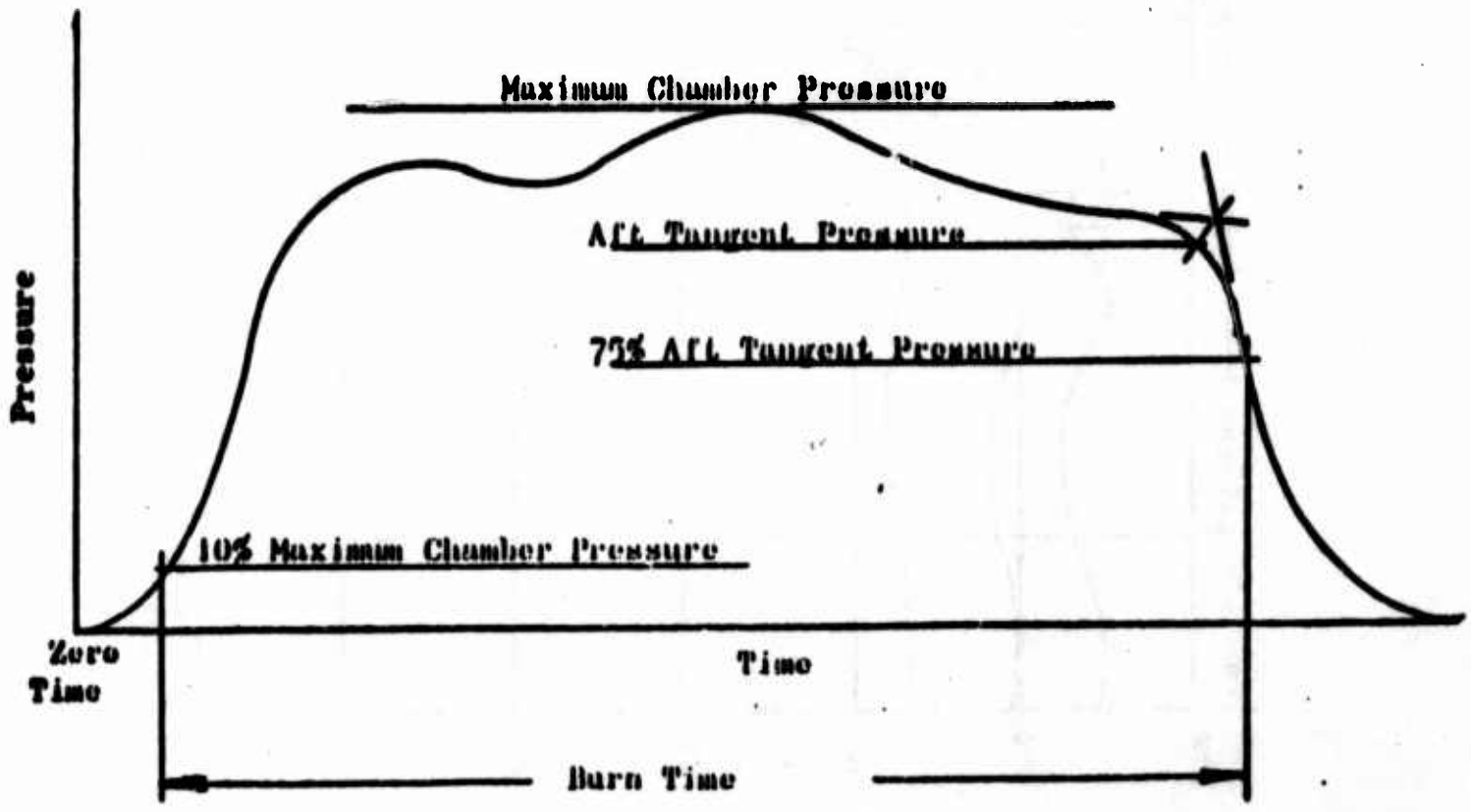


Figure 4. Illustration of Ballistic Definitions

CONFIDENTIAL

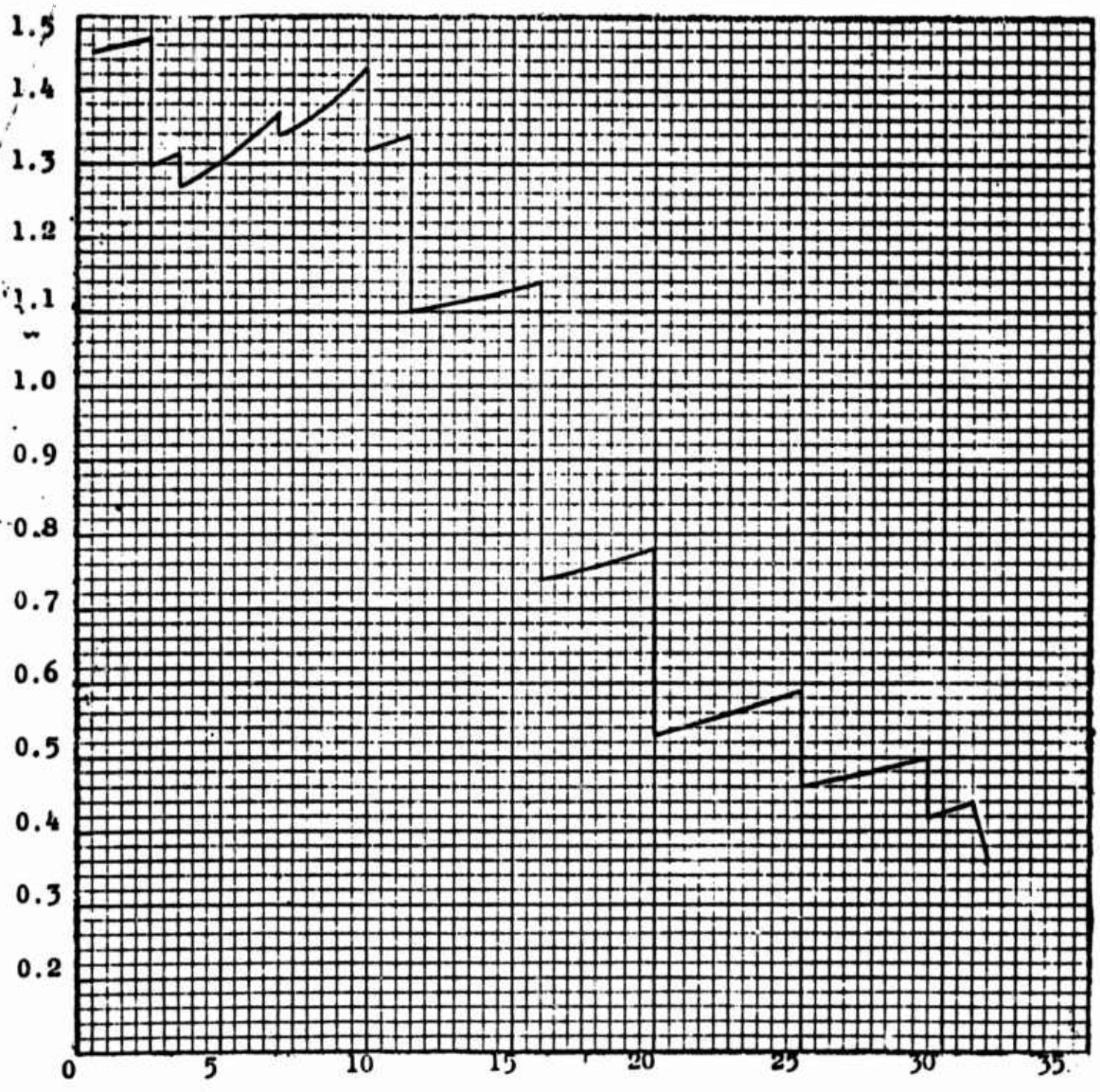


Figure 5 - Induced Acceleration* vs Time

*Acceleration normal to motor centerline due to nozzle vectoring. Determined at a point 14 inches aft of nozzle mounting flange.

CONFIDENTIAL

FORM 131-H-2 NEW 12-62

PREVIOUS PAGE WAS BLANK, THEREFORE WAS NOT FILMED

APPENDIX IV

ESTIMATION OF ENERGY REQUIRED FOR SOLID PROPELLANT MOTOR IGNITION

PREVIOUS PAGE WAS BLANK, THEREFORE WAS NOT FILMED

APPENDIX IV

ESTIMATION OF ENERGY REQUIRED FOR SOLID PROPELLANT MOTOR IGNITION

An extremely useful relationship between certain rocket motor parameters and the energy required to obtain satisfactory ignition has been developed by the U. S. Naval Ordnance Laboratory. (Reference: NavOrd Report 6134, G. J. Bryan and E. K. Lawrence). The above referenced report presents the methods utilized in obtaining data, and the empirical relationship which was developed. The equation derived has been further reduced and adapted for use by SPO through the combined efforts of the Propellant Research Unit and the Structures Design Unit.

DERIVATION OF FORMULA FOR ENERGY REQUIREMENTS

From Equation 3, NavOrd Report 6134,

$$Q = 38 \left[(A q_c) \left\{ \frac{L_g \sqrt{4\pi A_p}}{A} \right\}^{0.59} \right]^{1.06} \qquad (1)$$

Where

Q = Total energy required for ignition in calories

A = Total area exposed to products of ignition, cm^2

L_g = Length of grain, cm

A_p = Port area, cm^2

q_c = Ignitiability of propellant, cal/cm^2

Dimensional analysis of the above formula indicates the units of the term

$$\left[(A q_c) \left\{ L_g \sqrt{\frac{4\pi A_p}{A}} \right\}^{0.59} \right]^{1.06}$$

are $cal^{1.06}$. Therefore, to yield cal for Q, the dimensions of the constant 38 are $cal^{-.06}$. To make the above equation valid for British units, convert as follows:

$$\left(\frac{38}{\text{Cal}^{.06}}\right)\left(252\ \text{cal}/_{\text{BTU}}\right)^{.06} = (38)\ (1.39)/_{\text{BTU}}{}^{.06}$$

$$= 52.8\ \text{BTU}^{-.06}$$

For British Units, then

$$Q = 52.8\left[(A_{qc})\left\{L_g\sqrt{\frac{4\pi A_p}{A}}\right\}^{0.59}\right]^{1.06}$$

$$= 52.8\left[A^{1.06}\ q_c{}^{1.06}\left\{\frac{L_g\sqrt{4\pi A_p}}{A}\right\}^{0.6254}\right]$$

$$= (52.8)(4\pi)^{0.3127}\left[\frac{A^{1.06} q_c{}^{1.06} L_g{}^{0.6254} A_p{}^{0.3127}}{A^{0.6254}}\right]$$

$$= 116.5\ q_c{}^{1.06}\left[A^{0.4346}\ L_g{}^{0.6254}\ A_p{}^{0.3127}\right]$$

For a single type propellant (e.g. RDS-135), q_c may be assumed constant. Thus for a single propellant, the term $116.5\ q_c{}^{1.06}$ may be considered a single constant, K, and equation (1) becomes:

$$Q = K\ A^{0.4346} L_g{}^{0.6254} A_p{}^{0.3127} \qquad (2)$$

Where

$$K = 116.5\ q_c{}^{1.06} \qquad (3)$$

Once q_c is determined, then K may be calculated, determining the linear relationship between Q, the energy required for ignition, and the term $(A^{0.4346} L_g{}^{0.6254} A_p{}^{0.3127})$. This relationship is shown graphically in Figure 1.

The ignitability of Rocketdyne's propellants (q_c) has not been determined in such a manner that values are available for using directly in equation (1). However, the constant K may be approximated from the results of previous motor tests utilizing the same propellant, and on which satisfactory results were obtained. This is illustrated as follows.

If we assume that the Mk 25 rocket motor utilized the optimum weight of ignition material, then

$$Q = \left(\frac{96 \text{ gms}}{454 \text{ gms/lb}}\right)\left(2600 \text{ BTU/}_{\text{lb}}\right) = 550 \text{ BTU}$$

Since 96 gms = wt. of P120A ignition material used and 2600 BTU/lb = heat of explosion (approximate available energy) per lb of P120A.

For Mk 25:

$A = 2717 \text{ in.}^2$

$L_g = 40.3 \text{ in.}$

$A_p = 33.1 \text{ in.}^2$

From equation (2),

$$K = \frac{Q}{A^{0.4346} L_g^{0.6254} A_p^{0.3127}}$$

$$= \frac{550}{(2717)^{0.4346}(40.3)^{0.6254}(22.1)^{0.3127}}$$

$$= \frac{550}{(31.08)(10.09)(2.633)}$$

$$= 0.667$$

Or, utilizing the basic formula

$$Q = 550 = 52.8 \left\{(2717)\, q_c \left[\frac{40.3\ \sqrt{4\pi(22.1)}}{2717}\right]^{0.59}\right\}^{1.06}$$

$$= 52.8\ (1190 q_c)^{1.06}$$

$$q_c^{1.06} = \frac{550}{(52.8)(1190)^{1.06}}$$

$$q_c = 0.00769 \text{ BTU/in.}^2$$

From equation (3),

$$K = 116.5\, q_c^{1.06}$$

$$= (116.5)(0.00769)^{1.06} = 0.667$$

In order to obtain the best estimate, the K value was determined for several motor configurations tested which used RDS 135 propellant, and the best average value was approximated at 0.60.

CALCULATION OF ENERGY REQUIREMENTS

Once the constant, K, is determined, then the energy required to obtain ignition can be estimated if the port area (A_p), the length of the propellant grain (L_g), and the total area exposed to the products of ignition (A) are known. Application of this equation is illustrated in the following example.

For the M-34, the grain length (L_g) is 142 inches, the port area is 172 square inches, and the surface area is 53,000 square inches. The propellant formulation for M-34 is RDS-135, for which K value is placed at 0.60. The energy required for ignition (Q) then becomes

$$Q = (0.60)(53{,}000)^{0.435}(142)^{0.625}(172)^{0.313}$$

$$= 7560 \text{ BTU of available energy}$$

Since the ignition material, P-120A, has an available energy of 2600 BTU/lb, the weight of ignition material required is $\frac{7560}{2600} = 2.91$ pounds, or 1320 grams. (Note: Present design used 1000 grams, since relatively long ignition delay of 400 milliseconds at -75°F is permissible). The volume required to contain this amount of ignition material can readily be calculated from the bulk density of the particular ignition material involved. In this illustration 1/4" diameter P120A pellets were used, which has a bulk density of 22 grams/cubic inch. The volume required is then $\frac{1320 \text{ grams}}{22 \text{ grams/in.}^3}$ or 60 cubic inches.

The charts in figures 1 and 2 have been prepared to facilitate computation of the required energy, ignition material, and volume. Once the factor $A^{0.435}{}_L{}_g{}^{0.625}A_p{}^{0.313}$ has been calculated, these three variables may be obtained directly from the applicable chart by reading up to the line designated for the propellant concerned then across to the variable desired. Thus, for the M-34 the factor would be $(53,000)^{0.435}\ (142)^{0.625}(172)^{0.313}$, or 12,600.

On Figure 2, read up from 12,600 on the X-axis to the line designated as RDS-135, then across to the Y-axis. The ignition energy required is approximately 7600 BTU's, the ignition material required is 1320 grams, and the volume required is 60 cubic inches.

DISCUSSION

The authors of the referenced article have estimated that a satisfactory charge for 92% of the ignition systems could be obtained by a two trial method. First a value of one standard estimate of error below the nominal would be used, and, if unsuccessful (should be successful or under-ignition) a value of one standard error above the nominal would be tried. An even higher probability of success (99%) is estimated where tests previously conducted on similar configurations have proven satisfactory.

In application of the equation at SPO, it must be recognized that values of q_c are, at best, estimates based on previous firing data rather than analytical determinations. As additional information on this property is gained, values of q_c (and consequently, K) which are shown here will be adjusted to reflect the improved estimates. It is also evident that many factors, other than these three variables shown, should be considered before making a final decision as to the quantity and type of ignition to be employed. A suggested approach is to estimate the requirements from this equation to obtain approximate quantities of energy. The weight of ignition material may then be raised or lowered to compensate for other variables not previously considered, such as unusual or extreme ignition times, proximity of ignition medium to propellant surface, ignition shock limitations, starter diaphragms, etc.

CORRELATION CHART FOR ESTIMATION OF IGNITION ENERGY REQUIREMENTS

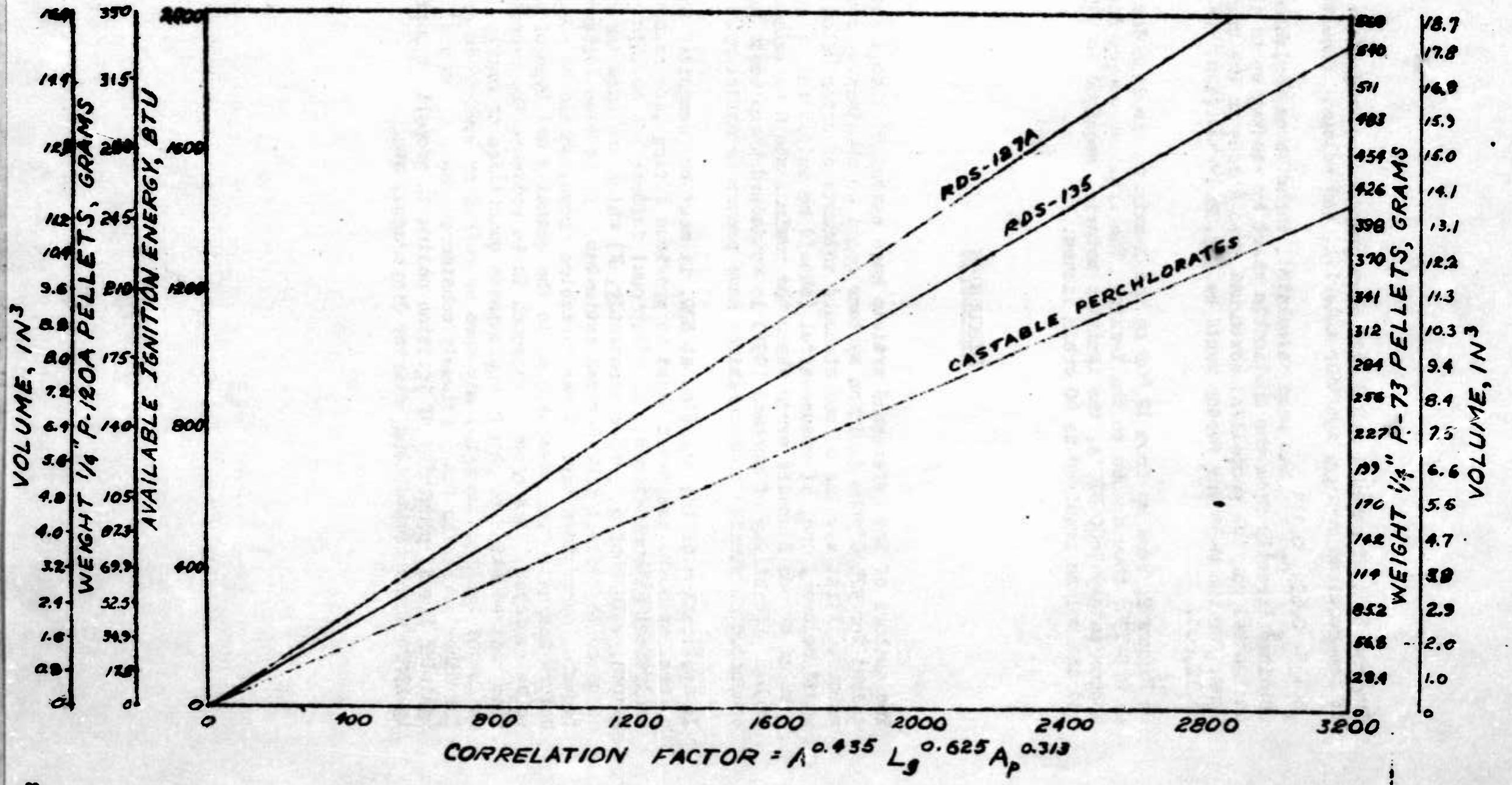


FIGURE 1

CORRELATION CHART FOR ESTIMATION OF ENERGY REQUIREMENTS

VOLUME IN M³

GRAMS REQUIRED X 1000

BTUX 1000 REQUIRED

CORRELATION FACTOR

FIG 1

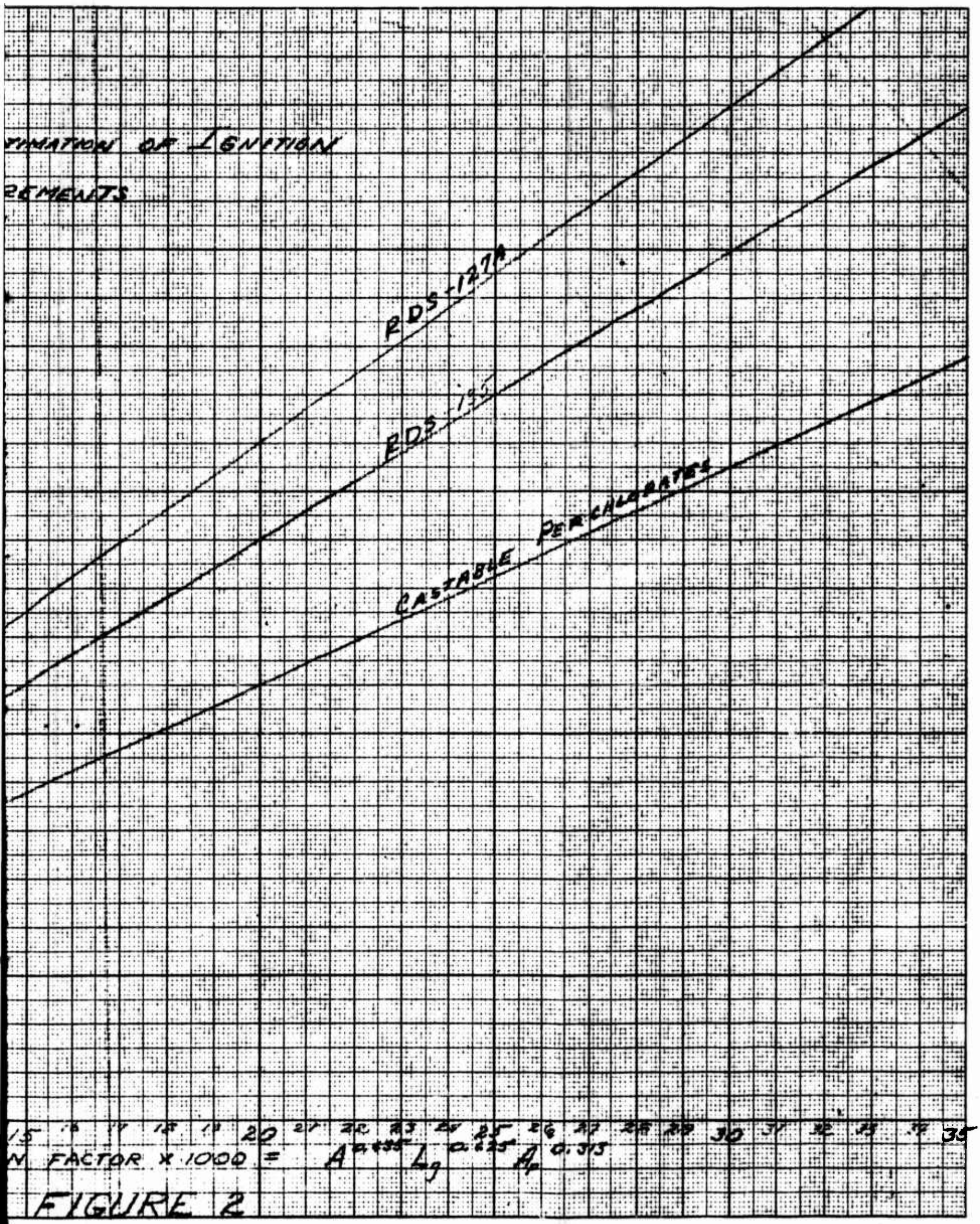

TIMATION OF IGNITION
REMENTS
RDS-127A
RDS-135
CASTABLE PERCHLORATES
15 16 17 18 19 20 21 22 23 24 25 26 27 28 29 30 31 32 33 34 35
N FACTOR X 1000 = A^0.435 Lg^0.225 Ap^0.315

FIGURE 2

2

PREVIOUS PAGE WAS BLANK, THEREFORE WAS NOT FILMED

APPENDIX V

WINDING MACHINES

PREVIOUS PAGE WAS BLANK, THEREFORE WAS NOT FILMED

APPENDIX V
WINDING MACHINES

The company developed a number of winding machines for the reinforced grain program. The 6-, 10-, 36-, and 40-inch winding machines were designed and fabricated. Design of the 72-inch winding machine was also initiated and approximately 75% completed.

SIX-INCH WINDING MACHINE

This machine was designed as a laboratory research tool to wind small cylindrical grains for grain studies, propellant matrix evaluation, development of fabrication techniques, and evaluation of process controls. It is capable of winding cylindrical grains 6 inches in diameter by 14 inches long with variable web thicknesses. The 6-inch grain was chosen to allow use of Rohm and Haas-type test hardware for standardized ballistic data.

The winding unit and all accessories are mounted on a mobile bench. The unit is capable of winding 16 wires simultaneously with considerable flexibility as to wire spacing and winding angles. Each wire is provided with individual tensioning by means of a frictional drag on the wire spool.

This unit has been successfully used to wind grains for burning rate studies, evaluating 5- and 10-mil wire, and study of process variables such as optimum wire volume, helix angles, and propellant viscosity.

TEN-INCH WINDING MACHINE

This unit was designed as a process development machine to wind grains for reproducibility studies, development of fabrication techniques, evaluation of process variables, and glass filament case development. The machine is capable of winding cylindrical grains 10 inches in diameter by 30 inches long. The 10-inch size was chosen to allow use of standard 10-inch test hardware.

This machine is a scaleup of the 6-inch unit and has similar capabilities and flexibility. Like the 6-inch unit, its mandrel rotation and traversing mechanism are operated through separate transmissions controlled by mechanical linkage, variable-speed-control units. This type design allows great flexibility in winding patterns; however, it is more difficult to develop reproducible wire patterns. The wire feed system is the same as on the 6-inch machine; however, the number of wires wound can be augmented as required. Wire application is in a continuous helical pattern, traversing back and forth along the grain length.

This unit was also designed for glass filament winding. It has a glass filament feed system capable of winding either preimpregnated rovings or "wet" rovings. The system has a two-spool capacity with tensioning devices for controlling the roving tension. In wet winding, a water-jacketed resin pot is provided to allow control of the resin temperature. The rovings, after passing through the resin bath, are stripped of excess resin and oriented for application on the cylinder.

This 10-inch machine was used for experimental winding of hydrotest cylindrical grain with special end bosses, the winding of glass filament cases, and the winding of glass filament cases on reinforced grains.

THIRTY-INCH WINDING MACHINES

This polar machine was designed and fabricated under a preceding study authorization; however, the design, fabrication, and evaluation of auxiliary equipment such as the wire feed system and propellant feed system were carried out under the RFG program. This is also true of modifications and improvements made on the unit. This machine has been in operation at the McGregor plant since November 1961 and all 10-inch, domed-end grains fabricated to date were made on this machine. Due to schedule delays in delivery of the 6-inch machine, this unit was also used to wrap 6-inch cylindrical grains for laboratory studies.

The unit was designed to wind grains up to 20 inches in diameter with cylindrical length-to-diameter ratios to 1.5, but it is capable of winding grains up to 30 inches in diameter with L/D ratios less than 1.0.

The polar-type winding machine winds grains with domed ends by alternating between polar winding and helical winding. In polar winding the wire is wound lengthwise from pole to pole as the grain rotates around its center of gravity on an axis normal to its longitudinal axis.

In helical winding the wire is wound on the horizontal rotating grain as the wire feed traverses back and forth along the cylindrical length of the grain. Winding angles are determined by change gears in the gear transmission which determine the ratio between mandrel rotation and the spindle speed, in the case of polar winding, and the ratio between mandrel rotation and carriage traverse movement in the case of helical winding.

THIRTY-SIX INCH WINDING MACHINE

This unit is capable of winding grains up to 36 inches in diameter and 5 feet long. It is a reciprocating helical winding type, employing hydro-mechanical means for actuation and winding control.

The general configuration of the machine consists of two upright structures, the headstock and tailstock. An overhead bridge joins the top of these structures and serves as a track for the carriage. The mandrel is positioned horizontally between the headstock and tailstock and rotates about its longitudinal axis. The headstock houses all power units, drive transmission, programming cams, and hydraulic winding control. The carriage moves bi-directionally and parallel to the axis of mandrel rotation. The delivery head, which is capable of laying down 50 individual wires, is mounted on a boom which moves vertically up and down and rotates about the vertical axis of the boom.

The horizontal position of the carriage and the vertical and rotational position of the carriage boom are controlled by cams. Precise tracer valves follow the cam surfaces and the movement of the tracer valves determines the motion of the carriage and boom. Thus, these cams orient and position the delivery head on a predesigned path at any instant in the winding cycle. The winding angle is controlled through a gear system with change gears that establish the speed ratio between mandrel revolutions and cam revolutions. The unit is able to develop high- and low-angle helix patterns as well as polar and circumferential windings.

FORTY-INCH WINDING MACHINE

Two 40-inch winding machines were designed and developed with company funds to support the extensive grain fabrication requirements of the Reinforced Grain Advanced Development Program. These units are advanced versions of the 36-inch winding machine which served as a development prototype. Due to the tight design and fabrication schedule, all possible basic components were used from the 36-inch machine. Operational experience on the 36-inch unit allowed a number of improvements to be built into the 40-inch machine.

Like its prototype, the 40-inch winding machine is a reciprocating, helical-winding type, employing hydro-mechanical means for actuation and winding control. It is capable of winding domes or cylindrical grains up to 40 inches in diameter and 80 inches long. It can develop helical patterns from low to high angles, including polar and circumferential patterns.

The general configuration of the machine consists of two upright structures, the headstock and tailstock. An overhead bridge joins the top of these structures and serves as a track for the carriage. The mandrel is positioned horizontally between the headstock and tailstock and rotates about its longitudinal axis. The headstock houses all drive transmission, programming cams, and hydraulic winding controls. The carriage moves bi-directionally and parallel to the axis of mandrel rotation. The delivery head is mounted on a boom which moves vertically up and down and rotates about the vertical axis of the boom.

The horizontal position of the carriage and the vertical and rotational position of the carriage boom are controlled by cams. Hydraulic tracer valves follow the cam surfaces and the movement of the

tracer valves through hydraulic cylinders and mechanical components determines the motion of the carriage and boom. The cams orient and position the delivery head on a predesigned path at any instant in the winding cycle. The winding angle is controlled through a gear system with a set of change gears providing the required gear ratios that establishes the speed ratio between mandrel revolutions and cam revolutions.

Two power units each consisting of a hydraulic reservoir, electric motor, and two hydraulic pumps are located adjacent to the headstock end of the machine.

Design requirements for the 40-inch machine were based on program motor sizes, increased operating capabilities, improved process controls, improved winding precision, and experience gained in the development and operation of the 36-inch unit. Design responsibility was assigned the design function of the Structural Plastics Group, located at the Van Nuys Facility. The two units were built by the Manufacturing Department of the Los Angeles facility.

APPENDIX VI

CAM DESIGN

PREVIOUS PAGE WAS BLANK, THEREFORE WAS NOT FILMED

APPENDIX VI
CAM DESIGN

GENERAL

It was apparent early in the RFG program that existing methods of developing cams for filament winding were inadequate for the scope and number of cams required. Since a GFW case required a single cam, or a set of two cams (X and Y), the problem hadn't been serious. Most of the industry scribed the desired path on the winding mandrel surface and forced the follower through the required motion. The follower motion generated the required contour on the cam blank mounted on the winding machine. This was obviously impractical for a multi-layer grain since the cost of repeating the operation for many mandrel diameters and shapes would be prohibitive. Cut-and-try approaches to cam design also proved unreliable, costly, and time consuming.

Therefore, it became necessary to theoretically develop the precise follower motion required to generate a specific filament path on a domed mandrel. The first approach was a geometric solution in which a helix angle defined by the design diameters is wound in plane over the domes and as a helix over the cylindrical section.

Along with the theory, it was necessary to develop a method of converting the theory to practice, and a graphical method of cam design was developed concurrently. In turn, the cam design was naturally adjusted to the existing SRD winding machines since the practical aspects were dependent on machine limitations of size, rate, mounting, and tracing. On SRD three-axis machines the "X" cam defines the variable horizontal (longitudinal) traverse of the follower carriage, the "Y" cam defines the variable transverse (vertical)

movement of the follower boom and the Z axis defines the variable rotational movement of the follower guide. The Z axis orientation was necessary for winding multi-wire warps to prevent roping and gaping of the wire patterns.

MOTOR A

Cams for Motor A were designed by the graphical approach and though tedious it proved very effective. The grain was divided into 9 geodesic layers and 8 intermediate layers. Each geodesic layer required an X, Y, and Z cam. Each intermediate layer was divided into 3 to 5 layers with different dome termination points and winding angles. Usually those layers with winding angles below 45 degrees were wound with X, Y, and Z cams while above 45 degrees the Y cam was not necessary. This resulted in a large number of cams and improved methods of cam fabrication were developed (see Cam Fabrication).

Design and winding of Motor A disclosed, and allowed solution of, many problems that were previously ignored or considered insignificant. It showed that more refined methods of determining warp width, layer dome thickness, dome in-plane angle ($\bar{\alpha}$) and winding patterns were necessary to improve cam design and grain design techniques.

A typical cam design package included the layout in rectangular coordinates, the polar coordinate data, and sketches of the three cams on polar graph paper. The raw data developed by graphical means or obtained from the cam computer program were plotted on the rectangular graph paper (cam rotation vs cam radius). The points were joined to form the cam contours and the contours corrected to allow for the radius of the cam follower normal to the curve. The radii for

appropriate cam angles were transferred to the data sheets and sketches plotted on polar graph paper. The sketches were used to show the cam configuration and the size blank required.

CAM COMPUTER PROGRAMS

Development of computer programs for cam design resulted in three basic programs: (1) a program (JWCKRT) for iterating the winding angle until a suitable winding geometry is obtained, (2) a program for cam design with 3-axis machine control (JJSCOT), and (3) a program with 2-axis machine control (RQSCOT).

The program for selection of the winding geometry was fairly straightforward. All acceptable winding patterns expected to be encountered, i.e., turns and circuits per pattern, were stored within the program. The winding angle was adjusted in increments equal to 0.01% of the total mandrel rotation until the resulting winding pattern was acceptably close to the stored values. The tolerance for this agreement was 0.5% of the total mandrel rotation for one circuit. This program also calculates the winding ratio and selects change gears which will yield this ratio. Various values are also calculated within this program which serve as input to the cam design programs. Development of computer programs for cam design was basically the same for both the 2- and 3-axis operation with the 2-axis operation simply maintaining the Y axis constant. The primary problem involved in each case was definition of the filament path over the domed ends to be readily usable. The geodesic dome is readily defined; however, occasions arise when the object to be wound upon is not a geodesic. The filament path was therefore defined in terms of the in-plane dome angle and the

dome coordinates. Follower head position and orientation was determined for each dome coordinate value except the first and last. For a given dome coordinate the filament path was approximated by defining the filament path as a quadratic of the form $y = ax^2 + bx + c$ passing through the given point and the points immediately before and after the given point. Follower position and orientation for the cylindrical portion of the mandrel were determined, as required, for simple spiral winding. After determination of follower position and orientation for one complete filament, this data was converted to cam coordinates using appropriate winding machine conversion factors. Cam follower correction was made at this point within the program; however, the technique for this correction has not yielded accurate results and needs further development. A plot of the cam contours was obtained by plotting the data on an SC-4020 plotter. An improved program combining all the computations necessary for a complete winding setup from winding geometry determination to cam coordinates for 3-axis operation (JJWBIG) was compiled; however, it was also plagued with the erroneous cam follower correction and required further development.

MOTOR B

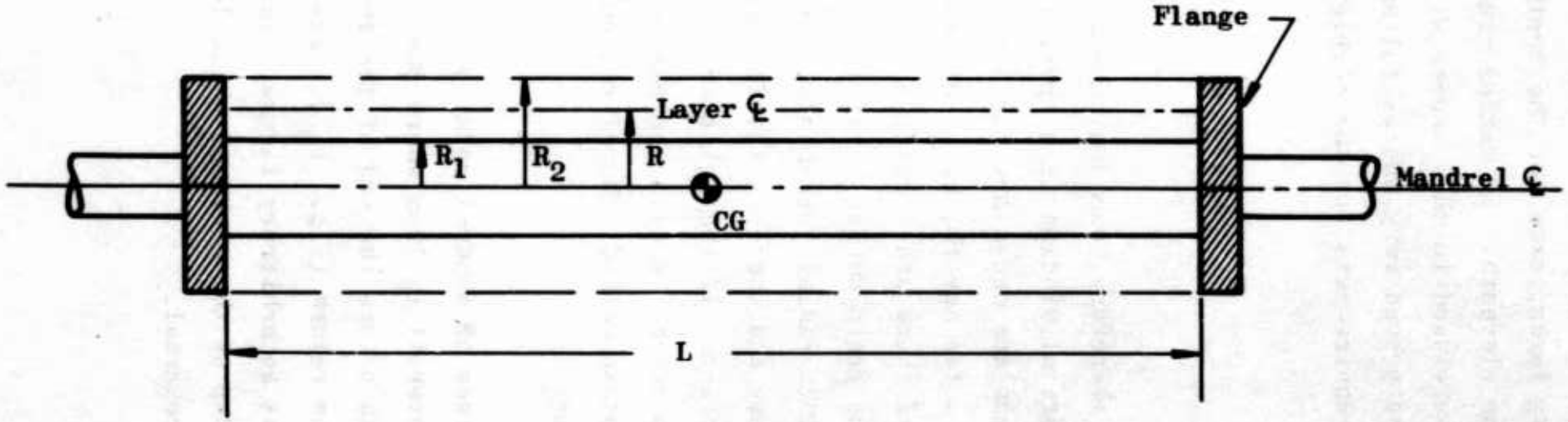
The major improvement in Motor B cam design, beside the use of the cam design computer program described above, was the reduction in the number of cams required. Study of all the cam designs for Motor A showed it feasible to reduce the number of cams required for a grain of a similar type due to the high degree of similarity in winding patterns between layers in adjacent cycles. The reduction was accomplished by designing a cam set for the middle layer of any series of three sequential layers, or for the outer layer for a series of two sequential layers. For example, cams for the first, second, and third geodesic

layer were designed for the second geodesic layer; cams for the tenth and eleventh geodesic were designed for the eleventh. By making minor machine adjustments during winding, cams were used in this manner without affecting pattern accuracy. The method proved very successful and resulted in a 50 to 60% reduction in cam requirements for the complete grain.

MOTOR D

All Motor D grains were cylindrical; therefore, cam design was considerably simplified. A cam for cylindrical winding is a special case of dome cam design. Only X and Z cams are necessary for straight cylindrical winding. The X cam can be used for any thickness of web; however, more than one Z cam is required if there are significant variations in the follower height above the grain surface. If the end plates are built up in 0.50- to 0.75-inch radial increments, the follower height stays near the grain surface and there is little warp foreshortening. Thus, one Z cam is sufficient. If the follower clearance varies considerably over the web then several Z cams are needed. The Motor D grains used the built-up end plate method; therefore, only one Z cam per grain was considered necessary.

The cams were designed using 180 degrees of mandrel rotation during follower reversal. In this case reversal is from where the wire warp contacts the grain one warp width before the end of the grain to one warp width past the grain end on the return (Fig. 1). Experience dictated the use of 180 degrees as an arbitrary figure. The use of greater rotation caused extra buildup at the reversal while less rotation usually caused wire slippage at reversal.



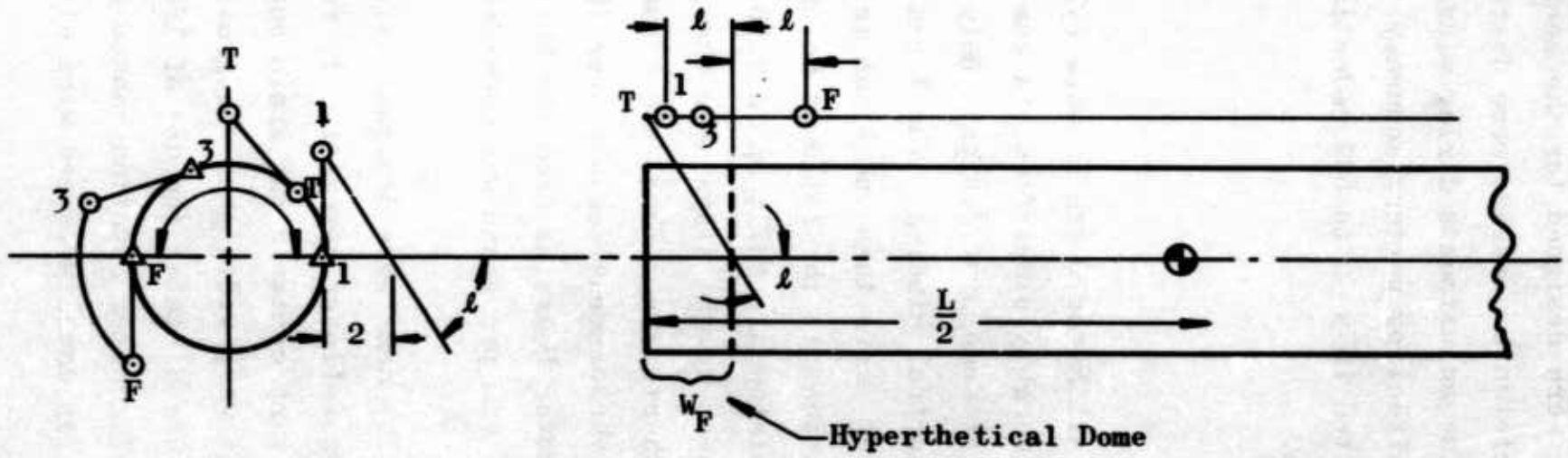


Figure 1 . Cam Design

CAM FABRICATION

Several design features applicable to fabricating and final use were worth discussing. The cam design called out the angle increments and radii for these angles and the shop fabricated the cam from this information. The following standards were established for the 36- and 40-inch winding machine cams.

1. Generally the X cams were large and made of 3/16-inch aluminum sheet while the Y and Z cams were made from 1/8-inch aluminum sheet. Steel cams were too heavy to handle. Some plastic (phenolic) cams were successful; however, the contour edges usually wore faster, were more easily damaged and couldn't be filed smooth like aluminum cams.

2. To fit the cam support shafts and driving stud, accurate hub holes were necessary. The shop drilled the hub diameter in a cam blank on a milling machine and used a transfer fixture to accurately position the drive hole.

3. A cam template, which consisted of a plate with radially scribed lines for each degree of angle (0--360), was made. The cam blank was mounted on the template by means of the drilled holes. The 3/8-inch diameter drive hole was always located on the 270 degree line of the cam. The cam was radially scribed for each angle called out on the design and a precision measuring scale with scribe mounted at the hub laid out the required radii at each angle. Ship curves were used to lay out the cam surface through the points located. The cam was then cut out with a band saw and a sanding wheel used to rough finish the required contour. The cam was finished by hand filing.

4. One technique used to add flexibility to the X cam and resultant horizontal carriage movement was to slot the X cam. This allowed the use of cam inserts with variable spacing of the hub hole and drive hole with respect to the slot. The inserts were made with 1/8-inch increments of spacing. The slot length was always towards the 270 degree mark on the cam which was also the smallest radius of the cam contour. The 0 cam insert was the same as the standard hole position.

The plus inserts increased the length of carriage travel at each end, depending on the amplification factor of the machine (1/2 to 5/8 inch for each 1/8-inch increment), and the minus inserts decreased the travel by the same degree. These slots were only needed on X cams for domes grains and for special cylindrical grains.

Since the cam contour had to be corrected for the difference of the normal distance between the cam follower centerline and the contour, the cam follower or stylus was kept at a standard 3/8-inch diameter. It was preferable to machine a weak point in the stylus so it broke before damaging the valve or cam in case of malfunction.

APPENDIX VII

AUTOMATIC PROPELLANT FEED SYSTEM

PREVIOUS PAGE WAS BLANK, THEREFORE WAS NOT FILMED

APPENDIX VII

AUTOMATIC PROPELLANT FEED SYSTEM

DEVELOPMENT

From the early research phase of the reinforced grain program considerable thought and effort were given to the best method of applying and spreading the matrix propellant. An adaptation of a commercial caulking gun was found to be an excellent tool for applying propellant to the grain. The propellant was loaded into polyethylene cartridges which were inserted in the gun. Extrusion pressure was obtained by either air or nitrogen.

As development progressed storage tests showed that Flexadyne propellants could be frozen at -70 F and stored for months without harm to properties. This technique permitted mixing propellant in advance and storing until needed.

The manual application of propellant on the grain by use of pressurized guns proved a simple and effective method of operation. The propellant could be applied when and where needed and at a rate compatible with the winding speed. This feed system was very satisfactory until grains became so large that propellant application became a limiting factor in grain winding. Pressure spraying, using a precoated ribbon, and employing mechanically held mobile extruders were among the feed techniques investigated. In all cases the difficulties appeared to outweigh the advantages. Concurrent with the application problem, the use of hand spatulas for spreading and smoothing the propellant was an increasing problem as grain size increased. Teflon rollers were tried

first, then differential speed-braked rollers were used. Neither was very satisfactory because of sticky binder accumulation which pulled propellant from the grain. It was apparent that a new concept in propellant feeding was required to improve the thickness uniformity and reduce the time lapse between start and finish of a layer of propellant. These factors are important in maintaining uniformity in web buildup.

DESCRIPTION

A new propellant feed system was designed and developed with features to overcome previous shortcomings. The advantages sought were:

1. Mechanical and semi-remote operation to reduce personnel exposure to potential hazard
2. Simultaneous propellant application along the entire grain cylindrical length to improve build-up uniformity and reduce possibility of air clusion
3. Improved temperature control and viscosity reduction through heating the spreader blade
4. Fabrication cost reduction by reducing manhours as much as 30%

The automatic feed system was composed of a spreader blade assembly, an extrusion unit, and necessary auxiliary equipment. The blade assembly consisted of two heated blades, positioned in a vee, and held against the grain by regulated pneumatic cylinders. The extruder unit was positioned relative to the spreader blade by a mechanical linkage. The extruder contained a series of rectangular propellant cartridges which were aligned to apply propellant evenly across the full grain length so the complete cylindrical section was covered in one revolution of the grain. The propellant was extruded from the cartridges by pneumatically controlled pistons or rams. A schematic diagram of the feed system is

shown in Fig. 1 . The side of the unit showing the battery of extrusion rams is shown in Fig. 2 . A view from the other side of the unit (Fig. 3) shows the nozzles of the plastic propellant cartridges. An end view of the unit is shown in Fig. 4 .

EVALUATION

The feed system unit was completed and undergoing shakedown evaluation when the grain fabrication work ceased. Results of the evaluation indicated the feed unit was usable; however, some potential problem areas were encountered.

With the extruders aimed on an upward angle, propellant tended to leak into the extruder and down the ram rods whenever pressure was released for any interruption of feeding. This was a nuisance and would make maintaining a clean unit very difficult over an extended winding period.

Under certain conditions of propellant "heat history" and grain surface, freshly applied propellant tended to pull loose from the grain before contact with the spreader blade. It then rolled up and resulted in a very uneven surface. This might be eliminated by some experimentation with a secondary smoothing blade located closer to the extruders. Some preliminary trials did show promise.

A third problem was the bulging of the cartridges after being filled. This caused a misalignment of the cartridge holding panel preventing it from seating tightly. Thus the cartridge nozzle or lip was not supported adequately to provide the necessary spreading action during propellant application.

Partly due to the preceding soft nozzle effect and partly as a result of low sensitivity in the controls, the thickness of the propellant layer was difficult to control. This would undoubtedly have improved with operating experience. Use of the unit was limited to inert propellant. This program was stopped which precluded use of the unit with live propellant.

Item	Descriptive Name
1	Cylindrical Grain or Mandrel
2	Extruder Head
3	Spread or Blade
4	Frame
5	Linkage Cable
6	Actuating Cylinder (Pneumatic)
7	Propellant Filled Cartridge
8	Extruder Ram
9	Extruder Cylinder (Pneumatic)
10	Wedge Angle
11	Pressure Safety Switch

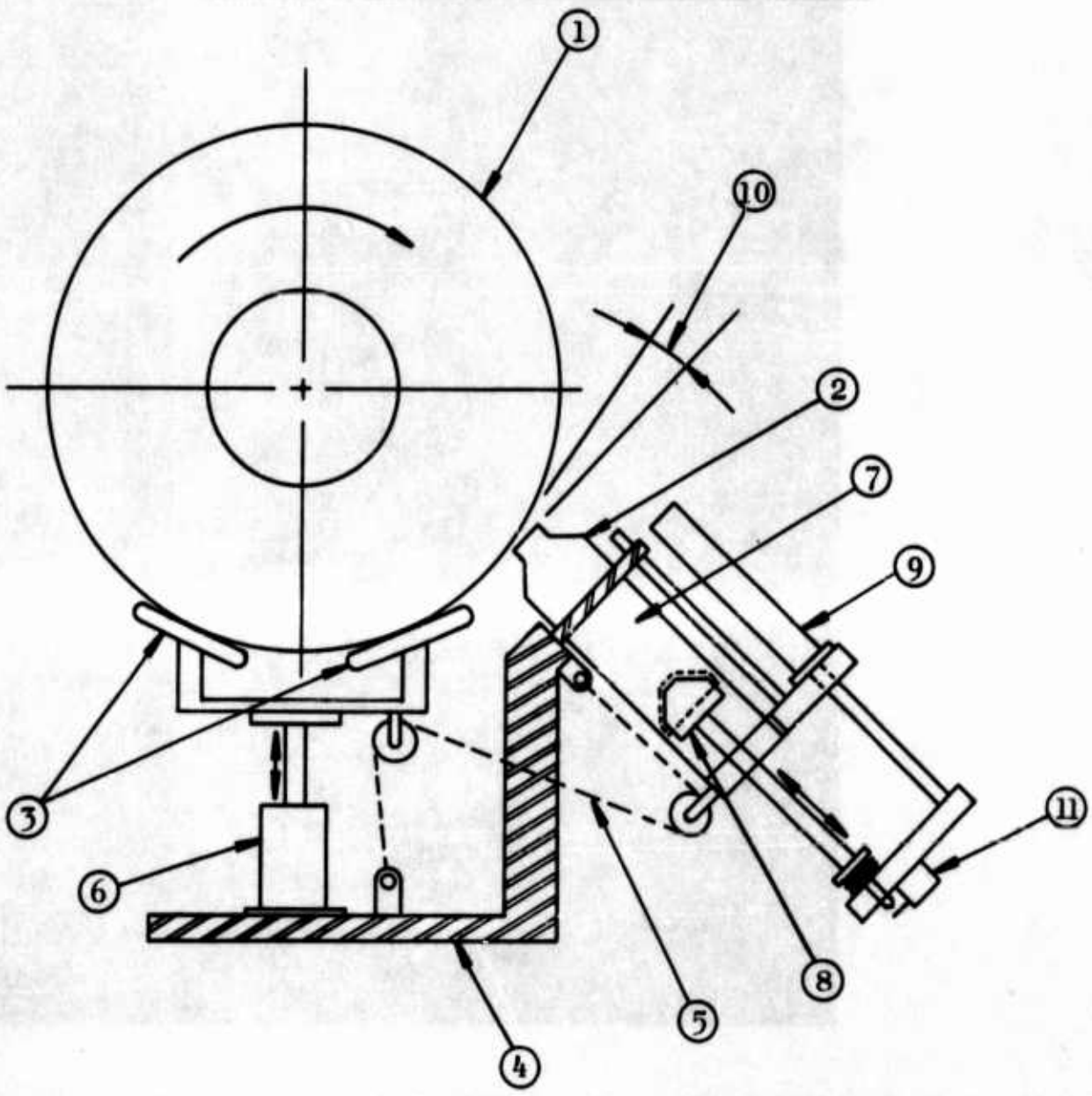
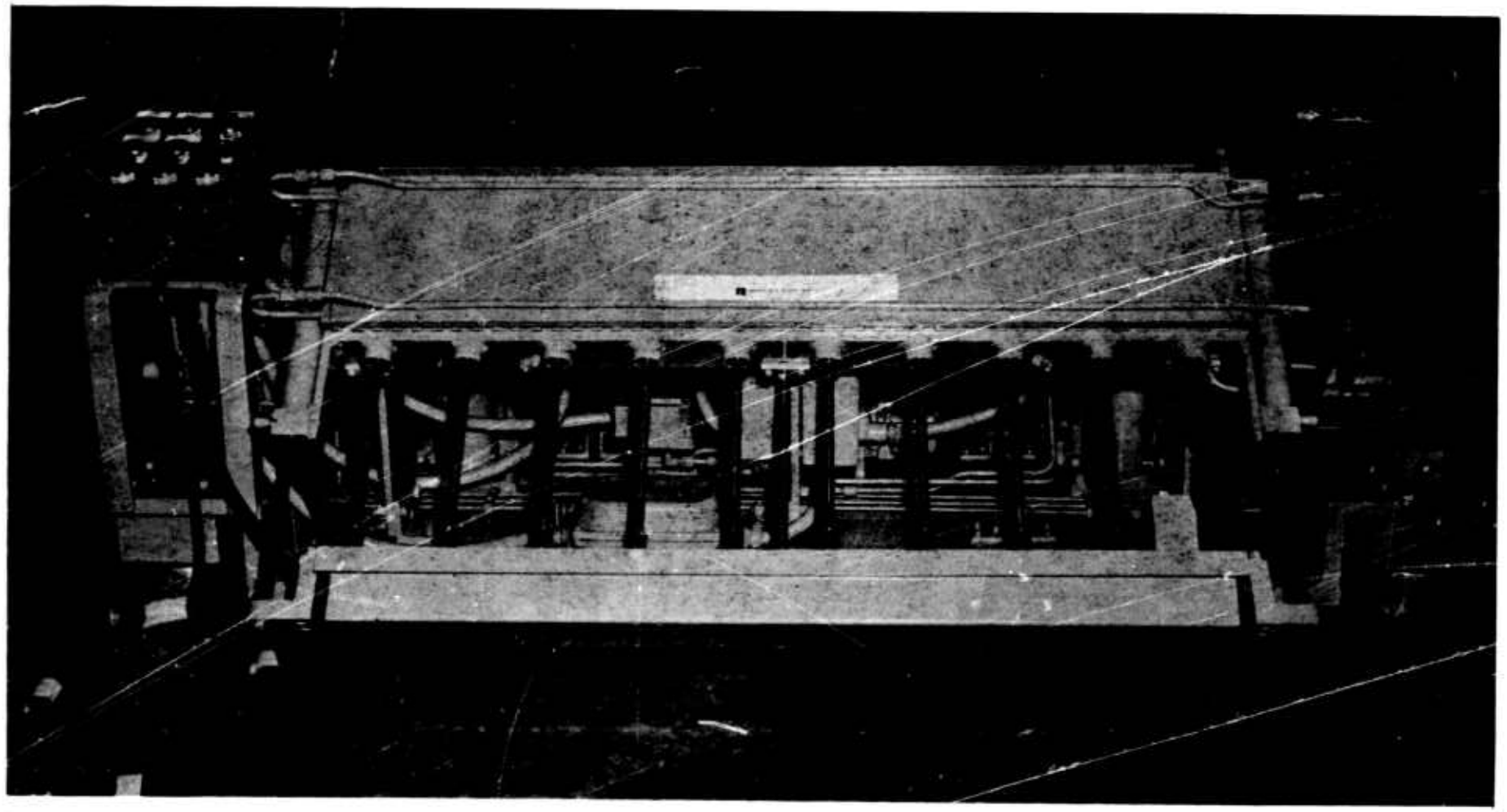
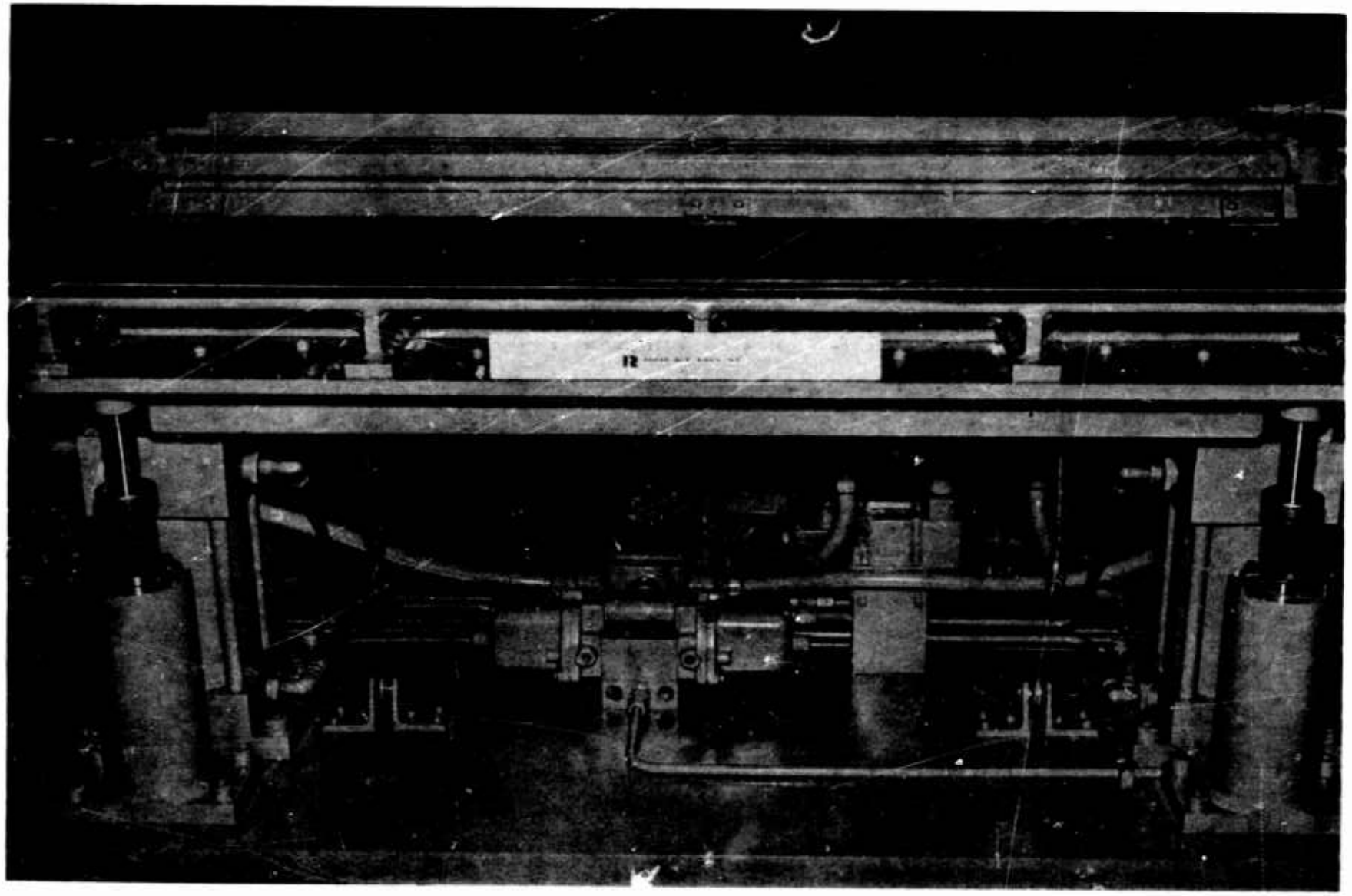


Figure 1 . Schematic of Propellant Feed System for Reinforced Grain



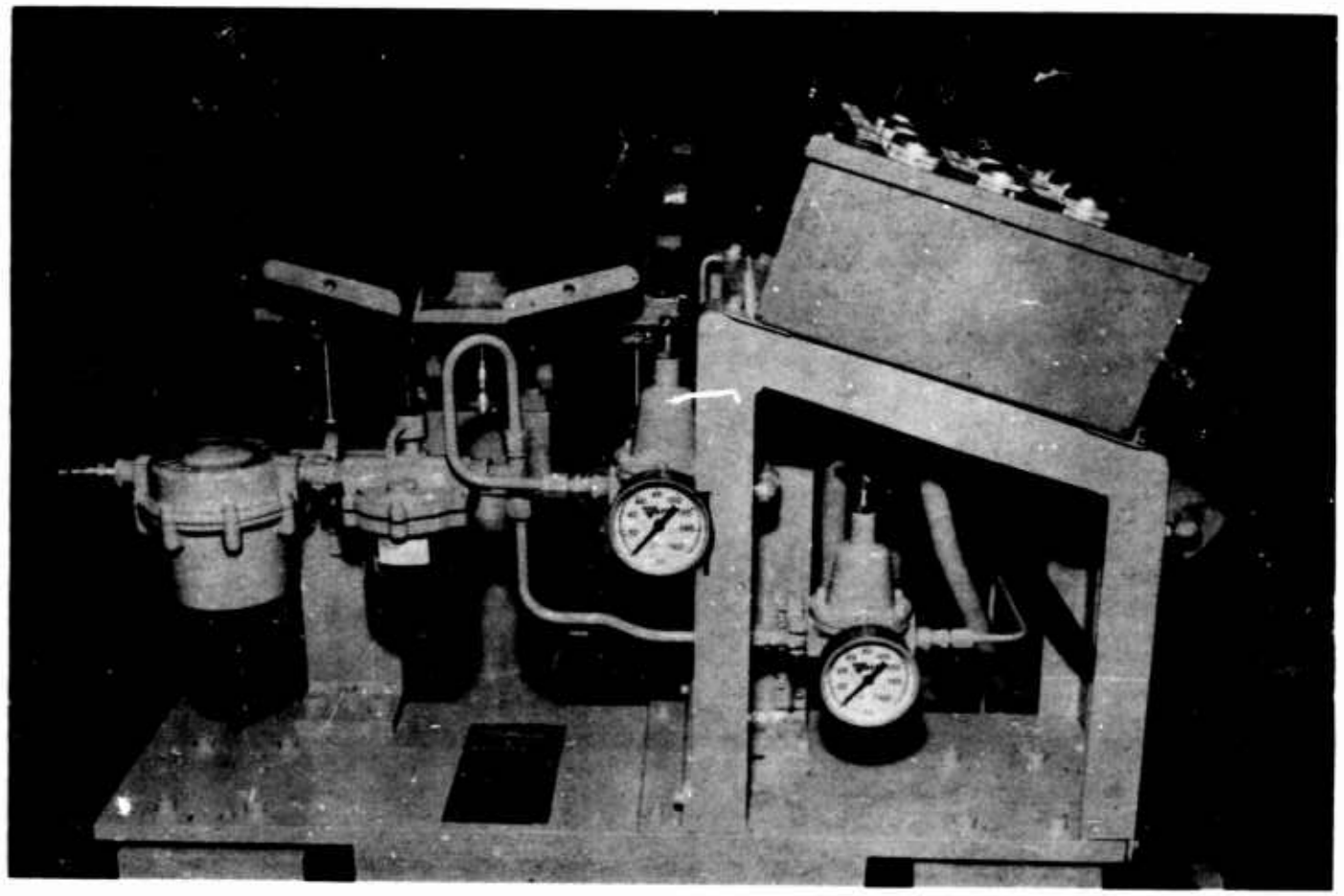
2/YA91-2/20/64M1A

Figure 2 . Extruder Unit Showing Extrusion Rams



2/YA91-2/20/64M1G

Figure 3 . Plastic Propellant Cartridge Nozzles



2/YA91-2/20/64M1C

Figure 4 . Extruder Unit End View

PREVIOUS PAGE WAS BLANK, THEREFORE WAS NOT FILMED

APPENDIX VIII

WIRE FEED SYSTEM FOR REINFORCED GRAIN

PREVIOUS PAGE WAS BLANK, THEREFORE WAS NOT FILMED

WIRE FEED SYSTEM FOR REINFORCED GRAIN

The wire feed system for the Reinforced Grain Advanced Development Program consists of several components, each of which are important to wire process control. These components are a tension control fixture, a tension monitor, a wire weight totalizer, a wire gathering fixture and a final wire guide.

The control of the wire tension during grain fabrication is important because of its effect upon the quality and structural capabilities of a reinforced grain. Furthermore, the tension must be held constant to insure winding buildup reproducibility and required wire volume percentage.

The tension monitoring system is used to set the winding tension initially, continuously monitor the tension of one wire and check intermittently the tension of all wires during grain fabrication. The wire weight totalizer was developed to monitor the in-process weight of wire used. The gathering fixture and the final wire guide enable the wire to be fed from the wire tension control to the grain in an orderly predetermined fashion with a minimum of wire friction.

This wire feed system has resulted in a controlled wire tension during winding operations. The previous system allowed only erratic control of wire tension and the tension fluctuated as much as 100 percent of the desired tension. The present system fluctuates no more than 2 percent of the desired tension.

The ability to maintain constant tension has contributed to the improved structural capabilities, web buildup reproducibility, and wire content repeatability of program grains.

DISCUSSION

WIRE TENSION CONTROL

The wire tension control (Fig. 1) is an electro-mechanical servo-system that automatically controls wire tension by varying the driving or retarding torque to the wire spool spindle (see Fig. 2). This unit maintains the preset tension within ± 2 percent. The unit has an adjustable spring loaded servo-arm for each spindle. This arm spring force is balanced by the wire loop from the spindle to the feed position. If tension varies, the loop allows the servo-arm to move from the equilibrium position. This sends an electrical signal to the servo motor which brings the system back to equilibrium by increasing or decreasing the driving torque of the wire spool spindle. This system works very well and is capable of compensating for an accelerating or decelerating wire feed rate.

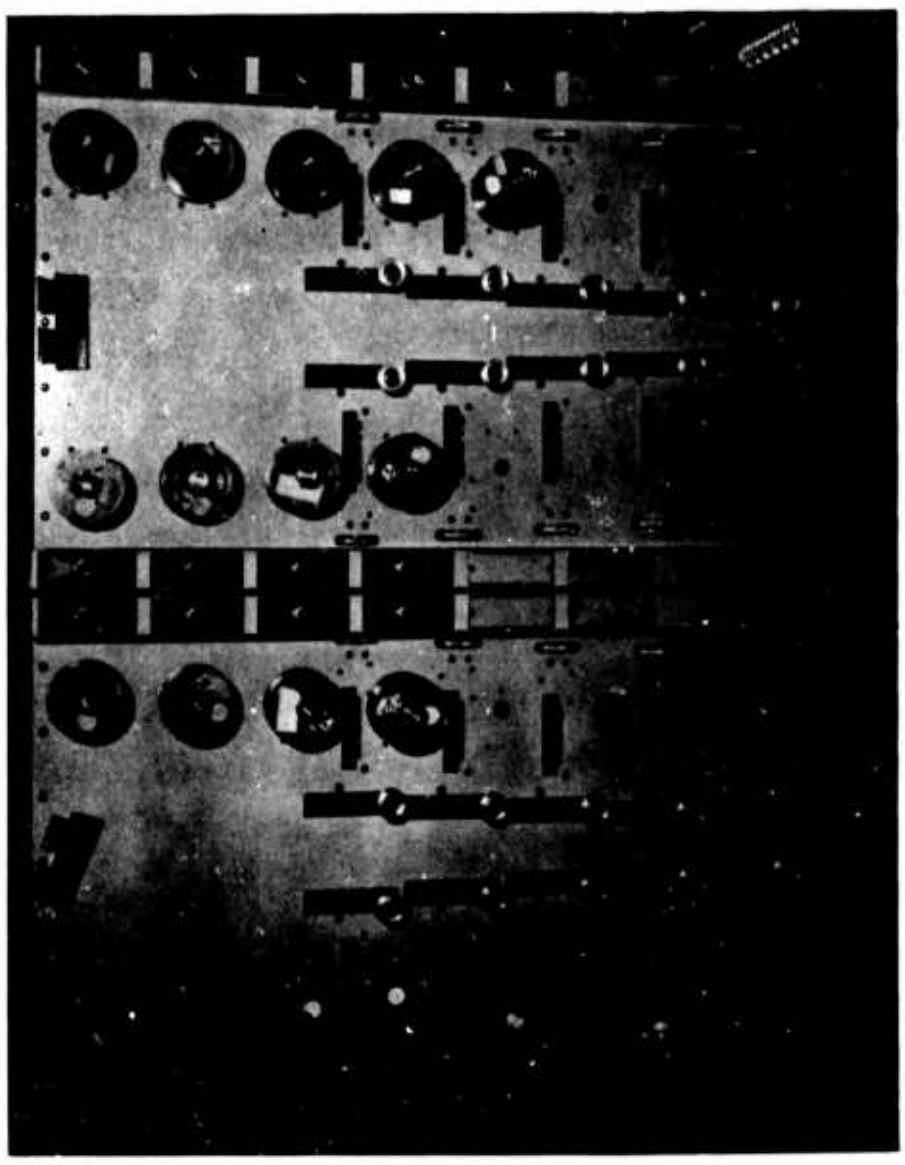


Figure 1. Tension Control Fixture

This tension control fixture was custom designed to Rocketdyne Specifications by Eastern Equipment and Controls Company, Roselle Park, New Jersey. Standard components were incorporated into a design package which would be compatible with the complete wire feed system requirements. The fixture was designed to accommodate 5 pounds of wire per spindle. The unit is capable of delivering wire at any rate up to 240 feet per minute. The tension range is adjustable from 200 to 800 grams with independent adjustments for each spindle.

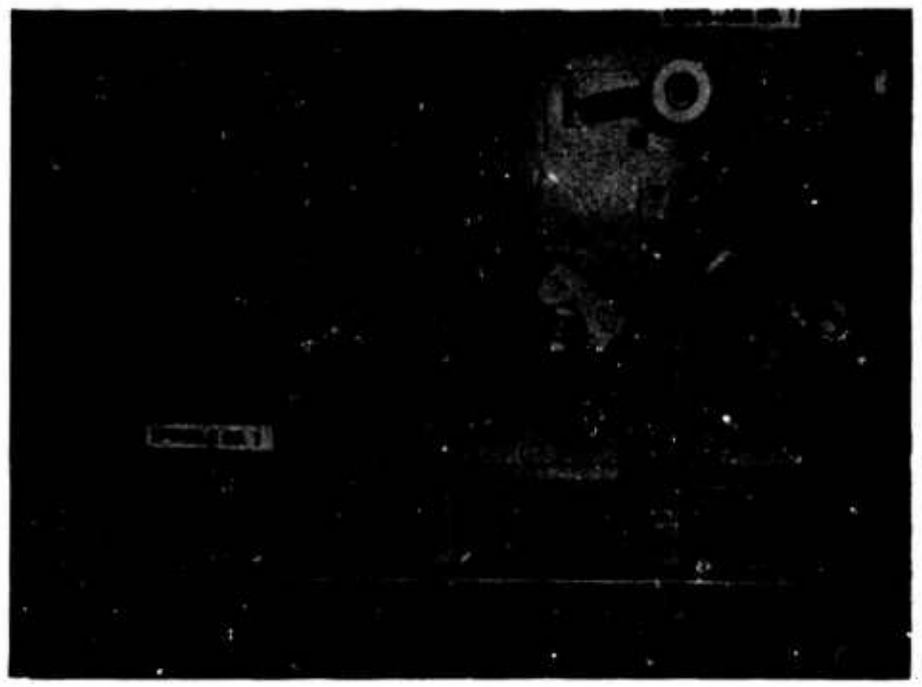


Figure 2. Control System, Tension Control Fixture

An alarm system which signals a wire break was included in the design. Actuation of the system rings a bell and illuminates a red light located by the spindle involved. This system may be bypassed for any spindle not being used.

The complete unit has 36 spindle assemblies with space provisions for 12 additional spindles for future requirements. Spare spindle assemblies were ordered and will be available for use in the event of a component malfunction during winding operations.

This wire tension control fixture has eliminated most of the wire breakage problems experienced with mechanical tension controls previously used. The mechanical controls were not capable of close tension control

and the tension constantly fluctuated, particularly during acceleration and deceleration. The mechanical controls had to be reset frequently to compensate for the change in spool feed diameter as the wire was depleted.

The servo-system tension control has decreased winding time by decreasing the amount of wire breakage and virtually eliminating the need to reset the tension during winding. Changing spools is much faster because of the quick release system used for securing the spools. This ability to maintain constant tension allowed better evaluation of other components of the wire feed system, and pointed out the need for improvements in these components.

WIRE GATHERING SYSTEM

The wire gathering system (Fig. 3) is an important component of the wire feed system. It enables the wire to be fed from the wire tension control to the grain in an orderly fashion. The gathering system must be designed in such a manner as to be as frictionless as possible so as not to offset the advantages of a good tension control system.

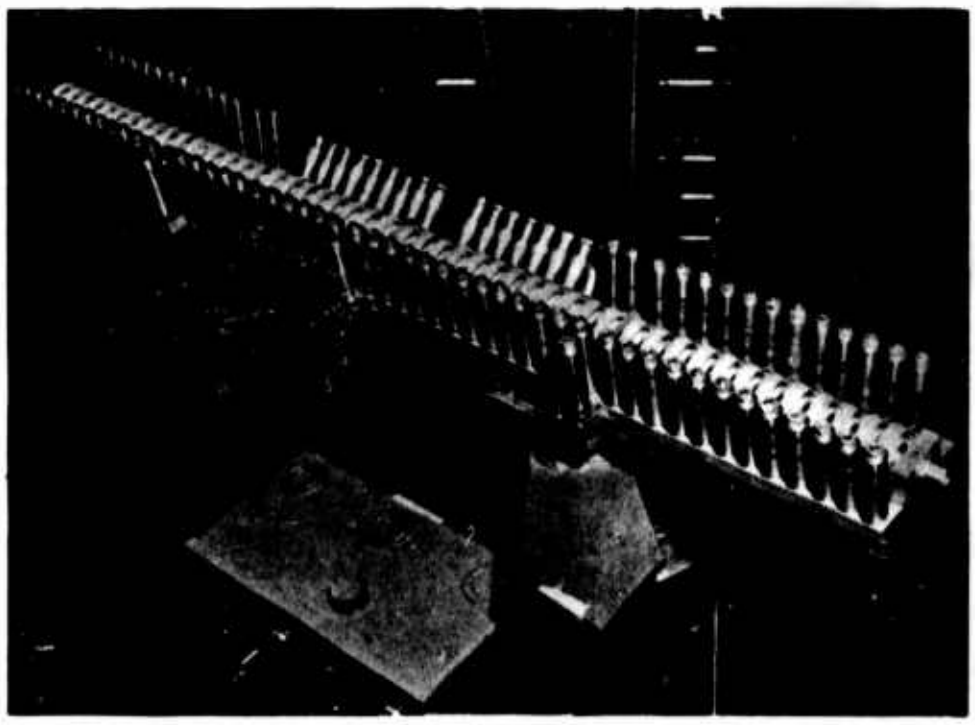


Figure 3. Wire Gathering Fixture

The gathering system has individual feed paths for each wire being used. This is necessary because all the wires do not feed at the same rate during dome winding. Each feed path for the wires is composed of ball bearing rollers and pulleys.

The gathering system is a considerable improvement over that previously used. The individual ball bearing feed paths do not cause the large tension variation during winding previously experienced. The design concept was not changed radically from the previous gathering system, the improvement being basically due to the use of the ball bearing rollers and pulleys.

FINAL WIRE GUIDE

The final wire guide (Fig. 4) is the fixture which dictates the wire spacing within the wire warp being wound on the grain. The final wire guide, usually referred to as the follower head, is attached to the boom of the winding machine. This gives the follower head the tri-axial motion required for laying the wire warp on the mandrel in the desired location.

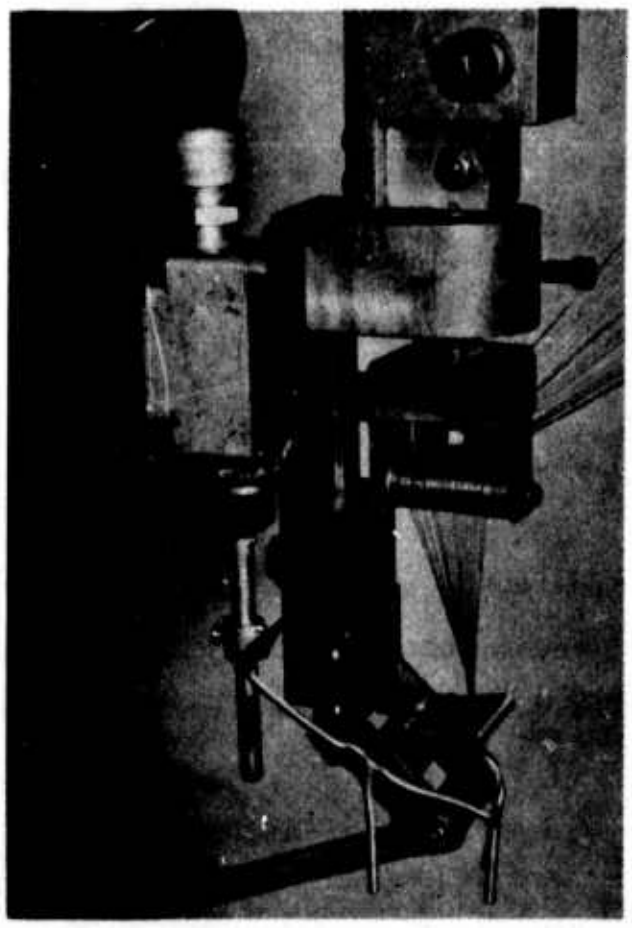


Figure 4. Follower Head

The wire is fed to the follower head from the wire gathering system which remains stationary while the follower head is traversing the length of the mandrel being wound upon. This causes the wire to be fed from the gathering system into the follower head at a constantly varying angle. The wire is then fed from the follower head to the grain at another varying angle which is determined by the winding geometry.

The follower head design must allow for these variations in wire feed angles. Two spacer combs and rollers are used to guide the wire with the least amount of drag while moving through the various feed angles. The initial comb and roller set is free swiveling so that it is always oriented at the optimum position with the gathering system. The final comb and roller set is controlled by the machine winding cams so that it is oriented as required by the winding geometry. The swiveling comb and roller was located at the axis of rotation of the cam oriented comb and roller. This location keeps the friction variation, caused by the combs, at a minimum. Ball bearings have been used in the rollers to keep the drag to a minimum.

The previous design for the follower head did not allow for this minimum friction variation. The comb and roller sets were not oriented on the same axis of rotation so severe wire feed angles resulted at the spacer comb as the follower head traversed the length of the grain. The rollers had sleeve bearings rather than ball bearings which also caused considerable drag.

WIRE TOTALIZER

The wire totalizer (Figure 5) is used to record the amount of wire wound into a grain. The amount used may be determined at any time during the winding process. This capability allows an in-process monitoring of an important process control variable.

The wire totalizer is nothing more than a calibrated wheel over which the wire runs. Each revolution of the wheel is recorded by an electric counter. The counter is actuated by a proximity sensor located at the calibrated wheel. The wheel has an element located near the periphery which energizes the proximity switch each revolution. This proximity switch is a stock item offered by Honeywell.

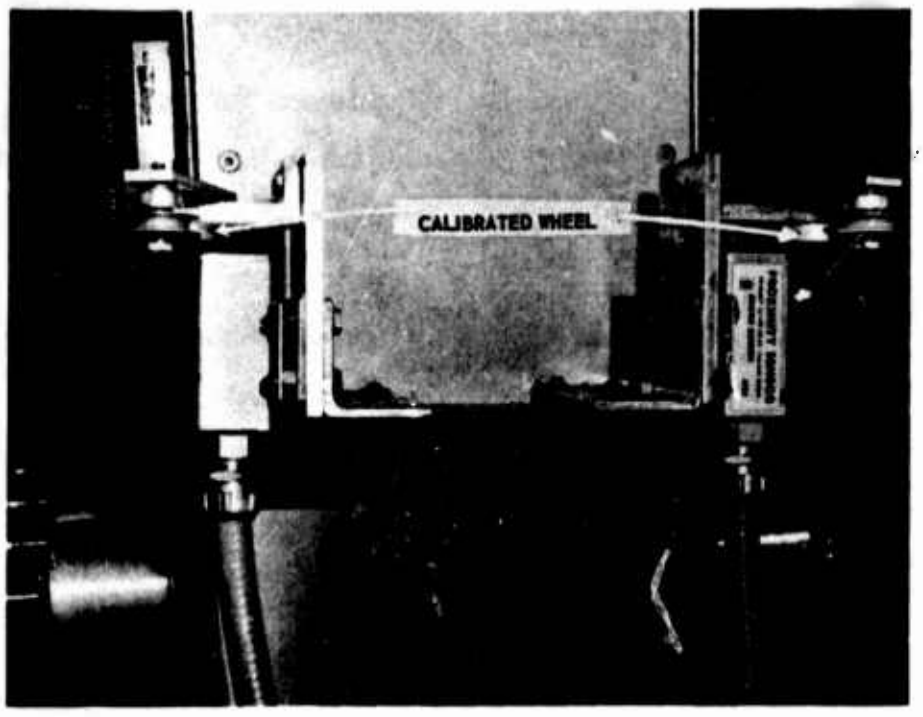


Figure 5. Wire Totalizer

This system has been calibrated so that each revolution of the wheel, when multiplied by a conversion factor, represents the wire weight used. The calibration of the system indicated that errors due to variations in wire diameter and wire density caused no more than $\pm$ 0.3 percent error in weight.

The results of this system were very good when checked during a grain winding. The wire weight obtained by this system varied only 0.8 percent from the weight obtained by actual weighings of the wire spools before and after winding.

TENSION MONITOR

An accurate and reliable system for measuring wire tension is a very important requirement for any wire feed system. Figure 6 illustrates the tension monitoring system chosen for this wire feed system. It consists of a tension transducer and an indicator. The transducer is a shelf item offered by Tensitron, Inc., Harvard, Massachusetts. It is essentially a cantilever beam with a full-bridge strain gage. The indicator is a Sanborn Transducer Amplifier-Indicator Model 311 which was obtained from the Sanborn Company, Waltham, Massachusetts.

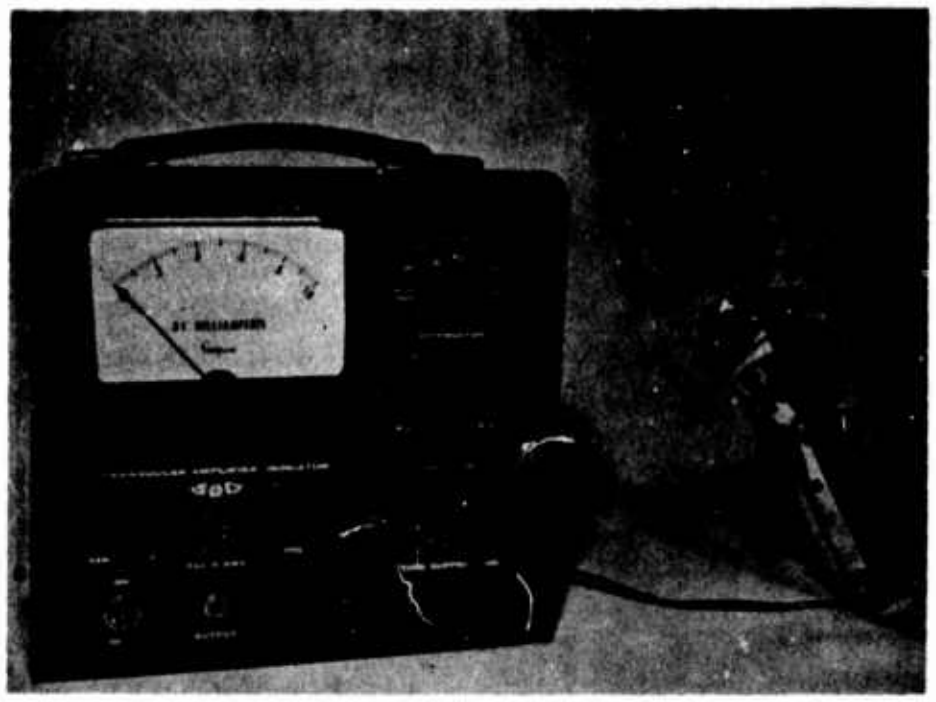


Figure 6. Tension Monitoring System

The system has proven to be a considerable improvement over the previously used tensiometers which were mechanical in nature and consisted of springs and gears. All of the components were subject to damage and wear which soon resulted in erroneous readings.

COMPARATIVE TESTS

A series of tests were conducted to compare the new wire feed system with the previous system. The results of these tests are shown in Tables 1 and 2. These tests were conducted with a follower head setting which would be required for winding a 60 degree helix angle pattern. The follower head positions are referenced to a Motor A mandrel.

TABLE 1

PREVIOUS TENSION CONTROL SYSTEM

	Tension at Control	Tension After Gathering System	Tension After Follower Head
Follower Head at Grain Mid Point	350 grams	350 grams	650 grams
Follower Head at Headstock Tangent Point	350 grams	450 grams	1000 grams
Follower Head at Tailstock Tangent Point	350 grams	450 grams	1000 grams

TABLE 2

NEW TENSION CONTROL SYSTEM

	Tension at Control	Tension After Gathering System	Tension After Follower Head
Follower Head at Grain Mid Point	350 grams	350 grams	380 grams
Follower Head at Headstock Tangent Point	350 grams	350 grams	380 grams
Follower Head at Tailstock Tangent Point	350 grams	350 grams	380 grams

The data shown in the columns headed Tension at Gathering Systems was obtained by feeding wire through the gathering system only. This shows how the tension varied as the feed angle from the gathering system to the grain varied. The data shown in the columns headed Tension After Follower Head was obtained by feeding wire through the gathering system and follower head. This shows the increase in tension caused by the follower head as the feed angle from the gathering system to the grain varied. Comparison of Table 1 and Table 2 shows the benefits of the design improvements of the wire gathering system and follower head.

The results in Table 1 and Table 2 were obtained by dynamic wire tension measurements with the follower head remaining static. Tests were also performed during actual winding conditions. These tests compared very well with the data shown in Table 1 and Table 2.

DOCUMENT CONTROL DATA · R&D

(Security classification of title, body of abstract and indexing annotation must be entered when the overall report is classified)

1 ORIGINATING ACTIVITY (Corporate author)
North American Aviation, Inc.
Rocketdyne Division
McGregor, Texas

2a REPORT SECURITY CLASSIFICATION
CONFIDENTIAL

2b GROUP
4

3 REPORT TITLE

Reinforced Grain Advanced Development Program

4 DESCRIPTIVE NOTES (Type of report and inclusive dates)

5 AUTHOR(S) (Last name, first name, initial)

Engineering Department, Rocketdyne, Solid Rocket Division, McGregor, Texas

6 REPORT DATE	7a TOTAL NO. OF PAGES	7b NO. OF REFS
October 1966	940	None

8a CONTRACT OR GRANT NO.	9a ORIGINATOR'S REPORT NUMBER(S)
AF 04(611)-9090 b PROJECT NO.	R-4233-22
c d	9b OTHER REPORT NO(S) (Any other numbers that may be assigned this report)

10 AVAILABILITY/LIMITATION NOTICES In addition to security requirements which must be met, this document is subject to special export controls and each transmittal to foreign nations may be made only with prior approval of AFRPL (RPPR/STINFO), Edwards, California 93523.

11 SUPPLEMENTARY NOTES	12 SPONSORING MILITARY ACTIVITY

13 ABSTRACT

The program originally outlined the development of three designs of lightweight, upper-stage motors using wire as grain reinforcement. Eventually, one of the original three upper-stage designs was replaced by a testweight air-launched demonstration motor with extreme environmental requirements. One of the upper-stage designs included a supersonic split-line gimbaled nozzle. Static firing test results of the upper-stage motors showed the design approach yielded high mass fraction goals. However, fabrication experience proved that unusual care and development approaches were necessary. Limitations and areas of risk, as well as preferred approaches, were established from the wide range of tests conducted during this Advanced Development Program. (Unclassified Abstract).

DD FORM 1 JAN 64 1473

14 KEY WORDS	LINK A		LINK B		LINK C	
	ROLE	WT	ROLE	WT	ROLE	WT
Solid Fuel Rocket Motor Wire Reinforced Grain, Upper-Stage Motor Advanced Development						

INSTRUCTIONS

1. **ORIGINATING ACTIVITY:** Enter the name and address of the contractor, subcontractor, grantee, Department of Defense activity or other organization *(corporate author)* issuing the report.

2a. **REPORT SECURITY CLASSIFICATION:** Enter the overall security classification of the report. Indicate whether "Restricted Data" is included. Marking is to be in accordance with appropriate security regulations.

2b. **GROUP:** Automatic downgrading is specified in DoD Directive 5200.10 and Armed Forces Industrial Manual. Enter the group number. Also, when applicable, show that optional markings have been used for Group 3 and Group 4 as authorized.

3. **REPORT TITLE:** Enter the complete report title in all capital letters. Titles in all cases should be unclassified. If a meaningful title cannot be selected without classification, show title classification in all capitals in parenthesis immediately following the title.

4. **DESCRIPTIVE NOTES:** If appropriate, enter the type of report, e.g., interim, progress, summary, annual, or final. Give the inclusive dates when a specific reporting period is covered.

5. **AUTHOR(S):** Enter the name(s) of author(s) as shown on or in the report. Enter last name, first name, middle initial. If military, show rank and branch of service. The name of the principal author is an absolute minimum requirement.

6. **REPORT DATE:** Enter the date of the report as day, month, year; or month, year. If more than one date appears on the report, use date of publication.

7a. **TOTAL NUMBER OF PAGES:** The total page count should follow normal pagination procedures, i.e., enter the number of pages containing information.

7b. **NUMBER OF REFERENCES:** Enter the total number of references cited in the report.

8a. **CONTRACT OR GRANT NUMBER:** If appropriate, enter the applicable number of the contract or grant under which the report was written.

8b, 8c, & 8d. **PROJECT NUMBER:** Enter the appropriate military department identification, such as project number, subproject number, system numbers, task number, etc.

9a. **ORIGINATOR'S REPORT NUMBER(S):** Enter the official report number by which the document will be identified and controlled by the originating activity. This number must be unique to this report.

9b. **OTHER REPORT NUMBER(S):** If the report has been assigned any other report numbers *(either by the originator or by the sponsor)*, also enter this number(s).

10. **AVAILABILITY/LIMITATION NOTICES:** Enter any limitations on further dissemination of the report, other than those imposed by security classification, using standard statements such as:

(1) "Qualified requesters may obtain copies of this report from DDC."

(2) "Foreign announcement and dissemination of this report by DDC is not authorized."

(3) "U. S. Government agencies may obtain copies of this report directly from DDC. Other qualified DDC users shall request through _____."

(4) "U. S. military agencies may obtain copies of this report directly from DDC. Other qualified users shall request through _____."

(5) "All distribution of this report is controlled. Qualified DDC users shall request through _____."

If the report has been furnished to the Office of Technical Services, Department of Commerce, for sale to the public, indicate this fact and enter the price, if known.

11. **SUPPLEMENTARY NOTES:** Use for additional explanatory notes.

12. **SPONSORING MILITARY ACTIVITY:** Enter the name of the departmental project office or laboratory sponsoring *(paying for)* the research and development. Include address.

13. **ABSTRACT:** Enter an abstract giving a brief and factual summary of the document indicative of the report, even though it may also appear elsewhere in the body of the technical report. If additional space is required, a continuation sheet shall be attached.

It is highly desirable that the abstract of classified reports be unclassified. Each paragraph of the abstract shall end with an indication of the military security classification of the information in the paragraph, represented as *(TS)*, *(S)*, *(C)*, or *(U)*.

There is no limitation on the length of the abstract. However, the suggested length is from 150 to 225 words.

14. **KEY WORDS:** Key words are technically meaningful terms or short phrases that characterize a report and may be used as index entries for cataloging the report. Key words must be selected so that no security classification is required. Identifiers, such as equipment model designation, trade name, military project code name, geographic location, may be used as key words but will be followed by an indication of technical context. The assignment of links, rules, and weights is optional.